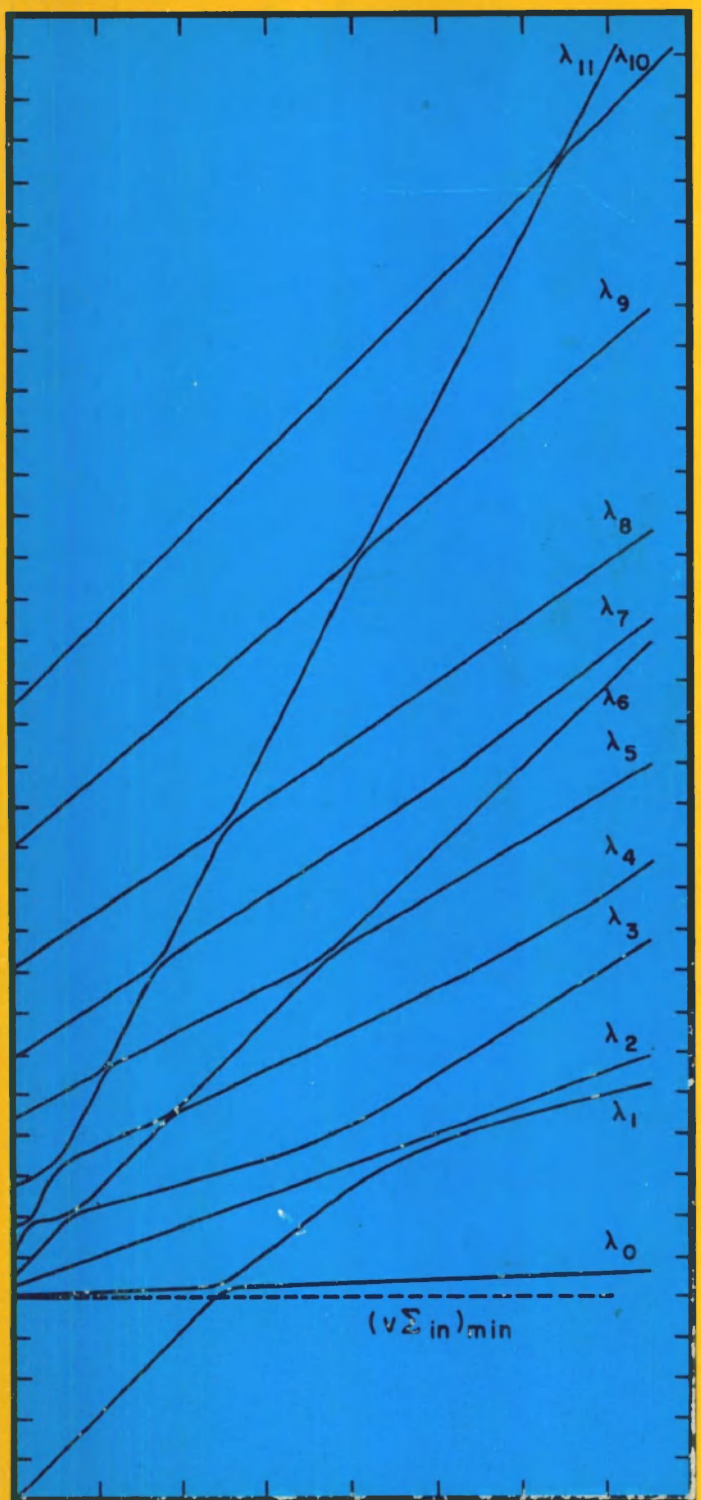

Vol. I

PULSED NEUTRON RESEARCH

Proceedings of a Symposium, Karlsruhe, 10-14 May 1965

INTERNATIONAL ATOMIC ENERGY AGENCY, VIENNA, 1965

PULSED NEUTRON RESEARCH

VOL.I

The following States are Members of the International Atomic Energy Agency:

AFGHANISTAN
ALBANIA
ALGERIA
ARGENTINA
AUSTRALIA
AUSTRIA
BELGIUM
BOLIVIA
BRAZIL
BULGARIA
BURMA
BYELORUSSIAN SOVIET SOCIALIST REPUBLIC
CAMBODIA
CAMEROON
CANADA
CEYLON
CHILE
CHINA
COLOMBIA
CONGO, DEMOCRATIC REPUBLIC OF
COSTA RICA
CUBA
CYPRUS
CZECHOSLOVAK SOCIALIST REPUBLIC
DENMARK
DOMINICAN REPUBLIC
ECUADOR
EL SALVADOR
ETHIOPIA
FINLAND
FRANCE
FEDERAL REPUBLIC OF GERMANY
GABON
GHANA
GREECE
GUATEMALA
HAITI
HOLY SEE
HONDURAS
HUNGARY
ICELAND
INDIA
INDONESIA
IRAN
IRAQ
ISRAEL
ITALY
IVORY COAST
JAPAN
KENYA
REPUBLIC OF KOREA
KUWAIT
LEBANON
LIBERIA
LIBYA
LUXEMBOURG
MADAGASCAR
MALI
MEXICO
MONACO
MOROCCO
NETHERLANDS
NEW ZEALAND
NICARAGUA
NIGERIA
NORWAY
PAKISTAN
PARAGUAY
PERU
PHILIPPINES
POLAND
PORTUGAL
ROMANIA
SAUDI ARABIA
SENEGAL
SOUTH AFRICA
SPAIN
SUDAN
SWEDEN
SWITZERLAND
SYRIA
THAILAND
TUNISIA
TURKEY
UKRAINIAN SOVIET SOCIALIST REPUBLIC
UNION OF SOVIET SOCIALIST REPUBLICS
UNITED ARAB REPUBLIC
UNITED KINGDOM OF GREAT BRITAIN AND NORTHERN IRELAND
UNITED STATES OF AMERICA
URUGUAY
VENEZUELA
VIET-NAM
YUGOSLAVIA

The Agency's Statute was approved on 23 October 1956 by the Conference on the Statute of the IAEA held at United Nations Headquarters, New York; it entered into force on 29 July 1957. The Headquarters of the Agency are situated in Vienna. Its principal objective is "to accelerate and enlarge the contribution of atomic energy to peace, health and prosperity throughout the world".

Printed by the IAEA in Austria
August 1965

PROCEEDINGS SERIES

PULSED NEUTRON RESEARCH

PROCEEDINGS OF THE SYMPOSIUM ON
PULSED NEUTRON RESEARCH
HELD BY THE
INTERNATIONAL ATOMIC ENERGY AGENCY
AT KARLSRUHE, 10-14 MAY 1965

In two volumes

VOL.I

INTERNATIONAL ATOMIC ENERGY AGENCY
VIENNA, 1965

Symposium on Pulsed Neutron Research, Karlsruhe, 10 - 14 May 1965.
Proceedings . . . held by the International Atomic Energy Agency, Vienna, the Agency, 1965.
2 vols. (IAEA Proceedings series)

621.039.512
539.125.5

PULSED NEUTRON RESEARCH
IAEA, VIENNA, 1965
STI/PUB/104

FOREWORD

In recent years there has been growing interest in transient, as opposed to static, techniques of neutron and reactor physics investigation. Perhaps the most notable example of the newer transient techniques is the pulsed neutron source method which has been applied to various studies of the detailed interaction of neutrons with non-multiplying as well as multiplying media.

More than 230 scientists from 22 countries and 3 international organizations participated in this IAEA Symposium held at the Kernforschungszentrum Karlsruhe, at the invitation of the Government of the Federal Republic of Germany. Although there have been previous meetings concerned with pulsed neutron measurements (notably at Berkeley in 1958 and at Brookhaven in 1962), this was the first international meeting on pulsed neutron research in which working scientists from all parts of the world participated.

This Symposium has provided not only new and significant pulsed neutron data, but also, what is equally important, fresh viewpoints of interpretation pointing toward useful directions for future pulsed neutron investigation. The general opinion of participants at Karlsruhe was that the potential value of pulsed neutron studies, on fast systems particularly, has scarcely been tapped and that much greater effort in this direction can be expected in the coming years.

EDITORIAL NOTE

The papers and discussions incorporated in the proceedings published by the International Atomic Energy Agency are edited by the Agency's editorial staff to the extent considered necessary for the reader's assistance. The views expressed and the general style adopted remain, however, the responsibility of the named authors or participants.

For the sake of speed of publication the present Proceedings have been printed by composition typing and photo-offset lithography. Within the limitations imposed by this method, every effort has been made to maintain a high editorial standard; in particular, the units and symbols employed are to the fullest practicable extent those standardized or recommended by the competent international scientific bodies.

The affiliations of authors are those given at the time of nomination.

The use in these Proceedings of particular designations of countries or territories does not imply any judgement by the Agency as to the legal status of such countries or territories, of their authorities and institutions or of the delimitation of their boundaries.

The mention of specific companies or of their products or brand-names does not imply any endorsement or recommendation on the part of the International Atomic Energy Agency.

CONTENTS OF VOL. I

NON-MULTIPLYING SYSTEMS - EXPERIMENT (Session I)

NON-MULTIPLYING SYSTEMS - THEORY (Session II)

NEUTRON THERMALIZATION AND SPECTRA (Session III)

NON-MULTIPLYING SYSTEMS – EXPERIMENT

(Session I)

A REVIEW OF PULSED NEUTRON EXPERIMENTS ON NON-MULTIPLYING MEDIA

K.H. BECKURTS
KERNFORSCHUNGSZENTRUM, KARLSRUHE,
FEDERAL REPUBLIC OF GERMANY

Abstract — Résumé — Аннотация — Resumen

A REVIEW OF PULSED NEUTRON EXPERIMENTS ON NON-MULTIPLYING MEDIA. For the last twelve years, the technique of pulsed neutron sources has been employed with increasing success for the study of the kinetic behaviour of neutrons in matter. Although the most useful applications of the technique are now in the field of reactivity measurements on multiplying media, there is a continuing interest in its use for studying transient and asymptotic neutron phenomena in non-multiplying assemblies.

A condensed review of this latter type of experiment is given, with particular emphasis on progress since the International Conference on Neutron Thermalization which was held in 1962 at the Brookhaven National Laboratory. This review includes a detailed discussion of the experimental condition for the observation of clean "transient" and "asymptotic" modes. Results for diffusion parameters are summarized and, wherever possible, compared with calculations based on experimental values of the scattering law.

Some new applications of the technique are discussed, for example :

(1) Friedmann's method for the determination of thermalization parameters;

(2) The simultaneous observation of space and time transients in pulsed moderators;

(3) Fast neutron field decay in non-multiplying assemblies of heavy materials.

Finally, a critical comparison between the pulsed source technique and other methods for the investigation of transient and asymptotic neutron phenomena (static methods; harmonically modulated sources) is made.

APERÇU D'ENSEMBLE DES EXPÉRIENCES SUR DES MILIEUX NON MULTIPLICATEURS AU MOYEN DES NEUTRONS PULSÉS. Depuis une douzaine d'années, on utilise avec un succès croissant la méthode des sources de neutrons pulsés pour l'étude du comportement cinétique des neutrons dans la matière. Les applications les plus utiles de cette méthode portent actuellement sur les mesures de la réactivité de milieux multiplicateurs, mais on s'intéresse toujours à son emploi pour l'étude des phénomènes neutroniques transitoires et asymptotiques dans des assemblages non multiplicateurs.

L'auteur donne un aperçu d'ensemble des expériences de ce deuxième type en insistant surtout sur les progrès accomplis depuis la Conférence internationale sur la thermalisation des neutrons, tenue à Brookhaven en 1962. Il discute en détail la condition expérimentale nécessaire pour l'observation des modes « transitoire » et « asymptotique » sans poison. Il fait la synthèse des résultats concernant les paramètres de diffusion et, chaque fois que c'est possible, les compare aux résultats des calculs fondés sur les valeurs expérimentales de la loi de diffusion.

Il décrit certaines applications nouvelles de la méthode et notamment:

1. La méthode de Friedmann pour la détermination des paramètres de thermalisation.

2. L'absorption simultanée des états transitoires variables dans l'espace et dans le temps, dans les ralentisseurs pulsés.

3. La décroissance du champ des neutrons rapides dans des assemblages non multiplicateurs en matières lourdes.

Il procède enfin à une comparaison critique de la méthode de la source pulsée avec d'autres méthodes utilisées pour l'étude des états transitoires et asymptotiques des neutrons (méthodes statiques; sources à modulation harmonique).

ОБЗОР ЭКСПЕРИМЕНТОВ С ИМПУЛЬСНЫМИ НЕЙТРОНАМИ В НЕРАЗМНОЖАЮЩЕЙ СРЕДЕ. В последние двенадцать лет все более успешно используется метод источников импульсных нейтронов для изучения кинетического поведения нейтронов в веществе. Хотя наиболее успешно этот метод применяется теперь в области измерений реактивности в размножающей среде, проявляется постоянный интерес к его использованию при изучении переходных и асимптотических нейтронных явлений в неразмножающих сборках.

Дается подробный обзор этого последнего типа экспериментов, особо отмечаются успехи, достигнутые со времени Международной конференции по термализации нейтронов в Брукхейвене в 1962 году. Обзор включает детальное обсуждение экспериментальных условий для наблюдения чистых "переходных" и "асимптотических" форм. Результаты по диффузионным параметрам суммируются и, когда это возможно, сравниваются с расчетами, основанными на экспериментальных значениях закона рассеяния.

Обсуждаются некоторые новые методы, например:

1. Метод Фридмана для определения параметров термализации.
2. Метод одновременного наблюдения переходных характеристик во времени и пространстве при импульсе в замедлителе.
3. Метод спада поля быстрых нейтронов в неразмножающих сборках из тяжелых материалов.

В заключение критически сравнивается метод импульсных источников с другими методами исследования переходных и асимптотических нейтронных явлений (статические методы, гармонически модулированные источники).

ESTUDIO PANORAMICO DE DIVERSOS EXPERIMENTOS CON NEUTRONES PULSADOS EN MEDIOS NO MULTIPLICADORES. En el curso de los últimos doce años la técnica de los neutrones pulsados se ha venido empleando con éxito creciente para estudiar el comportamiento cinético de los neutrones en la materia. Aunque las aplicaciones más útiles de esta técnica corresponden actualmente a la esfera de las mediciones de la reactividad realizadas en medios multiplicadores, subsiste el interés por su empleo en el estudio de los fenómenos *neutrónicos transitorios y asintóticos en conjuntos no multiplicadores.*

El autor ofrece un estudio resumido de esta última clase de experimentos, atendiendo especialmente a los progresos conseguidos desde 1962, año en que se celebró en Brookhaven la Conferencia Internacional sobre *Termalización Neutrónica. El estudio panorámico incluye un examen* detallado de las condiciones experimentales necesarias para la observación de los modos «transitorios» y «asintóticos», sin deformaciones. En él se resumen, además, los resultados obtenidos para los parámetros de difusión, y se comparan - cuando es posible - con los de cálculos realizados partiendo de *valores experimentales obtenidos con arreglo a la ley de* dispersión.

El autor examina algunas de las nuevas aplicaciones de la mencionada técnica, entre ellas las siguientes:

1. Determinación de los parámetros de termalización por el método de Friedmann.
2. Observación simultánea de los fenómenos transitorios de carácter espacial y temporal en moderadores sometidos a los efectos de los neutrones pulsados.
3. Decrecimiento del campo de neutrones rápidos en conjuntos no multiplicadores de materiales pesados.

Por último, el autor establece una comparación entre la técnica de los neutrones pulsados y otros métodos de investigación de los fenómenos neutrónicos transitorios y asintóticos (métodos estáticos, fuentes armónicamente moduladas).

1. INTRODUCTION

For the last twelve years, there has been an increasing interest in the use of pulsed source techniques for the study of neutron migration, thermalization and absorption in matter. For instance, about twenty different determinations of the diffusion parameters of ordinary water and ice, more than thirty experiments on various "organic" moderators – many of them as a function of temperature – and nine experiments on graphite have been published. Much of the data determined in this way is in disagreement and it appears doubtful if its use in reactor design has justified this enormous effort. There is no doubt, however, that these studies have, probably more than any other class of experiments, contributed to a better understanding of the kinetic behaviour of neutrons in matter. In particular, they have stimulated important developments in transport and thermalization theory, some of which are reviewed at this Symposium [1]. Furthermore, neutron kinetic studies

with pulsed sources have proved to be a useful and rather inexpensive field for student training and in fact a growing percentage of the work is being carried out at university laboratories. Finally, the good success which the pulsed source technique is having for reactivity determinations on reactor systems would probably not have been encountered without the important developments in instrumentation and analysis techniques achieved during the early studies on non-multiplying media.

In this paper some recent developments in this field are summarized, especially the progress made since the last major international conference which was held at Brookhaven in 1962 [2]. Section 2 deals mainly with decay measurements on thermalized neutron fields, to which by far the greatest research activity has been devoted. In section 3 transient phenomena in moderators, i.e. experiments to measure slowing-down and thermalization times, are considered. Section 4 deals with the fairly new field of "quasi-asymptotic" decay of monoenergetic neutron fluxes in heavy scattering substances.

This is not a reporter-type conference, and a considerable number of individual contributions are to be presented. In order not to anticipate too much the following papers we restrict ourselves to areas which are not otherwise covered. The paper is therefore far from a complete survey.

2. DECAY OF A THERMALIZED NEUTRON FIELD

Under certain limitations, which are now fairly well understood theoretically [3], a thermalized neutron field in a moderator is in a true asymptotic state and decays strictly exponentially with time. The classical approach is to measure the time constant α of this decay and to correlate it with the geometrical buckling B^2 of the assembly. The resulting α versus B^2 curve is analysed in terms of the diffusion parameters of the moderating material. Instead of varying the size of the system, one also can vary the concentration N of an added non-1/v absorber; analysing the resulting α versus N curve one observes parameters characteristic of the thermalization properties of the scattering medium. There are closely related stationary techniques, i.e. measurement of the diffusion length as a function of concentration of a 1/v or non-1/v absorber. The α versus B^2 method is hampered by three basic difficulties: The first is a purely experimental one, viz. the precise determination of α in the presence of non-asymptotic neutrons and background. The second problem is a theoretical one and consists in the calculation of the geometrical buckling from the given dimensions of the scattering medium. Thirdly, there is the problem of analysing the α versus B^2 curve properly. The difficulty to define the geometrical buckling does not necessarily arise in α versus N or stationary poisoning experiments, since they can be performed on nearly infinite media. The other two problems, however, arise in both latter techniques in an analogous form.

2.1. Problems arising in α-determinations

An asymptotic spectrum is rapidly established in hydrogenous moderators, because of their extremely good thermalization properties. "Waiting

time" problems thus do not seriously affect α-measurements if care is taken to eliminate higher spatial modes. Room-return background can be annoying but the assemblies can be easily shielded, since they tend to be quite small. Another source of background, as noted by SILVER [4], may be photoneutrons from the decay of 7.35-s N^{16} produced by the $O^{16}(n, p)N^{16}$ reaction on the oxygen present in water. This reaction has a threshold at 9.6 MeV and will occur if the neutron source employs the $H^3(d, n)He^4$ reaction. Other authors did not find this background troublesome; it can be eliminated completely by using a $H^2(d, n)He^3$ or other low-energy neutron source. The advantage of using lower energy sources is that shielding against room-return neutrons becomes simpler, and it is for this reason that OGRZEWALSKI et al. [5] used a fast chopper at a research reactor as a neutron source. It should be kept in mind, however, that the elimination of higher spatial modes will be the more difficult the lower the energy of the neutron source.

The situation is quite different in crystalline moderators, such as beryllium and graphite, where the trapping of low energy neutrons creates a serious limit beyond which the decay constant cannot grow. This limiting value, $\lim_{v \to 0} v\Sigma_t$, is about 2600 s^{-1} in graphite and 3800 s^{-1} in beryllium; the critical values of the buckling are about 15×10^{-3} cm^{-2} and 40×10^{-3} cm^{-2}, respectively. The above figures for the $\lim_{v \to 0} v\Sigma_t$ are based on very old measurements of the scattering cross-section below the Bragg cut-off and may therefore be greatly in error [6]. Nevertheless, it is obvious that at very high bucklings no clean asymptotic mode will exist. This is borne out in Fig. 1 where the decay of the neutron density in a beryllium block of $B^2 = 73 \times 10^{-3}$ cm^{-2} is plotted according to FULLWOOD, SLOVACEK and GAERTTNER [7]. The decay is nearly exponential at times between 300 and 700 μs after the pulse injection but tends to be slower later on. To demonstrate that the latter effect cannot be attributed to improper background subtraction, these authors measured, in the same set-up, the neutron decay in a polyethylene assembly whose size was chosen to give approximately the same decay rate. This decay rate was purely exponential as may be seen in Fig. 1. A similar experiment on a small graphite stack was performed by KÜCHLE [8]. He found a similar deviation from a purely exponential decay but the statistical accuracy of the data was not sufficient to support any far-reaching conclusion.

Being aware of these difficulties, most recent experimentalists working on crystalline media have confined their measurements to the low B^2 range. They have also established criteria to ensure that the observed decay corresponds to a true asymptotic state. Other groups experimenting on graphite [9-12] have determined the waiting time which must elapse after the injection of the neutron pulse before beginning the evaluation of the decay curve for α. Figure 2 shows the waiting time required to obtain good exponential decay in graphite according to SERDULA [12].

Recently, there has been some conflicting information. DAVIS, DE JUREN and REIER [13] have used a paraffin shield around their graphite stacks, in addition to the usual cadmium lining. Furthermore, their experimental area was shielded by walls of cans filled with borated water. Using a $H^2(d, n)He^3$ neutron source and collimating these neutrons directly on their graphite assemblies to avoid direct leakage of source neutrons into the experimental

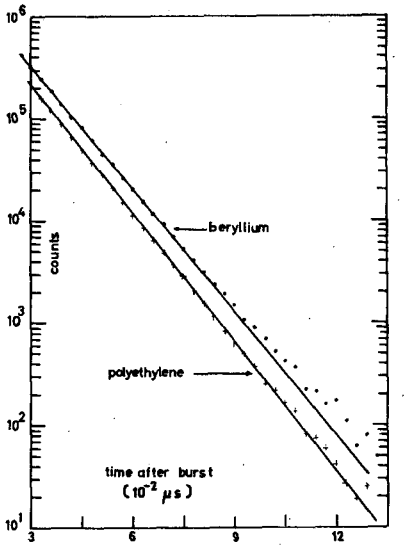

Fig. 1

Neutron die-away in beryllium and in a test assembly of polyethylene selected to give approximately the same decay time (from [7])

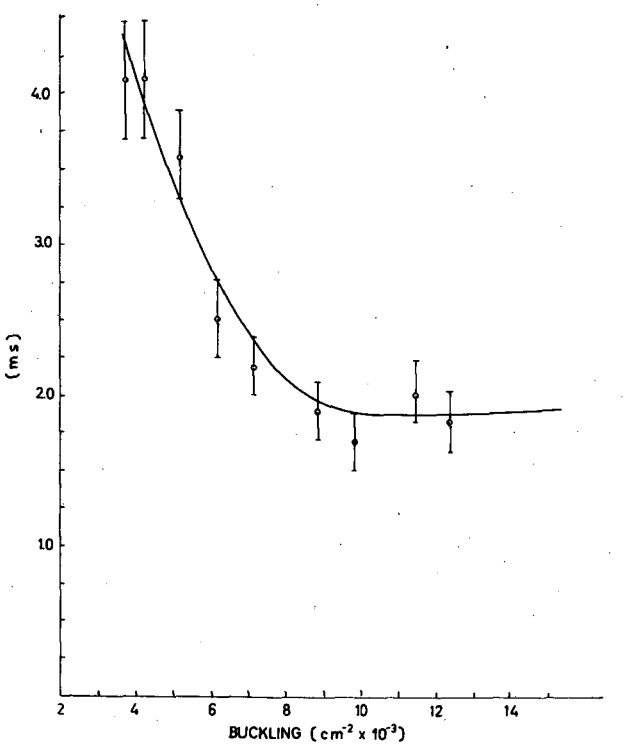

Fig. 2

Time after neutron pulse required for the attainment of an asymptotic spectrum as a function of buckling (from [12])

area, Davis, De Juren and Reier obtained clean exponential decay curves after waiting times of 1 ms or less at bucklings as high as 10×10^{-3} cm^{-2}. They state that "waiting times probably are an artifact of the shielding and the initial neutron energy rather than a property of a graphite stack in space". ZHEZHERUN et al. [14] were able to observe clean exponential decays over up to four decades in beryllium systems at bucklings up to 110×10^{-3} cm^{-2}. This corresponds to α-values up to 10^4 s^{-1}, i.e. figures highly above the critical limit stated before! This is in direct contradiction to the above-mentioned experiment of the R.P.I. (Rensselaer Polytechnic Institute, Troy, N.Y.) group and also violates the critical limit theorem to an extent which would be difficult to explain from inaccuracies in the measured low energy cross-section.

2.2. Definition of the geometrical buckling

The geometrical buckling can be defined in a most straightforward manner if the full space-time distribution can be measured and analysed in terms of Fourier modes. Such measurements are conveniently performed on rather large systems. Experiments on graphite [12, 13] have proved that the relation $d = 2.13\ D_0/\overline{\nu}$ is a very good approximation for the extrapolated endpoint, irrespective of the buckling. For very small water systems, a strong dependency of the extrapolated endpoint on the size and shape of the scattering medium is borne out by the remarkable differences in the α versus B^2 curves measured on "flat" and on "cubic" systems [15-18] whose bucklings were calculated using the simple formula $d = 2.13\ D_0/\overline{\nu}$. Theoretical calculations of the extrapolated endpoint in H_2O show that it decreases with increasing B^2 due to the diffusion cooling effect [19]; these calculations have partly been verified by experiments [18]. However, to explain the measured discrepancies on flat and on cubic systems, the extrapolated endpoint had to increase again considerably at high bucklings. An increase of the extrapolated endpoint for very thin slabs has indeed been predicted from an exact one-group theory treatment of the one-dimensional case [20, 21]. Also, it is known that in one-group theory, in the limit of very small dimensions, the behaviour of the decay constant for slabs and spheres is quite different. To resolve the discrepancies observed on small water systems, a multi-group transport theory treatment of the three-dimensional case would be of great help. Unfortunately, direct measurements of the space-time neutron distribution in these very small systems are not possible for experimental reasons.

2.3. Analysis of α versus B^2 measurements

The usual procedure of evaluating measured α versus B^2 curves is to approximate them by an expression

$$\alpha = \overline{\nu \Sigma_a} + D_0 B^2 - C B^4 + F B^6 + - \ldots \qquad (1)$$

using a method of least squares fitting. Some authors use statistical weight

factors on the individual α_i-values (preferably $\sim 1/\alpha_i^2$); others do not. It has been noted that the variation in the diffusion parameters derived in this way may be several times the most probable statistical error, according to the length of the B^2 interval used, the way in which weight factors were applied, or according to whether or not a B^6 form was included. This is especially the case in graphite where the α versus B^2 curves measured by some authors were in agreement whilst the derived diffusion parameters were not. The most popular explanation for these discrepancies is that the above procedure results in a "global" fit which represents the whole measured α versus B^2 region in the best possible way, thus not yielding necessarily the most probable diffusion parameters. Several authors have therefore used different evaluation procedures. For instance, if the absorption cross-section is known, the simpler relation

$$\frac{\alpha - \overline{v\,\Sigma_a}}{B^2} = D_0 - C\,B^2 + F\,B^4 + - \ldots \qquad (2)$$

is fitted to the corrected data. Other authors use iterative procedures, where the weight given to an experimental point is dependent on the influence which the diffusion parameter to be determined has on α. Most of these procedures, however, do not seem to be free of ambiguities, and for the time being the author would prefer a least squares fitting according to Eq. (1), with appropriate weighting of the individual points.

In view of these difficulties, it has been proposed that measured α versus B^2 curves, after the elementary correction for density and temperature deviations, be compared directly with each other or with the theoretically predicted curves. Apart from the fact that experimentalists will not like this proposal, since they want to produce meaningful physics data instead of unanalysed curves, there are several objections to this procedure. Our main interest in these comparisons is to see the effect of diffusion cooling, i.e. the deviation of the data from the straight-line behaviour. We aim at a theoretical prediction of these effects (i.e. of the coefficients C and F) to, say, 15-25%. To realize these small differences between measured and predicted diffusion cooling by direct comparison of calculated and measured α versus B^2 curves, the accuracy of the theoretical value of D_0 must be very high, say 1%. This high accuracy in the theoretical prediction of D_0 seems difficult to attain, especially in crystalline moderators where the scattering cross-section may vary slightly according to varying grain size. For the latter reason, direct comparisons between various experimental curves may show a larger disagreement in the amount of diffusion cooling than actually exists. In liquid moderators with a well-defined chemical composition, comparisons between experimental curves are reasonable whereas comparisons with theory may be hampered by inaccurate knowledge of D_0.

2.4. Some recent data on ordinary water

Some results of previous experiments are plotted in Fig. 3. Shown at $B^2 > 0$ are the results of pulsed experiments by KUCHLE [15]. At

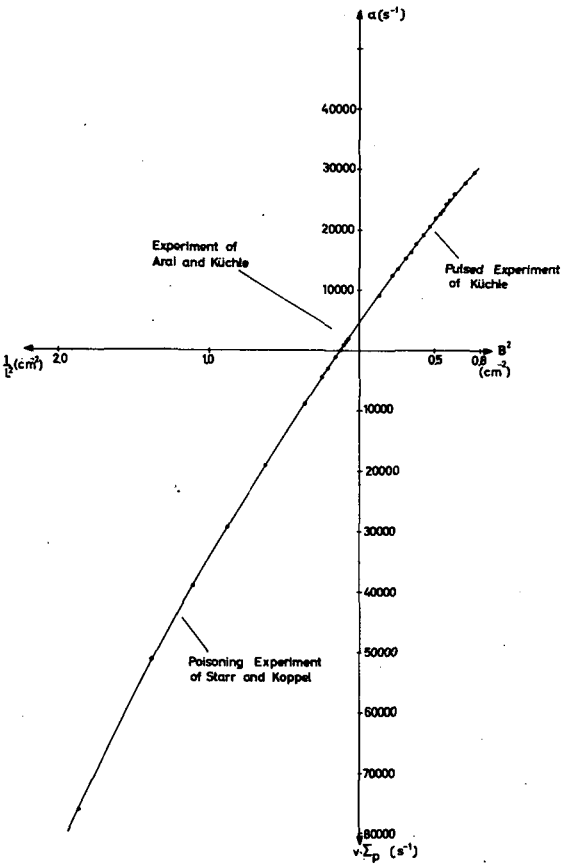

Fig. 3

The enlarged α versus B^2 curve for H_2O

$1/L^2 (= -B^2) > 0$, the results of a careful poisoning experiment by STARR and KOPPEL [22] are plotted. It had been assumed so far that measurements in the upper left quadrant of this co-ordinate system were not possible. However, as JOEST and MEMMERT [24] have pointed out, this region is accessible to experiments by measuring the diffusion length L in a non-stationary neutron field which is excited by a neutron source with a time behaviour $S(t) \sim e^{-\alpha t}$, $0 < \alpha < v\Sigma_a$. Their statement is easy to prove: Assume an infinite medium with a plane source $S(t) \sim e^{-\alpha t}$ at $z = 0$. Then in diffusion theory approximation, the flux $\phi(E, t, z)$ will be governed by

$$\frac{1}{v}\frac{\partial \phi(E,t,z)}{\partial t} = -v\Sigma_a\,\phi(E,t,z) + D(E)\frac{\partial^2 \phi(E,t,z)}{\partial z^2} + \mathcal{M}\phi + A\delta(z)e^{-\alpha t} \quad (3)$$

where $\mathcal{M}$ is the thermalization operator. Since $\alpha < v\Sigma_a$, the homogeneous

solutions of Eq. (3) will decay faster than the source term and the asymptotic time behaviour of the neutron flux will be $\sim e^{-\alpha t}$. Putting $\phi(E, t, z) = \phi(E, z)e^{-\alpha t}$, we obtain

$$(v\Sigma_a - \alpha)\ \phi(E, z) = D(E)\ \frac{\partial^2 \phi(E, z)}{\partial z^2} + \ \phi + A\,\delta(z) \qquad (4)$$

which is identical to a stationary diffusion problem in a moderator with $\Sigma_a^* = \Sigma_a - \alpha/v$. It is thus seen that the trick of using an exponentially decaying source expands the region of poisoning experiments until $\Sigma_a^* = 0$, i.e. $\Sigma_p = -\Sigma_a$.

ARAI and KÜCHLE [23] have recently performed measurements of this type on water. To realize an exponentially decaying source, they used a graphite assembly together with a large water reflector (Fig. 4). The neutrons

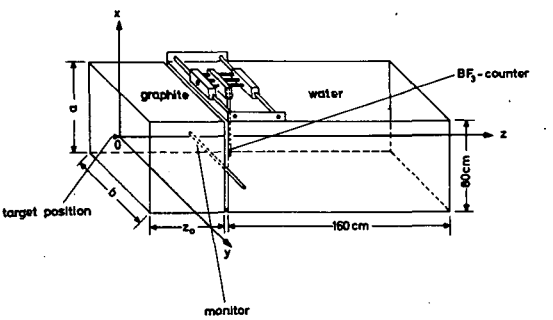

Fig. 4

Experimental arrangement of Arai and Küchle for measurement of diffusion length in a time-dependent neutron field in H_2O

from a 14-MeV source were injected into the graphite stack whose size was such that, after die-away of the transients, the composite system decayed with a time constant $\alpha < (v\Sigma_a)_{H_2O}$. The neutron density was measured in the H_2O as a function of distance from the graphite-H_2O interface with a small BF_3 counter. Time gates were used to suppress the transients. The resulting decay is exponential with distance and, after a small correction for lateral leakage, yields the diffusion length of the time-decaying neutron field. The resulting values of $1/L^2$ as a function of α are included in Fig. 3. The full curve is the result of a least-squares four-parameter fit of all the data. The corresponding diffusion parameters at 20°C are: $v\Sigma_a = 4782 \pm 15\ s^{-1}$; $D_0 = 35\,630 \pm 80\ cm^2\ s^{-1}$; $C = 3420 \pm 170\ cm^4\ s^{-1}$; and $F = 214 \pm 139\ cm^6\ s^{-1}$. The high statistical accuracy of these parameters indicates a good internal consistency of the data; the authors nevertheless recommend an increase of the limits of error by a factor of three. In Table I, these data are compared with various recent calculations of the diffusion parameters for H_2O.

From an inspection of Table I, the following conclusions can be drawn[1]:

[1] It was shown by Arai that the experimental diffusion parameters change only very slightly if, instead of Küchle's pulsed data, those of LOPEZ and BEYSTER [16] are used. Also, no large change occurs if the region $B^2 > 0.4\ cm^{-2}$, where the discrepancies in the α versus B^2 curves have been observed, is not used for the evaluation procedure.

TABLE I

MEASURED AND CALCULATED DIFFUSION PARAMETERS IN H_2O AT 20° C

D_0 ($cm^2\ s^{-1}$)	C ($cm^4\ s^{-1}$)	F ($cm^6\ s^{-1}$)	Remarks
37 045	3361	169	Calculated by GHATAK and HONECK [25] using Nelkin model
37 570	3380	210	Calculated by CLENDENIN [26] using Nelkin model [a]
38 230	2730	250	Calculated by CLENDENIN [26] using Radkowski model [a]
37 400	3080	144	Calculated by KALLFELZ [27] using Goldman-Nelkin model
33 900	3350	218	Calculated by KALLFELZ [27] using the Haywood-Thorson scattering law
35 630 ± 80	3420 ± 170	214 ± 139	Evaluation of ARAI and KÜCHLE [23]
35 300 ± 300	-	-	Calculated by SPRINGER et al. [29] from $\Sigma_s(E)$ and $\bar{\mu}(E)$

[a] These calculations were done at 23°C. The value of D_0 was therefore decreased by 400 $cm^2\ s^{-1}$; C and F were not corrected.

(a) The diffusion cooling coefficients predicted using either the Nelkin or the Goldman-improved Nelkin model agree very well among themselves and with the prediction derived from the experimental scattering law of water. All these predictions are in good agreement with the experimental value.
(b) The diffusion coefficient as predicted by the Nelkin model is about 4-5% higher than the experimental value. As KOPPEL and YOUNG [28] have pointed out, the agreement between the Nelkin model prediction and the measurement of neutron cross-sections and spectra in H_2O is considerably improved if the anisotropy of the molecular vibrations is accounted for in the model. Their modification of the Nelkin model reduces the predicted D_0 by about 4%, i.e. it practically removes the discrepancy between experiment and theory completely! The diffusion coefficient as derived from the experimental scattering law for water is about 4% lower than the directly measured value. This discrepancy is not very disturbing in view of the fact that D_0 depends very critically on the low β-portion of the $S(\alpha, \beta)$ function which is difficult to measure accurately. SPRINGER et al. [29] carefully measured $\bar{\mu}(E)$, the average cosine of the scattering angle, as a function of incident energy, and computed D_0 from $\bar{\mu}(E)$ and $\Sigma_s(E)$ by averaging $1/3\Sigma_s(E)[1-\mu(E)]$

over an equilibrium Maxwellian. The result is also compatible with the Arai and Küchle experiment.
(c) The Radkowski kernel calculations predict a diffusion cooling coefficient about 12% lower and a diffusion coefficient about 8% higher than the experiment.

2.5. New data on various moderators

2.5.1. Organic substances

Some data on Dowtherm A, benzene and diphenyl at room temperature are given in Tables II, III and IV, respectively. It is seen that for each of these moderators there are fortunately two measurements which are in

TABLE II

DIFFUSION PARAMETERS IN DOWTHERM A AT ROOM TEMPERATURE

$\overline{v\Sigma_a}$ (s^{-1})	D_0 ($cm^2\ s^{-1}$)	C ($cm^4\ s^{-1}$)	Remarks
2870 ± 40	49 200 ± 600	11 900 ± 2100	Measured by KÜCHLE [15]
2985 ± 85	51 000 ± 1650	16 500 ± 7000	Measured by BROWN [18]
-	51 500	12 200	Calculated by KALLFELZ [27]

TABLE III

DIFFUSION PARAMETERS IN BENZENE AT ROOM TEMPERATURE

$\overline{v\Sigma_a}$ (s^{-1})	D_0 ($cm^2\ s^{-1}$)	C ($cm^4\ s^{-1}$)	Remarks
2886 ± 111	48 694 ± 1373	13 869 ± 3849	Measured by PÁL et al. [30]
3120 ± 50[a]	48 500 ± 800	13 300 ± 2400	Measured by KÜCHLE and KUSSMAUL [31]
-	55 500	8 260	Calculated by KALLFELZ [27]

[a] This would yield a microscopic absorption cross-section of 348 mb per H atom. Presumably, impurities were present in the liquid.

reasonably good agreement. D_0 and C were calculated by KALLFELZ [27] using experimental scattering law data measured by GLÄSER [34]. In the case of diphenyl, a value of D_0 calculated from the measured $\Sigma_s(E)$ and $\mu(E)$ by Springer et al. is also listed. It is seen that the diffusion cooling co-

TABLE IV

DIFFUSION PARAMETERS IN DIPHENYL AT ROOM TEMPERATURE (density 1.053 g/cm³)

$\overline{v\Sigma_a}$ (s^{-1})	D_0 ($cm^2\ s^{-1}$)	C ($cm^4\ s^{-1}$)	Remarks
3700 ± 150	42120 ± 1160	7700 ± 1800	Measured by BAYER, ČERVENÁ and SCHÄFERLINGOVÁ [32]
3470 ± 280	43370 ± 1800	13700 ± 2900	Measured by ÁDÁM, BOD and PÁL [33]
-	48500	10340	Calculated by KALLFELZ [27]
-	48500 ± 1000	-	Calculated by SPRINGER et al. [29] from $\Sigma_s(E)$ and $\bar{\mu}(E)$

efficients based on the experimental scattering law are in the right order of magnitude. The values of D_0 derived from the scattering law in diphenyl and benzene are about 15% too high. The reason for this discrepancy is probably the same as discussed at the end of section 2.4.

Without much further comment we mention some other recent experiments on organic moderators: YUROVA et al. [35] have performed temperature-dependent experiments over a large T-range on benzene, diphenyl, diphenylmethane, diphenylether, gasoil, isopropyldiphenyl, anisole and tetradecane. From these experiments, they were able to derive a simple relationship

$$\frac{\rho}{\rho_0} D_0\,(T) = AT^{a/2} \tag{5}$$

for the dependency of the diffusion coefficient D_0 on the absolute temperature T. Here ρ and ρ_0 are the densities of the liquid at temperatures T and T_0, respectively, whereas A and a are characteristic constants which were determined for each of the above liquids. PÁL et al. [30] measured the diffusion parameters of benzene, toluene, xylene, cyclohexane, hexane at 22°C and of diphenyl at 85°C. For the same substances, they measured the total cross-section as a function of energy between 2 and 100 MeV and derived the diffusion coefficient by using the classical Radkowski prescription. Agreement within better than 20% between the calculated and measured values of D_0 was found. Measurements on diphenyl at 77°C and in MIPB at 30°C were reported by BLACKSHAW and WALTNER [36], on liquid ammonia by CHARLES [37] and on heptane between 17.5 and 80°C by NILSSON and SJÖSTRAND [38]. Some new results on terphenyl and paraffin are quoted in [39].

2.5.2. Graphite

Table V lists some more recent data on graphite. All parameters have been reduced to a density of 1.6 g/cm³. For comparison, the theoretical

TABLE V

DIFFUSION PARAMETERS OF GRAPHITE AT ROOM TEMPERATURE
(density 1.6 g/cm³)

D_0 (10^5 cm² s⁻¹)	C (10^5 cm⁴ s⁻¹)	F[a] (10^7 cm⁶ s⁻¹)	Buckling value B^2 (10^{-3} cm⁻²)	Experiment performed by
2.13 ± 0.02	26 ± 5	-	≤ 6	KLOSE, KÜCHLE and REICHARDT [10][b]
2.11 ± 0.02	16 ± 5	-20 ± 10	≤ 12	
2.14 ± 0.01	39 ± 3	-	≤ 18.9	STARR and PRICE [9]
2.19 ± 0.03	39 ± 4	-	≤ 15.4	SAGOT and TELLIER [11]
2.30 ± 0.06	45.6 ± 4.7	-	≤ 12.8	SERDULA [12]
2.26 ± 0.27	34.4 ± 38.8	- 6.9 ± 17.7	≤ 12.8	
2.187 ± 0.008	30 ± 1	-	≤ 5.3	DAVIS, DE JUREN and REIER [13][b]
2.20 ± 0.009	44.3 ± 4	+12.7 ± 5	≤ 12	
2.178	24.6	- 8.3	-	Calculated by HONECK [40] using Parks model

[a] Entries are given for four-parameter fits. There are no entries for three-parameter fits.
[b] A measurement of the stationary diffusion length was included in the evaluation procedure.

values predicted by HONECK [40] on the basis of the Parks model are included. The following comments can be made on the data in Table V: Apart from the data measured most recently by Davis, De Juren and Reier, the four other α versus B^2 curves, if plotted together, are in reasonably good agreement. The differences are essentially a result of different methods of evaluation. If Klose, Küchle and Reichardt would evaluate their experiment by a three-parameter fit up to $B^2 \approx 12 \times 10^{-3}$ cm^{-2}, they would obtain $D_0 \approx 2.17 \times 10^5$ cm^2 s^{-1} and $C \approx 40 \times 10^5$ cm^4 s^{-1}, i.e. results compatible with those of the following three authors. However, Klose, Küchle and Reichardt found that a three-parameter least squares fit did not work very well above $B^2 \approx 6 \times 10^{-3}$ cm^{-2}; i.e. above $B^2 = 6 \times 10^{-3}$ cm^{-2}, they found a continuous increase of the value of C with the length of the B^2 interval used in the evaluation. Above $B^2 = 6 \times 10^{-3}$ cm^{-2}, it was necessary to include a negative B^6 term in order to perform a consistent analysis. The existence of a negative B^6 term in graphite is predicted by theory; the experiments of STARR, HONECK and DE VILLIERS [41] on the average asymptotic velocity as a function of B^2 in graphite also give strong evidence for a negative B^6 term. Neither Starr and Price nor Sagot and Tellier found it necessary to include such a term in the analysis of their α versus B^2 curves; they used, however, a different evaluation technique than Klose, Küchle and Reichardt. The results of Serdula's analysis seem to confirm the results of Klose, Küchle and Reichardt; the statistical accuracy however is very low. Davis, De Juren and Reier have also mentioned that a four-parameter fit is superior to a three-parameter fit above $B^2 \approx 6 \times 10^{-3}$ cm^{-2}. However, they report a positive B^6 term. The reason for this discrepancy is probably the fact that in this most recent determination an α versus B^2 curve was found which looks quite different at high B^2 values. This is shown in Fig. 5 where these data are compared with those of Starr and Price. The difference in the experimental set-up, as was mentioned in section 2.1, is the increased shielding and the fact that 2.5-MeV neutrons were used; the procedure was different since Davis, De Juren and Reier used short waiting times.

In summary, the situation in graphite appears to be still very confused, partly because of the different results of evaluation procedures, partly because of the deviations in the α versus B^2 curves above $B^2 \approx 6 \times 10^{-3}$ cm^{-2}. One possible, though improbable, explanation might be derived from a recent paper of GHATAK and HONECK [25]. These authors note that the critical limit for the eigenvalues in graphite as derived from the Parks model is ≈ 1000 s^{-1} instead of the value ≈ 2600 s^{-1} derived from the measured cross-section. This may be the result of inaccuracies in the Parks model or in the measured cross-section. If the latter were true and 1000 s^{-1} were the actual critical limit, no stable asymptotic mode would exist for $B^2 \gtrsim 5 \times 10^{-3}$ cm^{-2}, i.e. only the region $0 < B^2 < 5 \times 10^{-3}$ cm^{-2} could be used for analysis.

2.5.3. Heavy water

Recent results on D_2O at room temperature are summarized in Table VI. It is seen that the measurements are in reasonable agreement among themselves and that the parameters are well represented by the theoretically predicted parameters. The latter are for pure D_2O and should be slightly

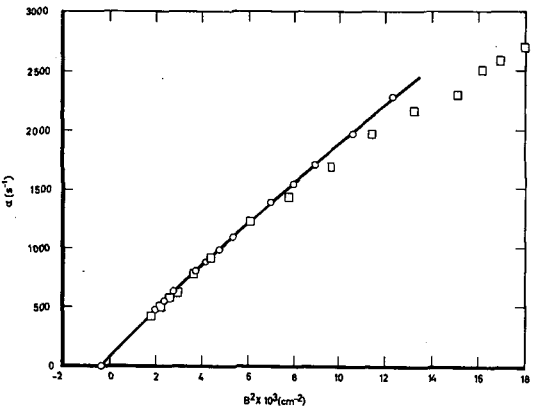

Fig. 5

α versus B^2 curves observed in graphite

□ STARR and PRICE [9]

O DAVIS, DE JUREN and REIER [13]

decreased which makes the agreement even better. Ganguly, Cobb and Waltner have also reported diffusion parameter measurements in the temperature range 10 - 50°C.

2.5.4. Other moderators

In Table VII some more recent data reported on various other moderators are listed. Many data on measurements published before 1962 are summarized in [45].

The new experiments in the USSR on beryllium and beryllium oxide indicate a much higher amount of diffusion cooling than previous experiments. The Czech data on water and ice at 0°C are impressive, since they reveal the strong effect which the phase transition has on the thermalization power. A similar observation was made by the group in the USSR.

2.6. Friedman's method

The most elementary thermalization property of a scattering medium is the inelastic part of the P_0 component of its scattering law, i.e. the quantity

$$\sigma_s(E' \to E) = \int_{-1}^{+1} \sigma_s(E' \to E, \cos\vartheta_0)\, d\cos\vartheta_0.$$

As is well known, the classical pulsed source technique is not the ideal method to measure quantities which depend sensitively on the above $\sigma_s(E' \to E)$. Rather, α versus B^2 curves are also strongly dependent on the transport properties of the medium, viz. the elastic scattering angular distribution. The diffusion cooling coefficient is a particularly complicated function of both the transport and the thermalization properties. Early attempts have

TABLE VI

DIFFUSION PARAMETERS OF D_2O (99.8%) AT ROOM TEMPERATURE

D_0 (10^5 cm^2 s^{-1})	C (10^5 cm^4 s^{-1})	Buckling range (10^{-3} cm^{-2})	Experiment performed by
2.00 ± 0.01	5.25 ± 0.25	3-par. fit, 1.3 < B^2 < 45 22°C	KUSSMAUL and MEISTER [42]
2.045 ± 0.044	4.706 ± 0.381	3-par. fit, [a] 16 < B^2 < 85 21°C	MALAVIYA and PROFIO [43]
2.039 ± 0.013	4.18 ± 0.18	3-par. fit, [b] 30 < B^2 < 90 28°C	WESTFALL and WALTNER [57]
2.06 ± 0.05	3.72 ± 0.5	3-par. fit, [b] 60 < B^2 < 100 20°C	GANGULY, COBB and WALTNER [44]
2.069	4.852 5.13	-	Calculated by HONECK [40] using incoherent scattering model for D_2O
2.09 ± 0.02	-	-	Calculated by SPRINGER et al. [29] from Σ_s (E) and $\bar{\mu}$(E) 20°C

[a] $\alpha_0 = 10$ s^{-1} assumed in evaluation of α versus B^2 curve.
[b] $\alpha_a = 0$ assumed in evaluation of α versus B^2 curve.

been made to separate both effects in a simple way, for instance the famous NELKIN [48] formula

$$C = \frac{D_0^2 \sqrt{\pi}}{v_0 M_2} (p + 1/2)^2 \qquad (6)$$

has frequently been used where M_2 is the second moment of the scattering law in an equilibrium Maxwellian,

$$M_2 = \iint \Sigma_s(E' \to E) \frac{(E' - E)^2}{(kT_0)^2} \frac{E}{kT_0} e^{-E/kT_0} \frac{dE}{kT_0} dE' \qquad (7)$$

TABLE VII

DIFFUSION PARAMETERS OF VARIOUS MODERATORS

Material	Density (g/cm^3)	Temperature (°C)	$\overline{v\Sigma_a}$ (s^{-1})	D_0 (10^5 cm^2 s^{-1})	C (10^5 cm^4 s^{-1})	Ref.
Be	1.79	20	262 ± 11	1.24 ± 0.013	3.68 ± 0.20	[14]
BeO	2.79	20	174 ± 6	1.56 ± 0.01	4.12 ± 0.27	[14]
Water	-	0	4740 ± 90	0.324 ± 0.01	0.042 ± 0.01	[46]
Ice	-	0	4470 ± 80	0.346 ± 0.01	0.083 ± 0.02	[46]
Ice	0.917	-80	4656 ± 200	0.266 ± 0.009	0.066 ± 0.01	[47]
Ice		-196		0.095 ± 0.004	0.02 ± 0.01	

and p is the exponent in the approximate relationship

$$\lambda_{tr}(E) \sim E^{p}. \tag{8}$$

However, Eq. (6) holds only approximately; it depends sensitively on the assumption that $\lambda_{tr}(E)$ can be represented by Eq. (8). To derive M_2 from a measured C, p must be known accurately. Thus it is difficult to derive direct information on thermalization properties from measured α versus B^2 curves and people have searched for other suitable methods.

An obvious approach is to measure the decay of a thermalized pulse in an infinite medium which contains a non-1/v absorber. In the presence of a 1/v absorber or in a non-absorbing medium the asymptotic spectrum is strictly Maxwellian; a non-1/v absorber will deform the asymptotic spectrum. Stated simply, the spectrum will be "cooler" for σ_a decreasing slower than 1/v and "hotter" for σ_a decreasing faster than 1/v. Whereas the relation between the decay constant α as a function of the absorber concentration N is linear in the case of a pure 1/v absorber, it will actually show a downward curvature as a result of the fact that the apparent absorption cross-section becomes smaller. This downward curvature will be the stronger, the stronger the deviations of $\sigma_a(E)$ from the 1/v law are; it is also greatly influenced by the isotropic part of the thermalization kernel.

Although measurements of this type have been done several times in the past [49, 50], the first author who realized the full possibilities of this approach was FRIEDMAN [51-53]. He described the α versus N relationship in an infinite medium by the expression

$$\alpha = \alpha_0 + \frac{2v_0}{\sqrt{\pi}} N (a + b N + \ldots) \quad , \tag{9}$$

where $\alpha_0 = [v\Sigma_a(v)]_{1/v}$ describes the fixed 1/v absorption of the "solvent". a is the Maxwell-averaged absorption cross-section of the added absorber,

$$a = \int_0^\infty \frac{E}{kT_0} e^{-E/kT_0} \sigma_a(E) \frac{dE}{kT_0} \tag{10}$$

and the higher coefficients b, c etc. depend on the thermalization properties of the solvent and the non-1/v behaviour of $\sigma_a(E)$. Describing the deviations of the asymptotic spectrum $\phi(E)$ from the equilibrium Maxwellian by means of an expansion into Laguerre polynomials of order unity,

$$\phi(E) = \frac{E}{(kT_0)^2} e^{-E/kT_0} \sum_k A_k L_k\left(\frac{E}{kT_0}\right), \tag{11}$$

Friedman could express b (and in principle the higher terms c, d, etc.) in terms of matrix elements

$$\gamma_{ik} = \int_0^\infty L_i \frac{E}{kT_0} \mathcal{M} L_k \frac{E}{kT_0} \frac{E}{kT_0} e^{-E/kT_0} \frac{dE}{kT_0}, \tag{12}$$

where $\mathcal{M}$ is the isotropic thermalization operator, and

$$S_k = \int_0^\infty \left[\frac{2v_0}{\sqrt{\pi}}\frac{a}{v} - \sigma_a(E)\right] L_k \frac{E}{kT_0}\frac{E}{kT_0} e^{-E/kT_0} \frac{dE}{kT_0} \qquad (13)$$

Since the S_k are well known if $\sigma_a(E)$ is carefully measured, b (and c, etc.) can be calculated to an accuracy depending only on the accuracy of the γ_{ik}, i.e. on the isotropic part of the scattering law. Conversely, if b is derived from a fit of the α versus N curve, information on the γ_{ik} can be obtained. The relation between b and the γ_{ik} and S_k is however complex. If one assumes that the two Laguerre polynomials k = 0 and k = 1 are sufficient to describe the disturbed spectrum[2], the relation between the b- and the γ-matrix simply becomes

$$b = -S_1^2/\gamma_{11} \qquad (14)$$

and γ_{11} can be derived immediately. As one can easily show, $\gamma_{11} = 0.25\ M_2$ and we thus have a simple method for the determination of the second moment of the scattering kernel.

Experimentally, the method is not as simple as this. The measurements are not performed at infinite geometry. To eliminate the effects of diffusion on α, α is determined at each absorber concentration as a function of B^2 and an extrapolation to $B^2 = 0$ is made. Friedman investigated aqueous solutions of Cd, Sm, Gd and Sm-Gd mixtures. He performed measurements in the range $0.096\ cm^{-2} < B^2 < 0.15\ cm^{-2}$. The paramount problem in this type of measurement is the elimination of spatial modes in the rather large vessels filled with strongly absorbing solutions. Unfortunately, no decay curves are shown in his publications. From the measurements on the above-mentioned solutions, he derived $M_2 = 0.84 \pm 0.1\ cm^{-1}$ for H_2O using Eq. (14). By a similar method, VERDAGUER et al. [54] found $M_2 = 1.46 \pm 0.43\ cm^{-1}$ for water. Both results are much lower than those derived by Eq. (6) from "standard" pulsed experiments, which are $\approx 3\ cm^{-1}$. The value calculated on the basis of the Nelkin model is $3.2\ cm^{-1}$. GLÄSER [55] has calculated M_2 from the Haywood-Thorson experimental scattering law of water and found $M_2 = 3.1\ cm^{-1}$. Thus there is strong evidence against the M_2 values derived by Friedman's method. There might be an error in the above value due to the use of the approximate Eq. (14) instead of the more accurate original equation. However, CALAME [56] has calculated accurate b-values on the basis of the Nelkin model; comparing his results with those derived from Eq. (14) one observes that the approximation is a very good one. The explanation of the discrepancies might be: (a) errors in the input values of $\sigma_a(E)$ used for the determination of the S_k (According to Calame, who did some numerical experiments, this is not very probable.); (b) errors in the α-determination caused by higher spatial modes; or (c) errors in the extrapolation to zero buckling. It would be extremely useful to investigate these questions further, since basically this method appears very attractive. The proposal to per-

[2] This assumption, as is well known, corresponds to the "shifted neutron temperature concept".

form a spatial Fourier analysis on large D_2O systems [58] appears to be excellent to meet some of these objectives.

2.7. Buckling determinations by the pulsed technique

It is well known that once the α versus B^2 relation is known for a substance, bodies of arbitrary shape can be built from this material and their B^2 determined by α-measurements. Such investigations have been done frequently, but since their results are of a highly specialized nature, not many results have been published. The interest lies mainly in the effect of oddly-shaped control elements and in streaming effects caused by holes and voids in homogeneous media.

3. TRANSIENT PHENOMENA

3.1. Measurements of the slowing-down time to definite energies

Depending on the availability of suitable resonance detectors, measurements of the slowing-down time to definite energies in the epithermal and near-thermal range can be made. Such experiments have been performed using In (1.46 eV), Pu(0.3 eV), Cd(0.178 eV) and Sm(0.0976 eV) as resonance detectors; some authors have also used a thick cadmium indicator which has an "edge" in the absorption cross-section at 0.5 eV[3]. Indication of resonance capture is either "positive", i.e. by observation of capture γ-rays or fissions, or "negative", i.e. by observation of the neutron transmission through the resonance absorber. In any case, a time-dependent reaction rate curve of the type illustrated in Fig. 6 is obtained. There are several ways to derive a slowing-down time from this curve; most authors consider the time displacement of the maximum as the proper slowing-down time while some authors use the average displacement. Which of the two definitions is used is irrelevant if the proper theoretical value is used in the comparison. Theoretical calculations for the time-energy distribution of neutrons slowed down by free nuclei at rest were performed by ORNSTEIN and UHLENBECK [60], DYAD'KIN and BATALINA [61] and by KOPPEL [62], among others. The ideal experiment is performed by measuring the space-integrated resonance reaction rate in a sufficiently large scattering medium. If localized resonance absorbers are used, the results are affected by diffusion times. Corrections for this effect can be made but are difficult to formulate.

The most recent measurements of this type which have been reported are those of ZHEZHERUN et al. [14]. These authors observed the neutron transmission through indium, cadmium and samarium, as well as the time-dependent fission rate of a Pu chamber shielded by Sm and Cd. Their experimental results (slowing-down times defined by the displacement of the maximum of the resonance reaction rate curves) are summarized in Table VIII. Theoretical values for slowing-down by free nuclei at rest are shown for

[3] Using the slowing-down time spectrometer, time-dependent capture rates in resonances in the high eV and low keV range have also been observed [59]; this technique is however outside the scope of this review.

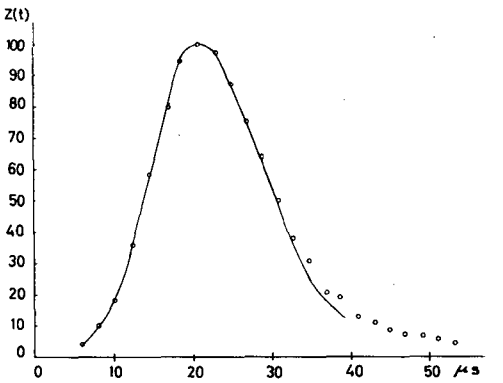

Fig. 6

Neutron flux distribution at 0.3 eV as a function of time in beryllium as observed with a Sm-Cd shielded Pu fission chamber (from [14])

TABLE VIII

SLOWING-DOWN TIMES IN Be AND BeO [14]

Energy (eV)	t (μs) in Be		t (μs) in BeO	
	Experiment	Theory	Experiment	Theory
1.46	7.5 ± 1	7.2	9.5 ± 1	9.3
0.3	17.5 ± 1	15.7	26 ± 2	19.2
0.178	40 ± 3	20.4	51 ± 3	20.3
0.0976	73 ± 5	27.6	88 ± 5	34.8

comparison; for 1.46 eV the agreement is excellent, but the lower the resonance energy falls the more this theory underestimates the experimental values. This is of course a consequence of the thermal motion of the moderator atoms and of their chemical binding which is very strong in Be and BeO.

Some experiments on slowing-down to Cd and In energies have been performed recently in H_2O and D_2O. Since slowing-down proceeds very fast in these moderators, especially in H_2O, the experiments are difficult to perform and require a high timing accuracy for the source burst and the neutron detection equipment. Results of PROFIO and ECKARD [63] are shown in Table IX. Slowing-down times were defined by the displacement of the maximum. It is seen that agreement between measured and calculated values is good except for the Cd-D_2O value. This difference is attributed to diffusion time effects (which were not corrected for) rather than to effects of chemical binding or thermal motion. MÖLLER and SJÖSTRAND [64] found independently that chemical binding and thermal motion play no important role in the slowing-down to the cadmium edge in H_2O.

TABLE IX

SLOWING-DOWN TIMES IN H_2O AND D_2O [63]

	Measured t (μs)		Calculated t (μs)	
	In resonance	Cd edge	In resonance	Cd edge
H_2O	0.75 ± 0.5	1.75 ± 0.5	0.6	1.65
D_2O	4.0 ± 1.0	10.5 ± 1.0	4	8

Profio and Eckard have suggested the use of time-dependent reaction rate measurements in moderating assemblies as a more general tool for reactor physics studies. For instance, they suggest the determination of resonance capture probabilities in this way and the separation of the thermal and epithermal activation of flux indicators from the time dependency. No work of this type has been published so far.

3.2. Investigation of time-dependent neutron thermalization

The most powerful tool for investigating the time-dependent neutron thermalization is the detailed measurement of the time-dependent spectrum using a pulsed source and synchronized chopper. This method necessitates very strong neutron sources and a time-of-flight spectrometer and does not belong to the class of simple pulsed source experiments reviewed in this paper[4]. Considerably simpler, though less informative, are measurements of the approach to equilibrium of certain spectral indices after the injection of a fast source burst. Three different kinds of spectral indices have been in use, viz. (a) the average neutron velocity, as determined by the counting rate ratio between a thick (black) and a thin (1/v) BF_3 counter; (b) the average cross-section of non-1/v absorbers, such as Cd and Gd, as measured by the intensity of capture γ-rays; and (c) the effective cross-section of 1/v absorbers as determined by a transmission experiment. The interpretation of these time-dependent spectral indices is difficult. Early workers have assumed that the spectrum at any time could be described by a Maxwellian, and they have derived a time-dependent neutron temperature T(t) from their measured spectral indices. After the elementary relation

$$T(t) - T(t = \infty) \sim e^{-t/t_{th}} \tag{15}$$

was applied, values of "thermalization time" t_{th} were deduced. Later on, it became evident that the effective temperature concept was inappropriate since the spectra deviate greatly from pure Maxwellian distribution, especially in moderators with strong chemical binding. Then, the "energy mode

[4] Cf. the review article of POOLE [65].

concept" was introduced, in which it is assumed that the time-dependent spectrum $\phi(E,t)$ can be represented by a superposition of separate modes, viz.

$$\phi(E,t) = \phi_{as}(E) \cdot e^{-\alpha t} + \phi_1(E)\, e^{-\lambda_1 t} + \phi_2(E)\, e^{-\lambda_2 t} + \ldots . \qquad (16)$$

α is the fundamental mode decay constant which is usually observed in pulsed source experiments, whereas the higher modes characterize the transients during the thermalization process. The $\lambda_{1,2,..}$ are dependent on the thermalization power of the moderator and in particular λ_1 is considered to be a characteristic quantity. $1/\lambda_1$ is sometimes called the "thermalization time constant". If the fundamental mode decay constant α is known, the contribution of the fundamental mode to a time-dependent spectral index can be "peeled off" and λ_1 can be determined. This evaluation, however, presupposes that a representation of the time-dependent spectrum by separate modes is possible. Unfortunately, theory has recently shown [25, 66] that in most crystalline moderators, especially in graphite and beryllium, no such representation is possible. In the media the fundamental mode decay constant is the only discrete eigenvalue below the critical limit, and even that only at sufficiently small bucklings, as repeatedly stated; all other eigensolutions belong to the continuum which extends above the critical limit and none of these can be isolated. Fortunately, in H_2O at least λ_1 and λ_2 are predicted to be discrete.

The experimental results reflect the difficulties in the evaluation procedure. In water, MÖLLER and SJÖSTRAND [64, 67] were able to isolate the first energy mode by reaction rate measurements on Cd and Gd; they found $1/\lambda_1 \approx 4\ \mu s$ for a large geometry. This agrees remarkably well with the theoretical prediction based on the Nelkin model [66], in which $1/\lambda_1 = 5.4\ \mu s$.

In graphite, several new results exist which are discrepant: SERDULA [12] determined time-dependent neutron temperatures by neutron transmission through silver absorbers. He interpreted his data according to Eq. (15) and determined t_{th} as a function of B^2 in the range $4 \times 10^{-3}\ cm^{-2} < B^2 < 14.5 \times 10^{-3}\ cm^{-2}$. After extrapolation to $B^2 = 0$, it was found that $t_{th} = 750 \pm 200\ \mu s$. KÜCHLE and SCHWEIKERT [68] performed transmission measurements through silver absorbers and analysed their data according to Eq. (16). Their values of λ_1 versus B^2 are shown in Fig. 7; note that some of them are $> 2600\ s^{-1}$. After extrapolation to $B^2 = 0$, it was found that $1/\lambda_1 = 550 \pm 50\ \mu s$. STARR, HONECK and DE VILLIERS [41] measured the average

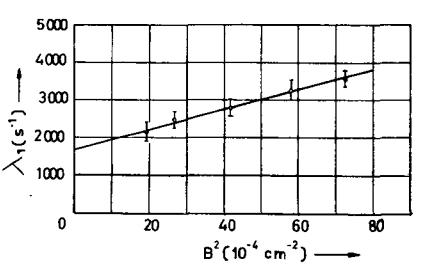

Fig. 7

The first higher eigenvalue λ_1 in graphite as a function of geometrical buckling
Note that the two largest values of λ_1 are above the "critical limit"

neutron velocity as a function of time for graphite stacks in the buckling range $(1.77\text{-}15.05)\times 10^{-3}$ cm^{-2}. Although the main purpose of their experiment was the determination of the asymptotic average velocity, they tried to derive information on the speed of the thermalization process. It was found that the average velocity approaches its asymptotic value nearly exponentially, with a time constant of about 525 μs which was found to be quite independent of B^2. In view of the large discrepancies of these various results and furthermore in view of the fact that no clear definition of the thermalization time can be given at present, the problem of time-dependent thermalization in graphite must be considered as still largely unsolved. The only conclusion which can be drawn from more recent studies is that the time scale of the thermalization process in graphite is about two to three times slower than that observed in the very first studies. The reasons for this have been discussed previously [69].

In the framework of their very careful work on diffusion and slowing-down in Be and BeO, ZHEZHERUN et al. [14] have determined time-dependent neutron temperatures by the transmission method. After Eq. (15) was applied and extrapolated to infinite geometry, it was found that $t_{th} = 185 \pm 20$ μs for Be and $t_{th} = 204 \pm 20$ μs for BeO. No detailed theoretical analysis of these values, which are higher than previously determined t_{th} figures, has been performed so far.

4. PULSED NEUTRON STUDIES IN THE FAST NEUTRON RANGE

In view of the increasing interest in fast reactor physics and with the availability of intense nanosecond-bunched fast neutron generators, some groups have lately started to apply the pulsed technique to the study of neutron diffusion and moderation in the keV and MeV range. There are several possibilities in this field, for instance measurements of the time-dependency of inelastic moderation, time-of-flight measurements of the neutron spectrum or studies of monoenergetic neutron diffusion. We shall restrict ourselves to the latter application.

The pioneer work in this field was done by BEGHIAN et al. at the Massachusetts Institute of Technology [70, 71]. This group studied the time decay of monoenergetic neutron fields (energy range 0.8 - 1.6 MeV) in assemblies of iron, bismuth, lead and natural uranium. Apart from iron which is discussed below, these are very heavy materials and the slowing-down by elastic collision can be neglected at least to a good approximation. If inelastic scattering is disregarded for the moment, the time-dependency of the diffusion of a burst of fast monoenergetic neutrons can be described by the usual one-group theory. After decay of spatial harmonics, the neutron field will therefore die away exponentially with time and the decay constant will be given by

$$\alpha = v\Sigma_r + D_0 B^2 + C_T B^4 \qquad (17)$$

where Σ_r and D_0 are the removal cross-section (see below) and the diffusion coefficient, evaluated at the proper energy. C_T is the well-known transport theory correction to the elementary diffusion theory,

$$C_T = \frac{v}{45\,\Sigma_t^3} \tag{18}$$

for isotropic scattering according to SJÖSTRAND [72].

The experimental arrangement used by BEGHIAN et al. [71] is shown in Fig. 8. Monoenergetic neutrons were produced by bombarding ~ 50-keV thick lithium targets with monoenergetic protons from a pulsed Van de Graaff generator. Neutrons emerging from the assemblies were detected by a

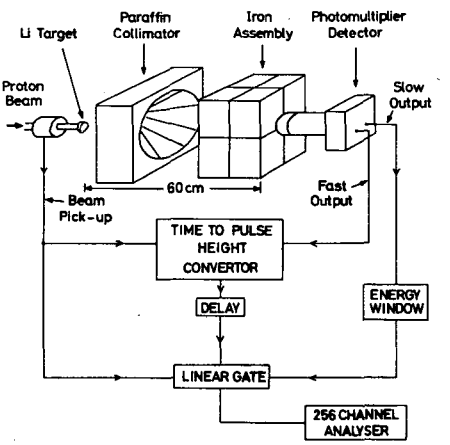

Fig. 8

Experimental set-up used by BEGHIAN et al. [71] for fast neutron flux decay studies on iron

1 in × 1 in plastic scintillation counter. This was biased in such a way that neutrons which had undergone an inelastic scattering process and thus had lost an appreciable amount of energy were not detected. Σ_r as defined by Eq. (17) thus represents removal processes, i.e. absorption as well as inelastic scattering, and is essentially equal to the non-elastic cross-section[5] usually determined by spherical shell transmission measurements. A typical decay curve for a lead block 8 in × 8 in × 8 in at 1.24 MeV is shown in Fig. 9; the decay is nearly exponential, allowing a value of α to be derived. An α versus B^2 curve in uranium at E = 0.84 MeV is shown in Fig. 10. The full curve is a least squares fit according to Eq. (17). Since three experimental points are not sufficient to determine three parameters, a calculated value of D_0 derived from scattering data of U^{238} was used. From this evaluation, $\sigma_r = 0.76 \pm 0.08$ b was obtained; this is roughly consistant with $\sigma_r = 0.6 \pm 0.14$ b which is obtained by adding up $\sigma_{n,\gamma}$ and the inelastic cross-sections for the excitation of the 700-keV and (partly) for the 150-keV level. Similar results were obtained for lead.

In the case of iron the elastic moderation cannot be neglected (A = 56). This has two consequences on the observed neutron decay: First, due to the

[5] Since the biased scintillation detector is not an ideal threshold detector, there remains an appreciable detection probability for neutrons which have been inelastically scattered, forming low-lying excited states. For instance, scattering processes leading to the 44 keV 2^+ level in U^{238} are not registered as removals and the measured Σ_r must be interpreted accordingly.

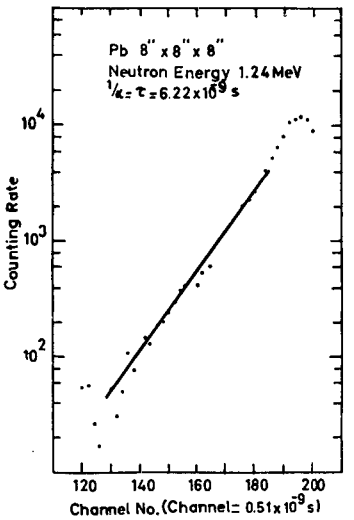

Fig. 9

Decay of 1.24-MeV neutron flux in lead as observed by BEGHIAN et al. [71]

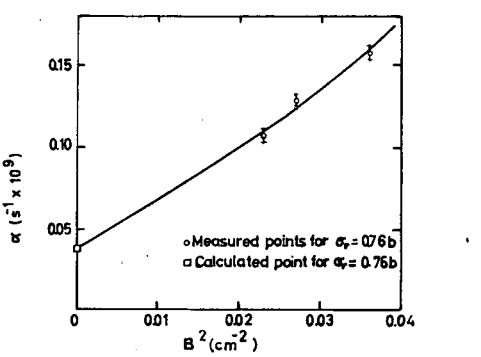

Fig. 10

α versus B^2 curve in U^{238} at 0.84 MeV (BEGHIAN et al. [71]

decreasing neutron velocity, the decay of the neutron density will not be strictly exponential. Rather, the decay constant will slowly decrease with time (since the D_0B^2 term normally represents the main contribution to α). This effect was considered to be negligible by Beghian et al. Secondly, since the sensitivity of the neutron detector decreases markedly with the neutron energy, the counting rate will decrease faster than the neutron density. Beghian et al. were able to show that this effect can be described by introducing an additional "effective elastic removal cross-section" term, $\Sigma_p = b\overline{\Delta E}/\lambda_{tr}$, into Eq. (17). Here $\overline{\Delta E}$ is the average energy loss in an elastic collision, λ_{tr} is the transport mean free path and b is a constant characteristic for the shape of the detectors' energy-dependent efficiency curve. After

the data was corrected in this way, the measured removal cross-sections were found to agree with other measurements.

Recently, Miessner at Karlsruhe has started similar experiments in the low kilovolt range. The objectives of his work are to measure capture cross-sections and to investigate the effect of the cross-section resonance structure on integral neutron behaviour. The first of these objectives was mainly initiated by the lack of reliable methods to measure keV capture cross-sections absolutely. In these experiments, monoenergetic neutrons at energies below the threshold for inelastic scattering are injected into assemblies of heavy absorbers such as uranium, tantalum, antimony or gold. The experimental set-up is similar to the one shown in Fig. 8. The $Li^7(p,n)Be^7$ reaction under 0° at threshold (E = 30 keV) has been used so far but some feasibility studies using the $Sc^{45}(p,n)Ti^{45}$ reaction at threshold (E = 5.5 keV) have been performed. The detector is a Li^6-loaded glass scintillator; it has a very high sensitivity for γ-rays and thus a rather poor signal-to-noise ratio; no better solution has been found so far. A decay curve observed in lead which was used as a test case is shown in Fig. 11.

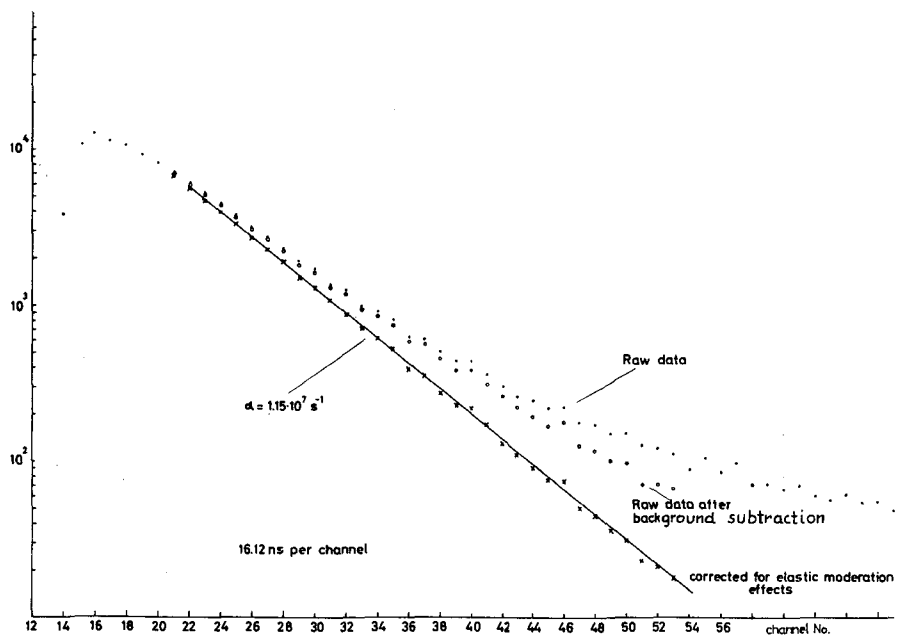

Fig. 11

Decay of 30-keV neutron field in a 15 cm x 20 cm x 30 cm lead block

A closer inspection of the decay curve after background correction shows that it is not exponential. This is due to the effect of elastic moderation which becomes appreciable after a sufficiently long time. In the particular example shown in Fig. 11, the decay was observed up to 800 ns after injection of the neutron pulse. A neutron of ~ 30 keV undergoes about 60 collisions during this time interval in lead, whereby its average velocity will decrease by about 35%. Of the two resulting effects on the observed decay mentioned

above, the first one, i.e. the reduction of the decay rate, is considered to be the more important.[6] Since elastic moderation at kilovolt energies is a rather transparent process, it is fairly simple to correct the measured time decay to account for elastic moderation. In [73], a correction factor F(t) is calculated which yields

$$n_{obs}(t)/F(t) \sim e^{-\alpha t}. \tag{19}$$

F(t) depends on the scattering and absorption cross-sections of the medium which must be known at least to first order. Arai has written an on-line computer programme to calculate this factor and to correct measured data immediately. It is seen in Fig. 11 that after this correction the measured densities die away exponentially.

Figure 12 shows a preliminary α versus B^2 curve which was observed in this way on natural uranium[7]. No upward curvature as in the work of Beghian et al. is observed here; this is because Σ_t is much larger in the keV than in the MeV region. The slope of the straight line yields $D_0 \approx 9.1 \times 10^7$ cm^2 s^{-1} which is much smaller than what would be expected on the basis of the known total cross-section. The reason for this discrepancy is unclear at present. The extrapolation to zero buckling yields $\sigma_a \approx 0.44$ b, in rough agreement with what might be expected on the basis of the known uranium cross-sections.

An analysis of these experiments must take into account the resonance structure of the cross-sections. The treatment is considerably simplified by the fact that in the range of energies and mass numbers considered here, the widths of the individual resonances are small compared with the average energy loss in an elastic collision. Therefore, simple approximations can be used. Under certain simplifying assumptions, the following relations [73] can be derived for the diffusion parameters:

$$\Sigma_a = f_c \langle \Sigma_a \rangle \tag{20}$$

$$D_0 = \frac{v}{3} \frac{1}{f_t \langle \Sigma_t \rangle}\,.^{8} \tag{21}$$

Here, the brackets mean averaging over an energy interval which is large enough to contain many resonances, but small enough that the average values do not change appreciably. $\langle \Sigma_a \rangle$ and $\langle \Sigma_t \rangle$ are "infinite dilution" average values of the type listed normally in cross-section tables. f_c and f_t are the self-shielding factors as defined by ABAGJAN et al. [74], viz.

---

[6] *This is so because the $Li^6(n, \alpha)H^3$ cross-section is assumed to be still nearly 1/v in this energy range.*

[7] Actually, the experiment was performed on natural uranium, but the effect of U^{235} is considered to be negligible.

[8] *Isotropic scattering in the laboratory system was assumed here.*

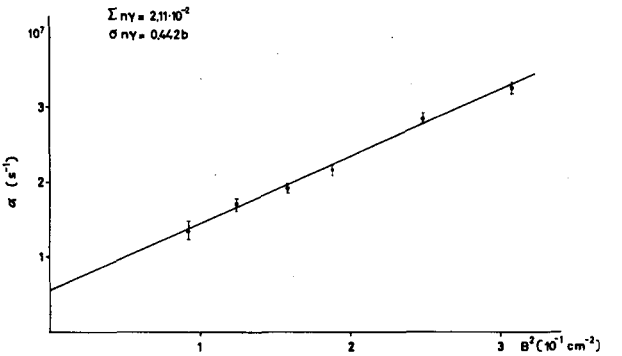

Fig. 12

α versus B^2 curve for 30-keV neutrons in natural uranium

$$f_c = \frac{1}{\langle \sigma_a \rangle} \frac{\left\langle \frac{\sigma_a}{\sigma_t} \right\rangle}{\left\langle \frac{1}{\sigma_t} \right\rangle} \tag{22}$$

$$f_t = \frac{1}{\langle \sigma_t \rangle} \frac{\left\langle \frac{1}{\sigma_t} \right\rangle}{\left\langle \frac{1}{\sigma_t^2} \right\rangle} \tag{23}$$

Values of f_t and f_c are tabulated for many nuclides in [74].

For U^{238} at 30-keV, f_t and f_c are very close to 1 and the self-shielding effects are easily eliminated. In going to lower energies, the self-shielding factors however decrease considerably; at 5 keV, for instance, $f_c \approx 0.55$ and $f_t \approx 0.7$ for U^{238}. Since at these low energies $\langle \Sigma_a \rangle$ and $\langle \Sigma_t \rangle$ can be accurately determined by other methods, pulsed source methods might be able to determine self-shielding factors in a rather straightforward manner.

5. SUMMARY AND CONCLUSIONS

Although a considerable amount of work on the asymptotic decay of thermalized neutron fields has been done, some of the basic problems still seem to be unsolved, for example, the question of the decay constant in small crystalline media, the shape dependency of B^2 in small water systems, and the analysis technique for α versus B^2 curves. In some regions good progress has been made. In many cases there is agreement between different measurements on liquid moderators; in H_2O the accuracy of the experiments, which are, however, largely poisoning experiments of the stationary type, is sufficient to permit very detailed comparisons with theory. Friedman's method has been shown to be a very useful tool; there are however large discrepancies between theory and experiment which represent a challenge to experimentalists.

Slowing-down time measurements above 0.5 eV are now available for a few moderators and generally corroborate the elementary theory for slowing-down by free nuclei at rest. Thermalization time measurements in water seem to be in a good state while measurements in graphite suffer from the

fact that no reasonable definition of a thermalization time is presently offered from theoreticians.

The new field of quasi-asymptotic decay of fast monoenergetic neutron fields deserves further attention. Many more developments in the theory and techniques of these experiments are required. In view of the steadily improving techniques for fast neutron differential cross-section measurements, it is somewhat doubtful if the pulsed technique will result in substantial improvements of fast reactor data. Rather, it will contribute to a better understanding of the behaviour of fast neutrons in matter.

REFERENCES

[1] CORNGOLD, N., "Theoretical interpretation of pulsed neutron phenomena", these Proceedings I.
[2] CORNGOLD, N. (Ed.), Proceedings of the Brookhaven Conference on Neutron Thermalization, BNL 719 (1962), especially Volume III: Experimental Aspects of Transient and Asymptotic Phenomena.
[3] CORNGOLD, N., Nucl. Sci. Engng 19 (1964) 80.
[4] SILVER, E., Rpt. ORNL-3499 (1963) 33.
[5] OGRZEWALSKI, Z. et al., Nukleonika VIII (1963) 595.
[6] CORNGOLD, N., private communication.
[7] FULLWOOD, R.R., SLOVACEK, R.E. and GAERTTNER, E.R., Nucl. Sci. Engng 18 (1964) 137.
[8] KÜCHLE, M., unpublished.
[9] STARR, E. and PRICE, G.A., Rpt. BNL 719, Vol. III (1962) 1034.
[10] KLOSE, H., KÜCHLE, M. and REICHARDT, W., Rpt. BNL 719, Vol. III (1962) 935.
[11] SAGOT, M. and TELLIER, H., Rpt. CEA 2210 (1962); cf. also J. nucl. Energy A/B 17 (1963) 347.
[12] SERDULA, K.J., Ph.D. Thesis, Birmingham (1963).
[13] DAVIS, S.K., DE JUREN, J.A. and REIER, M., submitted for publication in Nucl. Sci. Engng.
[14] ZHEZHERUN, I.F. et al., Proc. 3rd UN Int. Conf. PUAE, 1964, P/362a.
[15] KÜCHLE, M., Nukleonik 2 (1960) 131.
[16] LOPEZ, W.M. and BEYSTER, J.R., Nucl. Sci. Engng 12 (1962) 190.
[17] HALL, R.S., SCOTT, A. and WALKER, J., Proc. phys. Soc. 79 (1962) 257.
[18] BROWN, J.C.B., Ph. D. Thesis, Birmingham (1963).
[19] GELBARD, E.M. and DAVIS, J.A., Nucl. Sci. Engng 13 (1962) 237.
[20] KLADNIK, R., Nukleonik 6 (1964) 147.
[21] JUDGE, F.D. and DAITCH, P.B., Nucl. Sci. Engng 20 (1964) 428.
[22] STARR, E. and KOPPEL, J.U., Rpt. BNL 719, Vol. III (1962) 1012.
[23] ARAI, E. and KÜCHLE, M., submitted for publication in Nukleonik.
[24] JOEST, K.H. and MEMMERT, G., Proc. 3rd UN Int. Conf. PUAE, 1964, P/762.
[25] GHATAK, A.K. and HONECK, H., Nucl. Sci. Engng 21 (1965) 227.
[26] CLENDENIN, W.W., Nucl. Sci. Engng 18 (1964) 351.
[27] KALLFELZ, J., unpublished internal Karlsruhe report (1965).
[28] KOPPEL, J.U. and YOUNG, J.A., Nucl. Sci. Engng 19 (1964) 412.
[29] SPRINGER, T. et al., Proc. 3rd UN Int. Conf. PUAE, 1964, P/763.
[30] PÁL, L. et al., Proc. 3rd UN Int. Conf. PUAE, 1964, P/651.
[31] KÜCHLE, M. and KUSSMAUL, G., Nukleonik 6 (1964) 329.
[32] BAYER, R., ČERVENÁ, J. and SCHÄFERLINGOVÁ, W., Czech. J. Phys. B 12 (1962) 107.
[33] ÁDÁM, A., BOD, L. and PÁL, L., Acta Phys. Hung. XIII (1961) 25.
[34] GLÄSER, W., Nukleonik 7 (1965) 64.
[35] YUROVA, L.N. et al., Proc. 3rd UN Int. Conf. PUAE, 1964, P/356.
[36] BLACKSHAW, G.L. and WALTNER A.W., J. nucl. Energy A/B 17 (1963) 341.
[37] CHARLES, M.P., J. nucl. Energy 18 (1964) 305.
[38] NILSSON, T. and SJÖSTRAND, N.G., Ark. Fys. 24 (1963) 543.

[39] MURGATROYD, W. et al., Proc. 3rd UN Int. Conf. PUAE, 1964, P/564.
[40] HONECK, H., Rpt. BNL 719 Vol. IV (1962) 1186.
[41] STARR, E., HONECK, H. and DE VILLIERS, J., Nucl. Sci. Engng 18 (1964) 230.
[42] KUSSMAUL, G. and MEISTER, H., J. nucl. Energy A/B 17 (1963) 411.
[43] MALAVIYA, B.K. and PROFIO, A.E., Trans. Amer. nucl. Soc. 1 (1963) 58.
[44] GANGULY, N.K., COBB, F.C. and WALTNER, A.W., Nucl. Sci. Engng 17 (1963) 223.
[45] BECKURTS, K.H. and WIRTZ, K., in Neutron Physics, Springer-Verlag, Berlin (1964).
[46] DLOUHÝ, Z. and KVITEK, J., J. nucl. Energy A/B 16 (1962) 376.
[47] ANTONOV, A.V. et al., Atomnaja Energija 12 (1962) 1,22.
[48] NELKIN, M., J. nucl. Energy A 8 (1958) 48.
[49] SANTANDREA, E., TOSELLI, F. and VIANO, G., Proc. 2nd UN Int. Conf. PUAE 16 (1958) 265.
[50] MEADOWS, J.W. and WHALEN, J.F., Nucl. Sci. Engng 9 (1961) 132.
[51] FRIEDMAN, E., Nucl. Sci. Engng 14 (1962) 420.
[52] FRIEDMAN, E., Proc. 3rd UN Int. Conf. PUAE, 1964 P/509.
[53] FRIEDMAN, E., Nucl. Sci. Engng 19 (1964) 203.
[54] VERDAGUER, F. et al., Proc. 3rd UN Int. Conf. PUAE, 1964, P/678.
[55] GLÄSER, W. and BECKURTS, K.H., Nucl. Sci. Engng 20 (1964) 235.
[56] CALAME, G.P., Nucl. Sci. Engng 20 (1964) 352.
[57] WESTFALL, F.R. and WALTNER, A.W., Trans. Amer. nucl. Soc. 5 (1962) 386.
[58] DÖLLGAST, T., FEDERIGHI, F.D. and ZUMBRUNN, K., "Application of Friedman's method to heavy water", withdrawn from these Proceedings.
[59] BERGMAN, A.A. et al., Proc. 3rd UN Int. Conf. PUAE, 1964, P/642.
[60] ORNSTEIN, L.S. and UHLENBECK, G.E., Physica 4 (1957) 478.
[61] DYAD'KIN, G. and BATALINA, E.P., Atomnaja Energija 10 (1961) 5.
[62] KOPPEL, J.U., Nucl. Sci. Engng 8 (1960) 157.
[63] PROFIO, A.E. and ECKARD, J.D., Nucl. Sci. Engng 19 (1964) 321.
[64] MÖLLER, E. and SJÖSTRAND, N.G., AB Atomenergi Rpt RFX-248 (1963).
[65] POOLE, M.J., "Review of the application of pulsed sources to the measurement of neutron spectra in moderators and reactor lattices", these Proceedings I.
[66] SHAPIRO, C.S. and CORNGOLD, N., submitted for publication in Phys. Rev.
[67] MÖLLER, E. and SJÖSTRAND, N.G., Rpt. BNL 719, Vol. III (1962) 966.
[68] KÜCHLE, M. and SCHWEICKERT, E., unpublished.
[69] BECKURTS, K.H., Rpt. BNL 719 Vol. III (1962) RE 1.
[70] BEGHIAN, L.E. et al., Nucl. Sci. Engng 15 (1963) 375.
[71] BEGHIAN, L.E. et al., Nucl. Sci. Engng 17 (1963) 82.
[72] SJÖSTRAND, N.G., Ark. Fys. 15 (1959) 147.
[73] BECKURTS, K.H., unpublished internal Karlsruhe report (1964).
[74] ABAGJAN, L.P. et al., INDSWG 17 (1963).

DISCUSSION*

M. NELKIN: In connection with Friedman-type experiments, I think it is important to bear in mind that the theoretical α versus N curve has a very small curvature, which might be extremely difficult to measure.

K.H. BECKURTS: I don't think that the curvature is as small as all that. Even if it is small, it should nevertheless be possible for it to be detected accurately since the first-order effect, the coefficient a, should be very well known.

* See also the comment by R. Bednarz in the discussion following paper SM-62/74. (BEGHIAN, L.E. and WILENSKY, S., "The pulsed neutron technique applied to fast non-multiplying assemblies", these Proceedings II).

S.N. PUROHIT: Again in connection with the Friedman method, I should like to point out that because of the correction factors in the formula there is liable to be some uncertainty about determinations of M_2 made by means of this method on the basis of the experimental value of the diffusion cooling coefficient C_{Σ_a}.

K.H. BECKURTS: That is quite true. On the other hand, as Calame from the Rensselaer Polytechnic Institute has shown, this error is much smaller than the discrepancy in M_2, which amounts to a factor of 2–4.

M.N. MOORE: Would you say that spatial Fourier modal decontamination has proved successful in practice?

K.H. BECKURTS: Yes, I would. I would refer, for example, to the work of Meister on D_2O systems and to the investigations of Beyster and Lopez in connection with H_2O systems. Of course, detector perturbations are liable to be a problem and have to be kept small.

PULSED NEUTRON MEASUREMENT OF THE DIFFUSION PARAMETERS IN ORDINARY ICE AS A FUNCTION OF TEMPERATURE*

E. G. SILVER
OAK RIDGE NATIONAL LABORATORY,
OAK RIDGE, TENN., UNITED STATES OF AMERICA

Abstract — Résumé — Аннотация — Resumen

PULSED NEUTRON MEASUREMENT OF THE DIFFUSION PARAMETERS IN ORDINARY ICE AS A FUNCTION OF TEMPERATURE. The parameters λ_a, D and C in the familiar equation $\lambda = \lambda_a + DB^2 (1 - CB^2)$ have been measured by the "classical" pulsed neutron method in ice, over the buckling range 0.039 to 0.738 cm^{-2}, in an absorber-lined cryostat at temperatures down to -85°C. Techniques for producing accurately shaped ice cylinders of uniform density have been developed and are described.

A 300-keV deuteron accelerator, both pre- and post-acceleration pulsed, was used to produce bursts of D-D neutrons 20 to 200 μs long. D-T neutrons could not be used, despite intensity advantages, because they caused a high quasi-flat background due to photoneutrons from the decay of 7.35-s N^{16} produced by the O^{16} (n, p) N^{16} reaction. Each of 65 decays was measured with at least 10^6 counts in an 18-channel time analyser after waiting times ranging from 533 μs (largest cylinder) to 140 μs (smallest cylinder).

The results were analysed by use of a non-linear least squares fitting to a two-exponential decay model. A small-amplitude accelerator-derived component of $(6.5 \pm 2.5) \times 10^{-3} s^{-1}$ was found and corrected for. The corrected data had slopes constant within 1.5% over the time observed.

The results show that the absorption cross-section has 1/v dependence over the measured temperature range, making λ_a a constant and yielding an average value of (331.5 ± 3.1) mb for σ_a(H). (vD) may be fitted to a linear temperature relation yielding (vD) = (3.30 + 0.0123 T(°C)) x 10^4 cm^2/s. The diffusion cooling coefficient C has large uncertainties, but fits a linear temperature dependence: C = (4.55 + 0.025 T (°C)) x 10^3 cm^4/s.

MESURE DES PARAMETRES DE DIFFUSION DE LA GLACE ORDINAIRE EN FONCTION DE LA TEMPERATURE, AU MOYEN DES NEUTRONS PULSES. L'auteur a mesuré les paramètres λ_a, D et C de l'équation bien connue $\lambda = \lambda_a + DB^2(1-CB^2)$ pour la glace, par la méthode classique des neutrons pulsés dans une gamme de laplaciens allant de 0,039 à 0,738 cm^{-2}, à l'intérieur d'un cryostat revêtu intérieurement d'un absorbant, à des températures descendant jusqu'à -85°C. Il a mis au point une méthode permettant d'obtenir des cylindres de glace de dimension fixée avec précision et de densité uniforme.

Il a utilisé un accélérateur de deutérons de 300 keV, pulsé avant et après l'accélération, pour produire des bouffées de neutrons D-D ayant une durée de 20 à 200 μs. Il est impossible d'utiliser les neutrons D-T malgré les avantages que présente leur intensité, parce qu'ils produisent un fort bruit de fond quasi uniforme dû aux photoneutrons émis par la désintégration de ^{16}N (7,35 s), lequel résulte de la réaction ^{16}O(n, p) ^{16}N. Chacune des 65 désintégrations a été mesurée avec au moins 10^6 coups dans un analyseur en temps à 18 canaux, après que se furent écoulés des temps allant de 533 μs (cylindre le plus grand) à 140 μs (cylindre le plus petit).

Pour analyser les résultats, l'auteur a procédé à un ajustement non linéaire à un modèle de décroissance exponentielle à deux groupes par la méthode des moindres carrés. Il a trouvé une composante de faible amplitude, dérivée de l'accélérateur: $(6,5 \pm 2,5) \cdot 10^{-3} s^{-1}$, et il a fait la correction correspondante. Les résultats corrigés avaient des pentes constantes à 1,5% près sur tout l'intervalle de temps observé.

Ces résultats montrent que la section efficace d'absorption varie comme 1/v sur toute la gamme des températures mesurées, ce qui rend λ_a constant et donne pour σ_a(H) une valeur moyenne de (331,5 ± 3,1) mb. (vD) est ajusté à une fonction linéaire de la température: (vD) = (3,30 + 0,0123 T (°C))·10^4 cm^2/s. Le coefficient de refroidissement par diffusion, C, conserve un degré élevé d'incertitude, mais peut aussi être ajusté à une fonction linéaire de la température: C = (4,55 + 0,025 T (°C))·10^3 cm^4/s.

* Research sponsored by the United States Atomic Energy Commission under contract with the Union Carbide Corporation.

ИЗМЕРЕНИЕ С ПОМОЩЬЮ ИМПУЛЬСНЫХ НЕЙТРОНОВ ПАРАМЕТРОВ ДИФФУЗИИ В ОБЫЧНОМ ЛЬДУ КАК ФУНКЦИИ ТЕМПЕРАТУРЫ. Параметры λ_a, D и C в известном уравнении $\lambda = \lambda_a + DB^2(1 - CB^2)$ измерены "классическим" методом с применением импульсных нейтронов во льду в диапазоне лапласиана 0,039 – 0,738 $см^{-2}$ в наполненном поглотителем криостате при температурах вплоть до -85° С. Разработаны и описаны методы изготовления ледяных цилиндров с точной формой и равномерной плотностью.

Ускоритель дейтронов с энергией 300 кэв в импульсном режиме как до, так и после ускорения использовался для получения вспышек нейтронов D–D продолжительностью от 20 до 200 мксек. Нельзя было использовать нейтроны D–T, несмотря на преимущества, связанные с интенсивностью, так как они порождали высокий квази-плоский фон благодаря фотонейтронам в результате распада N^{16}, образуемого в ходе реакции $O^{16}(n, p)N^{16}$. Каждый из 65 распадов измеряли по крайней мере в размере 10^6 отсчетов в 18-канальном временном анализаторе после периодов выдержки в пределах от 533 (самый большой цилиндр) до 140 мксек (самый малый цилиндр).

Результаты анализировали с помощью метода нелинейных наименьших квадратов, соответствующих модели двухэкспоненциального распада. Выведена и уточнена полученная на ускорителе компонента с небольшой амплитудой в размере $(6,5 \pm 2,5) \cdot 10^{-3}$ $сек^{-1}$. Среди уточненных данных отмечалась постоянная наклонов в пределах 1,5% в течение времени наблюдения.

Результаты показывают, что сечение поглощения проявляет 1/v зависимость от диапазона измеряемой температуры, при этом λ_a является постоянной, а среднее значение $\sigma_a(H)$ достигает величины (331,5 ± 3,1). (vD) может соответствовать линейной температурной связи, в результате $(vD) = (3,30 + 0,0123\ T(°C)) \cdot 10^4$ $см^2/сек$. Значение коэффициента диффузионного охлаждения C отличается большой неопределенностью, однако соответствует линейной температурной зависимости: $C = (4,55 + 0,025\ T(°C)) \cdot 10^3$ $см^4/сек$.

MEDICION CON NEUTRONES PULSADOS DE LOS PARAMETROS DE DIFUSION EN HIELO ORDINARIO EN FUNCION DE LA TEMPERATURA. El autor ha medido, por el método « clásico » de los neutrones pulsados y para el caso del hielo, los parámetros λ_a, D y C de la conocida ecuación $\lambda = \lambda_a + DB^2(1 - CB^2)$, en el intervalo de laplacianos de 0, 039 a 0, 738 cm^{-2}; las mediciones se realizaron, a temperaturas de hasta -85° C, en un criostato revestido interiormente de un absorbente. El autor describe las técnicas que se han ideado para obtener bloques cilíndricos de hielo ajustados a tolerancias muy estrictas y de densidad uniforme.

Se utilizó un acelerador de deuterones de 300 keV, pulsado tanto antes como después de la aceleración, para producir ráfagas de neutrones de 20 a 200 μs, obtenidos en virtud de reacciones D-D. No era posible utilizar neutrones D-T, pese a la ventaja que ofrecían respecto a intensidad, porque producían un elevado fondo de carácter casi uniforme debido a los fotoneutrones resultantes de la desintegración del ^{16}N con período de 7, 35 s producido en la reacción $^{16}O(n, p)\ ^{16}N$. Se midió cada una de las 65 desintegraciones, con un número de impulsos de por lo menos 10^6, en un analizador de tiempo de 18 canales, después de tiempos de espera comprendidos entre 533 μs (para el cilindro de mayores dimensiones) y 140 μs (para el cilindro más pequeño).

Los resultados se analizaron mediante el ajuste no lineal por el método de los cuadrados mínimos a un modelo de desintegración exponencial doble. Se halló, y se corrigió, un componente de pequeña emplitud derivado del acelerador de $(6, 5 \pm 2, 5) \cdot 10^{-3} s^{-1}$. Las curvas halladas presentaban una pendiente que se mantuvo constante, dentro de un margen del 1, 5%, durante el período de observación.

Los resultados obtenidos demuestran que la sección eficaz de absorción es función de 1/v en el intervalo de temperaturas medido, haciendo que λ_a sea una constante y proporcionando un valor promedio de (331, 5 ± 3, 1) mb para $\sigma_a(H)$. El coeficiente vD puede ajustarse a una variación lineal en función de la temperatura, dando $(vD7 = (3, 30 + 0, 0123\ T(°C)) \cdot 10^4\ cm^2/s$. El coeficiente C de enfriamiento por difusión ofrece considerable indeterminación, pero su variación en función de la temperatura es de carácter lineal: $C = (4, 55 + 0, 025\ T(°C)) \cdot 10^3\ cm^4/s$.

1. INTRODUCTION

The method of time-dependent neutron diffusion measurements as a means to determine the diffusion parameters in moderators is by now well established through the work of numerous investigators [1-8] who have worked with a number of materials including H_2O, D_2O, Be, graphite, and others. In particular, light water has been investigated by VON DARDEL and SJÖSTRAND

[9], ANTONOV et al. [10, 11] DIO and SCHOPPER [12], BRACCI and COCEVA [13], LOPEZ and BEYSTER [14], and KÜCHLE [15]. In VON DARDEL's [1] first paper on the method a crude measurement of the temperature effect in ice is given, and ANTONOV et al. [11] report a measurement at -80° C and at the temperature of liquid nitrogen (-196° C).

In the investigations of DE SAUSSURE [16] and SILVER [17] on beryllium at low temperatures it was found that long-persisting changes in the effective mean neutron velocity made measurement of the asymptotic spectrum impossible at times when the neutron density in the assembly was still sufficiently high to be accessible to measurement. The "trapping effect" which was proposed to explain the observations depends on the existence of narrow energy domains in which the ratio of the transport cross-section to the inelastic scattering cross-section, $\sigma_{tr}/\sigma_{inel}$, is very high. In particular, in the first Bragg peak the ratio approaches ≈ 36. Neutrons inelastically scattered to this energy will diffuse slowly, and have low probabilities of scattering out of the energy trap. A quasi-independent sub-population is thus formed, whose relative density, as compared to that of the main population, continues to increase with time. The very large rise in the diffusion cooling constant which has been predicted by SINGWI [18] but has not been observed experimentally would be due to an asymptotic spectrum of "trapped" neutrons.

If this mechanism is the correct one to explain the observed effects in beryllium, then in H_2O ice, where the inelastic scattering is relatively much larger, this trapping effect should be substantially absent, and asymptotic spectra, evidenced by an unchanging decay period, should be observed at low temperatures. The present work was therefore undertaken to determine (1) whether the spectrum does, indeed, become asymptotic in relatively short times at low temperatures and (2) what the temperature effects on the diffusion coefficient and the diffusion cooling coefficients are.

2. EXPERIMENTAL ARRANGEMENTS

All the test bodies were cylinders of ice made from distilled water. Initial experiments showed that density reductions of up to 7.8% occurred in the last-freezing top-central portion of the cylinder as compared with the lower and outer regions which froze first. This was a result of the entrapment of gas that evolved from the solution during freezing. Further problems were encountered from stress cracking and irregularities in the shapes of the ice surface as frozen.

For the large cylinders (with radii >10 cm) these problems were solved by development and use of a "plug" shown in Fig. 1. The water in each cylinder was boiled for about 1 h under a surface layer of melted paraffin about 5 cm thick. Then the plug was set into the container and lowered by means of the leveling screws until the 0.3-cm-thick space between the cylinder wall and plug was filled with paraffin as seal. A tube extended about 2.0 cm into the water to allow expansion into the volume above, which was covered with a $\approx$ 3-cm-thick layer of viscous mineral oil to prevent re-absorption of air. Room-temperature water was circulated through a spiral coil soldered

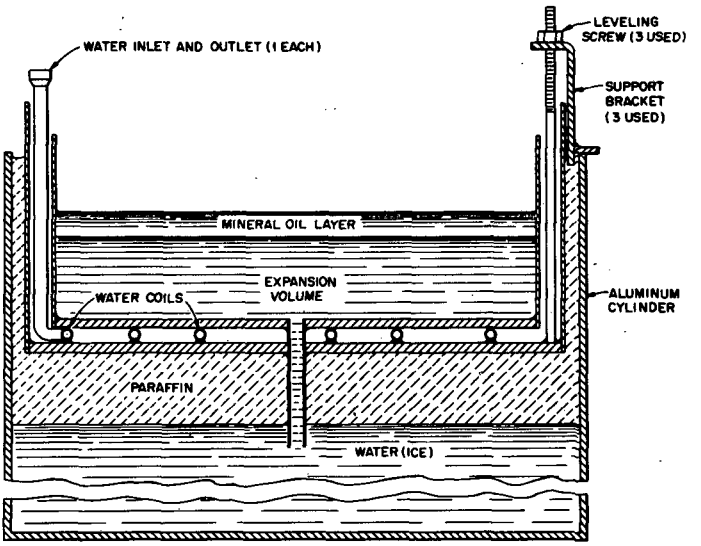

Fig. 1

Diagram of the plug used to produce large ice cylinders
The plug is shown in place in the aluminium water container.

to the plug plate to prevent freezing of the water from the top, and consequently cracking due to expansion of trapped water. A thick layer of paraffin between the coil-warmed plate and the water was required for freezing to occur. Without this layer the water would not freeze even in a refrigerator at -50° C because of convective circulation and heat exchange with the top plate. After freezing was complete the plug and paraffin were removed, the remaining small irregularities were filled with water and the cylinder was refrozen.

The small cylinders were made by a different technique, indicated in Fig. 2. For each ice cylinder to be formed an aluminium cylinder with accurately machined thin walls (approximately 0.1 cm thick) and accurately flat, parallel end planes, was placed on a glass plate and sealed to it with a vacuum sealing compound (Apiezon Q) around the outside. In each case the aluminium cylinder was about 12 cm longer than the ice cylinder to be produced. A flange connected to the vacuum system was placed on top of the cylinder with a neoprene gasket seal. Water and mineral oil flasks were then connected to the system as shown in the figure and the system was pumped for several hours. The water and oil were then transferred into the cylinder to a water height of about 1 cm above the desired level, with the oil layer ≈ 5 cm thick. The cylinder was then removed from the flange and placed in a refrigerator at about -5°C. Once freezing was complete, the cylinder was cooled further to -80°C. At this temperature the vacuum sealing material was brittle and the base plate could be removed by a sharp blow, leaving the bottom surface accurately flat and smooth. The entire cylinder was then sawed off at just above the desired height, removing the solidified oil and the uppermost portion of the ice with its non-uniform surface and any residual air inclusions. The cylinder was then placed in a lathe and the upper

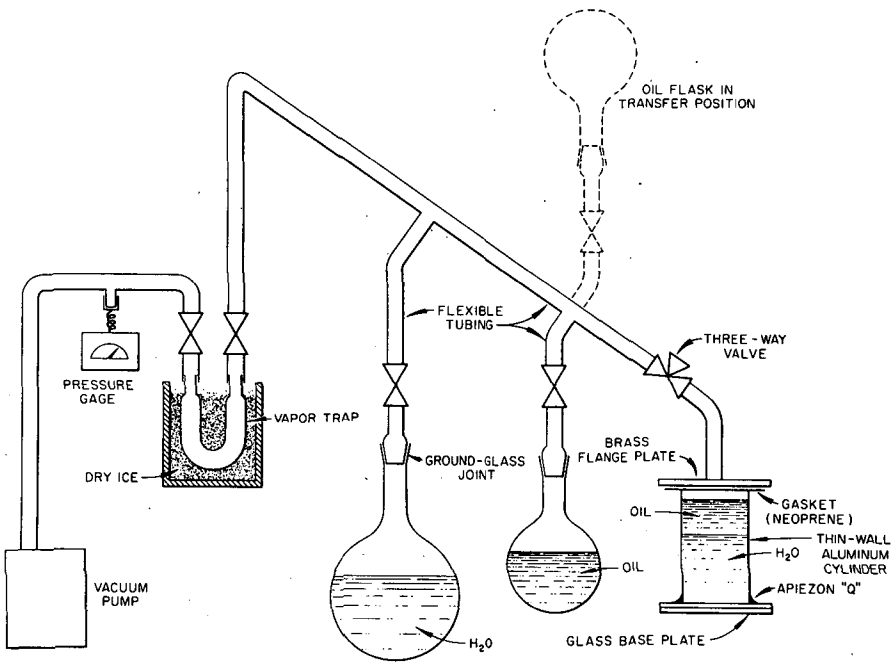

Fig. 2

Diagram of system used to produce small ice cylinders
Both flasks can be shifted to transfer position
The aluminium cylinder is shown filled and ready to be removed from the vacuum.

plane faced off to produce the final accurately shaped body. The outer aluminium remained in place, and the ends were sealed with aluminium foil to prevent sublimation of the ice. The presence of the aluminium, amounting to a reflector savings of 0.005 cm, had only negligible effect on the bucklings.

All cylinders were completely covered with cadmium, except for a circular hole at the centre of one plane face, just large enough to permit a detector to be placed in contact with the ice.

The measurements were performed in a refrigerated test chamber which had inside dimensions of about 60 cm × 60 cm × 50 cm and was lined with Boral (a dispersion of boron in aluminium) about 0.63 cm thick. Deuterons from a 300-kV accelerator entered the chamber through a beam tube and struck a water-cooled deuterium target positioned within 0.5 cm of the curved surface of the ice cylinder on the plane of symmetry. The detector was a 4.45-cm-diam. by 0.3-cm-thick $Li^6I(Eu)$ crystal attached to a photomultiplier.

The accelerator beam was pulsed both by a pre-acceleration beam deflector in the ion source and a post-acceleration deflector operated in synchronism with it. With this arrangement, beam on-off ratios of 5×10^4 to 5×10^5 were attained. The pulse width and repetition rates were controlled by a circuit which also served to gate the detector pulses into the 18 channels of the time analyser. The time from the end of the neutron pulse to the beginning of counting in the first channel and the widths of both the

pulse and counting channels were all adjustable within wide limits. For the work under discussion the detector channel widths ranged from 18.18 to 40 μs. The waiting times, to allow for establishment of the asymptotic spectrum and for a higher spatial mode decay, ranged from 440μs for the largest cylinder to 140μs for the smallest.

TABLE I

DIMENSIONS AND BUCKLINGS OF THE CYLINDERS USED IN THE EXPERIMENT

Cylinder No.	Height (cm)	Radius (cm)	B^2(at -45°C) (cm^{-2})
1	24.95 ±0.31	15.13 ±0.17	0.0394±0.0010
2	18.54 ±0.20	12.55 ±0.12	0.0620±0.0008
3	25.30 ±0.22	10.035±0.10	0.0689±0.0011
4	21.27 ±0.18	10.035±0.10	0.0748±0.0011
5	16.51 ±0.13	10.035±0.10	0.0880±0.0013
6	16.05 ±0.12	7.325±0.04	0.1352±0.0012
7	10.44 ±0.06	5.575±0.025	0.2489±0.0017
8	9.069±0.05	4.190±0.02	0.3933±0.0028
9	6.400±0.040	4.001±0.015	0.5161±0.0032
10	4.196±0.040	5.550±0.032	0.6058±0.0076
11	7.520±0.040	3.073±0.012	0.6606±0.0039
12	7.188±0.027	2.858±0.012	0.7460±0.0046

Table I lists the cylinders investigated and their bucklings. The latter are temperature dependent (see below) and are given for -45°C. The neutron time decay was measured for cylinder temperatures of -5, -25, -45, -65, and -85° C. At each temperature 2 to 5×10^6 counts were recorded in the analyser.

3. DATA ANALYSIS

The decay data were analysed by use of a non-linear least-squares fit computer program, using the model

$$C(t) = P_1 + P_2 \exp(-P_3 t) + P_4 \exp(-P_5 t), \quad (1)$$

where C(t) is the count rate t seconds after the pulse and P_1 through P_5 are parameters to be fitted.

Direct attempts to fit the data to such a model usually failed to converge even after many iterations, so an alternative process was adopted whereby a number of fits was performed with a range of fixed values for P_5, the exponent of the second decay component. The "best" fit, that is, the one giving the smallest sum of weighted residuals, was found and the corresponding value of P_3 was taken to be the decay constant λ. In all cases $|P_4/P_2|$, the ratio of the amplitudes of the two components at t = 0 (the end of the neutron pulse), was less than 4% for the best fit. In the largest cylinders the second component appears to be mostly due to small dead-time counting losses as evidenced by negative values of P_4. The source in the smallest cylinders is uncertain, but is most likely due either to imperfect beam cut-off or to room return. Either would be consistent with the observed buckling and temperature independence of the values of P_5. Figure 3 is a

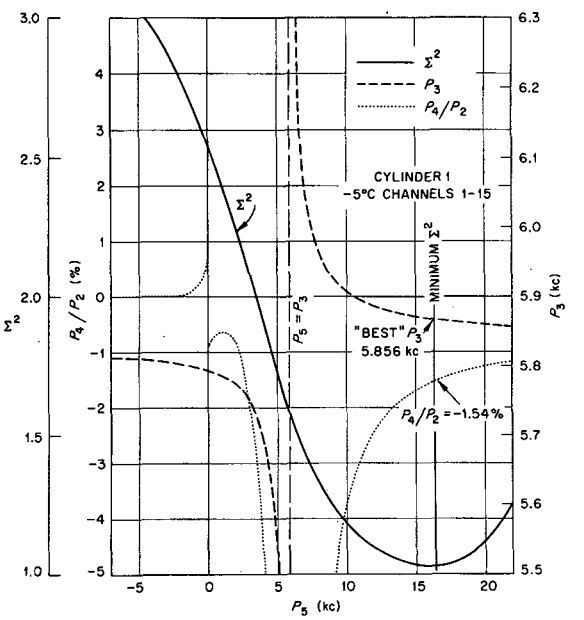

Fig. 3

The weighted sum of residuals squared Σ^2 the parameter P_3, and the ratio $|P_4/P_2|$, as a function of P_5 for a typical example of the results of a series of non-linear least-squares fits of the neutron decay data to the equation $C(t) = P_1 + P_2 e^{-P_3 t} + P_4 e^{-P_5 t}$. P_5 is fixed, and t = 0 at the end of the neutron pulse.

typical example of the effect of varying P_5 in a series of fixed-P_5 least-squares calculations. For each of the decay measurements analyses were carried out using all 18 channels and overlapping sections consisting of the data in channels 1-15, 2-16, 3-17, and 4-18, respectively. The latter series were used as a check for time trends in the measured decay constants. Where no such trends were found, it was concluded that asymptotic spectra had been obtained. Some cylinders at various temperatures were pulsed with

TABLE II

EFFECT OF EXTENDED WAITING TIME ON MEASURED DECAY CONSTANT

Cylinder No.	Temp. (C°)	Waiting time from end of pulse (μs)	Decay constant, λ ($10^3 s^{-1}$)
6	-65	280	7.891±0.064
		400	7.864±0.078
8	-85	175	13.290±0.100
		250	13.199±0.180
9	-45	180	16.085±0.129
		220	16.117±0.220
11	-85	140	19.412±0.321
		220	19.561±0.570

extended waiting times, as well as with the waiting times used for the main work. The results of these extended-waiting-time tests are shown in Table II. In all cases the effect of a longer waiting time was less than the uncertainties in the decay constant. The final values of P_3, the dominant decay constant, were taken from the results of analyses of channels 1-18 and from analyses using only the odd- or even-numbered channels. The latter procedure yielded two independent values from which the uncertainties from counting errors could be inferred.

Figure 4 shows the measured decay constants obtained for each buckling and temperature.

The diffusion parameters were then calculated from the measured cylinder dimensions and decay periods by an iterative procedure to obtain consistency between the transport mean free path entering the extrapolation distance calculations and the diffusion coefficient obtained. First the buckling for the i-th cylinder at a given temperature T was found by the equation

$$(B^2)_i^{(o)} = \frac{\pi^2}{\left[H_i + \frac{2\,(vD)^{(o)}\,K\,P_i}{\sqrt{T}}\right]^2} + \frac{\nu_o^2}{\left[R_i + \frac{(vD)^{(o)}\,K\,Q_i}{\sqrt{T}}\right]^2}, \qquad (2)$$

where

$$K = \frac{3 \times 0.7103\sqrt{T_o}}{\bar{V}_o} = 6.9024 \times 10^{-5} \text{ sec } (^\circ K)^{\frac{1}{2}} \text{ cm}^{-1}, \qquad (3)$$

H_i and R_i are the height and radius of the i-th cylinder, P_i and Q_i are extrapo-

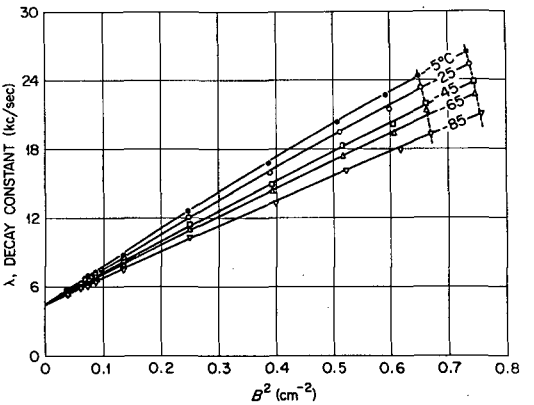

Fig. 4

Measured values of the decay constants λ as a function of B^2 for all cylinders and temperatures
Note the change in buckling with temperature caused by the change
in extrapolation distance with temperature.

lation distance correction factors discussed below, T_o is the temperature in °K, and $(vD)^{(o)}$ is a first estimate of the diffusion coefficient.

The pairs of numbers $[(B^2)_i^{(o)}, \lambda_i]$ were then least-squares fitted to the equation

$$\lambda = \sum_{j=o}^{n} a_j [(B^2)^{(o)}]^j \tag{4}$$

using n = 1, 2, 3. The coefficient of the linear term, a_1, was then used as an improved estimate, $(vD)^{(1)}$ in Eq. 2, and the process was repeated until the values of vD from successive trials differed by less than a pre-assigned value.

The errors associated with the coefficients a_j are obtained directly from the least-squares fitting procedure, which allows explicit specification of values of both $\delta(B_i^2)$ and $\delta\lambda_i$ [19]. The former are given by

$$\delta(B_i^2) = \left| \frac{4\pi^4}{\left[H_i + \frac{2(vD)\,K P_i}{\sqrt{T}}\right]^6} (\delta H_i)^2 + \frac{4\nu_o^4}{\left[R_i + \frac{(vD)\,K Q_i}{\sqrt{T}}\right]^6} (\delta R_i)^2 \right|^{\frac{1}{2}} \tag{5}$$

and the latter are obtained from the results of the decay curve analyses. In all cases the attempt to find terms of order B^6 (the coefficient a_3) resulted in much larger errors in all the coefficients and in errors in a_3 several times as large as a_3. Therefore the present results were all based on a three-parameter fit to the $\lambda(B^2)$ data, of the explicit form:

$$\lambda = v\Sigma_a + (vD)B^2 + C\,B^4. \tag{6}$$

The familiar extrapolation distance factor $0.7103\lambda_{tr}$ is obtained from one-velocity transport theory for flat surfaces and large media. In the case

of dimensions of only a few diffusion lengths and large surface curvature, corrections are needed to improve the calculation of the extrapolation distance. GELBARD and DAVIS [20] have made careful investigation of this effect for water and have obtained extrapolation distances as a function of buckling for infinite slabs and cylinders. The ratio of the Gelbard-Davis extrapolation distance to the one-velocity transport-theory extrapolation distance in water was computed for each geometry and applied to the buckling calculation. The resulting correction factors are shown in Fig. 5, where P and Q refer to the slab and cylinder geometries and are applied to the axial and radial buckling calculations, respectively.

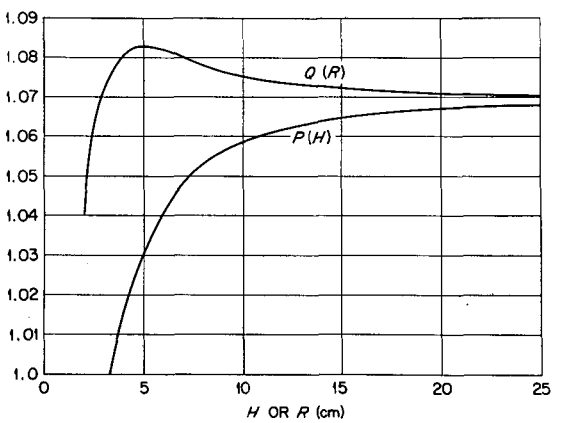

Fig. 5

The correction factors P and Q used to correct axial and radial extrapolation distances λ, respectively, in ice cylinders
The values are obtained from the work of GELBARD and DAVIS [20].

4. RESULTS AND DISCUSSION

4. 1. Asymptotic decay

As is seen from Table II, one result of the experiment is that no noticeable trapping effect appears in ice. At all bucklings and temperatures an equilibrium spectrum was attained at times of the order of 140 μs or less. This is in accord with the expectation based on the ratio $\sigma_{inel}/\sigma_{tr}$ in water.

4. 2. Inverse absorption Lifetime $v\Sigma_a$

Since the absorption cross-section of oxygen, $\sigma_a(O)$, is negligibly small and since the absorption cross-section for hydrogen is inversely proportional to the velocity, the value of $v\Sigma_a$ would be expected to be independent of temperature and was found to be so within the limits of accuracy, as shown in Fig. 6. Care was taken in the experiment to preserve water purity and to extend the data to small bucklings to obtain an independent measurement of the proton-neutron absorption cross-section. The result is $\sigma_a(H) = (331.5^{+3}_{-1}\frac{1}{6})$mb. The uncertainty is divided into ± 1.6 mb, caused by measurement errors, and

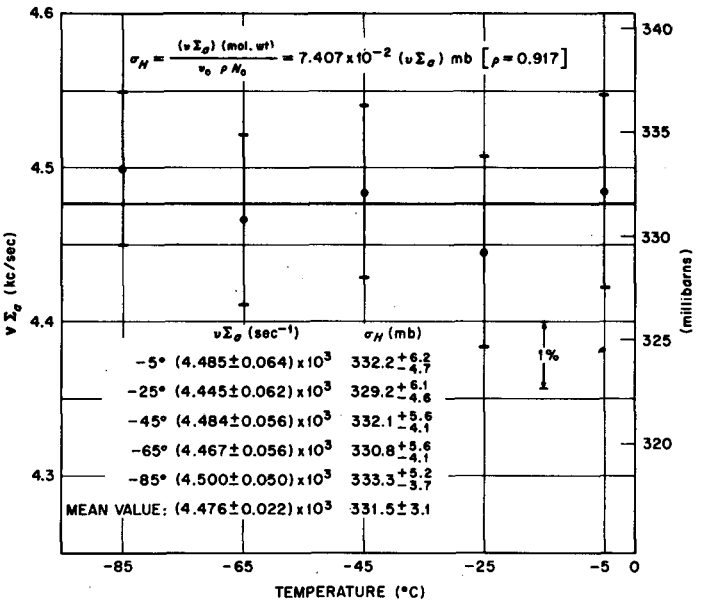

Fig. 6

Measured values of ($v\Sigma_a$) as a function of temperature
The corresponding microscopic hydrogen absorption cross-section is indicated on the right-hand ordinate scale (based on $\rho_i = 0.917$ g/cm^3).

±1.5 mb, by uncertainty in the ice density. This value is in excellent agreement with the value 332 ± 2 mb given by STEHN et al. [21] who quoted numerous other workers.

4.3. Diffusion coefficient vD

The diffusion coefficient has been measured by several workers in liquid water and by Antonov in ice at 0° C, -80° C, and -196°C. Several measurements of the temperature dependence of vD above the freezing point are also found in the literature. However, below the freezing point there is only Antonov's report (see [11]) which gives ratios for the values in ice to those in water at 0°C. This, combined with 0°C values of ANTONOV et al. [10], was used to infer absolute values. The errors therefore appear large.

Figure 7 shows the results of the present experiment, and, for comparison, the data of other workers. All data in water were adjusted to the density of ice by the relation $D_w/D_{w(i)} = \rho_i/\rho_w$, where w, i, and w(i) refer, respectively, to water, ice, and water of the artificial density of ice.

The data from the present work are consistent with a linear fit, yielding the coefficients

$$(vD)(T^\circ K) = (0.047 \pm 0.202) \times 10^4 + (1.225 \pm 0.087) \times 10^2\ (T^\circ K).$$

This fit is shown in Fig. 7.

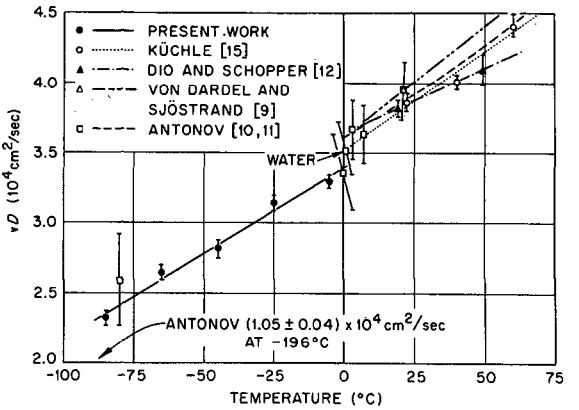

Fig. 7

Measured values of the diffusion coefficient vD
Results obtained by other workers in ice and water are also shown
All values in water are modified by $(\rho i/\rho w)^{-1}$ to compensate for the density difference.

Antonov found a discontinuity in vD at the freezing point of $(vD)_i/(vD)_w = 1.04 \pm 0.02$; after correction of this for the difference in density it was found that at 0°C $(vD)_i/(vD)_{w(i)} = 0.95 \pm 0.02$, where i, w, and w(i) are as defined above. When $(vD)_{w(i)} = (3.58 \pm 0.14) \times 10^4$ cm^2/s is used as a best value obtained from the results of Antonov and the extrapolated data of Von Dardel, Küchle, and Dio and Schopper, the present data lead to a value $(vD)_i/(vD)_{w(i)} = 0.95 \pm 0.15$. This is in agreement with Antonov's results.

Extrapolation of the data for D to -196°C yields a value of $D(-196°C) = (0.99 \pm 0.11) \times 10^4$ cm^2/s, which is, within the limits of error, in agreement with Antonov's value. Antonov's value at -80°C is also seen to agree, within the limits of error, with the results of the measurements reported here.

4.4. Diffusion cooling coefficient C

Figure 8 shows the values of C obtained in the present work, as well as data of other workers. The same sources as were quoted for vD above are available here. Antonov finds a ratio $(C)_i/(C)_w = 2.5 \pm 0.4$ at 0°C and also gives ratio values at -80°C and -196°C. In comparing the diffusion cooling coefficient in water with that in ice it is necessary to correct for the density difference. Since C has dimensions of cm^4/s = cm^3 × (velocity), the value of C is proportional to the inverse cube of the density. Hence the water data have been multiplied by $(1.0905)^3$ to correspond to the density of ice. This correction makes the 0°C ratio of Antonov $(C)_i/(C)_{w(i)} = 1.9 \pm 0.3$.

Because of the large scatter of the points, the extrapolation of the data of Küchle and Dio to 0°C has large associated uncertainties. However, surely fortuitously, the results of both investigators (based on four and three points, respectively) agree almost exactly on a value of -3.8×10^3 cm^4/s, with a combined uncertainty of about 1.15×10^3 cm^4/s. Antonov found, for water at 0.5°C, a value of $-(5.2 \pm 1.3) \times 10^3$ cm^4/s, whereas a linear fit to all his C-data up to 200°C yields a 0°C-value of -4.7×10^3 cm^4/s.

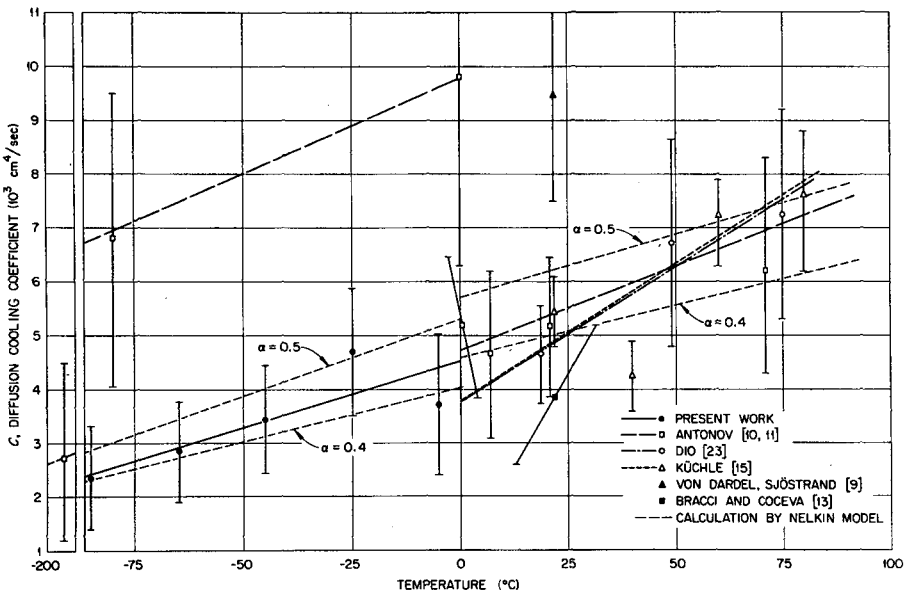

Fig. 8

Measured values of the diffusion cooling coefficient C
Values obtained by other workers in ice and water are also shown
All values in water have been scaled by $(\rho i/\rho w)^{-3}$ to compensate for the density difference.

The present data were fitted to a linear model which yielded the relation

$$C(T^\circ C) = -\left[(4.55 \pm 0.62) \times 10^3 + (0.025 \pm 0.011)(T^\circ C)\right] \text{ cm}^4/\text{s}.$$

This gives

$$C(0^\circ C) = -(4.55 \pm 0.63) \times 10^3 \text{ cm}^4/\text{s},$$

which falls between the values of Dio and Küchle on the one hand and of Antonov on the other. However, since the present data disagree considerably with the Antonov values at lower temperatures, the Antonov water values are probably also of low relative significance. Restricting consideration to the other results, we arrive at a ratio of $(C)_{w(i)}/(C)_i = (1.2 \pm 0.4)$ from which it cannot be concluded unequivocally that there is a discontinuity in C. However, the discontinuity of a factor of (1.9 ± 0.3) found by Antonov appears inconsistent with the present results. The present absolute data for C in ice can be compared only with those of Antonov and are seen to disagree seriously outside the large error limits.

For comparison, the figure includes computed values of C obtained by the following equation from NELKIN [22]:

$$C = \frac{(\alpha + \frac{1}{2})^2 \sqrt{\pi}\,(vD)^2}{M_2\, v}, \tag{7}$$

where α is a parameter obtained from $\lambda_{tr}(E) \propto E^{\alpha}$, and M_2 has the dimensions

of a macroscopic cross-section, i.e. $M_2 = N\sigma$. The calculations were made for α-values of 0.4 and 0.5, using a constant value of M_2 corresponding to a microscopic cross-section of 31.2 b per hydrogen atom. These values correspond to those found by Küchle over a temperature range from 22 to 80°C. It is to be noted that for $\alpha = 0.4$ a good fit to the present ice data is obtained. The calculation is based on the linear fit to the present data for vD in ice, and on a linear fit to the published data in water. However, the calculated values exhibit a discontinuity at the phase transition of the opposite direction from that found in the experiment.

REFERENCES

[1] VON DARDEL, G.F., Kungl. Tekniska Hogskolans Handlingar Nr. 75 (1954).
[2] SCOTT, F.R., THOMSON, D.B. and WRIGHT, W., Phys. Rev. 95 (1954) 582.
[3] CAMPBELL, E.C. and STELSON, P.H., Oak Ridge National Laboratory Rpt ORNL-2076 (1956) 32.
[4] BECKURTS, K.H., Nucl. Sci. Engng 2 (1957) 516-22.
[5] KOMOTO, T.T. and KLOVERSTROM, F., Trans. Amer. nucl. Soc. (1958) 94.
[6] DE SAUSSURE, G. and SILVER, E.G., Nucl. Sci. Engng 6 (1959) 159.
[7] ANDREWS, W. M., University of California Radiation Laboratory Rpt UCRL-6083 (1960) 193.
[8] BECKURTS, K.H., Nucl. Sci. Engng 2 (1957) 516-22.
[9] VON DARDEL, G. and SJÖSTRAND, N.G., Phys. Rev. 96 (1954) 1245.
[10] ANTONOV, A.V. et al., Inelastic Scattering of Neutrons in Solids and Liquids, IAEA, Vienna (1961) 377-94.
[11] ANTONOV, A.V. et al. At. Energ. 13 (1962) 373-74.
[12] DIO, W.H. and SCHOPPER, E., Nucl. Phys. 6 (1958) 175-76.
[13] BRACCI, A. and COCEVA, C., Nuovo Cim. IV (1956) 59.
[14] LOPEZ, W.M. and BEYSTER, J.R., Nucl. Sci. Engng 12 (1962) 190-202.
[15] KÜCHLE, M., Nukleonik 2 (1958); No.IV (1960) 131.
[16] DE SAUSSURE, G., Proc. Brookhaven Conf, on Neutron Thermalization, BNL 719 IV (1962) 1158/74.
[17] SILVER, E.G., Proc. Brookhaven Conf. on Neutron Thermalization, BNL 719 III (1962) 981-96.
[18] SINGWI, K.S. Ark. Fys. 16 (1960) 385-411.
[19] JARRARD, J.D. and CHAPMAN, G.T., Oak Ridge National Laboratory Rpt ORNL-TM-659 (see DEMING, W.E., Statistical Adjustment of Data, Wiley, N.Y. (1944) 50-55).
[20] GELBARD, E.M. and DAVIS, J.A., Nucl. Sci. Engng. 13 (1962) 237-44.
[21] STEHN, J.R., GOLDBERG, M.D., MAGURNO, B.A. and WIENER-CHASMAN, R., Neutron Cross Sections, BNL-325, 2nd ed., Suppl. 2 (1964) 1-0-1/1-0-2.
[22] NELKIN, M., J. nucl. Energy 5 (1958) 48.
[23] DIO, W.H., Nukleonik 1 (1958) 13.

EXTRAPOLATION DISTANCES FOR PULSED NEUTRON EXPERIMENTS

J. WALKER, J.B.C. BROWN* AND J. WOOD
UNIVERSITY OF BIRMINGHAM, UNITED KINGDOM

Abstract — Résumé — Аннотация — Resumen

EXTRAPOLATION DISTANCES FOR PULSED NEUTRON EXPERIMENTS. Attention has been drawn in earlier work to the effect of uncertainty in extrapolation distance on the results of pulsed neutron experiments and hence to the need for more accurate knowledge of this parameter. The extrapolated endpoints can be obtained from flux plots and the value for large systems can be deduced from diffusion coefficients. Information from both approaches is given and the dependence of extrapolated endpoint on temperature and on buckling is discussed.

Decay times and time-dependent flux plots have been measured in pulsed source experiments on small, accurately-known, volumes of water and Dowtherm A (thermex) by the use of a small scintillation detector and a time analyser; a separate scintillation detector or a BF_3 counter has been used as a monitor. Spatial harmonic analysis of the flux plots was performed by the method of least squares to obtain the extrapolated endpoints once appropriate corrections have been made to the recorded counts. Some consideration was given to the possibility of testing for the effect of flux distortion near the boundary by successive removal of the outer points and to the effects on extrapolated endpoint of the flux perturbation produced by the detector.

The results presented are mainly for measurements at 20°C in 4-in and 7-in cubic containers lined with cadmium, but very preliminary information was obtained for water at temperatures up to 80°C and equipment is being designed to extend the range of temperatures still further.

LONGUEURS EXTRAPOLÉES POUR LES EXPÉRIENCES A L'AIDE DES NEUTRONS PULSÉS. Dans un article déjà publié, les auteurs avaient signalé que les incertitudes concernant la longueur extrapolée avaient un effet sur les résultats d'expériences au moyen des neutrons pulsés, et que, par conséquent, il fallait connaître ce paramètre d'une manière plus précise. Les points extrapolés aux extrémités peuvent être obtenus à partir des courbes de flux et les valeurs pour des sytèmes de grandes dimensions peuvent être déduites des coefficients de diffusion. Les auteurs donnent des renseignements obtenus par ces deux méthodes et discutent les variations des points extrapolés en fonction de la température et du laplacien.

Ils ont déterminé les temps de décroissance et les courbes du flux en fonction du temps dans des expériences, au moyen d'une source pulsée, sur de petits volumes (mesurés exactement) d'eau et de « Dowtherm A » (thermex) en se servant d'un petit détecteur à scintillation et d'un analyseur en temps; un autre détecteur à scintillation ou un compteur BF_3 a été utilisé pour le contrôle. Ils analysent les courbes de flux du point de vue des harmoniques spatiaux par la méthode des moindres carrés, afin d'obtenir les points extrapolés, après avoir corrigé de façon appropriée les nombres de coups enregistrés. Ils étudient également la possibilité de vérifier l'effet des distorsions du flux au voisinage de la limite par suppressions successives des points extérieures, et les effets sur les points extrapolés des perturbations du flux dues au détecteur.

Les résultats présentés portent principalement sur des mesures faites à 20°C sur ces liquides contenus dans des récipients cubiques de 10 cm et de 18 cm revêtus intérieurement de cadmium, mais des informations très provisoires ont été obtenues sur l'eau à des températures allant jusqu'à 80°C; des appareils sont actuellement mis au point en vue d'étendre encore davantage la gamme des températures.

ДЛИНЫ ЭКСТРАПОЛЯЦИИ ПРИ ЭКСПЕРИМЕНТАХ С ИМПУЛЬСНЫМИ НЕЙТРОНАМИ. В более ранней работе было обращено внимание на влияние неточности длины экстраполяции на результаты экспериментов с импульсными нейтронами и на необходимость в связи с этим более точного значения этого параметра. Экстраполированные конечные точки могут быть получены по графикам потоков и данные для больших систем могут быть выведены из коэф-

* Now at the Central Electricity Generating Board, Berkeley Nuclear Laboratories, Berkeley, United Kingdom.

фициентов диффузии. Приводятся данные, полученные с помощью этих методов и рассматривается зависимость экстраполированных конечных точек от температуры и лапласиана.

Время распада и зависящие от времени графики потоков были измерены при проведении экспериментов с импульсными нейтронами в небольших точно известных объемах воды и вещества "Даутерм А" с помощью небольшого сцинтилляционного детектора и временного анализатора; в качестве регистратора использовался отдельный сцинтилляционный детектор или счетчик BF_3. Анализ пространственной гармоники графиков потоков осуществляется по методу наименьших квадратов, чтобы получить экстраполированные конечные точки после внесения необходимых поправок в результаты счета. Высказываются некоторые соображения относительно возможности определения эффекта искажения потока вблизи границы путем последовательного удаления внешних точек и относительно экстраполированных точек пертурбации потока, вызванной счетчиком.

Предварительные результаты касаются главным образом измерений при температуре 20°C в кубических контейнерах размером 4 и 7 дюймов, покрытых кадмием. Однако весьма приблизительные результаты были получены для воды при температуре до 80°C, и разработано оборудование для дальнейшего расширения диапазона температур.

LAS DISTANCIAS DE EXTRAPOLACION EN LOS EXPERIMENTOS CON NEUTRONES PULSADOS. Los autores señalaron ya en un trabajo anterior el efecto que sobre los resultados de los experimentos realizados con neutrones pulsados ejerce la incertidumbre respecto de la distancia de extrapolación, y a la consiguiente necesidad de conocer este parámetro con mayor precisión. Los puntos finales extrapolados pueden obtenerse partiendo de las representaciones gráficas de flujos y los valores para sistemas de grandes dimensiones pueden deducirse de los coeficientes de difusión. Los autores facilitan información sobre ambas formas de abordar el problema y examinan la variación del punto final extrapolado en función de la temperatura y del laplaciano.

En diversos experimentos realizados con fuentes de neutrones pulsados aplicadas a pequeñas masas de agua y de Dowtherm A (thermex) conocidas con toda precisión, se determinaron los tiempos de decrecimiento y las gráficas de flujo en función del tiempo empleando un pequeño detector de centelleo y un analizador de tiempo; como monitor se utilizó otro detector de centelleo o bien un contador de BF_3. Empleando el método de los cuadrados mínimos, se procedió al análisis de los armónicos espaciales de los diagramas de flujo, a fin de obtener el punto final extrapolado una vez introducidas las correcciones oportunas en los resultados de los recuentos. Se prestó también alguna atención a la posibilidad de determinar el efecto de la distorsión del flujo en las proximidades del límite por supresión sucesiva de los puntos exteriores y a los efectos que la perturbación del flujo debida al detector ejerce sobre el punto final extrapolado. Los resultados presentados se refieren principalmente a las mediciones realizadas a 20°C en recipientes cúbicos de 10,1 y de 17,7 cm de arista, con revestimiento interior de cadmio, pero se han obtenido resultados preliminares a 80°C, empleando agua, y se está modificando el equipo con miras a ampliar más aún el intervalo de temperaturas.

1. INTRODUCTION

The decay constant (α) of the fundamental spatial mode of the asymptotic thermal neutron distribution in a pulsed moderator can be related to the fundamental geometrical buckling by the expression

$$\alpha = v\Sigma_\alpha + D_0 B^2 - CB^4 + O(B^6) \qquad (1)$$

where $v\Sigma_\alpha$ is the absorption probability, D_0 the diffusion coefficient, C the diffusion cooling coefficient and $O(B^6)$ indicates higher-order buckling terms. The buckling B^2 is defined for a parallelepiped system of sides a, b, c by

$$B^2 = \left(\frac{\pi}{a+2Z_{01}}\right)^2 + \left(\frac{\pi}{b+2Z_{02}}\right)^2 + \left(\frac{\pi}{c+2Z_{03}}\right)^2 \qquad (2)$$

where Z_{01}, Z_{02}, Z_{03} are the extrapolated endpoints (or augmentation distances in the terminology of GELBARD and DAVIS [1]) to be added to the geometrical dimensions to give the points at which the flux distribution well inside the system would go to zero if extrapolated beyond the boundaries. The extrapolated endpoints are frequently taken to be the same for the different directions but the more general form is retained here for the moment.

The effect of uncertainty in extrapolated endpoints on the diffusion parameters extracted from pulsed source experiments was emphasized in earlier work [2, 3] and it was clear that more accurate measurements were required; Beckurts stated this need quite explicitly in his review paper at the Brookhaven Conference in 1962 [4]. The differences reported between extrapolated endpoints obtained by flux plotting in pulsed and steady-state experiments also called for further investigation. Early pulsed measurements in water at about 20°C [2, 5, 6] gave values in the range 0.4-0.46 cm which are well above the upper limits now indicated by steady state values (in the range 0.32-0.35 cm) [7] and the values obtained indirectly from diffusion coefficients in pulsed experiments. To help resolve these inconsistencies further measurements have been made at room temperatures with the Birmingham pulsed accelerators and a start has also been made on extending the techniques to higher temperatures. So far temperatures up to only 80°C have been used and the expected change in extrapolated endpoints, approximately 10%, is within the error of the preliminary measurements mainly because of instabilities in the present detectors.

2. EXPERIMENTAL DETAILS

The liquid moderators investigated were contained in accurately constructed parallelepiped boxes made from cadmium sheet bonded to aluminium to give rigidity to the cadmium. The bond was formed either by rolling the cadmium and aluminium together [8] or by the use of a suitable adhesive. Cubic boxes of approximately 4-in and 7-in side were used. Each box had a fitted lid with a central hole through which the detector could be inserted, so that flux plots could be made along a vertical line through the centre of the system. The boxes were filled to the brim so that the lids fitted flush to the liquid surface. This ensured that the geometrical dimension was well defined by two identical plane cadmium boundaries and this dimension could be measured accurately.

The sensitive part of the detector was a small boron-loaded or lithium-loaded ZnS (Ag) phosphor (N.E. 401) mounted on the end of a long perspex light-guide 0.5 in in diameter and sheathed in 0.01-in thick pure aluminium or 0.005-in stainless steel. The light guide led to a photomultiplier and transistor cathode follower and the pulses were fed through a conventional amplifier and discriminator to an 18-channel time analyser. The detecting phosphor itself was in the boron case a thin disc 8 mm in diameter and 0.3 mm thick attached to the end of the perspex and in the lithium case was painted as a thin layer directly onto the light guide. In both cases the phosphor was in the horizontal plane so that it formed a thin detector with good spatial resolution in the vertical direction along which the flux plots were made.

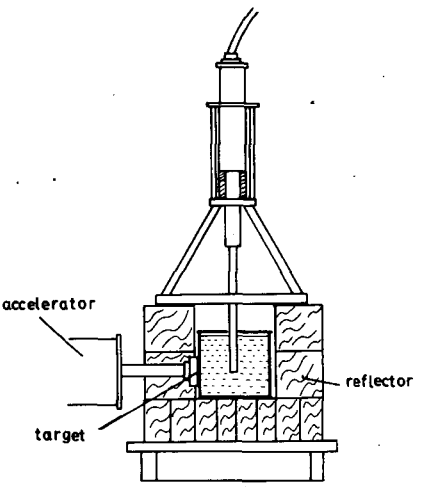

Fig. 1

Schema of experimental arrangement

The detector was held in a supporting frame and could be positioned at any desired height by a combination of spacers. The moderator system was surrounded by a 6-in thick reflector made of JABROC-N boron-loaded wood laminate blocks, which acted as a shield against room-return neutrons (see Fig. 1). The boron content of the shield caused the thermal flux set up inside it to die away rapidly and this, combined with the comparatively low energy of capture gamma rays, kept any interference with the scintillation detector to a negligible level. A second detector in a separate water-filled container near the target acted as a source-strength monitor so that the counts recorded at each point on the flux plot could be normalized to the same number of monitor counts. In the actual flux plotting the centre point was repeated between each of the other points to minimize the effect of any detector drifts. Examples of flux plots are shown in Fig. 2.

Thermostatically controlled heating tapes around the outside of the measuring volume were used for the higher temperatures. For all the results reported in this paper a minimum delay of 50 μs was used before the first counting channel opened. This ensured that thermalization was complete and an experimental check of this was made by time-dependent cadmium ratio measurements. No attempt is made here to analyse for any time-dependence of the extrapolated endpoint but this will be done with the improved information now being obtained.

3. METHOD OF ANALYSIS

The procedure used to analyse the flux plots followed closely the method of least squares described by DEMING [9], whereby the sum (S) of the weighted squares of the residuals is minimized. The weight of an observation is defined to be inversely proportional to its variance.

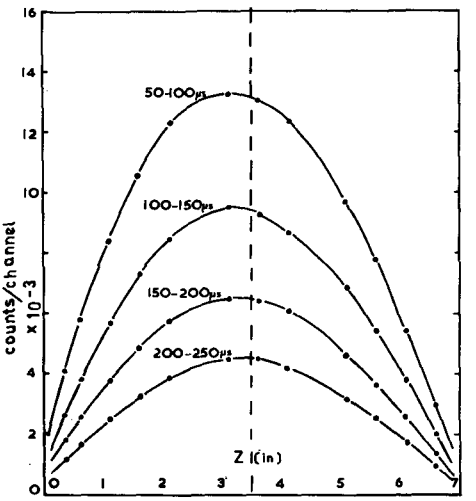

Fig. 2

Flux plots in 7-in cadmium box for water at 20°C

If we assume that all corrections for background, perturbation effect of counter, dead time etc. have been made, then the function to be fitted is

$$\phi(x) = \sum_n A_n \sin\left[\frac{n\pi(x+Z_0)}{a+2Z_0}\right] \qquad (3)$$

where x is measured from one boundary of the system, a is the physical width along the axis of measurement and Z_0 is the extrapolated endpoint, assumed the same for all harmonics.

A computer programme was written (in Mercury Autocode) to perform the least squares fitting of the data to Eq.(3). The programme included an iterative scheme which calculated better values of the amplitudes (A_n) from their previous values until there was no change in, say, the fourth significant figure. The number of harmonic terms included in the series could be varied and each calculation for a particular number of harmonics was independent of the previous number of harmonics used. Two methods of determining the extrapolated endpoint were used. In the first method the amplitudes were adjusted using various assumed values of Z_0, and a curve (Fig. 3) was then drawn of the minimum sum S versus Z_0. The value of Z_0 corresponding to the minimum of S was taken to be the best fitted value. The second method was an extension of the above to include the direct adjustment of the extrapolated endpoint and to calculate the corresponding standard error. It has been found that satisfactory convergence of the parameters can be achieved in about five iterations.

The effect of random error, number of measuring positions and magnitude of counts on the extrapolated endpoint for a hypothetical design experiment was investigated in the following way. Exact data for three harmonics with Poisson weighting but with a deliberately erroneous initial estimate

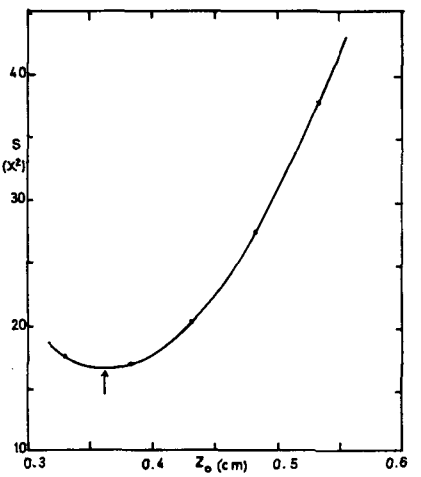

Fig. 3

Effect on minimum sum S of varying extrapolated endpoint

for Z_0 were analysed by the programme using the second method. It was found to be capable of computing the exact values of the amplitudes and extrapolated endpoint for three harmonics. When asked to fit the same data to four harmonics, the first three were found exactly, a negligibly small fourth harmonic was found with large standard error and the extrapolated endpoint was again calculated exactly. This indicated that the analysis was capable of providing the harmonic content of a flux plot. Similar data were again analysed but with random errors introduced into the hypothetical counts; the errors were derived from the standard deviation for a Poisson distribution and a table of normal deviates given in units of standard error [9]. The results of this analysis, given in Table I, show the effect that the increase in number of counts per position has on reducing the standard error of the extrapolated endpoint. It also indicates the desirability of having measurements at more than 14 evenly distributed points across this 18-cm wide system. This design investigation did not, of course, give any guidance as to the optimum distribution of time in an experiment but it indicated the conditions necessary for an accurate measurement of extrapolated endpoint. Fourteen points were selected, as this was the largest number used in our early measurements, but this has now been increased to 18 in current measurements.

Table II shows the results of fitting actual experimental data to various harmonics, using the second method. This can be compared with Fig. 3 and it is clear that there is excellent agreement between the value of Z_0 at the minimum of the curve and the result of the second method, with Poisson weighting and either three or four harmonics. This agreement gave confidence in the analytical procedure and indicated that three harmonics were adequate for the experimental arrangement used. The counts used in Table II were recorded for times greater than 100 μs after the end of the fast neutron burst.

TABLE I

ANALYSIS OF HYPOTHETICAL DESIGN EXPERIMENT (POISSON WEIGHTING WITH RANDOM ERRORS)

"Correct" amplitudes	Calculated amplitudes	Standard error	"Correct" Z_0 (cm)	Calculated Z_0 (cm)	Standard error (cm)	Number of points
100	103.2	3.61	0.3	0.215	0.194	14
1	3.94	3.39				
20	20.90	3.72				
	103.2	3.61	0.3	0.216	0.194	14
	4.08	3.62				
	20.89	3.73				
	- 0.342	3.08				
	98.04	2.89	0.3	0.309	0.171	20
	- 2.87	2.77				
	21.24	3.19				
	97.97	2.89	0.3	0.318	0.170	20
	- 2.50	2.84				
	21.17	3.18				
	- 1.5	2.52				
10000	10030	36.03	0.3	0.293	0.0207	14
100	131.7	33.67				
2000	2005	37.4				
	10030	36.03	0.3	0.292	0.0208	14
	133.0	36.02				
	2005	37.4				
	3.12	30.8				
	10010	29.12	0.3	0.294	0.0172	20
	109.5	27.8				
	2035	32.2				
	10010	29.14	0.3	0.294	0.0172	20
	108.4	28.48				
	2036	32.21				
	4.18	25.27				

TABLE II

EXTRAPOLATED ENDPOINT IN WATER AT 20°C
ANALYSIS OF EXPERIMENTAL PLOTS
WITH DIFFERENT HARMONICS
(Cube with 18-cm side)

Harmonic number	Amplitude of harmonic	Standard error	Z_0 (cm)	Standard error (cm)	S	Weighting	Number of points
1	5196.9	30.878	1.557	0.053	495.6	Poisson	11
2	-51.321	23.185					
1	5491.8	29.561	0.363	0.034	16.417	Poisson	11
2	11.794	25.991					
3	890.37	34.465					
1	5492.2	29.585	0.362	0.034	16.312	Poisson	11
2	9.936	26.616					
3	891.26	34.545					
4	7.9312	24.499					
1	5118.8	217.0	2.010	0.61[a]	1.713	Unit	11
2	- 19.05	180.8			$\times 10^6$		
1	5500.3	45.5	0.346	0.075[a]	7.158	Unit	11
2	10.541	42.05			$\times 10^4$		
3	898.21	56.96					
1	5500.5	53.8	0.345	0.088[a]	7.125	Unit	11
2	10.536	49.6			$\times 10^4$		
3	898.55	67.2					
4	7.598	49.63					

[a] Estimated standard error.

4. PERTURBATION PRODUCED BY THE DETECTOR

Two approaches were used to estimate the effects of detector perturbation. The first was a highly simplified model in which only the change

in decay constant produced by the detector was used to correct the measured fluxes and the analytical fits were then made to the corrected points. The second approach was to calculate in a more refined way a correction factor by which the Z_0 obtained from the uncorrected fluxes, had to be multiplied.

Both approaches showed that a reduction of approximately 10% had to be made in Z_0 for the measurements with the boron crystal in the 4-in cube. For this detector in the 7-in box the correction reduced to about 5%. With the thinner lithium detector the corrections will be smaller still.

For the decay time method let us assume that the neutron spectrum is not altered by the very small detector. The change in decay constant due to the detector will be

$$d\alpha = w(r)\overline{\Sigma'_a v},$$

where w(r) is a weighting factor depending on the position of the detector and $\overline{\Sigma'_a v}$ gives the absorption probability.

On simple perturbation theory and assuming that the depressed flux in the detector can be put in the form $F\phi$, where F is a constant depression factor and ϕ is the unperturbed flux, the weighting factor becomes

$$w(r) = \frac{F\phi^2(r)\Delta V}{\int_y \phi^2(r)dV},$$

where V is the volume of the moderator and ΔV that of the detector.

Thus the changes in decay constant produced by the detector in different positions should be nearly proportional to ϕ^2 if this highly simplified assumption of constant depression is at all justified. Experimental values for the changes in decay constant were obtained by using external detectors to measure the decay constant when the normal measuring crystal was placed inside at different positions.

The changes observed were in agreement with the ϕ^2 law when a nearly pure fundamental spatial mode was present and hence the flux measurements were corrected for decay time changes only. Similar measurements with plain light guides showed that they had a quite negligible effect on the decay constant and hence that only the crystal had any effect.

For the second method of correction preliminary calculations were based on a simple model of flux perturbation suggested by WILLIAMS [10]. In this model, the detector is considered as a concentrated point absorber of certain strength η and represented mathematically by a Dirac delta function. The one-velocity time-dependent diffusion equation with detector then becomes

$$\frac{1}{v}\frac{\partial\phi}{\partial t} = D\nabla^2\phi - \Sigma_a\phi - \eta\delta(r-r_0)\phi + S(r,t), \qquad (4)$$

where η is the strength of the detector absorption located at the general point r_0 and is shown [10] to be given by

$$\eta = \frac{D}{\bar{\phi}} \int_S \nabla\phi \, dS, \tag{5}$$

where $\bar{\phi}$ is the average flux in the detector and D is the diffusion coefficient for the moderator.

A useful practical formula for calculating η for a particular detector is

$$\eta = \frac{DS}{f\lambda}, \tag{6}$$

where S is the surface area of the detector, f is the self-shielding factor, λ is the linear extrapolation length of the flux at the detector surface and D is as above.

Equation (4) was solved numerically with the aid of a computer to give the perturbed flux at a particular time after the end of the pulse and also the perturbation correction to each harmonic of the flux of the equivalent unperturbed system. The initial spatial distribution was calculated from the formula given by BEYSTER in Ref. [3] which is for a system in which the axis of measurement is parallel to the direction of the beam current and where higher spatial modes are therefore emphasized. The perturbed flux was then analysed by the second method described earlier to give the uncorrected extrapolated endpoint. The percentage error to be subtracted from uncorrected Z_0 is shown in Table III for various sizes of a cubic system and for various values of η. For the boron detector used in the flux plots, Eq.(6) (with values of λ and f calculated for a foil in a medium with constant source) gave 0.15 as a value for η.

5. VARIATION OF EXTRAPOLATION DISTANCE WITH BUCKLING

It has been shown theoretically by WILLIAMS [11] that Z_0 is a function of buckling, and the relationship has been derived numerically for various water geometries by GELBARD and DAVIS [1]. A variational method has been used by KLADNIK [12] to calculate Z_0 for various slab thicknesses.

We have assumed the simple relationship

$$Z_0(B^2) = \text{const.} \times \bar{\lambda}_{tr}(B^2) \tag{7}$$

where the transport mean free path is averaged over the asymptotic energy spectrum in a pulsed system of buckling B^2. These spectra have been calculated by WOOD [13] using the diffusion approximation and the Egelstaff effective width kernel for water.

NELKIN [14] has used a variational method to calculate Z_0 for an infinite half-space (Milne problem) and obtained the expression

$$Z_0 = \left[\frac{3}{8}\frac{\bar{\lambda}_{tr}^2}{(\bar{\lambda}_{tr})^2} + \frac{1}{3}\right]\bar{\lambda}_{tr}, \tag{8}$$

TABLE III

PERTURBATION CORRECTIONS IN WATER
(200 μs after end of pulse)

Side (cm)	B^2 (cm^{-2})	η	Percentage error in Z_0
26	0.0417	1.0	3
		0.85	2
		0.62	1.5
		0.55	1
20	0.0695	0.7	38
		0.3	13
		0.1	5
11	0.396	0.5	40
		0.3	25
		0.1	8

Note: Detector used had $\eta \doteqdot 0.15$

where the transport mean free path is averaged over a Maxwellian flux. We have computed the expression inside the square brackets of Eq.(8) for the effective width kernel (reciprocal of effective width = 0.215) and found it to be 0.7378. Hence, for Eq.(7) to have the correct value for an infinite water slab as $B^2 \to 0$, we must use the expression

$$Z_0(B^2) = 0.7378\,\bar{\lambda}_{tr}(B^2) \tag{9}$$

In Fig.4 we compare the results of using Eq.(9), with other theoretical calculations. The values of GELBARD and DAVIS [1], were obtained using the Radkowsky kernel, whereas those of KLADNIK [12] were obtained using the gas kernel, but with values of the parameters ($A = 1.9$ and $\Sigma_s = 2.5\ cm^{-1}$) considered to represent well the thermalizing properties of water. The variation of $Z_0(B^2)/\bar{\lambda}_{tr}(0)$ obtained from Eq.(9) is in good agreement with the calculations of Kladnik; particularly as he also found the value of $Z(0)/\bar{\lambda}_{tr}(0)$ to depend on the kernel used.

If we make the reasonable assumption that the asymptotic flux in a parallelepiped system can be resolved into separable components along the x, y, z axes, and that each face, at the centre, can be considered to approximate to an infinite slab, then our results should be applicable to

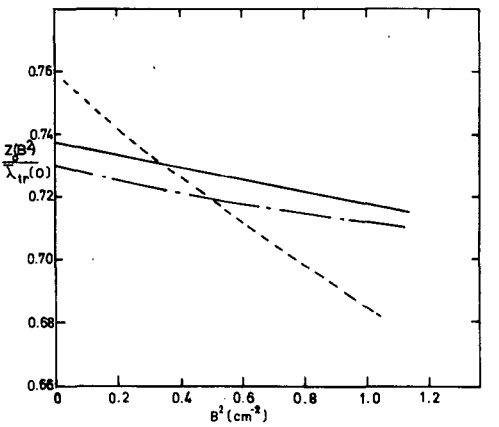

Fig.4

Variation of normalized extrapolated endpoint with buckling in water

---------- GELBARD and DAVIS [1]
———————— Equation (9)
—·—·—·— KLADNIK [12]

parallelepiped systems of equivalent total buckling. Further experiments on moderators of different shapes would be valuable to test this hypothesis.

6. BOUNDARY EFFECTS

A factor which could lead to errors is the distortion of flux near the boundaries of the system and for this reason flux plot analyses excluded points near the boundary. To illustrate the effect of including such points, a flux plot was performed in a 4-in cubic water system in which a large number of points at 1/8-in intervals from the boundary were plotted. This plot was analysed, successively including more of these points, and best-fit values of extrapolated endpoints were plotted against the distance d (measured from the boundary) of the last point included. Figure 5 illustrates how the derived value of extrapolated endpoint varies as the 'boundary region' points acquire greater statistical significance in the analysis. A further contribution to the distortion of the flux as measured near the upper boundary was that at the upper surface of the system the 'boundary' in the immediate neighbourhood of the detector was not cadmium but the perspex light guide. This effect will be checked separately by making measurements in an orthogonal direction.

7. EXTRAPOLATION DISTANCES FROM DIFFUSION COEFFICIENTS AND THE DEPENDENCE ON TEMPERATURE

Extrapolated endpoints can be obtained indirectly from the diffusion coefficient D_0 which, as shown earlier, is given by decay time measurements at different bucklings. D_0 can also be obtained from steady-state

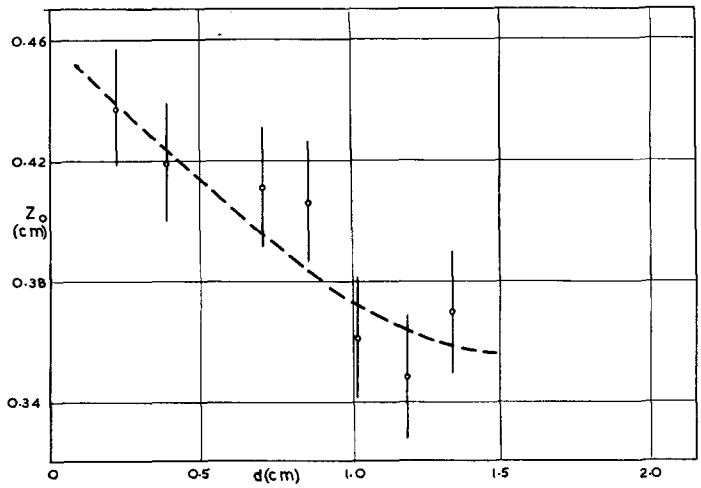

Fig. 5

Boundary effect on extrapolated endpoint for water

diffusion-length measurements with different degrees of poisoning of the moderator.

If $D_0 = 35\,800 \pm 200$ cm^2 s^{-1}, the transport mean-free-path for thermal neutrons in water at 20°C is

$$\bar{\lambda}_{tr} = 0.432 \pm 0.002 \text{ cm}$$

using $\bar{\lambda}_{tr} = 3D_0/\bar{v}$, where $\bar{v}$ is the mean neutron velocity for a Maxwellian distribution at 20°C. Hence, from Fig. 4, $Z_0 = 0.74\,\bar{\lambda}_{tr}$ for a very large system gives $Z_0 = 0.320 \pm 0.002$ cm.

To estimate the dependence of extrapolated endpoint on temperature the following expression is of sufficient accuracy

$$\frac{Z_0(T_2)}{Z_0(T_1)} = \sqrt{\frac{T_1}{T_2}}\,\frac{D_0(T_2)}{D_0(T_1)} \tag{10}$$

where T is in degrees Kelvin.

Table IV shows the expected percentage increase in Z_0 with temperature relative to the value at 25°C, using experimental and theoretical values of $D_0(T)$ for water. The experimental information available is very limited and as mentioned earlier, we have made preliminary measurements of flux distributions up to 80°C as a first step in temperature investigations. As expected the differences in flux plots over this range are very small and, indeed, for the first results the variations in points at each temperature were as large as those between temperatures, and the full analysis for changes in extrapolated endpoints was therefore not worthwhile. Table IV

TABLE IV

PERCENTAGE INCREASE IN EXTRAPOLATED ENDPOINT IN WATER AS TEMPERATURE IS CHANGED FROM 25°C TO T°C

Temp. T (°C)	Experiment [15]	Nelkin kernel [16]	Effective width kernel	Radkowsky kernel [16]
50	4	3	3	5
75	10	7	11	11
100	16	12	11	16
150	32	23	19	29
200	51	33	31	43
250	71	51	45	63
300	94	72	64	90

also draws attention to the need for further experiments on D_0 at high temperatures to test theoretical predictions.

8. SUMMARY OF EXPERIMENTAL RESULTS FOR WATER AND THERMEX AT 20°C WITH DISCUSSION

The extrapolated endpoints obtained from flux plots in 4-in and 7-in cubes of water and thermex (Dowtherm A) are shown in Table V. Thermex is an

TABLE V

EXTRAPOLATED ENDPOINTS AT 20°C

Material	Side of cube (cm)	Buckling (cm^{-2})	Detector	Extrapolated endpoint Z_0 (cm)	Theoretical Z_0 (cm)	
					Equation (9)	GELBARD and DAVIS [1]
Water	10.20	0.25	Boron	0.35 ± 0.02	0.317	0.340[a]
	17.65	0.087	Boron	0.38 ± 0.04	0.319	0.348[a]
Thermex	10.20	0.24	Boron	0.45 ± 0.02		
	17.65	0.085	Boron	0.48 ± 0.03		

[a] *Slab of equivalent total buckling.*

organic moderator of composition 26.5 wt.% diphenyl and 73.5 wt.% diphenyl oxide.

It is clear from the flux plots that the values for water in pulsed experiments are lower than the values reported in earlier work. The early values were too high because of inadequate corrections for detector perturbations, the influence of boundary effects and, in some cases, the black boundary not being immediately adjacent to the moderator.

For large systems pulsed values of extrapolated endpoints could be taken; for example, water (20°C) 0.36 ± 0.03 cm and thermex (20°C) 0.48 ± 0.03 cm. The water value is in good agreement with CARROLL and STOOKSBERRY's [7] steady-state measurement with a mock plane thermal source; their value for a semi-infinite slab of water was 0.35 ± 0.03 cm. Both their values and ours are in reasonable agreement with that from the diffusion coefficient.

Table V shows also that, although the trends are correct, better accuracy is required in the pulsed measurements if satisfactory tests are to be obtained for the various theoretical predictions of the variation of extrapolated endpoint with buckling. This improvement is also required to study effects of temperature.

ACKNOWLEDGEMENTS

This work is part of a programme supported financially by the Department of Scientific and Industrial Research, London. We are grateful for this support and also for that given by the Atomic Energy Establishment, Winfrith.

REFERENCES

[1] GELBARD, E.M. and DAVIS, J.A., Nucl. Sci. Engng 13 (1962) 237.
[2] HALL, R.S., SCOTT, S.A. and WALKER, J., Proc. phys. Soc. 79 (1962) 257.
[3] LOPEZ, W.M. and BEYSTER, J.R., Nucl. Sci. Engng 12 (1962) 190.
[4] BECKURTS, K.H., Proc. Brookhaven Conf., 1962, BNL 719, Vol. III.
[5] CAMPBELL, E.C. and STELSON, P.H., Rpt. ORNL 2204 (1956) 34-36.
[6] DE JUREN, J.A., STOOKSBERRY, R W. and CARROLL, E.E., Proc. Brookhaven Conf., 1962, BNL 719, Vol. III.
[7] CARROLL, E.E. and STOOKSBERRY, R.W., Nucl. Sci. Engng 20 (1964) 455.
[8] BROWN, J.B.C. and HALL, R.S., J. Sci. Instrum. 38 (1961) 381.
[9] DEMING, W.E., in Statistical Adjustment of Data, J. Wiley, Inc., N.Y. (1946).
[10] WILLIAMS, M.M.R., in Physics Department Report, University of Birmingham (1964).
[11] WILLIAMS, M.M.R., J. nucl. Energy 17 (1963) 55.
[12] KLADNIK, R., NIJS Rpt. - R435 (preprint) (1964).
[13] WOOD, J., "Time and space eigenvalues of the Boltzmann equation", these Proceedings I.
[14] NELKIN, M., Nucl. Sci. Engng 7 (1960) 552.
[15] ANTONOV, A.V., GRANATKIN, B.V., MERKULEV, Yu.A. and SMOLIK, Ch.K., Atomnaja Energija 12 1 (1962) 22.
[16] CLENDENIN, W.W., Nucl. Sci. Engng 18 (1964) 351.

THE DIFFUSION PARAMETERS OF HEAVY WATER

J. W. DAUGHTRY* AND A. W. WALTNER
NORTH CAROLINA STATE UNIVERSITY,
RALEIGH, N.C., UNITED STATES OF AMERICA

Abstract — Résumé — Аннотация — Resumen

THE DIFFUSION PARAMETERS OF HEAVY WATER. The diffusion parameters of heavy water have been measured at North Carolina State University over a temperature range of 25-250°C by means of the pulsed source method. A 1-MeV HVEC Van de Graaff, pulsed at the ion source, was used to generate the neutron pulses by means of the Be^9 (d, n) reaction. Neutrons were injected into cylindrical volumes of D_2O, and the decay constants of the neutrons were determined by means of a BF_3 counter located under the D_2O container and oriented along its diameter, operating into a 26-channel time analyser.

The time required to establish the asymptotic spectrum in D_2O was first measured by means of a transmission experiment involving a boron absorber and a LiI (Eu) scintillator. It was observed that a time of 200 μs was sufficient to establish the asymptotic spectrum. The approach to the asymptotic spectrum can be approximated by a time constant of 36 μs.

The diffusion parameters, D_0 and C, were determined by fitting the measured decay constants to the equation $\lambda = \lambda_0 + D_0B^2 - CB^4$. The infinite medium decay constant was calculated from known density and cross-section data. An iterative process was used to make the value of the extrapolation distance compatible with the diffusion coefficient D_0.

The values of D_0 obtained were somewhat lower than those of Baumann, who measured D by a static method utilizing a copper poisoning technique. These values were converted to D_0 by multiplying D by the average temperature of the moderator. The theoretical values of Honeck and Michael, obtained by direct solution of the transport equation, fall between the results of Baumann and those of this experiment.

PARAMÈTRES DE DIFFUSION DE L'EAU LOURDE. Les auteurs ont mesuré les paramètres de diffusion de l'eau lourde à l'Université de l'Etat de Caroline du Nord, pour une gamme de températures allant de 25 à 250°C, par la méthode de la source pulsée. Des deutérons pulsés au moyen d'une machine Van de Graaff HVEC de 1 MeV produisaient les bouffées de neutrons par la réaction $^9Be(d, n)$. Les neutrons étaient injectés dans des volumes cylindriques de D_2O, et les constantes de décroissance des neutrons mesurées à l'aide d'un compteur au BF_3 placé sous le récipient contenant l'eau lourde, orienté dans le sens de son diamètre et fournissant les données à un analyseur en temps à 26 canaux.

Les auteurs ont mesuré tout d'abord le temps nécessaire pour obtenir un spectre asymptotique dans l'eau lourde au moyen d'une expérience de transmission mettant en jeu un absorbeur de bore, un scintillateur de LiI (Eu). Ils ont observé que 200 μs suffisaient pour établir le spectre asymptotique. On peut caractériser approximativement l'approche du spectre asymptotique par une constante de temps égale à 36 μs.

Les auteurs ont déterminé ensuite les paramètres de diffusion D_0 et C en ajustant les constantes de décroissance mesurées à l'équation $\lambda = \lambda_0 + D_0B^2 - CB^4$. La constante de décroissance pour un milieu infini à été calculée pour une densité et une section efficace connues. Par un calcul d'itération, ils ont pu rendre la valeur de la longueur extrapolée compatible avec le coefficient de diffusion D_0.

Les valeurs obtenues pour D_0 étaient légèrement inférieures à celles trouvées par Baumann qui a mesuré D par une méthode statique en utilisant un procédé d'empoisonnement par du cuivre. Ces valeurs étaient converties en D_0 en multipliant D par la température moyenne du ralentisseur. Les valeurs théoriques obtenues par Honeck et Michael qui ont résolu directement l'équation de transport se situent entre les résultats de Baumann et ceux des auteurs.

ДИФФУЗИОННЫЕ ПАРАМЕТРЫ ТЯЖЕЛОЙ ВОДЫ. Методом пульсирующего источника в шт. Северная Каролина измерены диффузионные параметры тяжелой воды в интервале температур 25–250°C. Для получения импульсных нейтронов при помощи реакции Be^9(d, n) был использован ускоритель Ван де Граафа HVEC с энергией 1 Мэв, пульсированный у источника

---

* Present address: Argonne National Laboratory, Argonne, Ill.

ионов. Нейтроны вводили в цилиндрические объемы из D_2O, а постоянные распада нейтронов определяли при помощи счетчика BF_3, помещенного под содержащим D_2O контейнером, расположенным в направлении диаметра и подающим сигналы в 26-канальный анализатор времени.

Время, необходимое для установления асимптотического спектра в D_2O, прежде всего измеряли при помощи эксперимента передачи с использованием поглотителя из бора и сцинтиллятора из LiI(Eu). Опыт показал, что 200 мксек достаточно для установления асимптотического спектра. Приближение к асимптотическому спектру может быть приблизительно выражено константой времени 36 мксек.

Диффузионные параметры D_0 и C определяли путем подстановки измеренных постоянных распада в уравнение: $\lambda = \lambda_0 + D_0B^2 - CB^4$.
Постоянную распада в бесконечной среде рассчитывали на основании известных данных относительно плотности сечения. Использован повторный процесс для того, чтобы сделать величину расстояния экстраполяции совместимой с коэффициентом диффузии D_0.

Полученные значения D_0 оказались несколько ниже величин, найденных Бауманом, который измерял D по статическому методу с использованием способа отравления медью. Эти значения пересчитаны на D_0 путем умножения D на среднюю температуру замедлителя. Теоретические значения, полученные Конеком и Майкелом путем непосредственного решения уравнения переноса, занимают среднее между результатами Баумана и результатами, полученными в настоящем эксперименте.

LOS PARAMETROS DE DIFUSION EN AGUA PESADA. En la Universidad del Estado de Carolina del Norte se han medido los parámetros de difusión en agua pesada, para un intervalo de temperaturas de 25-250° C, empleando el método de los neutrones pulsados. Para generar esos impulsos neutrónicos mediante una reacción ^9Be (d, n), se empleó un acelerador Van de Graaff de 1 MeV construido por la High Voltage Engineering Corporation. Los neutrones se hicieron incidir sobre masas cilíndricas de D_2O y se determinaron las constantes de desintegración de los neutrones mediante un contador de BF_3 situado debajo del recipiente que contenía el D_2O, en sentido transversal, y conectado con un analizador de tiempo de 26 canales.

Primeramente se midió el tiempo necesario para establecer el espectro asintótico del D_2O, mediante un experimento de transmisión en el que se empleó boro como absorbente, así como un centelleador de LiI (Eu). Se comprobó que para establecer dicho espectro bastaban 200 μs. La manera más acertada de obtener un espectro asimétrico es utilizar una constante de tiempo de 36 μs.

Se determinaron los parámetros de difusión D_0 y C ajustando las constantes de desintegración halladas a la ecuación $\lambda = \lambda_0 + D_0B^2 - CB^4$. La constante de desintegración para un medio infinito se calculó partiendo del valor conocido de la densidad y de otros datos relativos a la sección eficaz. Para que el valor de la distancia de extrapolación fuese compatible con el coeficiente de difusión D_0, se siguió un proceso de iteración.

Los valores obtenidos para D_0 fueron algo inferiores a los calculados por Baumann, quien había medido D por un método estático empleando una técnica de envenenamiento con cobre. Estos últimos valores se transformaron en valores de D_0 multiplicando D por la temperatura media del moderador. Los valores téoricos obtenidos directamente de la ecuación de transporte por Honeck y Michael quedan comprendidos entre los resultados de Baumann y los del experimento descrito en la presente memoria.

1. INTRODUCTION

Very little experimental data are available on the neutron diffusion parameters of heavy water at elevated temperatures. CLENDENIN [1] has shown how measurements of the temperature dependence of these parameters may provide a method for discriminating between different theoretical scattering models. The research reported herein consists of an experimental determination of the neutron diffusion parameters in heavy water over a temperature range of 25 to 250°C by the pulsed-source method. A summary of parts of this report was presented at the 1964 meeting of the American Nuclear Society [2].

The method consists essentially of injecting bursts of neutrons into different sizes of heavy water systems and recording the exponential decay

of the neutron counting rate with a thermal neutron detector external to the medium. The exponential decay is caused by leakage and absorption and depends on the size and shape of the system, the temperature and the neutron properties of D_2O. The size and shape of the system can be described by the geometric buckling B^2. The decay constants were obtained for different bucklings and temperatures with a multichannel time analyser. It was assumed that the variation of the decay constant λ with buckling at a given temperature can be expressed by

$$\lambda = \lambda_0 + D_0 B^2 - CB^4. \qquad (1.1)$$

The infinite-medium decay constant λ_0 was calculated at each temperature from known density and cross-section data. The coefficients D_0 and C were obtained at each temperature by fitting the experimental values of λ and B^2 to Eq.(1.1) by the method of least squares.

HONECK and MICHAEL [3] reported values of D_0 and C for heavy water at 20, 77, 127 and 177°C. These results were obtained by solving the Boltzmann equation, using a theoretical scattering model previously proposed by HONECK [4].

One set of experimental data is available for heavy water in this temperature range. This is the work reported by BAUMANN [5], in which measurements were made by a static method utilizing a copper-poisoning technique. Results were obtained at 20, 100, 165 and 220°C.

The only pulsed data available before the research reported in this paper are the measurements by GANGULY et al. [6] in the temperature range of 10 to 50°C.

Tables I and II are a summary of diffusion-parameter measurements for heavy water. The quantity D_0 in Table I is related to the quantity D in Table II by the expression

$$D_0 = D\bar{v}, \qquad (1.2)$$

where both D and D_0 refer to Maxwellian neutron spectra and $\bar{v}$ is the average neutron velocity.

2. EXPERIMENTAL EQUIPMENT

2.1. Van de Graaff

Neutrons were produced for the experiment with a 1-MeV High Voltage Engineering Corporation Van de Graaff, using a deuteron beam on a beryllium target. The Van de Graaff was pulsed at the ion source. For the diffusion-parameter measurements the pulse duration was 250 μs with a repetition rate of about 400 pulses/s. This pulsing mode provided adequate counting rates, as well as sufficient time for the neutrons from one pulse to be dissipated before the next pulse.

TABLE I

NEUTRON DIFFUSION PARAMETERS OF HEAVY WATER BY THE PULSED METHOD

Author	D_2O purity (%)	Temp. (°C)	D_0 (10^5 cm^2/s)	C (10^5 cm^4/s)	100% D_2O		Buckling range (cm^{-2})
					D_0 (10^5 cm^2/s)	C (10^5 cm^4/s)	
SJÖSTRAND [7] (1959)	99.25 99.40	20				3.5 0.8[a]	0.0864 0.0966
STARR and DE VILLIERS [8] (1962)				5[b]			0.0076
WESTFALL and WALTNER [9] (1962)	99.81	29	2.040 ± 0.013	4.19 ± 0.18			0.030-0.090
GANGULY et al. [6] (1963)	99.88	10 20 31 40 50	1.87 ± 0.04 1.95 ± 0.07 2.00 ± 0.09 2.06 ± 0.10 2.13 ± 0.19	2.95 ± 0.35 3.72 ± 0.21 6.66 ± 0.25 7.04 ± 0.26 5.57 ± 0.47	2.00 ± 0.04 2.08 ± 0.05 2.14 ± 0.09 2.21 ± 0.10 2.28 ± 0.19	2.95 ± 0.43 3.72 ± 0.50 6.67 ± 1.44 7.04 ± 1.57 6.57 ± 1.72	0.063-0.100
KUSSMAUL and MEISTER [10] (1963)	99.82	22	2.000 ± 0.009	5.25 ± 0.25			0.0013-0.0470
MALAVIYA and PROFIO [11] (1963)	99.80	21	2.045 ± 0.044	4.706 ± 0.381			0.0160-0.0850
HONECK and MICHAEL [3] (1963)[c]		20 77 127 177			2.057 2.354 2.658 3.011	4.73 5.31 6.05 7.43	

[a] D_0 assumed to be 2.08×10^5 cm^2/s from references [14], [15], and [16].
[b] Obtained from a measurement of the average neutron velocity of one value of B^2.
[c] Theoretical.

TABLE II

NEUTRON DIFFUSION PARAMETERS OF HEAVY WATER BY OTHER THAN THE PULSED METHOD

Author	D_2O purity (%)	Temp. (°C)	D (cm)	λ_{tr} (cm)	100% D_2O			Method
					L (cm)	D (cm)	λ_{tr} (cm)	
SARGENT et al. [12] (1947)					171 ±20			Extrapolated value from diffusion length measurements with boron poisoning
AUGER et al. [13] (1947)	99.4	22		2.31 ± 0.09			2.4 ± 0.1	Measurement of extrapolation distance
DEXTER et al. [14] (1951)		18				0.83 ±0,03 0.84 ±0.03[a]		Diffusion length measurement with boron poisoning
KASH and WOODS [15] (1963)	99.7	24	0.842 ± 0.013[a]	2.49 ± 0.04		0.855 ± 0.013[a]	2.52 ± 0.04	Diffusion length measurement with boron poisoning
RAIEVSKY and HOROWITZ [16] (1954)		13				$D_0 = 2.000 \pm 0.005$ x 10^5 cm²/s	2.45 ± 0.07	Modulated source
BAUMANN [5] (1962)	99.3	20 100 165 220	0.816 ± 0.010 0.823 ± 0.010[a] 0.877 ± 0.011 0.895 ± 0.011[a] 0.963 ± 0.012 0.969 ± 0.012[a] 1.063 ± 0.013 1.070 ± 0.013[a]			0.841 ± 0.010 0.848 ± 0.010[a] 0.912 ± 0.011 0.920 ± 0.011[a] 0.989 ± 0.012 0.995 ± 0.012[a] 1.091 ± 0.013 1.098 ± 0.013[a]		Diffusion length measurement with copper poisoning
LUTZ and MEIER [17] (1962)					136 ± 7			Exponential pile Variable H_2O content

[a] Corrected values computed by Honeck and Michael (1963).

2.2. Pressurized system

Figure 1 is a cross-sectional drawing of the apparatus that was used in this research. For the measurements at temperatures above 100°C a pressurized system was necessary. The inside diameter of the pressure

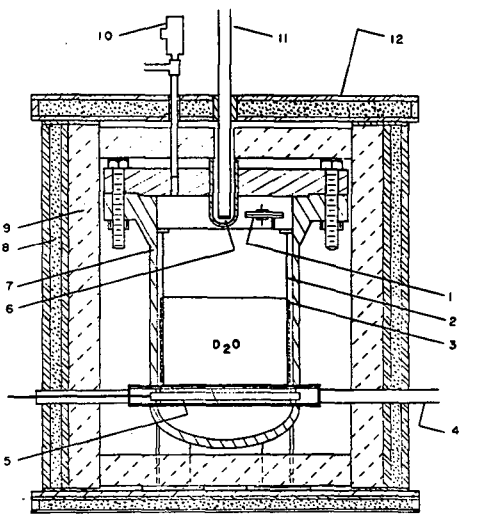

Fig. 1

Simplified cross-section of the experimental system

1. Diaphragm actuator
2. Stainless steel D_2O container
3. Heating tapes
4. Air hose for cooling counter
5. BF_3 proportional counter
6. Be target
7. Pressure vessel
8. Borax
9. Thermal insulation
10. Safety relief valve
11. Van de Graaff drift tube
12. Plywood

vessel was 13 in with a wall thickness of 0.5 in. Basically, it consisted of a 1-ft section of steel pipe with a cap welded to the bottom and a neck flange welded to the top. The vessel lid was a blind flange. A short length of pipe passed through the lid and was capped at the bottom. This served as a re-entry tube for the Van de Graaff target. Another pipe passed through the bottom of the vessel for placement of the neutron detector. The pressure vessel had a working-pressure rating of 820 lb/in^2 at 510°F and 960 lb/in^2 at room temperature.

For all diffusion-parameter measurements the D_2O was in a thin-walled, cylindrical, stainless steel container. The inside diameter of the container was 11.963 (+0.024, -0.043) in. The inside height was 15.188 in. The bottom and sides of the container were 0.078 in thick, and the lid was 0.063 in

thick. The lid was sealed with an o-ring made from a fluorocarbon elastomer compound rated for use to 265°C.

As the heavy water was heated, the pressure increased in the sealed stainless steel container. Since this container was incapable of withstanding the pressures encountered at the higher temperatures, an automatic regulating system was designed to maintain a pressure differential of less than 7 lb/in^2 between the pressure vessel and the heavy water container.

The stainless steel container was lined externally with cadmium except for an opening at the bottom, 1.0 in wide and 11.5 in long, which was aligned with the neutron detector tube to permit the passage of thermal neutrons from the heavy water system to the detector.

As shown in Fig. 1, the entire pressure-vessel system was enclosed in a neutron-shield box consisting of an approximately 1-in thick layer of borax contained between plywood walls.

2.3. Temperature-control system

The heavy water was heated by a set of flexible electric heating tapes. The tapes were 1 in wide, supplied approximately 100 W/ft of length, and were rated for use at temperatures up to 900°F. They were wrapped around the outside of the cadmium-clad stainless-steel container to a height approximately equal to the height of the D_2O inside the container. In cases where the water level was low, additional heat was provided by a 500-W heater element clamped to the bottom of the stainless steel container.

The temperature of the D_2O was measured by a thermocouple assembly mounted on the bottom of the stainless steel container. Additional thermocouples were used to measure the neutron-detector and heating-tape temperatures. The measured temperatures were recorded on a strip-chart recorder. The temperature of the heavy water was controlled by adjusting the voltage supplied to the heating units. In this manner the recorded temperature could be maintained within ±1.5°C of the desired temperature. The thermocouple wires and the power leads for the heating units entered the pressure vessel through high-temperature electrical-lead sealing glands. To minimize heat losses the neutron-shield box was lined with a 3-in thickness of thermal insulation.

2.4. Neutron-detection system

A BF_3 proportional counter with a filling-gas pressure of 167 cm Hg was used. The filling gas was enriched to 96% in the B^{10} isotope. The counter tube had a diameter of 1 in and a sensitive length of 12 in. It was inserted in a holder that provided proper positioning in the pressure-vessel pipe shown in Fig. 1. The counter was wrapped in cadmium except for an opening 1.0 in wide and 11.5 in long that was aligned with the opening in the cadmium lining of the D_2O container. This allowed free passage of neutrons from the D_2O to the neutron detector. The detector was cooled by a flow of room-temperature air. During the experiment the temperature of the neutron counter did not exceed 50°C.

Figure 2 is a schematic diagram of the neutron-counting electronics. The pulse produced by the ion beam is amplified and used to trigger

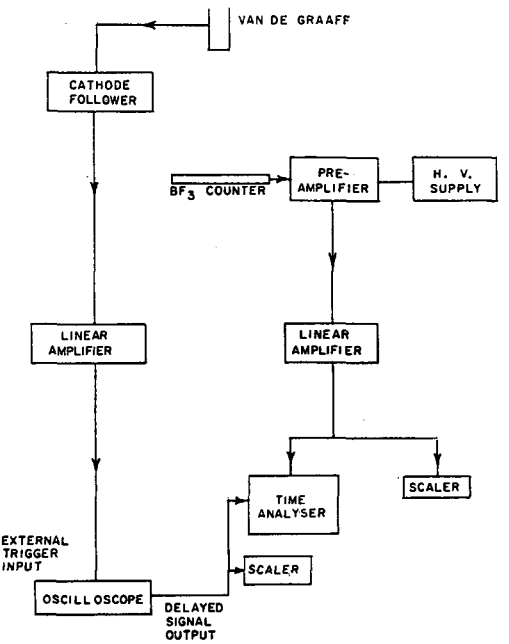

Fig. 2

Block diagram of the system electronics

a Tektronix 535 Oscilloscope, the triggering slope being selected to trigger at the end of the ion pulse. A delayed-trigger pulse is generated by this oscilloscope with a time delay which is variable over a wide range. This delayed-trigger pulse was used to trigger the time analyser. This provided a method for obtaining the desired waiting time after the end of a beam pulse before the initiation of the time analysis.

The 26-channel time analyser had no dead-time between channels and had variable channel width. In this research channel widths of approximately 10 and 20-μs duration were used. The data accumulated by the analyser were recorded on 26 Dekatron scalers. The analyser also incorporated a background channel with a width of approximately 170 μs. This channel recorded the neutron counting rate during the period of time just before a Van de Graaff beam pulse.

The beam pulses and various wave forms of the multichannel analyser were monitored for proper operation on the dual-sweep display of the oscilloscope. The analyser channel width was measured periodically by triggering the analyser and oscilloscope simultaneously with a square-wave generator and feeding the delayed-trigger output of the oscilloscope to the neutron-pulse input of the analyser. By observing the time delay required to record counts in the individual channels, the width of each channel could be measured.

3. EXPERIMENTAL PROCEDURE

3.1. Preliminary measurements

The neutrons produced by a 1-MeV deuteron beam and a beryllium target have energies of several MeV. The slowing-down time to the cadmium cut-off (approximately 0.4 eV) has been found to be about 10 μs in D_2O [18]. Those neutrons that do not leak out of the system and are not absorbed during the slowing-down process asymptotically approach an equilibrium distribution in energy (or velocity) that is approximately Maxwellian. It is important to know the length of time required after the neutron burst before the equilibrium distribution is established (to within the experimental accuracy).

STARR and DE VILLIERS [8] proposed a method of determining the time necessary to establish an equilibrium spectrum in a moderator. The method involves a comparison of the responses of two neutron detectors with sensitivities that differ as a function of the neutron energy. As long as the neutron-energy spectrum is changing the ratio of the counting rates of the two detectors will change. But as the neutron spectrum approaches its equilibrium distribution the ratio approaches a constant value.

This method was used in this experiment to determine the amount of delay that was necessary between the end of the Van de Graaff target pulse and the beginning of the time analyser counting period.

The two neutron detectors used in the ratio measurements were (1) a He^3 proportional counter with a filling-gas pressure of six atmospheres; and (2) a BF_3 proportional counter employing a filling gas enriched in B^{10} to 96% at a pressure of 45 cm Hg. The sensitivity of the BF_3 counter was considerably less than that of the He^3 counter. The ratio of the He^3 to BF_3 counting rates was about seven after the ratio had become constant.

Measurements were made on two D_2O geometries with bucklings of 0.03153 cm^{-2} and 0.05956 cm^{-2}. The D_2O was at room temperature. The Van de Graaff beam pulses were 250 μs long. The results are reproduced in Fig. 3. The ratios appear to reach a constant value about 150 μs after the end of the target pulse. This is in disagreement with the value of 600 μs reported by Starr and de Villiers.

As an additional check another measurement was made using a boron absorber method. Two runs were made in which a LiI(Eu) scintillator was used with the time analyser to observe the neutron decay from a D_2O system. In one run a boron absorber was placed between the crystal and the moderator. The other run was made with no absorber. For thermal neutrons the scintillator efficiency was approximately 96.3 per cent and the absorber transmission was about 28 per cent. The D_2O buckling was 0.038 cm^{-2}. The Van de Graaff beam pulse length was about 15 μs (full width at half maximum). A channel-by-channel ratio was computed for the two runs and these ratios were fitted by the method of least squares to a single exponential plus a constant. The results are shown in Fig. 4. The least-squares curve is within one per cent of the final ratio at 200 μs after the Van de Graaff beam pulse. The time constant of the exponential portion of the curve is 37.68 ± 0.68 μs.

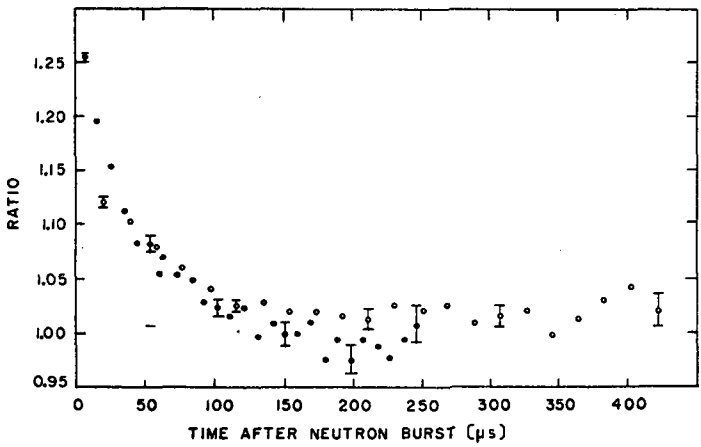

Fig. 3

Time variation of He^3-BF_3 counting ratio

○ $B^2 = 0.03153\ cm^{-2}$
● $B^2 = 0.05956\ cm^{-2}$

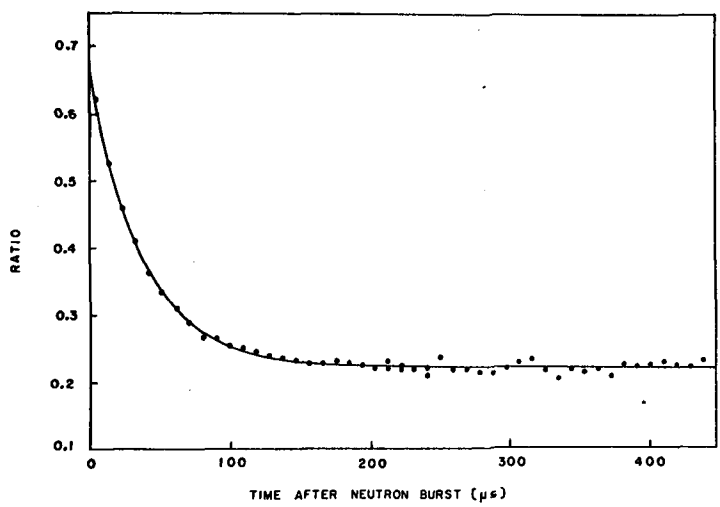

Fig. 4

Time variation of boron transmission

● Experimental points
— Least squares curve

3.2. Pressurized run procedures

The heavy water for this research was supplied by the United States Atomic Energy Commission, Savannah River Operations Office, under the university loan programme. Before initiation of the experimental measure-

ments samples of the D_2O were analysed to determine the purity, which was 99.69± 0.02 mole per cent. Later analyses during the course of the research showed no noticeable deterioration. An argon atmosphere was maintained in the experimental container to prevent degradation of the D_2O purity resulting from the presence of water vapour.

Measurements were made at temperatures from 25 to 250°C in 25°-increments. A minimum of two time-analyser runs was made at each temperature. The buckling was computed from the dimensions of the container, the weight of water in the container and the density of the water at the given temperature. It was also necessary to calculate the amount of D_2O in the vapour phase at each temperature.

4. ANALYSIS OF DATA

4.1. Decay constant evaluation

The number of counts recorded in each channel of the time analyser was corrected for dead-time losses and background. A weighted least-squares analysis of the corrected data was used to obtain the value of the decay constant and its standard error. These operations were all performed by a digital computer. An additional feature incorporated in the computer code was a channel-dropping option. After the decay constant was computed from the given data the first channel was dropped and a second decay constant was computed. Then the first two channels were dropped and another decay constant was computed and so on. The number of channels to be dropped was specified with the data input.

This technique was useful for detecting situations in which the neutron density was not in a pure exponential decay. For the data taken at the lowest buckling values the water level was near the top of the container. In these runs the higher spatial harmonics persisted for several hundred microseconds. This was detected by the channel-dropping method and delays up to 500 μs were used to obtain the fundamental mode decay.

4.2. Diffusion parameter evaluation

As mentioned in section 1 the infinite medium decay constant λ_0 was calculated for each temperature from known density and cross-section data. In computing λ_0 it was assumed that the absorption cross-sections are proportional to $1/v$ so that the variation of λ_0 with temperature is due only to the change in density. The calculated values of λ_0 are listed in Table III along with the densities of liquid D_2O and of saturated D_2O vapour.

Corrections were applied for neutron backscattering from the container walls. This correction was based on the thin shell reflector model frequently used in calculating reflector savings. The container is considered equivalent to an added amount of moderator weighted on the basis of the diffusion coefficients of the two media according to the relation

$$R' = R + \left(d + \frac{D_1}{D_2} T\right), \qquad (4.1)$$

where

R' = corrected radius
R = moderator radius
d = 0.7104 d_{tr}
D_1 = diffusion coefficient of moderator
D_2 = diffusion coefficient of container material
T = thickness of wall

R' was computed for all temperatures and similar corrections were made for the axial dimension, neglecting, however, from solid angle considerations, backscattering from the top of the vessel.

TABLE III

DENSITIES OF LIQUID HEAVY WATER AND SATURATED HEAVY WATER VAPOUR AND CALCULATED VALUES OF THE INFINITE MEDIUM DECAY CONSTANT

Temp. (°C)	Density of liquid D_2O (g/cm^3)	Density of saturated D_2O vapour (g/cm^3)	Infinite medium decay constant λ_0 (s^{-1})
25	1.10437	0.00003	21.7
50	1.09562	0.00009	21.5
75	1.08148	0.00029	21.2
100	1.06339	0.00059	20.8
125	1.04125	0.0014	20.4
150	1.0167	0.0028	19.9
175	0.9888	0.0051	19.4
200	0.9570	0.0087	18.8
225	0.9205	0.0142	18.0
250	0.881	0.022	17.3

The coefficients D_0 and C and their standard errors were obtained for each temperature by a least-squares analysis. These calculations were performed by computer using as input the experimental decay constants, the corrected dimensions of the D_2O geometries, and the calculated values of λ_0. An iterative procedure was necessary to make the value of D_0 used in the expression for the extrapolation distance ($d = 2.1312\ D_0/\bar{v}$) consistent with the results of the least-squares fit.

5. RESULTS AND DISCUSSION

5.1. Decay constants and diffusion parameters

The decay constants and the depth of D_2O in the container used in the least-squares analysis to obtain the parameters D_0 and C are tabulated in the Appendix. Also included in this tabulation are the iterated buckling

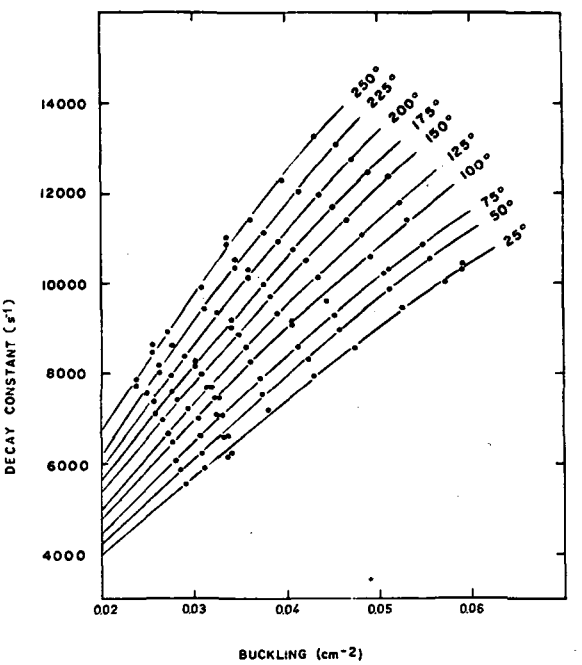

Fig. 5

Variation of λ with B^2

● Experimental points
— Least squares curves

values and estimates of the standard errors of the decay constants. Figure 5 shows the variation of λ with B for all ten temperatures. The curves are the results of the least-squares analyses of the experimental points.

The results obtained for D_0 and C are presented in Table IV. Values of D_0 for pure D_2O were obtained by correcting the measured values of D_0 for the H_2O content with the relationship

$$\frac{1}{D_0\,(\text{measured})} = \frac{1-f}{D_0\,(D_2O)} + \frac{f}{D_0\,(H_2O)} \qquad (5.1)$$

where f is the mole fraction of H_2O. The values of D_0 for H_2O were obtained from data published by ANTONOV et al. [19]. A comparison with

TABLE IV

EXPERIMENTAL VALUES OF D_0 AND C FOR 99.69 MOLE PER CENT HEAVY WATER

Temp. (°C)	D_0 (10^5 cm²/s)	C (10^5 cm⁴/s)
25	1.955 ± 0.027	4.65 ± 0.54
50	2.158 ± 0.033	6.39 ± 0.74
75	2.299 ± 0.038	7.08 ± 0.85
100	2.440 ± 0.043	7.47 ± 1.02
125	2.550 ± 0.048	7.43 ± 1.16
150	2.682 ± 0.054	7.69 ± 1.32
175	2.870 ± 0.061	8.83 ± 1.53
200	3.020 ± 0.068	9.26 ± 1.76
225	3.212 ± 0.076	10.16 ± 2.05
250	3.481 ± 0.086	12.41 ± 2.42

the results reported by GANGULY et al. [6] revealed what appeared to be an over-correction of their data for the effect of the light-water contamination. This correction was recalculated and the results are presented in Table V. Table VI contains values of D_0, λ_{tr}, and σ_{tr} for pure D_2O from the present research. The values of the transport mean free path λ_{tr}, obtained from the relationship

$$\lambda_{tr} = \frac{3D_0}{\bar{v}} , \tag{5.2}$$

and the microscopic transport cross-sections σ_{tr} were obtained from the expression

$$\lambda_{tr} = \frac{1}{\Sigma_{tr}} = \frac{1}{N\sigma_{tr}} , \tag{5.3}$$

where N is the number of D_2O molecules per cubic centimetre at each temperature. The significance of σ_{tr} in this case lies in the fact that it is not an explicit function of the average neutron velocity or the D_2O density as is the quantity D_0. The fractional errors in λ_{tr} and σ_{tr} should be about the same as that of D_0.

For comparison, the values of D_0 obtained for pure D_2O are plotted in Fig. 6 along with BAUMANN's [5] experimental values and HONECK and MICHAEL's [3] theoretical values. Also included are the experimental values of D_0 by Ganguly et al. from Table V. Although the agreement between the values reported for D_0 in this experiment and those reported by Ganguly et al. as corrected in this paper is quite good, the uncertainties reported in the earlier experiment are large.

TABLE V

VALUES OF D_0 FOR PURE D_2O OBTAINED FROM THE RESULTS OF GANGULY et al. [6] BY A RECALCULATION OF THE H_2O CORRECTION

Temp. (°C)	D_0 (10^5 cm²/s)
10	1.88 ± 0.04
20	1.96 ± 0.07
31	2.01 ± 0.09
40	2.07 ± 0.10
50	2.14 ± 0.19

TABLE VI

VALUES OF D_0, λ_{tr} AND σ_{tr} FOR PURE HEAVY WATER

Temp. (°C)	D_0 (10^5 cm²/s)	λ_{tr} (cm)	σ_{tr} (b)
25	1.983 ± 0.029	2.378	12.66
50	2.189 ± 0.035	2.521	12.04
75	2.331 ± 0.040	2.587	11.88
100	2.473 ± 0.045	2.651	11.79
125	2.582 ± 0.050	2.679	11.92
150	2.714 ± 0.056	2.732	11.97
175	2.903 ± 0.063	2.839	11.84
200	3.053 ± 0.070	2.906	11.95
225	3.246 ± 0.078	3.011	12.00
250	3.517 ± 0.088	3.184	11.85

The values of D reported by Baumann have been converted to values of D_0 by multiplying by the average neutron velocity $\bar{v}$. The values of D_0 reported in this paper are lower at all temperatures than Baumann's results and the difference increases with increasing temperature. The theoretical values of D_0 by Honeck and Michael lie within the experimental uncertainties reported here. Until more accurate experimental data become available, one can assume that the present Honeck scattering model is adequate for calculations of the diffusion coefficient of heavy water.

The major uncertainty remaining in the pulsed measurements appears to be in the definition of the extrapolation distance. It does, however, ap-

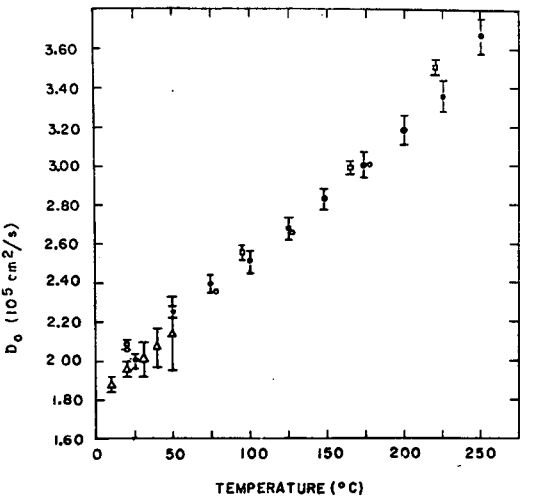

Fig. 6

Temperature dependence of D_0 for pure D_2O

○ Honeck and Michael △ Ganguly et al.
● This experiment □ Baumann

pear unlikely that the error in the extrapolation distance could be large enough to account for the difference between the two sets of experimental data. Corrections have been made on Baumann's results by Honeck and Michael as indicated in Table II; however, these corrections were small and actually increased the disagreement between Baumann's results and the results of the previous experiment.

Figure 7 shows the temperature dependence of σ_{tr}. The results from this experiment are essentially constant over the temperature range from 50 to 250°C. The sharp rise at 25°C has not been explained.

The values of C obtained in this research are the only experimental values reported to date for high-purity D_2O above 25°C. The method by which C may be corrected for the light-water contamination is not clear. The uncorrected values are plotted in Fig. 8 with the theoretical values of C for pure D_2O as calculated by Honeck and Michael. Since C for H_2O is much smaller than C for D_2O, the correction for H_2O is much smaller than for D_2O; the correction for H_2O contamination would tend to raise the experimental values, making the agreement between the theoretical and experimental results even poorer. The errors listed in Table IV were obtained from estimates of the uncertainties in the decay constants, the bucklings, the temperatures, and the values of λ_0.

Estimates of the standard errors of the decay constants are included with the tabulation of data in the Appendix. These errors include contributions from the following sources:

(a) Time analyser distortion,
(b) Neutron return from pressure vessel and insulation,
(c) Backscattering from stainless steel walls and
(d) Backscattering from D_2O vapour at higher temperatures.

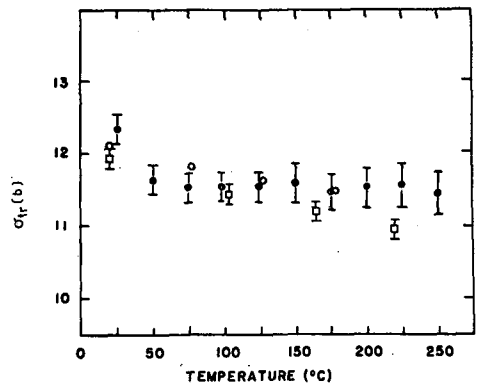

Fig. 7

Temperature dependence of σ_{tr} for pure D_2O

○ Honeck and Michael
● This experiment
□ Baumann

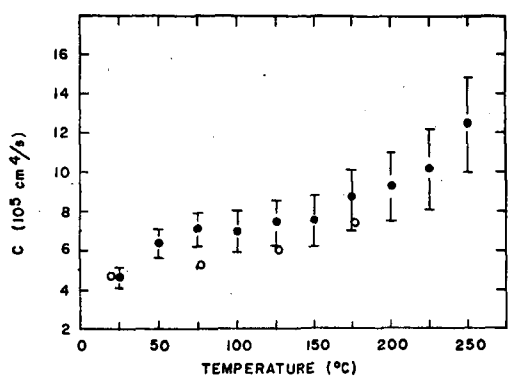

Fig. 8

Temperature dependence of C

○ Honeck and Michael (100%D_2O)
● This experiment (99.69% D_2O)

Separate measurements were made to determine the magnitude of each of the above effects and corrections to the data were made where necessary. In particular, small corrections were found necessary for a, c and d.

Uncertainties in the following quantities contributed to the errors estimated for the geometric buckling values:

(a) Density of the D_2O,
(b) Dimensions of the experimental container,
(c) Extrapolation distance and
(d) Quantity of D_2O in the container.

Errors in the D_2O density were negligible below 125°C. From 125 to 175°C the error was 0.25% and from 200°C through 250°C the error was 0.6% [20]. Expansion of the container with temperature caused an estimated increase in the linear dimensions of about 0.2% in going from 25 to 250°C.

The error in the extrapolation distance d, as defined by

$$d = 0.7104\,\lambda_{tr} = 2.1312\,D_0/\overline{v}, \tag{5.4}$$

is proportional to the error in D_0. The resulting errors in B^2 caused by errors in d were significant only for large buckling values at high temperatures.

The combined error in B^2 from the above sources was found to be negligible below 150°C, but added a small contribution to the errors in D_0 and C at the higher temperatures.

The error in the temperature was estimated to be ± 2°C at room temperature, increasing to ± 5°C at 250°C. This included constant errors of 1.1°C in the thermocouple accuracy and 1.5°C in maintaining the desired millivolt indications on the temperature recorder. The remainder of the error was caused by the temperature gradient within the D_2O.

Although the uncertainties of the λ_0 values were rather large, they did not contribute significantly to the errors in D_0 and C. The error in λ_0 was about 10% and resulted mainly from the uncertainty in the D_2O absorption cross-section. This error in λ_0 produced an error in D_0 of less than 0.1%.

Recent theoretical studies by GELBARD et al. [21], KLADNIK [22], and WILLIAMS [23] indicate that Eq.(5.4) may not be an adequate definition of the extrapolation distance d. These studies suggest that the proper expression should be a function of the buckling or the molecular mass of the moderator, or both. In the absence of a generally accepted expression that includes these factors, Eq.(5.4) has been used. The experimental dimensions and decay constants have been listed in the Appendix so that the data may be re-analysed at some later date if a more accurate definition of d, or a more suitable method of analysis becomes available.

ACKNOWLEDGEMENT

We wish to thank the United States Atomic Energy Commission for the loan of the D_2O under the university loan programme and for the partial support of this work under contract AT(30-1)-267.

APPENDIX

TABULATION OF DECAY CONSTANTS

T (°C)	B^2 (m^{-2})	H (cm)	λ (s^{-1})	T (°C)	B^2 (m^{-2})	H (cm)	λ (s^{-1})
25	291.1	28.15	5476 ± 34	75	283.2	28.69	6067 ± 79
	291.1	28.15	5491 ± 69		283.2	28.69	6092 ± 79
	314.3	24.94	5843 ± 71		304.4	25.46	6564 ± 85
	314.3	24.94	5878 ± 74		304.4	25.46	6628 ± 87
	337.5	22.51	6290 ± 77		326.2	22.98	7002 ± 93
	337.5	22.51	6292 ± 78		326.2	22.98	7027 ± 93
	338.9	22.38	6269 ± 78		327.5	22.85	7058 ± 95
	338.9	22.38	6342 ± 79		327.5	22.85	7075 ± 96
	385.6	18.97	7203 ± 98		371.1	19.37	7887 ± 104
	385.6	18.97	7212 ± 95		371.1	19.37	7946 ± 106
	430.8	16.68	7936 ± 106		413.2	17.03	8619 ± 121
	430.8	16.68	7963 ± 112		413.2	17.03	8665 ± 123
	474.5	15.02	8594 ± 97[a]		453.9	15.33	9255 ± 120[a]
	528.4	13.44	9454 ± 96[a]		504.1	13.71	10239 ± 121[a]
	576.6	12.32	10190 ± 86[a]		515.3	13.40	10375 ± 125
	593.3	11.98	10314 ± 134		548.5	12.57	10880 ± 118[a]
	593.3	11.98	10412 ± 62	100	279.0	29.17	6407 ± 81
50	286.9	28.32	5870 ± 76		279.0	29.17	6425 ± 83
	308.7	25.14	6267 ± 79		305.2	25.14	6852 ± 89
	308.7	25.14	6239 ± 85		305.2	25.14	6883 ± 90
	331.1	22.69	6670 ± 87		320.5	23.37	7326 ± 97
	331.1	22.69	6709 ± 93		321.7	23.24	7329 ± 96
	332.5	22.56	6700 ± 93		321.7	23.24	7361 ± 98
	332.5	22.56	6721 ± 94		363.8	19.70	8247 ± 110
	377.5	19.12	7530 ± 100		363.8	19.70	8269 ± 112
	377.5	19.12	7596 ± 99		364.2	19.67	8205 ± 107
	421.1	16.81	8303 ± 121		364.2	19.67	8242 ± 114
	421.1	16.81	8345 ± 114		404.6	17.31	8996 ± 125
	463.1	15.13	8952 ± 117[a]		404.6	17.31	9098 ± 127
	514.7	13.54	9837 ± 117[a]		443.9	15.58	9694 ± 125[a]
	560.7	12.41	10460 ± 114[a]		492.1	13.94	10592 ± 123[a]

[a] The decay constant listed is an average of two or three values with somewhat larger errors.

APPENDIX (cont.)

T (°C)	B^2 (m^{-2})	H (cm)	λ (s^{-1})	T (°C)	B^2 (m^{-2})	H (cm)	λ (s^{-1})
100	534.9	12.79	11340 ± 121[a]	175	281.3	27.80	7605 ± 97
125	274.7	29.79	6655 ± 85		281.3	27.80	7641 ± 99
	274.7	29.79	6684 ± 86		300.7	24.93	8120 ± 107
	294.4	26.43	7106 ± 94		300.7	24.93	8205 ± 110
	294.4	26.43	7116 ± 93		337.9	21.07	9079 ± 123
	314.7	23.85	7598 ± 101		337.9	21.07	9142 ± 125
	314.7	23.85	7624 ± 103		373.3	18.53	9903 ± 135
	317.0	23.59	7606 ± 116		373.3	18.53	9967 ± 136
	317.0	23.59	7631 ± 116		408.0	16.88	10737 ± 116[a]
	356.8	20.07	8496 ± 121		450.6	14.88	11509 ± 133[a]
	356.8	20.07	8516 ± 123		490.8	13.56	12461 ± 133[a]
	395.6	17.67	9326 ± 130	200	257.3	32.37	7381 ± 91
	395.6	17.67	9370 ± 132		257.3	32.37	7410 ± 96
	433.6	15.90	10054 ± 122[a]		274.4	28.66	7858 ± 101
	480.2	14.22	10949 ± 127[a]		274.4	28.66	7899 ± 99
	521.8	13.03	11750 ± 126[a]		292.6	25.71	8398 ± 110
150	269.8	30.50	6868 ± 88		292.6	25.71	8408 ± 106
	269.8	30.50	6869 ± 87		327.9	21.71	9320 ± 124
	288.6	27.06	7362 ± 96		327.9	21.71	9333 ± 124
	288.6	27.06	7383 ± 98		361.7	19.07	10160 ± 137
	308.1	24.41	7905 ± 105		361.7	19.07	10256 ± 141
	309.2	24.27	7841 ± 104		394.7	17.13	10982 ± 110[a]
	309.2	24.27	7872 ± 105		435.4	15.29	11850 ± 137[a]
	348.4	20.53	8792 ± 121		473.6	13.93	12711 ± 131[a]
	348.4	20.53	8793 ± 120	225	250.3	33.63	7655 ± 100
	385.7	18.07	9675 ± 133		250.3	33.63	7680 ± 99
	385.7	18.07	9685 ± 134		266.4	29.72	8083 ± 102
	422.3	16.25	10369 ± 117[a]		266.4	29.72	8138 ± 104
	467.1	14.53	11230 ± 132[a]		283.3	26.67	8640 ± 109
	507.1	13.31	12114 ± 130[a]		283.3	26.67	8655 ± 110
175	263.4	31.34	7177 ± 91		316.6	22.48	9596 ± 127
	263.4	31.34	7200 ± 93		316.6	22.48	9596 ± 126

[a] The decay constant listed is an average of two or three values with somewhat larger errors.

APPENDIX (cont.)

T (°C)	B^2 (m^{-2})	H (cm)	λ (s^{-1})	T (°C)	B^2 (m^{-2})	H (cm)	λ (s^{-1})
225	348.4	19.72	10481 ± 139	250	272.1	27.79	8926 ± 115
	348.4	19.72	10511 ± 141		272.1	27.79	8937 ± 115
	379.7	17.69	11246 ± 112[a]		303.0	23.37	9910 ± 137
	418.3	15.77	12075 ± 139[a]		303.0	23.37	9928 ± 131
	455.5	14.32	13043 ± 137[a]		332.7	20.46	10733 ± 145
250	241.6	35.13	7883 ± 101		332.7	20.46	10820 ± 149
	241.6	35.13	7991 ± 106		362.0	18.32	11421 ± 109[a]
	256.6	30.98	8383 ± 110		398.3	16.29	12360 ± 140[a]
	256.6	30.98	8457 ± 111		434.5	14.72	13300 ± 142[a]

[a] The decay constant listed is an average of two or three values with somewhat larger errors.

REFERENCES

[1] CLENDENIN, W.W., Nucl. Sci. Engng 18 (1964) 351-62.
[2] DAUGHTRY, J.W. and WALTNER, A.W., Trans. Amer. nucl. Soc. 7 (1964) 231-33.
[3] HONECK, H.C. and MICHAEL, P., Nucl. Sci. Engng 16 (1963) 140-42.
[4] HONECK, H.C., Trans. Amer. nucl. Soc. 5 (1962) 47-48.
[5] BAUMANN, N.P., Nucl. Sci. Engng 14 (1962) 179-85.
[6] GANGULY, N.K., COBB, F.C. and WALTNER, A.W., Nucl. Sci. Engng 17 (1963) 223-26.
[7] SJÖSTRAND, N.G., Ark. Fys. 15 (1959) 145-46.
[8] STARR, E. and DE VILLIERS, J.W.L., Rpt. BNL 5987 (1962).
[9] WESTFALL, F.R. and WALTNER, A.W., Trans. Amer. nucl. Soc. 5 (1962) 386.
[10] KUSSMAUL, G. and MEISTER, H., Reactor Sci. Tech. (J. nucl. Energy, Parts A/B) 17 (1963) 411-15.
[11] MALAVIYA, B.K. and PROFIO, A.E., Trans. Amer. nucl. Soc. 6 (1963) 58-59.
[12] SARGENT, B.W., BOOKER, D.V., CAVANNAGH, P.E., HEREWARD, H.G. and NIEMI, N.J., Canad. J. Res. 25A (1947) 134-42.
[13] AUGER, P., MUNN, A.M. and PONTECORUO, B., Canad. J. Res. 25A (1947) 143-56.
[14] DEXTER, A.H., HAMMERMESH, B., HONES, E.W., MORRIS, P.A. and RINGO, G.R., Rpt. ANL 4746 (1951) 14-16.
[15] KASH, S.W. and WOODS, D.C., Phys. Rev. 90 (1953) 564-66.
[16] RAIEVSKY, V. and HOROWITZ, J., C.R. Acad. Sci., Paris 238 (1954) 1993-95.
[17] LUTZ, H.R. and MEIER, R.W., Nukleonik 4 (1962) 108-10.
[18] PROFIO, A.E. and ECKARD, J.E., Nucl. Sci. Engng 19 (1964) 321-28.
[19] ANTONOV, A.V., GRANATKIN, B.V., MERKUL'EV, Yu.A. and SMOLIK, Ch.K., Soviet J. atomic Energy 12 (1962) 17-25.
[20] HEIKS, J.R., BARNETT, M.K., JONES, L.V. and ORBAN, E., J. phys. Chem. 58 (1954) 488-91.
[21] GELBARD, E.M., DAVIS, J.A. and SCHMIDT, E., Proc. Brookhaven Conf. on Neutron Thermalization, BNL 719 4 (1962) 1175-85.
[22] KLADNIK, R., Proc. Brookhaven Conf. on Neutron Thermalization, BNL 719 4 (1962) 1211-31.
[23] WILLIAMS, M.M.R., Nucl. Sci. Engng 18 (1964) 260-70.

DISCUSSION

(on the foregoing three papers)

W. REICHARDT: I would like to make a comment in connection with the temperature dependence of the diffusion parameters given in the abstract of Dr. Silver's paper (SM-62/72). When the moderator temperature approaches absolute zero, the diffusion coefficient must obviously go to zero. If a value of -273°C is inserted into the expression obtained by Dr. Silver for the temperature dependence of the diffusion coefficient of ice, the expression does in fact almost yield zero, although the extrapolation is very large. This suggests that the diffusion coefficient may be proportional to the absolute temperature within the whole temperature range from absolute zero up to 273°K. The same may be true for the diffusion cooling coefficient.

We have measured the lifetime in a single ice block at various temperatures from 20°K to the melting point of ice. The λ-values we obtained can be well fitted by an expression $\lambda = A + BT$, where A and B are constants. This means that the absorption cross-section of H_2O follows the $1/v$ law down to very small energies and that the leakage term, that is DB^2 plus higher-order terms, is proportional to the absolute temperature.

E. SILVER: It is quite true that the results of my measurements are fully consistent with a proportionality of D_0 with absolute temperature. The range of temperature covered by these measurements is, however, too small to enable such a conclusion to be drawn solely on the basis of my results. On the other hand, I am not surprised that the measurements you describe support such a conclusion, and it is very gratifying to have this information.

S. SCOTT: I was interested in the technique employed by Dr. Waltner (paper SM-62/62) for analysing higher-harmonic components. He appears to use a channel-cutting method instead of the more usual technique of a least-squares fit to several harmonics. Could he perhaps comment on this?

A. WALTNER: The decay constants are determined in the following manner. The complete set of channel counts is first corrected for dead time and background. These data are then fitted to a single exponential by a weighted least-squares computer programme. The procedure is repeated, the early time channels (the first one, then the first two, then the first three, etc.) being dropped to any channel number specified in the programme. From the plot of the decay constant against the number of channels dropped we can readily ascertain the presence of higher-order harmonics and introduce additional delay if needed.

L.G. KEMENY: Could Dr. Wood comment on the relative importance of energy-dependent and transport effects in his measurements of the extrapolation lengths in the geometries of these experiments (SM-62/42)?

J. WOOD: We have not been able to achieve a sufficient degree of accuracy with our measurements to enable us to distinguish between the theoretical methods referred to in the paper. Equation (9) and the results of Kladnik appear to be in good agreement, and this suggests that the variation with B^2 of the transport effect on Z_0 is less important than energy-dependent effects. The advantage of Eq. (9) is that it might be applicable to real systems.

A. HENRY: I may mention that Gelbard and Schmidt have extended their calculations to spheres and to the use of the Nelkin kernel. They find that the extrapolation distance is about 0.32 cm for water and is rather insensitive to buckling and to the many theoretical corrections made. Their conclusion is that a significantly different kernel would have to be used if calculated values were to be found as high as 0.40 cm. Your lower results help therefore to lessen a serious discrepancy.

M. NELKIN: I have a question on Mr. Silver's paper (SM-62/72). How large is the effect of making corrections to the extrapolation distance on the diffusion parameters D_0 and C in H_2O?

E. SILVER: I used the Gelbard-Davis result separately for the cylindrical and plane surfaces and found that the effect of applying the correction was insignificant for D_0 and about 20% (±10%) in the case of C. This is based on direct calculations with and without the correction. For the correction used I would refer you to Fig. 5 of the paper.

K.H. BECKURTS: I would like to point out that the generalized α versus B^2 curve of H_2O shown in my paper (SM-62/1) gives parameters, especially a diffusion cooling coefficient, which do not change very much if different methods are used to calculate B^2. In particular, the buckling region above 0.5 cm^{-2} can be dropped. This is possible, of course, because the stationary poisoning experiments have an extremely high weight in the evaluation.

ÉTUDE DU GRAPHITE ET DE L'OXYDE DE BÉRYLLIUM PAR LA MÉTHODE DE LA SOURCE PULSÉE DE NEUTRONS

G. CUNY, V. DENIZ, J. LALANDE, J. G. LE HO ET M. SAGOT
CENTRE D'ÉTUDES NUCLÉAIRES DE CADARACHE, FRANCE

Abstract — Résumé — Аннотация — Resumen

STUDY OF GRAPHITE AND BERYLLIUM OXIDE USING THE PULSED NEUTRON SOURCE METHOD. This paper contains diffusion parameter values (λ_t, C, F) for graphite, obtained from measurements made in the buckling range of 5.6 to 190 m^{-2} and supplemented by determination of anisotropy. It also takes into account the results of a systematic study (based on out-put current measurements) of the spectral stabilization of a neutron burst in relation to the stack dimensions and, for large stacks, in relation to the position of the point of measurement. The value of the transport mean free path for beryllium oxide is also given.

ÉTUDE DU GRAPHITE ET DE L'OXYDE DE BÉRYLLIUM PAR LA MÉTHODE DE LA SOURCE PULSÉE DE NEUTRONS. Les auteurs présentent les valeurs des paramètres de diffusion (λ_t, C, F) obtenues sur le graphite à la suite de mesures effectuées dans la gamme de laplaciens de 5, 6 à 190m^{-2} et complétées par la détermination de l'anisotropie. Ils rendent également compte de l'étude systématique, fondée sur la mesure du courant sortant, de la mise à l'équilibre spectral d'une bouffée de neutrons en fonction des dimensions des empilements et, pour les grands empilements, en fonction de la position du point de mesure. Ils donnent également la valeur du libre parcours moyen de transport obtenue sur l'oxyde de béryllium.

ИЗУЧЕНИЕ ГРАФИТА И ОКИСИ БЕРИЛЛИЯ МЕТОДОМ ИМПУЛЬСНОГО НЕЙТРОННОГО ИСТОЧНИКА. Приводятся значения параметров диффузии (λ_t, C, F), полученные на графите в результате измерений, проведенных в диапазоне лапласианов от 5,6 до 190 m^{-2} и дополненных определением анизотропии. Уделяется также внимание систематическому изучению (основанному на измерении потока) и приведению в спектральное равновесие нейтронного импульса в зависимости от размеров загрузки реактора, а в отношении больших загрузок — в зависимости от положения точки измерения. Приводится также значение среднего свободного транспортного пробега, полученного для окиси бериллия.

ESTUDIO DEL GRAFITO Y DEL OXIDO DE BERILIO MEDIANTE EL METODO DE LA FUENTE DE NEUTRONES PULSADOS. Los autores presentan los valores de los parámetros de difusión (λ_t, C, F) obtenidos para el grafito como résultado de mediciones efectuadas en el intervalo de laplacianos de 5, 6 a 190 m^{-2}, completadas con una determinación de la anisotropía. También dan cuenta del estudio sistemático, basado en la medición de un flujo de salida, del equilibrio espectral de una ráfaga de neutrones en función de las dimensiones de los impulsos acumulados y, en el caso de grandes acumulaciones, en función de la posición del punto de medida. También indican el valor del libre recorrido medio de transporte obtenido para el óxido de berilio.

1. INTRODUCTION

Un examen des résultats obtenus par différentes équipes montre qu'il subsiste un certain désaccord sur les valeurs des paramètres, en particulier sur la valeur de C et sur la possibilité de déceler un terme en B^6. Le désaccord peut provenir de trois sources:

a) les valeurs expérimentales, par exemple la présence des erreurs systématiques dans la détermination de la constante de décroissance provenant de présence d'harmoniques, des neutrons réfléchis, etc,

b) la méthode de dépouillement,

c) la difficulté d'obtenir les valeurs vraies des paramètres, à partir des valeurs expérimentales données, suivant la mise en œuvre de la méthode de dépouillement.

Dans le but d'éclaircir cette question, nous avons entrepris une campagne de mesures sur le graphite quasi-homogène en cherchant à éliminer au mieux les sources possibles d'erreur. Nous avons analysé d'une manière détaillée les courbes de décroissance pour vérifier que la décroissance asymptotique était bien atteinte. Nous avons enfin analysé la courbe de la constante de décroissance en fonction du laplacien pour déterminer l'incertitude inhérente dans la détermination des paramètres.

2. DISPOSITIF EXPÉRIMENTAL

2.1. La cellule

La cellule dans laquelle les expériences ont été faites a comme dimensions 8 m × 5,5 m, et 5 m de hauteur. Les empilements étaient construits sur un marbre de dimensions 2,40 m × 2,40 m recouvert d'une feuille de cadmium de 0,8 mm d'épaisseur, ce marbre étant à 1,50 m du sol. La cellule est climatisée à 20°C ± 2°C; le graphite n'est pas stocké dans cette cellule.

Pour blinder les empilements, une cage de cadmium d'une épaisseur de 0,8 mm est construite; la partie supérieure de la cage est fixe, tandis que les côtés latéraux sont composés de panneaux coulissants pour permettre un accès facile aux empilements. Des couvre-joints en cadmium éliminent tout effet de fente.

2.2. Source de neutrons

Le générateur de neutrons est un accélérateur électrostatique SAMES de 150 kV fournissant des neutrons de la réaction D-T. La pulsation est obtenue en pulsant l'oscillateur qui ionise le deutérium.

Pour éviter au maximum la perturbation créée par les neutrons réfléchis par les murs de la cellule, on a blindé la cible sur tous les côtés, sauf sa face avant, par 10 cm de fer qui à son tour est entouré de 10 cm de paraffine, le tout recouvert de cadmium.

2.3. Détection de neutrons

Les neutrons sortant de l'empilement sont détectés par des compteurs BF_3 associés à des chaînes électroniques classiques. L'analyse en temps est effectuée par deux analyseurs en temps TMC CN 110 à 256 canaux. La largeur des canaux est variable de 10 μs à 256 μs par sauts binaires. Un temps de mise en mémoire de 10 μs constitue en temps mort entre deux canaux consécutifs. La largeur du premier canal (canal de mesure du bruit de fond) et le retard entre le premier et le deuxième canal sont réglables indépendamment l'un de l'autre par des facteurs binaires multiplicatifs de

la largeur des autres canaux. Le temps de résolution de la chaîne complète est de 1,6 μs.

2.4. Définition du cycle élémentaire

La base de temps d'un analyseur est utilisée pour définir le déroulement du cycle.

La fermeture du premier canal envoie une impulsion à un tiroir de retard qui déclenche la bouffée de neutrons de largeur variable à volonté et qui est en général de l'ordre du temps de vie dans l'empilement étudié. On pallie ainsi l'inconvénient du retard à l'analyse par le fait que le TMC est réglable par bond binaire. Le déclenchement du cycle est obtenu par un générateur d'impulsions qui ouvre le premier canal des analyseurs.

3. LES EMPILEMENTS DE GRAPHITE

Les mesures ont porté sur 53 empilements constitués de briques de section 20 × 20 cm et de longueurs 60 cm, 40 cm et 20 cm, qui ont été filées avant cuisson dans le sens de la longueur et qui sont percées d'un canal de 14 cm de diamètre. Chaque brique dispose d'un ensemble de chemises qui permet d'obtenir des canaux de diamètres 3, 5, 7, 9 et 11 cm, le jeu entre chemises étant de l'ordre de 0,02 cm. Les mesures rapportées ici ont été effectuées sur ces briques dont les canaux étaient bouchés par ces chemises et un rondin de graphite.

La densité de chaque élément a été obtenue à partir des pesées individuelles et des relevés de cote par échantillonage. Les briques de même longueur, avec leurs chemises et noyaux, ont été numérotées en tenant compte de leur densité, de sorte qu'en les prenant dans l'ordre de numérotation on obtient une densité globale à peu près constante et indépendante du nombre de briques utilisées. Lors du montage des différents empilements, la densité moyenne de chacun d'eux a été déterminée à partir du poids total et des dimensions extérieures. Pratiquement tous les empilements ont une densité moyenne comprise dans la bande $1{,}6725 \pm 0{,}0005$. Les lits de briques qui les constituent ne sont pas croisés, ce qui entraîne une légère anisotropie neutronique.

Le tableau I donne la liste des divers empilements étudiés, leurs dimensions et leur densité.

4. LES MESURES

La cible est centrée sur l'une des faces latérales, et les compteurs BF_3 sont placés sur la face supérieure, un compteur au milieu de celle-ci, et l'autre au nœud de l'harmonique 3 dans le sens perpendiculaire à l'axe de tir et de l'harmonique 2 dans le sens du tir. Ceci nous permet d'obtenir deux mesures du temps de vie par expérience, les comptages étant faits indépendamment sur deux analyseurs synchronisés. Comme chaque expérience est répétée, on obtient en fait quatre mesures du temps de vie sur chacun des empilements.

TABLEAU I

DÉTAIL DES MESURES DES CONSTANTES DE DÉCROISSANCE

N° de l'empilement	A (cm)	B (cm)	C (cm)	α (s^{-1})	B_u^2 (m^{-2})	B_L^2 (m^{-2})	B^2 (m^{-2})	φ
1	220	240	220	190,68	1,97	3,64	5,61	1,6730
2	200	240	240	195,25	2,38	3,33	5,71	1,6726
3	220	220	220	198,57	1,97	3,95	5,92	1,6725
4	180	240	240	204,92	2,92	3,33	6,25	1,6728
5	220	200	220	206,52	1,97	4,36	6,33	1,6726
6	200	240	200	207,10	2,38	4,04	6,42	1,6728
7	220	180	220	217,74	1,97	4,90	6,88	1,6724
8	160	240	240	221,76	3,69	3,33	7,01	1,6727
9	200	200	200	222,53	2,38	4,76	7,14	1,6727
10	220	160	220	233,05	1,97	5,67	7,64	1,6722
11	180	220	180	236,28	2,93	4,91	7,83	1,6721
12	140	240	240	244,37	4,78	3,33	8,11	1,6729
13	180	200	180	245,36	2,93	5,31	8,24	1,6721
14	220	140	220	254,62	1,97	6,77	8,74	1,6721
15	180	180	180	256,49	2,93	5,86	8,79	1,6720
16	180	160	180	271,08	2,93	6,62	9,55	1,6719
17	120	240	240	275,24	6,45	3,32	9,77	1,6734
18	220	120	220	287,91	1,97	8,44	10,42	1,6720
19	160	160	160	301,53	3,69	7,38	11,07	1,6722
20	160	140	160	323,64	3,69	8,48	12,17	1,6720
21	240	100	240	329,33	1,66	10,87	12,52	1,6727
22	100	240	240	331,64	9,20	3,33	12,52	1,6724
23	220	100	220	341,74	1,97	11,17	13,14	1,6729
24	100	220	220	344,97	9,20	3,95	13,14	1,6722
25	140	160	140	342,88	4,79	8,48	13,27	1,6721
26	160	120	160	356,26	3,69	10,16	13,85	1,6721
27	140	140	140	366,63	4,79	9,59	14,37	1,6718
28	180	100	180	380,31	2,93	12,14	15,07	1,6719
29	140	120	140	399,57	4,79	11,26	16,04	1,6724
30	120	160	120	408,77	6,46	10,15	16,61	1,6726

TABLEAU I (Suite)

N° de l'empilement	A (cm)	B (cm)	C (cm)	α (s^{-1})	B_{II}^2 (m^{-2})	$B_{\perp}^2$ (m^{-2})	B^2 (m^{-2})	φ
31	240	80	240	423,98	1,66	15,80	17,46	1,6727
32	80	240	240	429,36	14,12	3,33	17,45	1,6726
33	100	140	160	431,23	9,19	8,48	17,67	1,6725
34	120	140	120	433,03	6,46	11,25	17,70	1,6729
35	80	220	220	440,33	14,13	3,95	18,08	1,6720
36	220	80	220	438,15	1,97	16,10	18,08	1,6729
37	140	100	140	452,58	4,79	14,00	18,78	1,6724
38	120	120	120	465,27	6,46	12,93	19,39	1,6723
39	120	100	120	518,67	6,46	15,67	22,13	1,6723
40	100	140	100	534,87	9,19	14,00	23,19	1,6724
41	100	120	100	567,22	9,20	15,67	24,87	1,6723
42	100	100	100	623,09	9,20	18,41	27,60	1,6723
43	100	80	100	710,16	9,20	23,34	32,54	1,6723
44	80	120	80	750,73	14,12	20,60	34,72	1,6726
45	80	100	80	803,03	14,12	23,34	37,45	1,6726
46	60	100	60	1166,14	24,39	33,62	58,01	1,6729
47	60	80	60	1238,12	24,39	38,56	62,95	1,6729
48	60	60	60	1390,3	24,39	48,85	73,24	1,6729
49	60	40	60	1768,4	24,39	76,44	100,8	1,6730
50	40	80	40	1926,2	51,94	66,19	118,1	1,6725
51	40	60	40	2041,9	51,94	76,49	128,4	1,6725
52	50	40	40	2212,5	34,36	104,1	138,5	1,6725
53	40	40	40	2373,7	51,94	104,1	156	1,6725

A = Cote parallèle au sens du filage
B = Autre cote horizontale
C = Hauteur

Nous avons été amenés à prendre des dispositions particulières sur les huit empilements de dimensions les plus faibles en raison de la présence des neutrons réfléchis qui indiquait que les précautions normalement prises n'étaient plus suffisantes: à l'intérieur de la cage de cadmium chacun de ces empilements est édifié dans une enceinte en paraffine d'une épaisseur de 5 cm doublée intérieurement de cadmium et percée d'une fenêtre en face de la cible. De plus, la sensibilité de la détection neutronique est améliorée

par l'utilisation d'un ensemble de quatre compteurs en parallèle dont les impulsions sont mélangées avant comptage dans le même analyseur. Les quatre compteurs sont placés côte à côte de façon à centrer la section active de l'ensemble sur la face supérieure de l'empilement.

On voudrait souligner ici la difficulté de faire une mesure précise sur de petits empilements. Du fait que le temps de vie est faible, c'est-à-dire que les fuites sont importantes, la mesure devient plus sensible à l'effet des neutrons réfléchis, d'autant plus qu'il est nécessaire d'attendre pendant une durée de l'ordre de six temps de vie pour que le spectre puisse atteindre son équilibre. En conséquence, le système de comptage doit être d'une grande sensibilité et d'un bas niveau de bruit de fond. Le compteur doit également être de dimensions données de façon à ne pas constituer un élément perturbateur dans le voisinage.

Malgré les précautions que nous avons prises, nous envisageons de refaire des mesures sur les petits empilements dans un autre lieu où il n'y aura pas à proximité des murs réfléchissants en utilisant un système de comptage de dimensions plus réduites.

5. ANALYSE DES MESURES ET RÉSULTATS

5.1. Détermination de la constante de décroissance

On procède par étapes successives:

a) Une première visualisation sur le scope de l'analyseur nous permet de dépister les canaux aberrants.

b) Pour éliminer les points mauvais qui peuvent encore subsister, un code IBM-704 permet de tracer dans un système semi-logarithmique les points corrigés du temps de résolution et du bruit de fond donné par le premier canal. Les points portés ici sont les moyennes prises sur cinq canaux consécutifs. Ce graphique nous permet d'avoir une première idée de l'intervalle de temps (t_1, t_2) pendant lequel la courbe est rectiligne.

c) Un autre code permet d'effectuer ensuite le travail suivant:

- Correction des mesures du temps de résolution et du bruit de fond du premier canal, et passage en logarithme.
- Détermination par moindres carrés, dans l'intervalle (t_1, t_2) défini précédemment, de la pente α_0 et de l'ordonnée à l'origine A_0.
- Soustraction du contenu du premier canal de la décroissance résiduelle correspondant à $A_0 \exp(-\alpha_0 t)$ donnant ainsi une meilleure valeur du bruit de fond. Le contenu de chaque canal est maintenant corrigé avec ce nouveau bruit de fond.
- Détermination d'un certain nombre d'intervalles (40 à 60 canaux), les centres des intervalles étant équidistants d'environ 10 canaux, et détermination par moindres carrés de la pente α_j de la droite ajustée dans l'intervalle j.
- Positionnement sur le papier des valeurs α_j dans un système centré sur α_0, ayant en abscisse l'écart relatif $(\alpha_j - \alpha_0)/\alpha_0$ et en ordonnée le canal sur lequel est centré l'intervalle j.

Dans la mesure où il existe un intervalle de temps pour lequel le fondamental subsiste seul et où le bruit de fond a été bien corrigé, nous observons un palier sur la courbe $\alpha_j = f(t_j)$. Par contre, si la valeur du bruit de fond n'est pas bien choisie, nous observons une dérive de cette courbe vers les faibles taux de comptage. Dans ce cas-ci, la comparaison entre les valeurs de α_j pour $t_j > t_2$ et la moyenne de celles pour $t_1 < t_j < t_2$ nous donne une correction à apporter au bruit de fond. Cette nouvelle valeur étant introduite dans le calcul, l'itération se poursuit jusqu'au redressement de la courbe.

L'examen de ces divers graphiques nous donne l'intervalle valable pour calculer ultérieurement α et la valeur du bruit de fond à utiliser. La figure 1 donne un aperçu de la durée entre la fin de la bouffée et le début de l'intervalle, en fonction du laplacien.

d) Un troisième code fait le calcul par moindres carrés sur l'ensemble des points dans l'intervalle déterminé, et donne la valeur de α et son erreur $\Delta\alpha$. Dans ces calculs par moindres carrés, la pondération utilisée tient compte d'une part de l'erreur statistique du comptage, et d'autre part de l'incertitude sur la valeur du temps de résolution.

e) La valeur de la constante de décroissance, pour un empilement donné, est obtenue par moyenne pondérée des différentes valeurs de α et $\Delta\alpha$ déterminées pour cet empilement (en général quatre valeurs). Ces moyennes pondérées sont données dans le tableau I.

5.2. Analyse de α en fonction de la taille de l'empilement

Comme les empilements ont une légère anisotropie qui provient d'une part du sens de filage et d'autre part de la présence du faible jeu entre les chemises, nous en avons tenu compte en dissociant le terme D_0B^2 en une composante parallèle au sens du filage et une composante perpendiculaire:

$$\alpha = v\Sigma_a + D_{\parallel} B_{\parallel}^2 + D_{\perp} B_{\perp}^2 - CB^4 + FB^6. \qquad (1)$$

Le dépouillement est effectué pour une densité $\varphi_0 = 1{,}672$ après multiplication du α_i mesuré par le rapport $R_i = (\varphi_0/\varphi_i)$, et des B_i^2 par R_i^2.

Les valeurs de $B_{\parallel}^2$ et $B_{\perp}^2$ sont calculées en utilisant comme longueurs d'extrapolations $0{,}71\,\lambda_t$ où

$$\lambda_{t_{\parallel}} = \frac{3D_{\parallel}}{\bar{v}}, \quad \lambda_{t_{\perp}} = \frac{3D_{\perp}}{\bar{v}}, \qquad (2)$$

$\bar{v}$ étant la vitesse moyenne de la densité maxwellienne en équilibre à $T = 20{,}2$°C, température moyenne pendant les expériences.

Tous les calculs par moindres carrés sont effectués en admettant une erreur relative constante.

Nous avons tout d'abord examiné dans la région où l'influence du terme en B^6 n'est pas à craindre si nous pouvions définir des bandes étroites d'incertitude pour les différents paramètres, à l'exclusion de F: on fixe a priori une valeur de C qui permet l'évaluation du terme en CB^4, et l'adjustement par moindres carrés des paramètres $v\Sigma_a$, $D_{\parallel}$ et $D_{\perp}$ à l'expression

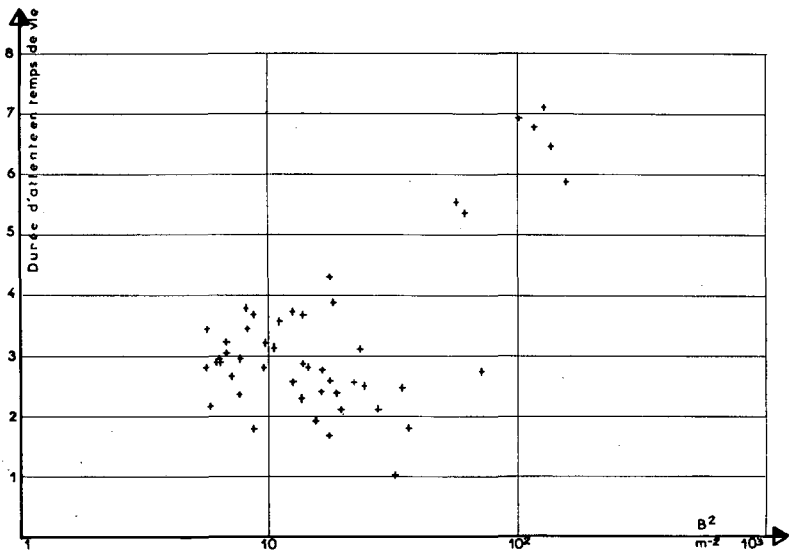

Figure 1

Durée d'attente pour le calcul de α.
Durée en fonction du laplacien.

$$\alpha_c = v\Sigma_a + D_{\parallel} B_{\parallel}^2 + D_{\perp} B_{\perp}^2 \qquad (3)$$

dans laquelle $\alpha_c = \alpha + CB^4$.

Bien entendu on itère entre les coefficients de diffusion et les longueurs d'extrapolation jusqu'à rendre le système cohérent. On procède à cet ajustement en utilisant les x premières valeurs de α_c pour diverses valeurs de x. S'il est effectivement possible de déterminer C avec précision, on doit voir, dans le cas où la valeur fixée de C est trop grande, que les valeurs de D augmentent et les valeurs de $v\Sigma_a$ décroissent en fonction de x. Par contre si C est trop petit, l'inverse doit se produire. Une famille de courbes calculées pour diverses valeurs de C doit alors nous permettre de fixer la région dans laquelle se trouve la bonne valeur de C.

Nous avons effectué ce genre de calcul pour des valeurs de C allant de $30 \cdot 10^5$ $cm^4 \cdot s^{-1}$ à $40 \cdot 10^5$ $cm^4 \cdot s^{-1}$, et en faisant varier x entre 20 et 45. Nous avons également tracé la famille des courbes calculées jusqu'au 40^e en supprimant successivement les 14 premiers points. Nous avons constaté que la détermination exacte, à partir de ces familles de courbes, des bonnes valeurs des paramètres n'est pas du tout évidente. Le fait de changer la valeur de C n'a pratiquement pour effet que de déplacer les courbes avec une légère divergence systématique seulement. Ceci laisse à penser qu'on pourrait trouver des ensembles de valeurs ($v\Sigma_a$, $D_{\parallel}$, $D_{\perp}$, C) sensiblement différents les uns des autres mais tels que chaque ensemble donne des écarts relatifs entre courbe correspondante et points expérimentaux, écarts peu sensibles dans l'ensemble utilisé. Nous avons examiné les écarts relatifs obtenus avec différents ensembles de paramètres et constaté qu'effectivement

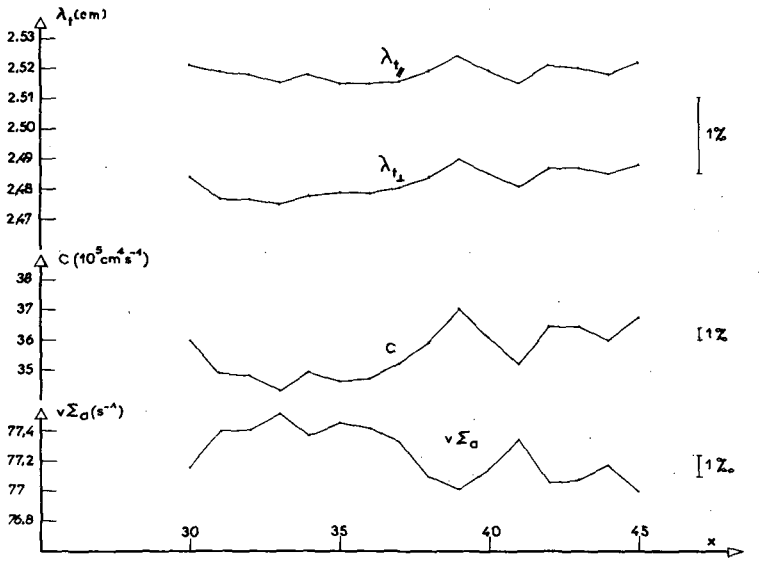

Figure 2

Valeurs des paramètres en fonction de la borne x de la première zone (de 30 à 45).
C calculé en seconde zone (30 à 45).

cette incertitude existe, qui dans le fond reflète l'incertitude inhérente à la détermination des paramètres. Nous avons tenu compte de ce fait dans les marges d'erreurs affectées aux valeurs données plus loin.

Nous avons mené le dépouillement final de la manière suivante: on fixe d'abord deux zones, la première, qui comprend les faibles laplaciens, dans laquelle on détermine $\nu\Sigma_a$, $D_{\parallel}$ et $D_{\perp}$, la seconde, qui comprend les laplaciens élevés, pour le calcul de C. Nous choisissons une valeur raisonnable de λ_t pour le premier calcul des laplaciens. En fixant une valeur de départ de C, on calcule la correction CB^4 à apporter aux points de la première zone dans laquelle on ajuste par moindres carrés $\nu\Sigma_a$, $D_{\parallel}$, $D_{\perp}$. Les valeurs qui en résultent permettent de préciser les laplaciens et le coefficient de refroidissement, calculé en utilisant les points dans la deuxième zone. Cette seconde valeur de C est utilisée pour une nouvelle détermination de $\nu\Sigma_a$, $D_{\parallel}$, $D_{\perp}$. On procède ainsi à des itérations entre les deux zones jusqu'à cohérence des résultats.

Nous avons fait une série de calculs en déplaçant successivement la borne supérieure de la première zone du 30e au 45e point, la seconde zone étant toujours comprise entre ces deux points.

Les résultats sont portés sur la figure 2. Nous nous sommes limités au point 45 puisque des calculs préliminaires et des courbes d'écarts relatifs ont montré que les plus petits empilements étaient influencés par la présence du terme en B^6. Nous avons également fait d'autres calculs en utilisant d'autres zones, notamment pour le calcul de C. Les résultats de ces calculs sont donnés dans le tableau II.

TABLEAU II

VALEUR DES PARAMÈTRES POUR DIFFÉRENTES ZONES

Limites pour calcul de		$v\Sigma_a$ (s^{-1})	$D_{\parallel}$ ($cm \cdot s^{-1}$)	$D_{\perp}$ ($cm \cdot s^{-1}$)	$\frac{D_{\parallel}}{D_{\perp}}$	C ($cm^4 \cdot s^{-1}$)
$v\Sigma_a$, $D_{\parallel}$, $D_{\perp}$	C					
1-40	40-45	77,14	$208,49 \cdot 10^3$	$205,68 \cdot 10^3$	1,0136	$36,29 \cdot 10^5$
1-30	30-45	77,16	$208,55 \cdot 10^3$	$205,57 \cdot 10^3$	1,0145	$36,11 \cdot 10^5$
1-29	29-45	76,78	$209,30 \cdot 10^3$	$206,20 \cdot 10^3$	1,0150	$37,90 \cdot 10^5$
1-28	28-44	76,82	$209,24 \cdot 10^3$	$206,13 \cdot 10^3$	1,0151	$37,93 \cdot 10^5$
1-27	27-43	77,32	$208,52 \cdot 10^3$	$205,00 \cdot 10^3$	1,0172	$34,69 \cdot 10^5$
1-26	26-42	77,42	$208,32 \cdot 10^3$	$204,80 \cdot 10^3$	1,0172	$33,73 \cdot 10^5$
1-25	25-42	77,48	$208,29 \cdot 10^3$	$204,70 \cdot 10^3$	1,0175	$33,79 \cdot 10^5$
1-24	24-41	76,55	$210,18 \cdot 10^3$	$206,63 \cdot 10^3$	1,0172	$41,20 \cdot 10^5$
1-23	23-40	77,00	$208,95 \cdot 10^3$	$205,85 \cdot 10^3$	1,0150	$37,44 \cdot 10^5$
1-22	22-39	77,02	$208,82 \cdot 10^3$	$205,79 \cdot 10^3$	1,0147	$36,56 \cdot 10^5$
1-21	21-38	76,66	$209,77 \cdot 10^3$	$206,55 \cdot 10^3$	1,0156	$40,59 \cdot 10^5$
1-20	20-38	76,55	$209,83 \cdot 10^3$	$206,84 \cdot 10^3$	1,0145	$41,26 \cdot 10^5$
1-19	19-37	76,81	$209,38 \cdot 10^3$	$206,31 \cdot 10^3$	1,0149	$39,64 \cdot 10^5$
1-18	18-36	76,85	$209,32 \cdot 10^3$	$206,24 \cdot 10^3$	1,0149	$39,63 \cdot 10^5$

Après étude de l'ensemble de ces résultats, les valeurs des paramètres $v\Sigma_a$, $D_{\parallel}$, $D_{\perp}$, $\lambda_{t_{\parallel}}$, $\lambda_{t_{\perp}}$ et C sont les suivantes:

$$v\Sigma_a = 77,2 \pm 0,6 \ s^{-1},$$

$$D_{\parallel} = (208,3 \pm 0,8) \cdot 10^3 \ cm^2 \cdot s^{-1},$$

$$D_{\perp} = (205,5 \pm 0,8) \cdot 10^3 \ cm^2 \cdot s^{-1},$$

$$C = (36 \pm 3) \cdot 10^5 \ cm^4 \cdot s^{-1},$$

$$\lambda_{t_{\parallel}} = 2,518 \pm 0,01 \ cm,$$

$$\lambda_{t_{\perp}} = 2,483 \pm 0,01 \ cm,$$

$$\lambda_{t_{\parallel}} / \lambda_{t_{\perp}} = 1,014 \pm 0,004,$$

ces valeurs étant données à une densité de 1,672 et à une température de 20, 2°C.

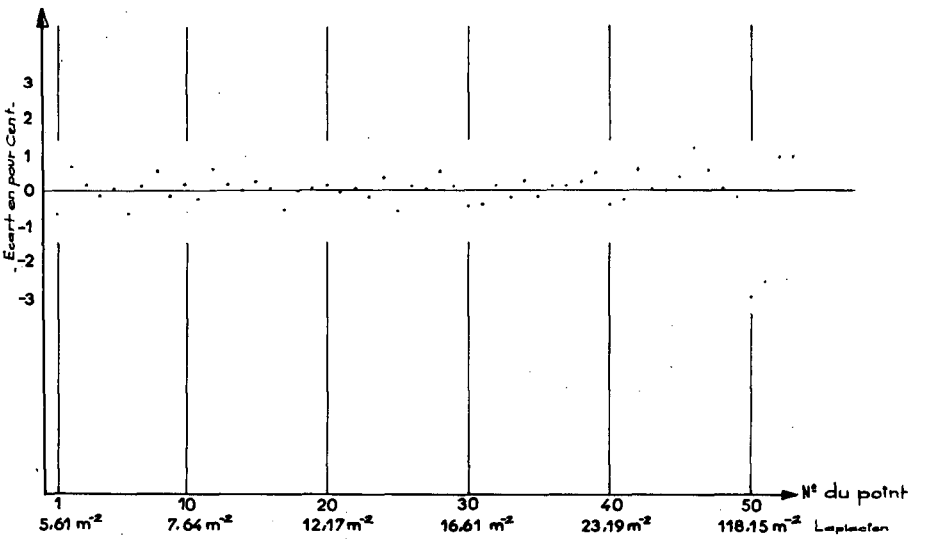

Figure 3

Ecarts relatifs des points expérimentaux par rapport à la courbe ajustée.

Ramenées à un graphite de densité 1,60, les valeurs de la section microscopique d'absorption, azote compris, du libre parcours de transport moyen dans un milieu cubique et du coefficient de refroidissement deviennent

$$\sigma_a = (4{,}18 \pm 0{,}03) \cdot 10^{-3} \text{ b} \quad \text{à } 2{,}2 \cdot 10^5 \text{ cm/sec},$$

$$\lambda_t = 2{,}606 \pm 0{,}01 \text{ cm},$$

$$C = (41 \pm 3) \cdot 10^5 \text{ cm}^4 \cdot \text{s}^{-1}.$$

Etant donné qu'aucune influence du terme en FB^6 n'a pu être décelée précédemment sur les 45 premiers empilements, nous avons déterminé le coefficient F sur les 8 empilements qui restent en adoptant pour les autres paramètres les valeurs qui viennent d'être données. On obtient une valeur égale à $-2 \cdot 10^7 \text{ cm}^6 \cdot \text{s}^{-1}$ avec une marge d'incertitude importante, $\pm 4 \cdot 10^7 \text{ cm}^6 \cdot \text{s}^{-1}$. Les déterminations de la constante de décroissance sont en effet moins précises dans la gamme des laplaciens élevés pour les raisons déjà indiquées: présence possible de neutrons réfléchis, retard à l'analyse important par rapport au temps de vie, perturbation possible due à la présence des compteurs et du blindage de cadmium-paraffine, et enfin faible contribution relative de ce terme en FB^6.

La figure 3 présente les écarts relatifs des points expérimentaux par rapport à la courbe calculée d'après les valeurs que nous publions ici. On peut voir que la précision des points expérimentaux est de l'ordre de 5‰ pour les 45 premiers empilements. Au-delà elle est moins bonne.

6. DÉTERMINATION DU TEMPS DE MISE EN ÉQUILIBRE

Nous présentons ici des mesures préliminaires du temps de mise en équilibre sur des empilements de diverses dimensions, avec un système de mesure très sensible au changement de spectre.

L'appareil de mesure consiste essentiellement en un ou plusieurs compteurs BF_3, d'un diamètre de 5 cm, enrichis à 90% de B^{10}, complètement recouverts de cadmium, et un petit compteur BF_3 appauvri en B^{10} (10%) qui, lui, est nu. Les deux compteurs sont placés sur la face supérieure de l'empilement, le compteur enrichi verticalement et le compteur appauvri couché. Le rapport du taux de comptage dans ces deux détecteurs en fonction du temps, après la bouffée de neutrons, varie très rapidement pendant environ 2 ms et beaucoup plus lentement pendant encore environ 2 ms, puis il se stabilise. La figure 4 montre une courbe typique de cette décroissance.

Jusqu'à maintenant nous n'avons fait que quelques expériences qui nous permettent de constater, grâce à l'amélioration apportée à la sensibilité du système de mesure, que l'approche à l'équilibre ne peut être considérée comme une exponentielle pure.

Bien que nos efforts dans l'étude des transitoires aient porté surtout, jusqu'à maintenant, sur l'amélioration de la sensibilité au spectre du système de détecteurs, quelques expériences ont été réalisées sur des empilements de laplaciens différents en faisant varier l'endroit de la détection. Les résultats présentés sur la figure 5 indiquent une augmentation de la durée de mise à l'équilibre lorsque le laplacien diminue ou, sur un empilement donné, lorsque le point de mesure s'éloigne de la face de tir.

7. RÉSULTATS OBTENUS SUR L'OXYDE DE BÉRYLLIUM

Nous avons effectué des mesures sur 14 blocs dont les laplaciens s'échelonnent entre 15 m^{-2} et 65 m^{-2}. La densité de l'oxyde de béryllium était 2,96 et la température moyenne 21,5°C.

La méthode d'analyse de α en fonction de B^2 est essentiellement la même que celle utilisée pour le graphite, qui a été décrite en détail dans une section précédente. On a utilisé les résultats sur les 11 premiers massifs (15 m^{-2} à 38 m^{-2}) pour obtenir $v\Sigma_a$ et D_0, et sur les trois derniers massifs pour obtenir la valeur de C, des itérations étant effectuées entre les deux régions pour obtenir l'ensemble de résultats cohérents suivants:

$$v\Sigma_a = 145 \pm 3 \ s^{-1},$$

$$D_0 = (132{,}7 \pm 2) \cdot 10^3 \ cm^2 \cdot s^{-1},$$

$$C = (4{,}2 \pm 1{,}5) \cdot 10^5 \ cm^4 \cdot s^{-1},$$

$$\lambda_t = 1{,}59 \pm 0{,}03 \ cm.$$

Ces résultats sont en bon accord avec ceux présentés par M. B. V. Joshi à ce colloque, à l'exception de l'absorption [1].

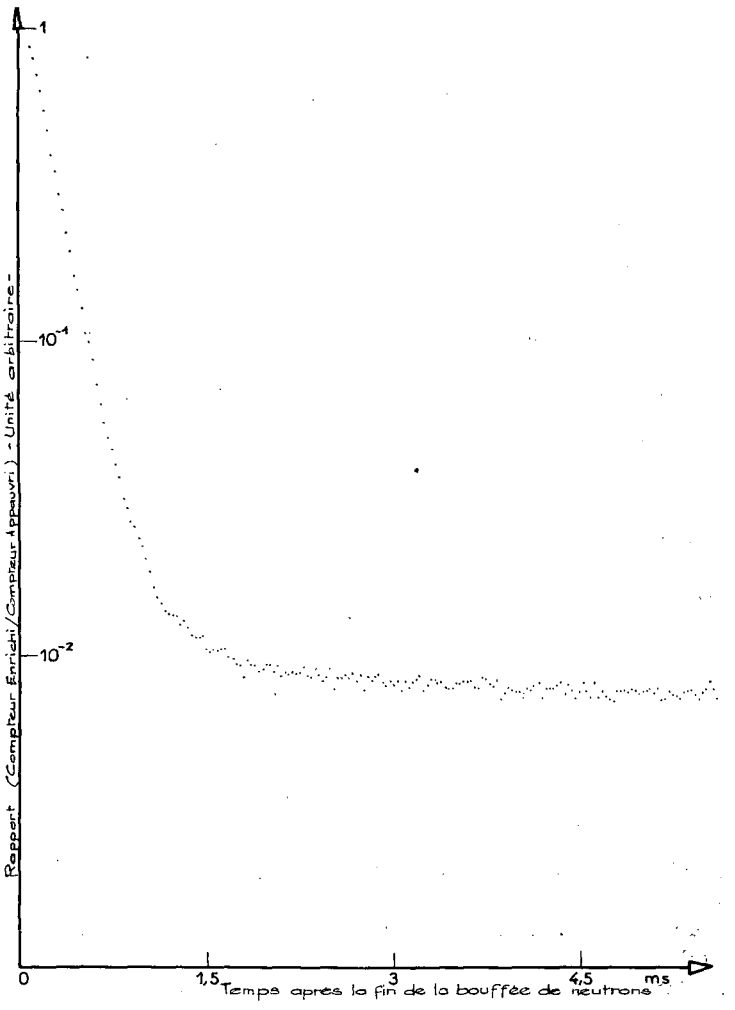

Figure 4

Mise à l'équilibre du spectre dans l'empilement 200 x 200 x 200 cm.

8. CONCLUSION

Nous croyons avoir obtenu une valeur très précise des libres parcours moyens de transport dans le graphite. L'anisotropie que nous avons mesurée est vraisemblablement celle du graphite, les jeux entre les chemises n'y contribuant que pour très peu; la valeur obtenue est en bon accord avec celles données dans les références [2, 3, 4].

Nous obtenons de nouveau une valeur élevée du coefficient de refroidissement en accord avec [2, 4, 5], mais toujours en désaccord avec le résultat obtenu par KLOSE et al. [3]. Les dépouillements effectués à partir des ré-

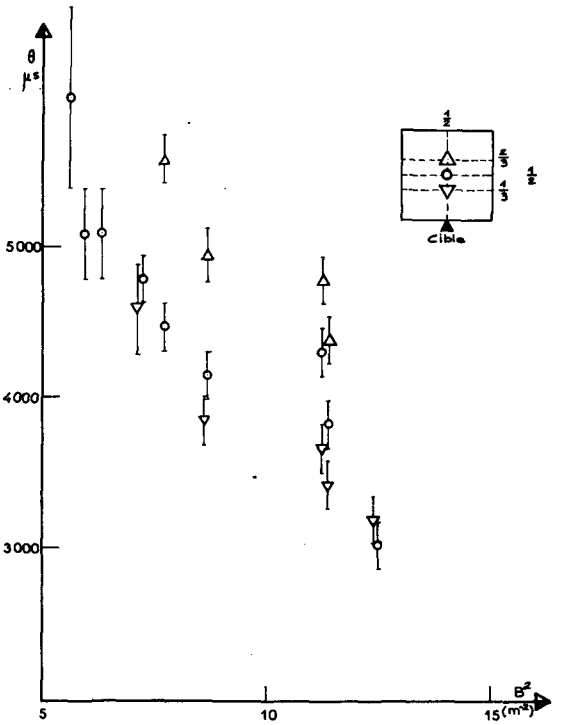

Figure 5

Durée de mise à l'équilibre θ en fonction du laplacien et du point de mesure.

sultats expérimentaux de ces auteurs sans utiliser le point obtenu par expérience exponentielle aboutissent en effet à une valeur de C voisine de la nôtre lorsque l'on ne tient pas compte d'un terme en FB^6; ils amènent à la réduire notablement, de l'ordre de $20 \cdot 10^5$ $cm^4 \cdot s^{-1}$ si l'on tient compte de ce terme. Parallèlement, la valeur absolue du coefficient F que nous obtenons est beaucoup plus faible que celle issue de ces dépouillements. Il ne nous est en effet pas possible dans le domaine des empilements étudiés de confirmer expérimentalement l'existence de ce terme.

Nos mesures de durée de mise à l'équilibre du spectre indiquent que cette durée varie avec le laplacien et est plus longue que les 2 ms précédemment admises [4, 6]. Le système de détection utilisé était alors nettement moins sensible aux variations du spectre que le nôtre et ne pouvait donc pas déceler de légères variations pendant la dernière partie de la mise à l'équilibre. Nous avons l'intention d'étudier cette question d'une manière plus systématique, particulièrement en ce qui concerne l'influence des harmoniques.

Nous avons par ailleurs commencé un programme très complet d'étude de l'anisotropie du graphite percé d'un réseau de canaux vides à diamètre variable (30 à 140 mm), qui sera mené parallèlement à l'étude des milieux absorbants et multiplicateurs.

RÉFÉRENCES

[1] JOSHI, B. V., "Diffusion Parameters of BeO by Pulsed Neutron Method", these proceedings.

[2] STARR, E. and PRICE, G. A., Measurement of the Diffusion Parameters of Graphite and Graphite Bismuth by Pulsed Neutron Method, BNL 719, III (1962) 1034-73.

[3] KLOSE, H., KUCHLE, M. and REICHARDT, W., Pulsed Neutron Measurement on Graphite, BNL 719 III (1962) 935-45.

[4] SAGOT, M. et TELLIER, H., Mesure des paramètres de diffusion et de l'anisotropie du graphite à l'aide d'une source pulsée de neutrons, Rapport C. E. A. n° 2210 (1963).

[5] STARR, E. and DEVILLIERS, J. W. L., Determination of Diffusion Cooling in Graphite by Measurements of the Average Neutron Velocity, BNL 719 III (1962) 997-1011.

[6] STARR, E., HONECK, J. and DEVILLIERS, J. W. L., Determination of Diffusion Cooling in Graphite by Measurements of the Average Neutron Velocity, NSE 18 (1964) 230-35.

DISCUSSION

K. H. BECKURTS: Were the evaluations of your data on α versus B^2 curves performed by a least-squares fit? Or did you employ a zoning technique in which various regions of the α versus B^2 curve were used for the determination of D_0 and C and, if so, what is the statistical justification of the method?

M. SAGOT: We did not determine any parameters using a least-squares fit to a parabola. What we did was to employ successive iterations on two zones (the method is described in the paper) and for this we used the least-squares method. We compared the two techniques for a set of experimental data that were different from ours and we found that they produced the same result. If, however, the measured points are eliminated one after the other on the basis of high B^2 values, the results obtained for the parameters are much more stable and much less subject to fluctuation with the iteration method than with the least-squares fit to a parabola. This is a result of the inherent lack of precision of the experimental points. The two methods would produce identical results if the experimental points were known to a high degree of accuracy.

P. DAITCH: Was there any energy bias or discrimination, particularly against low-energy neutrons, in the experiments described in your paper? This could be important if one considers the time-dependent spectra in theory or in experimental measurements, e.g. those presented in paper SM-62/52*.

M. SAGOT: There is no discrimination against cold neutrons. The detectors are BF_3 counters and there is only γ-discrimination. However, the spectral index measurements made on the graphite clearly show that after a reasonable period of time following the pulse one obtains a plateau, i.e. an equilibrium, which remains during the whole period of the α-measurement. This seems to indicate that there is no trapping effect, or at least none that can be detected, for the cold neutrons. No spectrum measurements were made with BeO.

M. KÜCHLE: In an article** by Davis, De Juren and Reier, it is pointed out that the difference in decay time of small assemblies is probably caused

* GAERTTNER, E.R., DAITCH, P.B., FULLWOOD, R.R., LEE, R.R. and SLOVACEK, R.E., "The effects of coherent scattering on the thermalization of neutrons in beryllium", these Proceedings I.

** To be published in Nucl. Sci. Engng.

by the different shieldings of the assemblies used by the different authors. Have you studied this point?

M. SAGOT: We did study the effect of neutron shielding on the eight smallest graphite stacks, because the reflected neutron effect interferred with the exponential decay despite shielding of the source. The measurements were carried out on stacks that were shielded by cadmium and by various thicknesses of paraffin and cadmium. We finally used a shield consisting of 5 cm of paraffin lined with cadmium on both sides, i.e. on the stack and the outside faces. In all cases it always takes a long time for the spectrum to achieve equilibrium and there seems to be no connection with the shielding.

DIFFUSION PARAMETERS OF BeO BY THE PULSED NEUTRON METHOD

B. V. JOSHI, V. R. NARGUNDKAR AND K. SUBBARAO
ATOMIC ENERGY ESTABLISHMENT TROMBAY,
BOMBAY, INDIA

Abstract — Résumé — Аннотация — Resumen

DIFFUSION PARAMETERS OF BeO BY THE PULSED NEUTRON METHOD. The use of the pulsed neutron method for the precise determination of the diffusion parameters of moderators is described. The diffusion parameters of BeO have been obtained by this method. The neutron bursts were produced from a cascade accelerator by pulsing the ion source and using the Be (d, n) reaction. The detector was an enriched boron trifluoride proportional counter. It is shown that by a proper choice of the counter position and length, and the source position, most of the space harmonics can be eliminated. Any constant background can be accounted for in the calculation of the decay constant. Very large bucklings were not used to avoid time harmonics. Any remaining harmonic content was rendered ineffective by the use of adequate time delay. The decay constant of the fundamental mode of the thermal neutron population was determined for several bucklings. Conditions to be satisfied for an accurate determination of the diffusion cooling constant C are discussed. The following values are obtained for BeO:

λ_0 = absorption constant = 156.02 ± 4.37 s^{-1}

D = diffusion coefficient = (1.3334 ± 0.0128) × 10^5 cm^2/s

C = diffusion cooling constant = (-4.8758 ± 0.5846) × 10^5 cm^4/s.

The effect of neglecting the contribution of the B^6 term on the determination of the diffusion parameters was estimated and is shown to be considerable. The reason for the longstanding discrepancy between the values of C obtained for the same moderator by different workers is attributed to this.

CALCUL DES PARAMÈTRES DE DIFFUSION DE BeO PAR LA MÉTHODE DES NEUTRONS PULSÉS. Les auteurs décrivent l'emploi de la méthode des neutrons pulsés pour la détermination précise des paramètres de diffusion des ralentisseurs. Ils ont calculé ceux de la glucine par cette méthode. Des deutérons pulsés au moyen d'*un accélérateur à cascade produisaient les bouffées de neutrons par la réaction Be (d, n)*. Le détecteur était constitué par un compteur proportionnel au BF_3 enrichi. En choisissant convenablement la position et la longueur du compteur d'une part, la position de la source d'autre part, il est possible d'éliminer la plupart des harmoniques spatiaux. Il est également possible de tenir compte de n'importe quel bruit de fond constant pour le calcul de la constante de décroissance. Il faut éviter les laplaciens très élevés afin de ne pas avoir d'harmoniques du temps. Tous les harmoniques qui restent sont rendus inopérants par un retard en temps adéquat. Les auteurs ont déterminé la constante de décroissance du mode fondamental de la population de neutrons thermiques pour plusieurs laplaciens. Ils discutent les conditions à remplir pour une détermination exacte de la constante du refroidissement par diffusion C. Pour la glucine, ils ont obtenu les constantes suivantes:

λ_0 (constante d'absorption) = 156, 02 ± 4, 37 s^{-1},

D (coefficient de diffusion) = (1, 3334 ± 0, 0128)·10^5 cm^2/s,

C (constante du refroidissement de diffusion) = (-4, 8758 ± 0, 5846)·10^5 cm^4/s.

Les auteurs ont étudié le rôle que peut jouer, dans la détermination des paramètres de diffusion, le fait que la contribution du terme en B^6 est négligé; ils montrent qu'il est considérable. Ce serait là probablement la cause des écarts entre les valeurs de C obtenues pour un même ralentisseur par différents chercheurs.

ОПРЕДЕЛЕНИЕ ДИФФУЗИОННЫХ ПАРАМЕТРОВ BeO С ПОМОЩЬЮ МЕТОДА ИМПУЛЬСНЫХ НЕЙТРОНОВ. Описывается применение метода импульсных нейтронов для точного определения диффузионных параметров замедлителей. С помощью этого метода были получены диффузионные параметры BeO. Импульсы нейтронов получались с помощью каскадного ускорителя в результате пульсирования источника ионов и использования реакции Be (d, n). Детектором служил пропорциональный счетчик из обогащенного трехфтористого бора. Показано, что при правильном выборе положения и длины счетчика, а также положения источника, можно устранить большую часть пространственных гармоник. Любой постоянный

фон может быть учтен при расчете постоянной распада. Чтобы избежать временных гармоник, очень большие лапласианы не использовались. Все оставшиеся гармоники были сведены на нет благодаря использованию правильного времени запаздывания. Постоянная распада основного состояния плотности тепловых нейтронов была определена для нескольких лапласианов. Рассматриваются те условия, которые должны быть соблюдены для точного определения константы диффузионного охлаждения (C). Для BeO получены следующие величины:

λ_0 = постоянная поглощения = 156,02 ± 4,37 сек$^{-1}$,

D = коэффициент диффузии = (1,3334 ± 0,0128)·10^5 см^2/сек,

C = постоянная диффузионного охлаждения = (-4,8758 ± 0,5846)·10^5 см^4/сек.

Выявлены последствия пренебрежения B^6 при определении диффузионных параметров, показано, что эти последствия являются значительными и объясняют существовавшее в течение длительного времени расхождение между значениями C, полученными для одного и того же замедлителя различными исследователями.

DETERMINACION DE LOS PARAMETROS DE DIFUSION EN EL BeO POR EL METODO DE LOS NEUTRONES PULSADOS. Los autores describen el empleo del método de los neutrones pulsados para determinar con precisión los parámetros de difusión en moderadores. Con ayuda de este método, han obtenido los parámetros de difusión en el BeO. Las ráfagas de neutrones se generaron mediante un acelerador en cascada pulsando la fuente iónica y empleando la reacción Be (d, n). Como detector se utilizó un contador proporcional de BF_3 enriquecido. Los autores demuestran que por selección adecuada de la posición y longitud del contador y de la ubicación de la fuente, pueden eliminarse la mayoría de los armónicos espaciales. En el cálculo de la constante de decrecimiento, fue posible tener en cuenta toda actividad de fondo constante. Para evitar armónicos temporales se prescindió de los laplacianos de valor muy elevado. Se eliminó el efecto de todo contenido armónico remanente mediante el empleo de un retardo adecuado. Se determinó, para varios laplacianos, la constante de decrecimiento del modo fundamental de la población de neutrones térmicos. Los autores examinan las condiciones que han de satisfacerse para determinar con precisión la constante C de enfriamiento por difusión. Los valores obtenidos para el BeO fueron los siguientes:

λ_0 = constante de absorción = 156, 02 ± 4, 37 s^{-1},

D = coeficiente de difusión = (1, 3334 ± 0, 0128)·10^5 cm^2/s,

C = constante de enfriamiento por difusión = (-4, 8758 ± 0, 5846)·10^5 cm^4/s.

Los autores calcularon el efecto de despreciar la influencia del término B^6 sobre la determinación de los parámetros de difusión, demostrando que es considerable. Atribuyen a ese efecto la persistente discrepancia entre los valores de C obtenido para el mismo moderador por distintos investigadores.

INTRODUCTION

Diffusion parameters of BeO at room temperature have been determined by the static method by KOECHLIN et al. [1] (1956) and by the pulsed neutron method by IYENGAR et al. [2] (1957) and ZHEZHERUN [3] (1964). Their results are summarized in Table I, along with theoretical calculations of SINGWI [4] (1959) and SINGWI and KOTHARI [5] (1958).

These results show that the diffusion length obtained by the static method is in considerable disagreement with that obtained by the pulsed neutron method. The theoretical estimate of the diffusion cooling constant is almost half the experimental value. In an attempt to resolve these discrepancies, the experiment was repeated using a wide buckling range and a precision time analyser. The statistical accuracy was improved and the data was subjected to rigorous analysis. The theory underlying the experiment has been discussed adequately elsewhere [6, 7, 8, 9, 10].

EXPERIMENTAL APPARATUS

The fast neutrons were produced from a 1-MeV Cockroft Walton accelerator using a deuteron beam and a beryllium target. The deuteron beam

TABLE I

DIFFUSION PARAMETERS OF BeO

Author	Absorption constant λ_0 (s^{-1})	Diffusion coefficient D (10^5 cm^2/s)	Diffusion length L (cm)	Diffusion cooling constant C (10^5 cm^4/s)	Buckling range B^2 (cm^{-2})
Koechlin (static method)			(32.7 ± 0.5)		0.003
Singwi (theoretical)		1.32		-2.0	
Iyengar (pulsed method)	(131.6 ± 2.6)	(1.18 ± 0.02)	(29.9 ± 0.6)	(-3.85 ± 0.08)	0.02 to 0.08
Zhezherun	175	(1.557)	(29.9 ± 1.0)	(-4.117 ± 0.270)	0.005 to 0.095
Present authors	(156.02 ± 4.37)	(1.333 ± 0.012)	(29.23 ± 0.44)	(-4.875 ± 0.585)	0.0028 to 0.0245

was pulsed by pulsing the extraction voltage of the RF ion source. The pulse width varied from 100 μs to 4 ms and the repetition rate from 25 to 250 s^{-1}.

A precision, 30-channel time analyser, incorporating square loop ferrite cores and transistor circuitry throughout, was used. It had a facility to provide an initial delay up to a maximum of 20 channel widths. A 100 kc/s quartz-crystal-controlled oscillator was used as a time standard for generating the channel widths. The detector pulses were passed through a "de-randomizer" to ensure exactly equal channel widths. The equality of the channel widths was confirmed to better than 0.1% by random counting. The channel width varied from 10 μs to 1 ms in steps of 10 μs. Counting in each channel was done by a scale of ten followed by a mechanical register. The scale of ten was a ring counter using ferrite memory cores and transistors. The mechanical registers were tested to be working satisfactorily up to 25 counts/s.

The BeO investigated had a mean density of 2.95 g/cm^3 and was in the form of rectangular bricks of size 10 cm × 10 cm × 5 cm (tolerance ± 0.01 cm). The variation in the weight of individual bricks was at most 2%. A total of 2000 bricks was used for the largest assembly weighing about 3 t. The buckling range was 0.0028 cm^{-2} (100 cm × 100 cm × 100 cm) to 0.245 cm^{-2} (40 cm × 30 cm × 30 cm). Throughout the experimental investigation the room temperature was maintained between 75 and 79°F.

CHOICE OF COUNTING RATE, CHANNEL WIDTH, PULSE WIDTH AND DELAY

The counting rate in the first channel was adjusted to be about 30 counts/s (3 mechanical register counts per second) so that the dead-time correction in that channel was less than 1%. Dead-time was due to the de-randomizing unit and was 5 μs. The counting was corrected for dead-time losses.

It can be shown that the statistical accuracy on the decay constant λ for a given counting time depends only on the number of relaxation times over which counts are accumulated and does not depend on the number of channels. The optimum counting period is about two and a half relaxation times. For convenience, ten channels were accommodated in about two and a half relaxation times of the decay.

The counting rate increases with increasing pulse width, an optimum being reached when the pulse width is about twice the relaxation time. Increasing the pulse width beyond this does not result in increased counting rate as the contribution of the earlier portion of the pulse becomes insignificant compared with the contribution of the later part.

An initial delay of approximately three relaxation times was used so that the contribution to the counting from the higher harmonics was negligible compared with the fundamental.

For each buckling, counting was stopped when a total of 100 000 counts were accumulated in the first channel. This was done in three sets, for the purpose of cross-checking.

ELIMINATION OF THE SPACE AND TIME HARMONICS

Space harmonics

The target was arranged at the centre of the top surface of the assembly as shown in Fig. 1. This prevents the excitation of even harmonics along lateral dimensions. The second and third harmonics in the z-direction were

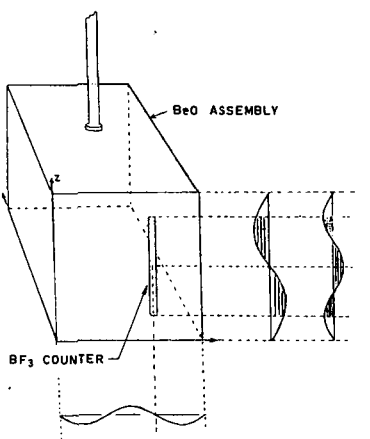

Fig. 1

Arrangement of source and detector in the assembly

eliminated by placing the BF_3 counter vertically; the position and the length of the counter were such that the positive and negative contributions of each harmonic were cancelled. The third harmonic in the x-direction was eliminated by placing the counter at a nodal point. The contribution from the third harmonic in the y-direction was minimized by giving adequate delay. Higher harmonics would be insignificant.

The elimination of the third harmonic was tested as follows. The sum of two exponentials, fundamental and third harmonic, can be considered as a single exponential and a decay constant can be obtained for it. The presence of the third harmonic effectively changes the true value of the fundamental decay constant slightly. However, since the third harmonic dies out faster, the decay constant determined as a function of delay will asymptotically reach a steady value which is the decay constant of the fundamental. This served as a test for checking the presence of higher harmonics also.

Time harmonics

The ratio of the zeroth eigenvalue (fundamental) to the first eigenvalue [8] for our lowest and highest buckling was about 0.1 and 0.3, respectively. The initial delay of three relaxation times was sufficient for the time-harmonic contribution to be negligible.

CALCULATION OF DECAY CONSTANT

The decay constants and their standard deviations were calculated by BEHREN's [11] method (1951) on the CDC-3600 computer. The constant background B was eliminated by the following subtraction method: Let $(C_1 + B)$, $(C_2 + B) \ldots (C_n + B) \ldots (C_{30} + B)$ be the observed counts in 1st, 2nd, ... n-th ... 30th channels, respectively.

$$C_n^1 = (C_n + B) - (C_{n+10} + B) = C_n - C_{n+10}$$

are the counts which are free from background. If T is the channel width, C_0 a constant and λ the decay constant, then

$$\begin{aligned} C_n^1 &= C_0 e^{-\lambda nT} - C_0 e^{\lambda (n+10) T} \\ &= C_0 e^{-\lambda nT} (1 - e^{-10\lambda T}) \\ &= C_0^1 e^{-\lambda nT}, \end{aligned}$$

where $C_0^1 = C_0 (1 - e^{-10\lambda T})$ is also a constant.

Thus the decay constant can be obtained from C_n^1 values. After ten values of C_n^1 were taken, eleven different values of the decay constant were calculated, each with a different initial delay. These decay constants were plotted and the decay constant, free from harmonics, was selected (Fig. 2). The bucklings, the observed decay constants and their standard deviations for various sizes are shown in Table II.

CALCULATION OF DIFFUSION PARAMETERS

The expression for the decay constant is

$$\lambda = \lambda_0 + DB^2 + CB^4 + FB^6 + \text{higher terms},$$

where $\lambda_0 = v \Sigma_a$ (v being the mean velocity of the Maxwellian spectrum at 77°F), D the diffusion coefficient, C the diffusion cooling constant, F the spectrum hardening coefficient and B^2 the buckling. A total of nineteen different sizes was used. Bucklings B^2 were calculated using a trial value of λ_{tr} where

$$\lambda_{tr} = \frac{3D}{v}, \qquad B^2 = \sum_{i=1}^{3} \frac{\pi^2}{(a_i + 2 \times 0.7104\, \lambda_{tr})^2}.$$

The extrapolation distance $0.7104\, \lambda_{tr}$ is only an approximation, which holds good for one-velocity theory. This approximation did not involve any appreciable error for the buckling range studied here. The value of the extrapolation distance to be used in the pulsed neutron work has received some

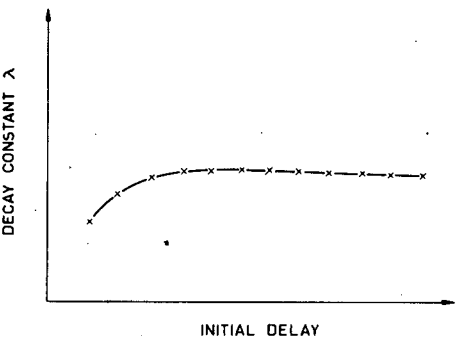

Fig. 2

Variation of decay constant with delay time

theoretical attention also [12, 13]. With these trial bucklings a second-degree least-squares fit was made to calculate λ_0, D and C. From this value of D, a fresh λ_{tr} was obtained to calculate new bucklings and a fresh least-squares fit made. The process was repeated until the two successive λ_{tr} values agreed to better than 0.001 cm. In the least-squares fit the decay constants λ_i were given weights $W_i = (\sigma_{\lambda i})^{-2}$, where $\sigma_{\lambda i}$ was the standard deviation on λ_i.

An estimation of the corrections on λ_0, D and C, due to neglecting the FB^6 contribution when the order of F is known, and their dependence on the buckling B^2 is given in Appendix I.

The equation to the parabola is,

$$\lambda = \lambda_0 + DB^2 + CB^4 .$$

The standard deviations on λ_0, D and C are given by [14]

$$\sigma_{\lambda_0} = \left(\frac{\Sigma w_i \delta_i^2}{N-a} S_{11}\right)^{\frac{1}{2}}$$

$$\sigma_D = \left(\frac{\Sigma w_i \delta_i^2}{N-a} S_{22}\right)^{\frac{1}{2}}$$

$$\sigma_C = \left(\frac{\Sigma w_i \delta_i^2}{N-a} S_{33}\right)^{\frac{1}{2}},$$

where N is the number of points used in the least-squares fit, "a" the number of parameters to be determined, δ_i = (λ_i calculated) - (λ_i observed) and S_{11}, S_{22} and S_{33} are the inverse matrix diagonal elements (Appendix I).

It is therefore seen that (1) for a given B^2 set of measurements the standard deviations on λ_0, D and C are linearly dependent on the standard deviations on the decay constants and (2) the standard deviations on λ_0, D and C have a dependence on B^2 of the nature $\sigma_{\lambda_0} \rightarrow B^0$, $\sigma_D \rightarrow B^{-2}$ and $\sigma_C \rightarrow B^{-4}$ as

TABLE II

DECAY CONSTANTS FOR VARIOUS SIZE ASSEMBLIES

Size (cm)	Buckling B^2 (10^{-2} cm^{-2})	Decay constant λ (s^{-1})	Standard deviations σ_λ (s^{-1})
100 x 100 x 100	0.283065	530.228	1.972
100 x 100 x 90	0.304624	557.419	2.639
100 x 90 x 90	0.326183	592.039	2.343
90 x 90 x 90	0.347742	611.479	1.616
90 x 90 x 80	0.377632	655.010	2.179
90 x 80 x 80	0.407522	687.292	2.417
80 x 80 x 80	0.437412	726.400	2.328
80 x 80 x 70	0.480550	785.231	2.016
80 x 70 x 70	0.523688	846.899	3.277
60 x 60 x 60	0.763484	1140.846	4.596
60 x 60 x 50	0.870165	1265.987	7.130
60 x 60 x 40	1.061245	1528.606	4.803
50 x 50 x 40	1.274608	1780.285	4.670
50 x 40 x 40	1.465688	2004.916	7.649
50 x 50 x 30	1.669847	2238.951	8.719
50 x 40 x 30	1.860928	2444.348	9.740
40 x 40 x 30	2.052008	2700.839	9.489
50 x 30 x 30	2.256167	2911.576	7.888
40 x 30 x 30	2.447248	3139.192	13.597

shown in Appendix II. Thus statistical accuracy on D and C is improved by using small sizes, while the statistical accuracy on λ_0 is independent of size.

For a good determination of C, the average cooling contribution $C\bar{B}^4$ to $\bar{\lambda}$ should be very much larger compared with the average standard deviation

on $\overline{\lambda}$; otherwise large statistical errors, comparable with C itself, are incurred on C, as shown in Appendix III.

For verifying these points, we divided our assemblies into three groups.

(1) 9 large sizes, 100 cm × 100 cm × 100 cm to 80 cm × 70 cm × 70 cm

(2) 10 small sizes, 60 cm × 60 cm × 60 cm to 40 cm × 30 cm × 30 cm

(3) All 19 sizes.

For large sizes, a linear least-squares fit and second-degree least-squares fit were made. For small sizes and all 19 sizes a second-degree least-squares fit was made. The results are shown in Table III.

DISCUSSION

According to CORNGOLD [15], no fundamental exponential decay can exist with a decay constant greater than $(v\Sigma)_{min}$. From the available data this is about 3800 s^{-1} for BeO. Our maximum decay constant, 3139 s^{-1}, is below this limit.

Generally three points are sufficient to determine a parabola. Thus it may be thought that the results for λ_0, D and C, whether determined from 9 large sizes, 10 small sizes or all 19 sizes, should be nearly the same. However, this is not the case as seen from results shown in Table III.

For the nine large sizes which we have considered, the average cooling contribution $C\overline{B}^4$ is of the order of the average standard deviation $\overline{\sigma}_\lambda$; thus very large statistical errors are incurred on λ_0, D and, in particular, on C. Actually this is an overfit and not a case of ill-conditioning as can be seen when a linear fit is made for the same assemblies. The linear-fit results are in agreement, within the statistical errors, with the final results obtained for all 19 sizes (parabolic fit).

The results of 10 small sizes by parabolic fit are also in agreement, within statistical errors, with the final results. However it may be seen that the statistical errors in constants determined from small sizes alone are comparatively large, as expected.

The results of all 19 sizes (9 large and 10 small) have a good balancing effect, that is, they not only allow a good determination of $C(C\overline{B}^4 \gg \sigma_\lambda)$, but the statistical accuracy on λ_0 and D is also improved considerably. Thus by a proper choice of small and large sizes we can achieve a desirable statistical accuracy on λ_0, D and C.

It should be noted that for our smallest assembly, (assuming [4, 10] $F = 1.0 \times 10^6$ cm^6/s) the B^6 correction term FB^6 is of the order of 16 for $\lambda = 3129$, or 0.5%. For larger assemblies it is very much smaller. Thus the average B^6 term, FB^6, is very small and it may be thought that neglecting this term would not result in significant errors on λ_0, D and C. But this is not true. Though the individual FB^6 terms are small, they are all systematic errors in the same direction and their cumulative effect is rather drastic. Our calculations show that, for the case of all 19 sizes, the errors on λ_0, D and C resulting from neglect of this term are $\delta_{\lambda_0 F} = -0.6\%$, $\delta_{DF} = +0.4\%$, $\delta_{CF} = -9\%$, for $F = +10^6$ cm^6/s. Though the highest FB^6 contribu-

TABLE III

DIFFUSION PARAMETERS OBTAINED BY VARIOUS LEAST-SQUARES FITTING METHODS

Assembly range (dimensions in cm)	Number of assemblies	Degree and type of least-squares fit	Absorption constant $\lambda_0 \pm \sigma_{\lambda_0}$ (s^{-1})	Diffusion coefficient $D \pm \sigma_D$ (10^5 cm^2/s)	Diffusion cooling constant $C \pm \sigma_C$ (10^5 cm^4/s)	Diffusion length $L \pm \sigma_L$ (cm)
100 × 100 × 100	9	Linear (first)	165.08 ± 6.33	1.2880 ± 0.0165	-	27.93 ± 0.56
to		Linear, corrected for CB^4 term	157.86 ± 6.33	1.3280 ± 0.0165	-	29.00 ± 0.56
80 × 70 × 70		Parabola (second)	201.16 ± 36.50	1.0953 ± 0.1880	-22.4063 ± 23.5600	23.33 ± 2.95
60 × 60 × 60 to 40 × 30 × 30	10	Parabola (second)	140.04 ± 32.89	1.3589 ± 0.0483	-5.5873 ± 1.6029	31.15 ± 3.70
100 × 100 × 100 to 40 × 30 × 30	19	Parabola (second)	156.02 ± 4.37	1.3334 ± 0.0128	-4.8758 ± 0.5846	29.23 ± 0.43

tion is only 0.5%, the C value is reduced by 9%. If we consider smaller and smaller sizes these errors increase enormously. If we include a size of 25 cm × 20 cm × 20 cm, the C value would be reduced by 50% or half the true value.

This perhaps explains a longstanding discrepancy of different values of the diffusion cooling constant C obtained by various workers for the same moderator. The larger the buckling used, the smaller the value of C obtained, since no correction for the FB^6 contribution is made. This tendency is shown in Table IV for various moderators (if F is assumed positive [4]). The $(v\Sigma)_{min.}$ values for different moderators are shown in Table V. It may be noted that previous experimenters have included values of $\lambda > (v\Sigma)_{min.}$ for Be, BeO and graphite, when analysing their data. This can be another reason for the discrepancy in their C values. However for H_2O and D_2O the maximum values of λ of the experimenters were less than $(v\Sigma)_{min.}$.

In conclusion, for a good determination of C the moderator size must be sufficiently small so that $C\overline{B}^4 \gg \overline{\sigma}_\lambda$, but it should not be so small that the FB^6 correction is very large. An optimum should be chosen to meet the two conflicting requirements. Further, the inclusion of large sizes is in general not necessary for a good determination of C, but it improves the statistical accuracy on λ_0 and D. The maximum value of λ should be less than $(v\Sigma)_{min.}$. A very interesting analysis of pulsed-source measurements is discussed by KOPPEL and LOPEZ [35] and KEEPIN [36].

Our experimental value of λ_{tr} agrees closely with 1.58 cm quoted by SINGWI and KOTHARI [5]. Our final values of the diffusion parameters are

$$\lambda_0 = (156.02 \pm 4.37)\ s^{-1}$$

$$D = (1.3334 \pm 0.0128) \times 10^5\ cm^2/s$$

$$C = (-4.875 \pm 0.584) \times 10^5\ cm^4/s$$

$$L = (29.23 \pm 0.44)\ cm$$

$$\lambda_{tr} = (1.600 \pm 0.016)\ cm$$

The effect of neglecting the contribution of the FB^6 term on the evaluation of the diffusion parameters λ_0, D and C is estimated for three different assumed values of F, using SINGWI's [4] formula as a guide. The results are shown in Table VI. An experimental determination of F is being attempted.

ACKNOWLEDGEMENTS

We are grateful to M.S. Kamath, S.K. Eligar and S.S. Padamadan for their help with electronics, maintenance of the accelerator and the read-outs. We are also grateful to the accelerator staff for running the accelerator, to Krishnan Kutty for programmes on the CDC-3600 and to Miss B.G. Mythili for programmes on TIFRAC computers.

TABLE IV

DISCREPANCIES IN VALUES OF DIFFUSION COOLING CONSTANT FOR VARIOUS MODERATORS

Moderator	Author	Year	Diffusion cooling constant, -C (cm^4/s)	B^2 range (cm^{-2})
Water 22°C	BRACCI and COCEVA [19]	1956	3000 ± 1000	0.09 to 0.96
	DIO [20]	1958	3600 ± 700	0.09 to 0.87
	ANTONOV et al. [21]	1955	4000 ± 1000	0.09 to 0.93
	KÜCHLE [22]	1960	4200 ± 800	0.09 to 0.87
	LOPEZ and BEYSTER [23]	1961	5116 ± 776	0.14 to 0.59
	VON DARDEL and SJÖSTRAND [24]	1954	7300 ± 1500	0.01 to 0.7
Beryllium 1.85 g/cm^3	DE SAUSSURE and SILVER [25]	1959	$(1.40 \pm 1.0) \times 10^5$	0.008 to 0.072
	ANTONOV et al. [21]	1955	$(2.93 \pm 1.0) \times 10^5$	0.008 to 0.061
	KLOVERSTROM et al. [26]	1958	$(3.90 \pm 0.8) \times 10^5$	0.003 to 0.041
Graphite 1.6 g/cm^3 1.7 g/cm^3	ANTONOV et al. [21]	1955	$(12.5 \pm 2.0) \times 10^5$	0.001 to 0.04
	STARR and PRICE [27]	1960	$(12.4 \pm 2.2) \times 10^5$	0.0016 to 0.0275
	BECKURTS [28]	1956	$(16.3 \pm 2.5) \times 10^5$	0.0007 to 0.0055
	KLOSE et al. [29]	1962	$(26.0 \pm 5.0) \times 10^5$	0.0007 to 0.024
	STARR and PRICE [30]	1962	$(34.0 \pm 3.0) \times 10^5$	0.0018 to 0.018
	STARR and DE VILLIERS [31]	1962	$(38.0 \pm 5.0) \times 10^5$	0.0018 to 0.013

TABLE IV (cont.)

Moderator	Author	Year	Diffusion cooling constant, -C (cm^4/s)	B^2 range (cm^{-2})
Heavy water, 20°C	GANGULY and WALTNER [32]	1961	$(3.72 \pm 0.5) \times 10^5$	0.064 to 0.094
Water, 22°C	KUSSMAUL and MEISTER [33]	1963	$(5.25 \pm 0.25) \times 10^5$	0.0013 to 0.047
ZrH	MEADOWS and WHALEN [34]	1962	$(1.58 \pm 0.27) \times 10^5$	0.03 to 0.11
	B^8 fit		$(2.12 \pm 0.35) \times 10^5$	0.03 to 0.39

TABLE V

$(v\Sigma)_{min.}$ VALUES FOR VARIOUS MODERATORS

Moderator	$(v\Sigma)_{min.}$ (s^{-1})
H_2O [15]	300 000
Be [15]	3 800
Graphite [15]	2 600
BeO	3 800
D_2O	500 000

We thank the Commissariat à l'Energie Atomique for the beryllium oxide bricks which were made in France under the general agreement between the Commissariat and the Indian Atomic Energy Commission for the study of beryllium oxide as a moderator.

We gratefully thank Dr. R. Ramanna for his valuable guidance, helpful suggestions, continued interest and constant encouragement, without which this paper would not have been possible, and also Dr. Ajoy Ghatak for interesting discussions.

APPENDIX I

The least squares normal equations for the estimation of λ_0, D and C are

$$\Sigma w\lambda = \lambda_0 \Sigma w + D\Sigma wB^2 + C\Sigma wB^4$$

$$\Sigma wB^2\lambda = \lambda_0 \Sigma wB^2 + D\Sigma wB^4 + C\Sigma wB^6$$

$$\Sigma wB^4\lambda = \lambda_0 \Sigma wB^4 + D\Sigma wB^6 + C\Sigma wB^8$$

Let the matrix be denoted by

$$\Delta = \begin{bmatrix} \Sigma w & \Sigma wB^2 & \Sigma wB^4 \\ \Sigma wB^2 & \Sigma wB^4 & \Sigma wB^6 \\ \Sigma wB^4 & \Sigma wB^6 & \Sigma wB^8 \end{bmatrix}$$

The inverse matrix elements S_{lm} are obtained by taking co-factors of lm and dividing by the determinant Δ

TABLE VI

COMPARISON OF LEAST-SQUARE FITTED DIFFUSION PARAMETERS WITH AND WITHOUT THE FB^6 TERM FOR THREE ASSUMED VALUES OF F

Assembly range (dimensions in cm)	Assumed F-value	$\lambda_0 \pm \sigma_{\lambda_0}$ (s^{-1})	$\delta\lambda_{0F}$ (s^{-1})	$(D \pm \sigma_D)$ (10^5 cm^2/s)	δ_{DF} (10^5 cm^2/s)	$(-C \pm \sigma_C)$ (10^5 cm^4/s)	δ_{CF} (10^5 cm^4/s)
100 × 100 × 100	0	156.02 ± 4.37	-	1.3334 ± 0.0128	-	4.8758 ± 0.5846	-
	1×10^6	155.23 ± 4.37	-0.79	1.3368 ± 0.0128	0.0033	5.2286 ± 0.5846	-0.3528
to	2×10^6	154.44 ± 4.37	1.58	1.3401 ± 0.0128	0.0067	5.5814 ± 0.5846	-0.7057
40 × 30 × 30	3×10^6	153.64 ± 4.37	-2.38	1.3434 ± 0.0128	0.0100	5.9342 ± 0.5846	-1.0585
60 × 60 × 60	0	140.04 ± 32.89	-	1.3585 ± 0.0483	-	5.5873 ± 1.6029	-
	1×10^6	137.37 ± 32.89	-2.67	1.3648 ± 0.0483	0.0063	6.0372 ± 1.6029	-0.4499
to	2×10^6	134.70 ± 32.89	-5.34	1.3710 ± 0.0483	0.0125	6.4871 ± 1.6029	-0.8997
40 × 30 × 30	3×10^6	132.03 ± 32.89	-8.01	1.3773 ± 0.0483	0.0188	6.9369 ± 1.6029	-1.3496

$$S_{lm} = \frac{\text{co-factor of lm}}{\Delta} \qquad l, m, = 1, 2, 3$$

$$S_{11} = \frac{(\Sigma wB^4 \Sigma wB^8 - \Sigma wB^6 \Sigma wB^6)}{\Delta}$$

$$S_{12} = -\frac{(\Sigma wB^2 \Sigma wB^8 - \Sigma wB^6 \Sigma wB^4)}{\Delta}$$

$$S_{13} = \frac{(\Sigma wB^2 \Sigma wB^6 - \Sigma wB^4 \Sigma wB^4)}{\Delta}$$

Similarly S_{21}, S_{22}, S_{23}, S_{31}, S_{32}, S_{33} can be obtained. The inverse matrix is denoted by

$$\Delta^{-1} = \begin{bmatrix} S_{11} & S_{12} & S_{13} \\ S_{21} & S_{22} & S_{23} \\ S_{31} & S_{32} & S_{33} \end{bmatrix}$$

$$\lambda_0 = \Sigma w\lambda S_{11} + \Sigma w\lambda B^2 S_{12} + \Sigma w\lambda B^4 S_{13}$$

$$D = \Sigma w\lambda S_{21} + \Sigma w\lambda B^2 S_{22} + \Sigma w\lambda B^4 S_{23}$$

$$C = \Sigma w\lambda S_{31} + \Sigma w\lambda B^2 S_{32} + \Sigma w\lambda B^4 S_{33}$$

To make allowance for the contribution of the FB^6 term we replace λ by $(\lambda - FB^6)$ in these equations to a first approximation. The matrix Δ and inverse matrix Δ^{-1} remain unchanged as their elements are independent of λ. The new diffusion parameters obtained are denoted by λ_0', D' and C'

$$\lambda_0' = \Sigma w(\lambda - FB^6) S_{11} + \Sigma w(\lambda - FB^6) B^2 S_{12} + \Sigma w(\lambda - FB^6) B^4 S_{13}$$

$$D' = \Sigma w(\lambda - FB^6) S_{21} + \Sigma w(\lambda - FB^6) B^2 S_{22} + \Sigma w(\lambda - FB^6) B^4 S_{23}$$

$$C' = \Sigma w(\lambda - FB^6) S_{31} + \Sigma w(\lambda - FB^6) B^2 S_{32} + \Sigma w(\lambda - FB^6) B^4 S_{33}$$

Therefore

$$\delta_{\lambda_0 F} = \lambda_0' - \lambda_0 = -F(\Sigma wB^6 S_{11} + \Sigma wB^8 S_{12} + \Sigma wB^{10} S_{13})$$

$$\delta_{DF} = D' - D = -F(\Sigma wB^6 S_{21} + \Sigma wB^8 S_{22} + \Sigma wB^{10} S_{23})$$

$$\delta_{CF} = C' - C = -F(\Sigma wB^6 S_{31} + \Sigma wB^8 S_{32} + \Sigma wB^{10} S_{33})$$

If a substitution is made for S_{11}, S_{12}... S_{33} etc. we see the dependence of these errors is related to buckling B^2 as follows:

$$\delta_{\lambda_0 F} \rightarrow B^6$$

$$\delta_{DF} \rightarrow B^4$$

$$\delta_{CF} \rightarrow B^2$$

APPENDIX II

From the expression for S_{11} given in Appendix I, it is seen that S_{11} has a dependence on B^2 to the zeroth power. Similarly, $S_{22} \rightarrow B^{-4}$ and $S_{33} \rightarrow B^{-8}$. Now [8]

$$\sigma_{\lambda_0} \propto (S_{11})^{\frac{1}{2}} \propto (B^0)^{\frac{1}{2}} \propto B^0$$

$$\sigma_D \propto (S_{22})^{\frac{1}{2}} \propto (B^{-4})^{\frac{1}{2}} \propto B^{-2}$$

$$\sigma_C \propto (S_{33})^{\frac{1}{2}} \propto (B^{-8})^{\frac{1}{2}} \propto B^{-4}$$

APPENDIX III

$$\overline{\lambda} = \lambda_0 + D\overline{B^2} + C\overline{B^4}$$

where the bars indicate average. By the law of proportion of errors

$$\overline{\sigma^2_{\lambda C}} = \sigma^2_{\lambda_0} + (\overline{B^2}\sigma_D)^2 + (\overline{B^4}\sigma_C)^2$$

Let the average cooling term be expressed in terms of $\overline{\sigma}_\lambda$ as $C\overline{B^4} = N\overline{\sigma_\lambda}$, where N is a number. Then

$$\overline{\sigma^2_{\lambda C}} = \sigma^2_{\lambda_0} + (\overline{B^2}\,\sigma_D)^2 + \left(\frac{N}{C}\,\overline{\sigma}_\lambda \,.\sigma_C\right)^2$$

and

$$\sigma_C^2 = \frac{\overline{\sigma^2_{\lambda C}} - (\sigma^2_{\lambda_0} + \overline{B^2}\,\sigma^2_D)}{\overline{\sigma^2_\lambda}} \times \frac{C^2}{N^2}$$

If N is not a sufficiently large number $\sigma_C \gtrsim C$, where C is the true value of the diffusion cooling constant.

REFERENCES

[1] KOECHLIN, J.C. et al., Proc. UN Int. Conf. PUAE 5 (1956) 20-23.
[2] IYENGAR, S.B.D. et al., Proc. Ind. Ac. Sci. XLV (1957) 215.
[3] ZHEZHERUN, I.F., J. nucl. Energy A/B 18 (1964) 279.
[4] SINGWI, K.S., Ark. Fys. 19 (1960) 147.
[5] SINGWI, K.S. and KOTHARI, L.S., Proc. 2nd. UN Int. Conf. PUAE 16 (1958) 325.
[6] NELKIN, M., J. nucl. Energy 8 (1958) 48.
[7] SINGWI, K.S. and KOTHARI, L.S., J. nucl. Energy 8 (1958) 59.
[8] PUROHIT, S.N., Nucl. Sci. Engng 9 (1961) 157.
[9] NELKIN, M., Nucl. Sci. Engng 7 (1960) 210.
[10] WILLIAMS, M.M.R., Proc. Brookhaven Conf. on Neutron Thermalisation, BNL 719 4 (1962) 1331.
[11] BEHRENS, D.J., AERE Rpt. T/R-629 (1951).
[12] WILLIAMS, M.M.R., J. nucl. Energy A/B 17 (1963) 55.
[13] GELBARD, E.M. and DAVIS, J.A., Nucl. Sci. Engng 13 (1962) 237.
[14] DEMING, W.E., Statistical Analysis of Data, John Wiley and Co., N.Y. (1943).
[15] CORNGOLD, N., Nucl. Sci. Engng 19 (1964) 91.
[16] FERMI, E. et al., Phys. Rev. 71 (1947) 589.
[17] WHITTEMORE, W.L. and McREYNOLDS, A.W., Rpt. GA-1687 (1960).
[18] BHANDARI, R.C. et al., J. nucl. Energy 7 (1958) 45.
[19] BRACCI, A. and COCEVA, C., Nuovo Cim. 4 X (1956) 59.
[20] DIO, W.H., Nukleonik 2 (1958) 131.
[21] ANTONOV, A.V. et al., Proc. UN Int. Conf. PUAE 5 (1956) 3-13.
[22] KÜCHLE, M., Nukleonik 2 (1960) 131.
[23] LOPEZ, W.M. and BEYSTER, J.R., Nucl. Sci. Engng 12 (1962) 190.
[24] VON DARDEL, G.F. and SJÖSTRAND, N.G., Phys. Rev. 96 (1954) 1245.
[25] DE SAUSSURE, G. and SILVER, E.G., Rpt. ORNL-2641, (1959).
[26] KLOVERSTROM, F. and KOMOTO, T.T., Trans. Amer. nucl. Soc. 1 1 (1958).
[27] STARR, E. and PRICE, G.A., Trans. Amer. nucl. Soc. 2 2 (1959) 125.
[28] BECKURTS, K.H., Nucl. Sci. Engng 2 (1957) 516.
[29] KLOSE, H. et al., Proc. Brookhaven Conf. on Neutron Thermalisation,BNL 719 3 (1962) 935.
[30] STARR, E. and PRICE, G.A., Proc. Brookhaven Conf. on Neutron Thermalisation,BNL 719 3 (1962) 1034.
[31] STARR, E. and DE VILLIERS, J.W.L., Proc. Brookhaven Conf. on Neutron Thermalisation, BNL-719 3 (1962) 997.
[32] GANGULY, N.K. and WALTNER, A.W., Trans. Amer. nucl. Soc. 4 2 (1961) 282.
[33] KUSSMAUL, G. and MEISTER, H., J. nucl. Energy A/B, 17 (1963) 411.
[34] MEADOWS, J.W. and WHALEN, J.F., Nucl. Sci. Engng 13 (1962) 230.
[35] KOPPEL, J.U. and LOPEZ, W.M., Proc. Brookhaven Conf. on Neutron Thermalisation, BNL 719 3 (1962) 946.
[36] KEEPIN, G.R., Atomic Energy Review 2 2 (1964) 75.

MEASUREMENTS AND CALCULATIONS OF THE SLOWING-DOWN AND MIGRATION TIME

A.E. PROFIO AND J.U. KOPPEL
GENERAL ATOMIC DIVISION OF GENERAL DYNAMICS CORPORATION,
JOHN JAY HOPKINS LABORATORY FOR PURE AND APPLIED SCIENCE,
SAN DIEGO, CALIF.
AND
A. ADAMANTIADES
MASSACHUSETTS INSTITUTE OF TECHNOLOGY, CAMBRIDGE, MASS.
UNITED STATES OF AMERICA

Abstract — Résumé — Аннотация — Resumen

MEASUREMENTS AND CALCULATIONS OF THE SLOWING-DOWN AND MIGRATION TIME. The mean time and variance in time for neutrons from an impulse source to slow down and migrate to the energy, angle and position of observation are important quantities in many experiments. The mean time is a correction in time-of-flight measurements of neutron spectra in bulk media, and the variance limits the ultimate resolution of such experiments. These parameters are equally significant in detectors which depend on moderation, in time-of-flight experiments where low energy neutrons are provided by a moderator placed near the pulsed source, and in slowing-down-time spectrometry.

Various analytical and numerical methods have been developed to calculate the space-energy-angle-time dependence, or integrals thereof. It is shown that the time moments,

$$\phi^{(n)}(\vec{r}, \vec{\Omega}, v, t) = \int_0^\infty t^n \phi(\vec{r}, \vec{\Omega}, v, t)\,dt,$$

can be calculated by repeated application of a steady state transport code. The source term for the calculation of the n^{-th} moment is equal to $nv^{-1}\phi^{(n-1)}$. Results are presented for multiplying and non-multiplying mock-ups of the TRIGA reactor. Another powerful calculational method is the time-dependent Monte Carlo code. Results of a calculation of leakage flux from a thin lead slab are presented.

Measurements have been made of the slowing-down time to the cadmium edge and to the 1.46-eV resonance of indium in water and in toluene. Capture gamma rays are detected by a scintillation counter. The technique requires a fairly intense source and efficient detector because of the low duty cycle (short burst width for resolution of the slowing-down time, large interpulse period for thermal neutron die-away) and the small probability for capture.

MESURES ET CALCUL DU TEMPS DE RALENTISSEMENT ET DE MIGRATION. Dans le phénomène de ralentissement et de migration des neutrons pulsés, amenés à l'énergie, à l'angle et à la position d'observation, le temps moyen et la variance en temps sont des grandeurs importantes pour beaucoup d'expériences. Le temps moyen est une correction pour les mesures par la méthode du temps de vol des spectres de neutrons dans des milieux de grande diffusion, et la variance a pour effet d'imposer une limite à la résolution des expériences. La grandeur de ces paramètres est également importante pour les détecteurs qui dépendent du ralentissement, dans les expériences par la méthode du temps de vol où des neutrons de faible énergie sont fournis par un ralentisseur placé près de la source pulsée, et en spectrométrie du temps de ralentissement.

Diverses méthodes analytiques et numériques ont été mises au point pour calculer la fonction espace-énergie-angle-temps ou des intégrales de cette fonction. Les auteurs montrent que les moments

$$\phi^{(n)}(\vec{r}, \vec{\Omega}, v, t) = \int_0^\infty t^n \phi(\vec{r}, \vec{\Omega}, v, t)\,dt$$

peuvent être calculés par application répétée d'un code de transport pour un état stationnaire. Le terme de la source pour le calcul du nième moment est égal à $nv^{-1}\phi^{(n-1)}$. Les auteurs présentent des résultats pour des modèles multiplicateurs et non multiplicateurs du réacteur Triga. Une autre méthode de calcul très utile est

le code de Monte-Carlo variable dans le temps. Les auteurs présentent les résultats d'un calcul de flux de fuite à partir d'une mince plaque de plomb.

Les auteurs ont mesuré le temps de ralentissement jusqu'au seuil cadmium et jusqu'à la résonance 1,46 eV de l'indium dans l'eau et dans le toluène. Ils ont décelé les rayons gamma de capture avec un compteur à scintillation. La méthode nécessite l'utilisation d'une source assez intense et d'un détecteur efficace à cause de la brièveté du cycle de fonctionnement (petite largeur de bouffée pour la résolution du temps de ralentissement, grand intervalle entre les bouffées pour l'évanouissement des neutrons thermiques) et de la faible probabilité de capture.

ИЗМЕРЕНИЯ И РАСЧЕТЫ ВРЕМЕНИ ЗАМЕДЛЕНИЯ И МИГРАЦИИ. Среднее время и изменение во времени жизни нейтронов, получаемых от импульсного источника, с целью их замедления и миграции до величины энергии, угла и положения, удобного для наблюдения, являются существенными количественными величинами во многих экспериментах. Среднее время является поправкой в измерениях нейтронных спектров по методу времени пролета в больших объемах материалов, а изменение ограничивает максимальную разрешающую способность таких экспериментов. Эти параметры одинаково важны в детекторах, зависящих от замедления, в экспериментах по времени пролета, где нейтроны с малой энергией поступают из замедлителя, находящегося вблизи пульсирующего источника, а также спектрометрии времени замедления.

Разработаны различные аналитические и цифровые способы для вычисления зависимости пространственного-энергетического-углового и временного распределения или интегралов по ним. Показано, что моменты времени

$$\phi^{(n)}(\vec{r}, \vec{\Omega}, v, t) = \int_0^\infty t^n \phi(\vec{r}, \vec{\Omega}, v, t)dt$$

можно высчитать путем повторного применения программы расчета для стационарного состояния переноса. Условие источника для вычисления момента "n" равно $nv^{-1}\phi^{(n-1)}$. Приводятся результаты для размножающих и неразмножающих моделей реактора "Трига". Другим методом энергетического расчета является метод временной зависимости Монте Карло. Даются также результаты вычисления потока утечки из тонкой свинцовой пластины.

Измерения проводили на замедлении по времени по отношению кадмиевой грани и резонанса в 1,46 эв индия в воде и толуоле. Захватное гамма-излучение детектируется с помощью сцинтилляционного счетчика. Этот метод требует исключительно интенсивного источника и эффективного детектора в связи с низкой полезно используемой долей времени цикла (короткая продолжительность вспышки для разрешающей способности замедления, большой период промежуточного пульса для затухания тепловых нейтронов) и небольшой вероятности для захвата.

MEDICION Y CALCULO DEL TIEMPO DE MODERACION Y DE MIGRACION. En muchos experimentos, reviste gran importancia el tiempo medio que transcurre hasta que la velocidad de los neutrones pulsados disminuya en la medida necesaria para que éstos alcancen la energía, el ángulo y la posición de observación apetecidas. El tiempo medio es una corrección de las mediciones de espectros neutrónicos en la masa hechas según el método del tiempo de vuelo, y la variación impone límites al poder de resolución efectivo de tales experimentos. Estos parámetros son igualmente importantes en los detectores cuyo funcionamiento se base en la moderación, en los experimentos con el método de tiempo de vuelo en los que un moderador situado cerca de la fuente de neutrones pulsados proporciona neutrones de baja energía, y en la espectrometría del tiempo de moderación.

Se han ideado diversos métodos analíticos y numéricos para calcular la distribución espacio-energía ángulo-tiempo o sus integrales. Ha podido demostrarse que los momentos temporales

$$\phi^{(n)}(\vec{r}, \vec{\Omega}, v, t) = \int_0^\infty t^n \phi(\vec{r}, \vec{\Omega}, v, t)\, dt,$$

pueden calcularse aplicando repetidamente una clave de transporte en régimen estacionario. El término de la fuente para el cálculo del momento « n »es igual a $nv^{-1}\phi^{(n-1)}$. Los autores presentan los resultados correspondientes a maquetas del reactor TRIGA en las que se emplean medios multiplicadores y no multiplicadores. Otro valioso método de cálculo consiste en emplear una clave de Monte Carlo en función del tiempo. Los autores exponen los resultados del cálculo de un flujo que escapa de una delgada placa de plomo.

Se han hecho mediciones del tiempo de moderación hasta la energía de corte del Cd y hasta la resonancia de 1, 46 eV del In en agua y en tolueno. Los rayos gamma de captura se detectaron con un contador de centelleo. Esta técnica exige disponer de una fuente de suficiente intensidad y de un detector eficaz debido a la brevedad del ciclo de trabajo (escasa anchura de las ráfagas para la resolución del tiempo de moderación y amplio intervalo entre los impulsos para observar la atenuación neutrónica de carácter térmico) y a las escasas probabilidades de captura.

1. INTRODUCTION

In many pulsed neutron experiments it is important to know the mean time for neutrons to slow down and migrate to the energy, angle and position of observation. It is often important to know the spread about the mean as well. For example, in the pulsed source, time-of-flight method for measuring spectra in bulk media, the mean time of emission (leakage) into the flight path is subtracted from the measured time delay to obtain the flight time. The variance in emission time may well be the largest component in the time uncertainty, which in turn determines the resolution attainable.

Another example of where the emission time must be known is in the design of a moderator to obtain neutrons at lower energies than are emitted by the pulsed source itself, e.g. an accelerator target or pulsed reactor. The size and composition of the moderator are chosen to balance the efficiency for moderation against the time delay and spread.

Detectors are sometimes provided with a moderator to slow down neutrons to lower energies where they may be more efficiently captured. In this case the mean time-to-capture and deviation, and the capture efficiency, are the quantities of interest. If the detector is used in a time-of-flight experiment, the moderator should be designed for best overall efficiency at a given time resolution.

In slowing-down-time spectrometry, the quantities desired are the average energy and relative deviation in energy as a function of time, or better still the time-dependent scalar flux $\phi(\vec{r}, v, t)$.

In this paper we review and extend calculations of neutron slowing-down and spatial migration, discuss experimental techniques, and compare theoretical with experimental results, where this can be done. We are primarily concerned with free-atom scattering without upscattering or multiplication, although examples are given of applications to thermal multiplying media as well. The discussion is divided for convenience into theory versus experiment, and into space-independent versus space-dependent theory.

2. THEORY

2.1. Space-independent theory

The space-independent problem arises when the volume-integrated flux in an infinite medium, or the local flux in an infinite medium with a uniformly distributed source density, is considered.

(a) Analytical methods

Formally, it is always possible to reduce a time-dependent problem to an equivalent stationary one by taking the Laplace transform. Under certain simplifying assumptions, it is possible to obtain an analytical solution for the inverse transform [1, 2]:

(1) Elastic scattering only, isotropic in the centre-of-mass system.
(2) Constant scattering mean free path, $\ell = \Sigma_s^{-1}$ = constant.
(3) No capture or multiplication, or else 1/v capture.
(4) Unit monoenergetic impulse source $q_0 = \delta(v - v_0)\delta(t)$, 1 n/cm^3 s (this is not a real restriction since other sources can be handled by superposition).
(5) Single nucleus, mass divided by neutron mass = A.
(6) $v \ll v_0$, where v_0 is the source velocity,

For hydrogen (A = 1), and $\Sigma_a = 0$, an exact solution can be obtained,

$$\phi(v,t) = \left(\frac{vt}{\ell}\right)^2 e^{-\frac{vt}{\ell}}\left(1 - \frac{v}{v_0} + \frac{2\ell}{v_0 t}\right) \tag{1}$$

for the collided flux. The solution was obtained explicitly by MARSHAK [2], who also gave an expression for the case Σ_s = constant/v. In the following we consider the "asymptotic" solution, where $v_0 \gg v$, $v_0 \gg 2\ell/t$ and hence Eq. (1) is independent of v_0.

The slowing-down time to a given velocity is often defined as the time-of-maximum,

$$t_m = 2\frac{\ell}{v}. \tag{2}$$

The mean time, or first time-moment, however, is

$$\langle t \rangle = \frac{\int_0^\infty t\phi(v,t)dt}{\int_0^\infty \phi(v,t)\,dt} = \frac{\phi^{(1)}}{\phi^{(0)}} = 3\frac{\ell}{v} \tag{3}$$

The time-integrated flux $\phi^{(0)} = 2\ell/v$, which converted to the more familiar flux per unit energy is seen to equal the stationary solution $\phi(E) = 1/\Sigma_s E$, as it must. The second time-moment is

$$\langle t^2 \rangle = \frac{\int_0^\infty t^2\phi(v,t)dt}{\int_0^\infty \phi(v,t)dt} = \frac{\phi^{(2)}}{\phi^{(0)}} = 12\left(\frac{\ell}{v}\right)^2. \tag{4}$$

The variance is

$$\sigma^2 = \langle t^2 \rangle - \langle t \rangle^2 = 3\left(\frac{\ell}{v}\right)^2 \tag{5}$$

and the relative deviation,

$$\frac{\sigma}{\langle t \rangle} = \frac{\sqrt{3}}{3} . \tag{6}$$

BECKURTS and WIRTZ [3] derive the corresponding integrals for the mean velocity and energy (and mean squared velocity and energy) versus time, with the normalization

$$\int_0^\infty n(v,t)dv = \int_0^\infty \frac{\phi(v,t)}{v} dv = 1. \tag{7}$$

They obtain

$$\langle E \rangle = 3m\left(\frac{\ell}{t}\right)^2 \tag{8}$$

and

$$\frac{\Delta E}{E} = \frac{\sqrt{\langle E^2 \rangle - \langle E \rangle^2}}{\langle E \rangle} = \sqrt{\frac{7}{3}}. \tag{9}$$

For heavier elements, approximate solutions can be obtained by synthesis from the time-moments. However, the moments are known exactly, and often only the first and second moments are required. These are given in Table I in terms of the parameter

$$x = vt/\ell . \tag{10}$$

It can be seen that the mean time increases with A as does the variance, but the relative deviation is smaller for larger A. Thus in slowing-down-time spectrometry, it is advantageous to make A as large as possible, and lead (A = 207) is usually chosen [4, 5]. However, it is not feasible to make a lead block effectively infinite, and the decrease in flux due to leakage has to be considered. This has been done within the framework of the age theory.

The time-to-maximum has been found [1] to be given very nearly by

$$t_m = \frac{A\ell}{v} (A > 1) \tag{11}$$

and for heavy elements $t_m = \langle t \rangle$. For $A \ll 1$ the slowing-down spectrum is

TABLE I

Time Moments in Infinite Medium, $\sum_s$ = Const. $\sum_a = 0$

	General A	A = 1	A>>1
$\langle x \rangle$	$\frac{3A(A+1)}{3A-1}$	3	A
$\langle x^2 \rangle$	$\frac{3(A+1)^3}{3A-1}$	12	A^2
$\frac{\sigma(x)}{\langle x \rangle}$	$\frac{\sqrt{3(2A-1)}}{3A}$	$\sqrt{\frac{3}{3}}$	$\sqrt{\frac{2}{3A}}$

essentially a narrow Gaussian distribution whose average energy decreases with time [3] according to

$$\langle E \rangle \cong \frac{m}{2}\left(\frac{A\ell}{t}\right)^2 \tag{12}$$

and

$$\frac{\Delta E}{E} \cong \sqrt{\frac{8}{3A}} \tag{13}$$

The first and second time-moments (defined for the slowing-down density rather than the flux) have been calculated by KOSALY and NEMETH [6] for heavy moderators with zero absorption and arbitrary variation of the scattering mean free rate with energy. ERIKSSON [7] has derived expressions for the moments with $\Sigma_s = \text{const.}/v^n$, where n is any positive integer.

For 1/v capture, it is always true for an impulse source that

$$\phi(v,t) = \phi_0(v,t)e^{-v\Sigma_a t} \quad , \tag{14}$$

where ϕ_0 refers to the solution with zero absorption. This can be verified by substituting Eq. (14) into the time-dependent Boltzmann equation with absorption, and noticing that it reduces to the equation without absorption. Absorption decreases $\langle t \rangle$ and σ.

The theoretical results are compared with experiment in section 3.

(b) Stepwise integration of the diffusion equation

It is possible to solve the time-dependent transport equation numerically by direct stepwise integration over the time variable as with the other variables. This has been done [8, 9] in the diffusion approximation. Results are presented for $\phi(v,t)$ in infinite non-absorbing water, and the reaction rate curves R(t) for cadmium and gadolinium absorbers in the water.

(c) Time-dependent Monte Carlo calculation

Infinite medium calculations have been carried out [10] in a mixture HCd_α ($\alpha = 0.001$ to 0.01) to obtain the time-response for captures in cadmium dissolved in a large liquid scintillation detector. The Monte Carlo technique is discussed in more detail in section 2.2(c).

2.2. Space-dependent theory

The migration of neutrons, hence the space-dependence, becomes important whenever the flux is observed as a function of distance from a localized source, or in any finite medium. The more powerful methods developed for these problems can, of course, be applied to the space-independent situation as well. In particular, the volume-integrated solution must equal the infinite medium result.

(a) Analytical methods

DYAD'KIN and BATALINA [11] obtained a solution for the space-energy-time distribution about a point isotropic source in an infinite homogeneous medium, under the assumptions of constant mean free path and isotropic elastic scattering. Numerical results are presented for the time-dependent flux at 1.46 eV (indium resonance energy) in water and water-sand mixtures, as a function of distance up to 30 cm.

CLAESSON [12] obtained results for plane and point isotropic sources in an infinite medium, evaluating the density at 1.46 eV for distances in water up to 20 cm from the source. Constant mean free path and isotropic scattering were assumed, but the calculation of the spatial dependence was improved by use of a transport mean free path.

A hydrogen cross-section varying as $1/v$ was assumed by SYKES [13] who calculated $\langle t \rangle$ and σ for a plane isotropic source in an infinite medium, again for isotropic elastic scattering.

The Claesson calculations, for example, clearly show the importance of migration in the time distribution. For a point source, t_m varies from $0.7\,\mu s$ at $r = 0$ to $1.65\,\mu s$ at $r = 20$ cm. The volume-integrated value from Eq.(2) is $0.87\,\mu s$.

(b) Time moments

The time-dependent Boltzmann equation for the neutron flux from an impulse source may be written as

$$\frac{1}{v}\frac{\partial \phi}{\partial t}(\vec{r}, v, \vec{\Omega}, t) = H\phi + S(\vec{r}, v, \vec{\Omega})\,\delta(t), \tag{15}$$

where H is a time-dependent operator such that $H\phi$ is

$$-\vec{\Omega}\cdot\nabla\phi - \Sigma_T\phi + \int dv' \int d\Omega' \Sigma_s(v' \to v, \vec{\Omega}' \to \vec{\Omega})\phi. \tag{16}$$

Taking the Laplace transform with respect to time yields

$$H\bar{\phi}(\vec{r}, v, \vec{\Omega}, s) + S(\vec{r}, v, \vec{\Omega}) - \frac{s}{v}\bar{\phi}(\vec{r}, v, \vec{\Omega}, s) = 0, \tag{17}$$

if $\phi = 0$ at $t = 0$. The n-th moment of the flux is defined as

$$\langle t^n \rangle = \frac{\int_0^\infty t^n \phi(\vec{r}, v, \vec{\Omega}, t)dt}{\int_0^\infty \phi(\vec{r}, v, \vec{\Omega}, t)dt} = \frac{\phi^{(n)}}{\phi^{(0)}}, \tag{18}$$

From the Laplace transform

$$\int_0^\infty e^{-st} t^n \phi(t)dt = (-1)^n \left[\frac{\partial^n \bar{\phi}(s)}{\partial s^n}\right] \tag{19}$$

we have

$$\phi^{(n)} = (-1)^n \lim_{s \to 0} \left[\frac{\partial^n \bar{\phi}(s)}{\partial s^n}\right] \tag{20}$$

Differentiating Eq. (17) n times with respect to s and letting s go to zero allows one to find the recursion relations

$$H\phi^{(n)} + \frac{n}{v}\phi^{(n-1)} = 0 \tag{21a}$$

$$H\phi^{(0)} + S(\vec{r}, v, \vec{\Omega}) = 0 \tag{21b}$$

The procedure for obtaining the moments in the case of an impulse source is then to solve the identical problem with a steady source $S(\vec{r}, v, \vec{\Omega})$, obtaining the time-integrated flux or $\phi^{(0)}$. Since Eq. (21a) is identical with Eq. (21b), if the source is replaced by

$$S^{(n)} = \frac{n}{v}\phi^{(n-1)}, \tag{22}$$

we see that any moment can be obtained by iteration. The procedure can be applied with any calculational method suitable for the stationary problem, allowing for scaling in the computer if this becomes necessary. Although implicit in the work of KOPPEL [1], the generality of the method does not appear to have been widely appreciated.

In many transport codes the scattering kernel and also the source are expressed in terms of coefficients of spherical harmonics, or in one-dimension, Legendre polynomials:

$$S(\vec{r}, v, \vec{\Omega}) = \sum_{\ell} \frac{2\ell+1}{2} P_{\ell}(\mu) S_{\ell}(\vec{r}, v) \qquad (23)$$

To apply Eq. (21a) to find $\phi^{(1)}$, it is necessary to express $\phi^{(0)}$ in its P_{ℓ} components, e.g. it is not correct to use merely the scalar flux.

Examples of time-moment calculations are given in Fig. 1, for an assembly representing a mock-up intended for measurements of the neutron spectrum bythe time-of-flight. The assembly considered is a 70-element TRIGA Mark III core surrounded by a 5-cm thick water reflector. To reduce the number of thermal fissions, the reactor was poisoned either with a solution of cadmium nitrate (75% of saturation) in the core and reflector, or with 0.75-mm thick cadmium sleeves around the fuel elements. The Linac target which would be used in the experiment was represented by an impulse source with a fission spectrum, distributed in a 4.3-cm diameter uranium sphere at the centre of the core.

Neutron cross-sections below 2.38 eV were generated by the GATHER code [14]. The scattering kernel used in the code properly describes the scattering from hydrogen as bound in water and in zirconium hydride. Cell disadvantage factors were obtained from a P_1, S_4 calculation with the GAPLSN code [15]. Fast cross-sections were generated from a B_1 calculation using the GAM code [16]. The stationary flux $\phi^{(0)}$ was calculated for an equivalent spherical geometry in P_1, S_4 with GAPLSN, and $\phi^{(1)}$ and higher moments were obtained as discussed above. The moments were calculated throughout the assembly but only leakage is considered here.

In the figure $<t>$ is plotted versus lethargy ($u = 0$ at 10 MeV) for three cases: a cadmium sleeve poisoned multiplying assembly, the same with ν arbitrarily set to zero (non-multiplying), and the cadmium solution poisoned assembly. The large increase in $<t>$ due to recycling through thermal fission is evident, even with the poison. Cadmium in the water, especially in the reflector, decreases the mean emission time but it is still about 10 μs. The deviation $\sigma = \sqrt{<t^2> - <t>^2}$ for the poisoned solution case is also shown in Fig. 1, and is seen to be large so that very long flight paths would be required for good energy resolution in a time-of-flight measurement.

(c) Monte Carlo

The Monte Carlo method is especially useful for calculations in small assemblies (in terms of mean free paths) or in highly absorbing materials, where the neutrons make only a few collisions during their lifetime. The computation time is then not too large, and furthermore in these systems ordinary transport calculation may not be very reliable. The time-dependence is incorporated in a Monte Carlo code by:

(1) Setting $t = 0$ in the source particle generator,

(2) After choosing the distance d to the next collision from the exponential distribution of free paths about the mean free path, calculating the flight time $\Delta t = d/v$ and adding it to the total time the neutron has lived since starting from the source.

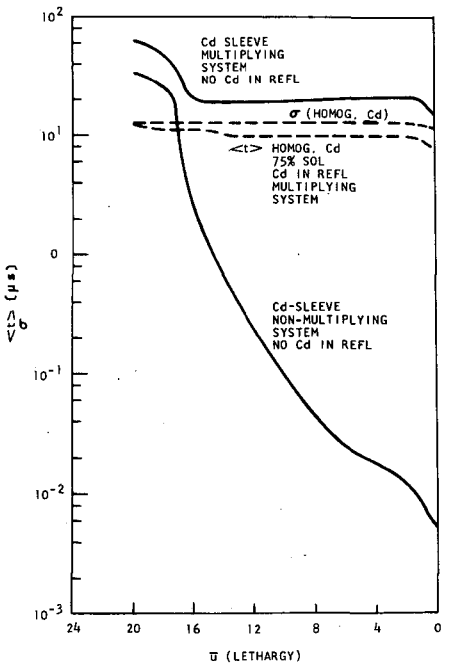

Fig. 1

Time-moments versus lethargy in poisoned TRIGA assemblies

(3) When the next collision would lie in a different region or outside the assembly, the particle is placed at the boundary and the distance to the boundary from the last collision D is calculated. The time increment is then $\Delta t = D/v$.

(4) In the event of regeneration or splitting, the starting time for the new particles becomes the lifetime to that point of the original particle.

(5) The time to exit, e.g. by leakage, absorption, falling below some weight standard or minimum speed, or exceeding a specified maximum time to follow one particle, is carried along and printed in the output. The time moments can also be calculated from

$$<t^n> = \sum_{i=1}^{I} \frac{(t_i)^n}{I} , \qquad (24)$$

where t_i is the lifetime of the i-th neutron and I is the total number of neutrons.

MICHAUDON [17] has reported calculations made in slabs of water from 1 to 20 initial mean-free-paths (ℓ) thick. The impulse source, energy E_0, generated neutrons incident on one face at a given angle θ to the normal. The hydrogen cross-section was taken as constant below 35 keV and varying as 1/v above that. Oxygen was assumed to be an isotropic elastic scatterer

with constant cross-section. Expectation values of $\langle t \rangle$, σ and N(E), the number of neutrons transmitted with exit energy E, were calculated. Some of the principal conclusions are:

(1) The angle of incidence has little effect on σ or on N for thick slabs, but for thin slabs a larger θ appreciably increases the probability for scattering, hence increases N.

(2) At normal incidence and exit, and for given E_0 and E, increasing the thickness increases $\langle t \rangle$, σ and N. However, the variation is such that the figure of merit as a moderator, $F = N/\sigma^2$, has a maximum at some optimum thickness. At $E_0 = 1$ MeV, $E = 1$ eV, there is a broad maximum from 6 to 12 ℓ. The optimum thickness decreases with decreasing E_0 while F increases, hence it is advantageous to make the source energy as small as possible. The optimum thickness increases with decreasing E, while F decreases.

(3) Increasing the proportion of heavy scatterer decreases F, and pure hydrogen is better than water. At a high exit energy (100 keV) from a slab 1 mean-free-path-thick , an increase in the proportion of oxygen over that in water eventually increases F once more.

(4) Addition of a homogeneous 1/v absorber, such as B^{10}, always decreases F, the decrease in N exceeding any improvement in σ due to preferential absorption of neutrons which have spent a relatively long time at a given energy.

(5) At an increasing angle of exit from the normal, N decreases and σ increases, so that F decreases.

These conclusions are interesting, but the problem reported does not consider anisotropic scattering, resonances or inelastic scattering. A computer programme called PULSE has been written by Profio which can include these effects. The code consists of a number of sub-routines (in the FORTRAN IV language) which perform most of the computations, linked by a main programme which takes care of input and output and calls the sub-routines in sequence. The code can be modified easily, but the present version provides options for point isotropic or monodirectional, monoenergetic sources, and for reading source neutron parameters from a magnetic tape prepared previously. The number of speed groups is 20, with arbitrarily specified lower boundaries. Geometry sub-routines are provided for a single-region infinite slab and a single-region sphere. The material may consist of one or two nuclides. Input includes the probabilities for elastic scattering from nuclide 1, for elastic scattering from nuclide 2, for inelastic scattering from nuclide 1, and for inelastic scattering from nuclide 2. Capture is found by subtraction. The total mean free path must also be given.

Elastic scattering can be either isotropic in the centre of mass system, or the scattering angle chosen from a cumulative probability table with 21 entries for each speed group and nuclide. The scatterer may be heavy or light; in the latter case a conversion is made from the centre of mass to the laboratory system. A special algorithm is used for hydrogen. Inelastic scattering is handled in much the same way. An option is provided to calculate the excitation energy from up to five resolved levels, or from a statistical model. Output is in the form of collision (and leakage) parameters on magnetic tape, for subsequent analysis. In addition, $\langle t \rangle$ and $\langle t^2 \rangle$ are computed for capture and for leakage, in each speed group.

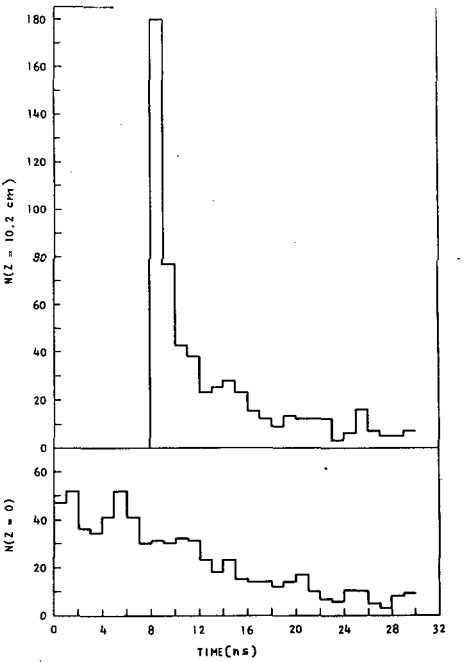

Fig. 2

Leakage versus time in 10.2-cm lead slab, E_0 = 0.84 MeV

A problem was run with PULSE for an 0.84-MeV source normally incident on an infinite slab of lead 10.2 cm thick, which is 1.91 mean free paths. Total, elastic, and inelastic cross-sections were taken from a General Atomic tabulation [18], except inelastic scattering below the 0.57-MeV level was set to zero. The division between the 0.57-MeV and the 0.805-MeV level was estimated from Brookhaven National Laboratory Rpt. BNL-325. The angular distribution for elastic scattering above 0.60 MeV was assumed to be equal to the 0.9-1.0-MeV distribution given in Rpt. BNL-400 (2nd ed), which is strongly peaked in the forward direction. Other angular distributions were assumed to be isotropic. Two thousand neutron histories were run with a maximum time cut-off of 100 ns and a lower speed cut-off corresponding to 0.25 MeV.

Results are shown in Fig. 2. The number of neutrons which have suffered only elastic collisions and then leak from the source face (z = 0) or the opposite face (z = 10.2 cm) are plotted versus time. Note that no neutrons leak from the z = 10.2-cm face until after 8.03 ns, the transit time of 0.84-MeV neutrons. The fraction of neutrons transmitted without collision is 15.4%, in good agreement with exp (-1.91) = 15%. The fraction of elastically collided neutrons which leak from the source face is 46%. The mean time of leakage for all neutrons (except the 3% which are inelastically scattered) is 12.6 ns. This is consistent with the exponential die-away time constant of 13.2 ns measured by Beghian and Wilensky at the Massachusetts Institute of Technology for a lead slab 10.2 cm × 71 cm × 81 cm.

TABLE II

Time to Maximum in Toluene and Water

	t_m (In), μs		t_m (Cd), μs	
	Measured	Calculated	Measured	Calculated
Toluene	1.5 ± 0.3[a]	1.3[d]	3.25 ± 0.3[a]	2.5[d]
			2.8[b]	2.8[e]
Water	0.75 ± 0.5[a]	0.9[d]	1.75 ± 0.5[a]	1.7[d] (0.4eV)
		0.9[f]	4.0 ± 0.2[c]	2.4[d] (0.2eV)
				~4[f]

a Profio and Eckard [19].
b Reines, F., et al. [10].
c Möller and Sjöstrand [20]
d Calculated from $2\ell/v$ (eq. 2).
e Monte Carlo [10].
f Stepwise time integration [9].

3. EXPERIMENT

Infinite medium conditions, and the restrictions of isotropic scattering and constant mean free path, are probably best satisfied by low energy neutrons in a large hydrogenous moderator. Measured and calculated results for water and toluene are listed in Table II.

REINES [10] measured the time distribution of capture gamma rays from a solution of cadmium in a large (75 cm diameter by 75 cm long), toluene-base scintillation detector. Cosmic ray neutrons were the source; zero-time was obtained from the recoil proton pulse. Thus the source density was uniform and the captures were automatically volume-integrated. An infinite medium, time-dependent Monte Carlo calculation at the experimental Cd-H ratio, 0.00323, agreed well with the measurement except at the long times corresponding to the die-away of the thermal neutron flux.

PROFIO and ECKARD [19] measured the time-to-maximum of the capture gamma counting rate in a 69-cm diameter by 69-cm long toluene-base scintillation detector containing thick foils of either indium or cadmium. A point source of D(d,n) neutrons from a 150-kV Cockcroft-Walton accelerator was located at the centre; pulse width was 0.25 μs. The calculated t_m at the indium resonance energy (1.46 eV) is seen to agree reasonably well with experiment, while the cadmium results do not. The probable explanation is the effect of chemical binding, although it is possible that the volume integration was in error. Measurements were also made in a small (16 cm × 20 cm × 21 cm) volume of water containing indium or cadmium foils. The source and the NaI(Tl) scintillation detector were external to the volume. These are not really infinite medium measurements, but there is approximate integration over the volume, and over a limited energy range near ther-

mal, leakage will not vary much with energy. Agreement between calculation and experiment is satisfactory, but the measurement is not very accurate. The small slowing-down time demands short bursts and a fast detection system. The time between bursts has to be long enough for most of the thermal flux to die away. Counting rates are low because of the small duty cycle, and because only a fraction of the neutrons are captured in the resonance and the gamma ray detected. The sodium iodide detector is sensitive to fast neutrons because of inelastic scattering in iodine; however, it has good efficiency and its good energy resolution allows discrimination against the hydrogen capture gamma ray (2.2 MeV).

MÖLLER and SJÖSTRAND [20] measured the capture gamma rays from a solution of cadmium in a 1.5-l vessel located in a 1-m cube of water. The source was a lithium target at the centre of the cube, bombarded by a pulsed proton beam from a Van de Graaff accelerator. A similar system has been put into operation by Adamantiades at the Massachusetts Institute of Technology. The solution is dilute, hence the time distribution should correspond to slowing-down past the cadmium resonance at 0.18 eV. The measured time-to-maximum was 4 μs; free-atom stationary nucleus scattering gives only 2.4 μs, while taking into account the thermalization properties, gives a t_m slightly less than 4 μs. The experimenters find that the absorption by the cadmium is quite large, decreasing the overall thermal die-away time constant, while net diffusion into the absorber solution increases the time constant in the solution. The spatial dependence near 0.2 eV was found to be small for source-absorber separations greater than 6 cm. A measurement with cadmium dissolved in the 1-m^3 of water indicated that the measurement was characteristic of an infinite medium, although perhaps there is some question since integration is not done over the entire volume, but over some volume corresponding to a mean free path or so of the gamma rays.

At high energies (keV-MeV) the capture gamma technique becomes more difficult to apply, since many resonances may contribute, and the radiative capture cross-sections are generally small. On the other hand, one could measure the neutron spectrum by time-of-flight, and observe time delays and broadening in scattering (or absorption) resonances. The resonance may occur in the moderator material itself, or in a filter in the flight path. Spectrum measurements by time-of-flight have been made recently at the General Atomic Linear Accelerator Facility in liquid hydrogen [21] and in depleted uranium [22]. The corrections to these measurements caused by the slowing-down time can be calculated, but the experiments themselves are not well suited to testing the theory.

Neglecting spatial and angular variation, we can use the results of section 2.1(a) to estimate the magnitude of $\langle t \rangle$ and σ in the large volume of liquid hydrogen. So far the spectrum measurements have been made down to 500 keV, with an instrumental time resolution (including burst width) of 37 ns. The source spectrum extends over the entire range, so that $\langle t \rangle$ could hardly be measured. However, the spectrum may be extended to thermal energies later. The main contribution to the slowing-down time comes from the last few collisions and we can assume $\sigma(H) = 20$ b. For liquid hydrogen at 20°K, $\ell = 1.2$ cm. Then from Eqs.(3) and (5), $\langle t \rangle = 3.6/v$ and $\sigma^2 = 4.32/v^2$.

Thus the time uncertainty σ is equivalent to a flight distance of only 2.08 cm. Even at 1 keV, σ = 48 ns.

In uranium, capture and fission are not negligible and the lowest inelastic scattering level is at 44 keV. Inelastic scattering decreases $<t>$ and σ, while fission tends to increase them. The time-moments method of section 2.2(c) can handle these complications, of course. However, it is interesting to calculate as for an elastic scatterer, A = 238, below 44 keV, with ℓ = 2.2 cm. From Table I, $<t> = A\ell/v = 524/v$ and $\sigma = \sqrt{2/3A}\,<t> = 0.053\,<t>$. Evaluated at 1 keV, $<t> = 12\ \mu s$ and $\sigma = 0.636\ \mu s$. The flight time over the 50-m distance used is 115 μs. The instrumental time resolution was about 125 ns. Thus σ is the main contributor to the time uncertainty. However, inelastic scattering distributes neutrons at keV energies in a very short time interval, and it is believed that the source emission is still quite significant in this range.

4. CONCLUSIONS

Theoretical methods are available to calculate both spatially-independent and spatially-dependent fluxes as a function of time. In many cases the time-moments only are needed; these can be obtained from repeated application of any code developed for steady-state problems. More calculations should be done to investigate the effect of absorption and inelastic scattering on the time behaviour and moderation efficiency.

There are few measurements of slowing-down versus time, and even fewer including spatial migration. Satisfactory agreement is obtained between theory and experiment at low epithermal energies in hydrogenous moderators with the resonance capture gamma counting technique. However, more accurate measurements should be made, and the spatial dependence should be investigated. The uncertainty in the slowing-down and migration time in the intermediate energy range may limit the resolution of spectrum measurements by time-of-flight; measurements of transmission resonance displacement and broadening are needed but the source should be monoenergetic, or should lie well above the energy range being investigated.

ACKNOWLEDGEMENTS

We wish to thank Mr. Gordon B. West of General Atomic for the use of his results in the time-moment calculations in the TRIGA assembly. Part of the development of the PULSE code was done at the Massachusetts Institute of Technology Computation Center.

The TRIGA calculations were performed on a programme sponsored by the Defense Atomic Support Agency.

REFERENCES

[1] KOPPEL, J., Nucl. Sci. Engng 8 (1960) 157-63.
[2] MARSHAK, R.E., Rev. mod. Phys. 19 (1947) 185-238.

[3] BECKURTS, K.H., and WIRTZ, K., Neutron Physics, Springer-Verlag, N.Y. (1964) 168-73.
[4] BERGMAN, A.A., et al., Proc. UN Int. Conf. PUAE 4 (1956) 135-46.
[5] MITZEL, F. and PLENDL, H.S., Nukleonik 6 (1964) 371-79.
[6] KOSALY, G. and NEMETH, G., Nukleonik 1 (1959) 225-27.
[7] ERIKSSON, K.E., Ark. Fys. 16 (1959) 1-14.
[8] OHANIAN, M.J. and DAITCH, P.B., Nucl. Sci. Engng 19 (1964) 343-52.
[9] GHATAK, A.K. and KRIEGER, T.J., Nucl. Sci. Engng 21 (1965) 304-11.
[10] REINES, F. et al., Rev. Sci. Instrum. 25 (1954) 1061-70.
[11] DYAD'KIN, I.G. and BATALINA, E.P., Atomnaja Energija 10 (1961) 5-12.
[12] CLAESSON, A., AB Atomenergi Rpt. AE-71 (1962).
[13] SYKES, J.B., J. nucl. Energy 2 (1955) 31-37.
[14] JOANOU, G.D., et al., General Atomic Rpt. GA-4132 (1963).
[15] ALEXANDER, J.H., et al., General Atomic Rpt. GA-4972 (1964).
[16] JOANOU, G.D. and DUDEK, J.S., General Atomic Rpt. GA-4265 (1963).
[17] MICHAUDON, A., J. nucl. Energy (A/B) 17 (1963) 165-86.
[18] JOANOU, G.D., et al., General Atomic Rpt. GA-2156 (1961).
[19] PROFIO, A.E. and ECKARD, J.D., Nucl. Sci. Engng 19 (1964) 321-28.
[20] MÖLLER, E. and SJÖSTRAND, N.G., Ark. Fys. 37 (1964) 501-30.
[21] RUSSELL, J.L., et al., "Neutron spectra in bulk media by time-of-flight", these Proceedings II.
[22] KATO, W.Y., et al., "Fast reactor physics parameters from a pulsed source", these Proceedings II.

NEUTRON SLOWING-DOWN TIME AND THERMALIZATION TIME CONSTANT IN GRAPHITE

Y. KANEKO AND K. SUMITA*
JAPAN ATOMIC ENERGY RESEARCH INSTITUTE,
TOKAI-MURA, IBARAKI-KEN, JAPAN

Abstract — Résumé — Аннотация — Resumen

NEUTRON SLOWING-DOWN TIME AND THERMALIZATION TIME CONSTANT IN GRAPHITE. The classical mechanics are able to describe the energy decrease of fast neutrons in their collision with moderator nuclei. However, when those neutrons are slowed down into the energy range of chemical binding of the moderator, such a simple model in which the collision of neutrons is treated as that of billiard balls is not valid; therefore more extended models have been suggested, including phonon exchange between the neutron and moderator lattice.

In order to prove their validity, a series of pulsed neutron experiments was performed to investigate neutron moderation and thermalization in a graphite pile. The graphite pile is of nuclear reactor grade with density 1.54 and is 240 cm in height and 120 cm in a side of its hexagonal cross-section. Bursts of neutrons of width 1 microsecond were generated at the centre of the pile. The slowing-down and diffusing neutrons were detected by bare and energy-selective, filter-covered BF_3 counters and analysed with a 256-channel time analyser. By interpreting that the increment of the difference of the events between the bare and the filter-covered counter is due to the contribution made by that fraction of the neutrons slowing down at the time of measurement below the cut-off energy of the filter, slowing-down times in graphite were determined.

As the results of the experiment, slowing-down times below 1.46, 0.61, 0.50, 0.41 and 0.21 eV were determined as 23, 36.9, 41.6, 45.8 and 87.5 μs respectively. The thermalization time constant in graphite was also determined as $(296 \pm 50)\,\mu$s by using the silver filter transmission method.

It is concluded that the crystal model is capable of describing most satisfactorily the slowing-down and thermalization phenomena in graphite.

TEMPS DE RALENTISSEMENT ET CONSTANTE DE TEMPS DE THERMALISATION DES NEUTRONS DANS LE GRAPHITE. La mécanique classique permet de décrire la diminution d'énergie des neutrons rapides lorsqu'ils entrent en collision avec des noyaux du ralentisseur. Mais lorsque cette diminution est telle que l'énergie des neutrons tombe dans la gamme des énergies de liaisons chimique du ralentisseur, le modèle simple dans lequel la collision des neutrons est traitée à la manière du choc entre deux boules de billard cesse d'être valable; on a donc proposé des modèles plus précis dans lesquels il y a échange de phonons entre le neutron et le réseau du ralentisseur.

Afin de prouver leur validité, les auteurs ont fait des expériences à l'aide de neutrons pulsés pour étudier le ralentissement et la thermalisation des neutrons dans un empilement graphite. Il s'agissait d'un graphite de pureté nucléaire dont la densité était de 1,54; l'empilement avait une hauteur de 240 cm; sa section était un hexagone régulier de 120 cm de côté. Des bouffées de neutrons d'une largeur d'une microseconde étaient produites au centre de l'empilement. Les neutrons qui subissaient le ralentissement et la diffusion étaient décelés à l'aide de deux compteurs au BF_3 dont l'un était revêtu d'un filtre sélecteur d'énergie et analysés au moyen d'un analyseur en temps à 256 canaux. En admettant que l'accroissement de la différence des événements entre le compteur revêtu d'un filtre et l'autre compteur est dû à la contribution de la fraction des neutrons dont l'énergie tombe au moment de la mesure au-dessous de l'énergie de coupure du filtre, on a déterminé les temps de ralentissement dans le graphite.

L'expérience a permis de constater que les temps de ralentissement pour des énergies inférieures à 1,46, 0,61, 0,50, 0,41 et 0,21 eV étaient respectivement de 23, 36,9, 41,6, 45,8 et 87,5 μs. On a également déterminé la constante de temps de thermalisation dans le graphite (296 ± 50 μs) par la méthode de transmission par un filtre en argent.

* Present address: Osaka University, Faculty of Engineering, Higashinoda, Miyakojima-ku, Osaka, Japan

Les auteurs concluent que le modèle du cristal permet de décrire d'une manière tout à fait satisfaisante les phénomènes de ralentissement et de thermalisation dans le graphite.

ВРЕМЯ ЗАМЕДЛЕНИЯ НЕЙТРОНОВ И ПОСТОЯННАЯ ВРЕМЕНИ ТЕРМАЛИЗАЦИИ В ГРАФИТЕ. Классическая механика дает возможность описать уменьшение энергии быстрых нейтронов при их столкновении с ядрами замедлителя. Однако при замедлении таких нейтронов в диапазоне энергии химической связи замедлителя такая простая модель, в которой столкновение нейтронов рассматривается как столкновение бильярдных шаров, является недействительной, поэтому предложены более широкие модели, включающие обмен фононов между нейтроном и решеткой замедлителя.

Чтобы доказать их пригодность, проведена серия экспериментов с импульсными нейтронами по изучению замедления нейтронов и их термализации в графитовой призме ядерной чистоты с плотностью 1,54, высотой 240 см и стороной 120 см в гексагональном поперечном сечении. В центре призмы отмечались вспышки шириной в 1 мксек. Замедленные и рассеянные нейтроны обнаруживались с помощью неэкранированного счетчика BF_3 и счетчика BF_3 с фильтром, избирающим энергию, и анализировались с помощью 256-канального анализатора времени. Путем интерпретации увеличения различия явлений между неэкранированным счетчиком и счетчиком с фильтром объясняется влияние доли нейтронов, замедленных во время измерения ниже пороговой энергии фильтра. Определено время замедления в графите.

В результате проведения эксперимента было установлено, что время замедления ниже 1,46; 0,6; 0,49; 0,41 и 0,2 эв составляло соответственно 22; 35,5; 39,8; 42,9 и 78,2 мксек. Постоянная времени термализации в графите также определялась с помощью метода пропускания серебряного фильтра и составила 335 ±80 мксек.

Вывод таков, что модель кристалла дает возможность весьма удовлетворительно описать явления замедления и термализации в графите.

EL TIEMPO DE MODERACION NEUTRONICA Y LA CONSTANTE DE TIEMPO DE TERMALIZACION EN EL GRAFITO. La pérdida de energía de los neutrones rápidos como consecuencia del choque con núcleos de un agente moderador puede explicarse en términos de mecánica clásica. Sin embargo, cuando la moderación de esos neutrones es tal que su energía corresponde al intervalo de energías de enlace químico del moderador, deja de ser válido un modelo tan simple en el que se considera que el choque de los neutrones se produce como si éstos fueran bolas de billar, por lo que se han sugerido modelos más complejos, comprendido el intercambio fonónico entre el neutrón y el reticulado moderador.

A fin de demostrar la validez de esos modelos, se ha realizado una serie de experimentos mediante neutrones pulsados con miras a estudiar la moderación y la termalización neutrónicas en una pila de grafito. El grafito era de pureza nuclear, con una densidad de 1, 54, y la pila tenía una altura de 240 cm y una sección hexagonal de 120 cm de lado. En su centro se generaron ráfagas de neutrones con una anchura de 1 μs. Los neutrones que intervenían en los procesos de moderación y de dispersión se detectaron mediante dos contadores de BF_3, el segundo de ellos provisto de un filtro selector de energías, y se analizaron con un analizador de tiempo de 256 canales. Se determinaron los tiempos de moderación en el grafito en el supuesto de que el aumento de la diferencia entre el número de sucesos detectado por el contador desprovisto de filtro y los detectados por el contador con filtro se debe a la contribución de la fracción de los neutrones que en el momento de la medición han perdido velocidad en grado suficiente para quedar por debajo de la energía de corte del filtro.

Como resultado del experimento se determinaron, para energías inferiores a 1, 46, 0, 61, 0, 50, 0, 41 y 0, 21 eV, tiempos de moderación de 23, 36, 9, 41, 6, 45, 8 y 87, 5 μs, respectivamente. También se halló un valor de 296 ± 50 μs para la constante de tiempo de termalización en el grafito, empleando el método de transmisión con filtro de plata. Los autores llegan a la conclusión de que el modelo de cristal permite describir muy satisfactoriamente los fenómenos de moderación y termalización en el grafito.

1. INTRODUCTION

One of the most important problems in nuclear reactor physics is the determination of neutron slowing-down and the thermalization properties of reactor materials. Classical mechanics describes the energy decrease of

fast neutrons in their collision with moderator nuclei. However, when those neutrons are slowed down into the energy range of the chemical binding of the moderator, such a simple model, in which the collision of neutrons is treated as that of billiard balls, is no longer valid; therefore more elaborate models have been proposed, which include phonon exchanges between the neutron and moderator lattice. Much work has been devoted to proving the validity of these models. The effect of chemical binding on the neutron slowing-down time and the thermalization time constant was investigated by pulsed neutron experiments in this work.

1.1. Slowing-down time

Theoretical work on the time-dependent neutron velocity distribution during slowing down has been performed by several authors. MARSHAK [1] calculated the approximate n-th moment of the slowing-down time from the Laplace transform of the time-dependent diffusion equation. VON DARDEL [2] and KAZARNOVSKY [3] obtained similar results. KRIEGER and FEDERIGHI [4] calculated the slowing-down spectrum in H_2O by using numerical Laplace inverse transformation on the diffusion equation with the heavy gas kernels. CROUCH [5] has measured the slowing-down time in H_2O using a Po-Be constant source. After his work, VON DARDEL [2] and HIRAKAWA [6] tried to determine the slowing-down time in H_2O and other materials by using pulsed neutron sources. They used 1/v counters with the filters having different cut-off energies for neutron detection. MÖLLER and SJÖSTRAND [7] and PROFIO and ECKARD [8] measured the prompt gamma rays of characteristic energies accompanying neutron captures by the absorbers in H_2O systems. KOPPEL [9] has measured the slowing-down time in graphite by observing the capture gamma rays from cadmium sheets interleaved in the graphite system. But in his work, comparison with the theoretical prediction has been done only at a single energy.

In this work, neutron slowing-down times to five energy points were determined by the transmission method and were compared with theoretical values.

1.2. Thermalization time constant

Theoretical work on the time-dependent neutron velocity distribution during thermalization has been done by several authors. KAZARNOVSKY [10], KATZURAGI [11] and PUROHIT [12] introduced the concept of characteristic spectra. FURUHASHI [13] showed that in an infinite system the Maxwellian component of the spectrum did not couple with the higher modes, which were orthogonal to the former, and contributed nothing to the actual neutron density. SINGWI and KOTHARI [14] and PUROHIT [12] calculated the thermalization time constants t_{th} in beryllium, graphite and light water. TAKAHASHI [15] also calculated t_{th} in graphite using the YOSHIMORI-KITANO model [16], with the conclusion that the higher moments of the scattering kernel played as important a role in the calculation of that value as the second moment did. VON DARDEL [2] and SJÖSTRAND [7] have made some experiments on beryllium, light water and ice. BECKURTS [17] has measured t_{th} in graphite by using the silver filter transmission method.

MÖLLER and SJÖSTRAND [7] have measured t_{th} in light water by obtaining information on the change of the neutron spectrum with time from the reaction rate with spectrum indicators dissolved in the system. Beckurt's result, (185±45) μs, agreed well with Purohit's theoretical value, 209.98 μs, and is accepted at present; however it did not agree with Takahashi's theoretical value of 307 μs. The authors of this paper have also undertaken the measurement of t_{th} in graphite by the silver filter transmission method.

2. THEORY

In the diffusion approximation, the neutron flux $\phi(E, \vec{r}, t)$ in a bare homogeneous moderator obeys the following equation:

$$\frac{1}{v}\frac{\partial \phi(E, \vec{r}, t)}{\partial t} = D(E)\nabla^2\phi(E, \vec{r}, t) - \Sigma_a(E)\phi(E, \vec{r}, t) - \Sigma_s(E)\phi(E, \vec{r}, t)$$

$$+\int_0^\infty \Sigma_s(E' \to E)\phi(E', \vec{r}, t)\,dE' + \delta(E_s)\,\delta(t), \qquad (1)$$

where $\vec{r}$ is the space co-ordinate, v the neutron velocity, E the neutron energy, E_s the energy of the pulsed neutrons, t the time after neutron injection, and Σ_s the scattering cross-section.

In the slowing-down region, this equation has been solved only for infinite systems and for the free-hydrogen scattering atoms at rest, with no absorption and constant scattering cross-sections. Rigorous solutions have not been obtained for the heavy atoms. MARSHAK [1] presented Eq. (2) to calculate an approximate first time moment of neutron flux under the above-mentioned conditions.

$$\langle t \rangle^1 \text{ (0°K free gas)} = \frac{\int_0^\infty t\,\phi(E_c, t)\,dt}{\int_0^\infty \phi(E_c, t)\,dt}$$

$$\simeq \frac{1}{\Sigma_s\sqrt{\frac{2E_c}{m}}}\left[1 - \frac{2}{1+2}\,\frac{1 - \left(\frac{M-1}{M+1}\right)^{1+2}}{1 - \left(\frac{M-1}{M+1}\right)^2}\right]^{-1}, \qquad (2)$$

where m and M are masses of neutron and scattering atoms, respectively.

In addition, the slowing-down density $q(E_c, t)$ should be determined from the following equation:

$$q(E_c, t) = \int_{E_c}^\infty \phi(E', t)\,dE' \int_0^{E_c} \Sigma_s(E' \to E'')\,dE'', \qquad (3)$$

where E_c is the energy under consideration, i.e. the cut-off energy of the filter. In the case of the graphite system, a first-energy decrement moment of the slowing-down density caused by a collision at E_c is 0.09 E_c for the 0°K free-gas case. Thus, $q(E_c, t)$ can be replaced approximately by ϕ (1.09 E_c), when slowing-down time below the cut-off energy E_c is evaluated by the following equation:

$$t^1 \text{ (0°K free gas)} = \int_0^\infty t\, q(E_c, t)\, dt \Big/ \int_0^\infty q(E_c, t)\, dt \tag{4}$$

$$t^1 \text{(0°K free gas)} \simeq \int_0^\infty t\, \phi(1.09\, E_c, t)dt \Big/ \int_0^\infty \phi(1.09\, E_c, t)dt \tag{5}$$

Marshak also calculated the ratio of the approximate first moment to the exact moment for M = 9 and 15. After his results were interpolated, t^1 (0°K free gas) was obtained. Slowing-down times, including thermal agitations or chemical binding, were also estimated on the assumption that slowing-down time was proportional to the integral $\int_{E_c}^{E_s} \frac{dE}{\xi\, Ev}$, where ξ was a logarithmic energy decrement.

Furuhashi has given a general formalism for the thermalization region, whereby the characteristic spectra are determined as eigenfunctions of a self-adjoint integral operator governing the thermalization and operating in the function space composed of modified density spectra. The time-dependent neutron flux is given as a series of characteristic spectra, decaying by the associated time constant λ_{mn}.

$$\phi(E, \vec{r}, t) = \sum_{mn} A_{mn}\, e^{-\lambda_{mn} t}\, v N_{mn}(E)\, R_m(\vec{r}), \tag{6}$$

where subscripts m and n indicate the m-th spatial and n-th energetic harmonic mode. Then the neutron spectrum approaches asymptotic form as follows:

$$\phi(E, \vec{r}, t) = A_{00}\, e^{-\lambda_{00} t}\, v N_{00}(E) + A_{01}\, e^{-\lambda_{01} t}\, v N_{01}(E) R_0(\vec{r}). \tag{7}$$

The reciprocal of λ_{01} in the infinite case with no absorption is defined as t_{th}. It was also ensured that the energetically higher mode of decay in the infinite system could not be detected when 1/v detectors were used [13]. Therefore, λ_{01} as a relaxation time constant could possibly be determined by the ratio of the response for a non-1/v detector to that of a 1/v detector. However, the measured data must be fitted to a single exponential function for a rather short time interval because components of N_{02}, N_{03}, ... have a tendency to contribute more strongly to the above-mentioned ratio than N_{01} and N_{00}. In addition to this data processing, another method, based

on the rather classical treatment which employs the concept of neutron temperature, is adopted in this work.

Von Dardel introduced the assumption that when the neutron gas was sufficiently close to thermal equilibrium, its velocity spectrum was approximately represented by a Maxwellian distribution with a temperature T different from the moderator temperature T_0. For a monatomic gaseous moderator of constant scattering cross-section, Von Dardel obtained,

$$\frac{dT}{dt} = -\frac{2}{3}\left(\frac{2kT_0}{m}\right)^{\frac{1}{2}} \Sigma_s \frac{A^{\frac{1}{2}}}{(A+1)} \left[1 + \frac{A}{A+1}\frac{T-T_0}{T_0}\right]^{\frac{1}{2}} (T - T_0) \qquad (8)$$

which, for $T(t) - T_0 \ll T_0$, reduces to

$$\frac{dT}{dt} = -\frac{1}{t_{th}}\left[1 + \frac{1}{2}\frac{A}{A+1}\frac{T-T_0}{T_0}\right](T - T_0) \qquad (9)$$

Thus, we obtain

$$(T - T_0)\, C(t) = e^{-t/t_{th}} , \qquad (10)$$

where

$$C(t) = \text{const.} \left(1 + \frac{A}{2(A+1)}\frac{T-T_0}{T_0}\right)^{-1} \qquad (11)$$

The results of the above discussion show that the change of neutron temperature with time can be represented by an exponential function with a relaxation constant, the reciprocal of t_{th}, if the small correction of Eq. (11) is also valid for the crystalline materials, graphite, and is applied to $T - T_0$.

PUROHIT [12] and TAKAHASHI [15] calculated t_{th} in graphite with results of 209.98 and 307 μs, respectively.

3. EXPERIMENTAL ARRANGEMENT

In this experiment, pulsed neutrons were generated near the centre of the graphite pile. The slowing-down and diffusing neutrons were detected by bare and energy-selective, filter-covered BF_3 counters; pulses were analysed alternately with a 256-channel time analyser. A block diagram for the measurement is shown in Fig. 1.

3.1. Pulsed neutron source [18]

A 200-kV Cockcroft-type compact pulsed neutron source was used in this experiment. Using a thin tritium target, the bursts of 14-MeV neutrons were produced with a 1-μs pulse width in the slowing-down experiment and with a 50-μs pulse width in the thermalization time constant experiment.

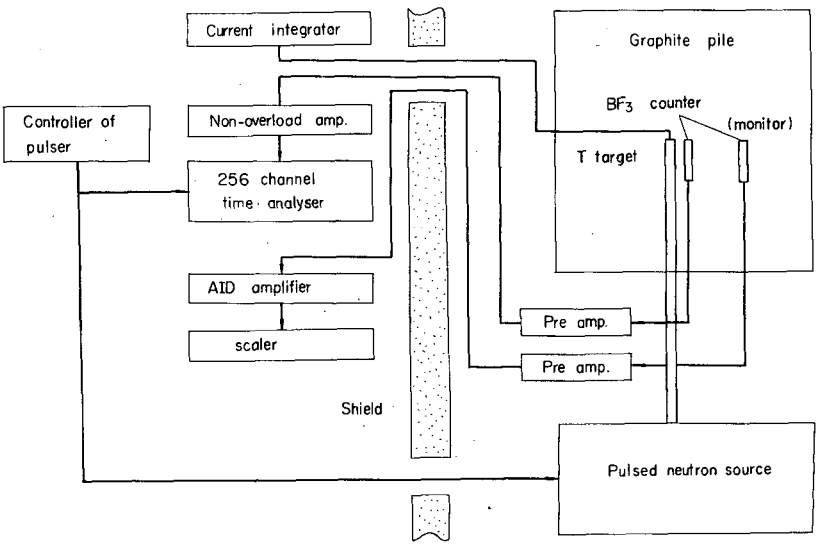

Fig. 1

Block diagram for the measurement

3. 2. Graphite pile

The graphite pile is of nuclear grade with a density of 1.54 g/cm^3, 240 cm in height and 120 cm on a side of its hexagonal cross-section. 2400 graphite rods of 6.5-cm diameter were stacked to make up this pile. Several hollow graphite tubes were also stacked for providing void channels into which an extension tube of the accelerator and neutron detectors was inserted. The distance from the wall of the graphite channel to the centre axis of the detector was 2.0 cm. A thin tritium target and neutron detectors were located on a mid-plane of the graphite pile in a manner shown in Fig. 2.

3. 3. Neutron detectors and time analyser

The slowing-down neutrons associated with pulsed neutron injection were detected by bare and energy-selective, filter-covered BF_3 counters (2.5 cm diameter, 36 cm Hg). In the case of the thermalization time constant measurement, a small BF_3 counter (1.3 cm diameter, 40 cm Hg) was used. The cut-off energy of the filter was calculated as the energy at which the counting efficiency of the filter-covered BF_3 counter for a uniformly incident unit flux amounted to half of that of the bare BF_3 counter (see Table I). Neutron pulses in the detector were amplified by the preamplifier and non-overloading amplifier with 0.1-μs rise time and its pulse height selector outputs were fed to a 256-channel time analyser. Analysis channel lengths of the time analyser were 0.25, 0.5 and 1.0 μs in the slowing-down time measurement and 50 μs in the t_{th} measurement. The time origin of the experiment was determined as an instant time at which a counting rate for the bare BF_3 counter amounted to half of the step increment caused by

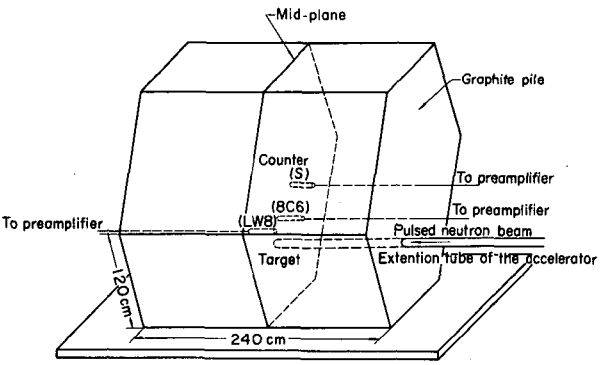

Fig. 2

Graphite pile

TABLE I

CUT-OFF ENERGY OF THE FILTERS*

Filter nuclide	Inner radius (mm)	Thickness (mm)	Cut-off energy (eV)
Indium	15.05	0.0137	-
Cadmium	15.85	1.36	0.61
Cadmium	15.85	0.68	0.50
Cadmium	15.05	0.3	0.41
Gadolinium	15.05	0.05	0.21
Silver	7.50	2.0	-

* The gadolinium filter was made by dispersing Gd_2O_3 in the resin layer on the aluminium cylinder. The other filter was made by using metals.

the injection of the pulsed neutrons. The delay time of pulsed neutron injection to the trigger of the time analyser was chosen as 8 -10 μs. One monitor channel was provided to measure the total neutron yield in a run of the experiment. A current integrator was also provided for the same purpose.

4. RESULTS OF THE EXPERIMENT

4.1. Slowing-down time

The counting rates of a bare, an indium filter-covered and a 1.36-mm cadmium filter-covered BF_3 counter as functions of time are shown in

Figs. 3, 4 and 5, respectively. The dip in the response with an indium filter is accounted for by the resonance captures at 1.46 eV. The increment of the difference of the events between the bare and the 1.36-mm cadmium filter-covered BF_3 counter with time can be considered as a result of the

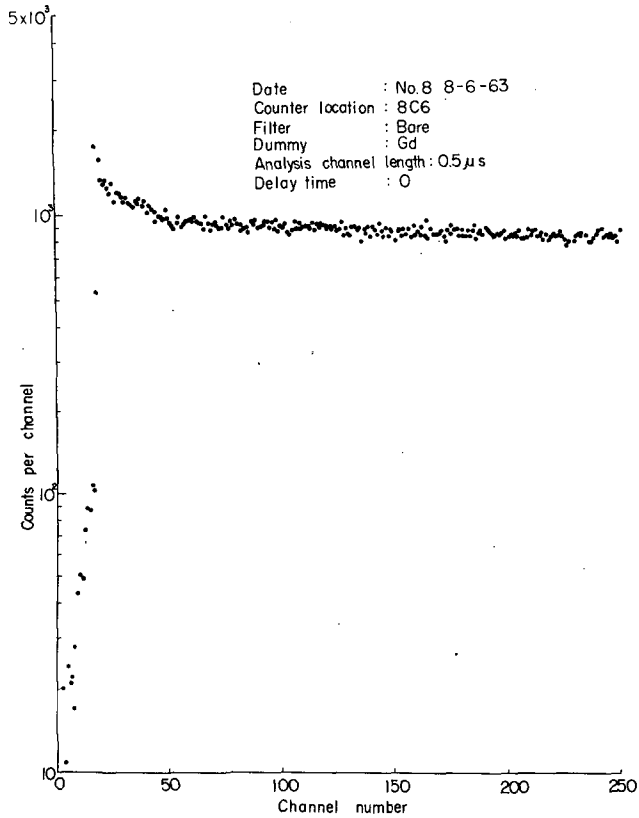

Fig.3

Time response for the bare BF_3 counter in the core diminished SHE

contribution of the fraction of the neutrons slowing down at the instant time of the measurement below the cut-off energy of the filter, 0.50 eV. The same interpretations were made with other filters. The increments of difference with the 1.36-mm cadmium filter and those with other filters are shown in Figs. 6, 7, 8 and 9. Slowing-down time to 1.46 eV and below 0.61, 0.50, 0.41 and 0.21 eV was determined from the results of Figs. 3, and 6, 7, 8 and 9 respectively, and are listed in Table II together with the theoretically predicted values. The experimental errors were estimated within 3%. The following corrections were considered: (1) leakage of some neutrons from the finite graphite pile before slowing-down below the cut-off energy, (2) time-of-flight effect from the wall of the graphite channel to the BF_3 counter, (3) background neutrons caused by the post-accelerated beam and (4) slowing down by hydrogen contained in the graphite. The effect

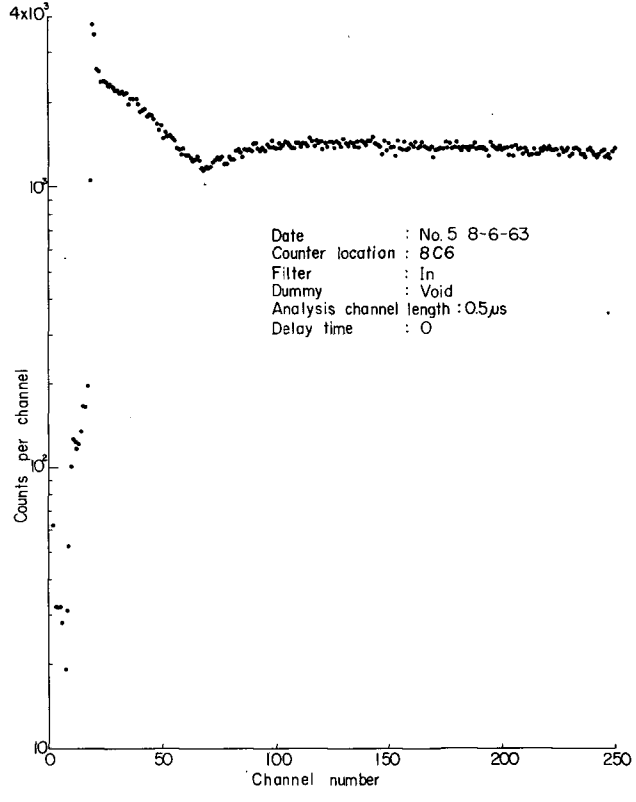

Fig. 4

Time response of the indium filter-covered BF_3 counter

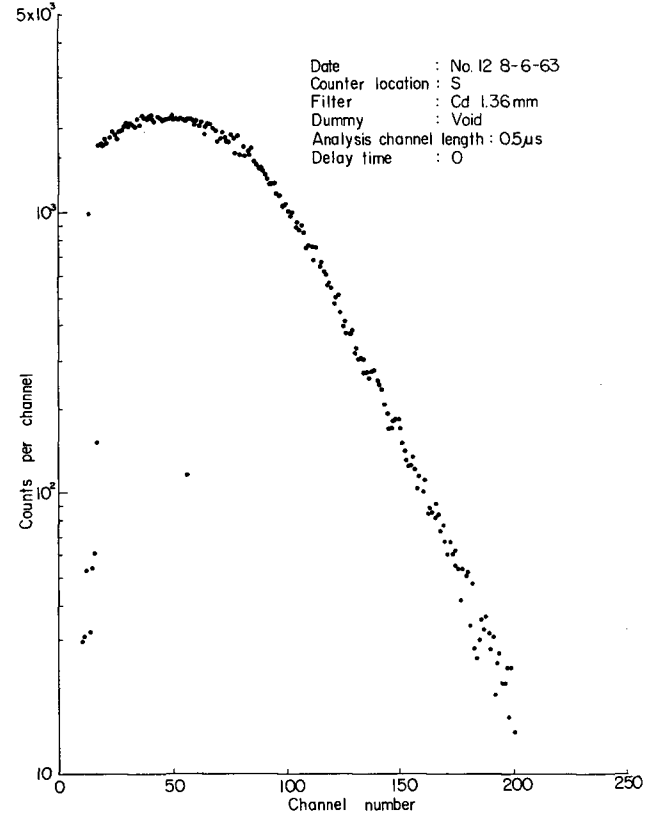

Fig. 5

Time response of the cadmium filter-covered BF_3 counter

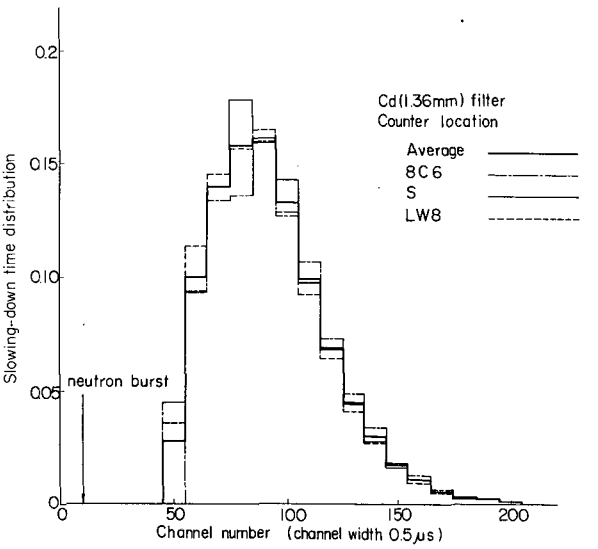

Fig. 6

Slowing-down time distribution below 0.61 eV

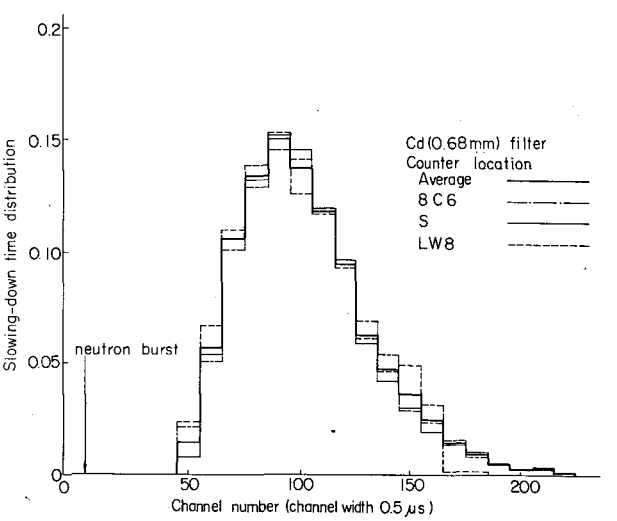

Fig. 7

Slowing-down time distribution below 0.50 eV

of the void space between the stacked graphite rods on the slowing-down time was taken into account by homogenizing the void with the graphite rods. Those experimental values of the slowing-down time did not show appreciative dependence on the detector positions. It was presumed that slowing-down time in graphite could be well evaluated with the crystal model.

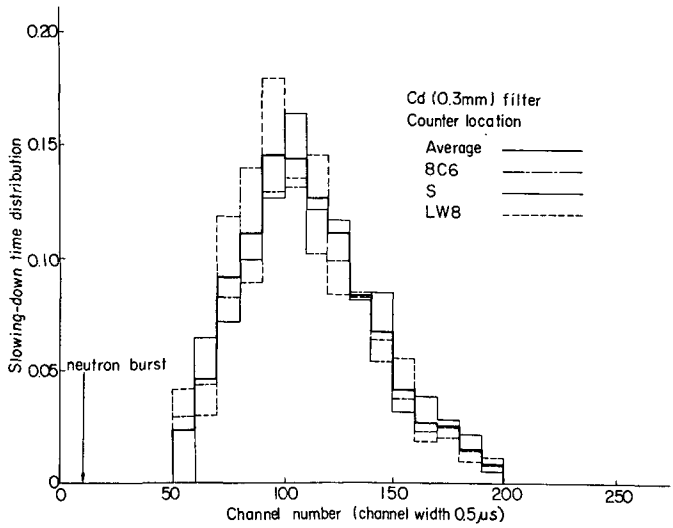

Fig. 8

Slowing-down time distribution below 0.41 eV

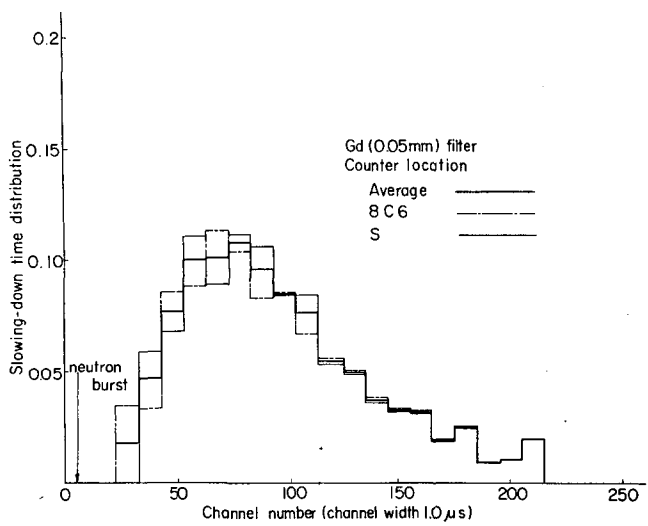

Fig. 9

Slowing-down time distribution below 0.21 eV

4. 2. Thermalization time constant

The counting ratio of the silver filter-covered BF_3 counter to the bare one, (silver ratio)$^{-1}$, should be related to the decrease of the neutron temper-

TABLE II

SLOWING-DOWN TIME IN GRAPHITE OF DENSITY 1.54 g/cm^3

Cut-off energy, or resonance energy (eV)	Detector position	Experimental results[a] (μs)	Theoretical values Free, 0°K (μs)	Free, 300°K (μs)	Crystal (μs)
1.46	8C6	23	23.3	23.3	23.3
	S	23			
0.61	8C6	37.1(35.9)	34.3	34.7	36.0
	S	37.1(35.8)			
	LW8	36.5(34.9)			
0.50	8C6	41.6(39.9)	38.1	38.7	40.1
	S	41.4(39.6)			
	LW8	41.9(39.8)			
0.41	8C6	45.7(42.2)	42.1	43.0	44.7
	S	45.8			
	LW8	45.8(43.5)			
0.21	8C6	86.7(77.8)	62.5	65.7	69.6
	S	87.7(78.8)			
	LW8	88.0(78.0)			

[a] Values in parentheses show the time in microseconds at which cadmium ratios amount to two.

ature T of the assumed Maxwellian neutron distribution [2] by the following equation.

$$\frac{(\text{silver ratio})^{-1}}{D\,(t)} = \frac{\int_0^\infty f_{Ag}\,(E)\,E\,e^{-E/kT}\,dE}{\int_0^\infty f_{bare}\,(E)\,E\,e^{-E/kT}\,dE}\,; \qquad (12)$$

where D (t), f_{Ag} (E) and f_{bare} (E) were flux depression factor, counting efficiencies of the silver filter-covered and the bare BF_3 counters, respectively.

The authors calculated the right-hand side of Eq. (8) for T from 300 to 600°K. The flux depression factor, D (t) was measured time-dependently as the ratio of the counting rate of the small BF_3 counter, which was located tangentially on the filter, to the rate, in turn, on the thin aluminium hollow cylinder having the same outer radius as that of the filter. Measured neutron temperatures T from 448 to 330°K obtained for times t from 0.4 to 0.9 ms were fitted to Eq. (10) with

$$t_{th} = (296 \pm 50)\,\mu s\,,$$

after the contributions of the higher harmonics were reduced by applying the correction factor of Eq. (11) on the measured $T-T_0$. A T_0 (asymptotic)

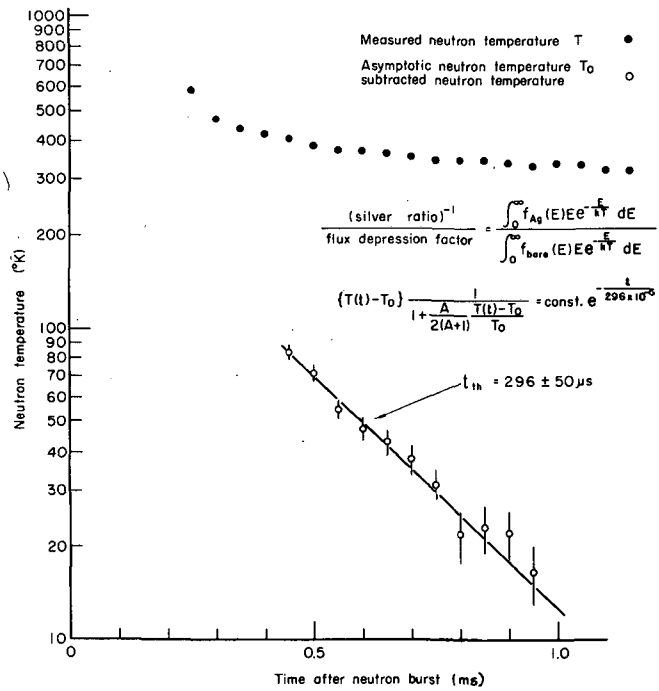

Fig. 10

Neutron temperature versus time after neutron bursts

of 330°K (the average of the neutron temperature for t from 1.5 to 2.0 ms) was used instead of the moderator temperature of 299°K (see Fig. 10). Disagreement between T_0 (asymptotic) and moderator temperature is attributed to the errors in the measurement of the flux depression factor D (t). To check the dependence of measured t_{th} on the detector position, some experiments were undertaken by placing detectors in the other places, 8C6 and LW8. Thereby, some of the experimental results showed fairly larger values than 296 μs, but agreed well within the experimental error, 50 μs. The experimental value of (296± 50) μs showed a fairly good agreement with the theoretical value of 307 μs, based on the Yoshimori-Kitano model, obtained by TAKAHASHI [15].

5. CONCLUSION

Slowing-down times of 1.46 and below 0.61, 0.50, 0.41 and 0.21 eV and thermalization time constants in graphite were measured by the transmission method. These experimental results showed a fairly good agreement with the theoretical values, including chemical binding in the graphite lattice.

ACKNOWLEDGEMENTS

The authors wish to express their appreciation to Messrs. R. Kurokawa and F. Akino for their aid in the experiment and, their gratitude to Dr. H. Takahashi for his helpful advice and discussions.

REFERENCES

[1] MARSHAK, R.E., Rev. mod. Phys. 19 (1947) 185.
[2] VON DARDEL, Trans. roy. Inst. Technol. Stockholm. No. 75 (1954).
[3] KAZARNOVSKY, M.V. et al., Thesis of the Lebedev Institute of Physics of the Academy of Science (1955)
[4] KRIEGER, T.J. and FEDERIGHI, F.D., Trans. Amer. nucl. Soc. 2 2 (1959) 102.
[5] CROUCH, M.F., Nucl. Sci. Engng 2 (1957) 631-39.
[6] HIRAKAWA, N., Fall Meeting of Atomic Energy Society of Japan 33 (1961).
[7] MÖLLER, E. and SJÖSTRAND, N.G., Rpt. AE-21 (1963).
[8] PROFIO, A.E. and ECKARD, J.D., Nucl. Sci. Engng 19 (1964) 321-28.
[9] KOPPEL, J., Trans. Amer. nucl. Soc. 3 2 (1960).
[10] KAZARNOVSKY, M.V. et al., Proc. 2nd UN Int. Conf. PUAE 16 (1958) 279.
[11] KATZURAGI, S., Nucl. Sci. Engng 13 (1962) 215-29.
[12] PUROHIT, S.N., Nucl. Sci. Engng 9 (1961) 157-67.
[13] FURUHASHI, A., J. nucl. Sci. Techn. 4 (1962) 677-84.
[14] SINGWI, K.S. and KOTHARI, L.S., J. nucl. Energy 8 (1958) 59.
[15] TAKAHASHI, H., Rpt. BNL-719(C-32) (1962).
[16] YOSHIMORI, A. and KITANO, Y., J. phys. Soc. Japan 11 (1956) 352-61.
[17] BECKURTS, K.H., Nucl. Sci. Engng 2 (1957) 516-22.
[18] SUMITA, K. et al., JAERI-Memo 1290.

DISCUSSION

M. KÜCHLE: The thermalization time of graphite which you measured, 296 μs, is much shorter than the value obtained by Schweickert*. This may be due to the fact that your source was not strong enough and that you were measuring essentially the second energy harmonic.

Y. KANEKO: We tried to reduce the contribution of the second energy mode by applying a correction factor $[1 + A(T - T_0)/2\,T_0(A+1)]^{-1}$ to measured $T - T_0$. This is discussed in the paper.

K.H. BECKURTS: Your value of 296 μs is not very far off from a value of about 200 ± 50 μs which I obtained about ten years ago in a transmission experiment. We also measured between 0 and 1 ms only, and we now believe that we obtained the second energy mode. To measure the fundamental mode, one should measure the transmission between 1 and 3 ms. This is extremely difficult, however, because the deviations of the spectrum from the asymptotic state are very small.

* SCHWEICKERT, H., Diploma Thesis, Karlsruhe, 1964.

NEUTRON MODERATION STUDIED BY THE TIME-DEPENDENT REACTION RATE METHOD

E. MÖLLER
AB ATOMENERGI, STUDSVIK, SWEDEN

Abstract — Résumé — Аннотация — Resumen

NEUTRON MODERATION STUDIED BY THE TIME-DEPENDENT REACTION RATE METHOD. Time-dependent neutron spectra have been studied in water, ice and heavy water, using the 5.5-MeV Van de Graaff accelerator at Studsvik as a pulsed neutron source. The change of the spectrum with time, after the injection of the neutrons in the moderator, has been followed by the detection and time analysis of prompt gamma rays which come from the reaction between the flux and the neutron-capturing, spectrum indicators (with known capture cross-section) which have been distributed in small quantities in the moderator. Earlier measurements on the thermalization in water have been extended to the slowing-down region by the use of indium as a spectrum indicator and by measuring with a time resolution of 0.05 μs. The results are in good agreement with the theory for the slowing-down caused by collisions with free protons. The space-dependence near the source of the time-dependent neutron density has been compared with recent theoretical work. In ice the thermalization time constant has been measured. The value obtained, 5 μs, deviates only slightly from the earlier value obtained for water, after correction for the density difference. This implies only a small difference in the integral parameters of the scattering law for the two states of water. Time-dependent reaction rate curves have also been measured for heavy water, using a volume of 900 l and indium, cadmium and gadolinium as indicators. Von Dardel's trial function for the time-dependent density during slowing down has been verified. The thermalization proceeds with a time constant of 33 μs and has been completed after 200 μs.

ÉTUDE DU RALENTISSEMENT DES NEUTRONS PAR LA MÉTHODE DE LA VITESSE DE RÉACTION. L'auteur a étudié les spectres des neutrons en fonction du temps dans l'eau, la glace et l'eau lourde, en utilisant l'accélérateur Van de Graaff de 5,5 MeV de Studsvik comme source de neutrons pulsés. Il a observé les modifications du spectre dans le temps, après l'injection des neutrons dans le ralentisseur, par la détection et l'analyse en temps des rayons gamma instantanés provenant de la réaction entre le flux et des indicateurs de spectre ayant une section efficace de capture connue, qui avait été répartis en petites quantités dans le ralentisseur. Il a étendu les mesures antérieures sur la thermalisation dans l'eau à la région de ralentissement en utilisant l'indium comme indicateur de spectre et en procédant à des mesures avec une résolution en temps de 0,05 μs. Les résultats concordent bien avec ceux que l'on obtient par la théorie du ralentissement par collisions avec des protons libres. L'auteur a également vérifié si les variations dans l'espace du nombre volumique des neutrons (variable aussi dans le temps) au voisinage de la source étaient conformes aux résultats des récents travaux théoriques. Dans la glace, la constante de temps de thermalisation a été mesurée. La valeur obtenue, 5 μs, n'est que très légèrement différente de la valeur obtenue précédemment pour l'eau et corrigée pour tenir compte de la différence de densité. Il n'y a donc qu'une petite différence entre les paramètres intégraux de la loi de diffusion pour ces deux états de l'eau. L'auteur a déterminé les courbes de la vitesse de réaction pour l'eau lourde en utilisant 900 litres de D_2O et de l'indium, du cadmium et du gadolinium comme indicateurs. La fonction préliminaire de Von Dardel, donnant la variation dans le temps de la densité au cours du ralentissement, a été vérifiée. La thermalisation s'effectue avec une constante de temps de 33 μs ; elle est terminée au bout de 200 μs.

ИЗУЧЕНИЕ ЗАМЕДЛЕНИЯ НЕЙТРОНОВ ПО МЕТОДУ ВРЕМЕННОЙ ЗАВИСИМОСТИ СКОРОСТИ РЕАКЦИЙ. Зависящие от времени спектры нейтронов изучены в воде, во льду и в тяжелой воде с помощью имеющегося в Студсвике ускорителя Ван де Граафа мощностью 5,5 Мэв в качестве источника импульсных нейтронов. Изменение спектра во времени после инжекции нейтронов в замедлитель прослеживалось путем детектирования и временного анализа мгновенных гамма-лучей, образующихся в результате реакции между пучком и индикаторами спектра захвата нейтронов с известным сечением захвата, которые были распределены в небольших количествах в замедлителе. Более ранние измерения термализации в воде были распространены на область замедления путем использования индия в качестве ин-

дикатора спектра и измерений с разрешающей способностью по времени 0,5 мксек. Результаты хорошо согласуются с теорией замедления в результате столкновения со свободными протонами. Пространственное распределение вблизи источника зависящей от времени плотности нейтронов сопоставлено с результатами последних теоретических работ. Измерена постоянная времени термализации во льду. Полученное значение (5 мксек) лишь немного отличается от ранее полученного значения для воды после внесения поправки на разницу в плотности. Это говорит о наличии лишь небольшой разницы между интегральными параметрами закона рассеяния для этих двух состояний воды. Измерены также кривые временной зависимости скорости реакции для тяжелой воды, для чего использовался объем 900 л и индий, кадмий и гадолиний в качестве индикаторов. Подтверждена функция Дардела для зависящей от времени плотности во время замедления. Термализация протекает с постоянным временем 33 мксек, и она была завершена после 200 мксек.

ESTUDIO DE LA MODERACION NEUTRONICA CON EL METODO DE LA VELOCIDAD DE REACCION EN FUNCION DEL TIEMPO. Empleando como fuente de neutrones pulsados el acelerador Van de Graaff de 5, 5 MeV de Studsvik, el autor ha estudiado los espectros neutrónicos en función del tiempo correspondientes a la difusión en agua ordinaria, en hielo y en agua pesada. La variación del espectro en función del tiempo, después de inyectar los neutrones en el moderador, se observó por detección y análisis de tiempo de los rayos gamma inmediatos procedentes de la reacción entre los neutrones incidentes y los indicadores del espectro neutrónico con sección eficaz de captura conocida que se habían distribuido en pequeñas cantidades en el moderador. Las mediciones de la termalización en el agua realizadas previamente se ampliaron a la región de moderación, empleando In como indicador espectral y efectuando las mediciones con un tiempo de resolución de 0, 05 μs. Los resultados concuerdan con los valores teóricos de la moderación de los neutrones por choque con los protones libres. El autor compara la variación espacial de la densidad neutrónica en función del tiempo en las proximidades de la fuente, con los resultados de recientes trabajos teóricos. Se ha medido la constante de tiempo de termalización en el hielo; el valor obtenido, 5 μs, sólo difiere ligeramente del hallado previamente para el agua, después de corregido para tener en cuenta la diferencia de densidad. Esto quiere decir que entre los parámetros integrales de la ley de dispersión para los dos estados del agua hay sólo una pequeña diferencia. También se han medido las curvas de la velocidad de reacción en función del tiempo correspondientes al agua pesada, empleando un volumen de 900 l e indio, cadmio y gadolinio como indicadores. Se ha verficado la función de prueba de Von Dardel para la variación de la densidad en función del tiempo durante la moderación. La termalización comienza con una constante de tiempo de 33 μs y queda completada al cabo de 200 μs.

1. INTRODUCTION

The principle of the time-dependent reaction rate method for the study of the time-dependent flux $\phi(E, t)$ is to measure as a function of time the reaction rate of the flux with a spectrum indicator, a neutron capturing element, which is distributed in small quantities in the moderator. The reaction rate is detected by the emitted gamma rays and recorded by a time analyser, synchronized to the pulsed fast neutron source. The recorded quantity will be

$$R(t) = \int \phi(E, t)\Sigma_a(E)dE \ , \qquad (1)$$

where $\Sigma_a(E)$ is the energy-dependent capture cross-section of the spectrum indicator. The reaction rate curve will display transients when the flux passes energy regions, where the cross-section deviates from the 1/v law. Combined with fast pulsing of the neutron source, the method allows neutron moderation studies to be extended into the slowing-down region even for the lightest moderators. The information obtainable consists mainly of scatter-

ing cross-sections, integral parameters of the scattering law and transport effects on slowing-down.

In earlier work by MÖLLER and SJÖSTRAND [1-3], the thermalization in water was studied by the use of cadmium, samarium and gadolinium as spectrum indicators. These studies have been extended to the electron volt region for light water. The corresponding measurements have been made in heavy water. Thermalization studies have also been performed in ice.

2. THE TIME-DEPENDENCE OF SLOWING-DOWN IN WATER

2.1. Theory

MARSHAK [4] has given an equation for the density $n(v, t)$ of neutrons of velocity v at the time t after the injection of fast neutrons in hydrogen:

$$n(v, t) = \frac{vt^2}{l_s^2} e^{-vt/l_s} . \tag{2}$$

l_s is the scattering mean free path, assumed to be constant. The equation implies integration of the histories of all the emitted neutrons. For a velocity v, the density will be at a maximum when the time

$$t_{max,n} = 2l_s/v \tag{3}$$

Another interesting function is the slowing-down density, $q(v, t)$, which can be derived from Eq.(2).

$$q(v, t) = \frac{v^2 t}{l_s^2} e^{-vt/l_s} \tag{4}$$

The slowing-down density is at maximum when the time

$$t_{max,q} = l_s/v \tag{5}$$

In an experimental situation, the neutron pulse is emitted from a point in the medium. The above equations should then include the space-dependence, due to diffusion during the moderation. CLAESSON [5] has obtained an expression for $n(r, v, t)$ in a P_1-approximation. The equation is quite complicated; the space-dependence of $t_{max,n}$ is given graphically. DYAD'KIN and BATALINA [6] have given a general treatment of the time variation of the space-energy distribution for the case of mixtures of different nuclei. Both theories show an increase with the distance from the source of $t_{max,n}$, the latter work to a greater extent than the former.

2.2. Earlier experiments

Attempts to verify Eq.(2) by direct measurement have been made by ENGELMANN [7] and PROFIO and ECKARD [8]. They detected gamma rays from the neutron capture in the resonance of indium at 1.46 eV. Due to low source intensity, a detailed curve could not be obtained, but the existence of the peak and its approximate position were clearly established.

2.3. The present investigation

Measurements of the reaction rate for indium were performed in a 1-m cube of water, in the centre of which short pulses of neutrons with a mean energy of 1 MeV were produced by means of a Van de Graaff accelerator and the $Li^7(p,n)Be^7$ reaction in a thick lithium target. To reduce the overlap between the cycles, the water was poisoned with boric acid to give a mean lifetime for the neutrons of 60 μs. The measurements were made with a time resolution of 0.04 μs. A weak indium sulphate solution, mixed with boric acid solution, in a plastic container was placed in the tank with a gamma-ray detector situated above. The position of the container relative to the detector could be varied. Time analysis of the detector pulses was performed by time-to-pulse-height conversion and pulse-height analysis. Discrimination was applied against 2.2-MeV gamma rays from the water. Two container sizes were used, 1.5 l and 0.4 l.

The use of a weak solution is very important. A measurement with a thick plate of indium would result in the recording of the time-dependent slowing-down density, not the density, succeeded by the effects of diffusion into the region of flux depression. The reaction rate curve would have its maximum at half the time given by Eq.(3). A strong solution will also cause peak-shifts to shorter times if the probability of resonance capture is comparable to that of scattering.

Figure 1 shows the result of a measurement at a distance of about 11 cm from the source. Correction for the dead-time of the time analyser and subtraction of the background measurement have been included. The indium concentration was such as to result in a macroscopic cross-section at the resonance of 0.237 cm^{-1}, which would change the decay time constant $(v\Sigma_t)^{-1}$ at the resonance energy of 1.46 eV from 0.450 μs to 0.385 μs, thus introducing a time shift not greater than 0.065 μs.

A theoretical curve may be obtained by calculating Eq.(1) for different times, deriving $\phi(E,t)$ from Eq.(2) and taking $\Sigma_a(E)$ from the Brookhaven National Laboratory Report BNL-325. The calculation can be continued to long times with an accuracy of a few per cent although Eq.(2) becomes invalid, since the cross-section becomes proportional to 1/v. The asymptotic reaction rate is proportional to the neutron density, independent of the spectrum shape. If the 1/v absorption in the water is taken into account, the result may be written

$$R(t) = (A_1 t^2 e^{A_2 t} + A_3)\, e^{-\lambda_a t} \quad , \tag{6}$$

where λ_a is the decay constant for absorption. To establish the value of $t_{max,n}$ at different distances from the source, least squares fits of Eq.(6)

were made to the recorded curves. In Fig. 1 the solid line is the fitted curve for this measurement. The resulting value of $t_{max,n}$ at this position is 0.95 μs. The value for the space-independent case obtained from Eq. (3) with $l_s = 0.75$ cm is 0.90 μs. It is seen that the shape of the curves is very well reproduced by a function of the type given in Eq. (2).

The $t_{max,n}$-values from measurements at a number of distances have been plotted in Fig. 2, where also theoretical values from CLAESSON [5] (Theory I) and DYAD'KIN and BATALINA [6] (Theory II) are shown. Since the experimental source is not monoenergetic, an exact comparison cannot be made. Time-shift correction should also be added to the experimental values. Claesson's curve is seen to reproduce the experiment rather well. The other curve could, by a reasonable change of a parameter in the (approximate) equation for $t_{max,n}$ in [6], be brought down by 8%; the space-dependence seems to be overestimated anyhow. The horizontal line at 0.90 μs represents the infinite medium value. A measurement with very small indium concentration in the whole tank and with the detector placed 9 cm from the source gave a $t_{max,n}$ close to the theoretical value. Since the efficiency of the gamma-ray detector influences the spatial weighting of the reaction rate curves, a better agreement would be fortuitous.

3. THE TIME-DEPENDENCE OF MODERATION IN HEAVY WATER

3.1. Theory

The time scale of the slowing down to the eV region in heavy water will essentially be given by the theory for slowing down in a deuteron gas. MARSHAK [4] also treated this case, and gave a function for the density, which can be made to approach the exact solution by the adjustment of the parameter b. VON DARDEL [9] also studied the properties of this function and found an optimum value for the parameter b of 0.903. The time-dependent neutron density will then be given by the following equation:

$$n(v,t) = \frac{t}{l_s}\left(\frac{vt}{l_s}\right)^{1.25} \exp\left[-\left(\frac{vt}{l_s} + \frac{0.903\, l_s}{vt}\right)\right] \qquad (7)$$

The maximum neutron density is found at the time when

$$t_{max,n} = 2.597\, l_s/v \quad . \qquad (8)$$

There are other papers on this topic; for references see KOPPEL [10] and BOFFI [11]. The space-dependent case has been treated by DYAD'KIN and BATALINA [6].

The approach-to-equilibrium has been studied by many authors. See VON DARDEL [9] and BECKURTS and WIRTZ [12]. The earlier theory relates the temperature of the spectrum to time by the following equation:

$$T(t) - T_0 \sim e^{-t/t_T}, \qquad (9)$$

where t_T is the time constant for thermalization. Later theoretical work has concentrated on the expansion of the flux as a sum of eigenfunctions which decay, each with its own decay constant (eigenvalue). The temperature concept treatment results in a time constant of 58 μs, if the molecule is considered as rigid [13]. For a recent review of thermalization parameters, see PUROHIT and SJÖSTRAND [14].

3.2. Earlier measurements

VON DARDEL [9] measured the time-dependence of the transmission of neutrons in heavy water through cadmium. Although many effects limit the applicability of Eq.(7) to the experimental results, good agreement was found with the transmission derived therefrom. EICHELBERGER [15] and PROFIO and ECKARD [8] measured the time distribution of indium capture-gamma-rays in small geometries of heavy water. They found an increased counting rate in the region 5-8 μs. The expected value of $t_{max,n}$, calculated from Eq.(8), is 7.0 μs.

3.3. The present measurements on D_2O

Measurements have been made of the time-dependent reaction-rate curves for indium, cadmium and gadolinium to obtain (a) curves for n(v, t), which could be compared to the existing theories for the space-dependence of slowing-down and (b) space- and time-dependent reaction-rate curves during the thermalization, which could be compared to theoretical curves for R(t, r) that can be obtained if ϕ(E, r, t) can be calculated. The first step would be to perform a space integration to compare with infinite medium calculations.

Preliminary experiments in a 50-l volume revealed that the effects of the source spectrum, the geometry and the leakage would make the results difficult to interpret. Measurements have therefore been completed in a 1-m^3 tank. The water had a light water content of 0.5%. The indicator concentration was varied in some of the measurements. The volume of the indicator container was 5 l in most of the measurements. The gamma-ray detector was kept 6 cm above the container, which could be moved horizontally.

Low concentrations had to be used for several reasons, and this caused a rather bad signal-to-background ratio. The analysis of the results has not yet been finished. The following figures should therefore be regarded as preliminary.

Figure 3 shows the result of a measurement with indium. The position was about 25 cm from the source, and the concentration corresponds to $\Sigma_a = 0.237$ cm^{-1}. The shift to shorter time, caused by this, is less than 0.7 μs. The solid line curve is the theoretical curve for n(v, t), Eq.(7). The agreement between theory and experiment is quite good. Since this is the spatial region where most neutrons having energies of 1.46 eV are found, this is to be expected.

Figure 4 shows cadmium curves, measured with a concentration which would give a thermal lifetime in the infinite medium of 600 μs. The position in the tank is indicated for each curve. The curves have been normalized

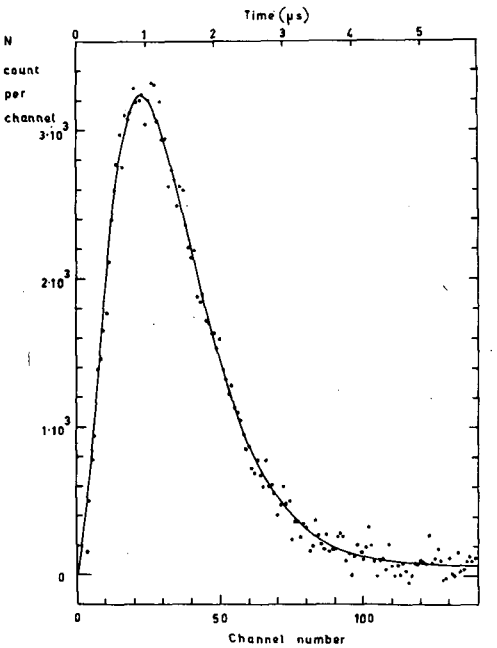

Fig. 1

Measurement of n(v, t) in H_2O, using the indium resonance at 1.46 eV

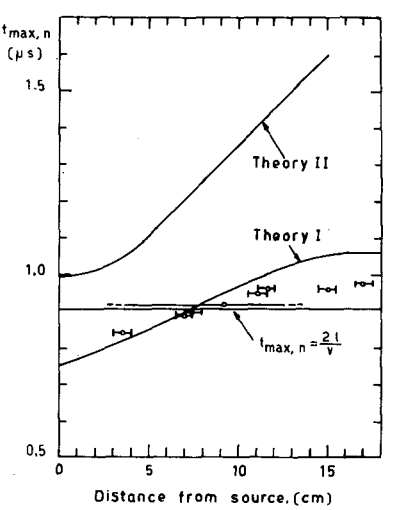

Fig. 2

Space-dependence of the time for maximum neutron density in H_2O

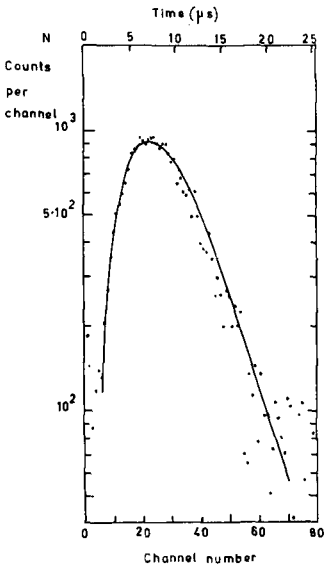

Fig. 3

Measurement of n(v, t) in D_2O, using the indium resonance at 1.46 eV

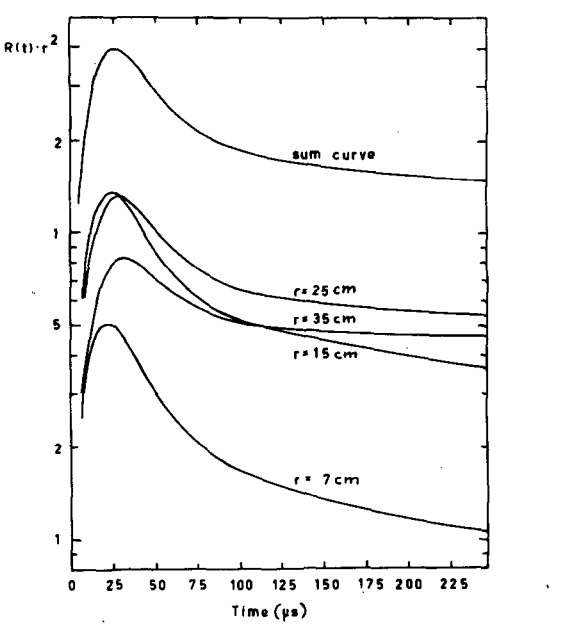

Fig. 4

Reaction rate curves for cadmium at various positions in D_2O

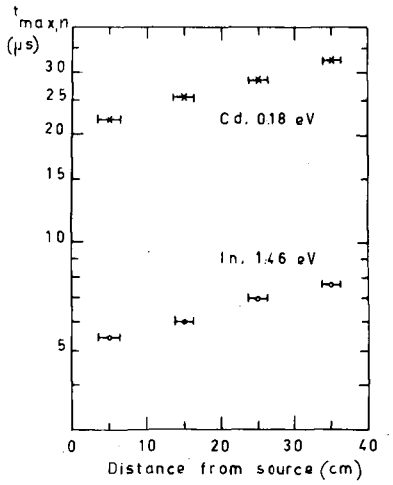

Fig. 5

Space-dependence of the time for maximum neutron density at the indium and cadmium energies in D_2O

and multiplied by r^2 before plotting. The upper curve is the sum of the four lower curves, and should represent the integral curve for the tank. The leakage should not exceed about 10% when all the neutrons have become thermalized. For r = 7 cm the peak in the cadmium curve is quite early in time; with increasing distance, the peak comes later. The decay of the neutron energy and density is fast at short distances. At the greatest distance it is seen that the number of neutrons leaking out is compensated by the neutron wave from the centre, which even causes a tendency for the density to increase at longer times.

The sum curve may be analysed by comparison with a calculated R(t) curve. This may be a useful way to judge different D_2O models. Such work is in progress [16]. By fitting a sum of exponentials to the curve after a time of about 75 μs, one may obtain the thermalization time constant. Two measurements with cadmium solutions with absorption corresponding to a thermal lifetime of 600 and 1800 μs and one measurement with a gadolinium solution of 600-μs lifetime yielded a thermalization time constant of 33 ± 4 μs. The thermalization was completed after 200 μs.

Figure 5 shows the time for the peak in the measured curves as a function of the distance from the source. The effects of the diffusion are quite large in heavy water, and a comparison with a suitable theory is of great interest. The expression for $t_{max,n}$ in Ref. [6] gives also a too-strong dependence of $t_{max,n}$ on the distance from the source. The absolute values also come out rather high.

4. THE THERMALIZATION TIME CONSTANT FOR ICE

A measurement has also been made of the thermalization time constant for ice of 268°K. The volume of the moderator was 15 l, and the indicator

was distributed in a volume of 1.5 l at the centre. Two methods of distributing the indicator were tried. In one case, a cold solution of cadmium sulphate was frozen very quickly. In the other case, a fine powder of cadmium oxide was frozen into the water. The outer region was matched in thermal cross-section by freezing boron powder into it. The results of the measurements were compared to liquid water measurements in the same geometry. The powder measurements gave distorted curves due to the imperfect distribution. The measurement with the frozen solution gave a thermalization time constant of 4.8 ± 0.5 μs. Thus, these measurements do not show the effects of a doubling of the time constant at the water-ice transition, as derived by ANTONOV et al. [17] from diffusion cooling measurements.

5. CONCLUSIONS

The results obtained in the reaction rate measurements above give results which verify directly the theoretical expressions for the time-dependence of slowing down in light and heavy water. The value of the thermalization time constant is in good agreement with the results from the calculations by PUROHIT [16] and also with the recently published results from the Rensselaer group. For detailed analysis of the results, further theoretical work on space- and time-dependent thermalization is needed.

These measurements have all been made with weak concentrations of spectrum indicator. One may, however, reverse the situation and put large amounts of indicator into the moderator, in which case the time constant is not measured directly. However, if such measurements are compared with multigroup calculations of the reaction rate, one may check different scattering models in a way similar to that for the stationary spectrum. Work along this line is planned.

REFERENCES

[1] MÖLLER, E. and SJÖSTRAND, N.G., Rpt. BNL 719 (C-32) (1962) 966-76.
[2] MÖLLER, E. and SJÖSTRAND, N.G., Nucl. Sci. Engng 15 (1963) 221.
[3] MÖLLER, E. and SJÖSTRAND, N.G., Ark. Fys. 27 (1964) 501.
[4] MARSHAK, R.E., Rev. mod. Phys. 19 (1947) 194-98.
[5] CLAESSON, A., AB Atomenergi Rpt. AE-129 (1963).
[6] DYAD´KIN, I.G. and BATALINA, E.P., Reactor Sci. Technol. 16 (1962) 103-09.
[7] ENGELMANN, P., Nukleonik 1 (1958) 125-28.
[8] PROFIO, A.E. and ECKARD, J.D., Nucl. Sci. Engng 19 (1964) 321-28.
[9] VON DARDEL, G.F., Trans. Roy. Inst. Techn., Stockholm No. 75 (1954).
[10] KOPPEL, J., Nucl. Sci. Engng 8 (1960) 157-63.
[11] BOFFI, V.C., Ann. Phys. (N.Y.) 27 (1964) 297-330.
[12] BECKURTS, K.H. and WIRTZ, K., Neutron Physics, Springer-Verlag, Berlin (1964) 226-32.
[13] VON DARDEL, G. and SJÖSTRAND, N.G., Prog. nucl. Energy, Ser. 1, 2 (1958) 183-221.
[14] PUROHIT, S.N. and SJÖSTRAND, N.G., "Neutron thermalization parameters", these Proceedings 1.
[15] EICHELBERGER, W., Nukleonik 4 (1962) 326-31.
[16] PUROHIT, S.N., private communication.
[17] ANTONOV, A.V., GRANATKIN, B.V., MERKULEV, Yu.A., PUSANOV, V.V. and SMOLIK, C.K., Soviet J. atom. Energy 13 (1963) 983-84.

DATA EVALUATION PROBLEMS IN THE PULSED NEUTRON SOURCE METHOD

L. PÁL, L. BOD AND Z. SZATMÁRY
CENTRAL RESEARCH INSTITUTE FOR PHYSICS,
HUNGARIAN ACADEMY OF SCIENCES, BUDAPEST, HUNGARY

Abstract — Résumé — Аннотация — Resumen

DATA EVALUATION PROBLEMS IN THE PULSED NEUTRON SOURCE METHOD. To determine the diffusion parameters of thermal neutrons the pulsed method has been in use for more than a decade. This method proves to be particularly suitable for the investigation of hydrogenous moderators. Results of measurements in water, benzene, toluene, xylene, cyclohexane, n-hexane and diphenyl are reported and the methods by which the diffusion parameters of interest can be evaluated from the measured data with the least error are discussed.

The time-of-flight effect, manifesting itself, for technical reasons, in the investigation of moderators at elevated temperatures and influencing the value of the decay constant, is investigated in detail both theoretically and experimentally, and the geometrical conditions under which proper accuracy can be achieved are given. The effect of the dead-time of the neutron detector and amplifier system on the value of the decay constant is also determined and it is shown that the effect of dead-time can be neglected when $[i(t)\,\tau]^2 \ll 1$, where $i(t)\,dt$ is the number of neutrons detected in the time interval $(t,\ t+dt)$ and τ is the dead-time.

For the evaluation of the decay constant the maximum likelihood method is used. For unambiguous determination of the likelihood function, the multi-channel analyser was operated in such a way as to store a maximum of one pulse per analysing cycle and per channel. It is of primordial importance to incorporate the parameter characterizing the background into the likelihood function. The parameters of the maximum likelihood function were evaluated by Newton iteration on a computer. If the background is not properly taken into account, this may cause apparent higher harmonic contamination, while higher harmonic contamination, in turn, may be taken for an apparent background. Therefore, it is particularly important to determine the parameter characterizing the background directly from the decay data obtained at several delay times.

The diffusion parameters were computed by the weighted least-squares method using the decay constants of minimum standard deviation evaluated from the maximum likelihood function. Since, for the materials investigated, the values of the transport mean free path were not known, a fast converging iteration procedure was elaborated for the determination of the transport mean free path. The computer evaluation made it possible to determine the coefficients of the B^6 and higher order terms of the decay constant. The diffusion parameters of the hydrogenous materials investigated were calculated by the Radkowsky prescription from the energy dependence of the integral scattering cross-sections. The calculations have shown that the Radkowsky prescription is a useful empirical method for the evaluation of the transport mean free path of numerous hydrogenous materials.

PROBLÈMES D'ÉVALUATION DES DONNÉES DANS LES APPLICATIONS DE LA MÉTHODE DE LA SOURCE PULSÉE. Pour obtenir les paramètres de diffusion des neutrons thermiques, on emploie depuis plus de dix ans la méthode des neutrons pulsés. Cette méthode convient tout particulièrement pour l'étude des ralentisseurs hydrogénés. Les auteurs donnent les résultats des mesures pour l'eau, le benzène, le toluène, le xylène, le cyclohexane, le n-hexane et le diphényle et discutent les méthodes permettant d'évaluer avec le minimum d'erreurs les paramètres de diffusion intéressants, à partir des données mesurées.

Ils étudient en détail au point de vue théorique et expérimental l'effet du temps de vol qui se fait sentir lors des recherches sur les ralentisseurs à des températures élevées pour des raisons techniques, et influe sur la valeur de la constante de décroissance; ils indiquent les conditions géométriques dans lesquelles on peut obtenir une bonne précision. Ils déterminent en outre l'effet du temps mort du détecteur de neutrons et du système d'amplification sur la valeur de la constante de décroissance: l'effet du temps mort peut être négligé si $[i(t)\,\tau]^2 \ll 1$, où $i(t)\,dt$ est le nombre des neutrons détectés dans l'intervalle de temps $(t,\ t+dt)$ et τ le temps mort.

Pour évaluer la constante de décroissance, on applique la méthode de la probabilité maximum. Pour déterminer la fonction de probabilité de façon non ambiguë, les auteurs ont réglé l'analyseur multicanal de manière qu'un acte d'enregistrement au maximum puisse être stocké par cycle d'analyse et par canal. Ils ont constaté qu'il est d'une importance primordiale d'incorporer le paramètre caractérisant le bruit de fond dans

la fonction de probabilité. Ils ont évalué les paramètres de la fonction de probabilité maximum par itération de Newton à l'aide de la calculatrice. Faute de tenir compte du bruit de fond d'une manière convenable, il peut se produire une contamination harmonique apparente plus élevée, et cette contamination risque d'être prise à son tour pour un bruit de fond apparent. Il est donc particulièrement important de déterminer directement le paramètre caractérisant le bruit de fond à partir de données concernant la décroissance obtenues après plusieurs temps de retard.

Les auteurs ont calculé les paramètres de diffusion par la méthode des moindres carrés pondérés, en utilisant les constantes de décroissance d'écart type minimum évaluées à partir de la fonction de probabilité maximum. Comme ils ne connaissaient pas, pour les matières faisant l'objet des expériences, les valeurs du libre parcours moyen de transport, ils ont mis au point une formule d'itération rapidement convergente, pour déterminer le libre parcours moyen de transport. L'évaluation à l'aide d'une calculatrice a permis de déterminer les coefficients du terme en B^6 et des termes d'ordre supérieur de la constante de décroissance. Les auteurs ont calculé les paramètres de diffusion pour les matières hydrogénées par la formule de Radkowsky à partir des variations des sections efficaces de diffusion intégrales selon l'énergie. Ces calculs montrent que la formule de Radkowsky constitue une méthode empirique qui a son utilité pour évaluer le libre parcours moyen de transport dans de nombreuses matières hydrogénées.

ПРОБЛЕМЫ ОЦЕНКИ ДАННЫХ ПРИ ПРИМЕНЕНИИ МЕТОДА ИСТОЧНИКА ИМПУЛЬСНЫХ НЕЙТРОНОВ. Для определения диффузионных параметров тепловых нейтронов уже более десяти лет применяется импульсный метод. Этот метод оказался весьма подходящим для исследования гидрогенных замедлителей. Сообщаются результаты измерений в воде, бензоле, толуоле, ксилон-циклогексане, n-гексане и дифениле; обсуждаются методы, с помощью которых на основании измеренных данных с наименьшей погрешностью можно определить параметры диффузии, представляющие интерес.

Ввиду того, что при исследовании замедлителей при высоких температурах встречаются *затруднения технического характера* из-за проявления воздействия времени пролета, что оказывает влияние на величину константы распада, то это явление подробно исследуется как теоретически, так и экспериментально; указываются геометрические условия, дающие возможность обеспечить надлежащую точность. Определяется также влияние времени отставания детектора нейтронов и усилительной схемы на величину константы распада и доказывается, что временем отставания можно пренебречь, если $[i(t)\tau]^2 \ll 1$, где $i/t/dt$ выражает число нейтронов, обнаруженных за промежуток времени $(t, t+dt)$, а τ обозначает время отставания.

Для оценки константы распада применяется метод максимальной вероятности. Для однозначного определения функции вероятности был выбран многоканальный анализатор, который работал таким образом, что для каждого цикла анализа и для каждого канала заносилось в память только одно зарегистрированное событие. Обнаружено, что введение в функцию *вероятности параметра, характеризующего фон, имеет первостепенное значение*. Параметры функции максимальной вероятности были определены на счетно-решающем устройстве по Ньютоновскому методу повторений.

Если не принимать в расчет фоновые шумы, то это может вызвать явное, более сильное гармоническое загрязнение, а оно в свою очередь, может быть принято за явный фон. Поэтому представляется особенно важным определить характеризующий фон параметр непосредственно из данных распада, полученных для разных времен замедления.

Диффузионные параметры подсчитывали по методу взвешенных наименьших квадратов с использованием констант распада наименьшего стандартного отклонения, определенных по функции максимальной вероятности. Так как для исследуемых материалов не были известны величины среднего свободного пути переноса, то для определения среднего свободного *пути переноса была выработана быстро конвергирующая повторная формула*. Использование счетно-решающего устройства дало возможность определить коэффициенты константы распада порядка B^6 и даже более высоких порядков. Диффузионные параметры исследуемых гидрогенных материалов были подсчитаны с помощью осаждения по методу Радковского на основании зависящих от энергии глобальных поперечных сечений рассеяния. Расчеты показали, что осаждение по методу Радковского является полезным эмпирическим методом для определения среднего свободного пути переноса многих гидрогенных материалов.

PROBLEMAS DE EVALUACION DE DATOS EN EL METODO DE LA FUENTE DE NEUTRONES PULSADOS. Desde hace más de diez años se viene empleando el método de los neutrones pulsados para determinar los parámetros de difusión de los neutrones térmicos. Este método ha resultado especialmente idóneo para el estudio de los moderadores hidrogenados. Los autores dan los resultados de las mediciones hechas en agua, benceno,

tolueno, xileno, ciclohexano, n-hexano y difenilo, y examinan los métodos para evaluar con el mínimo error los parámetros de difusión de interés partiendo de los datos obtenidos en las mediciones.

Se examina detenidamente, tanto en el plano teórico como en el experimental, el efecto de tiempo de vuelo que se manifiesta por razones técnicas cuando se investigan moderadores a elevadas temperaturas, y que influye en el valor de la constante de desintegración, y se exponen las condiciones geométricas en que se ha de operar para obtener resultados satisfactorios. Los autores determinan también el efecto que sobre la constante de desintegración ejerce el tiempo muerto del detector neutrónico y del amplificador, y demuestran que es despreciable cuando $[\, i(t)\, \tau\,]^2 \ll 1$, siendo i/t/dt el número de neutrones detectados en el intervalo de tiempo/t, t+dt/, y τ el tiempo muerto.

Se evaluó la constante de desintegración empleando el método de la máxima probabilidad. Para determinar inequívocamente la función de probabilidad, se eligió un analizador multicanal que acumulaba como máximo una sola señal por ciclo de análisis y por canal. Se comprobó que la incorporación del parámetro característico del fondo a la función de probabilidad tiene primordial importancia. Los parámetros de la función de máxima probabilidad se evaluaron en una calculadora aplicando el método de iteración de Newton. Cuando no se tiene debidamente en cuenta el fondo, éste puede causar una mayor contaminación aparente de armónicos, la cual, a su vez, puede interpretarse como un fondo aparente. Por ello es muy importante determinar directamente el parámetro característico del fondo, partiendo de los datos de desintegración obtenidos empleando diversas demoras.

Los parámetros de difusión se calcularon con el método de los cuadrados mínimos ponderados, empleando las constantes de desintegración de desviación tipo mínima obtenidas según la función de máxima probabilidad. Como no se conocían los valores del recorrido libre medio de transporte para los materiales investigados, se ideó un procedimiento de iteración rápidamente convergente para determinarlo. Con la calculadora se pudieron determinar los coeficientes de orden B^6 y los términos superiores de la constante de desintegración. Los parámetros de difusión de los materiales hidrogenados investigados se calcularon con la fórmula de Radkowsky, partiendo de la variación de las secciones eficaces integrales de dispersión en función de la energía. Los cálculos demuestran que la fórmula de Radkowsky proporciona un método empírico muy útil para evaluar el recorrido libre medio de transporte en gran número de materiales hidrogenados.

1. INTRODUCTION

In the last decade the pulsed neutron source technique has been used extensively for investigating the thermal neutron diffusion parameters in moderators. This method proved to be particularly useful for hydrogenous moderators. The advantage of this method over the stationary technique is that it permits the simultaneous determination of different parameters, such as absorption cross-section, transport mean free path and diffusion cooling coefficient.

The primary objective of the investigations continuing over several years at the Central Research Institute for Physics, Budapest, has been to clarify the influence of chemical binding on the diffusion parameters in a number of hydrogenous moderators. The measurements were carried out on water, benzene, cyclohexane, n-hexane, toluene, xylene and diphenyl. The values obtained for the transport mean free path were compared with those calculated from the measured cross-section data [1].

The present paper deals with the data evaluation methods by which the diffusion parameters can be calculated with the least error. In section 2 the experimental technique is briefly described; in section 3 the effect of time-of-flight is estimated; in section 4 the problems of statistical evaluation are discussed; and in section 5 the results of measurements are presented.

2. EXPERIMENTAL TECHNIQUE

The 14-MeV neutrons for the experiments were obtained from a pulsed 200-keV accelerator [2]. The pulse duration was 20 μs with a repetition rate of 300 or 600 pulses/s, according to the actual value of the decay constant. The mean current on the target was 15 or 30 μA, depending on the repetition rate. The yield was 10^6 neutrons per pulse. By pulsing not only the extracting voltage but also the ion source it was possible to avoid detection of fast neutrons between the individual pulses.

The measuring vessel was a straight cylinder with a piston (Fig. 1). The inside diameter and the height of the cylinder were 220 and 180 mm,

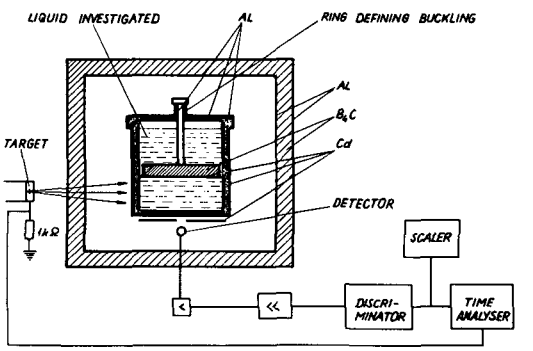

Fig. 1

Schematic view of the measuring apparatus

respectively. The position of the piston, thus the height of the liquid, was set with the aid of 14 to 16 rings of various heights. The use of these rings made it possible to reproduce accurately the same height at any time. The measuring vessel was protected from room-return thermal neutrons by a B_4C shield. A wall of paraffin bricks around the measuring vessel did not change the value of the decay constant, which proves the high efficiency of the cadmium coating and B_4C shield. To minimize the amplitude of the first axial harmonics, the neutrons were always injected symmetrically to the mid-plane of the actual liquid height.

A BF_3 proportional counter was used for measurements on benzene and cyclohexane and a scintillator containing B^{10} for measurements on the other moderators.

Special care must be taken in setting the discriminator level. Should the discriminator transmit pulses produced in the detector by the gammas from the cadmium coating, the diffusion taking place in the liquid above the piston would interfere with the measurement.

The channel width of the (20+4)· channel time analyser [3] was set to 40 or 100 μs, depending on the actual value of the decay constant. The time analyser was triggered by the ion pulses on the target. The 4 "background channels" could be delayed with respect to the 20 "effective channels". Before starting the measurements the detecting system and the time analyser

were checked by a Poisson test for randomness of counts and equivalency of channels.

3. THE TIME-OF-FLIGHT EFFECT

When there is an appreciable distance between the detector and the measuring vessel (necessarily so, for example, in high temperature experiments) or the detector is too thick, then, because of the finite flight time of the neutrons, the detection is somewhat delayed with respect to the neutron emergence. Since the flight time varies with neutron velocity, the measured decay will not show an exponential character. To study the time-of-flight effect, see Fig. 2, where H is a cut in the cadmium sheet covering the bottom

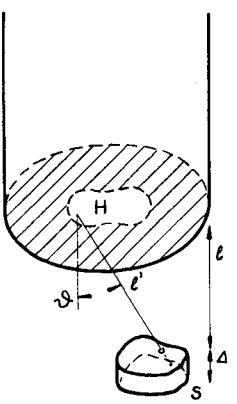

Fig. 2

Relative position of the measuring vessel to the detector

of the vessel, S the detector, l the distance between the detector and the vessel, Δ the thickness of the detector, l' the flight path between the points of emergence and detection and ϑ the angle between the normal to the bottom and the path l'.

Let i(t)dt be the number of neutrons detected in the interval (t, t+dt). The probability that a neutron with a velocity in the interval (v, v+dv) and a flight path in the interval (l', l'+dl') will be detected in the time interval (t, t+dt) is proportional to

$$\exp\left[-\alpha\left(t-\frac{l'}{v}\right)\right]dt\, f(l')dl'\, v\, \Sigma_a^d\, M(v)dv\ , \qquad (1)$$

where Σ_a^d is the absorption cross-section of the detector, M(v) the neutron spectrum and f(l') the probability density function of the flight path. Summing over all velocities above l'/t, averaging over l' and assuming $\Sigma_a^d \sim 1/v$ and M(v) to be the Maxwellian velocity spectrum, we obtain

$$i(t)dt = \text{const} \int f(l')dl' \int_{l'/t}^{\infty} \exp\left[-\alpha\left(t - \frac{l'}{v}\right)\right] v^2 \exp\left(-\frac{v^2}{v_0^2}\right) dv dt \,, \tag{2}$$

and finally

$$i(t) = \text{const} \; \exp\left(-\alpha t\right) \langle F(l', t) \rangle \,. \tag{2'}$$

Let us consider in Eq. (2') the function

$$F(l', t) = \int_{l'/t}^{\infty} \exp(\alpha l'/v) \, v^2 \exp(-v^2/v_0^2) dv \tag{3}$$

to find the extent of deviation from the exponential law. The brackets $\langle \rangle$ denote the averaging over l'.

By simple transformation one obtains from Eq. (3)

$$F(l', t) = \int_{0}^{v_0 t/l'} \exp\left(\frac{\alpha l'}{v_0} u\right) \frac{1}{u^4} \exp\left(-\frac{1}{u^2}\right) du \,. \tag{3'}$$

Plotting the function $F(l', t)$ for various l' and taking $\alpha = 10^4 \; s^{-1}$ and $v_0 = 2.2 \times 10^5$ cm/s we obtain the set of curves seen in Fig. 3.

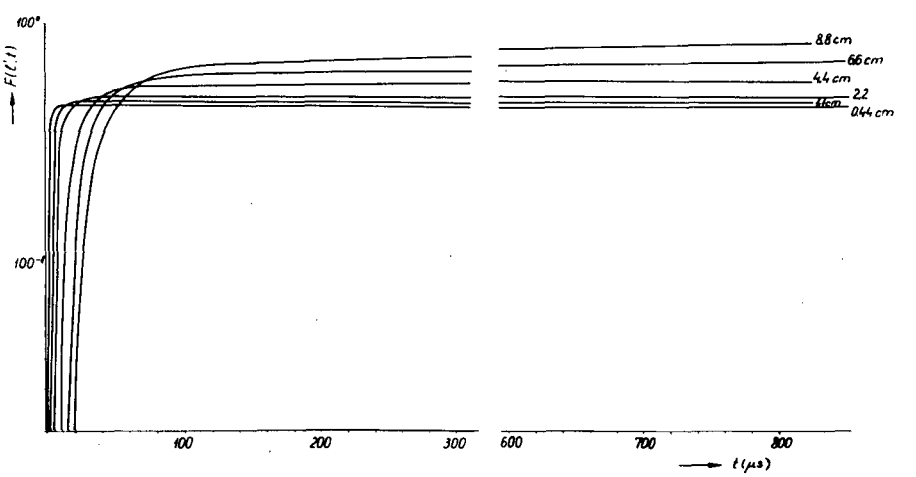

Fig. 3

$F(l', t)$ versus time at different values of l'

First, it is apparent that for a given value of t the function $F(l', t)$ depends slightly and fairly linearly on l'; thus in Eq. (2') we can write

$$\langle F(l', t) \rangle \approx F(\langle l' \rangle, t) \,. \tag{4}$$

The probability-density function of the flight path in the detector and the angular distribution of the emerging neutrons [4] are necessary to determine $\langle l' \rangle$.

If $\Sigma_a^d \Delta \ll 1$, the actual detector can be replaced by an ideal plane detector in the mid-plane of the actual detector.

It must be noted that in the case of a thick detector ($\Sigma_a^d \Delta > 1$), $f(l')$ depends on v and Eq. (2') is not correct. This, however, does not qualitatively affect the conclusions.

It can also be seen from Fig. 3 that there exists an interval where $F(l', t)$ is relatively constant; thus in this range i(t) will depart but slightly from $\exp(-\alpha t)$. In Fig. 4 the function log i(t) has been plotted as a function of t

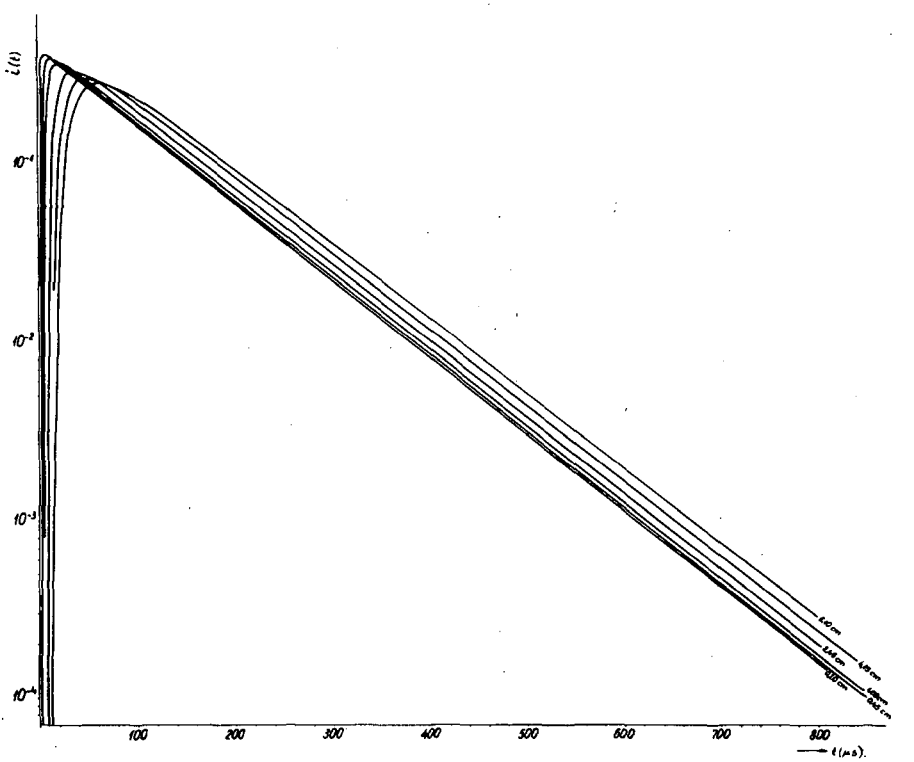

Fig. 4

Log i(t) versus time at different values of $(1+\Delta/2)$

for different values of $(1+\Delta/2)$. The characteristic feature of the curves is the appearance of a maximum and its shift to higher values of t with increasing l. After the maximum the curves continue in apparently straight lines. In fact, the slope of these straight lines is obtained in the measurements. It is of interest to note that the $-d/dt \log i(t)$ is always less than α and its deviation from α increases rapidly with increasing l. The deviation

$$\delta\alpha = \alpha - \left[-\frac{d}{dt} \log i(t) \right]$$

exhibits a minimum, $\delta\alpha_{\min.}$, at $t = 400\ \mu s$ which is essentially independent of l. Let us denote by $\overline{\delta\alpha}/\alpha$ the relative deviation

$$\frac{\overline{\delta\alpha}}{\alpha} = 1 - \frac{1}{\alpha(t_2 - t_1)} \log \frac{i(t_1)}{i(t_2)} ,$$

where $t_1 = 100\ \mu s$ and $t_2 = 800\ \mu s$. The values of the relative deviations are listed in Table I for different $(l+\Delta/2)$.

TABLE I

DEVIATIONS IN THE MEASURED DECAY CONSTANT CAUSED BY THE TIME-OF-FLIGHT EFFECT

$l+\frac{\Delta}{2}$ (cm)	$\overline{\delta\alpha}/\alpha$ (%)	$\delta\alpha_{\min}/\alpha$ (%)
0.20	9.9×10^{-4}	3.76×10^{-4}
0.45	8.3×10^{-3}	5.67×10^{-3}
1.00	8.4×10^{-2}	4.28×10^{-2}
2.45	0.62	0.30
4.15	1.83	0.89
6.10	3.72	1.82

A further interesting feature is that

$$\lim_{t \to \infty} - \frac{d}{dt} \log i(t) = 0 .$$

The reason for this is that the $F(l', t)$ starts to increase rapidly past the region where it is nearly constant. Therefore the set of curves in Fig. 4 cannot be approximated by a straight line for large values of t. However, this part of the curve has no practical importance, since for large t the background is predominant. The slopes of the nearly constant regions of the curves $F(l', t)$ increase both with α and l, while the length of these regions is roughly independent of l and inversely proportional to α. This means that the relative deviations, $\overline{\delta\alpha}/\alpha$, listed in Table I will be about the same for any α and only the length of the constant part of $F(l', t)$ will change. The change in the length is favourable to the accuracy of the measurement, since smaller values of α are associated with greater lengths.

The results of the measurements are in agreement with the theoretical considerations. In Fig. 5 a decay curve measured at $l = 4$ cm is shown. The maximum at about $t \sim 50\ \mu s$ is in agreement with Fig. 4.

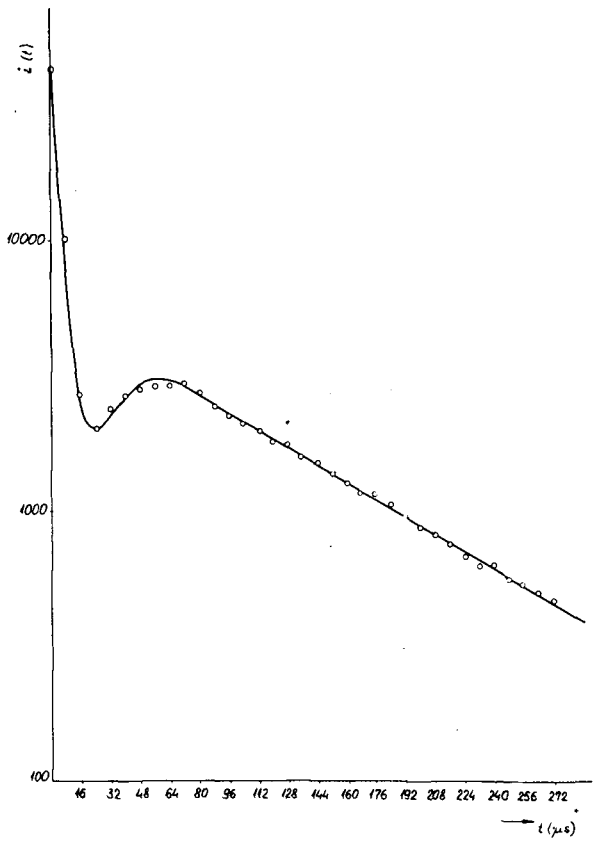

Fig. 5

Decay curve measured with a BF_3 counter at l=4 cm

In actual measurements the detector had been placed close to the bottom of the vessel. In this case the total thickness of the vessel wall and the detector, i.e. $(l+\Delta/2)$, was 0.5 cm and the relative error was of the order of 10^{-4}, which is extremely small.

4. METHOD OF EVALUATION

4.1. Maximum-likelihood estimation

First, it is necessary to construct the likelihood function $L(\vec{x}, \vec{a})$, which is the probability, or probability density, that the measured data are the actual components of the vector $\vec{x}$. When measuring the decay constant, the components of $\vec{x}$ are the counts $n_1, n_2, \ldots, n_s$ (s is the number of the channels in the time analyser). Let Θ be the channel width and N the number of analysing cycles. $L(\vec{x}, \vec{a})$, of course, contains parameters to be measured, which in the present case are symbolized by the vector $\vec{a}$ (here a_1 and a_2 are the background and intensity parameters, respectively, and a_3 is the

decay constant). An actual measurement yields an exposure for $\vec{x}$; the components of $\vec{a}$ are estimated by finding the vector $\tilde{\vec{a}}$ which maximizes the function $L(\vec{x}, \vec{a})$ at the measured $\vec{x}$. The components of $\tilde{\vec{a}}$ are evaluated from the set of equations:

$$\vec{F}(\vec{x}, \vec{a}) = \operatorname{grad}_{\vec{a}} \log L(\vec{x}, \vec{a}) = 0 \tag{5}$$

Equations (5) can be solved by Newton's iteration. The k-th step in the iteration is given by

$$\vec{a}_{k+1} = \vec{a}_k - \underline{\underline{R}}(\vec{x}, \vec{a}_k)\, \vec{F}(\vec{x}, \vec{a}_k)\,, \tag{6}$$

where $\underline{\underline{R}}(\vec{x}, \vec{a}_k)$ is the inverse of a matrix with elements

$$\frac{\partial^2 \log L(\vec{x}, \vec{a})}{\partial a_i\, \partial a_j}$$

The variance of the estimate $\tilde{\vec{a}}$ for the vector $\vec{a}$ is

$$\langle (\delta \tilde{a}_i)^2 \rangle = R_{ii}(\vec{x}, \tilde{\vec{a}})\,. \tag{7}$$

The iteration procedure is stopped at that k for which the value of each component of $\tilde{\vec{a}}$ satisfies the condition

$$|a_{k+1,i} - a_{k,i}| \ll \sqrt{\langle (\delta a_{k,i})^2 \rangle}. \quad (i = 1, 2, 3)$$

The most attractive features of the maximum-likelihood estimation are that it is (a) undistorted, i.e. $\langle \tilde{\vec{a}} \rangle = \vec{a}$, (b) efficient (since of all the estimation methods it involves the minimum variance), and (c) the distribution of the random variable $\vec{a}$ is normal.

It should be noted that (a), (b) and (c) are valid only asymptotically when $s \to \infty$. The function $L(\vec{x}, \vec{a})$ must be chosen to reflect the actual conditions of the measurements.

The time sequence of the neutrons initiating pulses in the detector is a Poissonian process. This process is filtered by the dead-time τ of the detector-amplifier-discriminator chain. The pulses of the filtered process are passed to the time analyser, the dead-time of which continues the filtering of the pulse sequence. The dead-time of the storers is of the same order of magnitude as the channel widths used. To obtain a likelihood function of unambiguous and relatively simple form, the analyser was operated to store a maximum of one pulse per channel and per analysing cycle. First,

we have to formulate the probability p_k that in an analysing cycle no pulse will be stored by the k-th channel. It can be shown that

$$p_k = e^{-I_k}\{1+\tfrac{1}{2}[i((k-1)\Theta)\tau]^2\} - \tfrac{1}{2}[i(k\Theta)\tau]^2 + O(\tau^2), \tag{8}$$

where i(t) is the pulse density from the detector at the time t and

$$I_k = \int_{(k-1)\Theta}^{k\Theta} i(t)dt = \int_{(k-1)\Theta}^{k\Theta} [i_0 \exp(-\alpha t)+b]\,dt = a_1 + a_2 \exp(-a_3 k\Theta)\,.$$

In the present case $[i(t)\tau]^2 < 10^{-4}$; thus it can be neglected in Eq. (8). This small order of correction for the dead-time τ is easy to understand, considering that in the chosen mode of operation counts are lost because of dead-time only if two or more pulses are produced in the detector within the time τ. In the case of Poisson distribution the probability of this event is

$$1-\exp(-i\tau)\frac{(i\tau)^0}{0!} - \exp(-i\tau)\frac{(i\tau)^1}{1!} = \frac{(i\tau)^2}{2} + O[(i\tau)^2]\,.$$

The number of counts n_k stored in the k-th channel is equal to the number of the analysing cycles in which at least one pulse is passed to the channel. Now, since the effect of the dead-time τ can be neglected, the individual channels are statistically independent and the likelihood function can be given by

$$L(\vec{n}, \vec{a}) = \prod_{k=1}^{s} \binom{N}{n_k} (1-p_k)^{n_k} p_k^{N-n_k}\,, \tag{9}$$

where

$$\vec{n} = (n_1, \ldots, n_k, \ldots, n_s)$$

and N is the number of analysing cycles.

This mode of analyser operation involves some counting losses but it is not appreciable, since, for example, for $n_1/N = 0.1$ about 5% of the pulses passed to the first channel are lost, which hardly increases the measuring time. The error induced by ignoring the dead-time amounts to about 1% for $n_1/N = 0.1$.

4. 2. Effects of background and higher harmonics

To find the origin of the background the decay curve was measured at a given liquid height, first under the normal measuring conditions, then with the vessel fully covered by cadmium and finally with both the detector and vessel completely surrounded by cadmium. After the measurement was normalized to constant monitor counts, the data plotted in Fig. 6 was obtained. The counts plotted for the second and third cases are the same,

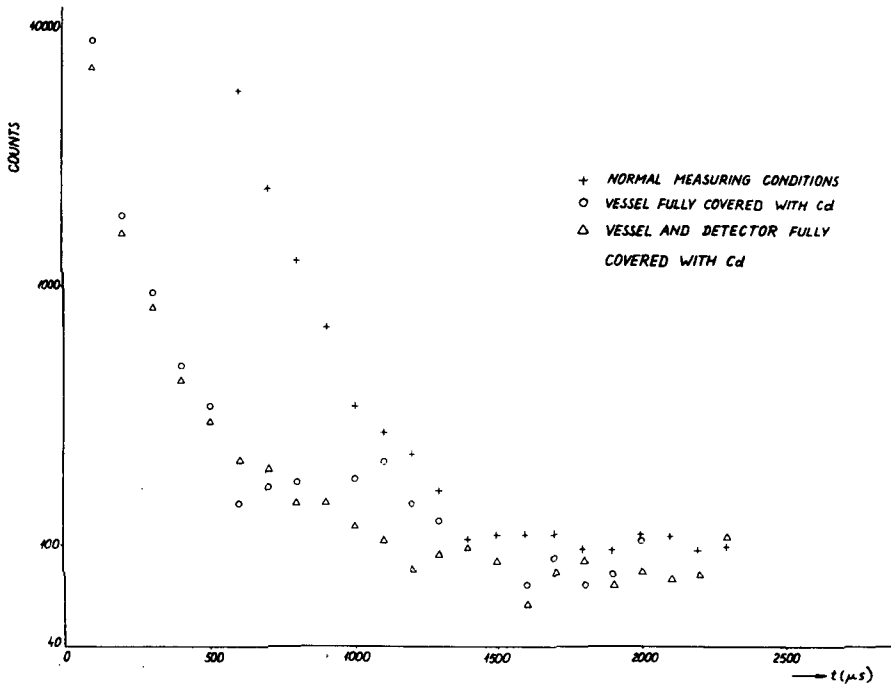

Fig. 6

i(t) versus time for neutrons and gammas

within statistical error, and eventually go over into the background of the first run. This implies that the main contribution to background comes from gamma radiation, since in the third measurement no neutrons could be detected. It also can be seen that the background is not constant. The rapidly varying contribution to the background is caused by the neutrons captured by cadmium, while the nearly constant contribution can be attributed to the activation of the construction materials. By adequate discrimination the influence of the rapidly varying part of the background can be considerably reduced.

It follows from the above that the information about the background has to be obtained during the decay process. In addition, the channel number has to be chosen so as to have the background predominate in the last few channels. This provides the most favourable conditions for the three-parameter fit.

There is a strong correlation between the estimations for $\tilde{a}_1$, $\tilde{a}_2$ and $\tilde{a}_3$. If $\tilde{a}_1$ is estimated to be larger than its true value, then $\tilde{a}_3$ will also be too large. This error may be enlarged by the fact that a decay curve with harmonic contamination can be well fitted by a considerably higher than true decay constant and some fictitious background (Fig. 7). Consequently a two-exponential fit cannot be reasonable unless the background is zero.

The estimate of the decay constant $\tilde{a}_3$ can be accepted only if the background evaluated from counts in the "effective channels" is consistent with the value obtained from the "background channels".

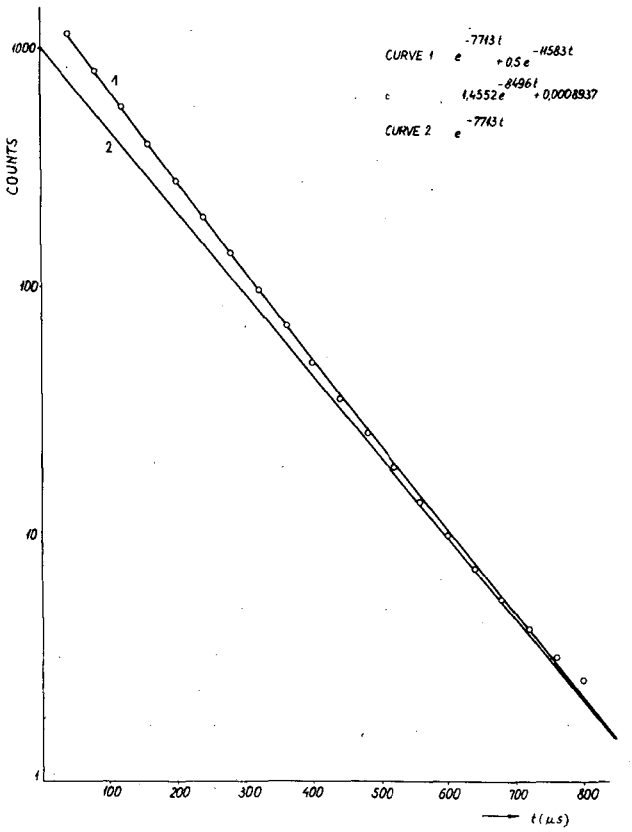

Fig. 7

Relation between higher harmonic and background

The delay time required for the harmonic contamination to die away was established by the "omission" method, already used by several authors. Upon gradual omission of the data registered by the first few channels, the parameter values obtained must satisfy two conditions: first, the successive values of the decay constant have to converge within experimental error to a definite value and secondly, the successive background estimations have to converge within experimental error to the value obtained from the background channels.

With properly chosen delay times, n_1/n_s was about 10^3, that is the exponential decay was covered to three orders of magnitude (about 8-12 channels). It has been shown [5] that no appreciable reduction of the statistical error in the decay constant can be achieved by covering the exponential decay for more than three orders of magnitude, or by using more than 4-5 channels.

4.3. Evaluation of the diffusion parameters from the decay constants by the least squares method

The decay constants were determined for different moderator heights (different bucklings B_i^2). Let us denote the decay constant for B_i^2 by α_i.

The likelihood function $L(\vec{\alpha}, \vec{a})$, where now the components of $\vec{a}$ are the diffusion parameters $v\Sigma_a$, D, C, etc. and the components of $\vec{\alpha}$ are the decay constants α_i, has the following form

$$L(\vec{\alpha}, \vec{a}) = \text{const} \cdot \exp\left[-\sum_{i=1}^{l} \frac{(\alpha_i - \langle\alpha_i\rangle)^2}{2\langle(\delta\alpha_i)^2\rangle}\right], \tag{10}$$

where

$$\langle\alpha_i\rangle = v\Sigma_a + DB_i^2 - CB_i^4 + FB_i^6 + \cdots . \tag{11}$$

This function will obviously be at a maximum if

$$Q = \sum_{i=1}^{l} \frac{(\alpha - \langle\alpha_i\rangle)^2}{\langle(\delta\alpha_i)^2\rangle} = \sum_{i=1}^{l} \rho_i(\alpha_i - \langle\alpha_i\rangle)^2 = \min. \tag{12}$$

This means that we have to apply a weighted least squares fit. The weights ρ_i are the reciprocals of the variances of the decay constants. Any other kind of weighting seems to be unjustified.

In the case of cylindrical geometry the buckling is given by

$$B^2 = \left(\frac{2.405}{R+d}\right)^2 + \left(\frac{3.14}{H+2d}\right)^2, \tag{13}$$

where

$$d = 0.758\,\lambda_{tr} = 2.274\,\frac{D}{v}, \tag{13'}$$

according to [6].

Since B^2 depends from Eq.(13') on the unknown parameter D, the fitting defined in Eq.(12) is most conveniently performed by iteration. In practical calculations it was found that the iteration procedure showed a bad convergence in several cases.

It can be readily shown that the vector $\vec{a}$ minimizing Eq.(12) is given by the set of equations

$$\underline{\underline{M}}\vec{a} = \vec{G}, \tag{14}$$

where

$$M_{pq} = \sum_{i=1}^{l} \rho_i B_i^{2(p+q-2)} . \tag{15}$$

and

$$G_p = \sum_{i=1}^{1} \rho_i \alpha_i B_i^{2(p-1)} \qquad (15')$$

Equations (14) determine the co-ordinates of the point of intersection of three planes in the space of the vectors $\vec{a}$. The vectors perpendicular to these planes are the row vectors of the matrix $\underline{\underline{M}}$. The position of the planes depends through B_i^2 on D. It can be seen that for nearly parallel planes even a small change in position will cause a considerable shift in the co-ordinates of the intersection point. Thus, if during the iteration there is a small change in D the co-ordinates of the intersection points may undergo a significant change. In the iteration then the new value of D may be considerably different from the preceding one and the difference may increase instead of decrease. This event is called "the case of ill condition". The poor convergence which has been observed is due to numerical reasons inherent in the structure of matrix $\underline{\underline{M}}$. Therefore it cannot be remedied by an equation solving techniques, but by changing the structure of the matrix $\underline{\underline{M}}$.

This can be done by the transformation of the buckling variables; for example, by shifting the origin on the axis of B^2 to the point B_i^2 (see Fig. 8) the structure of matrix $\underline{\underline{M}}$ will change to increase the angle of inclination between the planes. Using the method of orthogonal polynomials (see below) the matrix $\underline{\underline{M}}$ can be rewritten even in a diagonal form.

Improved convergence is manifested by a decrease in the subtractional loss of digits when solving Eqs. (14). Of course, there remains a loss of digits even in the ideal case, i.e. if $\underline{\underline{M}}$ is diagonal, namely in the evaluation of vector $\vec{G}$, and this loss is the higher the larger the exponent of B^{2q}, the coefficient of which is evaluated.

4.4. The coefficient of B^6

The evaluation of the coefficients of higher order terms is a problem frequently dealt with in the literature. The method of orthogonal polynomials [7] lends itself not only to improving the convergence but is of help also in considering the problem of higher order terms.

The elements of the inverse of the matrix $\underline{\underline{M}}$ in Eqs. (14) yield the correlation coefficients ($p \neq q$) and variances ($p = q$) of the diffusion parameters $\tilde{\vec{a}}$ as

$$(\underline{\underline{M}}^{-1})_{pq} = \langle (\delta \tilde{a}_p \delta \tilde{a}_q) \rangle \frac{Q_{min}}{1-3} \,. \qquad (16)$$

We try to find a procedure by which the parameters can be estimated independently of one another and the estimate of any parameter does not interfere with that of the rest. In this case the effect of introducing a new parameter is the most apparent. By Eq. (16) this condition is satisfied if both the matrices $\underline{\underline{M}}^{-1}$ and thus $\underline{\underline{M}}$ are diagonal. Let us replace the "polynomials" B^0, B^2, B^4, B^6, ... by the polynomials $\varphi_0(B^2)$, $\varphi_1(B^2)$, $\varphi_2(B^2)$, $\varphi_3(B^2)$, ..., where $\varphi_p(x)$ is a polynomial of order p and we write

$$\langle \alpha_i \rangle = v\Sigma_a + DB^2 - CB^4 + FB^6 + \ldots$$

$$= c_0 \varphi_0(B^2) + c_1 \varphi_1(B^2) + c_2 \varphi_2(B^2) + c_3 \varphi_3(B^2) + \ldots \qquad (17)$$

The diffusion parameters $v\Sigma_a$, D, C, F, etc. can be expressed in terms of

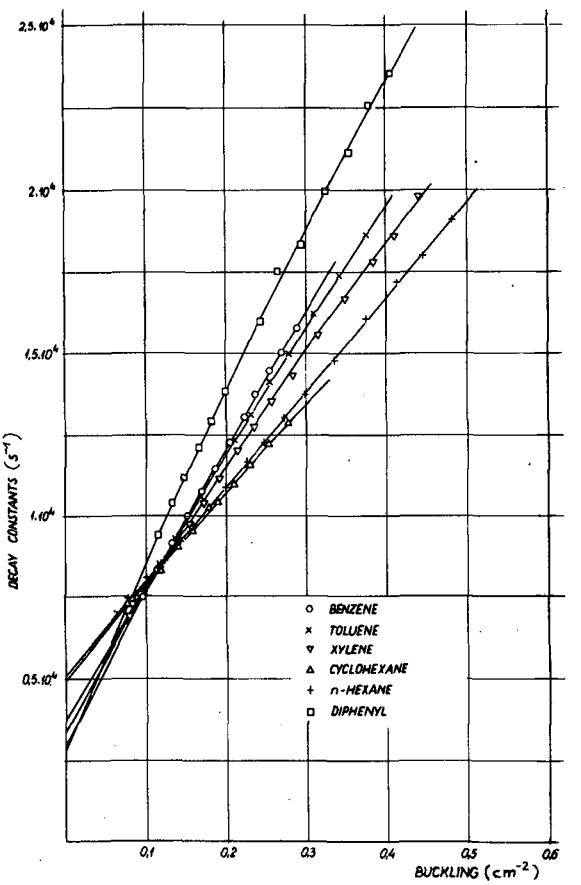

Fig. 8

α versus B^2 for benzene, toluene, xylene, cyclohexane, n-hexane and diphenyl

the parameters c_0, c_1, c_2, c_3, etc.. With the polynomials $\varphi_p(x)$ Eqs.(14), (15) and (15') take the form

$$\underline{\underline{M}}'\vec{c} = \vec{G}' , \qquad (18)$$

where

$$M'_{pq} = \sum_{i=1}^{l} \rho_i \varphi_p(B_i^2) \varphi_q(B_i^2) \qquad (19)$$

and

$$G'_p = \sum_{i=1}^{1} \rho_i \alpha_i \varphi_p(B_i^2) \qquad (19')$$

The polynomials $\varphi_p(x)$ can be chosen such that $M'_{pq} = 0$ for $p \neq q$.

It is obvious that one obtains more information about F the higher the values for which B^2 are measured. Therefore, we have chosen as an example the measurement in xylene, for which the highest value of B^2 is $0.44\ cm^{-2}$. The estimated parameters are

$c_0 = 11135.8 \pm 12.9$	$c_2 = 11165.8 \pm 1450$
$c_1 = 36157.4 \pm 151.3$	$c_3 = 9730.0 \pm 15760$
Three-parameter fit	Four-parameter fit
$v\Sigma_a = 3718.9 \pm 66.5$	$v\Sigma_a = 3632.4 \pm 150$
$D = 41140.0 \pm 648.4$	$D = 42585.9 \pm 2430$
$C = 11165.8 \pm 1415.0$	$C = 18079.1 \pm 12100$
	$F = c_3$

It is of interest to note that in the evaluation of G'_3 and G'_4 the losses of digits were two and three, respectively. This explains the large error in c_2 and c_3 showing that the value of c_3 is quite uncertain.

This example will be used also to show that the losses of digits cannot be further reduced. This implies that while the chosen measurement still yields useful information for C none is obtainable for F. It is of importance to show this, since even without knowing anything about the value of F it may happen that the measured data are better fitted by four parameters; in that case, however, considerably larger errors must be assigned to the values $v\Sigma_a$ and D, which are physically the most interesting quantities, than in the three-parameter fit.

The distribution of the minimum value of Q defined in Eq. (12) is χ^2_{l-3} for three, and χ^2_{l-4} for four parameters. For an appreciable improvement in the estimation in comparison with the three-parameter fit the inequality $Q^{(4)}_{min.}/(l-4) < Q^{(3)}_{min.}/(l-3)$ must be satisfied. In our example $Q^{(4)}_{min.}/(l-4) = 2.72$ and $Q^{(3)}_{min.}/(l-3) = 2.59$; therefore it is not reasonable to involve a B^6 term in the evaluation.

The statistical error of the measured values of α_i range from 0.3 to 0.5%. The measured data may fluctuate within this range but this fluctuation must not induce an appreciable fluctuation in the values of the parameters which can be reasonably determined. The measured α_i values were therefore increased or reduced by 0.5% at random and the parameters c_p in Eq. (17) were evaluated again. The results of ten tests are listed in Table II. The strong fluctuation of c_3 and the relative stability of the other parameters are immediately apparent. It is of interest to note that the spread even in c_2 does not exceed the statistical error, thus the estimation of error seems to be adequate.

TABLE II

FLUCTUATIONS IN THE DIFFUSION PARAMETERS FOR RANDOM CHANGES IN THE DECAY CONSTANTS

Test	c_0	c_1	c_2	c_3
1	11136.4	36298.9	-10200.9	22527.4
2	11136.8	36260.0	-11223.5	-12033.3
3	11122.1	36033.0	- 9494.9	18998.4
4	11127.1	36078.8	-11615.4	13341.0
5	11118.5	35935.8	-12817.0	6054.9
6	11139.1	35904.0	-12509.5	- 6236.3
7	11140.5	36038.9	- 9604.0	18553.5
8	11116.7	36091.3	-13426.7	28600.7
9	11116.2	35903.4	-11048.6	30088.9
10	11139.5	36247.9	- 9996.2	25281.4

This last result implies also that an accuracy of 0.5% in the measurement of α is sufficient to obtain an acceptable value for C but for the evaluation of F a wider range of B^2 values or a measurement of the decay constant with better than 0.05% accuracy would be needed.

5. DATA

The actual measurements were performed on various hydrogenous liquids. Diphenyl was measured at 85°C while the other liquids (water, benzene, toluene, xylene, cyclohexane, n-hexane) were measured at 22°C. The curves for α versus B^2 are shown in Fig. 8 and the values measured are listed in Table III. The results for water are consistent with those obtained by other authors (see, for example [8, 9, 10]). The results for benzene are in good agreement with the recent data reported by KÜCHLE and KUSSMAUL [11]. The diffusion length of diphenyl was found to be less than the values obtained by a stationary method [12, 13], or that predicted by PETRIE et al. [14] but are in fair agreement with the data obtained by BLACKSHAW and WALTNER [15] who used the pulsed method.

The effective cross-sections σ_a^H computed from the values of $v\Sigma_a$ obtained for the materials investigated are in good agreement with one another (Table III). The average value is 333.1 ± 3.0 mb, in good agreement with $331.5 + 1.7$ mb, which is the average of the results of several measurements performed by various direct and indirect methods [16]. The value of N_H

TABLE III

DIFFUSION PARAMETERS OF THERMAL NEUTRONS MEASURED BY THE PULSED METHOD

Material	$\langle v\Sigma_a \rangle$ (s^{-1})	$\langle \lambda_{tr} \rangle \langle v \rangle /3$ (cm^2/s)	C (cm^4/s)	L_D (cm)	σ_a^H (mb)	$N_H \langle \lambda_{tr} \rangle \times 10^{-21}$ (cm^{-2})
Water 22°C	4859 ± 123	36533 ± 1362	5939 ± 3148	2.74 ± 0.09	321.6 ± 8.1	29.32 ± 0.8
Benzene 22°C	2886 ± 111	48649 ± 1373	13869 ± 3849	4.11 ± 0.10	318.7 ± 12.1	23.61 ± 0.8
Toluene 22°C	3357 ± 80	44229 ± 847	9359 ± 2007	3.63 ± 0.06	335.8 ± 8.0	23.97 ± 0.8
Xylene 22°C	3719 ± 66	41140 ± 648	11165 ± 1415	3.32 ± 0.04	344.4 ± 6.1	24.11 ± 0.8
Cyclo-hexane	4925 ± 103	29944 ± 1382	5603 ± 4185	2.47 ± 0.06	335.1 ± 7.0	23.91 ± 0.8
n-hexane 22°C	5046 ± 67	28818 ± 546	927 ± 975	2.39 ± 0.03	349.2 ± 4.6	22.36 ± 0.8
Diphenyl 85°C	2778 ± 72	59529 ± 1534	20336 ± 3632	4.63 ± 0.08	327.2 ± 8.5	25.03 ± 0.8

λ_{tr} (N_H is the number of hydrogen atoms per cm^3) is independent of the chemical bond within the experimental error, as shown in an earlier paper [1]. The measured values of λ_{tr} are in agreement with those calculated by Radkowsky's prescription from the measured energy dependence of the cross-sections of the given materials [1].

REFERENCES

[1] PÁL, L., KISDI-KOSZÓ, É., BOD, L., SZATMÁRY, Z. and VIZI, I., Proc. 3rd. UN Int. Conf. PUAE, 1964, P/651.

[2] ÁDÁM, A., BOD, L., SZABÓ, Z. and SZEGHŐ, L., Acta phys. hung. 12 2 (1960) 107-18.

[3] SZLÁVIK, F., PALMAI, I., Kernenergie 6 (1963) 6-53, 209-14.

[4] DARDEL, G., Trans. Roy. Inst. Techn., Stockholm (1954) 75.

[5] JÁNOSSY, L. and RUPP, E., Reports of the Central Research Institute for Physics (in Hungarian) 8 (1960) 2-3, 75-81.

[6] VÉRTES, P., Nucl. Sci. Engng 16 4 (1963) 363-68.

[7] ЛИННИК Ю.В.: Метод наименьших квадратов и основы теории обработки наблюдений, Физматгиздат, Москва (1962) 275–90.

[8] ANTONOV, A.V., ISACOFF, A.I., MURIN, I.D., NEUPOCOYEV, B.A., FRANK, I.M., SHAPIRO, F.L. and SHTRANIKH, I.V., Proc. UN Int. Conf. PUAE 5 (1956) 3, 82.

[9] KÜCHLE, M., Nukleonik 2 (1960) 131.

[10] LOPEZ, W.M. and BEYSTER, J.R., Nucl. Sci. Engng 12 2 (1962) 190-202.

[11] KÜCHLE, M. and KUSSMAUL, G., Nukleonik 6 7 (1964) 239-330.

[12] ЮРОВА Л.Н., ПОЛЯКОВ А.А., СТЕПАНОВ Ц.Б., ТРОЯНСКИЙ В.Б., Нейтронная физика, Госатомиздат, Москва (1961) 192–97.

[13] BROWN, W.W., NAA-SR-MEMO (1956) see [14].

[14] PETRIE, C.D., STORM, M.L. and ZWEIFEL, P.F., Nucl. Sci. Engng 2 (1957) 728-44.

[15] BLACKSHAW, G.L. and WALTNER, A.W., Reactor Sci. Technol. 17 8 (1963) 341.

[16] BAKER, A.R. and WILKINSON, D.H., Phil. Mag. 3 (1958) 647-51.

DISCUSSION

S. SCOTT: I would like to comment on the time-of-flight effect mentioned in this paper. Some time ago in Birmingham we measured an effect of this sort, using both an internal scintillation counter and an external BF_3 counter with water systems. As far as I know this work was not followed up.

L.G. KEMENY: I believe that some of the more difficult theoretical problems of mathematical statistics involved in the data-evaluation problems reported in this paper are discussed in a new book by Professor Jánossy of the Central Research Institute of Physics, Budapest. This book, which has now been published in English by the Oxford University Press, contains a direct reference to pulsed-neutron measurements.

E. SILVER: I think it is important to bear in mind that the application of the criterion $[i(t)\tau]^2 \ll 1$ does not guarantee the absence of dead-time effects. Even if the criterion applies in channel 1, we have found that there may be an error of several per cent due to dead-time.

MEDIDA DE M_2 EN LIQUIDOS ORGANICOS *

L. SANCHO, B. GARCIA-CASTAÑER Y F. VERDAGUER
JUNTA DE ENERGIA NUCLEAR, MADRID, ESPAÑA

Abstract — Résumé — Аннотация — Resumen

MEASUREMENT OF M_2 IN ORGANIC LIQUIDS. This paper deals with the experimental study, using the pulsed neutron source method, of the effect of non-1/v capture on the diffusion parameters or organic liquids.

Cadmium is used to introduce the non-1/v capture, cadmium iodide being dissolved in tributyl phosphate and then dissolved in the liquid. The study is made with six different concentrations of cadmium, in addition to measuring the pure liquid. Benzene, a non-polar liquid, was used for the first measurement, and chlorobenzene, a polar liquid, for the following one. Measurements are carried out with internal counters situated at zero of the first harmonic; successive measurements are made with four, three, two and one counters, thus making it possible to determine the interference caused by the counters. The results of the measurements enable the value of M_2, the mean-square energy transfer, to be calculated for the liquid used.

MESURE DE M_2 DANS LES LIQUIDES ORGANIQUES. Les auteurs présentent l'étude expérimentale de l'influence de la capture non 1/v sur les paramètres de diffusion des liquides organiques, par la méthode de la source pulsée.

Pour introduire la capture non 1/v, ils utilisent le cadmium. Pour cela, ils dissolvent de l'iodure de cadmium dans du phosphate de tributyle et mélangent ensuite cette solution au liquide. Les expériences portent sur le liquide pur et sur six concentrations différentes de cadmium allant jusqu'à 50%. Pour la première mesure ils utilisent le benzène, liquide non polaire, pour la suivante le chloro-benzène, liquide polaire. Les mesures se font avec des compteurs internes situés au zéro du premier harmonique; on mesure successivement avec quatre, trois, deux et un compteur, ce qui permet de mesurer la perturbation produite par les compteurs. Les résultats de ces mesures permettent de calculer les valeurs de M_2 (transfert quadratique moyen d'énergie) pour le liquide utilisé.

ИЗМЕРЕНИЕ M_2 В ОРГАНИЧЕСКИХ ЖИДКОСТЯХ. Дается описание экспериментального исследования с использованием метода источника импульсных нейтронов влияния непропорционального 1/v захвата на диффузионные параметры органической жидкости.

Для введения непропорционального 1/v захвата использовали кадмий, причем йодид кадмия растворяли в трибутил-фосфате, а затем — в жидкости. Исследовали шесть различных концентраций кадмия в дополнение к измерению чистой жидкости. Для первого измерения использовали бензол и неполярную жидкость, а для следующего — хлоро-бензол и полярную жидкость. Измерения проводили с помощью внутренних счетчиков, расположенных в нулевом положении первой гармоники; последующие измерения проводили с четырьями, тремя, двумя и одним счетчиком, таким образом, давая возможность определить влияние счетчиков. Результаты измерений позволяют оценить значение M_2, то есть среднего квадрата передачи энергии, который рассчитывается для использованной жидкости.

MEDIDA DE M_2 EN LIQUIDOS ORGANICOS. En este trabajo se presenta el estudio experimental de la influencia de una captura no 1/v sobre los parámetros de difusión de líquidos orgánicos utilizando el método de la fuente pulsada de neutrones.

Para introducir la captura no 1/v se utiliza el cadmio. Para ello se disuelve yoduro de cadmio en fosfato de tributilo, disolviéndolo después en el líquido. El estudio se efectúa con seis concentraciones distintas de cadmio además de la medida sobre el líquido puro. Para la primera medida se ha utilizado el benceno, líquido no polar, y en la que sigue el clorobenceno, líquido polar. Las medidas se efectúan con contadores internos

* Este trabajo ha sido subvencionado, en parte, por el OIEA.

situados en el cero del primer armónico y se mide sucesivamente con cuatro, tres, dos y un contador, permitiendo así la medida de la perturbación producida por los contadores. Los resultados de las medidas permiten calcular el valor de M_2, transferencia cuadrática media de energía, del líquido utilizado.

1. INTRODUCCION

Según se ha visto en un trabajo anterior [1], al integrar aproximadamente la ecuación de transporte aplicada a un medio moderador con captura 1/v, envenenado con Cd, cuya captura no sigue la ley 1/v, se obtiene la siguiente expresión para la constante de decrecimiento exponencial del flujo de neutrones después de introducir en el medio un impulso de neutrones

$$\lambda_i = \sum_0 v_0 + v_T D_T B^2 - \frac{\sqrt{\pi}(D_T v_T)^2}{v_T M_2} B^4 + \left(\sum_{ef}^{Cd}\right)_{0i} \left(g(T) v_0 - \right.$$

$$\left. -2 v_0 \frac{\sqrt{\pi}}{v_T M_2} T\left(\frac{dg(T)}{dT}\right) D_0 B^2 \right) - \left(\sum_{ef}^{Cd}\right)^2_{0i} \frac{\sqrt{\pi}}{v_T M_2} v_0^2 T^2 \left(\frac{dg(T)}{dT}\right)^2 \qquad (1)$$

donde:

$\sum_0$ es la sección eficaz macroscópica del medio, que sigue la ley 1/v;

$\left(\sum_{ef}^{Cd}\right)_{0i}$ g(T) es la sección eficaz del cadmio en un espectro maxwelliano a la temperatura T [2];

v_0 y v_T son las velocidades medias de los neutrones en un espectro maxwelliano a las temperaturas de 20°C y T°K respectivamente;

D_T es la constante de difusión del moderador a la temperatura T;

M_2 es el coeficiente de transferencia cuadrática media de energía.

El término

$$\lambda_0 = \sum_0 v_0 + v_T D_T B^2 - \frac{\sqrt{\pi}(D_T v_T)^2}{v_T M_2} B^4$$

representa la constante de decrecimiento exponencial del moderador puro, o sea sin envenenar con Cd. Para utilizar esta expresión en el caso del benceno hay que suponer que D_T varía linealmente con la temperatura, lo mismo que el agua. Midiendo las constantes de decrecimiento para distintas concentraciones de Cd puede calcularse el valor de M_2. En este trabajo, dentro de un plan de medidas con líquidos orgánicos, se presenta el resultado de la aplicación de este método al caso del benceno.

2. MEDIDAS

Como fuente de neutrones se ha utilizado el blanco de un acelerador Cockcroft-Walton de 600 kV. Los impulsos de neutrones se consiguen pulsando la fuente. Los detectores de neutrones son de BF_3 y el analizador

TABLA I

CONCENTRACIONES DE CADMIO
Y VALORES DE λ_i

$B^2 = 0{,}06517 \pm 0{,}0004\ cm^{-2}$			
i	$N_i(at.Cd/cm^3)$	$(\Sigma_{ef}^{Cd})_0(cm^{-1})$	$\lambda_i(s^{-1})$
1	$1{,}52523 \cdot 10^{18}$	$3{,}8222 \cdot 10^{-3}$	7042,0 ± 21,5
2	$6{,}17756 \cdot 10^{18}$	$15{,}4809 \cdot 10^{-3}$	10051,8 ± 31,2
3	$9{,}39491 \cdot 10^{18}$	$23{,}5436 \cdot 10^{-3}$	12071,0 ± 37,1
4	$13{,}62380 \cdot 10^{18}$	$34{,}1412 \cdot 10^{-3}$	14662,5 ± 44,7

de tiempos es un TMC-220 de 256 canales. Las distintas concentraciones de Cd se han obtenido disolviendo en el benceno distintas soluciones de I_2Cd en fosfato de tributilo.

Para la determinación de λ_i se han situado los detectores simétricamente en el interior del moderador, midiendo sucesivamente con distinto número de contadores y haciendo posteriormente la extrapolación a «cero contador» [2]. Se ha determinado λ_i en cuatro concentraciones de cadmio, y los resultados pueden verse en la tabla I. Las medidas de λ_i que aparecen en la tabla I han sido corregidas por distintos efectos: a) variación de B^2 con la concentración del Cd debida a la variación de D_T y por tanto de la longitud extrapolada de d_t; b) variación del número de átomos de hidrógeno por cm^3 de la disolución a causa del fosfato de tributilo que se emplea para ello; c) captura debida al iodo. Estas correcciones han sido siempre inferiores a un 0,8%. Todas las medidas se han efectuado a una temperatura de 20°C, luego en (1) tenemos $v_T = v_0$.

3. CALCULO DE M_2

Para calcular M_2 escribimos la ecuación (1) en la siguiente forma:

$$Y_i = \lambda_0 - \frac{1}{M_2} S_i \qquad (2)$$

donde teniendo en cuenta que $v_T = v_0$

$$Y_i = \lambda_i - g(T) v_0 \left(\sum_{ef}^{Cd}\right)_{0i}$$

$$S_i = \left(\sum_{ef}^{Cd}\right)_{0i} \sqrt{\pi} T \frac{dg(T)}{dT} \left(2D_0 B^2 + \left(\sum_{ef}^{Cd}\right)_{0i} v_0 T \frac{dg(T)}{dT}\right)$$

obtenemos para S_i e Y_i los valores que aparecen en la tabla II y en la figura 1.

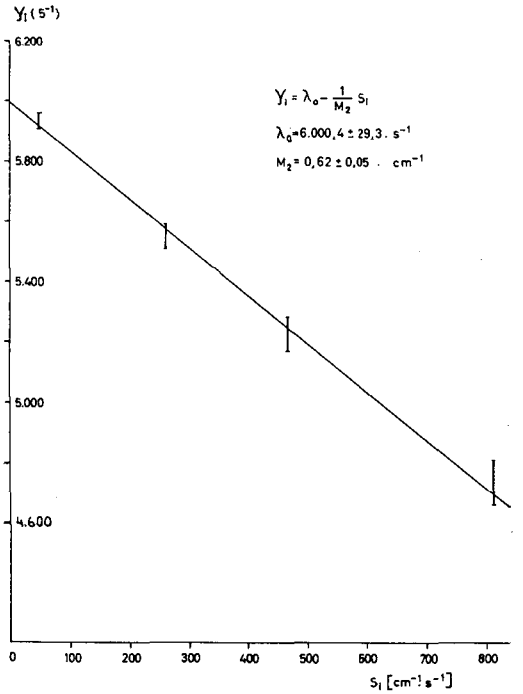

Figura 1

Variación de Y_i.

TABLA II

VALORES CALCULADOS DE S_i E Y_i

	$S_i (cm^{-1}s^{-1})$	$Y_i (s^{-1})$
1	48,0	5930,8 ± 22,5
2	261,3	5551,0 ± 41,5
3	467,8	5226,2 ± 55,5
4	812,7	4736,6 ± 75,2

Los parámetros utilizados para el cálculo de S_i e Y_i son los siguientes:

$$g(T) = 1,3215$$
$$T \frac{dg(T)}{dT} = 0,9753 \qquad [3]$$

$$D_0 = 48649 \pm 1362 \text{ cm}^2 \text{ s}^{-1}$$
$$B^2 = 0,06517 \pm 0,0004 \text{ cm}^{-2} . \qquad [4]$$

Ajustando por mínimos cuadrados los valores de la tabla II en la expresión (2) obtenemos los siguientes resultados:

$$\lambda_0 = 6000{,}4 \pm 29{,}3 \ s^{-1}$$
$$M_2 = 0{,}62 \pm 0{,}05 \ cm^{-1}. \qquad (3)$$

Los errores de estos valores han sido calculados por propagación de errores en la fórmula de mínimos cuadrados y combinando en ella linealmente los sistemáticos y cuadráticamente los estadísticos. Independientemente de este método, se ha medido experimentalmente el valor de λ_0, constante de decrecimiento para el benceno puro con $B^2 = 0{,}06517 \ cm^{-2}$, y hemos obtenido el valor $\lambda_0' = 6036{,}2 \pm 17{,}0 \ s^{-1}$ que como se ve está en buen acuerdo con el resultado de (3) dentro de los errores experimentales.

4. DISCUSION

Hay que hacer constar que la ecuación (1) es solamente aproximada en primer orden. Pero ahora bien, nuestros puntos experimentales se ajustan bien a una recta, dentro de los errores experimentales; por lo tanto y como las concentraciones de cadmio con las que hemos trabajado son pequeñas, los términos en que aparezcan potencias superiores de $\left(\sum_{ef}^{Cd}\right)_{0i}$ en un desarrollo superior de (1) no tienen influencia sobre el valor de λ_i.

Otra probable causa de error es la deformación del espectro de neutrones debida a la presencia del cadmio, ya que para llegar a (1) se ha supuesto siempre un espectro maxwelliano. Pero según se ve en [5], las desviaciones de la maxwelliana sufridas por el espectro de neutrones, para las concentraciones de cadmio utilizadas por nosotros, que representan en el caso máximo una captura por átomo de H de 1,2b, son despreciables.

Si a partir del valor de M_2 se calcula el valor de c, coeficiente de enfriamiento, resulta

$$c = 30711 \ cm^4 \ s^{-1}$$

valor muy superior que el dado en [4]. Esta discrepancia es en el mismo sentido que la que se presenta en el agua puesto que de [2] y [6] se ve que los valores de M_2 calculados a partir del coeficiente de enfriamiento y a través del enfriamiento producido por una captura no 1/v difieren también en factores.

REFERENCIAS

[1] VERDAGUER, F., An. Real Soc. Esp. Fís. y Quím. LX(A) (1964) 135-140.

[2] VERDAGUER, F., Enfriamiento de los neutrones por captura y su aplicación al estudio de su termalización en el agua ligera, Informe JEN 127-DF/I, 39 (1963).

[3] WESTCOTT, C.H., Effective Cross-Section Values for well Moderated Thermal Reactor Spectra, Informe CRRP-787 (1958).
[4] PAL, L. y col, Thermal Neutron Cross-Sections and Diffusion Parameters in Several Organic Materials, Actas 3ª Conf. int. util. EAFP, A/CONF. 28/651 (Ginebra, 1964) (por publicarse).
[5] BEYSTER, J.A. y col., Nuclear Sci. and Engng, 9 (1961) 168-184.
[6] FRIEDMAN, E., Nuclear Sci. and Engng, 14 (1962) 420-422.

DISCUSSION

K.H. BECKURTS: Did you compare the M_2 values obtained in your experiment with these calculated from the experimental scattering law?

L. SANCHO: Yes. The values differ by a factor of about three.

THE USE OF THE CHOPPER FOR PULSED NEUTRON MEASUREMENTS

A. GRAFFSTEIN, Z. OGRZEWALSKI, T. RZESZOT AND E. WARDA
INSTITUTE OF NUCLEAR RESEARCH, SWIERK, POLAND

Abstract — Résumé — Аннотация — Resumen

THE USE OF THE CHOPPER FOR PULSED NEUTRON MEASUREMENTS. The diffusion parameters of the organic glass have been measured using the pulsed neutron technique. A neutron pulse introduced into the moderating medium of certain dimensions (geometrical buckling) generates the time-dependent neutron flux, the asymptotic decay constant of which is measured. As a neutron detector the BF_3 miniature proportional counter has been used in typical amplifying and supplying electronic equipment. The pulses from the counter were recorded by the 256-channel time analyser of the At-4 type using a channel width of 4-16 μs. The exponential decay curves were elaborated by means of digital computer GIER.

The chopper operating at the horizontal channel of the EWA reactor has been used as a pulsed neutron source. The rotor of the chopper is constructed of steel, with a diameter of 43 cm. The rotor was rotated at a speed of 6000 rpm. The width of the neutron pulse was about 160 μs and the repetition rate 200 s^{-1}. The investigated sample was placed before the rotor slit. Since the neutron beam from the horizontal channel of the reactor was chopped by the rotor, the neutron pulses used for measurements consisted of neutrons of near thermal energy.

Due to small leakage of neutrons from the investigated sample during the slowing-down process, this method permitted to measure asymptotic decay constants even for great bucklings. The measurements have been carried out for rectangular geometry and the asymptotic decay constant as a function of buckling has been obtained.

EMPLOI D'UN HACHEUR DANS LES MESURES AU MOYEN DES NEUTRONS PULSÉS. Les auteurs ont mesuré les paramètres de diffusion dans le verre organique par la méthode de la source pulsée. Une bouffée de neutrons pénétrant dans un milieu ralentisseur ayant certaines dimensions (un certain laplacien géométrique) engendre un flux de neutrons variable dans le temps, dont on peut mesurer la constante de décroissance asymptotique. Comme détecteur de neutrons, les auteurs ont utilisé le compteur proportionnel miniature à BF_3 avec un ensemble électronique courant d'alimentation et d'amplification. Les impulsions du compteur ont été enregistrées par un analyseur en temps de 256 canaux, du type At-4, la largeur de canal étant de 4 à 16 μs. Les courbes de décroissance exponentielle ont été déterminées à l'aide d'une calculatrice numérique GIER.

Un hacheur fonctionnant sur le canal horizontal du réacteur EWA a été utilisé comme source pulsée. Le rotor du hacheur est une pièce d'acier de 45 cm de diamètre. La vitesse de rotation du rotor était de 6000 tours/min. La largeur de la bouffée de neutrons était d'environ 160 μs et la vitesse de répétition de 200 s^{-1}. L'échantillon à étudier était placé devant la fente du rotor. Comme le rotor hachait le faisceau de neutrons provenant du canal horizontal du réacteur, les bouffées utilisées pour les mesures étaient constituées par des neutrons d'une énergie proche de l'état thermique.

La fuite de neutrons hors de l'échantillon étudié pendant le processus de ralentissement restant faible, cette méthode a permis de mesurer les constantes de décroissance asymptotique, même pour les laplaciens élevés. Les auteurs ont procédé aux mesures pour une géométrie rectangulaire, et ils ont déterminé la constante de décroissance asymptotique en fonction du laplacien.

ИСПОЛЬЗОВАНИЕ СЕЛЕКТОРА БЫСТРЫХ НЕЙТРОНОВ ДЛЯ ИЗМЕРЕНИЯ ИМПУЛЬСНЫХ НЕЙТРОНОВ. При помощи метода импульсных нейтронов измерены диффузионные параметры органического стекла, а также графита. Введение импульсных нейтронов в замедляющую среду известных размеров (геометрический лапласиан) вызывает зависящий от времени нейтронный поток, константа асимптотического распада которого измеряется. В качестве детектора нейтронов использован миниатюрный пропорциональный счетчик BF_3, а также обычное усилительное и питающее электронное оборудование. Импульсы счетчика регистрировались 256-канальным анализатором времени типа At-4 при ширине канала

8–16 мксек. Экспоненциальные кривые распада получены на цифровом счетно-решающем устройстве GIER.

В качестве источника импульсных неитронов использован прерыватель, работающий на горизонтальном канале реактора EWA. Стальной ротор прерывателя диаметром 43 см вращался со скоростью 6000 об/мин. Ширина нейтронного импульса составляла около 160 мксек, а скорость повторения составляла 200 сек. Исследуемая проба помещалась перед щелью ротора.

Так как пучок неитронов из горизонтального канала реактора прерывался ротором, то использованные для измерений импульсные нейтроны состояли из нейтронов, близких к тепловым. Вследствие небольшой утечки нейтронов из исследуемой пробы во время процесса замедления, этот метод дал возможность измерять константы асимптотического распада для больших лапласианов. Измерения были проведены для различных геометрий, например для цилиндрической и прямоугольной конфигураций, причем была установлена зависимость константы асимптотического распада от лапласиана.

EMPLEO DEL SELECTOR EN LAS MEDICIONES CON NEUTRONES PULSADOS. Los autores han medido, empleando la técnica de los neutrones pulsados, los parámetros de difusión en el vidrio orgánico. Para ello inyectaron neutrones pulsados en un medio moderador de dimensiones determinadas (laplaciano geométrico), los cuales generaron un flujo neutrónico que variaba en función del tiempo, y midieron la constante de decrecimiento asintótico de ese flujo. En calidad de detector neutrónico emplearon un contador proporcional de BF_3 tipo miniatura, junto con circuitos electrónicos de amplificación y alimentación. Los impulsos del contador se registraron en un analizador de tiempo tipo At-4, de 256 canales, empleando anchuras de canal de 4-16 μs. Las curvas de decrecimiento exponencial se prepararon mediante una calculadora numérica GIER.

Como fuente de neutrones pulsados se utilizó el selector instalado en el canal horizontal del reactor EWA. El rotor de ese selector es de acero y tiene un diámetro de 43 cm. Se le hizo girar a 6000 rev/min. La anchura del impulso neutrónico era de unos 160 μs y la velocidad de repetición de 200 s^{-1}. La muestra investigada se colocó delante de la ranura del rotor. Dado que el haz neutrónico procedente del canal horizontal del reactor quedaba interrumpido de manera intermitente por el rotor, los impulsos neutrónicos empleados para las mediciones estaban constituidos por neutrones de energías próximas a la térmica.

Debido al pequeño escape de neutrones de la muestra investigada durante el proceso de moderación, fue posible medir con este método las constantes de decrecimiento asintótico incluso para grandes laplacianos. Las mediciones se llevaron a cabo para una geometría rectangular, determinándose la constante de decrecimiento asintótico en función del laplaciano.

INTRODUCTION

The decay constants of the thermal neutrons in organic glass have been measured for small geometries by the pulsed neutron technique. Similar measurements have been made already for water [1]. Organic glass was chosen as a moderator because of the small sizes of the samples which could be used and the simplicity of obtaining given dimensions. A chopper of special construction was used as a pulsed neutron source. The main advantage of this chopper is that it produces a neutron energy spectrum above 0.4 eV. The leakage of neutrons from the sample during the slowing-down process is relatively low, which is especially important for small samples of a moderator.

The diffusion theory cannot give a good interpretation of our results with respect to samples of small dimension. For example, the interpretation of extrapolation length and its dependence on buckling in the range of large bucklings is not well known. A more exact solution of the time-dependent problem can be reached on the basis of the neutron transport theory. This theory is being developed now by many authors, but the results of calculation are not available yet for the interpretation of experiments.

The first numerical calculations were made only for simple cases, namely, one-velocity approximation and infinite plane geometry [2].

EXPERIMENT

A chopper operating at the horizontal channel of the reactor EWA was used as a pulsed neutron source. The rotor of the chopper is constructed of steel and its diameter is 43 cm. Its construction was based on the ordinary fast chopper used in earlier pulsed measurements and an examination of different types of chopper rotors. Information about these measurements will be published in the near future [3].

The chopper with the collimator produces almost square neutron pulses of 160-μs duration. The repetition rate is 200 s^{-1}. It was experimentally confirmed that the neutron background is constant (time-independent) during the measurements. The starting pulse for the time analyser is produced simultaneously with the neutron pulse and in this way the high stability of the chopper velocity is not necessary. Two miniature proportional BF_3 counters were used for detection of neutrons.

The pulses from the counters were recorded by a 256-channel time analyser with channel widths from 4 to 16 μs. The samples under investigation were placed behind the chopper on the axis of the neutron beam from the horizontal channel of the reactor. The neutron beam was filtered by cadmium sheets of 1-mm thickness to eliminate the influence of the time-of-flight effect of the thermal neutrons on the shape of the neutron pulse.

The samples of organic glass were well shielded by cadmium sheets and bricks filled with borated paraffin. The measurements were elaborated by means of the weighted least squares fitting method using the digital computer GIER. The scheme of the experiment is presented in Fig. 1.

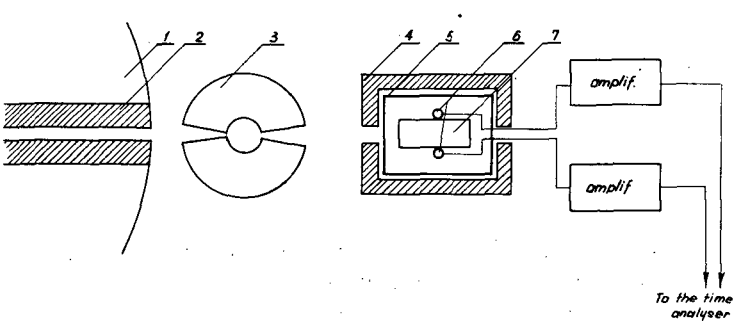

Fig. 1

The schematic layout of the experiment

1. Reactor
2. Collimator
3. Fast-chopper rotor
4. Shield
5. Cadmium
6. BF_3 counters
7. Organic glass

RESULTS

The set of rectangular parallelepipeds made in the organic glass has two constant dimensions a, and a third variable dimension z; a = 20, 10, 8, 6, 5, 4.5 cm and z is in the range of 2-18 cm. For fixed a and varying z the dependence of the decay constant as a function of buckling ($\alpha = \alpha(B^2)$) was obtained for the fixed extrapolation length d = 0.35 cm and is presented in Fig. 2. The exact results of measurements are presented in Table I. The

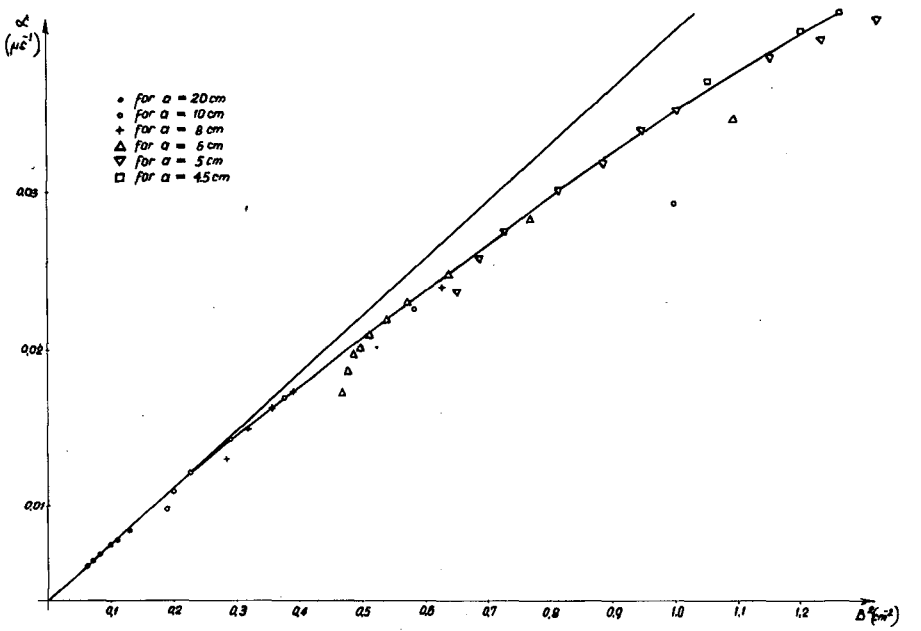

Fig. 2

The α-decay constant as a function of buckling

$C = -4800 \pm 2000$ cm^4/s
$L = 2.90 \pm 0.10$ cm
$\alpha_0 = 4100 \pm 200$ s^{-1}
$D_0 = 35\,900 \pm 10\,000$ cm^2/s

exponential decay curves were observed 200 μs after the end of the neutron burst. These exponentials were measured during three decades. The examples of the decay curves in semi-logarithmic scale are presented in Fig. 3.

REMARKS

Our measurements in the range of small dimensions should be interpreted by using the results based on the neutron transport theory calculated for finite sizes and defined geometry. In the near future we will try

TABLE I

MEASUREMENTS OF DECAY CONSTANT α AS A FUNCTION OF BUCKLING

a = 20 cm		a = 10 cm		a = 8 cm		a = 6 cm		a = 5 cm				a = 4.5 cm	
α (μs^{-1})	B^2 (cm^{-2})	α (μs^{-1})	B^2 (cm^{-2})	α (μs^{-1})	B^2 (cm^{-2})	α (μs^{-1})	B^2 (cm^{-2})	α (μs^{-1})	B^2 (cm^{-2})	α (μs^{-1})	B^2 (cm^{-2})	α (μs^{-1})	B^2 (cm^{-2})
0.0062	0.0609	0.0108	0.198	0.0130	0.286	0.0174	0.464	0.0218	0.628	0.0353	1.022	0.0369	1.045
0.0066	0.0705	0.0122	0.228	0.0149	0.317	0.0188	0.475	0.0239	0.650	0.0380	1.149	0.0407	1.217
0.0070	0.0802	0.0144	0.291	0.0157	0.332	0.0197	0.483	0.0258	0.686	0.392	1.23	0.0426	1.347
0.0077	0.0979	0.0169	0.374	0.0165	0.354	0.0204	0.494	0.0275	0.727	0.0406	1.33		
0.0082	0.1113	0.0221	0.583	0.0176	0.388	0.0211	0.509	0.0300	0.810	0.0424	1.47		
0.0087	0.1315	0.0328	1.431	0.0193	0.446	0.0218	0.533	0.0318	0.877	0.0440	1.63		
				0.0241	0.626	0.0230	0.570	0.0334	0.937	0.0453	1.86		
						0.0249	0.636						
						0.0283	0.766						
						0.0345	1.089						

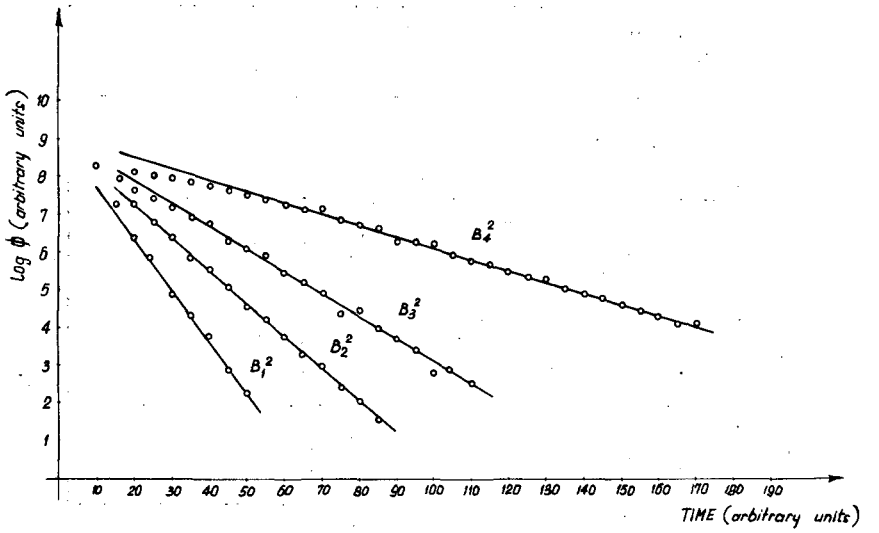

Fig. 3

Neutron decay curves for different bucklings

to measure higher modes for different geometries using the chopper technique.

ACKNOWLEDGEMENTS

The authors are indebted to Dr. J. Mika for his valuable remarks and discussion in the course of the preparation of this paper. We also thank S. Białowas and L. Szadkowski for their technical aid and assistance in the measurements.

REFERENCES

[1] OGRZEWALSKI, Z., RZESZOT, T., WARDA, E. and GRAFFSTEIN, A., Measurements of neutron diffusion parameters in water using a fast-chopper, Nukleonika 8 9 (1963) 595.

[2] BOWDEN, L., Ph.D. Thesis, Virginia Polytechnic Institute.

[3] OGRZEWALSKI, Z. and RZESZOT, T., The application of the fast chopper as a pulsed neutron source for neutron diffusion parameter measurements, Rpt. No. 539/IX of the Institute of Nuclear Research, Swierk.

NON-MULTIPLYING SYSTEMS - THEORY

(Session II)

THEORETICAL INTERPRETATION OF PULSED NEUTRON PHENOMENA*

N. CORNGOLD
BROOKHAVEN NATIONAL LABORATORY,
UPTON, N.Y., UNITED STATES OF AMERICA

Abstract — Résumé — Аннотация — Resumen

THEORETICAL INTERPRETATION OF PULSED NEUTRON PHENOMENA. The author discusses the present understanding of transient effects in the variation of neutron distributions in space, time and energy. In the analysis, particular attention is given to the pulsed neutron experiment in non-multiplying media, and to its interpretation in terms of space-energy modes and (time) decay constants.

Theoretical research in this field, much of which has come from the Brookhaven National Laboratory, has been built upon the exact solution of several special problems, and approximate, numerical solutions in more realistic situations. Recently, a unified point of view, based on the Van Hove-Glauber theory of the scattering of slow neutrons, has been proposed. It has been found that the long-time behaviour of the pair-correlation function, which enables one to distinguish between different types of moderating materials, also controls the type of decay-constant spectrum that one finds. In his discussion the author emphasizes the case of infinite medium solutions that are proportional to $\exp(i\vec{B}\cdot\vec{r})$, in media having 1/v absorption. The analytical work is concerned with modal solutions, proportional to $\exp(\lambda t)$ as well, while the numerical work is directed at the full, "life-history" solution, as well as the modal solutions. The author also remarks on phenomena encountered when the absorption is not 1/v and when the moderator sample is so small that the long-time solutions are no longer separable in space and energy.

Finally, the paper discusses the bearing of these recent developments upon the interpretation of pulsed experiments. Particular reference is made to the measurement of diffusion and diffusion cooling coefficients, and to the nature of the approach to the asymptotic distribution.

INTERPRÉTATION THÉORIQUE DES PHÉNOMÈNES DUS AUX NEUTRONS PULSÉS. L'auteur examine la conception actuelle des effets transitoires dans la variation des distributions des neutrons dans l'espace, dans le temps et selon l'énergie. Dans son étude, il accorde une attention particulière aux expériences, au moyen des neutrons pulsés, portant sur des milieux non multiplicateurs, ainsi qu'à leur interprétation en fonction des modes espace-énergie et des constantes de décroissance (en temps).

Les études théoriques dans ce domaine, dont la plupart one été exécutées au Laboratoire national de Brookhaven, sont fondées sur la solution exacte de plusieurs problèmes particuliers et sur des solutions numériques approximatives de problèmes serrant la réalité de plus près. A une data récente, on a proposé une interprétation uniforme fondée sur la théorie de la diffusion des neutrons lents établie par Van Hove et Glauber. On a constaté que le comportement à long terme de la fonction de corrélation de paire, qui permet de distinguer entre les différents types de ralentisseurs, détermine également le genre du spectre des constantes de décroissance que l'on obtient. Au cours de son examen critique, l'auteur met en évidence le cas des solutions relatives à un milieu infini, qui sont proportionnelles à $\exp(i\vec{B}\cdot\vec{r})$ dans les milieux à absorption 1/v. Le calcul analytique porte sur des solutions modales, également proportionnelles à $\exp(\lambda t)$, alors que le calcul numérique vise à obtenir la solution complète pour toute la durée depuis l'origine, ainsi que les solutions modales. Le mémoire traite aussi de phénomènes qui se produisent lorsque l'absorption n'est pas 1/v et que l'échantillon de ralentisseur est si petit que les solutions à long terme ne peuvent plus être séparées selon l'espace et l'énergie.

Enfin, l'auteur examine l'influence de ces faits nouveaux sur l'interprétation des expériences au moyen de neutrons pulsés - il mentionne notamment la mesure des coefficients de diffusion et de refroidissement par diffusion - ainsi que sur la nature de la méthode à employer pour étudier la distribution asymptotique.

ТЕОРЕТИЧЕСКАЯ ИНТЕРПРЕТАЦИЯ ЯВЛЕНИЙ, СВЯЗАННЫХ С ИМПУЛЬСНЫМИ НЕЙТРОНАМИ. Рассматривается современное толкование переходных эффектов в изме-

* This work was performed under the auspices of the United States Atomic Energy Commission.

нении пространственных, временных и энергетических распределений нейтронов. Особое внимание обращается на эксперимент с импульсными нейтронами в неразмножающих средах и на его интерпретацию с точки зрения пространственно-энергетических распределений и постоянных спада (во времени).

Теоретические исследования в этой области, большую часть которых проводит Брукхейвенская национальная лаборатория, основаны на точном решении нескольких специальных проблем, а также на приближенных численных решениях в более реальных ситуациях. Недавно предложена единая точка зрения, основанная на теории Ван Хов-Глаубера о рассеянии медленных нейтронов. Выяснено, что временная зависимость парно-корреляционной функции, которая позволяет проводить разницу между различными замедлителями, также регулирует обнаруживаемый спектр постоянной спада. В работе подчеркивается случай решения для бесконечной среды, которые пропорциональны экспоненте $(iB\cdot r)$, в средах с поглощением, подчиненным закону 1/v. Аналитическая работа связана с наиболее вероятными решениями, пропорциональными также экспоненте (λt), а численный расчет направлен на решение, учитывающее полную "историю процесса", а также на модальные решения. Затрагиваются также явления, с которыми сталкивались, когда поглощение не подчиняется закону 1/v и когда образец замедлителя настолько мал, что временные решения не разделяются больше в пространственно энергетическом отношении.

Наконец, обсуждается значение этих результатов для интерпретации импульсных экспериментов. В частности, авторы имеют в виду измерение диффузии, коэффициенты диффузионного охлаждения, а также, в зависимости от характера подхода, асимптотическое распределение.

INTERPRETACION TEORICA DE LOS FENOMENOS DEBIDOS A NEUTRONES PULSADOS. El autor discute los conocimientos y las teorías modernas sobre los efectos transitorios en las variaciones de la distribución de los neutrones en el espacio, en el tiempo y en la energía. El análisis se refiere principalmente a los experimentos con neutrones pulsados en medios no multiplicadores y a su interpretación según los modos espacio-energía y según las constantes de decrecimiento (de tiempo).

Una gran parte de las investigaciones teóricas en este campo se han realizado en el Brookhaven National Laboratory; se ha tratado de encontrar la solución exacta de varios problemas especiales y soluciones aproximadas, numéricas, para situaciones más reales. Recientemente se ha propuesto un punto de vista unificado que se basa en la teoría de Van Hove-Glauber sobre la dispersión de neutrones lentos. Se ha encontrado que el comportamiento a largo plazo de la función de correlación de pares, que permite distinguir entre diferentes tipos de moderadores, controla también el tipo de espectro de constante de decrecimiento que se encuentra. En su discusión, el autor destaca el caso de las soluciones relativas a un medio infinito que son proporcionales a $\exp(i\vec{B}\cdot\vec{r})$ en medios cuya absorción obedece a la ley 1/v. Los estudios analíticos se ocupan de las soluciones modales, también proporcionales a $\exp(\lambda t)$, mientras que los estudios numéricos se refieren tanto a la solución completa, la solución «historial», como a las soluciones modales. También habla de fenómenos que se observan cuando la absorción no obedece a la ley 1/v y cuando la muestra de moderador es tan pequeña que las soluciones a largo plazo no se pueden separar ya en el espacio ni en la energía.

Por último se discuten las consecuencias de estos últimos desarrollos para la interpretación de los experimentos con neutrones pulsados. En particular se trata de la medición de la difusión y de los coeficientes de enfriamiento por difusión, y de la naturaleza de la aproximación a la distribución asintótica.

1. INTRODUCTION

The pulsed neutron technique was introduced into reactor physics about fifteen years ago as a technique for measuring diffusion parameters of thermal neutrons [1]. It is particularly suited to the measurement of the average diffusion coefficient $\langle vD(v)\rangle$ and the average absorption rate, $\langle v\Sigma_a(v)\rangle$. In a sense, it complements the exponential experiment, which yields values for the diffusion length.

The analysis of the pulsed experiment appears, at first, to be delightfully simple. If $n(\underline{r}, t)$ is the number of thermal neutrons in the volume $d^3\underline{r}$ about $\underline{r}$, at time t, the equation

$$\frac{\partial n}{\partial t} - vDv^2 n + v\Sigma_a n = 0 \tag{1}$$

describes the evolution of $n(\underline{r}, t)$ after the cessation of the pulse. Then, a little analysis shows that when t is very large $n(\underline{r}, t)$ assumes the form $e^{-\lambda t} \times \phi(r)$, where $(\nabla^2 + B^2)\,\phi(\underline{r}) = 0$, and B^2 is the "buckling" of the fundamental mode. When this result is combined with Eq. (1) we obtain

$$\lambda = v\Sigma_a + vDB^2, \tag{2}$$

a simple equation which enables one to extract the thermal absorption and diffusion coefficients from a graph of λ versus B^2.

Of course, the difficulty lies in interpreting the quantities which appear in Eq. (2). Both $v\Sigma_a$ and vD represent averages over the asymptotic distribution, and, therefore, depend upon B^2. We must untangle this dependence, if we want the Maxwell-averaged quantities $\langle v\Sigma_a \rangle_0$ and $\langle vD(v) \rangle_0$. Even then, one must be careful, for the ratio $L^2 = \langle vD \rangle_0 / \langle v\Sigma_a \rangle_0$ is not equal to the L^2 measured in an exponential experiment. The latter refers to an average over a different type of (non-Maxwellian) spectrum [2]. While these distinctions were understood in the "early days" of the science, the uncertainties introduced by neglecting them were tolerable. Today, the increase in precision that stems from the use of sources of high intensity has changed our point of view. We wish to understand these phenomena. To do so, we must work with the theory of neutron thermalization in its modern and complicated form.

Our aim, in this survey paper, is to describe the present status of the theory that underlies the pulsed neutron experiment. The analysis, which depends on the spectral theory of the scattering operator, involves some rather heavy mathematics. Since the author is a physicist, addressing physicists, his aim must be to steer a sensible course between the Scylla of mathematical rigour[1], and the Charybdis of physicist's "hand-waving". Most of the discussion will concern infinite medium solutions proportional to $\exp(i\underline{B} \cdot \underline{r})$. This restriction enables us to go farther in our analysis without sacrificing too much, for these special solutions do represent many experimental situations.

Much of our analysis can be applied to the exponential experiment, but we have neither time nor space enough to work through the details here. Once again, the two types of experiment complement each other. As the pulsed spectrum is "diffusion-cooled", so the exponential spectrum is "diffusion-heated". In the former, we shall be concerned with the behaviour of the scattering kernel as $(v, v') \to 0$. In the latter, the important range is $(v, v') \to \infty$, which is much easier to discuss, since behaviour there is independent of atomic binding. However, there is a compensation. Instead of being sensitive to moderator type, L^2 versus Σ_a is found to depend critically upon the variation of absorption cross-section with energy, as $v \to \infty$.

The theory of the pulsed neutron experiment has grown considerably in the past three years. It is a striking coincidence that the kinetic theory

[1] The interested reader is invited to consult the papers of JÖRGENS [39] and SHIZUTA [40], for example.

of gases has undergone similar development, and that the spectral theory of the linearized Boltzmann equation has played a crucial role in both theories [3]. Many of the key theorems are similar, though the points of view in the two theories are different, indeed almost complementary. In neutron transport theory, there is no doubt about the nature of the interaction between neutron and nucleus; one is interested in the effect of the chemical state of the moderator atom upon the diffusion of neutrons. In kinetic theory, however, there is no doubt about the state of the "moderator", for it is composed of the "other" gas molecules. Rather, one's interest lies in the effect of different molecular force laws upon diffusion. In both fields, we find that small, inessential changes in the physical models cause considerable difficulty in the mathematical analysis. In classical kinetic theory, unless the force law is cut off, the scattering cross-section is divergent, while in the case of neutrons diffusing in crystalline media, the Bragg reflections cause special analytical difficulties. Thus, there are two aspects of our discussion of decay constants. We should describe the eigenvalue spectra belonging to different physical models, and those aspects of the spectra which do not change when we make small changes in the model.

2. THE MODAL APPROACH

The most obvious way to discuss solutions of the equation:

$$\frac{\partial}{\partial t}\, n(\underline{r},\underline{v},t) + \underline{v}\cdot\text{grad}\, n + v\Sigma n = \int d\underline{v}'v'\Sigma_s(\underline{v}',\underline{v})n + S \qquad (3)$$

is to construct them out of solutions to the homogeneous version of Eq. (3) which are exponential in time. With the Ansatz $n(\underline{r}, \underline{v}, t) \sim \exp(i\underline{B}\cdot\underline{r} - \lambda t)N(\underline{v})$, we are led to an eigenvalue equation

$$\lambda N(\underline{v}) = (i\underline{B}\cdot\underline{v} + v\Sigma)N(\underline{v}) - \int d\underline{v}'v'\Sigma_s(\underline{v}',\underline{v})N(\underline{v}'), \qquad (4)$$

$$= AN$$

where Σ is the total macroscopic cross-section, and $v'\Sigma_s(\underline{v}', \underline{v})$ is the scattering kernel. The fundamental eigenvalue, for fixed B^2, is to be compared with the asymptotic decay constant of experiment, while averaging its associated eigenfunction yields the effective vD of the simple model discussed earlier. However, we wish to go much deeper than the "simple" model.

To prepare Eq. (4) for analysis, we write $N(V) = \exp(-\frac{1}{2}v^2)\Psi(\underline{v})$. The kernel, $H(\underline{v}', \underline{v})$, which replaces $v'\Sigma_s(\underline{v}', \underline{v})$ is then symmetric. (Note that the unit of velocity is chosen so that the Maxwellian has a simple form.) We must now describe the eigenvalue problem, Eq. (4), more precisely.

To what space of functions should the eigensolutions, $N(\underline{v}, \lambda, B^2)$, belong? The conditions which they must satisfy are dictated by physical reasoning and, when possible, by mathematical convenience. In quantum mechanics $\Psi^*\Psi$ and its integral must exist; we are led naturally to a Hilbert space of

functions. In neutron transport theory, the key quantities are reaction rates; we demand that

$$\int d\underline{v} w(v) n(\underline{v})$$

exist for a large class of w(v) (cross-sections). This requirement leads to a Banach space of functions. However, the analysis of integral equations with which most of us are familiar takes place in Hilbert space [4]. (The theorems are easier to find!) Therefore, we shall use that space, and demand that the eigenfunctions belonging to the discrete spectrum be square integrable. Of course, what actually happens is that the eigenfunctions are well behaved at the origin, and decrease exponentially as $|v| \to \infty$, so that they are both integrable and square integrable. As a final remark about the choice of function space, we note that Professor Birkhoff, in his important studies on reactor criticality [5], points out that there is a space, $\mathscr{L}(\Delta)$, more general and more appropriate than the space $L(\Delta)$ of integrable density functions. It is "the space ... of all bounded σ-additive set-functions defined on the Boolean σ-algebra of all Borel subsets of Δ". This space contains elements which represent delta functions. It is not likely, however, that physicists will feel at home in it.

2.1. The continuous spectrum

A general, and elegant way to discuss the continuous spectrum rests upon a theorem of Weyl and von Neumann (see [5a]), which we shall use in an "engineering" manner. Roughly speaking, it states that if we add a well-behaved self-adjoint operator B to a self-adjoint operator C, the continuous spectrum of C is not altered. For us, the integral term in Eq. (4) which we call the "kernel" term will be the operator B. It is real and symmetric, and will be sufficiently well-behaved in the Hilbert space, if we can show that the kernel or one of its iterates is square integrable. $i\underline{B} \cdot \underline{r} - v\Sigma$ is the operator C; it is not self-adjoint, but is "normal", in that it commutes with its adjoint. There is reason to believe that the theorem holds in this case. We shall begin with the scattering by liquids and monatomic gases.

In these cases, the norm,

$$\|H\|^2 \equiv \int d\underline{v}' \int d\underline{v}\, H^2(\underline{v}', \underline{v})$$

can diverge only at the origin of velocities, or at infinity. All realistic models give the same behaviour at high velocity, and direct calculation shows that the integral diverges there [6]. However, one can show that the third iterate of the gas kernel is square integrable [7]. Thus, the gas kernel is acceptable, and the third iterate of all kernels will converge at high velocity.

There remains only the low velocity behaviour of the liquid kernel, which may be represented by the scattering from a diffusing atom. This investigation is not yet complete, but one can verify that the isotropic part of the

kernel converges, and the full angular kernel diverges. It is very likely that an iterated form of the liquid kernel will converge, and we shall assume the truth of this conjecture. With this collection of facts and assumptions in hand, we shall declare that the gas and liquid kernels are sufficiently well-behaved ("compact") for the Weyl-von Neumann theorem to be applicable.

Thus, the continuous spectrum of A, Eq. (4), is the continuous spectrum of $(i\underline{B}\cdot\underline{v}+v\Sigma)$, which is the set of all values assumed by that quantity as $\underline{v}$ is varied. If the minimum value of $v\Sigma$ occurs at $v = 0$, the continuous spectrum occupies the shaded portion of the λ-plane, as shown in Fig. 1. This is the case for most thermalization models. As the temperature of the moderator is decreased, $(v\Sigma)_{min}$ decreases, until it is equal to zero at $T = 0$. Then, the shaded region touches the origin, and (to anticipate a later discussion) there are no proper eigenfunctions. This should not be a surprise, since at $T = 0$ the thermalization equations become slowing-down equations, which resemble integral equations of Volterra type.

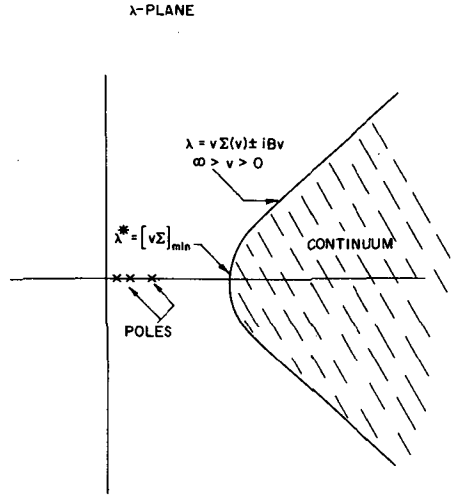

Fig. 1

Spectrum of time eigenvalues [6]

When the moderator is a polycrystal, the scattering kernel contains delta functions which spoil the property of square integrability. They appear as delta functions of energy change in the incoherent scattering, and as delta functions of energy change and angle of scattering, in the coherent scattering. These functions must be subtracted before we can use the Weyl-von Neumann theorem. The subtraction may be carried out in the incoherent case, but we have not yet carried it through for the coherent scattering. Thus, the analysis that follows would hold for a "super-incoherent" approximation in the theory of slow neutron scattering. Write

$$H_1(\underline{v}',\underline{v}) = \tilde{H}_1(\underline{v}',\underline{v}) - v\Sigma_{e\ell}(v)\,\frac{\delta(v'^2-v^2)}{2\pi v}\,, \qquad (5)$$

where an iterate of $\tilde{H}_1$ will turn out to be square integrable, and $\tilde{H}_1$ will be

"compact". If we substitute Eq. (5) into Eq. (4), we find that we must discuss the continuous spectrum of the operator $\tilde{C}$, where

$$\tilde{C} = \left(i\underline{v}\cdot\underline{B} + v\Sigma - v\Sigma_{el} \int \frac{d\Omega}{4\pi} \cdots \right) . \tag{6}$$

This may be done by writing $\tilde{C}\phi = \lambda\phi$, and manipulating the equation as one does in the "B_1-method" of transport theory. One finds that the continuous spectrum occupies a region of the λ-plane that differs from Fig. 1 only in that $(v\Sigma)_{min}$ is replaced by $(v\Sigma - v\Sigma_{el})_{min}$. In those cases where $(v\Sigma)_{min} = (v\Sigma)_{v=0}$, $\tilde{C}$ has the same continuous spectrum as C, because $(v\Sigma_{el})_{v=0} = 0$.[2] In future discussion we shall not distinguish between the polycrystal moderator and others but simply assume that the smoothed kernel, $\tilde{H}_1(\underline{v}', \underline{v})$ is being used.

We should make two additional points before closing the discussion of the continuous spectrum. First, we have made no restriction upon the absorption cross-section; it may have 1/v shape, resonance shape, etc. Second, we have not mentioned fission cross-sections. A prompt fission term, F, added to Eq. (4), has the form of a projection operator. The operator, B + F, which results, will be bounded and 1 : 1, but unfortunately, no longer self-adjoint. Thus, the Weyl - von Neumann theorem is not applicable, though it seems likely that the continuous spectrum of A + F remains that of C.

2.2. Discrete spectrum

It is easy enough to verify that the discrete eigenvalues are real and positive [6]. We are particularly concerned with those lying in the interval $0 \leq \lambda \leq \lambda^* = (v\Sigma)_{min}$ though there may be discrete eigenvalues embedded in the continuous spectrum as well. Of course, the presence of a continuous spectrum indicates that the discrete modes alone cannot form a complete set of functions.

Consider first the case $B^2 = 0$. Then, the operators appearing in Eq. (4) are invariant with respect to rotation of the velocity vector, and the eigensolutions will be of the form $N(\underline{v}) \sim f_l(v) Y_l(\Omega)$, where Y_l is a spherical harmonic of order l, and $\underline{v} = v\Omega$. The Boltzmann equation is replaced by a set of uncoupled equations for the $f_l(v)$, and we find a set of eigensolutions f_{lj} belonging to each value of l. The associated eigenvalues, λ_{lj} are $(2l+1)$-fold degenerate. In view of this "richness" of λ's the reader will permit us to limit our discussion to the $l = 0$ solutions only. These are generated by the "isotropic" part of the scattering kernel.

When $B^2 \neq 0$, rotational invariance exists only with respect to an axis parallel to $\underline{B}$, and the simple classification of solutions is lost. An attempt to expand the eigenfunctions in terms of spherical harmonics leads to a set of coupled integral equations [8]. When we discuss the case $B^2 \neq 0$, we shall nevertheless restrict ourselves to the isotropic part of the scattering kernel. The eigenvalues $\lambda_{oj}(B^2)$ which we obtain depart from the true λ_{oj}, but, we hope, not markedly. We shall devote most of our analysis of the isotropic

[2] $\tilde{C}$ is obviously not normal. We assume that the Weyl-von Neumann theorem may be applied when C is the sum of a normal operator and a bounded projection operator.

kernel to the $B^2 = 0$ case, and indicate, at the end, the changes induced by $B^2 \neq 0$.

Our aim, here, is to understand how the state of the moderator influences the discrete spectrum in the range $0 \leq \lambda_k \leq \lambda^*$. Much of what follows stems from the recent Brookhaven research of KUŠČER [9] of the University of Ljubljana. We begin by using a trick introduced by Lehner and Wing (see [10]). The eigenvalue equation is written as:

$$C\ \Psi(v) = \int_0^\infty dv' K_\lambda(v,v')\Psi(v') \ , \tag{7}$$

where

$$\Psi(v) = \sqrt{v\Sigma - \lambda}\ v e^{\frac{1}{2}v^2} \int d\Omega\ N(\underline{v}) \tag{8}$$

and

$$K_\lambda(v,v') = \frac{vv'\ e^{\frac{1}{2}(v^2 - v'^2)}}{\sqrt{(v\Sigma(v) - \lambda)\ (v'\Sigma(v') - \lambda)}} \int d\Omega\ \Sigma_s(\underline{v}', \underline{v}) \ . \tag{9}$$

One then regards λ as a parameter, and studies the eigenvalues $C_n(\lambda)$ as λ is varied $0 \leq \lambda \leq \lambda^*$. The intersection of the curves $C_n(\lambda)$ with the line $C = 1$ gives the eigenvalues λ_k. The key to the behaviour of the $C_n(\lambda)$ for fixed λ is $||K_\lambda||$, the norm of the kernel. At large v, v', the integral of K_λ^2 converges, due to the extra factors in the denominator of Eq. (9), which were absent from the symmetric, isotropic kernel considered earlier. At small v, v' and $\lambda < \lambda^*$, the integral converges for gas, liquid, and polycristalline moderators. One can show in most cases that the K_λ is positive definite, and that it cannot be a degenerate kernel. Thus, when $\lambda < \lambda^*$, we will find an infinite set of positive eigenfunctions, C_n, bounded as follows:

$$\int_0^\infty dv \int_0^\infty dv'\ K_\lambda^{\,2}(v,v') > C_0 > C_1 \geq \ldots > 0 \tag{10}$$

and which can accumulate only at zero. Figure 2 shows a typical family of curves $C_n(\lambda)$.

The behaviour of $C_n(\lambda)$ as λ approaches λ^* is particularly interesting. It is different for the three types of moderators that we consider, and reflects the fact that the low-energy scattering is markedly different in the three cases. This, in turn, may be traced back via the VAN HOVE theory [11] of slow neutron scattering to the behaviour of the scatterer's pair-correlation function at long times. Thus, the density of decay constants, λ_n, in the interval $0 \leq \lambda < \lambda^*$, will reflect the ease with which a moderator atom can diffuse through its environment.

2.2.1. The polycrystal

Consider first the harmonic solid, in the approximation noted earlier. Direct calculation shows that $||K_\lambda||$ remains finite as $\lambda \to \lambda^*$; there is nothing

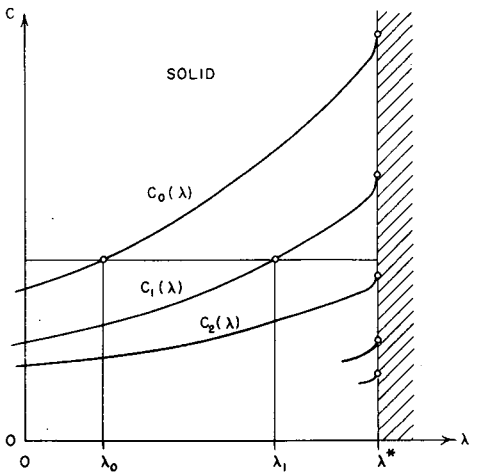

Fig. 2

Curves, $C_n(\lambda)$, for solid (polycrystal) [9]

singular about the limit. Thus, the family of curves, $C_n(\lambda)$, resembles those shown in Fig. 2, and the discrete spectrum contains only a finite number of points in the interval $0 \leq \lambda \leq \lambda^*$. (As we shall see later, the "finite number" is likely to be very small.) As the crystal is made "softer" (by weakening its binding forces, or raising its temperature) the values of the λ_n are found to decrease, while their number increases. When the binding forces are totally dissolved, we obtain the monatomic gas, where $||K_{\lambda^*}||$ diverges. The spectrum $C_n(\lambda^*)$ is not discrete, which indicates that none of the iterates of K_{λ^*} have finite norm.

2.2.2. The monatomic gas

The singular behaviour of K_{λ^*} for the gas is no surprise, for, as the binding is decreased, the inelastic scattering in the low velocity region increases rapidly. Thus, the "numerator" of Eq. (9) increases, while the "denominator" changes little, since $v\Sigma_s(v) \approx \lambda^* + bv^2$ in both cases. One can study the $C_n(\lambda)(\lambda \approx \lambda^*)$ in the gas case in greater detail than in the polycrystal, because the integral Eq. (7) may be reduced to a second order differential equation (for all moderator masses!) in that region. The eigensolution is seen to be closely related to a confluent hypergeometric function, and the imposition of boundary conditions leads to a critical equation for the $C_n(\lambda)$. Before the analysis was complete, Dr. Kuščer and I were sure that the C_n would become infinite as $\lambda \to \lambda^*$. Instead, the critical equation showed that they densely filled an interval $(0, C^*)$ as $\lambda \to \lambda^*$. (See Fig. 3.) When there is no absorption other than "1/v", C^* turns out to be equal to $6\sqrt{\pi}(1 + m/M)^2$, which is considerably greater than unity. Thus, the gas model gives an infinite number of discrete eigenvalues, λ_n, which are packed very close to λ^*. The finite limit point, C^*, is responsible for the close-packing, which had already been observed in studies of the proton gas model

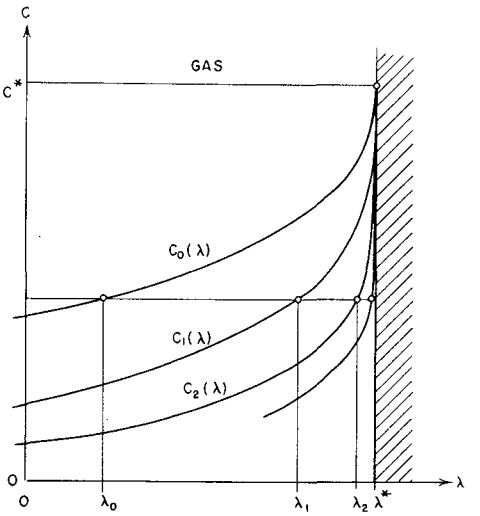

Fig. 3

Curves, $C_n(\lambda)$, for monatomic gas [9]

[12]. Only a few of the modes may be resolved by computer or experiment, and we had been troubled by this point for some time before the discovery of C*.

2.2.3. The liquid

The liquid provides a complicated intermediate case. $||K_{\lambda^*}||$ diverges, and the important behaviour at low velocity is governed by the diffusive part of the correlation function. In this case, we cannot go directly to a differential equation, but analysis based upon the Mellin transform of Eq. (7) shows that $C_0(\lambda)$ approaches a finite limit, C*, as $\lambda \to \lambda^*$. C* is greater than unity and, for η large - which is the case in most liquids -

$$C^* \approx \frac{\eta^2 + 1}{\eta^2 - 1} . \tag{11}$$

The dimensionless constant $\eta = \hbar/2mD$. D is the self-diffusion coefficient.

We are unable to show, using the proper kernel, that the interval (0, C*) is densely filled as $\lambda \to \lambda^*$. However, by replacing K_{λ^*} by another kernel, which preserves the essential features of the scattering, we can get an explicit equation for the $C_n(\lambda)$. The equation, similar to the one derived for the monatomic gas, predicts that the interval will be filled, as conjectured. Thus, the liquid also exhibits an infinite number of decay constants, packed extremely close to λ^*. (In fact, Kuščer has estimated that, for large n, $(\lambda^* - \lambda_n)/(\lambda^* - \lambda_{n+1}) \sim 10^4$!)

The transition from liquid to solid, via $\eta \to \infty$, is not simple. In that limit, C* approaches unity, and it would appear that the set of discrete eigen-

values is empty. However, as $\eta \to \infty$, the diffusive kernel, at low velocities, resembles a kernel for elastic scattering. As we noted earlier, this portion of polycrystal scattering tells us little - hence the empty spectrum. To go properly to the solid limit, one must consider the truly inelastic, as well as the quasi-elastic scattering. Then, if we consider the eigenvalue problem for the $C_n(\lambda^*)$ under the aspect of the Weyl - von Neumann theorem, we conjecture that the well-behaved inelastic scattering will add a finite number of discrete points, $C_n(\lambda^*) > 1$, to the continuous spectrum which fills (0, 1). In this way, the solid-behaviour will be reproduced. To summarize, though the liquid moderator has an infinite number of discrete decay constants, all but a few are packed so close to λ^* as to be unobservable, in practice. The liquid resembles a solid more than it does a gas.

2.2.4. Absorption

We have so far ignored the effects of absorption, which make themselves felt through the factors $(v\Sigma(v)-\lambda)$. For simplicity, we assume that the absorption rate also has its minimum at $v = 0$. Thus, $v\Sigma_a = \lambda_a + dv + ev^2 + \ldots$ The first, or "1/v" term causes λ^* and the family of curves $C_n(\lambda)$ to be shifted to the right. The second has an interesting effect upon the gas kernel, whose scattering rate, as we noted earlier, is $v\Sigma_s = \lambda_s + bv^2 + \ldots$ One finds that $||K_{\lambda^*}||$ is finite for any d, no matter how small. The addition of a constant absorption cross-section thus causes the discrete spectrum to have only a finite number of points. No such effect occurs in the liquid model, which already has a term proportional to v in the scattering rate series. There, the effect of absorption is to lower C^*, and to increase λ_n until the discrete disappears entirely. Roughly speaking, this is the effect of non-1/v absorption in all of the models. As one might guess, the amount of absorber that would be required to erase the discrete spectrum entirely is prohibitive.

2.3. Calculation of discrete eigenvalues ($B^2 = 0$)

Let us halt the general discussion at this point, before going on to the case $B^2 \neq 0$, to discuss the computation of discrete eigenvalues ($B^2 = 0$) for various models. The first computation that we are aware of, and which took slow neutron scattering seriously, was published by VON DARDEL in 1954 [1]. In his work, the approach-to-equilibrium was based upon the exchange of energy between a neutron gas, having a Maxwellian spectrum at temperature $T_n(t)$, and a gas of moderator atoms. This sensible, physically-motivated calculation gives the "M_2" estimate for λ_1, which is accurate to about 30% over the range of m/M [13].

To obtain more accurate results, one must go to a more formal treatment of the eigenvalue problem. This step was taken by BAILLY du BOIS, HOROWITZ and MAURETTE in 1958 [14]. Their analysis was based upon the expansion of the unknown eigenfunction in terms of a complete set of functions. The set of equations which ensued, led, upon truncation, to an eigenvalue problem for a finite-dimensional matrix. The French investigators used Hermite polynomials. They were followed by others [15] who used Laguerre polynomials in v^2 as a basis. These seemed particularly

appropriate to the problem, since they bore the Maxwellian, $v^2\exp(-v^2)$ as weight function. Unfortunately, the polynomial technique gave misleading and unreliable results until the singular nature of the eigenvalue spectrum was appreciated. Then investigators became aware of the extremely slow convergence of the method. Many eigenvalues which appeared to be "converged" were, in fact, greater than λ^*.

Accurate calculations of the λ_n followed soon upon the recognition of λ^*. Several methods were used, and, as one might guess, computational difficulty increased inversely as $(\lambda^* - \lambda_n)$. OHANIAN and DAITCH [16] studied the proton gas and Nelkin's model of H_2O [17] using a discrete ("multi-group") representation, while SHAPIRO and the author [13] discussed the gas model for all mass ratios, and the "heavy-crystal", with Debye spectrum of frequencies. The polynomial method was assessed in one section of the Brookhaven research. One saw that the poor convergence of the method was caused primarily by the choice of polynomials in v^2 rather than v. Though the former set was complete, one had the difficulty of representing $\sqrt{v^2}$ through a series in v^2, compounded with the restrictions induced by λ^*. However, expansion in a series of polynomials in v, with Maxwellian weight function, gives quite acceptable convergence.

In another section of the paper, an approach introduced earlier by the author is generalized [12]. This is the expansion of the scattering kernel (rather than the eigenfunction) into a series of degenerate kernels, chosen to duplicate successively higher moments of the kernel. One obtains a set of algebraic equations, in which λ_n is naturally restricted to lie in the interval $(0, \lambda^*)$. Approximations of low order give quite accurate results in this method, but, since the λ's are contained implicitly, a large amount of computation is required in each order. The discrete eigenvalues for the gas model, as resolved by computation, are shown in Fig. 4.

The most striking results of all occur in the crystalline case. There, Shapiro found that the set of discrete eigenvalues was empty (except for $\lambda_0 = 0$) for heavy crystal moderators, when the Debye temperature exceeded $\frac{1}{4}kT$. This result was verified for Parks' model of graphite [18] by GHATAK and HONECK [19], who used the multigroup approach. Shapiro's results may be seen in Fig. 5.

2.4. Discrete eigenvalues ($B^2 \neq 0$)

As B^2 is increased, the λ_n increase, as they would following an increase in absorption. The expansion about $B^2 = 0$.

$$\lambda_n(B^2) = \lambda_n(0) + \langle vD(v) \rangle_n B^2 - C_n B^4 + \ldots, \qquad (12)$$

defines the usual pulsed neutron parameters, and it is easy enough to prove that λ_n achieves the value λ^* at a finite B_n^2, called B_n^{*2}, and, subsequently, disappears [6]. Before the critical buckling is reached, $\lambda_0(B^2)$ describes the decay of a mode whose shape has been fixed by a balance between leakage and thermalization. Since the leakage rate increases with neutron speed, the equilibrium spectrum is "cooled" below kT. As B^2 is increased, the mean energy of the asymptotic mode sinks toward zero. At $\lambda_0(B^2) = \lambda^*$, a limit has been reached, and from the point of view of $\lim_{t\to\infty} N(v, t)$ two types

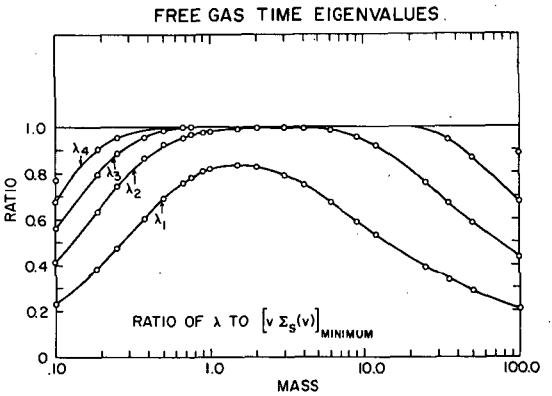

Fig. 4

Discrete eigenvalues for monatomic gas, as function of mass ratio, $B^2 = 0$ [13b]

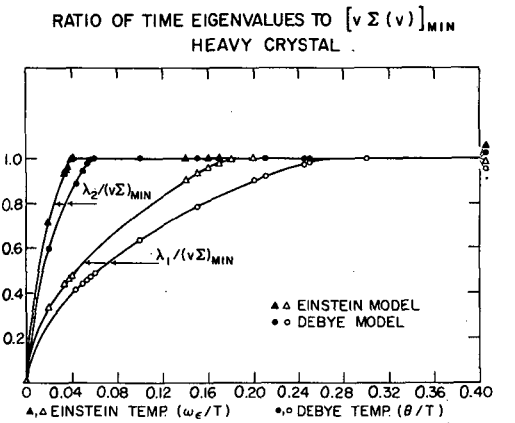

Fig. 5

Discrete eigenvalues for heavy crystal, as function of Debye temperature, $B^2 = 0$ [13b]

of behaviour are possible. Either $\exp(\lambda^* t)\,N(v, t)$ approaches a function which is independent of time and is peaked about $v = 0$, or it approaches a function that is concentrated in the neighbourhood of $v = 0$, but which decays with time. The first is the case of a discrete mode (at λ^*) embedded in the continuum, while the second is, roughly speaking, "pure continuum" behaviour.

Let us return to Eq. (12), which may be regarded as a perturbation series for $\lambda_n(B^2)$. We may write C_n in terms of the eigenfunctions and eigenvalues of the $B^2 = 0$ case. Then, if we neglect the small difference between transport and diffusion theory expressions for C_n, we find [20]:

$$C_o = \sum_{j=1}^{\infty} \frac{\left[\langle 0 | vD(v) | j \rangle\right]^2}{\lambda_j(0)} \qquad (13)$$

in an obvious notation. (The sum should be taken as an integration over the continuous spectrum, and a sum over discrete modes.) While Eq. (13) is not particularly useful when used directly, it leads to some interesting estimates for C; which can help to interpret data, especially when taken in crystalline moderators. For example, two simple estimates are [21]:

$$C_o < \frac{1}{\lambda_1} \left\{ \langle 0 | (vD)^2 | 0 \rangle - \left[\langle 0 | vD | 0 \rangle \right]^2 \right\} \tag{14a}$$

$$C_o > \frac{\langle 0 | vD | 1 \rangle^2}{\lambda_1} \tag{14b}$$

In the crystalline case, we may take $\lambda_1 = \lambda^*$, whence Eq. (14a) depends only upon Maxwell-averages of known cross-sections. Further, the second term in (14a) is easily measured in experiment. A rough calculation based upon (14a) then gives $C < 25 \times 10^5 \, cm^4/s$ for graphite, which is not a trivial result. Estimate (14b) which does require some knowledge of the first mode, may be seen to be a generalization of the "M_2" estimate for C_o [22, 23].

2.5. Laboratory experiments and theory

Almost all of the experimental data that is available gives λ_o as a function of the size of the moderator sample. Let us assume from the start that these λ_o's can be put 1 : 1 with $\lambda_o(B^2)$. Then, we can begin to discuss the experiments by saying that those data which are far below λ^* agree fairly well with theory, while those which are not, do not. Experiments in hydrogenous (and deuterogenous) moderators fall into the first category, while those in the coherent, crystalline materials (beryllium, graphite) fall into both.

Then, there are no difficulties "in principle" with the pulsed experiments in water. All of the measured λ's lie below λ^*, and the latest analysis of $\lambda_o(B^2)$ [19] which is based upon the Nelkin model, agrees to better than 5% in $\langle vD(v) \rangle$ and predicts a value of C_o that falls within the widely spread experimental values. The experiments in D_2O [24] have been analysed on the basis of a similar model; again, theory and experiment agree. Recently, MÖLLER and SJÖSTRAND [25] have reported a measurement of λ_1 for H_2O which presents the theoreticians with a challenge. The most reliable estimate, a direct calculation of λ_1 for the Nelkin model gives a number that is about 33% too low [19]. The discrepancy is rather too large to be ignored. We might add that there is also a discrepancy between theory and experiment in another type of experiment, when λ_0 is measured in H_2O as a function of the concentration of non-1/v absorber [26].

If there are marked discrepancies in the hydrogenous case, where we believe we are on firm ground, the difficulties in the crystalline case can only be called "fundamental". There is no agreement among experimenters as to a "best" value of C_o for beryllium or graphite, where the reported values range from zero to $3.3 \times 10^5 \, cm^4/s$ [27] and from 12 to $40 \times 10^5 cm^4/s$ respectively [28]. Further, much of the λ_o versus B^2 data lies well above λ^*. The only encouraging report we have heard has been from STARR,

HONECK and de VILLIERS [29], who have measured the approach-to-equilibrium in graphite, and find that it is not exponential. Yet, we are beginning to understand the reasons for these discrepancies. To explain, we proceed to the next section.

2.6. Computer experiments and theory

It is essential that we understand the role played by the continuous spectrum of eigenvalues, in the approach of the neutron pulse to equilibrium. Clearly, the behaviour of the function

$$\int_{\lambda^*}^{\infty} d\lambda \; e^{-\lambda t} \; F(v,\lambda) \; = \; N(v,t) \,, \tag{15}$$

depends critically upon the variation of $F(v, \lambda)$ with λ. If the function has several sharp peaks, $N(t)$ will be well represented by a few discrete exponentials, while if $F(v, \lambda)$ is smooth $N(t)$ will be far from exponential. Both cases occur in thermalization. One can argue that the weighting function in Eq. (15) has the form [30, 31]

$$F(v,\lambda) \; = \left[P \; \frac{1}{(v\Sigma - \lambda)} \; + \; f(\lambda) \; \delta(v\Sigma - \lambda) \right] g(v,\lambda) \tag{16}$$

where P denotes "principal value", and g is "smooth" in λ. (We shall handle the $B^2 \neq 0$ case via "diffusion theory".) This form suggests that in a discrete representation, Eq. (15) will have the form

$$N(v_n, t) = \frac{g_n}{\left| \frac{d}{dv} \; v\Sigma(v) \right|_n} \; e^{-v_n \Sigma(v_n) t} \,. \tag{17}$$

Thus, moderators with fluctuating "$v\Sigma$" ($= v\Sigma_{\text{inel.}} + \frac{v}{3\Sigma_s} B^2$) will have a continuum integral, part of which resembles a sum of discrete modes. These moderators are, of course, the polycrystals, and the important v_n occur near the Bragg cut-off. The quasi-modes should suggest to the reader the trapping modes introduced some time ago by de SAUSSURE [32]. In hydrogenous moderators one will find that the amplitudes of the exponential terms in Eq. (17) vary very slowly with n. As a result, $N(v_n, t)$ has markedly non-exponential behaviour.

The idea that the continuum contribution may exhibit some discrete aspects - in coherent moderators - is given credence by the recent work of GHATAK and HONECK [19]. There, the evolution of $N(v, t)$ was studied, in detail, using the multigroup approach, and the Parks' model of graphite. The emptiness of the set of discrete eigenvalues was verified, but one found that for a considerable interval of time (several milliseconds) after the pulse became thermalized, its velocity distribution held a particular, non-equilibrium shape. The decay constant for this quasi-mode was, roughly, $v\Sigma_{\text{inel.}}$, evaluated near the Bragg cut-off. After sufficient time, $N(v, t)$

achieved its final, diffusion-cooled form ($\lambda_0(B^2) < \lambda^*$) in which an appreciable fraction of the neutron population was below the Bragg cut-off. These results suggest that at least one of the terms in Eq. (17) is quite strong.

Another graph from these papers, Fig. 6, helps us to explain why one might "observe" a smooth curve, $\lambda_0(B^2)$ which transcends λ^* without hesi-

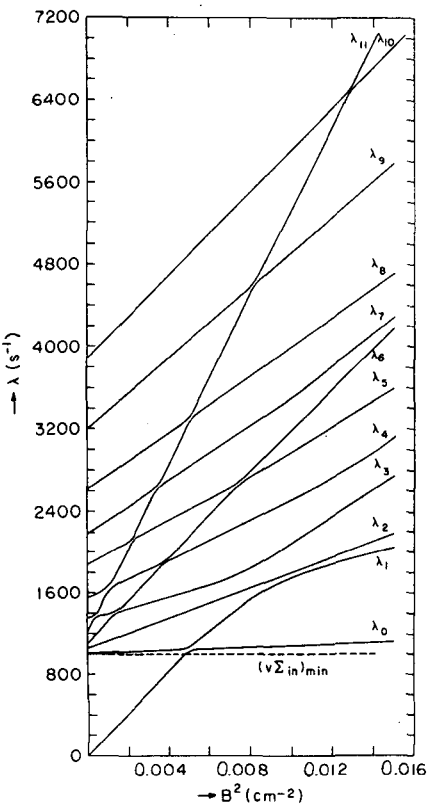

Fig. 6

Dependence of eigenvalues upon B^2 for Parks' model of graphite, as seen by 50-group calculation [19b]

tation. The analysis leading to Fig. 6 is "multi-group", and the continuum appears as in Eq. (17). (Though the modes with $\lambda > \lambda^*$ appear similar to discrete modes in this picture, we know that they are fundamentally different. The mode shape and "eigenvalue" are extremely sensitive to the order of the multi-group approximation.) Since $v\Sigma$ has a minimum at $v = 0$, we expect a strong contribution from $\exp(-\lambda^* t)$ independent of group structure, and this is found to be so. Indeed, we can use $d\lambda_n/dB^2 = \langle n|vD|n\rangle + 0(B^2)$ to verify that the decay constant of the lowest multi-group mode will depend little upon B^2. Thus, there will be a degeneracy at B_δ^{*2}, for the discrete mode, $\lambda_0(B^2)$ will collide with the multi-group mode. If we choose to continue these curves for $B^2 > B_0^{*2}$, when only the continuum remains, we must take the $\exp(-\lambda^* t)$ mode as the proper continuation of $\lambda_0(B^2)$, for that is the lowest mode and,

in the multi-group sense, it is always positive. Thus, the "true-mode" has a sudden change of slope upon reaching λ^*, while the curve that appears to be the smooth continuation of $\lambda_0(B^2)$ is, in fact, a higher mode. (A similar phenomenon is seen in the early two-group calculations of de SAUSSURE [32] and DAITCH and EBEOGLU [33].)

The two modes can be distinguished in a hand calculation only upon using great care. The higher mode is not everywhere positive, but the change in sign occurs at very low velocity. Thus, if one is not careful, one will be switched onto the wrong track[3] at B_0^{*2}. If we can assume that the pulsed neutron experiment follows the computer experiment, and that the trajectory of the multi-group mode for $B^2 > B_0^{*2}$ has a meaning independent of multi-group structure (in terms of the weight-function of the continuum integral, etc.) we shall have understood a puzzle that has troubled us for several years.

3. SUMMARY

Our aim, in this essay, has been to discuss the present state of our understanding of the decay constants in pulsed neutron experiments. One of the reasons for limiting our attention to the infinite medium solutions is that they form a well-defined and useful set, about which we have learned much in the past five years. While the study of these solutions is not yet complete, their general features are now understood.

The theoretician will no doubt be turning his attention to the time-dependent problem in a finite medium [34]. Several preliminary calculations have appeared [35], but there is no doubt that a rigorous (or demi-rigorous!) analysis will require very heavy mathematics. A particularly important aspect of the analysis will be the connection between the finite medium and infinite medium solutions. For example, we know that for sufficiently large B^2, no discrete λ's exist. If the infinite-medium solutions form a complete set, we might expand the finite-medium solution in terms of them, and might conjecture - on the basis of "superposition" - that a sufficiently small sample has no discrete decay constant. Yet, we know that this conclusion is false [10]; there is no simple relation between the $\lambda_n(B^2)$ and the true λ_n.

In any case, it is becoming clear that the quantities which appear in the modal representation of $N(v, t)$ do not lend themselves easily to measurement. Other representations are certainly possible, and should be exploited. The most popular of these seems to be the moments method [36, 37, 38], which is particularly appropriate in joining the slowing-down and asymptotic region, but does not give "diffusion parameters" readily. Perhaps the time has come for the experimenter to ask himself why he wishes to do pulsed neutron experiments. Surely, there are easier ways to "check" a scattering kernel, and the reactor design information one extracts is hardly worth the effort. The final justification is surely the thing-in-itself. The approach-to-equilibrium has fascinated scientists for many years, and, since Boltzmann, has posed some very interesting problems for the theoretician. Only recently

---

[3] This is surely the case in the calculations of JHA [41] and others similar to it. Jha's energy scale is cut off at "ten degree" neutrons. Under these conditions one could continue λ to values several times larger than λ^* without noticing that the fundamental mode had become one which changed sign.

have the experimenters, through the techniques of neutron physics, been able to provide so much valuable and detailed information.

ACKNOWLEDGEMENTS

Stimulating conversations with Drs. Ivan Kuščer, Paul Michael, Henry Honeck and Charles Shapiro have, in the past few years, improved the author's understanding of the matters discussed in this paper. He is also grateful to Dr. Joel Pincus for having helped him to avoid gross mathematical barbarisms.

REFERENCES

[1] VON DARDEL, G.F., Phys. Rev. 94 (1954) 1272; ANTONOV, A.V. et al., Proc. UN Int. Conf. PUAE 5 (1956) 3.
[2] STARR, E. and KOPPEL, J., Nucl. Sci. Engng 14 (1962) 224.
[3] GRAD, H., Proc. 3rd Int. Rarefied Gas Dynamics Symp., Academic Press, N.Y. (1963).
[4] TRICOMI, F.G., Integral Equations, Interscience, N.Y. (1957).
[5] BIRKHOFF, G., "Reactor Criticality in Neutron-Transport Theory" (Oct. 1961); also, Proc. Nat. Acad. Sci. 45 (1959) 567.
[5a] RIESZ, F. and NAGY, B.Sz., Functional Analysis, Frederick Ungar, N.Y. (1955).
[6] CORNGOLD, N., Nucl. Sci. Engng 19 (1964) 80.
[7] DORFMAN, R., Proc. Nat. Acad. Sci. 50 (1963) 804.
[8] NELKIN, M., Nucl. Sci. Engng 7 (1960) 210; HONECK, H.C., Proc. BNL Conf. Neutron Thermalization IV (1962) 1186.
[9] KUŠČER, I. and CORNGOLD, N., "Discrete Relaxation Times in Neutron Thermalization", (Feb. 1965), Phys. Rev., to be published.
[10] WING, G.M., An Introduction to Transport Theory, J. Wiley, N.Y. (1962).
[11] VAN HOVE, L., Phys. Rev. 95 (1954) 249; VINEYARD, G.H., Phys. Rev. 110 (1958) 999.
[12] CORNGOLD, N., MICHAEL, P. and WOLLMAN, W., Nucl. Sci. Engng 15 (1963) 13.
[13] NELKIN, M., J. nucl. Energy 8 (1958) 48; (b) SHAPIRO, C.S. and CORNGOLD, N., Phys. Rev. 137 (1965) 1686.
[14] BAILLY du BOIS, B., HOROWITZ, J., MAURETTE, C., Saclay Rpt SPM-525 (1958).
[15] KAZARNOVSKII, M.V., STEPANOV, A.V. and SHAPIRO, F.L., Proc. 2nd UN Int. Conf. PUAE 16 (1958) 279; HÄFELE, W. and DRESNER, L., Nucl. Sci Engng 7 (1960) 304; PUROHIT, S.N., Nucl. Sci. Engng 9 (1961) 157-305; WEISS, Z., Nukleonika 6 (1961); TAKAHASHI, H., Proc. BNL Conf. Neutron Thermalization IV (1962) 1299.
[16] OHANIAN, M.J. and DAITCH, P.B., Nucl. Sci. Engng 19 (1964) 343.
[17] NELKIN, M., Phys. Rev. 119 (1960) 791.
[18] PARKS, D.E., BEYSTER, J.R., WIKNER, N.F., Nucl. Sci. Engng 13 (1962) 306.
[19] GHATAK, A.K. and HONECK, H.C., (a) Nucl. Sci. Engng 21 (1965) 227; (b) J. nucl. Energy 19 (1965) 1.
[20] TAKAHASHI, H., Proc. BNL Conf. Neutron Thermalization IV (1962) 1299.
[21] CORNGOLD, N. and MICHAEL, P., Nucl. Sci. Engng 19 (1964) 91.
[22] NELKIN, M., J. nucl. Energy 8 (1958) 48.
[23] CORNGOLD, N., Lectures from 2nd Neutron Physics Conf. 1962, Univ. of Michigan (1964).
[24] HONECK, H.C., Trans. Amer. nucl. Soc. 5 (1962) 47.
[25] MÖLLER, E. and SJÖSTRAND, N.G., Ark. Fys. 27 (1964) 501.
[26] CALAME, G.P., Nucl. Sci. Engng 20 (1964) 352.
[27] ZHEZHERUN, I.F., Soviet atom. Energy 16 (1964) 264.
[28] PRICE, G.A., Nucl. Sci. Engng 18 (1964) 410.
[29] STARR, E., HONECK, H., de VILLIERS, J., Nucl. Sci. Engng 18 (1964) 230.

[30] CORNGOLD, N., MICHAEL, P. and WOLLMAN, W., Nucl. Sci. Engng 15 (1963) 13; KOPPEL, J., Nucl. Sci. Engng 16 (1963). 101.
[31] BEDNARZ, R. and MIKA, J., J. math. Phys. 4 (1964) 1285.
[32] de SAUSSURE, G., Nucl. Sci. Engng 12 (1962) 433.
[33] DAITCH, P.B. and EBEOGLU, D.B., Proc. BNL Conf. Neutron Thermalization IV (1962) 1132.
[34] JÖRGENS, K., Comm. pure appl. Math 11 (1958) 219; NELKIN, M., Physica 29 (1963) 261.
[35] WILLIAMS, M.M.R., J. nucl. Energy 17 (1963) 55; KLADNIK, R., Nukleonik 6 (1964) 137; JUDGE, F.D. and DAITCH, P.B., Nucl. Sci. Engng 20 (1964) 428.
[36] KOPPEL, J.U. and NALIBOFF, Y.D., Trans. Amer. nucl. Soc. 5 (1962) 337; KOPPEL, J.U., Nucl. Sci. Engng 12 (1962) 532.
[37] GHATAK, A.K. and KRIEGER, T.J., Nucl. Sci. Engng 21 (1965) 304.
[38] WILLIAMS, M.M.R., Nucl. Sci. Engng 19 (1964) 221.
[39] JÖRGENS, K., Comm. pure appl. Math. 11 (1958) 219.
[40] SHIZUTA, Y., Prog. theor. Phys. 32 (1964) 489.
[41] JHA, S.S., J. nucl. Energy 12 (1960) 89.

DISCUSSION

S.N. PUROHIT: What kind of model was used for the solid calculations?

N. CORNGOLD: The specific calculations of C. Shapiro and the author were based upon the heavy-crystal approximation. The general analysis of I. Kuščer and the author is based on the Van Hove theory of scattering from crystals and depends only on the properties of the "width function". It is quite general, except for a somewhat crude treatment of the coherent scattering.

W. REICHARDT: Was I correct in understanding you to say that an originally discrete eigenvalue can disappear when you poison the moderator even with a 1/v absorber?

N. CORNGOLD: I should say that only a non-1/v absorber will produce this effect. You are quite right in reminding us that 1/v absorbers affect the spectrum only trivially.

K.H. BECKURTS: I would like to comment on the eigenvalue calculations of GHATAK and HONECK [22]. It should be borne in mind that these calculations are largely qualitative in nature and need to be done with more realistic scattering kernels. For instance, the critical eigenvalue limit obtained by these authors in graphite is 1000 s^{-1}, whereas the experimental value seems to be 2600 s^{-1}. I think it is a challenge to theoreticians to find out which features of the scattering kernel are important here.

N. CORNGOLD: I quite agree. I believe that when certain deficiencies in the Parks' model are remedied the discrepancy will be reduced. The results I have mentioned still need to be corroborated by direct analysis, which is a difficult matter.

P. ZWEIFEL: Where do you use the assumption that the eigenfunctions are square-integrable?

N. CORNGOLD: This assumption appears in the general analysis of Dr. Kuščer and the author. The square-integrability of the kernel plays a key role there.

TIME AND SPACE EIGENVALUES OF THE BOLTZMANN EQUATION

J. WOOD
UNIVERSITY OF BIRMINGHAM, UNITED KINGDOM

Abstract — Résumé — Аннотация — Resumen

TIME AND SPACE EIGENVALUES OF THE BOLTZMANN EQUATION. Two problems in neutron thermalization have aroused considerable experimental and theoretical interest. The experiments are the pulsed source in a pure moderator and the measurement of diffusion length. In a recent paper Corngold discusses the theory of the spectra of the eigenvalues (decay constants) arising from the consideration of these two problems.

We examine from the viewpoint of Corngold's theory the temporal and spatial eigenvalues of a number of kernels. We use three methods of solving the Boltzmann transport equation and compare their accuracy. The methods studied are:

(i) The diffusion approximation;
(ii) The P_3 approximation;
(iii) The B_0 approximation.

The equations are solved numerically and in the case of the B_0 method a new iterative scheme is applied to the resulting non-linear eigenvalue problem which gives good convergence.

The kernels used include (a) the gas model, (b) the effective width model of Schofield and Egelstaff and (c) the crystal model (incoherent approximation).

The effect on the scattering cross-sections of varying parameters in these models is shown graphically. The effective width model is used to represent light water, and the dependence of thermalization parameters on the effective width parameter has been calculated. The value of the effective width parameter giving optimum agreement with experimental values of these thermalization parameters is obtained.

Results are tabulated of the variation of the time-dependent eigenvalues with size of system (B^2) and the variation of the spatial eigenvalues with increased absorber concentration. The approach of the eigenvalues to a limiting value is shown graphically. The energy spectra of space- and time-dependent transients in a pulsed slab are also shown.

VALEURS PROPRES TEMPORELLES ET SPATIALES DE L'ÉQUATION DE BOLTZMANN. Dans la thermalisation des neutrons, deux problèmes ont suscité un intérêt considérable chez les expérimentateurs et les théoriciens. Les expériences portent sur la source pulsée dans un ralentisseur pur et sur la mesure de la longueur de diffusion. Dans un travail récent, Corngold discute la théorie des spectres des valeurs propres (constantes de décroissance) résultant de l'étude de ces deux problèmes.

L'auteur examine du point de vue de la théorie de Corngold les valeurs propres temporelles et spatiales pour plusieurs noyaux. Pour résoudre l'équation de transport de Boltzmann, il emploie trois méthodes et compare l'exactitude des résultats. Les méthodes étudiées sont les suivantes:

1. Approximation de diffusion;
2. Approximation P_3;
3. Approximation B_0.

Les équations sont résolues numériquement; dans le cas de la méthode d'approximation B_0, on applique au problème non linéaire des valeurs propres un nouveau procédé d'itération assurant une bonne convergence.

Les noyaux employés comprennent: a) le modèle de gaz, b) le modèle de largeur effective de Schofield et Egelstaff, c) le modèle de cristal (approximation incohérente).

L'effet sur les sections efficaces de diffusion, que l'on obtient en faisant varier les paramètres dans ces modèles, est indiqué graphiquement. Le modèle de largeur effective est employé pour représenter l'eau légère; on a calculé les variations des paramètres de thermalisation en fonction du paramètre de largeur effective. Pour ce paramètre, on a déterminé la valeur qui assure la meilleure concordance avec les valeurs expérimentales des paramètres de thermalisation.

On présente sous forme de tableaux les résultats de la variation des valeurs propres temporelles en fonction des dimensions du système (B^2) et de la variation des valeurs propres spatiales en fonction de la concentration de l'absorbant. L'évolution des valeurs propres vers une limite est représentée graphiquement. L'auteur indique

également les spectres énergétiques des états transitoires dépendant de l'espace et du temps dans une plaque exposée à des neutrons pulsés.

ВРЕМЕННЫЕ И ПРОСТРАНСТВЕННЫЕ СОБСТВЕННЫЕ ЗНАЧЕНИЯ УРАВНЕНИЯ БОЛЬЦМАНА. Две проблемы в области термализации нейтронов вызвали значительный экспериментальный и теоретический интерес. Эксперименты касаются распада импульсных источников в чистом замедлителе и измерения длины диффузии. В последней своей работе Корнгольд рассматривает теорию спектров собственных значений (постоянные распада), вытекающую из этих двух проблем.

С точки зрения теории Корнгольда рассматриваются временные и пространственные собственные значения ряда ядер. Применены три метода решения уравнения переноса Больцмана и сравнена их точность. Исследуемыми методами являются:

1. Диффузионная аппроксимация.
2. P_3-аппроксимация.
3. B_0-аппроксимация.

Для уравнений получены цифровые значения, а в случае метода B_0 применена новая итерационная схема для решения результатирующей нелинейной задачи о собственных значениях, позволяющая получить хорошую сходимость.

Используемыми ядрами являются: a) модель газа; b) модель эффективной ширины Шофильда и Эгельстаффа; c) кристаллическая модель (некогерентная аппроксимация).

Влияние меняющихся параметров на сечения рассеяния в этих моделях показано графически. Чтобы представить легкую воду, использовали модель эффективной ширины. Рассчитана зависимость параметров термализации от параметра эффективной ширины. Получено значение параметра эффективной ширины, согласующееся наилучшим образом с экспериментальными значениями этих параметров термализации.

Результаты изменения зависящих от времени собственных значений при изменении размера системы (B^2) и изменения пространственных собственных значений при увеличении концентрации поглотителя сведены в таблицу. Приближение собственных значений к предельному значению изображено графически. Показаны также энергетические спектры зависящих от пространства и времени переходных процессов в пульсирующей пластине.

VALORES PROPIOS TEMPORALES Y ESPACIALES DE LA ECUACION DE BOLTZMANN. La termalización de neutrones plantea dos problemas que han suscitado considerable interés experimental y teórico. Los experimentos consisten en el empleo de la fuente pulsada en un moderador puro, y en la medición de la longitud de difusión. En un artículo reciente, Corngold discute la teoría de los espectros de los valores propios (constantes de decremento) que se deriva del estudio de esos dos problemas.

El autor examina con arreglo a la teoría de Corngold los valores propios temporales y espaciales de una serie de núcleos. Emplea tres métodos para resolver la ecuación de transporte de Boltzmann y compara su exactitud; los métodos son:

1. La aproximación de difusión.
2. La aproximación P_3.
3. La aproximación B_0.

Las ecuaciones se resuelven numéricamente, y en el caso del método B_0 se aplica al resultado (un problema no lineal de valores propios) un nuevo procedimiento de iteración que da una buena convergencia.

Los núcleos empleados incluyen a) el modelo gaseoso, b) el modelo de la anchura efectiva de Schofield y Egelstaff, y c) el modelo del cristal (aproximación incoherente).

La memoria muestra gráficamente cómo varían en estos modelos las secciones eficaces de dispersión cuando se modifican los parámetros. El autor emplea el modelo de la anchura efectiva para representar el agua ligera, y ha calculado cómo los parámetros de la termalización dependen del parámetro de anchura efectiva. También obtiene el valor de este último parámetro que mejor concuerda con los valores experimentales de los de la termalización.

Se dan en cuadros los resultados de la variación de los valores propios dependientes del tiempo en función del tamaño del sistema (B^2), así como la variación de los valores propios espaciales cuando aumenta la concentración del absorbedor. Un gráfico muestra la aproximación de los valores propios al valor límite. También se indican los espectros de energía de los fenómenos transitorios dependientes del espacio y del tiempo en una placa sometida a impulsos neutrónicos.

1. INTRODUCTION

Two important experiments in neutron thermalization are the pulsed-source in a pure moderator and the measurement of diffusion length. CORNGOLD [1] has discussed the eigenvalue spectra associated with these problems and, in particular, he shows that for the pulsed problem the discrete eigenvalues (decay constants) cannot exceed $(v\Sigma)_{min}$. We have solved numerically the homogeneous Boltzmann transport equations arising from these experiments using realistic kernels to represent liquid and crystalline moderators. We have examined the limiting behaviour of the discrete eigenvalues for the existence of a maximum value of buckling for the pulsed system, and a maximum value of absorption in the diffusion-length problem. It has been usual when considering the pulsed problem to consider only the fundamental spatial mode which can be described by a buckling and derive the fundamental and higher time-dependent eigenvalues for various values of B^2. In fact the general solution (assuming only discrete eigenvalues) is composed of terms of the form

$$\phi(E, \mu)e^{-\lambda \pm Sx}$$

The general form gives rise to a multiple eigenvalue problem which we have considered in two ways: the conventional, in which we fix S as iB and solve for all permissible values of λ, and the less usual in which we fix λ as λ_0 and seek all allowable values of S.

Three methods of solution were used: (i) the diffusion approximation, (ii) the spherical harmonic (P_3) approximation and (iii) the B_0 approximation. To enable a direct comparison of (i) and (ii) with (iii) we have restricted all solutions to isotropic scattering, except for the curve shown in Fig. 4. The assumption of isotropy makes (iii) in principle exact.

2. THE SCATTERING KERNELS

2.1. Liquid moderator

To represent water we have used the effective width kernel of EGELSTAFF in Ref. [2]. The differential scattering cross-section is, in the usual notation

$$\sigma(E \to E', \theta) = \frac{\sigma_b}{2kT}(E'/E)^{\frac{1}{2}} e^{-\beta/2} S(\alpha, \beta),$$

where

$\alpha = E' + E - 2\mu\sqrt{E\,E'}$ and

$\beta = (E' - E)/kT$.

The scattering law $S(\alpha, \beta)$ for this model is given by

$$S(\alpha, \beta) = \frac{1}{\pi} \exp(2d^2\alpha) \frac{2(d^2 + \frac{1}{4})^{\frac{1}{2}}}{[\beta^2 + (2d\alpha)^2]^{\frac{1}{2}}} d\alpha K_1 \{(d^2 + \tfrac{1}{4})^{\frac{1}{2}}[\beta^2 + (2d\alpha)^2]^{\frac{1}{2}}\},$$

where K_1 is the modified Bessel function of the second kind and d is the reciprocal of the effective width parameter q.

The value of d(=1/q) can be chosen to give agreement with some physical property of the material which depends upon the actual phonon frequency distribution for its value, such as the specific heat or kinetic energy ($\bar{K}$). However, for our purpose it is convenient to use the pulsed parameter D_0 as a means of fitting the width parameter. The effect of the oxygen in the water is allowed for by assuming it contributes as a gas of mass 16. The variation of D_0 with 1/q is shown in Fig. 1. Some experimental values (with

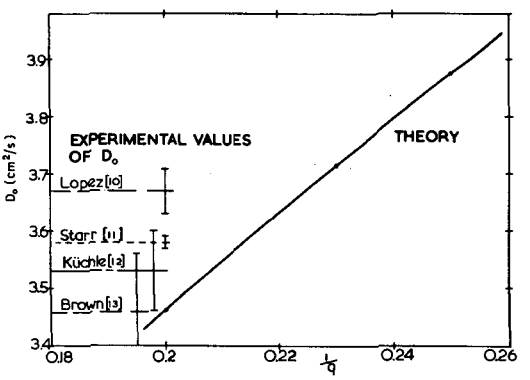

Fig. 1

The variation of the pulsed parameter D_0 for water with the reciprocal of the effective width, d = 1/q at 21°C.

errors) are indicated on the vertical axis. The theoretical values were calculated from the familiar relationship

$$D_0 = \frac{\int_0^\infty (\lambda_{tr}/3)M(E)dE}{\int_0^\infty (1/v)M(E)dE}.$$

From Fig. 1. and other considerations which will be mentioned later, we conclude that d = 0.215 is a suitable value to take. The experimental and calculated cross-sections for two values of the effective width are shown in Fig. 2.

2. 2. Crystalline moderator

To represent a crystalline material we have used the incoherent approximation, where the first phonon term is treated exactly and the phonon energy distribution for the higher phonon terms is approximated by a Gaussian distribution, as suggested by SCHOFIELD in Ref. [3]. For the particular case of beryllium we used a Debye phonon energy spectrum (with $\Theta = 1000°K$) for the first phonon term. At each energy, the higher phonon terms were included until their contribution to the total incoherent cross-section became

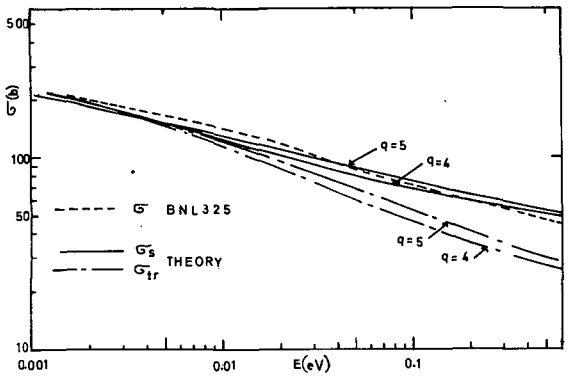

Fig. 2

The scattering cross-section of water at 21°C.
The theoretical values are for the effective width kernel.
σ_s is the scattering cross-section and σ_{tr} the transport cross-section.

negligible. In the incoherent model, the incoherent elastic cross-section is

$$\sigma_{EL}(E) = \frac{\sigma_b}{4\alpha E}\,[1 - \exp(-4\alpha E)],$$

where

$$\alpha = \frac{1}{M}\int_0^\infty \frac{\rho(w)}{w}\,\coth\,(w/2T)\,dw.$$

To reproduce broadly the effect of the abrupt change in cross-section in the neighbourhood of the Bragg cut-off, we have taken $\sigma_{EL} = 0$ for $E < 0.005$ eV. The calculated and measured cross-sections for beryllium are compared in Fig. 3. Such a device cannot produce the numerous maxima above the Bragg

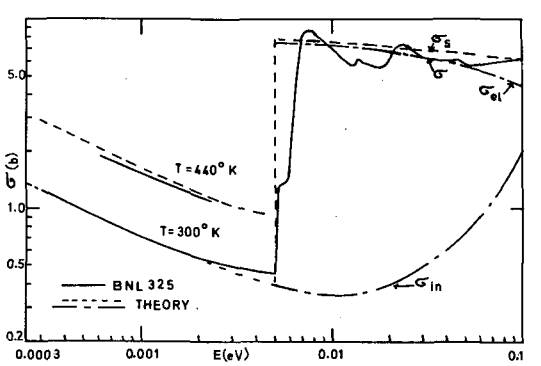

Fig. 3

The scattering cross-sections of beryllium.
The theoretical values are for the incoherent approximation
with Bragg cut-off at 0.005 eV.
σ_{el} is the elastic and σ_{in} the inelastic cross-section.

peak caused by coherent effects, but it does enable the importance of the sudden rise in the cross-section to be demonstrated as shown by Figs. 7 and 8. As is well known a simple Debye frequency is inadequate to represent graphite. We have made some preliminary calculations which suggest that a considerable improvement can be obtained by using the phonon distribution function of EGELSTAFF (see Ref. [4]). We intend to incorporate this within the framework of the incoherent approximation to produce scattering data for graphite.

3. MATHEMATICAL PROCEDURE

To solve the homogeneous integral equations we have replaced them by eigenvalue problems in matrix algebra, and solved these numerically by computer, using either the Q.R. algorithm method [5] or the method of inverse iteration. Where possible we have symmetrized the matrices by applying the detailed balance condition satisfied by the kernels. Because it is particularly important to our results we describe in the Appendix the method used to obtain the B_0 solution.

4. RESULTS AND DISCUSSION

4.1. Effective width and gas kernels

The method of quadrature used in all the matrix calculations is the generalized Simpson's rule of DAITCH [6]. This has the merit of concentrating the energy mesh points in a desired region. The lowest energy value was always very small, being of the order of 10^{-7} eV; for the water calculations the upper energy cut-off always exceeded 1 eV and for beryllium 0.35 eV. As a means of assessing the accuracy of the results, the number of energy points was varied and the convergence of the eigenvalues checked. The methods of obtaining the theoretical values of $(v\Sigma)_{min}$ for the various kernels are described by WILLIAMS in Ref. [7]. These values of $(v\Sigma)_{min}$ also provided a useful check on the accuracy of the computations, since the upper bound being observed was indicated by the one eigenvalue which remained independent of the buckling.

The excellent agreement between the calculated and measured values of λ_0 versus B^2 for water is shown in Fig. 4. The kernel is the effective width one with $d = 0.215$. The diffusion approximation was used with (linear) anisotropy. The agreement is of course mainly but not entirely the result of fitting the gradient of the curve at the origin; nevertheless, it does demonstrate that this model can accurately predict the integral properties of water measured by such pulsed experiments. In contrast to λ_0, the thermalization time τ_{th} is independent of the transport cross-section of the material: it is a measure of the energy exchange processes and hence provides an independent check on the choice of d. The thermalization time is given by the expression [8]

$$\lambda_1 = v\Sigma_a + 1/\tau_{th} \quad (B^2 = 0) .$$

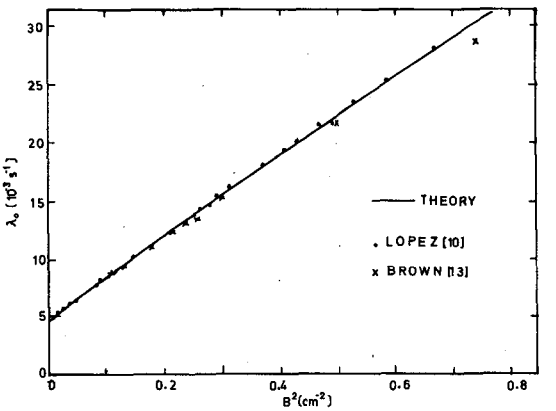

Fig. 4

λ_0 versus B^2 for water at 21°C.
The theoretical curve was calculated using the effective width model, d = 0.215.
Diffusion approximation solution, including (linear) anisotropy.

From Table I we can see that the value of thermalization time for d = 0.21 is in good agreement with the experimental value of 4.1 μs, reported

TABLE I

VARIATION OF THERMALIZATION TIME, τ_{th}, FOR WATER WITH THE RECIPROCAL OF EFFECTIVE WIDTH

d	τ_{th} (μs)
0.2	4.55
0.21	4.50
0.27	4.13
0.5	3.71

by MÖLLER in Ref. [9]. The values of τ_{th} for water considered as a gas of various effective masses are shown in Table II. The time-dependent eigenvalues for the three methods of solution are compared in Tables III and IV. It should be noted that for the effective width and gas kernels, higher eigenvalues exist below $(v\Sigma)_{min}$. These increase with buckling and disappear into the continuum as does finally the fundamental eigenvalue. The limiting behaviour of K_0 and λ_0 is shown in Figs. 5 and 6. It is clear from Fig. 5 that, despite anisotropy, the maximum value of buckling for water would be reached well beyond the experimental range. However, for the diffusion-

TABLE II

THERMALIZATION TIME OF WATER AS A GAS

Mass	τ_{th} (μs)
1.0	3.603
1.884	4.886
2.0	5.054

TABLE III

VALUES OF NORMALIZED TIME EIGENVALUES FOR WATER AT 21°C GIVEN BY EFFECTIVE WIDTH KERNEL, d = 0.21 (Number of energy mesh points = 41)

B^2 (cm^{-2})	Diffusion approximation				B_0
	$\frac{\lambda_0}{(v\Sigma)min}$	$\frac{\lambda_1}{(v\Sigma)min}$	$\frac{\lambda_2}{(v\Sigma)min}$	$\frac{\lambda_3}{(v\Sigma)min}$	$\frac{\lambda_0}{(v\Sigma)min}$
0	0.01612	0.7550	0.9631	1.0000	0.01612
0.2	0.0305	0.7634	0.9651	1.0000	
0.5	0.0517	0.7765	0.9684	1.0000	
1.0	0.0863	0.7967	0.9732	1.0000	0.0867
3.0	0.2145	0.8605	0.9852	1.0000	
5.0	0.3277	0.9033	0.9918	1.0000	0.3326
8.0					0.4848
13.0	0.6537	0.9727	1.0000		0.6870
14.0	0.6825	0.9761	1.0000		
14.8	0.7038	0.9784	1.0000		
18.0					0.8323
23.0					0.9253
27.0	0.8950	0.9960	1.0000		0.9655
30.0	0.9164	0.9987			
36.0	0.9444	1.0000			

TABLE IV

VALUES OF $(\lambda_1/v\Sigma_s)$ FOR GAS KERNEL
Diffusion and B_0 approximation
using 35 energy points and P_3 using 23

Mass ratio	A = 1			A = 2		
$B^2 \times \Sigma_f^{-2}$	Method			Method		
	Diff.	P_3	B_0	Diff.	P_3	B_0
0	0.8190			0.8257		
0.001	0.8192	0.8193	0.8194	0.8260	0.8261	0.8262
0.01	0.8210	0.8229	0.8231	0.8283	0.8305	0.8307
0.05	0.8284	0.8387	0.8393	0.8384	0.8500	0.8506
0.1	0.8374	0.8578	0.8587	0.8505	0.8734	0.8745
Mass ratio	A = 4			A = 10		
$B^2 \times \Sigma_f^{-2}$	Method			Method		
	Diff.	P_3	B_0	Diff.	P_3	B_0
0	0.7456			0.5672		
0.001	0.7461	0.7460	0.7463	0.5681	0.5663	0.5682
0.01	0.7500	0.7756	0.7523	0.5754	0.5748	0.5772
0.05	0.7670	0.7772	0.7784	0.6074	0.6121	0.6161
0.1	0.7874	0.8082	0.8102	0.6459	0.6577	0.6635

length problem the maximum value of $\Sigma_a(v_0)$ as shown in Fig. 6 is reached at about $\Sigma_f/\Sigma_f + \Sigma_a) = 0.77$, for the gas of mass 1 (see Table V).

4. 2. Incoherent approximation kernel for beryllium

The importance of the Bragg effect on the time-dependent eigenvalues is shown in Table VI and Fig. 7. In contrast to water, we found that no higher eigenvalues existed, and hence only one exponentially decaying energy mode is present even in an infinite medium. It is clear from Fig. 7 that experimental measurements have been made in the region where no simple exponential decay (and asymptotic energy mode) exists. The marked effect of the Bragg cut-off on the asymptotic energy mode for two sizes of buckling is shown in Fig. 8.

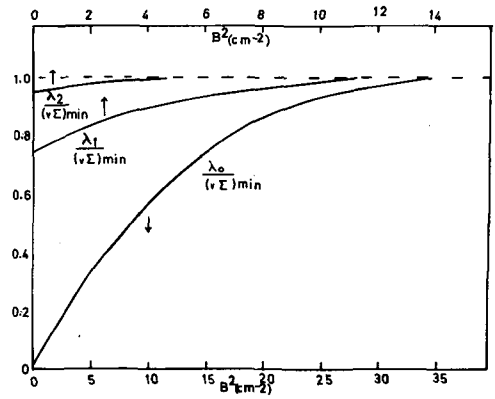

Fig. 5

Approach of normalized time eigenvalues to limiting value.
Effective width kernel for water at 21°C with d = 0.21; B_0 solution.

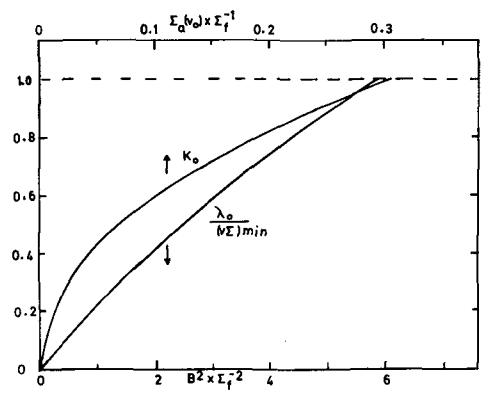

Fig. 6

Limiting behaviour of fundamental eigenvalues for diffusion-length problem (K_0) and pulsed-source problem (λ_0).
Gas kernel with mass 1; B_0 solution.

By extending CORNGOLD's [1] discussion of an upper limit for eigenvalues of the diffusion-length problem to the higher spatial eigenvalues corresponding to a decay constant λ, we see that $S < (\Sigma - \lambda/v)_{min}$. For moderators such as beryllium, due to the Bragg effect, the minimum value depends strongly on λ. This can be seen from Figs. 9 and 10. The values of the first few spatial eigenvalues shown in Table VII lie in the region between the B_0 and P_3 limits. For the case of $\lambda_0 = 0$, that is the diffusion-length problem, we found for the B_0 solution a discrete value for K_0 of 0.0434 cm^{-1}, but no higher spatial eigenvalues which satisfied the transport upper bound. Figure 11 shows the energy spectra of the time and spatial transients having eigenvalues λ_1 and K_1 respectively for a gas of mass 10. Both of these

TABLE V

MEAN ENERGY OF EQUILIBRIUM FLUX
(Gas kernel, mass = 1)

Pulsed				Diffusion length			
$B^2 \times \Sigma_f^{-2}$	Method			$\Sigma_a(v_0) \times \Sigma_f^{-1}$	Method		
	Diff.	P_3	B_0		Diff.	P_3	B_0
0.5	1.8985	1.9038	1.9037	0.001	2.0003	2.0003	2.0003
1.0	1.805	1.824	1.825	0.02	2.0152	2.0153	2.0153
2.0	1.641	1.690	1.701	0.2	2.1642	2.1746	2.1750

Note: For the pulsed problem in an infinite medium and the diffusion length problem with no absorption, the mean energy = 2.

TABLE VI

VALUES OF NORMALIZED TIME EIGENVALUES $(\lambda_0/v\Sigma)_{min}$ FOR BERYLLIUM
(Number of energy points = 51)

B^2 (cm^{-2})	Diffusion approximation		B_0	
	Without Bragg (cm^{-1})	Bragg cut-off 0.005 eV (cm^{-1})	Without Bragg (cm^{-1})	Bragg cut-off 0.005 eV (cm^{-1})
0.008685	0.2946	0.3285	0.2945	0.3239
0.01737	0.5080	0.5645	0.5086	0.5578
0.02605	0.7087	0.7875	0.7103	0.7811
0.03040	0.8029	0.8946	0.8051	0.8895
0.03350				0.9649
0.03474	0.8911	1.0000	0.8944	
0.03882	0.9654	1.0000	0.97028	

modes decay exponentially, one in time, the other in space, to leave the fundamental spatial mode (cos Bx) decaying exponentially with decay constant λ_0.

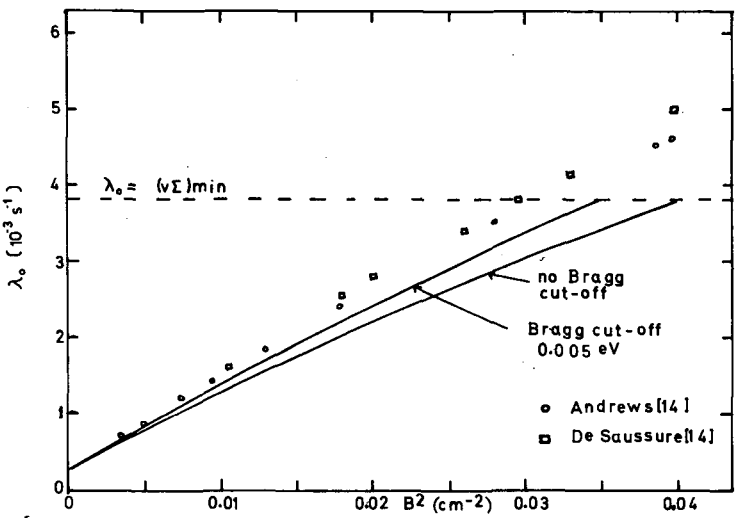

Fig. 7

λ_0 versus B^2 for beryllium at 21°C.
Incoherent approximation kernel with Debye temperature = 1000°K; B_0 solution.

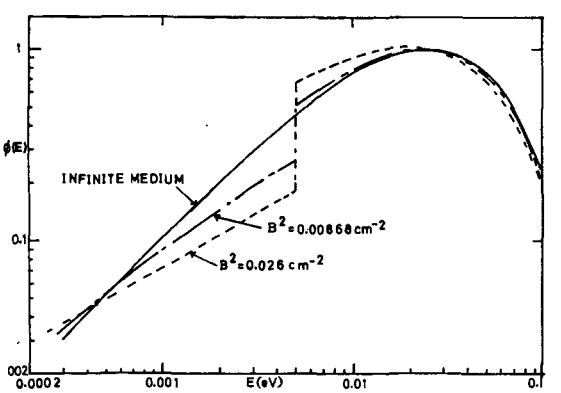

Fig. 8

Asymptotic energy spectra for beryllium system with pulsed-source, showing effect of introducing Bragg cut-off at 0.005 eV.
Spectra normalized to have unity as maximum ordinate; B_0 solution.

5. CONCLUSIONS

The results of our calculations are in general agreement with Corngold's theory. For the pulsed source in water, the effective width kernel gave two higher eigenvalues in addition to the fundamental. All of these disappeared for a sufficiently large value of buckling which was well beyond the experimental range. This general behaviour was also shown by the gas kernel.

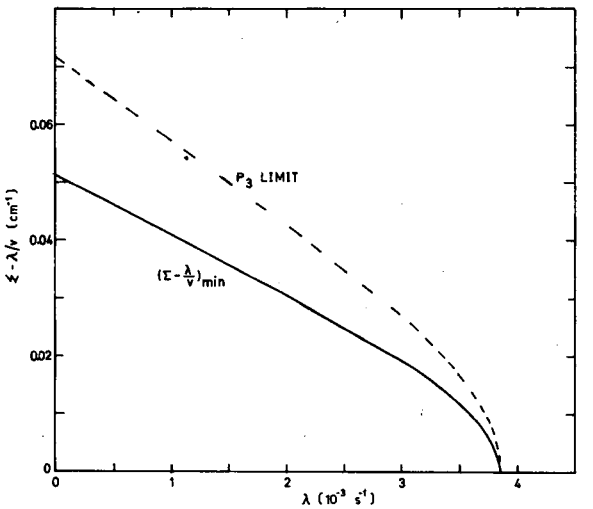

Fig. 9

The effect on $\Sigma - \lambda/v$ of varying the decay constant λ, for beryllium with Bragg cut-off at E = 0.005 eV.

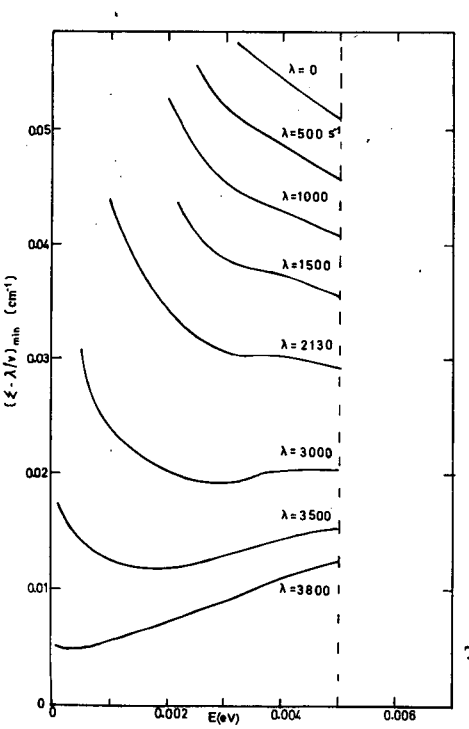

Fig. 10

The variation of $(\Sigma - \lambda/v)_{min}$ with λ, for beryllium

- - - - P_3 upper limit

——— Transport limit

TABLE VII

SPATIAL EIGENVALUES OF TIME-DEPENDENT PROBLEM FOR BERYLLIUM
($\lambda_0 = 2100\ s^{-1}$, 45 energy points)

P_3 solution		
	Without Bragg (cm^{-1})	Bragg cut-off 0.005 eV (cm^{-1})
iB	0.139	0.129
S_1	0.275	0.0339
S_2	0.276	0.0347
S_3	0.277	0.0362
S_4	0.278	0.0377
S_5	0.279	0.0399

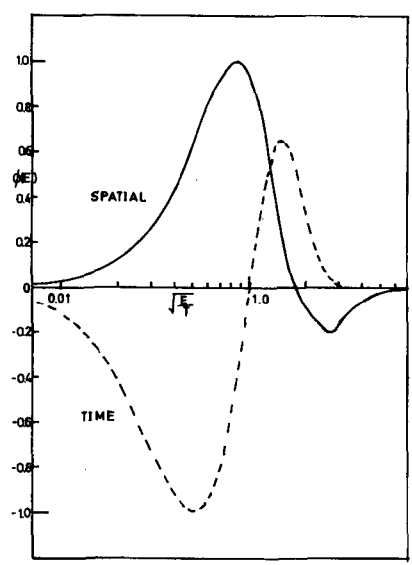

Fig. 11

Energy spectra of transients in a pulsed system, $B^2 = 0.001\ \Sigma_f^2$
Gas kernel, mass = 10;
Spectra normalized to have a maximum magnitude of unity; B_0 solution.

We have shown that the effective width model with d = 0.215 gives excellent agreement with the experimental values of λ_0 over a wide range of B^2, and the measured λ_1 in an infinite water system.

For beryllium we could only find a fundamental time-dependent eigenvalue. This disappeared at a value of B^2 which has been considerably exceeded by experimentalists seeking to measure a simple exponential decay. The importance of including the Bragg effect in beryllium calculations has been demonstrated. We have calculated higher spatial eigenvalues associated with the fundamental time decay constant in a pulsed system and suggest that such systems should not be analysed only in terms of a fundamental spatial mode characterized by a value of B^2.

ACKNOWLEDGEMENTS

The author wishes to thank Dr. M.M.R. Williams for many valuable discussions.

This work is part of the general programme of the Applied Nuclear Science Group at the University of Birmingham and has received financial support from the Atomic Energy Establishment, Winfrith and the Department of Scientific and Industrial Research, London; appreciation is expressed for this support.

APPENDIX

THE B_0 APPROXIMATION SOLUTION

1. THE TIME-DEPENDENT PROBLEM

For the time-dependent problem, the equation to be solved is the Boltzmann transport equation with a pulsed source, which for slab geometry is given by

$$\frac{1}{v}\frac{\partial \phi}{\partial t}(x, E, \mu, t) + \left[\mu\frac{\partial}{\partial x} + \Sigma_a(E) + \Sigma_s(E)\right]\phi(x, E, \mu, t)$$

$$= \int_{-1}^{1} d\mu' \int_{0}^{\infty} \Sigma(E' \to E, \mu_0)\,\phi(x, E', \mu', t)\,dE', \qquad (1)$$

where the symbols have their usual meaning, in particular $\Sigma(E' \to E, \mu_0)$ is the scattering kernel and μ_0 is the cosine of the angle between μ and μ'. We consider solutions of the form

$$\phi(x, E, \mu, t) = \phi(E, \mu, B)e^{-\lambda t + iBx}, \qquad (2)$$

where B^2 is the geometric buckling in the x-direction. Substituting Eq. (2) into Eq. (1), we obtain

$$[-\lambda/v + \Sigma_a(E) + \Sigma_s(E) + iB\mu]\,\phi(E,\mu,B)$$

$$= \int_{-1}^{1} d\mu' \int_0^\infty \Sigma(E' \to E, \mu_0)\,\phi(E',\mu',B)\,dE'. \tag{3}$$

We next expand the flux and scattering kernel in Legendre polynomials.

$$\phi(E,\mu,B) = \sum_{l=0}^{\infty} \frac{2l+1}{2}\,\phi_l(E,B)P_l(\mu) \tag{4}$$

$$\Sigma(E' \to E, \mu_0) = \sum_{l=0}^{\infty} \frac{2l+1}{2}\,\Sigma_l(E' \to E)P_l(\mu_0). \tag{5}$$

We now assume isotropic scattering, that is on the right-hand side of Eq. (5) only the term with $l = 0$ is non-zero.

Inserting Eqs. (4) and (5) into (3), using the addition theorem and dividing by the terms in the square brackets, we obtain

$$\sum_{n=0}^{\infty} \frac{2n+1}{2}\,P_n(\mu)\,\phi_n(E,B) = \frac{\frac{1}{2}P_0(\mu)\int_0^\infty \Sigma_0(E' \to E)\,\phi_0(E',B)dE'}{[-\lambda/v + \Sigma_a(E) + \Sigma_s(E) + iB\mu]} \tag{6}$$

Multiplying by $P_1(\mu)$ and integrating over μ, the result is

$$\phi_0(E,B) = \frac{1}{2iB}\log\left[\frac{-\lambda + v\Sigma_a(E) + v\Sigma_s(E) + iBv}{-\lambda + v\Sigma_a(E) + v\Sigma_s(E) - iBv}\right]$$

$$\times \int_0^\infty \Sigma_0(E' \to E)\,\phi_0(E',B)dE' \tag{7}$$

That is

$$\phi_0(E,B) = \frac{1}{B}\tan^{-1}\left[\frac{Bv}{-\lambda + v\Sigma_a(E) + v\Sigma_s(E)}\right]\int_0^\infty \Sigma_0(E' \to E)\,\phi_0(E',B)dE' \tag{8}$$

We now replace the integral in Eq. (8) by a finite sum, say,

$$\sum_{j=1}^{N} w_j \Sigma_0(E_j' \to E)\,\phi_0(E_j', B),$$

where the w_j and E_j' depend on the method of quadrature used. By choosing the values of E to give agreement with the E_j' we obtain the following system of linear equations

$$\phi_0(E_i, B) = \frac{1}{B}\tan^{-1}\left[\frac{v_i B}{-\lambda + v_i\Sigma_a(E_i) + v_i\Sigma_s(E_i)}\right]\sum_{j=1}^{N} w_j\,\Sigma_{ij}(E_j' \to E_i)\,\phi(E_j', B) \tag{9}$$

$$i = 1, 2, \ldots N.$$

Writing Eq. (9) in matrix notation we have

$$\Phi = A\Phi \tag{10}$$

where

$$\Phi = \begin{bmatrix} \phi_0(E_1, B) \\ \phi_0(E_2, B) \\ \vdots \\ \phi_0(E_N, B) \end{bmatrix} \tag{10'}$$

$$A = TK,$$

T is diagonal

$$T_i = \frac{1}{B} \tan^{-1} \left[\frac{v_i B}{-\lambda + v_i \Sigma_a(E_i) + v_i \Sigma_s(E_i)} \right],$$

and

$$K_{ij} = w_j \Sigma_{ij}(E_j \to E_i)$$

For a fixed value of B and $0 < \lambda < (v\Sigma)_{min}$, Eq. (10) is a matrix eigenvalue problem where the eigenvalue is transcendental. We now require the solution (using an obvious notation)

$$A(\lambda)\Phi = w(\lambda)\Phi \tag{11}$$

for values of λ which make $w(\lambda) = 1$. It is desirable to deal with the matrix A in a symmetric form. This we can achieve by means of the following substitution. Let us define the diagonal matrix D as

$$D_i = \sqrt{w_i / M_i T_i}, \tag{12}$$

where w_i and T_i are as above and $M_i = (E_i/T^2)e^{-E_i/T}$.

Let

$$Y = D\Phi \tag{13}$$

Substituting Eq. (13) into Eq. (11), we obtain

$$TKD^{-1}Y = w(\lambda)D^{-1}Y$$

i.e.

$$DTKD^{-1}Y = w(\lambda)Y$$

i.e.

$$BY = w(\lambda)Y, \tag{14}$$

where

$$B_{ij} = \sqrt{T_i}\sqrt{T_j}\sqrt{w_i}\sqrt{w_j}\,K_{ij}\sqrt{M_j/M_i} \tag{15}$$

Clearly, B is symmetric since all scattering kernels satisfy the detailed balance condition that

$$\Sigma(E_j \to E_i)\sqrt{M_j/M_i} = \Sigma(E_i \to E_j)\sqrt{M_i/M_j}.$$

Having solved Eq.(14) for values of λ which make $w(\lambda) = 1$, we can obtain Φ from Eq.(13). To solve Eq.(14) we proceed as follows. From Eq.(14) we have

$$[B(\lambda) - w(\lambda)]Y = 0 \tag{16}$$

To find the rate of change of w with λ, we differentiate and obtain

$$\left[B - w(\lambda)I\right]\frac{dY}{d\lambda} = \left[\frac{dw}{d\lambda}I - \frac{dB}{d\lambda}\right]Y \tag{17}$$

Equation (17) determines both $dY/d\lambda$ and $dw/d\lambda$. From Eq.(16) the matrix on the left-hand side of Eq.(17) is singular, and since B is symmetric

$$Y^T[B - wI] = 0 \tag{18}$$

Therefore, after pre-multiplying Eq.(17) by Y^T, we have

$$0 = Y^T\left[\frac{dw}{d\lambda}I - \frac{dB}{d\lambda}\right]$$

and hence

$$\frac{dw}{d\lambda} = \frac{Y^T\frac{dB}{d\lambda}Y}{Y^TY}. \tag{18'}$$

Our iteration scheme is to solve Eq.(14), using an approximate value of λ, by the method of inverse iteration to find the eigenvalue nearest to 1. We then obtain an improved value of λ from

$$\lambda_{i+1} = \lambda_i - (w_i - 1)/(dw/d\lambda)_i \tag{19}$$

where $dw/d\lambda$ is given by Eq.(18'). The iteration process is repeated until the value obtained for w is sufficiently close to 1.

2. THE SPATIAL PROBLEM

For the spatial problem we seek solutions of the form

$$\phi(x, E, \mu) = \phi(E, \mu)e^{-Kx}$$

to the equation

$$[\mu\partial/\partial x + \Sigma_a(E) + \Sigma_s(E)]\,\phi(x, E, \mu)$$

$$= \int_{-1}^{1} d\mu' \int_{0}^{\infty} \Sigma(E' \to E, \mu_0)\,\phi(x, E', \mu')dE'. \tag{20}$$

By using methods similar to those described in [1], we obtain for the expression analogous to Eq. (9)

$$\phi_0(E_i, \Sigma_a(v_0)) = \frac{1}{2K} \log \left[\frac{\Sigma_a(v_0)/v_i + \Sigma_s(E_i) + K}{\Sigma_a(v_0)/v_i + \Sigma_s(E_i) - K}\right] \sum_{j=1}^{N} w_j \Sigma_{ij}(E_j \to E_i)\,\phi(E_j) \tag{21}$$

$$i = 1, 2, \ldots N.$$

where we have assumed

$$\Sigma_a(E) = v_0 \Sigma_a(v_0)/v.$$

In matrix notation Eq. (21) becomes

$$C(K)\Phi = K\Phi, \tag{22}$$

where L is diagonal,

$$L_i = \frac{1}{2} \log \left[\frac{v_0 \Sigma_a(v_0)/v_i + \Sigma_s(E_i) + K}{v_0 \Sigma_a(v_0)/v_i + \Sigma_s(E_i) - K}\right]$$

and

$$K_{ij} = w_j \Sigma_{ij}(E_j \to E_i).$$

The matrix C can be transformed to give a symmetric matrix E in a way similar to that described in [1]. Thus we have to solve

$$E(K)X = \beta(K)X \tag{23}$$

for values of K such that $\beta = K$.

The iteration scheme now becomes

$$E(K_i)X_i = \beta_i(K_i)X_i$$

$$K_{i+1} = K_i - (\beta_i - K_i)/[(d\beta/dK)_i - 1] \tag{24}$$

$$\frac{d\beta}{dK} = X^T \frac{dE}{dK} X / X^T X .$$

For the spatial eigenvalues (real) associated with a fundamental decay constant λ_0, we can adapt the above procedure in an obvious way.

REFERENCES

[1] CORNGOLD, N., Nucl. Sci. Engng 19 (1964) 80-90.
[2] EGELSTAFF, P. A. and SCHOFIELD, P., Nucl. Sci. Engng 12 (1962) 260-70.
[3] SCHOFIELD, P. and HASSIT, A., Proc. 2nd UN Int. Conf. PUAE 16 (1958) 217-22.
[4] WIKNER, N. F., JOANOU, G. D. and PARKS, D. E., Nucl. Sci. Engng 19 (1964) 108-29.
[5] FRANCIS, J. G. F., Computer Journal 4 (1961) 265.
[6] DAITCH, P. B., Trans. Amer. nucl. Soc. 6 1 (1963).
[7] WILLIAMS, M. M. R. and WOOD, J., to be published in J. nucl. Energy.
[8] PUROHIT, S. N., Nucl. Sci. Engng 9 (1961) 157-67.
[9] MÖLLER, E. and SJÖSTRAND, N. G., Ark. Fys. 27 31 (1964).
[10] LOPEZ, W. M. and BEYSTER, J. R., Nucl. Sci. Engng 12 (1962) 190-202.
[11] STARR, E. and KOPPEL, J. U., Nucl. Sci. Engng 14 (1962) 224-29.
[12] KÜCHLE, M., Nukleonik 2 (1960) 131.
[13] BROWN, J. C. B. (1963) Ph. D. Thesis, Birmingham University, England.
[14] ANDREWS, M. M., in University of California Rpt UCRL 6803 (1960).

DISCUSSION

P. SCHOFIELD (Chairman): Could you comment on the applicability of the infinite medium solution exp(iBx) to the finite medium problem, concerning the big change in the cross-section which is usual with a Bragg cut-off?

J. WOOD: The general solution referred to in the paper is only for the case of an infinite slab. Even for a smoothly varying cross-section, I have not seen it proved that a simple expression for buckling (B^2) is meaningful in the case of general geometry. For the case of the infinite slab we have shown that, say, for a P_3 solution it is possible to find an "asymptotic" and "transient" part. The importance of these may be affected by the existence of a Bragg cut-off. This could be found by solving for the boundary conditions.

SOME SPECTRAL PROPERTIES OF THE TRANSPORT EQUATION AND THEIR RELEVANCE TO THE THEORY OF PULSED NEUTRON EXPERIMENTS

S. ALBERTONI
UNIVERSITY OF MILAN AND
APPLICAZIONI E RICERCHE SCIENTIFICHE,
AND
B. MONTAGNINI
UNIVERSITY OF MILAN AND SNAM,
MILAN, ITALY

Abstract — Résumé — Аннотация — Resumen

SOME SPECTRAL PROPERTIES OF THE TRANSPORT EQUATION AND THEIR RELEVANCE TO THE THEORY OF PULSED NEUTRON EXPERIMENTS. The pulsed neutron experiments rest, as is well known, on the assumption that the neutron transport equation, in a finite bare body, possesses at least one discrete eigenvalue. Nelkin and then Corngold pointed out that this assumption could no longer be true if the sample is very small. Their arguments, however, were based on certain simplifying assumptions about the scattering kernel or the spatial dependence of the neutron density, which could, in principle, greatly restrict the validity of their results when dealing with realistic problems. We have thus preferred to attack the problem from a quite general point of view, which resembles, in many aspects, the approach of Lehner and Wing's paper, "On the spectrum of an asymmetric operator arising in the transport theory of neutron", relating to the one-velocity theory.

We have considered the integro-differential transport equation in a finite homogeneous convex body of an arbitrary shape, surrounded by vacuum. The free gas-scattering kernel (averaged over the angles, so that the scattering is isotropic) has been adopted, and then the absorption has been assumed to follow the "1/v" law. Let then $\lim_{v \to 0} v\Sigma_s(v) = h_0$, where h_0 results in a positive constant.

The eigenvalue spectrum of the transport equation can be shown to have the following structure: the half-plane Re $\lambda \leq -h_0$ is occupied by a densely distributed spectrum (let us say "continuous spectrum"), while the remaining half-plane Re $\lambda > -h_0$ contains at most a finite number of real eigenvalues λ_i. It has been shown that the number of the discrete eigenvalues can reduce to zero if the body is small enough (of the order of a mean free path).

Thus we see that Nelkin's idea on the disappearing of the decay modes for samples of very small size is correct also within our general assumptions. As far as we know the experimental results do not seem to provide an unambiguous answer pro or contra this theoretical assertion. We are now developing a numerical method to get a suitable correlation of experimental measurements within the framework of our theoretical approach.

QUELQUES PROPRIÉTÉS SPECTRALES DE L'ÉQUATION DE TRANSPORT ET LEURS RAPPORTS AVEC LA THÉORIE DES EXPÉRIENCES AU MOYEN DES NEUTRONS PULSÉS. On sait que les expériences au moyen des neutrons pulsés reposent sur l'hypothèse selon laquelle dans un corps sans réflecteur de dimension finie, l'équation de transport des neutrons possède pour le moins une valeur propre discrète. Nelkin, puis Corngold ont fait ressortir que cette hypothèse n'est plus valable si l'échantillon est très petit. Cependant, leurs arguments sont fondés sur certaines hypothèse simplificatrices concernant le noyau de diffusion ou les variations du nombre volumique dans l'espace, ce qui peut en principe restreindre sensiblement la validité de leurs résultats lorsque les problèmes serrent de près la réalité. Les auteurs ont donc préféré aborder la question d'une manière très générale analogue par maints côtés à celle que Lehner et Wing on choisi pour leur article intitulé «On the spectrum of an asymmetric operator arising in the transport theory of neutrons» (Spectre d'un opérateur asymétrique intervenant dans la théorie de transport des neutrons) et concernant la théorie à une seule vitesse.

Les auteurs ont étudié l'équation de transport intégro-différencielle pour un corps convexe, homogène et fini de configuration quelconque, dans le vide. Après avoir choisi le modèle de gaz libre pour le noyau de diffusion (moyenne calculée sur les angles de manière que la diffusion soit isotrope), ils ont supposé que l'absorption s'opère selon la loi «1/v» et ont posé ensuite $\lim_{v \to 0} v\Sigma_s(v) = h_0$, d'où il résulte que h_0 est une constante positive.

On peut montrer que le spectre des valeurs propres de l'équation de transport a la structure suivante: le demi-plan Re $\lambda \leq -h_0$ est occupé par un spectre à distribution dense (ou «spectre continu»), alors que l'autre demi-plan Re $\lambda > -h_0$ contient tout au plus un nombre fini de valeurs propres réelles λ_i. Il est prouvé que le nombre des valeurs propres discrètes peut tomber à zéro si le corps est suffisamment petit (de l'ordre d'un libre parcours moyen).

Les auteurs concluent que l'idée de Nelkin selon laquelle les modes de désintégration disparaissent pour des échantillons de dimension très petite reste également valable pour les hypothèses générales qu'ils ont adoptées. Pour autant que les auteurs le sachent, les résultats expérimentaux ne semblent ni confirmer ni contredire de façon absolue cette affirmation théorique. Ils élaborent actuellement une méthode numérique de manière à obtenir une corrélation appropriée des données expérimentales dans le cadre de leur théorie.

О НЕКОТОРЫХ СПЕКТРАЛЬНЫХ СВОЙСТВАХ УРАВНЕНИЯ ПЕРЕНОСА И ИХ СВЯЗИ С ТЕОРИЕЙ ЭКСПЕРИМЕНТОВ С ИМПУЛЬСНЫМИ НЕЙТРОНАМИ. Как хорошо известно, эксперименты с импульсными нейтронами основываются на предположении, что уравнение переноса нейтронов в конечном теле без отражателя имеет по крайней мере одно дискретное собственное значение. Нелкин, а затем Корнгольд отмечали, что это предположение не может быть верным, если образец очень мал. Их аргументы, однако, основывались на некоторых упрощенных предположениях относительно ядра рассеяния или пространственной зависимости плотности нейтронов, что может в принципе в значительной степени ограничить пригодность их результатов при решении реальных проблем. В связи с этим мы предпочли приступить к проблеме с весьма общей точки зрения, которая во многих отношениях напоминает подход, изложенный в докладе Ленера и Винга "О спектре асимметричного оператора, возникающего в теории переноса нейтронов" относительно теории одной скорости.

Рассмотрено интегродифференциальное уравнение переноса в конечном выпуклом гомогенном теле произвольной формы, помещенном в вакуум. Было принято ядро рассеяния свободного газа (усредненное в углах, так что рассеяние является изотропическим), затем было сделано предположение, что поглощение подчиняется закону "1/v". Пусть затем $\lim_{v \to 0} v\Sigma_s(v) = h_0$, где h_0 в результате является положительной константой.

Можно показать, что спектр собственного значения уравнения переноса имеет следующую структуру: полуплоскость Re $\lambda \leq -h_0$ занимается плотно распределенным спектром (скажем, "непрерывным спектром"), в то время как другая полуплоскость Re $\lambda > -h_0$ содержит по крайней мере конечное число действительных собственных значений λ_i. Показывается, что число собственных значений можно уменьшить до нуля, если тело является достаточно малым (порядка среднего свободного пути пробега).

Таким образом, мы видим, что идея Нелкина относительно исчезновения форм распада для образцов очень малого размера является правильной также в рамках наших общих предположений. Как известно, экспериментальные результаты, по-видимому, не дают ясного ответа за или против этого теоретического предположения. В настоящее время разрабатывается числовой метод с целью получения соответствующей поправки к результатам экспериментальных измерений в рамках нашего теоретического подхода.

ALGUNAS PROPIEDADES ESPECTRALES DE LA ECUACION DE TRANSPORTE Y SU RELACION CON LA TEORIA DE LOS EXPERIMENTOS CON NEUTRONES PULSADOS. Como es bien sabido, los experimentos con neutrones pulsados se basan en la suposición de que la ecuación de transporte neutrónico en un cuerpo desnudo y finito posee por lo menos un valor propio discreto. Nelkin y más tarde Corngold afirmaron que este postulado no es cierto si la muestra es muy pequeña. No obstante, sus argumentos se basaban en ciertas hipótesis simplificadas acerca del núcleo de dispersión o acerca de la dependencia espacial de la densidad neutrónica, lo que, en principio, puede restringir mucho la validez de los resultados obtenidos si se quieren extrapolar para aplicarlos en la práctica. Por esta razón los autores han preferido enfocar el problema desde un punto de vista más general y que, en muchos aspectos, se parece al adoptado por Lehner y Wing en su artículo «On the spectrum of an asymmetric operator arising in the transport theory of neutrons» (Espectro de un operador asimétrico en la teoría de transporte neutrónico), que propugna la teoría de la velocidad única.

Los autores han considerado la ecuación de transporte integrodiferencial en un cuerpo convexo, homogéneo y finito de forma arbitraria, rodeado de vacío; adoptaron el núcleo de dispersión gaseoso libre (promediado sobre todos los ángulos para que la dispersión sea isotrópica) y supusieron que la absorción obedece a la ley «1/v». Entonces, si $\lim_{v \to 0} v\Sigma_s(v) = h_0$, h_0 resulta ser una constante positiva.

Se puede demostrar que el espectro de los valores propios de la ecuación de transporte tiene la estructura siguiente: el semiplano $\mathrm{Re}\,\lambda \leq -h_0$ está ocupado por un espectro muy denso (que los autores denominan «espectro continuo»), mientras que el otro semiplano $\mathrm{Re}\,\lambda > -h_0$ contiene a lo sumo un número finito de valores propios λ_i. Se ha demostrado que el número de valores propios discretos puede llegar a cero si el cuerpo es suficientemente pequeño (del orden del recorrido libre medio).

Así, pues, la idea de Nelkin sobre la desaparición de los modos de desintegración en muestras muy pequeñas es correcta también si se aplican los postulados generales de los autores. Al parecer, los resultados experimentales no corroboran ni refutan categóricamente esta afirmación teórica. Los autores están desarrollando un método numérico para encontrar una correlación adecuada de las mediciones experimentales dentro del marco de su teoría.

1. INTRODUCTION

Most theoretical investigations on the eigenvalue spectrum of the neutron transport equation originate from LEHNER and WING's [1, 2] fundamental papers, where the time-dependent one-velocity transport equation in a bare slab was first fully and rigorously treated. These authors showed that the eigenvalue spectrum of this equation (considered in a Hilbert space of square summable functions) is made of the following parts (Fig. 1): a continuous spectrum occupying the half-plane $\mathrm{Re}\lambda \leq -\Sigma_0 v_0$, where v_0 is the

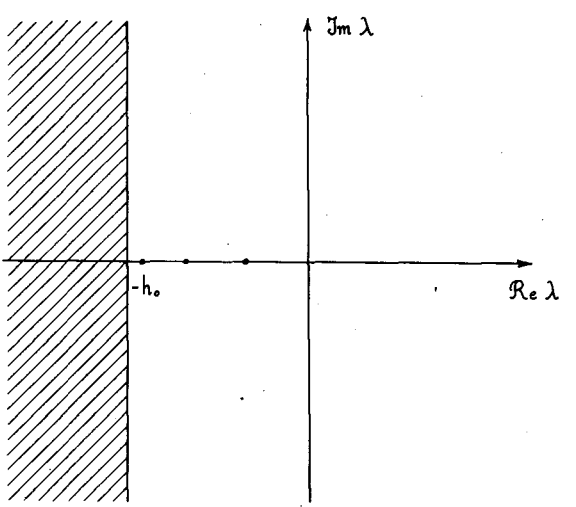

Fig. 1

LEHNER and WING [1] spectrum

neutron speed and Σ_0 the total cross-section of the slab, and a point spectrum consisting of a finite (but not zero) number of real eigenvalues. The same authors showed that an entirely different result is achieved, if a finite body is considered. The spectrum is then purely discrete, the eigenvalues

whose real part is larger than $-\Sigma_0 v_0$ (if existing) being real. Moreover, there are eigenvalues with $\mathrm{Re}\lambda \leqq -\Sigma_0 v_0$ which form an infinite sequence of negative real numbers without accumulation points, except for $\lambda = -\infty$, but it cannot be excluded that also complex eigenvalues exist [3] (see Fig. 2).

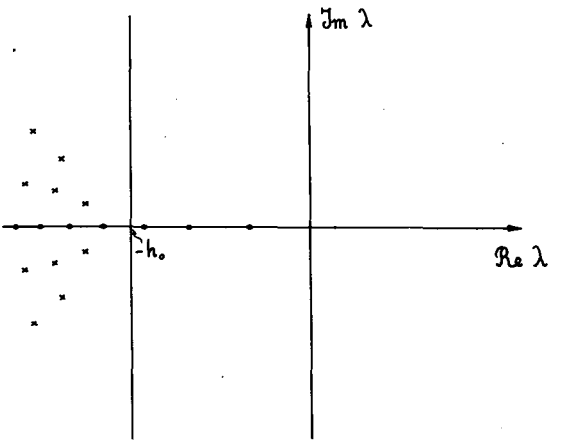

Fig. 2
VAN NORTON [3] spectrum

The nature of the spectrum in the slab case or the finite-body case does not change in an essential way when passing to n velocity groups [4, 5], or also to continuous velocity dependence, provided that the set of admissible neutron speeds is bounded away from zero [5].

The appearance of the continuous spectrum in the slab case is related to the fact that a neutron can spend an indefinitely large time in the slab without undergoing collisions or escaping, provided it moves fairly parallel to the slab sides. These long-uncollided neutrons form an exceptional class of neutrons which cannot be treated like the ordinary neutron population and can hardly be expected to allow for a discrete eigenfunction expansion. Since the first investigations, it has thus been clear that the continuous spectrum is related to the unboundedness of the time that a neutron can spend in crossing the infinite slab. This concept was found to be of much use in another case. In 1963, NELKIN [6] observed that the theory of pulsed neutron experiments involves the solution of an initial value problem relating to a finite sample, but without any lower bound for the speed of the neutrons moving in it, since thermal neutrons can have all the energies between zero and infinity. We see that the transit time increases indefinitely, as neutrons of vanishingly small energy are considered, and thus a continuous spectrum is to be expected, in analogy with Lehner and Wing's case, if $[v\Sigma_t(v)]_{\min} = h_0 > 0$ and $\mathrm{Re}\lambda \leqq -h_0$. The most striking result of Nelkin's study, however, concerns the discrete spectrum: if the body in which thermal diffusion occurs is small enough, then, contrary to Lehner and Wing's case, the discrete spectrum is a void set. Thus fundamental decay modes should no longer be present in samples of very small size. The validity of Nelkin's arguments, however, is restricted in principle by the fact that a very simple (and rather

unphysical) degenerate scattering kernel has been used. Such a kernel allows the transformation of the space-energy integral (Peierls) equation into an integral equation in the space variables only, whose behaviour can be easily checked at least in the very important limiting case $\lambda = -h_0$. This is no longer possible if more complicated kernels are used.

Otherwise, one could introduce some simplifying assumptions on the space-dependence of the problem. CORNGOLD [7] assumes that the flux has a prescribed behaviour of the exp ($i\underline{B} \cdot \underline{r}$) type: the spatial variable is thus readily eliminated, and there is room for considering a rather complex kernel such as the free gas scattering kernel. The results are sketched in Fig. 3. The curve Γ represents a line of singularities of the Laplace

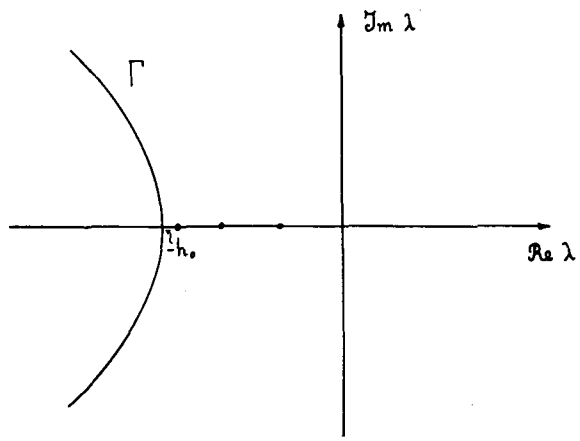

Fig. 3

CORNGOLD [7] spectrum

transform of the neutron distribution and plays the same role as the edge of the continuous spectrum in the Lehner and Wing case, while the points on the real axis represent isolated singularities (poles), i.e. the discrete eigenvalues of the problem. The number of these eigenvalues is finite for $B_2 \neq 0$, decreases steadily as B^2 is increased ("the eigenvalues move into the continuum"), and vanishes when $B^2 \geq B^{*2}$, where B^{*2} is a "critical" value of the buckling which depends on the physical characteristics of the medium. Here again we are faced with the disappearance of the fundamental mode for small sample sizes. Some discrepancy, however, exists between the results of Corngold and Lehner and Wing, namely, that a curve Γ of singularities is found, instead of a continuous spectrum occupying a half plane. This should be a result, roughly speaking, of the fact that Corngold has made use of the "one Fourier component approximation", instead of treating the full spatial dependence of the flux with the exact boundary conditions ([7], p. 85).

Here we will study the eigenvalue spectrum of the transport equation from a more general standpoint. We adopt the free gas model and consider an arbitrary homogeneous finite body (surrounded by vacuum) as the domain for the space variables. In a previous work [8], we assumed that the scat-

tering was isotropic in the laboratory system; in other works we replaced the exact free gas scattering kernel, which depends on the scattering angle, with the angle-integrated kernel, which depends only on the energy change. This was necessary to put the transport equation into the integral form and obtain more detailed properties of the spectrum. Here we summarize the results obtained in [8] and then suspend the isotropic scattering assumption and show that two, at least, of the main results of [8] are still valid.

2. SUMMARY OF PREVIOUS RESULTS

Let us consider a finite, homogeneous, convex body V surrounded by vacuum. We assume that a single nuclide is present, and let N be the number of nuclei per unit volume, M their mass and σ_s the scattering cross-section for a free nucleus at rest (assumed to be independent of the velocity of the neutron moving towards it).

If we assume that isotropic scattering is present, then the transport equation reads

$$\frac{\partial n(\underline{r}, v\underline{\Omega}, t)}{\partial t} + v\underline{\Omega} \cdot \operatorname{grad}_{\underline{r}} n(\underline{r}, v\underline{\Omega}, t) + v\Sigma_t(v) n(\underline{r}, v\underline{\Omega}, t)$$

$$= \frac{1}{4\pi} \int v' \Sigma_s(v' \to v) n(\underline{r}, v'\underline{\Omega}', t) dv' d\Omega' , \qquad (1)$$

where, in the free gas scattering approximation [9, 10]

$$\Sigma_t(v) = N\sigma_s \cdot \frac{1}{\beta v} \left[\frac{e^{-\mu\beta^2 v^2}}{\sqrt{\pi\mu}} + \left(\beta v + \frac{1}{2\mu\beta v}\right) \operatorname{erf}\left(\sqrt{\mu}\beta v\right) \right] + \frac{\gamma}{v} \qquad (2)$$

$$\Sigma_s(v' \to v) = N\sigma_s \cdot \frac{(\mu+1)^2}{4\mu} \cdot \frac{v}{v'^2} \left\{ \operatorname{erf}\left(\beta \frac{\mu+1}{2\sqrt{\mu}} v - \beta \frac{\mu-1}{2\sqrt{\mu}} v'\right) \pm \operatorname{erf}\left(\beta \frac{\mu+1}{2\sqrt{\mu}} v + \beta \frac{\mu-1}{2\sqrt{\mu}} v'\right) \right.$$

$$\left. + e^{\beta^2(v'^2 - v^2)} \left[\operatorname{erf}\left(\beta \frac{\mu+1}{2\sqrt{\mu}} v' - \beta \frac{\mu-1}{2\sqrt{\mu}} v\right) \mp \operatorname{erf}\left(\beta \frac{\mu+1}{2\sqrt{\mu}} v' + \beta \frac{\mu-1}{2\sqrt{\mu}} v\right) \right] \right\} \qquad (3)$$

Here $\mu = M/m$ and $\beta = \sqrt{m/2kT}$, m being the neutron mass, k the Boltzmann constant and T the temperature of the body. The macroscopic absorption cross-section was assumed to have the form γ/v, where γ is a constant and the upper or lower signs in Eq. (3) refer to $v \leq v'$ or $v > v'$.

The unknown $n(\underline{r}, v\underline{\Omega}, t)$ is the usual "angular" density of neutrons ([14] p. 15), which is related to the phase density $u(\underline{r}, \underline{v}, t)$ of the kinetic theory of gases by the relationship

$$n(\underline{r}, v\underline{\Omega}, t)\, dV dv d\Omega = u(\underline{r}, \underline{v}, t)\, dV v^2 dv\, d\Omega \qquad (4)$$

For reasons of homogeneity with paper [8], we make use of the last variable.

By substituting into Eq. (1), setting

$$u(\underline{r},\underline{v},t) = e^{-\frac{1}{2}\beta^2 v^2}\psi(\underline{r},\underline{v},t) \tag{5}$$

and using the following independent variables

$$\underline{\rho} = \beta \underline{v} \tag{6}$$

$$\tau = \beta^{-1} t \tag{7}$$

we obtain the equation

$$\frac{\partial \psi(\underline{r},\underline{\rho},\tau)}{\partial \tau} + \underline{\rho}\cdot \operatorname{grad}_{\underline{r}} \psi(\underline{r},\underline{\rho},\tau) + h(\rho)\psi(\underline{r},\underline{\rho},\tau) = \int_{\omega} R(\rho,\rho')\psi(\underline{r},\underline{\rho}',\tau)\,d\omega', \tag{8}$$

where $d\omega' = \rho'^2\, d\rho'\, d\Omega'$ denotes the element of the new dimensionless velocity space ω (or ω'), and

$$h(\rho) = N\sigma_s\left[\frac{e^{-\mu\rho^2}}{\sqrt{\pi\mu}} + \left(\rho + \frac{1}{2\mu\rho}\right)\operatorname{erf}(\sqrt{\mu}\,\rho)\right] + \beta\gamma \tag{9}$$

$$R(\rho,\rho') = \frac{S(\rho,\rho')}{4\pi\rho\rho'} \tag{10}$$

$$S(\rho,\rho') = N\sigma_s \frac{(\mu+1)^2}{4\mu}\left\{ e^{\frac{\rho^2-\rho'^2}{2}}\left[\operatorname{erf}\left(\frac{\mu+1}{2\sqrt{\mu}}\rho - \frac{\mu-1}{2\sqrt{\mu}}\rho'\right) \pm \operatorname{erf}\left(\frac{\mu+1}{2\sqrt{\mu}}\rho + \frac{\mu-1}{2\sqrt{\mu}}\rho'\right)\right]\right.$$

$$\left. + e^{\frac{\rho'^2-\rho^2}{2}}\left[\operatorname{erf}\left(\frac{\mu+1}{2\sqrt{\mu}}\rho' - \frac{\mu-1}{2\sqrt{\mu}}\rho\right) \mp \operatorname{erf}\left(\frac{\mu+1}{2\sqrt{\mu}}\rho' + \frac{\mu-1}{2\sqrt{\mu}}\rho\right)\right]\right\} \tag{11}$$

This form of the transport equation has the advantage that the collision operator is symmetric.

It remains to specify the boundary and initial conditions. The boundary condition is the usual one, namely, that no neutrons may cross the boundary surface Γ of the body V coming from outside

$$\psi(\underline{r},\underline{\rho},\tau) = 0 \quad \text{if} \quad \underline{r} \in \Gamma, \tag{12}$$

$\underline{\rho}$ entering the body. The initial condition is that ψ is known at some initial instant $\tau = 0$

$$\psi(\underline{r},\underline{\rho},0) = \psi_0(\underline{r},\underline{\rho}) \tag{13}$$

Now, an initial value problem such as that just formulated can be solved, under very general assumptions, by means of a Laplace transform technique [11]: Let $\mathcal{H}$ be the Hilbert space of the complex-valued functions which are

defined and square-summable on the domain $V \otimes \omega$, the norm and the scalar product being defined, as usual, by Eqs. (14) and (15) respectively.

$$\| f \| = \left\{ \int\int_{V\omega} |f(\underline{r},\underline{p})|^2 \, dV \, d\omega \right\}^{1/2} \tag{14}$$

$$(f, g) = \int\int_{V\omega} f(\underline{r},\underline{p}) \, \overline{g(\underline{r},\underline{p})} \, dV \, d\omega \tag{15}$$

Equation (8) can be written in the form

$$\frac{\partial \psi}{\partial \tau} = A\psi \, , \tag{16}$$

where A denotes the integro-differential operator

$$A \cdot = -\underline{p} \cdot \mathrm{grad}_{\underline{r}} \cdot - h(p) \cdot + \int_{\omega} R(p,p') \cdot d\omega' \tag{17}$$

defined on the domain D_A of the functions f in $\mathcal{H}$, which admit the directional derivative $\underline{p} \cdot \mathrm{grad}_{\underline{r}} f$, satisfy the boundary condition $f(\underline{r}, \underline{p}) = 0$ for $\underline{r} \in \Gamma$ ($\underline{p}$ entering the body) and are such that Af is also in $\mathcal{H}$. Then, under some general assumptions which are all satisfied by our A and upon which we shall not insist here, one can take the Laplace transform of Eq. (16), solve the non-homogeneous equation so obtained by means of the resolvent of A, and find the solution of the problem in the form of an inverse Laplace integral

$$\psi(\underline{r},\underline{p},\tau) = \lim_{\eta \to \infty} \frac{1}{2\pi i} \int_{\kappa - i\eta}^{\kappa - i\eta} e^{\lambda \tau} (\lambda I - A)^{-1} f_0(\underline{r},\underline{p}) \, d\lambda \, . \tag{18}$$

Here κ is such that the vertical line $\mathrm{Re}\lambda = \kappa$ lies on the right of all the singularities of the resolvent $(\lambda I - A)^{-1}$ (I = identity operator), i.e. on the right of the spectrum of A. By shifting the integration path to the left and collecting the residues at the poles of the integrand, i.e. the eigenvalues of A, one can obtain the desired eigenfunction expansion. Facts such as the existence or non-existence of the decay modes have their spectral counterparts in terms of the existence of poles, so that the study of the spectrum of A will provide any information we need. Here we summarize the results obtained in [8].

Let us consider the function h(p). This function has a finite limit as $p \to 0$

$$\lim_{p \to 0} h(p) = 2N\sigma_s / \sqrt{\pi\mu} + \beta\gamma = h_0 > 0 \tag{19}$$

The spectral plane is then decomposed by A as follows (see Fig. 4):

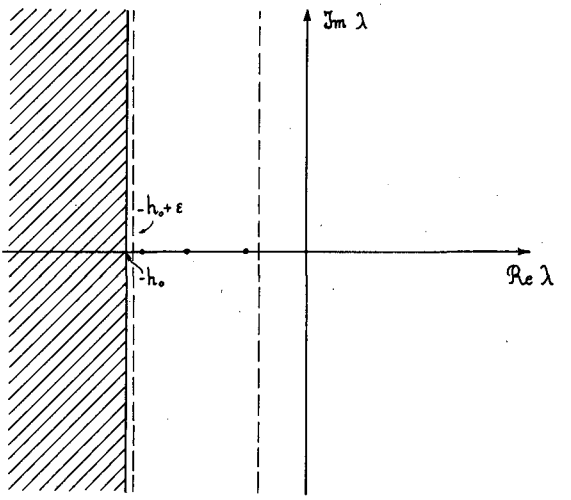

Fig. 4

Spectrum from Ref. [8]

(a) The entire half-plane $\mathrm{Re}\lambda \leq -h_0$ is contained in the spectrum. Thus a "continuously distributed spectrum" exists and occupies a half-plane, just as in the Lehner and Wing problem. (We do not say "continuous spectrum", since nothing has been ascertained about the existence and domain of definition of the resolvent: the less stringent locution "band spectrum" will therefore be used henceforth).

(b) The points in the half-plane $\mathrm{Re}\lambda > -h_0$ belong either to the point spectrum of A or to the resolvent set (on which the integrand of Eq. (18) is a regular analytic function of λ).

(c) The point spectrum contained in $\mathrm{Re}\lambda > -h_0$ consists of at most a finite number of eigenvalues β_m, $m = 1, 2, \ldots n$, which lie on a finite interval of the real axis $-h_0 < \beta < \beta_M$. A positive constant a_0 (of the order of a mean free path) exists, such that, if the diameter (the maximum chord) of the body V is smaller than a_0, then $n = 0$, i.e. A has no discrete eigenvalues.

From (a) we can see, without entering into a detailed analysis, that the shifting of the integration path of Eq. (18) to the left must stop at some $\mathrm{Re}\lambda = -h_0 + \epsilon$, $0 < \epsilon < \min_m(\beta_m + h_0)$ since the band spectrum is certainly not a region of regularity of the resolvent. The solution of our initial value problem could then be written (possibly) as a finite sum of discrete modes (the residues collected at the n poles of the resolvent) plus an inverse Laplace integral taken on the path $\mathrm{Re}\lambda = -h_0 + \epsilon$, which is all we can do for representing the contribution of the band spectrum. If, however, at least one discrete mode is present, the effect of the band spectrum, which is $O(e^{-h_0 t})$, will decay faster than the discrete mode itself and it is yet possible, after a sufficiently long time, to get an exponential decay. If, on the contrary, the size of the body is such that no eigenvalues exist (no poles), then the behaviour of the time-dependent solution is determined only by the band spectrum and no simple interpretation of a pulsed experiment with such a sample is possible.

3. THE BAND SPECTRUM OF A IN THE CASE OF THE EXACT FREE GAS SCATTERING KERNEL

Now we shall suspend the assumption of isotropic scattering made in [8] and make use of the exact free gas scattering kernel. The operator A is still given by Eq. (17), where the kernel R(p, p') is replaced by the exact kernel

$$H(\underline{p},\underline{p}') = N\sigma_s \frac{(\mu+1)^2}{4(\pi\mu)^{3/2}} \frac{1}{\rho} e^{-\frac{1}{4}\left[\frac{\rho^2}{\mu} + \frac{\mu}{\rho^2}(p^2-p'^2)^2\right]} \tag{20}$$

with $\rho = |\underline{p} - \underline{p}'|$ (see [12, 13]).

We shall first show that our "exact" A still possesses a band spectrum for $\mathrm{Re}\,\lambda \leq -h_0$. The proof, very similar to that given in [8], rests on the following theorem [11]: If, for a given λ, a family of functions $u_\delta \in D_A$ exists, such that

$$\|u_\delta\| \geq C > 0 \quad , \quad C = \text{constant} \tag{21}$$

$$\|(\lambda I - A)u_\delta\| \to 0 \quad \text{as} \quad \delta \to 0 \tag{22}$$

then λ is in the spectrum of A.

Let, then, $\underline{\Omega} = \underline{p}/p$ and let $\alpha_{\underline{\Omega}}$ be a plane perpendicular to $\underline{\Omega}$, $V_{\underline{\Omega}}$ the projection of V on $\alpha_{\underline{\Omega}}$. Any point $\underline{r} \in V$ can be written as $\underline{r}_0 - s\underline{\Omega}$, where $\underline{r}_0 \in V_{\underline{\Omega}}$ and $s_1(\underline{r}_0, \underline{\Omega}) \leq s \leq s_2(\underline{r}_0, \underline{\Omega})$, s_1 and s_2 being the values of s for which the line $\underline{r} = \underline{r}_0 - s\underline{\Omega}$ intersects the boundary surface Γ of V. We assume that the plane $\alpha_{\underline{\Omega}}$ is placed in such a way that $0 < s_1 \leq s_2$ (Fig. 5). Then, an integral of the type $\int_\omega \int_V F(\underline{r}, \underline{p})\, dV d\omega$ can also be written

$$\int_0^\infty p^2 dp \int_{4\pi} d\Omega \int_{V_{\underline{\Omega}}} d\alpha \int_{s_1}^{s_2} F(\underline{r}_0 - s\underline{\Omega}, p\underline{\Omega})\, ds \,.$$

Let us now consider the following family of functions u_δ $(0 < \delta < 1/2)$

$$u_\delta(\underline{r}, \underline{p}; \lambda) = \frac{s_2 - s}{a} e^{(s-s_1)\frac{h_0+\lambda}{r}} g(p),$$

where a is the diameter of V, and

$$g(p) = \begin{cases} 1/\delta^2 & \text{if } \delta^2 \leq p \leq \delta \\ 0 & \text{otherwise} \end{cases}.$$

It is easily verified that $u_\delta \in D_A$. For $\beta = \mathrm{Re}\,\lambda < -h_0$ we have

$$\|u_\delta\|^2 = \int_\omega \int_V |u_\delta(\underline{r}, \underline{p}; \lambda)|^2 dV d\omega$$

$$= \frac{1}{a^2\delta^4} \int_{\delta^2}^{\delta} p^2 dp \int_{4\pi} d\Omega \int_{V_{\underline{\Omega}}} d\alpha \int_{s_1}^{s_2} e^{2(s-s_1)\frac{h_0+\beta}{r}} (s_2 - s)^2 ds \,.$$

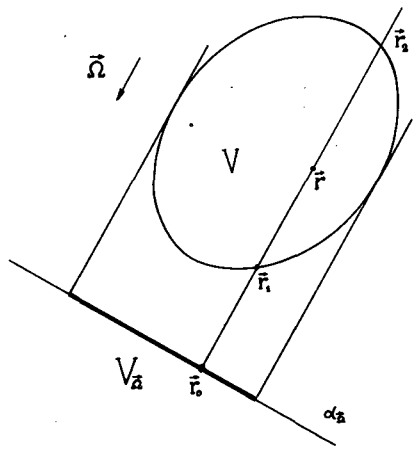

Fig. 5

Geometrical layout for section 3

Let b be a lower bound for the maximum length of the chords drawn in the direction $\underline{\Omega}$, as $\underline{\Omega}$ varies (b > 0 for a convex body), and let $V_{\underline{\Omega}}^*$ be the sub-set of $V_{\underline{\Omega}}$ for which $s_2(\underline{r}_0, \underline{\Omega}) - s_1(\underline{r}_0, \underline{\Omega}) \geq (3/4)b$. We can also assume, without any loss of generality, that δ satisfies the inequality $\exp\{-b|h_0+\beta|/\delta\} \leq \frac{1}{2}$. Then

$$\|u_\delta\|^2 \geq \frac{b^2}{16a^2\delta^4} \int_{\delta^2}^{\delta} p^2 dp \int_{4\pi} d\Omega \int_{V_{\underline{\Omega}}^*} d\alpha \int_{s_1}^{s_1 + b/2} e^{2(s-s_1)\frac{h_0+\beta}{p}}\, ds$$

$$= \frac{b^2}{16a^2\delta^4} \int_{4\pi} d\Omega \int_{V_{\underline{\Omega}}^*} d\alpha \int_{\delta^2}^{\delta} \frac{p^3}{2|h_0+\beta|} \left(1 - e^{-b\frac{|h_0+\beta|}{p}}\right) dp$$

$$\geq \frac{b^2}{64a^2\delta^4|h_0+\beta|} \int_{4\pi} d\Omega \int_{V_{\underline{\Omega}}^*} d\alpha \int_{\delta^2}^{\delta} p^3 dp$$

$$= \frac{b^2}{256a^2|h_0+\beta|} (1-\delta^4) \int_{4\pi} d\Omega \int_{V_{\underline{\Omega}}^*} d\alpha \geq C_1 > 0,$$

since the measure of $V_{\underline{\Omega}}^*$ is certainly not zero for a convex body. We have, on the other hand,

$$(A - \lambda I)u_\delta = \left[p\frac{\partial}{\partial s} - h(p) - \lambda \right] u_\delta(\underline{r}, \underline{p}; \lambda) + \int_\omega H(\underline{p}, \underline{p}') u_\delta(\underline{r}, \underline{p}'; \lambda)\, d\omega'$$

$$= z_1 + z_2 ,$$

where the symbol $p\partial/\partial s$ has been used instead of $-\underline{p} \cdot \mathrm{grad}_{\underline{r}}$. By using formula (A.1) (see the Appendix) we get

$$\|z_1\|^2 = \frac{1}{a^2\delta^4}\int_{\delta^2}^{\delta} p^2 dp \int_{4\pi} d\Omega \int_{V_\Omega} d\alpha \int_{s_1}^{s_2} \{[h(p)-h_0](s_2-s)+p\}^2 e^{2(s-s_1)\frac{h_0+\beta}{p}} ds$$

$$\leq \frac{(N\sigma_2 a+1)^2}{a^2\delta^4}\int_{4\pi} d\Omega \int_{V_\Omega} d\alpha \int_{\delta^2}^{\delta} \frac{p^5}{2|h_0+\beta|}\left(1 - e^{-2(s_2-s_1)\frac{|h_0+\beta|}{p}}\right) dp$$

$$\leq \frac{C_2}{|h_0+\beta|\delta^4}\int_{4\pi} d\Omega \int_{V_\Omega} d\alpha \int_{\delta^2}^{\delta} p^5 dp \leq \frac{C_3(\delta^2-\delta^8)}{|h_0+\beta|} \to 0 \quad as \quad \delta \to 0.$$

We have, furthermore,

$$\|z_2\|^2 = \int_\omega d\omega \int_V \left| \int_{\omega_\delta} H(\underline{p},\underline{p}')\, u_\delta(\underline{r},\underline{p}';\lambda)\, d\omega' \right|^2 dV,$$

where ω_δ denotes the spherical shell $\delta^2 \leq p \leq \delta$. By the aid of the Schwarz inequality and the inequality of Eq. (A.4) we obtain

$$\|z_2\|^2 \leq \int_\omega d\omega \int_V \left\{ \int_{\omega_\delta} H^2(\underline{p},\underline{p}')\, d\omega' \right\} \cdot \left\{ \int_{\omega_\delta} |u_\delta(\underline{r},\underline{p}';\lambda)|^2 d\omega' \right\} dV$$

$$\leq C_4(\delta^3-\delta^6)\int_V dV \int_{\omega_\delta} |u_\delta(\underline{r},\underline{p};\lambda)|^2 d\omega$$

$$= C_4 \frac{\delta^3-\delta^6}{a^2\delta^4}\int_{\delta^2}^{\delta} p^2 dp \int_{4\pi} d\Omega \int_{V_\Omega} d\alpha \int_{s_1}^{s_2} e^{2(s-s_1)\frac{h_0+\beta}{p}} (s_2-s)^2 ds$$

$$\leq C_5 \frac{(1-\delta^4)}{|h_0+\beta|}(\delta^3-\delta^6) \to 0 \quad as \quad \delta \to 0.$$

Thus we see that the family u_δ satisfies Eqs. (21) and (22), so that any point λ with $\mathrm{Re}\lambda < -h_0$ is contained in the spectrum of A. But, since the spectrum is a closed set, we conclude:

Theorem 1: The entire half-plane $\mathrm{Re}\lambda \leq -h_0$ is contained in the spectrum of A.

4. NON-EXISTENCE OF THE EIGENVALUES FOR SMALL BODIES

Let λ belong to the half-plane $\mathrm{Re}\lambda \geq -h_0$ and consider the eigenvalue equation $A\varphi = \lambda\varphi$, i.e.

$$-p\frac{\partial\varphi}{\partial s} + (h+\lambda)\varphi = \int_\omega H(\underline{p},\underline{p}')\,\varphi(\underline{r},\underline{p}')\, d\omega', \tag{23}$$

where $\varphi \in D_A$. By integrating along s, as customary ([14], p. 24), and taking account of the boundary condition, the following equation is obtained

$$\varphi(\underline{r},\underline{p}) = \frac{1}{p}\int_0^{s(\underline{r},\underline{\Omega})} e^{-\frac{h(p)+\lambda}{p}s}\, ds \int_\omega H(\underline{p},\underline{p}')\,\varphi(\underline{r}-s\underline{\Omega},p')\,d\omega', \quad (24)$$

where $s(\underline{r},\underline{\Omega})$ is the value of s for which the half-line $\underline{r}-s\underline{\Omega}$, $\underline{r}\in V$, $s\geq 0$ intersects the boundary surface Γ. Equation (24) can also be written

$$\varphi = T_\lambda K \varphi\ , \quad (25)$$

where

$$T_\lambda f \overset{def}{=} \int_0^{s(\underline{r},\underline{\Omega})} e^{-\frac{h(p)+\lambda}{p}s} f(\underline{r}-s\underline{\Omega},\underline{p})\,ds \quad (26)$$

$$K f \overset{def}{=} \int_\omega \frac{1}{p} H(\underline{p},\underline{p}')\, f(\underline{r},p')\,d\omega' \quad (27)$$

We shall prove that $||T_\lambda||\leq a$ for $Re\lambda \geq -h_0$, where a is the diameter of V. We have, in fact, by the Schwarz inequality,

$$|T_\lambda f(\underline{r},\underline{p})|^2 \leq \int_0^{s(\underline{r},\underline{\Omega})} ds \cdot \int_0^{s(\underline{r},\underline{\Omega})} |f(\underline{r}-s\underline{\Omega},\underline{p})|^2 ds \leq a\int_0^{s(\underline{r},\underline{\Omega})} |f(\underline{r}-s\underline{\Omega},\underline{p})|^2 ds$$

and, if we extend the definition of f to all $\underline{r}$-space by setting $f(\underline{r},\underline{p})=0$ when $\underline{r}\notin V$, we obtain

$$\begin{aligned}
\|T_\lambda f\|^2 &\leq a\int_0^\infty p^2 dp \int_{4\pi} d\Omega \int_{\alpha_{\underline{\Omega}}} d\alpha \int_{s_1(\underline{r}_0,\Omega)}^{s_2(\underline{r}_0,\Omega)} ds' \int_{-\infty}^{\infty} |f(\underline{r}_0-(s+s')\underline{\Omega},\underline{p})|^2 ds \\
&\leq a^2\int_0^\infty p^2 dp \int_{4\pi} d\Omega \int_{\alpha_{\underline{\Omega}}} d\alpha \int_{-\infty}^{\infty} |f(\underline{r}_0-t\underline{\Omega},\underline{p})|^2 dt \\
&= a^2\int_\omega d\omega \int_V |f(\underline{r},\underline{p})|^2 dV = a^2\|f\|^2\ , \quad \text{q.e.d.}
\end{aligned}$$

We have also, from Eqs. (A.3) and (A.5),

$$\begin{aligned}
\|Kf\|^2 &= \int_V dV \int_\omega \frac{1}{p^2}\left|\int_\omega H(\underline{p},\underline{p}')\, f(\underline{r},\underline{p}')\,d\omega'\right|^2 d\omega \\
&\leq \int_V dV \int_{p\leq 1} \frac{1}{p^2}\left\{\int_\omega H^2(\underline{p},\underline{p}')\,d\omega' \cdot \int_\omega |f(\underline{r},\underline{p}')|^2 d\omega'\right\} d\omega \\
&+ \int_V dV \int_{p>1} \left|\int_\omega H(\underline{p},\underline{p}')\, f(\underline{r},\underline{p}')\,d\omega'\right|^2 d\omega \\
&\leq \int_{4\pi} d\Omega \int_0^1 dp \int_\omega H^2(\underline{p},\underline{p}')\,d\omega' \cdot \int_V dV \int_\omega |f(\underline{r},\underline{p}')|^2 d\omega'
\end{aligned}$$

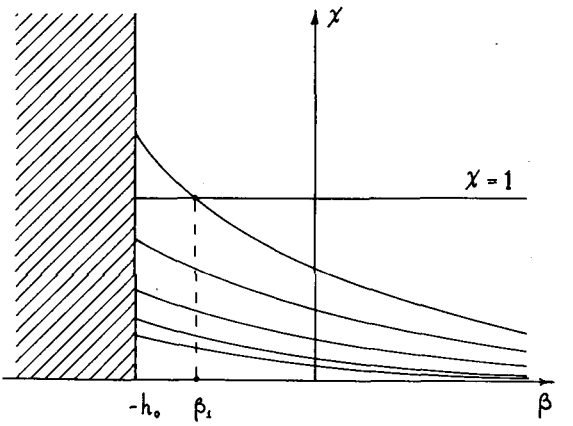

Fig. 6

$\chi_i(\lambda)$ curves

$$+ \int_v dV \int_\omega \left| \int_\omega H(\underline{\rho},\underline{\rho}') f(\underline{r},\underline{\rho}')\, d\omega' \right|^2 d\omega$$

$$\leq \left(4\pi^2 \sqrt{8\pi\mu} + 64\pi^2\mu^2 \right) C^2 \|f\|^2 = C'^2 \|f\|^2$$

Taking the norms of both members of Eq. (25) we obtain

$$\|\varphi\| = \|T_\lambda K \varphi\| \leq \|T_\lambda\| \cdot \|K\| \cdot \|\varphi\| \leq a C' \|\varphi\| \qquad (28)$$

Let

$$a_0 = \frac{1}{C'} = \left(\frac{1}{4\sqrt{8\pi\mu}} + \frac{4\mu}{\pi} \right)^{-1/3} \frac{\mu}{(\mu+1)^2} \cdot \frac{1}{N\sigma_s} \qquad (29)$$

Inequality (28) then shows that Eq. (25) cannot have a solution $\varphi \neq 0$ if $a < a_0$, which implies in its turn that also Eq. (23) has not a non-trivial solution for such values of a. We conclude:

Theorem 2: If $a < a_0$, then no eigenvalue of A exists in the half-plane $\mathrm{Re}\lambda > -h_0$. The vertical line $\mathrm{Re}\lambda = -h_0$, which lies in the band spectrum, must necessarily belong to the continuous or residual spectrum.

Let us now suppose $a < a_0$, $\mathrm{Re}\lambda > -h_0$ and consider the inhomogeneous equation

$$Af - \lambda f = g \,, \quad g \in \mathcal{H} \qquad (30)$$

By using the same procedure as for Eq. (23), this equation can be transformed into the following

$$f = T_\lambda K f + \ell \,,$$

where

$$\ell(\underline{r},\underline{p}) = \frac{1}{p}\int_0^{s(\underline{r},\underline{\Omega})} e^{-\frac{h(p)+\lambda}{p}s}\, g(\underline{r}-s\underline{\Omega},\underline{p})\,ds \tag{31}$$

We say that $\ell \in \mathcal{H}$. By extending the definition of $g(\underline{r},\underline{p})$ to all $\underline{r}$-space V_∞ and taking $g(\underline{r},\underline{p}) \equiv 0$ if $\underline{r} \notin V$, we obtain, in fact,

$$\|\ell\|^2 \le \int_\omega \frac{1}{p^2}\,d\omega \int_V \left\{ \int_0^\infty e^{-\frac{h_0+\beta}{p}s}\,ds \cdot \int_0^\infty e^{-\frac{h_0+\beta}{p}s}\,|g(\underline{r}-s\underline{\Omega},\underline{p})|^2 ds \right\} dV$$

$$\le \frac{1}{h_0+\beta}\int_\omega \frac{1}{p}\,d\omega \int_0^\infty e^{-\frac{h_0+\beta}{p}s}\,ds \int_{V_\infty} |g(\underline{r}-s\underline{\Omega},\underline{p})|^2\,dV$$

$$= \frac{1}{(h_0+\beta)^2}\int_\omega d\omega \int_V |g(\underline{r},\underline{p})|^2\,dV = \frac{1}{(h_0+\beta)^2}\|g\|^2 < \infty \tag{32}$$

Since $\|T_\lambda K\| < 1$ for $a < a_0$, the resolvent $(I - T_\lambda K)^{-1}$ exists, is bounded and is defined over the entire space $\mathcal{H}$. Then Eq. (31) can be solved with respect to f and gives

$$\|f\| \le \|(I - T_\lambda K)^{-1}\| \cdot \|\ell\| \le C(h_0+\beta)^{-1}\|g\| \tag{33}$$

This shows that Eq. (30) has a uniquely determined solution belonging to $\mathcal{H}$, for any $g \in \mathcal{H}$, $\mathrm{Re}\lambda > -h_0$, i.e.

Theorem 3: If $a < a_0$, then the half-plane $\mathrm{Re}\lambda > -h_0$ is contained in the resolvent set of A. The spectrum is therefore restricted to the band spectrum $\mathrm{Re}\lambda \le -h_0$. Thus we see that the most relevant results of paper [8], summarized in section 2, are still valid if the isotropic scattering assumption is suspended, and the exact free gas scattering kernel is used.

5. FURTHER RESULTS: A NUMERICAL METHOD

More detailed information about the eigenvalues of A (in the case in which their existence cannot be excluded a priori) seems to be obtainable only if the isotropy of scattering is assumed, so that we must return to the definition of A in Eq. (17). Equation (24), with $H(\underline{p},\underline{p}')$ replaced by $R(p,p')$ and after integration over $\underline{\Omega}$, gives the Peierls equation

$$\xi(\underline{r},p) = \frac{1}{p}\int_V \frac{e^{-\frac{n(p)\sigma|\underline{r}-\underline{r}'|}{p}}}{|\underline{r}-\underline{r}'|^2}\,dV \int_0^\infty R(p,p')\,\xi(\underline{r}',p')\,p'^2\,dp', \tag{34}$$

where $\xi(\underline{r},p) = \int_{4\pi} \varphi(\underline{r},\underline{p})\,d\Omega$. By setting $q(\underline{r},p) = p\xi(\underline{r},p)$ and remembering Eq. (10), we can put Eq. (34) into the form

$$q = G_\lambda S q \,, \tag{35}$$

where

$$G_\lambda f \stackrel{def}{=} \int_V \frac{e^{-\frac{h(p)+\lambda}{p}|\underline{r}-\underline{r}'|}}{4\pi p\,|\underline{r}-\underline{r}'|^2} f(\underline{r}', p)\, dV' \tag{36}$$

$$S f \stackrel{def}{=} \int_0^\infty S(p,p') f(\underline{r}, p')\, dp' \tag{37}$$

(Operators such as G_λ or S act on the Hilbert space $\mathcal{H}_0$ of the functions $f(\underline{r}, p)$ square-summable on $V \otimes E$, where E is the interval $0 \leq p < \infty$; norms and scalar products in this space will be affected by the index O.)

The following results have been derived in [8] and are stated here briefly.

(a) The eigenvalues of A, if existing, are real. We first observe that the symmetry of S implies that

$$(q, Sq)_0 = (G_\lambda S q, Sq)_0 = (G_\lambda \vartheta, \vartheta)_0$$

is real. But

$$(G_\lambda \vartheta, \vartheta)_0 = \int_0^\infty dp \iint_{V\,V} \frac{e^{-\frac{h(p)+\lambda}{p}|\underline{r}-\underline{r}'|}}{4\pi p\,|\underline{r}-\underline{r}'|^2} \vartheta(\underline{r}', p)\, \overline{\vartheta(\underline{r}, p)}\, dV dV' \,, \tag{38}$$

where the right-hand member can be written, by means of the Lehner-and-Wing Fourier transform technique [1], as follows:

$$\int_0^\infty dp \int_{V_\infty} \frac{1}{p w} \arctan \frac{p w}{h(p)+\lambda} \left|\tilde{\vartheta}(\underline{w}, p)\right|^2 dV_{\underline{w}} \,, \tag{39}$$

where $\tilde{\vartheta}(\underline{w}, p)$ is the Fourier transform of $\vartheta(\underline{r}, p)$, assumed to be zero if $\underline{r} \notin V$, and $(1/pw)\arctan\{pw/[h(p)+\lambda]\}$ is the transform of $(1/4\pi p) r^{-2} \exp\{-[h(p)+\lambda] r/p\}$. It is easily seen that the imaginary part of the latter function is $\gtrless 0$ as $\mathrm{Im}\lambda$ is $\lessgtr 0$. Then λ must be a real number, in order that $(G_\lambda \vartheta, \vartheta)_0$ may be real (the alternative $\vartheta = Sq = 0$ is readily excluded; because $Sq = 0$ would imply $q = 0$ by Eq. (35)).

(b) There is at most a finite number of eigenvalues of A. The proof is rather delicate and cannot be shortened to a reasonable extent. If, however, we introduce the supplementary condition that S is positive definite (a property which has been established for the monatomic hydrogen, but is probably true for all values of the scatterer mass) at least the plan of a Lehner-Wing type proof [4] can be given. In this case, in fact, the square root, $S^{1/2}$, of S exists, and Eq. (35) can be written (the parameter λ is now real, with $-h_0 \leq \lambda < \infty$)

$$\psi = L_\lambda \psi \,, \tag{40}$$

where $\psi = S^{1/2} q$, $L_\lambda = S^{1/2} G_\lambda S^{1/2}$. From Eqs. (38) and (39) we see that $(L_\lambda f, f)_0 = (G_\lambda S^{1/2} F, S^{1/2} f)_0 > 0$, i.e. L_λ is a self-adjoint positive definite operator. We take for granted that L_λ is bounded and completely continuous in the interval $-h_0 \leq \lambda < \infty$ (this is not difficult to be proven, but rather long: we may only cite paper [8], in which $G_\lambda S$ is shown to be completely continuous, so that $L_\lambda^2 = S^{1/2} G_\lambda S G_\lambda S^{1/2}$ is also completely continuous, and finally L_λ itself (by [15], p. 432). The boundedness should be easily admitted (see section 4). Then L_λ has a denumerable infinity of positive eigenvalues $\chi_1(\lambda) \geq \chi_2(\lambda) \geq \ldots$ converging towards zero. The difference $L_\lambda - L_{\lambda'} = S^{1/2} (G_\lambda - G_{\lambda'}) S^{1/2}$ is also positive definite, for $\lambda < \lambda'$, as can be seen from Eq. (39), since

$$\frac{1}{pw} \arctan \frac{pw}{h(p) + \lambda} - \frac{1}{pw} \arctan \frac{pw}{h(p) + \lambda'} > 0, \quad \lambda < \lambda'$$

(see [1]). It follows [16] that the eigenvalues of $L_\lambda = L_{\lambda'} + (L_\lambda - L_{\lambda'})$ must exceed the corresponding eigenvalues of $L_{\lambda'}$ ("the addition of a positive definite operator increases all the eigenvalues"). The curves $\chi_i(\lambda)$ are thus steadily decreasing and tend to zero as $\lambda \to +\infty$ as seen by Eq. (39). Since all these curves are bounded for $-h_0 \leq \lambda < \infty$ and accumulate only towards the λ-axis (see Fig. 6), they cannot have more than a finite number of intersections $\beta_1, \ldots, \beta_n$ with the horizontal line $\chi = 1$ in this interval. These are the eigenvalues of A.

A numerical method has been elaborated, which follows directly from the theory here expounded. We sketch it in a few words. Let us consider Eq. (35) or, better, the eigenvalue equation $\chi \zeta = S G_\lambda \zeta$, i.e.

$$\chi \zeta(\underline{r}, p) = \int_0^\infty \frac{S(p,p')}{p'} dp' \int_V \frac{e^{-\frac{h(p)+\lambda}{p'}|\underline{r}-\underline{r}'|}}{4\pi |\underline{r}-\underline{r}'|^2} \zeta(\underline{r}', p') d\underline{r}', \qquad (41)$$

where $\zeta = Sq$. We know that the eigenvalues of A are determined by the intersections of the line $\chi = 1$ with the curves $\chi_i(\lambda)$ of the eigenvalues of Eq. (41). The problem is thus to calculate these $\chi_i(\lambda)$ or at least the principal eigenvalue $\chi_1(\lambda)$; a suitable technique for this is the Feynman method ([14], p. 302). For any fixed λ, p we consider the following auxiliary eigenvalue problem

$$\eta \varrho(\underline{r}) = \int_V \frac{e^{-\sigma|\underline{r}-\underline{r}'|}}{4\pi |\underline{r}-\underline{r}'|^2} \varrho(\underline{r}') dV', \quad \sigma = \frac{h(p)+\lambda}{p}. \qquad (42)$$

This equation has a denumerable infinity of positive eigenvalues η_j and the corresponding eigenfunctions ρ_j form a complete orthogonal system. Both η_j and ρ_j can be computed by numerical methods. Then we put $\zeta(\underline{r}, p | \gamma) = \Sigma_j \zeta_j(p|\lambda) \rho_j(\underline{r}|p|\lambda)$. By substituting into Eq. (41) and making use of the orthogonality relations, we obtain the following system of infinite integral equations:

$$\chi \zeta_j(p|\lambda) = \Sigma_k \int_0^\infty S(p,p') \frac{\eta_k(p'|\lambda)}{p'} M_{jk}(p,p'|\lambda) \zeta_k(p'|\lambda) dp', \qquad (43)$$

where

$$M_{jk}(p,p'|\lambda) = \int_v \varrho_j(\underline{r},p|\lambda)\varrho_k(\underline{r},p'|\lambda)dV .$$

Since ρ_j and ρ_k are orthogonal for $j \neq k$, $p = p'$ and vary relatively slowly as p varies, we may assume that $M_{jk}(p, p'|\lambda) = \delta_{jk} + \epsilon \tilde{M}_{jk}(p, p'|\lambda)$, where $\epsilon\tilde{M}_{jk}$ is a small perturbation. We also set $\zeta_i(p|\lambda) = \Sigma_s \epsilon^s \zeta_i^{(s)}(p|\lambda)$, $\chi(\lambda) = \Sigma_s \epsilon^s \chi^{(s)}(\lambda)$, then substitute into Eq. (41) and collect the terms with the same power of ϵ. The zeroth approximation gives, for the principal eigenvalue, the following equation,

$$\chi_i^{(0)}(\lambda)\zeta_i^{(0)}(p|\lambda) = \int_0^\infty S(p,p')\frac{\eta_i(p'|\lambda)}{p'}\zeta_i^{(0)}(p'|\lambda)dp' \qquad (44)$$

which can be solved by numerical methods. Although the Feynman method should not be sufficiently accurate for very small bodies, our first calculations show that the $\chi_1^{(0)}(\lambda)$ curve has the correct behaviour, as shown in Fig. 6, and remains below the line $\chi = 1$ if the diameter of the sample (a sphere) is less than two or three mean free paths.

APPENDIX

We give some estimates concerning the functions h(p) and $H(\underline{p}, \underline{p}')$. We have, from Eq. (9)

$$\lim_{p\to 0} h(p) = \frac{2N\sigma_s}{\sqrt{\pi\mu}} + \beta\gamma = h_0 > 0$$

$$h'(p) = N\sigma_s \cdot \frac{2}{\sqrt{\pi}}\int_0^{\sqrt{\mu}p}\left(1 - \frac{t^2}{\mu p^2}\right)e^{-t^2}dt > 0$$

Hence

$$\begin{aligned} 0 \leq h(p) - h_0 &= N\sigma_s\left[\frac{e^{-\mu p^2} - 2}{\sqrt{\pi\mu}} + p\,\mathrm{erf}(\sqrt{\mu}p) + \frac{1}{2\mu p}\mathrm{erf}(\sqrt{\mu}p)\right] \\ &\leq N\sigma_s\left[\frac{e^{-\mu p^2} - 2}{\sqrt{\pi\mu}} + p + \frac{1}{\sqrt{\pi\mu}p}\int_0^{\sqrt{\mu}p} dt\right] \qquad (A.1) \\ &= N\sigma_s\left[\frac{e^{-\mu p^2} - 1}{\sqrt{\pi\mu}} + p\right] \leq N\sigma_s p \end{aligned}$$

Now we consider the kernel $H(\underline{p}, \underline{p}') = H(\underline{p}', \underline{p})$. We have

$$0 \leq H(\underline{p}, \underline{p}') \leq \frac{C}{\varrho}e^{-\varrho^2/4\mu}, \qquad C = N\sigma_s\frac{(\mu+1)^2}{4(\pi\mu)^{3/2}}$$

Thus

$$\int_\omega H(\underline{p},\underline{p}')\,d\omega' \le 4\pi C \int_0^\infty \varrho\, e^{-\varrho^2/4\mu}\,d\varrho = 8\pi\mu C \tag{A.2}$$

$$\int_\omega H^2(\underline{p},\underline{p}')\,d\omega' \le 4\pi C^2 \int_0^\infty e^{-\varrho^2/2\mu}\,d\varrho = 2\pi\sqrt{2\pi\mu}\,C^2 \tag{A.3}$$

Let ω_δ denote the spherical shell $\delta^2 \le p' \le \delta$, $\delta \le 1/2$. Then

$$\int_\omega d\omega \int_{\omega_\delta} H^2(\underline{p},\underline{p}')\,d\omega' \le 2\pi\sqrt{2\pi\mu}\,C^2 \int_{\omega_\delta} d\omega' = C_1(\delta^3 - \delta^6) \tag{A.4}$$

Let us now consider the symmetric operator

$$Hf \overset{\text{def}}{=} \int_\omega H(\underline{p},\underline{p}')f(\underline{r},\underline{p}')\,d\omega'$$

and let f be an arbitrary element in $\mathcal{H}$ with $\|f\| = 1$. Then we have

$$\begin{aligned}
|(Hf,f)| &\le \int_V dV \int_\omega\int_\omega H(\underline{p},\underline{p}')|f(\underline{r},\underline{p}')||f(\underline{r},\underline{p})|\,d\omega\,d\omega' \\
&\le \tfrac{1}{2}\int_V dV \int_\omega\int_\omega H(\underline{p},\underline{p}')\{|f(\underline{r},\underline{p}')|^2 + |f(\underline{r},\underline{p})|^2\}\,d\omega\,d\omega' \\
&\le 4\pi\mu C \int_V dV \int_\omega |f(\underline{r},\underline{p}')|^2 d\omega' + 4\pi\mu C \int_V dV \int_\omega |f(\underline{r},\underline{p})|^2 d\omega \\
&= 8\pi\mu C
\end{aligned} \tag{A.5}$$

so that $\|H\| \le 8\pi\mu C$.

REFERENCES

[1] LEHNER, J. and WING, G. M., "On the spectrum of an asymmetric operator arising in the transport theory of neutrons", Comm. on pure appl. Math. 8 (1955) 217-234.

[2] LEHNER, J. and WING, G. M., "Solution of the linearized Boltzmann equation for the slab geometry", Duke math. J. 23 (1956) 125-42.

[3] VAN NORTON, R., "The spectrum of a neutron transport operator", N. Y. Univ., Rpt NYO 9085 (1960).

[4] PIMBLEY, G., "Solution of an initial value problem for the multi-velocity neutron transport equation with a slab geometry", J. Math. Mech. 8 (1959) 837-66.

[5] JÖRGENS, K., "An asymptotic expansion in the theory of neutron transport", Comm. pure appl. Math. 11 (1958) 219-42.

[6] NELKIN, R. S., "Asymptotic solutions of the transport equation for thermal neutrons", Physica 29 (1963) 261-73.

[7] CORNGOLD, N., "Some transient phenomena in thermalization", Nucl. Sci. Engng. 19 (1964) 80-90.
[8] ALBERTONI, S. and MONTAGNINI, B., "On the spectrum of neutron transport equation in finite bodies", to be published in J. math. Anal. and Applications.
[9] COHEN, E.R., "A survey of neutron thermalization theory", Proc. UN Int. Conf. PUAE 5 (1956) 405-16.
[10] BECKURTS, K.H. and WIRTZ, K., Neutron Physics, Springer Verlag, Berlin (1964).
[11] HILLE, E. and PHILLIPS, R.S., "Functional analysis and semigroups", Amer. math. Soc. Coll. Publ. 34 (1957).
[12] JAFFÉ, G., "Diffusion of neutrons", Phys. Rev. 88 (1952) 603 - 11.
[13] OSBORN, R.K., "Some characteristics of the thermal neutron scattering probability", Nucl. Sci. Engng 3 (1957) 29 - 37.
[14] *DAVISON, B., Neutron Transport Theory, Oxford Univ. Press (1957)*
[15] ZAANEN, A.C., Linear Analysis, North Holland, Amsterdam (1960).
[16] WING, G.M., "An introduction to transport theory", John Wiley & Sons, N.Y. (1962).

SPECTRUM OF THE BOLTZMANN OPERATOR WITH AN ISOTROPIC THERMALIZATION KERNEL

R. BEDNARZ
INSTITUTE OF NUCLEAR RESEARCH,
SWIERK, POLAND

Abstract — Résumé — Аннотация — Resumen

SPECTRUM OF THE BOLTZMANN OPERATOR WITH AN ISOTROPIC THERMALIZATION KERNEL. The spectrum of the transport operator with an isotropic thermalization kernel has been studied in the Hilbert space of the square integrable functions over the six-dimensional set. The set is a Cartesian product of the unbounded velocity space and a convex bounded body. The operator has a domain with functions permitting the directional derivative and vanishing at the boundary for velocity directions entering the body. The kernel has been symmetrized according to the detailed balance condition and assumed to be square integrable. The total collision rate must reach its minimum value (bound of the point spectrum) at zero velocity and must behave like a linear function for large velocities. With an additional assumption that the total collision rate has a positive derivative on the set of positive measurements including zero velocity, the spectral theorem is proved. The spectral plane is divided into two half planes by the straight line perpendicular to the real axis. This line crosses the negative real axis at the bound of the point spectrum. The left half-plane including this line is all contained in the spectrum. The right open half-plane belongs to the resolvent set of the real axis on which the point spectrum may be situated. It is found that the point spectrum exists for sufficiently large samples but vanishes for sufficiently small samples. The first result is equivalent to the absence of a normal mode, and has been obtained by Nelkin for a separable thermalization kernel and by Albertoni and Montagnini for the free gas kernel. Finally, the applicability of the spectral theorem to the interpretation of pulsed neutron experiments with solids and liquids is discussed.

SPECTRE DE L'OPÉRATEUR DE BOLTZMANN A NOYAU DE THERMALISATION ISOTROPE. Le spectre de l'opérateur de transport à noyau de thermalisation isotrope a été étudié dans l'espace de Hilbert des fonctions de carré sommables dans un ensemble à six dimensions. Cet ensemble est un produit cartésien de l'espace des vitesses non limité et d'un corps convexe limité. L'opérateur possède un domaine ayant des fonctions qui permettent de dériver par rapport à la direction et cessent d'exister à la limite pour les directions de vitesse orientées vers le corps. On a symétrisé le noyau selon la condition du bilan détaillé et supposé qu'il s'agit d'un carré sommable. Le taux de collision total doit atteindre sa valeur minimum (limite du spectre ponctuel) pour une vitesse nulle et son comportement sera semblable à celui d'une fonction linéaire pour les grandes vitesses. Si l'on suppose en outre que le taux de collision total a une dérivée positive sur l'ensemble des mesures positives, y compris la vitesse nulle, on a démontré le théorème spectral. Le plan spectral est divisé en deux demi-plans par la droite perpendiculaire à l'axe réel. Cette droite coupe l'axe réel négatif à la limite du spectre ponctuel. Le demi-plan gauche qui comprend cette droite est entièrement contenu dans le spectre. Le demi-plan ouvert droit appartient à l'ensemble résolvant de l'axe réel sur lequel le spectre ponctuel peut être situé. Il a été constaté que le spectre ponctuel existe pour des échantillons suffisamment grands et cesse d'exister s'ils sont assez petits. Le premier résultat équivaut à l'absence d'un mode normal ; il a été obtenu par Nelkin pour un noyau de thermalisation séparable et par Albertoni et Montagnini pour le modèle de gaz libre du noyau. Enfin, l'auteur examine dans quelle mesure le théorème spectral permet d'interpréter les expériences, au moyen des neutrons pulsés, faites sur les solides et les liquides.

СПЕКТР БОЛЬЦМАНОВСКОГО ОПЕРАТОРА С ФУНКЦИЕЙ ВЛИЯНИЯ ИЗОТРОПИЧЕСКОЙ ТЕРМАЛИЗАЦИИ. Спектр оператора переноса с функцией влияния изотропической термализации изучен в гильбертовом пространстве квадратичных интегральных функций для шестимерного ряда. Этот ряд является картезианским произведением неограниченного скоростного пространства и ограниченного вогнутой поверхностью тела. Оператор имеет сферу с 8 функциями, дающими возможность образования направленных производных, исчезающих на пределе для направлений скоростей, поступающих в тело. Функции влияния была придана

симметричная форма на основании точных условий равновесия с предположением о возможности квадратичного интегрирования. Общее число соударений должно достичь минимальной величины (предел точечного спектра) при нулевой скорости и для больших скоростей должно выражаться линейной функцией. При наличии дополнительной гипотезы, что общее число соударений имеет положительную производную для ряда с положительным измерением, включая нулевую скорость, спектральная теорема может считаться доказанной. Спектральная плоскость разделяется на две полуплоскости прямой линией, перпендикулярной к действительной оси. Эта линия пересекает отрицательную ось на пределе точечного спектра. Левая полуплоскость, включая эту линию, входит полностью в спектр. Правая открытая полуплоскость принадлежит к результирующему ряду вне действительной оси, на которой может быть расположен точечный спектр. Было найдено, что точечный спектр существует для достаточно больших проб, но исчезает для достаточно малых.

Первый результат равнозначен отсутствию нормального вида, и он был получен Нелкином для отделимой функции влияния термализации, а также Альбертони и Монтаньини для функции влияния в свободном газе. Наконец, обсуждается применимость спектральной теоремы к истолкованию экспериментов с импульсными нейтронами в твердых телах и жидкостях.

ESPECTRO DEL OPERADOR DE BOLTZMANN CON NUCLEO ISOTROPICO DE TERMALIZACION. El autor ha estudiado el espectro del operador de transporte con núcleo isotrópico de termalización en el espacio de Hilbert de las funciones de cuadrado integrable sobre un conjunto de seis dimensiones. Este conjunto es un producto cartesiano del espacio de velocidad ilimitada y un cuerpo limitado convexo. El operador cubre una región con funciones que permiten la derivada direccional y que desaparecen en los límites para las direcciones de velocidad orientadas hacia el cuerpo. El núcleo se ha simetrizado de acuerdo con la condición de balance detallado y se supone que constituye un cuadrado integrable. La frecuencia total de colisiones tiene que alcanzar su valor mínimo (límite del espectro de puntos) a la velocidad cero, y a velocidades grandes tiene que comportarse como una función lineal. Si se supone además que la frecuencia total de colisiones tiene una derivada positiva en el conjunto de medidas positivas, inclusive la velocidad cero, queda probado el teorema espectral. La recta perpendicular al eje real divide el plano espectral en dos semiplanos, y cruza el eje real negativo en el límite del espectro de puntos. El semiplano izquierdo, que incluye esta línea, queda contenido en el espectro. El semiplano derecho, abierto, pertence al conjunto resolvente del eje real en que se puede situar el espectro de puntos. El espectro de puntos existe cuando la muestra es suficientemente grande pero desaparece cuando es suficientemente pequeña. El primer resultado equivale a la falta de un modo normal y ha sido obtenido por Nelkin para un núcleo de termalización separable, y por Albertoni y Montagnini para el núcleo de gas libre. Finalmente, se discute hasta qué punto es posible interpretar los experimentos con neutrones pulsados en sólidos y en líquidos aplicando el teorema espectral.

I. INTRODUCTION

The theory of pulsed neutron experiments for a long time was based mainly upon the diffusion approximation. The first qualitative information based upon the Boltzmann equation was obtained by NELKIN [1]. In the case of spherical geometry, isotropic scattering and a separable thermalization kernel, he proved that there is no point spectrum of the Boltzmann operator for sufficiently small spheres. This result is equivalent to the lack of the exponentially decaying fundamental mode. Further investigation has been carried out by ALBERTONI and MONTAGNINI [2]. Using the functional analysis methods developed in neutron transport by LEHNER and WING [3, 4] PIMBLEY [5] and JÖRGENS [6], they studied isotropic free gas model in the bounded geometry. They obtained two spectral properties of the transport operator. First, the closed left half-plane ($\mathrm{Re}\,\lambda \leqq -[v\,\Sigma(v)]_{\min.}$) is contained in the spectrum. This result is important, since it implies the non-existence of the point spectrum surrounded by the resolvent set in the left half-plane, and therefore the non-existence of the normal mode with the decay constant greater than the minimum collision rate. The second property

concerns the open right half-plane; namely, the point spectrum does not exist for sufficiently small samples. Hence there is no asymptotic neutron distribution depending exponentially on time for small samples.

We consider also isotropic thermalization models in the bounded geometry, but do not specify dependence of the scattering kernel and total macroscopic cross-section on velocity. The models must satisfy only the conditions listed in section II. In section III we discuss the importance of the spectrum investigation for the solution of the initial value problem. In this section the Hilbert space is introduced and the domain of the transport operator is defined. Section IV contains four theorems concerning the spectrum of the transport operator and two theorems describing properties of the generalized Peierls operator. The proofs of these theorems are contained in [7]. In section V we discuss applicability of the spectral theorems to various isotropic thermalization models.

II. PHYSICAL ASSUMPTIONS

We will consider the time behaviour of the neutron density $N(\vec{r}, v, \vec{\Omega}, t)$ in the convex bounded sample (body) of the moderating material. Let us assume that the initial density is a given function of the position $\vec{r}$, velocity v, and direction of the neutron flight $\vec{\Omega}$, at time $t = 0$:

$$N(\vec{r}, v, \vec{\Omega}, 0) = F(\vec{r}, v, \vec{\Omega}) . \tag{1}$$

The time evolution of the density is described by the Boltzmann equation which has, in the absence of sources, the following form [8]:

$$\frac{\partial}{\partial t} N(\vec{r}, v, \vec{\Omega}, t) + v\vec{\Omega} \cdot \operatorname{grad} N(\vec{r}, v, \vec{\Omega}, t) + v\Sigma(v) N(\vec{r}, v, \vec{\Omega}, t)$$

$$= \int_0^\infty dv' \int_U d\vec{\Omega}' v' \Sigma_s(v') f(v'\vec{\Omega}' \to v\vec{\Omega}) N(\vec{r}, v, \vec{\Omega}, t), \tag{2}$$

where $\Sigma(v)$, and $\Sigma_s(v)$ are the total and scattering macroscopic cross-sections respectively, U is the surface of the unit sphere, and $f(v'\vec{\Omega}' \to v\vec{\Omega}) dv\, d\vec{\Omega}$ may be described as the probability that a neutron entering a collision with velocity (vector) $v'\vec{\Omega}'$ will belong to $dv\, d\vec{\Omega}$ after collision.

The following homogeneous boundary condition is satisfied at the boundary S of the body:

$$N(\vec{r}, v, \Omega, t) = 0 \tag{3}$$

for $\vec{r} \in S$, $t \geq 0$ and $\vec{\Omega}$ entering the body.

The theorems of section IV are proved under the following assumptions concerning thermalization kernels and total macroscopic cross-sections:

(a) Isotropy of the thermalization kernel

$$f(v'\vec{\Omega}' \to v\vec{\Omega})\Sigma_s(v') = \frac{1}{4\pi}\Sigma(v, v') \tag{4}$$

(b) Detailed balance condition

$$\Sigma(v, v')v'M(v') = \Sigma(v, v')vM(v), \tag{5}$$

where

$$M(v) = \frac{4}{\sqrt{\pi}}\beta^2 v^2 e^{-\beta^2 v^2} \tag{6}$$

$T = 1/2\beta^2$ (neutron mass = Boltzmann constant = 1); T is the temperature of the sample.

(c) Square-integrability after symmetrization

$$K(v, v') = \sqrt{\frac{v'M(v')}{vM(v)}}\,\Sigma(v, v') = K(v', v)$$

$$\int_0^\infty dv \int_0^\infty dv' \left|K(v, v')\right|^2 < \infty \tag{7}$$

(d) Existence of the quantity

$$N_\delta = \int_0^\infty dv \int_{\delta^2}^{\delta} dv' \left|vK(v, v')\right|^2, \tag{8}$$

where $N_\delta \to 0$ as $\delta \to 0$.

(e) The collision rate $h(v) = v$ is a continuous function of v and for $v > 0$ satisfies the condition

$$h(v) > \lim_{v \to 0} h(v) = -\alpha_0 > 0, \tag{9}$$

where α_0 is a finite negative number.

(f) The derivative of the collision rate exists on an open interval $(0, v_0)$ of a positive measure and is positive

$$\frac{d}{dv}h(v) > 0 \qquad v \in (0, v_0) \tag{10}$$

III. MATHEMATICAL SETTING

Introducing the new function

$$\psi(\vec{r}, v, \vec{\Omega}, t) = \frac{v}{\sqrt{vM(v)}}\,N(\vec{r}, v, \vec{\Omega}, t) \tag{11}$$

we can write Eq. (2) in the form

$$\frac{\partial \psi}{\partial t} = A\psi \tag{12}$$

$$A \cdot = -v\vec{\Omega}\,\mathrm{grad}\cdot - v\Sigma(v)\cdot + \frac{1}{4\pi}\int_0^\infty dv' \int_U d\vec{\Omega}' \cdot vK(v, v')\cdot .$$

The conditions of Eqs. (1) and (3) can be rewritten as

$$\psi(\vec{r}, v, \vec{\Omega}, 0) = \frac{v}{\sqrt{vM(v)}} F(\vec{r}, v, \vec{\Omega}) = F_1(\vec{r}, v, \vec{\Omega}) \tag{13}$$

and

$$\psi(\vec{r}, v, \vec{\Omega}, t) = 0 \tag{14}$$

respectively, for $\vec{r} \in S$, $t \geq 0$ and $\vec{\Omega}$ entering the sample.

Now we discuss the importance of a knowledge of the spectrum for the solution of the above initial value problem. The operator A does not depend on time. An application of the Laplace transform to Eq. (12) gives a formal solution of the problem

$$\psi(\vec{r}, v, \vec{\Omega}, t) = \frac{1}{2\pi i} \int_{b-i\infty}^{b+i\infty} d\lambda e^{\lambda t} [(\lambda - A)^{-1} F_1], \tag{15}$$

where b is taken right of the integrand singularities. The evaluation or estimation of Eq. (15) depends on a knowledge of the behaviour of $(\lambda - A)^{-1}F_1$. The singularities of this function are of particular importance. Thus we must study the operator $(\lambda - A)^{-1}$. This implies that we must study the spectrum [9] of the operator A. In fact HILLE [9] has shown that Eq. (15) has the definite mathematical meaning for operators which are infinitesimal generators of the strongly continuous semi-groups. We are not going to prove in this paper that A is a generator of a strongly continuous semi-group. We hope that it will be done in the near future. The information contained in our paper will be helpful for a presentation of Eq. (15) in a form useful for interpretations of experiments.

The action of the linear operator A is defined by Eq. (12). To proceed effectively in its study we must agree on the space of functions with which to work. Let $\mathscr{H}$ be the Hilbert space of the complex-valued functions $g(\vec{r}, v, \vec{\Omega})$ which are defined and square-integrable over the Cartesian product $V \otimes (0, \infty) \otimes U$, where the set V is open and its closure $\overline{V}$ is the convex sample. The scalar product and the norm are defined by Eqs. (16) and (17) respectively.

$$(g, h)_{\mathscr{H}} = \int_V d\vec{r} \int_0^\infty dv \int_U d\vec{\Omega}\, g(\vec{r}, v, \vec{\Omega}) \overline{h(\vec{r}, v, \vec{\Omega})} \tag{16}$$

$$||g||_{\mathscr{H}} = \sqrt{(g, g)_{\mathscr{H}}} \tag{17}$$

We investigate Eq. (12) on $\mathscr{H}$, together with the boundary conditions given by Eqs. (13) and (14) given on $S \otimes (0, \infty) \otimes U_e$, where $S = \overline{V} - V$ and U_e is a sub-set of U containing directions entering the sample.

The operator A on $\mathscr{H}$ has a domain D(A) for the set of functions $f \in \mathscr{H}$, which are absolutely continuous on all chords of the sample for each velocity v, which satisfy $S \otimes (0, \infty) \otimes U_e$ the homogeneous boundary conditions and are such that $Af \in \mathscr{H}$.

The operator $\frac{1}{4\pi} \int_U d\vec{\Omega}' \cdot$ is a projection on $\mathscr{H}$ to a sub-space defined as follows: L is the space of square-integrable functions defined on the domain $V \otimes (0, \infty)$ with the scalar product

$$(g, h)_L = \int_V d\vec{r} \int_0^\infty dv\, g(\vec{r}, v)\, \overline{h(\vec{r}, v)} \tag{18}$$

and the norm

$$||g||_L = \sqrt{(g, g)_L} \tag{19}$$

IV. SPECTRAL THEOREMS

First, we formulate two theorems describing properties of the generalized Peierls operator defined on L:

$$P_\lambda \cdot = \int_V d\vec{r}' \int_0^\infty dv' \left[\exp\left(- \frac{\lambda + h(v)}{v} |\vec{r} - \vec{r}'| \right) \Big/ 4\pi |\vec{r} - \vec{r}'|^2 \right] K(v, v') \cdot \tag{20}$$

and secondly we formulate four theorems concerning decomposition of the spectral plane of A on $\mathscr{H}$. The proofs of the theorems which are given below are contained in [7].

Theorem I: A necessary and sufficient condition that $\psi \in D(A)$ be an eigenfunction of A corresponding to λ with $\mathrm{Re}\,\lambda > \alpha_0$ is that there be a function $\theta \in L$ which satisfies the equation $(I - P_\lambda)\theta = 0$ for that λ-value.

Theorem II: The generalized Peierls operator P_λ on L is compact for $\mathrm{Re}\,\lambda > \alpha_0$.

Theorem III: The closed left half-plane $\mathrm{Re}\,\lambda \leq \alpha_0$ is contained in the spectrum of A.

Theorem IV: The open right half-plane $\mathrm{Re}\,\lambda > \alpha_0$ permits only a resolvent set and point spectrum of A .

Theorem V: There is no point spectrum of A with $\mathrm{Re}\,\lambda > \alpha_0$ and $\mathrm{Im}\,\lambda \neq 0$.

Theorem VI: There is no point spectrum of A on the open right half-plane $\mathrm{Re}\,\lambda > \alpha_0$ for sufficiently small samples.

Theorem I enables us to investigate the Peierls operator instead of the much more complicated unbounded operator A for $\mathrm{Re}\,\lambda > \alpha_0$. Theorem II is necessary to prove theorem IV. In fact, the Peierls operator exists for $\mathrm{Re}\,\lambda \leqq \alpha_0$ but it is not compact for $\mathrm{Re}\,\lambda < \alpha_0$. Theorem III eliminates the resolvent set for $\mathrm{Re}\,\lambda \leqq \alpha_0$ and therefore even if the point spectrum exists in this region, it cannot be separated from continuous or residual spectra. Since we are discussing the properties of A in the Hilbert space, we will never be allowed to move the contour of integration in Eq. (15) to the region $\mathrm{Re}\,\lambda \leqq \alpha_0$. Physically, the contribution from the contour $\mathrm{Re}\,\lambda = \alpha_0 + \epsilon$ (ϵ – small and positive number) will describe the transient phenomena in the case when the asymptotic mode exists. Theorem IV eliminates continuous and residual spectra for $\mathrm{Re}\,\lambda > \alpha_0$. It will enable us to deform the contour of integration in Eq. (15), taking into account only contributions from the point spectrum. Theorem V claims that these contributions can be located only on the real axis. In other words, there are no fundamental modes and "higher harmonics" with oscillating parts. Finally, theorem VI shows the lack of the normal modes of the following form:

$$N_i(\vec{r}, v, \vec{\Omega}, t) = C_i e^{\alpha_i t} n_i(\vec{r}, v, \vec{\Omega}), \tag{21}$$

where only C_i depends on the initial condition for small samples. Therefore we should be pessimistic about the meaning of pulsed experiments with small samples, as well as about consideration of "higher harmonics" with $\alpha_i < \alpha_0$.

V. APPLICABILITY OF SPECTRAL THEOREMS TO THE VARIOUS THERMALIZATION MODELS

We discuss now the applicability of the spectral theorems to the various thermalization kernels. In the last ten years a great amount of information has been obtained on the scattering of thermal neutrons in solids and liquids. Not all of these data are necessary for checking the validity of the assumptions contained in section II. Therefore we are going to discuss these special physical effects which decide the behaviour of the scattering kernel for large and small velocities or introduce singularities to the scattering kernel.

Because of assumption (a) in section II we are restricted to the isotropic thermalization kernels. In fact for light moderators, the anisotropy of scattering cannot be neglected in practical calculations. However, the anisotropy of scattering may not change the spectral properties of the transport operator. Some support for this opinion is given by the results obtained by MIKA [10] in the case of the one-velocity transport.

The condition (b) is valid for all media which are in the thermal equilibrium [11].

The discussion of assumption (c) is much more complicated. It is obvious that kernels including the effect of the elastic scattering in solids are not square-integrable, since they contain the delta function depending on energy transfer.

Now we prove that the isotropic part of the free gas kernel is square-integrable after symmetrization is performed.

The free gas kernel has the following form [12]:

$$\Sigma(v, v') = \sigma_0 \frac{(M+1)^2}{4M} \frac{v}{v'^2} \{\mathrm{erf}(\beta\theta v - \beta\eta v') \pm \mathrm{erf}(\beta\theta v + \beta\eta v')$$

$$+ e^{\beta^2(v'^2 - v^2)} [\mathrm{erf}(\beta\theta v' - \beta\eta v) \mp \mathrm{erf}(\beta\theta v' + \beta\eta v)]\}, \tag{22}$$

where σ_0 is the scattering nucleus-neutron cross-section independent of energy in the centre of the mass system, the upper sign being for $v < v'$ and the lower for $v > v'$. M is the mass of the nucleus, $\theta = (M+1)/2\sqrt{M}$ and $\eta = (M-1)/2\sqrt{M}$. Let us notice that for $v' > v$ the term

$$\mathrm{erf}(\beta\theta v' - \beta\eta v) - \mathrm{erf}(\beta\theta v' + \beta\eta v) = -\frac{2}{\sqrt{\pi}} \int_{-\beta\theta v' + \beta\eta v}^{\beta\theta v' + \beta\eta v} dt\, e^{-t^2} \tag{23}$$

is negative and since $\Sigma(v, v')$ is positive we have

$$\Sigma(v, v') \leq \sigma_0 \frac{(M+1)^2}{4M} \frac{v}{v'^2} [\mathrm{erf}(\theta\beta v - \eta\beta v') + \mathrm{erf}(\theta\beta v + \eta\beta v')]. \tag{24}$$

By introducing two parameters v_1 and γ, such that $0 < v_1 < \infty$ and $0 < \gamma < 1$, we obtain

$$I = \int_0^\infty dv' \int_0^\infty dv\, |K(v, v')|^2 = 2 \int_0^\infty dv' \int_0^{v'} dv \frac{v' M(v')}{v M(v)} (\Sigma(v, v'))^2$$

$$\leq \frac{\sigma_0^2 (M+1)^4}{8M^2} (k_1 + k_2 + k_3), \tag{25}$$

where

$$k_1 = \int_0^{v_1} dv' \int_0^{v'} dv \frac{\exp[\beta^2(v^2 - v'^2)]}{vv'} [\mathrm{erf}(\theta\beta v - \eta\beta v') + \mathrm{erf}(\theta\beta v + \eta\beta v')]^2$$

$$k_2 = \int_{v_1}^\infty dv' \int_{\gamma v'}^{v'} dv \frac{\exp[\beta^2(v^2 - v'^2)]}{vv'} [\mathrm{erf}(\theta\beta v - \eta\beta v') + \mathrm{erf}(\theta\beta v + \eta\beta v')]^2 \tag{26}$$

$$k_3 = \int_{v_1}^\infty dv' \int_0^{\gamma v'} dv \frac{\exp[\beta^2(v^2 - v'^2)]}{vv'} [\mathrm{erf}(\theta\beta v - \eta\beta v') + \mathrm{erf}(\theta\beta v + \eta\beta v')]^2.$$

Now

$$k_1 = \int_0^{v_1} dv' \int_0^{v'} dv \, \frac{\exp[\beta^2(v^2 - v'^2)]}{vv'} \left[\frac{2}{\sqrt{\pi}} \int_{-\theta\beta v + \eta\beta v'}^{\theta\beta v + \eta\beta v'} dt \, e^{-t^2} \right]^2$$

$$\leq \int_0^{v_1} dv' \int_0^{v'} dv \, \frac{\exp[\beta^2(v^2 - v'^2)]}{vv'} \left[\frac{2}{\sqrt{\pi}} \int_{-\theta\beta v + \eta\beta v'}^{\theta\beta v + \eta\beta v'} dt \right]^2$$

$$\leq \int_0^{v_1} dv' \int_0^{v'} dv \, \frac{1}{vv'} \left[\frac{2}{\sqrt{\pi}} \, 2\theta\beta v \right]^2 = \frac{\eta\theta^2\beta^2 v_1^2}{\pi} < \infty \qquad (27)$$

$$k_2 = \int_{v_1}^{\infty} dv' \int_{\gamma v'}^{v'} dv \, \frac{\exp[\beta^2(v^2 - v'^2)]}{vv'} \left[\frac{2}{\sqrt{\pi}} \int_{-\theta\beta v + \eta\beta v'}^{\theta\beta v + \eta\beta v'} dt \, e^{-t^2} \right]^2$$

$$\leq \int_{v_1}^{\infty} dv' \int_{\gamma v'}^{v'} dv \, \frac{v}{v^2} \, \frac{\exp[\beta^2(v^2 - v'^2)]}{vv'} \left[\frac{2}{\sqrt{\pi}} \int_{-\infty}^{\infty} dt \, e^{-t^2} \right]^2$$

$$\leq 4 \int_{v_1}^{\infty} dv' \, \frac{1}{\gamma^2 v'^3} \int_{\gamma v'}^{v'} dv \cdot v \cdot \exp[\beta^2(v^2 - v'^2)]$$

$$\leq \frac{2}{\beta^2\gamma^2} \int_{v_1}^{\infty} dv' \, \frac{1}{v'^3} (1 - \exp[-(1 - \gamma^2)\beta^2 v'^2)]$$

$$\leq \frac{2}{\beta^2\gamma^2} \int_{v_1}^{\infty} \frac{dv'}{v'^3} = \frac{\eta}{\beta^2\gamma^2} \, \frac{1}{v_1^2} < \infty$$

(27) (cont.)

$$k_3 = \int_{v_1}^{\infty} dv' \int_0^{\gamma v'} dv \, \frac{\exp[\beta^2(v^2 - v'^2)]}{vv'} \left[\frac{2}{\sqrt{\pi}} \int_{-\theta\beta v + \eta\beta v'}^{\theta\beta v + \eta\beta v'} dt \, e^{-t^2} \right]^2$$

$$\leq \int_{v_1}^{\infty} dv' \int_0^{\gamma v'} dv \, \frac{\exp[-\beta^2(1 - \gamma^2)v'^2]}{vv'} \left[\frac{2}{\sqrt{\pi}} \, 2\theta\beta v \right]^2$$

$$= \frac{4\theta^2\gamma^2}{\pi(1 - \gamma^2)} \exp[\beta^2(1 - \gamma^2)v_1^2] < \infty .$$

Finally from Eqs. (25) and (27) we have

$$I = \int_0 dv' \int_0 dv \left| K(v, v') \right|^2 < \infty \tag{28}$$

Hence we proved assumption (c) for the free gas kernel.

Now it will be shown that assumption (c) is not satisfied for those thermalization models where the effect of the molecular diffusion in liquids is taken into account. For these models the scattering laws have the following property [13] for small values of v and v':

$$S(\alpha,\gamma) = D\alpha/\gamma^2, \tag{29}$$

where

$$\alpha = \frac{v^2 + v'^2 - 2vv' \cos\theta}{2MT}$$

$$\gamma = \frac{v^2 - v'^2}{2T} \tag{30}$$

$$\cos\theta = \vec{\Omega} \cdot \vec{\Omega}'$$

D is a constant. We consider only the motions of the atoms so we can write

$$\Sigma(v, v') = v \int_U d\vec{\Omega}' \frac{\sigma_b}{4\pi} \frac{v}{v'} e^{-\gamma/2} S(\alpha, \gamma) \tag{31}$$

where σ_b is the bound-atom cross-section. By taking a number v_2, positive and sufficiently small so that Eq. (29) can be used, we have

$$\int_\epsilon^{v_2} dv \int_\epsilon^{v_2} dv' \left| K(v, v') \right|^2 = \left(\frac{2\sigma_b TD}{M} \right)^2 \int_\epsilon^{v_2} dv \int_\epsilon^{v_2} dv' \frac{vv'(v^2 + v'^2)}{(v^2 - v'^2)^4} \tag{32}$$

By introducing the polar co-ordinate system, one can easily check that the above integral diverges for $\epsilon \to 0$. Hence the diffusion in liquids leads to the kernel which is not square-integrable after symmetrization.

The proof of assumption (c) given by CORNGOLD [14] is valid in the case of inelastic scattering in solids.

Now we prove condition (d) for the free gas kernel. As for Eq. (24), we have for $v > v'$

$$\Sigma(v, v') \leq \frac{\sigma_0 (M+1)^2}{4M} \frac{v}{v'^2} \exp[\beta^2 (v'^2 - v^2)] \frac{2}{\sqrt{\pi}} \int_{-\theta\beta v' + \eta\beta v}^{\theta\beta v' + \eta\beta v} dt\, e^{-t^2} \tag{33}$$

Now

$$N_\delta = \int_{\delta^2}^{\delta} dv' \int_0^{\infty} dv \left| vK(v, v') \right|^2 < 2L_1 + L_2, \tag{34}$$

where

$$L_1 = \int_0^{\delta} dv \int_0^{v} dv' \left| vK(v, v') \right|^2 \leq \frac{\sigma_0^2 (M+1)^4}{16 M^2} \frac{2\theta^2 \beta^2 \delta^4}{\pi}$$

$$L_2 = \int_{\delta}^{\infty} dv \int_0^{\delta} dv' \left| vK(v, v') \right|^2 \leq \frac{\sigma_0^2 (M+1)^4}{16 M^2} \frac{4\theta^2 \beta^2 \delta^2}{\pi} . \tag{35}$$

The two above inequalities have been obtained similarly as the inequalities of Eqs. (27) using the relation (33). From Eqs. (34) and (35) we get

$$\lim_{\delta \to 0} N_\delta = 0 \tag{36}$$

as could have been expected.

Assumption (d) is also valid for the kernels describing inelastic scattering in solids since they are bounded [12] and have the same asymptotic behaviour as the free gas kernel.

The condition (e) is physically reasonable since the total collision rate h(v) should approach a minimum positive value in the limit where the neutron is still and is hit by moving scatterers. This condition has been discussed by NELKIN [1] and is valid for the free gas kernel [2].

Assumption (f) is necessary to prove theorem III. It is valid for the free gas kernel and from experimental data seems to be valid for solids.

In this section we have proved that the theorems of section IV are applicable to the isotropic part of the free gas kernel and to the isotropic models describing inelastic scattering in solids. It has been indicated that the models describing the diffusion in liquids and elastic scattering in solids do not satisfy the condition (c) and therefore the theorems of section IV are not applicable to them.

ACKNOWLEDGEMENT

It is a pleasure to thank Dr. R. Zelazny and Dr. A. Kuszell for several stimulating discussions and Dr. J. Mika for communicating his results before publication.

REFERENCES

[1] NELKIN, M., Physica 29 (1963) 261.
[2] ALBERTONI, S. and MONTAGNINI, B., On the time dependent transport equation for thermal neutrons in finite bodies, Università Degli Studi Di Milano (1964).
[3] LEHNER, J. and WING, G.M., Comm. pure appl. Math. 8 (1955) 217.
[4] LEHNER, J. and WING, G.M., Duke Math. J. 23 (1956) 125.
[5] PIMBLEY, G., J. Math. Mech. 8 (1959) 837.
[6] JÖRGENS, K., Comm. pure appl. Math. 11 (1958) 219.
[7] BEDNARZ, R., Report of Institute of Nuclear Research, Swierk, in print.
[8] DAVIDSON, B., Neutron Transport Theory, Clarendon Press, Oxford (1957).
[9] HILLE, E., Functional analysis and semi-groups, Amer. math. Soc., N.Y. (1948).
[10] MIKA, J., The initial value problem for a slab with anisotropic scattering, submitted for publication in J. math. Phys.
[11] HURWITZ, H., NELKIN, M.S. and HABETLER, G.J., Nucl. Sci. Engng 1 (1956) 280.
[12] TURCHIN, V.F., Slow Neutrons (in Russian), Moscow (1963).
[13] EGELSTAFF, P.A., Inelastic Scattering of Neutrons in Solids and Liquids, IAEA, Vienna (1961) 25.
[14] CORNGOLD, N., Rpt. BNL 7461 (1963).

DISCUSSION

(on the foregoing two papers)

N. CORNGOLD: Could Dr. Montagnini tell us what will happen to the point spectrum as the radius of the sphere becomes infinite?

B. MONTAGNINI: Our analysis is valid only for finite bodies. However, I think that the number of the eigenvalues will increase indefinitely as the radius of the sphere becomes infinite, in agreement with your own results relating to the infinite medium.

P. ZWEIFEL: Could Dr. Bednarz tell us which scattering he used and whether his results were the same as those of Dr. Montagnini?

R. BEDNARZ: I have shown that the results of Albertoni and Montagnini (except those which refer to a finite number of discrete roots) are valid for the square-integrable kernels after symmetrization. This class includes all models describing inelastic scattering in solids. The point spectrum disappears for sufficiently small samples in the case of all kernels belonging to the class.

J. MIKA: I would like to mention that the original results of Lehner and Wing for a slab can be extended to the case of anisotropic scattering, as pointed out by Dr. Montagnini. It turns out that the main spectral properties of the Boltzmann operator remain unchanged when anisotropic scattering is taken into account. The main peculiarity in the latter case is that the integral equation is replaced by a system of integral equations, which nevertheless conserves its compactness. A paper is to be published on this subject.

M. NELKIN: Does Mr. Bednarz' proof apply when Bragg scattering is included?

R. BEDNARZ: No, it does not.

M. NELKIN: When the apparent measured decay constants exceed $(v\Sigma)_{min}$ in crystalline assemblies, does this correspond to no fundamental mode, or would a fundamental mode with $\alpha < (v\Sigma)_{min}$ be established at later times? There have been indications pointing both ways in the papers we have heard.

P. SCHOFIELD (Chairman): In connection with the Bragg scattering, it seems to me that regardless of whether or not a fundamental mode exists, the whole phenomenon is going to be so complicated in a small assembly that it will not really be of much help in a physical situation to know whether it is there or not.

N. CORNGOLD: The precise analysis we have heard described fails in the case of the polycrystal because the appropriate scattering kernel is no longer square-integrable. It may be worth noting, however, that in the $\exp(iB \cdot r)$ theory the kernel may be made square-integrable by subtracting the elastic scattering from it right at the start. Perhaps a similar subtraction would work here, leaving us with a square-integrable kernel which satisfies the conditions of Dr. Montagnini and Dr. Bednarz. The analysis would proceed in the same way, with the total reaction rate being replaced by the inelastic part. But whether this can also be carried through in the case of the finite medium, I do not know.

M. KAZARNOVSKY: As pointed out in Dr. Corngold's paper and also in my lectures to the Summer School on Reactor Physics (Poland, September 1964), in the absence of a discrete spectrum of eigenvalues in the continuous spectrum range, quasi-discrete eigenvalues should exist close to the boundary of the continuous spectrum and should give rise almost to the same time dependence of the neutron density as normal discrete values. It would be interesting to elucidate the structure of the spectrum in the vicinity of these eigenvalues. It would be particularly interesting to know whether these values are shifted into the complex range.

P. SCHOFIELD: I should like to address an open question to the experts concerning the eigenvalues for the Einstein model. Since in this model only energies differing by a multiple of the oscillator energy are coupled, one will have a band of discrete time constants $\lambda_1(E)$ for $0<E<\theta$ (the oscillator energy). The question is what happens if we now introduce a low-frequency contribution which couples these modes together by allowing scattering between all energies?

M. NELKIN: I agree that an Einstein model does not give a proper approach-to-equilibrium, but I think that certain specific energy distributions can decay exponentially, thus giving well-defined eigenvalues.

N. CORNGOLD: What we have labelled an "Einstein model" is not the exact model that you are discussing. We first made the mass expansion and then specialized the frequency distribution to the Einstein shape. In this manner we avoided the subtle phenomena you mention.

TIME-DEPENDENT NEUTRON THERMALIZATION IN LIQUID MODERATORS H_2O AND D_2O

S. N. PUROHIT
AB ATOMENERGI,
STUDSVIK, NYKÖPING, SWEDEN

Abstract — Résumé — Аннотация — Resumen

TIME-DEPENDENT NEUTRON THERMALIZATION IN LIQUID MODERATORS H_2O AND D_2O. Theoretical studies of time-dependent thermal neutron spectra for the scattering models of H_2O and D_2O have been undertaken. Using the Boltzmann transport equation, these spectra have been numerically generated with a multigroup programme, NEFLUDI TDCS. From the calculated spectra, reaction rates for Cd, Sm and Gd, the resonance detectors, have been obtained.

In the case of light water studies, the free proton gas and the bound proton model of Nelkin have been employed as the scattering models. The source for thermal neutrons at $10^{-2}\mu s$, for these cases, has been obtained by the Ornstein-Uhlenbeck solution for the slowing down of a pulse of neutrons in hydrogen. Theoretical reaction rates obtained in these studies are compared with the results of the experiments of Möller and Sjöstrand. The proton gas model is found to be inadequate to explain the measured reaction rates. The oscillator model of Nelkin, for the bound protons in H_2O, improves the agreement between theory and experiment. However, some disagreement still persists. The effect of variation of the relative weight between the intramolecular vibrations and hindered rotations on the reaction rates has also been studied.

Theoretical reaction rates have also been determined for the neutron-scattering model of Butler for D_2O. The Von Dardel expression for the time-dependent neutron flux, in an infinite medium of deuterons, has been used to compute the source for the thermal neutrons in this study. A comparison of the theoretical reaction rates for H_2O and D_2O is also given.

The improvement of the Nelkin model with regard to two factors, (i) the relative weight between the dynamical modes and (ii) the structure of hindered rotations, is considered. The effect of the replacement of the delta function representation, for the hindered rotations in H_2O and D_2O, with the structure on the integral parameters has been discussed. The analysis of the integral experiments to obtain a parameter of the neutron scattering law for a moderator is proposed.

THERMALISATION D'UN FLUX DE NEUTRONS VARIABLE DANS LE TEMPS, AU MOYEN DES RALENTISSEURS LIQUIDES H_2O ET D_2O. L'auteur a fait des études théoriques sur les spectres des neutrons thermiques variables dans le temps pour les modèles de diffusion dans H_2O et D_2O. En utilisant l'équation de transport de Boltzmann, il a exprimé ces spectres numériquement à l'aide du programme à plusieurs groupes NEFLUDI TDCS. A partir du spectre calculé, il a obtenu les vitesses de réaction pour Cd, Sm et Gd, servant de détecteurs par résonance.

Lors des études sur l'eau légère, il a employé comme modèles de diffusion le modèle du gaz de protons libres et celui des protons liés établis par Nelkin. Il a alors obtenu la source pour les bouffées de neutrons thermiques d'une durée de $10^{-2}\mu s$ par la solution de Ornstein-Uhlenbeck relative au ralentissement d'une bouffée de neutrons dans l'hydrogène. Il compare les vitesses de réaction théoriques établies par ces études aux résultats des expériences de Möller et Sjöstrand. Il a constaté que le modèle du gaz de protons ne suffit pas pour expliquer les vitesses de réaction mesurées. Le modèle de l'oscillateur élaboré par Nelkin, pour les protons liés dans H_2O, assure une meilleur concordance entre la théorie et l'expérience. Cependant, plusieurs divergences continuent de subsister. L'effet que la variation du poids relatif entre vibrations intramoléculaires et rotations inhibées exerce sur les vitesses de réaction a également fait l'objet d'une étude.

Les vitesses de réaction théoriques ont été en outre déterminées pour le modèle de la diffusion des neutrons dans D_2O, élaboré par Butler. L'expression de von Dardel du flux de neutrons en fonction du temps dans un milieu deutéronique infini a permis de calculer la source pour les neutrons thermiques au cours de ces travaux. L'auteur compare aussi les vitesses de réaction théoriques pour H_2O et D_2O.

Il examine la possibilité d'améliorer le modèle de Nelkin en ce qui concerne les deux facteurs suivants: a) poids relatif entre les modes dynamiques; b) structure des rotations inhibées. L'effet d'une substitution de cette structure à la représentation au moyen de la fonction delta, pour les rotations inhibées dans H_2O et

D_2O, sur les paramètres intégraux fait l'objet d'une discussion. L'auteur propose d'analyser les expériences intégrales en vue d'obtenir un paramètre de la loi de diffusion des neutrons dans un ralentisseur.

ЗАВИСЯЩАЯ ОТ ВРЕМЕНИ ТЕРМАЛИЗАЦИЯ НЕЙТРОНОВ В ЖИДКИХ ЗАМЕДЛИТЕЛЯХ H_2O и D_2O. Проведены теоретические исследования зависящих от времени спектров тепловых нейтронов для моделей рассеяния H_2O и D_2O. С помощью больцмановского уравнения переноса цифровое выражение этих спектров получено в виде многогрупповой программы NEFLUDI TDCS. На основании рассчитанных спектров получены скорости реакций для Cd, Sm и Gd, являющихся резонансными детекторами.

При исследовании легкой воды в качестве моделей рассеяния использовали модель свободного протонного газа и модель связанных протонов Нелкина. Источник тепловых нейтронов со временем 10^{-2}мксек для этих исследований получен благодаря решению Орнштейна-Уленбека для замедления импульса нейтронов в водороде. Теоретические скорости реакций, полученные в результате этих исследований, сопоставляются с результатами экспериментов Меллера и Сьестранда. Модель протонного газа оказалась непригодной для объяснения измеренных скоростей реакций. Модель осциллятора Нелкина для связанных протонов в H_2O уменьшает расхождение между результатами теоретических расчетов и экспериментов. Однако все еще остается некоторое расхождение. Изучено также влияние изменения относительного веса между внутримолекулярными колебаниями и естественными вращениями на скорости реакций.

Определены теоретические скорости реакций для моделей рассеяния нейтронов Батлера для D_2O. Выражение Дарделла для зависящего от времени потока нейтронов в бесконечной среде дейтронов использовано для расчета источника тепловых нейтронов. Дается также сравнение теоретических скоростей реакций для H_2O и D_2O. Рассматривается вопрос об улучшении модели Нелкина в отношении двух факторов: 1) относительно веса между динамическими колебаниями и 2) структуры естественных вращений. Рассмотрено влияние на интегральные параметры замены выражения для дельта-функции для естественных вращений в H_2O и D_2O структурой. Предлагается анализ результатов интегральных экспериментов для получения параметра закона рассеяния нейтронов для замедлителя.

TERMALIZACION DE LOS NEUTRONES EN FUNCION DEL TIEMPO EN LOS MODERADORES LIQUIDOS H_2O Y D_2O. El autor ha estudiado teóricamente las variaciones temporales de los espectros de neutrones térmicos en los modelos de dispersión en H_2O y en D_2O. Los espectros se generaron numéricamente con un programa de grupos múltiples NEFLUDI TDCS basándose en la ecuación de transporte de Boltzmann, y a partir de ellos se obtuvieron las velocidades de reacción para los detectores por resonancia Cd, Sm y Gd.

Se estudia también el agua ligera empleando como modelos de dispersión el gas de protones libres y el modelo de protones enlazados de Nelkin. La fuente para los neutrones térmicos, de impulsos de $10^{-2}\mu s$, se obtuvo mediante la solución de Ornstein-Uhlenbeck para la moderación de una ráfaga de neutrones en hidrógeno. El autor compara las velocidades de reacción obtenidas teóricamente en estos estudios con los resultados de los experimentos de Möller y Sjöstrand. El modelo del gas de protones no explica las velocidades de reacción medidas; en cambio, el modelo del oscilador de Nelkin para los protones enlazados en H_2O hace concordar mejor la teoría con el experimento pero no elimina todas las discrepancias. También se estudia el efecto que se ejerce sobre la velocidad de reacción al variar las ponderaciones relativas entre las vibraciones intramoleculares y las rotaciones inhibidas.

Se determinaron las velocidades teóricas de reacción en el modelo de dispersión neutrónica de Butler para D_2O. Para calcular la fuente de neutrones térmicos se empleó en este estudio la expresión de von Dardel para la variación del flujo neutrónico en función del tiempo en un medio infinito de deuterones. La memoria compara también las velocidades teóricas de reacción en H_2O y D_2O.

El autor analiza el perfeccionamiento del modelo de Nelkin con respecto a dos factores: a) la ponderación relativa de los modos dinámicos, y b) la estructura de las rotaciones inhibidas. Se ha discutido el efecto que se produce en los parámetros integrales al sustituir con la estructura la representación de la función delta en el caso de rotaciones inhibidas en H_2O y D_2O. El autor propugna el análisis de los experimentos integrales para obtener un parámetro de la ley de dispersión de neutrones en un moderador.

1. INTRODUCTION

The early theoretical and experimental time-dependent neutron thermalization studies were limited only to the study of the transient spectrum in the diffusion period. The recent experimental measurements on the thermal neutron spectrum in graphite and reaction rates in H_2O covering the thermalization period, as reported at the last Brookhaven thermalization conference held in May 1962, have also generated considerable theoretical interest in the study of the time-dependent Boltzmann equation. In addition to the interpretation of the experiments, the theoretical studies also aim at the solution of the initial value problem for a set of scattering models.

In this paper, we present results for the theoretical reaction rates for Cd, Sm and Gd resonance detectors using the various scattering models for H_2O and D_2O. These reaction rates have been obtained from time-dependent thermal neutron spectra generated from the numerical solution of the Boltzmann equation. This study has been undertaken to interpret the integral time-dependent neutron thermalization experiments in liquid moderators, which are being performed at the AB Atomenergi. We have also attempted to discuss the importance of the study of the integral parameters, such as the Debye-Waller factor, the effective temperature and the second energy transfer moment weighted by the Maxwellian distribution, in order to investigate the details of the scattering law of a moderator. As an example, we have treated the bound proton model for H_2O in detail.

2. TIME-DEPENDENT BOLTZMANN EQUATION

The time behaviour of a pulse of neutrons undergoing moderation, thermalization and diffusion in a moderating medium is described by the time-dependent Boltzmann equation. Based upon the orthogonal space mode expansion and the diffusion theory approximation, we obtain

$$\sum_p \psi_p(\underline{r}) \left[\frac{1}{v} \frac{\partial \phi_p(E,t)}{\partial t} = -\left\{ \Sigma_{a_{eff}}(E) + \Sigma_s(E) \right\} \phi_p(E,t) + \int_0^\infty \Sigma_s(E' \longrightarrow E)\, \phi_p(E',t)\, dE' + Q\, \delta(E-E_s)\, \delta(t) \right]. \quad (1)$$

Assumptions involved in deriving this equation are given in the accompanying paper of PUROHIT and SJÖSTRAND [1]. $\phi_p(E,t)$ is the flux associated with the p-th spatial mode of geometrical buckling, B_p^2. Total and differential scattering cross-sections are represented by $\Sigma_s(E)$ and $\Sigma_s(E' \rightarrow E)$ terms respectively. $\Sigma_{a_{eff}}(E)$ is the effective absorption cross-section, $\Sigma_a(E)$ a sum of absorption cross-sections, and $D(E)B_p^2$ the leakage cross-sections.

In principle, one may construct the complete solution of $\phi(E,r,t)$ from the superposition of $\phi_p(E,t)$ solutions. However, in practice the study is usually limited to the fundamental spatial mode ($p = 0$) [2-5]. This paper is limited to the consideration of the infinite medium problem, $B^2 = 0$.

Alternatively, one may adopt the normal mode technique to obtain $\phi_p(E, t)$, as discussed in the accompanying paper [1]. However, this approach is more suitable for studying the transient spectra.

To determine $\phi(E, t)$ for thermal neutrons, the source for thermal neutrons and the scattering matrix for the scattering model under study are required.

2. 1. *The thermal neutron source, S(E, t)*

$$S(E, t) = \int_{E_T}^{E/\alpha} \Sigma_s(E' \to E)\, \phi(E', t)\, dE', \tag{2}$$

where E_T, the thermal cut-off energy, is assumed to be equal to 1. 02 eV, α is equal to $[(A - 1)/(A + 1)]^2$, with A equal to the ratio between the scattering atom and neutron masses.

For hydrogenous moderators, the time-dependent solution for the infinite medium problem as given by ORNSTEIN and UHLENBECK [6] may be used. For H_2O results presented in this paper, we assumed

$$\phi(E', t) = \Sigma_{s_0}^2\, t^2 \sqrt{E'} \exp(- t \Sigma_{s_0} \sqrt{E'}). \tag{3}$$

Σ_{s_0} is the free particle scattering cross-section taken to be equal to 1. 33 cm^{-1}. To account for the effect of binding for energies above E_T, the proton gas with an effective temperature (T_{eff}/T) has been used to calculate S(E, t) in Eq. (2).

$$\frac{T_{eff}}{T} = \int_0^\infty \left(\frac{\hbar\xi}{2k_BT}\right) f(\xi)\, \mathrm{Coth} \frac{\hbar\xi}{2k_BT} d\xi \tag{4}$$

$f(\xi)$ is the frequency spectrum of the dynamical modes. For the proton gas, $T_{eff}/T = 1$, and for the bound proton model of NELKIN [7] $T_{eff}/T = 4.66$.

For D_2O, $\phi(E', t)$ given by VON DARDEL [8] may be employed to obtain the thermal neutron source.

$$\phi(E', t) = (\Sigma_{s_0} t)^{\frac{2}{1-\alpha}} (\sqrt{E'})^{\left(\frac{1+\alpha}{1-\alpha}\right)} \exp\left\{ - \Sigma_{s_0} t \sqrt{E'} - \frac{b}{\Sigma_{s_0} t \sqrt{E'}} \right\} \tag{5}$$

According to ERIKSSON [9], the Von Dardel expression is in good agreement with the Swartholm's exact function for A = 2 and A = 12. The value of b is equal to 0. 903 for A = 2.

2. 2. *Thermal neutron scattering matrix*

In the neutron scattering formalism of VAN HOVE [10], the differential scattering cross-section, using the Gaussian incoherent approximation is given by the following well-known expression

$$\Sigma_s(E \rightarrow E') = \frac{\Sigma_b}{4\pi} \int_{-1}^{+1} \left(\frac{E'}{E}\right)^{1/2} \int_{-\infty}^{+\infty} \exp i\omega t \exp\left(\frac{\hbar^2 K^2}{2M}\ \gamma(t)\right) dt\, d\mu, \qquad (6)$$

where Σ_b is the bound atom scattering cross-section and $\hbar K$ and $\hbar\omega$ are the momentum and energy transfers between the neutron and moderating atom, respectively. For harmonic vibrations, the width function (mean square displacement of the vibrating atom)

$$\gamma(t) = -\lambda + \int_{-\infty}^{+\infty} \frac{f(\xi) \exp(-i\xi t\, d\xi)}{\hbar\xi \left(\exp \frac{\hbar\xi}{k_B T} - 1\right)}, \qquad (7)$$

where λ is the Debye-Waller integral.

$$\lambda = \int_0^{\infty} \frac{f(\xi)}{\hbar\xi} \operatorname{Coth} \frac{\hbar\xi}{2k_B T}\ d\xi. \qquad (8)$$

As noted earlier, $f(\xi)$ is the generalized frequency distribution (the frequency spectrum of phonons in solids and of the velocity auto-correlation function in liquids) and T is the thermodynamic temperature. $\hbar$ and k_B are the Planck and Boltzmann constants, respectively.

The dynamics of atomic motions in the bound proton model of NELKIN [7] and the BUTLER model [11] for D_2O are represented by the translational motion of the whole molecule plus the harmonic vibrations of four oscillators representing three intra-molecular vibrations and hindered rotations. For these models,

$$\frac{f(\xi)}{M} = \left[\frac{f_{gas}}{M_{mol}} + \sum_{i=1}^{4} \frac{\delta(\xi - \xi_i)}{M_i}\right]. \qquad (9)$$

In Table I, we give the weights of vibrations for the standard NELKIN model [7] and the two modified Nelkin models I and II used in this study. For the Butler model, the weights of vibrations for studying the neutron scattering by deuterons and oxygen atoms separately are also given.

Based upon the ZEMACH-GLAUBER formalism [12] using the above frequency spectrum one obtains

$$\Sigma_s(E \rightarrow E') = \int_{-1}^{+1} d\mu \left[\left(\frac{E'}{E}\right)^{1/2} \exp(-2W) \prod_{i=1}^{4} \left\{\sum_{n_i=-\infty}^{+\infty} I_{n_i}(Z_i) \exp\left(\frac{-\hbar\alpha}{2k_B T}\right) S_{gas}(K, \omega')\right\}\right]. \qquad (10)$$

TABLE I

PARAMETERS OF THE SCATTERING MODELS OF H_2O AND D_2O

Parameter	H_2O			D_2O (Butler)	
	Nelkin	Nelkin I	Nelkin II	Deuteron	Oxygen
x	0.397	0.222	0.674	0.325	0.424
M_r/m	2.32	1.764	3.195	4.39	181.8
M_v/m	5.84	7.94	4.74	13.52	428.6

Note: $x = \frac{M_r \text{ (effective mass for hindered rotations)}}{M_v \text{ (effective mass for each intra-molecular vibration)}}$

In the above expression, $2W$, $I_{n_i}(Z_i)$ and $S_{gas}(K, \omega')$ represent the Debye-Waller factor (for four oscillators), the modified Bessel function of the first kind and the scattering law for the gas model, respectively. Z_i, ω' and α are defined as follows

$$Z_i = \frac{\hbar K^2}{2M_i \xi_i \operatorname{Sinh} \frac{\hbar \xi_i}{2k_B T}} \tag{11}$$

and

$$\omega' = \omega - \alpha \quad \text{and} \quad \alpha = \sum_i n_i \xi_i \tag{12}$$

The scattering matrices for the Nelkin and Butler models with the parameters listed in Table I were obtained from the Gaker code of HONECK [13]. This code calculates the incoherent scattering matrix for the model of free translational mass and two harmonic oscillators based upon the simplified version of the above Eq. (10). In the case of H_2O, the contribution of oxygen atoms is neglected. However, for D_2O separate matrices for oxygen and deuterons have been obtained and added together.

2.3. Numerical solution

The Boltzmann equation for thermal neutrons is transformed into a set of linear algebraic equations using the multigroup formalism. The numerical solution of the transformed equations is obtained by two multigroup programmes - NEFLUDI and NEFLUDI TDCS prepared by L. Persson in collaboration with K. Nyman, for the Ferranti Mercury computer. Both programmes require the thermal group cross-sections and the thermal neutron source as the input data and handle twenty-two energy groups, because of the machine storage capacity.

The NEFLUDI code generates the flux distribution $\phi(E, t)$ and reaction rates for 1/v absorbers and for three resonance detectors (Cd, Sm and Gd), using the given scattering matrix at each time point. However, in the modified version NEFLUDI TDCS, the group-sections are obtained with the calculated time- and energy-dependent fluxes at a few time points during the run as the weighting factors. Detailed results obtained with the NEFLUDI have been given elsewhere [14]. In this paper, we shall present the results obtained with the NEFLUDI TDCS.

3. REACTION RATES FOR H_2O

Time-dependent thermal neutron spectra have been numerically generated for the proton gas model and three cases of the bound proton model given in Table I (Nelkin model, modified Nelkin I and II) using the source integral for thermal neutrons as described in section 2.1. Qualitatively, the proton gas and the Nelkin model spectra are similar. However, quantitative differences exist. The thermal groups between 0.1 and 1.02 eV reach a distinct maximum before decaying, which indicates strong downward scattering. On the other hand, each group below 0.1 eV has a broad maximum (which disappears with the decrease in energy) followed by an asymptotic level.

In this paper, we present detailed numerical results only for the reaction rates from the above spectra. Time-dependent thermal neutron spectrum results will be given elsewhere. To undertake a comparative study of different scattering models, a set of reaction rate parameters are listed in Table II. The available experimental results are also given.

3.1. Proton gas and Nelkin model

In Fig. 1, we present the theoretical reaction rates for the proton gas and the Nelkin model for H_2O for three resonance detectors, Cd, Sm and Gd.

TABLE II

REACTION RATE PARAMETERS FOR Cd AND Sm FOR H_2O

Model	Cd			Sm		
	R_{peak}/R_{level}	t_{peak}	t_{th} (μs)	R_{peak}/R_{level}	t_{peak}	t_{th} (μs)
Proton gas	1.84	3.49	3.39 ± 0.16	1.25	5.73	3.56 ± 0.05
Nelkin	1.96	3.49	4.51 ± 0.15	1.31	5.73	4.88 ± 0.16
Nelkin I	1.94	3.49	-	1.29	5.73	-
Nelkin II	2.06	3.49	-	1.36	5.73	-
Experiment	1.91	4.1 ± 0.2	4.1 ± 0.4	1.29	6.1	-

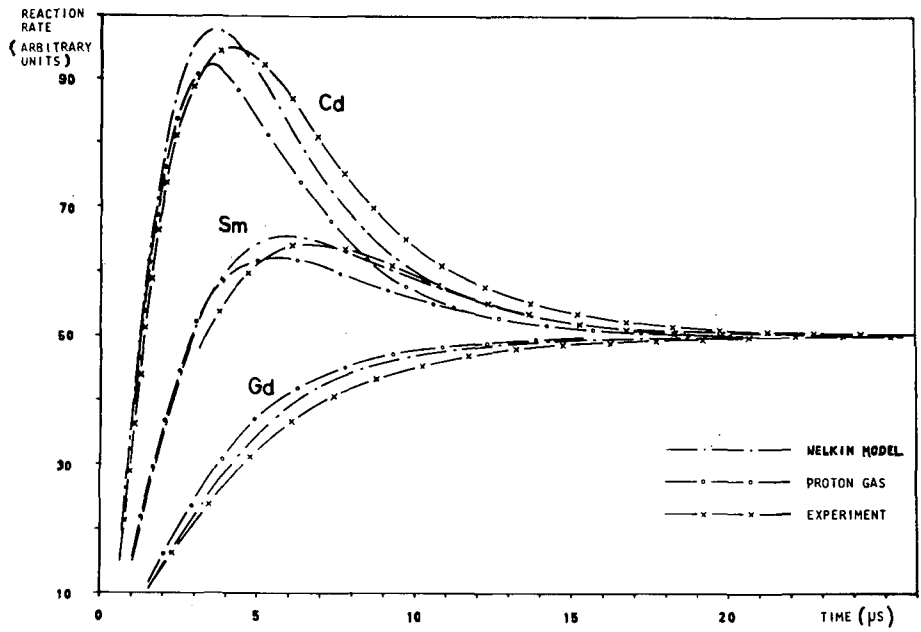

Fig. 1

Reaction rate curves for Cd, Sm and Gd corrected to zero absorption for H_2O
All the curves are normalized at the final level.

The experimental results of MÖLLER and SJÖSTRAND [15] are also shown. All the curves have been normalized to a level value of 50 and correspond to the zero absorption case.

The comparison between theoretical and experimental results demonstrates that the proton gas model is inadequate to explain the experimental results for all three detectors. The ratios of R_{peak}/R_{level} for Cd and Sm, using the gas model, are equal to 1.84 and 1.25 respectively compared to the experimental values of 1.91 and 1.29 respectively. The average thermalization time constant for the proton gas model is estimated to be equal to 3.48 ± 0.1 μs (see Table II), while the experimental value of Möller and Sjöstrand is equal to 4.1 ± 0.4 μs.

The Nelkin model reaction rates are in better agreement with the experimental results than the gas case. Nevertheless, there still exists some disagreement. (See Fig. 1 and also Table II.) The estimated average thermalization time constant for the Nelkin model is equal to 4.69 ± 0.15 μs. It is higher than the experimental value. The difference between theoretical and experimental values lies outside the range of the uncertainty involved in the fitting of the exponential. Thermalization time constant values for the gas and Nelkin models have been obtained by fitting the reaction rate beyond 10 μs by a single exponential, as has been undertaken in the experiment. The average of several fittings is given in Table II.

3. 2. Modified Nelkin models

It is well-known that the application of the Sachs-Teller mass tensor concept has introduced some uncertainty in the assignment of the relative weight, x, between one intra-molecular vibration and hindered rotations in the Nelkin model. To investigate the effect of the variation of x on the reaction rates, we repeated the calculations for the modified Nelkin models I and II. In Fig. 2, R(t) for these two cases I and II (corresponding to x = 0. 222 and 0. 674 respectively) along with the original Nelkin model (x = 0. 397) and experimental results are also shown.

From the study of the results given in Fig. 2 and Table II we note that an increase in the contribution of intra-molecular vibrations (in modified Nelkin II) enlarges the disagreement between theory and experiment around the peak. On the other hand, an increase in the contribution of the hindered rotations in modified Nelkin I slightly diminishes this disagreement.

4. REACTION RATES FOR THE MODELS OF D_2O

To make a comparative study of three scattering models of D_2O (the Butler model with the parameters of Table I and two gas models of masses equal to 3. 6 (BROWN and ST. JOHN [16]) and 2, with the contribution of oxygen as a gas of mass 16 for both the gas models) time-dependent thermal

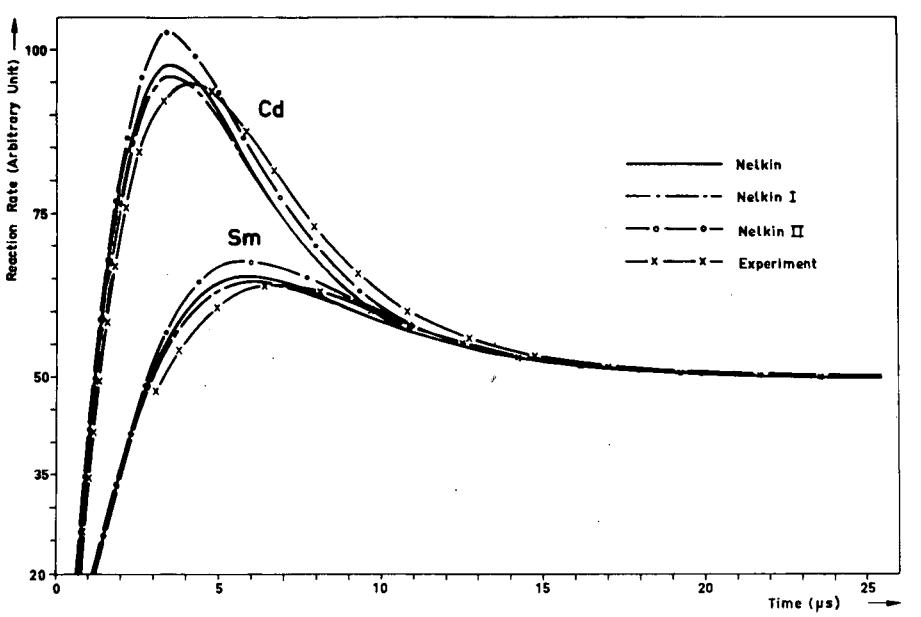

Fig. 2

Reaction rate curves for Cd and Sm corrected to zero absorption for H_2O obtained by varying the relative weight between one intra-molecular vibration and hindered rotations (See Table I.)

neutron spectra and the reaction rates for three resonance detectors Cd, Sm and Gd were obtained.

The Von Dardel expression given in section 2.1 has been used to obtain the thermal neutron source with an initial time of 1 μs. The contribution of the scattering of neutrons by oxygen atoms in the calculation of thermal neutron source has been neglected. The scattering matrices for the above three models of D_2O have been calculated assuming the free-particle scattering cross-section to be equal to 3.46 cm^{-1}.

In Fig. 3, we plot the reaction rates for Cd and Sm for three scattering models of D_2O. The Cd reaction rate from the preliminary experiments of D_2O, as communicated by Möller is also shown. All the curves have been normalized to a value of 50, assuming the level at 410 μs and are for the zero absorption case. The values of t_{peak} for Cd are equal to 24.2, 25, 8 and 22.6 μs for the Butler model and for the two gas models of mass 3.6 (Brown and St. John) and of mass 2, respectively. For Sm similar values are 41.8, 41.8 and 35.4 μs. R_{peak}/R_{level} for Cd corresponding to the above three models in the same order are equal to 2.50, 2.52, and 2.28 and for Sm, these values are equal to 1.49, 1.47 and 1.39. The experimental value of t_{peak} for Cd is equal to 26.6 μs and R_{peak}/R_{level} is equal to 1.11*

From the reaction rate curves in Fig. 3 as well as from the above results we conclude that the difference between the results given by the Butler and gas (mass 2) models is significant. On the other hand, the Butler and the Brown and St. John models give similar reaction rates. It is of interest to compare R_{peak}(Butler)/R_{peak}(deuteron gas) for Cd and Sm, which is equal to 1.09 and 1.07 respectively, with R_{peak}(Nelkin)/R_{peak}(proton gas) for these cases which is equal to 1.065 and 1.048 respectively. This demonstrates that the experimental reaction rate studies may also confirm the existence of the similar dynamics of atomic motions in H_2O and D_2O.

5. MODIFICATION OF THE NELKIN MODEL FOR H_2O

The NELKIN model [7] in the present form has proved extremely valuable in the interpretation of the early integral measurements on the total scattering cross-section and the infinite medium thermal neutron spectra. However, it is now being recognized that the model needs improvement along two lines: (i) the replacement of the delta function representation of the hindered rotations by the structure, and (ii) the assignment of the realistic relative weight between the intra-molecular vibrations and hindered rotations.

---

* The preliminary value of the average thermalization time constant is estimated to be equal to 33 μs compared to 33 ± 4 μs given by Möller [MÖLLER, E., "Neutron moderation studied by the time-dependent reaction rate method", these Proceedings I.; See also POOLE, M. J. and WYDLER, P., "Measurement of the time-dependent spectrum in heavy water" and WALKER, J., BROWN, J. B. C. and WOOD, J., "Extrapolation distances for pulsed neutron experiments", these Proceedings I.] The time required for the establishment of the asymptotic neutron distribution in H_2O and D_2O is estimated to be equal to 30 and 230 μs, respectively.

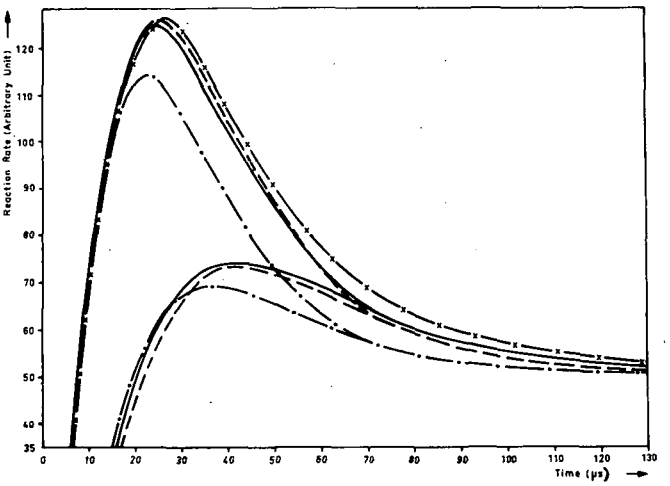

Fig. 3

Reaction rate curves for Cd and Sm corrected to zero absorption for three models of D_2O

- - - - - Brown and St. John (gas mass 3.6)

——— Butler model

-.-.-.- Gas model 2

-x-x- Möller

5. 1. Structure of hindered rotations of H_2O and D_2O

The cold neutron scattering studies of LARSSON and DAHLBORG [17], and EGELSTAFF, HAYWOOD and THORSON [18] have demonstrated the existence of a structure for the hindered rotations of H_2O and D_2O molecules. The experimentally derived frequency spectra are handicapped by the limitation of the extrapolation method in Egelstaff's case and by approximations involved in obtaining the Debye-Waller factor and multiphonon corrections in Larsson's case. Nevertheless, these spectra do provide detailed information about the structure of hindered rotations which perhaps play the predominant role in the process of neutron thermalization.

To investigate the effect of replacing the delta function representation by the structure for hindered rotations it may be useful to study the integral parameters such as the Debye-Waller integral (λ) and the effective temperature T_{eff}/T. In Table III, we present results for the contribution of hindered rotations to λ and T_{eff}/T for H_2O at 365, 295 and 275°K and for D_2O at 428 and 295°K. For each temperature, two cases are given. The first case corresponds to the structure for hindered rotations as given by the experiments of Larsson and Dahlborg and the second to the oscillator representation. The equivalent oscillator energies obtained from the first case are also listed for comparison.

From these results, it is evident that to duplicate even two integral parameters the representation of hindered rotations by a delta function is

TABLE III

DEBYE-WALLER INTEGRAL (λ) AND T_{eff}/T FOR HINDERED ROTATIONS OF H_2O AND D_2O

Moderator (°K)	$(\hbar\xi_0)_{peak}$ (eV)	$(\lambda T)_{Exp}$	$(\lambda T)_{Osc}$	$\left(\frac{T_{eff}}{T}\right)_{Exp}$	$\left(\frac{T_{eff}}{T}\right)_{Osc}$	$(\hbar\xi_0)_{D.W.}$ (eV)	$(\hbar\xi_0)_{T_{eff}}$ (eV)
D_2O							
428	0.043	1.65	1.61	1.20	1.11	0.042	0.059
295	0.05	0.73	0.67	1.47	1.30	0.047	0.064
H_2O							
365	0.06	1.04	0.71	1.33	1.29	0.048	0.066
295	0.063	0.67	0.47	1.50	1.47	0.05	0.066
275	0.073	0.56	0.35	1.64	1.69	0.052	0.069

inadequate. This is supported by the study of $\Sigma_s(E \rightarrow E')$ in [18] which has shown that the inclusion of the structure for hindered rotations for H_2O improves the agreement between theoretical and experimental results.

The calculation of the scattering matrix using the experimental frequency spectrum would require the multiphonon treatment of SJÖLANDER [19] or of EGELSTAFF and SCHOFIELD [20]. This will involve the use of a large machine programme such as the LEAP of Harwell. Alternatively, it is proposed that the Zemach-Glauber formalism Eq. (10) may be employed with the correct value of the Debye-Waller factor taking into account the structure for hindered rotations. This is feasible as this factor appears explicitly in Eq. (10). At the same time one may assign an equivalent oscillator energy to the hindered rotations from the T_{eff}/T parameter. This procedure will enable the use of the present oscillator codes and will also take into account the structure of hinderd rotations in an approximate manner.

5. 2. Relative weight between dynamical modes

At present, the exact theoretical and experimental estimates of relative weights between various dynamical modes of the H_2O molecule are not available. The present neutron scattering experiments do not cover the energy transfers of the magnitude of intra-molecular vibrations. Attempts have been made to obtain the relative weight, x, between one intra-molecular vibration and hindered rotations from the neutron scattering law data. (See [18] and [21].) In the latter study,the value of $x = 0.674$ has been obtained. This value is the basis of the modified Nelkin model II used in the reaction rate studies described in section 3. 2.

Theoretically, the problem is complicated by the lack of understanding of the hindered rotations. In a recent paper, YIP and OSBORN [22] treated hindered rotations as small angle rotations of a molecule having the permanent electric dipole moment μ in the local electric field of intensity ϵ generated by the neighbouring molecules. The energy associated with the torsional oscillator has been found to be equal to $\sqrt{2\lambda B}$, where $\lambda = \mu x \epsilon$ and B is the rotational constant. Using $\lambda = 0.825$ eV and $B = 2.2 \times 10^{-3}$ eV, one obtains the oscillator energy equal to 0. 06 eV. It may be of interest to compare the weight of the oscillator in the Yip-Osborn and Nelkin models. Though a direct comparison is not feasible, one may compare the coefficient of the K^2 term in the intermediate scattering function for the two cases and obtain an effective mass for the hindered rotations in the Yip-Osborn case. It is found to be equal to $\frac{3}{4} Bb^2$, with b equal to the nuclear distance from the centre-of-mass. For $b = 0.9 \times 10^{-9}$ cm and $B = 2.2 \times 10^{-3}$ eV, one obtains $M_r/m = 1.764$ compared to 2. 32 in the Nelkin model. The former value is the basis of the modified Nelkin model I. (See also [23].)

In Fig. 4, the variations of λ(structure)/λ(oscillator), $T_{eff}/T4t$ and M_2(bound proton)/M_2(proton gas) are plotted as a function of the relative weight between one intra-molecular vibration and hindered rotations. The value of M_2 has been obtained by calculating the first term of the mass expansion exactly and the correction factor due to the Doppler approximation. This procedure has been discussed in detail in [23] and [1]. It is of interest to note that λ and M_2 decrease by a factor of 1. 16 and 1. 43 respectively,

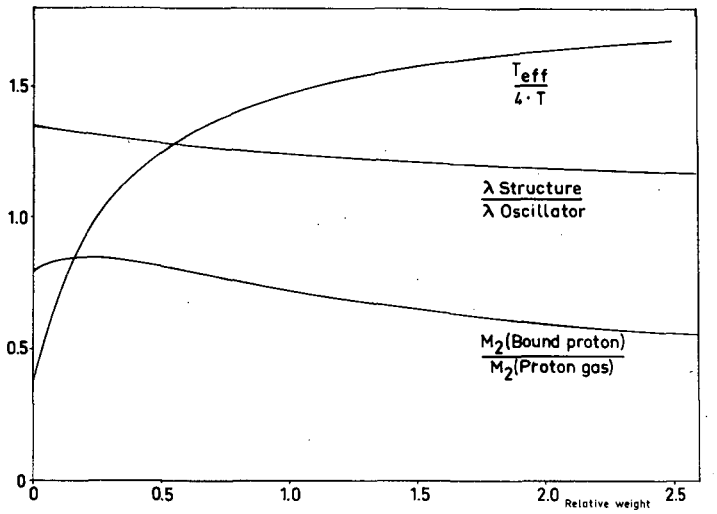

Fig. 4

The variation of M_2, T_{eff}/T and λ, the Debye-Waller integral with relative weight between one intra-molecular vibration and hindered rotations of H_2O.

when x varies from zero to 2.5. On the other hand, $T_{eff}/4T$ increases by a factor of 4.5 over the same range of x. One may therefore conclude that T_{eff}/T is strongly dependent on the contribution of the intra-molecular vibrations, M_2 depends primarily upon the contribution of hindered rotations and λ is sensitive to the variation in structure for hindered rotations.

6. INTEGRAL EXPERIMENTS AND SCATTERING LAW

The study of the variation of a parameter of thermal neutrons, such as the thermalization time constant (or the diffusion cooling coefficient, the diffusion length and the re-thermalization cross-section) with a parameter of epithermal neutrons, such as the effective temperature of the moderator, may be employed to investigate the details of the scattering law for a moderator. The thermal neutron parameters are given by the time and space transient experiments. The effective temperature is given by the deviation of the total scattering cross-section $\Sigma_s(E)$ from the free particle value Σ_{s_0}, as shown by PLACZEK [24] and also by the deviation of the asymptotic flux from the Fermi spectrum, as given by CORNGOLD [25].

In Fig. 5, the thermalization time constant $t_{th}/t_{th}(\text{gas})$ is plotted as a function of T_{eff}/T for six moderators - H_2O, D_2O, Be, BeO, graphite and CH_2. For the crystalline moderators the frequency spectra described in the accompanying paper [1] have been used. Results for CH_2 are based upon the parameters of GOLDMAN and FEDERIGHI [26]. $t_{th}/t_{th}(\text{gas})$ has been obtained by estimating t_{th} in the L_1^1 approximation and using the exact values of $t_{th}(\text{gas})$.

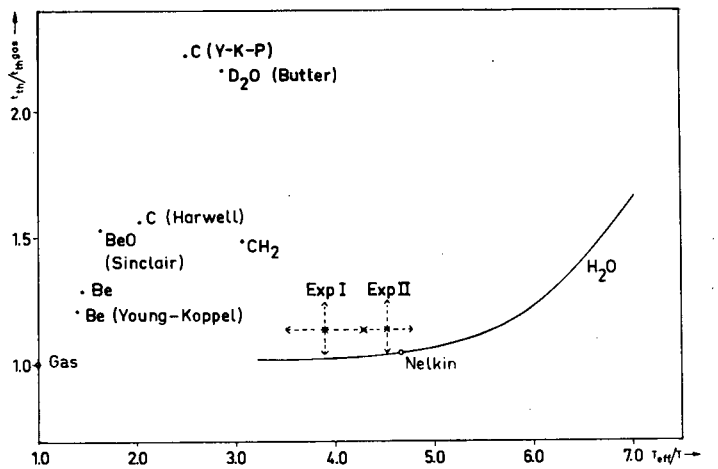

Fig. 5

Thermalization time constant $t_{th}/t_{th}(gas)$ versus T_{eff}/T for several moderators at room temperature

For H_2O, theoretical results obtained by varying the relative weight between one intra-molecular vibration and hindered rotations are also given. Two points, Exp. I and II, corresponding to available experimental results are also shown. In Exp. I and II T_{eff}/T values given by POOLE et al. [27] and BEYSTER et al. [28] have been used. These values are equal to 3.9 ± 0.4 and 4.52 ± 0.24 respectively. The time constant value of (4.1 ± 0.4) μs in both cases corresponds to the experimental results of MÖLLER and SJÖSTRAND [15]. The theoretical curve is fixed in the horizontal direction, as T_{eff}/T can be exactly calculated. The L_1^1 approximation gives the lowest value of the thermalization time constant, therefore, the effect of higher polynomials is to raise this curve. As the theoretical curve is flat within the range of experimental uncertainty, even if we raise the theoretical curve by 20% the theoretical model predicted from the experimental results does not alter. Exp. II point agrees with the Nelkin model; however, Exp. I point is in better agreement with the modified Nelkin model I.

7. CONCLUSION

The present reaction rate and integral parameter studies are sensitive enough to distinguish between the gas model and the bound model of a moderator. The investigation of the effect of the details of a scattering law (such as the structure of hindered rotations in H_2O and D_2O) on the reaction rates of the resonance detectors would require further studies of the factors which contribute to the uncertainty in theoretical and experimental results. The study of two integral parameters, as discussed in section 6, may be exploited to discriminate between two frequency spectra of the dynamical modes of

the same moderator or to investigate a specific detail of a scattering law (such as the relative weight between one intra-molecular vibration and hindered rotations in the H_2O molecule). As shown in Fig. 5, there is always one point in this study given by the experiments which corresponds to the real moderator. The theoretical problem is therefore reduced to matching this point.

The study of the degree of chemical binding for protons in various hydrogenous moderators at several temperatures is feasible with the help of the reaction rate and integral parameter studies as shown by the example of H_2O in this paper.

ACKNOWLEDGEMENTS

The author extends his thanks to Drs. R. Pauli and E. Möller and Professor N. G. Sjöstrand for many stimulating discussions. He also appreciates the effort of the numerical group in undertaking the computations, especially those of Mr. L. Persson.

REFERENCES

[1] PUROHIT, S. N. and SJÖSTRAND, N. G., "Neutron thermalization parameters", these Proceedings I.
[2] PUROHIT, S. N., Nucl. Sci. Engng 9 (1961) 305.
[3] BERNARD, E. et al., Nucl. Sci. Engng 17 (1963) 513.
[4] GHATAK, A. K. and HONECK, H. C., J. nucl. Energy A/B 19 (1965) 1.
[5] OHANIAN, M. J. and DAITCH, P. B., Nucl. Sci. Engng 19 (1964) 329.
[6] ORNSTEIN, L. S. and UHLENBECK, G. E., Physica 4 (1937) 478.
[7] NELKIN, M. S., Phys. Rev. 119 (1960) 741.
[8] VON DARDEL, G. F., Trans. roy. Inst. Techn., Stockholm No. 75 (1954).
[9] ERIKSSON, K. E., Ark. Fys. 16 (1958) 1.
[10] VAN HOVE, L., Phys. Rev. 95 (1954) 249.
[11] BUTLER, D., Proc. phys. Soc. 81 (1963) 276.
[12] ZEMACH, A. C. and GLAUBER, R. J., Phys. Rev. 101 (1956) 118.
[13] HONECK, H., Rpt. BNL-5826 (1961).
[14] PUROHIT, S. N. and PERSSON, L., Time dependent thermal neutron spectra and reaction rates for scattering models of H_2O (NEFLUDI) Part I, (RFR-283, AB Atomenergi internal report) (1964).
[15] MÖLLER, E. and SJÖSTRAND, N. G., Ark. Fys. 27 (1964) 501.
[16] BROWN, H. D. and St. JOHN, D. S., Rpt. DP-33 (1954).
[17] LARSSON, K. E. and DAHLBORG, U., J. nucl. Energy 16 (1962) 81.
[18] EGELSTAFF, P. A., HAYWOOD, B. C. and THORSON, I. M., Inelastic Scattering of Neutrons in Solids and Liquids I IAEA, Vienna (1963) 343-56.
[19] SJÖLANDER, A., Ark. Fys. 14 (1958) 315.
[20] EGELSTAFF, P. A. and SCHOFIELD, P., Nucl. Sci. Engng 12 (1962) 260.
[21] BEYSTER, J. R., Integral neutron thermalization, Rpt. GA-3853 (1963).
[22] YIP, S. and OSBORN, R. K., Phys. Rev. 130 (1963) 1860.
[23] PUROHIT, S. N., Integral parameters of the thermal neutron scattering law, Rpt. AE-154 (1964).
[24] PLACZEK, G., Phys. Rev. 96 (1954) 1228.
[25] CORNGOLD, N., Ann. Phys. 6 (1959) 368, 11 (1960) 338.
[26] GOLDMAN, D. T. and FEDERIGHI, F. D., Rpt. BNL-719, 1 (1962) 100.
[27] POOLE, M. J., SCHOFIELD, P. and SINCLAIR, R. N., Exponential and Critical Experiments III (1963) 87-110.
[28] BEYSTER, J. R. et al., Integral neutron thermalization, Rpt. GA-4659 (1964).

NEUTRON THERMALIZATION PARAMETERS

S. N. PUROHIT
AB ATOMENERGI, STUDSVIK, NYKÖPING
AND
N. G. SJÖSTRAND
CHALMERS UNIVERSITY OF TECHNOLOGY, GÖTEBORG, SWEDEN

Abstract — Résumé — Аннотация — Resumen

NEUTRON THERMALIZATION PARAMETERS. A critical discussion of the neutron thermalization parameters employed to describe the transient time and space-dependent phenomena is presented. These parameters are (i) M_2, the second energy transfer moment of the scattering kernel weighted by the Maxwellian distribution, (ii) the thermalization time constant, (iii) the diffusion cooling coefficient, (iv) the absorption cooling coefficient, (v) the rethermalization length, (vi) the diffusion heating coefficient, and (vii) the limit of the decay constant $(v\Sigma_s)_{min}$. The determination of the time and space transient parameters using the polynomial representation for the energy part of the neutron flux is discussed. Based upon the low-order polynomial expansion, interrelationships between various parameters are obtained. Limitations of these expressions in the analysis of transient phenomena are pointed out.

An attempt is made to compare theoretical and experimental results for several moderators. Theoretical M_2 values are obtained using the first term of the Placzek mass expansion and the correction with the generalized Doppler approximation. In these calculations available theoretical or derived frequency spectra of the dynamical modes of the moderators are used.

Various experimental methods for the determination of neutron thermalization parameters are compared. The uncertainties and limitations of the different methods are pointed out. Available experimental data are surveyed and a list of "best values" is suggested. The comparison between theoretical and experimental data shows that a large theoretical and experimental effort is needed to obtain a full understanding of the results.

PARAMÈTRES DE LA THERMALISATION DES NEUTRONS. Les paramètres de la thermalisation des neutrons utilisés pour décrire les phénomènes transitoires dépendant du temps et de l'espace font l'objet d'un examen critique. Ces paramètres sont les suivants: a) M_2 moment de transfert d'énergie du deuxième ordre du noyau de diffusion pondéré par la distribution maxwellienne; b) constante de temps de la thermalisation; c) coefficient de refroidissement par diffusion; d) coefficient de refroidissement par absorption; e) longueur de rethermalisation; f) coefficient d'échauffement par diffusion; g) limite de la constante de décroissance $(v\Sigma_s)_{min}$. Les auteurs examinent la possibilité de déterminer les paramètres des phénomènes transitoires dépendant du temps et de l'espace en représentant l'énergie du flux de neutrons sous la forme d'un polynôme. En se fondant sur le développement d'un polynôme de faible degré, on obtient des relations entre divers paramètres. Les auteurs indiquent les limitations de ces expressions dans l'analyse de phénomènes transitoires.

Ils essaient de comparer les résultats théoriques et expérimentaux pour plusieurs ralentisseurs. Ils obtiennent les valeurs théoriques de M_2 en utilisant le premier terme du développement de Placzek selon la masse et la correction au moyen de l'approximation généralisée de Doppler. Dans ces calculs, ils ont recours aux spectres de fréquence théoriques ou dérivés dont on dispose pour les modes dynamiques des ralentisseurs.

Ils comparent différentes méthodes expérimentales permettant de déterminer les paramètres de la thermalisation des neutrons et indiquent les marges d'incertitude et les limitations de ces méthodes. Ils donnent un aperçu des données experimentales disponibles et proposent une liste des «meilleures valeurs». La comparaison entre les données expérimentales et théoriques montre que d'importants travaux théoriques et expérimentaux sont encore nécessaires pour parvenir à une parfaite compréhension des résultats.

ПАРАМЕТРЫ ТЕРМАЛИЗАЦИИ НЕЙТРОНОВ. Критически рассматриваются параметры термализации нейтронов, используемые для описания зависящих от времени и пространства переходных явлений. Этими параметрами являются: 1) M_2 – второй момент передачи энергии интегрального ядра рассеяния, взвешенный по максвелловскому распределению; 2) постоянная времени термализации; 3) коэффициент диффузионного охлаждения; 4) коэффициент

абсорбции охлаждения; 5) длина ретермализации; 6) коэффициент диффузионного нагревания и 7) предел постоянной распада $(\nu \Sigma_s)_{мин}$. Рассматривается вопрос об определении переходных во времени и пространстве параметров с помощью полиномиального выражения для энергетической части нейтронного потока. На основании полиномиального разложения в ряд низкого порядка определена взаимозависимость между различными параметрами. Подчеркиваются недостатки этих выражений в отношении анализа переходных явлений.

Делается попытка сопоставить теоретические и экспериментальные результаты для нескольких замедлителей. Теоретические значения M_2 получены через посредство первого члена ряда Плачека для массы и внесения поправок по методу обобщенной аппроксимации Допплера. В этих расчетах используются имеющиеся теоретические или рассчитанные частотные спектры динамических колебаний замедлителей.

Сравниваются различные экспериментальные методы определения параметров термализации нейтронов. Указываются неточности и недостатки различных методов. Рассматриваются имеющиеся экспериментальные данные и предлагается перечень "наилучших значений". Сравнение теоретических и экспериментальных данных показывает, что для полного понимания этих результатов необходимо провести большой объем теоретических и экспериментальных работ.

PARAMETROS DE TERMALIZACION DE NEUTRONES. La memoria trata de los parámetros de termalización de neutrones que se emplean para describir los fenómenos transitorios en función del tiempo y del espacio. Dichos parámetros son a) M_2, momento de segundo orden de transferencia de energía del núcleo de dispersión ponderado por la distribución de Maxwell; b) la constante temporal de termalización; c) el *coeficiente de enfriamiento por difusión*; d) el coeficiente de enfriamiento por absorción; e) la longitud de retermalización; f) el coeficiente de calentamiento por difusión, y g) el límite de la constante de decrecimiento $(\nu \Sigma_s)_{min}$. Se discute la determinación de los parámetros transitorios en tiempo y espacio con la representación polinómica del componente energético del flujo neutrónico. Las relaciones entre diversos parámetros se obtienene basándose en el desarrollo polinómico de orden inferior. La memoria destaca los *límites de estas expresiones* en el análisis de los fenómenos transitorios.

Los autores intentan comparar los resultados obtenidos teórica y experimentalmente para varios moderadores. Empleando el primer término del desarrollo de Placzek según la masa y la corrección con la aproximación generalizada de Doppler se obtienen valores teóricos de M_2. Para estos cálculos emplean los espectros de frecuencia, teóricos o derivados, de los modos dinámicos de los moderadores.

Se comparan diversos métodos experimentales para determinar los parámetros de la termalización de neutrones y se destacan las ambigüedades y limitaciones de cada uno. La memoria revisa los datos experimentales de que se dispone y propone una lista de «valores recomendados». Al comparar los datos teóricos con los experimentales se ve que todavía habrá que desarrollar una extensísima labor teórica y experimental antes de poder llegar a comprender los resultados.

1. INTRODUCTION

In neutron thermalization studies the aim is usually to follow the history of a neutron spectrum, either as a function of a spatial variable or as a function of time. The asymptotic spectrum reached at sufficiently large values of the variable in question is of special importance and is often the main object of the investigation. A complete and realistic description of the history of the differential spectrum is difficult to determine experimentally. Only recently some initial studies of time-dependent neutron spectra have been made with powerful electron accelerators [1, 2]. With more conventional types of neutron sources one is limited to the still difficult task of making accurate experimental determinations of integral parameters, such as the diffusion cooling coefficient.

In view of this situation it is obvious that a parametric description of neutron thermalization is justified in many cases. It can give a good physical

insight into the phenomena and facilitates the comparison between theory and experiment. However, one must always be aware of the danger of over-simplification.

The aim of this paper is to examine various parameters used for describing neutron thermalization. Their intimate connection with each other is shown. The treatment is based on the polynomial method, which is very suitable for this purpose in spite of its limitations. Theoretical values for the thermalization parameters M_2 are estimated and compared with values obtained from experiments. For other aspects of the subject the reader is referred to other review articles, such as those by BECKURTS [3], KOTHARI and DUGGAL [4] and KEEPIN [5].

2. TIME AND SPACE TRANSIENTS

The analysis of transients associated with a decaying pulse of neutrons in a moderator or with the spatial variation of neutrons from a steady state source in an infinite moderator is usually undertaken by the Boltzmann transport equation. In the diffusion theory approximation, we write:

$$\frac{1}{v}\frac{\partial\phi(E,\underline{r},t)}{\partial t} = -[\Sigma_t(E) - D(E)\nabla^2]\,\phi(E,\underline{r},t) + \int_0^\infty \Sigma_s(E'\to E)\,\phi(E',\underline{r},t)\,dE' \quad (1)$$

$\phi(E,\underline{r},t)$ is the neutron flux as a function of energy E (or velocity v), space ($\underline{r}$) and time (t) variables. $\Sigma_t(E)$ and D(E) are the macroscopic total cross-section and diffusion coefficient respectively. $\Sigma_s(E'\to E)dE'$ is the neutron scattering probability governed by the energy transfer process between neutron and the colliding atom.

2.1. Time eigenvalues

To determine the time eigenvalues, we expand $\phi(E,\underline{r},t)$ in a complete set of orthogonal functions $\xi_p(\underline{r})$ of space variable ($\underline{r}$), and look for the solution of the following type:

$$\phi(E,\underline{r},t) = \sum_{p=o}^{\infty} \xi_p(\underline{r})\Psi_p(E)\exp(-\lambda_p t) \quad (2)$$

$$\nabla^2\xi_p(\underline{r}) = -B_p^2\xi_p(\underline{r}) \quad \text{and} \quad \xi_p(\underline{\tilde{r}}) = 0 \quad (3)$$

The above expansion implies that all the spatial modes vanish at the extrapolated boundary ($\underline{\tilde{r}}$) and that the latter is independent of neutron energy.

From the knowledge of the complete spectrum of eigenvalues and eigenfunctions, one may obtain $\phi(E,\underline{r},t)$ by the principle of superposition of the normal modes

$$\phi(E,\underline{r},t) = \sum_{p=0}^{\infty} \xi_p(\underline{r}) \left[\sum_{1} \Psi_{pi}(E) \exp(-\lambda_{pi} t) + \int_{\lambda^*}^{\infty} \exp(-\lambda_p t) \Psi_p(E,\lambda)\, d\lambda \right] \quad (4)$$

The sum represents the discrete part of the spectrum and the integral gives the contribution of the continuum. λ^* separates the two spectra and is equal to $(v\Sigma_s)_{min}$ for a non-absorbing medium. This is evident from the expression of $\Psi_p(E)$ obtained by substituting the above expansion for $\phi(E, \underline{r}, t)$ in the homogeneous integral equation.

$$\Psi_p(E) = \frac{v \int_0^{\infty} \Sigma_s(E' \to E) \Psi_p(E')\, dE'}{v(\Sigma_t + DB_p^2) - \lambda} \quad (5)$$

We note two cases.

Case (a): If $[v(\Sigma_t + DB_p^2)]_{min} > \lambda$, then λ belongs to the discrete set. Assuming $\Sigma_t(E)$ to be inversely proportional to v for small v and B_p^2 to be independent of energy, one obtains $\lambda^* = (v\Sigma_t)_{min}$ or equal to $(v\Sigma_s)_{min}$ for $\Sigma_a = 0$. As shown by NELKIN [6] and by CORNGOLD [7] the same limit also holds in transport theory. The eigenfunction $\Psi_p(E)$ for a particular value of λ is obtained by solving the above integral equation.

Case (b): If $[v(\Sigma_t + DB_p^2)]_{min} < \lambda$, then λ belongs to the continuum and

$$\Psi_p(E,\lambda) = P\left[\frac{v \int_0^{\infty} \Sigma_s(E' \to E) \Psi_p(E')\, dE'}{v(\Sigma_t + DB_p^2) - \lambda}\right] + g(\lambda)\, \delta(\lambda - v\Sigma_t - v\, DB_p^2) \quad (6)$$

P implies the principal value of the integral whenever the denominator appears as the integrand. The delta functions give the contribution of singularities other than the poles.

Only for a proton gas case a satisfactory discussion of the character of the time eigenvalues associated with the energy modes, as given by CORNGOLD et al. [8] and SHIZUTA [9], exists. According to these authors the number of discrete eigenvalues between zero and $(v\Sigma_s)_{min}$ is infinite for an infinite medium. SHAPIRO [10] has obtained extensive numerical results for the existence and convergence of discrete eigenvalues for the monatomic gas model, the Nelkin water model and for the heavy crystal model. Numerical results for the eigenvalues of the bound proton model have been obtained by OHANIAN and DAITCH [11] and by GHATAK and HONECK [12]. The quoted papers indicate that the first eigenvalue always exists for a finite medium. There are also strong indications that there is always at least a second eigenvalue, even though it may lie close to the limiting decay constant.

2.2. Estimation of the time eigenvalues

Expanding $\Psi_p(E)$ in a complete set of orthogonal polynomials one obtains the secular determinant for solving the eigenvalue problem. The choice of these polynomials is arbitrary. The Laguerre polynomials have been widely used in the literature, as they are the exact eigenfunctions of the Wilkins heavy gas scattering operator. Let

$$\Psi_p(E) = \sum_{n=o}^{\infty} a_{np} L_n^1 \left(\frac{E}{T}\right) M(E, T) \tag{7}$$

$$M(E, T) = \frac{E}{T^2} \exp\left(-\frac{E}{T}\right) \tag{8}$$

Equation (8) defines a Maxwellian distribution at the thermodynamic temperature T.

Following the treatment given in Ref. [13], one obtains the following secular determinant

$$\left| G_{mn} - F_{mn} - \lambda W_{mn} \right| = 0 \tag{9}$$

The matrix elements G_{mn}, W_{mn} and F_{mn} are defined as follows:

$$G_{mn} = (\Sigma_a + DB_p^2)_{mn} \tag{10}$$

$$W_{mn} = \left(\frac{1}{v}\right)_{mn} \tag{11}$$

$$F_{mn} = \int_o^{\infty} \int_o^{\infty} \Sigma_s(E \to E') M(E, T) \left\{ L_n^1\left(\frac{E'}{T}\right) - L_n^1\left(\frac{E}{T}\right) \right\} L_m^1\left(\frac{E}{T}\right) dE' dE \tag{12}$$

The following integral defines the G_{mn} and W_{mn} matrix elements:

$$X_{mn} = \int_o^{\infty} X(E) L_m^1\left(\frac{E}{T}\right) L_n^1\left(\frac{E}{T}\right) M(E, T) dE \tag{13}$$

We note the following properties of F_{mn}, the matrix elements of the scattering operator

1. $F_{mn} = F_{nm}$ and $F_{mo} = F_{on} = 0$

2. $F_{11} = - M_2/4$

where the important parameter M_2 is defined as:

$$M_2 = \frac{1}{T^2} \int_0^\infty \int_0^\infty \Sigma_s(E \to E') M(E, T) (E' - E)^2 \, dE' \, dE \tag{14}$$

2.3. Space eigenvalues

The space transients from a steady source in an infinite medium may also be analysed as an eigenvalue problem. Let

$$\phi(E, x) = \Psi(E) \exp(- x\sqrt{\alpha}) \tag{15}$$

Expanding $\Psi(E)$ in a set of orthogonal polynomials along the lines of the time-dependent problem one obtains the secular determinant from Eq. (1) by putting $\partial\phi/\partial t = 0$. Alternatively, one may set $\lambda = 0$ and $B^2 = -\alpha$ in the time eigenvalue secular determinant.

$$| (\Sigma_a)_{mn} - F_{mn} - D_{mn} \alpha | = 0 \tag{16}$$

It must be emphasized that the determination of time and space eigenvalues involves exactly the same matrix elements.

2.4. Eigenvalues in L_1^+ approximation

In the L_1^+ approximation, there are only two eigenvalues for time-and space-dependent cases.

Time eigenvalues

$$\lambda_o = \frac{2 v_o G_{oo}}{\sqrt{\pi}} - \frac{G_{oo}^2 v_o}{M_2 \sqrt{\pi}} K^2 \tag{17}$$

$$\lambda_1 = \frac{2 M_2 v_o}{3\sqrt{\pi}} + \frac{8 G_{oo} v_o}{3\sqrt{\pi}} \left[\frac{G_{11}}{G_{oo}} - \frac{G_{1o}}{\sqrt{2} G_{oo}} + \frac{1}{8} \right] + \frac{G_{oo}^2 v_o}{M_2 \sqrt{\pi}} K^2 \tag{18}$$

$$K^2 = \left[1 - 2\sqrt{2} \frac{G_{1o}}{G_{oo}} \right]^2 \tag{19}$$

In the case of 1/v absorption, $G_{mn} = D_{mn}B_p^2$ and the expressions for λ_o and λ_1 reduce to the well-known expression for the decaying pulse in a finite moderator. The effect of the 1/v absorption term is to increase the eigenvalues by a constant term. In the case of a finite medium the preferential leakage of neutrons with large velocities leads to the well-known diffusion cooling effect [14]. The presence of a non-1/v absorber will give an additional spectrum change, called absorption cooling. This effect has been studied by FRIEDMAN [15] and by VERDAGUER [16].

Space eigenvalues

$$\alpha_o = \frac{\Sigma_{aoo}}{D_{oo}} [1 - H \Sigma_{aoo}] \tag{20}$$

$$\alpha_1 = \frac{M_2}{4} [1 - J(\Sigma_a)] \frac{D_{oo}}{D_{oo}D_{11} - D_{1o}^2}, \tag{21}$$

where

$$H = \frac{4}{M_2} \left[\frac{\Sigma_{a1o}}{\Sigma_{aoo}} - \frac{D_{1o}}{D_{oo}}\right]^2 \tag{22}$$

is the diffusion heating coefficient.

The expression for J is straightforward but complicated. In the absence of absorption J = 0.

It must be remarked that the zeroth eigenvalue α_o determines the rate of the diffusion of the asymptotic neutron distribution in space. The reciprocal of $\sqrt{\alpha_o}$ is the diffusion length L. The first eigenvalue α_1 governs the establishment of the asymptotic distribution of thermal neutrons in space. In analogy to the diffusion length one may define $1/\sqrt{\alpha_1}$ as the relaxation length. It may be pointed out that α_1 governs the thermalization process in two adjoining media kept at different temperatures and is identical to the rethermalization area as discussed by SELENGUT [17].

2.5. Limitations of the polynomial method

In principle the expansion of the neutron flux in a complete set of orthogonal polynomials of velocity or energy variables is quite general, but in practice one encounters the problem of convergence. The low-order approximations, such as the L_1^1 approximation discussed here, give a good physical insight into the neutron thermalization problems and especially the relationship between different parameters. This approximation also expresses all the thermalization parameters in terms of the integral parameter of the scattering law, M_2, and is therefore useful in studying the effect of the details of atomic motions on thermalization processes. It has been

established that the theoretical results obtained with the Rayleigh-Ritz variational method, using a Maxwellian distribution with the neutron temperature as the trial function [18], can also be derived using the L_1^1 approximation. It is well known that the L_1^1 approximation gives an upper limit for the eigenvalues and is therefore useful for rough quantitative discussion of the parameters. However, higher order approximations are usually needed for a detailed quantitative comparison between theory and experiment.

As pointed out by TAKAHASHI [19] and PUROHIT [20] the use of energy polynomials gives a slow rate of convergence for the time eigenvalues of a heavy crystal. However, the energy polynomials give better convergence for the space eigenvalues. The detailed numerical calculations undertaken by SHAPIRO [10] using velocity as well as energy polynomials have clearly demonstrated that the velocity polynomials give much better convergence in time-dependent problems.

In the following we will use the L_1^1 relationships derived but introduce f-factors which correct the non-converged parameters.

3. THERMALIZATION PARAMETERS

From the above results for the eigenvalues one may obtain the explicit expressions for the thermalization parameters.

3.1. Time transient parameters

Diffusion cooling coefficient (C_d). The coefficient of the B^4 term in the expression of λ_o as a function of B^2 for 1/v absorption (Eq. (17)) gives C_d, when corrections have been made for transport theory effects.

$$C_d = \frac{D_{oo}^2 v_o}{M_2 \sqrt{\pi}} \left[1 - 2\sqrt{2} \frac{D_{1o}}{D_{oo}} \right]^2 f_c \tag{23}$$

where f_c is a correction factor due to higher order polynomials than L_1^1.

Absorption cooling coefficient (C_{abs}). The coefficient of N^2 (where N is the number of absorber atoms per unit volume) in the expression of λ_o (Eq. (17)) when $B^2 = 0$ yields:

$$C_{abs} = \frac{\sigma_{aoo}^2}{M_2 \sqrt{\pi}} \left[1 - 2\sqrt{2} \frac{\Sigma_{a1o}}{\Sigma_{aoo}} \right]^2 f_a \tag{24}$$

The expressions for C_d and C_{abs} are exactly identical if $(D)_{mn}$ is replaced by $(\sigma_a)_{mn}$.

Thermalization time constant. The reciprocal of λ_1 (Eq. (18)) for $\Sigma_a = 0$ and $B_p^2 = 0$ provides the thermalization time constant for the establishment of the Maxwellian distribution.

$$t_{th} = \frac{3\sqrt{\pi}}{2 M_2 v_o} f_t \tag{25}$$

3.2. Space transient parameters

Diffusion heating coefficient. The coefficient H in the expression of α_0 (Eq. (20)) is defined to be the diffusion heating coefficient.

$$H = \frac{1}{2M_2}\left(1 - 2\sqrt{2}\,\frac{D_{1o}}{D_{oo}}\right)^2 f_h \tag{26}$$

(For 1/v absorption $\Sigma_{a1o}/\Sigma_{aoo} = 1/2\sqrt{2}$).

Thermalization relaxation length. From Eq. (21) one obtains, assuming zero absorption,

$$a_1 = \frac{M_2}{4}\, f_r\, \frac{D_{oo}}{D_{oo}D_{11} - D_{1o}^2} \tag{27}$$

3.3. Interrelationships

By eliminating M_2 between some of the above equations we obtain the following interrelationships between various parameters:

$$t_{th} = \frac{3\pi C_d}{2D_{oo}^2 v_o^2}\,\frac{f_t}{f_c}\left(1 - 2\sqrt{2}\,\frac{D_{1o}}{D_{oo}}\right)^{-2} \tag{28}$$

A similar expression would result between t_{th} and C_a.

$$H = \frac{\sqrt{\pi} C_d}{2D_{oo}^2 v_o}\,\frac{f_h}{f_c} \tag{29}$$

The above result is exact in the L_1^1 approximation. It is interesting to note that the same expression can be obtained from

$$\lambda_o = \Sigma_{ao} v_o + \frac{2D_{oo} v_o B^2}{\sqrt{\pi}} - C_d B^4 \tag{30}$$

by putting $\lambda_o = 0$ and $B^2 = -\alpha$. The derivation given in this paper brings out the limitation of the relation between C_d and H employed extensively to infer C_d from the measured value of H.

$$a_1 = \frac{3\sqrt{\pi}}{8 v_o t_{th}}\, f_t\, f_r\, \frac{D_{oo}}{D_{oo}D_{11} - D_{1o}^2} \tag{31}$$

4. THEORETICAL ESTIMATION OF THE PARAMETERS M_2 AND $(v\Sigma_s)_{min}$

Using the neutron scattering formalism of VAN HOVE [21], M_2 and $(v\Sigma_s)_{min}$ are represented by the following time integrals:

$$M_2 = \frac{\sigma_b}{8}\left[\left(\frac{d}{i\,d\eta}\right)^2 \int_{-\infty}^{+\infty} \frac{dt}{\left[\frac{\rho(t,\eta)}{T} + (t+\eta)^2\right]^{3/2}}\right]_{\eta=0} \tag{32}$$

$$(v\Sigma_s)_{min} = \frac{v_o \Sigma_b}{4\sqrt{T}} \int_{-\infty}^{+\infty} \frac{dt}{[\rho(t,o)]^{3/2}}, \tag{33}$$

where

$$\rho(t,\eta) = -\left[\, i(t+\eta) + \frac{m}{M}\gamma(t)\right] \tag{34}$$

$\rho(t, \eta)$ is given in terms of the width function $\gamma(t)$ (the mean square displacement of atoms) for the scattering model. For harmonic vibrations in a moderator

$$\gamma(t) = \int_{-\infty}^{+\infty} \frac{\exp(-i\xi t - 1) f(\xi)\, d\xi}{\xi \exp\left(\frac{\xi}{T} - 1\right)} \tag{35}$$

In the case of a Bravais lattice, $f(\xi)$ is the frequency spectrum of phonons and for a liquid $f(\xi)$ may be considered to be the frequency spectrum of the velocity auto-correlation function.

4.1. Estimation of M_2

A comparative study of the scattering laws for moderators may be undertaken by estimating M_2, using the first term of the mass expansion M_2^1 and the correction factor A(D) according to the detailed balanced Doppler approximation. Let

$$M_2 = M_2^1\, A(D) \tag{36}$$

$$\lambda T = \int_0^{\infty} \frac{f(x)\,(\cosh x/2 - 1)\, dx}{x \sinh x/2} \tag{37}$$

$$A(D) = \frac{1}{\left(1 + \frac{m}{M}\,\frac{a}{T}\right)^{3/2} \left(1 + 4\frac{m}{M}\lambda T\right)^2} \tag{38}$$

and

$$M_2^D = 8\sigma_b \frac{m}{M} \frac{a}{T} A(D) , \tag{39}$$

where

$$M_2^1 = \frac{\sigma_b m}{2MT^3} \int_0^\infty \frac{f(\xi)\xi^3 K_2(\xi/2T)\, d\xi}{\sinh \xi/2T} \tag{40}$$

$$\frac{a}{T} = \int_0^\infty \frac{x f(x)\, dx}{2 \sinh x/2} \tag{41}$$

$$x = \xi/T \tag{42}$$

For a monatomic gas model $\alpha/T = 1$ and $\lambda T = 1/4$. In the limit of weak binding, for the heavy mass case M_2^1 and $M_2(D)$ reduce to the well-known expression of $8\sigma_b \cdot m/M$. For a discussion of the Doppler approximation, see PUROHIT and RAJAGOPAL [22] and for the mass expansion case Ref. [23].

In Table I, we list the values of M_2^1, M_2^D, M_2 and M_2 (gas) for five moderators. For graphite, the Yoshimori-Kitano frequency spectrum, used by Parks (see [24]) and his group in the United States, and the Harwell spectrum [25], obtained from the Chalk River measurements, were used. In the case of beryllium, the theoretical spectrum of YOUNG and KOPPEL [26] and the experimental spectrum as derived by SINCLAIR [27] were used. The beryllium oxide results are based upon the Sinclair spectrum [27]. For H_2O, the Nelkin model [28] parameters and for D_2O the incoherent scattering law parameters as given by BUTLER [29] have been used. The results for H_2O and D_2O have been obtained using the structure for the hindered rotations as give by the Stockholm experiments of LARSSON and DAHLBORG [30].

SCHOFIELD in [25] has estimated M_2^1 for the Yoshimori-Kitano and Harwell spectra for graphite equal to 1.15 and 1.696 b respectively. The corrected M_2 value according to SCHOFIELD [31] for the Yoshimori-Kitano spectrum is 0.97 b and the General Atomic value is 0.9784 b [24]. The method of obtaining the latter value is not clear from that reference. Using the Brooks-Krumhansl model for graphite, KOTHARI [32] estimated M_2 equal to 0.80 b.

In the case of H_2O, M_2^1 for the Nelkin model according to SCHOFIELD in [25] is equal to 208 b. The exact value of M_2, as given by HONECK [33] after neglecting the contribution of oxygen atoms is equal to 49.05 b. According to GLÄSER and BECKURTS [34], M_2 for H_2O is equal to 46.5 b.

TABLE I

VALUES OF M_2 AND $(v\Sigma_s)^D_{min}$
FOR MODERATORS AT ROOM TEMPERATURE

Moderator	M_2^1 (b)	M_2 Doppler corrected (b)	M_2^D (b)	M_2 (gas) (b)	$(v\Sigma_s)^D_{min}$ (10^{-4} s^{-1})
H_2O					
(a) Nelkin	201.3	47.31	63.44		42.0
(b) Proton gas	-	-	-	57.56	-
D_2O					
(a) Butler	24.73	10.71	13.98	-	4.67
(b) Gas	-	-	-	28.78	-
Beryllium					
(a) Young-Koppel	4.33	3.14	3.98	-	5.80
(b) Sinclair	4.03	2.94	3.87	-	5.79
(c) Gas	-	-	-	4.88	
Beryllium oxide					
(a) Sinclair	4.42	3.38	4.52		4.58
(b) Gas	-	-	-	6.61	
Graphite					
(a) Yoshimori-Kitano	1.17	0.98	1.54	-	2.07
(b) Harwell	1.695	1.39	1.90	-	2.29
(c) Gas	-	-	-	2.79	-

Note: For BeO and D_2O, the M_2 values are for the whole molecule, for H_2O the M_2 values are per hydrogen atom, for Be and graphite per moderator atom.

4.2. *Estimation of* $(v\Sigma_s)_{min}$

The expressions for $(v\Sigma_s)_{min}$ for the detailed balance Doppler approximation and the heavy mass cases are as follows:

$$(v\Sigma_s)^D_{min} = \frac{v_o\Sigma_b\left(\frac{4}{\pi}\frac{m}{M}\frac{a}{T}\right)^{1/2}}{\left(1+\frac{m}{M}\frac{a}{T}\right)^2+\left(\frac{m}{M}\right)^2\frac{a}{T}\left(4\lambda T-\frac{a}{T}\right)} \tag{43}$$

$$(v\Sigma_s)^1_{min} = v_o \Sigma_b \frac{m}{M} \int_0^\infty \frac{x^{1/2} f(x) \exp\left(-\frac{x}{2}\right) dx}{2 \sinh \frac{x}{2}} \qquad (44)$$

λ, α and x are given by Eqs.(40-42).

In Table I $(v\Sigma_s)^D_{min}$ for five moderators are listed. The values of $(v\Sigma_s)^1_{min}$ for three crystalline moderators are as follows. For the Yoshimori-Kitano and Harwell spectra of graphite, $(v\Sigma_s)^1_{min}$ is equal to 1.05×10^3 and 1.64×10^3 s^{-1} respectively. For Be, the Young-Koppel and Sinclair spectra give 4.73×10^3 and 4.10×10^3 s^{-1}, respectively. The value for BeO is equal to 2.18×10^3 s^{-1}. CORNGOLD and MICHAEL [35] have given $(v\Sigma_s)_{min}$ for H_2O, Be and C equal to 3.0×10^5, 3.8×10^3 and 2.6×10^3 s^{-1} respectively. All data in Table I are based on bound atom cross-sections taken from BNL 325.

4.3. λ_1 versus $(v\Sigma_s)_{min}$

Is λ_1, the second eigenvalue, also discrete and less than $(v\Sigma_s)_{min}$? According to SHAPIRO [10], λ_1 is discrete for a gas model for all masses and for a heavy Debye crystal λ_1 is no longer discrete above θ/T equal to 0.28. CORNGOLD and SHAPIRO [36] therefore concluded that λ_1 may not be discrete for most of the crystalline moderators and the approach-to-equilibrium takes place with a time constant of $(v\Sigma_s)_{min}$.

For λ_1 to be discrete Δ must be less than one, where

$$\Delta = \frac{2 v_o M_2}{3\sqrt{\pi}\,(v\Sigma_s)_{min}} \quad \frac{1}{f_t} = \frac{\Delta_1}{f_t} \qquad (45)$$

It is easy to establish that Δ is less than one for the gas model, therefore λ_1 is discrete. From the values of M_2^D and $(v\Sigma_s)^D_{min}$ one can show that Δ_1 is less than one for the five moderators. Therefore, λ_1 is discrete in the Doppler approximation. For a heavy crystal case, using M_2^1, $(v\Sigma_s)^1_{min}$ and f_t values, one obtains Δ_1 greater than one.

It must be noted that in the heavy mass limit Δ is proportional to $(m/M)^{\frac{1}{2}}$ for the Doppler approximation and is independent of the mass term for the heavy crystal case. The latter fact does not give the correct weak binding limit.

5. COMPARISON WITH EXPERIMENTS

Considering the many reported experiments on the determination of thermalization parameters one might imagine that there exists a wealth of experimental data useful for comparison with theory. Unfortunately, this is not so. The reason is partly trivial: several experiments have not been made with sufficient accuracy, or their presentation is not detailed enough for a careful evaluation. There are also other difficulties, which are connected with the parametric description given here. To determine the para-

meter M_2 from a measured quantity the correction factor f must be known (see section 3 above). However, only for a few moderator models such factors have been calculated. Similarly, the transport correction to the B^4 term in the expression for the fundamental time constant (Eq. (17)) and the correction due to a B^6 term are not very well known either. In addition, the temperature dependence of the diffusion constant must be known for an evaluation of M_2 from C_d (see below). The determination of M_2 from the thermalization time seems to involve fewer uncertainties. However, the experimental determination of the thermalization time constant is more difficult and, as discussed in section 2, the existence of a unique second eigenvalue λ_1 has been questioned, especially for crystalline media.

In view of all this, we have limited our comparison of theory and experiment to the room temperature data of the five important moderators treated in section 4. Only M_2-values obtained from diffusion cooling coefficients and from thermalization time constants are included. We hope to be able to make a more complete comparison in the future, involving more moderators, other temperatures and also results from the measurements of other parameters.

5.1. Table of experimental results

In Table II we have for various parameters given values which represent reasonable averages of the best available experimental information. From the diffusion cooling coefficient the parameter M_2 has been obtained through the formula

$$M_2 = \frac{(a + \frac{1}{2})^2 \sqrt{\pi}\, D_o^2}{v_o\, C_d}\, f_c \tag{46}$$

which is a slightly changed form of Eq. (23). Here $D_o = 2D_{bo}\, v_o/\sqrt{\pi}$ and the coefficient α gives the variation of the transport mean free path l_{tr} with neutron energy E according to

$$l_{tr}(E, T_m) \cdot \rho(T_m) = b E^a \tag{47}$$

where b is a constant. No other direct influence of the moderator temperature T_m than through the density ρ is assumed (see KOZHEVNIKOV [37]). The coefficient α is derived from measurements of the diffusion constant or diffusion length as a function of temperature. From the thermalization time constant, t_{th}, the parameter M_2 is obtained directly from Eq. (25).

The f_c and f_t values used are the following: For H_2O and D_2O $f_c = 1.35$ (heavy gas), for H_2O $f_t = 1.15$ (proton gas). The heavy crystal approximation has been used for the three solid moderators Be, BeO and C, giving $f_c = 3.42$, 3.97 and 6.36 respectively and $f_t = 9.77$, 11.3 and 17.8 respectively, where the Debye-temperatures have been assumed to be $\theta/T = 10/3$, 4 and 7, respectively. All data refer to the densities of 1.85, 2.79 and 1.60 g/cm^3 respectively for these moderators.

The value listed for the diffusion cooling coefficient of H_2O is an average based on several recent measurements, of which those described in Ref. [38-

TABLE II

VALUES OF M_2 AT ROOM TEMPERATURE DERIVED FROM EXPERIMENTS

Moderator	C_d (10^5 cm^4/s)	D_0 (10^5 cm^2/s)	α	t_{th} (μs)	M_2 (b)
H_2O	0.044 ± 0.008	0.36 ± 0.01	0.45 ± 0.05		43 ± 9
				4.1 ± 0.4	51 ± 5 (per hydrogen atom)
D_2O	5.0 ± 1.0	2.05 ± 0.04	0.16 ± 0.05		12 ± 3 (per molecule)
Be	3.0 ± 0.5	1.24 ± 0.03	0.20 ± 0.05		1.0 ± 0.3
				185 ± 20	5.2 ± 0.6
BeO	4.0 ± 0.8	1.55 ± 0.04	0.0 ± 0.1		7.2 ± 2.4
				204 ± 20	10 ± 1
C	40 ± 5	2.15 ± 0.03	0.00 ± 0.05		1.8 ± 0.4
				400 ± 100	6.7 ± 1.7

40] are representative. Also the temperature coefficient α is an average, including in addition the work of REIER and De JUREN [41] and of ANTONOV [42]. The thermalization time constant is that determined by MÖLLER and SJÖSTRAND [43].

The diffusion cooling coefficient for D_2O is based on the work done by SJÖSTRAND [44], GANGULY et al. [45] and KUSSMAUL and MEISTER [46]. The temperature dependence reported by BAUMANN [47] was assumed.

For beryllium we have used the data by ANDREWS [48] and by ZHEZHERUN [49]. The last author has also furnished data for BeO and for the thermalization time constant of the two moderators. Lacking reliable knowledge of the temperature dependence of the diffusion parameters for BeO we have assumed $\alpha = 0$ for this moderator.

In the case of graphite there seems to be no doubt that $\alpha = 0$, as several measurements indicate. The value of C_d is an average of the values given by STARR and PRICE [50], SAGOT and TELLIER [51] and WALKER [52]. The thermalization time constant was taken from BARNARD et al. [1].

It is seen from Table II that the two methods of measurement give consistent results only for H_2O and D_2O and possibly also for BeO, whereas the two M_2 values for Be and graphite disagree very much. The reason may to some extent be the experimental difficulty to isolate the energy mode giving the thermalization time when the decay constant lies close to the limit of the continuous modes. Also the correction factors f are uncertain for the heavy crystal model.

5.2. Discussion

A comparison between the Doppler corrected M_2 values of Table I and the experimental ones of Table II shows that theory and experiment agree satisfactorily only for light and heavy water. For the other three moderators the theoretical values are of the same order of magnitude as the experimental ones, but the agreement is poor. There is no clear tendency that the theoretical values agree better with results obtained from one type of experiment than with those from the other type. The source of discrepancy is probably the correction factors for higher polynomials. In the case of crystalline moderators, a calculation of eigenvalues using the second and even third term of the mass expansion is required to derive more reliable values for these correction factors. Such a study will perhaps also clear up the problem of the character of the first eigenvalue for the crystalline moderators. As pointed out earlier the $(v\Sigma_s)_{min}$ expression using the first term of the mass expansion does not reduce to the heavy gas formula in the weak binding limit. Therefore, the character of the first eigenvalue for the crystalline moderators can not be concluded on the basis of the heavy crystal study. It is our contention that $(v\Sigma_s)_{min}$ is perhaps proportional to $(m/M)^{\frac{1}{2}}$ for all degrees of binding. This will always ensure that the first eigenvalue λ_1 is discrete and less than $(v\Sigma_s)_{min}$. Further theoretical and experimental studies of M_2 and $(v\Sigma_s)_{min}$ are required to improve the situation.

REFERENCES

[1] BARNARD, E. et al., Nucl. Sci. Engng 17 (1963) 513.
[2] MOSTOVOY, V. I. et al., Proc. 3rd UN Int. Conf. PUAE, 1964, P/367.
[3] BECKURTS, K. H., Proc. Brookhaven Conf. on Neutron Thermalization, BNL 719 (1962).
[4] KOTHARI, L. S. and DUGGAL, V. P., Advances in Nucl. Sci. and Techn. 2 (1964) 186.
[5] KEEPIN, G. R., Atomic Energy Rev. 2 (1964) 75.
[6] NELKIN, M., Physica 29 (1963) 261.
[7] CORNGOLD, N., Nucl. Sci. Engng 19 (1964) 80.
[8] CORNGOLD, N. et al., Nucl. Sci. Engng 15 (1963) 13.
[9] SHIZUTA, Y., Progr. theor. Phys. 32 (1964) 489.
[10] SHAPIRO, C. S., Rpt BNL 8433 (1964).
[11] OHANIAN, M. J. and DAITCH, P. B., Nucl. Sci. Engng 19 (1964) 343.
[12] GHATAK, A. K. and HONECK, H. C., Rpt BNL 8115 (1964).
[13] PUROHIT, S. N., Nucl. Sci. Engng 9 (1961) 157.
[14] VON DARDEL, G. and SJÖSTRAND, N. G., Nucl. Phys. Rev. 96 (1954) 1245.
[15] FRIEDMAN, E., Nucl. Sci. Engng 19 (1964) 203.
[16] VERDAGUER, F., J. E. N. 127-DF/I 39 (1963).
[17] SELENGUT, D. S., Proc. R. P. I. Symp. Neutron Physics, Academic Press, N. Y. (1962) 162.
[18] NELKIN, M., J. nucl. Energy 8 (1958) 48.
[19] TAKAHASKI, H., Rpt BNL 719 4 (1962) 1299.
[20] PUROHIT, S. N., Applications of the polynomial method in the study of neutron thermalization, Rpt BNL (1962) (unpublished).
[21] VAN HOVE, L., Phys. Rev. 95 (1954) 249.
[22] PUROHIT, S. N. and RAJAGOPAL, A. K., Nucl. Sci. Engng 13 (1962) 250.
[23] PUROHIT, S. N., Rpt BNL 719 1 (1962) 203.
[24] WIKNER, N. F. et al., Nucl. Sci. Engng 19 (1964) 108.
[25] POOLE, M. J., SCHOFIELD, P. and SINCLAIR, R. N., Exponential and Critical Experiments III IAEA, Vienna (1964) 87-110.

[26] YOUNG, J. A. and KOPPEL, J. U., Nucl. Sci. Engng 19 (1964) 363.
[27] SINCLAIR, R. N., Inelastic Scattering of Neutrons in Solids and Liquids II IAEA, Vienna (1963) 199.
[28] NELKIN, M., Phys. Rev. 119 (1960) 741.
[29] BUTLER, D., Proc. Phys. Soc. 81 (1963) 276.
[30] LARSSON, K. E. and DAHLBORG, U., Reactor Sci. 16 (1962) 81.
[31] SCHOFIELD, P., Rpt BNL 719, I RB 1 (1962).
[32] KOTHARI, L. S., Rpt BNL 719 I (1962) 117.
[33] HONECK, H. C., Nucl. Sci. Engng 18 (1964) 49.
[34] GLÄSER, W. and BECKURTS, K. H., Nucl. Sci. Engng 20 (1964) 236.
[35] CORNGOLD, N. and MICHAEL, P., Nucl. Sci. Engng 19 (1964) 91.
[36] CORNGOLD, N. and SHAPIRO. C. S., Approach to equilibrium of a neutron gas in crystalline material, unpublished 1963.
[37] KOZHEVNIKOV, D. A., Atomnaja Energija 14 (1963) 525.
[38] KÜCHLE, M., Nukleonik 2 (1960) 131.
[39] LOPEZ, W. M. and BEYSTER, J. R., Nucl. Sci. Engng 12 (1962) 190.
[40] STARR, E. and KOPPEL, J., Nucl. Sci. Engng 14 (1962) 229.
[41] REIER, M. and De JUREN, J. A., J. nucl. Engng 14 (1961) 18.
[42] ANTONOV, A. V. et al., Inelastic Scattering of Neutrons in Solids and Liquids, IAEA, Vienna (1961) 377.
[43] MÖLLER, E. and SJÖSTRAND, N. G., Ark. Fys. 27 (1964) 501.
[44] SJÖSTRAND, N. G., Ark. Fys. 15 (1959) 145.
[45] GANGULY, N. K. et al., Nucl. Sci. Engng 17 (1963) 223.
[46] KUSSMAUL, G. and MEISTER, H., Reactor Sci. 17 (1963) 411.
[47] BAUMANN, N. P., Nucl. Sci. Engng 14 (1962) 179.
[48] ANDREWS, W. M., Rpt UCRL-6083 (1960).
[49] ZHEZHERUN, I. F., Atomnaja Energija 14 (1963) 193 and also Proc. 3rd UN Int. Conf. PUAE, 1964, A/Conf. 28/P/362 a.
[50] STARR, E. and PRICE, G. A., Proc. Brookhaven Conf. on Neutron Thermalization Rpt BNL 719 (1962).
[51] SAGOT, M. and TELLIER, H., Reactor Sci. 17 (1963) 347.
[52] WALKER, J., Proc. 3rd UN Int. Conf. PUAE, 1964, A/Conf. /P/564.

DISCUSSION

(on the foregoing two papers)

K.H. BECKURTS: I have one brief comment on paper SM-62/32. It seems to me that the discrepancies found in the M_2 values for the crystalline moderators of carbon and tin are an indication of the fact that all the elementary relations between tin and carbon are inappropriate in crystalline moderators.

P. SCHOFIELD (Chairman): I would like to ask Mr. Purohit what numerical accuracy he claims for his computation. I should have thought that 22 energy groups was rather a small number for these time-dependent spectra calculations.

S.N. PUROHIT: I do not think that 22 thermal groups are a small number, provided that you weight the group cross-sections properly. We have weighted them with the calculated time- and energy-dependent flux during the run of the problem. The numerical accuracy is of the same order as that of the experiments. The difference between the gas-model results for H_2O and D_2O and the experimental results lies outside the range of numerical uncertainty. To resolve the difference between the bound-model and experimental results, further calculations would be required. In my opinion, however, the results for the reaction rate will not be altered qualitatively even if you increase the number of energy groups.

ANISOTROPIC MIGRATION IN SLAB LATTICES *

H. C. HONECK AND B. C. QUIQUEMELLE **
BROOKHAVEN NATIONAL LABORATORY,
UPTON, N.Y., UNITED STATES OF AMERICA

Abstract — Résumé — Аннотация — Resumen

ANISOTROPIC MIGRATION IN SLAB LATTICES. One of the newest applications of pulsed neutron experiments is the measurement of the thermal neutron diffusion coefficient in different directions in a heterogeneous medium. This paper describes a theoretical method developed to predict these diffusion coefficients and presents some results for experiments in progress at Brookhaven National Laboratory.

The interpretation of these experiments is considerably simplified if the experimental assembly is large. Diffusion cooling can then be ignored, the spectra taken to be Maxwellian, and a single energy group considered. With this simplification, it is possible to solve the transport equation numerically for the case of slab geometry. We insert a solution of the form

$$\phi(x, y, z, \vec{\Omega}, t) = \exp(iB_1 X + iB_2 y - \lambda t)\phi(x, \vec{\Omega})$$

into the transport equation and solve for $\phi(x, \vec{\Omega})$ by a combination of DSN and integral transport theory methods. The principal advantages of this method over existing methods is that absorption and anisotropic scattering are easily included, and the cell may be composed of many sub-regions.

While we might attempt to find the eigenvalue λ, given B_1 and B_2, it is more convenient to replace iB_1 by κ_1, iB_2 by κ_2, and determine κ_1, given κ_2 and λ. The λ can then be expressed as a power series in κ_1^2 and κ_2^2 (or equivalently B_1^2 and B_2^2). The diffusion coefficients are then given by $D_n = -d\lambda/d\kappa_n^2$.

Experiments are in progress at Brookhaven National Laboratory on alternating slabs of aluminium and polyethylene. We have selected the following one-group cross-sections: aluminium, $\Sigma_a = 0.01228$ cm^{-1}, $\Sigma_s = 0.08428$ cm^{-1}, $\bar{\mu} = 0$; polyethylene, $\Sigma_a = 0.01947$ cm^{-1}, $\Sigma_s = 2.593$ cm^{-1}, $\bar{\mu} = 0.25$.

MIGRATION ANISOTROPE DANS LES RÉSEAUX A PLAQUES. Une des dernières applications des expériences au moyen des neutrons pulsés est la mesure des coefficients de diffusion anisotrope des neutrons thermiques dans un milieu hétérogène. Les auteurs exposent une méthode théorique élaborée pour prévoir ces coefficients de diffusion et ils indiquent quelques résultats obtenus au cours des expériences qui sont actuellement faites au Laboratoire national de Brookhaven.

L'interprétation de ces expériences se trouve grandement simplifiée si l'assemblage expérimental est de grande dimension. On peut alors négliger le refroidissement par diffusion, admettre que les spectres sont maxwelliens et ne considérer qu'un seul groupe d'énergies. Grâce à cette simplification, il est possible de résoudre numériquement l'équation de transport pour le cas d'une géométrie à plaques. Dans l'équation de transport, les auteurs introduisent une solution ayant la forme

$$\phi(x, y, z, \vec{\Omega}, t) = \exp(iB_1 x + iB_2 y - \lambda t)\phi(x, \vec{\Omega})$$

et ils la résolvent par rapport à $\phi(x, \vec{\Omega})$ en combinant la méthode DSN et des méthodes fondées sur la théorie du transport. Les principaux avantages de ce procédé par rapport aux méthodes existantes sont les suivants: il permet d'inclure facilement l'absorption et la diffusion anisotrope et la cellule peut être composée de nombreuses subdivisions.

Les auteurs auraient pu essayer de déterminer la valeur propre λ pour B_1 et B_2 donnés, mais il est plus commode de remplacer iB_1 par κ_1 et iB_2 par κ_2, puis de déterminer κ_1 pour κ_2 et λ donnés. La valeur de λ peut alors être exprimée sous la forme d'une série de puissances en κ_1^2 et κ_2^2 (ou de manière équivalente en B_1^2 et B_2^2). Dans ce cas les coefficients de diffusion sont donnés par la formule $D_n = -d\lambda/d\kappa_n^2$.

---

* This work was performed under the auspices of the United States Atomic Energy Commission.

** Permanent address: EURATOM, Ispra, Italy

Au Laboratoire national de Brookhaven des expériences sont actuellement en cours sur des plaques alternées d'aluminium et de polyéthylène. Les auteurs ont choisi les sections efficaces à un groupe ci-après: aluminium, $\Sigma_a = 0,01228$ cm^{-1}, $\Sigma_s = 0,08428$ cm^{-1}, $\bar{\mu} = 0$; polyéthylène, $\Sigma_a = 0,01947$ cm^{-1}, $\Sigma_s = 2,593$ cm^{-1}, $\bar{\mu} = 0,25$.

АНИЗОТРОПИЧЕСКАЯ МИГРАЦИЯ В РЕШЕТКАХ ИЗ ПЛАСТИН. Одной из самых новых областей применения экспериментов с импульсными нейтронами является измерение коэффициента диффузии тепловых нейтронов в различных направлениях в гетерогенной среде. Описывается теоретический метод, разработанный с целью предсказания таких коэффициентов диффузии, и представляются некоторые результаты экспериментов, проводимых в настоящее время в Брукхейвене.

Интерпретация этих экспериментов в значительной степени упрощается, если экспериментальная сборка является большой. В этом случае можно пренебрегать диффузионным охлаждением, спектры считать максвелловскими и рассматривать единственную группу энергии. При таком упрощении можно численно решить уравнение переноса для случая пластинчатой геометрии. Мы подставляем решение модели

$$\Phi(x,y,z,\vec{\Omega},t) = \exp(iB_1 x + iB_2 y - \lambda t)\,\Phi(x,\vec{\Omega})$$

в уравнение переноса и решаем $\Phi(x,\vec{\Omega})$ путем сочетания методов фильтров для выравнивания данных и интегральной теории переноса. Основные преимущества этого метода по сравнению с существующими состоят в том, что легко включаются поглощение и анизотропическое рассеяние и ячейка может состоять из многих подобластей.

Хотя сделана попытка найти B_1 и B_2 с данным собственным значением λ, удобнее вместо iB_1 поставить κ_1 и вместо $iB_2 - \kappa_2$ и определить κ_2 с данным κ_1 и λ. В таком случае λ можно выразить в виде степенного ряда в κ_1^2 и κ_2^2 (или соответственно в B_1^2 и B_2^2). Коэффициенты диффузии затем выводятся из уравнения $D_n = -d\lambda/d\kappa_n^2$.

В настоящее время в БНЛ проводятся эксперименты с переменными пластинами из алюминия и полиэтилена. Отобраны следующие поперечные сечения одной группы: алюминий $\Sigma_a = 0,01228$ см$^{-1}$, $\Sigma_s = 0,08428$ см$^{-1}$, $\bar{\mu} = 0$; полиэтилен $\Sigma_a = 0,01947$ см$^{-1}$, $\Sigma_s = 2,593$ см$^{-1}$, $\bar{\mu} = 0,25$.

MIGRACION ANISOTROPICA EN RETICULADOS DE PLACAS. Una de las aplicaciones más modernas de los experimentos con neutrones pulsados es la medición en diferentes direcciones de los coeficientes de difusión anisotrópica de neutrones térmicos en un medio heterogéneo. La memoria describe un método teórico que se ha establecido para predecir estos coeficientes de difusión, y presenta algunos de los resultados obtenidos en los experimentos que se realizan en el Brookhaven National Laboratory.

La interpretación de los resultados se simplifica considerablemente si el conjunto experimental es de grandes dimensiones. En este caso cabe prescindir del enfriamiento por difusión, suponer que los espectros son maxwellianos y considerar un solo grupo energético. Gracias a esta simplificación se consigue resolver numéricamente la ecuación de transporte cuando se trata de una geometría de placas. Los autores introducen en esta ecuación una solución de la forma

$$\phi(x, y, z, \vec{\Omega}, t) = \exp(iB_1 x + iB_2 y - \lambda t)\phi(x, \vec{\Omega})$$

y despejan $\phi(x, \vec{\Omega})$ por una combinación de métodos DSN y de teoría integral del transporte. Las principales ventajas de este procedimiento son que permite fácilmente incluir la absorción y la dispersión anisotrópica, y que la celda se puede componer de muchas subregiones.

Es posible tratar de encontrar el valor propio λ cuando se conocen B_1 y B_2, pero conviene más sustituir iB_1 por κ_1 e iB_2 por κ_2, y determinar κ_1 una vez conocidos κ_2 y λ. En este caso, λ se puede expresar como serie exponencial de κ_1^2 y κ_2^2 (o, lo que es equivalente, de B_1^2 y de B_2^2). Entonces, la ecuación $D_n = -d\lambda/d\kappa_n^2$ dará los coeficientes de difusión.

En el Brookhaven National Laboratory se están haciendo experimentos con placas alternadas de aluminio y polietileno. Los autores han seleccionado las siguientes secciones eficaces en un solo grupo: aluminio, $\Sigma_a = 0,01228$ cm^{-1}, $\Sigma_s = 0,08428$ cm^{-1}, $\bar{\mu} = 0$; polietileno, $\Sigma_a = 0,01947$ cm^{-1}, $\Sigma_s = 2,593$ cm^{-1}, $\bar{\mu} = 0,25$.

INTRODUCTION

An important factor which enters the criticality condition of a reactor is the leakage.

It is well known that the diffusion theory applied to a large homogeneous reactor gives the non-leakage probability [1] of a thermal neutron as

$$\frac{1}{1 + L^2 B_g^2} \quad , \qquad L^2 = \frac{D}{\Sigma_a} \tag{1}$$

in which B_g^2 is the geometrical buckling and L, the diffusion length, is a characteristic of the infinite medium; L has been interpreted as:

(a) $L^2 = \frac{1}{6}\,\overline{r^2}$, where $\overline{r^2}$ is the mean square distance travelled by a thermal neutron between birth and capture in the finite homogeneous medium.

(b) $L = \frac{dx}{d\ell n\varphi}$, where φ is the asymptotic flux distribution far from a plane source in an infinite medium.

When heterogeneous reactors were considered, the first idea was to retain Eq. (1) for non-leakage probability in the equivalent homogeneous reactor. Equation (1) is equivalent to a definition for L^2 and, for example, WEINBERG and WIGNER [2] have found that for a stacked reactor this definition is

$$L^2 = L_m^2 (1-f) + L_f^2 f \quad , \tag{2}$$

which is equivalent to define $L^2 = \overline{D}/\overline{\Sigma}_a$, with $\overline{D}$ and $\overline{\Sigma}$ being the flux-volume averaged transport mean free path (m.f.p.) and macroscopic absorption cross-section. This is also the prescription found by RUSSELL [3] using a variational principle.

Others have suggested that $\overline{D}$ must be calculated from the flux-volume average of the microscopic transport cross-section which gives the correct homogeneous limit.

However, this method has not been found satisfactory in the case where the design of the reactor exhibits a strong anisotropy; the equivalent homogeneous medium is then better characterized by a diffusion tensor [4] and the non-leakage probability becomes

$$\frac{1}{1 + L_x^2 B_x^2 + L_y^2 B_y^2 + L_z^2 B_z^2} \tag{3}$$

with $D_x = L_x^2 \Sigma_{ax}$, $D_y = L_y^2 \Sigma_{ay}$, and $D_z = L_z^2 \Sigma_{az}$.

Several authors have given methods for finding the above homogeneous characteristics. In those methods, L_i has been given the interpretation of the mean square distance travelled in the direction i. For example, the successful BEHRENS' [5] theory has considered the case of holes in an homogeneous medium; the Behrens' correction to the homogeneous L^2 contains two parts: (1) a "homogeneous" correction which is simply a dilution factor correction $(1 + \phi)^2$, where ϕ is the volume ratio of hole to material; (2) an "anisotropic" correction containing a geometric factor which is the mean square chord of the holes in the considered direction.

Following the theory of Behrens, the effect of holes on the leakage of a reactor and then the critical mass was considered for many different situations. LALETIN [6] has studied the case of a cylindrical hole in an infinite slab reactor with diffusion theory, assuming that the radius of the hole is sufficiently small to neglect the perturbation of the radial flux. This perturbation has been taken into account by CARTER [7]. CHERNICK and KAPLAN [8] have calculated the case of a transverse air gap in a cylindrical reactor using both the diffusion and transport theory. Those results generally applied to the anisotropy caused by holes in fairly homogeneous reactors.

Now we are interested in the more general problem of finding an averaging procedure in a real homogeneous reactor with a periodic structure. Both interpretations of L have been used. The asymptotic decay rate interpretation is taken from SPINRAD [9], who applied diffusion theory to an infinite array of slabs, and also from SHEVELEV [10], who corrects the Spinrad results in the direction parallel to the slab by a transport theory treatment.

The interpretation of the mean-square-travelled distance has been given by FERZIGER et al. [11] who extended Behrens' ideas. This interpretation was also given by LESLIE [12], who considered a lattice with small geometrical buckling and found that the mean square distance can be expressed as an average of the m.f.p. over a new type of flux inside a unique cell. Further it has been recognized that the mean-square-distance interpretation is correct only in the case of small absorption (see BENOIST [13]).

More sophisticated approaches have been elaborated to calculate the average diffusion parameters, starting directly from the Boltzmann equation. A simple solution product of a macroscopic flux by the fine structure flux has not been found to be correct and BENOIST [13] has shown the existence of a term of interaction between the gradient of the macroscopic flux and the microscopic flux.

BEHRENS and OLDEKOP [14] have sought eigenfunction solutions of the form $\varphi(\underline{x}, \underline{B})\, e^{i\underline{B}\cdot\underline{x}}$ in the diffusion theory approximation. They found an expansion of the eigenvalue k as a function of the buckling for slab and rectangular lattices, thus giving the migration area in a closed form, since

$$\frac{1}{k_e} = \frac{1}{k_\infty}\left(1 + L_x^2 B_x^2 + L_y^2 B_y^2 + L_z^2 B_z^2\right) + 0(B^4) \qquad (4)$$

LESLIE [15] also has been able to work out similar solutions in the transport theory approximation and, from a balance equation inside the cell, the leakage, proportional to $\overline{D}B^2$, is found to give a suitable cell-averaged diffusion coefficient.

Finally we will mention the work of DAVISON [16] who also applied the balance equation inside a slab cell and averaged for all possible positions of the cell in the reactor.

ANISOTROPIC MIGRATION IN A SLAB SYSTEM

One of the simplest problems to be solved is the determination of the thermal diffusion parameters of a periodic system composed of slabs of two different non-multiplying materials.

If we consider, for example, a system of aluminium-water (or polyethylene) slabs, such as those used in the Brookhaven National Laboratory experiments, we expect to have a measurable anisotropy since aluminium with a large m.f.p. can be considered as void with respect to water. Then using the mean-square-distance picture the distance travelled parallel to slabs must be greatly increased as compared to the distance travelled perpendicular to the slabs. Quantitative Monte Carlo evaluation of this picture has been given by BEELER [17] for a void-material system.

We define the diffusion lengths from the asymptotic decay rates. Consider a semi-infinite slab lattice and a steady plane source. If the latter is parallel to the source, then deep within the medium the flux will approach the form

$$\phi(\underline{r},\underline{\Omega}) = \psi(x,\underline{\Omega})e^{-\kappa_\perp x} \tag{5}$$

where x is measured perpendicular to the slabs, ψ is the fine structure in each lattice cell, and $\kappa_\perp = 1/L_\perp$ is the inverse diffusion length. If the lattice is placed perpendicular to the source, then the asymptotic distribution is of the form

$$\phi(\underline{r},\underline{\Omega}) = \psi(x,\underline{\Omega})e^{-\kappa_\parallel y}\,, \tag{6}$$

where y is measured parallel to the slabs.

A similar experiment is the pulsed neutron experiment where a burst of neutrons is incident on a finite lattice characterized by bucklings $B_\perp^2$ and $B_\parallel^2$. The asymptotic flux is of the form

$$\phi(\underline{r},\underline{\Omega},t) = \psi(x,\underline{\Omega})e^{-\lambda t}\, e^{iB_\perp x}\, e^{iB_\parallel y} \tag{7}$$

We next insert these asymptotic solutions into the one-velocity transport equation

$$\left[\frac{1}{v_0}\frac{\partial}{\partial t} + \mu\frac{\partial}{\partial x} + \eta\frac{\partial}{\partial y} + \Sigma_a(x) + \Sigma_s(x)\right]\phi(x,y,\underline{\Omega})$$

$$= \int d\underline{\Omega}'\Sigma_s(x)f(x,\underline{\Omega}\,|\,\underline{\Omega}')\phi(x,y,\underline{\Omega}')\,, \tag{8}$$

where μ and η are the direction cosines with respect to the x and y axes and define the direction $\underline{\Omega}$. By inserting either Eq. (5), (6) or (7) one obtains the equation

$$\left[\mu \frac{\partial}{\partial x} + \Sigma_e(x,\underline{\Omega})\right] \psi(x,\underline{\Omega}) = \int d\underline{\Omega}' \Sigma_s(x) f(x,\underline{\Omega} \mid \underline{\Omega}') \psi(x,\underline{\Omega}'), \tag{9}$$

where

$$\Sigma_e(x,\underline{\Omega}) = \Sigma_a(x) + \Sigma_s(x) - \mu\kappa_\perp - \eta\kappa_\parallel \tag{10}$$

or

$$\Sigma_e(x,\underline{\Omega}) = \Sigma_a(x) - \frac{\lambda}{v_o} + \Sigma_s(x) + i\mu B_\perp + i\eta B_\parallel \tag{11}$$

Equation (9) is an eigenvalue equation. Either $\kappa_\perp$, $\kappa_\parallel$ or λ is the eigenvalue. Because of the arbitrary choice of the direction cosines μ and η, it is obvious that the results depend only on the square of κ or B. Thus, we might express the eigenvalue as some function of $B_\perp^2$ and $B_\parallel^2$.

$$\lambda = g(B_\perp^2, B_\parallel^2) \tag{12}$$

If we interpret $\kappa_\perp^2 = -B_\perp^2$, $\kappa_\parallel^2 = -B_\parallel^2$, and $\lambda = 0$, then we obtain the results for the diffusion length experiment.

The point of this discussion is that the pulsed neutron and diffusion length experiments are equivalent and that if the solutions of Eq. (9) are found for one experiment for a wide range of λ, $B_\perp$ and $B_\parallel$ (or Σ_a, $\kappa_\perp$ and $\kappa_\parallel$), then the solutions also apply to the other experiment. For convenience we choose Eq. (10) since it contains only real terms. We also will add a constant absorption cross-section to simulate the λ/v_o term.

We next comment on the applicability of a one-velocity model. Equation (12) can be written as

$$\lambda = \lambda_o + v_o D_\perp B_\perp^2 + v_o D_\parallel B_\parallel^2 + \ldots, \tag{13}$$

where $D_\perp$ and $D_\parallel$ are the directional diffusion coefficients. The terms given involve cross-sections averaged over a Maxwellian distribution; the higher order terms give corrections for shifts in the neutron spectrum. Thus, if the one-velocity theory is valid, it is in those regions where the time or actual absorption is small, and Eq. (13) applies.

SOLUTION OF THE EIGENVALUE EQUATION

A variety of methods exists for solving Eqs. (9) and (10). We use a combination of the S_n method with integral transport theory. A straightforward

solution by S_n methods would be quite time-consuming, since $\psi(x,\mu,\eta)$ is a three-dimensional function. Hence we first cast Eq. (9) into an integral equation [18].

$$\psi(x,\underline{\Omega}) = \int_0^a dx' T(x|x',\underline{\Omega}) H(x',\underline{\Omega})$$

$$H(x',\underline{\Omega}) = \int d\underline{\Omega}' \Sigma_s(x') f(x',\underline{\Omega}|\underline{\Omega}') \psi(x',\underline{\Omega}'), \tag{14}$$

where a is the width of a lattice cell. We next expand the angular dependence in terms of ortho-normal angular polynomials of which we will need:

$$P_1(\underline{\Omega}) = \sqrt{1/4\pi}$$

$$P_2(\underline{\Omega}) = \sqrt{3/4\pi}\ \mu$$

$$P_2(\underline{\Omega}) = \sqrt{3/4\pi}\ \eta \tag{15}$$

$$P_3(\underline{\Omega}) = \sqrt{3/4\pi}\ \xi\ ,$$

where ξ is the direction cosine to the z-axis. A typical expansion is

$$H(x,\underline{\Omega}) = \sum_{k=1}^{\infty} H_k(x) P_k(\underline{\Omega}) \tag{16}$$

We restrict the scattering function $f(x,\underline{\Omega}|\underline{\Omega}')$ to be linear in $\mu_0 = \underline{\Omega} \cdot \underline{\Omega}'$. In this case the infinite sum in Eq. (16) reduces to only four terms, since

$$H_1(x) = \Sigma_s(x)\psi_1(x)$$

$$H_n(x) = \bar{\mu}(x)\Sigma_s(x)\psi_n(x), \quad n = 2,3,4 \tag{17}$$

$$H_n(x) = 0, \quad n > 4$$

Insert these expansions in Eq. (9), multiply by $P_\ell(\underline{\Omega})$, and integrate over $\underline{\Omega}$. There results

$$\psi_\ell(x) = \sum_{n=1}^{4} \int_0^a dx' H_n(x') T_{\ell n}(x|x') \qquad (18)$$

$$T_{\ell n}(x|x') \equiv \int d\underline{\Omega} P_\ell(\underline{\Omega}) T(x|x', \underline{\Omega}) P_n(\underline{\Omega})$$

We compute the $T_{\ell n}(x|x')$ by S_n methods [19]. This is quite straightforward and requires no iteration since by definition $T_{\ell n}(x|x')$ is the P_ℓ component of the flux at x, due to a unit source at x' shaped like $P_n(\underline{\Omega})$ in a non-scattering medium whose total cross-section is $\Sigma_e(x,\underline{\Omega})$ from Eq. (10). Since $\psi(x,\underline{\Omega})$ is periodic, the boundary condition is that $\psi(0,\underline{\Omega}) = \psi(a,\underline{\Omega})$.

The spatial integration is done by subdividing the cell into small slabs and assuming ψ to be constant in each small slab. The integration over the small slabs is also done by the S_n part of the calculation.

CALCULATION OF THE EIGENVALUE

Equation (18) is now in the form of a matrix equation which can be solved by the usual iteration methods [20]. Actually, the following equation is solved,

$$\theta\psi_\ell(x) = \sum_{n=1}^{4} \int_0^a dx' H_n(x') T_{\ell n}(x|x'), \qquad (19)$$

where θ is an auxiliary eigenvalue. If we wish to compute $\kappa_\perp$, we set $\kappa_\parallel = 0$, insert a trial value of $\kappa_\perp$ and compute θ. This procedure is repeated until a $\kappa_\perp$ is found such that $\theta = 1$. We next set $\kappa_\parallel$ to some arbitrary value and iterate on $\kappa_\perp$ until $\theta = 1$. In this way we obtain pairs of values of $\kappa_\perp$ and $\kappa_\parallel$ which are the eigenvalues of Eq. (9). The entire procedure is then repeated using several values of a constant absorption cross-section to simulate the time absorption. These results are collected and fit to an expression like Eq. (13) and the values of $D_\perp$ and $D_\parallel$ obtained. In this paper we will present only the results for the eigenvalues $\kappa_\perp$ and $\kappa_\parallel$.

RESULTS

There are two main sources of numerical error in our calculations. The first involves the number of subdivisions used in the spatial treatment. In nearly all cases the error in the eigenvalue was less than 0.5% if the spatial subdivisions were less than 0.5 mean free paths. The second error involves the order of the S_n approximation used. An S_4 calculation always gave accurate results for $\kappa_\perp$ but the errors in $\kappa_\parallel$ were an order of magnitude larger and errors of a few per cent were noted in some S_8 calculations of $\kappa_\parallel$. The calculations reported here were done with S_8.

TABLE I

EIGENVALUES FOR ALUMINIUM WATER SLAB LATTICES

$\Sigma_w t_w$ *	$\rho = t_{Al}/t_w$	$\kappa_\perp$ (cm^{-1})	$\kappa_\parallel$ (cm^{-1})	$\kappa_\perp^2/\kappa_\parallel^2$
0.5	0.5	0.3064	0.3008	1.038
	1.0	0.2574	0.2473	1.083
	2.0	0.2046	0.1915	1.142
	4.0	0.1573	0.1441	1.192
	9.0	0.1152	0.1047	1.210
1.0	0.5	0.3060	0.2890	1.077
	1.0	0.2566	0.2284	1.262
	2.0	0.2031	0.1697	1.432
	4.0	0.1550	0.1247	1.545
	9.0	0.1121	0.0909	1.519
	23.0	0.0834	0.0705	1.399
2.0	0.5	0.3054	0.2664	1.314
	1.0	0.2549	0.1981	1.656
	2.0	0.1997	0.1412	2.002
	4.0	0.1540	0.1032	2.226
	9.0	0.1102	0.0780	1.995
3.0	0.5	0.3046	0.2479	1.511
	1.0	0.2528	0.1777	2.024
	2.0	0.1952	0.1249	2.443
	4.0	0.1500	0.0924	2.637

* $\Sigma_w = 2.234$ cm^{-1} (transport cross-section).

A series of calculations was done on a system of alternating slabs of water and aluminium. The following thermal cross-sections were used.

Aluminium: $\Sigma_a = 0.01228$ cm^{-1}

$\Sigma_s = 0.08428$ cm^{-1}

$\bar{\mu} = 0$

Water: $\Sigma_a = 0.01947$

$\Sigma_s = 2.593$

$\bar{\mu} = 0.25$

We define ρ as the ratio of the thickness of aluminium to the thickness of water, and the quantity $\Sigma_w t_w$ as the thickness of the water region in trans-

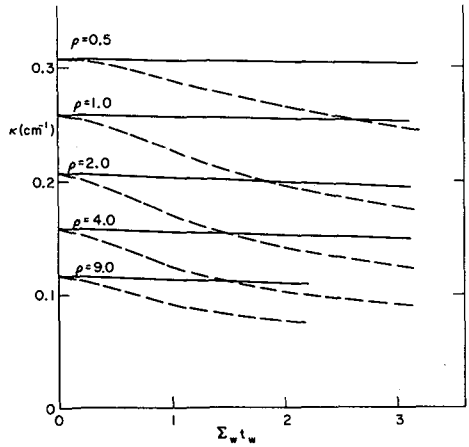

Fig. 1

Eigenvalues for aluminium-water slab lattices

$\kappa_\perp$

$\kappa_{\parallel}$

$\Sigma_w = 2.234\ cm^{-1}$

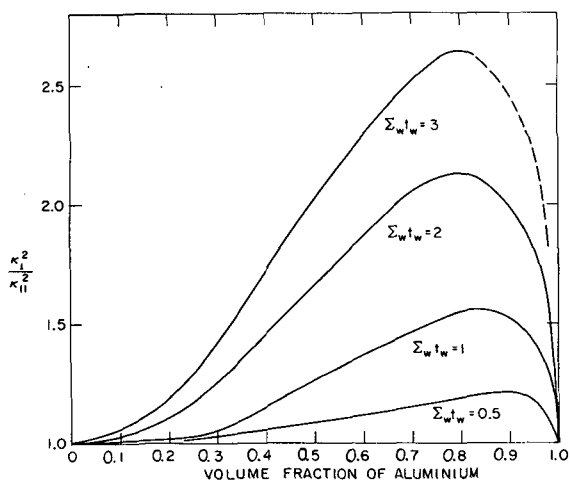

Fig. 2

Anisotropy in aluminium-water slab lattices

$\Sigma_w = 2.234\ cm^{-1}$

(Transport cross-section)

port mean free paths. Our results for $\kappa_\perp$, $\kappa_{\parallel}$, and the anisotropy $(\kappa_\perp/\kappa_{\parallel})^2$ are given in Table I and plotted in Figs. 1 and 2.

In Fig. 1 we observe that $\kappa_\perp$ is insensitive to the slab thickness and deviates only slightly from the homogeneous value. The anisotropy is mainly

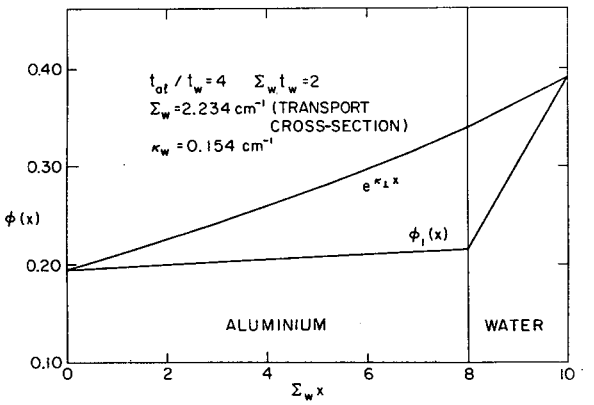

Fig. 3

Scalar flux distribution in a cell

$t_{al}/t_w = 4$;

$\Sigma_w t_w = 2$;

$\kappa_w = 0.154\ cm^{-1}$

$\Sigma_w = 2.234\ cm^{-1}$

(Transport cross-section)

a result of the decrease in κ_{11} with increasing slab thickness. The anisotropy is nearly linear with slab thickness and for thick slabs is maximum when the volume fraction of aluminium is near 0.8. As the slab thickness decreases, the point of maximum anisotropy appears to shift toward higher aluminium-water ratios. It is interesting to note that a large anisotropy (≈ 2) can be obtained in experimentally realizable situations. For example, $t_w = 1.34$ cm, $\rho = 1$; $t_w = 0.9$, $\rho = 2$ or 9. The curves presented in Figs. 1 and 2 should aid in the design of future experiments.

It is of considerable theoretical interest to know the shape of the flux within a cell. The scalar flux distribution in a cell is shown in Fig. 3 and it is evident that the flux is very linear in each region. This linearity is probably a result of the weak absorption in the system. Nevertheless, the indication is that linear trial functions for the flux in a variational calculation should give excellent results. Note that it is the flux $\phi(x)$ that is linear rather than the periodic flux $\psi(x)$.

CONCLUSION

We have developed a numerical method for computing anisotropic leakage in a slab lattice. Results have been presented for a wide range of slab thicknesses and volume ratios of aluminium-water lattices. These results can be used to design either a pulsed neutron experiment or diffusion length experiment.

REFERENCES

[1] GLASSTONE, S. and EDLUND, M.C., The Elements of Nuclear Reactor Theory, D. Van Nostrand Co., Inc., Princeton, N.J. (1952).

[2] WEINBERG, A.M. and WIGNER, E.P., The Physical Theory of Neutron Chain Reactors, The University of Chicago Press, Chicago, Ill. (1958).

[3] RUSSELL, J.L., Trans. Amer. nucl. Soc. 2 (1959) 19-28.

[4] BEELER, J.R., Diffusion Tensor for Slab Geometry, Apex. 488.

[5] BEHRENS, D.J., The effects of holes in a reacting material on the passage of neutrons, Proc. phys. Soc. A62 (1949) 607-16.

[6] LALETIN, N.I., The effect of a cylindrical channel on neutron diffusion, J. nucl. Energy 13 (1960) 57-64.

[7] CARTER, C., Streaming due to holes in a reactor, J. nucl. Energy 15 (1961) 76-80.

[8] CHERNICK, J. and KAPLAN, I., J. nucl. Energy 2 (1955) 41.

[9] SPINRAD, B.I., Anisotropic diffusion lengths in diffusion theory, J. appl. Phys. 26 (1955) 548-50.

[10] SHEVELEV, Ya.V., Neutron diffusion in a one-dimensional uranium-water lattice, J. nucl. Energy 6 (1957) 132-41.

[11] FERZIGER, J.H. et al., Diffusion lengths in heterogeneous media, Nucl. Sci. Engng 10 (1961) 285-94.

[12] LESLIE, D.C., The weighting of diffusion coefficients in cell calculations, J. nucl. Energy 16 (1962) 1-11.

[13] BENOIST, P., Theorie du coefficient du diffusion dans un reseau comportant des cavites, CEA.

[14] BEHRENS, H. and OLDEKOP, W., Calculation of migration areas in heterogeneous reactors with periodic structure, Nukleonik 6 3 (1964).

[15] LESLIE, D.C., The calculation of leakage and of flux distributions in systems with surimposed buckling, Rpt. AEEW-M292.

[16] DAVISON, B., The effective thermal diffusion length in a sandwich reactor, J. nucl. Energy 7 (1958) 51-68.

[17] BEELER, J.R., Diffusion anisotropy in singly- and doubly-periodic lattices, Nucl. Sci. Engng 14 (1962) 254-65.

[18] HONECK, H.C., Internal memo (27 April 1964).

[19] CARLSON, B.G., Numerical formulation and solution of neutron transport problems, Rpt. LA-2996.

[20] HONECK, H.C., Rpt. BNL-5826 (1961).

[21] TRLIFAJ, L., A variational method for the homogenization of a heterogeneous medium, J. nucl. Energy 6 (1957) 142-54.

[22] SELENGUT, D.S., Diffusion coefficients for heterogeneous systems, Rpt. HW-60220 (1959) 65-84.

DISCUSSION

M.N. MOORE: It would be surprising if the only solution to the Boltzmann equation in slab geometry with a source at the boundary was $e^{-\kappa x}$. By using $e^{-\kappa x}$ as an Ansatz, one finds κ as a function of the buckling. However, one does not see other solutions. Have you investigated the uniqueness of $e^{-\kappa x}$, and, if so, how large are these other solutions compared to $e^{-\kappa x}$?

H.C. HONECK: The solutions looked for here are asymptotic solutions of the form $e^{-\kappa x}\psi(x)$, where $\psi(x)$ is the fine structure in the lattice. The results presented are for the lowest eigenvalue or smallest κ. The method can and has been used to obtain some higher eigenvalues.

L.G. KEMENY: May I ask Dr. Honeck whether his calculations will ultimately lead to the definition of a "diffusion tensor" for cases of anisotropic diffusion in multi-dimensional geometries? In such a case the "diffusion coefficient" might take the form of a 3×3 matrix, for example. I understand

that this approach has already been tried in similar geometries on a numerical – Monte Carlo – basis.

H.C. HONECK: This type of calculation would certainly lead to a "diffusion tensor" which could be used in reactor calculations. The most practical systems are, of course, rod lattices and the present theory is only for slabs. Here, Monte Carlo calculations may be necessary and some have been done by Beeler.

A. HENRY: In any multiregion assembly it can be shown that there is no such thing as equivalent homogeneous κ's. In view of this I don't know whether it is going to be practical to work with tensor diffusion constants.

E.G. SILVER: Do you know of any pulsed-neutron experiments in slab lattices to compare with your calculations?

H.C. HONECK: I believe that experiments on lucite-aluminium slabs have been done at North Carolina State University; others have been done on polyethylene-aluminium slabs at Brookhaven National Laboratory but final results are not yet available.

M. KAZARNOVSKY: In this investigation one might have expected a characteristic diffusion-cooling effect in some slabs and a heating effect in others. This effect would be expected to increase as the thickness of the slabs decreased. Have any estimates been made of this effect?

H.C. HONECK: No. The present study involved only one energy group and was intended to investigate the mathematical and numerical problems encountered in describing the spatial and angular distributions.

SPECTRAL CORRECTION ANALYSIS OF PULSED NEUTRON DIFFUSION PARAMETERS

J. A. DE JUREN
ATOMICS INTERNATIONAL, CANOGA PARK, CALIF.,
UNITED STATES OF AMERICA

Abstract — Résumé — Аннотация — Resumen

SPECTRAL CORRECTION ANALYSIS OF PULSED NEUTRON DIFFUSION PARAMETERS. The conventional expansion of the decay constant as a power series of the buckling in moderator die-away experiments is abandoned. Instead the decay constant is expressed as

$$\alpha_B = v\Sigma_a + D_B B^2,$$

where $D_B = \lambda_B v_B/3$, and for $B^2 = 0$, $D_0 = \lambda_0 v_0/3$.

The assumption will be made that the cooling from neutron leakage in a finite moderator reduces the effective Maxwellian temperature of the neutron spectrum, T_B, from the moderator temperature T_0. To take into account the variation of transport mean free path λ_B and the velocity with buckling the temperature dependence of the diffusion coefficient is assumed as

$$D_B = D_0(T_B/T_0)^w,$$

where w may be evaluated from diffusion length (or pulsed) measurements at different temperatures.

These expressions may be related by means of the heat transfer coefficient, γ. The average heat transfer from the moderator to a neutron is

$$\frac{dE}{dt} = \frac{3}{2}k\gamma(T_0 - T_B).$$

The following relations are derived:

$$\frac{T_0}{T_B} = 1 + \frac{2w}{3\gamma} D_B B^2,$$

or

$$\frac{v_0}{v_B} \left[1 + \frac{2w}{3\gamma} D_B B^2\right]^{\frac{1}{2}},$$

$$D_0 = D_B\left(1 + \frac{2w}{3\gamma} D_B B^2\right)^w.$$

A code has been developed to determine $v\Sigma_a$, D_0, γ, and v_B/v_0 from these relationships. Results are given for carbon, beryllium, light water and heavy water.

ANALYSE A CORRECTION SPECTRALE DES PARAMÈTRES DE DIFFUSION DES NEUTRONS PULSÉS. L'auteur a abandonné la méthode classique du développement de la constante de décroissance en série de puissances du laplacien dans les expériences sur l'«évanouissement» dans le ralentisseur. Il exprime cette constante par la formule

$$\alpha_B = v\Sigma_a + D_B B^2,$$

où $D_B = \lambda_B v_B/3$, et pour $B^2 = 0$, $D_0 = \lambda_0 v_0/3$.

Il suppose que le refroidissement dû à une fuite de neutrons dans un ralentisseur fini réduit la température maxwellienne effective du spectre des neutrons, T_B, à partir de la température du ralentisseur T_0. Pour tenir compte de la variation du libre parcours moyen de transport λ_B et de la vitesse en fonction du laplacien, il admet que la variation du coefficient de diffusion en fonction de la température est définie par la loi

$$D_B = D_0(T_B/T_0)^w,$$

où w peut être évaluée par des mesures au moyen des neutrons pulsés pour différentes températures.

Entre ces expressions on peut établir une relation en faisant intervenir le coefficient de transfert de chaleur γ. Le transfert de chaleur moyen du ralentisseur à un neutron est

$$\frac{dE}{dt} = \frac{3}{2} k\gamma (T_0 - T_B),$$

d'où les relations suivantes:

$$\frac{T_0}{T_B} = 1 + \frac{2w}{3\gamma} D_B B^2,$$

ou

$$\frac{v_0}{v_B} = \left[1 + \frac{2w}{3\gamma} D_B B^2\right]^{\frac{1}{2}},$$

$$D_0 = D_B\left(1 + \frac{2w}{3\gamma} D_B B^2\right)^w.$$

L'auteur a élaboré un code permettant de déterminer $v\Sigma_a$, D_0, γ, et v_B/v_0 à partir de ces relations. Il indique les résultats qu'il a obtenus pour le carbone, le béryllium, l'eau légère et l'eau lourde.

АНАЛИЗ СПЕКТРАЛЬНЫХ ПОПРАВОК ДИФФУЗИОННЫХ ПАРАМЕТРОВ ИМПУЛЬСНЫХ НЕЙТРОНОВ. При экспериментах исчезновения активности в замедлителе обычное разложение постоянной распада в экспоненциальный ряд лапласиана больше не употребляется. Вместо этого, постоянная распада выражается следующей формулой:

$$\alpha_B = v\Sigma_a + D_B B^2,$$

где

$$D_B = \frac{\lambda_B v_B}{3}, \quad \text{а для} \quad B^2 = 0,$$

$$D_0 = \frac{\lambda_0 v_0}{3}.$$

Делается предположение о том, что охлаждение, вызываемое утечкой нейтронов в замедлителе конечных размеров, уменьшает температуру T_0 замедлителя на эффективную максвелловскую температуру нейтронного спектра T_B. Чтобы учесть изменение величины среднего свободного пути переноса λ_B и скорость в зависимости от лапласиана, температурная зависимость коэффициента диффузии записывается следующей формулой:

$$D_B = D_0\left(\frac{T_B}{T_0}\right)^w,$$

где w может быть определено на основании измерений длины диффузии или импульсных измерений при разных температурах.

Эти выражения могут быть объяснены с помощью γ-коэффициента теплопередачи. Средняя теплопередача замедлителя нейтрону определяется по формуле:

$$\frac{dE}{dt} = \frac{3}{2} k\gamma (T_0 - T_B).$$

Выводятся следующие отношения:

$$\frac{T_0}{T_B} = 1 + \frac{2w}{3\gamma} D_B B^2$$

или

$$\frac{v_0}{v_B} = \left[1 + \frac{2w}{3\gamma} D_B B^2 \right]^{1/2}, \quad D_0 = D_B \left(1 + \frac{2w}{3\gamma} D_B B^2\right)^w .$$

На основании этих соотношений был выработан код для определения $v\Sigma_a$, D_0, λ и v_B/v_0. Сообщаются результаты для углерода, бериллия, обыкновенной и тяжелой воды.

ANALISIS DE PARAMETROS DE DIFUSION DE NEUTRONES PULSADOS POR CORRECCION ESPECTRAL. En vez de desarrollar la constante de decremento en forma de serie exponencial del laplaciano, como se suele hacer en los experimentos de atenuación en el moderador, el autor la expresa con la ecuación:

$$\alpha_B = v\Sigma_a + D_B B^2,$$

siendo $D_B = \lambda_B v_B/3$, y cuando $B^2 = 0$, entonces $D_0 = \lambda_0 v_0/3$.

El postulado es que el enfriamiento por escape neutrónico en un moderador finito hace que la temperatura efectiva de Maxwell del espectro neutrónico, T_B, sea inferior a la temperatura T_0 del moderador. Para incluir la variación del libre recorrido medio de transporte, λ_B, y la velocidad, teniendo en cuenta el laplaciano, se supone que el coeficiente de difusión en función de la temperatura queda expresado por

$$D_B = D_0 (T_B/T_0)^w,$$

pudiéndose calcular w por medición de la longitud de difusión (o pulsada) a distintas temperaturas.

Estas fórmulas se pueden relacionar entre sí por medio del coeficiente de transferencia de calor γ. La transferencia media de calor del moderador a un neutrón es

$$\frac{dE}{dt} = \frac{3}{2} k\gamma (T_0 - T_B).$$

De esta fórmula se pueden derivar las siguientes relaciones:

$$\frac{T_0}{T_B} = 1 + \frac{2w}{3\gamma} D_B B^2,$$

o bien:

$$\frac{v_0}{v_B} = \left[1 + \frac{2w}{3\gamma} D_B B^2 \right]^{\frac{1}{2}},$$

$$D_0 = D_B \left(1 + \frac{2w}{3\gamma} D_B B^2\right)^w.$$

Se ha confeccionado una clave para determinar $v\Sigma_a$, D_0, γ, y v_B/v_0 a partir de estas ecuaciones. Se dan los resultados obtenidos para el carbono, el berilio, el agual ligera y el agua pesada.

1. INTRODUCTION

In the past few years the pulsed neutron technique has become a powerful tool in studying neutron diffusion. An analytic fit is made to the decay constant of the fundamental mode α for a series of bucklings in a given moderator. At first, attempts were made to use the relationship $\alpha = v\Sigma_a + D_0 B^2$;

however, it was soon apparent that the decay constants for large bucklings fell below the tangent to the values for small bucklings. As the size of the moderator is decreased, the ratio of neutron leakage to capture increases. The leakage neutrons have a higher average energy than the neutrons remaining since the chance of escape is proportional to the velocity (flux weighting). As a result, the neutrons in a small moderator should have a lower temperature than those in a larger volume and the diffusion constant should decrease as the size decreases. To account for the spectral change a diffusion cooling coefficient C was introduced [1].

A least-squares fit was made to the parabola

$$\begin{aligned} \alpha &= v\Sigma_a + D_0B^2 - CB^4 \\ &= v\Sigma_a + D_0B^2\left(1 - \frac{C}{D_0}B^2\right). \end{aligned} \tag{1}$$

For a small range of bucklings this type of fit seemed adequate; however as the buckling values were increased and a steady-state point was included at $\alpha = 0$, it appeared that a three-parameter fit was inadequate. Accordingly extra terms were added,

$$\alpha = v\Sigma_a + D_0B^2 - CB^4 + FB^6 + \ldots \tag{2}$$

In most moderators the picture is clouded by the difficulty in obtaining reliable decay constants for the larger bucklings. In the case of water reliable extrapolation lengths for different geometric bucklings must also be obtained [2, 3]. Values of C are often in disagreement and higher order parameters are conjectural. If the last term in the buckling expansion is negative, it will dominate at very large bucklings. Since the decay constant will always increase with buckling, the range of a satisfactory fit will be limited if $-CB^4$ is the last term.

2. SPECTRAL CORRECTION ANALYSIS

In an effort to find a better functional form, the conventional power series expansion of the decay constant is abandoned. Instead the expression

$$\alpha_B = v\Sigma_a + D_BB^2 \tag{3}$$

will be retained, where

$$D_B = \frac{\lambda_B v_B}{3},$$

and for $B^2 = 0$,

$$D_0 = \frac{\lambda_0 v_0}{3}.$$

An attempt will be made to find a relationship between D_B and D_0. We will assume that the cooling from leakage reduces the effective Maxwellian temperature of the neutron spectrum to a value T_B compared with the moderator temperature T_0. To take into account the variation of the diffusion coefficient with temperature the relation

$$D_B = D_0\left(\frac{T_B}{T_0}\right)^w \tag{4}$$

is introduced, where the constant w may be evaluated from diffusion length (or pulsed) measurements at different temperatures.

BECKURTS [4] has introduced a simple thermalization theory to take into account temperature changes caused by diffusion cooling. A temperature equilibrium is reached when the neutron population has as much energy gain by heat transfer from the moderator as the energy loss in excess of the average, due to leakage. The rate of energy loss in excess of the average per escaping neutron is

$$-\frac{dE}{dt} = D_B B^2(\bar{E}_a - \frac{3}{2}kT_B)$$

where $\bar{E}_a$ is the mean neutron energy of the leakage flux. The heat transfer from the moderator to a neutron is

$$\frac{dE}{dt} = \frac{3}{2}\,k\gamma(T_0 - T_B)$$

where the γ is the heat transfer coefficient defined by this equation. At equilibrium we have

$$\frac{3}{2}k\gamma(T_0 - T_B) = D_B B^2(\bar{E}_a - \frac{3}{2}kT_B) \tag{5}$$

with

$$\bar{E}_a = \frac{\frac{m}{2}\int_0^\infty D(v)v^2n(v)dv}{\int_0^\infty D(v)n(v)dv}.$$

If the neutron density is expressed as a function of temperature

$$n(T)dT = \frac{2\pi}{(\pi T_B)^{3/2}}\,e^{-T/T_B}T^{1/2}dT.$$

Since $\frac{1}{2}mv^2 = kT$ and $D(T) = D_0\left(\frac{T}{T_0}\right)^w$ the mean energy becomes

$$\bar{E}_a = \frac{k\int_0^\infty T^{(3/2+w)}\,e^{-T/T_B}dT}{\int_0^\infty T^{(1/2+w)}\,e^{-T/T_B}dT} = (\frac{3}{2} + w)kT_B. \tag{6}$$

Then Eq. (5) reduces to

$$\frac{3}{2}k\gamma(T_0 - T_B) = wD_B B^2 kT_B$$

and

$$\frac{T_0}{T_B} = 1 + \frac{2w}{3\gamma} D_B B^2, \tag{7}$$

or

$$\frac{v_0}{v_B} = \left[1 + \frac{2w}{3\gamma} D_B B^2 \right]^{1/2}. \tag{8}$$

As a result Eqs. (4) and (7) may be combined to give

$$D_0 = D_B(1 + \frac{2w}{3\gamma} D_B B^2)^w. \tag{9}$$

The decay constants corrected for the spectral change, $\alpha(v_0)$, become

$$\alpha(v_0) = v\Sigma_a + D_0 B^2 \tag{10}$$

$$= D_B B^2(1 + \frac{2w}{3\gamma} D_B B^2)^w + v\Sigma_a$$

$$= (\alpha_B - v\Sigma_a) \left[1 + \frac{2w}{3\gamma}(\alpha_B - v\Sigma_a) \right]^w + v\Sigma_a \tag{11}$$

In our early work [5] initial choices were made of $v\Sigma_a$ and γ to obtain corrected decay constants and a weighted straight-line least-squares fit was made using Eq. (10). For a given γ, iterations were made until the sum of the weighted deviations, $\sigma_f^2 = \Sigma w_i \delta_i^2$, reached a minimum value. Then γ was varied until σ_f^2 was minimized. The errors in D_0 and γ were difficult to evaluate and approximations were used. Equations (9) and (11) are not sensitive to the value of w, which is usually between 0.4 and 1.0 for most moderators at or above room temperature. If the first term of the binomial approximation is used,

$$\alpha(v_0) = v\Sigma_a + (\alpha_B - v\Sigma_a) \left[1 + \frac{2w^2}{2\gamma}(\alpha_B - v\Sigma_a) \right] \tag{12}$$

results. A poor choice of w will yield an incorrect γ, but the ratio w^2/γ obtained and therefore $v\Sigma_a$ and D_0 are independent of the choice of w in the approximation. For the exact expression $v\Sigma_a$ and D_0 are unchanged when w is close to 1.0, as in the case of water, and are barely changed (within statistical errors) in other moderators by a poor choice of w; however,

an accurate value of w is needed to obtain temperature and velocity ratios. In deriving the weights for a fit, it was assumed that $\alpha(v_0)$ has the same relative error as α_B, which is not strictly true.

A code has been developed based on a method suggested by VAUGHAN [6] which obviates this difficulty by fitting the experimental decay constants directly. A new variable η is introduced defined as

$$\eta = \frac{2w}{3\gamma} D_0. \tag{13}$$

The temperature is eliminated between Eqs. (4) and (7) with the result

$$\frac{D_B}{D_0} = \left[1 + \eta B^2 \frac{D_B}{D_0} \right]^{-w} \tag{14}$$

or

$$\frac{D_B}{D_0} = f(\eta B^2) \tag{15}$$

Then Eq. (3) becomes

$$\alpha_B = v\Sigma_a + D_0 B^2 f(\eta B^2). \tag{16}$$

An initial guess, η_0, is made for the value of η, and η is set equal to $\eta_0 + \delta$ where δ is the error in the estimation so that the best value of δ is zero. If δ is assumed small, a Taylor's expansion gives

$$f(\eta B^2) = f(\eta_0 B^2) + \delta B^2 f'(\eta_0 B^2). \tag{17}$$

Then

$$\alpha_B = v\Sigma_a + D_0 B^2 f(\eta_0 B^2) + D_0 \delta B^4 f'(\eta_0 B^2). \tag{18}$$

If we let $x = \eta B^2$, Eq. (14) may be expressed as

$$f(x) = [1 + xf(x)]^{-w} \tag{19}$$

and differentiating with respect to x we obtain

$$f'(x) = \frac{-wf^2(x)}{1 + (1 + w)xf(x)}. \tag{20}$$

By successive approximations, values of $f(\eta_0 B^2)$ and $f'(\eta_0 B^2)$ can be determined for the various bucklings. Then a weighted least-squares fit is made to Eq. (18), and $v\Sigma_a$, D_0 and $D_0\delta$ and their errors are determined. The value of δ obtained from the last two parameters is added to η_0, and iteration continues until the δ obtained from a fit is sufficiently small compared to η_0 to determine the parameters with negligible computational error.

The error in γ has been calculated by the code with the assumption that the error in w is zero. In the moderators to be discussed w was not always known, and trial values were inserted in the code. To get the composite error in γ, the relative error from the code result should be compounded with the relative error in w^2 since w^2/γ is essentially determined by the fit.

3. APPLICATION TO MODERATORS

3. 1. Graphite

The results for the corrected decay constants have been given previously [5]. Using the latest approach with the uncorrected experimental decay constants, σ_f dropped to 1. 22 from 1. 31 with the corrected constants, and the errors in the parameters were reduced slightly. For AGOT graphite at 23. 5°C and a density of 1. 689 g/cm^3 the values obtained for w = 0. 48 ± 0. 01 [7] are:

$$v\Sigma_a = 77.89 \pm 0.47 \text{ sec}^{-1}$$

$$D_0 = (2.0948 \pm 0.0056) \times 10^5 \text{ cm}^2 \text{ sec}^{-1}$$

$$\gamma = 1620 \pm 57 \text{ sec}^{-1}$$

$$\sigma_f = 1.22.$$

The decay data and velocity ratios are included in Table I for completeness.

Without the steady state point the parameter values were:

$$v\Sigma_a = 80.7 \pm 6.1 \text{ sec}^{-1}$$

$$D_0 = (2.079 \pm 0.034) \times 10^5 \text{ cm}^2 \text{ sec}^{-1}$$

$$\gamma = 1708 \pm 228 \text{ sec}^{-1}$$

$$\sigma_f = 1.27.$$

The usual quadratic fit for the pulsed data only gave the following parameters:

$$v\Sigma_a = 89.9 \pm 3.9 \text{ sec}^{-1}$$

$$D_0 = (2.008 \pm 0.017) \times 10^5 \text{ cm}^2 \text{ sec}^{-1}$$

$$C = (21.2 \pm 1.6) \times 10^5 \text{ cm}^4 \text{ sec}^{-1}$$

$$\sigma_f = 1.19.$$

Based on the goodness of fit, σ_f, and the size of the errors one would conclude that this fit is superior; however when the steady state point is

TABLE I

PULSED NEUTRON DATA IN GRAPHITE

B^2 (cm^{-2})	α_B (sec^{-1})	v_B/v_0
-3.685×10^{-4}	0.00 ± 0.43	1.0077 ± 0.0003
1.944×10^{-3}	473.0 ± 2.4	0.9632 ± 0.0013
2.360	547.8 ± 2.1	0.9566 ± 0.0015
2.561	592.4 ± 1.2	0.9527 ± 0.0016
2.762	626.3 ± 1.7	0.9499 ± 0.0017
3.714	807.2 ± 1.6	0.9349 ± 0.0021
4.112	879.4 ± 1.8	0.9291 ± 0.0023
4.712	987.3 ± 2.0	0.9207 ± 0.0025
5.312	1095.7 ± 3.2	0.9125 ± 0.0027
6.928	1382.1 ± 2.8	0.8917 ± 0.0033
8.862	1705.4 ± 3.9	0.8699 ± 0.0038
10.57	1971.9 ± 5.4	0.8531 ± 0.0042

included, σ_f jumps to 1.67, indicating that the function does not adequately fit the full data. When the FB^4 term is added, σ_f drops to 1.35 and the following parameters are obtained:

$$v\Sigma_a = 77.41 \pm 0.60 \text{ sec}^{-1}$$

$$D_0 = (2.0863 \pm 0.0097)\times10^5 \text{ cm}^2 \text{ sec}^{-1}$$

$$C = (35.4 \pm 3.8)\times10^5 \text{ cm}^4 \text{ sec}^{-1}$$

$$F = (7.6 \pm 3.1)\times10^7 \text{ cm}^6 \text{ sec}^{-1}.$$

Errors because of temperature and density variations in the graphite were not included, causing σ_f to level off at about 1.2 for a good fit rather than 1.0

3.2. Light water

Some unpublished decay data (Table II) of Stooksberry and De Juren in cylinders of water at 23° are treated next. The value of $w = 0.87 \pm 0.01$ and $L = 2.781 \pm 0.006$ cm was obtained from previously published steady state data [8]. Extrapolation lengths used to obtain the bucklings were derived from Gelbard's treatment [2] and varied from 0.32 to 0.35 cm. Values of the parameters were:

TABLE II

PULSED NEUTRON DATA IN WATER

B^2 (cm^{-2})	α_B (sec^{-1})	v_B/v_0
-1.293×10^{-1}	0.00 ± 22	1.0038 ± 0.0009
3.068×10^{-2}	5797 ± 28	0.9991 ± 0.0002
1.126×10^{-1}	8863 ± 89	0.9967 ± 0.0008
1.540	10190 ± 85	0.9956 ± 0.0011
2.078	12120 ± 82	0.9941 ± 0.0014
3.962	18680 ± 140	0.9890 ± 0.0026
6.458	27320 ± 130	0.9823 ± 0.0042

$$v\Sigma_a = 4699 \pm 20 \text{ sec}^{-1}$$

$$D_0 = 36110 \pm 150 \text{ cm}^2 \text{ sec}^{-1}$$

$$\gamma = (3.61 \pm 0.85) \times 10^5 \text{ sec}^{-1}.$$

The parameters derived without the steady state point are in agreement with these values, but the statistical errors are of course higher. The value of D_0 obtained is in agreement with representative pulsed measurements and with steady state measurements corrected for diffusion hardening [9]. A good set of pulsed extrapolation length measurements in representative bucklings is still needed.

3.3. *Beryllium*

ANDREWS [10] has made a series of pulsed measurements in beryllium at five different temperatures. No steady-state data were taken. At the three highest temperatures the transport mean free path is in a region where it is quite flat, corresponding to a value of $w = 0.5$. At lower temperatures the spectrum is distorted by the drop-off of the scattering cross-section below 0.007 eV and the spectrum loses its Maxwellian appearance [11]. Here the effective transport mean free path is longer, and values of w lower than 0.5 must be used. Results of the analysis appear in Table III. The errors assumed for w are estimates and the values marked by asterisks were included to show the insensitivity of $v\Sigma_a$ and D_0 to the choice of w. The value of γ, of course, depends markedly on the choice of w. Andrews increased the errors of his decay constants to one or two per cent, and the numbers in parentheses are internal errors based on the input errors of the decay constants. Removing points at high bucklings did not change the parameters appreciably. Andrews, using the conventional three-parameter fits, lists the variation in $v\Sigma_a$ from 285 ± 8 sec^{-1} at 292°K to 270.5 ± 8 sec^{-1} at 478°K where the densities are corrected to 1.85 g/cm^3. The present results vary

TABLE III

PULSED NEUTRON DIFFUSION PARAMETERS IN BERYLLIUM

Points	T	w	γ (10^3 sec^{-1})	$\nu\Sigma_a$ (sec^{-1})	D_0 (10^5 cm^2 sec^{-1})
11	292°K	0.32 ± 0.08	2.06 ± 0.22 (0.49)	275.5 ± 5.6 (12.6)	1.270 ± 0.012 (0.028)
11		0.50* ± 0.08	5.67 ± 0.51 (1.20)	277.3 ± 5.2 (12.0)	1.264 ± 0.011 (0.026)
9	354°K	0.48 ± 0.04	8.08 ± 0.73 (2.23)	273.8 ± 4.1 (12.4)	1.336 ± 0.009 (0.027)
7		0.48 ± 0.04	9.65 ± 1.11 (4.43)	277.7 ± 3.5 (13.9)	1.325 ± 0.008 (0.033)
9		0.32* ± 0.04	3.31 ± 0.34 (0.99)	272.8 ± 4.3 (12.8)	1.340 ± 0.010 (0.029)
9	394°K	0.50 ± 0.02	12.55 ± 1.1 (4.1)	274.4 ± 3.3 (12.2)	1.375 ± 0.007 (0.026)
9	437°K	0.50 ± 0.02	13.39 ± 0.95 (4.4)	267.8 ± 2.7 (12.6)	1.437 ± 0.006 (0.027)
9	478°K	0.50 ± 0.02	13.94 ± 2.2 (4.4)	269.3 ± 6.5 (12.9)	1.493 ± 0.014 (0.028)

from 275.5 ± 5.6 to 271.3 ± 6.5 with the same density correction, or $v\Sigma_a$ may be assumed constant within experimental errors. The difference in the zero buckling extrapolation is again illustrated for the two methods of fitting. Using either method of analysis the results at 292°K may be questionable because of the distortion of the spectrum with increase in buckling. This distortion may have occurred for the two highest bucklings at 354°K, which were eliminated in the seven-point analysis. The velocity ratio distributions are similar at the three highest temperatures and the 437°K case is illustrated in Fig. 1.

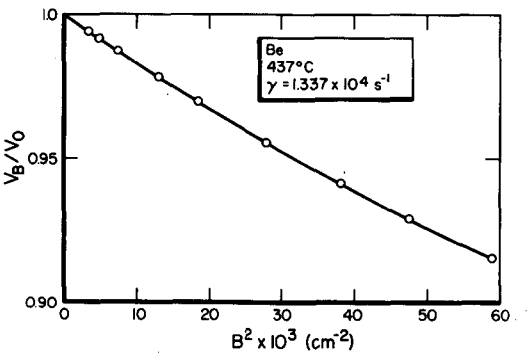

Fig. 1

Neutron velocity ratio with buckling in beryllium

3.4. Heavy water

In the case of heavy water most experimentalists have not measured many bucklings at a given temperature. MEISTER and KUSSMAUL [12] have investigated heavy water at 22°C for 15 sizes. The analysis of their data is summarized in Table IV. When the four highest bucklings were removed, D_0 dropped to $(1.997 \pm 0.013) \times 10^5$ cm^2 sec^{-1}. This change in D_0 was also noted with conventional fitting.

Meister and Kussmaul obtained the following values from conventional fitting for the whole buckling range, 13×10^{-4} cm^{-2} to 466×10^{-4} cm^{-2}.

$$v\Sigma_a = 19.0 \pm 2.5 \text{ sec}^{-1}$$

$$D_0 = (2.000 \pm 0.009) \times 10^5 \text{ cm}^2 \text{ sec}^{-1}$$

$$C = (5.25 \pm 0.25) \times 10^5 \text{ cm}^4 \text{ sec}^{-1}.$$

The heavy water was 99.82 mole% D_2O and Meister and Kussmaul list the absorption cross-section calculated from nuclear cross-sections as $v\Sigma_a = 16.5$ sec^{-1}. Once again the spectral correction technique gives values of $v\Sigma_a$ slightly lower and D_0 slightly higher than the power series approach. The value of $w = 0.95$ was inferred from the measurements of DAUGHTRY and WALTNER [13].

TABLE IV

PULSED NEUTRON DIFFUSION PARAMETERS IN D_2O

Points	w	γ (10^4 sec^{-1})	$v\Sigma_a$ (sec^{-1})	D (10^5 cm^2 sec^{-1})
15	0.95 ± 0.05	3.38 ± 0.26	17.53 ± 2.0	2.020 ± 0.012
15	0.70 ± 0.10	1.78 ± 0.14	17.35 ± 2.0	2.022 ± 0.012

4. THERMALIZATION TIME CONSTANT

For the non-equilibrium case, a solution must be found for the equation

$$\frac{3}{2}k\frac{dT_B}{dt} = \frac{3}{2}k\gamma(T_0 - T_B) - D_B B^2(\bar{E}_a - \frac{3}{2}kT_B)$$

$$= \frac{3}{2}k\gamma(T_0 - T_B) - wkT_B D_B B^2 \qquad (21)$$

$$\frac{dT_B}{dt} = \gamma T_0 - T_B(\gamma + \frac{2w}{3}D_B B^2)$$

$$= -(\gamma + \frac{2w}{3}D_B B^2)\left[T_B - T_0\left(\frac{\gamma}{\gamma + \frac{2w}{3}D_B B^2}\right)\right]$$

$$T_B - T_0\frac{1}{1 + \frac{2w}{3\gamma}D_B B^2} = \text{Const. } e^{-t/\tau}$$

where τ is the thermalization time constant.

$$1/\tau = \gamma + \frac{2w}{3}D_B B^2 = \gamma\frac{T_0}{T_B}. \qquad (22)$$

This expression has been previously given [14] for a constant λ_t, which corresponds to $w = 1/2$ in this notation. The thermalization results are tabulated (see Table V) with the error in w included.

Starr and de Villiers have obtained a composite thermalization time constant of 525 μsec for five graphite stacks with bucklings from 5.5×10^{-3} to 15×10^{-3} cm^{-2}. Using Eq. (7), a value of 450 μsec is obtained for a buckling of 10.6×10^{-3} cm^{-2}. Considering the difficulty of the experiment the agreement is not bad. Möller and Sjöstrand have measured τ_0 in water by a spectrum indicator technique. Various resonance abosrbers are dissolved in the medium. They obtained a value of $\tau_0 = 4.1 \pm 0.4$ μsec.

TABLE V

SUMMARY OF THERMALIZATION CONSTANTS

Moderator	w	T	$\gamma(\text{sec}^{-1})$	τ_0 (μsec)
Graphite	0.48 ± 0.01	23.5°C	1620 ± 86	617 ± 33
H_2O	0.87 ± 0.01	23°C	$(3.61 \pm 0.85) \times 10^5$	2.77 ± 0.65
D_2O	0.95 ± 0.05	22°C	$(3.38 \pm 0.43) \times 10^4$	29.6 ± 3.8
Be	0.50 ± 0.02	394°K	$(12.6 \pm 1.5) \times 10^3$	79.7 ± 9.5
	0.50 ± 0.02	437°K	(13.4 ± 1.4)	74.7 ± 7.8
	0.50 ± 0.02	478°K	(13.9 ± 2.5)	71.7 ± 12.8

REFERENCES

[1] VON DARDEL, G.F. and SJÖSTRAND, N.G., Phys. Rev. 96 (1954) 1245.

[2] GELBARD, E.M. and DAVIS, J.A., Nucl. Sci. Engng 13 (1962) 237.

[3] DE JUREN, J.A., STOOKSBERRY, R.W. and CARROLL, E.E., Proc. of the Brookhaven Conf. on Neutron Thermalization, Vol. III, BNL-719 (1962).

[4] BECKURTS, K.H., Nucl. Sci. Engng 2 (1957) 516.

[5] DAVIS, S.K., DE JUREN, J.A. and REIER, M., Nucl. Sci. Engng, to be published.

[6] VAUGHAN, E.U. and PASCHALL, R.K., private communication.

[7] LLOYD, R.C., CLAYTON, E.D. and RICHEY, R.C., Nucl. Sci. Engng 4 (1958) 690.

[8] REIER, M. and DE JUREN, J.A., J. nucl. Energy 14 (1961) 18.

[9] BECKURTS, K.H., Proc. of the Brookhaven Conf. on Neutron Thermalization, Vol. III, BNL-719 (1962) RE-1.

[10] ANDREWS, W.M., UCRL-6083 (1960).

[11] FULLWOOD, R.R., SLOVACEK, R.E. and GAERTTNER, E.R., Nucl. Sci. Engng 18 (1964) 138.

[12] MEISTER, H. and KUSSMAUL, G., J. nucl. Energy 17 (1963) 411.

[13] DAUGHTRY, J.W. and WALTNER, A.W., Trans. Amer. nucl. Soc. 7 (1964) 232.

[14] BARNARD, E., KHAN, N.A., McLATCHIE, R.C.F., POOLE, M.J. and TAIT, J.H., Nucl. Sci. Engng 17 (1963) 513.

GENERAL DISCUSSION

P. SCHOFIELD (Chairman): I shall now call on Mr. Čopić, who wishes to comment briefly on some work in Yugoslavia.

M. ČOPIĆ: This is a short comment on recent work aiming at the development of a programme for computing the regular eigenfunctions and the discrete eigenvalues for time- and velocity-dependent slab problems. The solutions are sought in the form:

$$n(x, \mu, v, t) = \exp(-\lambda t)\, M(v)\, \psi_\lambda(x, \mu, v),$$

where the function $\psi_2(x, \mu, v)$ is decomposed into the infinite medium solution $\psi_B(x, \mu, v)$ and a transition function $h(x, \mu, v)$ needed for proper description of the exact boundary condition at the slab surfaces. The infinite medium solution is obtained by the expansion method of Nelkin, using the truncated kernel approximation and taking anisotropic scattering into account. The velocity polynomials, ortho-normal on the interval $(0, \infty)$ with the weight function $M(v)$, are used. The convergence is much better than in the case of Laguerre or Hermite polynomials. The transition function $h(x, \mu, v)$ is obtained in the first order approximation from a system of coupled Fredholm equations.

In testing the programme, use has been made of the free proton gas model and the results for 7th and 9th approximations in velocity coincide very well with those obtained by other methods. (See NIJS Rpt. R-449.)

ГРАФИЧЕСКИЙ МЕТОД РЕШЕНИЯ НЕКОТОРОГО КЛАССА ЗАДАЧ НЕЙТРОННОЙ ФИЗИКИ

А.В. СТЕПАНОВ
ФИЗИЧЕСКИЙ ИНСТИТУТ ИМ П.Н. ЛЕБЕДЕВА
АН СССР. МОСКВА,
СССР

Abstract — Résumé — Аннотация — Resumen

GRAPHIC METHOD OF SOLVING A CERTAIN CLASS OF NEUTRON PHYSICS PROBLEM. The author considers the passage of neutrons through an inhomogeneous moderator with scattering properties which undergo space-time fluctuations. A graphic method is devised for solving a Boltzmann equation possessing parameters which vary in an irregular manner, i.e. are random functions. An equation is derived for averaged neutron density and the problem is formulated in terms of the characteristic values for a heterogeneous moderator system. It is shown in particular that the relaxation length of neutron density in an inhomogeneous moderator differs from the relaxation length calculated for systems with averaged, "levelled" properties.

SOLUTION, AU MOYEN DE DIAGRAMMES, DE CERTAINS PROBLÈMES RELATIFS A LA PHYSIQUE DES NEUTRONS. L'auteur étudie le passage des neutrons à travers un ralentisseur non homogène dont les propriétés de diffusion subissent des fluctuations dans l'espace et le temps. Il a élaboré une méthode permettant de résoudre, au moyen de diagrammes, une équation de Boltzmann, dont les paramètres accusent des variations irrégulières et, autrement dit, sont des fonctions aléatoires. Il a obtenu une relation exprimant le nombre volumique moyen des neutrons et formulé le problème relatif aux valeurs propres pour des systèmes ralentisseurs non homogènes. Il montre notamment que la longueur de relaxation du nombre volumique des neutrons dans un ralentisseur non homogène diffère de celle qui a été calculée pour des systèmes à propriétés intégrées ou «aplanies».

ГРАФИЧЕСКИЙ МЕТОД РЕШЕНИЯ НЕКОТОРОГО КЛАССА ЗАДАЧ НЕЙТРОННОЙ ФИЗИКИ. Рассмотрено прохождение через неоднородный замедлитель, рассеивающие свойства которого испытывают пространственно-временные флуктуации. Развит графический метод решения уравнения Больцмана, параметры которого изменяются нерегулярным образом, т.е. являются случайными функциями. Получено уравнение для усредненной плотности нейтронов, и сформулирована задача на собственные значения для неоднородных замедляющих систем. Показано, в частности, что длина релаксации нейтронной плотности в неоднородном замедлителе отличается от длины релаксации, вычисленной для систем с усредненными "сглаженными" свойствами.

METODO GRAFICO PARA RESOLVER ALGUNOS PROBLEMAS DE FISICA NEUTRONICA. El autor considera el paso de neutrones a través de un moderador heterogéneo cuyas propiedades de dispersión fluctúan en el espacio y en el tiempo. Describe un método gráfico para resolver una ecuación de Boltzmann cuyos parámetros varían de manera irregular, es decir, son funciones aleatorias. Se deduce en la memoria una ecuación representativa de la densidad neutrónica media y se plantea el problema en términos de los valores característicos de un sistema de moderador heterogéneo. Se demuestra, en particular, que la longitud de relajamiento de la densidad neutrónica en un moderador heterogéneo difiere de la longitud calculada para sistemas con propiedades promedio «niveladas».

1. ВВЕДЕНИЕ

Исследование прохождения нейтронов через замедлитель как в стационарном случае, так и при наличии импульсного источника, является мощным методом изучения свойств вещества. Информация о диффузионных характеристиках вещества, получаемая при обработке экспериментальных данных,

необходима при конструировании и эксплуатации ядерных реакторов. Методы нейтронной физики успешно применяются и в других областях, например в ядерной геофизике. При этом в ряде случаев, например при изучении диффузии нейтронов в вибрирующих системах или в среде с развитыми пространственными неоднородностями, строго говоря, мы сталкиваемся с необходимостью рассмотреть задачу о прохождении нейтронов через замедлитель, рассеивающие свойства которого изменяются от точки к точке и с течением времени нерегулярным образом, флуктуируют, например в кипящей воде. Эти флуктуации происходят в макроскопических масштабах и приводят к тому, что плотность нейтронов также флуктуирует. Практический интерес представляет средняя плотность и средний квадрат плотности нейтронов. Найденные экспериментально значения плотности нейтронов обычно сравнивают с решением кинетического уравнения с усредненными параметрами. Строго говоря, это решение при определенных условиях может заметно отличаться от средней плотности нейтронов, что приводит к ошибкам при интерпретации экспериментальных данных.

В параграфе 2 методом, развитым ранее Буре [1] для описания прохождения электромагнитного излучения через флуктуирующие среды, получено кинетическое уравнение для усредненной плотности нейтронов. При выводе этого уравнения используется графическая техника, существенно облегчающая выкладки и проясняющая смысл сделанных приближений. В этом же параграфе сформулирована задача на собственные значения для среды с флуктуирующими рассеивающими свойствами. Показано, что вид функции распределения нейтронов существенным образом определяется корреляцией флуктуаций в веществе.

В параграфе 3 рассмотрена диффузия тепловых нейтронов от плоского стационарного источника в неограниченной неоднородной среде и показано, что флуктуации рассеивающих свойств вещества приводят к изменению ("перенормировке") *длины релаксации нейтронной плотности*. Из результатов, полученных в этом параграфе, следует заключить, что флуктуации в замедлителе по теории возмущений возможны лишь на малых расстояниях от источника. Для определения асимптотического поведения функции распределения нейтронов вдали от источника необходимо решение кинетического уравнения, полученного в результате суммирования определенного класса членов ряда теории возмущений во всех порядках.

В параграфе 4 рассмотрена диффузия нейтронов в двухскоростном приближении.

В приложении получено уравнение для среднего квадрата плотности нейтронов.

2. ВЫВОД ОБЩИХ ФОРМУЛ И ВВЕДЕНИЕ ГРАФИЧЕСКОГО ПРЕДСТАВЛЕНИЯ

Однородное кинетическое уравнение, описывающее перенос нейтронов в среде, свободной от источников, можно записать в символической форме:

$$\hat{A}\psi(x) = 0, \qquad (2.1)$$

где $\hat{A}$-линейный оператор действующий на x — совокупность переменных,

от которых зависит функция распределения нейтронов ψ. Частный вид оператора $\hat{A}$ определяется условиями той конкретной задачи, которую мы рассматриваем. Например, в случае стационарной диффузии тепловых нейтронов в однородной среде

$$\hat{A} = D\nabla^2 - \frac{1}{T}, \tag{2.2}$$

где D-коэффициент диффузии, а T-время жизни тепловых нейтронов по отношению к поглощению. Если рассеивающие свойства среды изменяются нерегулярно от точки к точке и с течением времени, то оператор $\hat{A}$ содержит компоненты, зависимость которых от пространственных координат $\vec{r}$ и времени t имеет флуктуирующий (или случайный) характер. Выделим из оператора $\hat{A}$ флуктуирующую часть $\hat{\mu}$:

$$\hat{A}(x) = \hat{B}(x) - \hat{\mu}(x), \tag{2.3}$$

где

$\hat{B}(x)$-регулярная часть оператора $\hat{A}(x)$ r;

$$\hat{B}(x) = \langle \hat{A}(x) \rangle; \tag{2.4}$$

$$\langle \hat{\mu}(x) \rangle = 0. \tag{2.5}$$

Скобки $\langle\ \rangle$ означают вычисление среднего по ансамблю (математическое ожидание)*; относительно закона распределения случайной функции $\hat{\mu}(x)$ предположим, что он имеет гауссову форму. Это предположение означает, что все корреляционные функции $\langle \hat{\mu}(x_1)\hat{\mu}(x_2)\ldots\hat{\mu}(x_k) \rangle$, содержащие нечетное число $\hat{\mu}$, равны нулю (а не только $\langle \hat{\mu} \rangle$), и все корреляторы от четного числа $\hat{\mu}$ выражаются через парные корреляционные функции $\langle \hat{\mu}(x_1)\hat{\mu}(x_2) \rangle$. Класс случайных величин с такими статистическими свойствами оказывается достаточно широким, в то время при ином законе распределения $\hat{\mu}$ задача резко усложняется, поскольку необходимо рассматривать корреляционные функции более высокого порядка. Обозначим через G(x/y) функцию Грина уравнения (2.1). Как известно

$$\hat{A}G(x/y) = -\delta(x-y), \tag{2.6}$$

где $\delta(x-y)$ есть произведение δ-функций по отдельным переменным. Запишем (2.6) с помощью (2.3) в следующем виде:

$$\hat{B}(x)G(x/y) = -\delta(x-y) + \hat{\mu}(x)\,G\,(x/y). \tag{2.7}$$

Это уравнение удобно представить в интегральной форме:

$$G(x/y) = G_0(x/y) - \int dx' G_0(x/x')\hat{\mu}(x')G(x/y). \tag{2.8}$$

---

* *Практически среднее по ансамблю совпадает со средним по интервалу совокупности переменных x. В условиях "плохого разрешения" это усреднение производит сам измерительный прибор.*

Операторы, содержащиеся в $\hat{\mu}$, действуют, как и обычно на выражение, стоящее справа от $\hat{\mu}$. Функция $G_0(x/y)$ удовлетворяющая уравнению:

$$\hat{B}(x)\, G_0(x/y) = -\delta(x-y), \tag{2.9}$$

или

$$G_0(x/y) = -\hat{B}^{-1}\, \delta(x-y). \tag{2.10}$$

есть функция Грина кинетического уравнения

$$\hat{B}(x)\, \psi(x) = 0, \tag{2.11}$$

описывающего перенос нейтронов в среде с регулярными, не флуктуирующими свойствами.

Практический интерес представляет функция $\langle G(x/y)\rangle$. Получим приближенное уравнение, которому удовлетворяет эта функция. Непосредственное усреднение уравнения (2.8), как легко видеть, не позволяет получить уравнение для функции $\langle G(x/y)\rangle$. Запишем решение уравнения (2.8) по методу последовательных приближений:

$$G(x/y) = G_0(x/y) - \int dx' G_0(x/x')\hat{\mu}(x') G_0(x'/y) + \tag{2.12}$$

$$+ \iint dx'dx'' G_0(x/x')\hat{\mu}(x') G_0(x'/x'')\hat{\mu}(x'') G_0(x''/y) + \ldots$$

Анализ выражения (2.12) удобно производить, перейдя к графическому представлению. Поставим в соответствие функции $G_0(x/y)$ прямую горизонтальную линию, соединяющую точки x и y, а функциям $G(x/y)$ и $\langle G(x/y)\rangle$ -двойную горизонтальную линию и жирную горизонтальную линию, соответственно, проведенные между теми же точками, т.е.

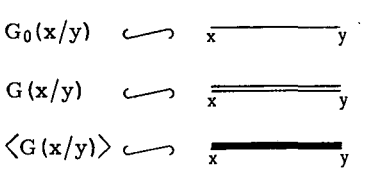

Операторную величину $\hat{\mu}(x)$ обозначим пунктирной вертикальной линией, идущей от точки x вверх. По переменным каждой узловой точки, из которой берет начало пунктирная линия, выполняется интегрирование. Тогда графический образ выражения (2.12) имеет вид:

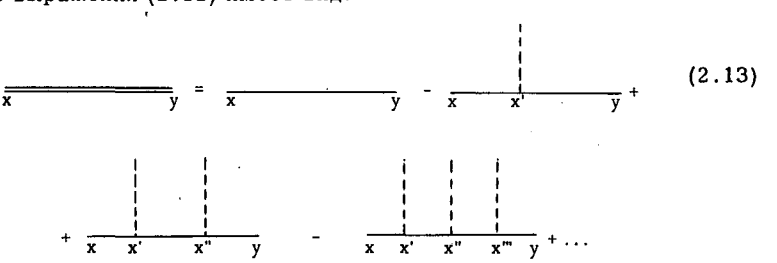

(2.13)

Напоминаем, что операторы, содержащиеся в $\overline{\hat{\mu}}$ действуют на выражение, стоящее справа от $\hat{\mu}$. Учитывая сделанные нами выше предположения о статистических свойствах $\hat{\mu}$, выполним усреднение выражения (2.13). Тогда вклад графиков, содержащих нечетное число пунктирных линий обратится в нуль. Усреднение остальных слагаемых сводится к попарному замыканию пунктирных линий. Учитывая эти замечания, получим следующее выражение для $\langle G(x/y)\rangle$

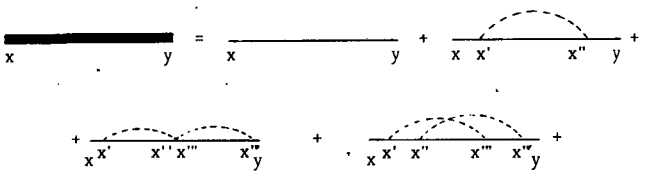

(2.14)

или

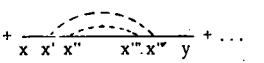

$$\langle G(x/y)\rangle = G_0(x/y) + \int\int dx'dx'' G_0(x/x') \times$$

$$\times \langle \hat{\mu}(x') G_0(x'/x'') \hat{\mu}(x'') \rangle G_0(x''/y) + \ldots \qquad (2.15)$$

Вклады графиков определенного типа удается просуммировать и получить уравнение для функции $\langle G(x/y)\rangle$. Так, если ограничиться рассмотрением графиков типа:

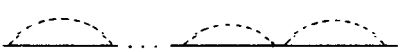

, (2.16)

то для функции $\langle G(x/y)\rangle$ получаем следующее уравнение:

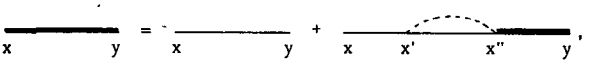

(2.17)

т.е.

$$\langle G(x/y)\rangle = G_0(x/y) +$$

$$+ \int\int dx'dx'' G_0(x/x') \langle \hat{\mu}(x') G_0(x'/x'') \hat{\mu}(x'') \rangle \langle G(x''/y)\rangle, \qquad (2.18)$$

или

$$\langle G(x/y)\rangle = G_0(x/y) + \int\int dx'dx'' G_0(x/x') M(x'/x'') \langle G(x''/y)\rangle, \qquad (2.19)$$

где

$$M(x/y) = \langle \hat{\mu}(x) G_0(x/y) \hat{\mu}(y) \rangle. \qquad (2.20)$$

Графический образ M(x/y)

(2.21)

M(x/y)-аналог массового оператора квантовой теории поля, а само уравнение (2.19) аналогично уравнению Дайсона [2]. Справедливость уравнений (2.17-2.20) проверяется непосредственной итерацией.

Графики типа

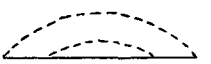

также удается просуммировать. В этом случае функция $\langle G\rangle$ удовлетворяет нелинейному интегральному уравнению (о суммировании графиков этого типа см., например [3]). В дальнейшем мы ограничимся приближением (2.16). В тех случаях, когда корреляционная функция $\langle\mu(x_1)\mu(x_2)\rangle$ затухает быстрее, чем функция $G_0(x_1/x_2)$, приближение (2.16) позволяет учесть основной вклад флуктуаций рассеивающих свойств среды в значение функции распределения нейтронов. Более подробный анализ уравнения (2.19) и приближения (2.16) удобно провести на примере конкретной задачи нейтронной физики, одну из которых мы рассмотрим в следующем параграфе.

В заключение этого параграфа получим однородное уравнение, которому удовлетворяет усредненная функция распределения нейтронов $\langle\psi(x)\rangle$ в среде, свободной от источников при наличии флуктуаций рассеивающих свойств.

Из определения функции Грина G(x/y) следует, что

$$\psi(x) = \int G(x/y)\,\psi_0(y)dy, \tag{2.22}$$

где $\psi_0(y)$ определено распределением источников. Далее из (2.22) непосредственно вытекает:

$$\langle\psi(x)\rangle = \int \langle G(x/y)\rangle\,\psi_0(y)dy. \tag{2.23}$$

В рамках приближения (2.16) из уравнения (2.19) получаем

$$\langle\psi(x)\rangle = \int G_0(x/y)\psi_0(y)dy + \iiint dx'dx''dy\, G_0(x/x')M(x'/x'')\times \tag{2.24}$$

$$\times\langle G(x''/y)\rangle\,\psi_0(y) =$$

$$= \int G_0(x/y)\psi_0(y)\,dy + \iint dx'dx''G_0(x/x')M(x'/x'')\langle\psi(x'')\rangle.$$

Действуя оператором $\hat{B}(x)$ на обе части этого уравнения и учитывая (2.7), преобразуем (2.24) к следующему виду:

$$\hat{B}\langle\psi(x)\rangle = -\psi_0(x) - \int dx'M(x/x')\langle\psi(x')\rangle \tag{2.25}$$

Если источники отсутствуют, то $\psi_0(x) = 0$ и мы приходим к задаче на собственные значения

$$\hat{B}\langle\psi(x)\rangle = -\int dx' M(x/x')\langle\psi(x')\rangle . \qquad (2.26)$$

3. ДИФФУЗИЯ ТЕПЛОВЫХ НЕЙТРОНОВ В СРЕДЕ С НЕРЕГУЛЯРНЫМИ СВОЙСТВАМИ

Прохождение тепловых нейтронов через вещество от плоского стационарного источника в неограниченной среде, как известно описывается уравнением диффузии:

$$\frac{d}{dz}\left[D(z)\frac{d}{dz}G(z/z_0)\right] - \frac{G(z/z_0)}{T(z)} + Q\,\delta(z - z_0) = 0, \qquad (3.1)$$

где $G(z/z_0)$-плотность нейтронов в точке z, D(z) и T(z) -соответственно, коэффициент диффузии и время жизни тепловых нейтронов по отношению к поглощению; $Q\delta(z-z_0)$ описывает действие источника нейтронов, расположенного в плоскости $z=z_0$ и обладающего мощностью Q.

Решение уравнения (3.1) можно получить известными методами, если D и T зависят от z некоторым регулярным образом. Если же свойства среды таковы, что D и T оказываются случайными функциями z с гауссовым законом распределения, то плотность нейтронов в такой среде может быть найдена с помощью процедуры, развитой в предыдущем параграфе. Чтобы избежать громоздких выкладок, предположим, что $D(z) = D_0 = \text{const}$, а неоднородность среды проявляется лишь в появлении флуктуирующей части T(z) т.е.

$$\frac{1}{T(z)} = \frac{1}{T_0} + \frac{1}{\tau(z)}, \qquad (3.2)$$

причем

$$\left\langle\frac{1}{T(z)}\right\rangle = \frac{1}{T_0} \text{ и } \left\langle\frac{1}{\tau(z)}\right\rangle = 0. \qquad (3.3)$$

При этих предположениях уравнение (3.1) можно записать в виде:

$$\frac{d^2}{dz^2}G(z/z_0) - \kappa_0^2 G(z/z_0) + \delta(z - z_0) = \frac{1}{t(z)}G(z/z_0), \qquad (3.4)$$

где $$\kappa_0^2 = 1/D_0 T_0, \quad t(z) = D_0\tau(z)$$

и для удобства нормировка источника нейтронов выбрана так, что $Q = D_0$. Таким образом, оператор $\hat{A}$ введенный в предыдущем параграфе, в нашем случае оказывается равным:

$$\hat{A} = \frac{d^2}{dz^2} - \kappa_0^2 - \frac{1}{t(z)}, \qquad (3.5)$$

а операторы $\hat{B}$ и $\hat{\mu}$ соответственно равны

$$\hat{B} = \frac{d^2}{dz^2} - \kappa_0^2 \tag{3.6}$$

$$\hat{\mu} = 1/t(z) \tag{3.7}$$

функция $G_0(z/z_0)$-решение уравнения

$$\left(\frac{d^2}{dz^2} - \kappa_0^2\right) G_0(z/z_0) + \delta(z-z_0) = 0, \tag{3.8}$$

как известно, имеет вид:

$$G(z/z_0) = \frac{1}{2\kappa_0} e^{-\kappa_0 |z-z_0|} \tag{3.9}$$

Пунктирной линии, соединяющей две точки на графиках предыдущего параграфа мы сопоставим корреляционную функцию

$$E(z_1/z_2) = \langle t^{-1}(z_1) t^{-1}(z_2) \rangle. \tag{3.10}$$

В дальнейшем для простоты ограничимся рассмотрением следующего специального вида функции $E(z_1/z_2)$:

$$E(z_1/z_2) = S e^{-q|z_1 - z_2|}, \tag{3.11}$$

где S-амплитудный множитель. Будем предполагать также, что корреляции величины $t^{-1}(z)$ затухают быстрее, чем плотность нейтронов в среде без флуктуаций, т.е.

$$\kappa_0 < q \tag{3.12}$$

"Массовый оператор" $M(z_1/z_2)$ (см.(2.20) и (2.21)) равен:

$$M(z_1/z_2) = G_0(z_1/z_2) E(z_1/z_2) = \frac{S}{2\kappa_0} e^{-\kappa_1 |z_1 - z_2|}, \tag{3.13}$$

где

$$\kappa_1 = \kappa_0 + q \tag{3.14}$$

Таким образом, усредненная плотность нейтронов $\langle G(z/z_0) \rangle$ удовлетворяет уравнению:

$$\langle G(z/z_0) \rangle = G_0(z/z_0) + \frac{S}{4\kappa_0^2} \iint_{-\infty}^{\infty} dz' dz'' e^{-\kappa_0 |z - z'|} \times e^{-\kappa_1 |z' - z''|} \langle G'(z''/z_0) \rangle, \tag{3.15}$$

которое в нашем частном случае непосредственно следует из уравнения (2.19). Интегрируя по z^1 в (3.15), получаем следующее интегральное уравнение для $\langle G(z/z_0)\rangle$

$$\langle G(z/z_0)\rangle = G_0(z/z_0) + \frac{S}{2\kappa_0^2}\cdot\frac{1}{\kappa_0^2-\kappa_1^2}\times$$
$$\times\left\{\kappa_0\int_{-\infty}^{\infty}dz''e^{-\kappa_1|z-z''|}\langle G(z''/z_0)\rangle - \kappa_1\int_{-\infty}^{\infty}dz''e^{-\kappa_0|z-z''|}\langle G(z''/z_0)\rangle\right\}. \tag{3.16}$$

Непосредственной итерацией уравнения (3.16) можно убедиться в том, что поправки к $G_0(z/z_0)$ оказываются пропорциональными $(z-z_0)^{\ell}$ (ℓ -целое). Таким образом, для описания асимптотического поведения $\langle G(z/z_0)\rangle$ на больших расстояниях от источника необходимо найти точное решение уравнения (3.16), что легко сделать с помощью преобразования фурье:

$$n(k) = \frac{1}{\sqrt{2\pi}}\int_{-\infty}^{\infty}dze^{ikz}\langle G(z/z_0)\rangle \tag{3.17}$$

$$n_0(k) = \frac{1}{\sqrt{2\pi}}\int_{-\infty}^{\infty}dze^{ikz}G_0(z/z_0) = \frac{1}{2\kappa_0}e^{ikz_0}\sqrt{\frac{2}{\pi}}\frac{\kappa_0}{\kappa_0^2+k^2}. \tag{3.18}$$

Уравнение для $n(k)$ оказывается алгебраическим

$$n(k) = n_0(k) + \frac{S\sqrt{\pi/2}}{\kappa_0^2(\kappa_0^2\kappa_1^2)}\{\kappa_0 V_{\kappa_1}(\kappa) - \kappa_1 V_{\kappa_0}(k)\}n(k), \tag{3.19}$$

где

$$V_{\kappa_i}(k) = \frac{1}{\sqrt{2\pi}}\int_{-\infty}^{\infty}dze^{-\kappa_i|z|+ikz} = \sqrt{\frac{2}{\pi}}\frac{\kappa_i}{\kappa_i^2+k^2}. \tag{3.20}$$

Окончательное выражение для $n(k)$ имеет вид

$$n(k) = \frac{1}{\sqrt{2\pi}}e^{ikz_0}\frac{\kappa_1^2+k^2}{(\kappa_1^2+k^2)(\kappa_0^2+k^2)-S\frac{\kappa_1}{\kappa_0}}. \tag{3.21}$$

Плотность нейтронов $\langle G(z/z_0)\rangle$ найдем, выполнив обратное преобразование Фурье

$$\langle G(z/z_0)\rangle = \frac{1}{\sqrt{2\pi}}\int_{-\infty}^{\infty}dk\,e^{-ikz}\,n(k) =$$
$$= \frac{1}{2\pi}\int_{-\infty}^{\infty}dk\,e^{-ik(z-z_0)}\frac{\kappa_1^2+k^2}{(k+k_1)(k-k_1)(k+k_2)(k-k_2)}, \tag{3.22}$$

где

$$k_{1,2}=\sqrt{-\frac{\kappa_1^2+\kappa_0^2}{2}\pm\frac{1}{2}\sqrt{(\kappa_1^2-\kappa_0^2)^2+4S\frac{\kappa_1}{\kappa_0}}}\,. \qquad (3.23)$$

Вычисляя интеграл в (3.22), получаем окончательный результат

$$\langle G(z/z_0)\rangle=\frac{1}{2(\beta_2^2-\beta_1^2)}\left\{\frac{\kappa_1^2\beta_1^2}{\beta_1}e^{-\beta_1|z-z_0|}-\frac{\kappa_1^2-\beta_2^2}{\beta_2}e^{-\beta_2|z-z_0|}\right\}. \qquad (3.24)$$

Здесь

$$\beta_{1,2}=\sqrt{\frac{\kappa_1^2+\kappa_0^2}{2}\mp\frac{1}{2}\sqrt{(\kappa_1^2-\kappa_0^2)^2+4S\frac{\kappa_1}{\kappa_0}}}\,. \qquad (3.25)$$

Из выражений (3.24) и (3.25) при $x_1\gg x_0$ следует, что на больших расстояниях от источника усредненная плотность нейтронов

$$\langle G(z/z_0)\rangle=\frac{1}{2\kappa_0}e^{-\kappa_0\left(1-\frac{S}{2\kappa_1\kappa_0^3}\right)|z-z_0|} \qquad (3.26)$$

т.е. убывает экспоненциально с длиной релаксации $\frac{1}{\kappa_0}\left(1+\frac{S}{2\kappa_1\kappa_0^3}\right)$. При написании (3.26) мы ограничились линейным по κ_0/κ_1 поправками в показателе экспоненты, а для предэкспоненциального множителя — нулевым приближением. Таким образом, флуктуации рассеивающих свойств среды привели к увеличению, по сравнению с диффузией в среде без флуктуаций, длины релаксации плотности нейтронов. Можно показать, что подобный эффект имеет место и в нестационарном случае.

В заключение этого параграфа приведем оценки точности приближения (2.16) в котором получено уравнение (2.19), а следовательно и уравнение (3.15). Сравнивая выражения, отвечающие графикам

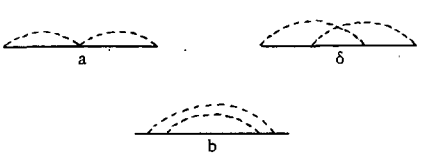

легко можно убедиться в том, что при $q\gg\kappa_0$ вклад графиков типа а превышает вклад графиков типа б и в в q/κ_0 раз.

4. ДИФФУЗИЯ ТЕПЛОВЫХ НЕЙТРОНОВ В НЕОДНОРОДНОЙ СРЕДЕ. ДВУХГРУППОВОЕ ПРИБЛИЖЕНИЕ

Сформулируем задачу о диффузии тепловых нейтронов в неоднородной среде в условиях, аналогичных оговоренным в предыдущем параграфе $D=D_0=\text{const}$, $\frac{1}{T(z)}=\frac{1}{T_0}+\frac{1}{\tau(z)}$ и т.д.), учитывая зависимость плотности нейтронов от энергии E.

Ранее [4] в двухгрупповом приближении была решена задача о диффузии нейтронов от плоского стационарного источника в однородной среде с поглощением по закону $1/v$ (v-скорость нейтрона). Было показано, что в этом приближении поток нейтронов можно представить в виде:

$$N(z/E) = \frac{E}{(kT)^2} e^{-\frac{E}{kT}} \left[n_0^0(z) L_0^{(1)}\left(\frac{E}{kT}\right) + \frac{n_1^0(z)}{\sqrt{2}} L_1^{(1)}\left(\frac{E}{kT}\right) \right], \qquad (4.1)$$

где $L_0^{(1)} = 1$ и $L_1^{(1)}(x) = 2 - x$ -полиномы Лагерра, T-температура среды, k-постоянная Больцмана.

Функции n_0^0 и n_1^0 являются решением системы уравнений

$$\begin{aligned} \hat{B}_{00}\, n_0^0(z) + B_{10}\, n_1^0(z) + Q_0(z/z_0) &= 0, \\ \hat{B}_{01}\, n_0^0(z) + B_{11}\, n_1^0(z) + Q_1(z/z_0) &= 0 \end{aligned} \qquad (4.2)$$

или

$$\begin{aligned} \frac{d^2 n_0^0(z)}{dz^2} - \kappa_0^2\, n_0^0(z) - p^2 n_1^0(z) + Q_0(z/z_0) &= 0. \\ \frac{d^2 n_1^0(z)}{dz^2} - \kappa_1^2\, n_1^0(z) - p^2 n_0^0(z) + Q_1(z/z_0) &= 0. \end{aligned} \qquad (4.2a)$$

Здесь

$$\kappa_0^2 = \frac{3}{v_0 T_0 \ell} \frac{\sqrt{\pi}}{2}, \quad \kappa_1^2 = \frac{3}{\ell} \gamma_{11} + \frac{21}{16} \sqrt{\pi} \frac{1}{v_0 T_0 \ell}, \quad v_0 = \sqrt{\frac{2kT}{m}};$$
$$p^2 = \frac{3\sqrt{\pi}}{4\sqrt{2}\, T_0 \ell v_0}, \quad Q_i = A_i\, \delta(z - z_0); \qquad (4.3)$$

ℓ-длина свободного пробега нейтрона по отношению к рассеянию.

В случае неоднородной среды функции n_0 и n_1 удовлетворяют следующей системе уравнений

$$\begin{aligned} \frac{d^2 n_0(z)}{dz^2} - \kappa_0^2\, n_0(z) - p^2 n_1(z) - \frac{1}{t_{00}(z)}\, n_0(z) - \frac{1}{t_{01}(z)}\, n_1(z) + Q_0(z/z_0) &= 0, \\ \frac{d^2 n_1(z)}{dz^2} - \kappa_1^2\, n_1(z) - p^2 n_0(z) - \frac{1}{t_{01}(z)}\, n_0(z) - \frac{1}{t_{11}(z)}\, n_1(z) + Q_1(z/z_0) &= 0, \end{aligned} \qquad (4.4)$$

$$\frac{1}{t_{00}(z)} = \frac{3\sqrt{\pi}}{2} \frac{1}{\tau(z)\ell v_0}; \quad \frac{1}{t_{01}(z)} = \frac{1}{t_{10}(z)} = \frac{3\sqrt{\pi}}{4\sqrt{2}} \frac{1}{\ell\tau(z) v_0}, \qquad (4.5)$$

$$\frac{1}{t_{11}(z)} = \frac{21\sqrt{\pi}}{16} \frac{1}{\tau(z) v_0 \ell}, \qquad (4.6)$$

которая в представлении, диагонализирующем матрицу $\hat{B}$, имеет вид:

$$\tilde{B}_0 n_0(z) - \tilde{\mu}_{00} n_0(z) - \tilde{\mu}_{01}\tilde{n}_1(z) + \tilde{Q}_0(z/z_0) = 0,$$

$$\tilde{B}_1 \tilde{n}_1(z) - \tilde{\mu}_{11}\tilde{n}_1(z) - \tilde{\mu}_{01}\tilde{n}_0(z) + \tilde{Q}_1(z/z_0) = 0. \qquad (4.7)$$

С помощью графической процедуры параграфа 2 в приближении (2.16) получаем для $\tilde{n}_0$ и $\tilde{n}_1$ приближенную систему уравнений

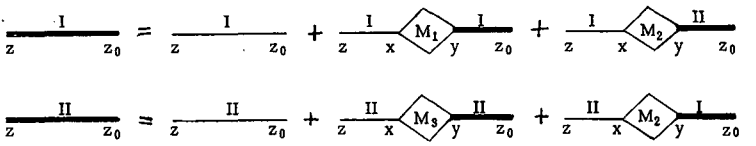

(4.8)

Были введены следующие обозначения:

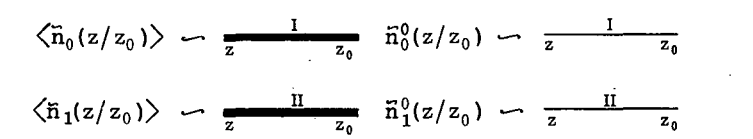

(4.9)

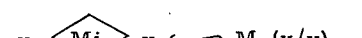

$$M_1(x/y) = \langle \tilde{\mu}_{00}(x)\tilde{\mu}_{00}(y)\rangle \tilde{n}_0^0(x/y) + \langle \tilde{\mu}_{01}(x)\tilde{\mu}_{01}(y)\rangle \tilde{n}_1^0(x/y)$$

$$M_2(x/y) = \langle \tilde{\mu}_{01}(x)\tilde{\mu}_{11}(y)\rangle \tilde{n}_1^0(x/y) + \langle \tilde{\mu}_{01}(x)\tilde{\mu}_{01}(y)\rangle \tilde{n}_0^0(x/y)$$

$$M_3(x/y) = \langle \tilde{\mu}_{11}(x)\tilde{\mu}_{11}(y)\rangle \tilde{n}_1^0(x/y) + \langle \tilde{\mu}_{01}(x)\tilde{\mu}_{01}(y)\rangle \tilde{n}_0^0(x/y).$$

И окончательно

$$\langle \tilde{n}_0(z/z_0)\rangle = \tilde{n}_0^0(z/z_0) + \iint dxdy\, \tilde{n}_0^0(z/x)\{M_1(x/y)\langle \tilde{n}_0(y/z_0)\rangle +$$

$$+ M_2(x/y)\langle \tilde{n}_1(y)z_0)\rangle\},$$

$$\langle \tilde{n}_1(z/z_0)\rangle = \tilde{n}_1^0(z/z_0) + \iint dxdy\, \tilde{n}_1^0(z/x)\{M_3(x/y)\langle \tilde{n}_1(y/z_0)\rangle + \qquad (4.10)$$

$$+ M_2(x/y)\langle \tilde{n}_0(y/z_0)\rangle\}.$$

5. ЗАКЛЮЧЕНИЕ

В публикуемой работе развит графический метод решения кинетического уравнения, описывающего прохождение нейтронов через флуктуирующие

среды. В области очень малых энергий нейтронов (холодные нейтроны) классическое уравнение Больцмана, не учитывающее волновых свойств нейтрона, которые проявляются в этой энергетической области неприменимо. Вместе с тем информация о характере взаимодействия холодных нейтронов с веществом существенна для определения асимптотического поведения решения кинетического уравнения [5]. Описание распространения холодных нейтронов в веществе возможно с помощью волнового уравнения Шредингера [6]. Прохождение нейтронной волны через среду с флуктуирующими рассеивающими свойствами также может быть рассмотрено [7] с помощью графической процедуры, описанной выше. В данной работе было обсуждено уравнение Больцмана, содержащее случайные функции пространственных координат и времени. Можно рассчитывать, что нахождение решения уравнений кинетики реактора, а также отыскание численного решения кинетического уравнения, коэффициенты которого – быстроменяющиеся функции энергии (например, транспортная длина рассеяния с кристаллическом замедлителе) удастся упростить, также используя графический метод.

В заключение автор выражает глубокую благодарность М.В.Казарновскому за плодотворные обсуждения и ценные советы.

ПРИЛОЖЕНИЕ

Получим уравнение для корреляционной функции

$$\langle D(x_2x_1/x_2'x_1')\rangle = \langle G(x_2/x_1)\,G(x_2'/x_1')\rangle \qquad (П.1)$$

Умножая уравнение (2.12) на аналогичное ему, получим после усреднения уравнение для коррелятора $\langle D\rangle$

$$\begin{aligned}\langle D(x_2x_1/x_2'x_1')\rangle &= G_0(x/y)\,G_0(x'/y') + \\ &+\iint dy_1\,dy_1'\,G_0(x_2/y_1)\,G_0(x_2'/y_1')\langle\hat{\mu}(y_1)\,\hat{\mu}(y_1')\rangle\times \\ &\times G_0(y_1/x_1)\,G_0(y_1'/x_1') + \iint dy_1dy_2G_0(x_2/y_1)\times \\ \times\langle\hat{\mu}/y_1)\,G_0(y_1/y_2)\,\hat{\mu}(y_2)\rangle\,G_0(y_2/x_1)\,G_0(x_2'/x_1') &+ \iint dy_1'dy_1'G_0(x_2'/y_1')\times \\ \times\langle\hat{\mu}(y_1')\,G_0(y_1'/y_2')\,\hat{\mu}(y_2')\rangle\,G_0(y_2'/x_1')\,G_0(x_2/x_1) &+ \ldots\end{aligned} \qquad (П.2)$$

Обозначая $\langle D(x_2x_1/x_2^1x_1^1)\rangle$ символом

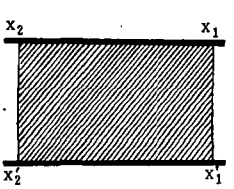

получим следующее графическое представление уравнения (П.2)

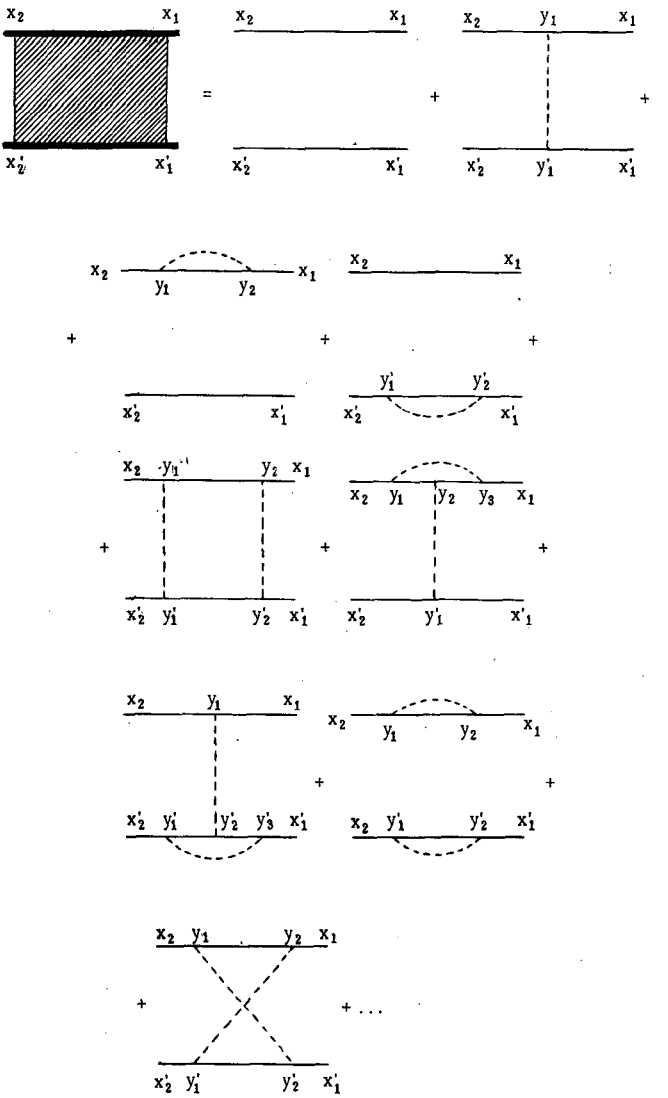

(П.3)

Обозначения те же, что и введенные в параграфе 2.

Просуммировать графики, содержащие пунктирные линии, можно, используя результаты параграфа 2. В приближении (2.16) получим

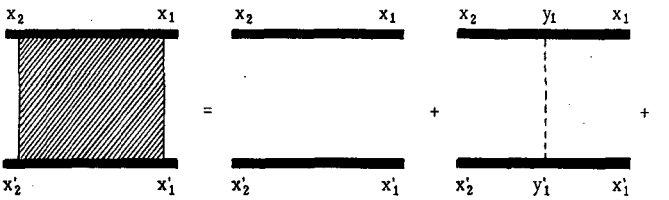

(П.4)

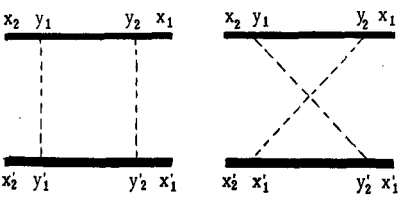

Первое слагаемое в (П.4) равно, очевидно, $\langle G(x_2/x_1)\rangle \langle G(x_2'/x_1')\rangle$ и не содержит корреляций между $G(x_2/x_1)$ и $G(x_2'/x_1')$. Учесть приближенно эти корреляции можно, суммируя графики типа

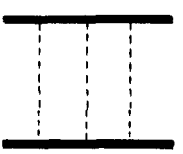

(П.5)

В этом так называемом "лестничном приближении", корреляционная функция $\langle D\rangle$ удовлетворяет уравнению

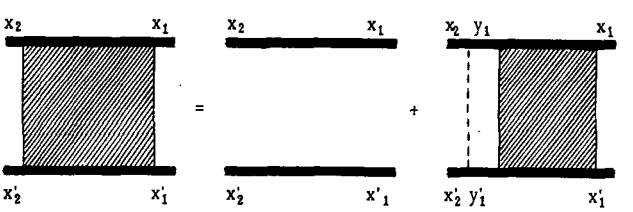

(П.6)

$$\langle D(x_2x_1/x_2'x_1')\rangle = \langle G(x_2/x_1)\rangle\langle G(x_2'/x_1')\rangle +$$

$$+\iint dy_1dy_1'\langle G(x_2/y_1)\rangle\langle G(x_2'/y_1')\rangle\times \qquad (П.7)$$

$$\times\langle\hat{\mu}(y_1)\hat{\mu}(y_2')\rangle\langle D(x_2x_1/x_2'x_1')\rangle.$$

Уравнение (П.7) аналогично квантово-механическому уравнению Бете-Сальпитера [8].

Средний квадрат плотности нейтронов (при наличии источника $\sim\delta(x-y)$), очевидно равен корреляционной функции $<D>$ при попарно совпадающих аргументах $<D(xy/xy)>$.

ЛИТЕРАТУРА

[1] BOURRET R.C., Nuovo Cim. XXVI, 1 (1962)
[2] АХИЕЗЕР А.И., БЕРЕСТЕЦКИЙ В.Б., Квантовая электродинамика физматгиз М., 1959.
[3] АБРИКОСОВ А.А., ГОРЬКОВ А.П., ДЗЯЛОШИНСКИИ И.Е., Методы квнтовой теории поля в статистической физике. Физматгиз, М., 1962.
[4] КАЗАРНОВСКИИ М.В., СТЕПАНОВ А.В., ШАПИРО Ф.Л., Вторая Международная конференция по мирному использованию атомной энергии. Женева (1958). Доклады советских ученых, т.1, стр. 469.
[5] NELKIN M., Physica 29 (1963) 261.
[6] ЮЗ Д., Нейтронная оптика. изд. иностр. лит., М., 1955 г.
[7] СТЕПАНОВ, А.В., К теории прохождения холодных нейтронов через вещество. Препринт ФИАН, 1965.
[8] SALPETER E., BETHE H., Phys. Rev. 84 (1951) 1232.

К ТЕОРИИ ПРОХОЖДЕНИЯ ХОЛОДНЫХ НЕЙТРОНОВ ЧЕРЕЗ ВЕЩЕСТВО

А.В. СТЕПАНОВ
ФИЗИЧЕСКИЙ ИНСТИТУТ им. П.Н. ЛЕБЕДЕВА АН СССР, МОСКВА СССР

Abstract — Résumé — Аннотация — Resumen

INVESTIGATIONS RELATED TO THE THEORY OF THE PASSAGE OF COLD NEUTRONS THROUGH MATTER. A study was made of the passage of cold neutrons through matter, account being taken of quantum effects. A solution was obtained for the wave equation of Schrödinger which describes the development of a pulse of neutrons of low energy in time. It is shown that correlation of the fluctuations in the scattering properties of the medium leads to a change in the law of dispersion and to additional attenuation of the neutron wave.

THÉORIE RELATIVE AU PASSAGE DES NEUTRONS FROIDS A TRAVERS LA MATIÈRE. L'auteur examine le passage des neutrons froids à travers la matière en tenant compte des effets quantiques. Il indique la solution de l'équation d'onde de Schrödinger qui exprime l'évolution dans le temps d'une bouffée de neutrons de faible énergie. Il montre que la corrélation entre les variations des propriétés de diffusion du milieu entraîne une modification de la loi de dispersion et un amortissement complémentaire de l'onde neutronique.

К ТЕОРИИ ПРОХОЖДЕНИЯ ХОЛОДНЫХ НЕЙТРОНОВ ЧЕРЕЗ ВЕЩЕСТВО. Рассмотрено прохождение холодных нейтронов через вещество с учетом квантовых эффектов. Получено решение волнового уравнения Шредингера, описывающего развитие во времени импульса нейтронов малой энергии. Показано, что корреляция флуктуаций рассеивающих свойств среды приводит к изменению закона дисперсии и дополнительному затуханию нейтронной волны.

INVESTIGACIONES SOBRE LOS ASPECTOS TEORICOS DEL PASO DE NEUTRONES FRIOS A TRAVES DE LA MATERIA. El autor estudió el paso de neutrones fríos a través de la materia, tomando en cuenta los efectos cuánticos. Obtuvo una solución para la ecuación ondulatoria de Schrödlinger, que describe el desarrollo en el tiempo de un impulso de neutrones de baja energía. Demuestra que la correlación de las fluctuaciones sufridas por las propiedades de dispersión del medio, lleva a un cambio en la ley de dispersión y a una atenuación adicional de la onda neutrónica.

1. ВВЕДЕНИЕ

Теоретическое описание прохождения нейтронов через вещество основано на представлении о функции распределения нейтронов $f(\vec{r}, \vec{v}, t)$ в пространстве координат $\vec{r}$ и скоростей $\vec{v}$. Функция f удовлетворяет уравнению баланса нейтронов

$$\frac{\partial f(\vec{r}, \vec{v}, t)}{\partial t} = -\vec{v}\nabla f(\vec{r}, \vec{v}, t) - f(\vec{r}, \vec{v}, t)[W_a(\vec{r}, v) + W_s(\vec{r}, v)] +$$

$$+ \int d\vec{v}' f(\vec{r}, \vec{v}', t) W(\vec{r}, \vec{v}' \to \vec{v}) + Q(\vec{r}, v, t) = 0, \qquad (1.1)$$

где W_a и W_s – вероятности поглощения и рассеяния нейтрона, соответст-

венно, отнесенные к единице времени, а $W(\vec{r}, \vec{v}' \to \vec{v})d\vec{v}$ вероятность того, что нейтрон, имеющий начальную скорость $\vec{v}'$, в результате рассеяния приобретает скорость $\vec{v}$ в интервале $(\vec{v}+d\vec{v}, \vec{v})$. Уравнение (1.1) является, по существу, полуклассическим, поскольку нейтроны рассматриваются как классические частицы одновременно обладающие определенной скоростью и координатой, и лишь ядро уравнения $W(\vec{r}, \vec{v}' \to \vec{v})$ вычисляется с помощью квантово-механической теории рассеяния. С уменьшением энергии нейтронов E растет длина нейтронной волны $\lambda = \hbar/\sqrt{2mE}$ (m – масса нейтрона) и все более существенными становятся проявления волновых свойств нейтрона. Поэтому последовательное рассмотрение прохождения достаточно медленных (холодных) нейтронов возможно лишь на основе уравнений квантовой механики.

Если длина волны нейтрона велика по сравнению с расстоянием между рассеивающими центрами, то приближенно рассеивающую среду можно рассматривать как однородную, а прохождение нейтронов описать с помощью показателя преломления n, который связан со средней энергией взаимодействия нейтронов с веществом $\langle V \rangle$ [1]:

$$n^2 = 1 - \langle V \rangle / E; \tag{1.2}$$

$$\langle V \rangle = \frac{2\pi\hbar^2}{m} aN, \tag{1.3}$$

где a – амплитуда рассеяния нейтрона изолированным бесконечно тяжелым ядром;
N – число ядер в 1 $см^3$. Вследствие поглощения нейтронов $\langle V \rangle$ – комплексно. Движение рассеивающих центров приводит к отклонению действующего потенциала от $\langle V \rangle$. Это отклонение δV обусловливает переходы между состояниями нейтрона в среднем потенциальном поле $\langle V \rangle$. Такой подход к описанию прохождения холодных нейтронов через вещество развивался М.В.Казарновским и автором [2] и по существу аналогичен методу деформируемых ионов, который позволяет рассмотреть рассеяние электронов на колебаниях кристаллической решетки (см. [3]). При этом мы, используя теорию возмущений, получаем выражение для вероятности перехода в единицу времени. Прохождение нейтронов через значительный объем вещества тогда можно описать как последовательность таких переходов (многократное рассеяние), каждый из которых рассматривается как независимое законченное "столкновение", приводящее к устойчивому эффекту, пропорциональному времени. Очевидно, что такой подход оправдан, когда эффективное время взаимодействия мало по сравнению со временем между последовательными взаимодействиями. В противном случае переходы нельзя рассматривать как независимые. Когда энергия нейтрона стремится к нулю, время между столкновениями остается конечным (хотя средняя длина свободного пробега стремится к нулю) [4], а эффективное время взаимодействия, обратно пропорциональное скорости нейтрона, обращается в бесконечность. Таким образом, рассмотрение прохождения холодных нейтронов через вещество как многократное рассеяние несправедливо и необходимо искать решение волнового уравнения. В параграфе 2 с помощью графического метода [5] выведено уравнение (2.22), описывающее распространение холодных нейтронов в среде с флуктуирующими свойствами.

Параграф 3 посвящен анализу решения основного уравнения (2.22). Показано, что в общем случае корреляции флуктуаций в среде приводят к изменению закона дисперсии и дополнительному затуханию нейтронной волны. Соответственно изменяется и показатель преломления. В этом же параграфе рассмотрены некоторые специальные типы корреляционных функций. В связи с тем, что для изучения распространения холодных нейтронов существенна информация о корреляциях в среде, относительно медленно меняющихся в пространстве и во времени, для отыскания таких корреляционных функций можно воспользоваться методами гидродинамики [6]. В свою очередь анализ прохождения холодных нейтронов через рассеивающие среды с нерегулярными свойствами позволяет определить важные характеристики атомного движения*.

В приложении дано уточнение приближения (2.14), сделанного при выводе основного уравнения (2.22).

2. ОБЩИЕ ФОРМУЛЫ

Уравнение Шредингера, которому удовлетворяет $\psi(\vec{r}, t)$ волновая функция нейтрона, проходящего через вещество, можно записать в виде:

$$i\hbar\frac{\partial\psi(\vec{r}, t)}{\partial t} = [\hat{H}_0 + V(\vec{r}, t)]\psi(\vec{r}, t), \qquad (2.1)$$

где $\hat{H}_0 = p^2/2m$ – оператор кинетической энергии нейтрона, а $V(\vec{r}, t)$ – оператор энергии взаимодействия нейтрона с атомами среды. Движение атомов вещества приводит к появлению зависимости этого оператора от времени. Выделим из оператора $V(\vec{r}, t)$ флуктуирующую часть:

$$\delta V(\vec{r}, t) = V(\vec{r}, t) - \langle V(\vec{r}, t)\rangle. \qquad (2.2)$$

Предположим, что $\langle V(\vec{r}, t)\rangle$ не зависит от времени. Из (2.2) непосредственно следует:

$$\langle \delta V(\vec{r}, t)\rangle = 0 \qquad (2.3)$$

Усреднение в формулах (2.2) и (2.3) выполняется по закону распределения случайной функции $V(\vec{r}, t)$, который задается динамикой атомов рассеивающей среды. Предположим, что этот закон распределения имеет гауссову форму. Тогда среднее от всех произведений нечетного числа функций δV равны нулю (а не только $\langle\delta V\rangle$) и все корреляторы от четного числа выражаются через парные корреляционные функции $\langle\delta V(\vec{r}', t')\ \delta V(\vec{r}'', t'')\rangle$. Это предположение оказывается достаточно общим, в то же время при ином законе распределения функции δV задача резко усложняется, поскольку необходимо учитывать корреляционные функции более высокого порядка.

Вернемся к уравнению (2.1). Если задано $\psi(\vec{r}', t')$ значение волновой функции в момент времени t', то во все последующие моменты времени $t > t'$:

---

* Разумеется, в такой среде должно преобладать когерентное рассеяние нейтронов.

$$\psi(\vec{r}, t) = \int K(\vec{r}t; \vec{r}'t')\psi(\vec{r}', t')d\vec{r}'. \qquad (2.4)$$

Здесь $K(\vec{r}, t; \vec{r}', t')$ – функция Грина уравнения (2.1), имеющая смысл полной амплитуды перехода из пространственно-временной точки $(\vec{r}', t')$ в точку $(\vec{r}, t)$ *(она называется также функцией распространения или пропагатором)*. При $t > t'$ функция K удовлетворяет уравнению

$$[i\hbar\frac{\partial}{\partial t} - \hat{H}_0 - V(\vec{r}, t)]\, K(\vec{r}, t; \vec{r}', t') = \delta(\vec{r} - \vec{r}')\delta(t - t'), \qquad (2.5)$$

а при $t < t'$

$$K(\vec{r}, t; \vec{r}', t') = 0. \qquad (2.6)$$

Таким образом, для изучения эволюции пакета нейтронных волн достаточно найти функцию $K(\vec{r}, t; \vec{r}', t')$, которая и будет предметом дальнейшего рассмотрения. Вводя обозначение

$$\hat{H} = \hat{H}_0 + \langle V(\vec{r}, t)\rangle \qquad (2.7)$$

и используя (2.2), перепишем уравнение (2.5) в следующем виде:

$$[i\hbar\frac{\partial}{\partial t} - \hat{H}_1]\, K(\vec{r}, t; \vec{r}', t') = \delta V(\vec{r}, t)K(\vec{r}, t; \vec{r}', t') + \delta(t - t')\delta(\vec{r} - \vec{r}'). \qquad (2.8)$$

Это уравнение удобно представить в интегральной форме:

$$K(\vec{r}, t; \vec{r}', t') = K_1(\vec{r}, t; \vec{r}', t') + \int d\vec{r}''dt'' K_1(\vec{r}, t; \vec{r}'', t'') \times$$

$$\times\, \delta V(\vec{r}'', t'')K(\vec{r}'', t''; \vec{r}', t'). \qquad (2.9)$$

Функция $K(\vec{r}, t; \vec{r}', t')$ *удовлетворяет уравнению*

$$\hat{B}K_1(\vec{r}, t; \vec{r}', t') = \delta(\vec{r} - \vec{r}')\delta(t - t'), \qquad (2.10)$$

где оператор

$$\hat{B} = i\hbar\frac{\partial}{\partial t} - \hat{H}_1, \qquad (2.11)$$

т.е. функция

$$K_1(\vec{r}, t; \vec{r}', t') = \hat{B}^{-1}\delta(\vec{r} - \vec{r}')\delta(t - t') \qquad (2.12)$$

описывает движение нейтронов в усредненном поле $\langle V(\vec{r}, t)\rangle$. Поскольку $V(\vec{r}, t)$ является случайной функцией $\vec{r}$ и t то и функция Грина $K(\vec{r}, t; \vec{r}', t')$ также испытывает флуктуации. Экспериментально определяемые величины пропорциональны усредненным квадратичным относительно $\psi(\vec{r}, t)$ выражениям. Например, вероятность найти нейтрон в точке $\vec{r}$ в момент времени t:

$$\langle|\psi(\vec{r}, t)|^2\rangle = \iint d\vec{r}'d\vec{r}''\langle K(\vec{r}, t; \vec{r}', t')K^*(\vec{r}t; \vec{r}''t')\rangle\psi(\vec{r}'t')\psi^*(\vec{r}'', t'). \qquad (2.13)$$

Пренебрегая корреляцией между $K(\vec{r}t;\ \vec{r}'t')$ и $K(\vec{r}t;\ \vec{r}''t')$, получим приближенно:

$$\langle K(\vec{r}t;\ \vec{r}'t')K^*(\vec{r}t;\ \vec{r}''t')\rangle \approx \langle K(\vec{r}t;\ \vec{r}'t')\rangle \langle K^*(\vec{r}t;\ \vec{r}'t')\rangle \tag{2.14}$$

и

$$\langle |\psi(\vec{r}, t)|^2\rangle \approx |\langle\psi(\vec{r}, t)\rangle|^2 . \tag{2.15}$$

Степень точности приближения (2.14) мы обсудим в конце этого параграфа. Таким образом, в этом приближении наша задача сводится к отысканию $\langle K(\vec{r}t;\ \vec{r}'t')\rangle$. Получим приближенное уравнение, которому удовлетворяет эта функция. Как легко видеть, непосредственное усреднение выражения (2.9) не позволяет получить уравнения для функции $\langle K(\vec{r}t;\ \vec{r}'t')\rangle$. Запишем решение уравнения (2.9) по методу последовательных приближений:

$$K(\vec{r}t;\ \vec{r}'t') = K_1(\vec{r}t;\ \vec{r}'t') + \int d\vec{r}''dt''K_1(\vec{r}t;\ \vec{r}''t'') \times \delta V(\vec{r}''t'')K_1(\vec{r}''t'';\ \vec{r}'t') +$$

$$+ \iint d\vec{r}''d\vec{r}'''dt''dt'''K_1(\vec{r}t;\ \vec{r}''t'')\delta V(\vec{r}''t'')K_1(\vec{r}''t'';\ \vec{r}'''t''')\times \delta V(\vec{r}'''t''')K_1(\vec{r}'''t''';\vec{r}'t') + \ldots \tag{2.16}$$

и, выполнив усреднение, получим следующее выражение для $\langle K(\vec{r}t;\ \vec{r}'t')\rangle$:

$$\langle K(\vec{r}t;\ \vec{r}'t')\rangle = K_1(\vec{r}t;\ \vec{r}'t') + \int d\vec{r}''dt''K_1(\vec{r}t;\ \vec{r}''t'') \times$$

$$\times \langle \delta V(\vec{r}''t''\rangle\ K_1(\vec{r}''t'';\ \vec{r}'t') +$$

$$+ \iint d\vec{r}''d\vec{r}'''dt''dt'''K_1(\vec{r}t;\vec{r}''t'')\langle \delta V(\vec{r}''t'')\delta V(\vec{r}'''t''')\rangle \times K_1(\vec{r}''t'';\vec{r}'''t''')K_1(\vec{r}'''t''';\vec{r}'t') + \ldots \tag{2.17}$$

Подинтегральные выражения в последующих приближениях содержат корреляционные функции типа $\langle \delta V(\vec{r}', t')\,\delta V(\vec{r}'', t'')\ldots\delta V(\vec{r}^{(n)}, t^{(n)})\rangle$, которые вследствие сделанных нами выше предположений о законе распределения функции δV либо равны нулю (n – нечетное), либо выражаются через парные корреляционные функции (n – четное).

Дальнейший анализ выражения (2.17) удобно производить, перейдя к графическому представлению [5]. Введены следующие обозначения:

$K_1(\vec{r}_2t_2;\ \vec{r}_1t_1)$ —

$\langle K(\vec{r}_2t_2;\ \vec{r}_1t_1)\rangle$ — 

$\langle \delta V(\vec{r}_2t_2)\delta V(\vec{r}_1t_1)\rangle$ —  (2.18)

Тогда, суммируя определенную последовательность членов ряда (2.17):

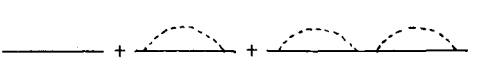 (2.19)

(см. также формулу (2.16) работы [5]) получим следующее приближенное уравнение для функции $\langle K(\vec{r}_2 t_2; \vec{r}_1 t_1)\rangle$:

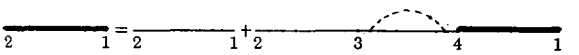

(2.20)

(В узлах 3 и 4 выполняется интегрирование) т.е.

$$\langle K(\vec{r}_2 t_2; \vec{r}_1 t_1)\rangle = K_1(\vec{r}_2 t_2; \vec{r}_1 t_1) + \int\int d\vec{r}_3 d\vec{r}_4 dt_3 dt_4 K_1(\vec{r}_2 t_2; \vec{r}_3 t_3) \times$$

$$\times K_1(\vec{r}_3 t_3; \vec{r}_4 t_4)\langle \delta V(\vec{r}_3 t_3)\delta V(\vec{r}_4 t_4)\rangle \langle K(\vec{r}_4 t_4; \vec{r}_1 t_1)\rangle, \qquad (2.21)$$

или

$$\langle K(\vec{r}_2 t_2; \vec{r}_1 t_1)\rangle = K_1(\vec{r}_2 t_2; \vec{r}_1 t_1) + \int\int d\vec{r}_3 d\vec{r}_4 dt_3 dt_4 K_1(\vec{r}_2 t_2; \vec{r}_3 t_3) \times$$

$$\times M(\vec{r}_3 t_3; \vec{r}_4 t_4)\langle K(\vec{r}_4 t_4; \vec{r}_1 t_1)\rangle, \qquad (2.22)$$

где

$$M(\vec{r}_3 t_3; \vec{r}_4 t_4) = K_1(\vec{r}_3 t_3; \vec{r}_4 t_4)\langle \delta V(\vec{r}_3 t_3)\delta V(\vec{r}_4 t_4)\rangle. \qquad (2.23)^*$$

В этом приближении (формула (2.19)) мы не учитываем вклады от графиков типа:

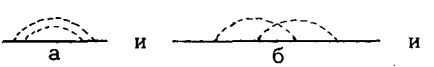

их различных комбинаций, что оправдано, когда корреляционная функция $\langle \delta V(\vec{r}_2 t_2)\, \delta V(\vec{r}_1 t_1)\rangle$ затухает (в пространстве и во времени) быстрее, чем функция распространения $K_1(\vec{r}_2 t_2; \vec{r}_1 t_1)$ [5].

В дальнейшем мы ограничимся приближением (2.19)* и найдем решение уравнения (2.22), которое и будет основным в нашем анализе прохождения холодных нейтронов через вещество.

Усредняя выражение (2.4) и используя (2.22) получим интегральное уравнение для $\langle \psi\rangle$:

$$\langle \psi(\vec{r}_1 t)\rangle = \int K_1(\vec{r}t; \vec{r}'t')\psi(\vec{r}'t')d\vec{r}' +$$

$$+ \int\int d\vec{r}''dt''d\vec{r}'''dt'''K_1(\vec{r}t; \vec{r}''t'')M(\vec{r}''t''; \vec{r}'''t''')\langle \psi(\vec{r}'''t''')\rangle, \qquad (2.24)$$

которое, учитывая (2.10) и (2.11), можно преобразовать к следующему виду:

$$\hat{B}\langle \psi(\vec{r}_1 t)\rangle = \psi(\vec{r}, t')\delta(t - t') + \int d\vec{r}''dt''M(\vec{r}t; \vec{r}''t'')\langle \psi(\vec{r}''t'')\rangle \qquad (2.25)$$

В общем случае это уравнение – интегральное, т.е. поведение $\langle \psi\rangle$ в точке

---

* M – аналог массового оператора квантовой теории поля, а уравнение (2.19) аналогично уравнению Дайсона [7].

** Графики типа а также удается просуммировать. В этом случае функция $\langle K\rangle$ удовлетворяет нелинейному интегральному уравнению (о суммировании графиков этого типа см. [8]).

$\vec{r}$ в момент времени t зависит не только от ее значений при $\vec{r}'$и t' близким к $\vec{r}$ и t соответственно, но и от значений $\langle\psi\rangle$ в точках пространства и моменты времени удаленные от $\vec{r}$ и t. Область значений ($\vec{r}''$, t''),которая дает основной вклад в величину интеграла в (2.25) определяется характерными радиусом ℓ и временем затухания τ корреляционной функции $\langle\delta V(\vec{r}_2 t_2)\delta V(\vec{r}_1 t_1)\rangle$

В заключение этого параграфа обсудим приближение (2.14). Если область локализации первоначального пакета нейтронных волн больше ℓ^3, что, как правило, имеет место и ℓ_1 – длина релаксации K_1 также больше ℓ, то в интеграл (2.13) основной вклад дают области $|\vec{r}_1' - \vec{r}_2'| \gg \ell$ и эффектом корреляции $K(\vec{r}t;\ \vec{r}'t')$ и $K^*(\vec{r}t;\ \vec{r}''t')$ можно пренебречь.

3. РЕШЕНИЕ ОСНОВНОГО УРАВНЕНИЯ

Перейдем теперь к отысканию решения уравнения (2.22) и ограничимся рассмотрением тех случаев, когда функции K_1 и M (а, следовательно, и $\langle K\rangle$) зависят лишь от разности своих аргументов, т.е. когда

$$K_1(\vec{r}_2 t_2;\ \vec{r}_1 t_1) = K_1(\vec{r}_2 - \vec{r}_1;\ t_2 - t_1), \tag{3.1}$$

$$M(\vec{r}_2 t_2;\ \vec{r}_1 t_1) = M(\vec{r}_2 - \vec{r}_1;\ t_2 - t_1), \tag{3.2}$$

и

$$\langle K(\vec{r}_2 t_2;\ \vec{r}_1 t_1)\rangle = \langle K(\vec{r}_2 - \vec{r}_1;\ t_2 - t_1)\rangle. \tag{3.3}$$

В отношении K_1 это предположение означает, что мы пренебрегаем зависимостью $\langle V\rangle$ от пространственных переменных и действие этого потенциала учитываем введением эффективной массы нейтрона μ и коэффициента затухания нейтронной волны δ (δ – не зависит от энергии нейтрона, если сечение поглощения изменяется по закону $1/v$, v – скорость нейтрона).

Тогда, как известно

$$K_1(\vec{r}, t) = \begin{cases} \int \frac{d\vec{p}}{(2\pi)^3} e^{i\vec{p}\vec{r} - i\frac{\hbar p^2}{2\mu}t - \delta t} & t \geq 0 \\ 0 & t < 0 \end{cases} \tag{3.4}$$

При этом (3.2) выполняется, если корреляционная функция $\langle\delta V(\vec{r}_2 t_2)\delta V(\vec{r}_1 t_1)\rangle$ зависит только от $\vec{r}_2 - \vec{r}_1$ и $t_2 - t_1$ т.е. в пространственно-однородном стационарном случае. Выполняя Фурье-преобразование по всем переменным:

$$\langle\tilde{K}(\vec{p}, \omega)\rangle = \int d\vec{r}dt\, e^{-i\vec{p}\vec{r} + i\omega\tau}\langle K(\vec{r}, t)\rangle \tag{3.5}$$

$$\langle K(\vec{r}, t)\rangle = \frac{1}{(2\pi)^4}\int d\vec{p}d\omega\, e^{i\vec{p}\vec{r} - i\omega\tau}\ \langle\tilde{K}(\vec{p}, \omega)\rangle \tag{3.5а}$$

$$\widetilde{M}(\vec{p},\omega)=\int d\vec{r}dt\, e^{-i\vec{p}\vec{r}+i\omega t}\, M(\vec{r},t) \tag{3.6}$$

$$M(\vec{r},t)=\frac{1}{(2\pi)^4}\int d\vec{p}d\omega\, e^{i\vec{p}\vec{r}-i\omega t}\, \widetilde{M}(\vec{p},\omega) \tag{3.6a}$$

$$\widetilde{K}(\vec{p},\omega)=\int d\vec{r}dt\, e^{-i\vec{p}\vec{r}+i\omega t}\, K_1(\vec{r},t)=$$

$$=\int\frac{d\vec{\kappa}}{(2\pi)^3}\int_0^\infty dt\int d\vec{r}\, e^{-i\vec{p}\vec{r}+i\vec{\kappa}\vec{r}}\; e^{-i\frac{\kappa^2\hbar}{2\mu}t-\delta t\, i\omega t}=\frac{i}{\omega-\hbar p^2/2\mu+i\delta}\,. \tag{3.7}$$

$$K_1(\vec{r},t)=\frac{1}{(2\pi)^4}\int d\vec{p}d\omega\, e^{i\vec{p}\vec{r}-i\omega t}\, \widetilde{K}_1(\vec{p},\omega)\,, \tag{3.7a}$$

преобразуем уравнение (2.22) к следующему виду:

$$\frac{1}{(2\pi)^4}\int d\omega d\vec{p}\, e^{i\vec{p}\vec{r}-i\omega t}\,\{\langle\widetilde{K}(\vec{p},\omega)\rangle-\widetilde{K}_1(\vec{p},\omega)\}=$$

$$=\frac{1}{(2\pi)^4}\int d\omega d\vec{p}\, e^{i\vec{p}\vec{r}-i\omega t}\,\widetilde{K}_1(\vec{p},\omega)\widetilde{M}(\vec{p},\omega)\langle\widetilde{K}(\vec{p},\omega)\rangle, \tag{3.8}$$

т.е.

$$\langle\widetilde{K}(\vec{p},\omega)\rangle=\frac{\widetilde{K}_1(\vec{p},\omega)}{1-\widetilde{K}_1(\vec{p},\omega)\widetilde{M}(\vec{p},\omega)}\,, \tag{3.9}$$

или

$$\langle\widetilde{K}(\vec{p},\omega)\rangle=\frac{1}{\widetilde{K}_1^{-1}(\vec{p},\omega)-\widetilde{M}(\vec{p},\omega)}\,. \tag{3.10}$$

Таким образом, функция $\langle\widetilde{K}(\vec{p},\omega)\rangle$ существенным образом зависит от вида "массового оператора" $M(\vec{p},\omega)$ а, следовательно, и от вида корреляционной функции $\langle\delta V(\vec{r}_1 t_1)\delta V(\vec{r}_2 t_2)\rangle$. Если появление флуктуирующей части $V(\vec{r},t)$ обусловлено распространением звуковых возмущений, то

$$\langle \delta V(\vec{r}_1 t_1)\delta V(\vec{r}_2 t_2)\rangle = Q\, e^{i\vec{q}\vec{r} - i\Omega t - \gamma t} + \text{компл. сопр.} \qquad (3.11)$$

$$\vec{r} = \vec{r}_2 - \vec{r}_1, \qquad t = t_2 - t_1$$

Здесь $\vec{q}$ и Ω соответственно волновой вектор и частота, а $e^{-\gamma t}$ описывает затухание флуктуаций вследствие диссипативных процессов в веществе, Q – множитель пропорциональности. Тогда, ограничиваясь для простоты первым слагаемым в (3.11), получим:

$$\widetilde{M}(\vec{p},\omega) = Q\int_0^\infty dt\, e^{it(\omega-\Omega)-\gamma t}\int\frac{d\vec{\kappa}}{(2\pi)^3}\int d\vec{r}\, e^{-i\vec{p}\vec{r}+i\vec{q}\vec{r}+i\vec{\kappa}\vec{r}} \times e^{-i\frac{\hbar\kappa^2}{2\mu}t-\delta t} =$$

$$= iQ\left[\omega - \Omega - \frac{\hbar}{2\mu}(\vec{q}-\vec{p})^2 + i(\gamma+\delta)\right] \qquad (3.12)$$

и

$$\langle K(\vec{p},\omega)\rangle = i\frac{\omega - \Omega - \frac{\hbar}{2\mu}(\vec{q}-\vec{p})^2 + i(\gamma+\delta)}{\left(\omega - \frac{\hbar p^2}{2\mu} + i\delta\right)\left(\omega - \Omega - \frac{\hbar}{2\mu}(\vec{q}-\vec{p})^2 + i(\gamma+\delta)\right) - Q}. \qquad (3.13)$$

Как нетрудно проверить, вычисляя $\langle K(\vec{r},t)\rangle$ или $\langle \psi(\vec{r},t)\rangle$ измененный закон дисперсии нейтронной волны определяется уравнением:

$$\omega^2 - \omega\left[\frac{\hbar p^2}{2\mu} + \Omega + \frac{\hbar}{2\mu}(\vec{q}-\vec{p})^2 - i(\gamma+2\delta)\right] +$$

$$+\left[\frac{\hbar p^2}{2\mu} - i\delta\right]\left[\Omega + \frac{\hbar}{2\mu}(\vec{q}-\vec{p})^2 - i(\gamma+\delta)\right] + Q = 0, \qquad (3.14)$$

из которого непосредственно следует, что кроме волны с $\omega \approx \frac{\hbar p^2}{2\mu} - i\delta$ возможно распространение волны с $\omega \approx \frac{\hbar(\vec{p}-\vec{q})^2}{2\mu} + \Omega - i(\gamma+\delta)$. Аналогичная картина наблюдается при распространении света в поле звуковых волн. Нейтронная волна со смещенной частотой соответствует одной из компонент дублета Мандельштама-Бриллюэна [9]. Наконец, в случае произвольной зависимости корреляционной функции от $\vec{r} = \vec{r}_2 - \vec{r}_1$ и $t = t_2 - t_1$*

$$\langle \delta V(\vec{r}_2 t_2)\delta V(\vec{r}_1 t_1)\rangle = \int\frac{d\vec{q}d\Omega}{(2\pi)^4}\, e^{i\vec{q}\vec{r} - i\Omega t}\, F(\vec{q},\Omega) \qquad (3.15)$$

* Фурье-образ корреляционной функции непосредственно связан с поперечным сечением рассеяния нейтронов.

$$\widetilde{M}(\vec{p},\omega)=\int_0^\infty dt\, e^{i\omega t-\delta t}\int d\vec{r}\, e^{-i\vec{p}\vec{r}}\int\frac{d\vec{\kappa}}{(2\pi)^3}\, e^{i\vec{\kappa}\vec{r}-i\frac{\hbar\kappa^2}{2\mu}}\times\int\frac{d\vec{q}\,d\Omega}{(2\pi)^4}\, e^{i\vec{q}\vec{r}-i\Omega t}\, F(\vec{q},\Omega) \tag{3.16}$$

Интегралы по $\vec{r}$, t и $\vec{q}$ вычисляются. В результате

$$\widetilde{M}(\vec{p},\omega)=\int\frac{d\vec{\kappa}}{(2\pi)^3}\int\frac{d\Omega}{2\pi}\, F(\vec{p}-\vec{\kappa},\Omega)\frac{i}{\omega-\frac{\hbar\kappa^2}{2\mu}-\Omega+i\delta} \tag{3.17}$$

и

$$\langle\widetilde{K}(\vec{p},\omega)\rangle=i\left[\omega-\frac{\hbar p^2}{2\mu}-i\mathrm{Re}\widetilde{M}(\vec{p},\omega)+i\delta+\mathrm{Im}\widetilde{M}(\vec{p},\omega)\right] \tag{3.18}$$

При получении (3.18) мы предполагали, что функция $F(\vec{q},\Omega)$ не содержит особенностей типа $(\omega-\omega_0+i\gamma)^{-1}$, как в предыдущем случае, и волна со смещенной частотой отсутствует. Таким образом, и в общем случае наличие флуктуаций потенциала $V(\vec{r},t)$ приводит к изменению закона дисперсии и постоянной затухания нейтронной волны.

В заключение этого параграфа получим в первом приближении теории возмущений выражение для $\langle\widetilde{K}(\vec{p},\omega)\rangle$:

$$\langle\widetilde{K}(\vec{p},\omega)\rangle=\widetilde{K}_1(\vec{p},\omega)=\widetilde{M}(\vec{p},\omega)\widetilde{K}_1^2(\vec{p},\omega). \tag{3.19}$$

Тогда при $t>0$

$$\langle K(\vec{p},t)\rangle=K_1(\vec{p},t)-\int_{-\infty}^{\infty}\frac{\widetilde{M}(\vec{p},\omega)\,e^{-i\omega t}\,d\omega}{\left[\omega-\frac{\hbar p^2}{2\mu}+i\delta\right]^2}=$$

$$=K_1(\vec{p},t)+2\pi i\frac{\partial}{\partial\omega}\left[\widetilde{M}(\vec{p},\omega)e^{-i\omega t}\right]\Bigg|_{\omega=\frac{\hbar p^2}{2\mu}-i\delta}+2\pi i\sum\text{выч.}\frac{e^{-i\omega t}}{\left[\omega-\frac{\hbar p^2}{2\mu}+i\delta\right]^2}M(\vec{p},\omega), \tag{3.20}$$

где последнее слагаемое есть сумма вычетов в полюсах $\widetilde{M}(\vec{p},\omega)$ в нижней полуплоскости ω. Даже если эти полюса простые, то уже второе слагаемое оказывается пропорциональным t и теория возмущений оказывается неприменимой при больших t.

4. ЗАКЛЮЧЕНИЕ

В работе исследовано уравнение Шредингера, описывающее прохождение холодных нейтронов через вещество, рассеивающие свойства которого изменяются случайным образом от точки к точке и с течением времени.

Флуктуации в среде приводят к изменению закона дисперсии и дополнительному затуханию (помимо обусловленного поглощением атомными ядрами вещества) нейтронных волн. Соответственно, изменяется и показатель преломления, что может оказаться существенным для анализа отражения нейтронных волн. Экспериментальное изучение распространения холодных нейтронов через вещество позволяет определить параметры корреляционной функции $\langle \delta V(\vec{r}t)\delta V(\vec{r}'t')\rangle$ и проанализировать свойства атомного движения в средах с нерегулярными свойствами (жидкости, стекла и т.п.).

В настоящей работе не рассматривался переход от квантово-механического описания к классическому, основанному на кинетическом уравнении. Эта задача, представляющая большой самостоятельный интерес, будет рассмотрена в дальнейшем.

В заключение автор выражает глубокую благодарность М.В. Казарновскому за плодотворные обсуждения.

ПРИЛОЖЕНИЕ

Для уточнения приближения (2.14) необходимо рассмотреть корреляционную функцию

$$\langle L(\vec{r}_2 t_2 \vec{r}_1 t_1; \vec{r}_2' t_2' \vec{r}_1' t_1')\rangle = \langle K(\vec{r}_2 t_2; \vec{r}_1 t_1) K^*(\vec{r}_2 t_2; \vec{r}_1 t_1)\rangle \qquad (\text{П}.1)$$

Умножая уравнение (2.16) на его комплексно сопряженное, получим после усреднения уравнение для коррелятора $\langle L\rangle$:

$$\langle L(\vec{r}_2 t_2 \vec{r}_1 t_1; \vec{r}_2' t_2' \vec{r}_1' t_1')\rangle = K_1(\vec{r}_2 t_2 \vec{r}_1 t_1) K_1(\vec{r}_2' t_2' \vec{r}_1' t_1') +$$

$$+ \iint d\vec{r}_3 dt_3 d\vec{r}_3' dt_3' K_1(\vec{r}_2 t_2; \vec{r}_3 t_3) K_1^*(\vec{r}_2' t_2' \vec{r}_3' t_3') \langle \delta V(\vec{r}_3 t_3) \delta V^*(\vec{r}_3' t_3')\rangle \times$$

$$\times K_1(\vec{r}_3 t_3; \vec{r}_1 t_1) K_1^*(\vec{r}_3' t_3'; \vec{r}_1' t_1') + \iint d\vec{r}_3\, dt_3 d\vec{r}_4\, dt_4 K_1(\vec{r}_2 t_2; \vec{r}_3 t_3) K_1(\vec{r}_3 t_3; \vec{r}_4 t_4) \times$$

$$\times \langle \delta V(\vec{r}_3 t_3) \delta V(\vec{r}_4 t_4)\rangle K_1(\vec{r}_4 t_4; \vec{r}_1 t_1) K_1^*(\vec{r}_2' t_2'; \vec{r}_1' t_1') +$$

$$+ K_1(\vec{r}_2 t_2; \vec{r}_1 t_1) \iint d\vec{r}_3' dt_3' d\vec{r}_4' dt_4' K_1^*(\vec{r}_2' t_2'; \vec{r}_3' t_3') \times$$

$$\times K_1^*(\vec{r}_3' t_3'; \vec{r}_4' t_4') \langle \delta V^*(\vec{r}_3 t_3) \delta V^*(\vec{r}_4' t_4')\rangle K_1^*(\vec{r}_4' t_4'; \vec{r}_1' t_1') + \ldots \qquad (\text{П}.2)$$

Обозначая

$$\langle L(\vec{r}_2 t_2 \vec{r}_1 t_1 / \vec{r}_2' t_2' \vec{r}_1' t_1') \rangle \rightarrow$$

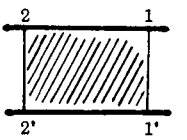

получим следующее графическое представление уравнения (П.2):

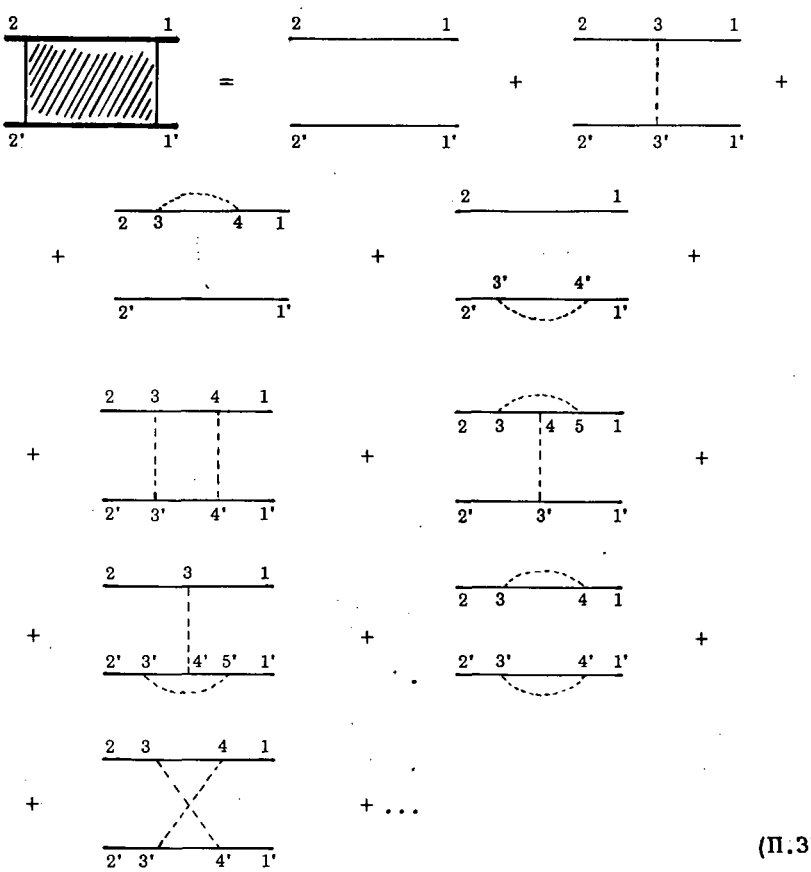

(П.3)

Нижние линии на графиках отвечают комплексно сопряженным величинам.

Пунктирные линии, относящиеся к какой-либо одной прямой линии, мы можем учесть в приближении (2.19), используя результаты параграфа 2. Получаем:

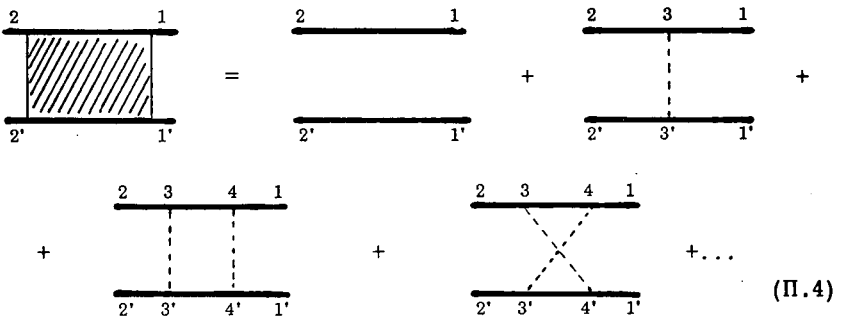

(П.4)

Очевидно, что приближению (2.14) (с учетом (2.19)) отвечает первое слагаемое в выражении (П.5). Получим теперь уточнение приближения (2.14), ограничиваясь учетом также всех графиков типа:

(П.5)

(так называемое "лестничное приближение").
В этом случае

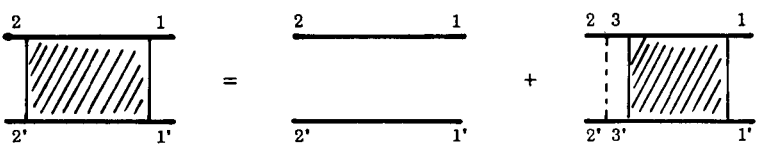

(П.6)

т.е.

$$\langle L(\vec{r}_2 t_2; \vec{r}_1 t_1/\vec{r}_2' t_2' \vec{r}_1' t_1') \rangle = L_1(\vec{r}_2 t_2 \vec{r}_1 t_1/\vec{r}_2' t_2' \vec{r}_1' t_1') +$$

$$+ \iint d\vec{r}_3 d\vec{r}_3' dt_3 dt_3' L_1(\vec{r}_2 t_2 \vec{r}_3 t_3/\vec{r}_2' t_2' \vec{r}_3' t_3') \times$$

$$\times \langle \delta V(\vec{r}_3 t_3) \delta V^*(\vec{r}_3' t_3') \rangle \langle L(\vec{r}_3 t_3 \vec{r}_1 t_1/\vec{r}_3' t_3' \vec{r}_1' t_1') \rangle, \qquad (П.7)$$

где

$$L_1(\vec{r}_2 t_2 \vec{r}_1 t_1/\vec{r}_2' t_2' \vec{r}_1' t_1') = \langle K(\vec{r}_2 t_2/\vec{r}_1 t_1) \rangle \langle K^*(\vec{r}_2' t_2' \vec{r}_1' t_1') \rangle \qquad (П.8)$$

Уравнение (П.7) аналогично квантово-механическому уравнению Бете-Сальпитера [10]. Если $\langle \delta V(\vec{r}_3 t_3) \delta V^*(\vec{r}_3' t_3') \rangle$ быстро затухает с увеличением расстояния между пространственно временными точками $\vec{r}_3 t_3$ и $\vec{r}_3' t_3'$, то уравнение (П.7) можно упростить, полагая в функциях L_1 и $\langle L \rangle$, $\vec{r}_3 = \vec{r}_3'$ и $t_3 = t_3'$

$$\langle L(\vec{r}_2 t_2 \vec{r}_1 t_1 / \vec{r}_2' t_2' \vec{r}_1' t_1') \rangle = L_1(\vec{r}_2 t_2 \vec{r}_1 t_1 / \vec{r}_2' t_2' \vec{r}_1' t_1') +$$

$$+ A \int d\vec{r}_3 dt_3 L_1(\vec{r}_2 t_2 \vec{r}_3 t_3 / \vec{r}_2' t_2' \vec{r}_3 t_3) \langle L(\vec{r}_3 t_3 \vec{r}_1 t_1 / \vec{r}_3 t_3 \vec{r}_1' t_1') \rangle, \qquad (П.9)$$

где

$$A = \int d\vec{r}_3' dt_3' \langle \delta V(\vec{r}_3 t_3) \delta V^*(\vec{r}_3' t_3') \rangle. \qquad (П.10)$$

Графическое представление уравнения (П.9) выглядит следующим образом:

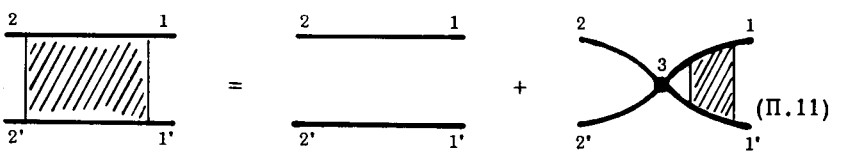

(П.11)

Зачерненному кружку отвечает множитель A. Нас интересует функция $\langle L \rangle$, когда $(r_2 t_2) = (\vec{r}_2' t_2')$.
В этом случае уравнение

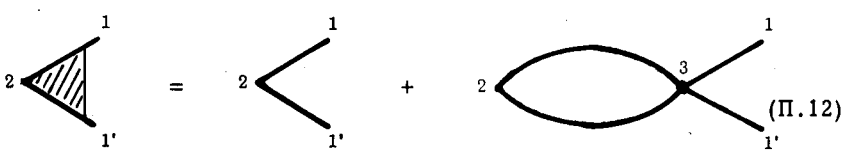

(П.12)

с помощью преобразования Фурье:

$$\langle \tilde{L}(\vec{p}_1 \vec{p}_2 \omega_1 \omega_2) \rangle =$$

$$= \int d\vec{r}_2 dt_2 d\vec{r}_1' dt_1' \, e^{i\vec{p}_1(\vec{r}_2 - \vec{r}_1') - i\vec{p}_2(\vec{r}_2 - \vec{r}_1') - i\omega_1(t_2 - t_1) + i\omega_2(t_2 - t_1')} \langle L(\vec{r}_2 t_2 \vec{r}_1 t_1 / \vec{r}_2 t_2 \vec{r}_1' t_1') \rangle$$

$$\tilde{L}_1(\vec{p}\omega) = \int d\vec{r}_2 dt_2 \, e^{i\vec{p}(\vec{r}_2 - \vec{r}_1) - i\omega(t_2 - t_1)} L_1(\vec{r}_2 - \vec{r}_1; t_2 - t_1)$$

сводится к алгебраическому, решение которого

$$\langle \tilde{L}(\vec{p}_1 \vec{p}_2 \omega_1 \omega_2) \rangle = \frac{\tilde{L}_1(\vec{p}_1 \vec{p}_2 \omega_1 \omega_2)}{1 - A \tilde{L}_1(\vec{p}_1 \omega_1)}. \qquad (П.13)$$

ЛИТЕРАТУРА

[1] Юз Д., Нейтронная оптика. Изд. иностр. лит., М., 1955
АХИЕЗЕР А., ПОМЕРАНЧУК И., Некоторые вопросы теории ядра. ГИТТЛ, М., 1950.
[2] КАЗАРНОВСКИЙ М.В., СТЕПАНОВ А.В., Труды ФИАН (в печати).
[3] ЗАЙМАН Д., Электроны и фононы. ИИЛ. М., 1962.
[4] NELKIN M., Physica 29 (1963) 261.
[5] СТЕПАНОВ А.В., Графический метод решения некоторого класса задач нейтронной физики. Препринт ФИАН, 1965.
[6] KADANOFF L., MARTIN P., Ann of Phys 24 (1963) 419.
[7] АХИЕЗЕР А.И., БЕРЕСТЕЦКИЙ В.Б., Квантовая электродинамика, Физматгиз, М., 1959.
[8] АБРИКОСОВ А.А., ГОРЬКОВ Л.П., ДЗОШИНСКИИ И.Е., Методы квантовой теории поля в статистической физике. Физматгиз, М., 1962.
[9] ЛАНДАУ Л.Д., ЛИФШИЦ Е.М., Электродинамика сплошных сред, ГИТТЛ, М., 1957.
[10] SALPETER E., BETHE H., Phys. Rev. 84 (1951) 1232.

ВОЗМОЖНЫЙ МЕТОД ИССЛЕДОВАНИЯ АНАЛИТИЧЕСКОЙ ЗАВИСИМОСТИ НЕЙТРОННОГО РАСПРЕДЕЛЕНИЯ ОТ ПАРАМЕТРОВ ЯДРА РАССЕЯНИЯ

М.В. КАЗАРНОВСКИЙ и Ш. КЕНЖЕБАЕВ
ФИЗИЧЕСКИЙ ИНСТИТУТ им. П.Н. ЛЕБЕДЕВА
АН СССР, МОСКВА,
СССР

Abstract — Résumé — Аннотация — Resumen

POSSIBLE METHOD FOR STUDYING THE ANALYTICAL DEPENDENCE OF NEUTRON DISTRIBUTION ON PARAMETERS OF THE SCATTERING NUCLEUS. One of the possible models for the scattering nucleus – $W_s(v, v')$ – convenient for studying the analytical properties of the functions of neutron distributions – is the expression $W_s(v, v')$ in the form of a superposition of the scattering nuclei represented by a gaseous model corresponding to different masses. Even in the simplest case involving the sum of two terms this superposition satisfies the general requirements (asymptotic character at high energies and the condition of detailed balance) and contains two arbitrary parameters.

Within the framework of the multi-velocity theory the total information on the law of scattering which is necessary to calculate the neutron distributions is contained in the set of parameters $\gamma_{ik}(\gamma_{ik}+\gamma_{ki}, \gamma_{io}=\gamma_{oi}=\gamma_{oo}=0)$. If these are known it is relatively easy to consider the behaviour of the neutron distributions in the thermal range. Within the framework of the gaseous (and consequently also the superposition) model the parameters γ_{ik} can be calculated in an analytical form (in the paper expressions are quoted for γ_{11}, γ_{12} and γ_{22}). The paper discusses the advantages, the drawbacks and the physical justification for the superposition model.

MÉTHODE POSSIBLE POUR L'ÉTUDE DE LA RELATION DE DÉPENDANCE ANALYTIQUE ENTRE LA DISTRIBUTION DES NEUTRONS ET LES PARAMÈTRES DU NOYAU DE DIFFUSION. Un des modèles possibles du noyau de diffusion $W_s(v, v')$, qui convient à l'étude des propriétés analytiques des fonctions de distribution des neutrons, consiste à exprimer $W_s(v, v')$ sous la forme d'une superposition des noyaux de diffusion conformes au modèle de gaz et correspondant à des masses différentes. On a constaté que même dans le cas le plus simple, qui est celui de la somme de deux termes, cette superposition satisfait aux exigences générales (caractère asymptotique en présence de hautes énergies et équilibre détaillé) et comporte deux paramètres arbitraires.

Dans le cadre du formalisme de la théorie à plusieurs vitesses, toutes les données relatives à la loi de diffusion, nécessaires pour le calcul de la distribution des neutrons, sont contenues dans l'ensemble des paramètres $\gamma_{ik}(\gamma_{ik}+\gamma_{ki}, \gamma_{io}=\gamma_{oi}=\gamma_{oo}=0)$, dont la connaissance permet d'examiner assez facilement la distribution des neutrons dans la région thermique. En s'appuyant sur le modèle de gaz (et par conséquent aussi sur celui de la superposition), on parvient à calculer les paramètres γ_{ik} sous une forme analytique (le mémoire donne les expressions pour γ_{11}, γ_{12} et γ_{22}). Les avantages, les inconvénients et les particularités physiques du modèle de superposition font l'objet d'un examen critique.

ВОЗМОЖНЫЙ МЕТОД ИССЛЕДОВАНИЯ АНАЛИТИЧЕСКОЙ ЗАВИСИМОСТИ НЕЙТРОННОГО РАСПРЕДЕЛЕНИЯ ОТ ПАРАМЕТРОВ ЯДРА РАССЕЯНИЯ. Одной из возможных моделей ядра $w_s(v, v')$, удобной для исследования аналитических свойств функций нейтронных распределений, является выражение $w_s(v,v')$ в виде суперпозиции ядер рассеяния по газовой модели, соответствующих различным массам. Оказывается, что даже в простейшем случае суммы двух членов, эта суперпозиция удовлетворяет общим требованиям (асимптотика при больших энергиях и условие детального равновесия) и содержит два произвольных параметра.

В рамках формализма многоскоростной теории вся информация о законе рассеяния, необходимая для расчета нейтронных распределений, содержится в наборе параметров γ_{ik}, $(\gamma_{ik}=\gamma_{ki}, \gamma_{io}=\gamma_{oi}=\gamma_{oo}=0)$, зная которые можно относительно просто рассмотреть пове-

дение нейтронных распределений в тепловой области. В рамках газовой (а следовательно и суперпозиционной) модели параметры γ_{ik} удается вычислить в аналитическом виде (в работе приведены выражения для γ_{11}, γ_{12} и γ_{22}.

Обсуждаются преимущества, недостатки и физическая обоснованность суперпозиционной модели.

METODO POSIBLE PARA ESTUDIAR LA RELACION ANALITICA ENTRE LA DISTRIBUCION NEUTRONICA Y LOS PARAMETROS DEL NUCLEO DISPERSOR. Uno de los modelos posibles del núcleo dispersor, que resulta conveniente para estudiar las propiedades analíticas de las funciones correspondientes a las distribuciones neutrónicas, es la expresión $W_s(v, v')$, en forma de una superposición de los núcleos dispersores representados por un *modelo gaseoso correspondiente a masas diferentes. Aun en el caso más simple, donde interviene* la suma de sólo dos términos, esta superposición satisface las exigencias generales (carácter asintótico a energías elevadas y condición de equilibrio detallado), y contiene dos parámetros arbitrarios.

En el marco de la teoría de las velocidades múltiples, la información total sobre la ley de la dispersión necesaria para calcular las distribuciones neutrónicas, está contenida en el conjunto de parámetros γ_{ik} ($\gamma_{ik} + \gamma_{ki}$, $\gamma_{io} = \gamma_{oi} = \gamma_{oo} = 0$). Si estos parámetros se conocen, resulta relativamente fácil considerar las distribuciones neutrónicas en el intervalo térmico. Con arreglo al modelo gaseoso (y por consiguiente también al de superposición), los parámetros γ_{ik} pueden calcularse en forma analítica (en la memoria, los autores presentan expresiones que dan los valores de γ_{11}, γ_{12} y γ_{22}). Se analizan en la memoria las ventajas, los inconvenientes y la justificación física del modelo de superposición.

1. В последнее время весьма актуальным стал вопрос об аналитических свойствах функций нейтронных распределений, в частности, временной зависимости нейтронного спектра. Для его решения очень важно найти аналитические выражения для этих функций. Однако в силу крайней сложности уравнения баланса нейтронов в общем случае это сделать невозможно. Поэтому представляется целесообразным попытаться подобрать такое более или менее реалистичное модельное выражение для ядра рассеяния, которое было бы достаточно простым, чтобы можно было искать распределение нейтронов в аналитической форме. В то же время это модельное выражение должно зависеть от одного или нескольких параметров, вариация которых отражала бы изменение закона рассеяния в достаточно широких пределах. Настоящая работа посвящена обсуждению возможного варианта такой модели.

2. Поскольку нас в основном интересует эффект изменения энергии нейтронов при рассеянии, влияние пространственного переноса нейтронов на функции нейтронного распределения $N(\vec{r}, v, t)$ (т.е. на число нейтронов в единичном элементе объема вблизи точки $\vec{r}$ в единичном интервале скоростей * вблизи v в момент t), мы рассмотрим пространственный перенос нейтронов в диффузионном приближении. Тогда в случае точечного импульсного моноэнергетического источника единичной интенсивности

$$S(\vec{r}, v, t) = \delta(\vec{r} - \vec{r}_s)\,\delta(v - v_s)\,\delta(t),$$

разлагая $N(\vec{r}, v, t)$ по собственным функциям оператора Лапласа

---

* Ниже предполагается, что скорость измеряется в единицах $\sqrt{2kT/m}$, где T-температура замедлителя, k—постоянная Больцмана, а m—масса нейтрона.

$$\nabla^2 R_k(\vec{r}) + B_k^2 R_k(\vec{r}) = 0,$$

$$\int R_k(\vec{r})\, R_{k'}(\vec{r}) d\vec{r} = \delta_{kk'},$$

обращающимся в нуль на экстраполированной границе,

$$N(\vec{r}, v, t) = \sum_k n_k(v, t) R_k(\vec{r}) R_k(\vec{r}_s),$$

получим для коэффициентов этого разложения известное уравнение:

$$\frac{\partial n(v, t)}{\partial t} + [W_c(v) + D(v)B^2 + W_s(v)]n(v, t) - \tag{1}$$

$$-\int_0^\infty W_s(v', v)n(v', t)dv' - \delta(t)\delta(v - v_s) = 0.$$

(индекс k для краткости опущен). Здесь

$W_c(v)$ — вероятность захвата нейтрона со скоростью v в единицу времени;

$W_s(v,v')$ — ядро рассеяния, т.е. вероятность того, что нейтрон со скоростью v в результате рассеяния в замедлителе перейдет в единицу времени в единичный интервал скорости вблизи v;

$W_s(v) = \int_0^\infty W_s(v,v')\, dv'$; $D(v)$ — коэффициент диффузии нейтронов со скоростью v.

Аналитическое решение этого уравнения в виде различных рядов и его исследование даже в простейшем случае бесконечной однородной замедляющей среды при $B^2 = 0$ возможно лишь при весьма частых предположениях о виде ядра рассеяния, например, в модели тяжелого газа [1] или протонного газа [2] или для вырожденного (разделяющегося) ядра рассеяния [3].

С другой стороны, решение этого уравнения можно искать в виде разложения по какой-либо полной системе функций, зависящих от скорости (энергии). Например [4], в качестве таких функций можно выбрать систему полиномов $L_i(v)$, ортонормированных с весом $M(v)$ (максвелловское распределение) в интервале $0 \leqslant v \leqslant \infty$

$$\int_0^\infty M(v)L_i(v)\, L_k(v)dv = \delta_{ik}\,, \tag{2}$$

$$M(v) = \frac{v}{\sqrt{\pi}} v^2 e^{-v^2}\,.$$

Тогда

$$n(v, t) = M(v) \sum_{i=0}^{\infty} n_i(t)L_i(v)\,, \tag{3}$$

причем n_0 характеризует полное число нейтронов, n_1 — их среднюю скорость, n_2 — средний квадрат скорости и т.д. Очевидно, что это разложение представляет интерес только в том случае, если оно быстро сходится. Оценки [4] показывают, что в случае модели тяжелого газа две, максимум три группы нейтронов n_i достаточны для вполне удовлетворительного описания

нейтронного распределения. Следует, однако, отметить, что в тех случаях, когда уравнение (1) не имеет дискретного спектра временных постоянных затухания, т.е. нейтронное распределение с ростом t стремится к сингулярной функции от v, сходимость разложения (2) при больших t должна ухудшаться с ростом t. Как было отмечено ранее [5] в этом случае нейтронное распределение от импульсного источника быстрых нейтронов сначала с ростом t приближается к спектру, близкому к максвелловскому, а затем при заметно больших временах начинает формироваться асимптотическое сингулярное распределение. Очевидно, что разложение (3) должно позволить описать конечную стадию первого процесса и начальную стадию второго. Для величин $n_i(t)$ как известно получается следующая система уравнений:

$$\frac{\partial n_i}{\partial t} + \sum_{k=0}^{\infty} D_{Ok} B^2 n_k + W_0 n_i + \sum_{k=0}^{\infty} \gamma_{ik} n_k - L_i(v_s)\delta(t) = 0,$$

$$D_{ik} = D_{ki} = \int_0^{\infty} D(v) M(v) L_i(v) L_k(v) dv, \qquad (4)$$

$$\gamma_{ik} = \int_0^{\infty} dv M(v) L_i(v) \int_0^{\infty} dv' W_s(v, v')[L_k(v) - L_k(v')] \quad i = 0; 1; \ldots$$

причем из условия детального равновесия $\gamma_{ik} = \gamma_{ki}$, $\gamma_{i0} = \gamma_{0i} = \gamma_{00} = 0$ (здесь для простоты предположено, что $W_c(v) = W_0$ не зависит от v).

В тех случаях, когда в разложении (3) можно ограничиться конечным (небольшим) числом j членов, приближенное решение системы (4) можно легко найти, обрезая суммирование по к на j−ом члене и рассматривая только первые j уравнений.

3. Вся информация о ядре рассеяния, необходимая для отыскания решения системы (4), содержится в постоянных γ_{ik}, и для исследования влияния закона рассеяния на нейтронное распределение необходимо найти эти постоянные. В общем виде нельзя для них получить аналитические выражения. Поэтому представляет интерес найти такую модель для ядра рассеяния, в которой это возможно. При этом оно должно удовлетворять двум основным требованиям:

1) условию детального равновесия:

$$M(v) W_s(v, v') = M(v') W_s(v', v)$$

2) при больших передаваемых энергиях ($|v^2 - v'^2| \gg 1$) оно должно совпадать с ядром рассеяния на свободных покоящихся атомах $W_{sf}(v, v')$. Согласно формализма Ван Хове [6] и Скофилда [7], ядро рассеяния можно представить в виде:

$$W_s(v, v') = B v' \int_{-\infty}^{\infty} dt e^{it(v'^2 - v^2)} \int_{-1}^{1} d\cos\theta S(v^2 + v'^2 - 2vv'\cos\theta, t), \qquad (5)$$

где

$$B = \frac{1}{2\pi}\left(\frac{A+1}{A}\right)^2 \sum_{sf} \sqrt{\frac{2kT}{m}}$$

(A-массовое число атомов замедлителя, а Σ_{sf} — макроскопическое сечение рассеяния нейтронов на свободных покоящихся атомах), а $S(q^2, t)$ — так называемая промежуточная корреляционная функция. Функция S должна удовлетворять следующим общим требованиям: из условия действительности следует, что

$$S(q^2, t) = S^*(q^2, -t). \tag{6}$$

Из условия

$$W_s(v, v') \to W_{sf}(v, v') \qquad |v^2 - v'^2| \gg 1$$
$$S(q^2, 0) = 1, \quad \left.\frac{\partial S(q^2, t)}{\partial t}\right|_{t=0} = i\frac{q^2}{A}. \tag{7}$$

Из условия детального равновесия

$$S\left(q^2, t + \frac{i}{2}\right) \qquad \text{— действительна.} \tag{8}$$

Простейшая модель ядра рассеяния удовлетворяющая требованиям — газовая модель, согласно которой

$$S(q^2, t) = S_g(q^2, t, A) = e^{-t(t-i)q^2/A}. \tag{9}$$

Оказывается, что для этой модели параметры γ_{ik} можно вычислить в аналитическом виде (см. приложение). В частности

$$\gamma_{11} = \frac{32}{3} \cdot \frac{\pi^{3/2} B}{3\pi - 8} \cdot \frac{A^y}{(A+1)^3}\left[1 - \frac{2A-1}{2A^{3/2}}(A+1)^{1/2}\right],$$

$$\gamma_{12} = \frac{2}{\sqrt{9\pi - 28}}\left[2\sqrt{\pi}B \cdot \frac{A^{3/2}}{(A+1)^3}\left(1 + \frac{2A}{A+1} + \frac{3A-1}{\sqrt{A}}\operatorname{arctg}\sqrt{A}\right) - \gamma_{11}\right], \tag{10}$$

$$\gamma_{22} = \frac{4}{9\pi - 28}\left[8(3\pi - 8)\sqrt{\pi}B\frac{A^{5/2}}{(A+1)^{7/2}} - \gamma_{11} - \sqrt{9\pi - 28}\,\gamma_{12}\right].$$

В частных случаях при A = 1

$$\gamma_{11} = \frac{4\pi^{3/2}}{3(3\pi - 8)}\left(1 - \frac{1}{\sqrt{2}}\right)B \approx 1,51\,B,$$

$$\gamma_{12} = \frac{\sqrt{\pi}}{\sqrt{9\pi - 28}}\left[1 + \frac{\pi}{4} - \frac{8\pi}{3(3\pi - 8)}\left(1 - \frac{1}{\sqrt{2}}\right)\right]B \approx 0,25\,B, \tag{11}$$

$$\gamma_{22} = \frac{4\sqrt{\pi}}{9\pi - 28}\left[\frac{3\pi - 8}{\sqrt{2}} + \frac{4\pi}{3\pi - 8}\left(1 - \frac{1}{\sqrt{2}}\right) - 1 - \frac{\pi}{4}\right]B \approx 2,0\,B,$$

при $A \to \infty$

$$\gamma_{11} = \frac{4\pi^{3/2}}{3\pi - 8} B\left(\frac{A}{A+1}\right)^2 \frac{1}{A}\left(1 - \frac{4}{3A}\right) = 15,6\, B\left(\frac{A}{A+1}\right)^2 \cdot \frac{1}{A} \cdot \left(1 - \frac{4}{3A}\right),$$

$$\gamma_{12} = \frac{2\sqrt{9\pi - 28}}{3\pi - 8}\, \pi^{3/2} B\left(\frac{A}{A+1}\right)^2 \frac{1}{A}\left(1 - \frac{4}{3A}\right) \approx 0,263\, \gamma_{11} \tag{12}$$

$$\gamma_{22} = \frac{16\,\pi^{3/2}}{(3\pi - 8)(9\pi - 28)} B\left(\frac{A}{A+1}\right)^2 \frac{1}{A}\left\{\frac{2(3\pi - 8)^2}{\pi} - \frac{9\pi - 26}{2} - \right.$$

$$\left. - \left[3\frac{(3\pi - 8)^2}{\pi} - \frac{2}{3}(9\pi - 26)\right] \frac{1}{A}\right\} \approx 35,3 B\left(\frac{A}{A+1}\right)^2 \frac{1}{A}\left(1 - \frac{2,8}{A}\right).$$

К сожалению функция $S_g(q^2, t, A)$ зависит только от одного параметра A. Пурохит [8] предложил обобщение газовой модели в виде

$$S_P(q^2, t) = e^{-\frac{q^2}{A}(a + bt + ct^2)}, \tag{13}$$

где a, b и c — некоторые константы. Однако любое отклонение (13) от (9) приводит к нарушениям требований (6)-(8). Значительно более общим и удобным кажется другое простое обобщение газовой модели, а именно представление $S(q^2, t)$ в виде суперпозиции $S_g(q^2, t, A)$, соответствующих различным A, т.е. в виде

$$S(q^2, t) = \sum_i a_i\, e^{-\tau(t - i)q^2/A_i} \tag{14}$$

(в общем случае суммирование по i может включать в себя и интегрирование по каким-либо участкам непрерывного спектра значений A). Выражение (14) автоматически удовлетворяет требованиям (6) и (8). Условие (7) удовлетворяется, если

$$\sum_i a_i = 1, \tag{15}$$

$$\sum_i a_i \frac{1}{A_i} = \frac{1}{A}. \tag{16}$$

При этом даже если в сумме (14) взять только два члена ($i = 1,2$), мы получаем наряду с выполнением требований (6-8) два дополнительных параметра (например, a_1/a_2 и A_1/A_2). Соответственно, параметры γ_{ik} в такой модели имеют вид:

$$\gamma_{ik} = \sum_i a_i\, \gamma_{ik}(A_i), \tag{17}$$

где $\gamma_{ik}(A)$ определяются формулами (10-12) или аналогичными им при i, $k > 2$. Таким образом, предлагаемое обобщение газовой модели позволяет

получить простые аналитические выражения для параметров γ_{ik}, что в свою очередь открывает возможности аналитического исследования нейтронных распределений в рамках многоскоростной теории [4].

4. В общем случае функция S может зависеть от двух независимых переменных q^2 и t более или менее произвольным образом (при условии выполнения (6-8). Формально введенное выше выражение (14) подразумевает, что эти переменные входят в S в виде одной вполне определенной линейной комбинации

$$q^2(t^2 - it).$$

Это является серьезным ограничением на возможный характер вариаций $S(q^2, t)$ в зависимости от свободных параметров. Поэтому возникает вопрос, является ли выражение (14) в какой-либо степени физически обоснованным, или оно представляет собой чисто формальную схему. В последнем случае может оказаться, что оно отражает реальное взаимодействие нейтронов с замедлителем, лишь в тривиальном случае, когда в сумме по i имеется только один член. т.е. когда S совпадает с S_g. Легко, однако, убедиться, что выражение (14) является физически естественным. Действительно, помимо тривиального случая, когда замедлитель представляет собой смесь газов с различными массовыми числами, и выражение (14) является точным, к этому выражению можно придти в следующих случаях:

1) если химическая связь рассеивающего атома изотропна, как это имеет место для одноатомных кубических кристаллических решеток, по-видимому, применимо так называемое гауссово приближение:

$$S(q^2, t) = e^{-\frac{q^2}{A} f(t)} \tag{18}$$

где $f(t)$ — некоторая, как правило, осциллирующая функция. При этом в интеграл (5) могут давать сравнимые вклады несколько минимумов функции $f(t)$. Вычисляя эти вклады методом перевала* мы немедленно придем к выражению, эквивалентному (14);

2) если же химическая связь рассеивающего атома анизотропна (как это почти всегда имеет место в молекулах и некубических кристаллах), то функция S является результатом усреднения по углам $\vec{\Omega}$, характеризующим ориентацию молекулы (кристалла) выражения вида (18), по q с $f(t)$, зависящей от $\vec{\Omega}$, т.е.

$$S(q^2, t) = \int e^{-\frac{q^2}{M} f(\vec{\Omega}, t)} \cdot \frac{d\vec{\Omega}}{4\pi} \cdot \tag{19}$$

Вычисление интеграла (5) методом перевала эквивалентно замене (19) на сумму $S(q^2,t) = \int d\vec{\Omega} \sum_k a_k(\vec{\Omega}) e^{-\frac{q^2}{A}} \varphi_k(\vec{\Omega})(t^2 - it)$ совпадающего с (14), если положить $A_i = A/\varphi_k(\Omega_i)$ и учесть, что суперпозиция (14) включает как суммирование, так и интегрирование по спектру массовых чисел A_i.

* При этом для выполнения (17) следует предположить также, что положения точек перевала не зависят от v и v', что также является серьезным ограничением.

Следует однако отметить, что химическая связь приводит только к увеличению эффективной массы замедлителя. Поэтому если в интеграле (5) дает вклад только область $|t| \ll 1$, то оценка этого интервала методом перевала приводит как для случая изотропной связи, так и для случая анизотропной связи к нарушению условия (16). Замену вычисленного методом перевала интеграла (5) от выражений (18) и (19) суперпозицией (14) можно трактовать как некоторую корректировку результатов приближенного расчета. Поэтому даже и в этом случае суперпозиция (14) представляется физически разумным приближением.

Наконец, отметим, что наличие чисто упругого рассеяния учитывается в рамках настоящей модели добавлением в сумме (14) члена с $A = \infty$.

ПРИЛОЖЕНИЕ

Расчет параметров γ_{11}, γ_{12} и γ_{22} по газовой модели.

Согласно (2) и (4), учитывая, что [4]

$$L_0(v) = 1, \quad L_1(v) = \sqrt{\frac{2\pi}{3\pi - 8}}\left(v - \frac{2}{\sqrt{\pi}}\right),$$

$$L_2(v) = \sqrt{\frac{6\pi - 16}{9\pi - 28}}\left(v^2 - \frac{2\sqrt{\pi}}{3\pi - 8}\, v + \frac{1}{2}\,\frac{32 - 9\pi}{3\pi - 8}\right),$$

имеем

$$\gamma_{11} = \frac{8\sqrt{\pi}}{3\pi - 8}\,(\delta_{20} - \delta_{11}),$$

$$\gamma_{12} = \frac{8}{\sqrt{9\pi - 28}}\,(\delta_{30} - \delta_{21}) - \frac{16\sqrt{\pi}}{(3\pi - 8)\sqrt{9\pi - 28}}\,(\delta_{20} - \delta_{11}),$$

$$\gamma_{22} = \frac{6\pi - 16}{9\pi - 28} \cdot \frac{4}{\sqrt{\pi}}\,(\delta_{40} - \delta_{22}) - \frac{32}{9\pi - 28}\,(\delta_{30} - \delta_{21}) +$$

$$+ \frac{32\sqrt{\pi}}{(3\pi - 8)(9\pi - 28)}\,(\delta_{20} - \delta_{11}).$$

При этом, согласно (5) и (9)

$$\delta_{k\ell} = \delta_{\ell k} = \int_0^\infty v^{k+2} \ell^{-v^2}\, dv \int_0^\infty W_s(v, v') v'^{\ell}\, dv' =$$

$$= \frac{AB}{2} \int_{-\infty}^{\infty} \frac{dt}{t(t - i)} \int_0^\infty dv \int_0^\infty dv' v^{k+1} v'^{\ell+1} \ell^{-v^2} \ell^{it(v'^2 - v^2)} \cdot$$

$$\cdot \{\exp[-t(t - i)(v - v')^2/A] - \exp[-t(t - i)(v + v')^2/A]\}.$$

Заменяя переменные $v' = vx$, изменяя порядок интегрирования и интегрируя по v, получим*

$$\delta_{k\ell} = \frac{AB}{4}\,\Gamma(v)\int_{-\infty}^{\infty}\frac{dt}{t(t-1)}\,I_{\ell v}(t),$$

$$I_{\ell,\,v}(t) = \int_0^{\infty} dx\, x^{\ell+1}\left[R^{-v}(t,x) - R^{-v}(t,-x)\right],$$

$$R(t,x) = 1 - it\,(x^2-1) + t(t-i)\,(1-x)^2/A,$$

$$v = 2 + (k+\ell)/2$$

В интересующих нас случаях интегралы $I_{\ell,v}(t)$ имеют вид:

$$I_{0,3} = \frac{3\pi}{8}\cdot\frac{\sqrt{A}}{\sqrt{t(t-i)}}\cdot\frac{1+\dfrac{A}{1+it}}{(A+1)^{5/2}},$$

$$I_{0,3\frac{1}{2}} = \frac{16}{15}\,\frac{\sqrt{A}}{\sqrt{t(t-i)}}\cdot\frac{\left(1+\dfrac{A}{1+it}\right)^{3/2}}{(A+1)^3},$$

$$I_{0,4} = \frac{5\pi}{16}\cdot\frac{\sqrt{A}}{\sqrt{t(t-i)}}\cdot\frac{\left(1+\dfrac{A}{1+it}\right)^{2}}{(A+1)^{7/2}},$$

$$I_{1,3} = \frac{3}{4(A+1)^2}\left\{\frac{1+\dfrac{1}{3}\cdot\dfrac{A(A+1)}{t(t-i)}}{\sqrt{\dfrac{A+1}{A}\,t(t-i)}}\ \operatorname{arctg}\frac{\sqrt{t(t-i)}}{\sqrt{A(A+1)}} + \frac{A}{t(t-i)}\right\},$$

$$I_{1,3\frac{1}{2}} = \frac{16}{15(A+1)^3}\cdot\frac{1}{\sqrt{1+it+\dfrac{t(t-i)}{A}}}\left[1+\frac{3}{4}\,\frac{A(A+1)}{t(t-i)}\right],$$

$$I_{2,4} = \frac{5\pi}{16}\left[1+\frac{3}{5}\,\frac{A(A+1)}{t(t-i)}\right]\frac{\sqrt{A}}{(A+1)^{3\frac{1}{2}}}\cdot\frac{1}{\sqrt{t(t-i)}}.$$

Последующее интегрирование по t приводит к выражениям (10).

---

* При этом необходимо, чтобы $R\,|\,R(t,x) > 0$, что выполняется при условии $0 < \mathrm{Im}\,t < 1$, т.е. при интегрировании по t особенности, лежащие на действительной оси, следует обходить сверху.

ЛИТЕРАТУРА

[1] WILKINS, J.E.Jr.CP-2431 (1944). E.R.Cohen. Nucl. Sci. Eng. 2 (1957) 227, HURWITZ, H. Jr. NELKIN, M.S.HABETLER, G.J. Nucl. Sci. Eng. 11 (1956) 180.
[2] WIGNER, E.P. WILKINS, J.E. Jr. AECD 2275 (1944) CORNCOLD, N. MICHAEL, P. WOLLMAN, W. Proc. BNL Conf. Neutron Thermalization IV, (1962) 1103.
[3] KOPPEL, J.U. Proc. BNL. Conf. Neutron Thermalization IV, (1962) 1103.
[4] КАЗАРНОВСКИЙ, М.В. ШАПИРО,Ф.Л. Нейтронная физика (сборник статей) Госатомиздат, Москва (1961),стр. 169.
[5] KAZARNOVSKY, M.V. Time-Dependent Problems in Neutron Transport, Lectures at the International Advanced Summer School on Reactor Physics, Poland.
[6] VAN HOVE, L. Phys. Rev. 95 (1954) 249.
[7] SCHOFIELD, P. Phys. Rev. Lett. 4 (1960) 239.
[8] PUROHIT, S.N. Nucl. Sci. Eng. 13 (1962) 250.

DISCUSSION

(on the foregoing three papers)

N. CORNGOLD: Are we to regard Dr. Stepanov's theory as expressing the successive collisions of a typical neutron, and does the averaging process then give us the usual density function for neutrons?

M. KAZARNOVSKY: Neutron propagation in this theory is described by the Green's function G_0 and not by the flight of the neutron between *collisions*.

P. ZWEIFEL (Chairman): In "ordinary" quantum field theory the solid line shown in paper SM-62/110 could represent the propagation of a neutron, and the dotted line its interaction with a potential. Is some such physical interpretation involved here?

M. KAZARNOVSKY: The solid line represents neutron propagation in the absence of fluctuations and the dotted line represents the effective "potential" created by the fluctuations. In this case, however, the problem is simpler since it is not necessary to use a secondary-quantization formalism.

P. SCHOFIELD: Dr. Stepanov's method seems to be very similar to that used by S. F. Edwards some years ago to discuss the nature of electronic energy levels in liquid metals. The random fluctuations in this latter method were those of the positions of the ions in the liquid.

M. KAZARNOVSKY: Yes, the method is similar to the techniques used for studying the passage of electrons through metals and the propagation of electro-magnetic waves.

NEUTRON THERMALIZATION AND SPECTRA

(Session III)

CALCULATION OF THERMAL SCATTERING KERNELS *

J. A. YOUNG AND J. U. KOPPEL
GENERAL ATOMIC DIVISION OF GENERAL DYNAMICS CORPORATION,
JOHN JAY HOPKINS LABORATORY FOR PURE AND APPLIED SCIENCE,
SAN DIEGO, CALIF., UNITED STATES OF AMERICA

Abstract — Résumé — Аннотация — Resumen

CALCULATION OF THERMAL SCATTERING KERNELS. A long-standing programme at General Atomic has been the development of physical models to describe the scattering of slow neutrons from the various moderators and the numerical methods necessary for the computation of thermal neutron cross-sections and scattering kernels. This paper contains a review of the recent developments and improvements in the scattering descriptions and subsequent kernels for the moderators Be, C, H_2O, D_2O, CH_2, H_2 and D_2. In particular for the moderators Be and C accurate phonon spectra, obtained by the root sampling technique, are presented along with comparisons to demonstrate how well the scattering models can predict the results of cross-section and spectral measurements. While the treatment of H_2O is essentially that of Nelkin, curves of calculated and experimental neutron spectra are shown, which demonstrate that the inclusion of anisotropic effects for the molecular vibrations improve the agreement between theory and experiment. Following Butler's description of neutron scattering by D_2O, a scattering kernel has been obtained which predicts quite accurately integral quantities such as neutron spectra and angular as well as total scattering cross-sections. An interesting result of the curves shown is that the inter- and intramolecular interference effects tend to cancel so that an incoherent approximation is quite adequate to calculate neutron spectra in D_2O for the case of infinite media or weakly space-dependent problems. By utilizing the treatment by Lin and Koenig of the vibrational modes of infinite CH_2 chains, a scattering kernel has been obtained which results in very good agreement between the predicted and experimental total cross-section and neutron spectra. Curves are presented to demonstrate this agreement between theory and experiment. Neutron spectra have been calculated for liquid hydrogen at boiling using a very accurate scattering description. These spectra are shown in the paper to be very sensitive both to geometry and the scattering model.

CALCUL DE NOYAUX DE DIFFUSION POUR LES NEUTRONS THERMIQUES. La General Atomic exécute depuis longtemps un programme de mise au point de modèles physiques pour décrire la diffusion de neutrons lents par divers ralentisseurs, ainsi que de méthodes numériques pour le calcul de sections efficaces et de noyaux de diffusion pour les neutrons thermiques. Les auteurs présentent une étude critique des améliorations apportées récemment aux descriptions de la diffusion et aux noyaux en découlant pour les ralentisseurs Be, C, H_2O, D_2O, CH_2, H_2 et D_2. Notamment, en ce qui concerne les ralentisseurs Be et C, ils présentent des spectres exacts de phonons, obtenus par une méthode d'échantillonnage appropriée, et font des comparaisons qui montrent que les modèles de diffusion permettent de prévoir correctement les résultats des mesures de sections efficaces et de spectres. Dans le cas de l'eau, on applique essentiellement le modèle de Nelkin, mais des courbes théoriques et expérimentales de spectres de neutrons montrent que l'inclusion des effets anisotropes pour les vibrations moléculaires améliore la concordance entre les résultats théoriques et les résultats expérimentaux. Sur la base de la description de la diffusion des neutrons par D_2O faite par Butler, on a obtenu un noyau de diffusion qui permet de prévoir assez exactement des quantités intégrales telles que les spectres de neutrons et les sections efficaces de diffusion angulaires aussi bien que totales. Un résultat intéressant des courbes présentées est que les effets des interférences intermoléculaires et intramoléculaires tendent à s'annuler, de sorte qu'une approximation incohérente est tout à fait suffisante pour calculer les spectres des neutrons dans D_2O lorsqu'on considère un milieu infini ou qu'il s'agit de fonctions peu variables dans l'espace. En traitant les modes vibrationnels des chaînes CH_2 infinies comme l'ont fait Lin et Koenig, on a obtenu un noyau de diffusion qui permet d'obtenir un bon accord entre les valeurs théoriques et expérimentales des sections efficaces totales et des spectres de neutrons. Les auteurs présentent des courbes qui montrent cette concordance

* Work supported by the United States Atomic Energy Commission under contract AT(04-3)-167.

entre la théorie et l'expérience. Ils ont calculé des spectres de neutrons pour l'hydrogène liquide au point d'ébullition, en utilisant une description très exacte de la diffusion. Les auteurs montrent que ces spectres sont très sensibles, à la fois, à la géométrie et au modèle de diffusion.

РАСЧЕТ ЯДЕР РАССЕИВАНИЯ ДЛЯ ТЕПЛОВЫХ НЕЙТРОНОВ. В долгосрочную программу отдела "Дженерал атомик" входила разработка физических моделей с целью описания рассеяния медленных нейтронов из различных замедлителей, а также числовых методов, необходимых для вычисления поперечных сечений тепловых нейтронов и ядер рассеивания. Дается обзор последних достижений и усовершенствований в области описаний рассеяния и ядер рассеяния для замедлителей Be, C, H_2O, D_2O, CH_2, H_2 и D_2. В особенности для замедлителей Be и C точные фононовые спектры, полученные посредством метода подбора корней, даются в сравнениях для того, чтобы показать, насколько хорошо рассеивающие модели могут предсказать результаты измерений поперечного сечения и спектра. В связи с тем, что обработка H_2O является более существенной, чем обработка Нелкина, показываются высчитанные кривые и спектр экспериментальных нейтронов, которые демонстрируют, что включение анизотропных эффектов для молекулярных вибраций улучшает совпадение между теорией и экспериментом. Придерживаясь описания Батлера по рассеянию нейтронов с помощью D_2O, были получены ядра рассеивания, которые точно предсказали целые количества, такие как нейтронный спектр и угол, а также общее количество поперечных сечений рассеивания. Одним из интересных результатов кривых является то, что эффекты меж- и интрамолекулярного проникновения имеют тенденцию к аннулированию так, что несвязная аппроксимация вполне достаточна для вычисления нейтронного спектра в D_2O для случая определенной среды или для проблем слабой космической зависимости. Используя обработку вибрационных моделей определенных цепочек CH_2 методом Лина и Кенига, было получено ядро рассеивания, которое очень хорошо согласуется с предсказанным и опытным общим поперечным сечением и нейтронным спектром. Даются кривые для того, чтобы продемонстрировать это совпадение между теорией и экспериментом. Нейтронный спектр рассчитывали для жидкого водорода при кипении, используя при этом очень точное описание рассеяния. Приводимые спектры являются очень чувствительными как к геометрии, так и к модели рассеяния.

CALCULO DE NUCLEOS DE DISPERSION TERMICOS. La General Atomic viene ejecutando desde hace bastante tiempo un programa relativo a la elaboración de modelos físicos que describen la dispersión de neutrones lentos en los diferentes moderadores, y de los procedimientos numéricos necesarios para el cómputo de las secciones eficaces neutrónicas y de los núcleos de dispersión térmicos. En la memoria se examinan los recientes adelantos y perfeccionamientos registrados en la descripción de la dispersión y en los núcleos resultantes aplicables a los moderadores Be, C, H_2O, CH_2, H_2 y D_2. En particular, en el caso del Be y del C se presentan espectros fonónicos exactos obtenidos por el método de muestreo cuadrático, así como comparaciones tendientes a demostrar la precisión con que los modelos de dispersión permiten predecir los resultados de las mediciones de secciones eficaces y de espectros. Si bien el análisis del H_2O sigue en esencia las teorías de Nelkin, se presentan curvas de espectros neutrónicos, calculados y obtenidos experimentalmente, que demuestran que la inclusión de los efectos anisotrópicos en las vibraciones moleculares mejora la concordancia entre los resultados teóricos y los experimentales. Con arreglo a la descripción de Butler para la dispersión de neutrones en D_2O, se ha obtenido un núcleo de dispersión que permite predecir con considerable exactitud cantidades integrales tales como los espectros neutrónicos y las seccions efficaces de dispersión angulares y totales. Un resultado interesante de las curvas que se presentan es que los efectos de interferencia inter e intramolecular tienden a anularse, por lo que una aproximación incoherente vale para calcular los espectros neutrónicos en D_2O, en el caso de medios infinitos o de variaciones ligeramente dependientes del espacio. Aplicando el método de Lin y Koenig para el análisis de los modos de vibración de cadenas infinitas de CH_2, se ha obtenido un núcleo de dispersión gracias al cual la concordancia entre los valores calculados y experimentales de las secciones eficaces totales y de los espectros neutrónicos es muy satisfactoria. Se presentan curvas que ponen de manifiesto esta concordancia entre los resultados teóricos y experimentales. Se han calculado los espectros neutrónicos del hidrógeno líquido en ebullición aplicando una representación muy precisa de la dispersión. Se demuestra que estos espectros son muy sensibles a la geometría y al modelo de dispersión.

1. INTRODUCTION

One of the more important physical quantities that occurs in the study of thermal reactors is the cross-section for the transfer of neutrons from one energy group to another when interacting with chemically bound moderators. This paper surveys the work performed by the authors for the purpose of obtaining scattering kernels (energy transfer cross-sections) that will accurately predict parameters that are of practical importance to the reactor designer. The principal approach toward obtaining models for the scattering of neutrons has been to utilize as far as possible all the physical information known about the scatterer. With the notable exception of beryllium, the direct coupling of the theory with neutron experiments has been rather weak, although for all moderators comparisons have been made with measurements of such integral quantities as neutron energy spectra, total cross-sections, etc. The double differential neutron measurements from polycrystalline solids, molecular liquids, and gases have, in our opinion, not always been of sufficient quality to satisfy theoretical needs. These measurements have had a practical application, however, usually through the extrapolation technique [1], which has been exploited mainly by the workers at Harwell.

To compute the scattering cross-section for neutrons interacting with a molecular system it is necessary to have some knowledge of the molecular dynamics. The type of physical knowledge one must have depends on whether the scatterer is a solid or a molecular liquid. Of course even when a very detailed description of the molecular dynamics exists, it is still necessary to make some assumptions and approximations in order to make calculations tractable. Perhaps the most universal approximation is the incoherent approximation, which neglects the effects of interference in the scattering. For a solid this approximation is often very useful, not only because of its success in predicting neutron spectra, but also because of the fact that, for a monatomic solid moderator that is sufficiently isotropic, the cross-section depends on the lattice dynamics only through the phonon spectrum. Molecular moderators in the liquid state, such as water, heavy water, etc., require a special treatment including the details of the molecular dynamics, yet the incoherent approximation has proved reasonably successful in these cases as well. This approximation also dominates the work of the present authors. In the following sections we discuss the moderators: beryllium, graphite, light and heavy water, polyethylene, zirconium hydride, and hydrogen. In section 2.1, a calculation is described of the one-phonon coherent cross-section of beryllium using a lattice dynamical model rather than the Debye approximation. This latter calculation casts strong doubt on the validity of the extrapolation technique for such coherent scatterers as beryllium and graphite.

The work of other authors is not discussed in this paper because of space limitations. This same constraint requires us to mention only briefly work that has been published for some time and also to omit work that is in progress and hence incomplete.

2. BERYLLIUM

The moderator beryllium is important because of its light weight and its low absorption cross-section for thermal neutrons. Although beryllium is an almost pure coherent scatterer, the incoherent approximation might be expected to predict adequately neutron spectra and other quantities of interest to the reactor physicist. However, the next section will show how poor this approximation is for predicting the double differential cross-sections. Neglecting interference, the scattering cross-section from a monatomic crystal at temperature T can be written as

$$\frac{d^2\sigma}{d\epsilon d\Omega} = a^2 \sqrt{\frac{E}{E_0}} \frac{1}{2\pi} \int_{-\infty}^{\infty} dt\, e^{i\epsilon t} \exp\left[\frac{\hbar\kappa^2}{2M} \int_{-\infty}^{\infty} \frac{f(\omega)e^{-\omega/2T}}{2\omega \sinh(\omega/2T)} (e^{i\omega t} - 1)\, d\omega\right], \tag{1}$$

where

ϵ = the energy transfer to the neutron,
κ^2 = the square of the momentum transfer,
a = the bound nuclear scattering length,
E_0, E = the initial and final neutron energies, respectively,
M = the atomic mass, and
$f(\omega)$ = the frequency spectrum.

While Eq. (1) is true only for an isotropic substance with one particle per unit cell, it is an excellent approximation for beryllium and much less severe than the incoherent approximation itself. By using the central force model of SCHMUNK et al. [2], the frequency spectrum of beryllium has been computed [3] by sampling the frequencies for 10 261 values of the wave vector in an irreducible segment of the first Brillouin zone. The phonon spectrum is shown in Fig. 1, and a comparison of the calculated and measured total cross-section is shown in Fig. 2, using the elastic scattering cross-section computed by means of the computer code HEXSCAT [4] and the inelastic scattering computed by means of the machine program GASKET [5]. Also shown in Fig. 1 is the phonon spectrum obtained by SINCLAIR [6] using the extrapolation technique. The neutron spectrum in beryllium with a poisoning of 0.4 barns per Be atom has been measured by NEILL [7]. Figure 3 compares the calculated and measured spectra for this finite beryllium assembly and shows that the scattering kernel described above is adequate for the prediction of neutron energy spectra in beryllium.

2.1. Coherent inelastic scattering from polycrystalline beryllium

Neutron scattering from polycrystalline solids has been the subject of intense interest to experimentalists in recent years. Part of this interest has been stimulated by the extrapolation technique [1], which is used to find the frequency spectrum of the solid from measurements of the double differential scattering cross-section. However, although lattice dynamical models have been known for various solids, the calculations of $d^2\sigma/d\epsilon\, d\Omega$ have all been in the incoherent approximation, i.e., with neglect of interference, even though results differ from experiment by large factors at low momentum transfer. Since interference effects are expected to dominate

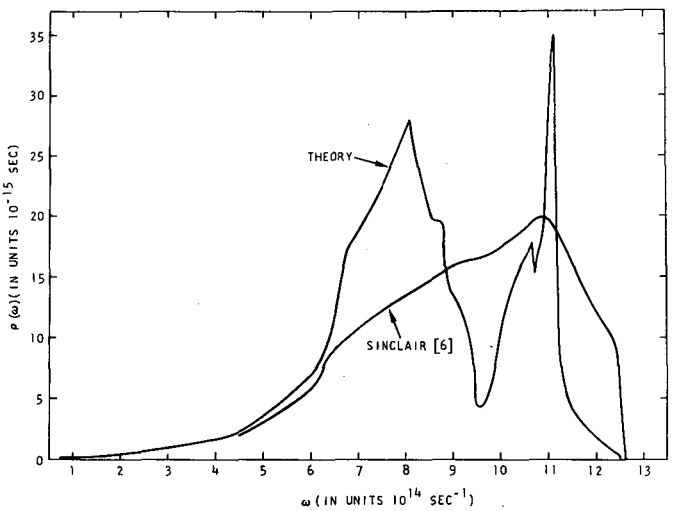

Fig. 1

Phonon spectrum of beryllium

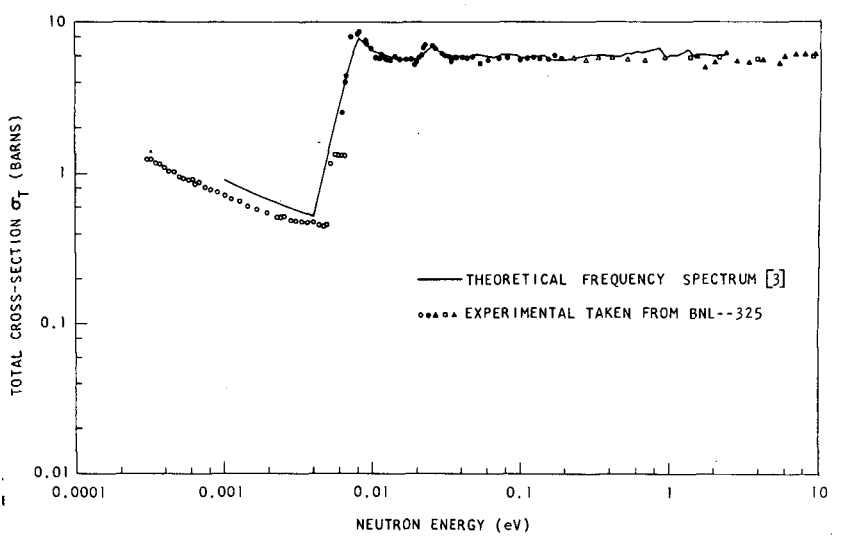

Fig. 2

Total cross-section of beryllium at room temperature

at just those momentum transfers where the extrapolation must be performed, it has been thought worthwhile to compute the one-phonon coherent double differential scattering cross-section from polycrystalline beryllium. In addition, such calculations are expected to indicate if the measurements on polycrystalline solids generally have the necessary precision for meaningful comparisons between theory and experiment.

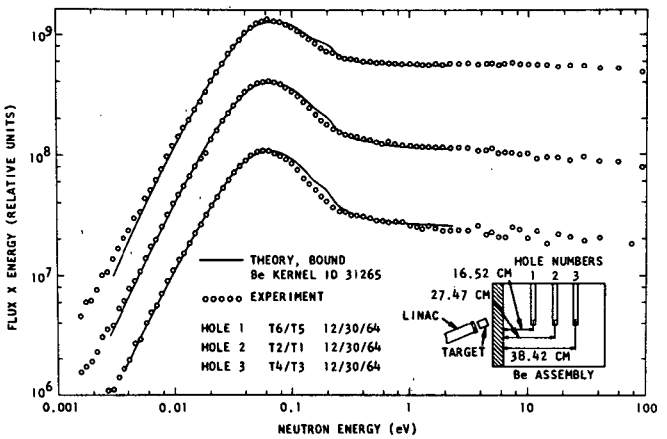

Fig. 3

The neutron spectra in a poisoned beryllium assembly

The one-phonon double differential neutron scattering cross-section from a monatomic polycrystalline solid at temperature T can be written in the following way:

$$\frac{d^2\sigma}{d\epsilon\, d\Omega} = \frac{a^2}{2M}\sqrt{\frac{E}{E_0}}\frac{1}{4\pi}\sum_j \int_{4\pi} d\mu\, d\phi \left| \sum_k e^{-W^k} e^{i\vec{\kappa}\cdot\vec{r}^k}\, \vec{\kappa}\cdot\vec{C}(k|_j^{\vec{\kappa}/2\pi}) \right|^2 \times$$

$$\times \frac{1}{1-e^{-\eta\epsilon/kT}} \frac{1}{\eta\epsilon}\, \delta\,[\epsilon - \hbar\eta\omega_j(\vec{\kappa}/2\pi)] \,. \qquad (2)$$

In this equation μ and ϕ define the polar angles of $\vec{\kappa}$, $\vec{r}^k$ is the position vector of the k-th particle of the elementary cell of the crystal, and W^k is the Debye-Waller factor for atom k. The quantity η is +1 (−1) for phonon emission (absorption) by the neutron.

In order to evaluate Eq. (2), it is necessary to have a dynamical model of the lattice vibrations. In our calculations for beryllium, we have used the central force model of SCHMUNK et al. [2] obtained from single crystal neutron measurements. The phonon energies and polarization vectors $\vec{C}(k|_j^{\vec{q}})$ are determined by the equations

$$\omega_j^2(\vec{q})\, C_\alpha(k|_j^{\vec{q}}) = \sum_{\beta,\, k'} D_{\alpha\beta}(_{kk'}^{\vec{q}})\, C_\beta(k'|_j^{\vec{q}}) \,, \qquad (3)$$

where $D_{\alpha\beta}(_{kk'}^{\vec{q}})$ is the dynamical matrix. From Eq. (2), it is seen that the cross-section $d^2\sigma/d\epsilon\, d\Omega$ is non-vanishing only if the sphere (in $\vec{\kappa}$ space) with

radius $|\vec{\kappa}|$ intersects the constant frequency surfaces $\omega(\vec{\kappa}/2\pi) = |\epsilon|/\hbar$, at least in one cell in reciprocal space. Clearly, for small energy transfer $|\epsilon|$ these constant frequency surfaces correspond to acoustical phonons and are approximate spheres at the centre of each cell. Since these centres are separated by reciprocal lattice vectors, it is seen that for small $|\epsilon|$ the cross-section must vanish unless $|\vec{\kappa}| \cong 2\pi|\vec{\tau}|$, where $|\vec{\tau}|$ is a reciprocal lattice vector. Thus the cross-section shows a series of peaks which become broader with increasing $|\epsilon|$, although centred at about the same $|\vec{\kappa}|$ for all $|\epsilon|$. A similar situation arises for $|\epsilon|$ of the order of the largest frequency of the crystal, since beryllium has at least one optical branch with its maximum at the centre of the zone.

The calculation of Eq. (2) is carried out by performing the integral over μ numerically along the intersections between the constant $|\vec{\kappa}|$ sphere and the constant $\omega_j = |\epsilon|/\hbar$ surfaces. Equation (2) has been programmed for computation on the IBM 7044. The accuracy of the calculation is limited only by the force model, which is expected to be quite good. Because of the relative expense of computation we have compared our results with the experiment of SCHMUNK [8] for beryllium powder at an energy transfer of 0.015 eV only. This low energy transfer is the most difficult of the experimental curves to compute since the peaks are narrowest. On the other hand, this case provides a severe test of our calculations. Since the data show a very large spread, the experimental points have been averaged by SCHMUNK [8]. These average experimental points, the present calculations, and the incoherent approximation are compared in Fig. 4. The quantities α and β

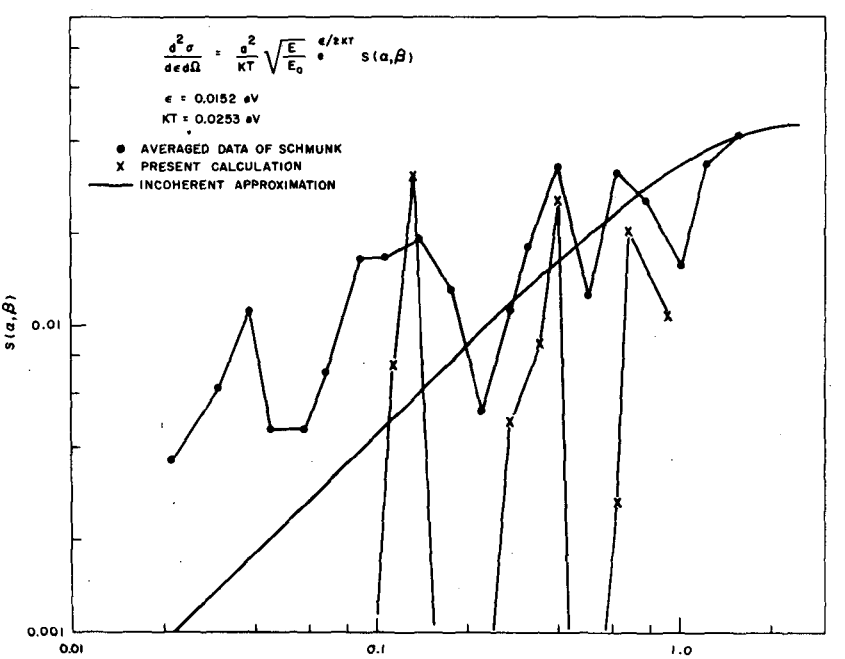

Fig. 4

The double differential scattering cross-section of beryllium at room temperature

are the dimensionless momentum and energy transfer, respectively. The experimental data have been corrected for multiple scattering only crudely, and this is most likely the reason that the valleys in the experimental curve are filled in. Thus the comparison between theory and experiment is not on a completely par basis, yet the agreement shown in Fig. 4 is fair considering the difficulties and inaccuracies of the experiment as evidenced by the spread in the unaveraged data points. The experimental peak showing at roughly $\alpha = 0.04$ seems to be spurious. This peak should correspond to the (0, 0, 1) plane at $\alpha = 0.028$, yet it does not appear experimentally at higher β values, and our calculations show the cross-section to be very small in this region owing to the structure factor. It seems clear that double differential scattering measurements from polycrystals as opposed to single crystals do not yet have the required precision to permit meaningful comparisons between theory and experiment.

It is well to remark here that the momentum transfers considered above have been too large to be in the first Brillouin zone, and the conclusions have been essentially independent of the shape of the constant frequency contours. However, for momentum transfers in the first Brillouin zone (small α), the neutron scattering depends very strongly on the shape of the constant frequency surfaces, and the curves of $S(\alpha, \beta)$ versus α at constant β become a series of peaks, one for each branch, ω_j, at all energy transfers. These peaks tend toward delta functions in the limit of a Debye crystal or as $|\vec{\kappa}| \to 0$ (for an isotropic crystal).

Figure 4 clearly shows that interference effects are so pronounced that an extrapolation to zero momentum transfer in order to obtain the phonon spectrum is just not possible. The incoherent approximation deviates from a straight line long before coherent effects die out, making the extrapolation technique meaningless. Since beryllium is relatively isotropic, and thus should provide a good example for this technique, one can only conclude that the extrapolation technique will give worse results for polyatomic moderators such as beryllium oxide.

3. GRAPHITE

For graphite, as for other monatomic crystalline moderators, the neutron scattering cross-section in the incoherent approximation is given adequately by the frequency spectrum of the lattice vibrations. However, graphite, like beryllium, is a coherent scatterer, and as a consequence the double differential scattering cross-section for small energy and momentum transfers will be very poorly described by this approximation. Since, however, the neutron spectrum is not sensitive to the detailed nature of the lattice dynamics, it is expected that the incoherent approximation will predict spectra accurately. The phonon spectrum of Ceylon natural graphite, obtained by YOSHIMORI and KITANO [9] by a series of approximations from a Born-Huang force model, was adjusted by PARKS [10] to predict the measured specific heat of reactor-grade graphite. This adjusted phonon spectrum predicted neutron spectra in very good agreement with experiment under a wide variety of conditions [10].

A new calculation of the phonon spectrum of reactor-grade graphite has been performed. This calculation [11] is essentially exact, and its accuracy depends only on that of the force model. The force model of YOSHIMORI and KITANO [9] was used for a sampling of 47 788 values of the wave-vector in an irreducible segment of the first Brillouin zone. The resulting phonon spectrum is shown in Fig. 5. The force constants were chosen so that the calculated and measured specific heat agreed very precisely over the temperature range from 100 to 1000°K. This calculation can be compared profitably with the results obtained from the extrapolation technique. In Fig. 5 the phonon spectrum of POOLE et al. [12] is shown compared with

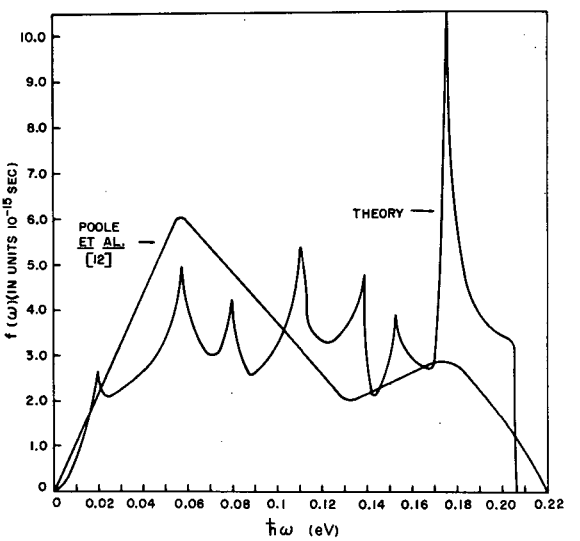

Fig. 5

Phonon spectrum of graphite

the calculated spectrum. Although the present authors feel that the results of the extrapolation technique will be poor for determining the quantitative features of the phonon spectrum, the results will perhaps suffice for the qualitative features. More recently, HAYWOOD and THORSON [13] have found structure in $f(\omega)$ at 0.02 eV and a cut-off at 0.075–0.080 eV that is associated with the cut-off in the TA planar distribution; both conclusions agree with the theory in Fig. 5. EGELSTAFF and HARRIS [14] find from a graphite scattering measurement at 1200°K that there is a definite peak at 0.08 eV and a broad unresolved peak centred at 0.175 eV; both observations agree with the theory shown in Fig. 5. It is clear that the peak at 0.175 eV is the dominant feature of the phonon spectrum and is the result of the very strong coupling between nearest neighbour atoms in the basal planes.

It has been shown in reference [15] that the most recent and more accurate phonon spectrum of graphite and the modified spectrum of YOSHIMORI and KITANO [10] give very nearly identical results in the calculation of neutron spectra and total cross-section. The total cross-section, again

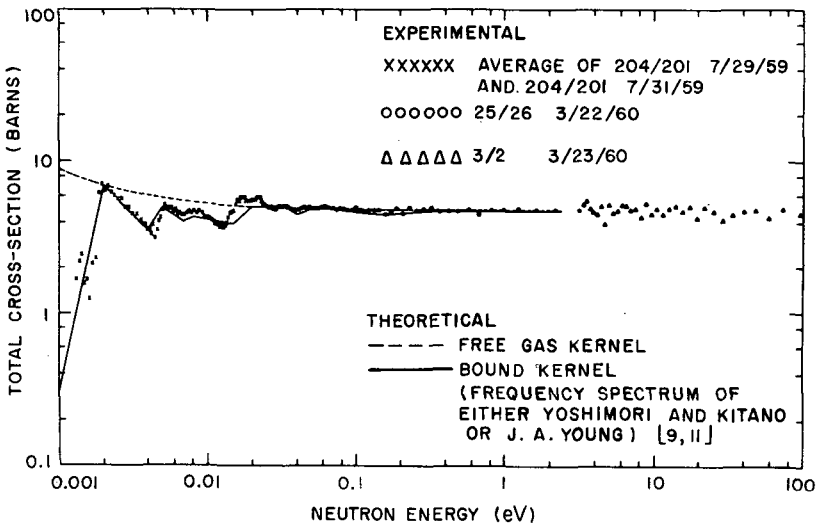

Fig. 6

Total cross-section of graphite at room temperature

computed using SUMMIT for the inelastic scattering and HEXSCAT for the elastic scattering, is shown in Fig. 6. A typical case is shown in Fig. 7, where the neutron spectrum in a poisoned infinite medium of graphite has been computed for the YOSHIMORI and KITANO [9], POOLE et al. [12], and YOUNG and KOPPEL [11] kernels at 300°K and compared with a measurement by NEILL and BARDES [16].

The coherent inelastic scattering cross-section is presently being computed and will be reported at a later date. The calculation is proceeding in the same manner as in the case of beryllium, but using the force model described in Ref. [11].

4. LIGHT WATER

The NELKIN model [17] for the dynamics of the H_2O molecule has proved quite successful in predicting neutron spectra in infinite media of aqueous solutions; however, experiment did show a discrepancy of about 10% for heavily 1/v and resonance poisoned solutions. Part of this discrepancy has been removed by eliminating the assumption of spatial isotropy of the molecular vibrations [18]. In this calculation the two protons are bound harmonically to an infinitely heavy oxygen atom. The restoring forces produced when the protons move away from their equilibrium positions are (1) a force in the direction of the O-H bond proportional to the change in bond length, and (2) a force normal to the O-H bond and proportional to the change in bond angle. Aside from the above internal motions, the rotations of the H_2O molecule about its principal axis of inertia are taken to be completely hindered by a harmonic torsional potential. This model yields

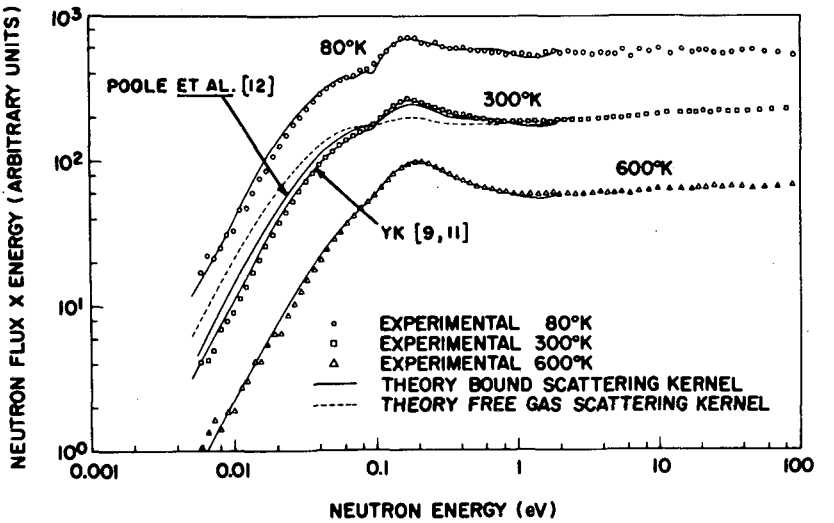

Fig. 7

Neutron spectra in graphite

six normal vibrational modes. In the rotational modes the H atoms move perpendicular to the O-H bond. With these considerations it is possible to write down the potential energy and thus to find the eigenvalues and eigenvectors of the normal modes. This model has been programmed for evaluation using a modification of the machine code GAKER [19] to compute the scattering kernel. The P_0 and P_1 kernels show important deviations from

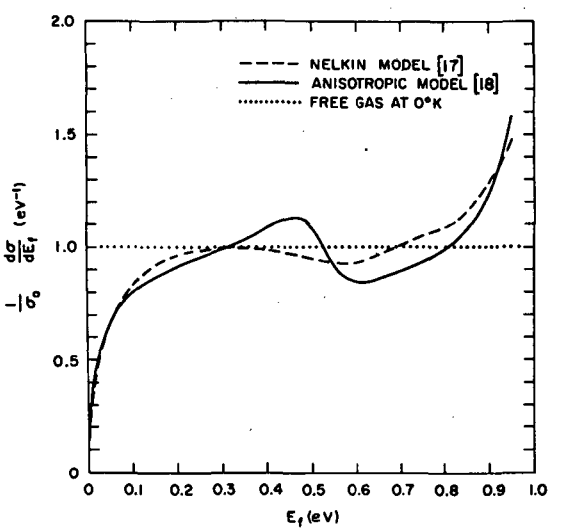

Fig. 8

P_0 scattering kernel corresponding to the isotropic (Nelkin) and anisotropic model
The free gas kernel for T = 0°K is also shown for comparison

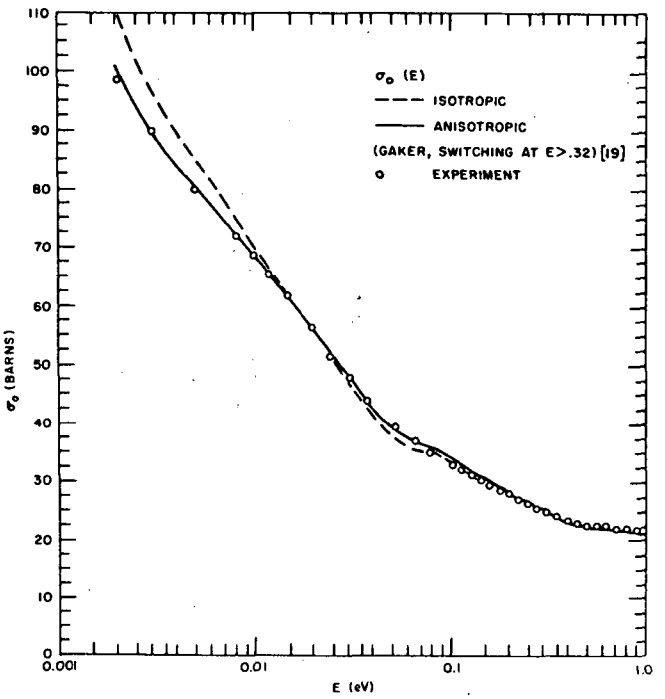

Fig. 9

Total scattering cross-section of H_2O

the isotropic model. Figure 8 shows the comparison for the P_0 kernel. The isotropic and anisotropic models are compared in Fig. 9 for the calculation of the total cross-section, and in Fig. 10 for the calculation of the neutron spectrum in a typical case of a solution poisoned with a low energy resonance absorber. The anisotropic model predicts a harder spectrum and thus comes closer to experiment, although there is still some residual discrepancy. More spectral comparisons are made in another paper at this Symposium [20].

5. HEAVY WATER

An incoherent scattering model for D_2O has been given by HONECK [21] by a simple adjustment of parameters in Nelkin's model for H_2O. Interference effects, which arise because of the large coherent scattering lengths of deuterium and oxygen, were considered by BUTLER [22], along with a more rigorous treatment of the molecular dynamics. The remaining question of how Butler's theory affects neutron spectra under various geometries and poison concentrations has been answered [23] by incorporating Butler's results in another modified version of the machine code GAKER. Calculations show that an unusual cancellation of intermolecular and intramolecular interference occurs so that, in all cases studied, the incoherent approximation will predict neutron spectra in very good agreement with experiment, and the

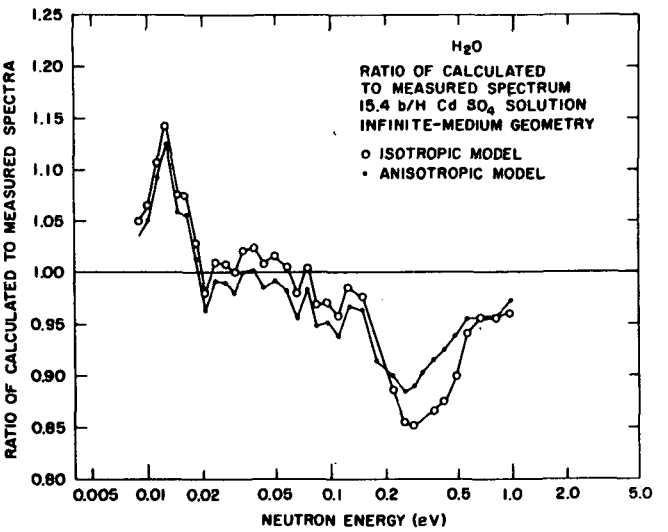

Fig. 10

Neutron spectra in water

effects of interference change things by at most about 3%. The angular cross-section $d\sigma/d\Omega$ did show the effects of interference, and in this case the theory agreed quite well with the experiment of SPRINGER [24] as demonstrated in Fig. 11. In addition, the calculated and measured total cross-sections agree very well, as shown in Fig. 12. Detailed comparisons with experimental neutron spectra are being reported by NEILL et al. in another paper at this Symposium [20].

6. POLYETHYLENE

The description of neutron scattering by polyethylene is considerably simplified due to its unusual crystal structure. The solid is made up of long, kinked chains of CH_2 radicals. The chains are coupled only weakly so that polyethylene does not act as a normal solid, and its phonon spectrum becomes Debye-like only at very low frequency. Assuming infinite, completely uncoupled chains, the dispersion relations of polyethylene consist of 9 different branches (2 acoustical and 7 optical), each one having the phase difference θ_i between corresponding elements of 2 neighbouring CH_2 radicals as the only parameter. This was shown by LIN and KOENIG [25], and using their results the frequency spectrum can be obtained from the simple formula

$$f(\omega) = c \sum_i \frac{d\,\theta_i(\omega)}{d\omega} ,$$

where c is a normalization constant. The calculated phonon spectrum [26] shown in Fig. 13, does not include the acoustical modes since they cannot be calculated correctly from the uncoupled chain model. A better approxi-

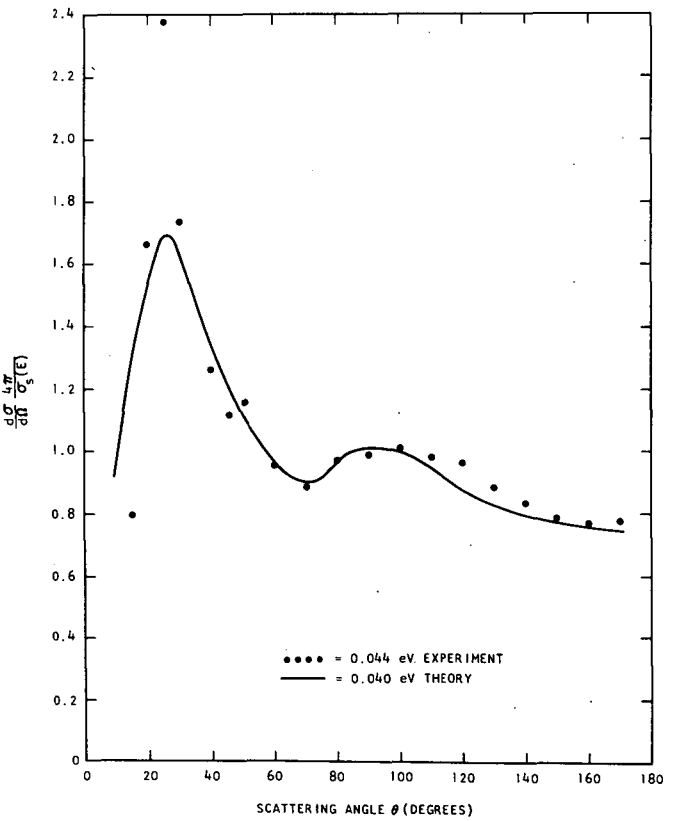

Fig. 11

The angular cross-section $d\sigma/d\Omega$ for D_2O at room temperature

mation for the acoustical modes is obtained from WUNDERLICH's work [27]. By means of the computer code SUMMIT [5] the scattering kernel can readily be obtained. Another method of approach is to use the code GAKER by breaking up the phonon spectrum into a small number of discrete modes. The acoustical modes are then treated in the short collision time approximation, with the effective temperature being that of room temperature. The results of the above procedure are quite satisfactory, as shown by comparison with the measured total cross-section [28] and measured neutron spectra [29] shown in Figs. 14 and 15, respectively. Figure 15 is for infinite-medium geometry of 1% borated polyethylene. Also shown in the figures are calculations using the kernel of GOLDMAN [28], who followed a similar procedure but used different frequencies and weights.

7. ZIRCONIUM HYDRIDE

Zirconium hydride has perhaps the simplest properties of all the moderators for neutron scattering. In ZrH_x the hydrogen atoms are situated at

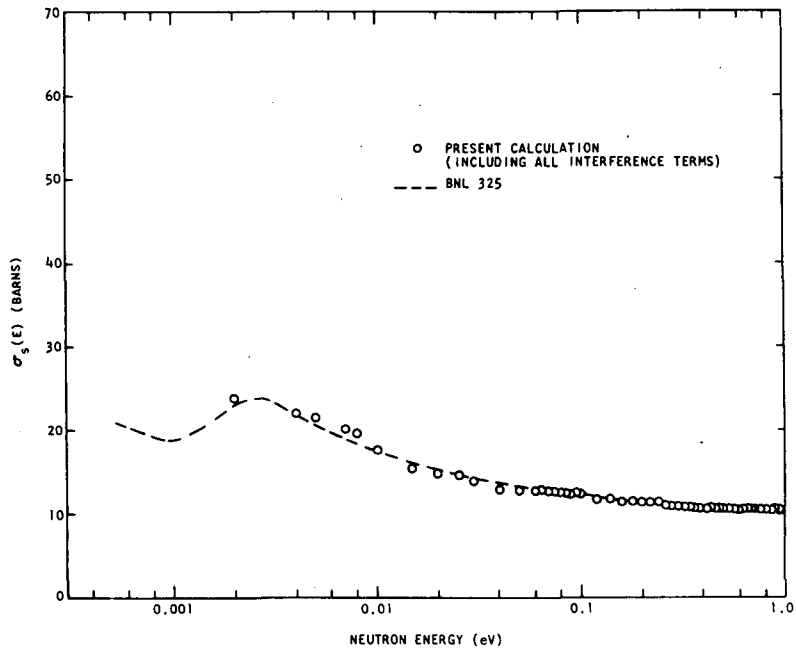

Fig. 12

Total cross-section of D_2O at room temperature

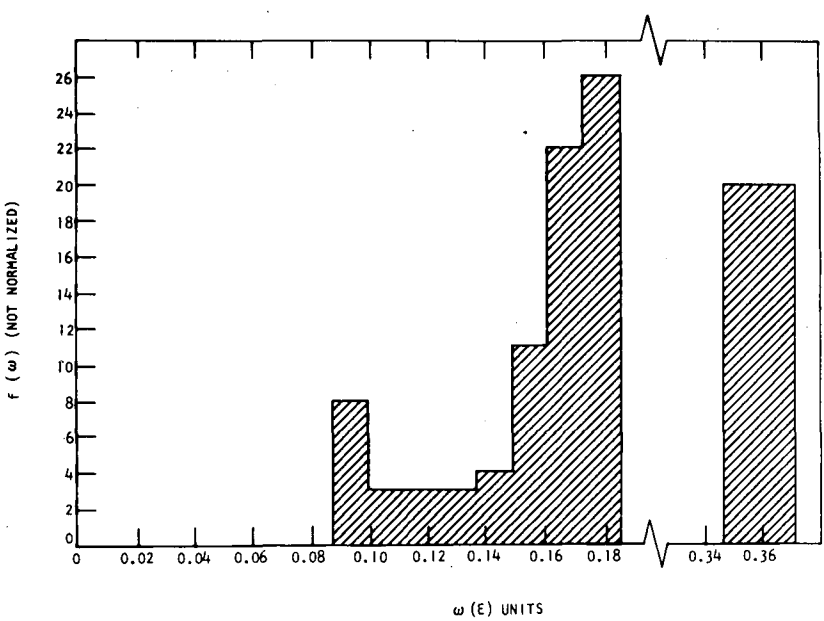

Fig. 13

Phonon spectrum of polyethylene

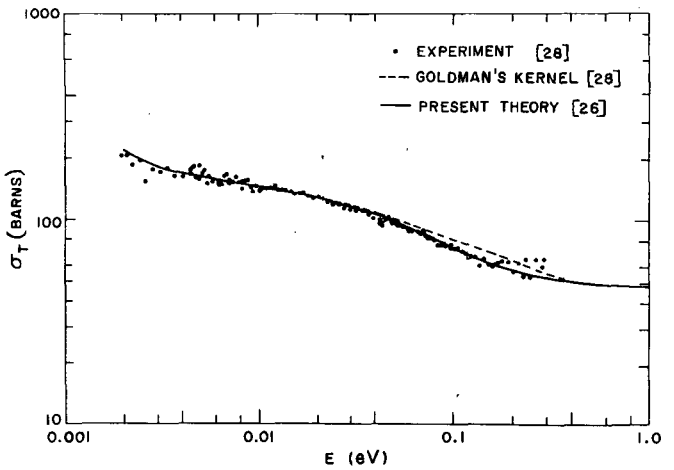

Fig. 14

Total cross-section of polyethylene at room temperature

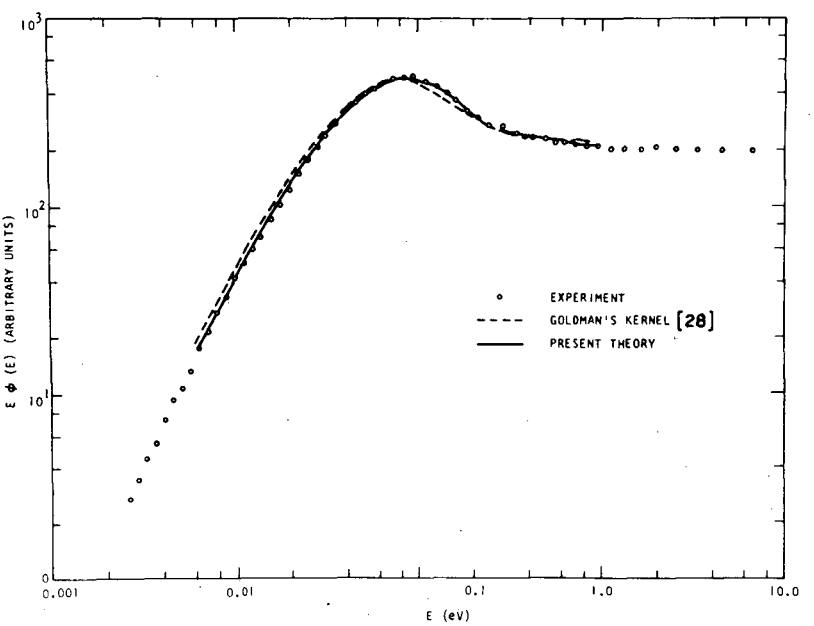

Fig. 15

Neutron spectrum in an infinite-medium geometry of 1% borated polyethylene

the centre of a tetrahedron formed by relatively massive zirconium atoms. Thus, as far as the hydrogen atoms are concerned, zirconium hydride behaves as an Einstein crystal, i. e. as an assembly of isotropic simple har-

monic oscillators. The distance between energy levels is 0.137 eV. The experiments of WOODS et al. [30] indicate that there is a natural width to the oscillator energy levels that is relatively independent of the moderator temperature. A reasonably accurate scattering kernel has been obtained [31] for zirconium hydride by considering the phonon spectrum to be the sum of two parts, one part being a Debye spectrum with a cut-off at 0.02 eV and the other a Gaussian distribution centred at 0.137 eV and having a natural width given by the data of WOODS et al. [30]. The relative weight attached to the acoustical modes is 1/360, and scattering by the zirconium atoms is not considered because of their relatively low cross-section. Figure 16 clearly demonstrates that the model described above predicts infinite-medium neutron spectra in very good agreement with experiment.

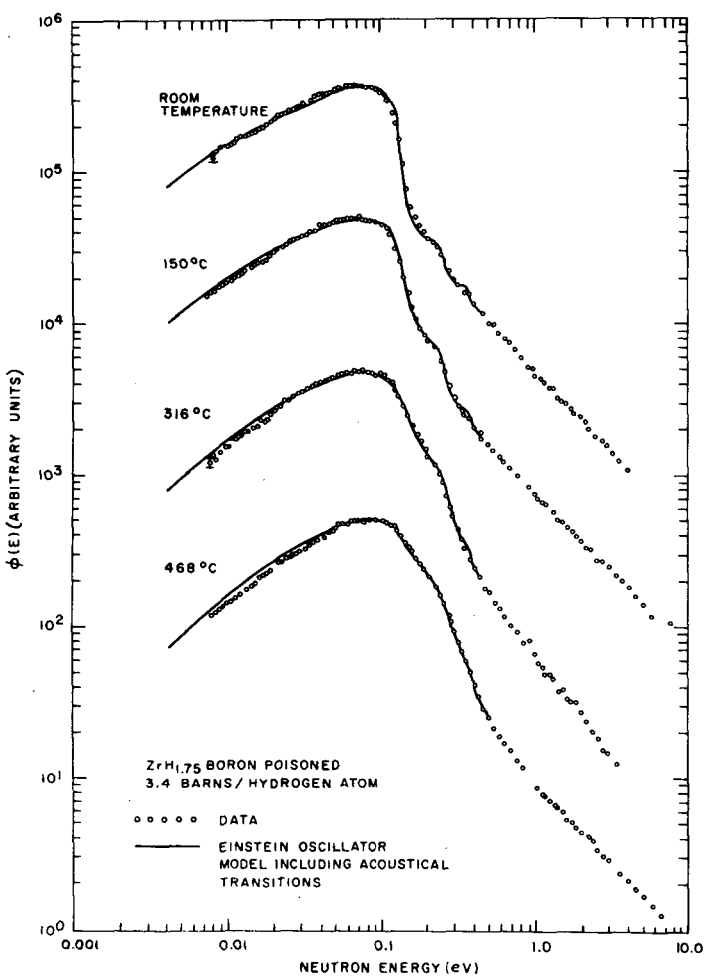

Fig. 16

Neutron spectra in poisoned zirconium hydride

8. MOLECULAR HYDROGEN

In working toward an understanding of neutron interactions in cold moderators, it has been considered worthwhile to compute the scattering cross-sections, and hence neutron spectra, in molecular hydrogen. Slow neutron scattering from hydrogen is quite different from that of other molecular moderators. While the hydrogen molecule is quite simple, it has very unusual properties, owing to the strong spin correlation between the two protons. In addition, the molecule has a small moment of inertia causing the rotational levels to be widely separated, and the incoherent scattering cross-section of the proton is about 40 times the coherent cross-section. Because of these properties, most of the approximations usually made in neutron scattering fail for the H_2 molecule. On the other hand, intermolecular interference scattering is essentially absent, owing to the small coherent cross-section. Also, because of the relatively small Debye temperature of liquid hydrogen, intermolecular correlations should not affect scattering except at very low neutron energies.

The calculation of the neutron scattering cross-section by the H_2 molecule has been done essentially exactly [32]. The only approximation is the assumption of harmonic H-H bond stretching forces and neglect of rotation-vibration coupling. For liquid hydrogen the approximations also include free translations and rotations of the molecules. Previous calculations have either neglected the vibrational and higher rotational transitions [33] or have performed the thermal average in the total cross-section only, in addition to neglecting the vibrations. An interesting result of the calculation is that the spin-conserving transitions for para-hydrogen are proportional to the coherent cross-section, while the spin-nonconserving transitions are proportional to the incoherent cross-section of a single hydrogen atom. This means that for para-hydrogen the scattering cross-section is very low unless the neutron has sufficient energy to cause a transition from para- to ortho-hydrogen. In the laboratory this energy is 0.022 eV.

The double differential cross-sections for para- and ortho-hydrogen at temperature T are given by [32]

$$\left(\frac{d^2\sigma}{d\Omega d\epsilon}\right)_{para} = \frac{k}{k_0}\left(\frac{M}{\pi\kappa^2 T}\right)^{\frac{1}{2}} \sum_n \frac{1}{n!}\left(\frac{\kappa^2}{4M\omega}\right)^n \sum_{J=0,2,4\ldots} P_J \left[a_c^2 \sum_{J'=0,2,4\ldots} + a_i^2 \sum_{J'=1,3,5\ldots}\right] (2J'+1) \exp\left\{-\frac{[\epsilon + \Delta E + (\kappa^2/4M)]^2}{\kappa^2 T/M}\right\}$$

$$\times \sum_{\ell=|J'-J|}^{J'+J} C^2(JJ'\ell;00)\,|A_{n\ell}|^2 \quad . \tag{4}$$

$$\left(\frac{d^2\sigma}{d\Omega d\epsilon}\right)_{ortho} = \frac{k}{3k_0}\left(\frac{M}{\pi\kappa^2 T}\right)^{\frac{1}{2}} \sum_n \frac{1}{n!}\left(\frac{\kappa^2}{4M\omega}\right)^n \sum_{J=1,3,5\ldots} P_J \left[a_i^2 \sum_{J'=0,2,4\ldots} + \left(3a_c^2 + 2a_i^2\right) \sum_{J'=1,3,5\ldots}\right] (2J'+1) \exp\left\{-\frac{[\epsilon + \Delta E + (\kappa^2/4M)]^2}{\kappa^2 T/M}\right\}$$

$$\times \sum_{\ell=|J'-J|}^{J'+J} C^2(JJ'\ell;00)\,|A_{n\ell}|^2 \,. \qquad (5)$$

In these expressions, k_0 and k are the initial and final neutron momenta respectively. M the proton mass. T the temperature. P_J the statistical weight of the angular momentum state J. ω the level spacing of the vibrations (0.54 eV), and a_c and a_i the proton coherent and incoherent scattering length, respectively. Also $C(JJ'\ell;00)$ is a Clebsch-Gordan coefficient, $\Delta E = E_{J'} - E_J + n\omega$, where $E_J = 0.0147\ J(J+1)/2$, and

$$A_{n\ell} = \int_{-1}^{1} d\mu\ \mu^n P_\ell(\mu) \exp -\left(\frac{\kappa^2\mu^2}{8M\omega} + \frac{i\kappa a\mu}{2}\right), \qquad (6)$$

where a is the equilibrium separation of the two protons.

At temperatures of the order of 20°K (liquid hydrogen) practically all of the H_2 molecules are in the ground state with J = 0. Hence, only the first term in the sum over J in Eq. (4) contributes to the para-hydrogen cross-section. Similarly, at such a low temperature only the term with J = 1 will contribute to $d^2\sigma/d\Omega\, d\epsilon$ for ortho-hydrogen. Although in a state of complete thermodynamical equilibrium the relative concentration of ortho- to para-hydrogen at 20°K is nearly zero, it still is possible to obtain a large ortho-concentration (by fast cooling of a room-temperature equilibrium mixture), because the ortho-to-para spontaneous transition probability is small. However, it is important to note that the scattering kernel obtained for this metastable moderator will not (and should not) satisfy detailed balance, which can only hold for the true equilibrium mixture of para- and ortho-hydrogen.

In Fig. 17 the total cross-section for both para- and ortho-hydrogen is shown at 20.4°K. The points shown are the experimental values of SQUIRES and STEWART [34]. A machine program called LHK [35] computes the scattering kernels from Eqs. (4) and (5). Using these kernels, space-independent spectra have been computed [36] in the buckling range $0 \leq B^2 \leq 0.1$ cm^2 for both para- and ortho-hydrogen, as shown in Figs. 18 and 19. Notice that not only are the para-hydrogen spectra very buckling-dependent, but also the spectra in ortho-hydrogen are remarkably different. Since ortho-hydrogen is not a substance in thermal equilibrium, the spectrum will always be far from Maxwellian, even for zero leakage and absorption, because of the large upscattering cross-section of ortho-to-para transitions.

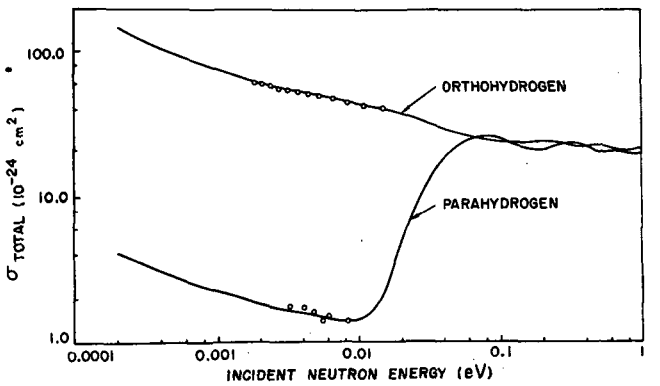

Fig. 17

Total cross-sections of ortho- and para-hydrogen at 20.4°K

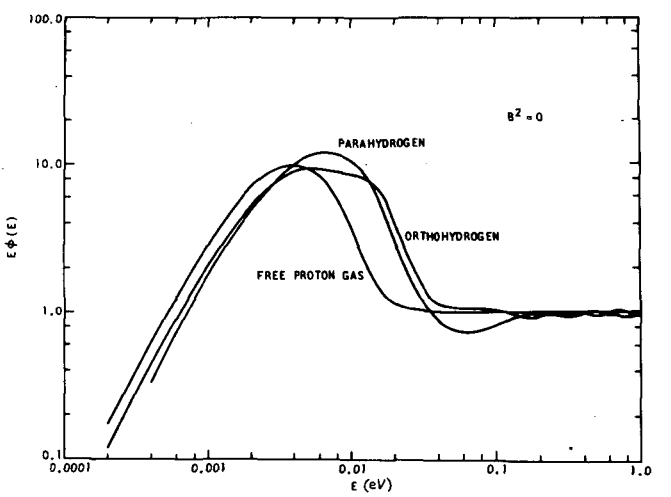

Fig. 18

Neutron spectra in para- and ortho-hydrogen at 20.4°K
with natural poisoning for zero buckling

9. SUMMARY

Accurate scattering kernels by which one can compute the parameters of interest for most moderators that are of importance to the reactor designer are now available. Nevertheless there remain some outstanding problems that require further study. For example, the moderator beryllium oxide does not yet have an accurate scattering representation. The present authors have evolved a lattice dynamical model for beryllium oxide and are in the process of obtaining numerical results. Beryllium oxide is especially complicated because the scattering does not depend simply on the phonon

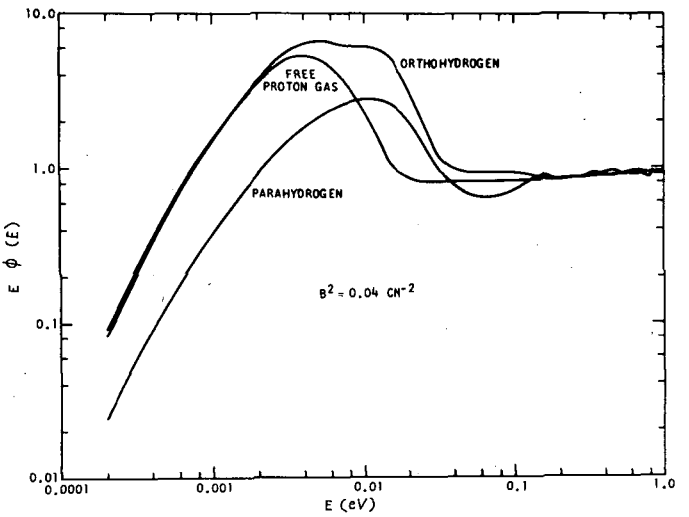

Fig. 19

Neutron spectra in para- and ortho-hydrogen at 20.4°K
with natural poisoning for a buckling of 0.04 cm^{-2}

spectrum even for the incoherent approximation, and this more complex dependence on the dynamics is being taken into account.

Also needed is an accurate method of treating the hindered rotational spectrum in light and heavy water. In this connection the very recent work of McMURRY is referenced [37].

The moderator zirconium hydride is very little understood except on simple physical grounds, although it is true that neutron spectra can be computed quite accurately for this moderator. The calculations in this case, however, are very phenomenological in nature and thus not very satisfactory.

It seems, then, that enough problems remain in the field of slow neutron scattering from reactor moderators to keep physicists busy for some time yet.

REFERENCES

[1] EGELSTAFF, P. A., Inelastic Scattering of Neutrons in Solids and Liquids, IAEA, Vienna (1961) 25-38.
[2] SCHMUNK, R. E., BRUGGER, R. M., RANDOLPH, P. D. and STRONG, K. A., Phys. Rev. 128 (1962) 562.
[3] YOUNG, J. A. and KOPPEL, J. U., Phys. Rev. 134 (1964) A1476; Nucl. Sci. Engng 19 (1964) 367.
[4] NALIBOFF, Y. D. and KOPPEL, J. U., HEXSCAT, A machine program for coherent elastic scattering of neutrons by hexagonal lattices, USAEC Rpt GA-6026, (15 Dec. 1964).
[5] TRIPLET, J. R., NALIBOFF, Y. D. and KOPPEL, J. U., private communication.
[6] SINCLAIR, R. N., Inelastic Scattering of Neutrons in Solids and Liquids II IAEA, Vienna (1963) 199-211.
[7] NEILL, J. M., private communication.
[8] SCHMUNK, R. E., Phys. Rev. 136 (1964) A1303.
[9] YOSHIMORI, A and KITANO, Y., J. phys. Soc. Japan 11 (1956) 352.
[10] WIKNER, N. F., JOANOU, G. D. and PARKS, D. E., Nucl. Sci. Engng 19 (1964) 108.
[11] YOUNG, J. A. and KOPPEL, J. U., J. chem. Phys. 42 (1965) 357.

[12] POOLE, M. J., SCHOFIELD, P., and SINCLAIR, R. N., Exponential and Critical Experiments III IAEA, Vienna (1964) 87-110.
[13] HAYWOOD, B. C. and THORSON, J. M., Inelastic Scattering of Neutrons in Solids and Liquids II IAEA, Vienna (1963) 111-21.
[14] EGELSTAFF, P. A. and HARRIS, D. H. C., Phys. Lett. 7 (1963) 220.
[15] YOUNG, J. A., WIKNER, N. F. and PARKS, D. E., to be published in Nukleonik.
[16] NEILL, J. M. and BARDES, R. E., private communication.
[17] NELKIN, M., Phys. Rev. 119 (1960) 741.
[18] KOPPEL, J. U. and YOUNG, J. A., Nucl. Sci. Engng 19 (1964) 412.
[19] HONECK, H. C., Rpt BNL-5826 (1961).
[20] NEILL, J. M., YOUNG, J. C., TRIMBLE, G. D. and BEYSTER, J. R., "Neutron spectra in H_2O, D_2O, BeO and CH_2", these Proceedings I.
[21] HONECK, H. C., Trans. Amer. nucl. Soc. 5 (1962) 47.
[22] BUTLER, D., Proc. phys. Soc. (London) 81 (1962) 276-94.
[23] KOPPEL, J. U. and YOUNG, J. A., to be published in Nukleonik.
[24] SPRINGER, T., Study Group Meeting of the IAEA on Research Reactor Utilization, Athens, 9-13 Sept. 1963.
[25] LIN, T. P. and KOENIG, J. L., J. mol. Spectry. 9 (1962) 228.
[26] KOPPEL, J. U. and YOUNG, J. A., Nucl. Sci. Engng 21 (1965) 257.
[27] WUNDERLICH, B., J. chem. Phys. 37 (1962) 1207.
[28] GOLDMAN, D. T. and FEDERIGHI, F. D., Nucl. Sci. Engng 16 (1963) 165.
[29] YOUNG, J. C., et al., Nucl. Sci. Engng 18 (1964) 376.
[30] WOODS, A. D. B., et al., Inelastic Scattering of Neutrons in Solids and Liquids II IAEA, Vienna (1963) 3-20.
[31] YOUNG, J. C., et al., Nucl. Sci. Engng 19 (1964) 230.
[32] YOUNG, J. A. and KOPPEL, J. U., Phys. Rev. 135 (1964) A603.
[33] SARMA, G., Inelastic Scattering of Neutrons in Solids and Liquids, IAEA, Vienna (1961) 397-409.
[34] SQUIRES, G. L. and STEWART, A. T., Proc. roy. Soc. (London) A230 (1955) 19.
[35] NALIBOFF, Y. D., LHK, An IBM-7044 code to calculate cross-sections and kernels for liquid para- and ortho-hydrogen, Rpt NASA-CR-54227, (30 July 1964).
[36] KOPPEL, J. U. and YOUNG, J. A., submitted to Nucl. Sci. Engng.
[37] McMURRY, H. L., Bull. Amer. phys. Soc. 10 (1965) 377.

DIFFERENTIAL NEUTRON SCATTERING FROM HYDROGENOUS MODERATORS*

J.R. BEYSTER, J.C. YOUNG, J.M. NEILL AND W.R. MOWRY
GENERAL ATOMIC DIVISION OF GENERAL DYNAMICS CORPORATION,
JOHN JAY HOPKINS LABORATORY FOR PURE AND APPLIED SCIENCE,
SAN DIEGO, CALIF., UNITED STATES OF AMERICA

Abstract — Résumé — Аннотация — Resumen

DIFFERENTIAL NEUTRON SCATTERING FROM HYDROGENOUS MODERATORS. The measurement of single differential neutron scattering cross-sections ($d\sigma/d\Omega$) for the common moderators is being carried out by time-of-flight techniques. The procedure utilizes an intense pulsed source of thermal neutrons produced by the General Atomic linear accelerator, and a 12-m flight path at the end of which is located a thin sample of the moderator under investigation. In addition there is a short final flight path for the scattered neutrons from the sample to several totally absorbing neutron detectors. The scattering angular distribution for over 50 incident neutron energies can be measured simultaneously using the above procedure. Intensities are high, background is low and well defined, and measurements may be made rapidly at all scattering angles from 10° to 155°.

Measurements of the differential scattering cross-section for vanadium, H_2O, D_2O and ZrH are presented. Vanadium has been studied as a check of the experimental apparatus. H_2O measurements for several sample thicknesses and orientations have been made for comparison with calculations based on various bound hydrogen scattering models and for comparison with the work of Springer and Reinsch. The experimental measurements have all been corrected for the serious effects of multiple scattering in the samples. At present the pronounced variation predicted at about 0.06 eV neutron energy by the Nelkin scattering model is not observed experimentally due to the fact that the assumed single hindered rotator at 0.06 eV is not physically realistic. In addition large angle scattering is not predicted correctly by this simple model.

The experimental data serve several useful purposes. First the angular distributions are quite sensitive to the physical properties of the scattering model and serve to verify their adequacy. Secondly the experimental results are sensitive to higher orders of the P_n scattering, in contrast to many integral experiments, which are sensitive mainly to P_0 scattering. In particular one may test the P_1 scattering kernel appropriate to a given molecular model. Third, the transport cross-section may be calculated directly from the experiments for use in multigroup reactor analysis.

DIFFUSION DIFFÉRENTIELLE DES NEUTRONS PAR DES RALENTISSEURS HYDROGÉNÉS. On mesure par les méthodes du temps de vol les sections efficaces différentielles de diffusion simple ($d\sigma/d\Omega$) pour les ralentisseurs usuels. On utilise des neutrons thermiques produits par une source pulsée intense (accélérateur linéaire de la General Atomic) avec un parcours de vol de 12 m à l'extrémité duquel est placé un échantillon mince du ralentisseur à l'étude. En outre, on a également prévu un petit parcours de vol terminal pour les neutrons diffusés, entre l'échantillon et plusieurs détecteurs de neutrons entièrement absorbants. Cette méthode permet de mesurer simultanément la distribution angulaire de diffusion pour plus de 50 énergies des neutrons incidents. Les intensités sont élevées, le bruit de fond est faible et bien défini et on peut procéder à des mesures rapides pour tous les angles de diffusion compris entre 10 et 155 degrés.

Les auteurs présentent des mesures de la section efficace différentielle de diffusion pour le vanadium, H_2O, D_2O et ZrH. On a étudié le vanadium pour contrôler le dispositif expérimental. On a fait des mesures avec H_2O pour diverses épaisseurs et orientations des échantillons en vue de les comparer aux calculs fondés sur divers modèles de diffusion par l'hydrogène lié et aux résultats obtenus par Springer et Reinsch. Toutes les mesures expérimentales ont été corrigées pour tenir compte des effets importants de la diffusion multiple dans les échantillons. Pour l'instant, on n'a pas observé expérimentalement la variation accusée que fait prévoir le modèle de diffusion de Nelkin lorsque l'énergie des neutrons est d'environ 0,06 eV; ceci est dû

* Work performed under the auspices of United States Atomic Energy Commission, Contract No. AT(04-3)-167, Project Agreement No. 2.

au fait que l'hypothèse du rotateur unique inhibé à 0,06 eV n'a pas de réalité physique. En outre, ce modèle simple ne permet pas de prévoir avec exactitude la diffusion selon de grands angles.

Les données expérimentales sont utilisées à diverses fins pratiques. Tout d'abord, les distributions angulaires sont très sensibles aux propriétés physiques du modèle de diffusion et elles servent à les vérifier. Deuxièmement, les résultats expérimentaux sont sensibles aux ordres supérieurs de la diffusion P_n, par opposition à *plusieurs expériences intégrales qui sont surtout sensibles à la diffusion* P_0. *En particulier, on peut vérifier* le noyau de diffusion P_1 approprié à un modèle moléculaire donné. Troisièmement, on peut calculer la section efficace de transport directement à partir des expériences en vue de l'utiliser dans l'analyse des réacteurs en théorie multigroupe.

ДИФФЕРЕНЦИАЛЬНОЕ РАССЕЯНИЕ НЕЙТРОНОВ ИЗ ВОДОРОДОСОДЕРЖАЩИХ ЗАМЕДЛИТЕЛЕЙ. Измерения сечений $(d\sigma/d\Omega)$ однократного дифференциального рассеяния нейтронов для замедлителей обычных видов проводится по методу измерения времени пролета. Метод предусматривает использование интенсивного пульсирующего источника тепловых нейтронов, производимых линейным ускорителем общества "Дженерал атомик" с длиной пролета в 12 м, в конце которого располагается тонкий образец исследуемого замедлителя. В дополнение к этому имеется еще конечный путь пролета для рассеянных образцов нейтронов по направлению к нескольким полностью поглощающим нейтроны детекторам. Метод позволяет измерять одновременно угловое распределение более чем для 50 энергий бомбардирующих нейтронов. Интенсивности высоки, фоновые шумы малы и хорошо определены, так что измерения могут производиться быстро при всех углах рассеяния от 10 до 155°.

Сообщаются результаты измерений сечений дифференциального рассеяния для ванадия, H_2O, D_2O и ZrH. Ванадий изучен для проверки экспериментального оборудования. Измерения с H_2O для образцов разной толщины в различных направлениях проведены для сопоставления с расчетами, основанными на различных моделях рассеяния со связанным водородом, и для сравнения с работами Шпрингера и Рейнша. Во все экспериментальные измерения были внесены поправки на наблюдаемое в образцах сильное воздействие многократного рассеяния. В настоящее время предсказываемое моделью рассеяния Нелкина сильное изменение при энергии нейтронов приблизительно в 0,06 эв экспериментально не наблюдается из-за того, что предположительный единый ротатор с торможением при мощности в 0,06 эв не представляется физически реальным. Кроме того, эта простая модель не предугадывает правильно рассеяние при больших углах.

Экспериментальные данные служат для целого ряда полезных надобностей. Прежде всего угловое распределение чрезвычайно чувствительно по отношению к физическим свойствам модели рассеяния и поэтому служит для проверки удовлетворительности этой модели. Во-вторых, экспериментальные результаты чувствительны к более высоким порядкам рассеяния P_n в противоположность многочисленным интегральным экспериментам, которые чувствительны главным образом к рассеянию P_0. В частности представляется возможным проверять ядро рассеяния P_1 так, чтобы оно подходило для данной молекулярной модели. В-третьих, на основании экспериментов представляется возможным подсчитывать непосредственно сечения переноса для использования их в анализе реакторов многих групп.

DISPERSION DIFERENCIAL DE NEUTRONES EN MODERADORES HIDROGENADOS. Los autores están midiendo, por el método del tiempo de vuelo, las secciones eficaces diferenciales de dispersión neutrónica $(d\sigma/d\Omega)$ de los moderadores de uso corriente. Para ello emplean una intensa fuente pulsada de neutrones térmicos producidos por el acelerador lineal de la General Atomic, y una trayectoria de vuelo de 12 m, al final de la cual se encuentra una muestra delgada del moderador. Además, hay una breve trayectoria final de vuelo para los neutrones dispersados que va desde la *muestra hasta varios detectores de neutrones totalmente* absorbentes. Con este procedimiento puede medirse simultáneamente la distribución angular de dispersión correspondiente a más de 50 energías de incidencia de los neutrones. Las intensidades son elevadas, la actividad de fondo es baja y bien definida, y las mediciones pueden efectuarse rápidamente en todos los ángulos de dispersión comprendidos entre 10° y 155°.

Se presentan mediciones de las secciones eficaces de *dispersión diferencial del vanadio*, H_2O, D_2O y ZrH. El V se ha investigado para comprobar el aparato experimental. Se han efectuado mediciones en H_2O, con muestras de espesor y orientación diferentes para cotejar los resultados con los cálculos basados en varios modelos de dispersión con enlaces hidrógeno, y para compararlos también con los trabajos de Springer y Reinsch. Las mediciones experimentales se han corregido para compensar los acusados efectos de la dispersión múltiple en las muestras. En la actualidad, la pronunciada variación prevista para una *energía neutrónica de 0,06 eV*,

aproximadamente, por el modelo de dispersión de Nelkin no se observa experimentalmente debido a que el rotor monorrestringido que se considera a 0,06 eV, no es realista desde el punto de vista físico. Además, este modelo simple no describe satisfactoriamente la dispersión a grandes ángulos.

Los datos experimentales sirven para varios fines. En primer lugar, las distribuciones angulares son muy sensibles a las propiedades físicas del modelo de dispersión y permiten verificar su validez. En segundo lugar, los resultados experimentales son sensibles a la dispersión P_n de orden superior, a diferencia de muchos experimentos integrales, que son sensibles sobre todo a la dispersión P_0; en particular es posible comprobar el núcleo de dispersión P_1 apropiado para un modelo molecular determinado. Por último, la sección eficaz de transporte puede calcularse directamente a partir de los datos experimentales y utilizarse para el análisis de reactores por el método de varios grupos.

1. INTRODUCTION

In principle many problems of practical importance utilizing thermal neutron scattering data could be resolved if one had complete measurements of the double differential scattering cross-sections, $d^2\sigma/d\Omega dE$. Although much data are available today from many research groups, problems often arise in correlating these data. For example, there exist significant differences between scattering law measurements at various laboratories and their interpretation in terms of lattice or molecular vibrational spectra. For water there are three independent and different measurements of the hindered rotational part of the frequency spectra [1]. In addition, frequency spectra deduced from scattering law data have, in general, been quite different in shape from those calculated from neutron dispersion measurements or from other well-known non-neutron data [2, 3]. While these difficulties are not discussed here, they have been considered serious enough to warrant the development of other experimental procedures for studying the important features of thermal neutron scattering during the last few years. Many of these procedures are integral in nature and are the subject of a number of papers at this Symposium. A procedure which we have adopted for investigating the physics of slow neutron scattering is to measure the single differential scattering cross-section defined as follows in terms of the conventional scattering law $S(\alpha,\beta)$.

$$\frac{d\sigma(E_o)}{d\Omega} = \frac{kT}{4\pi}\,\sigma_f\left(\frac{A+1}{A}\right)^2 \int_0^\infty e^{-\frac{\beta}{2}} \sqrt{\frac{E}{E_o}}\, S(\alpha,\beta)\, dE. \qquad (1)$$

The measurements reported here complement and extend to the free gas limit those recently reported by SPRINGER et al. [4] on the same moderators. The experimental procedure we used, however, is considerably different from that of Springer et al.

The measurement of $d\sigma/d\Omega$ is particularly appropriate for many moderators because: (1) generally available reactor and Linac neutron sources are intense enough to prove excellent experimental accuracy for absolute cross-section measurements; (2) the measurement can usually be made sensitive to the prominent features of the scattering description or model which one is trying to verify, and (3) multiple scattering corrections which are often large at thermal energies can be made with precision using approximate scattering models.

2. EXPERIMENTAL PROCEDURES

In this work it was desired to measure $d\sigma/d\Omega$ absolutely without recourse to normalization procedures. The experimental technique and the correction procedures developed for this programme are discussed in detail elsewhere [5] and will be only briefly outlined here. Thermal neutrons, produced in a high flux Linac target, stream along a 12-m neutron flight path, are collimated to a 5-cm diameter beam and are allowed to strike a thin scattering sample. After interaction, the neutrons are detected at scattering angles from 10° to 155° from the incident direction using "black" Li^6 glass detectors. The neutron energy is established by measuring the flight time. The flight path from the sample to the detector must be short (30 cm for example) since neutrons may change energy in collision and this energy change can distort the experimental energy resolution.

The absolute scattering cross-section can be determined from the measured counting rate at a given energy and angle $C(\theta, E)$ by dividing by the detector response at zero degrees with no sample $C(0°, E)$. $R(\theta, E)$ is defined as $C(\theta, E)/C(0°, E)$. The experimental differential cross-section is calculated from the expression:

$$\frac{d\sigma}{d\Omega} = \frac{R(\theta, E)\, R^2 \cos\alpha}{A_B N_o T} C_f C_R C_M, \qquad (2)$$

where all geometrical quantities are shown in Fig. 1. C_f is a correction for the fact that the neutron beam incident on the sample does not have infinitely steep edges. C_R is an angularly dependent correction factor due to the finite angular resolution of the experimental geometry, and C_M is the correction factor for multiple elastic and inelastic scattering.

The most important correction to the simple expression given in Eq. (2) is that for the multiple scattering in the material of the sample and its holder. There are several approximations that can be used in making this correction. This simplest procedure formulated years ago by VINEYARD [6] assumes isotropic scattering on all collisions and no energy change in collision. Another method is to use the measured angular distributions to formulate the multiple scattering correction for the first and second scattering, to assume the subsequent collisions are isotropic, but to retain the elastic scattering approximation. This is the method used by LEMMEL [7] and SPRINGER in [4]. A third procedure is to calculate the correction for multiple scattering (C_H) by using a theoretical scattering model for the moderator and one-dimensional transport theory. The latter was adopted for this work and uses the computer code MUSE II [8].

An intercomparison of various procedures may be found in Ref. [5]. The sizeable magnitude of the correction which must be applied to the data is illustrated in Fig. 2 where the transport multiple scattering correction factors $(C_H)(C_M)$ are given. $(C_H)(C_M)$ does not decrease linearly with sample thickness so that rather thin samples may not be really free from correction. Comparisons of the transport correction (C_H) with the Vineyard correction C_V have shown that in some cases there is not a large difference. Further, in view of general agreement obtained between the experimental work re-

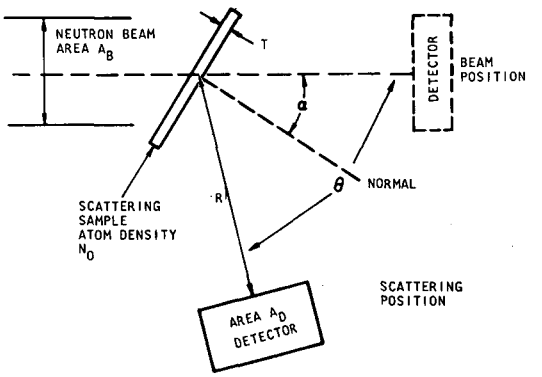

Fig. 1

Experimental arrangement used in measuring differential scattering cross-sections

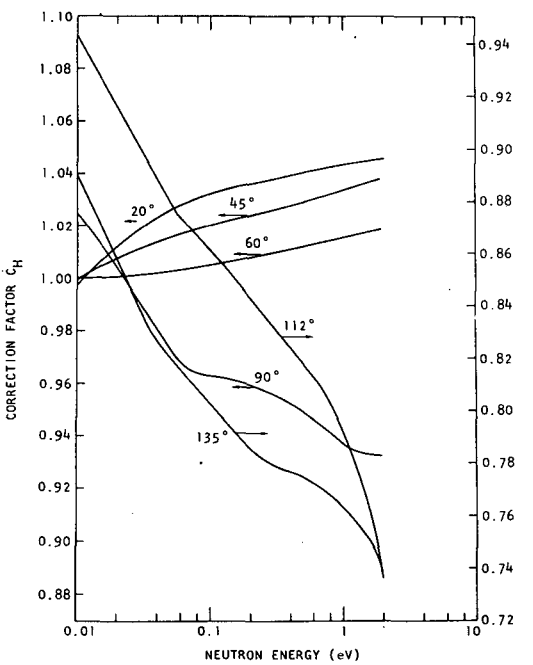

Fig. 2

Correction factor for scattering by a 21.5-mil H_2O sample

ported here and that of SPRINGER [4] who uses a more approximate method of performing the multiple scattering correction, it is believed that the Lemmel-Springer procedure tends to predict about the same magnitude correction for multiple scattering. The accuracy of the correction C_H used in the analysis of all data reported here is determined largely by the validity

of the theoretical scattering kernel. The detailed accuracy of the kernel is not as necessary for the measurements of $d\sigma/d\Omega$ as for the analysis of double differential scattering experiments. This results from the fact that cross-sections integrated over final energies are being studied rather than energy spectra and level widths. Great care will be required in applying this procedure, using an approximate scattering kernel, to the analysis of double differential scattering data.

One can see from Eq. (2) that to obtain absolute cross-sections directly from the angular scattering measurements, a sample of known uniform thickness must be used. In our experiment the walls of all samples were made of 5-mil aluminium (1100 H), stretched between two sets of heavy retaining rings which were subsequently removed [9]. If thick aluminium walls are used, a pronounced diffraction pattern for aluminium occurs in the background runs but is not usually present in the signal runs, thus producing an error when background is subtracted from signal. The average thickness of the sample is determined by measuring its area and weighing it before and after filling. The thickness of the samples is further checked by performing a neutron transmission measurement at many neutron energies.

3. SCATTERING FROM VANADIUM

The apparatus used in the scattering experiments has been checked by measuring the differential cross-section for vanadium (an incoherent scatterer), which can presumably be understood. A nearly isotropic scattering distribution is expected except for small effects caused by multiple scattering and preferential angular absorption. Conversion of these data to absolute cross-sections have been made with simple corrections for multiple scattering using the VINEYARD [6] technique. Angular distributions at all energies are generally isotropic to within 10% and integrate to the known scattering cross-section also to within 10%. It is uncertain whether the thin target angular distribution for vanadium should be completely isotropic since it is the sum of two rather anisotropic components. Further, the total scattering cross-section for vanadium is known to about 5% [10]. Thus, it is concluded that the present test experiments on vanadium give data which agree to within experimental error with the known properties of vanadium.

4. SCATTERING FROM H_2O

Single differential scattering cross-sections have been measured for H_2O for two samples (thicknesses of 0.019 and 0.013 in) at 55 neutron energies and at 30 scattering angles. The sample orientation was varied in several additional experiments to check on the validity of the multiple scattering correction procedures necessary for data analysis. A partial sampling of the experimental data obtained from 0.006 to 2.2 eV is shown in Figs. 3 and 4. To display a large amount of data in a compact manner the cross-sections given in this report have all been multiplied by adjustable constants. To obtain absolute cross-sections, the ordinate given must be multiplied by the factor in brackets at the right. Statistical error bars have been omitted

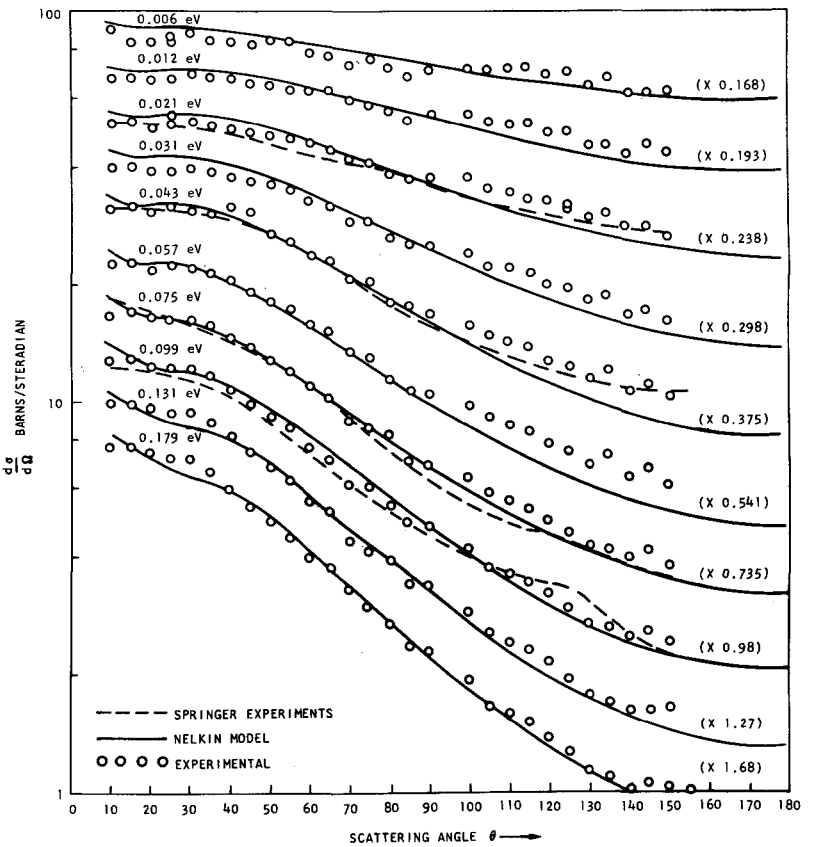

Fig. 3

Scattering cross-section for H_2O

from data shown in the figures for clarity. Generally statistical errors are 5% or less. Actually, data to 10 eV neutron energy were measured to study the transition to the free gas limit. The predictions of the free gas model and NELKIN [11] model are shown in Fig. 4 at 1 and 2.2 eV neutron energies. The bound hydrogen model agrees much better with experiment than the free gas model, even at these relatively high energies. Data analysis above 2.2 eV has not yet been completed. It can be seen that generally a larger scattering cross-section is measured at large scattering angles than is predicted by the bound hydrogen model. This indicates qualitatively the need for including increased molecular binding in the model for water; this might be accomplished if a distributed rotational spectrum were used in the theory. In the energy region of from 0.2-0.3 eV the Nelkin model seems to fit the experimental data almost exactly. Around 0.06 eV it appears to agree most poorly with experiment. A comparison of these new experimental data with those of SPRINGER et al. [4] is shown in Fig. 3. Generally the agreement with the measurements at the four energies of Springer is good although at some angles beyond 90° discrepancies of as much as 15% exist. In one

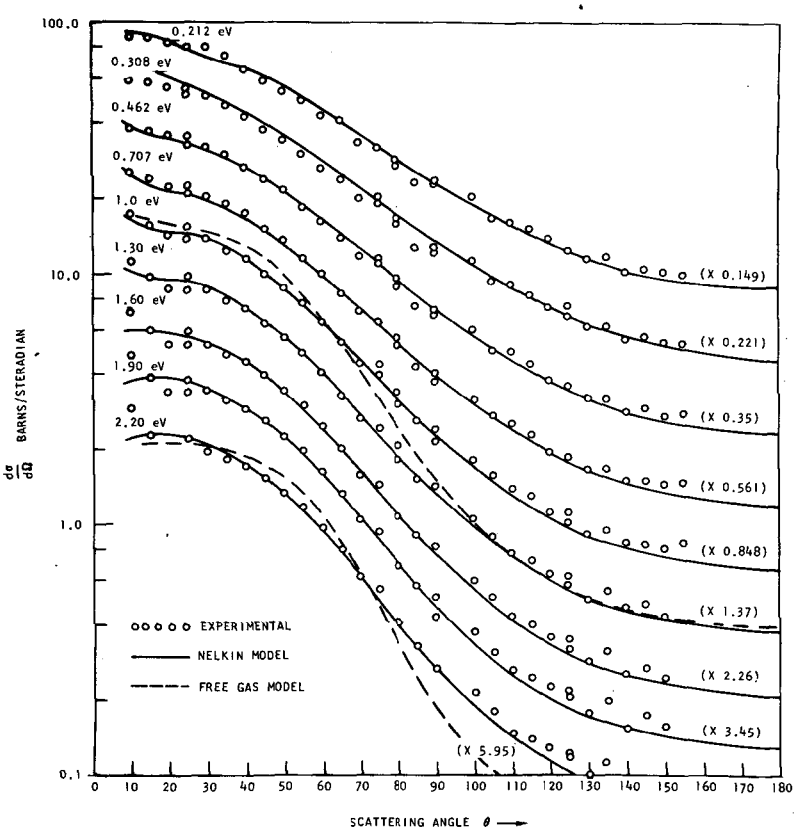

Fig. 4

Scattering cross-section for H_2O

of the cases shown, the structure seen by Springer at back angles was not observed here. The agreement of the WHITTEMORE and McREYNOLDS [12] data with the new data is rather poor probably because the former data were not corrected for multiple scattering. The former data were measured also with a long BF_3 counter so that an energy-dependent detector solid angle could have resulted. Differences in shape of the angular distribution in excess of 50% actually occur. The anomaly that the 0.06 eV angular distribution reported by WHITTEMORE and McREYNOLDS [12] was more forward peaked than higher energy distributions has not been observed. This anomaly is in fact not a prediction of the Nelkin model for water even though a discrete oscillator has been assumed at 0.06 eV to represent the rotational frequency band.

A useful comparison of various experimental and theoretical scattering results can be obtained by calculating $\bar{\mu}$ defined as follows:

$$\bar{\mu}(E) = \int \frac{d\sigma}{d\Omega} \cos\theta \, d\Omega. \tag{3}$$

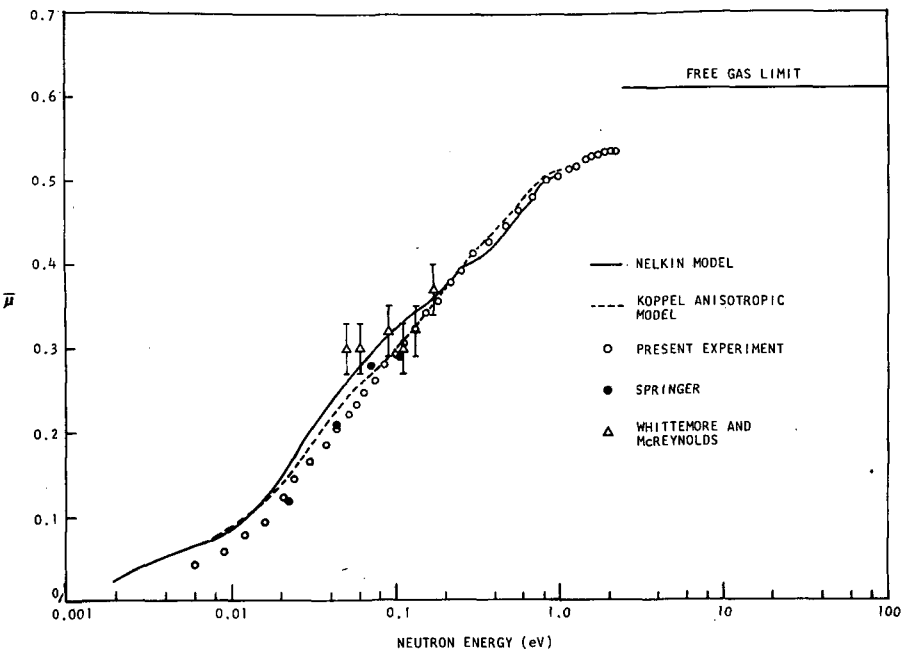

Fig. 5

$\bar{\mu}$ for H_2O

It will be recalled that the energy-dependent transport cross-section may be determined from $\bar{\mu}$ and this quantity can be used to obtain the thermal diffusion constant as follows:

$$\overline{Dv} = \frac{\int n(v) v \frac{\lambda_{tr}}{3} dv}{\int n(v)\, dv} \,. \tag{4}$$

In Fig. 5, $\bar{\mu}$ calculated using the results for the present experiments are shown. The data have not been extended to the high energy limit, even though angular distribution data exist, because the multiple scattering correction factors above 2 eV have not yet been calculated. The four solid points show the work of SPRINGER [4] which are in relatively good agreement with the present work. The triangles represent WHITTEMORE and McREYNOLDS' [12] data. The dashed line is the prediction of the Nelkin model. At roughly 0.3 eV, $\bar{\mu}$ for this model seems to deviate noticeably from experiment. This small discrepancy may still be numerical in origin and associated with the change-over criteria in the model. The dashed curve gives $\bar{\mu}$ calculated with the KOPPEL [13] anisotropic vibration model for water. Clearly this more realistic treatment of the vibrational motion removes at least half of the discrepancy with the Nelkin model above 0.02 eV. Due to the above effects the measured transport mean free path and that predicted by the Nelkin model tend to disagree in certain energy regions, particularly around 0.06 eV

where the theoretical model makes the assumption of a single torsional frequency. The agreement with measured total cross-sections above 0.02 eV was also improved considerably with the model of KOPPEL and YOUNG [13]. Below 0.02 eV both models give the same results and disagree with experiment. Predictions of $\bar{\mu}$ with the Haywood kernel [14] have not yet been made.

The thermal diffusion constant at 20°C has been calculated from the new experimental results; it is $\overline{D_0 v} = 35\,130$ cm^2/s. The SPRINGER [4] result is $35\,300 \pm 300$ cm^2/s. The theoretical predictions [13] are $\overline{D_0 v} = 37\,906$ cm^2/s for the Nelkin model and $\overline{D_0 v} = 36\,532$ cm^2/s for the anisotropic model of KOPPEL and YOUNG [13]. One would probably be justified in assigning an error of at least 1% to the theoretical calculations of $\overline{D_0 v}$ due to numerical problems with the models. Poisoned diffusion length measurements of STARR and KOPPEL [15] gave $35\,680 \pm 100$ cm^2/s and an analysis of pulsed measurements by KOPPEL and LOPEZ [16] gives $36\,630 \pm 370$ cm^2/s. The various determinations of $\overline{D_0 v}$ vary outside of the experimental error, and the total spread between the predictions of the anisotropic model and the result of this paper is 4%. To try to resolve remaining discrepancies in a really convincing manner by integral measurements of $\overline{D_0 v}$ would seem very difficult especially since the pulsed and steady state procedures may not determine the same quantity. It is our belief that the present method of determining $\overline{D_0 v}$ is inherently more accurate than the pulsed technique and appears to give results more nearly in agreement with the results from the other experimental sources.

5. SCATTERING FROM D_2O

Initial measurements of the single differential scattering cross-section for heavy water have been completed at 55 neutron energies ranging from 0.006 to 10 eV and for one sample configuration having a transmission of about 90%. Some of the new experimental data are shown in Figs. 6 and 7 together with the experimental measurements of SPRINGER [4] and the theoretical calculations of $d\sigma/d\Omega$ performed by KOPPEL [17] and Houston using essentially BUTLER's [18] formulation of the double differential scattering cross-section for D_2O. Generally, the results of this experiment do not agree with those of Springer as well as in the case of scattering from H_2O. The angular dependence shows the pronounced effect of coherent scattering. The cross-sections have been calculated ignoring coherence completely [19] and including it both for intra- and intermolecular scattering [17]. The theoretical predictions of cross-sections at angles less than 15-20° are at present still subject to some error. Measured interference peaks are generally somewhat less pronounced than those observed in Springer's experimental work but have the same characteristic deviation from the theoretical peaks; namely the experimental peaks are narrower. The narrower elastic interference peaks observed in the experiment indicate that the D_2O molecules are tending to cluster as in a solid.

For D_2O, $\bar{\mu}$ has been calculated using the experimental data for 14 of the 55 neutron energies and it is given in Fig. 8. $\bar{\mu}$ calculated by KOPPEL

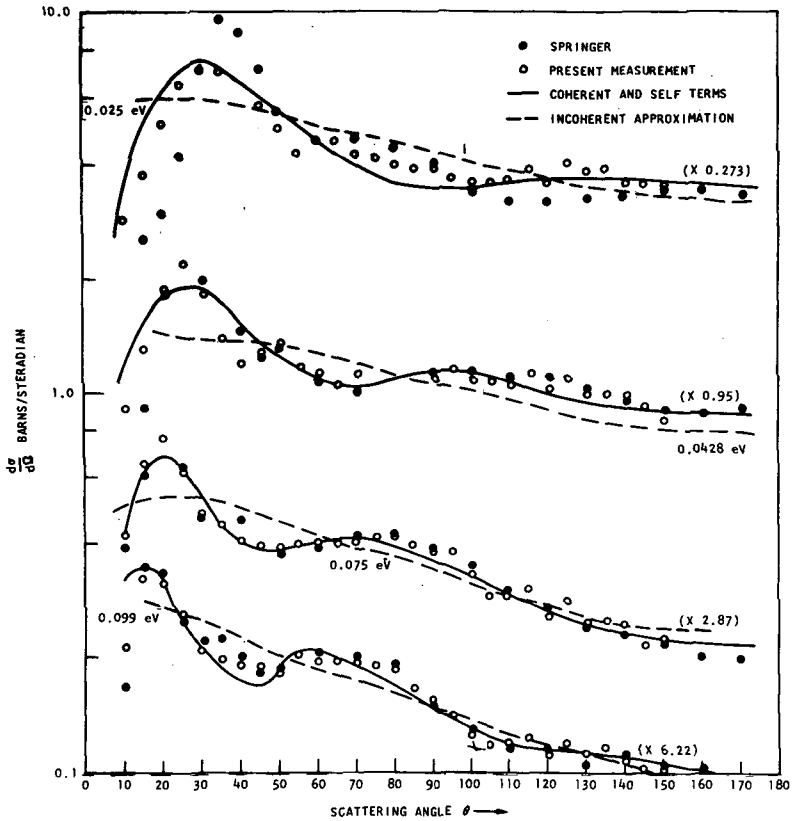

Fig. 6

Scattering cross-section for D_2O

[17] is also shown and the experiment and theory generally display many of the same characteristic variations due to coherent scattering.

In conclusion, our detailed understanding of neutron scattering from D_2O is not completely adequate as yet. While integral spectral data indicate that only a completely incoherent scattering kernel is required even for some space-dependent problems, the single differential scattering measurements indicate the importance of including coherent effects. The single scattering experiments for this important moderator need to be repeated and improved both by using thicker scattering samples (multiple scattering is very small for the work reported here) and by increasing the experimental angular resolution by at least a factor of two. Further work with the scattering model which would include the rotational frequency band properly is also in order.

6. SCATTERING FROM ZIRCONIUM HYDRIDE

Single differential scattering cross-sections have been measured using a thin pressed powder sample of $ZrH_{1.85}$ for 55 neutron energies from 0.006

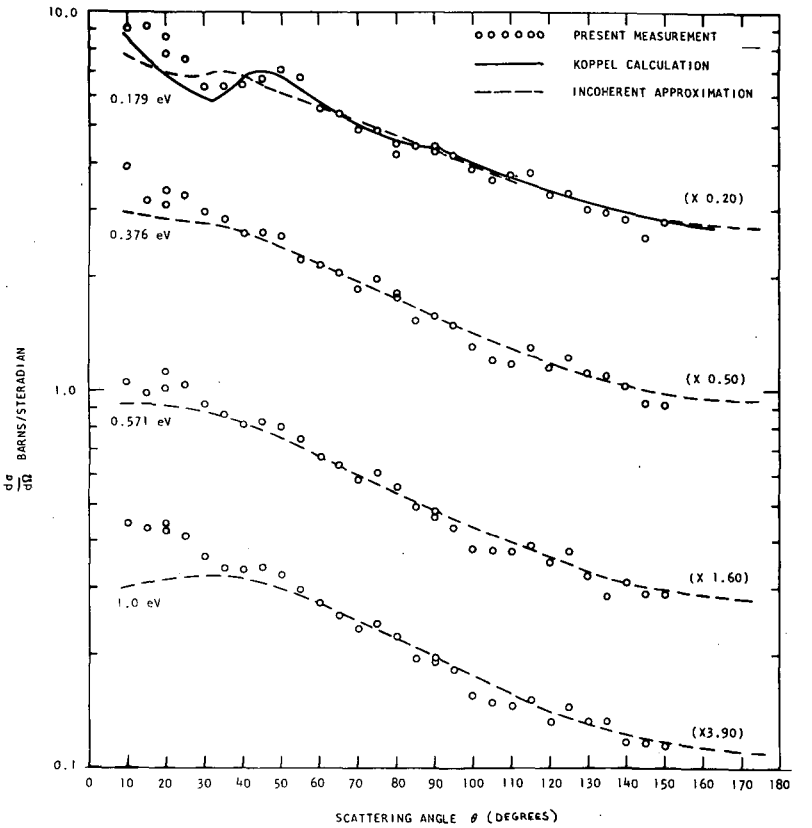

Fig. 7

Scattering cross-section for D_2O

to 10 eV neutron energy. C_H was appreciable as in the case of H_2O and in the range 0.75 to 1.10. The differential elastic and inelastic scattering cross-sections used for $ZrH_{1.85}$ in MUSE are used also to calculate the theoretical single scattering cross-section ($d\sigma/d\Omega$). Six selected angular distributions are given in Fig. 9. Statistical counting errors are less than 5% on all points shown. The solid curves are the theoretical calculation [19] and the three dashed curves represent the experimental work of SPRINGER et al. [4]. It will be observed that both sets of experimental points tend to show fine structure. This is due to the coherent scattering from zirconium and cannot be expected to be the same in both experiments unless the allotropic form of the samples and the experimental angular resolution are the same. Further, Springer's data consist of angular distribution shape measurements for $ZrH_{1.91}$ not $ZrH_{1.85}$ and have not been adjusted for the slight hydrogen difference in the comparison shown. The data are merely normalized to give the same total scattering cross-section for zirconium hydride as for our data. The general trend of both sets of experimental data is very similar although many substantial differences which must be

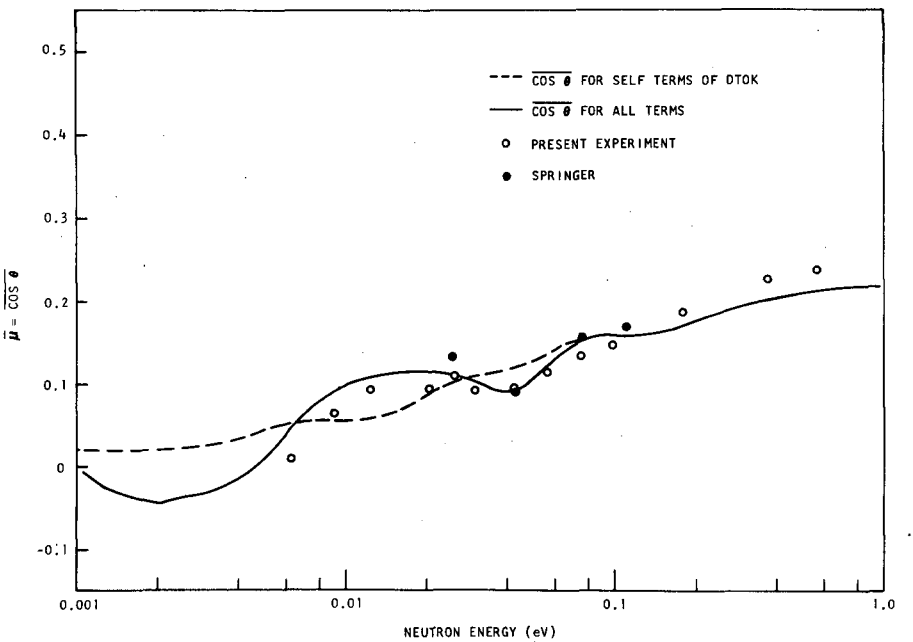

Fig. 8

$\bar{\mu}$ for D_2O

examined in detail exist. Since very little total cross-section data exist for zirconium hydride, it is difficult to thoroughly check the integral of the measured single differential cross-section. The integral of the experiment $d\sigma/d\Omega$ and theoretically calculated total cross-sections, however, disagreed generally by less than five per cent and in no case by more than 10% which is encouraging. It is apparent from Fig. 9 that $\bar{\mu}$ calculated from the experiment will be less than that given by the theoretical calculation. This is consistent with Springer's findings [4]. In addition, the large decrease (calculated by Memmert [4]) in $\bar{\mu}$ as the first level in zirconium hydride becomes excited by inelastic neutron scattering is clearly observable. One can see this from a comparison of the more forward peaked 0.105 eV curve with the 0.153 eV curve.

The theoretical calculations presented here are based on the natural width Einstein oscillator model [20] (SUMMIT model) used previously with some success in calculating temperature-dependent infinite medium neutron spectra. The zirconium scattering is calculated in the free gas limit ignoring coherence whereas the elastic scattering from the bound hydrogen is calculated in the incoherent approximation. The accuracy of this procedure has not been evaluated in detail yet, but as in previous cases the theoretical predictions are most subject to error at scattering angles less than 20°. It is not clear as yet if this experiment constitutes a confirmation or rejection of the phenomenological theoretical model. The variation between theory and experiment are larger than reported previously for H_2O or D_2O except just above the first excited vibrational state of the molecule where the agree-

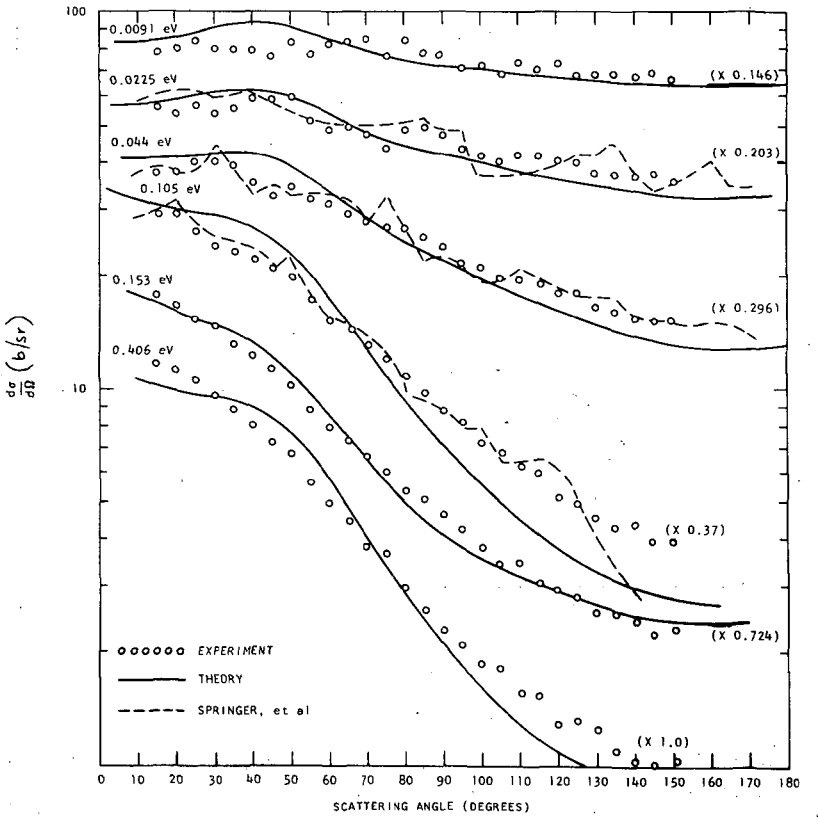

Fig. 9

Scattering cross-section for zirconium hydride

ment is quite good. At other energies it would appear that the model still somewhat underestimates the degree of the molecular binding. The calculational model used here is, however, much more elementary than that used for H_2O and D_2O and requires further development.

REFERENCES

[1] MOSTOVOY, V.I., DYKAREV, V.S., EVEMEER, I.P., ISHMAYER, S.P., SADIKOV, I.P., SALTYKOV, Yu. S., TARABANKO, V.A. and CHENYSKOV, A.P., Proc. 3rd UN Int. Conf. PUAE, 1964, P/367.

[2] YOUNG, J.A. and KOPPEL, J.U., "Calculation of thermal scattering kernels", these Proceedings I.

[3] WIKNER, N.F., JOANOU, G.D. and PARKS, D.E., Nucl. Sci. Engng 19 (1964) 108; BARDES, R.G., HOUGHTON, G.K., PARKS, D.E., BEYSTER, J.R., Neutron spectra in graphite poisoned with samarium, Rpt GA-4812 (Dec. 1963).

[4] SPRINGER, T., HOFMEYER, C., KORNBICHLER, S., LEMMEL, H.D., Proc. 3rd. UN Int. Conf. PUAE 1964, P/763.

[5] BEYSTER, J.R., et al., Integral neutron thermalization annual summary report, 1 Oct. 1963-31 Sep. 1964, USAEC Rpt GA-5798 (Oct. 1964).

[6] VINEYARD, C.H., Multiple scattering of neutrons, Phys. Rev. 96 (1954) 93.

[7] LEMMEL, H.D., Thesis, Munich, Institute of Technology, Munich, Germany.

[8] HONECK, H.C., MUSE, a computer code for multiple scattering corrections, Rpt GA-5968, (Nov. 1964).
[9] BEYSTER, J.R., Integral neutron thermalization, Rpt GA-6096 (Jan. 1965).
[10] BROCKHOUSE, B.N., Canad. J. Phys. 33 (1955) 889; Cross section compilation, Rpt BNL 325.
[11] NELKIN, M.S., Phys. Rev. 119 (1960) 741.
[12] WHITTEMORE, W.L. and McREYNOLDS, A.W., Inelastic Scattering of Neutrons in Solids and Liquids, IAEA, Vienna (1961) 511.
[13] KOPPEL, J.U. and YOUNG, J.A., Nucl. Sci. Engng 19 (1964) 412-17.
[14] POOLE, M.J., private communication.
[15] STARR, E. and KOPPEL, J.U., Nucl. Sci. Engng 14 (1962) 224.
[16] KOPPEL, J.U. and LOPEZ, W.M., Rpt BNL 719 III (1962) 946.
[17] KOPPEL, J.U. and YOUNG, J.A., The Role of Interference Scattering in Neutron Thermalization by Heavy Water, Rpt GA-6103 (March 1965).
[18] BUTLER, D., Proc. phys. Soc. 81 (1962) 276, 294.
[19] HONECK, H.C., Trans. Amer. nucl. Soc. 5 1 (1962) 47.
[20] YOUNG, J.C., et al., Nucl. Sci. Engng 19 (1964) 230.

DISCUSSION

(on the foregoing two papers)

W. GLASER: In connection with the frequency distribution of beryllium which you used in your calculations, we have seen that there is some disagreement between the calculated curve and the curve measured by Sinclair. Could you tell us how you derived your distribution or input data from measurements?

J. A. YOUNG: The theoretical phonon distribution of beryllium was determined from a theoretical force model, the constants of which were determined by the single-crystal dispersion-relation measurements of Schmunk.

W. REICHARDT: How did you arrive at the weighting factor of 1/360 for the acoustical part of the frequency distribution for zirconium hydride? Ehret at Karlsruhe, who has done scattering law measurements on zirconium hydride, got a 2% contribution of the acoustical part.

J. A. YOUNG: We chose this relative weight because it resulted in a good fit to the experimental data. While a lower mass, somewhere between 91 and 364, would perhaps be more realistic, the effect on the neutron spectra is not likely to be very significant.

I. SADIKOV: To what approximation did you solve the kinetic equation in the calculation of neutron spectra in Be?

J. A. YOUNG: It was solved in accordance with one-dimensional transport theory (GAPLSN).

M. NELKIN: Have you any information on the discrepancy between theory (1000 s^{-1}) and experiment (2600 s^{-1}) for $(v\Sigma)_{min}$ in graphite?

J. A. YOUNG: No, not at the moment.

S. N. PUROHIT: Would the intermediate scattering function for the hindered rotations in H_2O as given by the Yip and Osborn model improve the agreement between theory and experiment for the infinite medium spectra?

J. A. YOUNG: Yes. An accurate treatment of the hindered rotations and also the approach to the free rotation limit would be very useful.

M. CADILHAC: To interpret the experimental spectra, is it necessary to introduce a temperature-variable theoretical frequency distribution to take account of the anharmonicity effects? I am thinking mainly of graphite.

J. A. YOUNG: It is not necessary to introduce anharmonicities in the case of neutron spectra because, as the temperature rises, the neutron spectrum becomes less sensitive to the details of the scattering process.

M. KAZARNOVSKY (Chairman): The hydrogen molecule is very simple and neutron scattering by it can be calculated very exactly. Comparisons between theoretical and experimental data are therefore of great interest. What was the accuracy of the experimental data with which you compared your calculations?

J. A. YOUNG: While I do not recall off hand the accuracy of the Squires and Stewart experiment in 1954, it was sufficient to permit a comparison to be made between theory and experiment, thus providing a good test of the theory, especially in the case of ortho-hydrogen with its higher cross-section below 0.022 eV.

REVIEW OF THE APPLICATION OF PULSED SOURCES TO THE MEASUREMENT OF NEUTRON SPECTRA IN MODERATORS AND REACTOR LATTICES

M.J. POOLE
ATOMIC ENERGY RESEARCH ESTABLISHMENT,
HARWELL, DIDCOT, BERKS., UNITED KINGDOM

Abstract — Résumé — Аннотация — Resumen

REVIEW OF THE APPLICATION OF PULSED SOURCES TO THE MEASUREMENT OF NEUTRON SPECTRA IN MODERATORS AND REACTOR LATTICES. The employment of pulsed sources for neutron spectrum measurements is described with reference to applications for which the method is suitable. Emphasis is placed on the use of pulsed sources for basic studies of the process of neutron moderation. Various scattering laws which have been proposed for common moderators are mentioned and the corresponding predicted energy spectra are compared with experimental measurements.

APPLICATION DES SOURCES PULSÉES A LA MESURE DES SPECTRES DE NEUTRONS DANS LES RALENTISSEURS ET LES RÉSEAUX DE RÉACTEURS. L'auteur décrit l'emploi de sources pulsées pour mesurer des spectres de neutrons, du point de vue des applications que la méthode est susceptible de recevoir. Il étudie particulièrement l'emploi de sources pulsées dans les études fondamentales sur le processus de ralentissement des neutrons. Il mentionne diverses lois de diffusion qui ont été proposées pour les ralentisseurs usuels; les spectres d'énergie calculés d'après ces lois font l'objet d'une comparaison avec les résultats de mesures expérimentales.

ОБЗОР ПРИМЕНЕНИЯ ИМПУЛЬСНЫХ ИСТОЧНИКОВ ДЛЯ ИЗМЕРЕНИЯ НЕЙТРОННЫХ СПЕКТРОВ В ЗАМЕДЛИТЕЛЯХ И РЕАКТОРНЫХ РЕШЕТКАХ. Дается описание применения импульсных источников для измерения нейтронных спектров с указанием тех видов применения, для которых пригоден этот метод. Основное внимание уделено применению импульсных источников для фундаментальных исследований процесса замедления нейтронов. Указаны различные законы рассеяния, предложенные для обычных замедлителей, и соответствующие предсказанные теоретические энергетические спектры сравниваются с результатами экспериментальных измерений.

APLICACION DE FUENTES PULSADAS A LA MEDICION DE ESPECTROS NEUTRONICOS EN MODERADORES Y RETICULADOS DE REACTOR. En la memoria se describe el empleo de fuentes pulsadas para medir espectros neutrónicos y se indican los casos en que dicho método es adecuado. En especial, se expone la utilización de fuentes pulsadas en estudios básicos del proceso de moderación neutrónica. Se hace referencia a diversas leyes de dispersión propuestas para moderadores corrientes y se comparan los correspondientes espectros energéticos calculados con los que se han determinado experimentalmente.

1. INTRODUCTION

The separation of neutron spectrum measurements by time-of-flight into "pulsed source" and "chopper" measurements is artificial; most of the experiments described here could equally well be carried out using a chopper to analyse the spectrum in an assembly driven by a steady source (reactor). However, as in practice, it has been convenient to carry out spectrum studies using pulsed neutron sources (usually a source depending on an electron Linac)

and a description of such experiments is properly included in a symposium devoted to the use of pulsed sources in reactor physics.

The aim of spectrum measurements has been three fold. In the first place attempts have been made to measure spectra in reactor systems [4, 14] either to give information on the neutron spectrum to be expected in a specific reactor, or to provide information to set up a "correlation" type of recipe for reactor design (e.g. the Westcott formalism for spectra in reactors). Secondly spectra may be measured in simple systems with the object of testing a thermalization model by the comparison of experimental and theoretical spectra. The choice of a system for the experiment is now dictated by the particular features of the thermalization model that is being examined (e.g. spectra in infinite homogeneous systems are sensitive to the form of the energy transfer cross-section $\Sigma(E' \rightarrow E)$ for the moderator but give no information about the angular distribution of the scattering). Thirdly experiments may be made to test some aspect of the transport theory or to test the accuracy of a computer code used to calculate spectra.

Most of the experiments to be discussed in this paper are of the second type. Within this category two classes can be distinguished:

(a) Experiments in large (ideally infinite) homogeneous systems where loss of neutrons of any energy by diffusion from a volume element is small enough to be treated as a correction to loss by capture and scattering to another energy. As has already been mentioned these experiments are sensitive to the energy transfer kernel $\Sigma(E' \rightarrow E)$ but not to the angular distribution of scattering or to the energy dependence of the total scattering cross-section.

(b) Experiments in which the spectra near to boundaries are measured. The geometry should be kept simple (e.g. plane boundary between two media or between two regions at different temperatures) so that difficulties in handling the transport equation do not arise during the interpretation of the experiment. Now the spectrum depends not only on $\Sigma(E' \rightarrow E)$ but also on the angular dependence of the scattering law.

Measurements of spectra in homogeneous media have been extensively reported in the literature for most of the common moderators [42 to 47, 50 to 54]. Experiments of type (b) have been described by PARKS et al. [13] (angular dependence of leakage spectra and variation of spectra near to a simulated core-reflector interface), by Day (spectra near to a plane temperature discontinuity), by Beckurts (asymptotic spectra in finite water tanks) and by Sinclair et al. (spectra near to an absorbing boundary). Interpretation has always required a scattering kernel based on a model taking into account the chemical binding of the atoms in the moderator. Such models have been provided by PARKS (see [1]) and by EGELSTAFF (see [2]) for graphite, by Nelkin and by HAYWOOD (see [3]) for water and by BROWN and St. JOHN [4], by HONECK [5] and by HAYWOOD and THORSON [6] for heavy water. In addition models are available for benzene [7], polyethylene [8], zirconium hydride [9], beryllium oxide [10] and beryllium [11]. Differences between the models for the more common moderators (C, H_2O, D_2O) are discussed in a later section.

2. THE EXPERIMENTAL TECHNIQUE

Before considering any experimental details it is necessary to consider the resolution needed in a typical spectrum measurement. The spectrum is usually made up from a thermal group of more or less Maxwellian shape, joined to a high energy "tail" approximately to 1/E form, with possibly one or more relatively narrow dips caused by resonance absorption. It is established in an earlier paper [12] that the resolution required is almost entirely set by the need to see these resonance dips; if the 0.3-eV Pu^{239} and the 1-eV Pu^{240} resonances are taken as typical, a resolution of $\sim 2\ \mu s/m$ is desirable. For a spectrum without resonances $\sim 10\ \mu s/m$ is sufficient.

Pulsed sources can be used in three main ways for the measurement of spectra in moderating systems.

(a) The system can be driven by the pulsed fast neutron source and the spectrum of neutrons in an extracted beam measured by time-of-flight.

The pulsing of the assembly is used directly as the time reference for the time-of-flight experiment. The resolution of the experiment is then determined by the relaxation time of the system, so it is important to discuss the factors determining this relaxation time.

In an absorbing and finite system this relaxation time not only depends on the absorption and leakage but also on the energy of neutrons under consideration; at high energies the slowing-down time to that energy is the controlling factor, while at low energies the mean lifetime of the neutrons is the controlling factor. The time variation of neutron flux has been calculated by solving the time-dependent diffusion equation, and the results in infinite graphite-moderated and water-moderated systems, which have been poisoned to a value of $\Sigma_s = 0.1$ in each case, are shown in Fig. 1. This variation of emission time with energy leads not only to a resolution correction but also to a correction on the time-of-flight of the neutrons. This latter is usually done by calculating the mean time of emission of the neutrons by a method first proposed by PARKS [13]. The time-dependent diffusion equation is

$$\frac{1}{v}\frac{\partial \phi(E,t)}{\partial t} = -[\Sigma_a(E) + \Sigma_s(E) + D(E)\,B^2]\,\phi(E,t) + \int_0^\infty \Sigma(E' \to E)\,\phi(E',t)\,dE + S(E,t) \tag{1}$$

where $\phi(E,t)$ is the flux spectrum at time t, $\Sigma_a(E)$ and $\Sigma_s(E)$ are the macroscopic absorption and scattering cross-sections respectively and $\Sigma(E' \to E)$ is the energy transfer kernel.

Multiplying by t and integrating over all time with $S(E,t) = S(E)\,\delta(t)$ we have

$$\int_0^\infty \frac{1}{v} E \frac{\partial \phi}{\partial t}(E,t)\,dt = -[\Sigma_a(E) + \Sigma_s(E) + D(E)\,B^2] \int_0^\infty t\,\phi(E,t)\,dt$$

$$+ \int_0^\infty \Sigma(E' \to E) \int \phi(E',t)\,dt\,dE \tag{2}$$

Writing $\phi_0 = \int_0^\infty \phi(E, t)dt$ and $\phi_1 = \int_0^\infty t\,\phi(E, t)\,dt$, one obtains

$$\frac{\phi_0}{v} = -[\Sigma_a(E) + \Sigma_s(E) + D(E)B^2]\,\phi_1(E) + \int_0^\infty \Sigma(E' \to E)\,\phi_1(E')dE \qquad (3)$$

which has the same form as the steady state neutron balance equation with

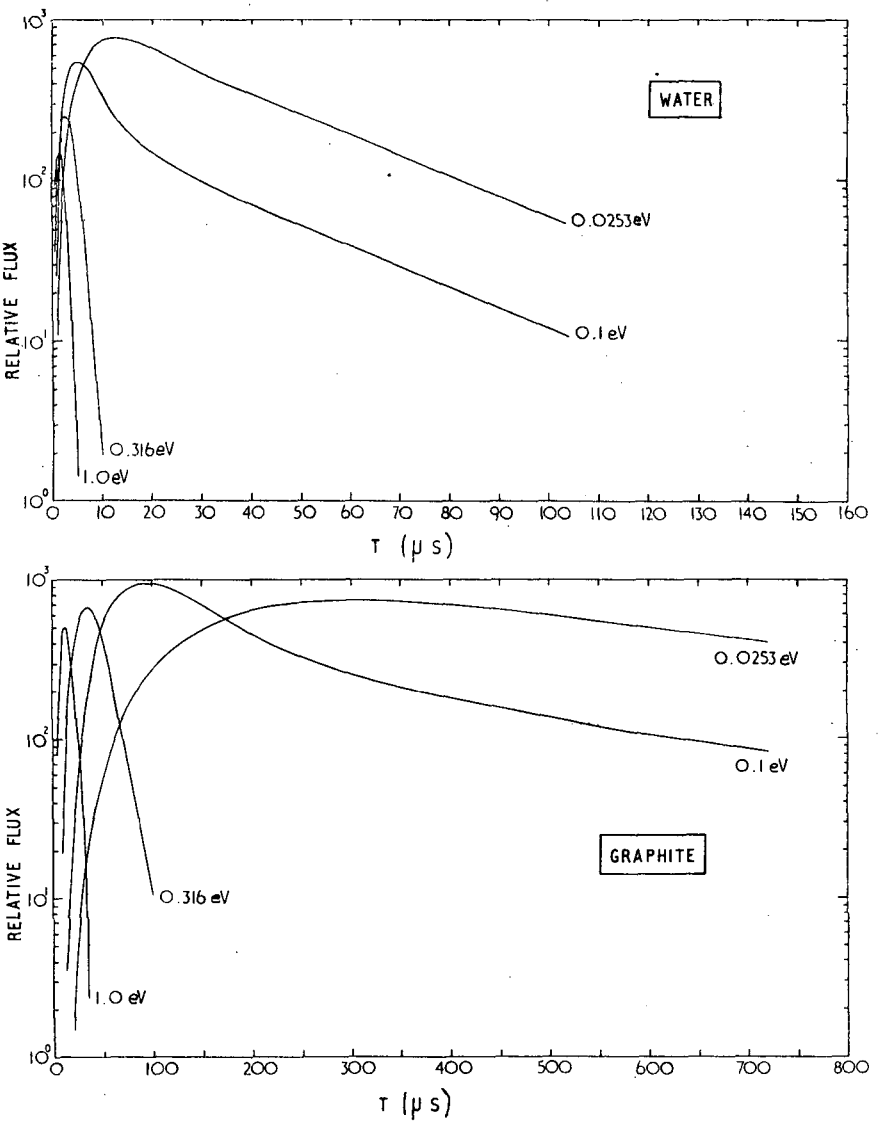

Fig. 1

Calculated neutron pulse shapes

its source replaced by ϕ_0/v_1, where ϕ_0 is itself a solution of the steady state equation.

Finally the mean time of emission is given by

$$\bar{t}(E) = \phi_1(E)/\phi_0(E) \tag{4}$$

If Eq. (1) is multiplied by t^2 and integrated, it is possible to obtain $\bar{t}^{-2}$ in a similar manner. Although this method of correction presupposes some knowledge of $\Sigma(E' \rightarrow E)$, in practice the correction is relatively small and any plausible model is adequate to give $\Sigma(E' \rightarrow E)$ for this purpose.

If the pulsed source method is to be used for measurements in a multiplying lattice the foregoing analysis of the relaxation time is no longer true. Now the time dependence of the fast source is tied to that of the thermal neutrons and it is correct to say that all neutrons die away with approximately the same relaxation time, which is equal to the product of the multiplication factor and the neutron lifetime in the system.

In general this leads to a considerable increase of lifetimes for multiplying systems over purely absorbing ones, and the method has, for this reason, been applied much less to measurement of the spectra for absorbing systems, a chopper and DC source being preferred. However in the cases where a pulsed source measurement is possible (usually water-moderated systems) it has the considerable advantage over steady methods of reducing the overall activation of the fuel, thus permitting higher peak fluxes. An interesting extension in this field has recently been described by SLOVACEK et al. [14] who excited a lattice with a pulsed source and measured the asymptotic spectrum set up using a synchronized chopper. By measuring the spectrum at a sufficiently long time after the pulse it was certain that the spatial distribution corresponded to a fundamental mode and relatively simple theory could be used in the interpretation. The spectrum obtained in this way is the same as that which would be obtained from a steady state measurement on the same system with the addition of an absorber whose macroscopic cross-section is reduced by λ/v, where λ is the asymptotic decay constant.

Figure 2 is a diagram of the usual experimental arrangement. Typically the flight path will be from 10 to 60 m long, according to the experiment, and the detector may consist of a bank of BF_3 counters having a cross-sectional area of 1000 cm^2 and an efficiency $\sim 50\%$ at a neutron velocity of 2200 m/s. The method has also been used for fast neutrons with flight paths up to 300 m long using a variety of detectors (B^{10} absorber plus gamma detector, plastic scintillator, lithium-loaded glass scintillator). In all cases a vital part of the experiment is the determination of the curve for counter sensitivity versus energy. It is rarely adequate to calculate this from the geometry of the counters and the known cross-sections.

(b) The system can be irradiated by the pulsed source and a chopper used to make the time-of-flight experiment.

The chopper is arranged to run so that all time intervals between source pulse and chopper burst occur with equal probability, under which conditions the experiment is equivalent to a spectrum measurement using a steady source and chopper. This method has been used by BEYSTER et al. [15]

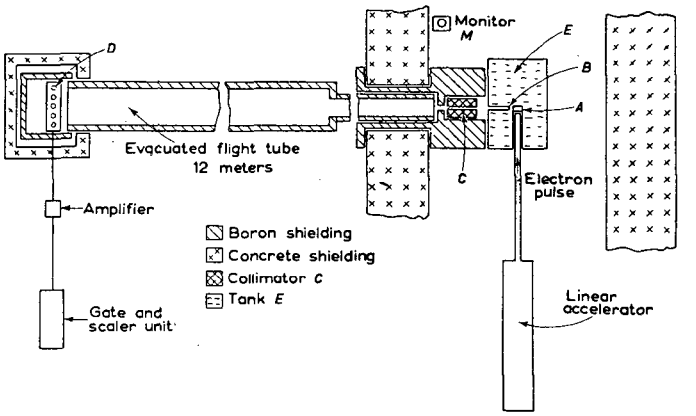

Fig. 2

Experimental arrangement

to measure spectra in systems whose relaxation time prevented the use of method (a). It appears to have no particular advantage over the use of a steady source to drive the assembly

(c) A combination of pulsed source and chopper is used to measure spectra at a definite time after the introduction of the source pulse.

This method has been used by BARNARD in [16], NICHOLSON in [17] and WYDLER in [18] for the determination of the time dependence of the spectrum, and by BECKURTS [19] and SLOVACEK in [14] for the measurement of asymptotic spectra. Two procedures have been described for the measurement of time-dependent spectra. Barnard synchronized the chopper and the accelerator and measured spectra referred to the chopper position at definite times after the source pulse. NICHOLSON and POOLE [20] have described a method in which the chopper and accelerator are run asynchronously and making use of a two-dimensional analyser the source-to-chopper burst delay is recorded separately for each cycle. This procedure gives very detailed information which has considerable advantage when calculating spectra at the beam origin from the measured spectra which are referred to the chopper position. It also has the advantage of eliminating the necessity for synchronizing equipment and ensuring that all spectra are correctly normalized together without the need for separate monitors.

3. EXTRACTION OF A NEUTRON BEAM

The extraction of a representative neutron beam is common to all time-of-flight spectrum measurements and it is important that it is done in such a way that the spectrum in the beam is simply related to the spectrum in the system under investigation. Differences can occur in a number of ways.

(a) The opening of a hole into the system removes material and this may alter the spectrum existing at the point of observation. Except in systems where the effect of heterogeneity is marked (e.g. close-packed water lattices)

it has been shown possible to use a probe tube as large as 5 cm in diameter in both water and graphite systems without distorting the spectrum at the point of observation*.

(b) If the probe tube passes through regions of widely differing spectra (e.g. perpendicular to the slabs in a slab lattice) then streaming down the probe tube can cause changes in the spectra at the point of observation. If the spectrum change is rapid, as e.g. near the surface of fuel, then this effect can be serious for much smaller tube sizes than the 5 cm mentioned above.

(c) Flux gradients can affect the beam spectrum. It must be remembered that the spectrum of the beam from a re-entrant tube is that of the directed flux in the direction of the flight tube. Only in the absence of flux gradients is this the same as the scalar flux spectrum. For cases in which diffusion theory applies, these quantities are simply related by

$$N(E) \alpha \phi(E) (1 + \lambda_{tr} \nabla \phi \cdot \Omega),$$

where N(E) is the directed flux in direction Ω, (E) the scalar flux and λ_{tr} the transport mean free path. In circumstances for which diffusion theory is not valid then it is essential to interpret the measurements by a full transport theory calculation designed specifically to give the directed flux along the flight tube.

(d) An alternative method of extracting a beam is to open a hole right through the assembly and produce the beam by a scatterer located in this tube [21, 22]. This technique provides a beam whose spectrum is proportional to the scalar flux spectrum (i) if the scatterer has negligible capture cross-section and a scattering cross-section constant with energy, (ii) if the scattering is isotropic in angle, (iii) if inelastic scattering can be neglected.

However most materials are crystalline and, in an anisotropic flux the effect of Bragg scattering will be to distort the spectrum. BEYSTER [22] has used zirconium as a scatterer but disregards all data below 0.01 eV, while JOHANNSON in his most recent experiments [23] attempted to avoid the difficulty by using liquid lead.

(e) The minimum size of probe tube required is dictated by the available experimental conditions (e.g. source strength, energy resolution). Where a beam is being extracted from a fuel rod (e.g. Zenith reactor experiments [24]) then it is important to remember that the spectrum obtained will be the average over the area viewed by the collimator, and will not necessarily correspond to the spectrum at any particular point.

4. NEUTRON DETECTORS

4.1. Thermal systems

Generally speaking the measurement of a thermal neutron spectrum does not set very stringent conditions on the performance of the neutron detector. Boron trifluoride proportional counters, because of their relative simplicity,

* This is not correct for energies near to the Bragg cut-off.

have been widely used. By the use of enriched BF_3 as filling gas it is easily possible to obtain efficiencies greater than 50% over an area 30 cm × 30 cm. The thickness required (~12 cm) is usually negligible compared to the flight path length which has to be large to contend with the long relaxation times of the pulsed systems. A particular advantage when using a Linac is that the proportional counter is less sensitive to X-rays than is the usual scintillation detector (e.g. lithium-loaded glass). A typical curve of sensitivity versus energy is shown in Fig. 3.

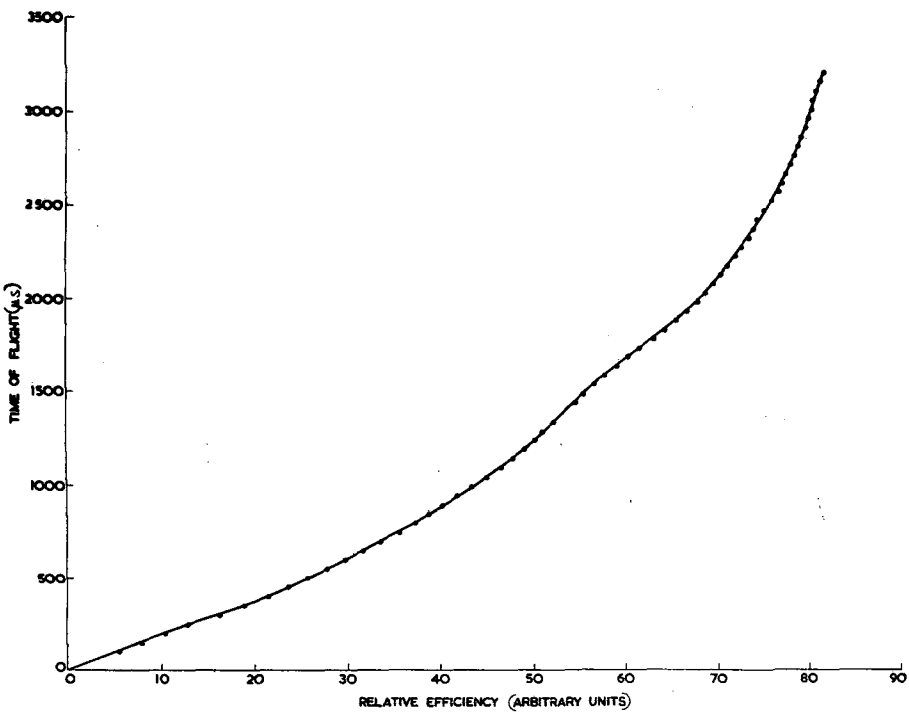

Fig. 3

Efficiency of BF_3 counters

5. EXPERIMENTS TO TEST THE SCATTERING LAW

5.1. *Scattering laws concerned*

It has been shown by many authors [26] that the scattering properties of a crystalline moderator can be derived from the spectrum of normal modes of vibration of the system $\rho(\beta)$ and that a formally similar quantity can be defined for a liquid. Scattering laws proposed for the moderators differ in the form of $\rho(\beta)$ assumed and in the method used to include the effects of coherent scattering when this takes place (and to a less extent in the accuracy of the approximation used in calculating the scattering cross-sections from $\rho(\beta)$). The real form of $\rho(\beta)$ can be complex, and it is often convenient to use simplified forms for which some of the integrations involved

can be carried out explicitly. It is therefore of considerable practical interest to see how far reactor properties are sensitive to the fine details of $\rho(\beta)$. This subject has already been extensively discussed by McDOUGALL [27] and by PARKS in [1] for the case of graphite reactors.

5.1.1. Water

Scattering laws used have been based on the monatomic gas model in which $\rho(\beta)$ becomes a δ-function at the origin, on the Nelkin model in which $\rho(\beta)$ contains four δ-functions (one at the origin to represent diffusive motion, one at 0.06 eV to represent the hindered rotations of the water molecule, and two at 0.205 eV and ~0.48 eV to take account of molecular vibrations) and on the Haywood model where β is between 0 and 10 and $\rho(\beta)$ is a continuous function derived in part from experiment, with which is combined a δ-function at 0.405 eV. Figure 4 shows $\rho(\beta)$ for the Haywood model, the

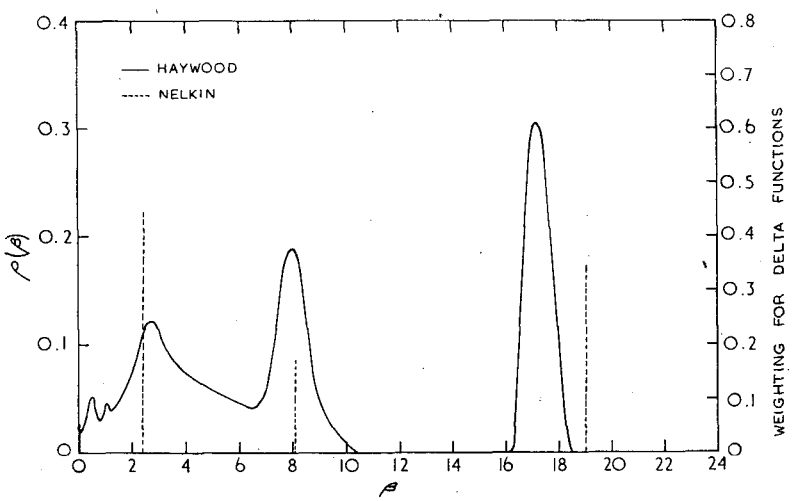

Fig. 4

$\rho(\beta)$ for H_2O at 295°K

positions of the δ-functions used in the Nelkin model being marked in. Two other models, the "width" model in which $\rho(\beta)$ is replaced by a Gaussian curve centred on the origin, and a model in which the Gaussian is displaced from the origin and a δ-function added at high energies have also been proposed [29, 39]. Although the former has the advantage that cross-sections can be explicitly calculated, because of the omission of all high energy vibrations, it does not reproduce the spectrum well.

5.1.2. Heavy water

A model has been proposed by Honeck which is similar to the Nelkin model, $\rho(\beta)$ being represented again by four δ-functions. A continuous $\rho(\beta)$ has been given by HAYWOOD in [6] and a preliminary form of this is illustrated in Fig. 5. A feature in which the treatment of the scattering from D_2O

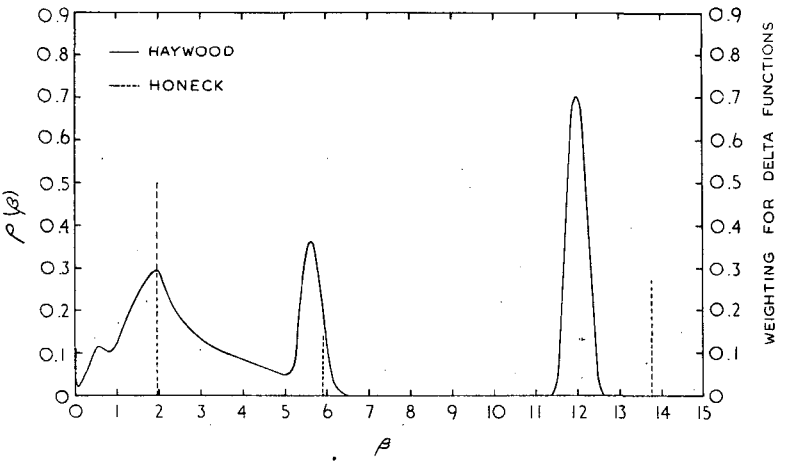

Fig. 5

$\rho(\beta)$ for D_2O at 295°K

differs significantly from that of H_2O is that in the case of D_2O it becomes necessary to account much more carefully for scattering from the oxygen.

An earlier model for D_2O proposed by BROWN and St. JOHN [4] was based on the concept of a mass tensor and for D_2O this is equivalent to an effective mass of 3.6 for the deuterium atom.

5.1.3. Graphite

Scattering laws used have been based either on a theoretical frequency distribution derived by YOSHIMARI and KITANO [36] or on a much simplified distribution proposed by EGELSTAFF in [2]. These are reproduced in Figs. 6 and 7. A somewhat different simplification, also proposed by EGELSTAFF [30], is shown in Fig. 8, but comparisons between this and experiment are still incomplete.

5.1.4. Beryllium and beryllium oxide

YOUNG in [33] has calculated $\rho(\beta)$ for crystalline beryllium using a central force model proposed by SCHMUNK et al. [34] including up to fifth nearest-neighbour interactions. Figure 9 shows the frequency distribution obtained. On the same figure is given a $\rho(\beta)$ derived by SINCLAIR [35] from measurements of the double differential scattering cross-section for polycrystalline beryllium.

5.1.5. Zirconium hydride

The scattering properties of zirconium hydride are of considerable interest because the structure is such that the hydrogen atoms are located in an almost isotropic potential well created by the heavy zirconium atoms and their normal modes of vibration should closely approximate those of the

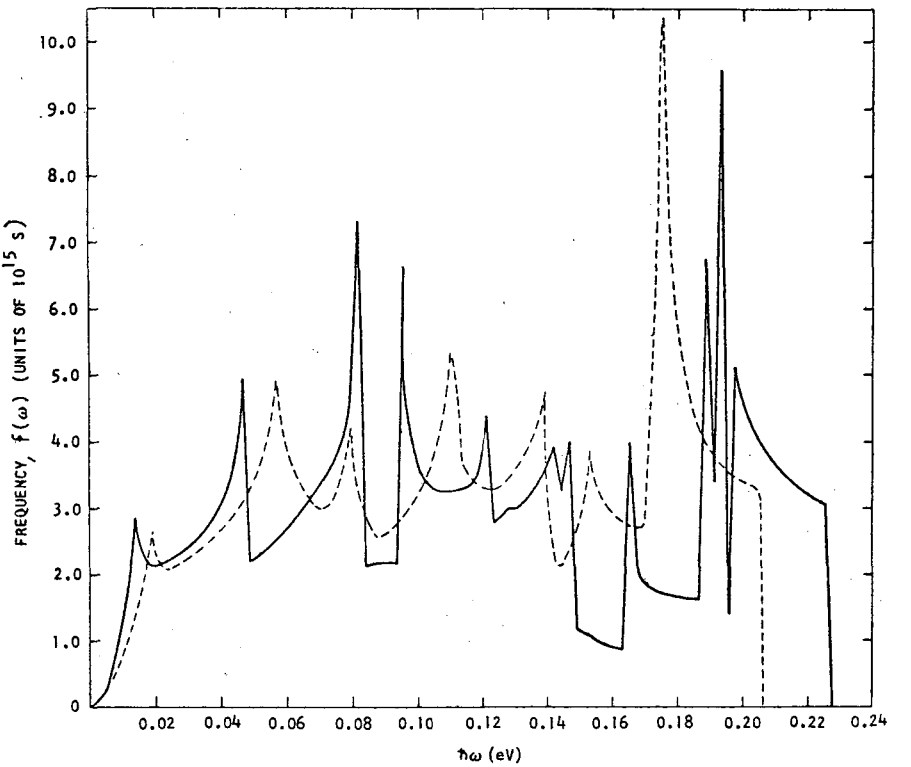

Fig. 6

Frequency spectra of graphite

----- Frequency spectrum from root sampling

——— Frequency spectrum from Yoshimori and Kitano

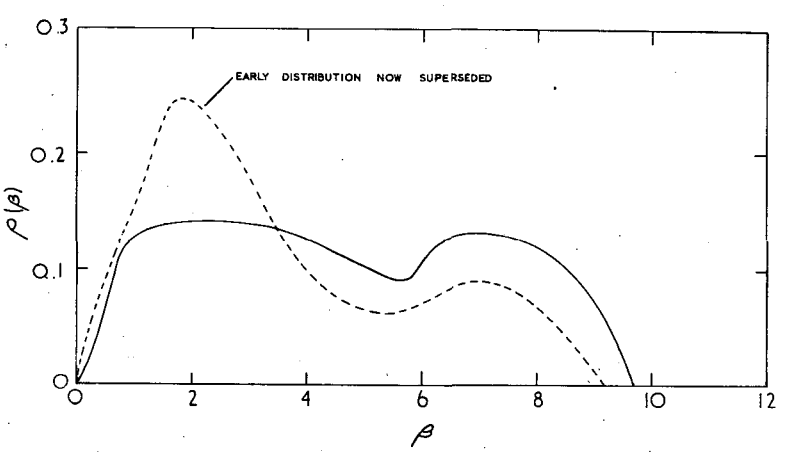

Fig. 7

ρ(β) for graphite at 295°K

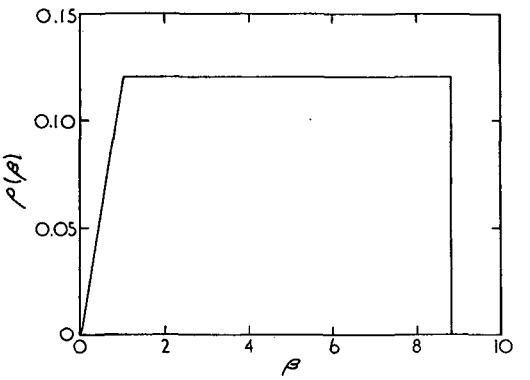

Fig. 8

Simplified $\rho(\beta)$ for graphite at 295°K

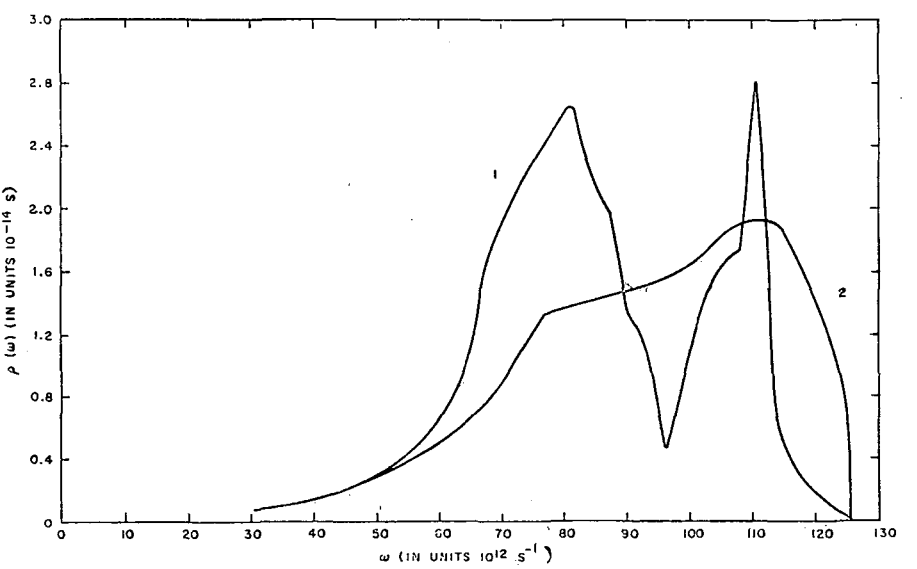

Fig. 9

Frequency spectra of beryllium

1. Obtained theoretically from a central force model
2. Obtained by Sinclair using the extrapolation procedure on $S(\alpha,\beta)$

simple Einstein oscillator, a situation very remote from the Debye spectrum of normal modes. The form of $\rho(\beta)$ is thus a single optical peak at 0.137 eV plus an acoustic branch (corresponding to "in phase" motion of the Zr and H atoms) with a Debye cut-off at 0.02 eV. Various detailed models have been proposed [9], the most recent discussion being given by BEYSTER et al. [37] who conclude that the model proposed by Young is best able to predict the spectrum in ZrH.

5.1.6. Polyethylene

The scattering from polyethylene is of practical interest because it is often used to "mock-up" water in zero energy reactor assemblies and it is important to know how much the substitution of polyethylene for water in the assembly will differ from that of the reactor due to the differences in the scattering laws. GOLDMAN and FEDERIGHI [8] have proposed a $\rho(\beta)$ consisting of a number of discrete frequencies representing a freely translating CH_2 molecule with vibrations corresponding to stretching and bending modes and with the rotational freedom strongly hindered. This model suffers from the same disadvantage as the Nelkin model for H_2O, namely it is not possible to choose a set of parameters which will at the same time reproduce accurately the diffusion coefficient, spectra and the total cross-section. PARKS [39] has therefore prepared a model based partly on the vibrational spectrum proposed by WUNDERLICH [40] and using the SUMMIT code to calculate the scattering kernel. Results obtained from this model are compared with experiment in a later section.

5.1.7. Benzene

A scattering law for benzene has been calculated on the basis of the frequency distribution of CRAWFORD and MILLER [41] shown in Fig. 10. Due to the similarity in structure this scattering law will go a long way towards describing thermalization in the polyphenyls.

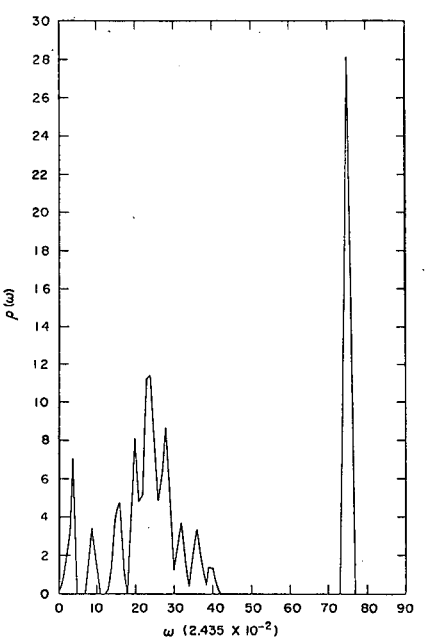

Fig. 10

Frequency distribution of molecular vibrations
in benzene from measurements by CRAWFORD and MILLER [41]

5.2. Spectra in homogeneously poisoned moderators

The spectrum of neutrons in an infinite homogeneously poisoned moderator with a uniform fast source is given by the neutron balance equation

$$0 = -[\Sigma_a(E) + \Sigma_s(E)]\,\phi(E) + \int_0^\infty \Sigma(E' \to E)\,\phi(E')\,dE' + S(E) \qquad (5)$$

in which $\Sigma_a(E)$ and $\Sigma_s(E)$ are the macroscopic absorption and scattering cross-sections respectively, $\Sigma(E' \to E)$ is the energy transfer kernel (i.e. the P_0 component of the scattering cross-section), $\phi(E)$ is the neutron flux spectrum and $S(E)$ the neutron source spectrum. For zero absorption (and zero source) detailed balance forces $\phi(E)$ into a Maxwellian distribution irrespective of any other properties of $\Sigma(E' \to E)$. Poisoning (i.e. non-zero Σ_a) causes distortion of the Maxwellian and the presence of a source adds an approximately $1/E$ slowing-down distribution to the spectrum which now depends quite strongly on the model used to calculate $\Sigma(E' \to E)$. Eventually the addition of excessive amounts of poison removes most of the thermal group and again little information can be obtained about $\Sigma(E' \to E)$. Spectra in homogeneously poisoned moderators have been measured by a number of authors [42 to 47, 51 to 54] and compared with spectra calculated from the scattering laws listed in section 5.1. In nearly all cases the spectra have been measured by time-of-flight using the pulsed source method. In practice the experimental condition deviated more or less from the ideal conditions of an infinite medium with a uniformly distributed fast source, and some procedure must be found to deal with leakage from the moderator and with the presence of a point source. Two cases may be distinguished. For media in which the diffusion length is much smaller than the slowing-down length, then at distances sufficiently far from the source the spectrum ceases to be strongly position sensitive and is given by the equation

$$0 = -\left[\Sigma_a(E) + \Sigma_s(E) - D(E)\,\frac{\nabla^2\phi}{\phi}\right]\phi(E) + \int_0^\infty \Sigma(E' \to E)\,\phi(E')\,dE' + S(E), \qquad (6)$$

where the quantity $\nabla^2\phi/\phi$ may by assumed to be independent of energy. The absolute value of $\phi(E)$ now falls off with distance from the source in the same way as the flux of fast neutrons. Under these circumstances it is sufficient to determine $\nabla^2\phi/\phi$ by making a flux scan using foil detectors (Mn or Au are often used). Several such scans should be made with different detectors and the assumption can only be accepted as valid if the same value for $\nabla^2\phi/\phi$ is obtained from each. PARKS (see [13]) in a more detailed diffusion theory treatment has shown that there is a small (and calculable) correction to the spectrum derived in this way, proportional to $(L_1/L_2)^4$, where L_1 and L_2 are the diffusion and slowing-down lengths respectively.

If, however, the diffusion length is not small compared to the slowing-down length then spectra must be obtained from a transport theory calculation capable of yielding the directed flux at the point of measurement for the detailed geometry and source condition employed. Typically slab geometry

DSN codes have been used for this purpose. Frequently the source is described in terms of a measured distribution of slowing-down neutrons at, for example, the indium resonance energy. This situation commonly arises for weakly-poisoned graphite or heavy water moderators. (Even for pure water the diffusion length is somewhat less than the slowing-down length.) A procedure which has been considerably used is to measure the spatial distribution of slowing-down neutrons at the indium resonance energy and use this to determine the source for a DSN calculation.

Most pulsed source measurements concern systems which are sufficiently poisoned to ensure that the diffusion length is small. There are three reasons for this choice of conditions, namely (i) it is desirable to keep the thermal neutron relaxation time as short as possible to minimize corrections to the time-of-flight experiment; (ii) the spectrum is most sensitive to the scattering law at fairly high poison concentrations; and (iii) it is simplest to allow for spatial dependence in highly poisoned systems.

5.2.1. Spectra in poisoned water

Spectra in poisoned water have been measured for a variety of poisons [42, 43, 44, 45, 46, 47] and some of the results are shown in Figs. 11 and 12. The earliest treatment of thermalization in water was given by WIGNER and WILKINS [48] who showed that for perfect gas scattering the integral neutron balance equation could be reduced to a second-order differential equation. Spectra were extensively calculated on this basis by Amster using

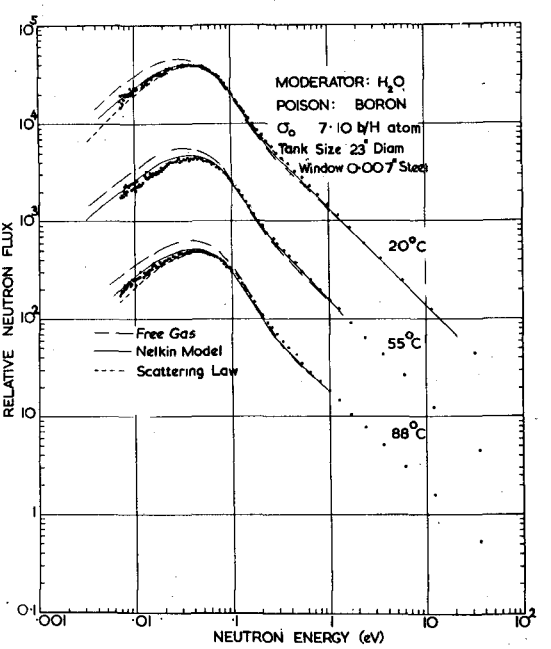

Fig. 11

Experimental and calculated spectra for highly poisoned water at various temperatures

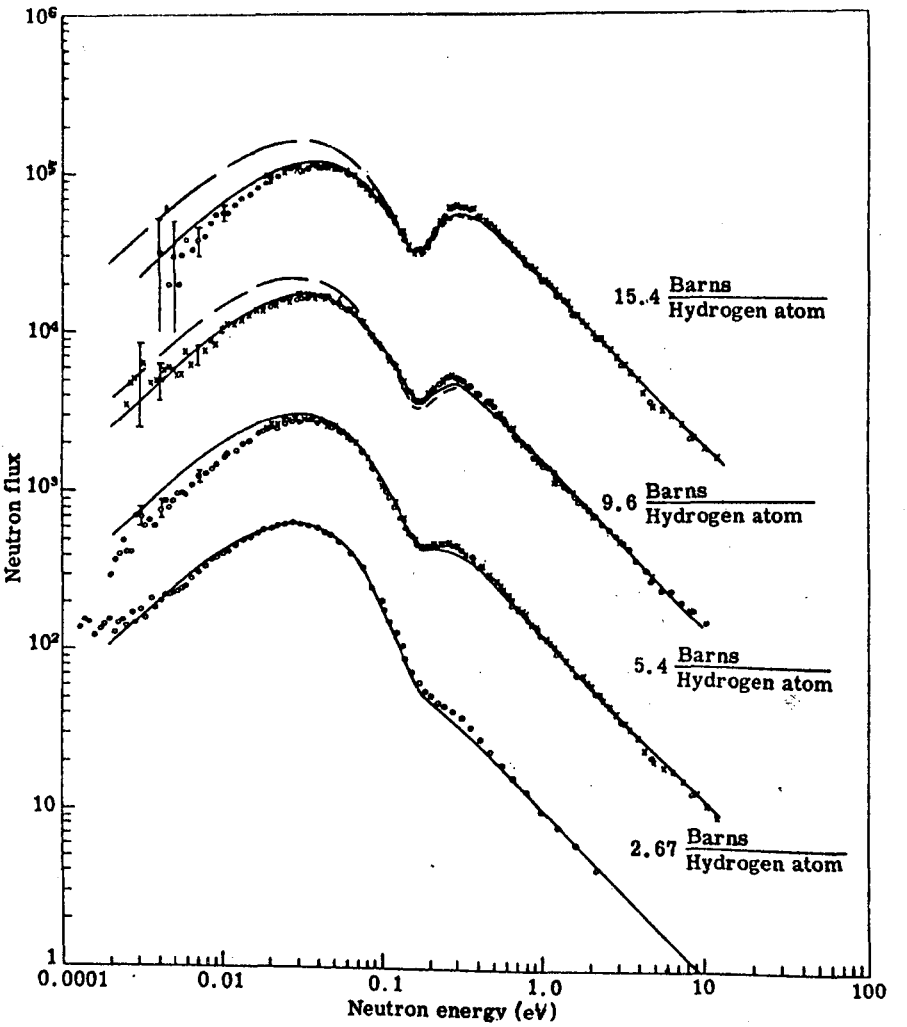

Fig. 12

Neutron spectra in water poisoned with cadmium sulphate

——— Bound hydrogen calculation of neutron spectrum
----- Free hydrogen calculation of neutron spectrum

the SOFOCATE and KATE codes, and perfect gas thermalization has been incorporated into a number of reactor codes. The most extensively used treatment of the chemical binding in water is that of Nelkin (see section 5.1) and spectra calculated using the Nelkin model are composed with measured spectra and with perfect gas calculations in Figs. 11 and 12. It will be seen that the Nelkin model is a considerable improvement over the perfect gas, but discrepancies still exist at low energies where too many neutrons are predicted and in the energy region around 0.1 to 0.3 eV. Attempts have been made to improve the kernel by altering the relative weights of the

δ-functions in the frequency distributions, but such attempts only lead to failure to predict the total cross-section. It is concluded that although the Nelkin model is adequate for many reactor calculations, it cannot yield both accurate spectra and accurate total cross-sections. Recently YOUNG in [49] has recomputed the Nelkin kernel taking into account the anisotropy of the molecular vibrations, and Haywood has proposed a kernel in which the hindered rotations and low-energy vibrations are represented by a continuous distribution. Spectra calculated from the Haywood kernel are given in Fig. 13. It will be seen that the Haywood kernel in particular appears capable of reproducing poisoned water spectra very accurately, although comparisons over a wider range than is at present available are needed to confirm this.

5.2.2. Spectra in poisoned heavy water

Poisoned heavy water has been investigated by NEILL et al. [50] and by SINCLAIR in [31] for both 1/v and resonant poisons. Figure 14 shows some representative spectra. Again the effect of chemical binding is shown by the lack of agreement with perfect gas calculations. An effective mass of 3.5 for the deuterium atom as proposed by BROWN and St. JOHN [4] gives somewhat better agreement over the thermal region for the boron-poisoned cases at the expense of misrepresenting the high-energy tail of the spectrum. Spectra calculated from HONECK's [5] modification to the Nelkin kernel agree well with measured spectra as can be seen from Figs. 14 and 15. The use of diffusion theory to calculate spectra in the way described in section 5.2 is only possible for the most highly poisoned cases, and it is usual to calculate spectra in lightly poisoned D_2O using a DSN code.

5.2.3. Spectra in poisoned graphite

Graphite, being a solid moderator, poses the problem of how to produce a uniformly poisoned assembly. Both PARKS et al. [13] and GAYTHER [52] have taken the viewpoint that it is better to use a closely defined slab geometry and deal explicitly with the heterogeneity introduced, than to attempt to make a homogeneous system in which an ill-defined poison grain size causes difficulty in estimating the self-shielding of the poison. In both cases layers of poison and graphite were interleaved, the thickness of the graphite layers being less than a mean free path (2.5 cm). The experiments described in [13] were carried out for one 1/v poison calculation in an assembly at different temperatures, while Gayther used different 1/v and resonant poison concentrations at room temperature. Results are shown in Figs. 16, 17 and 18, which also give theoretical spectra calculated using the Parks' kernel and those from a preliminary version of the EG2H kernel. The discrepancies observed by Gayther have not yet been fully explained. Although the kernel used to calculate the spectra was a preliminary one, it has been shown that spectra calculated on a later model given by Egelstaff (see Appendix to Ref. [1]) differ little from the calculated spectra shown here. It should also be noted that relatively good agreement is obtained with spectra in graphite poisoned with a 1/v absorber and the discrepancies only become serious when the more stringent test of a resonant poison is used. No dis-

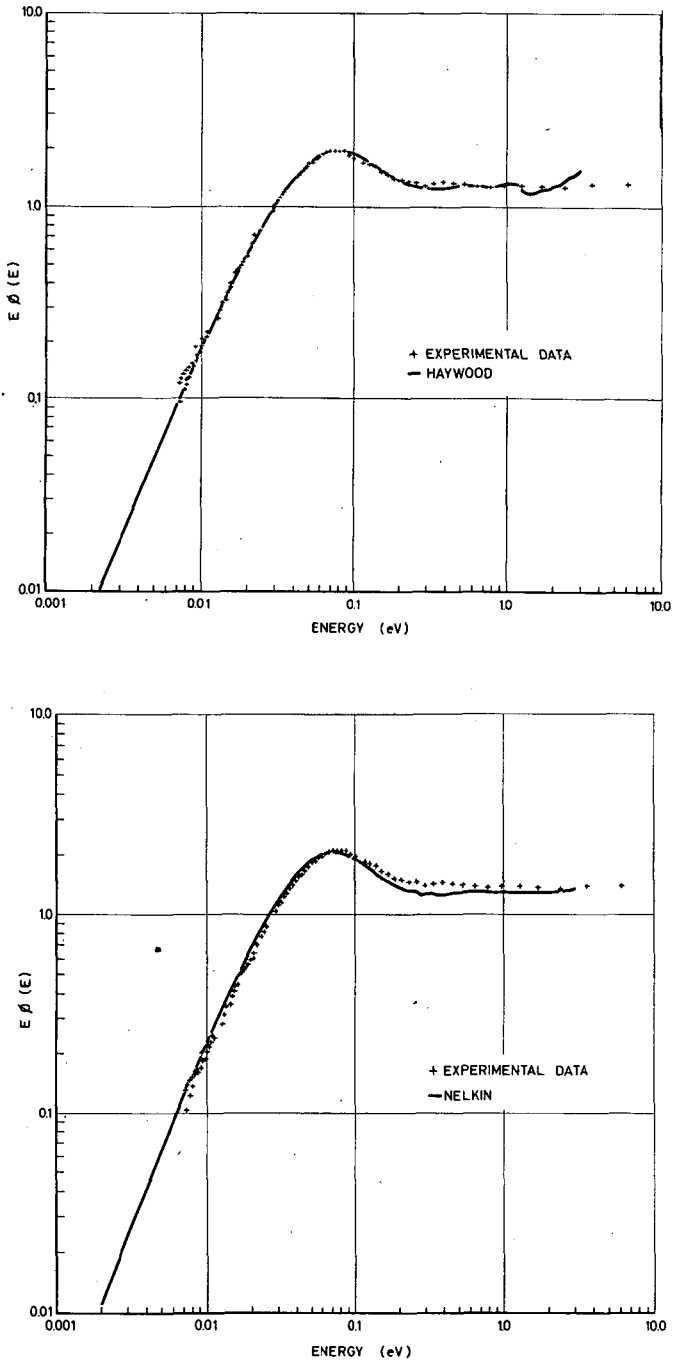

Fig. 13

Comparison between measured and calculated spectra in boron-poisoned light water (Poole and Sinclair)

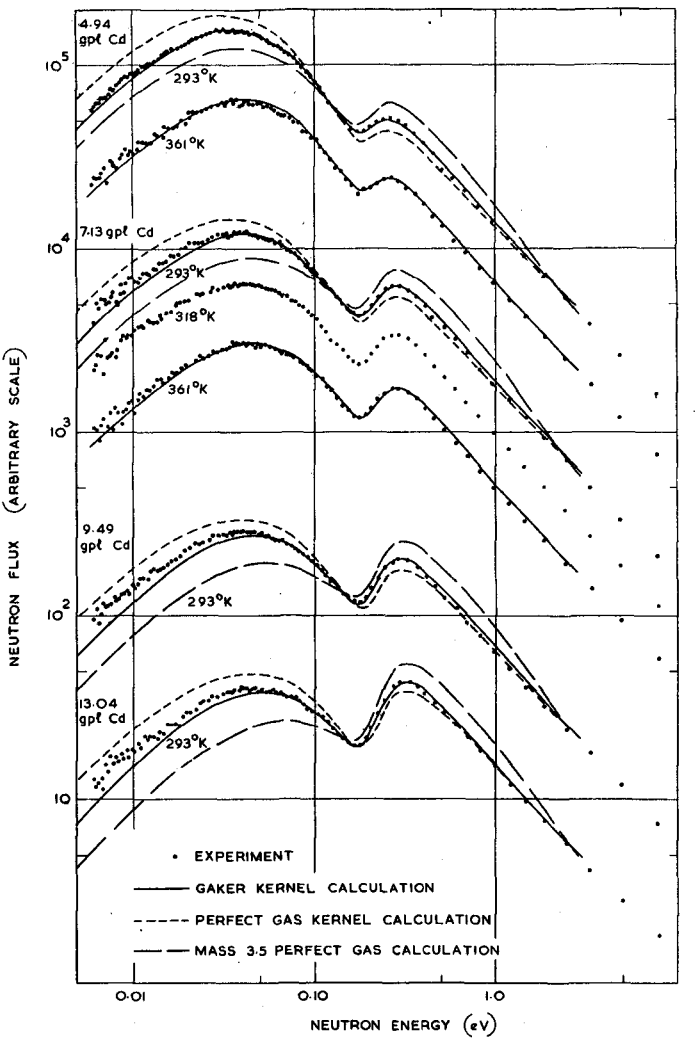

Fig. 14

Neutron spectra in heavy water poisoned by cadmium
(Measurements of Sinclair)

crepancy is observed by BEYSTER [32] between measured spectra and spectra calculated using the Parks' kernel for the case of graphite poisoned by samarium (Fig. 19). It is clear that the use of the Parks' kernel allows calculation of spectra in homogeneous systems with acceptable accuracy. What is not yet clear is whether this degree of complication is required or whether one of the simplified models will be adequate.

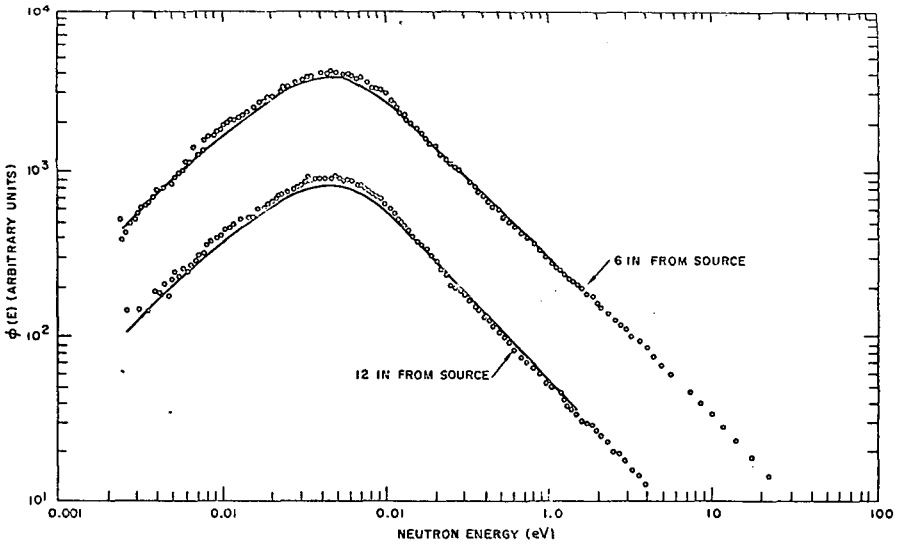

Fig. 15

90° angular flux in D_2O poisoned to 2.1 b/D atom

(Poisoned by boron aluminium plates at 1/8 in spacing
in a 18 in × 18 in × 8 in tank)

O Experimental data
—— GAPLSN calculations

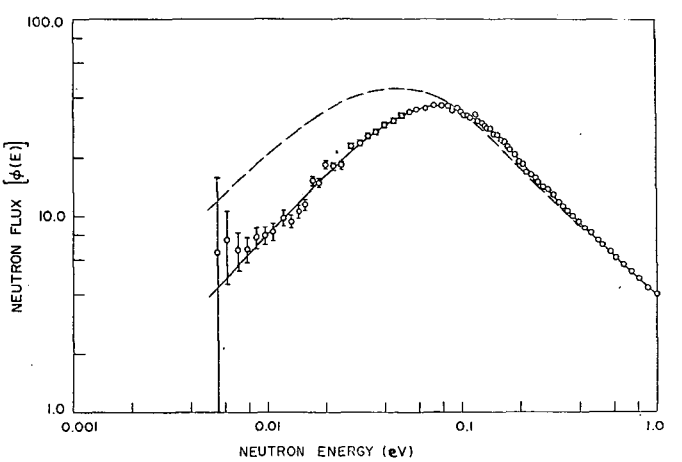

Fig. 16

Neutron flux versus neutron energy at 323°K

—— Crystal, 323°K
----- Free gas, 323°K
O Experimental, 323°K

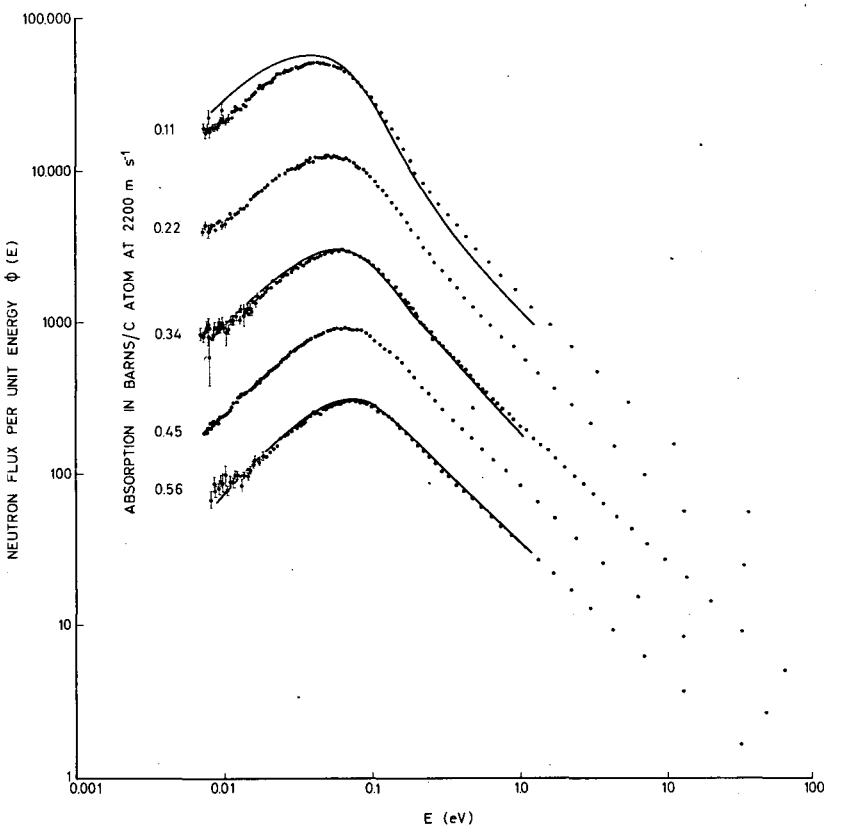

Fig. 17

Spectra in the copper-poisoned graphite assemblies at 290°K

● Experiment
—— Theory

5.2.4. Spectra in poisoned polyethylene

Spectra have been measured by YOUNG et al. [53] and compared with calculations made using both the GOLDMAN and FEDERIGHI [8] kernel and the KOPPEL and YOUNG[49] kernel. The results are shown in Fig. 20. Even though the frequency spectrum is approximated by four δ-functions, a simplification that has less physical basis than in the case of water, the agreement between measured and calculated spectra is excellent, particularly for the Koppel-Young kernel.

5.2.5. Spectra in poisoned zirconium hydride

As has already been mentioned, the behaviour of zirconium hydride is of great theoretical interest because of the belief that it will behave very similarly to a simple Einstein oscillator. From the point of view of reactor

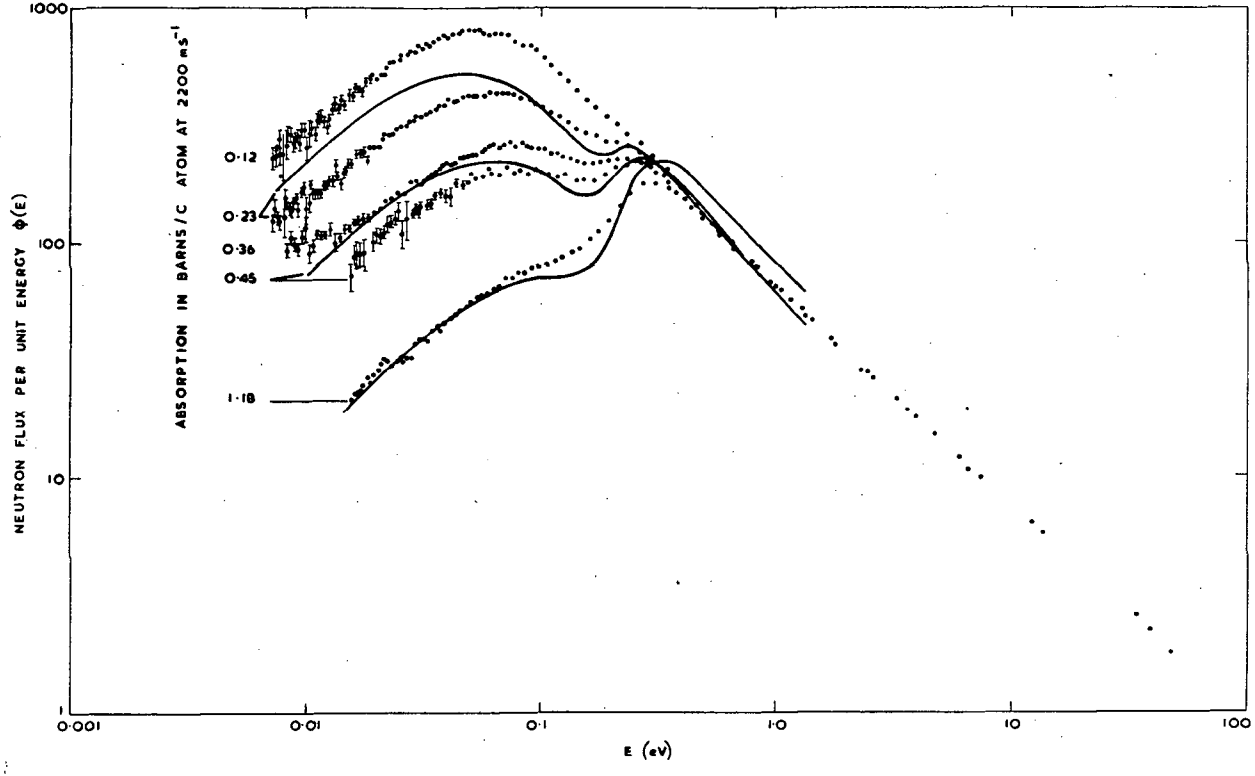

Fig. 18

Spectra in the cadmium-poisoned graphite assemblies at 290°K

● Experiment
—— Theory

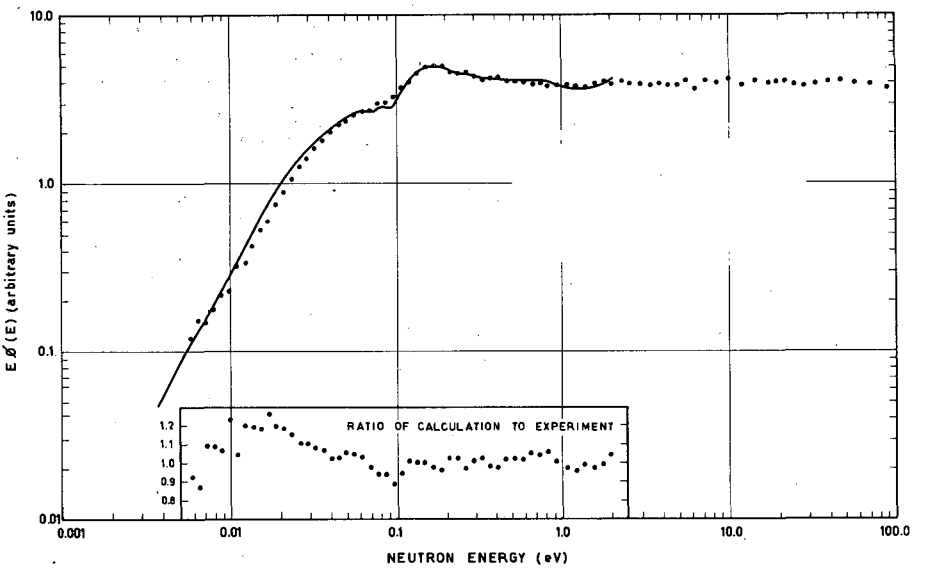

Fig. 19

90° angular neutron spectrum in samarium-poisoned graphite at 80°K

● Experiment (7/20/63; T6, T7)
—— Calculation (GAPLSN 8/20/63)

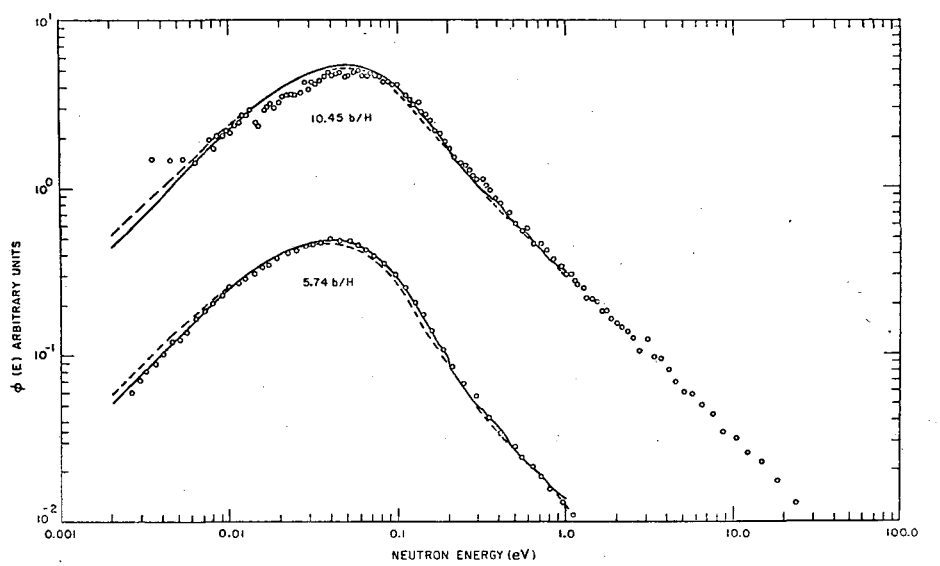

Fig. 20

Infinite-medium borated polyethylene spectra at room temperature

O Experiment
—— Summit (Parks)
----- GAKER (Goldman)

physics this property of zirconium hydride leads to the possibility of building a reactor with very large negative prompt temperature coefficient and utilizing this to prevent the occurrence of power transients. Spectra in poisoned zirconium hydride have been measured [54]. The material was in the form of carefully mixed powders (zirconium hydride and boron carbide) contained

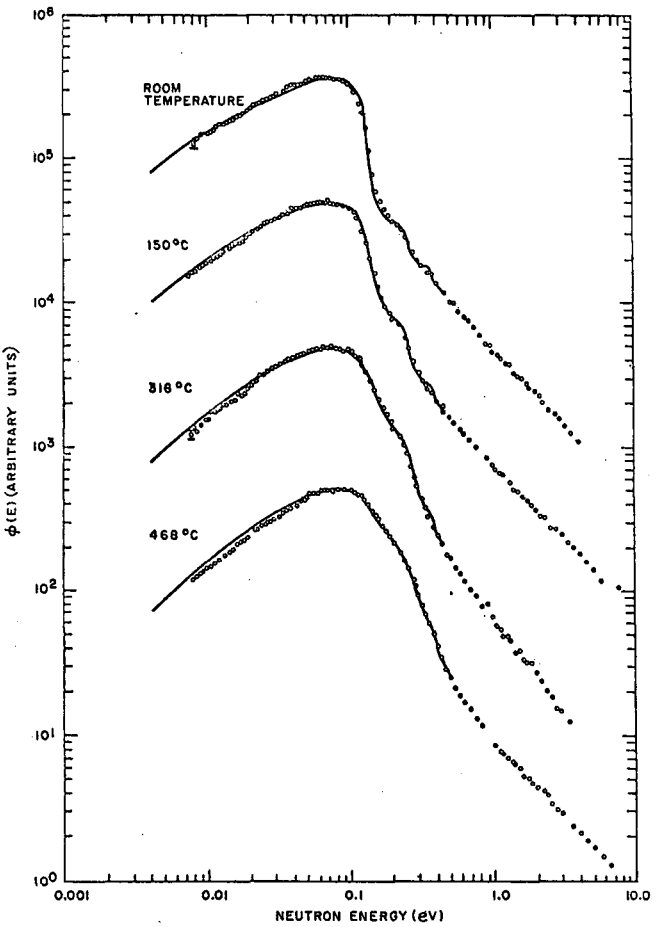

Fig. 21

Infinite-medium spectra at various temperatures in zirconium hydride poisoned to 3.4 b/H atom

O Data

—— Einstein oscillator model including acoustical transitions

in a box which could be heated to 470°C. These spectra are shown in Fig. 21, from which it is clear that the predictions of the Young model are verified. This result is in marked disagreement with predictions from the phenomenological model of MILLER et al. [55].

6. MEASUREMENT OF TIME-DEPENDENT SPECTRA

6.1. Theory

The spectrum of neutrons existing in a moderator after the injection of a pulse of fast neutrons can be obtained from the time-dependent diffusion equation

$$\frac{1}{v}\frac{\partial\phi(E,t)}{\partial t} = -\left[\Sigma_a(E)+\Sigma_s(E)-D(E)\frac{\nabla^2\phi}{\phi}\right]\phi(E,t)+\int_0^\infty \Sigma(E'\to E)\phi(E',t)dE'+S(E,t) \tag{7}$$

The spectra are sensitive to $\Sigma(E'\to E)$ and measurement of time-dependent spectra may be used as an alternative to measurement of spectra in poisoned systems to check the validity of energy transfer kernels, with the advantage in the case of solid moderators that the difficulty of obtaining uniform poisoning is avoided. It is also found that time-dependent spectra in finite systems are very sensitive to the exact form of D(E).

Equation (7) has been solved numerically by various methods. The simplest (i.e. stepping out the equation by the explicit method) appears adequate provided precautions are taken to ensure stability of the process, and a code (SPECTIM) has been written by the author to accomplish this. This code takes around 1.5 min on the IBM 7030 computer to carry out 250 time steps using 81 energy groups for the flux. McLATCHIE in Ref. [16] solves the equation by a method which in principle is more accurate; $\Sigma(E'\to E)dE'$ is first written as a square matrix. In this notation Σ_a Σ_s and D(E) are diagonal matrices, and the equation may be reduced to the form

$$\frac{\partial\phi}{\partial t} = F\phi + S \tag{8}$$

in which F is a matrix given by

$$F = v(-\Sigma_a - \Sigma_s + D B^2 + \Sigma_{inel}) \tag{9}$$

in which Σ_{inel} is the scattering kernel and is a square matrix, while Σ_a, Σ_s and D are diagonal matrices.

The solution to this equation is $\phi = e^{Ft}$ and a code has been written to exponentiate the matrix F. In the case of graphite, for 50 energy groups this code requires approximately 20 min computer time. Comparison between the output from this and from SPECTIM has revealed only a few per cent difference, which is then the usual experimental error in measuring the spectrum. For all practical purposes the simpler code can be taken as adequate.

6.2. Measurements in graphite

Time-dependent spectra in graphite have been reported by BARNARD et al. [16], by NICHOLSON and POOLE [17] and by MOSTOVOY et al. [56]

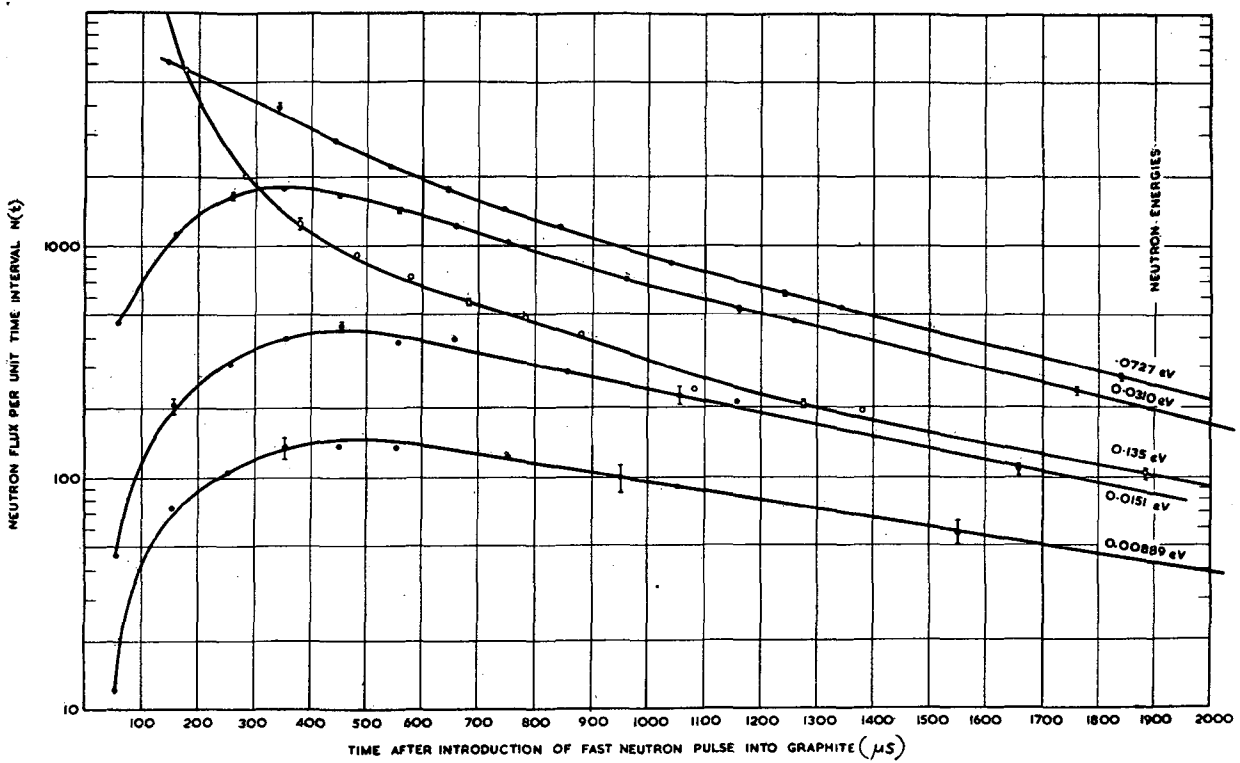

Fig. 22

Time behaviour of neutron flux for different energy groups (Barnard et al.)

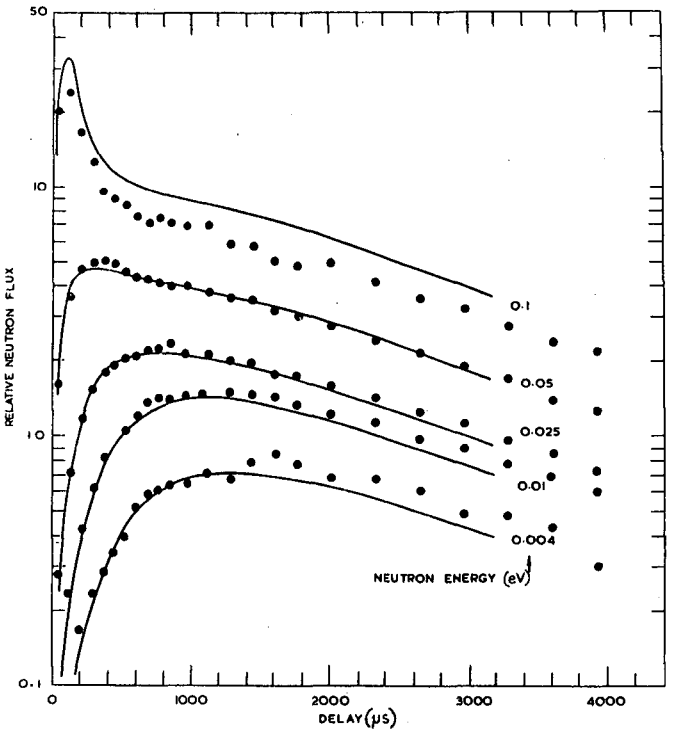

Fig. 23

Time decay curves (Nicholson and Poole)

—— Calculated

• Measured

0.1-eV neutron flux x 15

0.05-eV neutron flux x 1.5

and are shown in Figs. 22, 23 and 24. The experimental method has already been described (section 2). These spectra are compared with scattering kernels based on the work of Egelstaff et al. In the earlier work (Barnard), spectra were only measured at a few times with rather poor resolution, and the calculation was carried out using a very early scattering kernel and with a constant value for D(E). Nevertheless reasonable agreement between experiment and theory is obtained. Later work (Nicholson and Poole) has produced spectra at close time intervals, and it was found necessary to carry out the calculation taking into account the detailed behaviour of D(E) (Fig. 25) to obtain agreement between experiment and theory.

6.3. Time-dependent spectra in beryllium

Measurement of time-dependent spectra in beryllium have been reported by MOSTOVOY et al. [56] using a linear accelerator source and by FULLWOOD et al. [38] also using a Linac source. Results of Fullwood's measurements

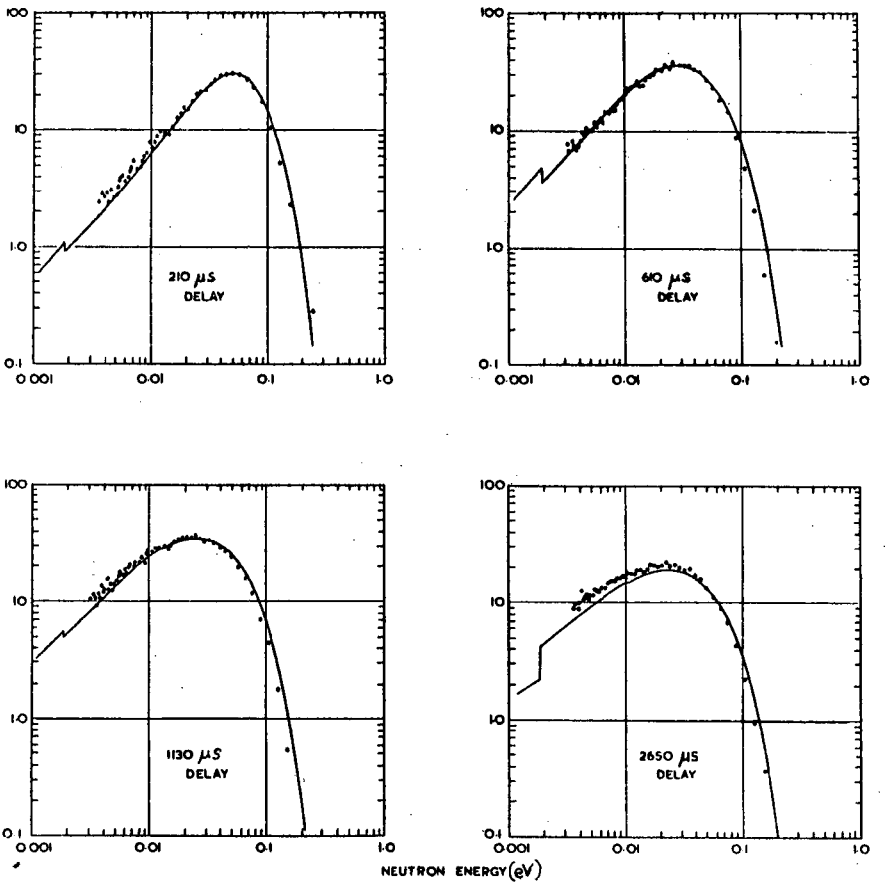

Fig. 24

A selection of neutron energy spectra

—— Calculated spectra
• Experiment

are shown in Fig. 26. No details were given of the calculations also shown in this figure.

6.4. *Asymptotic spectra in pure moderators*

The asymptotic spectrum obtained at long time in a finite moderator is given by the equation

$$0 = \left(\Sigma_a(E) + \Sigma_s(E) + D(E)B^2 - \frac{\lambda}{v} \right) \phi(E) - \int_0^\infty \Sigma(E' \to E)\phi(E')dE', \qquad (10)$$

in which λ is the asymptotic decay constant of the neutron density, i.e.

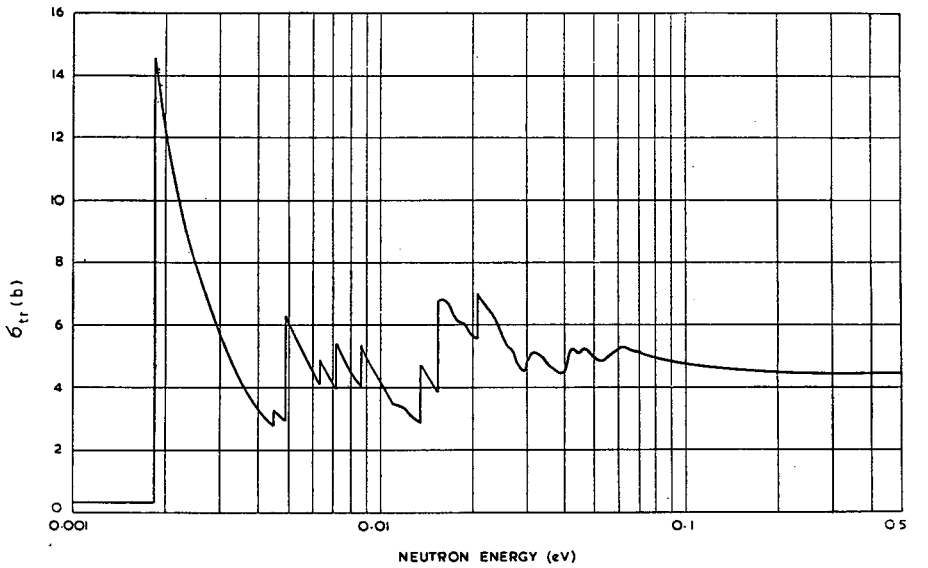

Fig. 25

Transport cross-section of graphite

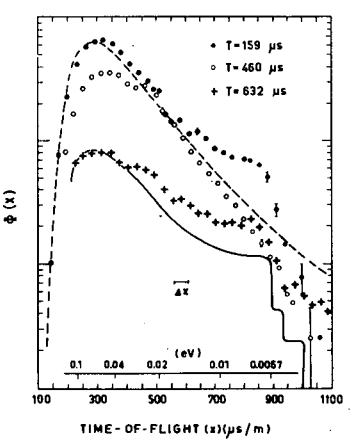

a)

Fig. 26(a)

Time-dependent neutron spectra in the centre of a parallelepiped of Be metal buckling 0.073 cm^{-2} for 30°C at times (T) after the primary burst from the linear electron accelerator. The curves are arbitrarily spaced for clarity

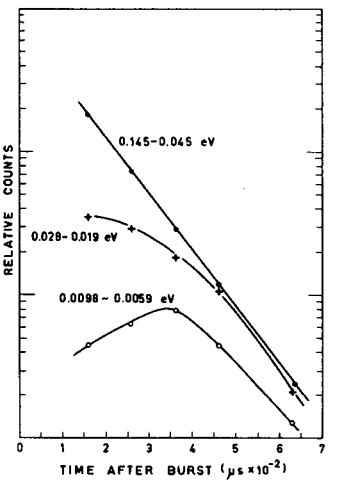

b)

Fig. 26(b)

Neutron die-away of several selected energy groups in beryllium

- Covering peaks of spectra
- \+ Covering Bragg energy 0.022 eV
- O Covering Bragg energy 0.0067 eV

$$\lambda = \frac{\int_0^\infty \phi(E)\,[\Sigma_a(E) + D(E)\,B^2]\,dE}{\int_0^\infty \frac{1}{v}\,\phi(E)\,dE} \qquad (11)$$

Such spectra are often easier to measure than the full time dependence. For example in water all thermalization effects are over in a few microseconds and the usual combined accelerator and chopper measurement becomes very difficult. However, after a few tens of microseconds the asymptotic spectrum is achieved, and BECKURTS [19] has measured this by interposing a simple rotating shutter in the neutron beam. This shutter prevented neutrons entering the flight tube for about the first 50 μs after the pulse of fast neutrons. Thus no measurements were made until the spectrum had reached its asymptotic value. Figure 27 shows the ratio of the asymptotic spectrum at the centre of a 5-cm cube of water as measured by Beckurts to a room temperature Maxwellian distribution. On the same graph is given the same quantity calculated from the perfect gas (mass 18) scattering kernel. Agreement is good below 0.08 eV, but as might be expected becomes progressively worse at higher energies.

7. MEASUREMENTS OF SPATIALLY-DEPENDENT SPECTRA

All the experiments so far described, except the asymptotic spectra of Beckurts, have been measurements in geometries intended as approxi-

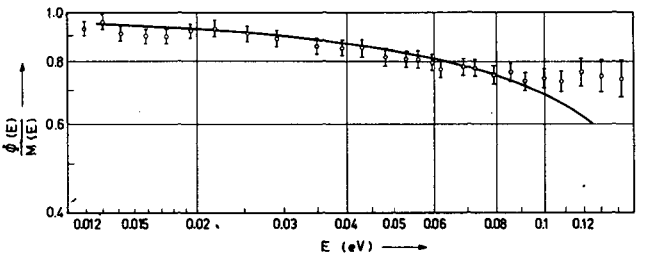

Fig. 27

Asymptotic spectrum in 5-cm cube of water plotted as a ratio to a room temperature Maxwellian (Beckurts)

mations to the infinite system, and spatial effects have only entered as correction terms. Angular dependence of the scattering is only of importance to these corrections and has been introduced through the choice of the diffusion coefficient employed. Even for the very small moderators used by Beckurts in measuring asymptotic spectra, the treatment assumes the existence of a single harmonic mode for the flux, leading to separability in space and energy. The experiments to be described now are specifically designed, firstly to test the sensitivity of the spectrum to the angular dependence of the scattering in situations where this might be expected to be important, and, secondly to check the validity of scattering models in predicting this angular dependence.

7.1. Spectra at a plane absorbing surface

One of the simplest situations in which a spatially-dependent spectrum occurs is at a plane highly absorbing surface immersed in an infinite moderator (or the spectrum at the boundary of a semi-infinite moderator). This configuration is usually referred to as the energy-dependent Milne problem. POOLE, SCHOFIELD and SINCLAIR [46] have described experiments in which the angular and spatial dependence of the thermal spectrum is investigated close to a cadmium sheet in water, and by considering the relation between the spectrum of neutrons travelling parallel and perpendicular to the surface, have demonstrated that an isotropic scattering kernel is not sufficient to describe the situation. These experiments have been extended by SINCLAIR in [31] with the same conclusion.

An extensive series of measurements has been made by Beyster et al. on the spectrum emerging from the surface of a slab of water containing dissolved boron as a poison. The geometry used is shown in Fig. 28. Attempts to reproduce the measured spectra using a 23 energy group and 82 spatial region transport theory code lead to errors of about 15%, even when P_1 terms were included in both the kernel and the source expressions. A more elaborate calculation employing P_3 terms in the kernel gave only minor improvement, but significant improvement was obtained by a proper treatment of the fast source, suggesting that the experiment as carried out was still sensitive to the energy and angular distribution of the source. The geometry was therefore changed in an attempt to reduce this sensitivity; the results of these experiments are shown in Figs. 29 and 30. Agreement

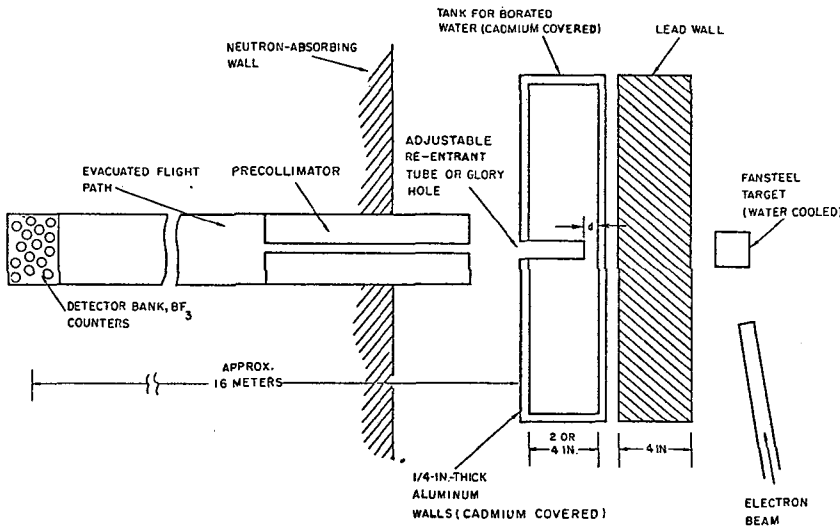

Fig. 28

Typical experimental arrangement for measuring spatially-dependent neutron spectra

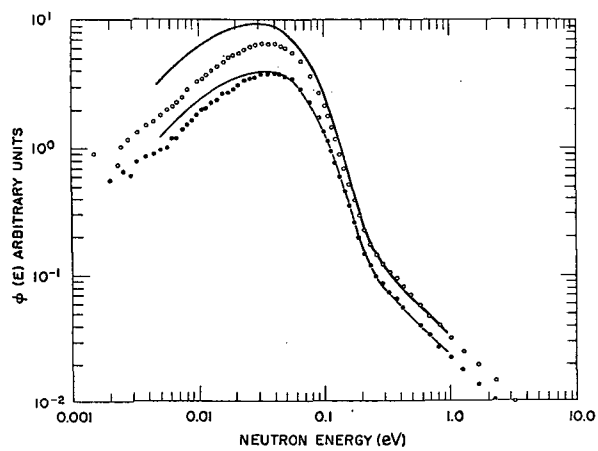

Fig. 29

Angular spectra in a 4-in slab of pure water (18 in × 18 in × 4 in tank)

O 0° angular spectrum at d = 9.5 cm
• Surface leakage
—— GAPLSN calculations

between theory and experiment is markedly better, confirming the dependence of spectrum on source position.

7.2. *Spectra at a plane temperature discontinuity*

BARDES et al. [57] and PARKS et al. [13] have measured spectra in the region of the interface between hot poisoned graphite and cold pure gra-

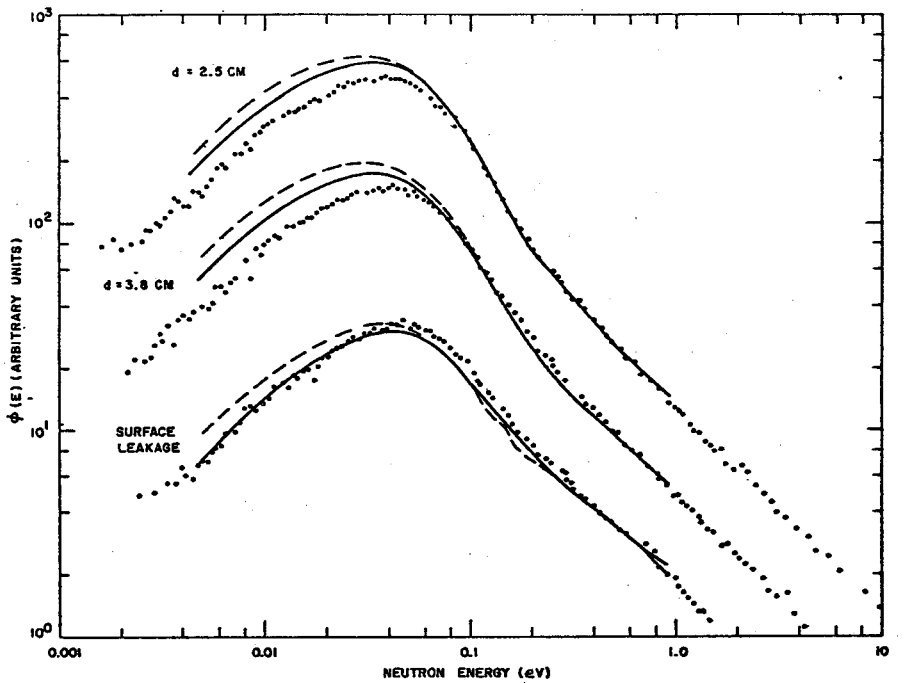

Fig. 30

90° angular flux in a 2-in slab of borated water, 5 b/H atom

—— GAPLSN calculation (Nelkin)
----- GAPLSN calculation (Radkowsky)
• Data

phite (to simulate a hot core in a reflector) while DAY [28] has measured the directed spectrum near to the interface between hot graphite and cold graphite. Some results of Bardes' experiments are shown in Fig. 31 compared with calculations using an S_n code and cross-sections based on the Parks' model for graphite. (It is not stated whether an isotropic kernel was employed.) Results show reasonable agreement with theory although there are persistent errors below 0.1 eV. The experiments of Day are not pulsed source measurements, being performed with a reactor source and chopper, but are included because of their similarity to the work reported by Parks and by Bardes. Two large graphite blocks (approximately 120 cm by 120 cm by 120 cm) were set up with a crumpled aluminium foil thermal barrier between them. The block furthest from the source could be heated to any temperature up to 400°C while the inner block was kept at room temperature. Neutron beams have been extracted from a series of positions on either side of the temperature discontinuity and spectra measured by time-of-flight. Directions of extraction both perpendicular to and parallel to the net neutron current were used. Spectra have been calculated using both a diffusion theory code (DIFF) and a slab geometry DSN code, and some results of these calculations are shown in Fig. 32. Differences are almost entirely the result of different group structures, that used in the DIFF code

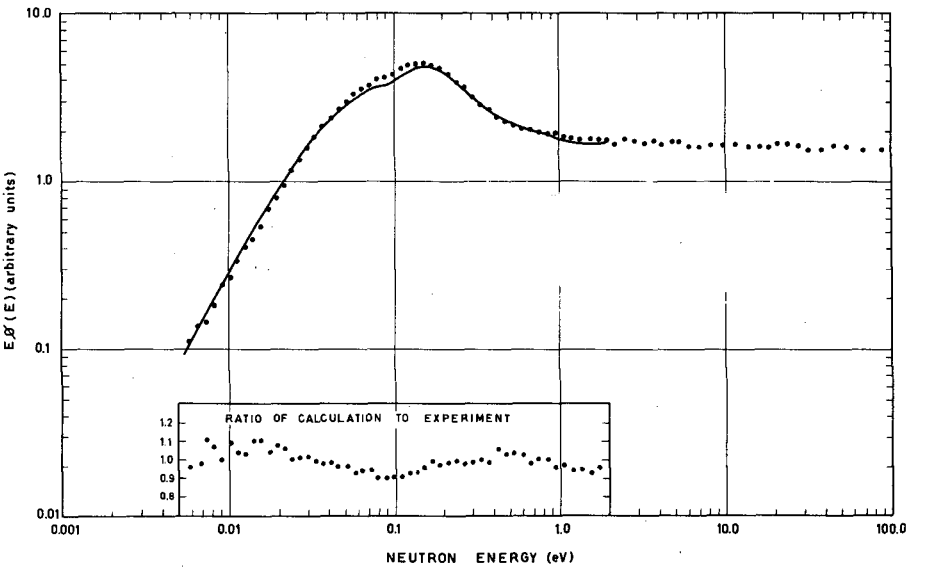

Fig. 31

90° angular neutron spectrum in poisoned 600°K graphite at 2 in from interface

● Experiment (7/11/63; T36, T35)
—— Calculation (GAPLSN 9/1/64)

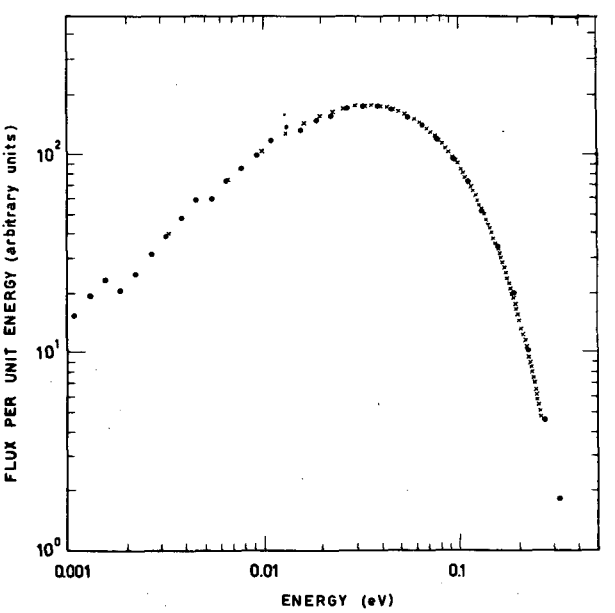

Fig. 32

Comparison of calculated spectra 5 cm from interface in graphite at 250°C

● Calculated using WDSN
X Calculated using DIFF

being too coarse at low energies to take account of the Bragg scattering in graphite. Comparison with experiment is shown in Fig. 33, the kernel used being a heavy gas kernel with effective mass of 33. Calculations using a more realistic kernel are proceeding.

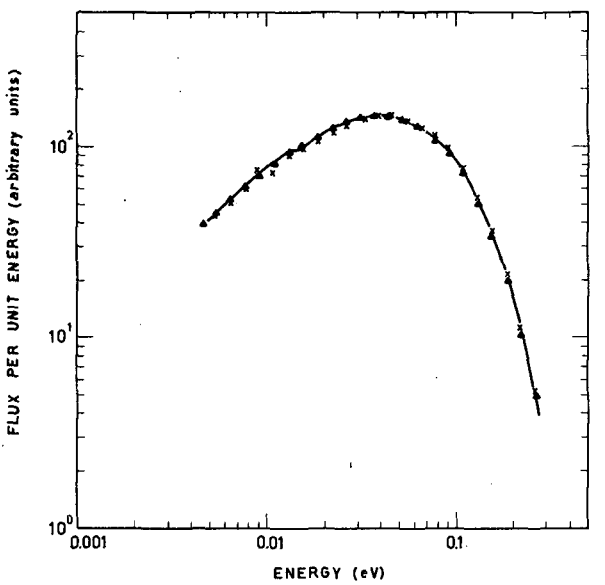

Fig. 33

Comparison of experimental and theoretical spectra 7 cm from the interface in graphite at 250°C

—— Experimental spectrum

Spectra calculated using WDSN

▲ Heavy gas mass 30 for 250°C graphite
▲ Heavy gas mass 30 for 35°C graphite
x Heavy gas mass 20 for 250°C graphite
x Heavy gas mass 30 for 35°C graphite

8. SPECTRA IN MULTIPLYING ASSEMBLIES

8.1. Stationary spectra

Because of the relaxation times involved, the measurement of spectra in multiplying assemblies is almost entirely confined to water-moderated assemblies. Some of the earliest pulsed source measurements of this kind were made by the author and reported at the 1958 Geneva Conference [51]. These were confined to close-packed water-moderated systems and were made with the object of confirming two group constants for the correlation then in use. Considerable difficulties arose in extracting representative beams from fuel (and these difficulties remain today) and meaningful data were only obtained from moderator positions. Attempts were made to obtain directed spectra emerging from probe tubes inserted axially and radially into a fuel bar. Both spectra differed from the moderator spectrum, the

former in particular being very much hardened and distorted. It was concluded that the axial spectra were not representative because of the amount of fuel removed in making the probe hole, and the radial suffered from streaming of neutrons into the point of observation from the moderator. As at that time there was no method readily available to calculate the directed spectrum these experiments were taken no further. Subsequent experiments in slab lattices also ran into difficulties from the streaming of neutrons along the probe tube from points of widely differing spectrum.

More recently BEYSTER et al. [25] have started measuring spectra in a subcritical assembly to investigate the variation of the spectrum in the presence of large flux gradients. It is claimed that the use of a fuelled system, by introducing a distributed source, eliminated the sensitivity of the results to the spectrum and position of the driving source (see section 7.1). Directed flux spectra are calculated using a DSN code, good agreement being obtained with experiment (see Fig. 34).

8.2. Asymptotic spectra

At long times after the introduction of a fast neutron pulse into a moderating and multiplying assembly, the spatial distribution becomes a funda-

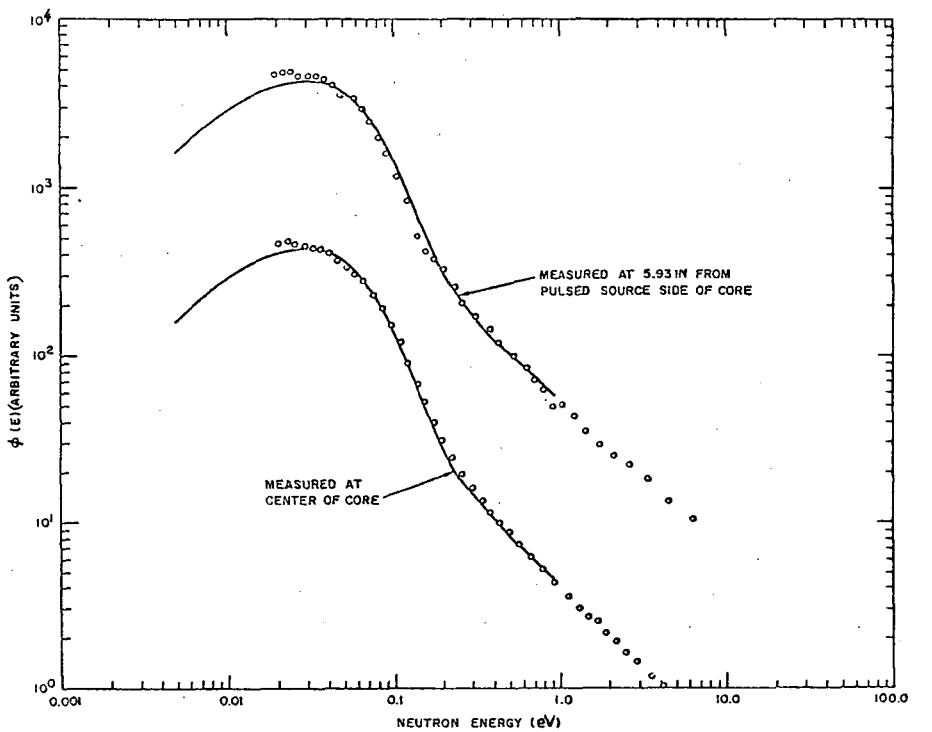

Fig. 34

Scalar neutron spectra in subcritical assembly

—— Calculated spectra using DSN

O Experimental data

mental mode distribution and the density everywhere decays exponentially with time constant. It is easy to see from the diffusion equation that the spectrum in these circumstances will be the same as the stationary fundamental mode spectrum which is in every way the same except for the introduction of an additional absorption given by λ/ν. Asymptotic spectra in multiplying systems differ from those in pure moderators in that the latter consist of a thermal group only, while the former show a 1/E slowing down "tail" due to the coupling between the thermal flux and the fast source. Measurements of asymptotic spectra in multiplying systems have been made by SLOVACEK et al. [14] using a chopper synchronized to a linear accelerator, and, provided beam extraction troubles do not arise, this should prove a very powerful technique for the investigation of reactor systems.

9. CONCLUSIONS

The measurement of spectra in moderators and lattices by the use of pulsed sources has proved an important technique for the study of thermalization problems. Measurement of stationary spectra in poisoned moderators and of time-dependent spectra in pure moderators has enabled scattering kernels to be put on a firm basis at least as far as their isotropic part is concerned, and the technique has proved of more widespread application than was first thought. Work on the understanding of spatially-dependent spectra is well under way but still not complete.

Although attempts have been made to use the method for the measurement of spectra in reactor lattices, it is less suited to this type of work than to the more basic studies. Probably the best approach is to use detailed spectrum measurements to consolidate the theoretical understanding of thermalization by means of well-planned, clearly interpretable experiments, and to verify that the theory thus set up does correctly predict all the important reaction rates in a reactor by means of direct measurement of these reaction rates.

REFERENCES

[1] WIKNER, N.F., JOANOU, G.D. and PARKS, D.E., Rpt GA-4169 (1963).
[2] EGELSTAFF, P.A. and COCKING, S.J., Inelastic Scattering of Neutrons in Solids and Liquids, IAEA, Vienna, (1961) 569-78; see also appendix to [1].
[3] EGELSTAFF, P A., HAYWOOD, B.C. and THORSON, I.M., "The motion of hydrogen in water", Inelastic Scattering of Neutrons in Solids and Liquids I IAEA, Vienna (1963) 343-56.
[4] BROWN, H.D. and St. JOHN, D.S., Rpt DP - 33 (1954).
[5] HONECK, H.C., Brookhaven National Lab., internal report.
[6] HAYWOOD, B.C. and THORSON, I.M., Rpt BNL 719(C32) (1962).
[7] BOFFI, V.C., MOLINARI, V.G. and PARKS, D.E., "Slow neutron scattering by benzene", Inelastic Scattering of Neutrons in Solids and Liquids I IAEA, Vienna (1963) 285-95.
[8] GOLDMAN, D.T. and FEDERIGHI, F.D., Nucl. Sci. Engng 16 (1963) 165.
[9] ROSENBLUTH, M.N. and NELKIN, M., Rpt GA-471 (1958).
[10] BEYSTER, J.R. et al., Rpt GA - 4659 (1964) 100.
[11] YOUNG, J.A. and KOPPEL, J.U., Nucl. Sci. Engng 19 (1964) 367.
[12] POOLE, M.J., BARNARD, E., COATES, M.S. and ROGERS, B.J., Neutron Physics, Academic Press, N.Y. (1962) 248.

[13] PARKS, D.E., BEYSTER, J.R. and WIKNER, N.F., Rpt. GA-2437 (1961).
[14] SLOVACEK, R.E., GAERTTNER, E.R., FULLWOOD, R.R. and BACH, D.R., Nucl. Sci. Engng 21 (1965) 329.
[15] BEYSTER, J.R. et al., Rpt GA-2544 (1960).
[16] BARNARD, E., KHAN, N.A., McLATCHIE, R.C.F., POOLE, M.J. and TAIT, J.H., Nucl. Sci. Engng 17 (1963) 513.
[17] NICHOLSON, K.P. and POOLE, M.J., Rpt AERE-R-4842.
[18] POOLE, M.J. and WYDLER, P., "Measurement of the time-dependent spectrum in heavy water", these Proceedings I
[19] BECKURTS, K.H., Z. Naturf. 16a (1961) 612.
[20] NICHOLSON, K.P. and POOLE, M.J., Proc. Symp. on the Automatic Acquisition and Reduction of Nuclear Data, EANDC, Karlsruhe (1964).
[21] JOHANSSON, E., LAMPA, E. and SJÖSTRAND, N.G., Ark. Fys. 18 (1960) 513.
[22] BEYSTER, J.R., Rpt BNL 719(C32) (1962).
[23] JOHANSSON, E., JONSSON, E., LINDBERG, M. and MEDNIS, J., Rpt. AE 123 (Oct. 1963).
[24] BARCLAY, F.R., COATES, M.S., DIMENT, K.M. and DURRANI, S.A., Rpt BNL 719 (C32) (1962).
[25] BEYSTER, J.R. et al., Rpt GA-4659 (1964).
[26] EGELSTAFF, P.A. and SCHOFIELD, P., Nucl. Sci. Engng 12 (1962) 260.
[27] McDOUGALL, J.D., J. nucl. Energy (parts A/B) 17 (1963) 48.
[28] DAY, D., *Rpt AERE - R4667 (1964).*
[29] EGELSTAFF, P.A., Rpt NP - Gen- 29.
[30] EGELSTAFF, P.A., private communication.
[31] SINCLAIR, R.N., and WILLIAMS, P.J., "Thermalization studies of ordinary and heavy water", these Proceedings I.
[32] BEYSTER, J.R., private communication.
[33] YOUNG, J.A. et al., Rpt GA - 4659 (1964); see also [11]
[34] SCHMUNK, R.E., BRUGGER, R.M., RANDOLPH, P.D. and STRONG, K.A., Phys. Rev. 128 (1962) 562.
[35] SINCLAIR, R.N., "The neutron scattering law and the frequency distribution of the normal modes of beryllium and beryllium oxide", Inelastic Scattering of Neutrons in Solids and Liquids II IAEA, Vienna (1963) 199-211.
[36] YOSHIMORI, A. and KITANO, Y., J phys. Soc. Japan II 4 (1956) 352.
[37] BEYSTER, J.R. et al. Rpt GA-4328 (1963).
[38] FULLWOOD, R.R., SLOVACEK, R.E. and GAERTTNER, E.R., Nucl. Sci. Engng 18 (1964) 138.
[39] YOUNG, J.C., TRIMBLE, G.D., NALIBOFF, Y.D., HOUSTON, D.H. and BEYSTER, J.R., Nucl. Sci. Engng 18 (1964) 376.
[40] WUNDERLICH, B.W., J. chem. Phys. 37 (1962) 1023.
[41] CRAWFORD, B.L. and MILLER, F.A., J. chem. Phys. 17 (1949) 249.
[42] POOLE, M.J., J. nucl. Energy 5 (1957) 325.
[43] BEYSTER, J.R., WOOD, J.L., LOPEZ, W.M. and WALTON, R.B., Nucl. Sci. Engng 9 (1961) 168.
[44] BURKART, K. and REICHARDT, W., Rpt BNL 719(C-32) (1962).
[45] SINCLAIR, R.N., Rpt AERE-PR-NP-6
[46] POOLE, M.J., SCHOFIELD, P. and SINCLAIR, R.N., Exponential and Critical Experiments III IAEA Vienna (1964) 87-110.
[47] JONES, R.H., Rpt AERE - R4776 (1964).
[48] WIGNER, E.P. and WILKINS, J.E., Rpt AECD-2275 (1948).
[49] KOPPEL, J.U. and YOUNG, J.A., Nucl. Sci. Engng 19 (1964) 412.
[50] NEILL, J.M., YOUNG, J.C. and BROUWER, W., Trans. Amer Nucl. Soc. 2 (1964); see also Rpt GA-4659 (1964).
[51] CAMPBELL, C.G., FREEMANTLE, R.G. and POOLE, M J , Proc. 2nd UN Int. Conf. PUAE 16 (1958) 233.
[52] GAYTHER, D., Rpt AERE - R4794 (1964).
[53] YOUNG, J.C., TRIMBLE, G.D., NALIBOFF, Y.D., HOUSTON, D.H. and BEYSTER, J.R., Nucl. Sci. Engng 18 (1964) 376.
[54] HOUTON, G.K., BEYSTER, J.R., YOUNG, J.C., TRIMBLE, J.D. and HOUSTON, D.H., Rpt GA-4328 (1963); YOUNG, J.C. et al., Nucl. Sci. Engng 19 (1964) 230.
[55] MILLER, J., BREHM, R.L. and ROBERTS, W.J., Rpt NAA-SR-7140 (1962).

[56] MOSTOVOY, V.I., DYKAREV, V.S., EREMEEV, I.P., ISHMAYEV, S.P., SADIKOV, I.P., SALTIKOV, Yu.S., TARAHAN'KO, V.A. and CHERNYSHOV, A.A., Proc. 3rd. UN Int. Conf. PUAE, 1964, P/367.
[57] BARDES, R.G., NEILL, J.M. and HOUGHTON, G.K., Trans. Amer. nucl. Soc. 7 (1964) 228.

DISCUSSION

N. CORNGOLD: Do you believe that data are available which would show a final mode (distribution) in crystalline moderators?

M.J. POOLE: I do not believe that experiments have been done for the specific purpose of determining this, nor do I think that existing experiments have sufficient statistical accuracy over the whole energy range to establish the point.

S.N. PUROHIT: Could anyone indicate whether, in addition to the difference in hindered rotation structure, there is also a difference in weight factors between the Nelkin model and the Haywood kernel for H_2O?

P. SCHOFIELD: The weights of the delta function in the Haywood model have been adjusted to give the generally accepted value of 4.6 for the parameter 'T'. This would imply that the weights must be similar to those of the Nelkin model.

J.A. YOUNG: The weights in the Haywood kernel are roughly as follows: distributed rotational modes, approximately 0.5; the first delta function, 0.166; the second delta function 0.333.

W. KATO: Are there any significant differences between the measured spectra obtained by the chopper method and the pulsed source technique?

M.J. POOLE: When the two experiments are properly carried out there should be no differences, and any that may arise will be a result of experimental technique. I believe General Atomic conducted a test in this connection some years ago and the results were satisfactory.

M. NELKIN: To what extent can spatial effects be made small in the measurement of time-dependent spectra?

M.J. POOLE: It is necessary to include the effect of space harmonics, possibly up to the seventh.

C.A. PRESKITT: In reactor design there is a great deal of interest in spectra for reactor lattices. Is there anything new to report on experiments on such lattices?

M.J. POOLE: Chopper experiments have been carried out with the Zenith reactor (United Kingdom) on a uranium-in-graphite lattice in which the uranium contained some percentage of plutonium, and with some fuelled BeO-moderated systems. There has also been a good series of experiments in Sweden using fuelled assemblies excited by the R1 reactor. However, most of the experiments were carried out with steady reactors and choppers and were therefore not included in the paper.

TIME-DEPENDENT THERMAL NEUTRON SPECTRA IN D_2O*

R.C. KRYTER**, G.P. CALAME, R.R. FULLWOOD AND E.R. GAERTTNER
RENSSELAER POLYTECHNIC INSTITUTE,
TROY, N.Y., UNITED STATES OF AMERICA

Abstract — Résumé — Аннотация — Resumen

TIME-DEPENDENT THERMAL NEUTRON SPECTRA IN D_2O. The thermalizing properties of heavy water have been studied by measuring the differential flux, $\phi(E,t)$, existing in a 50-cm cube ($B^2 = 0.0102$ cm^{-2}) of 99.76 mol.% D_2O maintained at 43.3°C, following a pulse of fast neutrons from an external source. The experimental technique utilizes a phased neutron chopper (3/4-in thick 1% boron-10 steel) in conjunction with the pulsed Rensselaer Polytechnic Institute linear electron accelerator for isolating the time variable, while energy determination is accomplished by measuring neutron time-of-flight over a 3.1-m shielded flight path. Fully corrected neutron spectra are presented, covering the time range $20\ \mu s \leqslant T \leqslant 200\ \mu s$ subsequent to the initiating pulse, while the energy range is limited to about $0.6\ eV \geqslant E \geqslant 0.006$ eV.

The early-time thermalization spectra display marked spectral shifts from the asymptotic diffusion-cooled Maxwellian. The flux-weighted mean energy at $T = 40\ \mu s$, for example, is about 0.137 eV. The thermalization process proceeds rapidly and is essentially complete at $T = 200\ \mu s$ following the fast pulse; the kinetic temperature of the diffusion-cooled Maxwellian distribution at that time differs by only 3°K from its asymptotic value (determined for $T = 1000\ \mu s$ and $T = 2000\ \mu s$ in a separate investigation). This compares with an experimentally determined thermalization time of 600 μs reported in recent literature.

Detailed calculations of the spectra have been made using an IBM 704 computer to obtain a numerical solution of the time- and energy-dependent diffusion equation. The experimental results are compared with calculations based on both a free gas scattering kernel of mass 3.597 and on a bound, incoherent scattering kernel for D_2O which employs the level parameters of Honeck. While neither kernel predicts spectra in agreement with experiment, it is clear that the bound kernel is superior to the free gas model. In the early-time region, the Honeck kernel appears to transfer energy too rapidly, while the opposite appears to be true of the free-gas kernel of mass 3.597. Both kernels, however, predict that the thermalization should be essentially complete at 200 μs.

SPECTRES DE NEUTRONS THERMIQUES VARIABLES DANS LE TEMPS, DANS D_2O. Les auteurs ont étudié les propriétés thermalisantes de l'eau lourde en mesurant le flux différentiel, $\phi(E,t)$, dans un cube de 50 cm de côté ($B^2 = 0,0102$ cm^{-2}) de D_2O à 99,76 moles %, maintenue à une température de 43,3°C, à la suite d'une bouffée de neutrons rapides émis par une source externe. Ils ont utilisé simultanément un hacheur de neutrons phasé (20 mm d'épaisseur, acier à 1% de ^{10}B) et l'accélératuer linéaire d'électrons pulsé du Rensselaer Polytechnic Institute pour isoler la variable temps, l'énergie étant déterminée par la mesure du temps de vol des neutrons sur un parcours blindé de 3,1 m. Les auteurs présentent des spectres de neutrons entièrement corrigés pour des temps compris entre 20 et 200 μs après l'impulsion de départ, l'énergie étant comprise entre 0,6 et 0,006 eV.

Les spectres aux temps initiaux de la thermalisation présentent des différences marquées par rapport au spectre maxwellian asymptotique de neutrons refroidis par diffusion. C'est ainsi que l'énergie moyenne pondérée par le flux au temps $T = 40\ \mu s$ est d'environ 0,137 eV. Le processus de thermalisation évolue rapidement et il est pratiquement terminé au temps $T = 200\ \mu s$, après la bouffée de neutrons rapides; la température cinétique de la distribution maxwellienne des neutrons refroidis par diffusion ne diffère, à ce moment, que de 3°K de sa valeur asymptotique (déterminée pour $T = 1000$ et pour $T = 2000\ \mu s$ dans une autre expérience). On peut comparer ces résultats au temps de thermalisation de 600 μs déterminé au cours de travaux dont les résultats ont été publiés récemment.

---

* This work performed under Atomic Energy Commission Contract No. AT(30-3)-328

** Based in part on R.C. Kryter's dissertation for Ph.D.

On a fait des calculs détaillés des spectres à l'aide d'un ordinateur IBM 704 en vue d'obtenir une solution numérique de l'équation de diffusion en fonction du temps et de l'énergie. Les auteurs comparent les résultats expérimentaux et les calculs fondés à la fois sur un noyau de diffusion de gaz libre, de masse 3,597, et sur un noyau de diffusion incohérent lié pour D_2O qui utilise les paramètres de niveau de Honeck. Si pour aucun des deux noyaux il n'y a concordance entre les spectres calculés et les spectres mesurés expérimentalement, il est néanmoins évident que le noyau lié est supérieur au modèle de gaz libre. Dans la région des temps initiaux, le noyau de Honeck semble transférer l'énergie trop rapidement, tandis que le noyau de gaz libre semble avoir la tendance opposée. Néanmoins, les deux noyaux permettent de calculer que la thermalisation devrait être pratiquement terminée en 200 μs.

СПЕКТРЫ ТЕПЛОВЫХ НЕЙТРОНОВ В D_2O В ЗАВИСИМОСТИ ОТ ВРЕМЕНИ. Изучались термализирующие свойства тяжелой воды путем измерения дифференциального потока $\varphi(E,t)$, существующего в кубе с ребром 50 см ($B^2 = 0{,}0102\ см^{-2}$) с 99,76% грамм-молекулы D_2O, при температуре 43,3°C в результате импульса быстрых нейтронов от внешнего источника. Экспериментальный метод использует фазовый селектор нейтронов (сталь с 1% бора-10, толщина 0,75 дюйма) совместно с импульсным линейным электронным ускорителем Ренселеерского политехнического института для выведения переменной времени, тогда как энергетическое определение осуществляется измерением нейтронов по времени пролета по экранированной траектории полета 3,1 м. Приводятся полностью скорректированные спектры нейтронов, охватывающие диапазон по времени $20 \leq T \leq 200$ мксек, после первоначального импульса, в то время как энергетический диапазон ограничивается примерно величинами до $0{,}6 \geq E \geq 0{,}006$ эв.

Первоначальные спектры термализации показали спектральные смещения от асимптотического максвеллиана с диффузионным охлаждением. Усредненная по потоку энергия при $T = 40$ мксек, например, составляет примерно 0,137 эв. Процесс термализации проходит быстро и по существу завершается при $T = 200$ мксек сразу же после быстрого импульса, кинетическая температура при максвелловском распределении с диффузионным охлаждением в это время отличается только на 3° K от ее асимптотической величины (определена при $T = 1000$, 2000 мксек в отдельном исследовании). Эта величина сравнивается с экспериментально определенным временем термализации в 600 мксек, о котором сообщается в новейшей литературе.

Приводятся подробные расчеты спектров с использованием счетной машины IBM 704 для получения цифрового решения уравнения диффузии в зависимости от энергии и времени. Экспериментальные результаты сравниваются с расчетами, основанными как на интегральном ядре рассеяния свободного газа с массой в 3,597, так и на связанном некогерентном ядре рассеяния для D_2O, при котором используются параметры уровней Хонека. Несмотря на то, что ни одно из ядер не предсказывает спектры в соответствии с экспериментом, ясно, что связанное ядро имеет преимущество перед моделью свободного газа. В диапазоне первоначального времени ядро Хонека, по-видимому, слишком быстро передает энергию, в то время как противоположное явление, по-видимому, остается верным для ядра свободного газа с массой в 3,597. Оба ядра, однако, предсказывают, что термализация по существу должна закончиться при 200 мксек.

ESPECTROS DE NEUTRONES TERMICOS DEPENDIENTES DEL TIEMPO EN D_2O. Se han estudiado las propiedades termalizadoras del agua pesada midiendo el flujo diferencial, $\phi(E,t)$, existente en un cubo de 50 cm de arista ($B^2 = 0{,}0102\ cm^{-2}$) de D_2O de 99,76 mol por ciento mantenido a 43,3°C, a raíz de un impulso de neutrones rápidos emitidos por una fuente externa. Para este experimento se utiliza un selector de neutrones en fase (acero con 1% de ^{10}B, de 3/4 de pulg de espesor), juntamente con acelerador lineal de electrones pulsados del Rensselaer Polytechnic Institute para aislar la variable tiempo, mientras que la energía se determina midiendo el tiempo de vuelo de los neutrones en una trayectoria de 3,1 m dentro de un tubo blindado. Se presentan espectros neutrónicos completamente corregidos correspondientes al intervalo $20 \leqslant T \leqslant 200$ μs consecutivo al impulso inicial, mientras que el intervalo de energía se limita a $0{,}6 \geqslant E \geqslant 0{,}006$ eV, aproximadamente.

Los espectros iniciales de termalización presentan acusadas desviaciones respecto de la distribución maxwelliana asintótica con enfriamiento por difusión. Por ejemplo, la energía media ponderada con respecto al flujo es de unos 0,137 eV para $T = 40$ μs. El proceso de termalización se desarrolla rápidamente y en esencia queda completado en el tiempo $T = 200$ μs siguiente al impulso de neutrones rápidos; para este tiempo, la temperatura cinética de la distribución maxwelliana con enfriamiento por difusión difiere solamente en 3°K de su valor asintótico (determinado para $T = 1000$, 2000 μs en otra investigación). En cambio, recientemente

se ha anunciado en la literatura especializada la determinación experimental de un tiempo de termalización de 600 μs.

Con una IBM 704 se han efectuado cálculos minuciosos de los espectros para obtener la solución numérica de la ecuación de difusión en función del tiempo y de la energía. Los resultados experimentales se comparan con los cálculos basados en un núcleo de dispersión constituido por un gas libre de masa 3,597 y en un núcleo de dispersión de D_2O enlazado e incoherente, en que se aplican los parámetros de nivel de Honeck. Si bien de ninguno de estos dos núcleos se deducen espectros que concuerden con los resultados experimentales, es evidente que el núcleo enlazado es preferible al modelo de gas libre. En la región inicial, la transmisión de energía resultante del núcleo de Honeck parece ser demasiado rápida, mientras que con el núcleo de gas libre de masa 3,597 sucede aparentemente lo contrario. En cambio, ambos núcleos permiten prever que la termalización debe quedar prácticamente completada al cabo de 200 μs.

1. INTRODUCTION

As reactor design calculational techniques become increasingly sophisticated and the designer is more often beset with the task of calculating quantities which are sensitive to flux nuances, one finds an ever increasing interest in the detailed differential neutron spectrum set up in a realistic nuclear system containing fuel, moderator, and absorbers. However, the problems associated with predicting the neutron spectrum within a practical reactor are immensely difficult, due to the complex interplay of neutron absorption, leakage from finite boundaries, temperature discontinuities, and heterogeneities. Likewise, though a great many experimental measurements have been performed in operating reactors and critical assemblies, the conditions under which the data are obtained are often too complex to allow simple physical interpretation. It is well, therefore, to investigate (both theoretically and experimentally) the simplest possible systems initially, and to advance to more complex configurations only when all aspects of the more pedestrian problems are fully understood. Accordingly, the work reported herein deals with a pure moderating medium in "clean" geometry amenable to theoretical treatment.

The motivations behind the present work were both experimental and theoretical. From the former point of view, we intended to develop techniques allowing us to extract the doubly-differential scalar flux $\phi(E,t)$ from a pulsed low-mass moderating assembly at relatively early times succeeding the initial burst of fast source neutrons. From the standpoint of reactor theory, we intended to investigate the effects of neutron transport, scattering kernel formulation, neutron leakage, and various approximations to the Boltzmann equation on the thermalization problem in D_2O. By appealing to a simplified form of this latter equation, the time-dependent diffusion equation, we may establish the compatibility of these goals. For a finite, absorbing, homogeneous medium (spatial modes higher than the fundamental neglected) the governing equation may be written

$$\frac{1}{v}\frac{\partial\phi(E,t)}{\partial t} = -[\Sigma_T(E)+D(E)B^2]\phi(E,t)+\int_0^\infty \Sigma_s(E'\rightarrow E)\,\phi(E',t)dE'+S(E,t), \quad (1)$$

where $\Sigma_T(E)$ is the total neutron macroscopic cross-section for the medium, $\phi(E,t)$ is the neutron scalar flux per unit energy and time interval centred

about energy E and time t, $\Sigma_s(E' \rightarrow E)$ is the macroscopic differential scattering cross-section for transfer from energy E' into energy element dE about E, B^2 is the geometric buckling, v is the scalar velocity corresponding to energy E, and S(E,t) is the source number density per unit time at energy E and time t. Equation (1) is valid, of course, only in those spatial regions far from strong sources or sinks; in the present experiment this means far from the assembly boundaries. It is well known that the asymptotic solution of Eq.(1) for long times subsequent to the burst and for $\Sigma_a = 0$ (or $\Sigma_a \propto 1/v$) and $B^2 = 0$ is simply the Maxwellian, $\phi(E) = M(E)$; furthermore, the scattering kernel plays no role in determining this distribution. In contrast, at relatively early times the time derivative term on the left-hand side of Eq.(1) so dominates that even if absorption and leakage are small (giving rise to high neutron intensity and hence good measurement statistics) the equilibrium M(E) will no longer satisfy Eq.(1) and accordingly the scattering kernel participates actively in determining the detailed $\phi(E,t)$. Thus direct measurement of these spectra provides information with which to confront theoretical predictions based on the solution of the diffusion equation (or more sophisticated approximations) in conjunction with various models describing the scattering kernel [1].

2. EXPERIMENTAL TECHNIQUE

Since strongly non-Maxwellian behaviour may be introduced at no sacrifice in the neutron intensity available for measurement, time-dependent differential flux measurements possess certain advantages over other experimental procedures (notably, measurements in heavily poisoned media) currently in vogue for determining the adequacy of proposed scattering kernels. However, $\phi(E,t)$ measurements are also fraught with difficulties, namely

(1) Low data acquisition rate – the result of stringent time resolution requirements;
(2) Large early-time background – the result of small temporal separation between the accelerator burst and data collection;
(3) Precise inter-run normalization requirement – the result of using a re-entrant tube to extract the scalar flux at the medium centre;
(4) Stringent time resolution requirements – the result of measuring a flux spectrum which changes rapidly with time after the initiating pulse.

To the authors' knowledge, only one time-dependent differential spectrum investigation has been performed and reported in the literature before the measurements reported herein: BARNARD et al. [2] have reproduced the spectrum of neutrons existing in a graphite block at times ranging from 300 to 1000 μs after the introduction of a fast pulse. In the present study, techniques which rather closely parallel the graphite work were tailored to meet the more severe requirements associated with the measurement of $\phi(E,t)$ in D_2O at times ranging from 20 to 300 μs subsequent to pulse injection.

The physical apparatus required to measure the time-dependent spectrum of neutrons in a moderator such as D_2O consists of three principal components: a spectrum-generating assembly containing the material under

TABLE I

PHYSICAL AND NUCLEAR PROPERTIES OF THE SPECTRUM SOURCE

Cubical assembly side length (cm)	50.0
Weight of D_2O (kg)	137.5
Assembly geometric buckling (cm^{-2})	0.0102
Thermal non-leakage probability, $1/(1+L^2B^2)$	0.0097
Fast non-leakage probability, $\exp(-B^2\tau)$	0.29
Measured die-away time (μs)	472 ± 5
Computed[a] die-away time (μs)	499
D_2O temperature (°C)	43.3 ± 1
Deuterium atom density (cm^{-3})	6.607×10^{22}
Hydrogen atom density (cm^{-3})	1.589×10^{20}
Oxygen atom density (cm^{-3})	3.311×10^{22}
Macroscopic absorption cross-section at 0.0254 eV (cm^{-1})	0.898×10^{-4}

[a] Using diffusion parameters of [14] in the usual buckling expansion (through B^4) of the asymptotic decay constant.

study, a pulsed source of high-energy neutrons with which to excite the medium, and a neutron spectrometer with which to analyse the time-varying stream of neutrons emanating from the medium. In the present investigation, the spectrum source consisted of a cubical box of thin aluminium, 50 cm on a side, containing liquid D_2O. Miscellaneous physical and nuclear properties of the heavy water spectrum source are recorded in Table I. A 1-in outer-diam. re-entrant tube terminating at the cube's centre allowed the examination of the central (scalar) flux with negligible perturbation to the system [3, 4]. A thermal neutron "vacuum" boundary was established by covering all six faces with 1/32-in cadmium sheet, and the medium under study was further protected from room return of neutrons by placing it inside a shield box having $1\frac{1}{4}$-in thick powdered B_4C walls. The medium was supplied with enough external (electric) heat to override the internal gamma ray heating generated during pulsing, thus allowing long-term temperature control to within ± 1 deg. C. Temperature gradients were avoided by continuously agitating the D_2O with a small motor-driven aluminium propeller located in an extreme corner of the tank. The pulsed neutron source was provided by the Rensselaer Polytechnic Institute high-intensity

TABLE II

PHYSICAL SPECIFICATIONS OF THE CHOPPER AND FLIGHT PATH

Chopper material	Stainless steel, 1 wt.% B^{10}
Disc diameter (cm)	18.4
Disc thickness (cm)	1.91
Transmission of 1-eV neutron (%)	~4
Chopper rotational speed (rps)	150
Large slit burst width (FWHM)[a] (μs)	18.75
Small slit burst width (FWHM) (μs)	7.2
"Asymptotic" disc burst width (FWHM) (μs)	122
Mean neutron flight path length (m)	3.1
Assembly-to-chopper drift distance (cm)	~33
Spectrometer acceptance angle (sr)	$\sim 1.7 \times 10^{-5}$
Flight-path thermal (inner) shield	3.2 cm B_4C + 0.8 mm Cd
Flight-path moderating (outer shield)	7.1 m^3 H_2O + 363 kg H_3BO_3
Die-away time of shield tank (μs)	~12
Gamma flash shadow shield (cm)	20

[a] FWHM, full width at half-maximum.

linear electron accelerator [5] in conjunction with a thick water-cooled tungsten conversion target. The spectrometer consisted of a slow neutron disc chopper (rotating in known, but variable, phase relationship with the accelerator firing) separated from a BF_3 gas neutron detector by a 3.1-m shielded flight path, thereby allowing velocity determination through measurement of neutron time-of-flight. The chopper was equipped with an electronically-selectable burst width, enabling the experimenter to keep the time resolution of the spectrometer consistent with requirements in the various time ranges studied. Some pertinent physical specifications of the neutron spectrometer are listed in Table II.

Figure 1 (not to scale) illustrates the manner in which the three fundamental components described above were integrated to form a working system. The Rensselaer Polytechnic Institute Linac was operated at an electron energy of 45-50 MeV with a peak electron beam current (at the target) of 600 mA; the square-shaped pulses of electrons were 4.5 μs in duration, and with a repetition rate of 150 pulses/s; the average power dissipation

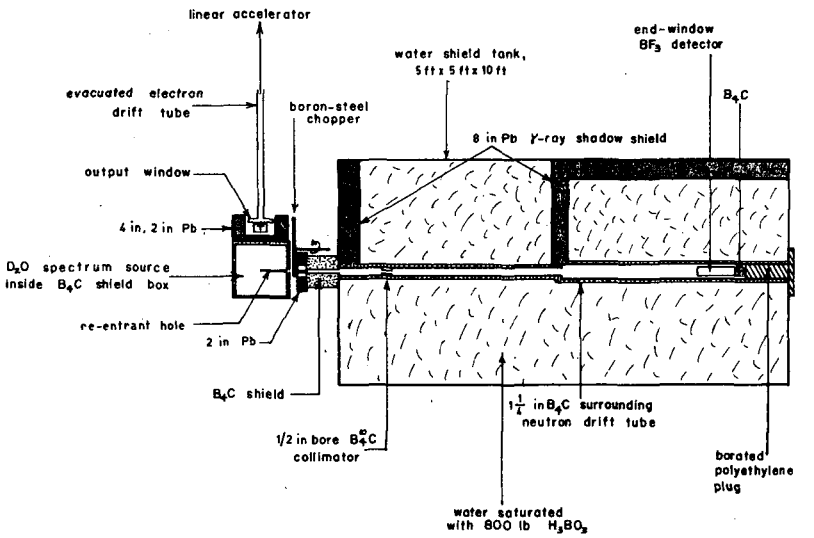

Fig. 1

Physical layout of the apparatus

in the neutron-producing tungsten conversion target was 18.5 kW. This primary target was, in turn, surrounded by 4 in of lead (2 in in the direction of the spectrum source), water-cooled by means of imbedded aluminium tubing. The purpose of the lead was twofold: first, it increased the available neutron intensity by means of the γ-n reaction with the incompletely converted Bremsstrahlen beam; second, it served as a personnel shield from the radioactive target assembly. The fast neutron pulse was injected right through the side of the B_4C shield box, such procedure being feasible because the B_4C is perhaps 80% transparent to neutrons having energies in excess of 1 MeV. Partially thermalized neutrons were allowed to leave the cubical assembly's centre in a direction perpendicular to the Linac axis, thereby avoiding contamination of the extracted beam with the neutron current component undoubtedly present along the source axis. Most such neutrons emanating from the spectrum source arrived at the chopper, which opened once per burst at a known (but experimentally variable) time delay following the accelerator pulse, only to find it closed and were therefore absorbed in the boron steel. However, if not intercepted by the chopper, those neutrons properly directed then passed through the bore of a 2-in long, $1\frac{1}{2}$-in outer-diam. sintered $B_4^{10}C$ cylinder situated in the chopper housing which served both as stationary slit for the chopper and neutron beam defining collimator. Immediately following this collimator, the neutrons passed through the 5/8-in tube penetrating a post-chopper shield box filled with B_4C powder which shielded the entrance to the neutron drift path against extraneous neutrons from the target area.

The air-filled main drift tube was constructed of aluminium conduit, 5 ft of $1\frac{1}{2}$-in diameter joined to a 5-ft section of $2\frac{1}{2}$-in diameter. This entire 10-ft length was lined on the inside with 1/32-in cadmium and on the

outside by a $1\frac{1}{4}$-in thickness of powdered B_4C supported by a wooden trough. The drift pipe assembly, in turn, was positioned centrally within a steel plate tank 5 ft × 5 ft × 10 ft containing 1800 gal of water saturated with 800 lb of boric acid; an immersion pump provided continuous closed circuit circulation. This heavy shielding was necessitated by the fact that the entire spectrometer, including the detector, was situated inside the Linac target room and was thereby subjected to intense gamma ray bombardment as well as a long-lived fast neutron background. Also within the large water shield tank were three walls of lead brick, a minimum of 8 in thick, to protect the spectrum detector from the target gamma flash and from Bremsstrahlen produced by electron beam rake-off along the accelerator drift tube. The front of the single end-window detector (6 in long, filled to 76 cm Hg pressure with BF_3 enriched to 96% B^{10}) was placed about 21 in within the shield tank and the access hole sealed with 2 in of B_4C backed up by 13 in of polyethylene, the last 2 in of which were heavily borated. A spiral groove cut in the polyethylene plug admitted the detector signal cable without presenting any straight-line leakage path for room neutrons. The acceptance solid angle of the system was such that the detector was capable of viewing a source area about 1/2-in in diameter at the bottom of the re-entrant tube, thus ensuring that only neutrons emanating from the assembly's centre would be detected.

A novel technique was used in normalizing with precision those spectral data collected at one time after the initial neutron injection with similar data received at another time. It should be stressed that simple procedures such as keeping data collection time constant for all runs do not ensure correct normalization, since the detector may gradually change its sensitivity, the associated amplifiers may change their gain, and source intensity changes may be introduced inadvertently by slight variations in both the electron beam energy and the manner in which it strikes the tungsten conversion target. Attempts to monitor the total neutron production from the γ-n target reaction by means of a remote detector and scaler gated off for about 700 μs following the accelerator trigger were largely unsuccessful; unaccountable discrepancies between monitors of 3-5% were typical. To circumvent the need for normalizing factors derived through external means, a device was constructed which sequentially incremented (on a burst-by-burst basis) the post-burst time at which the spectrum was measured and automatically routed the incoming information to the proper memory location of the multi-channel time analyser [6]. In the present experiment, a 1024 channel analyser[1] was employed, which divided conveniently into 8 sections of 128 channels each. The sequential delay/eight-group router thus allowed the "simultaneous" collection of eight different thermalization spectra (having "waiting" time increments of 32 μs); since the incrementing sequence was repeated every 8/150 s, system variations which took place over periods of hours or even minutes were applied equally to all eight spectra with the result being correct normalization. A test was performed to ensure that no member of the family of eight different thermalization spectra consistently received an undue share of the primary neutrons from the accelerator, caused by un-

[1] Model CN-1024 with type 211 plug-in, Technical Measurement Corporation, North Haven, Conn., United States of America.

intentional synchronization occurring between the 60-c/s power line supplying the Linac's 15-kV charging voltage power supplies and the 150 c/s repetition rate of the experiment. The results showed that phase interlocking was no problem. The importance of intensity normalizations which are absolutely above suspicion will be discussed in section 3.5.

3. CORRECTIONS TO THE RAW DATA

The raw data received in this experiment as counts per time channel on a time-of-flight analyser must be corrected for six sources of distortion in arriving at quantities which are directly proportional to the neutron flux per unit inverse velocity (or energy) and unit time intervals. The corrections applied deal with the time-dependent background, the flight path materials transmission, the energy-dependent detector efficiency, the energy-dependent flight path, the assembly-to-chopper drift distortion, and the finite system resolution capabilities in both energy-space and time-space. These topics are each considered in turn below.

3.1. Time-dependent background

Knowledge of the time-dependent background was quite important in this experiment because, as we stressed earlier, the signal-to-background ratio was marginal for higher energies at early post-burst times in spite of the extensive flight path shielding depicted in Fig. 1. This background had its origin, of course, in neutrons which managed to reach the detector by means of paths other than the desired one, in particular, neutrons directly from the target area which penetrated the water shield and the drift tube B_4C and cadmium liners. To subtract this unwanted component from the recorded data, blocked-beam background runs were obtained about once a day by either placing a 1/2-in thick $B_4^{10}C$ block over the mouth of the re-entrant hole or by stopping the chopper rotor in a closed position and firing the accelerator at the usual repetition rate from a pulse generator. Both methods produced identical results, demonstrating the opacity of the boron-steel rotor to the rather low-energy neutrons of interest in this investigation. The normalization of these background data to the signal-plus-background runs was effected by matching the heights of data in several early time channels which essentially recorded the rapid decay of the poisoned-water shield tank itself, a procedure which proved to be more accurate than relying on external neutron production monitors.

3.2. Flight path materials transmission

Since the flight path used in this work was not evacuated, a small fraction of the neutrons travelling from the spectrum source assembly to the detector were absorbed or scattered before reaching their destination by collisions with nitrogen and oxygen atoms and with water molecules. The thin aluminium window which formed the bottom of the re-entrant hole was also partially opaque to neutrons. While we were not concerned with absolute intensities in this experiment, the relative transmission of these beam

materials as a function of energy must be taken into account. It was assumed that a single scattering event removed a neutron from the beam just as effectively as an absorption event, since the entire flight path was lined with cadmium and B_4C; hence, the materials transmission was calculated from

$$\text{Transmission } (E) = \exp\left(-\sum_{i=1}^{4} N_i \sigma_i(E)\, X_i\right) , \qquad (2)$$

where the N_i, $\sigma_i(E)$, and X_i are the number densities, total cross-sections, and thicknesses, respectively, associated with the four materials.

3.3. Detector efficiency

The relative efficiency with which the spectrum counter detects neutrons of various energies was determined by comparing its response in a standard flux field with that of a counter "thin" enough to have a reciprocal velocity response. These measurements were performed through the courtesy of Mrs. S.B. Armstrong at the nearby Knolls Atomic Power Laboratory, who used a slow neutron chopper in conjunction with a 6.1-m flight path and the thermal column of the Thermal Test Reactor. The 1/v detector was identical in physical construction to that employed in the time-dependent D_2O measurements, but was filled to only 7 cm Hg pressure with BF_3 gas depleted to 11% B^{10}. While it is true that the detector efficiency corrections may be quite large (a ratio of about 4 exists between the efficiency at 1 eV and at 0.01 eV); this relative detector response is believed to be known quite precisely, a belief which is supported by our demonstrated ability to reproduce an asymptotic (in time) spectrum having good Maxwellian shape and the correct neutron temperature[2].

3.4. Energy-dependent flight path

Even though the distance separating the chopper and the detector was fixed, the "effective" flight path length for these experiments was non-constant because neutrons of higher energy penetrated (on the average) farther into the detector gas before suffering the $B^{10}(n,\alpha)Li^7$ reaction causing them to be counted than did neutrons of lower energy. Although the assumption of an energy-independent mean internal stopping position would have resulted in a maximum error of only 1% in the inverse velocity scale over the range of energies considered presently, this correction was not neglected in reducing the raw data. The mean internal stopping position (measured from the inside surface of the detector's end window) for a neutron of energy E was calculated by taking a spatial average over the one-collision absorption probability within the detector [7]

---

[2] See section 4 of this paper.

$$\overline{X}(E) = \frac{\int_0^L X\phi_0 e^{-\Sigma_a(E)X}\Sigma_a(E)\,dx}{\int_0^L \phi_0\, e^{-\Sigma_a(E)X}\,\Sigma_a(E)\,dx} = \frac{1}{\Sigma_a(E)}\left[1 - \frac{\Sigma_a(E)L\, e^{-\Sigma_a(E)L}}{1 - e^{-\Sigma_a(E)L}}\right], \quad (3)$$

where $\Sigma_a(E)$ is the macroscopic absorption cross-section of the filling gas, L is the length of the counter, X is a position variable, and ϕ_0 is the incident polyenergetic flux. The "effective" flight path was then taken as

$$P(E) = P' + \overline{X}(E), \quad (4)$$

where P' is the basic flight path length from the chopping plane to the inner surface of the detector's end window.

3.5. Assembly-to-chopper drift distortion

Because the chopping plane did not coincide physically with the bottom of the re-entrant hole from which the observed neutrons emanated, a spectral distortion occurred during the time required by the neutrons to traverse the depth of the extraction hole. This distortion was caused by the fact that the neutron population present in the D_2O assembly changed in magnitude with time. Since the slower neutrons required longer times to reach the chopper, the slow neutron population present at the chopping plane at any given instant in time, τ, was characteristic of conditions existing at the assembly's centre at a much earlier post-burst time than was the fast neutron population incident upon the chopper at this same instant. If we define a position axis with origin at the assembly centre and the chopping plane at a distance d, then the instantaneous flux observed at the chopper is related to the (unobservable) flux present at the re-entrant hole bottom at various earlier times, through the neutron velocity:

$$\phi(E, d, \tau) = \phi(E, 0, \tau - d/v). \quad (5)$$

Since we wished to present the flux spectra at the medium centre at unique time lapses subsequent to the accelerator pulse, $\phi(E, 0, \tau)$, and not the time-dependent spectra at the chopper, $\phi(E, d, \tau)$, we had to find a means of relating the two quantities. While this is easily done for the case of asymptotic (in time) spectra, where all neutron energies may be assumed to decay exponentially with the same die-away constant, a simple coupling relationship is not obtainable at non-asymptotic times and other methods were sought.

If one is willing to accumulate distorted spectra at a great number of "waiting" times, τ, subsequent to the accelerator pulse he may correct for the drift distance distortion by a simple graphical interpolation technique which involves no approximations to the time behaviour of the neutron flux other than its smoothness, a reasonable assumption for a non-crystalline moderator like D_2O. This "exact" technique was introduced by BARNARD et al. [2] and was used with complete success in the work presented herein.

The technique consists of first plotting a large number of neutron "life history" curves (one for each velocity measured by time-of-flight), i. e. graphs of the normalized flux versus the neutron emission time from the assembly centre (obtained through the velocity) with the energy as a parameter and then connecting the discrete points by smooth curves. One may then reconstruct the true differential flux spectrum existing in the medium at any unique time lapse subsequent to the accelerator burst simply by reading off the various ordinates at the desired abscissa value. In applying this technique the importance of the sequential delay/eight-group router [6] data collection procedure (section 2), which ensures normalizations correct to considerably less than 1%, cannot be over-emphasized; more conventional auxiliary neutron production monitors were found to be insufficiently reliable.

3.6. Finite system resolution

When we say that as a result of our measurements with the neutron spectrometer we find a certain value for the flux $\phi(E', t')$, where E' and t' are particular values of the energy and time variables, we realize that this flux value which we have measured is a composite of a continuum of elemental fluxes having energies and times distributed in some fashion about the values $E = E'$ and $t = t'$. This "smearing" effect of the imperfect system resolution may be described succinctly in mathematical terms by a double convolution integral:

$$\phi \text{ observed } (E', t') = \int_{-\infty}^{\infty} R'(\xi) \int_{-\infty}^{\infty} R(\lambda) \phi_{\text{true}} (E' + \xi, t' + \lambda) d\lambda \, d\xi \, , \qquad (6)$$

where R' and R are the resolution functions (not necessarily identical) associated with the neutron energy, E, and the time lapse subsequent to the accelerator pulse, t. By substituting the theoretical flux for ϕ_{true} and performing the indicated integrals of Eq. (6), one can resolution-broaden the calculated flux and thereby obtain spectra which may be compared validly with the experimental spectra. Although ϕ_{true} remains unknown, one can even calculate energy- and time-dependent correction factors $\phi_{\text{obs.}}(E', t')/\phi_{\text{theor.}}(E', t')$ with which to correct the experimental data to "perfect" resolution if the correction factors are small and if one feels his approximation to $\phi_{\text{true}}(E, t)$ is adequate to the task. At the time of submission of this paper, Eq. (6) has only been evaluated in the asymptotic limit wherein one has time-energy separability. However, for post-burst times in excess of 50 μs a comparison of spectra obtained using the 7 and 19 μs open times shows the resolution effects to be negligible; accordingly, these later spectra are presented with no reservations and may be compared validly with theoretical results.

4. EXPERIMENTAL RESULTS

We now turn our attention to selected data displayed on a "life history" curve basis; Fig. 2 follows the time-dependent growth and decay of neutrons

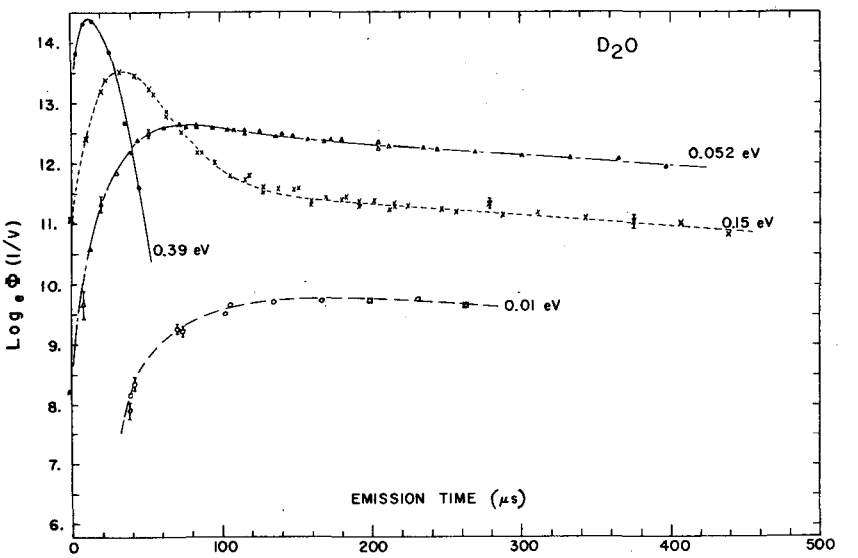

Fig. 2

Neutron build-up and decay curves for 0.39, 0.15, 0.052, and 0.01 eV

possessing energies of 0.39, 0.15, 0.052, and 0.01 eV. These data have been corrected for all sources of distortion except system resolution (which is why the curves do not display zero flux at zero emission time relative to the accelerator pulse) and are normalized to the same primary burst intensity. The curves connecting the discrete data points have been drawn only for conceptual clarity and do not represent theory. The statistical error bars represent one standard deviation, and are based on counting statistics alone. Figure 2 indicates that the higher energies build up rapidly with increasing time, and after reaching sharp, high peaks they decay rapidly; finally they level off to the slower asymptotic decay rate characteristic of the medium's absorption and leakage. In contrast, the lower energies grow in much more slowly, possess broad maxima, and never attain the peak flux levels reached by the higher energies. This behaviour is precisely what we might anticipate on physical grounds: neutrons scattered into the higher energy intervals have for the most part suffered relatively few collisions with moderator atoms since their birth at MeV energies, while the converse is true for neutrons scattered into the lower energy intervals. Accordingly, the rapid time variation of the higher energy groups reflects the transient existence of the small number of sources feeding these groups, while the slower time variation of the lower energies reflects the multiplicity of sources in energy-time space which are capable of feeding neutrons to these lower energy intervals.

We also note from Fig. 2 that the asymptotic decay rate for the various energies is unique (to within the statistical precision of the data) after approximately 200 μs have elapsed. It must therefore be concluded that under the present experimental conditions the neutron population achieved dynamic equilibrium with the moderator atoms after about 200 μs following the pulse;

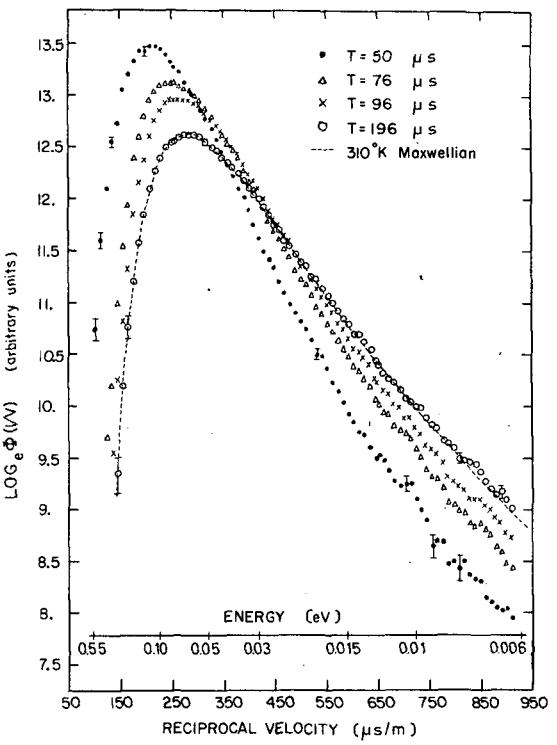

Fig. 3

Time-dependent neutron spectra in D_2O at 316.5°K

this value differs sharply with the 600 μs reported by STARR et al. [8], but agrees with the later measurements of DAUGHTRY and WALTNER [9], who found equilibrium after about 150-200 μs.

The neutron spectra present in the assembly at post-burst times of 50, 76, 96 and 196 μs are shown in Fig. 3, along with a Maxwellian distribution least-squares fitted to the latest spectrum[3]. These data are fully corrected[4] and are normalized to a standard primary neutron production rate. A Maxwellian distribution of neutron temperature 310°K is seen to fit the 196 μs experimental spectrum quite satisfactorily, which bolsters our confidence in the data collection and distortion correction procedures. Furthermore, this 310°K is only 3°K higher than the neutron temperature obtained by fitting a Maxwellian distribution to a spectrum measured at a "waiting" time of 2000 μs, which must surely be late enough for asymptotic conditions to prevail; this lends additional weight to the reported equilibrium attainment time of 200 μs.

---

[3] Spectra have been reproduced for times as late as 2000 μs, but since the spectrum shapes were found to be no different from the 196-μs data they have not been presented here.

[4] Regarding resolution corrections, see comment in section 3.6.

5. COMPARISON WITH THEORY

Time-dependent P_1 theory, as well as the diffusion approximation, was used in attempts to predict the transient spectra in D_2O. The computational method involved the standard technique of direct time integration of the set of time-dependent equations written in a 45-point discrete ordinates energy representation [10-11]; this scheme was tested and found to be stable against numerical round-off. The integration time step (0.2 μs) was so chosen that the higher-energy transients (higher-order eigenfunctions) were well represented when a first-order Taylor series approximation was used to extrapolate the flux forward in time. Leakage was allowed for by assuming a fundamental (cosine) spatial flux distribution and hence adding a $D(E)B^2$ term to the absorption. Two scattering kernels were employed: one was a free gas kernel of fictitious mass 3.597 and the other was a bound, incoherent Nelkin-type model using the level parameters of HONECK [12]. In each case, the oxygen was treated as a free gas of mass 16, and the slight (0.24%) light water contamination was allowed for by treating the hydrogen as a free gas of fictitious mass 2.74. A Selengut-Goertzel approximation to the P_1 component of the Honeck kernel was used in conjunction with both the bound and free gas P_0 kernels. This choice was dictated by the fact that free gas P_1 kernels are known to give incorrect results and also because the full P_1 bound kernel yielded an unreasonable asymptotic decay time. The transient spectra, on the contrary, were found to be relatively insensitive to the form chosen for the P_1 component; this is understandable on physical grounds because at early times the energy exchange process (governed by the scattering kernel's P_0 component) completely dominates the leakage (governed by the P_1 component), while the converse situation prevails at late times.

A source of the form $\delta(E-E_0)\times\delta(t)$ was employed, where E_0 is the highest energy point in the mesh (1.145 eV). Though this was an admittedly unrealistic source as compared to the experiment, the theoretical spectra at post-burst times of 20 μs or later were not found to be particularly sensitive to the time or energy distribution assumed for the source. The time scales between theory and experiment were made to coincide by adding to the time lapse following the delta-function-source introduction the slowing-down time to 1.145 eV, taken as 5.8 and 3.8 μs for the bound and free gas representations, respectively. It should also be pointed out that although time-dependent diffusion theory calculations resulted in transient spectra possessing large second time derivatives (indicating that the second-order Telegrapher's equation should be used), surprisingly little difference was found between the final spectra produced by solving the diffusion and P_1 approximations to the Boltzmann equation. Accordingly, the diffusion theory results are presented here.

5.1. The spectrum at early times

Figure 4 shows comparisons between experiment and time-dependent diffusion theory for post-burst times of 20, 30, 60, and 100 μs. These spectra have been arbitrarily displaced for clarity and both theoretical curves have been individually peak-normalized to the experimental data at each of the

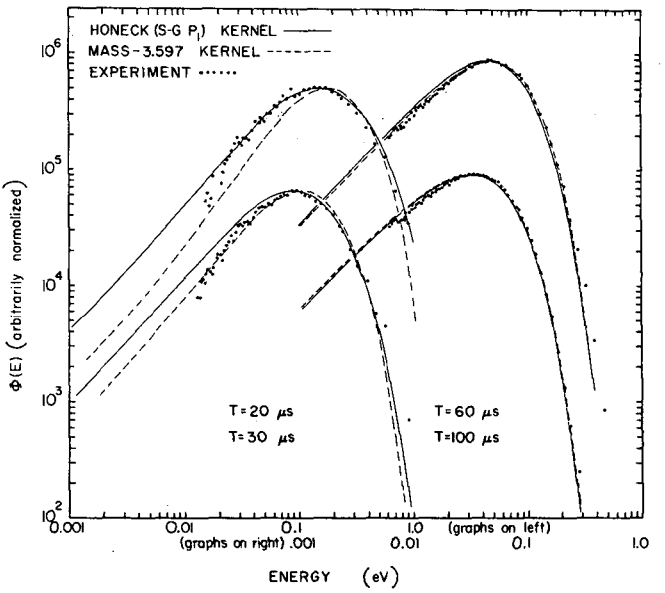

Fig. 4

Experiment versus theory at T = 20, 30, 60, amd 100 μs

four times. It is interesting to note that the thermalization rates predicted by the two scattering kernels change with time, according to the manner in which higher-energy transients are excited as a function of time. Specifically, it is seen that the bound kernel spectrum fits the earliest experimental data significantly better than the free gas kernel prediction (which has not downscattered neutrons rapidly enough during the time span $0 \leqslant t \leqslant 20$ μs), though neither is without fault (the anomalous positions of the data points above 0.5 eV at the two earlier times are attributed to the absence of resolution corrections). However, in comparing the 20- and 30-μs spectra, we find that during this time lapse the bound kernel spectrum has definitely thermalized too rapidly while no such firm conclusion may be drawn for the mass-3.6 free gas spectrum, which simply does not have the correct shape at either of the early times. The overly-rapid thermalization predicted by both the free gas and the bound kernels at the two later times shown in Fig. 4 would seem to indicate an insufficiently large diffusion cooling coefficient C or conversely too large a mean squared energy transfer M_2 for both kernels. One may draw this conclusion validly because as the spectrum approaches its asymptotic shape the higher-order energy transfer moments become insignificant and the second moment becomes a good measure of the rate of approach-to-equilibrium. The agreement between experiment and both theories is seen to improve with the passage of time, as one might expect; furthermore, it should be emphasized that both kernels are in agreement with experiment in that they predict that the thermalization process should be essentially complete at 200 μs.

Although the shapes of the calculated spectra are in fair agreement with their experimental counterparts, the amplitudes of the computed spectra

as a whole seem to decay too rapidly with time in the region $20 \leqslant t \leqslant 60$ μs. For example: after normalizing the theoretical and experimental spectra at 20 μs, each point of the theoretical curves at 30 and 60 μs had to be multiplied by factors of 1.14 and 1.27, respectively, to obtain the peak normalizations shown in Fig. 4. Oddly enough, the amplitude discrepancy levels off at about 28% and is not troublesome for times greater than 60 μs. This curious discrepancy between experiment and theory, regarding the total number of neutrons contained in the entire spectrum as a function of time, appears to be independent of the kernel used and has not been resolved at this writing, although it has been established that the apparent neutron loss is not caused by truncation errors resulting from too large a time step in the numerical integration procedure. It has been hypothesized that the apparent loss of neutrons in the calculated spectra at early times is a result of upscattering of neutrons beyond the highest point in the energy mesh (1.145 eV). This possibility is currently being investigated by extending the discrete energy mesh up to 3 eV in a 78-group calculation, the results of which are not yet available.

5.2. The asymptotic spectrum

The theory and experiment are in slight disagreement regarding the amount of diffusion cooling present in the asymptotic spectrum. Although it is apparent in Fig. 4 that at 100 μs subsequent to the burst either scattering kernel yields spectra which are slightly too "soft" in comparison to experiment, the opposite situation prevails at asymptotic times ($t > 200$ μs). By a least-squares fitting of the data to Maxwellian distributions[5], we found the theory (independent of the kernel used) to yield a diffusion cooling temperature shift[6] of about 2.5°C, while the experiment revealed about 9.8 ± 0.4°C. This result lends weight to our earlier observation that both kernels are characterized by too small a value of C.

The asymptotic spectrum was also computed with both the free gas and bound kernels in the P_3 rather than the P_1 approximation but no significant difference was noted, suggesting that at least at asymptotic times transport effects are unimportant. In addition, these P_3 calculations yielded directly values for the thermalization parameters α_0, D_0, C, and F in the usual buckling expansion of the asymptotic decay constant

$$\lambda = \alpha_0 + D_0 B^2 - CB^4 + FB^6 + \ldots \tag{7}$$

The numerical values of α_0 and D_0 were in agreement with experimental and theoretical values [12-14], but, as we anticipated, the value of C for both kernels was too small by almost a factor of two. If one assumes that the diffusion cooling temperature shift is, in first approximation, directly pro-

[5] In spite of the fact the $\Sigma_a(E)$ and $D(E)B^2$ are not zero or 1/v, this is an excellent approximation (see Fig. 3).

[6] The diffusion cooling temperature shift is defined as $T_m - T_n$, where T_m is the physical moderator temperature and T_n is the neutron temperature of the best-fit Maxwellian.

portional to C [15], then one can explain roughly half of the asymptotic spectrum temperature shift discrepancy as due to the small C value characteristic of these two kernels.

As a final observation, the asymptotic die-away time (measured as 472 ± 5 μs) was predicted satisfactorily (479 μs) by a diffusion theory calculation using a Selengut-Goertzel approximation to the P_1 component of the bound kernel but was predicted unsatisfactorily (437 μs) when the full P_1 bound kernel was employed. This again indicates a deficiency in this kernel.

6. CONCLUSIONS

Physical apparatus and measurement techniques were developed which allowed us to extract the doubly-differential scalar flux, $\phi(E, t)$, from a pulsed low-mass pure moderating assembly at relatively early post-burst times. The adequacy of calculational procedures was also tested, with the result that while present methods were deemed adequate to the task, care must be exercised regarding such areas as choice of approximation to the *Boltzmann equation, upscattering at early times, and integration time step* and stability. In addition, the transient spectra were shown to be sensitive to scattering kernel structure and deficiencies of two popular models for D_2O scattering were brought to light.

REFERENCES

[1] KOPPEL, J.U. and NALIBOFF, Y.D., Trans Amer. nucl. Soc. 5 2 (1962) 337-38.
[2] BARNARD, E., KHAN, N.A., McLATCHIE, R.C.F., POOLE, M.J. and TAIT, J.H., Nucl. Sci. Engng 17 (1963) 513-22.
[3] *GAERTTNER, E.R., FULLWOOD, R.R., MENZEL, J.H., TOTH, G.P., "Measurements of the spatially-dependent asymptotic spectra in water and polyethylene", these Proceedings I.*
[4] SLOVACEK, R.E., GAERTTNER, E.R., FULLWOOD, R.R., Nucl. Sci. Engng 21 (1965) 329-45.
[5] GAERTTNER, E.R., YEATER, M.L., FULLWOOD, R.R., IRE Trans. nucl. Sci. NS-9 5 (1962) 23.
[6] FULLWOOD, R., Nucl. Instrum Meth. 30 2 (1964) 206-08.
[7] STONE, R.S. and SLOVACEK, R.E., Nucl. Sci. Engng 6 (1959) 466-74.
[8] STARR, E., HONECK, H., DE VILLIERS, J., Nucl. Sci. Engng 18 (1964) 230-35.
[9] DAUGHTRY, J.W. and WALTNER, A.W., Trans. Amer. nucl. Soc. 7 2 (1964) 232.
[10] DAITCH, P.B. and OHANIAN, M.J., Trans. Amer. nucl. Soc. 6 2 (1963) 293.
[11] OHANIAN, M.J. and DAITCH, P.B., Nucl. Sci. Engng 19 (1964) 343-52.
[12] HONECK, H.C., Trans. Amer. nucl. Soc. 5 1 (1962) 47.
[13] GANGULY, N.K. and WALTNER, A.W., Trans. Amer. nucl. Soc. 4 2 (1961) 282-83.
[14] KUSSMAUL, G. and MEISTER, H., J. nucl. Energy A/B 17 (1963) 411-15.
[15] FULLWOOD, R.R., Trans. Amer. nucl. Soc. 7 2 (1964) 231.

THE EFFECTS OF COHERENT SCATTERING ON THE THERMALIZATION OF NEUTRONS IN BERYLLIUM*

E. R. GAERTTNER, P. B. DAITCH, R. R. FULLWOOD**, R. R. LEE**
AND R. E. SLOVACEK
RENSSELAER POLYTECHNIC INSTITUTE, TROY, N. Y.,
UNITED STATES OF AMERICA

Abstract — Résumé — Аннотация — Resumen

THE EFFECTS OF COHERENT SCATTERING ON THE THERMALIZATION OF NEUTRONS IN BERYLLIUM. Coherent scattering complicates the problem of thermalization in crystalline moderators by the trapping of neutrons at the Bragg energies. This effect arises because the whole microcrystal absorbs the recoil from the collision; also there is little up-scattering because the cross-section must be averaged over all atoms of the crystal. If the neutron is removed from a trapped peak by inelastic or incoherent elastic scattering, it is fairly probable that it will leak from the moderator in a small system because of the much smaller λ_{tr} for values away from the Bragg energies. These effects result in a neutron spectrum in beryllium metal which for buckling values of 0.072 and 0.1 cm^{-2} does not reach equilibrium at times as great as 5 mean-lifetimes in neutron die-away experiments. For bucklings of about 0.027 and 0.01 cm^{-2} the spectrum, although distorted in both cases from the Maxwellian, appears to be stable after about 600 μs. In all cases the spectrum is severely truncated for neutron energies below 0.0068 eV, the lowest Bragg peak.

The measurements are performed using the phased-neutron chopper pulsed-electron linear accelerator technique. The initial photo-neutron pulse injected into the moderator is sampled at a later time by a mechanical neutron chopper having a 130-μs sampling time at full-width, half-maximum. This sample of the neutron spectrum is energy analysed by time-of-flight over a 3-m flight path by means of a BF_3 detector and energy analysers.

A disc chopper consisting of B^{10} steel (3/4 in thick, 1 wt.% of B^{10}) is located as close as possible to the moderator to minimize the distance between the chopping plane and the bottom of the 0.5 in × 0.5 in re-entrant hole penetrating to the centre of the medium. This minimizes the difficult chopper flight path correction to the spectrum.

The data is background subtracted and corrected for the energy-dependent mean detector stopping distance, the energy response of the detector and the material in the flight path. The mean chopping time is calculated, based on an assumed flux time dependence which is obtained from the data by least squares fitting. Several iterations are required until self-consistency is obtained.

EFFETS DE LA DIFFUSION COHÉRENTE SUR LA THERMALISATION DES NEUTRONS DANS LE BÉRYLLIUM. La diffusion cohérente complique le problème de la thermalisation dans les ralentisseurs cristallins du fait du piégeage des neutrons aux énergies de Bragg. Ceci est dû au fait que l'ensemble du microcristal absorbe l'énergie de recul de la collision; en outre, la diffusion n'est pas beaucoup plus élevée, parce qu'il faut faire la moyenne de la section efficace sur tous les atomes du cristal. Si un neutron est éloigné d'un pic piégé par diffusion inélastique ou par diffusion élastique incohérente, il est fort probable que, dans un petit système, il sortira du ralentisseur du fait de la valeur beaucoup plus faible de λ_{tr} lorsqu'on s'écarte des énergies de Bragg. Ces effets se traduisent par un spectre de neutrons dans le béryllium métallique qui, pour des valeurs du laplacien égales à 0,072 et 0,1 cm^{-2}, ne parvient pas à l'équilibre, en un temps pouvant atteindre 5 durées de vie moyennes dans des expériences sur l'évanouissement des neutrons. Pour des laplaciens de 0,027 et 0,01 cm^{-2}, le spectre – bien que présentant dans les deux cas des distorsions par rapport au spectre maxwellien – semble se stabiliser après quelque 600 μs. Dans tous les cas, le spectre est très tronqué pour des énergies de neutrons inférieures à 0,0068 eV, pic de Bragg le plus bas.

* This work performed under United States Atomic Energy Commission Contract No. AT(30-3)-328.

** This work based in part on Ph. D. theses of R. R. Fullwood and R. R. Lee

Les mesures sont faites à l'aide d'un accélérateur linéaire d'électrons pulsé et d'un hacheur phasé de neutrons. La bouffée initiale de photoneutrons injectée dans le ralentisseur est échantillonnée ultérieurement par un hacheur mécanique de neutrons ayant un temps d'échantillonnage d'une largeur entière de 130 μs à la moitié du maximum. On analyse en énergie cet échantillon du spectre de neutrons par la méthode du temps de vol sur un parcours de 3 m, au moyen d'un détecteur à BF_3 et d'analyseurs d'énergie.

Un hacheur circulaire, en acier à 1% en poids de ^{10}B, de 200 mm d'épaisseur, est placé aussi près que possible du ralentisseur pour réduire au minimum la distance entre la plan du hacheur et le fond de la cavité de 13 mm × 13 mm qui pénètre jusqu'au centre du système. On réduit ainsi au minimum la correction délicate qu'il faut appliquer au spectre du fait du parcours de vol jusqu'au hacheur.

On déduit le bruit de fond des données obtenues et on leur applique une correction pour tenir compte de la distance moyenne d'arrêt du détecteur, qui est fonction de l'énergie, de la réponse en énergie du détecteur et de la matière présente sur le parcours de vol. On calcule le temps moyen de hachage en se fondant sur une hypothèse touchant la variation du flux en fonction du temps; on obtient cette hypothèse en ajustant les données par la méthode des moindres carrés. Il faut procéder à plusieurs itérations avant d'obtenir des résultats convergents.

ДЕЙСТВИЕ КОГЕРЕНТНОГО РАССЕЯНИЯ НА ТЕРМАЛИЗАЦИЮ НЕЙТРОНОВ В БЕРИЛЛИИ. Когерентное рассеяние усложняет проблему термализации в кристаллических замедлителях благодаря захвату нейтронов при энергиях Брэгга. Этот эффект возникает потому, что весь микрокристалл поглощает атомы отдачи в результате столкновения; имеет место также повышение рассеяния, так как сечение должно усредняться на все атомы кристалла. Если удаляется нейтрон из захваченного пика за счет неупругого или некогерентного упругого рассеяния, то вполне возможно, что будет наблюдаться утечка из замедлителя в небольшой системе ввиду очень малой величины λ_{tr} для значения энергий, отличающихся от брэгговских. Эти эффекты приводят к нейтронному спектру в металлическом бериллии, который для значений лапласиана 0,72 и 0,1/см^2 не достигает равновесия за время до 5 средних величин времени жизни нейтронов в экспериментах на затухание. Для лапласианов примерно 0,027 и 0,01/см^2 спектр, хотя он и искажен в обоих случаях по сравнению с максвелловским распределением, становится стабильным после примерно 600 мксек. Во всех случаях спектр резко обрезается для энергий нейтронов ниже 0,0068 эв, что является самым низким пиком Брэгга.

Осуществляются измерения с использованием фазового селектора нейтронов с импульсным электронным линейным ускорителем. Позже производится отбор первоначального фотонейтронного импульса, инжектированного в замедлитель, с помощью металлического селектора нейтронов с временем взятия образца FWHM 130 мксек. Этот образец нейтронного спектра анализируется по энергии методом времени пролета по трехметровой траектории полета с помощью детектора BF_3 и анализаторов энергии.

Дисковой селектор (сталь с 1% B^{10}, толщиной 0,75 дюйма), расположен по возможности ближе к замедлителю для уменьшения расстояния между селекторной пластиной и дном входного отверстия 0,5 × 0,5 дюйма, ведущего к центру среды. Это сводит к минимуму трудность введения поправки к спектру, связанной с траекторией полета в селекторе.

Данные квалифицированно извлекаются и исправляются для зависимого от энергии среднего расстояния детектора, энергетической характеристики детектора и материала на траектории полета. Рассчитывается среднее время селекции на основе предполагаемой зависимости потока-времени, которая получается на основе данных методом наименьших квадратов. Требуется несколько повторений до получения согласованности данных между собой.

EFECTOS DE LA DISPERSION COHERENTE EN LA TERMALIZACION DE NEUTRONES EN EL BERILIO. La dispersión coherente complica el problema de la termalización en moderadores cristalinos por la retención de los neutrones a las energías de Bragg. Este efecto se debe a que todo el microcristal absorbe las partículas de retroceso resultantes del choque; asimismo, el aumento de energía por dispersión es escaso, pues la sección eficaz ha de promediarse respecto de todos los átomos del cristal. Si el neutrón es desalojado de un pico de retención por dispersión inelástica o dispersión elástica incoherente, es bastante probable que escape del moderador en un sistema de dimensiones reducidas, pues λ_{tr} es mucho menor para valores distantes de las energías de Bragg. Estos efectos originan en el Be metálico un espectro neutrónico que, para valores del laplaciano iguales a 0,072 y 0,1/cm^2 aproximadamente no alcanza el equilibrio en intervalos de incluso 5 vidas medias en experimentos de atenuación neutrónica. Para laplacianos del orden de 0,027 y 0,01/cm^2 el espectro, si bien se aparta en ambos casos de la distribución maxwelliana, parece alcanzar la estabilidad al cabo de unos

600 μs. En todos los casos el espectro resulta muy perturbado cuando la energía neutrónica es inferior a 0,0068 eV, que es el pico menor de Bragg.

Las mediciones se efectúan por el procedimiento del selector de neutrones en fase y del acelerador lineal de electrones pulsados. El impulso inicial de fotoneutrones inyectado en el moderador es muestreado por un selector mecánico de neutrones cuyo tiempo de muestreo (amplitud total a la mitad del máximo) es de 130 μs. La energía de esta muestra del espectro neutrónico se analiza por el método del tiempo de vuelo en una trayectoria de 3 m con un detector de BF_3 y analizadores de energía.

Un selector de disco de acero al ^{10}B de 3/4 de pulg de espesor (1% en peso de ^{10}B) se coloca lo más cerca posible del moderador para reducir al mínimo la distancia entre el plano de selección y el fondo del orificio reentrante de 0,5 pulg × 0,5 pulg, que penetra hasta el centro del medio. Esto simplifica la difícil corrección de la trayectoria de vuelo en el selector para adaptarla al espectro.

La actividad de fondo se resta de los datos, que se corrigen para tener en cuenta la distancia media de frenado en el detector, dependiente de la energía, la respuesta energética del detector y el material situado en la trayectoria de vuelo. El tiempo medio de selección se calcula basándose en una dependencia hipotética del flujo con respecto al tiempo, que se determina ajustando los datos por cuadrados mínimos. Se precisan varias iteraciones para obtener resultados compatibles.

1. INTRODUCTION

When neutrons thermalize in a crystalline moderator, it is possible for the neutron density to be increased over the Maxwellian distribution in the vicinity of the Bragg coherent scattering peaks. This is called neutron trapping [1]. The phenomenon involved is that of the neutron wave interacting with a whole crystal which substantially eliminates any change of energy in such scattering interactions. The thermalization of neutrons in beryllium which exhibits marked coherent Bragg scattering peaks has led to the experimental and theoretical investigations of several ramifications of this phenomenon.

The disappearance of a discrete asymptotic decay constant and the existence of an upper bound on the asymptotic decay constant for small beryllium assemblies was first predicted by de SAUSSURE [1, 2, 3]. He also predicted on physical grounds the existence of a continuum of eigenvalues in the spectrum for materials exhibiting coherent Bragg peaks. The existence of a continuum in a rigorous theory has also been demonstrated [4, 5]. The disappearance of eigenvalues into the continuum has been demonstrated by means of some numerical calculations for tightly bound materials [6]. In this paper we will study evidence of these phenomena and also determine the nature of the asymptotic spectrum.

Our qualitative estimates for the occurrence of the upper bound on the asymptotic eigenvalue were based on the two group treatment of DAITCH and ĘBEOGLU [7], which is essentially the model of de SAUSSURE [1], using one group as the thermal group and the other as a delta function to represent the trapped group at about 0.007 eV. The eigenvalue of the broad thermal group increases linearly with B^2 (neglecting higher terms) in much the same manner as a non-crystalline moderator. The eigenvalue of the trapped group changes very little with buckling because of the very large value of the transport cross-section at the Bragg peak of about 0.007 eV. It is therefore possible for these eigenvalues to coincide for some critical buckling which appeared to be about 0.05 cm^{-2}. Further, for bucklings beyond this value the asymptotic eigenvalue would be that of the trapped group. If this picture

were enlarged to include all energy groups this trapped eigenvalue would appear in a continuum. For bucklings larger than the critical buckling, the dominant eigenvalues are the continuum and the thermal group eigenvalue appears to become buried in this spectrum.

The purpose of this investigation was to establish the situation as firmly as possible for beryllium for a series of bucklings including the range greater than 0.05 cm^{-2}. A considerable amount of data has been reported in this interesting range but the scatter in asymptotic eigenvalues for large bucklings [8, 9, 10, 11] was great and it was hoped to take advantage of the very high neutron intensity available from the Rensselaer Polytechnic Institute pulsed-Linac to perform experiments. Simultaneously, some quantitative calculations have been carried through using the same technique as OHANIAN and DAITCH [12]. The kernel employed was constructed by DAHLBERG [13]; the isotropic energy exchange kernel is based on the incoherent approximation and uses YOUNG and KOPPEL's frequency spectrum [14] for one phonon terms, the higher terms being based on a Debye spectrum; the calculation of the transport cross-section follows that of BHANDARI [15].

2. EXPERIMENTAL TECHNIQUE

The experimental set-up is shown in Fig. 1. A pulse of electrons of 0.5 A, 50 MeV was stopped in a thick water-cooled e-γ-n tungsten target. Some neutrons produced thereby were thermalized in the beryllium spectrum source. After a pre-determined waiting time, the neutron chopper opened, allowing a sample of the neutron flux extracted by a 1/2 in × 1/2 in re-entrant hole extending to the centre of each assembly to enter the time-of-flight spectrometer. The neutron spectrometer had a 3.1-m flight path which was shielded by a 5 ft × 5 ft × 10 ft tank of water. Inside of the tank were lead walls to provide gamma shielding of the detector. Further shielding of the spectrometer was provided by paraffin-boric acid and boron carbide collimators. The defining apertures were made of B^{10} sintered carbide with an aperture 1/8-in in diameter next to the chopper followed by a similar one with 1/2-in aperture located just inside the shielding tank.

The rotor of the neutron chopper was a disk, 7.25-in in diameter, 0.75-in thick, of stainless steel containing 1 wt.% of B^{10}. The slot was 0.392 in wide on the side facing the medium and 0.492 in wide away from it at the trailing edge to allow neutrons of energy as low as 0.0022 eV to pass through. The resulting burst width of the chopper was essentially trapezoidal, 121 μs full width at half maximum. The disk was mounted on one end of a quill bearing and driven at 9000 rpm by a synchronous motor with a five-to-one gear belt step-up. A time signal was obtained by a magnetic drum head pick-up from a piece of magnetized steel on the circumference of the disk located 572 μs ahead of the opening time of the chopper. Additional shielding was located around the chopper to reduce the background.

The neutron detector in the time-of-flight spectrometer was a ceramic end-window counter 2 in in diameter and 6 in long filled to one atmosphere of 96% enriched BF_3. The axis of the counter was in the neutron flight path.

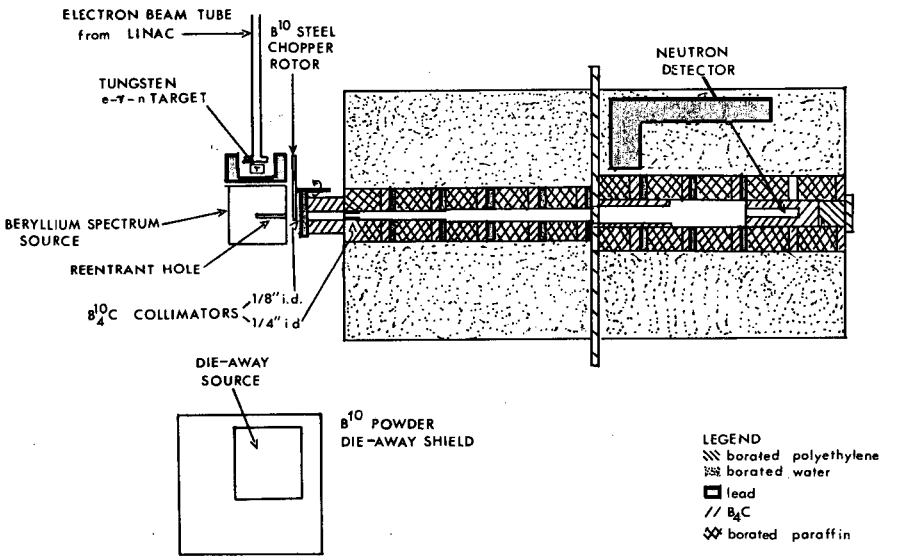

Fig. 1

The heavily shielded 3.1-m neutron spectrometer

Additional BF_3 counters located outside the shield tank were used as beam intensity monitors for normalization purposes.

The timing sequence began by the detection of a signal from the magnetic timing mark. This signal was amplified, shaped and sent to the control room where it triggered a binary count-down circuit that allowed operation at 150 pulses per second or sub-harmonics depending upon electron beam power restrictions. This signal triggered a digital delay generator which in turn fired the Linac; thus, this delay generator controlled the waiting period before sampling the spectrum. This delay generator in conjunction with another one was used to gate off and on the scalers that count the monitor signals. The scalers were gated off just before pulsing the Linac and were kept off for 700 μs to allow time for the stabilization of the monitor detectors and electronics. The signals from the spectrometer detector were appropriately amplified and shaped and sent to the control room for recording on a TMC CN110 digital computer using a type-212 time-of-flight plug-in with channel widths of 80 μs. The time-of-flight unit was triggered by the count-down circuit so that the gamma flash was recorded in the computer.

The four spectrum sources were constructed of beryllium of 99% purity, which was lent by Oak Ridge National Laboratory through the courtesy of Dr. Dixon Callahan. They were part of the same batch of beryllium used by de Saussure and Silver in their die-away measurements. The individual blocks were small and of several commensurate dimensions which permitted stacking to form the assemblies tabulated in Table I. The mean density was 1.85 g/cm^3. The individual blocks had a 0.199-in hole centred on the square face but by taking advantage of the different sizes, the blocks were stacked to break this hole in each layer so that neutron streaming would not influence the results. The buckling values presented in Table I were

TABLE I

SPECTRUM SOURCES

	Medium I	Medium II	Medium III	Medium IV
Dimensions (in)	2.87 x 12.06 x 12.13	4.31 x 11.88 x 12.02	12.94 x 12.13 x 12.00	18.63 x 17.31 x 17.75
Weight (kg)	13	19	57	173
Buckling (cm^{-2})	0.12	0.75	0.026	0.013

obtained from the stacked dimension with the addition of a buckling-dependent extrapolation length obtained from ANDREWS [10]. The buckling-dependent extrapolation length is not presented in Andrews but can be obtained from his data. The assemblies were surrounded by 1/32-in cadmium, enclosed in 1-in polyethylene to give mechanical strength and provide additional high energy neutron moderation and then clamped between 1/2-in aluminium plates. The upper plate had a large eye bolt to allow the moving of the assembly into position on the neutron spectrometer using an overhead crane.

3. CORRECTIONS TO THE DATA

The energy response of the spectrum detector was measured at the Knolls Atomic Power Laboratory by Mrs. Sara B. Armstrong using a 6.1 m flight path on the east thermal column of the Thermal Test Reactor by a comparison with a 1/v counter of the same geometry at the same position. The tabular results of this experiment were put into an analytic form by observing that the departure from a first collision calculation for the detector was only about 10%. Therefore, the data were least squares fitted to a power series using as a weight the first collision probability; namely

$$\mathrm{CORR}\,(1/v) = (1-e^{-\Sigma L}) \sum_{l=0}^{5} a_l (1/v)^l$$

where Σ is the macroscopic cross-section of the BF_3 gas, L is the counter length, and v is the neutron velocity (m/s). The neutron detector constituted a 5% variation in the neutron stopping position in the detector as a function of neutron energy. This effect was corrected by calculating the mean stopping position with a first collision weight; namely

$$\bar{x} = \frac{\int_0^L \Sigma_a \, x(1-e^{-\Sigma x})dx}{\int_0^L \Sigma_a \, (1-e^{-\Sigma x})\,dx} .$$

The 3.1-m flight path was not evacuated and a correction was made for material in the neutron beam. This correction was made by a FORTRAN code written by Mr. R. C. Kryter using the cross-section data in BNL-325. Corrections were made for aluminium, oxygen, nitrogen and water by using table look-up in resonance regions and fractional power of energy fitting in the smooth regions. This code covered the energy range 0.0008 to 10.0 eV.

It was also necessary to correct for the fact that the chopper time response was finite. The mean chopping time was calculated from the time averaged over the chopper response function and the time dependence of the spectrum; namely

$$\bar{t} = \frac{\int_0^\infty t\Phi(c_0, 1/v, t)C(t)dt}{\int_0^\infty \Phi(c_0, 1/v, t)C(t)dt} .$$

The quantity $\Phi(c_0, 1/v, t)$ is the flux incident upon the chopping plane as a function of reciprocal velocity and time after the neutron burst occurred, and C(t) is the chopper time response function as a function of time after the initial neutron burst.

It should be noted that the spectrum being sampled by the neutron chopper is not the same spectrum as that in the centre of the medium because of the transit time distortion due to the time required for the neutrons of different energies to travel the distance from the re-entrant hole bottom to the chopping plane. The correction for this distortion in the asymptotic time limit [16] is $\exp(\alpha l/v)$ where α is the decay constant, and l is the distance in meters from the centre of the medium to the chopping plane.

In the analysis of these experiments it was decided to use the following simplest a priori assumption on time dependence:

$$\Phi(0, 1/v, t) = a(e^{-\alpha_1 t} - e^{-\alpha_2(1/v)t}) ,$$

where a is a fitting parameter, α_1 is the "asymptotic" decay constant and $\alpha_2(1/v)$ is the "mother" decay constant. This dependence tacitly assumed the form of a two-group calculation with the thermal group feeding the trapped group and conformed with experimental measurements which showed an essentially single exponential decay. (It may actually be a composite

of continuous eigenvalues.) This form was integrable over the chopper function but analytically was much more complicated than the similar calculation for an asymptotic spectrum such as would be observed in an infinite non-crystalline homogeneous medium. One of the principal difficulties was due to the fact that the calculation must be done in retarded time, whereas, in the asymptotic calculation time zero may be arbitrarily located. Several times may be defined as follows:

$$\tau_1 = 574.2 - 1/v - \text{DELACC}$$
$$\tau_2 = 608.5 - 1/v - \text{DELACC}$$
$$\tau_3 = 693 - 1/v - \text{DELACC}$$
$$\tau_4 = 727 - 1/v - \text{DELACC}$$
$$S_{lm} = \frac{e^{-\alpha_l \tau_m}}{\alpha_l^2}$$
$$T_{lm} = \left(\tau_m + \frac{2}{\alpha_l}\right) S_{lm} .$$

Then the mean chopping time is:

$$\bar{t} = \frac{T_{11} + T_{14} - T_{12} - T_{13} + T_{22} + T_{23} - T_{21} - T_{24}}{S_{11} + S_{14} - S_{12} - S_{13} + T_{22} + T_{23} - T_{21} - T_{24}} + \frac{1}{v} + \text{DELACC}$$

where DELACC is the delay between the accelerator firing and the chopper opening.

Because the mean chopping time was energy dependent, it was necessary to reconstruct the spectrum at a fixed time which was chosen to be the centre of the chopper opening (t_{eff}). The spectrum must also be reconstructed at the centre of the medium. This was done by the following transformation:

$$\Phi(0, v, t_{eff}) = \frac{B\Phi(c_0, v, \bar{t}(v)[e^{-\alpha_1 t_{eff}} - e^{-\alpha_2 t_{eff}}]}{[e^{-\alpha_1(\bar{t}(v) - c_0/v)} - e^{-\alpha_2(\bar{t}(v) - c_0/v)}]} ,$$

where $\Phi(c_0, v, \bar{t}(v))$ was the flux at the chopping plane at the mean chopping time. All the previous corrections were performed in the FORTRAN code PROD and were applied to all data presented.

To obtain $\alpha_2(1/v)$, the data were first processed in PROD using the approximate form $\alpha_2(1/v) = 1/\xi\bar{\Sigma}_s v$, where ξ is the logarithmic energy decrement and Σ_s is the average macroscopic scattering cross-section over the region of interest. Then the results of PROD were least squares fitted by iteration to the mother-daughter time dependence in a code LSMFD which gave a better form for $\alpha_2(1/v)$. This result was inserted into PROD, and this process repeated until self consistency was obtained.

4. RESULTS

The results of the experiment are plotted as $\phi(E)$ versus E in Figs. 2-6. Figures 2 and 3 for bucklings of 0.12 and 0.075 cm^{-2} respectively show spectra for all the different time intervals that were practical to measure in each case. The curve 122 μs in Fig. 2 is too early in time for the spectrum

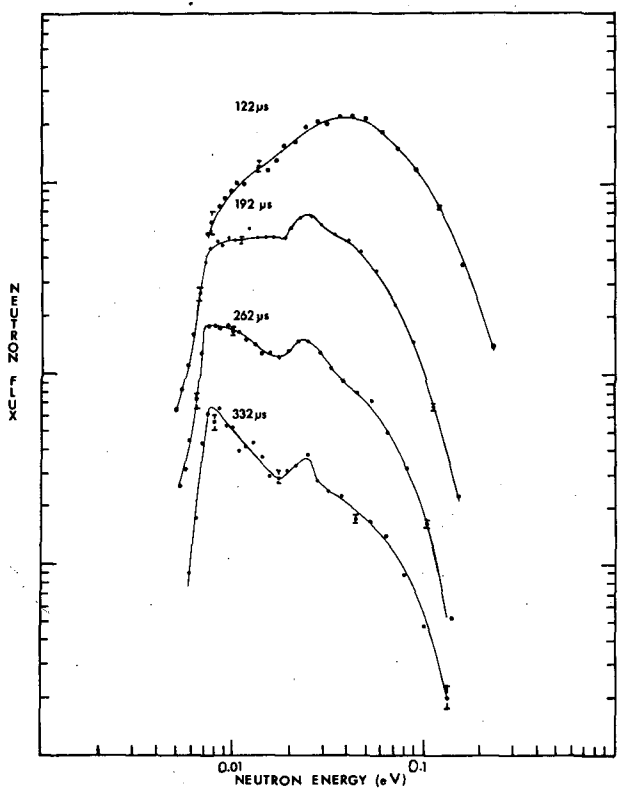

Fig. 2

Time-dependent spectra in beryllium metal, $B^2 = 0.12$ cm^{-2}. The error bars are statistical only; the normalization is arbitrary. The solid lines are used to assist the reader and relate to no theory.

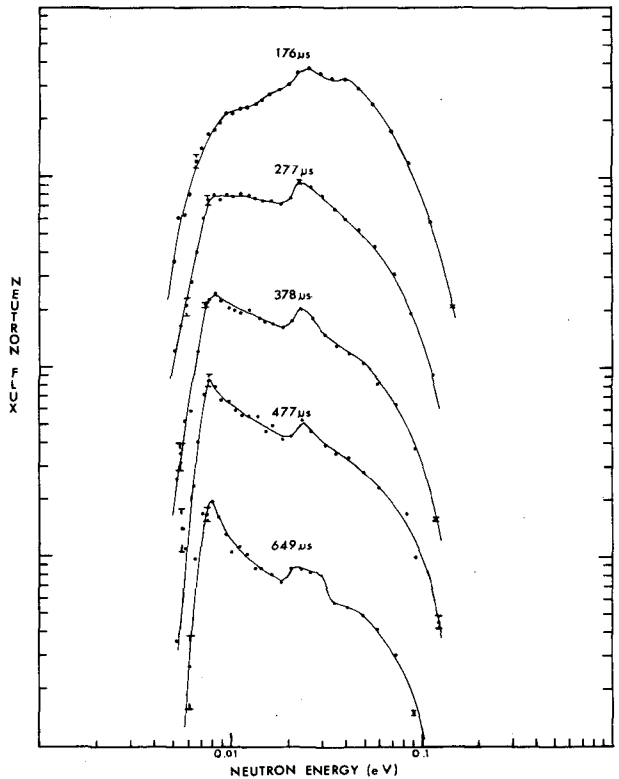

Fig. 3

Time-dependent spectra in beryllium metal, $B^2 = 0.075$ cm^{-2}. The error bars are statistical only; the normalization is arbitrary. The solid lines are used to assist the reader and relate to no theory.

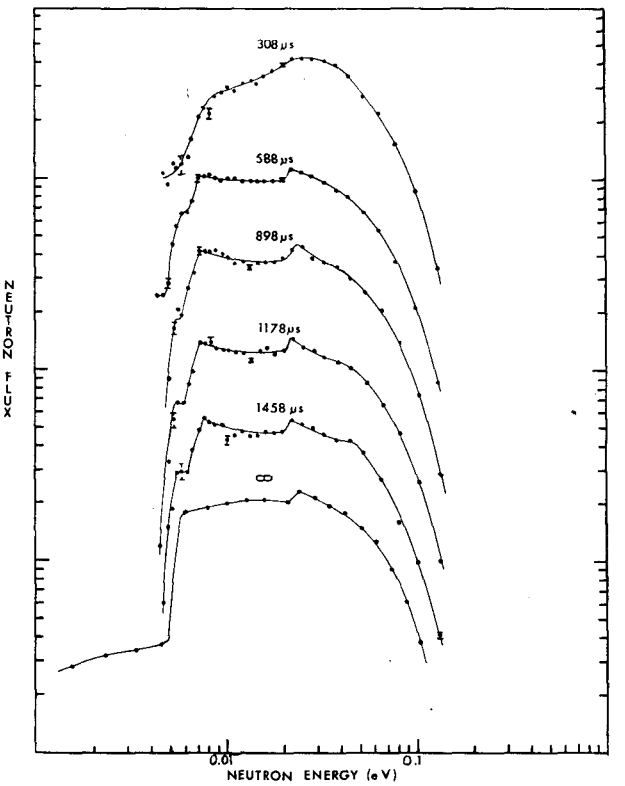

Fig. 4

Time-dependent spectra in beryllium metal, $B^2 = 0.026$ cm^{-2}. The error bars are statistical only; the normalization is arbitrary. The solid lines are used to assist the reader and relate to no theory. The points on the curve labelled ∞ are the theoretical results of the discrete ordinates method (see text).

to have thermalized in the usual sense and is not particularly pertinent to the object of this study. Figure 4 shows a considerable spectral change out to 588 μs or approximately 2 mean lifetimes after which it is quite stable. (The curves labelled ∞ are asymptotic calculations based on the discrete ordinate method of OHANIAN and DAITCH [12].) The agreement for this buckling is extremely good considering the number of discrete ordinates used. Figure 5 shows essentially stable spectra for all four times; therefore for this buckling (0.013 cm^{-2}) no information is available as to the thermalization time.

Figure 6 is the surface spectra measured for a buckling of 0.026 cm^{-2} and compared with the centre spectrum for this buckling at 898 μs after the burst. In general, peaks in the transport cross-section correspond to depressions in the surface spectrum and peaks in the centre spectrum.

To clearly bring out the trapping effect these spectra were fitted to a Maxwellian distribution by least squares techniques resulting in a neutron temperature in this sense. The fractional deviation from this fitted

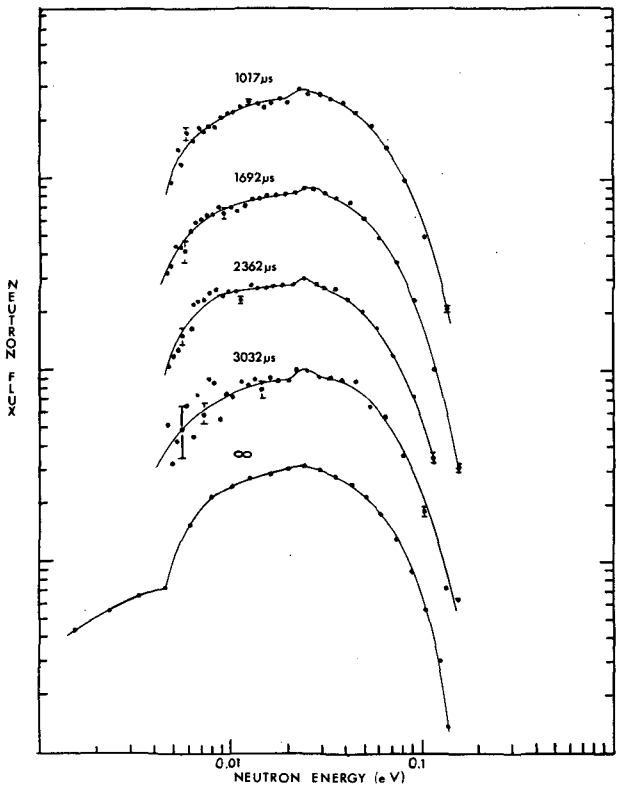

Fig. 5

Time-dependent spectra in beryllium metal, $B^2 = 0.013$ cm^{-2}. The error bars are statistical only; the normalization is arbitrary. The solid lines are used to assist the reader and relate to no theory. The points on the curve labelled ∞ are the theoretical results of the discrete ordinates method (see text).

Maxwellian was calculated and is presented in Figs. 7 to 11. This displays graphically the trapping phenomena. A great deal of the information in the spectrum at any one time is given by the temperature of the linearized Maxwellian fitted by means of least squares. Further, the meaningful deviations from this function are clearly visible in these plots. The temperature of the fitted Maxwellian varies approximately 20°K/mean lifetime in this range for the buckling 0.12 cm^{-2} and about 10°K/mean lifetime for the buckling 0.075 cm^{-2}. Figure 9 shows definitely that the spectrum is stable after 588 μs for the buckling 0.026 cm^{-2}. Figure 10 shows this same stability for the buckling 0.013 cm^{-2}.

To ensure the proper operation of the equipment and the correctional procedures, a slab of polyethylene of buckling 0.16 cm^{-2} was measured in the spectrometer under the same conditions that the beryllium was measured (Fig. 10). A Maxwellian, diffusion-cooled 1°K is expected [17]. The medium temperature measured by thermocouples also indicated 300°K with a probable

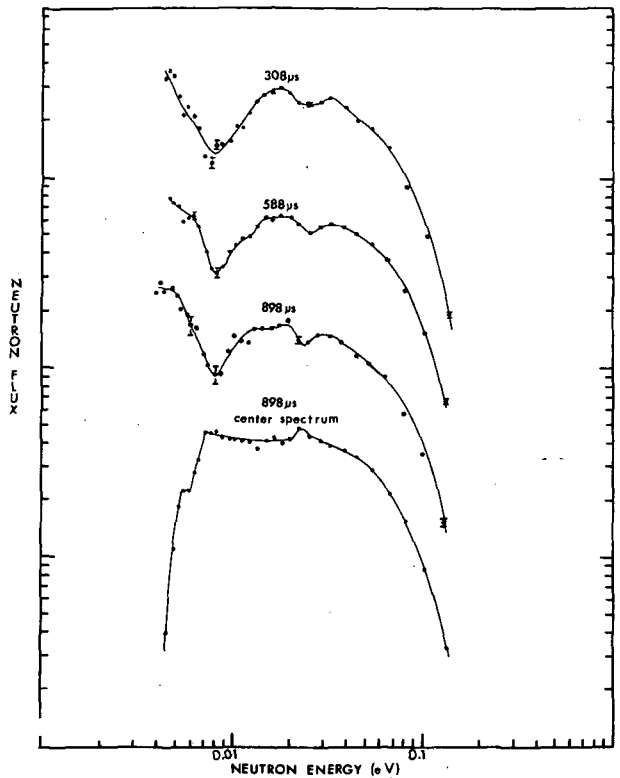

Fig. 6

Time-dependent surface spectra from beryllium metal, $B^2 = 0.026$ cm^{-2}.
The error bars are statistical only; the normalization is arbitrary.
The solid lines are used to assist the reader and relate to no theory.

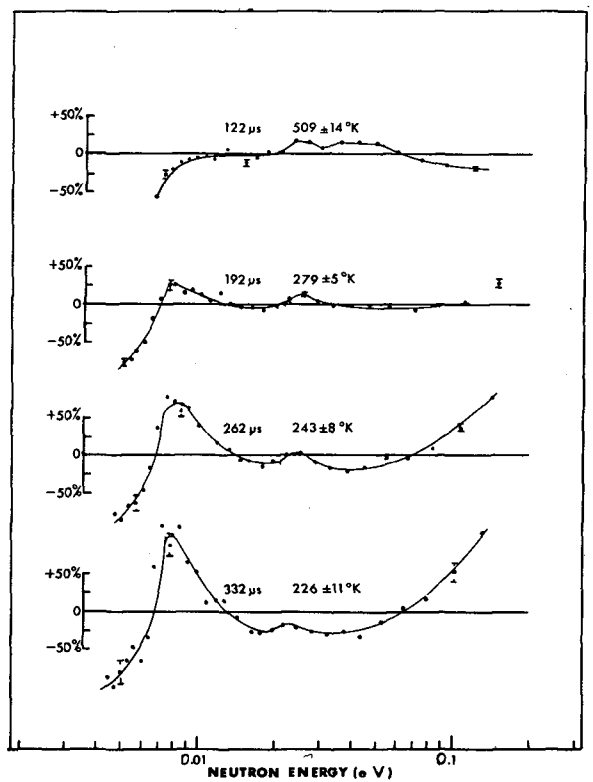

Fig. 7

Fractional deviation of beryllium neutron spectra from fitted Maxwellian distribution, $B^2 = 0.12$ cm^{-2}.
The error bars are statistical only. The medium temperature was 305°K.

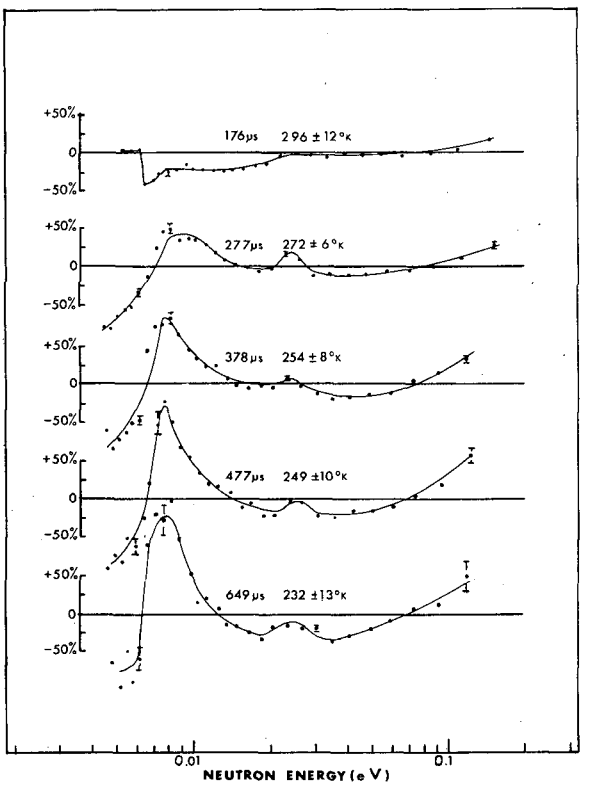

Fig. 8

Fractional deviation of beryllium neutron spectra from fitted Maxwellian distribution, $B^2 = 0.075\ cm^{-2}$.
The error bars are statistical only. The medium temperature was 305°K.

error of 1°K. It was therefore concluded that the equipment and corrections were performing correctly.

The theory employed uses a discrete set of energies which results in a lack of resolution in that certain peaks in the cross-sections and flux cannot be well represented. The points of the energy mesh are represented by solid circles on the theoretical curves, see Figs.4 and 5 labelled ∞ and Fig.12. These are multigroup diffusion theory calculations using 37 groups from 0.00005 to an upper limit of 2.0 eV. The geometry is taken to be that for the one dimensional slab case with a single buckling component equal to the total buckling of the experimental assembly. The kernel used is a full isotropic energy exchange kernel and a diagonal P_1 kernel as described in the introduction. There are limitations on the accuracy of the theoretical calculations involving besides the finite discrete mesh the inaccuracy involved in these particular calculations which set certain small matrix elements to zero; these inaccuracies might total as much as 0.1%. For this reason, the value of the asymptotic eigenfunctions much below one thousandth of the peak value of any particular asymptotic eigenfunction may be some-

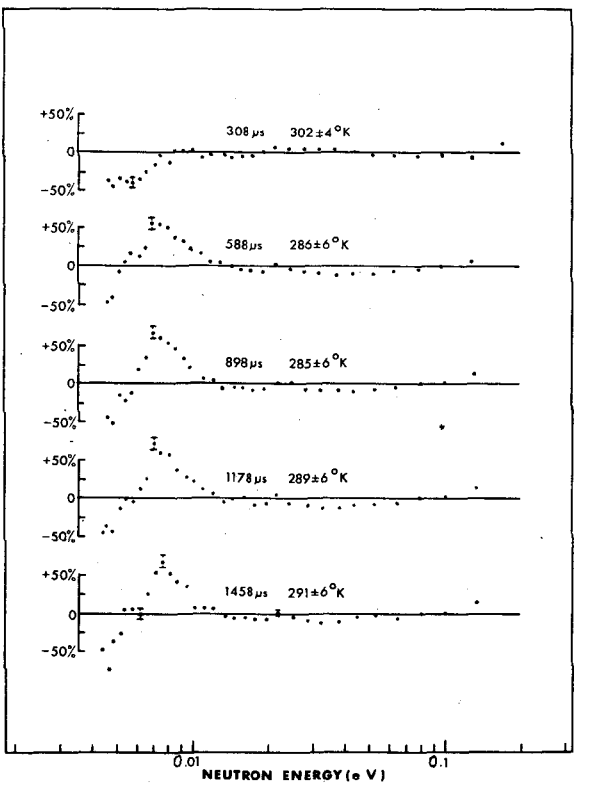

Fig. 9

Fractional deviation of beryllium neutron spectra from fitted Maxwellian distribution, $B^2 = 0.026\ cm^{-2}$.
The error bars are statistical only. The medium temperature was 295°K.

what questionable. The asymptotic eigenfunctions for the bucklings of 0.075 and 0.12 cm^{-2} in Fig. 12 are definitely identified as "continuum" eigenfunctions, as in reference [12], peaking at the lowest energy mesh point employed, 0.00005 eV. Conversely, the asymptotic eigenfunctions for the smaller bucklings are not "continuum" but rather discrete eigenfunctions.

5. CONCLUSIONS

Time-dependent spectra furnish a severe test of many phenomena in the thermal range. Although a great deal of the data may be represented by the temperature of the least squares fitted Maxwellian, the experiments presented here also show systematic deviations from the Maxwellian. The idea of neutron trapping is consistent with the experimental data. For bucklings less than or equal to 0.026 cm^{-2} an asymptotic spectrum is established within experimental error. For bucklings larger than or equal to 0.075 cm^{-2} an asymptotic spectrum was not found experimentally for

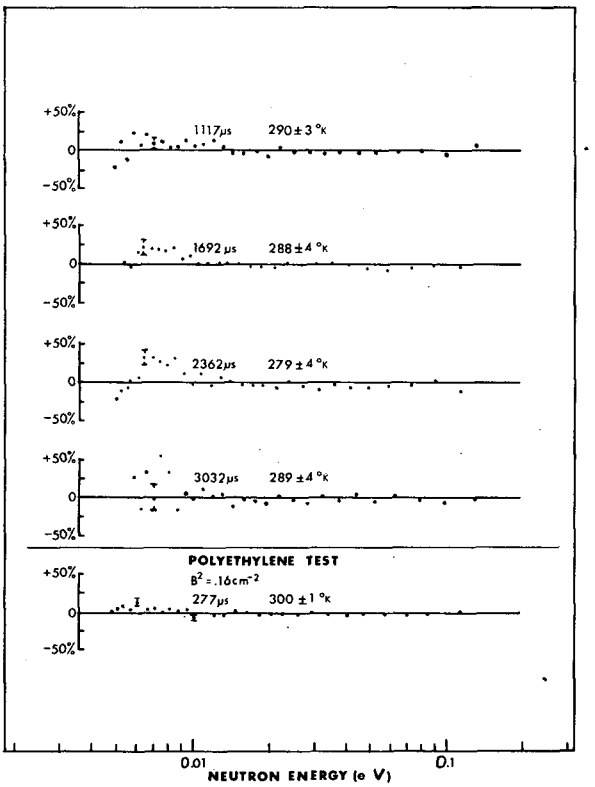

Fig.10

Fractional deviation of beryllium neutron spectra from fitted Maxwellian distribution, $B^2 = 0.013\ cm^{-2}$.
The error bars are statistical only. The beryllium medium temperature was 295°K; the polyethylene medium temperature was 300°K.

times up to six mean lives after the initial burst of neutrons. This is in agreement with simple theoretical models. Somewhat more complicated models suggest further interesting phenomena involving what might be called the extreme diffusion cooling case in that the neutron flux is tending towards a peak at zero energy. Over the energy range of measurement involved in our measurements, there is no large disagreement between theory and experiment. The fact that an asymptotic spectrum is not established in certain cases indicates that several eigenfunctions or perhaps a continuum of eigenfunctions are contributing in these cases. Certainly, as one goes from $B^2 = 0.026\ cm^{-2}$ to $B^2 = 0.075\ cm^{-2}$ the dominance of the lowest eigenfunction has been essentially lost.

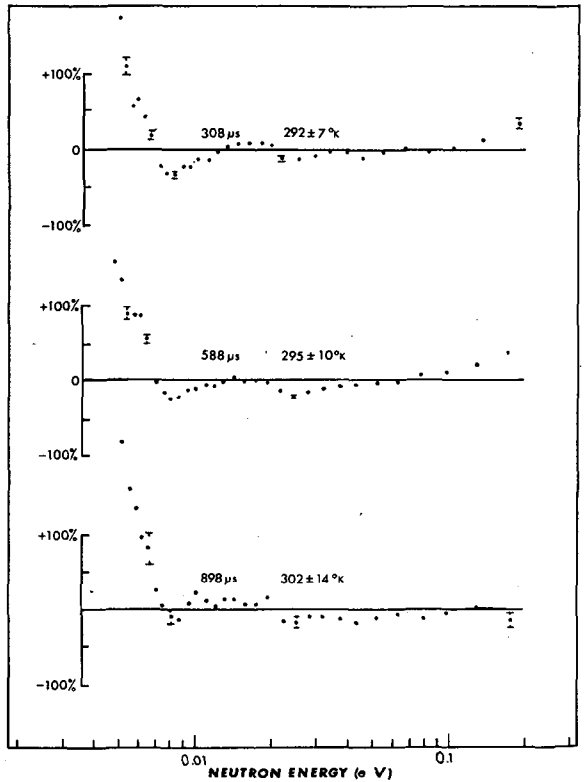

Fig. 11

Fractional deviation of beryllium neutron surface spectra from fitted Maxwellian distribution, $B^2 = 0.026\ cm^{-2}$.
The error bars are statistical only. The medium temperature was 297°K.

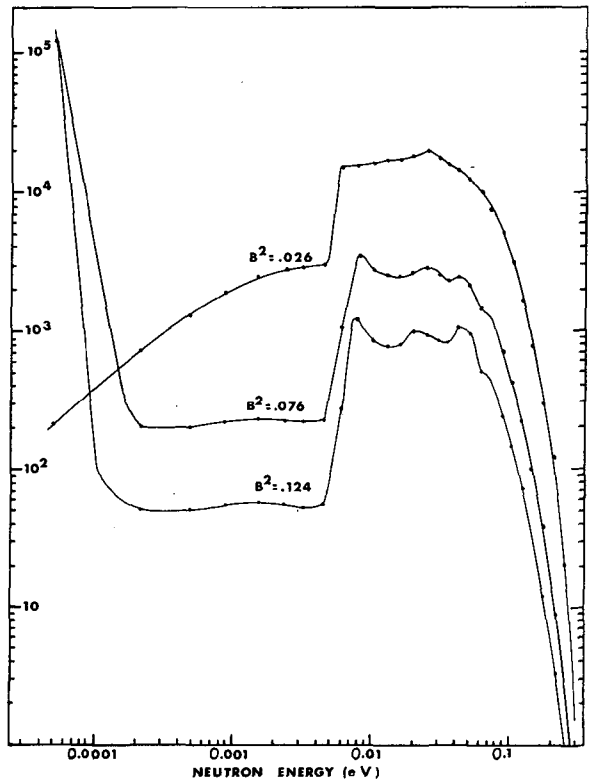

Fig. 12

Lowest theoretical eigenfunctions
Energy mesh points are indicated by solid circles.

REFERENCES

[1] de SAUSSURE, G., Rpt. ORNL-3193 (1961) 223-228.
[2] de SAUSSURE, G., Nucl. Sci. Engng 12 (1962) 433.
[3] de SAUSSURE, G., Proc. Brookhaven Conf., Neutron Thermalization, Rpt. BNL 719 (C-32) IV (1962) 1158.
[4] CORNGOLD, N., MICHAEL, P., WOLLMANN, W., Nucl. Sci. Engng 15 (1963) 13.
[5] KOPPEL, J., Nucl. Sci. Engng 16 (1963) 101.
[6] CORNGOLD, N., SHAPIRO, C., Trans. Amer. nucl. Soc. 7 (1964) 52.
[7] DAITCH, P., EBEOGLU, D., Proc. Brookhaven Conf. Neutron Thermalization, Rpt. BNL-719 (C-32) IV (1962) 1132.
[8] ANTONOV, A. et al., Proc. UN Int. Conf. PUAE 5 (1956) 3,82.
[9] de SAUSSURE, G. and SILVER, E., Rpt. ORNL-2641 (1959).
[10] ANDREWS, W., Rpt. UCRL-6083 (1960).
[11] SILVER, E., Proc. Brookhaven Conf. Neutron Thermalization, Rpt. BNL-719 (C-32) III (1962) 981.
[12] OHANIAN, M.J. and DAITCH, P.B., Nucl. Sci. Engng 19 (1964) 343.
[13] DAHLBERG, R., Ph.D. Thesis at Rensselaer Polytechnic Inst., 1964.
[14] YOUNG, J., KOPPEL, J., Nucl. Sci. Engng 19 (1964) 367.
[15] BHANDARI, R., J. nucl. Energy 6 (1958) 104.
[16] BECKURTS, K.H., Z. Naturf. 16a (1961) 611.
[17] FULLWOOD, R.R., Trans. Amer. nucl. Soc. 7 (1964) 231.

MEASUREMENTS OF THE SPATIALLY-DEPENDENT ASYMPTOTIC SPECTRA IN WATER AND POLYETHYLENE*

E. R. GAERTTNER, R. R. FULLWOOD, J. H. MENZEL AND G. P. TOTH
RENSSELAER POLYTECHNIC INSTITUTE,
TROY, N. Y., UNITED STATES OF AMERICA

Abstract — Résumé — Аннотация — Resumen

MEASUREMENTS OF THE SPATIALLY-DEPENDENT ASYMPTOTIC SPECTRA IN WATER AND POLYETHYLENE. Diffusion parameters except for Σ_a may be measured by studying the asymptotic neutron flux distribution as a function of the energy and space variables. In addition to the energy integral quantities which may also be obtained from a die-away experiment, the energy-dependent extrapolation length and energy-dependent transport mean-free-path length may also be obtained.

The time asymptotic spectrum is measured by the phased neutron chopper, pulsed-electron, linear-accelerator technique. The initial photo-neutron pulse is obtained by stopping the electron beam in a thick tungsten target. At a later time, a mechanical neutron chopper is allowed to open, sampling the spectrum at this time and defining a time zero for the time-of-flight neutron energy determination. The neutrons are detected in an end window BF_3 detector and time-sorted in a multichannel analyser. The neutron spectrum is extracted from the medium by the use of re-entrant holes extending to various depths.

The neutron spectra as a function of position are analysed according to first-order diffusion theory

$$F(X,E) = F(O,E)\left[\cos\frac{\pi x}{L} + \frac{\pi\lambda_{tr}}{L}\sin\frac{\pi x}{L}\right],$$

where $F(X,E)$ is the measured flux, $L = 2(a + \epsilon)$, a being the slab half-thickness and ϵ the extrapolation distance. The extrapolation distance is obtained by a least squares fit of the scalar flux to a cosine distribution for a given energy. The value of λ_{tr} is obtained by fitting the above equation using the previously obtained value of the extrapolation distance.

The value of the diffusion cooling coefficient is obtained by directly measuring the scalar flux neutron temperature. From a variational diffusion calculation the following may be obtained for the case of 1/v absorption and $\lambda_{tr} \sim E^{\alpha}$ where α is a constant:

$$C = \frac{D_0(T - T_n)(\alpha + \frac{1}{2})}{T_n B^2}$$

where D_0 is the average diffusion coefficient, T the medium temperature, T_n the neutron temperature and B^2 the buckling. This equation is valid to the first order in the temperature shift and to the second order in buckling. For those cases of more complicated energy dependence of λ_{tr}, more complex relations have been developed.

In addition to the above analyses, it is also possible to study the neutron temperature as a function of position and by adding and subtracting symmetrical spatial points to obtain the scalar and current flux. Present measurements give a constant scalar flux temperature up to a distance of about 1 cm from the surface for a polyethylene slab 7.5 cm thick. This has been interpreted by M. M. R. Williams as a breakdown of space-energy separability near the surface. If this is so, the diffusion theory approximation may indeed not be appropriate near the surface.

* Work performed under Atomic Energy Commission Contract AT (30-3) 328.

MESURES DE SPECTRES ASYMPTOTIQUES, VARIABLES DANS L'ESPACE, DANS L'EAU ET LE POLYÉTHYLÈNE. On peut mesurer les paramètres de la diffusion, à l'exception de Σ_a, en étudiant la distribution du flux de neutrons asymptotique en fonction de l'énergie et de l'espace. Outre les quantités intégrales d'énergie, que l'on peut aussi obtenir par une expérience sur l'évanouissement, on peut déterminer la longueur extrapolée et la longueur libre parcours moyen de transport variables selon l'énergie.

On mesure le spectre asymptotique dans le temps par la méthode du hacheur de neutrons phasé et de l'accélérateur linéaire d'électrons pulsé. On obtient la bouffée initiale de photoneutrons en arrêtant le faisceau d'électrons par une cible de tungstène épaisse. A un instant donné, un hacheur mécanique de neutrons commence à échantilloner le spectre et définit ainsi un temps zéro pour la détermination de l'énergie des neutrons par la méthode du temps de vol. Les neutrons sont mesurés par un détecteur à BF_3 à fenêtre en bout et analysés en temps par un sélecteur multicanal. On extrait le spectre de neutrons du système au moyen de cavités de différentes profondeurs.

On analyse les spectres de neutrons en fonction de la position d'après la théorie de la diffusion du premier ordre

$$F(X,E) = F(O,E)\left[\cos\frac{\pi x}{L} + \frac{\pi\lambda_{tr}}{L}\sin\frac{\pi x}{L}\right]$$

où $F(X,E)$ est le flux mesuré, $L = 2(a+\epsilon)$, a étant la moitié de l'épaisseur de la plaque et ϵ la distance extrapolée. On obtient la distance extrapolée en ajustant, par la méthode des moindres carrés, le flux scalaire à une distribution en cosinus pour une énergie donnée. On détermine la valeur de λ_{tr} en ajustant l'équation ci-dessus au moyen de la valeur précédemment déterminée de la distance extrapolée.

On détermine la valeur du coefficient de refroidissement par diffusion en mesurant directement la température des neutrons du flux scalaire. Par un calcul de variations, on peut obtenir l'équation suivante dans le cas d'une absorption $1/v$ lorsque $\lambda_{tr} \sim E^{\alpha}$, α étant une constante:

$$C = \frac{D_0(T - T_n)(\alpha + \frac{1}{2})}{T_n B^2}$$

où D_0 est le coefficient de diffusion moyenne, T la température du système, T_n la température des neutrons et B^2 le laplacien. Cette équation est valable jusqu'au premier ordre du changement de température et jusqu'au deuxième ordre du laplacien. Pour les cas où λ_{tr} dépend de l'énergie de manière plus complexe, on a établi des relations qui sont également plus complexes.

Outre les analyses ci-dessus, on peut étudier la température des neutrons en fonction de la position et obtenir le flux scalaire par addition ou soustraction de points symétriques dans l'espace. Les mesures actuelles donnent une température constante de flux scalaire jusqu'à une distance d'environ 1 cm de la surface pour une plaque de polyéthylène de 7,5 cm d'épaisseur. Selon une interprétation de ce résultat donnée par M.M.R. Williams, il se pourrait que l'approximation de la théorie de la diffusion ne soit pas applicable au voisinage de la surface.

АСИМПТОТИЧЕСКИЕ НЕЙТРОННЫЕ СПЕКТРАЛЬНЫЕ ИЗМЕРЕНИЯ В ПОЛИЭТИЛЕНЕ В ЗАВИСИМОСТИ ОТ ПРОСТРАНСТВА. Параметры диффузии за исключением параметров для Σ_α могут измеряться путем изучения асимптотического распределения нейтронного потока как функции переменных пространства и энергии.

Кроме интегральных количеств энергий, которые могут быть получены в результате экспериментов по затуханию, могут быть также получены длина экстраполяции в зависимости от энергии и длина средней свободной траектории переноса в зависимости от энергии.

Измеряется асимптотический спектр времени путем фазового селектора нейтронов с импульсным электронным линейным ускорителем. Первоначальный фото-нейтронный импульс получается путем остановки электронного пучка толстой мишенью из вольфрама. Позднее механический селектор нейтронов дает возможность начать отбор спектра в этот период времени и определяет нулевое время для определения энергии нейтронов по времени пролета. Нейтроны обнаруживаются в окошечном детекторе BF-3 и отбираются по времени в много-

канальном анализаторе. Спектр нейтронов выделяется из среды путем использования входных отверстий, простирающихся на различную глубину.

Спектры нейтронов как функция положения анализируются согласно теории диффузии первого порядка:

$$F(X,E) = F(O,E)\left[\cos\frac{\pi x}{L} + \frac{\pi\lambda_{tr}}{L}\sin\frac{\pi x}{L}\right]$$

F(X,E) является измеренным потоком, $L = 2(\alpha+\epsilon)$, α является толщиной половины пластины и ϵ является длиной экстраполяции. Длина экстраполяции получается подгонкой способом наименьших квадратов скалярного потока к косинусоидальному распределению для данной энергии. Значение λ_{tr} получается путем решения вышеприведенного уравнения с использованием ранее полученной величины для длины экстраполяции.

Значение коэффициента диффузионного охлаждения получается путем непосредственного измерения температуры нейтронов скалярного потока. Из расчета переменной диффузии может быть получено следующее уравнение для случая поглощения 1/v и $\lambda_{tr} \approx E^{\alpha}$, где α является постоянной:

$$C = \frac{D_0 (T - T_n)(\alpha + 1/2)}{T_n B^2}$$

является средним коэффициентом диффузии, T является температурой среды, T_n является температурой нейтронов, а B^2 является лапласианом. Это уравнение действительно для первого порядка при смещении температуры и для второго порядка при лапласиане. Для случаев более сложной энергетической зависимости λ_{tr} выведены более сложные соотношения.

Кроме вышеприведенных анализов возможно также изучить температуру нейтронов в качестве функции положения и путем прибавления и вычитания симметричных пространственных точек получить скалярный и постоянный поток. Настоящие измерения дают постоянную температуру скалярного потока до расстояния примерно в 1 см от поверхности для полиэтиленовой пленки толщиной в 7,5 см. Это было истолковано М.М.Р.Уильямсом как нарушение отделимости энергии–пространства вблизи поверхности. Если это так, то аппроксимация диффузионной теории может не подходить для положения вблизи поверхности.

MEDICIONES ESPECTRALES DEL FLUJO ASINTOTICO DEPENDIENTE DEL ESPACIO EN EL AGUA Y EN EL POLIETILENO. Los parámetros de difusión, salvo los correspondiente a Σ_a, pueden medirse estudiando la distribución asintótica del flujo neutrónico en función de las variables energía y espacio. Además de las cantidades integrales de energía, que pueden también obtenerse con experimentos de atenuación, es posible determinar la longitud de extrapolación en función de la energía y el libre recorrido medio de transporte en función de la energía.

El espectro asintótico en el tiempo se mide con ayuda de un selector de neutrones en fase y de un acelerador lineal de electrones pulsados. El impulso inicial de fotoneutrones se obtiene interceptando el haz electrónico con un blanco grueso de volframio. Ulteriormente, un selector mecánico de neutrones muestrea el espectro correspondiente a ese momento y define el tiempo cero para la determinación de la energía de los neutrones por el método del tiempo de vuelo. Los neutrones se detectan con un detector de BF_3 de ventana terminal y se clasifican con respecto al tiempo mediante orificios reentrantes de profundidad diversa.

Los espectros neutrónicos en función de la posición se analizan con arreglo a la teoría de difusión de primer orden:

$$F(X,E) = F(O,E)\left[\cos\frac{\pi x}{L} + \frac{\pi\lambda_{tr}}{L}\,\text{sen}\,\frac{\pi x}{L}\right]$$

donde F(X,E) es el flujo medido; en $L = 2(a+\epsilon)$, a es el semiespesor de la placa y ϵ es la distancia de extrapolación. Esta se obtiene ajustando por cuadrados mínimos el flujo escalar a una distribución cosenoidal para una energía dada. El valor de λ_{tr} se obtiene por ajuste de la ecuación indicada con el valor previamente determinado de la distancia de extrapolación.

El valor del coeficiente de enfriamiento por difusión se obtiene midiendo directamente la temperatura del flujo neutrónico escalar. Calculando la difusión variacional se obtiene la siguiente expresión para el caso de absorción según la ley 1/v y de $\lambda_{tr} \sim E^{\alpha}$, siendo α una constante:

$$C = \frac{D_0(T - T_n)(\alpha + \frac{1}{2})}{T_n B^2}$$

D_0 es el coeficiente de difusión media, T es la temperatura del medio, T_n es la temperatura neutrónica y B^2 es el laplaciano. Esta ecuación es válida para el término de primer orden del desplazamiento de la temperatura y para el término de segundo orden del laplaciano. Se han establecido relaciones más complejas para los casos en que la dependencia de λ_{tr} con respecto a la energía es más complicada.

Además de los anteriores análisis, también es posible estudiar la temperatura neutrónica en función de la posición y, sumando y restando puntos espaciales simétricos, obtener el flujo escalar y el lineal. Las mediciones que se realizan actualmente indican que la temperatura del flujo escalar es constante hasta una distancia de aproximadamente 1 cm de la superficie para una placa de polietileno de 7,5 cm de espesor. M.M.P. Williams ha interpretado este fenómeno como una falla del principio de la separabilidad de las variables espacio y energía en las proximidades de la superficie. De ser así, es muy posible que la aproximación según la teoría de difusión no sea válida cerca de la superficie.

1. INTRODUCTION

Time asymptotic measurements of the spatially-dependent neutron spectrum in moderators in slab geometry were performed by the pulsed electron Linac phased-neutron-chopper technique [1]. The mechanical chopper is a B^{10} loaded stainless steel disk spinning at 9000 rpm. The experimental layout is shown in Fig. 1*. A pulse of electrons of about 1/2 A, 4.5-μs duration, and 50-MeV energy was incident on a water cooled tungsten (e-γ-n) target. Neutrons which approximate a primary fission spectrum irradiated the spectrum source under investigation. After a sufficient time had elapsed to establish the time asymptotic spectrum (380 μs) the chopper opened and sampled the neutron spectrum for 122 μs at full width at half maximum. Neutrons were extracted from the medium at various depths by means of a 1/2-in diameter re-entrant hole and were detected by a BF_3 counter with a thin ceramic window. The energy of the neutrons was determined by measuring time-of-flight over a 3.1-m flight path. The time sorting of the neutrons was done by a Technical Measurements Corporation CN-1024 analyser, using data routing into eight groups of 128 channels. Details of this method will be described later. The energy response of the BF_3 counter was carefully measured using the Thermal Test Reactor (TTR) at the Knolls Atomic Power Laboratory. The data was further corrected for the mean stopping distance in the 6-in long detector, material in the flight path, the mean chopping time, and finite resolution. The spectral distortion caused by the distance between the bottom of the re-entrant hole and the chopping plane has been removed. The disk chopper was selected to minimize such distortion.

2. EXPERIMENTAL TECHNIQUE

The directional neutron flux at various spatial positions was extracted by means of re-entrant holes penetrating to the desired depths. As long as

* In Fig. 1 and all subsequent figures all wings represent the standard deviations and include only statistical errors due to counting. Dashed lines do not represent theoretical results but serve only as visual aid in connecting experimental points.

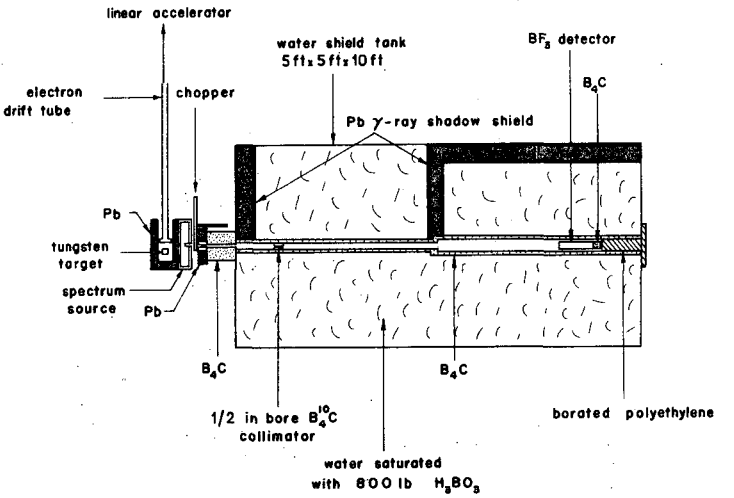

Fig. 1

Physical layout of the apparatus

it was necessary only to measure the energy distribution of the neutrons, the normalization of the data had to be accurate enough to make a proper background subtraction; since the background was a factor of about fifty less than the signal, no great precision was required. However, an accurate measurement of the spatial distribution of the various energy groups required much greater accuracy of the experimental data and was limited almost entirely by the precision of the normalization between measurements at various depths. When only a background subtraction is required, it is a common practice to use subsidiary neutron detectors of various types for monitoring the incident neutron flux. Thus, the system stability depends on the stability of both the spectrum detector and the monitor detectors. Failure of an amplifier in either system and the subsequent repair or replacement introduces a normalization change making it difficult to connect data measured before and after the event.

In the time-dependent measurements in D_2O [1a] this problem was overcome effectively by the use of the sequentially routing delay [2, 3]. This device sequentially increments the time between the neutron source pulse and the sampling time with each accelerator pulse in eight steps of 32 μs each and automatically routes the incoming information to the proper location in the memory of the TMC CN-1024 analyser. Since these measurements are made with a single detector and since a set of eight different time-dependent spectra can be taken in 8/150 s, any gain changes or even replacement of electronics causes no difficulty because the spectra are completely self-normalized. Other sets of spectra may be obtained and interlocked with the previous set by overlapping one of the spectra.

The successful performance of this device for the measurement of time-dependent spectra inspired the idea of an equivalent device for the self-normalization of the spatially-dependent spectra. After examining many

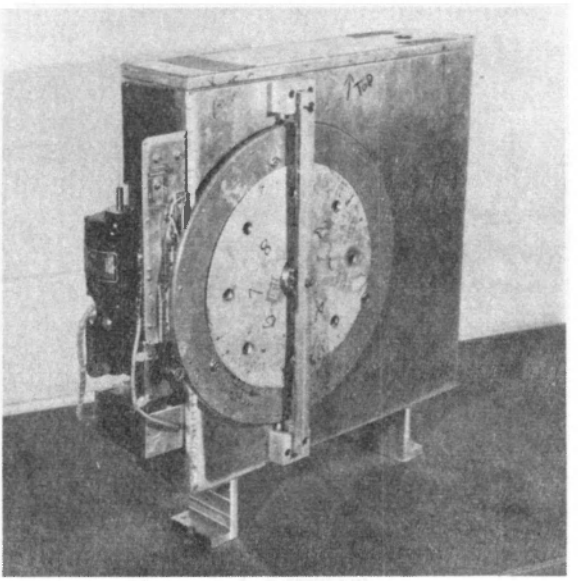

Fig. 2

Automatic re-entrant hole changer

designs, it was decided to construct an automatic re-entrant hole changer consisting of a slab with a rotating cylinder containing eight re-entrant holes, each extending to various depths (Figs. 2 and 3). The spectrum source was a slab measuring $17\frac{3}{4}$ in × $17\frac{3}{4}$ in × 3 in. It was shielded by 1/32-in cadmium and was surrounded by 5/8-in B_4C powder to eliminate room background. The choice of eight re-entrant tubes was demanded by the TMC CN-1024, which is capable of eight memory group routings. To employ this self-normalizing technique, it was necessary only to have two spatial positions and through the technique of overlapping measurements to link the data of as many positions as desired. On the other hand, data acquisition was greatly simplified and more efficiently obtained when all measurements were performed with one loading of the rotating cylinder. Physically attached to the cylinder was a 16-in diameter gear which was rotated at a speed of 88 seconds per revolution. The time required to change spatial positions was 11 s. The Linac beam output could be maintained very constant for the short periods of time involved. The indexing and routing was done by magnetic reed switches. One switch was used for indexing and three switches were used for setting up a binary code which controlled the memory location in which the data were stored.

The spatial positions loaded into the cylinder were ± 1-3/8 in, ± 1-1/8 in, ± 5/8 in, - 1-1/2 in and 0 based on the total thickness of 3 in and measured relative to the centre; therefore, four of the spatial positions were paired into mirror images about the centre of the slab. In this combination all eight positions were used. Consequently, the background measurement would have to be performed separately. Since the time necessary to rotate

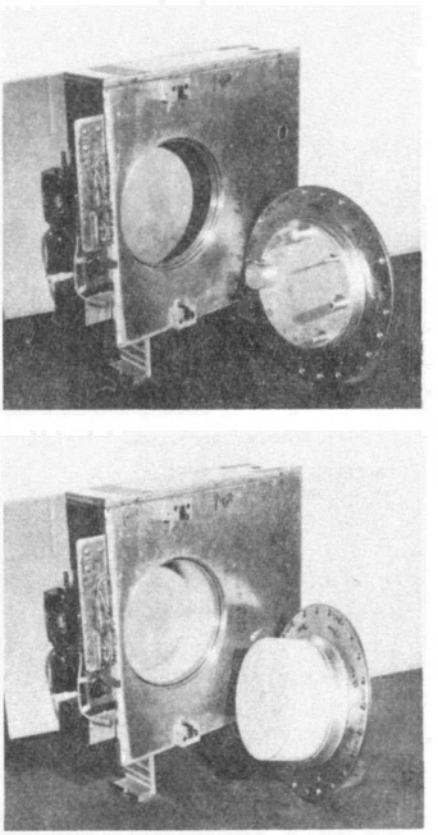

Fig. 3

Automatic re-entrant hole changer as used with water and polyethylene

the cylinder from one re-entrant hole to the next was considerable, it seemed profitable to use this time for background acquisition. Accordingly, the large gear was covered with a cadmium sheet. The spatially-dependent flux data were then taken for 49 s at each re-entrant hole. By means of electronic delays the data acquisition was inhibited for 2 s to be sure that the previously measured hole had time to move out of the spectrometer beam; background was then taken for 7 s and the analysers were inhibited until the next re-entrant hole came into place. The background data were acquired on a separate TMC CN-256 channel analyser using 128 data channels of 40-μs width, which was also the setting of the CN-1024. In this fashion nine groups of data were taken sequentially. When taking data in this manner and a precision of $\pm 1\%$ or better is desired, the relatively small number of sampling groups may become significant. To overcome this problem and to check the operation of the routing mechanism a region within each of the nine memory locations was set aside for recording the number of accelerator bursts fired at this location. This number was used to tie in the background data and to

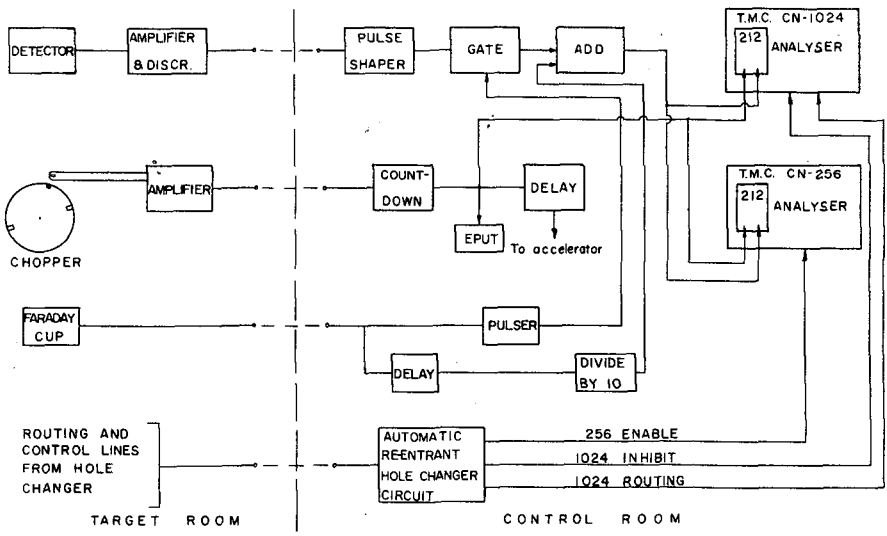

Fig. 4

Diagram of electronics

make small adjustments in the normalization of the data; i.e. adjust for small on-time variations.

Figure 4 shows a simplified overall block diagram. A magnetic pick-up signal was detected on the chopper which initiated the accelerator-phased-chopper timing sequence. This occurred 572 μs before the chopper opened; the time allowed for moderation was this time minus the delayed trigger sent to the accelerator. If a longer delay was needed, the preceding trigger was used. A count-down circuit was used when the experiment was performed at less than 150 pulses per second. This signal was the starting time for the analysers. The neutron spectrum signals were detected, amplified and sent to a gate which was closed long enough to blank out three channels from the detector signals. The detector signals passed through a linear adder and to both the analysers which could be inhibited depending upon the configuration of the automatic hole changer circuit. The pulse coming from the Faraday cup triggered the pulser which blanked out the three channels from the detector signals; the same pulse fired a time delay and this output was divided by ten to prevent channel overflow and then deposited in the second blanked out channel. This marked the number of accelerator bursts fired at each of the nine locations. The reason for triggering from the Faraday cup was to ensure that each marker was associated with the operation of the Linac. In case the Linac ceased operation, the markers stopped immediately.

3. RESULTS

When using this arrangement with eight re-entrant holes in the medium a major question was whether or not one hole perturbed the other. This was

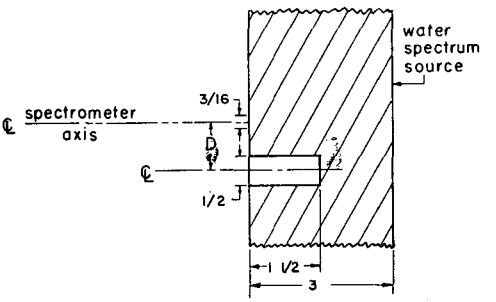

Fig. 5

Void perturbation study (all dimensions in inches)

tested by locating $\frac{1}{2}$-in diameter, $1\frac{1}{2}$-in long voids at varying distances from a location at which the surface spectrum was being measured (Fig. 5); this was a severe test designed to emphasize the problem. The distance D was varied from 1/2 in, 5/8 in, 3/4 in, 1 in, 2-3/16 in, 3-3/16 in and 6 in (nearest-neighbour distance). The integrals over the spectra agreed to within ± 2% which was about the experimental error and showed no general trends. It had been expected that the intensity would be slightly higher for the smallest values of D because of void streaming; this was not, however, observed over this range of values. From these measurements it was assumed that re-entrant holes spaced $3\frac{1}{4}$ in between centres would result in a negligible perturbation within the accuracy of the experiment and this was the re-entrant hole spacing used in the spatially-dependent measurement.

Perturbation effects of re-entrant centre spectrum holes with varying diameters had been studied previously [4, 5] in polyethylene and the measurements determined that a spectrum shift from a 2-in re-entrant hole could not be detected within the accuracy of the experiment; however, the normalization in this study did not permit quantitative statements about the effects of hole diameter on the amplitude. Therefore, the automatic re-entrant hole changer was consequently used to measure the effect of hole diameter on the amplitude of a scalar spectrum. Re-entrant aluminium tubes penetrating to the centre of the water slab with diameters of 1/4 in, 3/8 in, 1/2 in, 3/4 in, 1 in, and 2 in were used (see Fig. 3). The measurements were performed by the technique previously described. The effect on the amplitude is shown in Fig. 6. The qualitative explanation for the rise of the amplitude in going from 1/4 in to 1/2 in is the competition between the removal of absorption of the neutron by the moderator and the increase in solid angle for escape produced by the larger re-entrant tube. This effect would probably not have been observed in D_2O because of its extremely low absorption. The spectra were fitted to a Maxwellian distribution and the corresponding temperatures varied from 304 to 308°K with a standard deviation of 3 deg K as shown in Fig. 6.

Spatially-dependent asymptotic spectra were obtained for H_2O and polyethylene at the spatial positions ± 1-3/8 in, ±1-1/8 in, ± 5/8 in, - 1-1/2 in and 0 based on the slab thickness of 3 in and measured relative to the centre. Data acquisition was delayed until 380 μs or about 3.8 mean lifetimes after the primary neutron pulse. It must be emphasized at this point that the sub-

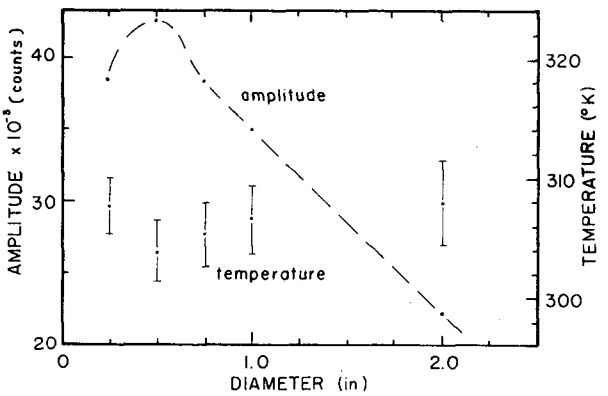

Fig. 6

Re-entrant hole diameter study

sequently discussed experimental results are of a preliminary nature since they are based on a maximum of only seven spatial positions; however, the apparent discrepancy between the calculated [6] and experimental [7, 8, 9, 10] values of the extrapolation length in small water systems and the question of space-energy separability [11] motivate their publication.

Assuming the existence of a time asymptotic spectrum and the validity of space-energy separability, the directional flux in a slab of pure moderator is represented in the diffusion theory approximation by

$$F(E, x, \mu = 1) = f(E)\, F(X = 0) \left[\cos \pi X/L + \lambda_{tr}(E) \frac{\pi}{L} \sin \pi X/L \right] \quad (1)$$

where $L = 2(a + \epsilon)$, a = slab half-thickness and ϵ = extrapolation distance. The directional flux is thus the sum of the scalar flux and the current flux times an energy-dependent function. Considering Eq.(1), one can see that the scalar flux can be obtained by adding the directional flux measured at symmetric spatial points and that the current flux can be obtained by subtracting the directional flux measured at symmetric spatial points. This method was applied to the directional flux spectra obtained for seven spatial positions. The resulting scalar and current spectra were then fitted to Maxwellian energy distributions, a procedure which makes it possible to characterize the shapes of the asymptotic spectra with a single parameter, namely the temperature. While it is easily shown theoretically that these finite medium spectra cannot be strictly Maxwellian in shape, the validity of this procedure is illustrated in Fig. 7 where $\phi(E)/E$ versus E is plotted for the scalar flux at the centre of the water slab and at 1/8 in from the boundary; both fit the Maxwellian distribution equally well.

Figure 8 shows the spatial distribution of the scalar flux amplitudes in water at a few selected energies, namely 0.1661, 0.1028, 0.0504, 0.0257, and 0.0210 eV. Figure 9 shows the spatial variations in flux shape for the directional flux, the scalar flux, and the current flux in water for the energy range from 0.20 to 0.005 eV as a function of the fitted temperature distance. The medium temperature was 300 ± 1°K. The fact that the temperature of

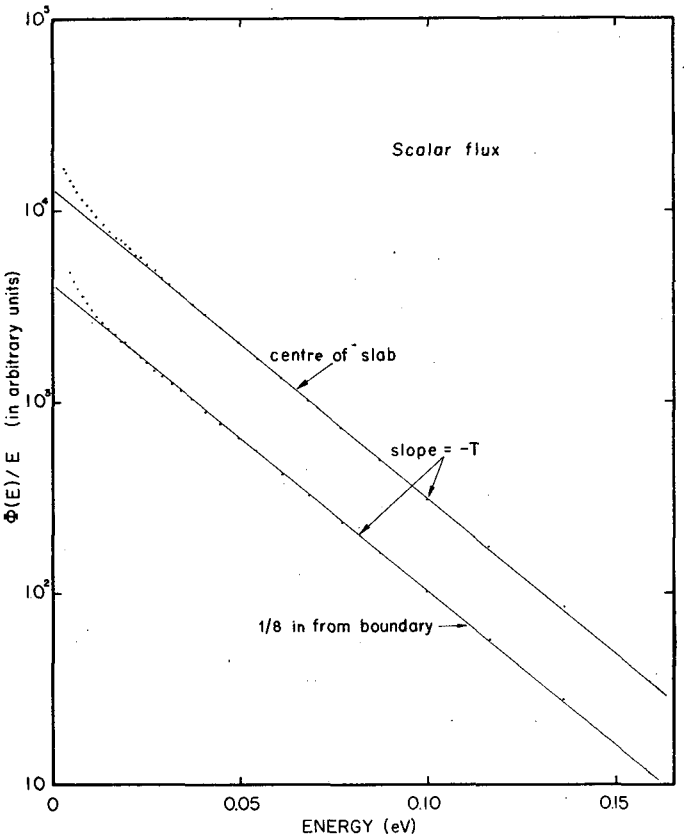

Fig. 7

Neutron temperature determination

the scalar flux is constant within the medium and rises near the boundary is in complete agreement with the results of WILLIAMS [11] who found that the average energy, defined as

$$\overline{E}_{\phi(X)} = \left[\int_0^\infty E\phi\,(E, X)\,dE \right] \Big/ \left[\int_0^\infty \phi\,(E, X)\,dE \right],$$

behaves in the same manner. Williams states that $\overline{E}_{\phi(X)}$ should remain constant up to a distance d of the order of 0.5 cm from the boundary, which implies that in the inner "asymptotic" region, space and energy are accurately separable. The distance d is a measure of the width of the transient zone near the boundary and varies slowly with the buckling B^2. If Williams' values of B^2 are interpolated linearly to fit $B^2 = 0.1635$ cm^{-2} used in the spatially-dependent measurements, the calculated distances are found to be d = 1.02 cm and d = 0.526 cm for effective masses of the water molecule of 18 and 5.3, respectively. The experiment showed that 0.318 cm < d $\lesssim$ 0.95 cm; a more

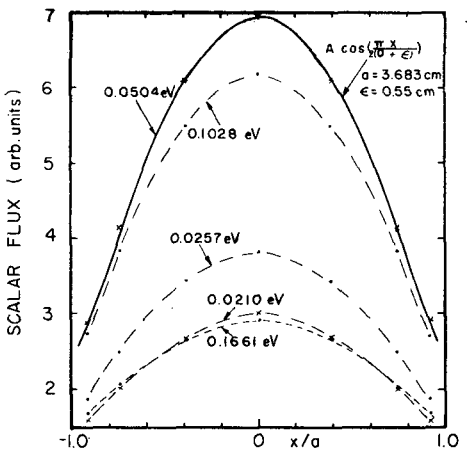

Fig. 8

Spatial distribution of the scalar flux amplitude

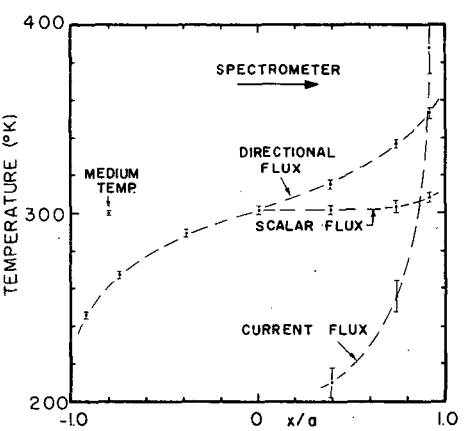

Fig. 9

Spatial variation of the directional, scalar and current flux shapes

definite value of d cannot be assigned because of the lack of more spatial positions.

As stated previously, the spatial distribution of the scalar flux was determined by symmetric measurements of the directional flux. The extrapolation length was then obtained by fitting the scalar flux to a cosine distribution by means of an iterative least squares fitting code. The extrapolation length is defined as the distance ϵ from the vacuum boundary of the slab at which the "asymptotic" flux would vanish if it were represented by the same analytic function in the vacuum as that which describes it in the medium far from the boundary [7]. This definition implies the existence of a unique extrapolation length and consequently a unique buckling. The extrapolation length based on this definition was obtained by omitting the scalar flux mea-

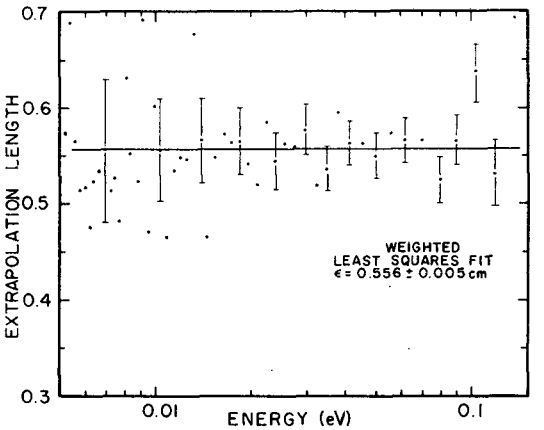

Fig. 10

Extrapolation length for water

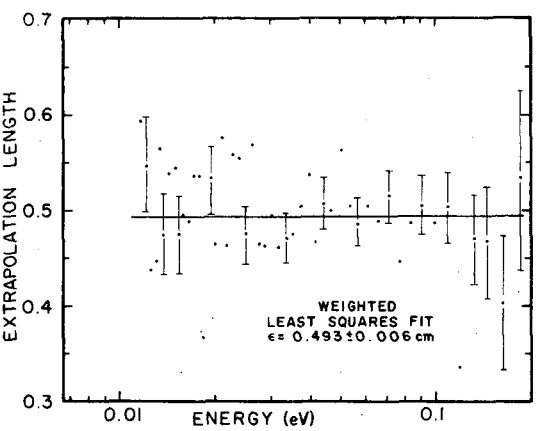

Fig. 11

Extrapolation length for polyethylene

surements at the spatial positions nearest to the boundary and will be referred to as a five-point fitted extrapolation length. The values of ϵ as a function of energy for water and polyethylene are shown in Figs. 10 and 11. respectively. Fitting these data to a constant in the weighted least squares sense gives $\epsilon = 0.556 \pm 0.005$ cm for water and $\epsilon = 0.493 \pm 0.006$ cm for polyethylene. The value for water is much higher than the calculated values [6] of 0.3 to 0.35 cm and is even higher than the experimental (die-away) values of 0.46 ± 0.05 cm [8] and 0.4 cm [10]. Also, it is interesting to note that using an extrapolation length of 0.55 cm, the disagreement between theoretical calculations of diffusion parameters in water [12] and experimental measurements is apparently reduced [13].

In spite of the fact that the energy and spatial flux were not separable at the two spatial positions 1/8 in from the boundaries, the scalar flux at these

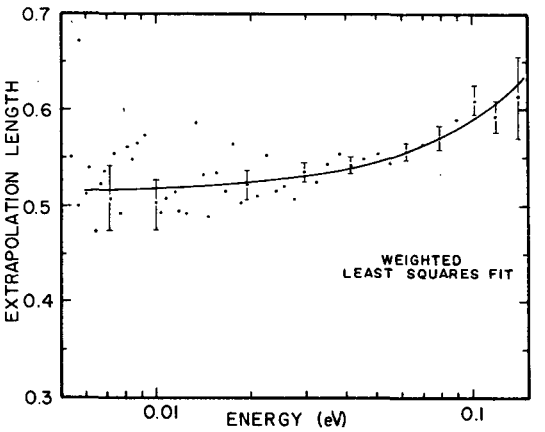

Fig. 12

Energy-dependent "extrapolation length" for water (transient effect)

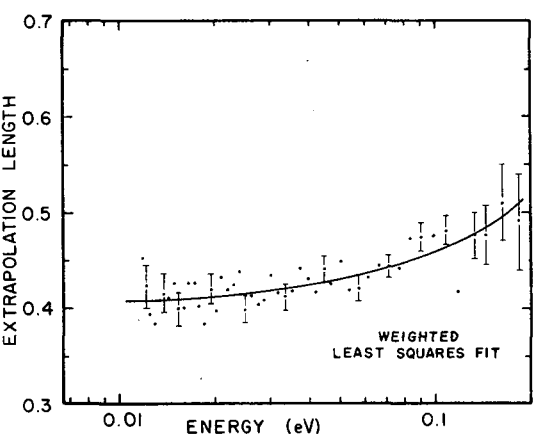

Fig. 13

Energy-dependent "extrapolation length" for polyethylene (transient effect)

positions was used in a seven-point iterative cosine fit for $\epsilon(E)$ and the results for water and polyethylene are shown on Figs. 12 and 13. This extrapolation length now apparently varies with energy; a quadratic weighted least squares fit, namely $\epsilon(E) = 0.513 + 0.632\,E + 1.43\,E^2$ for water and $\epsilon(E) = 0.401 + 0.591\,E - 0.388\,E$ for polyethylene, describes this energy dependence very well.

Figure 9 shows the results of fitting Maxwellian distributions to the directional flux, the scalar flux, and the current flux. The measurement of the scalar flux temperature is a check for asymptotic neutron spectrum measurements that few nuclear experiments have. The temperature of the neutron scalar flux must be in agreement with the following first-order relationship [14, 15]:

$$C = \left[(T-T_n)\, D_0\, (1+\alpha) \right] / T_n B^2 ,$$

where T is the moderator temperature, T_n is the neutron temperature, D_0 is the diffusion coefficient, B^2 is the buckling ($1/cm^2$) and α is the power of the energy used to approximate the energy dependence of λ_{tr}. This relationship is currently under study by CALAME [15] using a Laguerre power series expansion of the energy-dependent solution of the transport equation. This technique agrees with the variational calculation to the first order in B^2. It also yields higher order corrections to B^2 and established the energy range of validity.

4. SUMMARY

An experimental technique for spatially-dependent asymptotic spectra measurements has been discussed in detail. Its success in the preliminary investigations certainly justifies a further series of more precise measurements with a greater number of more closely spaced spatial positions. This technique provides an excellent tool to study the extent of the region of space-energy separability, to determine the dependence of the extrapolation length on the buckling, and to investigate intensively the apparent difference between the calculated and the experimental (pulsed) values of the extrapolation length.

REFERENCES

[1] BECKURTS, K.H., Naturf. 16a (1961) 611.
[1a] KRYTER, R.C., CALAME, G.P., FULLWOOD, R.R. and GAERTTNER, E.R., "Time-dependent thermal neutron spectra in D_2O", these Proceedings I.
[2] FULLWOOD, R.R., Nucl. Instrum. Meth. 30 2 (1964) 206-08.
[3] KRYTER, R.C., FULLWOOD, R.R., and GAERTTNER, E.R. J. nucl. Energy A/B (1965), in press.
[4] FULLWOOD, R.R., SLOVACEK, R., CERBONE, R. and GAERTTNER, E.R., Amer. nucl. Soc. Trans. 7 (June 1964) 77.
[5] SLOVACEK, R., Nucl. Sci. Engng 21 (1965) 329-45.
[6] GELBARD, E.M., DAVIS, J.A. and SCHMIDT, E., Proc. Brookhaven Conf. on Neutron Thermalization, BNL-719 (C-32) IV (1962) 1175.
[7] CARROLL, E.E. and STOOKSBERRY, R.W., Nucl. Sci. Engng 20 (1964) 455-61.
[8] CAMPBELL, E.C. and STELSON, P.H., Phys. Progr. Rpt ORNL-2204 (1956) 34-36.
[9] HALL, R.S., SCOTT, S.A. and WALKE, J., Proc. phys. Soc. 79 (1962) 257-63.
[10] DE JUREN, J.A., STOOKSBERRY, R. and CARROLL, E.E., Proc. Brookhaven Conf. on Neutron Thermalization, BNL-719 (C-32) III (1962) 895.
[11] WILLIAMS, M.M.R., J. nucl. Energy, Parts A/B 17 (1963) 55-66.
[12] CALAME, G.P., Nucl. Sci. Engng 19 (1964) 189-95.
[13] YEATER, M.L., private communication.
[14] FULLWOOD, R.R., Amer. nucl. Soc. Trans. 7 (1964) 231.
[15] CALAME, G.P. and FULLWOOD, R.R., in preparation.

MEASUREMENTS OF THE ASYMPTOTIC SPECTRUM OF A MULTIPLYING MEDIUM*

R. E. SLOVACEK**, R. J. CERBONE, E. R. GAERTTNER,
R. R. FULLWOOD AND D. R. BACH***
RENSSELAER POLYTECHNIC INSTITUTE, TROY, N. Y.,
UNITED STATES OF AMERICA

Abstract — Résumé — Аннотация — Resumen

MEASUREMENTS OF THE ASYMPTOTIC SPECTRUM OF A MULTIPLYING MEDIUM. The asymptotic (in time) spectrum of a multiplying medium is of interest not only for analysing pulsed neutron experiments but also for investigating the neutron diffusion properties of the medium. The pulse-neutron-source mechanical-chopper-technique has been developed to measure the asymptotic neutron spectrum in a multiplying assembly. The surface and centre (scalar) spectra were measured for each of four multiplying assemblies and comparisons were made with spectrum calculations.

All of the multiplying systems contained enriched U^{235} and hydrogen as the moderator. Two of the assemblies were constructed of zirconium-clad fuel strips in water; the other two assemblies consisted of a mixture of UO_2 and ZrO_2 powders dispersed in paraffin. The sizes and hydrogen-to-U^{235} ratios were made different so that absorption, leakage and scattering were varied.

The scalar spectrum was calculated by means of a steady state diffusion theory calculation. The agreement between the measured and scalar spectra was satisfactory when the measured value of the asymptotic decay constant was used to calculate the spectrum. The calculated asymptotic spectrum was found to be extremely sensitive to the decay constant; a 7% change in the decay constant for one of the assemblies resulted in a 47% change in the ratio of the thermal flux to the slowing-down flux.

The surface spectra for two of the assemblies were obtained using a double P_1 calculation. The surface spectrum calculation agreed with the data in the thermal region up to 0.2 eV. However, upon extending the range of comparison to higher energies, the measured leakage flux was about 50% harder than the calculated flux. Measurements of the surface spectrum have recently been obtained with better statistics to compare with other surface spectrum calculations.

The asymptotic-spectrum measuring technique has been demonstrated as a useful method for studying position-dependent spectra. Steady state spectrum measurements have also been obtained in one of the assemblies to compare the two techniques using the same spectrometer. These results are still being analysed. As the asymptotic neutron density has a persistent spatial distribution which is more amenable to analysis, the asymptotic technique applied to multiplying systems should be extremely useful for studying the space-dependent spectrum problem over a large energy range.

MESURES DU SPECTRE ASYMPTOTIQUE D'UN MILIEU MULTIPLICATEUR. Le spectre asymptotique (dans le temps) d'un milieu multiplicateur présente un intérêt non seulement pour l'analyse des expériences au moyen des neutrons pulsés, mais également dans la recherche sur les propriétés du milieu concernant la diffusion des neutrons. Les auteurs ont mis au point la méthode utilisant une source de neutrons pulsés et un hacheur mécanique de manière à pouvoir mesurer le spectre aymptotique des neutrons dans un assemblage multiplicateur. Ils ont mesuré les spectres à la surface et au centre (scalaire) pour 4 assemblages multiplicateurs et ils ont comparé les résultats à ceux des calculs.

Tous les systèmes multiplicateurs contenaient ^{235}U enrichi et de l'hydrogène comme ralentisseur. Deux de ces assemblages étaient construits avec des lames de combustible gainées de zirconium, immergées dans l'eau; les deux autres assemblages étaient constitués par une dispersion de poudres de UO_2 et de ZrO_2 dans de la paraffine. Les auteurs ont choisi des dimensions et des rapports $H/^{235}U$ différents de manière à faire varier l'absorption, la fuite et la diffusion.

* This work supported by the United States Atomic Energy Commission under contract AT(30-3)-328.

** Present address is Knolls Atomic Power Laboratory, Schenectady, N.Y., USA.

*** Now at the University of Michigan, Ann Arbor, Mich., USA.

Les auteurs ont calculé le spectre scalaire par la théorie de la diffusion à l'état stationnaire. Ils ont constaté que les spectres mesurés et les spectres scalaires étaient en bon accord s'ils utilisaient la valeur mesurée de la constante de décroissance asymptotique pour calculer le spectre. Il s'est avéré que le spectre asymptotique calculé était extrêmement sensible à la constante de décroissance; une variation de 7% de cette constante dans un des assemblages a donné lieu à une variation de 47% dans le rapport flux de neutrons thermiques-flux de ralentissement.

Les auteurs ont obtenu les spectres à la surface pour deux des assemblages au moyen d'un double calcul P_1. Les résultats du calcul du spectre à la surface sont en accord avec les données dans la région thermique jusqu'à 0,2 eV. Toutefois, pour des énergies plus élevées, le flux de fuite mesuré était environ 50% plus dur que le flux calculé. Des mesures du spectre à la surface ont été faites récemment; elles ont donné des résultats qui concordent mieux avec d'autres calculs du spectre à la surface.

La méthode qui consiste à mesurer le spectre asymptotique s'est révélée utile pour étudier les spectres qui varient selon la position. Les auteurs ont également obtenu des mesures du spectre à l'état stationnaire dans l'un des assemblages pour comparer les deux méthodes au moyen d'un même spectromètre. L'analyse des résultats est en cours. Etant donné que la densité asymptotique des neutrons présente une distribution spatiale fondamentale qui se prête mieux à l'analyse, la méthode asymptotique appliquée aux systèmes multiplicateurs devrait être d'une très grande utilité pour étudier le problème des spectres variables dans l'espace sur une large gamme d'énergies.

ИЗМЕРЕНИЯ АСИМПТОТИЧЕСКОГО СПЕКТРА УМНОЖАЮЩЕЙ СРЕДЫ. Асимптотический (по времени) спектр умножающей среды представляет интерес не только для проведения экспериментов по анализу пульсирующих нейтронов, но и также для изучения свойств нейтронной диффузии среды. Для измерения асимптотического нейтронного спектра в размножающей системе разработан источник пульсирующих нейтронов — механический прерыватель. Осуществлено измерение поверхности и центра (скаляра) спектра каждой из четырех размножающих систем, дается сравнение с расчетами спектра.

Во всех размножающих системах в качестве замедлителя использовался обогащенный уран-235 и водород. Две системы были изготовлены из топливных стержней, покрытых цирконием в воде; две других системы были изготовлены из смеси порошков UO_2 и ZrO_2, диспергированных в парафине. Размеры и пропорции водорода по отношению к урану-235 брали различные с тем, чтобы разнообразить абсорбцию, утечку и рассеяние.

Скалярный спектр высчитывали на основании теории статической диффузии. Совпадения между измеренным и скалярным спектром оказывались удовлетворительными, когда для вычисления спектра использовалась измеренная величина асимптотической постоянной распада. Найдено, что высчитанный асимптотический спектр является чрезвычайно чувствительным к постоянной распада; 7%-ное изменение в постоянной распада для одной из систем дало в результате 47%-ное изменение в тепловом состоянии к замедлению отношения потоков.

Поверхностный спектр для двух из систем получен при использовании двойного вычисления P1. Вычисление поверхностного спектра совпало с данными в тепловой области до 0,2 ev. Однако при расширении степени сравнения в более высоких энергиях измеренный поток утечки равнялся приблизительно 50 %, чем это предусматривалось расчетами. Измерения поверхностного спектра, полученные за последнее время, имеют более лучшие статистические данные по сравнению с другими расчетами поверхностных спектров.

Метод измерения асимптотического спектра был показан как метод, полезный для изучения спектра позиционной зависимости. Измерения статического спектра были также получены в одной из систем с целью сравнения обоих методов при использовании одного и того же спектрометра. Эти результаты пока еще анализируются. Поскольку плотность асимптотических нейтронов имеет постоянное пространственное распространение, которое гораздо лучше поддается анализу, то асимптотический метод, применяемый к размножающим системам, должен оказаться чрезвычайно полезным для изучения спектральных проблем космической зависимости при сверх больших энергиях.

MEDICIONES DEL ESPECTRO ASINTOTICO EN UN MEDIO MULTIPLICADOR. El espectro asintótico (en el tiempo) en un medio multiplicador ofrece interés no sólo para analizar los resultados de experimentos con neutrones pulsados, sino también para investigar las propiedades de difusión de los neutrones en ese medio. A fin de medir el espectro neutrónico asintótico en un conjunto multiplicador, se ha ideado una técnica de empleo combinado de una fuente de neutrones pulsados y de un selector mecánico. En este experimento se midieron los espectros (escalares) en la superficie y en el centro de cuatro conjuntos multiplicadores, comparándose los resultados obtenidos con los espectros calculados.

Todos los sistemas multiplicadores contenían uranio enriquecido en el isótopo ^{235}U y empleaban H como moderador. Dos de ellos se prepararon con tiras de combustible introducidas en agua; los dos restantes consistían en una mezcla de polvos de UO_2 y de ZrO_2 dispersa en parafina. Se puso cuidado en que las dimensiones de los sistemas y las razones $H/^{235}U$ fuesen distintos, a fin de que lo fueran también la absorción, el escape y la dispersión.

Se calculó el espectro escalar por un procedimiento basado en la teoría de la difusión en régimen estacionario. La concordancia entre los espectros medidos y los escalares fue satisfactoria cuando se empleó para calcular el espectro el valor medido de la constante de decrecimiento asintótico. Pudo comprobarse que el espectro asintótico calculado era muy sensible a la variación de esa constante; una modificación del 7% en el valor de la constante correspondiente a uno de los conjuntos se tradujo en una modificación del 47% en la razón flujo térmico/flujo de moderación.

Se obtuvieron los espectros superficiales para dos de los conjuntos empleando un cálculo de doble P-1. Los resultados del cálculo concordaron con los datos correspondientes a la región térmica para energías de hasta 0,2 eV. Ahora bien, al extender la gama de comparaciones a energías más altas, el flujo de escape medido resultó superior en un 50% al calculado. En fecha más reciente se obtuvieron valores del espectro superficial con menores desviaciones estadísticas que se emplearon en la comparación con el cálculo de otros espectros de esa índole.

La técnica de la medición del espectro asintótico ha resultado un instrumento muy valioso para el estudio de los espectros que varían en función de la posición de la fuente. En uno de los conjuntos, antes mencionados, se realizaron también mediciones del espectro en régimen estacionario con miras a comparar las dos técnicas empleando el mismo espectrómetro. El análisis de los resultados obtenidos no ha terminado aún. Como la densidad neutrónica asintótica presenta una distribución espacial persistente que se presta más al análisis, los autores estiman que la técnica de medición del espectro asintótico aplicada a sistemas multiplicadores ha de resultar en extremo útil en el estudio del problema del espectro espacial en un amplio intervalo energético.

1. INTRODUCTION

Following a burst of high energy neutrons into a moderating medium, the processes of neutron slowing down, thermalization, and diffusion occur, eventually resulting in a state in which the neutron spectrum no longer changes with time. This spectrum is the so-called asymptotic spectrum. In a non-multiplying medium, the shape of the asymptotic spectrum is closely approximated by a Maxwellian distribution; in a multiplying medium, the asymptotic spectrum is approximately a Maxwellian at thermal energies while at higher energies it is approximately 1/E due to the presence of the fission source. Therefore, it is possible by measuring the multiplying medium asymptotic spectrum to investigate the diffusion and transport properties of the medium over a wide energy range.

If observations of the neutron spectrum are not limited solely to the asymptotic region but are made at all times after the burst, the steady state neutron spectrum is obtained from the measurement [1] . These studies on infinite media have yielded valuable comparisons between calculations and measurements of the neutron spectrum up to about 10 eV. Extension of the steady state investigations to finite systems has pointed out the importance of the role of the primary fast neutron source on the shape of the low energy neutron distribution [2] . The asymptotic spectrum in a finite or infinite system, however, is characterized by the medium properties and does not retain any dependence on the primary neutron source.

BECKURTS [3] first employed the pulsed source, mechanical chopper technique to measure the asymptotic spectrum of water. He observed a pure Maxwellian distribution at the ambient temperature of the moderator

for assemblies with negligible leakage. He also observed directly the characteristic diffusion cooling for small assemblies. This technique was later extended and used at RPI to study other pure moderator characteristics such as the effect of coherent scattering on neutron thermalization in beryllium [4], heavy water [5], and the energy-dependent extrapolation distance and λ_{tr} of polyethylene [6] and water.

A large departure in the asymptotic spectrum from the ambient Maxwellian is not easily attained unless the pure moderator is either heavily poisoned with non-1/v absorbers or very small. These changes cause a large reduction in intensity which make the asymptotic spectrum difficult to measure. The situation is improved in a subcritical multiplying medium where the prompt fission source supplies neutrons over a wide energy range even in the asymptotic limit. In addition, since the asymptotic spectrum is essentially the same as the steady state spectrum but with a decreased 1/v poisoning, the non-1/v characteristics (leakage or absorption) of a medium may be emphasized.

The measurement of the asymptotic neutron spectrum in a pulsed subcritical assembly is also of direct practical value in reactor design and operation. Pulsed neutron techniques to determine the subcriticality of a reactor are used extensively; the analysis of these measurements requires a knowledge of the asymptotic spectrum. In addition, the validity of the spectrum computational methods used in reactor design can be tested.

This investigation was primarily concerned with the asymptotic spectrum in multiplying media although the steady state spectrum was also obtained for one of the media studied. Asymptotic neutron spectrum measurements at the centre and the surface of four subcritical assemblies have been obtained using the pulsed source, mechanical chopper technique. Two of the assemblies were water-moderated heterogeneous systems and the results of their asymptotic spectrum measurements have been published [7]. The present investigation was concerned with the measurement and calculation of the centre and surface spectra of two homogeneous multiplying media.

2. EXPERIMENTAL METHOD

Asymptotic spectrum measurements were made with bursts of high energy neutrons produced by the Rensselaer electron linear accelerator (Linac) in conjunction with a specially designed mechanical neutron chopper. Figure 1 illustrates one of the two experimental arrangements that was used.

The Linac was operated for spectrum measurements on multiplying media at an electron energy of 45 MeV at either a 15 or 30 pulses per second repetition rate with a peak electron current of 0.45 A in 4.5 μs burst. The electron beam incident on a thick water-cooled tungsten target produced photoneutrons which irradiated the spectrum source. The target was surrounded on five sides by 4 in of lead to shield the environment from the radioactive tungsten. To protect the BF_3 neutron detectors from the intense γ-ray flash 2 in of lead were used in the direction of the spectrum source. In the arrangement shown in Fig. 1, the effect of the γ-ray flash was further reduced by locating the target down-stream from the intersection of the electron beam axis and the neutron beam axis. The lead shield contributed to

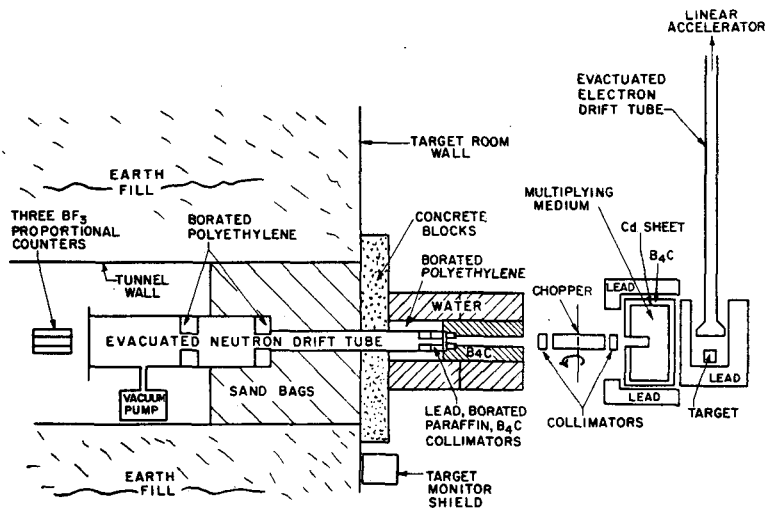

Fig. 1

Experimental arrangement for measuring the asymptotic and steady state spectra

the photoneutron yield by absorbing scattered Bremsstrahlen. The lead also scattered neutrons, resulting in a large diffusion source of high energy neutrons. In a second experimental arrangement used for both asymptotic and steady state measurements, the centre of the spectrum source was located at the intersection of the electron beam axis and the neutron beam axis and 34 BF_3 detectors were located in a building at a flight path distance of 24 m.

Neutrons left the centre of the spectrum source through a re-entrant hole to enter the neutron spectrometer. For surface spectrum measurements, the neutron source and shield were rotated 180°. Surrounding the spectrum source was a 1/32-in sheet of Cd and B_4C 1 in thick, which served to define a thermal and epithermal neutron boundary, simplifying the leakage calculations. There was also a 4-in thick lead wall to serve as a biological shield.

The neutron spectrometer acceptance angle, defined by four additional blocks in the back of the 14-in diameter chopper, was 1.5×10^{-6} steradians. The energy resolution of the neutron spectrometer was

$$\Delta E/E = 0.12\sqrt{E}$$

for a 11-m flight path and was about a factor of 2 better for the 24-m flight path.

The chopper design was a compromise between chopper speed, radius, slit height, and slit shape to satisfy as closely as possible all of the requirements on the spectrometer resolution, rotor dynamic transmission, pulse overlap, background transmitted through the rotor, and the re-entrant hole perturbation. A schematic diagram of the chopper is shown in Fig. 2. The upper and lower surfaces defining the slit were each formed by a pair of

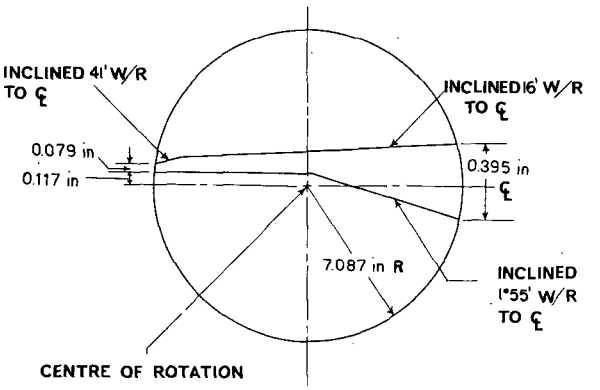

Fig. 2

Schematic of rotor slit shape

planes approximating the parabolic surfaces which were calculated to give the desired transmission. The centre of rotation of the rotor did not lie in the slit so that only one neutron burst could pass through the chopper per revolution.

For the measurement of an asymptotic spectrum, the neutron chopper served as a window which sampled the neutron flux from the spectrum source. The time separation between the initial neutron burst and the flux sampling was adjusted to be sufficient for the neutrons to thermalize, for the higher harmonic spatial transients to decay to a negligible value and for the neutrons to travel from the spectrum source to the chopping plane (entrance surface of the chopper).

A trigger signal obtained from a magnetic strip on the rotor initiated the timing sequences required for the asymptotic spectrum measurement. The time between triggering the Linac and opening the chopper was varied for each experimental arrangement by a delayed signal obtained from a Hewlett Packard H08 218A digital delay generator.

The neutron pulses from the BF_3 detector bank were fed into a TMC[1] 256 channel time analyser used with a Model 212 plug-in unit.

In the experimental arrangement shown in Fig. 1, the data were obtained with three thin end window RSN-108S counters[2] 12.75 in long in a horizontal array, covering a beam area 2 in high and 6 in wide at a distance of 11 m from the surface of the rotor. These counters were filled to a B^{10} concentration of 0.2364×10^{20} atoms/cm^3. In the second experimental arrangement, 34 end window counters were used at a distance of 24 m from the rotor surface. This arrangement permitted steady state spectrum measurements to be made with essentially the same equipment that was used for obtaining an asymptotic measurement.

Two homogeneous assemblies consisting of a dispersion of UO_2 and ZrO_2 particles uniformly distributed in paraffin [12] were constructed, The use of homogeneous assemblies having 90% of the fuel particles less than

[1] Technical Measurements Corporation, North Haven, Conn., USA.

[2] Reuter-Stokes Electronic Components Inc., Cleveland, Ohio, USA.

TABLE I

MULTIPLYING MEDIUM COMPOSITIONS

Element or isotope	Number density (atoms/b cm)
H	0.02555
O^{16}	0.03156
C	0.01235
U^{238}	0.00000834
Zr	0.01565
Al	0.0002481
U^{235}	0.0001116

10 microns in diameter eliminates the uncertainties in the calculated spectrum arising from the fuel self shielding experienced in the previous heterogeneous assemblies. These assemblies were constructed using 4 in × 4 in × 2 in compacts having a U^{235} fuel density of 0.0434 g/cm^3. The number densities are listed in Table I. The assemblies are:

A. Multiplying medium 3 (MM3)

This assembly was constructed of 18 fuel compacts to form a bare assembly 12 in × 12 in × 4 in. A re-entrant hole to the centre of the assembly (2 in) was made by milling a slot 7/8 in × 3/8 in through the centre of one block. A 0.002-in aluminium foil covered each end of the hole to contain fission products. Two thermocouples located over the centre of the assembly monitored the MM3 temperature which was (26 ± 2)°C for all spectrum measurements.

B. Multiplying medium 7 (MM7)

This assembly was constructed of 54 fuel compacts to form a bare assembly 12 in × 12 in × 12 in. A 7/8-in × 3/8-in re-entrant hole penetrated to the centre of the fuel assembly. The temperature was also monitored by two thermocouples to be (32 ± 2)°C during the spectrum measurements.

3. CORRECTIONS TO DATA

In addition to background and normalization, the following corrections to the data were taken into account for the asymptotic spectrum measurement: (1) the drift distance distortion, (2) the counter efficiency, (3) the rotor dynamic transmission function, (4) the time-of-flight error attributed

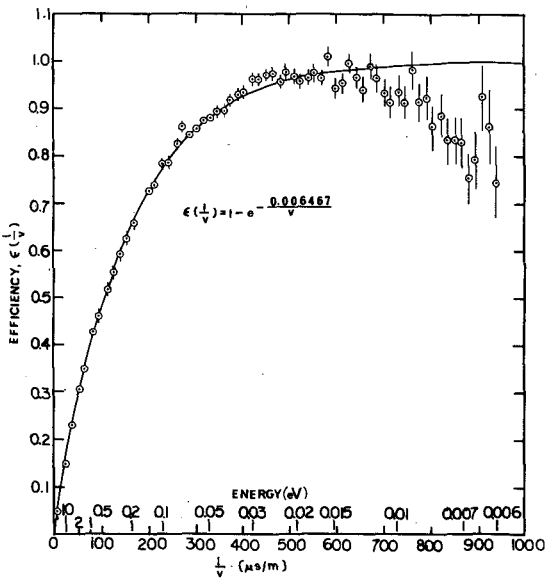

Fig. 3

Counter efficiency determined with 1/v detector

to the chopper, (5) the flight path correction, (6) the spectrometer resolution, and (7) the re-entrant hole perturbation.

A correction for the drift distance, d, between the origin of the neutrons in the spectrum source and the chopping plane was necessary [3] because of the time decay of the neutron density in the medium during the flight time of the neutrons over this distance. For the asymptotic spectrum this correction was easily applied because the neutron density at all energies decayed exponentially with the same decay constant α. The validity of this correction has been verified and has been discussed elsewhere [7].

The calculated efficiency, based on the counter length, B^{10} density and cross-section, was in good agreement with the measured efficiency up to an inverse velocity of 700 μs/m as shown in Fig. 3. For greater inverse velocities, the measured values were less than the calculated efficiency (the droop in the experimental points above 700 μs/m was apparently caused by scattering in the 0.080 in alumina ceramic end window of the counters). A lower energy limit of approximately 0.01 eV was therefore imposed on the spectrum data.

Corrections to the spectrum data had to be made for the chopper slit transmission which was not constant over the entire spectrum. This transmission function was measured experimentally and was described previously [7].

A correction to the neutron time-of-flight from the chopper to the counters was necessary because the source was decaying during the open time of the chopper. This resulted in a shift in the centroid of the neutron burst formed by the chopper. BECKURTS [3] calculated this correction for a chopper which did not close before the neutron density decayed com-

pletely. As the chopper in this experiment closed after a short time (59 μs full width at half maximum at 30 rps), the calculation was generalized to include this effect; neglecting this correction would result in an energy error of 8% at 1 eV.

A correction to the flight path was included to account for the energy-dependent penetration of neutrons into the counters (12.75 in length). The flight path from the entrance surface of the chopper to the mean detection centre for the neutron energy range 0.01 - 10 eV was determined to be (11.12 ± 0.10)m for the first experimental arrangement and (24.4 ± 0.1) m for the second arrangement. The error in the flight path was determined by calculating the mean variance in the detection position for this energy range.

A correction was also made for the energy-dependent transmission of the materials in the flight path (air and aluminium windows). This correction was 5% at 0.01 eV relative to 10 eV.

The correction for the energy resolution of the spectrometer was less than 1% and was therefore neglected. The time uncertainty was taken to be that which yielded one half of the total area under the calculated resolution function. With this energy resolution, the effect on the spectrum was less than 1% even at the joining region between the thermal and slowing-down parts of the spectrum. The resolution correction for the 24-m flight path was also neglected.

A possible spectrum perturbation arising from the presence of the re-entrant hole was also considered. STONE et al. [8] measured the cadmium ratio in a subcritical assembly constructed from the fuel strips that were used in previous asymptotic measurements and found less than a 6% hole effect [7]. BEYSTER et al. in a Poole type spectrum measurement [1] indicated that there was no measurable effect at the centre of a large homogeneous medium for hole sizes up to 5 cm in diameter. POOLE [9] observed a 20% change in the manganese-cadmium ratio at the inner end of a probe tube in a heterogeneous water-uranium slab lattice; however, he attributed this to streaming down the tube which passed down the tube which passed through a region where the spectrum was known to change appreciably.

To study the effect of re-entrant hole size on the asymptotic spectrum of a small homogeneous region, experiments were performed using a polyethylene slab 12 in × 12 in × 3-3/16 in thick as a spectrum source. The re-entrant hole depth was made equal to one half of the slab thickness and a 0.040-in diameter aperture in the cadmium shield around the slab allowed a beam to be brought out from the centre. The results indicated that there was no measurable effect on the shape of the spectrum for the hole diameters 0.125 in, 0.5 in, and 2 in.

Although the shape of the spectrum was the same for each hole size in the polyethylene measurements, the intensity does change as shown in Table II. The relative intensity was obtained by normalizing the area under the measured spectrum to the target monitor count; care was exercised to maintain the same spectrometer solid angle for each case.

The cross-section of the re-entrant hole in each of the multiplying media was 7/8 in × 3/8 in. Based on the above observations the measured scalar spectrum perturbation caused by the hole was therefore expected to be negligible and no correction was made for this effect.

TABLE II

RE-ENTRANT HOLE PERTURBATION ON SCALAR FLUX INTENSITY

Hole diameter (in)	Relative intensity
0.125	1.00
0.50	0.94 ± 0.05
2	0.47 ± 0.03

For the steady state spectrum measurements made only on MM7 using the 24.4-m flight path, the counter efficiency correction and the flight path correction were the same as discussed above for asymptotic measurements. The re-entrant hole perturbation and the resolution correction were also expected to be negligible.

The mean emission time for the multiplying medium was estimated by three methods.

(a) $\bar{t}(E) = (1-k_{eff})\ \bar{t}_{par}(E) + k_{eff}/\alpha$
(b) $\bar{t}(E) = \bar{t}_{par}(E)$
(c) $\bar{t}(E) = 1/\alpha$ for all energies.

The mean emission time $\bar{t}_{par}$ for the paraffin fuel blocks was obtained from the energy-dependent mean emission time calculations made for polyethylene [10] (since emission time calculations are not available for paraffin) and k_{eff} was obtained from a four-group two-dimensional diffusion theory eigenvalue calculation. Each of these mean emission time estimates was used to correct the nominal time-of-flight; no noticeable change in the measured spectrum shape was observed for the different emission times used in this correction.

4. AUXILIARY MEASUREMENTS

Some auxiliary experiments were performed to demonstrate the existence of an asymptotic spectrum. This was obviously essential in order to provide reasonable comparisons with the asymptotic spectrum calculations. In addition, both the time decay constant and the spectrum had to be asymptotic in time to make the drift distance correction to the data possible.

Time to establish an asymptotic spectrum

The determination of the existence of the asymptotic spectrum was carried out by measuring the spectrum as a function of time after the neutron burst for the first experimental arrangement. This measurement was made for each multiplying medium using large time increments (approximately a mean lifetime) and was made in greater detail (10-μs increments) for a

2-in polyethylene slab. The moderator provided a simple source in which the thermalization and diffusion times were comparable to those in a multiplying system.

The corrections to the data were checked by asymptotic scalar measurements made on a polyethylene slab 12 in × 12 in × 3-3/16 in at 26°C. The validity of the corrections were verified since the correct neutron temperature was observed for this slab.

Neutron die-away measurements

The purpose in determining the die-away time for each spectrum source was twofold. The decay constant was required for the source-to-chopper drift distance correction. Of more basic interest was the comparison of the measured and calculated decay constants.

The die-away time of each spectrum source was measured with a low intensity D-T source at the Knolls Atomic Power Laboratory (KAPL) [11]. Each lattice was shielded with 0.030 in of cadmium and a 2-in thick layer of natural boron carbide immediately adjacent to the medium. The adequacy of the shielding arrangement against the room scattered neutron background was determined by investigating the linearity of the measured decay constant as a function of boric acid concentration in water. This investigation was discussed in detail in reference [12]; at the highest concentration of natural boron (6 g/l), where background was emphasized due to absorption and resultant fast decay, the mean lifetime was about 16 μs. Linearity was demonstrated showing that the system was well shielded. The results are given in Table III. To evaluate the effectiveness of the neutron shield used in the actual spectrum measurement at Rensselaer Polytechnic Institute, a 4-in lead wall was placed around the shielded assembly; less than a 1% change in the decay time occurred. Therefore, the die-away time in the Linac experiments was not expected to differ from the KAPL measurement.

5. COMPARISON OF EXPERIMENTAL RESULTS WITH CALCULATION

In the calculation of the asymptotic spectrum, one fundamental assumption, well borne out by experiment, was used. This was the exponential decay of the neutron density, which reduced the time-dependent Boltzmann equation to a stationary equation. Consequently, readily available stationary methods could be used to obtain the solution if the physical absorption cross-section were decreased by α/v, where α is the prompt neutron decay constant of the assembly and v the neutron velocity. Conversely, the decay constant could be calculated by evaluating the quantity of 1/v absorber which had to be removed to render the system prompt critical with $k_{eff} = 1+\beta$.

Spectrum-averaged group constants were used to calculate the decay constant α_c. The decay constant and the asymptotic spectrum were obtained by an iterative procedure using the same series of calculations.

Previous calculations of the MM3 decay constant α yielded a value which was 7% higher than the measured value when the boundary of the core region was taken to be a free surface. Subsequently four-group, two-region dif-

TABLE III

SPECTRUM SOURCE DIE-AWAY TIME

Spectrum source	Slab size (in)	Re-entrant hole size (in)	Measured die-away time (μs)	Calculated die-away time (μs)
MM3	4 x 12 x 12	3/8 x 7/8	48.4 ± 0.5	48.9
MM7	12 x 12 x 12	3/8 x 7/8	122 ± 1	121.6

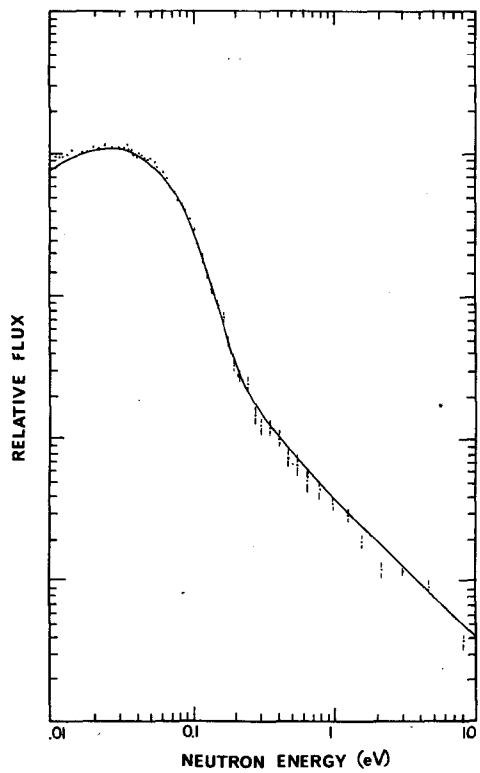

Fig. 4

MM3 centre asymptotic spectrum

fusion theory calculations for each of the two homogeneous assemblies (MM3 and MM7) have shown that the B_4C region adjacent to the core region must be properly accounted for in the treatment of the fast neutron leakage. The calculated decay constants for MM3 and MM7 now agree within 1% of the measured values.

For the present investigation, the asymptotic centre spectrum of MM3 and MM7 were calculated with a 78 group diffusion theory calculation (SWAK)

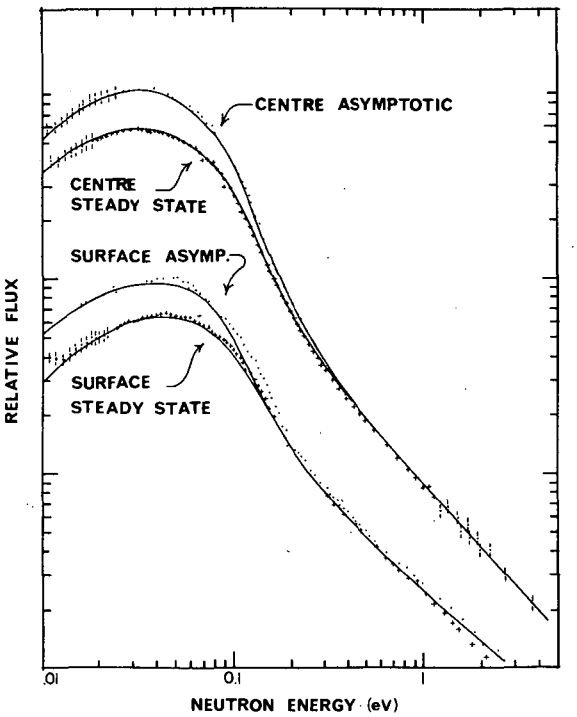

Fig. 5

MM7 asymptotic and steady state spectra

[13] which extended up to 3 eV using a polyethylene kernel to approximate the paraffin moderator characteristics; the calculated decay constant was used to reduce the time-dependent problem to a time-independent one. A comparison between the centre asymptotic calculation and the experimental data for MM3 is given in Fig. 4; for MM7 it is given in Fig. 5.

Figure 4 shows the good agreement (within 5%) that is possible between a diffusion theory calculation and a homogeneous system (MM3) with well-defined thermal boundaries. It should be noted that the calculated value of the decay constant was used in this spectrum calculation. Also, the use of a polyethylene kernel for this paraffin moderated assembly may account for the slight discrepancies from 0.3 to 1 eV and below 0.07 eV. This slight discrepancy also appears in the MM7 centre asymptotic spectrum.

A one-dimensional transport theory calculation (TET) [14] was also used to calculate the asymptotic and steady state spectrum at both the centre and surface of MM7. This thermal spectrum calculation had a 32 energy group structure which extended up to 0.625 eV. The source distribution for the thermal spectrum calculation was obtained from an epithermal transport calculation using a cosine distribution as the initial source for the asymptotic case; for the steady state case, an exponential distribution was used for the epithermal transport calculation.

Over the energy range 0.001 to 0.625 eV, the centre asymptotic spectrum as calculated using the diffusion theory (SWAK) agreed well with

the transport theory (TET) result. At the top of Fig.5 are shown the measured and calculated centre asymptotic spectra; the agreement is within 5% over the energy range from 0.01 to 1 eV.

The lower three curves in Fig.5 show the comparison of the data and the transport theory spectrum calculation for the steady state centre spectrum and for the asymptotic and steady state surface spectra. No transverse leakage corrections were made in these transport calculations. An estimate of the transverse leakage effect indicated that a spectrum will be hardened by less than 20% for any of the cases studied.

6. CONCLUSIONS

(1) In the calculation of the decay constant of a multiplying medium surrounded by a neutron shield, the fast neutron reflection from the shield must be properly taken into account to get good agreement with the measured value of the decay constant. The discrepancy amounted to 7% for MM3 without this correction.

(2) The decay constant of a system can be obtained from the measurement of the asymptotic spectrum. The calculated asymptotic spectrum was found to be extremely sensitive to the value of the decay constant used in the calculation. A 7% change in the MM3 calculated decay constant that was used to calculate the asymptotic spectrum resulted in a 47% change in the calculated thermal to slowing-down flux ratio. The calculated decay constant that was within 1% of the measured one yielded a calculated asymptotic spectrum that was within 5% of the measured one.

(3) The asymptotic spectrum of a paraffin moderated multiplying medium can be calculated to within 5% of the measured spectrum using a polyethylene kernel.

(4) The asymptotic centre spectrum of a homogeneous multiplying assembly can be calculated to within 5% without the use of an auxiliary measurement of the decay constant.

(5) The steady state spectrum of a homogeneous multiplying medium of the type considered here (MM7) can be calculated to within 20% if a reasonable approximation for the thermal steady state source distribution is made.

REFERENCES

[1] POOLE, M.J., J. nucl. Energy 5 (1957) 325; BEYSTER, J.R. et al., Nucl. Sci. Engng 9 (1961) 168.
[2] BEYSTER, J.R. et al., Nucl. Sci. Engng 18 (1964) 376.
BEYSTER, J.R. et al., Rpt. GA-5486 (1964).
[3] BECKURTS, K.H., Z. Naturf. 16a (1961) 611.
[4] FULLWOOD, R.R. et al., Nucl. Sci. Engng 18 (1964) 137.
[5] KRYTER, R. et al., J. nucl. Energy A/B, to be published.
[6] FULLWOOD, R.R. et al., ANS Trans. 7 (1964).
[7] SLOVACEK, R.E. et al., Nucl. Sci. Engng 21 (1965) 329.
[8] STONE, R.S. et al., Nucl. Sci. Engng 2 (1957) 626.
[9] POOLE, M.J., "Neutron time of flight methods", Proc. EANDC Symposium (SPAEPEN, J., Ed.) (1961) 221.
[10] BEYSTER, J.R. et al., Rpt. GA-4069 (1963).

[11] BACH, D.R. et al., Nucl. Sci. Engng 11 (1961) 199.
[12] BACH, D.R. et al., Exponential and Critical Experiments,II IAEA,Vienna (1964) 391.
[13] BOLLACOSA, D. and GOLDMAN, D.T., to be published.
[14] EDGAR, K.R. and RENO, T.T., Jr., TET-thermal energy transport theory spectrum code, Rpt. KRP-4 (KAPL).

DISCUSSION

(on the foregoing four papers)

K. H. BECKURTS: First, I would like to congratulate Dr. Gaerttner and his collaborators on their excellent results, which are all the more impressive when one considers that the Rensselaer Polytechnic Institute group was the last to embark upon thermalization work. Secondly, I would like to ask a question: how did you determine the chopper transmission function in these time-dependent spectrum measurements, or were these calculated functions?

E. R. GAERTTNER: The functions were measured. The chopper was designed with flat surfaces simulating parabolic surfaces, in order to provide a flat energy response from 0-680 μs/m at 15 rps, sufficient to cover the entire energy range of interest. Thus, no transmission correction was required at 15 rps. However, since the measurements were made at 30 rps, a ratio of the 30 rps to the 15 rps count rate in each time-of-flight interval was made experimentally to correct the 30 rps data.

I. SADIKOV: What was the total uncertainty in the determination of the slowing-down time in the measurements of the non-stationary spectra in D_2O for short times?

P. DAITCH: I do not recollect exactly, but it is small compared with the 4.5-μs burst width and negligible at the 50-μs and later time data reported in these papers.

I. SADIKOV: Did you estimate the effect of the highest spatial harmonics on the form of the non-stationary spectra in D_2O?

P. DAITCH: Our first estimates in this connection did not seem to improve the agreement between the theory and measurements. However, we shall look into the matter further.

I. SADIKOV: In what form did you use the source in calculating non-stationary spectra in D_2O?

P. DAITCH: We used several sources at energies of the order of 1 to 5 eV and carried them forward in time. We found, however, that there was very little difference after about 20 min. Moreover, as the experimental resolution is understood, it should be possible to use the earliest time measurements as a source for the later measurements.

N. CORNGOLD: I have a question relating to paper SM-62/52. How does the critical (maximum) discrete eigenvalue observed in beryllium compare with the experimental value of $(v\Sigma)_{min}$?

P. DAITCH: The paper to which you refer deals only with the spectrum, i.e. the eigenfunctions, and not the eigenvalues. However, mention may be made of certain experimental results, on the understanding, of course, that the whole analysis is subject to further review. Generally speaking, the experimental determination is a difficult one and a good deal depends on the interpretation. However, to the best of our judgement, the eigenvalue observed in our beryllium die-away experiments is fully consistent with your published value of $(v\Sigma)_{min} = 3800\ s^{-1}$.

N. G. SJÖSTRAND: In Dr. Gaerttner's oral presentation, he mentioned the effect of the re-entrant holes on the spatially-dependent spectra measurements, a matter which is discussed in greater detail in paper SM-62/55.

Does he have any idea of the extent to which this uncertainty affects the results of the measurements? I would think that this is a rather serious consideration in these small systems.

E. R. GAERTTNER: We believe that it is the re-entrant hole effect and not the third harmonic which is responsible for the measured extrapolation lengths which are apparently too large. It appears that in many cases re-entrant holes (which must, of course, be used to extract a beam) lead to reasonable results. In the space-dependent measurements reported here these may indeed be a problem. I feel personally that the problem of beam extraction is not fully understood. It is a difficult question and someone will have to resolve it.

M. J. POOLE: With reference to the time-dependent spectra in D_2O, did you take into account only the first harmonic? It is our experience that agreeement can never be obtained under these conditions, harmonics up to the seventh mode being required.

E. R. GAERTTNER: Our first estimates of this did not seem to improve agreement between the theory and the measurements. We shall look into the matter further.

MEASUREMENT OF THE TIME-DEPENDENT SPECTRUM IN HEAVY WATER

M. J. POOLE
ATOMIC ENERGY RESEARCH ESTABLISHMENT,
HARWELL, DIDCOT, BERKS., UNITED KINGDOM
AND
P. WYDLER
SWISS FEDERAL INSTITUTE FOR REACTOR RESEARCH,
WÜRENLINGEN, SWITZERLAND

Abstract — Résumé — Аннотация — Resumen

MEASUREMENT OF THE TIME-DEPENDENT SPECTRUM IN HEAVY WATER. The spectrum of neutrons emerging from the centre of a cylindrical tank containing 280 l of pure heavy water has been measured between 40 μs and 1.2 ms after the injection of a fast neutron pulse. A chopper time-of-flight spectrometer and magnetic tape recording and analysing facilities were used. Theoretical spectra calculated in the diffusion approximation using a scattering kernel for heavy water suggested by Honeck agree well with the experimental results.

MESURE DE SPECTRES VARIABLES DANS LE TEMPS, DANS L'EAU LOURDE. Les auteurs ont mesuré le spectre de neutrons provenant du centre d'un réservoir cylindrique contenant 280 litres d'eau lourde pure entre 40 μs et 1,2 ms après injection d'une bouffée de neutrons rapides. Ils ont utilisé un spectromètre à temps de vol, couplé à un hacheur, ainsi que des moyens d'enregistrement sur bande magnétique et d'analyse. Les spectres théoriques calculés dans l'approximation de diffusion à l'aide d'un noyau de diffusion pour l'eau lourde suggéré par Honeck sont en bon accord avec les résultats expérimentaux.

ИЗМЕРЕНИЕ СПЕКТРА В ТЯЖЕЛОЙ ВОДЕ, ЗАВИСЯЩЕГО ОТ ВРЕМЕНИ. Спектр нейтронов, выходящий из центра циллиндрического бака объемом в 280 л тяжелой воды, измерялся во временных пределах от 40 мксек до 1,2 мсек после того, как был введен импульс быстрых нейтронов. Использовались спектрометр времени полета с прерывателем, магнитофонная лента и аналитические устройства. Теоретический спектр, высчитанный в диффузионном приближении с использованием интегрального ядра рассеяния для тяжелой воды, предложенный Хонеком, хорошо согласуется с экспериментальными результатами.

MEDICION DEL ESPECTRO TEMPORAL EN EL AGUA PESADA. Los autores han medido el espectro de los neutrones provenientes del centro de un tanque cilíndrico que contenía 280 l de agua pesada pura, para el intervalo comprendido entre 40 μs y 1,2 ms, después de la aplicación de una ráfaga de neutrones rápidos. Se utilizaron un espectrómetro de tiempo de vuelo provisto de selector y aparatos adecuados de grabación magnetofónica y de análisis. Los espectros teóricos calculados con arreglo a la aproximación por difusión empleando el núcleo de dispersión para el agua pesada sugerido por Honeck concuerdan satisfactoriamente con los resultados experimentales.

1. INTRODUCTION

The behaviour of a pulse of fast neutrons approaching thermal equilibrium is known to be sensitive to the scattering properties of the moderator. Measurements of the time-dependent spectrum therefore provide a means of testing energy exchange kernels which are needed for thermal re-

actor calculations. Measurements on graphite have been reported by BARNARD et al. [1] and by NICHOLSON and POOLE [2]. MOSTOVOY et al. [3] have measured time-dependent spectra both in beryllium and graphite.

Although a knowledge of the thermalization process in heavy water is a fundamental requirement for the design of a heavy water reactor, the process is not yet well understood. Recently, however, theoretical scattering kernels have become available, but these still require experimental confirmation. Measurements of the time-dependent spectrum in heavy water have therefore been made. In the present paper the experimental technique used for these measurements is described and the results are compared with calculations based on diffusion theory.

2. EXPERIMENTAL ARRANGEMENT

The experimental arrangement is shown in Fig. 1. The spectra were observed in the centre of a tank which was 70 cm in diameter and 78 cm long, contained heavy water of 99.8% purity and was shielded with 0.2 cm of cadmium. The target of the Harwell electron linear accelerator was positioned at the centre of one face of the tank and provided bursts of fast neutrons of 1.7-μs duration at a repetition frequency of 96 pulses/s. Neutrons were extracted radially and perpendicular to the flux gradient through an aluminium probe tube 4.5 cm in diameter with an aluminium window 0.3 mm thick.

Neutrons emerging from the tube entered a chopper time-of-flight spectrometer [2]. The flight path was 5 m long and a bank of four BF_3 counters was used to detect the neutrons, the counts from each counter being recorded separately to improve the spectrometer resolution. Background was determined by inserting a boron carbide and cadmium shutter into the beam between the tank and the chopper. The chopper speed was not synchronized with the accelerator repetition frequency; instead, for each machine cycle the delay from accelerator burst to chopper opening was measured. This method has already proved to be very successful for normalizing spectra corresponding to different times and has the advantage that no monitoring of the accelerator output is required. The overall count rate, however, was slightly less than that which could have been achieved with a synchronized chopper. Magnetic tape equipment was used to record and analyse the data. A detailed description of this method has been given by NICHOLSON and POOLE [4]. The following quantities were simultaneously measured for each event and recorded as a 16 bit number on 1-in magnetic tape:

(a) Delay between the pulse of fast neutrons and the chopper burst,
(b) Time-of-flight for the neutron to travel from the chopper to the counters,
(c) Number of recording counter,
(d) Position of shutter, whether in spectrum or background position.

Seven bits (128 channels) were used to record the delay and 6 bits (64 channels) were allocated to the time-of-flight. The delay channel width was 10 μs for the first 64 channels and 20 μs for the remainder. The time-of-flight channels were 80 μs long. An overall spectrometer resolution

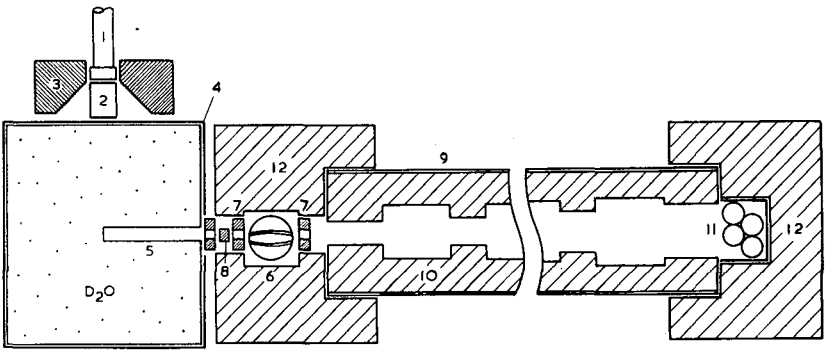

Fig. 1

Experimental arrangement

of 20 μs/m was used for the time-of-flight measurement. Delays were measured with an effective resolution which varied from 24 to 34 μs between 0.1 and 0.01 eV.

3. PROCESSING OF THE DATA

The magnetic tapes were analysed on a 4096 channel magnetic tape analyser, six passes being required for each tape to obtain a spectrum. The frequency distribution of chopper delays was checked and was found to be random. In addition to the usual corrections to time-of-flight data the following corrections were applied:

(a) Derivation of the spectrum

By recording delay and time-of-flight as defined above, a spectrum at the position of the centre of the chopper was measured. The flux in the centre of the tank was related to it through the equation $\varphi(v,t) = \varphi_0(v, t+a/v)$, $\varphi_0(v,t)$ being the observed spectrum and a the distance from the centre of the tank to the centre of the chopper.

(b) Resolution correction

By using STONE and SLOVACEK's method [10], a correction was applied to allow for the fact that each spectrum represents an average over a finite time. In the first order approximation the correction is proportional to the second time derivative of the observed flux, the factor of proportionality being $\frac{1}{2}(F_2/F_0 + C_2)$, where $F_n = \int dt\, t^n P(v,t)$ and $C_2 = \int d\epsilon\, \epsilon^2 R(\epsilon)$. $P(v,t)$ is the chopper transmission probability function and $R(\epsilon)$ is the delay resolution function. F_0 and F_2 were obtained from the theoretical functions $P(v,t)$ derived by MARSEGUERRA and PAULI [5]. Before calculating the second derivative a sum of exponentials was fitted to the decay curves for each energy group. The correction was important for short delays and changed the mean energy of the 44-μs spectrum, for example, by 11%.

4. THEORETICAL METHODS

In the diffusion approximation the distribution of neutrons in energy, space and time $N(E, \vec{r}, t)$ is governed by the equation

$$\frac{\partial}{\partial t}N(E,\vec{r},t) = -\left[\Sigma_a(E) + \Sigma_s(E) - D(E)\frac{\nabla^2 N(E,\vec{r},t)}{N(E,\vec{r},t)}\right] v(E)N(E,\vec{r},t)$$

$$+ \int_0^\infty dE'\,\Sigma(E' \to E)v(E')N(E',\vec{r},t) + S(E,\vec{r},t) \qquad (4.1)$$

where $\Sigma_a(E)$, $\Sigma_s(E)$ and $\Sigma(E' \to E)$ are the macroscopic absorption, total scattering and differential scattering cross-sections, respectively, $D(E)$ is the diffusion coefficient and $S(E, \vec{r}, t)$ represents the source. A Fortran programme SPECTIM has been written to integrate this equation by the explicit method. Provided care is taken to ensure the stability of the process this simple procedure has been found satisfactory over a wide range of conditions. Similar methods have been described by OHANIAN and DAITCH [6] and by GHATAK and HONECK [7] who calculated time-dependent spectra in water and graphite.

SPECTIM takes the leakage into account either

(a) By assuming an energy-independent buckling B^2. The flux is separated into a series of spatial modes to each of which is assigned a separate value of B^2, or

(b) By making the assumption that the leakage $\nabla^2 N(E, \vec{r}, t)/N(E, \vec{r}, t)$ can be written as $A(\vec{r}, t)$ which is time-dependent but still energy-independent.

Integration of the diffusion equation over energy shows [2] that $A(\vec{r}, t)$ can be related to the total neutron density $N(\vec{r}, t)$ in the following way:

$$-\frac{\partial}{\partial t}\ln N(\vec{r},t) \sim \overline{\Sigma_a v}(\vec{r},t) - A(\vec{r},t)\,\overline{Dv}(\vec{r},t),$$

where

$$\overline{Dv}(\vec{r},t) = \int_0^\infty dE\, D(E)\, v(E)\, N(E,\vec{r},t) \Big/ \int_0^\infty dE\, N(E,\vec{r},t)$$

and

$$\overline{\Sigma_a v}(\vec{r},t) = \int_0^\infty dE\, \Sigma_a(E)\, v(E)\, N(E,\vec{r},t) \Big/ \int_0^\infty dE\, N(E,\vec{r},t).$$

$\overline{\Sigma_a v}$ simplifies to $\Sigma_a v$ for a $1/v$ absorber. The value of method (b) is that $N(0, t)$ ($\vec{r} = 0$ for the centre of the tank) can easily be obtained from an integral measurement, whereas an accurate measurement of the relative

intensities of the spatial modes in the experimental tank is more laborious. If N(0, t) can be fitted by the sum of exponentials corresponding to the decay times of the harmonic modes, then the methods are equivalent.

Relaxation times and asymptotic spectra for different values of B^2 were also obtained from Eq. (4. 1) by writing $N(E, t) = N(E) \exp(-\mu t)$ and finding the lowest eigenvalue of the resulting equation

$$[\Sigma_a(E) + \Sigma_s(E) + D(E)B^2 - \mu/v]v(E)N(E) = \int_0^\infty dE' \, \Sigma(E' \to E)\, v(E')N(E') \qquad (4.2)$$

A heavy water scattering kernel proposed by HONECK [8] was used for the computations. The code GAKER was used to calculate a 81×81 scattering matrix. A perfect gas kernel was added separately to account for the scattering by the oxygen [11]. The energy-dependent diffusion coefficient was derived from the experimental measurement of the mean cosine of the scattering angle (see SPRINGER et al. [9]).

5. RESULTS AND CONCLUSIONS

A selection of both theoretical and experimental spectra is shown in Fig. 2. The theoretical curves were normalized by equating the intensities of the calculated and observed spectrum at 124 μs, the intensities of the remaining spectra were then found to be in good agreement. The calculation of the time-dependent spectrum has not been extended to very long delays. Instead, the 1000-μs spectrum was obtained by superimposing the asymptotic spectra obtained from the bucklings calculated for the fundamental and third harmonic modes and taking into account the measured intensities. This procedure is justified because after about 200 μs it was found that only the intensities, and not the shapes of the spectra for each mode, changed with time. Theoretical and experimental spectra agree quite well except for the 44-μs spectrum for which the calculated spectrum is harder than that observed.

Mean energies $\overline{E}(t) = \int_0^\infty dE\ E\ N(E) / \int_0^\infty dE\, N(E)$ and total neutron densities $N(t) = \int_0^\infty dE\, N(E)$ were evaluated for the experimental spectra. The contributions to the integrals below 0. 006 eV and above 0. 2 eV were calculated assuming the spectra to be Maxwellian. The neutron density N(t) agreed well with an integral measurement. To derive the experimental time constants a sum of exponentials was fitted to the observed neutron density, $N(t) = \Sigma\, a_n \exp(-b_n t)$; the parameters giving the best fit are shown in Table I. b_1, b_2 and b_3 agreed with the theoretical relaxation time constants for the fundamental mode and the third and seventh harmonic modes calculated from Eq. (4. 2); the bucklings were obtained from the expression $B^2 = (n\pi/L)^2 + (2.405/R)^2$. A (5, 1) mode, however, was not observed. Also shown in Table I is a calculation of the time constants based on the elementary formula of Beckurts. Again, the agreement with measured values is quite good.

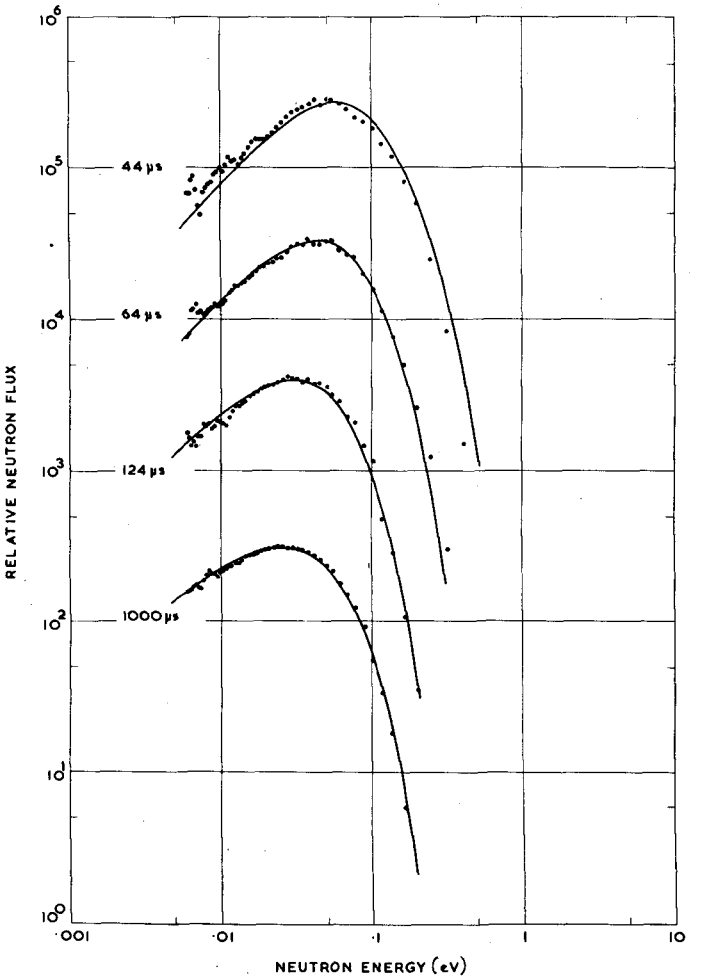

Fig. 2

Experimental and calculated spectra at four different times

Figure 3 shows the variation of the mean neutron energy with time. Some deviation which can be seen for the first two experimental points is believed to be caused by a lack of resolution and an uncertainty of ±3 μs in the time scale. Because of the strong third harmonic mode present with negative amplitude the spectrum does not reach equilibrium before 2 ms after the fast neutron pulse. Up to 400 μs the neutron density is still increasing which leads to a negative leakage term in Eq.(4.1) and therefore causes "diffusion heating". For delays below 400 μs the mean neutron energy was measured to be above 1.5 kT.

Theoretical curves for the relaxation time constant and the mean energy of the asymptotic spectrum are shown in Fig. 4. The thermalization parameters in the expansion $\mu = \Sigma_a v + D_0 B^2 - CB^4 + \ldots$ were obtained by fitting

TABLE I

TIME CONSTANTS CALCULATED TO FIT THE OBSERVED NEUTRON DENSITY

Spatial mode*	B^2 ($cm^{-2} \times 10^{-3}$)	Time constant (ms^{-1})			Observed intensity	Calculated mean energy
		GAKER (μ)	$\Sigma_a v + D_0 B^2 - CB^4$ **	Experimental (b_n)	(a_n)	(kT)
(1, 1)	5.78	1.199	1.20	1.16	3.31	1.477
(3, 1)	17.7	3.543	3.57	3.01	-2.58	1.417
(5, 1)	41.5	7.796	8.01	-	not observed	1.303
(7, 1)	77.3	13.195	13.9	14.0	0.27	1.147
					no radial "harmonics" observed	

* First and second index referring to axial and radial flux distributions, respectively.

** $D_0 = 20.7 \times 10^4$ $cm^2 s^{-1}$, $C = 3.5 \times 10^5$ $cm^4 s^{-1}$ (SJÖSTRAND [12]).

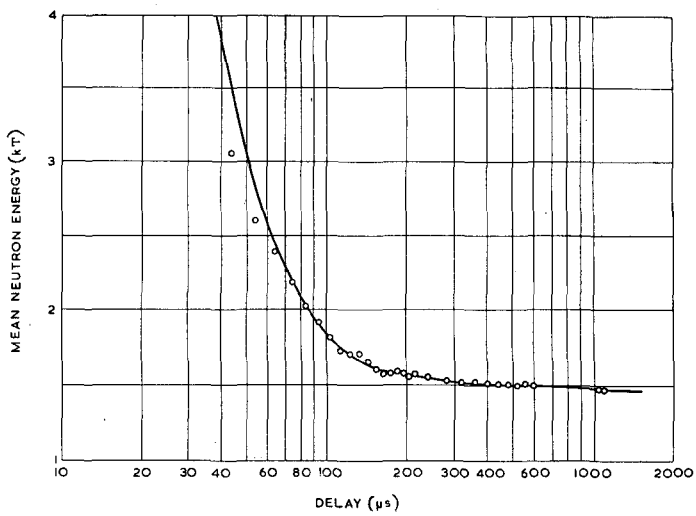

Fig. 3

Mean neutron energies of spectra

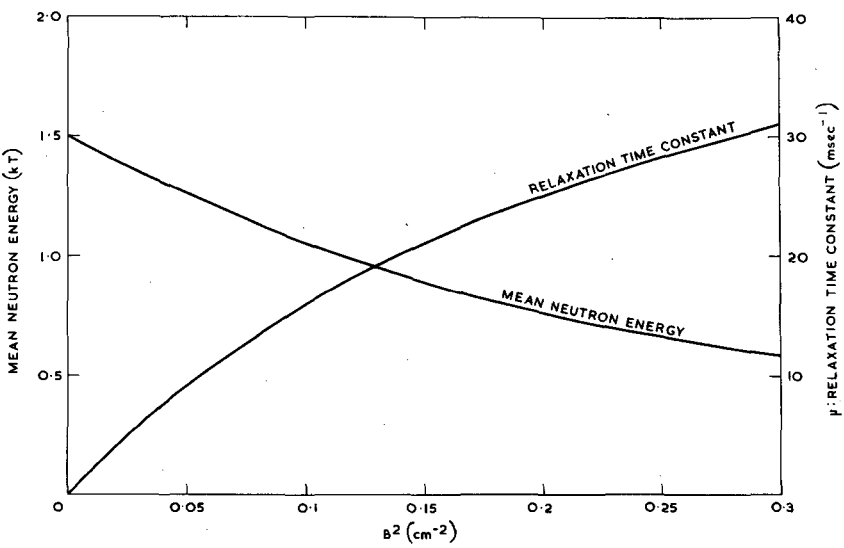

Fig. 4

Relaxation time constant and mean neutron energy
of the asymptotic spectrum as a function of B^2

the $\mu(B^2)$ curve over the range for B^2 indicated in Fig. 4. Results, given in Table II, are in good agreement with experimental values.

To summarize it can be said that agreement between theory and experiment is close even for delays below 200 μs where the spectrum is most sensitive to the scattering kernel.

TABLE II

THERMALIZATION PARAMETERS FOR HEAVY WATER

	D ($cm^2/s \times 10^5$)	C ($cm^4/s \times 10^5$)	F ($cm^6/s \times 10^5$)	G ($cm^8/s \times 10^5$)
Measured values				
[13]	2.09 ± 0.03			
[14]	2.09 ± 0.025			
[15]	2.08 ± 0.05	3.72 ± 0.5 (20°C)		
[16]	2.00 ± 0.01	5.25 ± 0.25 (22°C)		
[9]	2.09 ± 0.02			
[12]		3.5 ± 0.8		
Calculations (GAKER), kernel temperature 293°K				
(a) Two parameters	1.996	3.494		
(b) Three parameters	2.079	5.381	6.346	
(c) Four parameters	2.077	5.299	5.645	1.553

ACKNOWLEDGEMENTS

The authors wish to thank Dr. R.N. Sinclair and Mr. K. P. Nicholson for their advice and for stimulating discussions. Mr. R.H. Jones and Miss L. Baillie assisted with the theoretical calculations and Mr. P.R. Pitts with various parts of the experiment. The co-operation of the Linac operating team is gratefully acknowledged.

REFERENCES

[1] BARNARD, E., KHAN, N.A., McLATCHIE, R.C.F., POOLE, M.J. and TAIT, J.H., Nucl Sci. Engng 17 (1963) 513.

[2] NICHOLSON, K.P. and POOLE, M.J., Rpt. AERE-R 4842 (1965).

[3] MOSTOVOY, V.I., DYKAREV, V.S., EREMEEV, I.P., ISHMAYEV, S.P., SADIKOV, I.P., SALTYKOV, Y.S. TARABAN'KO, V.A. and CHERNYSHOV, A.A., Proc 3rd UN Int. Conf. PUAE, 1964, A/CONF.28/P/367.

[4] NICHOLSON, K.P. and POOLE, M.J., Conf. on Automatic Handling and Acquisition of Data, Karlsruhe, 1964.

[5] MARSEGUERRA, M. and PAULI, G., Nucl. Instrum. Meth. 4 (1959) 140.

[6] OHANIAN, M. J. and DAITCH, P. B., Nucl. Sci. Engng 19 (1964) 343.
[7] GHATAK, A. K. and HONECK, H. C., Rpt. BNL-8115 (1964).
[8] HONECK, H., Trans. Amer. nucl. Soc. 5 (1962) 47.
[9] SPRINGER, T., HOFMEYR, Ch., KORNBICHLER, S. and LEMMEL, H. D., Proc. 3rd UN Int. Conf. PUAE 1964, A/CONF. 28/P/763.
[10] STONE, R. S. and SLOVACEK, R. E., Nucl. Sci. Engng 6 (1959) 466.
[11] SINCLAIR, R. N., Private communication.
[12] SJÖSTRAND, N. G., Ark. Fys. 15 (1958) 145.
[13] KASH, S. W. and WOODS, D. C., Phys. Rev. 90 (1953) 564.
[14] BROWN, H. D. and HENNELLY, E. J., Rpt. BNL-719 III (1962) 879.
[15] GANGULY, N. K. and WALTNER, A. W., Trans. Amer. nucl. Soc. 4 (1961) 282.
[16] KUSSMAUL, G. and MEISTER, H., React. Sci. Technol. 17 (1963) 411.

DISCUSSION

S. N. PUROHIT: From your results for D_2O what is the estimated value of the average thermalization-time constant?

P. WYDLER: The value varies with time, being about 48 μs in the region between 40 and 80 μs. This observation was also confirmed by the calculations, which did not predict a constant for any of the spatial modes investigated.

I. SADIKOV: It seems to me that the finite width of the resolution of the apparatus should lead to an increase in the mean energy value as compared with the theoretical value. However, your experimental points are lower than the theoretical curve.

P. WYDLER: I think this depends on the properties of the chopper, on the burst width. In our experiment the total neutron density as a function of time was increasing rapidly below 40 μs. Under these conditions it was possible for the experimental points to lie below the theoretical curve.

I. SADIKOV: I think it may depend more on the slowing-down process than on the chopper.

P. WYDLER: Yes, I would agree on that point.

MEASUREMENTS OF NEUTRON SPECTRA IN HYDROGENOUS MODERATORS

J. KALLFELZ AND W. REICHARDT
KERNFORSCHUNGSZENTRUM KARLSRUHE,
FEDERAL REPUBLIC OF GERMANY

Abstract — Résumé — Аннотация — Resumen

MEASUREMENTS OF NEUTRON SPECTRA IN HYDROGENOUS MODERATORS. Measurements of neutron spectra have been made in various hydrogenous moderators, using a 400-keV Cockcroft-Walton pulsed neutron source, a slow chopper, and a 3-m flight path. The spectra measured include the following types:

(1) Asymptotic leakage spectra normal to the surface for water, benzene and Dowtherm A, for slab geometries with thickness varying from 2 to 15 cm.

(2) Asymptotic leakage spectra in water at various angles from the normal of the surface, for an effectively infinite geometry.

(3) Time-dependent spectra from the middle of an ice moderator at liquid nitrogen and liquid hydrogen temperatures, and from the middle and surface of a block of zirconium hydride ($ZrH_{1,65}$) at room temperature.

Spectra calculations were made using theoretical and experimental scattering kernels. Among the programmes used is a FORTRAN II code, ADALS, for the calculation of angular-dependent asymptotic leakage spectra. The scattering kernels used include the Nelkin and Haywood kernels for water, and kernels for benzene and Dowtherm A derived from scattering-law measurements made at Karlsruhe. The calculated spectra are compared with the experimental results.

MESURES DES SPECTRES DE NEUTRONS DANS DES RALENTISSEURS HYDROGÉNÉS. Les auteurs ont fait des mesures de spectres de neutrons dans divers ralentisseurs hydrogénés en utilisant une source de neutrons pulsés Cockcroft-Walton de 400 keV, un hacheur lent et un parcours de vol de 3 m. Ils ont mesuré notamment les types de spectre suivants:

1. Spectres de fuite asymptotiques normaux à la surface pour l'eau, le benzène et le Dowtherm A dans des géométries de plaques, l'épaisseur variant de 2 à 15 cm.
2. Spectres de fuite asymptotiques dans l'eau sous des angles divers par rapport à la normale à la surface, dans une géométrie infinie.
3. Spectres variables dans le temps, provenant du centre d'un bloc ralentisseur en glace aux températures de l'azote et de l'hydrogène liquides, et du centre et de la surface d'un bloc d'hydrure de zirconium ($ZrH_{1,65}$) à la température ambiante.

Les calculs des spectres ont été faits au moyen de noyaux de diffusion théoriques et expérimentaux. Parmi les programmes utilisés figure un code FORTRAN II, ADALS, pour le calcul des spectres de fuite asymptotiques variable selon l'angle. Parmi les noyaux de diffusion utilisés figurent les noyaux de Nelkin et de Haywood pour l'eau, et d'autres noyaux pour le benzène et Dowtherm A calculés à partir des mesures de la loi de diffusion faites à Karlsruhe. Les auteurs comparent les spectres théoriques aux résultats expérimentaux.

ИЗМЕРЕНИЕ НЕЙТРОННЫХ СПЕКТРОВ В ВОДОРОДНЫХ ЗАМЕДЛИТЕЛЯХ. Измерения нейтронных спектров производили на различных водородных замедлителях при использовании источника импульсных нейтронов Кокрофта-Уолтона с энергией 400 кэв, селектора медленных нейтронов и пути пролета 3 м. Измеренные спектры включали следующие виды:

1. Асимптотические спектры утечки, обычные для поверхности воды, бензола и "Даутерма" А, для пластинчатых геометрий с толщиной 2–15 см.

2. Асимптотические спектры утечки в воде при различных углах, начиная от обычного для воды, в отношении эффективной бесконечной геометрии.

3. Зависимые от времени спектры от середины ледового замедлителя при температурах жидкого азота и жидкого водорода и от середины и поверхности блока гидрида циркония ($ZrH_{1,65}$) при комнатной температуре.

Расчеты спектров производили при использовании теоретических и экспериментальных ядер рассеяния. Среди использованных программ находятся программа FORTRAN II, ADALS

для расчета зависящих от угла асимптотических спектров утечки. Использованные ядра рассеяния включают ядра Нелкина и Хэйвуда для воды, а также ядра для бензола и "Даутерма" А, полученные из измерений по закону рассеяния, проведенных в Карлсруэ. Расчетные спектры сравниваются с экспериментальными результатами.

MEDICION DE ESPECTROS NEUTRONICOS EN MODERADORES HIDROGENADOS. Se han medido espectros neutrónicos en varios moderadores hidrogenados con una fuente pulsada de neutrones Cockcroft-Walton de 400 keV, un selector lento y una trayectoria de vuelo de 3 m. Los espectros medidos eran de los siguientes tipos:

1. Espectros asintóticos de escape normales a la superficie en el caso del agua, del benceno y del Dowtherm A, para configuraciones geométricas en forma de placa con espesores comprendidos entre 2 y 15 cm.
2. Espectros asintóticos de escape en el agua a varios ángulos respecto de la normal a la superficie, para una geometría efectivamente infinita.
3. Espectros dependientes del tiempo desde el centro de un moderador de hielo a las temperaturas del hidrógeno y del nitrógeno líquidos, y desde el centro y la superficie de un bloque de hidruro de circonio ($ZrH_{1,65}$) a la temperatura ambiente.

Los espectros se calcularon aplicando núcleos de dispersión teóricos y experimentales. Entre los programas utilizados cabe citar el FORTRAN II, ADALS, para el cálculo de los espectros asintóticos de escape en función del ángulo. Los núcleos de dispersión aplicados son los de Nelkin y Haywood para el agua; para el benceno y el Dowtherm A se emplearon núcleos deducidos de las mediciones de la ley de dispersión hechas en Karlsruhe. Los espectros calculados se comparan con los resultados experimentales.

I. INTRODUCTION

The combined pulsed source chopper technique has proved to be a valuable tool for the investigation of neutron spectra in moderators. As is well known, the time asymptotic equilibrium state in an infinite moderator with 1/v absorption is completely governed by the principle of detailed balance, which causes the spectrum to be a Maxwellian. To get information about the scattering properties of the moderator, it is therefore necessary to study deviations from this state by enforcing a distortion of the spectrum. This situation is realized when neutron leakage from the moderator is present. For small moderator assemblies the spectrum inside is distorted by diffusion cooling. A direct measurement of this phenomenon has been made by BECKURTS [1]. For large moderators the leakage causes a distortion of the spectrum only near the surface. The leakage spectra correspond to those of the Milne problem without absorption and a Maxwellian source at infinity. This problem has been investigated experimentally and theoretically by various authors [1-5]. Of interest are the angular dependence of the spectra and how they are influenced by the detailed form of the scattering law.

A more direct method is to look into the approach to the equilibrium state, where the deviations are larger and therefore the influence of the scattering properties of the moderator becomes more apparent. Measurements of the time dependence of neutron spectra were first made by BARNARD et al. [6]. For large moderators such investigations yield information mainly about the isotropic part of the scattering law, whereas diffusion-cooled and leakage spectra are influenced by both transport effects and thermalization effects which causes a very complex dependence on the scattering law.

In the following two sections of this paper two different investigations of thermal neutron spectra by the combined pulsed source chopper technique

are described. Section II deals with time asymptotic leakage spectra. For a large moderator, angular-dependent measurements were made for water, and leakage spectra perpendicular to the surface were measured for water, benzene, and Dowtherm A. Furthermore for water and benzene, measurements of the perpendicular leakage spectra were performed for small slabs, where the spectra in the middle no longer are Maxwellian as a result of diffusion cooling. Section III concerns investigations of the neutron moderation through measurements of the time behaviour of neutron spectra after the injection of a short pulse of fast neutrons into a moderator. The moderators investigated were zirconium hydride at room temperature and ice at liquid nitrogen and liquid hydrogen temperature.

II. LEAKAGE SPECTRA*

1. *Experimental methods*

The pulsed neutron source and flight path have been described in [7]. The source, a 400-keV cascade deuteron accelerator, was developed by EYRICH [8]. At the end of the 3-m flight path is the neutron detector bank of eight high-pressure BF_3 counters. A cadmium chopper with a rotation rate of 7000 - 12 000 rpm is used. An electronic pulse given from the chopper is delayed, and then used to trigger the accelerator and the time analyser connected to the detector. Thus, by adjusting the time at which the accelerator pulse occurs, one can ensure the thermalization of the neutrons in the moderator before the chopper opens. Three long counters were used as monitors to determine the intensity of the source.

The measurements of the leakage spectra for neutrons emitted at angles from 0° to 72° from the surface normal were made on two large water samples, 15 cm×30 cm×30 cm and 12 cm×22 cm×22 cm. Figure 1 shows schematically the experimental set-up for this measurement. The different angles were obtained by turning the sample about the axis through the centre of the area from which the neutrons were extracted. For each angular adjustment, the apparatus was moved so that the position of the target relative to the moderator sample remained constant. The area from which the neutrons were extracted was fixed by windows of various sizes, such that the area of the surface seen by the detector bank was identical for all angles.

To measure at larger angles from the normal to the surface, rather large distances (up to 14 cm) were necessary. This causes a considerable correction for the different flight times between the moderator surface and the chopper. To check the accuracy of this correction, measurements of the spectrum for leakage perpendicular to the surface were made at three distances. The spectra obtained from these measurements were identical.

The measurements of the spectra for neutrons emitted parallel to the surface were made on a 22 cm×22 cm×12 cm H_2O sample, using the assembly shown in Fig. 2. The extraction channel was 2 cm wide, and had a cadmium lining, except for the last 8 mm from the extraction point; this

* Work performed by J. Kallfelz.

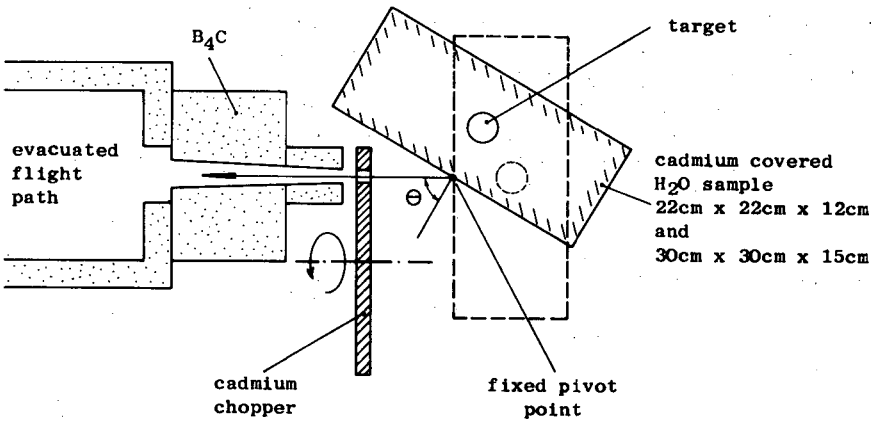

Fig. 1

Set-up for measurements of angular-dependent leakage spectra for θ-values between 0° and 72°

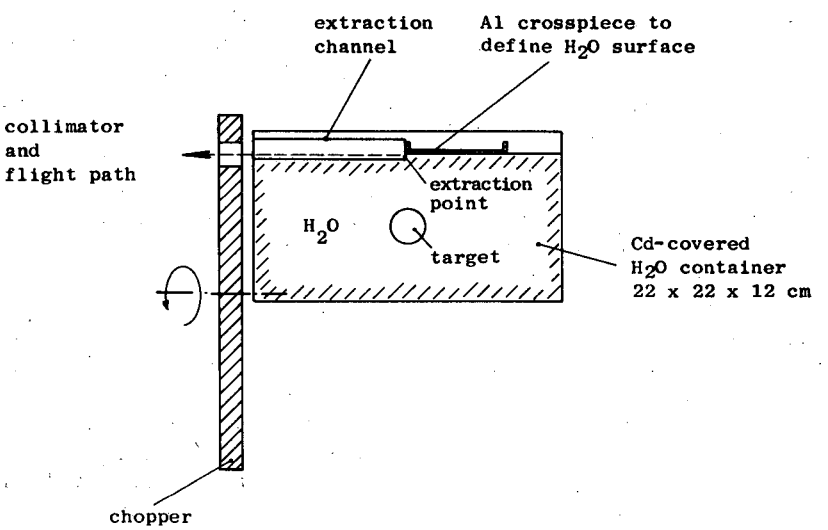

Fig. 2

Assembly for measuring the leakage spectra at the grazing angle

lining ensured that only neutrons from the extraction point could pass through the chopper. The water surface was sharply defined at the extraction point by an aluminium cross piece in contact with the surface. Measurements were made for channel intrusion depths of 2 and 4 mm below the surface.

2. *Results*

(a) Perpendicular leakage spectra

The results for the leakage spectra perpendicular to the surface for H_2O, benzene, and Dowtherm A at room temperature are shown in Figs. 3

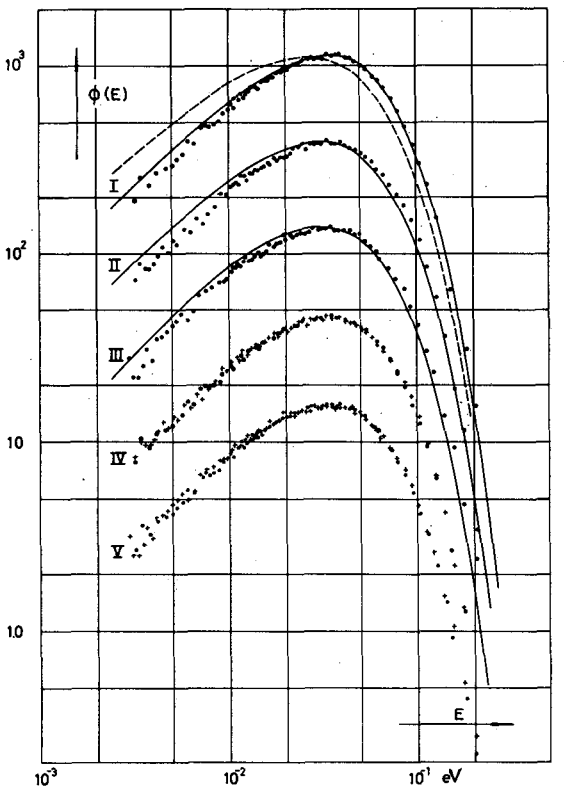

Fig. 3

Leakage spectra perpendicular to surface from a large sample at room temperature (24°C)
The solid curves are theoretical calculations.

I : H_2O (••••); Maxwellian at moderator temperature (– – – –)
II : Dowtherm A
III: benzene
IV: H_2O (••••) compared to Dowtherm A (++++)
V : H_2O (••••) compared to benzene (++++)

and 4. In these figures, and in Fig. 5, the solid curves are from theoretical calculations, which are discussed in part 3 of this section.

The spectra for the large sample (30 cm×30 cm×15 cm) are compared in Figs. 3-IV and 3-V for the three moderators. These spectra are practically identical, although the frequency distributions of the three moderators are quite different [9, 10]. All three spectra are about 15-17% hotter than a Maxwellian distribution at moderator temperature, shown by the dashed curve in Fig. 3-I.

The effect of diffusion cooling, first observed directly in spectra measurements of BECKURTS [1], is quite apparent in the spectra for small slabs. It can be seen in Fig. 4 that the maximum of the spectra for the smallest slabs is at about 0.025 eV, while that of the infinite medium is at 0.030 eV.

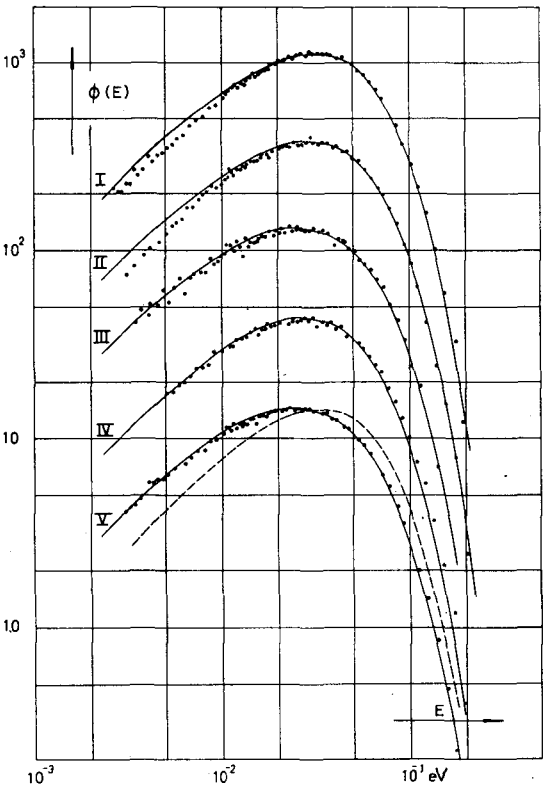

Fig. 4

Leakage spectra perpendicular to surface from thin slabs at 24°C
The solid curves are theoretical calculations.

I : H_2O, 4.2 cm x 30 cm x 30 cm slab
II : H_2O, 3 cm x 20 cm x 20 cm slab
III: H_2O, 2.1 cm x 20 cm x 20 cm slab
IV: benzene, 4.2 cm x 30 cm x 30 cm slab;
V : benzene (••••) 3.1 cm x 30 cm x 30 cm slab;
empirical curve fitted to points in Fig. 3-IV (– – – –)

(b) Angular-dependent spectra

The results of the angular-dependent spectra measurements are shown in Fig. 5, for various values of μ, the cosine of the angle θ between the emerging direction and the normal to the surface. The measurements for μ = 1.0, 0.7, 0.5, and 0.3 (θ = 0°, 45°, 60°, and 72°) are those from the 22 cm×22 cm×12 cm sample; the results with the 30 cm×30 cm×15 cm sample were essentially the same. There is very little angular dependence down to μ = 0.3, the spectra being all of nearly the same form. There is a very slight amount of cooling as μ decreases, which can be detected by dividing the μ = 1.0 curve into the other curves. As an example, Fig. 6 shows the quotient $\phi(\mu = 0.3, E)/\phi(\mu = 1.0, E)$. While the points scatter considerably,

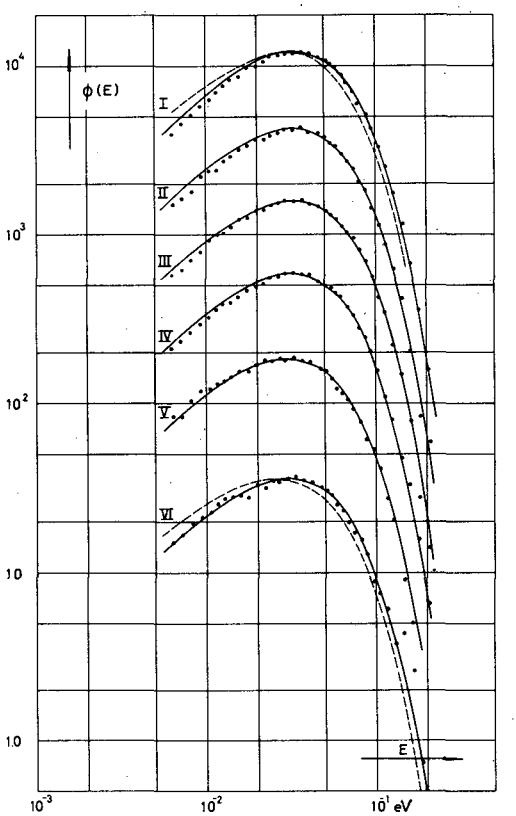

Fig. 5

Angular-dependent leakage spectra from H_2O at 24°C
The solid curves are theoretical calculations.

I : $\mu = 1.0$ (••••);
empirical curve fitted to points in Fig. 5-V (– – –)
II : $\mu = 0.7$ - III: $\mu = 0.5$ - IV: $\mu = 0.3$
V : $\mu = 0.0$, extraction channel penetrating 4 mm below surface
VI: $\mu = 0.0$, extraction channel penetration 2 mm (••••)
Maxwellian at moderator temperature (– – –)

a definite trend toward higher values for lower energies can be seen, which indicates that the $\mu = 0.3$ spectrum is cooler. For comparison, the quotient of two Maxwellians with T_0 differing by 2% is shown.

For $\mu = 0.0$, the container described in the previous section for measuring spectra emerging parallel to surface was used. The spectra shown were obtained from measurements in which the extraction channel penetration into the surface was approximately 2 and 4 mm. The results for both intrusion depths are practically the same. The intensity for the 2-mm measurement was very low, therefore the points scatter considerably. Theoretical calculations [4] predict that the transient flux, which describes the variation in the spectra form near the surface, dies off quite rapidly for increasing di-

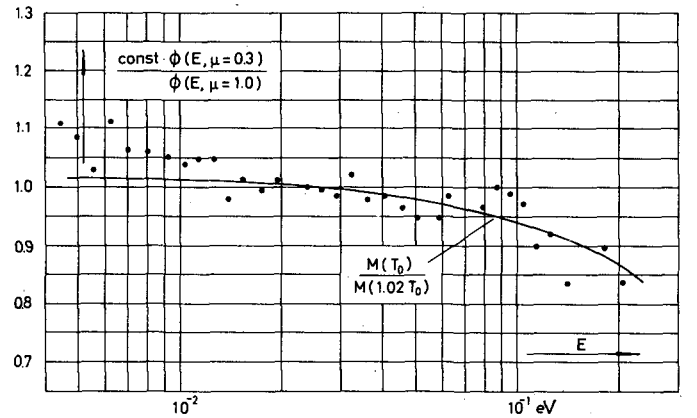

Fig. 6

φ(E, μ = 0.3)/φ(E, μ = 1.0), for the H_2O angular-dependent spectra measurements
The solid curve is the quotient of two Maxwellians with T_0 differing by 2%.

stance from the surface. Furthermore, the disturbing effect of the extraction channel becomes greater for increasing penetration depth. Hence, the results must be interpreted with care. However, since the variation between the 4-mm and 2-mm measurements is minimal, it was felt justified to extrapolate, and presume that the 2-mm measurement gives essentially the form of the spectra for zero penetration, which is the case of interest. It can be seen that the spectra at the grazing angle are cooler than that for $\mu = 1.0$. The dotted curve in Fig. 5-VI is a Maxwellian at moderator temperature; the spectrum is obviously hotter than this Maxwellian.

3. *Theoretical calculations and comparison with measurements*

The calculations for the buckling-dependent perpendicular leakage spectra were done with ADALS, a programme developed by KLADNIK [11, 12] for the time-asymptotic, angular-dependent leakage spectra for infinite slabs. The theory for the programme applies a variational technique. The influence of the surface on the spectra is described by a variational trial function, improved by one iteration.

The curves shown in Figs. 3 and 4 were calculated with ADALS, using linearly anisotropic scattering kernels. The water calculations shown are for the FEDERIGHI and GOLDMAN [13] version of the Nelkin kernel, while the Dowtherm A and benzene calculations were done with a kernel calculated by a Karlsruhe version of PIXSE [14] from GLÄSER's [9] scattering laws. For water, calculations were also done with the Haywood kernel [10]; the results were essentially the same as with the Nelkin kernel. For the large sample, the calculated spectra for the organic moderators are slightly cooler than those for H_2O, but otherwise of practically the same form. As can be seen, the agreement between measurements and calculations is good for H_2O, while for benzene and Dowtherm A the calculated spectra are a little cooler than the measurements. For thin slabs, the agreement is satisfactory for all cases; thus ADALS describes quite well the influence of diffusion

cooling. In general, it can be said that the agreement between ADALS calculations and experiment is satisfactory for the perpendicular leakage spectra.

The angular dependence of the leakage spectra calculated by ADALS, which predicts a Maxwellian for $\mu = 0.0$, was stronger than that which we detected experimentally. To obtain better agreement, modifications were made on another programme developed by Kladnik, which treats the Milne problem for a semi-infinite medium with zero absorption and a Maxwellian source at infinity. The spectra from our angular measurements, made in a large geometry, correspond to this situation. The theory for this problem is described in [2]. Since the geometry effects for this case are much simpler, the trial function describing the influence of the surface can be more involved. For the trial function used in [2], with one iteration, the spectrum for $\mu = 0.0$ is a Maxwellian. This programme was modified by using a more complex trial function, and performing two iterations. For the perpendicular leakage spectra ($\mu = 1.0$), the results of the modified programme agree well with the ADALS thick slab calculations. The results of a linearly anisotropic Haywood kernel calculation with the modified programme are shown in Fig. 5. The theoretical spectra are 17% and 11% hotter than a Maxwellian for $\mu = 1.0$ and 0.0, respectively. As can be seen in the figure, the agreement with the measured spectra is satisfactory in all cases.

4. *Summary*

Measurements of the leakage spectra perpendicular to the surface of H_2O, benzene, and Dowtherm A for a large geometry show that for these moderators the influence of differences in the scattering law on the leakage spectra is very small. Whereas the frequency distributions of the substances are quite different, the measured spectra are almost identical. The angular dependence of the leakage spectra in H_2O was found to be very weak. The spectrum perpendicular to the surface has a mean energy about 17% higher than that of a Maxwellian. This difference decreases with increasing angle to the normal, being about 10% for grazing emission.

The measured perpendicular leakage spectra can satisfactorily be described by theoretical calculations made with ADALS. A modified version of the programme for the Milne problem without absorption gives results which are in satisfactory agreement with the angular measurements. It is intended to improve this programme by using still more terms in the variational trial function. We plan to make calculations for other scattering kernels, to see whether the angular dependence of the leakage is markedly influenced by variations in the scattering law.

III. MEASUREMENTS OF TIME-DEPENDENT NEUTRON SPECTRA*

1. *Apparatus*

The investigations of the time dependence of neutron spectra in zirconium hydride and ice were made with essentially the same equipment de-

* Work performed by W. Reichardt

scribed above. For the zirconium hydride measurements we used a block of 20 cm×26 cm×28 cm of solid zirconium hydride ($ZrH_{1.65}$) which was in the form of small disc-shaped pellets (15.1 mm diameter, 2.5 mm height) with a density of $\rho = 5.43$ g/cm^3. The average density of the block was 4.929 g/cm^3.

The ice was kept at low temperatures by a cryostat which is shown in Fig. 7. The ice block was of cylindrical form (14.2 cm diameter, 14.6 mm

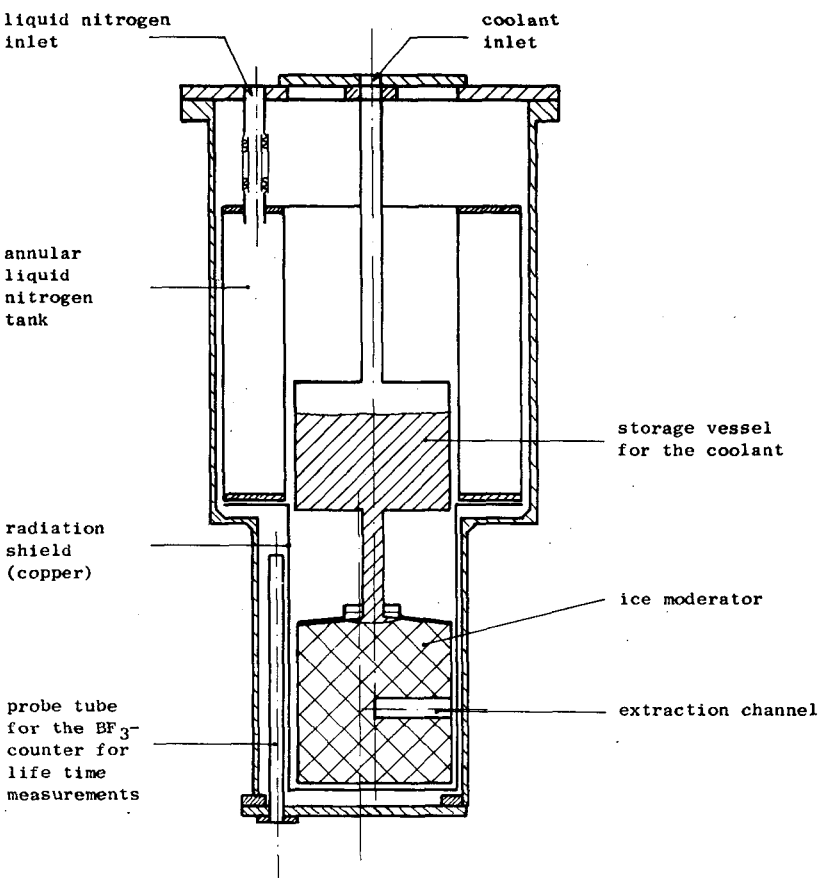

Fig. 7

Schematic drawing of the cryostat

height) encased in a cadmium clad aluminium container, which was flanged to the storage vessel of the coolant. Through the small tube connecting the storage vessel with the moderator vessel, the coolant was in direct contact with the ice but had a negligible disturbing effect on the measurements. The temperature of the ice block was determined by two copper-constantan thermocouples. It was only slightly above the coolant temperature (77 and 21°K, respectively). The radiation shield, made of 1-mm copper, and the outer vessel had thin aluminium windows to minimize the absorption and scattering of neutrons in the beam.

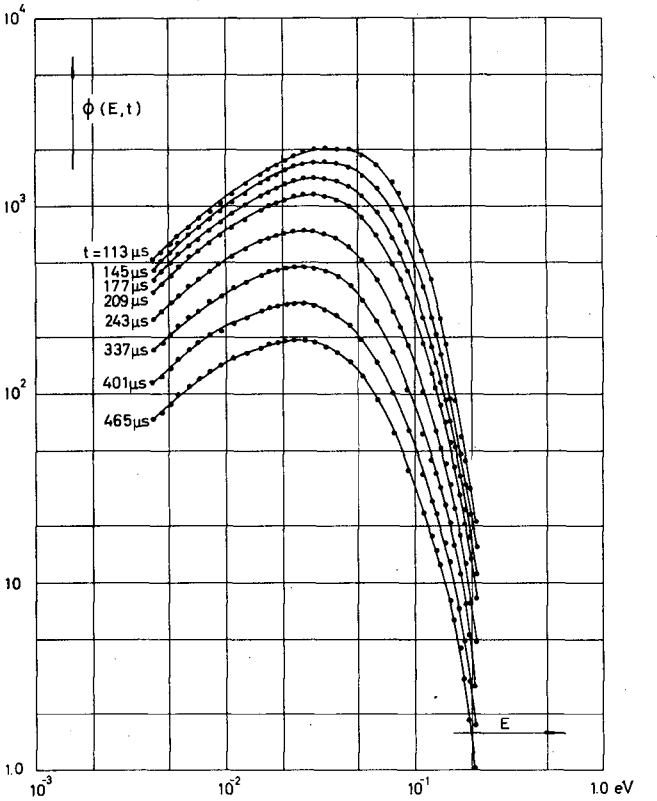

Fig. 8

Spectra in zirconium hydride at different times after the neutron pulse

2. *Results*

(a) Zirconium hydride

Figure 8 shows the spectra in the middle of the zirconium hydride block at times after the fast neutron burst varying from 113 to 465 µs. At the end of this time interval the spectra change only slightly with time, thus indicating that the asymptotic state has been approached. The spectra with the largest delay are cooler than a Maxwellian at moderator temperature (24°C) which can best be seen from Fig. 9, where the spectra divided by a Maxwellian of 20°C and corrected for the asymptotic decay $e^{-\lambda_0 t}$ are plotted versus flight time. This figure clearly shows the influence of the 0.13-eV resonance. Above 0.13 eV the neutrons are strongly scattered down to lower energies at early times which causes the sharp dip in the curves. At longer times, upscattering from lower energies becomes important and, therefore, the spectra only change slowly in this region. The dip in the nearly asymptotic spectra is caused by diffusion cooling, since the moderator block was not infinitely large. The "constriction" of the

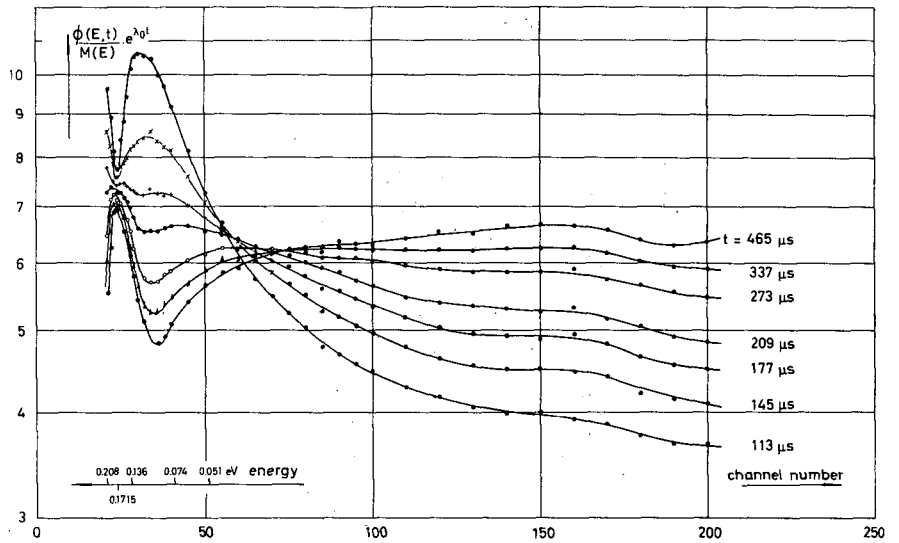

Fig. 9

Spectra in zirconium hydride divided by a Maxwellian of 20°C and corrected for the asymptotic decay versus flight time

curves occurs at 0.17 eV where the inelastic scattering cross-section has a maximum.

From these spectra the time dependence of the mean energy has been determined. These data can be described well by an exponential approach of the mean energy to its equilibrium value with a relaxation time of $\tau_{rel} = 97 \pm 7$ μs (see Fig. 10). The asymptotic value of the mean energy is 0.0493 eV and thus 4% below 2 kT_M.

In addition, the spectra from the surface were measured from 50 to 370 μs after the pulse (Fig. 11). The almost asymptotic leakage spectrum is harder than the spectrum from the middle of the block by 18%. The mean energy of these spectra can again be fitted by a relation $E(t) = E_\infty [1+a \exp(-t/\tau_{rel})]$ with $\tau_{rel} = (74 \pm 7)$ μs (Fig. 12).

(b) Ice

The results of the spectra measurements in ice at 77°K are shown in Fig. 13. The spectrum measured with the longest delay after the neutron burst can be well described by a Maxwellian of 75°K, thus indicating a small decrease in mean energy by diffusion cooling. Close to the asymptotic state, the mean energy calculated from these data shows an exponential behaviour with a relaxation time $\tau_{rel} = (77 \pm 7)$ μs (Fig. 14). Figure 15 shows the result of a transmission measurement through an indium foil, where $Q(t) - Q(\infty)$ is plotted versus time. (Q(t) is the ratio of the counting rate of the detector after transmission through the absorber to the counting rate of the bare detector.) The relaxation time obtained from these data is (67 ± 10) μs.

The results for ice at liquid hydrogen temperature given in Figs. 16 and 17 show that the moderation process at this low temperature is extremely

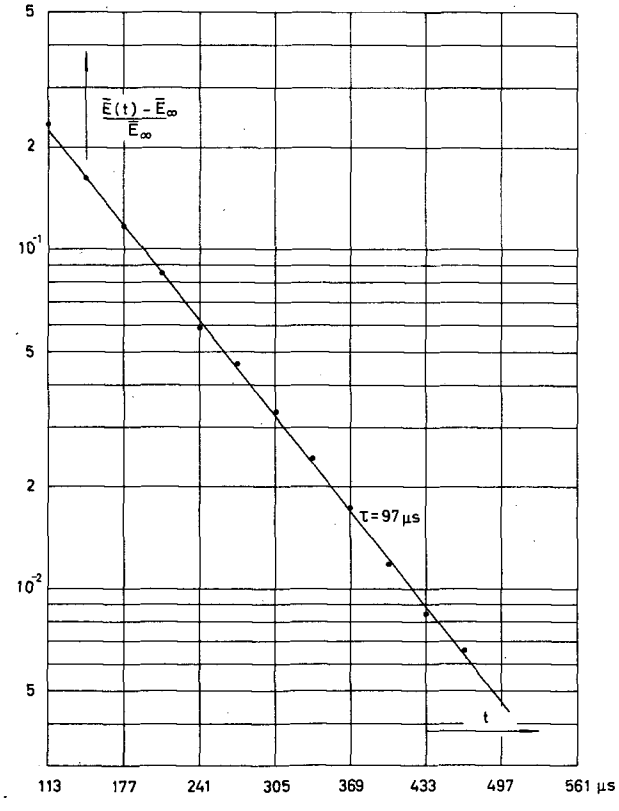

Fig. 10

Determination of the relaxation time of the mean energy in zirconium hydride

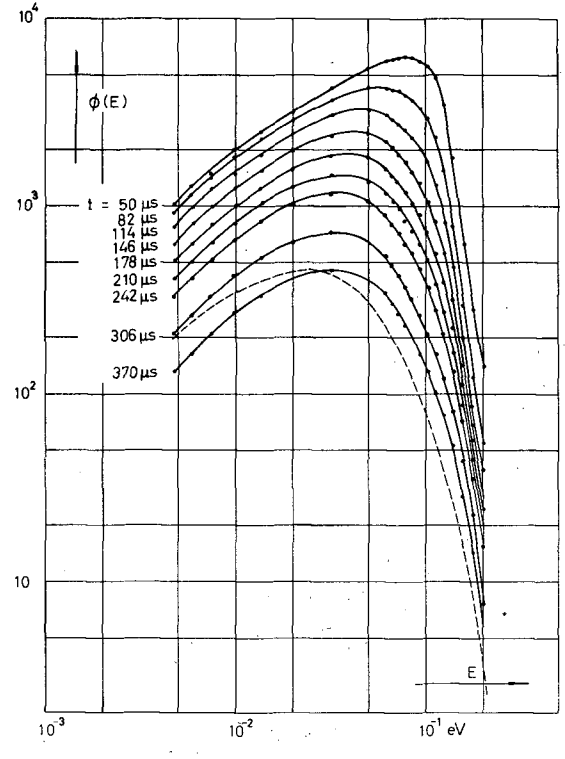

Fig. 11

Leakage spectra from zirconium hydride at different times after the neutron pulse

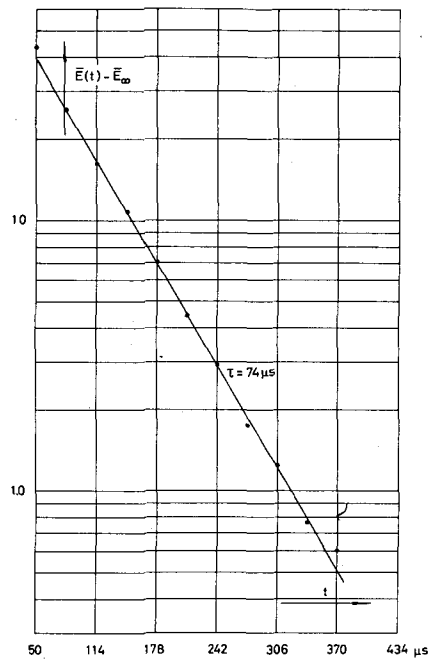

Fig. 12

Determination of the relaxation time of the mean energy of the leakage spectra from zirconium hydride

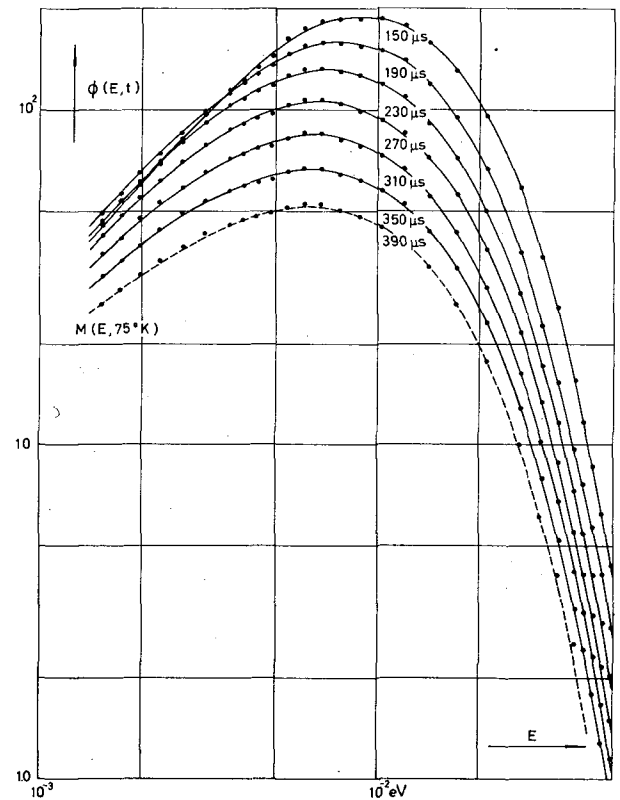

Fig. 13

Time-dependent neutron spectra in ice at 77°K

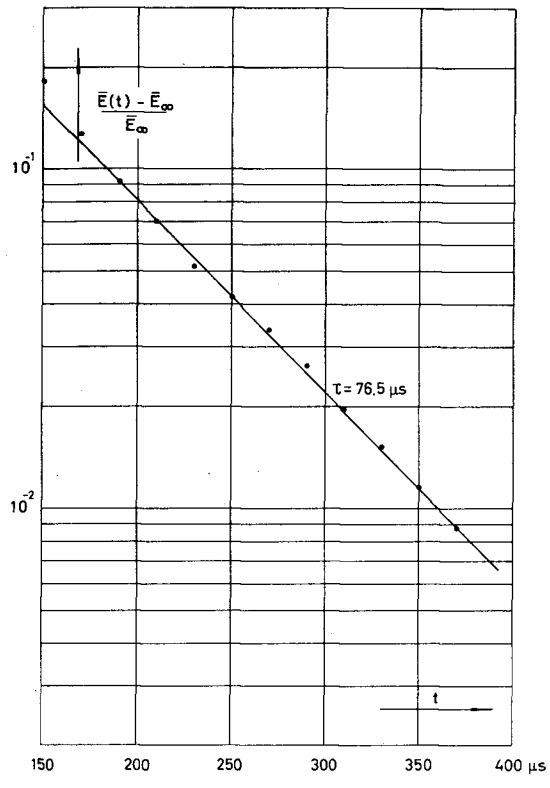

Fig. 14

Time dependence of the mean energy in ice at 77°K

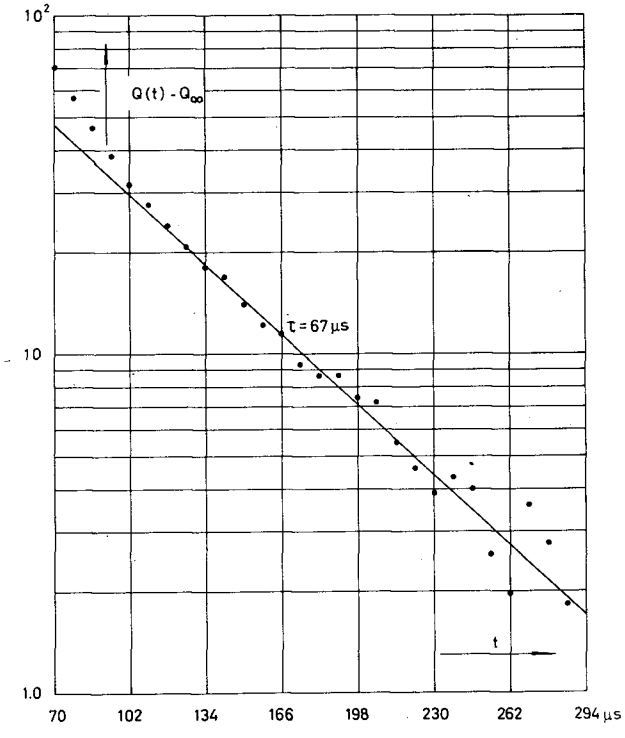

Fig. 15

Ice at 77°K: Determination of the relaxation time from a transmission measurement

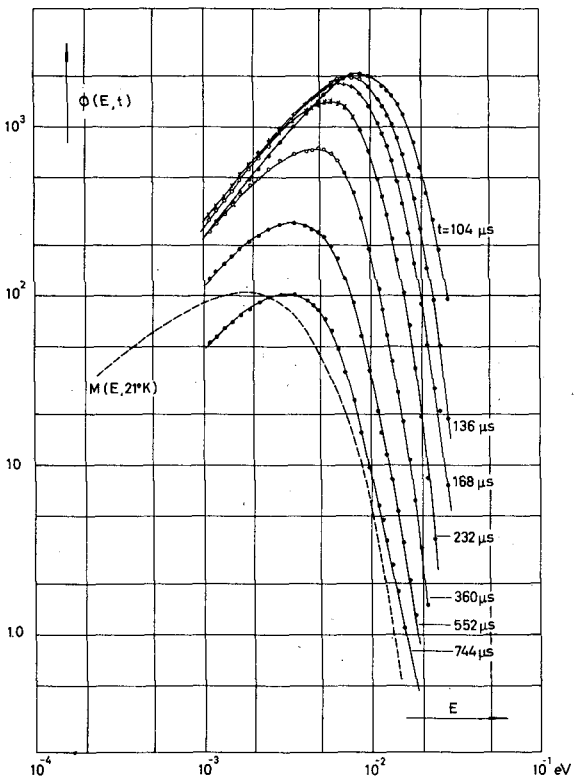

Fig. 16

Neutron spectra in ice at 21°K at different times after the neutron pulse

slow. The dotted line is a Maxwellian of 21°K. From this, one can see that the neutrons are still far from their equilibrium state even at 744 μs after the pulse. At this time, the mean energy of the spectrum is about 30% higher than that of a Maxwellian of 21°K. In Fig. 18 the data of the spectra measurements are presented in the form $\phi(E,t)e^{\lambda_0 t}/M(E)$; (M(E) = Maxwellian of 21°K, λ_0 = asymptotic decay constant). During the moderation process a dip successively appears in the curves in the vicinity of 0.01 eV. This phenomenon might be explained by a high density of states in the phonon energy distribution within this region. However, no confirmation for this could be found in the literature.

3. Discussion of the results and comparison with other measurements

(a) The energy mode concept

For a long time it has been believed that the solution of the time-dependent infinite medium diffusion equation without absorption can be decomposed into a set of discrete exponentially decaying energy modes

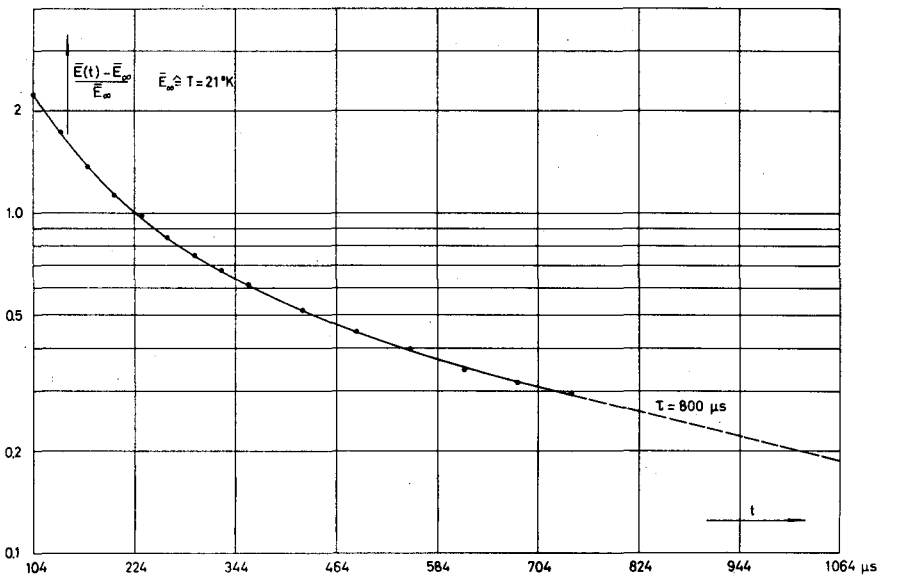

Fig. 17

Time dependence of the mean energy in ice at 21°K

$$\phi(E,t) = \sum_{i=0}^{\infty} a_i \phi_i(E)\, e^{-\lambda_i t}. \tag{1}$$

Among others CORNGOLD et al. [15] have shown that this concept is not true. Discrete eigenvalues exist only in the range $\lambda_i < (\Sigma_{inel} v)_{min}$ while above this limit the eigenvalues form a continuum. Therefore, the solution for the time-dependent flux is written as

$$\phi(E,t) = \sum_{i=0}^{i_{max}} a_i \phi_i(E) e^{-\lambda_i t} + \int_{(\Sigma_{inel} v)_{min}}^{\infty} a(\lambda)\phi_\lambda(E)\, e^{-\lambda t}\, d\lambda \tag{2}$$

Under the condition that the two lowest eigenvalues are discrete, the approach-to-equilibrium is governed by the two first terms of the expansion

$$\phi(E,t) = \phi_0(E)^{-\lambda_0 t} + \phi_1(E)\, e^{-\lambda_1 t} \tag{3}$$

with $\lambda_0 = 0$, $\lambda_1 = 1/\tau_{th}$, where τ_{th} = thermalization time. For a finite medium, where the spatial dependence can be taken into account by the geometric buckling B^2, with 1/v absorption the same representation as Eq. (2) holds, with the single exception that the lower limit of the integral is given by $\lambda_{min} = (\Sigma_{inel} v)_{min} + \Sigma_a v$.

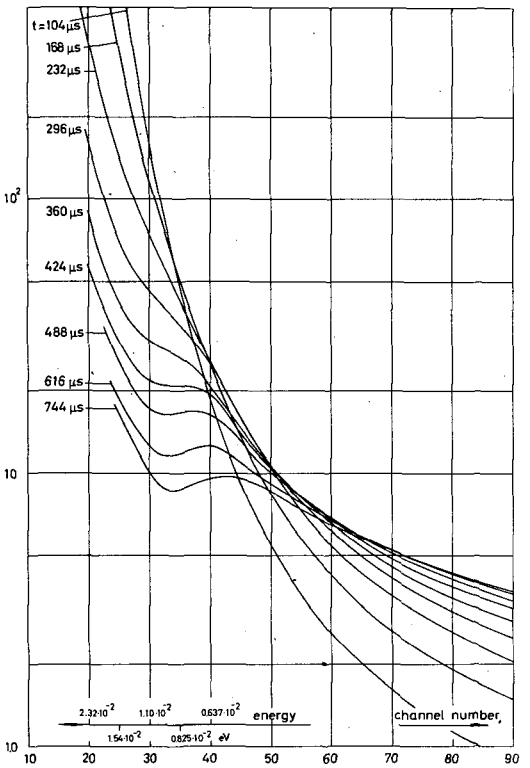

Fig. 18
Ice at 21°K: $\phi(E,t)e^{\lambda_0 t}/M(E, 21°K)$

The two lowest eigenvalues are given by

$$\lambda_0 = (\Sigma_a v)_0 + DB^2 + O(B^4)$$
$$\lambda_1 = (\Sigma_a v)_0 + \frac{1}{\tau_{th}} + gDB^2 + O(B^4) \tag{4}$$

where D = diffusion constant and g = dimensionless factor.

The resulting time dependence of the mean energy is

$$\bar{E}(t) = \frac{\int_0^\infty E\phi_0(E)dE\, e^{-\lambda_0 t} + \int_0^\infty E\phi_1(E)dE\, e^{-\lambda_1 t}}{\int_0^\infty \phi_0(E)dE\, e^{-\lambda_0 t} + \int_0^\infty \phi_1(E)dE\, e^{-\lambda_1 t}} = E_\infty \frac{1 + A\, e^{-(\lambda_1 - \lambda_0)t}}{1 + B\, e^{-(\lambda_1 - \lambda_0)t}}$$

$$= E_\infty \left(1 + (A - B)\, e^{-(\lambda_1 - \lambda_0)t} + (B^2 - AB)\, e^{-2(\lambda_1 - \lambda_0)t} + \ldots\right). \tag{5}$$

Therefore, the determination of the relaxation constant of the mean energy yields

$$\lambda_1 - \lambda_0 = \frac{1}{\tau_{th}} + (g - 1)DB^2 + O(B^4). \tag{6}$$

The analysis of transmission measurements, where the counting rate of the detector surrounded by an absorber is divided by the counting rate of the bare detector, leads to an expression similar to the second line of Eq.(5). Therefore, if the truncation of the expansion after the second term is justified, both methods should yield identical results.

(b) Determination of $(\Sigma_{inel} v)_{min}$

SHAPIRO and CORNGOLD [16] have investigated the solution of the time-dependent Boltzmann equation for the two models of a heavy Debye crystal and a heavy Einstein crystal. They found that only for $\theta_D/T \lesssim 0.28$ and $\theta_E/T \lesssim 0.20$ discrete λ_1 values can be obtained. This means that for practically no crystalline medium at room temperature will a λ_1-value exist.

Applying these results to ice of T = 77°K with an assumed Debye temperature of 215°K the value of $\theta_D/T = 2.79$ is far beyond this limit. The same holds for zirconium hydride under the assumptions that it can be represented by an Einstein crystal with an Einstein temperature which corresponds to 0.13 eV.

Unfortunately, little is known about the inelastic scattering cross-sections for ice and zirconium hydride. Ehret (see Ref. [17]) has done measurements on the inelastic scattering of zirconium hydride. The evaluation of the data has not yet been finished. Preliminary calculations of the total inelastic scattering cross-section with a width of 33 MeV for the 0.13-eV resonance and a 2% contribution of the acoustical part of the frequency distribution yield a value of $(\Sigma_{inel} v)_{min} = 5.0 \times 10^4\ s^{-1}$ [18]. A calculation taking into account only the 0.13-eV resonance, assuming its width as 28 MeV, and neglecting the acoustical part gives $(\Sigma_{inel} v)_{min} = 2.5 \times 10^4\ s^{-1}$. These values correspond to relaxation times of 20 and 40 μs, respectively. Therefore, the critical condition is well satisfied with the measured zirconium hydride values.

Recently, WHITTEMORE [19] has published a new value of the width of 18 MeV for the 0.13-eV resonance. This smaller value, however, will not appreciably change the inelastic scattering cross-section at very low energies. Calculations, taking into account this new width, are being made.

For the determination of $(\Sigma_{inel} v)_{min}$ of ice at 77°C the results of WHITTEMORE and McREYNOLDS [20] for the total cross-section of ice have been used. The total cross-sections of ice at 20°C and 76°K show a difference of about 10 b at 0.0009 eV. Assuming that this difference is a result of the inelastic scattering, which is essentially zero at 20°K, a value of $\sigma_{inel} = 10$ b is obtained at 0.0009 eV. This energy is probably small enough that the 1/v law for the inelastic scattering cross-section is valid. From this value a limiting relaxation time of 40 μs is obtained. The critical condition $\lambda_1 - \lambda_0 + DB^2 < (\Sigma_{inel} v)_{min}$ again is fulfilled.

(c) Zirconium hydride

Under the assumptions that a discrete λ_1-value exists and that all higher energy modes had died out before the time at which the analysis of the data starts, the measured relaxation time constants can be identified with

$$\lambda_1 - \lambda_0 = \frac{1}{\tau_{th}} + (g-1)DB^2.$$

The agreement between the value of 74 μs obtained from the leakage spectra and that of 97 μs obtained from the spectra in the middle of the block is not very good. The difference may be caused by the fact that higher energy modes are still present in the case of the leakage spectra. The time interval of the measurements begins at 50 μs after the pulse, whereas the analysis of the spectra from the middle starts at 113 μs after the pulse.

As the leakage from the block was small, these values will be close to the infinite medium values. Using the g-factor determined by MEADOWS and WHALEN [21], we obtain τ_{th} = 92 μs for the middle of the block and τ_{th}= 71 μs at the surface. These data can be compared with the results of MEADOWS and WHALEN [21]. Correcting our values for the difference in hydrogen density we get 126 μs and 98 μs for $ZrH_{1.7}$ with a density of 3.48 g/cm^3, which are in reasonable agreement with values of Meadows and Whalen, obtained from the transmission measurement, of 139 and 124 μs. The agreement with their thermalization time of 194 μs obtained from the lifetime measurements is not good.

(d) Ice

For ice at liquid nitrogen temperature the relaxation times of (67±10)μs determined from the transmission measurement and (77±7) μs from the time behaviour of the mean energy agree well. As the leakage from the block was very small, these values are almost equal to the infinite medium values. BROWN [22] has determined the thermalization time of ice at 76°K by a transmission method to be (20±2) μs which differs very much from our data.

A rough estimate of the thermalization time can be made by means of the relation $\tau_{th} \approx 6C/D^2$. With the diffusion parameters obtained by ANTONOV et al. [23], 136 μs are obtained. The above relation is only approximate and, therefore, the result gives only an idea of the order of magnitude for the thermalization time. It supports, however, our results which indicates that the energy exchange with the H_2O molecules is strongly hindered. In ice of liquid hydrogen temperature the mean energy does not show a purely exponential behaviour. This is to be expected as the neutrons are still far from equilibrium. If a first eigenvalue exists at all, a lower limit for the thermalization time can be obtained by the assumption that the region where the mean energy approaches its equilibrium value begins immediately after the end of the time interval of our measurements. This exponential approach is indicated by the dotted line in Fig. 18 from which a lower limit of about 800 μs is obtained.

4. *Summary*

The time dependence of neutron spectra in solid zirconium hydride of room temperature and ice at 77 and 21°K have been investigated. From the mean energy of the spectra the values of $1/(\lambda_1 - \lambda_0)$ which for the infinite medium are identical with the thermalization time have been determined. The results are given in the following Table:

TABLE

RELAXATION TIMES OF THE MEAN ENERGY

	Buckling B^2 (cm^{-2})	$\frac{1}{\lambda_1 - \lambda_0}$ (μs)	Remarks
$ZrH_{1.65}$ ($\bar{\rho}$ = 4.92 g/cm³)	0.0492	97 ± 7	
		74 ± 7	Leakage spectrum
Ice (77°K)	0.155	77 ± 7	
		67 ± 10	Transmission method
Ice (21°K)	0.155	> 800	

This analysis is based on the assumption that the concept of a thermalization time is reasonable and, if so, that it is possible to separate the two lowest energy modes from the contribution of higher modes. The results, however, are not accurate enough to state this with certainty. For zirconium hydride at 24°C and ice at 77°K a rough estimate indicates that the first condition might be fulfilled. The difference of the data for zirconium hydride shows that the contribution of higher modes might not be negligible. Because of these difficulties it seems more appropriate to compare the results of the spectra measurements directly with theory. Therefore, we intend to perform time-dependent spectra calculations for the investigated moderators.

ACKNOWLEDGEMENTS

The authors want to thank Professor K. H. Beckurts for initiating this work and for many helpful discussions during the performance of this work. The help of Dr. W. Eyrich during the experiments is appreciated. We are indebted to Dr. R. Kladnik for valuable discussions and support in the theoretical calculations. Thanks are due to Dr. D. T. Goldman who calculated for us the scattering matrices for the Nelkin kernel.

REFERENCES

[1] BECKURTS, K.H., Z. Naturf. 16a (1961) 611.
[2] KLADNIK, R. and KUŠČER, I., Nucl. Sci. Engng 11 (1961) 116.
[3] WILLIAMS, M.M.R., Nucl. Sci. Engng 18 (1964) 260.
[4] EISENHAUER, C., Nucl. Sci. Engng 19 (1964) 95.
[5] KIEFHABER, E., Nucl. Sci. Engng 18 (1964) 404.
[6] BARNARD, E. et al., Rpt. BNL-719 (1962) 805.

[7] BECKURTS, K.H. and REICHARDT, W., Proc. EANDC Symp. on Neutron Time-of-Flight Methods, Saclay (1961) 239.
[8] EYRICH, W., Nukleonik 4 (1962) 167.
[9] GLÄSER, W. and BECKURTS, K.H., Nucl. Sci. Engng 20 (1964) 235.
[10] HAYWOOD, B.C. and THORSON, I.M., Rpt. BNL-719 I (1962) 26.
[11] KLADNIK, R., The asymptotic angular dependent leakage spectrum of thermal neutrons. NIJS Rpt. R 435 (1964).
[12] KLADNIK, R., Nucl. Sci. Engng 17 (1963) 185.
[13] FEDERIGHI, F.D. and GOLDMAN, D.T., KERNEL and PAM-programs for use in the calculation of the thermal scattering matrix for chemically bound systems, Rpt. KAPL-2225 (1962).
[14] MacDOUGALL, J.D., PIXSE, Rpt. AEEW-M 318 (1963).
[15] CORNGOLD, N., MICHAEL, P. and WOLLMANN, W., Rpt BNL-719 (C-32) IV (1962) 1103.
[16] SHAPIRO, C.S. and CORNGOLD, N., The approach to equilibrium of a neutron gas, to be published in Phys. Rev.
[17] GLÄSER, W., EHRET, G. and MERKEL, A., Inelastic Scattering of Neutrons II IAEA, Vienna (1965) 167.
[18] EHRET, G., private communication.
[19] WHITTEMORE, W.L., Rpt. GA-9744 (1964).
[20] WHITTEMORE, W.L. and McREYNOLDS, A.W., Rpt. GA-2503 (1960).
[21] MEADOWS, J.W. and WHALEN, J.F., Nucl. Sci. Engng 13 (1962) 230.
[22] BROWN, J.B., Pulsed neutron source measurements with pure moderators, Doctorate Thesis, Birmingham (1963).
[23] ANTONOV, A.V. et al., Rpt. AEC-TR-5143.

DISCUSSION

N. CORNGOLD: The observation made by Kallfelz and Reichardt of a λ_1 below $(v\Sigma)_{min}$ is most interesting. The calculations made by Shapiro suggest that moderation by the optical mode in ZrH would not produce a λ_1. However, moderation by the acoustical modes, whose Debye temperature (according to Dr. Young) is less than kT, might possibly produce a λ_1.

W. REICHARDT: At the moment it is difficult to state with certainty that a discrete λ_1-value exists in zirconium hydride. All we can say is that the experimentally determined time behaviour of the mean energy shows a purely exponential approach to the asymptotic value. The relaxation-time constant obtained from these data lies well below the critical limit $(\Sigma_{inel}v)_{min}$ which we have determined from calculations based on measured scattering-law data. It might be valuable to make direct measurements of the inelastic scattering cross-section of zirconium hydride at low energies to be sure about the value of $(\Sigma_{inel}v)_{min}$.

M. NELKIN: I woulk like to point out that Mr. Kallfelz' experiment can be analysed to determine unambiguously the weight to be assigned to the acoustic branch of $f(\omega)$ in ZrH. Whether this corresponds to a well-defined λ_1 is a more difficult question. I would guess that there is not a truly discrete λ_1, but that the approach-to-equilibrium is very nearly exponential.

NEUTRON SPECTRA IN H_2O, D_2O, BeO AND CH_2*

J.M. NEILL, J.C. YOUNG, G.D. TRIMBLE AND J.R. BEYSTER
GENERAL ATOMIC DIVISION OF GENERAL DYNAMICS CORPORATION,
JOHN JAY HOPKINS LABORATORY FOR PURE AND APPLIED SCIENCE,
SAN DIEGO, CALIF., UNITED STATES OF AMERICA

(Presented by J. Russell)

Abstract — Résumé — Аннотация — Resumen

NEUTRON SPECTRA IN H_2O, D_2O, BeO AND CH_2. Thermal neutron spectral measurements in moderators of interest to reactor technology are being made at General Atomic. The purpose of these measurements is to provide an integral check of the adequacy of proposed scattering models for these moderators. At present the scattering kernels are obtained by measuring the double differential scattering cross-sections directly, or by inferring them from a study of the vibrational and rotational motions of the molecules in a liquid or the lattice vibrational spectrum in a solid. The direct measurement has suffered from some experimental difficulties, such as obtaining the desired intensity and resolution and making the proper corrections for multiple scattering in the sample. From the standpoint of the application to reactor technology, the latter procedure for obtaining the scattering kernel has been more satisfactory in many instances. The integral measurements that have been made, coupled to comparative calculations of the neutron spectra, allow comment to be made on the status of the theoretical scattering models for H_2O, D_2O and BeO.

In this paper, angular- and position-dependent spectra measured in H_2O and D_2O poisoned with boron or cadmium are presented and show improved agreement with the theoretical values. It appears that the Nelkin model for H_2O provides a reasonable first description for the scattering by that moderator. It also appears that the Honeck model for D_2O, an extension of the incoherent model for H_2O of Nelkin, is also an adequate description for some applications. This is surprising since deuterium, unlike hydrogen, is mostly a coherent scatterer; however it supports recent studies by Koppel which showed that the intramolecular and intermolecular interference scattering terms in D_2O tend to cancel.

Measured angularly-dependent neutron spectra in BeO poisoned with borated stainless steel are also presented. In general the agreement of measurement with calculations has been considerably improved. The theoretical scattering kernel is based on a Debye frequency spectrum with a cut-off frequency adjusted to satisfy the specific heat measurements for BeO. Significant Bragg trapping of low energy neutrons is observed in the measurements.

SPECTRES DE NEUTRONS DANS H_2O, D_2O, BeO ET CH_2. Des mesures de spectres de neutrons thermiques dans des ralentisseurs utiles en technologie des réacteurs sont en cours à la General Atomic. Ces mesures ont pour objet de vérifier si les modèles de diffusion proposés pour ces ralentisseurs conviennent bien. Actuellement, on obtient les noyaux de diffusion en mesurant directement les sections efficaces de diffusion différentielles doubles ou en les déduisant d'une étude des mouvements vibrationnels et rotationnels des molécules dans un liquide ou du spectre des vibrations du réseau dans un solide. La mesure directe s'est ressentie de quelques difficultés expérimentales auxquelles ont s'est heurté pour obtenir l'intensité et la résolution désirées et apporter les corrections voulues pour tenir compte de la diffusion multiple dans l'échantillon. Du point de vue de l'application à la technologie des réacteurs, le deuxième moyen d'obtention du noyau de diffusion est plus satisfaisant dans de nombreux cas. Les mesures intégrales qui ont été faites, combinées à des calculs comparatifs des spectres de neutrons, permettent de porter un jugement sur la qualité des modèles théoriques de diffusion pour H_2O, D_2O et BeO.

Les auteurs présentent des spectres variables selon l'angle et la position, qui ont été mesurés dans H_2O et D_2O empoisonnés par du bore ou du cadmium et sont en meilleur accord avec les valeurs théoriques. Il s'avère que le modèle de Nelkin pour H_2O constitue une bonne description préliminaire de la diffusion due

* Work performed under the auspices of United States Atomic Energy Commission, Contract No. AT(04-3)-167, Project Agreement No.2

à ce ralentisseur. Il s'avère de même que le modèle de Honeck pour D_2O, qui est un développement du modèle incohérent de Nelkin pour H_2O, représente également une description satisfaisante pour quelques applications. Cette constatation est surprenante du fait que le deutérium est avant tout un diffuseur cohérent, ce que n'est pas l'hydrogène, mais elle corrobore de récentes études de Koppel qui montrent que les termes de diffusion dus aux interférences intramoléculaires et intermoléculaires dans D_2O tendent à s'annuler.

Les auteurs présentent également des spectres de neutrons, variables selon l'angle, mesurés dans BeO empoisonné avec de l'acier inoxydable au bore. D'une manière générale, l'accord entre les mesures et les calculs a été considérablement amélioré. Le noyau de diffusion théorique est fondé sur un spectre de fréquences de Debye avec une fréquence de coupure ajustée de manière à satisfaire les mesures de chaleur spécifique pour BeO. Dans les mesures, les auteurs ont observé un important piégeage de Bragg de neutrons de faible énergie.

СПЕКТРЫ НЕЙТРОНОВ В H_2O, D_2O, $Be\overline{O}$ и $\overline{C}H_2$. В обществе "Дженерал атомик" производятся измерения спектров тепловых нейтронов в замедлителях, представляющих интерес для технологии реакторов. Цель измерений—обеспечить полную проверку удовлетворительности предлагаемых моделей рассеяния для этих замедлителей. В настоящее время ядра рассеяния получаются или путем непосредственного измерения сечений двойного дифференциального рассеяния, или посредством выведения их из изучения колебательных вращательных движений молекул в жидкости или колебательного спектра решетки в твердом теле. Непосредственные измерения были сопряжены с некоторыми экспериментальными затруднениями, как, например, получение желательной интенсивности и разрешения и введение надлежащих поправок на многократное рассеяние в образце. С точки зрения применения к технологии реакторов последний метод получения ядер рассеяния оказался во многих случаях более удовлетворительным. Проведенные интегральные измерения одновременно со сравнительными расчетами спектров нейтронов позволяют высказаться относительно состоятельности теоретических моделей рассеяния для H_2O, D_2O и BeO.

Даются указания относительно спектров, зависящих от угла и положения, измеренных в H_2O и D_2O и отравленных бором или кадмием; эти данные указывают на улучшение согласованности с теоретическими величинами. По-видимому, модель Нелкина для H_2O дает достаточно удовлетворительное в первом приближении описание рассеяния, производимого этим замедлителем. Нужно также думать, что модель Гонека для D_2O, являющаяся распространением некогерентной модели Нелкина для H_2O, также является удовлетворительным описанием для некоторых видов применения. Это представляется удивительным, так как в противоположность водороду дейтерий является в большинстве случаев когерентным рассеивающим веществом, но это обстоятельство подтверждает недавнее исследование Коппеля, который показал, что вклады внутримолекулярных и межмолекулярных интерференций рассеяния в D_2O имеют тенденцию аннулировать друг друга.

В докладе приводятся также полученные замером зависящие от угла спектры нейтронов в BeO, отравленной борированной нержавеющей сталью. Вообще говоря, согласованность измерений с расчетами была значительно улучшена. Теоретическое ядро рассеяния основано на дебаевском спектре частоты, порог которой был отрегулирован таким образом, чтобы согласоваться с измерениями удельной теплоемкости для BeO. При этих измерениях наблюдался значительный Брегговский захват нейтронов низких энергий.

ESPECTROS NEUTRONICOS EN H_2O, D_2O, BeO Y CH_2. En los laboratorios de la General Atomic se están midiendo espectros de neutrones térmicos en moderadores de interés para la tecnología nuclear. La finalidad de estas mediciones es verificar la validez de los modelos de dispersión propuestos para esos moderadores. En la actualidad, los núcleos de dispersión se determinan midiendo directamente las secciones eficaces de dispersión diferenciales dobles, o estudiando los movimientos de vibración y de rotación de las moléculas en los líquidos, o el espectro de vibraciones reticulares en los sólidos. La medición directa tropieza con algunas dificultades experimentales, tales como obtener la intensidad y el poder de resolución deseados e introducir las correcciones adecuadas para tener en cuenta la dispersión múltiple en la muestra. Para la tecnología de los reactores, el segundo procedimiento de determinación del núcleo de dispersión suele dar resultados más satisfactorios. Las mediciones integrales efectuadas, combinadas con el cálculo comparado de los espectros neutrónicos, permiten formular algunas observaciones sobre el estado actual de los modelos teóricos de dispersión correspondientes al H_2O, D_2O y BeO.

En la memoria se presentan los espectros dependientes del ángulo y de la posición medidos en H_2O y en D_2O envenenados con boro o con cadmio, espectros que muestran una mayor concordancia con los valores teóricos. Parece que el modelo de Nelkin para el H_2O constituye una primera descripción razonable de la dispersión en ese moderador. Asimismo, el modelo de Honeck para el D_2O, ampliación del modelo incoherente

de Nelkin para el H_2O, constituye una descripción apropiada para ciertas aplicaciones. Ello es un tanto sorprendente porque el deuterio, al contrario que el hidrógeno, suele ser un dispersor coherente, pero confirma recientes estudios de Koppel, que demostró que los términos de dispersión por interferencia intra e intermolecular en el D_2O tienden a anularse.

También se presentan espectros neutrónicos dependientes del ángulo, medidos en BeO envenenado con acero inoxidable borado. En general, la concordancia de los valores medidos con los datos calculados ha mejorado considerablemente. El núcleo teórico de dispersión se basa en un espectro de frecuencias de Debye con una frecuencia de corte adaptada a las mediciones del calor específico del BeO. En las mediciones se observa que la retención de Bragg afecta a una cantidad considerable de neutrones de baja energía.

1. INTRODUCTION

Thermal neutron spectral measurements in moderators of interest to reactor technology are being made at General Atomic. The purpose of these measurements is to provide an integral check of the adequacy of proposed scattering models for these moderators. The scattering kernels can be obtained by measuring directly the double differential scattering cross-sections, or by inferring them from a study of the vibrational and rotational motions of the molecule in a liquid or the lattice vibrational spectrum in a solid. From the standpoint of application to reactor technology, the latter procedure of obtaining the scattering kernel has been more satisfactory in many instances. Recent integral measurements in H_2O, D_2O, [1] BeO, and in polyethylene, coupled to comparative calculations of the neutron spectra allow comment to be made on the status of the theoretical scattering models for these moderators.

For H_2O, the gross features of the scattering model have been tested previously [2, 3] at room temperature under infinite medium conditions (in which leakage effects are insignificant). More critical tests have since been performed and are presented in this paper. These tests include spectral measurements H_2O under infinite-medium geometries at temperatures up to 600°F and position-dependent measurements in 1/v poisoned H_2O.

Spectral measurements in D_2O have been made to check the scattering model (essentially similar to that for H_2O) and include position-dependent measurements at room temperature in D_2O poisoned by either a 1/v absorber or a resonance absorber. A well-tested scattering model for BeO does not yet exist. Spectral measurements in 1/v-poisoned beryllium oxide have been made, however, to check the models based on a Debye frequency spectrum and the Sinclair [4] frequency spectrum.

Spectral measurements have been performed in a heterogeneous assembly of polyethylene to test the techniques for measurement of neutron spectra within a cell, and to check the scattering kernel for that moderator in cell geometry.

The above measurements show an improvement in the understanding of the neutron thermalization in these four moderators, and indicate that direct measurement of neutron spectra in a cell is feasible.

2. EXPERIMENTAL AND ANALYTICAL METHODS

All of the neutron spectra reported here have been measured by pulsed neutron time-of-flight techniques at the General Atomic Linear Accelerator Facility. The experimental and analytical methods are fairly standardized and are reported in Ref. [1].

Position-dependent spectral measurements are performed in a suitably sized tank or assembly of the moderator in question whose basic arrangement is illustrated in Fig. 1. The re-entrant hole allows the extraction of a vector flux. For the heated H_2O, the neutron beam is extracted from a thin walled cylindrical tube extending through a heavy walled 10 in diameter pressure vessel. (See Fig. 1). A zirconium scattering plug at the center of the tube allows the scalar spectrum to be obtained. However, the spectrum must be corrected for coherent scattering effects by the zirconium plug.

Neutrons emitted from the viewed surface or the scattering plug are collimated and timed along a 16-m flight path until detected by a calibrated bank of 32 stacked $B^{10}F_3$ counters. Since the neutron detector measures neutrons over each pulsing interval, it essentially integrates the time-dependent neutron spectrum. Consequently, the measured response corresponds to the response from a steady state source, and comparisons with theory are made on that basis. This technique is restricted to cases in which the mean emission time of the neutrons from the assembly is a small fraction of the flight time. Corrections are made for the mean emission time and appear to be adequate for the cases studied here.

The overall experimental arrangement for study of cell spectra in polyethylene is basically as shown in Fig. 1. The cell is located at the center of a 12 in × 12 in × 7 in assembly of seven slabs of polyethylene, alternately pure and borated. The usual time-of-flight procedure is employed; the main difference lies in the use of a small re-entrant hole and precollimator.

In the position-dependent measurements, activation of cadmium-covered indium foils allows the local buckling to be determined and provides a basis for the distributed source in the calculations.

The neutron spectra are calculated utilizing a variety of computer codes. The scattering kernel is generated by means of the GAKER [5, 6] code for H_2O, D_2O, and polyethylene. For BeO a scattering kernel is generated in the incoherent inelastic approximation by the SUMMIT [7] code using a Debye frequency spectrum with a cut-off frequency adjusted to satisfy the specific heat measurements for BeO. An alternative frequency spectrum used is that of SINCLAIR [4]. Group cross-sections, P_0 and P_1, are then calculated using these scattering kernels by the GATHER [8] code.

For the position-dependent cases, the procedure is then as follows: a distributed epithermal source, P_0 and P_1, in a single dimension, is calculated by the DSZ [9] code using smoothed flux plot data. The angular neutron spectra are then calculated by GAPLSN [10], a one-dimensional S_n transport theory code, using these group cross-sections and the distributed source.

$D(E)B^2$ terms are added to the group absorption cross-sections to account for leakage in directions normal to the direction of the S_n calculation. The P_1 source from the DSZ code is calculated from a diffusion theory approximation and is probably underestimated in H_2O. When the poison is

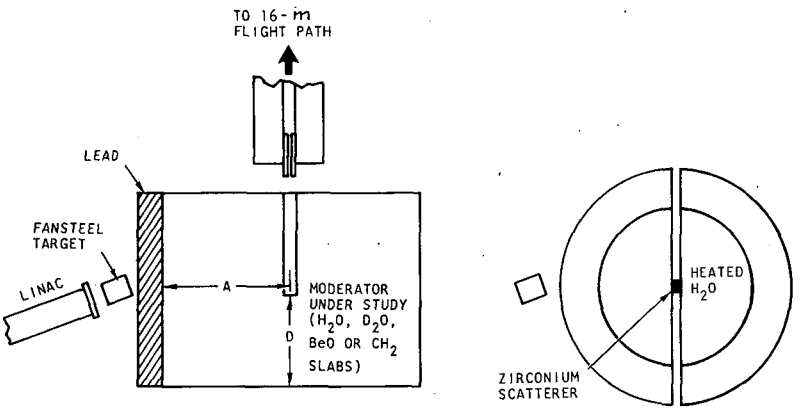

Fig. 1

Geometries for spectral measurements

non-homogeneously distributed, disadvantage factors for the cross-section averaging are obtained from a cell calculation employing the GAPLSN [10] code.

The calculated and measured spectra are presented as normalized by a simple fit in the 1/E region. This is approximately equivalent to a normalization on the basis of the same source intensity. In the position-dependent measurements, the relative intensity between each position has been preserved since the relative intensity as well as the spectral shape depends on the scattering properties of the moderator.

3. NEUTRON SPECTRA IN H_2O

Thermal neutron spectra have been measured under infinite medium conditions in water poisoned by a 1/v absorber as a function of moderator temperature. These measurements have been performed to determine the importance of molecular binding in establishing the neutron spectrum in high temperature water. It is known that molecular binding produces significant spectral shifts at room temperature, and so these measurements serve to establish the magnitude and importance of the binding effects at elevated temperatures. Comparisons of the theoretical and measured spectra at four different temperatures in water poisoned with boric acid to 5.15 b/H atom (at 2200 m/s) are shown in Fig. 2.

Two scattering models have been used in the determination of the theoretical spectra: (1) the free gas model and (2) NELKIN's [11] bound scattering model. Since the Nelkin model was formulated, an improvement has been made by KOPPEL [12] to include the spatial anisotropy of the vibrational modes of motion. Due to the computational expense, this new scattering kernel has been generated for room temperature only so that the above measurements at temperature have not been re-analysed in terms of the improved model. The difference between the two models is not large, however, as a companion paper [13] indicates, so that the temperature depen-

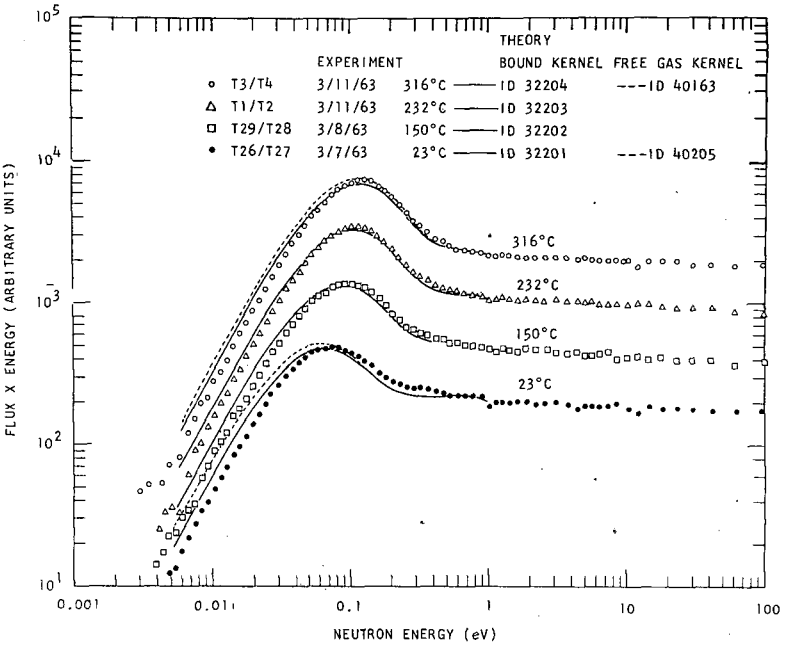

Fig. 2

Neutron spectra in borated water (5.15 b/H) at elevated temperatures

dence of the neutron spectra predicted by the Nelkin model is expected to be satisfactory for many applications. In the comparisons of Fig. 2, it can be stated that spectra calculated by the free gas model are less accurate than those based on the bound model. The difference between the bound and free gas model spectral calculations becomes less as the temperature is increased. It does appear that at sufficiently high temperatures and poisons (fuel loadings) the free gas model may permit adequate predictions of spectra under infinite medium conditions. The results shown in Fig. 2 do not, however, appear to support EGELSTAFF's [14] suggestion based on scattering law data that the Nelkin model parameters might need to be adjusted in going from 23 to 300°C. There is no marked change in the spectral shape as the moderator temperature is changed, and the discrepancies between measured and calculated spectra do not change significantly over the temperature range studied. Further measurements in H_2O are needed at elevated temperatures to investigate resonance absorption effects in neutron spectra; these measurements have been initiated at General Atomic.

Position-dependent spectral measurements have been performed in a 12 in × 12 in × 4 in tank of H_2O poisoned by boric acid to 5.15 b/H atom, the same concentration as in the measurements at temperature. Neutron spectra have been measured at 90° to the source-assembly axis across the 4 in dimension of the tank with D of Fig. 1 equal to 1, 2, 3 and 4 in (surface) and A equal to 6 in. The results of the spectral measurements are presented in Fig. 3 together with spectra calculated using the bound hydrogen model for H_2O; they show a fairly good agreement.

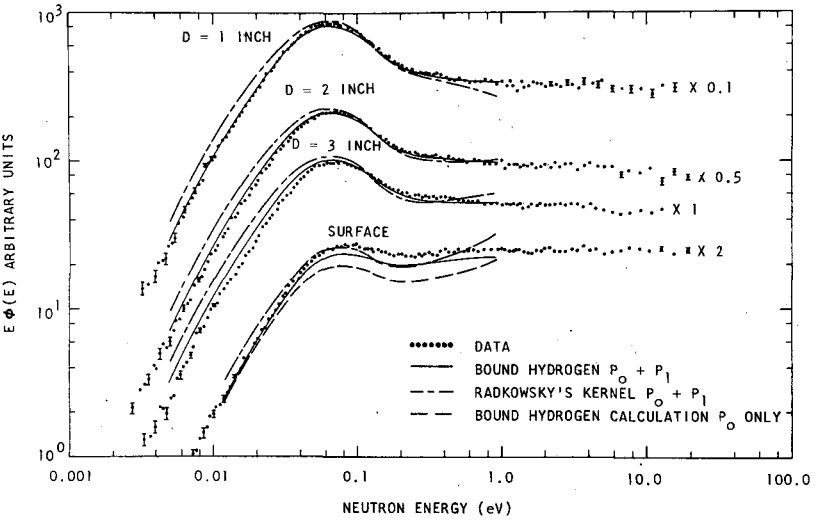

Fig. 3

Position-dependent neutron spectra in borated water (5.15 b/H)

In the calculations, both P_0 and P_1 scattering have been considered, and the 4 in axis is the direction accounted for in the one-dimensional S_n calculation. The lack of agreement in relative intensities between the theory and experiment at the surface may indicate that either the P_1 scattering matrix is incorrect or the reflection from the boundaries has boosted the source intensity at the surface. Alternately, the restriction of the cross-section anisotropy to P_1 only may have caused the observed discrepancy, although this is doubtful in view of numerical studies made previously [15]. A second calculation has been performed in which P_1 scattering is neglected. The neglect of P_1 scattering makes little or no difference at the center of the tank (D = 2 in); however, at the edge of the tank, the neutron spectrum calculated with only isotropic scattering is both lower in magnitude and has a changed shape as shown in Fig. 3. Since the calculated and measured spectra of Fig. 3 are all normalized with respect to their relative intensities, it becomes obvious that consideration of anisotropic scattering is essential if the surface leakage spectrum is to be calculated accurately.

The theoretical curves shown in Fig. 3 include the modification made by Koppel to the Nelkin model, although the resulting spectral changes are small. The agreement between theory and experiment in the position-dependent measurements reported here is sufficiently good, that it can be stated that the Nelkin model for H_2O appears to provide a reasonable description of the P_0 scattering. Also, in Fig. 3 are shown the neutron spectra calculated with the RADKOWSKY [16] prescription. Although the prescription may be useful in certain cases, its limitations are revealed in Fig. 3, where the Nelkin treatment clearly allows the calculation of more accurate spectra. The Radkowsky description generally appears to predict space-dependent spectra which are too thermal.

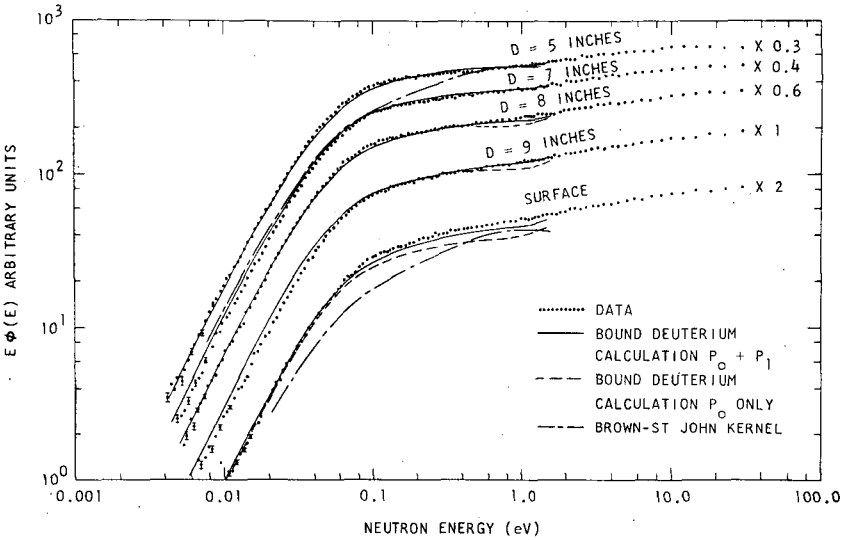

Fig.4

Position-dependent neutron spectra in boron-poisoned D_2O (1.94 b/D)

4. NEUTRON SPECTRA IN D_2O

Position-dependent measurements have been made in an 18 in × 18 in × 10 in tank of D_2O poisoned by boron-aluminium plates to 1.94 b/D atom at 2200 m/s. The purpose of these measurements was to test the adequacy of the bound kernel for D_2O which is based on a treatment by HONECK [17] following the Nelkin model for H_2O. The dynamical structures of the H_2O and D_2O molecules are similar, but hydrogen is mainly an incoherent scatterer whereas deuterium is mainly a coherent scatterer. Honeck has stated that if the scattering law is written as the sum of a self (incoherent) term and a difference (interference) term, then the latter term gives little contribution to the total cross-section above 0.01 eV. The incoherent approximation does not predict correct angular cross-sections, so that the P_1 scattering matrix will probably be in error.

Neutron spectra have been measured at different positions across the 10 in axis of the tank, with A of Fig. 1, equal to 6 in and D equal to 5, 7, 8, 9 and 10 in (surface). These measurements are shown in Fig. 4, together with the values calculated using the Honeck model for D_2O. Good agreement between theory and experiment is indicated except at the surface where the discrepancy in the relative intensity is about 12%. In the calculations, both P_0 and P_1 scattering are considered. Neglecting the P_1 scattering makes little difference at the center of the tank but gives rise to both a shape and magnitude change in the surface spectrum. Since the measurements at the center of the tank are well described by the P_0 scattering alone, the Honeck description of D_2O must then be adequate for the isotropic component. At the surface, however, where the flux gradient is strongest and a P_1 scatter-

ing dependence would be expected, the agreement is surprising in view of the incoherent treatment of deuterium. Recent studies by BUTLER [18] and KOPPEL and YOUNG [19] have shown that the intramolecular interference contribution to the D_2O total scattering cross-section is compensated by the intermolecular scattering due to liquid effects. Consequently, retention of the self-scattering terms alone as done by Honeck is a reasonable approximation for determination of neutron spectra. The BROWN-St. JOHN [20] scattering kernel for D_2O has also been used to calculate the spectra in Fig. 4. The kernel is obviously unsatisfactory in space-dependent geometries at high poisons.

Neutron spectra have also been measured in the same 18 in × 18 in × 10 in tank of D_2O but poisoned by cadmium nitrate to 2.44 b/D atom at 2200 m/s. Here D of Fig. 1 was held constant and A was 6, 9, and 12 in. The purpose of these measurements was to test the differential P_0 scattering matrix elements in the vicinity of the 0.175 eV cadmium resonance. The measurements are compared with the theoretical values in Fig. 5 and show good agreement. The good agreement between theory and experiment again supports the view that the P_0 scattering by D_2O is adequately described in Honeck's method and that the method is very suitable for calculating spectra in large assemblies in which leakage is relatively small and no discontinuities are present.

5. POSITION-DEPENDENT SPECTRA IN BeO

Position-dependent spectral measurements have been made in a 24.5 in cube of BeO in an arrangement similar to that of Fig. 1. The purpose of these measurements was to provide good spectral data for comparison now with existing scattering kernels for BeO and for comparison later with kernels to be developed. Two kernels are considered now: one is based on a Debye frequency spectrum with an adjusted cut-off frequency, and the other is based on the SINCLAIR [4] frequency spectrum derived from scattering law data by the extrapolation technique.

The beryllium oxide is poisoned by 10-mil sheets of 1 wt. % borated stainless-steel placed between each 0.42 in layer of BeO. This poisoning represents about 1.2 b/Be atom at 2200 m/s. Spectral measurements have been made at three positions corresponding to the A of Fig. 1 equal to 6, 12 and 18 in. The spatial distribution of the indium resonance flux shows that the local buckling at the 6 in position is less than that at the 12 and 18 in positions (where it was essentially the same). Since this would imply less inleakage at the 6 in position, the neutron spectrum can be expected to be harder there. This deduction is borne out by the measurements shown in Fig. 6. The calculated curves based on the Debye frequency spectrum show good agreement with the measured fluxes at the 6 in and 12 in positions, though obvious discrepancies are to be seen at the 18 in position. It is believed that these discrepancies are experimental in origin since there is no obvious reason for expecting such a large spectral difference between the 12 in and 18 in positions, and since the other two measurements agree so well with theory. The comparison of the measurements to the calculations based on the Sinclair kernel is not as satisfactory as is shown for the 12 in position

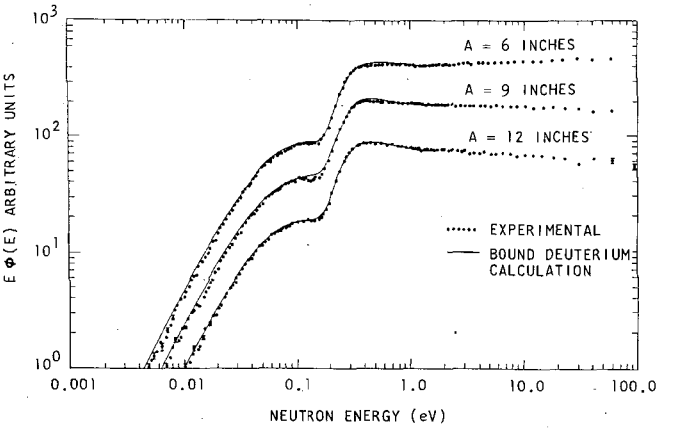

Fig. 5

Position-dependent neutron spectra in cadmium-poisoned D_2O

only in Fig. 6. This is surprising since the BeO does not behave like a Debye crystal and Sinclair's kernel is obtained from experimental data.

The measurements have been presented as flux $\phi(E)$ instead of the $E\phi(E)$, used elsewhere in this paper, in order to illustrate clearly the effects of Bragg scattering which give rise to observable low energy peaks. At the Bragg cut-off, the elastic scattering cross-section undergoes large changes and, due to the net inleakage, a peak can develop in the neutron spectrum. The calculated fluxes do not show these low energy peaks because the elastic coherent scattering has not yet been included into the BeO kernel.

6. NEUTRON SPECTRA ACROSS A POLYETHYLENE CELL

Neutron spectra have been measured as a function of position across a cell consisting of 1 in of pure polyethylene and 1 in of 1.3 wt.% borated polyethylene. The measurements serve as an integral check on KOPPEL's [21] scattering kernel for polyethylene and also advance the techniques toward the goal of direct measurement of neutron spectra within a fuel rod. Koppel's kernel is obtained by lumping into four discrete oscillators with appropriate weights the frequency spectrum calculated from the work of LIN and KOENIG [22]. The scattering kernel is then computed by means of the GAKER [5, 6] code and appears to be satisfactory [13, 23] for spectral calculations under infinite medium conditions.

The cell measurements were accompanied by studies in which the size of the re-entrant hole and precollimator were varied. No spectral changes could be observed between the three hole sizes of 0.359, 0.221, and 0.140 in in diameter. Calculations of the spectra were performed with the usual S_{16} transport theory approach considering both P_0 and P_1 scattering. The cell was treated as an infinite plane slab with reflective boundaries. Its actual physical size was accounted for by a $D(E)B^2$ correction to the group cross-sections. The comparison of measured and theoretical spectra is presented

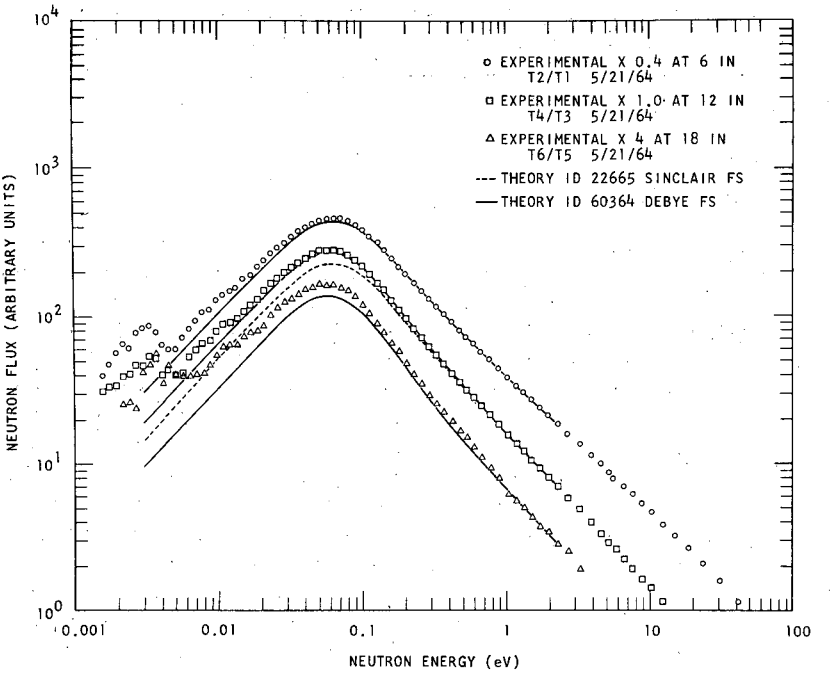

Fig. 6

Position-dependent neutron spectra in boron-poisoned BeO (1.2 b/Be)

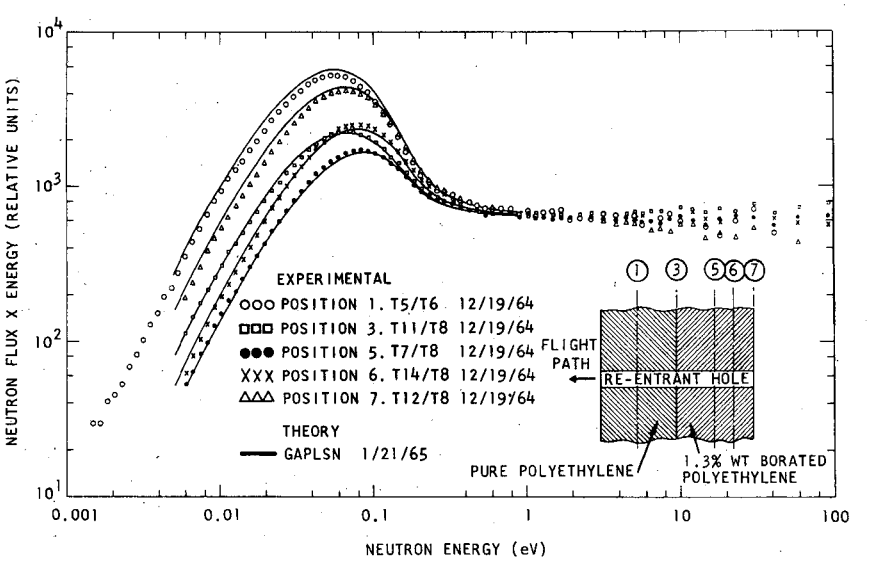

Fig. 7

Neutron spectra across a polyethylene cell

in Fig. 7. The agreement is very satisfactory. The whole structure of the spectral variation across the cell can be both calculated and measured without resort to any re-normalization procedure. This gives us confidence in proceeding to direct measurements in even smaller lattices.

7. CONCLUSIONS

The measurements have shown that the NELKIN [11] model predicts the neutron spectrum in H_2O reasonably accurately over temperatures which range up to 350°C. The agreement is better than with the free gas model. Some discrepancies remain which may possibly be experimental in origin, since the position-dependent measurements in H_2O are generally in better agreement. The latter measurements have shown that the Nelkin model modified by Koppel provides a reasonable description of P_0 scattering by light water. By comparing the calculated surface leakage spectrum with and without P_1 scattering to the measured spectrum, it would appear that the Nelkin model generally underestimates P_1 scattering. In addition, we have shown clearly that the Radkowsky [16] treatment of H_2O does not provide as accurate a description as do the bound hydrogen models.

For heavy water, we have found that the incoherent treatment of D_2O by Honeck is satisfactory for a variety of reactor spectral conditions. It provides a scattering kernel which permits accurate neutron spectra to be calculated in moderately space-dependent geometries. This permits confidence at least in the P_0 scattering matrix and also supports the conclusions of BUTLER [18] and KOPPEL [19] stating that the self-scattering terms are an adequate approximation to the scattering description of liquid D_2O for the calculation of neutron spectra. We have also shown the Brown-St. John [20] description of D_2O to be quite unsatisfactory in the experiments that have been reported here.

For BeO, the P_0 scattering matrix based on a kernel generated from an adjusted Debye frequency spectrum has been shown to be superior to that from the SINCLAIR [4] kernel and is quite satisfactory for the calculation of neutron spectra in geometries where the spatial dependence is not large. Differential scattering measurements could, however, be expected to indicate discrepancies in this scattering kernel.

In the polyethylene cell studies, KOPPEL's [21] scattering kernel for that moderator has again been shown to be satisfactory. The feasibility of direct spectral measurements in a 1 in cell has also been established, and it encourages measurements in smaller lattices.

Further refinements in the scattering models for these four moderators can be expected from the continuing theoretical effort at General Atomic. It is anticipated that integral measurements of the type reported here will continue to provide important checks on the adequacy of proposed scattering models. However, it appears that the spectral measurements will be required to be made in strongly positionally-dependent geometries to check the refinements that may be forthcoming in the models for H_2O, D_2O, BeO, and polyethylene.

REFERENCES

[1] YOUNG, J.C., NEILL, J.M., HOUSTON, D.H., and BEYSTER, J.R., Rpt. GA-6034 (Jan. 1965), to be published in Nucl. Sci. Engng.

[2] YOUNG, J.C. et al., Nucl. Sci. Engng. 18 (1964) 376.

[3] BEYSTER, J.R. et al., Nucl. Sci. Engng. 9 (1961) 168.

[4] SINCLAIR, R.N., Inelastic Scattering of Neutrons in Solids and Liquids II IAEA, Vienna (1963) 199-211.

[5] HONECK, H.C., THERMOS, A thermalization transport theory code for reactor lattice calculations, Rpt. BNL-5826 (1961).

[6] BEYSTER, J.R. et al., Integral neutron thermalization annual summary report, 1. Oct. 1963-31. Sept. 1964, USAEC Rpt. GA-5798.

[7] BELL, J., SUMMIT, an IBM-7090 program for the computation of crystalline scattering kernels, USAEC Rpt. GA-2492.

[8] JOANOU, G.D., SMITH, C.V. and VIEWEG, H.A., GATHER II, Rpt. GA-4132 (July 1963).

[9] BEYSTER, J.R. et al., Integral neutron thermalization, Annual summary report 1961-1962 Rpt. GA-3542.

[10] ALEXANDER, J.H., HINMAN, G.W. and TRIPLETT, J.R., GAPLSN: a modified DSN program for the solution of the one-dimensional anisotropic transport equation, Rpt. GA-4972 (March 1964).

[11] NELKIN, M., Scattering of slow neutrons by water, Phys. Rev. 119 2 (1960) 741.

[12] KOPPEL, J.U. and YOUNG, J.A., Nucl. Sci. Engng 19 (1964) 412.

[13] YOUNG, J.A. and KOPPEL, J.U., "Calculation of thermal scattering kernels", these Proceedings I.

[14] EGELSTAFF, P.A., Inelastic Scattering of Neutrons in Solids and Liquids, IAEA, Vienna (1961) 25.

[15] BEYSTER, J.R. et al., Integral neutron thermalization quarterly progress report, 1. Oct.-31 Dec. 1962, Rpt. GA-3853 (Feb. 1963).

[16] RADKOWSKY, A., Rpt. ANL-4476 (1960) 93-100.

[17] HONECK, H.C., Trans. Amer. nucl. Sci. 5 1 (1962) 47.

[18] BUTLER, D., The scattering of slow neutrons by heavy water, Proc. phys. Soc. 81 (1963).

[19] KOPPEL, J.U. and YOUNG, J.A., The role of interference scattering in neutron thermalization by heavy water, GA-6103 (March 1965), to be published in Nucl. Sci. Engng.

[20] BROWN, H.D. and ST.JOHN, D.S., Neutron energy spectrum in D_2O, Rpt. DP-33, E.I. du Pont de Nemours and Company (1954).

[21] KOPPEL, J.U. and YOUNG, J.A., Nucl. Sci. Engng 21 (1965) 268.

[22] LIN, T.P. and KOENIG, J.L., J. mol. Spectry 9 (1962) 228.

[23] YOUNG, J.C. and HUFFMAN, D., Spectrum Book, USAEC Rpt. GA-5319 (May 1964).

DISCUSSION

P. SCHOFIELD: With reference to the possible temperature dependence of the parameters of the Nelkin model, I would like to ask Dr. Russell if there are any recent accurate measurements of the total cross-section of water in the range 1-10 eV as a function of temperature, such as those which were obtained at room temperature. The variation of T might be obtained from these and we could have some idea of the variation of the parameters obtained.

J. RUSSELL: No measurements of the total cross-section of water at higher temperatures have been made at General Atomic. However, $\overline{T}$ in the Nelkin model was recently verified, to within experimental accuracy, by a measurement made at room temperature.

T. SPRINGER: Concerning the question of the temperature dependence of scattering on H_2O, we found that in an energy range between liquid nitrogen temperature and 200°C, and between 0.02 and 0.1 eV, $d\sigma(\theta)/d\Omega$ is extremely insensitive to temperature (less than a few per cent).

P. SCHOFIELD: I should point out that very accurate values of the cross-section (to within less than 1%) are required in the range 1-10 eV to obtain T.

THERMALIZATION STUDIES OF ORDINARY AND HEAVY WATER

R. N. SINCLAIR AND P. J. WILLIAMS
ATOMIC ENERGY RESEARCH ESTABLISHMENT,
HARWELL, DIDCOT, BERKS., UNITED KINGDOM

Abstract — Résumé — Аннотация — Resumen

THERMALIZATION STUDIES OF ORDINARY AND HEAVY WATER. Thermal neutron spectra in ordinary and heavy water have been studied by the time-of-flight technique using the 45-MeV Linac at Harwell. The experiments are designed to investigate the sensitivity of the spectra to the details of the scattering kernel in regions of isotropic flux and near to boundaries where the anisotropy is high.

Spectra in a large volume of heavy water poisoned with a 1/v absorber (boron) or a resonant absorber (cadmium) have been measured at 293 and 360°K. The results are compared with spectra calculated in the infinite medium approximation with the SIMPH code. A leakage correction is determined from the spatial flux variation as measured by gold and manganese activations. The scattering kernels used in the calculations are based on different models of the dynamics of the heavy water molecule.

Earlier measurements of the spectra incident on a totally absorbing surface immersed in ordinary water have been extended to include neutrons moving at glancing angles to the surface. The experiments demonstrate the effects of the finite moderator size and the source position on the leakage spectra and these effects are confined to energies greater than about 0.1 eV. Below this energy the combined results show that there is little change in the spectra as a function of angle μ greater than 0.2 (μ is the cosine of the angle between the neutron direction and the normal to the surface). For $\mu = 0$ the spectrum is very close to a Maxwellian distribution with $T_n = 1.05\ T_m$, where T_n and T_m are the neutron and moderator temperatures, respectively. The spectra are compared with calculations made with the Winfrith DSN code on the assumption that the scattering is isotropic.

ÉTUDES DE THERMALISATION SUR L'EAU ORDINAIRE ET L'EAU LOURDE. A Harwell, les auteurs ont étudié des spectres de neutrons thermiques dans l'eau ordinaire et dans l'eau lourde par la méthode du temps de vol, à l'aide de l'accélérateur linéaire de 45 MeV. Les expériences ont pour objet de déterminer dans quelle mesure les spectres sont sensibles aux détails du noyau de diffusion dans les régions de flux isotrope et au voisinage des limites où l'anisotropie est élevée.

Dans une grande quantité d'eau lourde empoisonnée par un absorbeur 1/v (bore) ou un absorbeur résonnant (cadmium), on a mesuré des spectres à des températures de 293 et 360°K. Les résultats sont comparés aux spectres calculés au moyen du code SIMPH dans l'approximation d'un milieu infini. La correction de fuite est déterminée à partir de la variation du flux dans l'espace, mesurée par activation de l'or et du manganèse. Les noyaux de diffusion utilisés dans les calculs sont basés sur différents modèles de la dynamique de la molécule d'eau lourde.

Des mesures antérieures des spectres tombant sur une surface complètement absorbante immergée dans de l'eau ordinaire ont été développées pour inclure les neutrons dont la trajectoire fait un angle de ricochet avec la surface. Les expériences démontrent l'influence du ralentisseur de dimension finie et de la position de la source sur les spectres de fuites, et indiquent que ces effets sont limités aux énergies supérieures à environ 0,1 eV. Au-dessous de cette énergie, les résultats combinés montrent que les spectres varient peu en fonction de l'angle formé par la direction des neutrons et de la normale à la surface, lorsque le cosinus de cet angle est supérieur à 0,2. Pour $\mu = 0$, le spectre est très proche d'une distribution maxwellienne avec $T_n = 1{,}05\ T_m$, T_n et T_m étant les températures des neutrons et du ralentisseur. Les auteurs comparent les spectres aux calculs faits à l'aide du code DSN de Winfrith à partir de l'hypothèse que la diffusion est isotrope.

ИЗУЧЕНИЕ ЯВЛЕНИЙ ТЕРМАЛИЗАЦИИ ОБЫЧНОЙ И ТЯЖЕЛОЙ ВОДЫ. В Харуэлле с помощью линейного ускорителя с энергией 45 Мэв изучались спектры тепловых нейтронов в обычной и тяжелой воде методом по времени пролета. Эксперименты предназначаются для исследования чувствительности спектра в отношении отдельных частей интегрального ядра рассеяния в областях изотропического потока и около границ, где велика анизотропия.

Спектры в большом объеме тяжелой воды, отравленной поглотителем 1/V (бор) или резонансным поглотителем (кадмий) измеряли при температуре 293 и 360° К. Результаты сравниваются со спектрами, рассчитанными в приближении бесконечной среды с помощью кода SIMPH. Поправка на утечку определяли из пространственного изменения потока, измеренного путем оценки активации золота и магния. Ядра интегрального рассеяния, используемые при расчетах, основываются на различных моделях динамики молекулы тяжелой воды.

Более ранние измерения спектров на полностью поглощающей поверхности, погруженной в обычную воду, расширены с целью включения нейтронов, перемещающихся под углами скольжения к поверхности. Эксперименты показывают влияние размера конечного замедлителя и положения источника на спектры утечки, такое воздействие ограничивается рамками энергии выше приблизительно 0,1 эв. Ниже этого уровня энергии, как показывают комбинированные результаты, имеется небольшое изменение спектров как функция угла μ больше чем 0,2 (μ – косинус угла между направлением перемещения нейтрона и нормалью к поверхности). Для $\mu = 0$ спектр весьма близок к максвелловскому распределению при $T_n = 1{,}05\ T_m$, где T_n и T_m – температуры нейтронов и замедлителя. Спектры сравниваются с расчетами, проведенными с помощью кода DSN в Винфрите, в предположении, что рассеяние является изотропическим.

ESTUDIOS DE TERMALIZACION EN EL AGUA ORDINARIA Y EN EL AGUA PESADA. Se han estudiado los espectros de neutrones térmicos en agua ordinaria y en agua pesada con el método del tiempo de vuelo utilizando el acelerador Linac de 45 MeV de Harwell. La finalidad de los experimentos es investigar la sensibilidad de los espectros a pequeñas variaciones de los núcleos de dispersión en regiones de flujo isotrópico y en las proximidades de los límites de separación en que la anisotropía es elevada.

Se han medido a 293 y 360°K espectros en un gran volumen de agua pesada envenenada con un absorbente que sigue la ley 1/v (boro) o con un absorbente por resonancia (cadmio). Los resultados se comparan con los espectros calculados según la aproximación del medio infinito con la clave SIMPH. La corrección de escapes se obtiene a partir de la variación espacial del flujo medida por activación de oro y de manganeso. Los núcleos de dispersión aplicados para el cálculo se basan en diferentes modelos dinámicos de la molécula de agua pesada.

Las mediciones anteriores de espectros de neutrones incidentes en una superficie totalmente absorbente sumergida en agua ordinaria se han ampliado para incluir los neutrones que inciden en la superficie según ángulos rasantes. Los experimentos muestran los efectos de las dimensiones finitas del moderador y de la posición de la fuente en los espectros de escape, efectos que se limitan a las energías superiores a 0,1 eV. Por debajo de este valor, los resultados combinados muestran que los espectros sufren escasas variaciones en función de μ (esto es, el coseno del ángulo formado por la dirección de los neutrones y la normal a la superficie) cuando éste es superior a 0,2. Cuando $\mu = 0$ la distribución espectral es muy parecida a la maxwelliana con $T_n = 1{,}05\ T_m$, siendo T_n y T_m las temperaturas de los neutrones y del moderador respectivamente. Los autores comparan estos espectros con cálculos hechos mediante la clave DSN de Winfrith partiendo del supuesto de que la dispersión es isotrópica.

1. INTRODUCTION

The effect of the chemical binding of the molecules of moderating materials on their thermalizing properties has been extensively studied using the pulsed neutron source technique to measure thermal neutron spectra [1, 2, 3]. The experiments fall broadly into two main categories. Firstly the measurement of neutron spectra in systems for which spatial effects are negligible. Measurements of spectra in highly poisoned moderators fall into this class. Such experiments provide a sensitive test of the accuracy of the energy transfer cross-section $\Sigma(E \rightarrow E')$ predicted from experimentally based models of the dynamics of the scattering system.

The second type of experiment involves the observation of the spatial and angular dependence of the directed flux spectrum in a region of moder-

ator where an absorption or temperature discontinuity has been deliberately introduced. This gives conditions similar to those in a thermal reactor near to a fuel element, coolant channel or control rod and the spectrum can now be expected to depend on the angular dependence of the scattering law. If the experimental geometry can be described in terms of one dimension, the directed flux is characterized by $\psi(z, \mu, E)$ where z is the distance from the perturbing surface, μ is the cosine of the angle between the neutron direction and the normal to the surface and E is the neutron energy. Calculation of these spectra involves solution of the transport equation. An example of each type of experiment is presented in this paper.

(a) Spectra in poisoned heavy water have been studied and compared with spectra calculated using scattering kernels based on various models of the dynamics of the heavy water molecule. This molecule is of particular interest because of the large coherent scattering from the deuterium and because scattering from oxygen cannot be neglected as is possible for ordinary water. Two different types of neutron absorber have been used as poison to highlight the effect of the scattering kernel in different energy regions. One was a $1/v$ absorber (boron) while the second (cadmium) was chosen because of the presence of a strong low-energy resonance.

(b) The variation with angle of the directed neutron flux near to a perfectly absorbing surface (the thermal neutron Milne problem) has been the subject of many theoretical investigations [4, 5, 6] but only the time-of-flight technique allows detailed experimental measurement. This problem is the simplest case of an absorption discontinuity and comparison of experiment and theory using a scattering kernel known to be satisfactory for the calculation of infinite medium spectra will demonstrate the importance of the angular dependence of the scattering.

In an earlier experiment the angular flux near to an absorption discontinuity was measured [3]. Using a different geometry these results have been confirmed and extended to include neutrons leaving the surface at grazing angles. Spectra calculated by the Carlson S_n method on the assumption of isotropic scattering are found to disagree with the experimental data.

2. EXPERIMENTAL TECHNIQUE

The 45-MeV Harwell electron Linac with a uranium target provided 1.7-μs bursts of fast neutrons for the time-of-flight experiments. The effective starting time for the time-of-flight measurement and the burst width which determines the basic resolution are both affected by the slowing-down and thermal neutron relaxation time of the moderator and are energy dependent. Calculation of these factors requires knowledge of the cross-section that the experiment is designed to test but, provided the experiment is designed to minimize such effects, any plausible model suffices to make the necessary corrections. A flight path length of 60.36 m was chosen so as to minimize possible errors from this cause. The flight path, which was evacuated, was shielded along its entire length with a boron-paraffin wax mixture canned in thin steel. Correction was made for the presence of 50 cm of air and 1 cm of aluminium in the neutron beam. The correction was never greater than 2%.

A bank of thirty-six enriched BF_3 counters of diameter 2.5 cm and length 30 cm were used as the neutron detector. The relative sensitivity of this detector as a function of neutron energy was measured by comparing a spectrum with that observed by a bank of counters containing enriched BF_3 at a low pressure and which could be assumed to have a variation of sensitivity with energy proportional to the $B^{10}(n,\alpha)Li^7$ cross-section, apart from a small correction for the absorption in the copper walls. Possible errors in this measurement lead to an uncertainty of about 3% in the relative sensitivity of the detector at 3 eV and 0.005 eV.

Various collimators were used to define the area viewed by the counter and it was established that the spectrum was independent of collimator material for those tested (borated wax, sintered boron-ten carbide, boron-epoxy resin mixture). For most of the experiments described a borated wax collimator 25 cm long with a 3 cm diameter hole was used. The flight path shielding closely followed the cone of the beam defined by the main collimator.

Background in the experiments arose from neutron leakage through the flight path and detector shielding. A boron shutter was introduced into the beam as close to the point of spectrum measurement as possible to enable a background determination to be made. The maximum value of the background observed in any experiment amounted to 1% at the peak of the spectrum rising to 30% at 0.006 eV where the spectrum intensity was lowest.

3. SPECTRA IN POISONED HEAVY WATER

3.1. The experiment

Solutions of boron and cadmium in heavy water were prepared by carefully drying either a mixture of boric oxide and borax or cadmium nitrate and adding it to the heated water under an inert atmosphere. In this way the isotopic purity of the heavy water was maintained above 99.65%. Figure 1 illustrates the geometry of the experiment. The solution was contained in a cylindrical tank with the fast neutron source placed on the axis in a through hole of diameter 7.5 cm. A probe tube of diameter 3.5 cm allowed the extraction of a beam from the centre of the tank. Previous work [7] has established that this size of tube does not affect the spectrum. A stainless steel window 0.006 in thick closed the end of the tube. Absorption in this window introduced less than $\frac{1}{2}$% distortion into the spectrum. A 4-kW stainless steel clad heater inserted into the bottom of the tank was used to heat the solution, the temperature being held to $\pm$ 1 deg C with a thermostat. To avoid degradation of the heavy water at the higher temperatures a reflux condenser was fitted to the tank and during the cooling period air was admitted through a drying agent.

The time resolution of the experiments was determined by the gate widths used in the time-of-flight analysis. In the energy region above 0.033 eV the resolution was 6.5 μs/m and below this energy 13 μs/m. The limiting resolution available in the spectrum measurement of the most lightly poisoned solution can be estimated from the slowing-down time and the

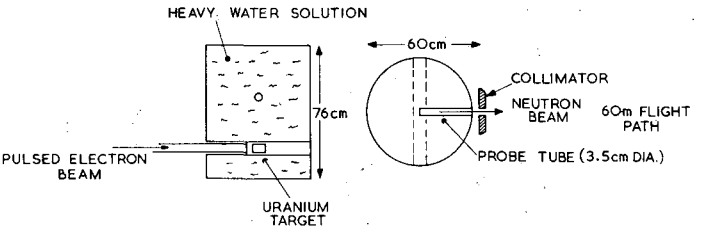

Fig. 1

The geometry of the poisoned heavy water experiment

thermal spectrum relaxation time and was less than 1.5 μs/m. Small corrections for the mean emission time of the neutrons as a function of energy have been estimated in a similar way and amount at worst to a 0.2% correction to the neutron flight time at 0.0253 eV.

Spectra were only measured for absorptions great enough to make the spectrum independent of position for an appreciable region around the probe tube. Under these conditions simple diffusion theory can be used to calculate the theoretical comparisons. Spectra in four boron solutions with absorptions in the range 1.23 b/D atom to 4.83 b/D atom were measured at 293°K (Fig. 2). For the weakest solution spectra were also observed at four distances between 14.6 and 28.0 cm from the source along the axis of the cylinder. These spectra are all different [8] and it was concluded that diffusion theory could not be used in this case. This conclusion was confirmed by activation measurements (see Fig. 4) and by a two-group diffusion theory calculation. Spectra in four cadmium solutions with concentrations in the range between 4.94 g/l and 13.04 g/l of cadmium are shown in Fig. 3.

Spectral changes in the neighbourhood of the probe tube were also investigated by measuring manganese and gold activations along a set of axes defined by the axis of the tank and the probe tube. Gold-manganese foils of diameter 0.25 in mounted on a thin aluminium framework were irradiated with and without cadmium covers and the activities of each component were analysed separately. These results both confirmed that the spectra were independent of position and allowed values of $\nabla^2\phi/\phi$ at the point of measurement to be determined. This value is required to allow for the effect of leakage on the calculated spectra. In the pseudo infinite medium calculation the leakage is represented by the term $-(\nabla^2\phi/\phi)\,D(E)\phi(E)$, where D(E) is the diffusion coefficient defined by

$$D(E) \approx \frac{1}{3[\Sigma_a(E)+\Sigma_s(E)(1-\bar{\mu}(E)]} ,$$

where $\bar{\mu}(E)$ is the mean scattering angle and $\Sigma_a(E)$, $\Sigma_s(E)$ are macroscopic cross-sections. Figure 4 shows the activations measured along the axis of the tank in the boron solutions. The second spatial derivatives of the flux at the position of the probe tube were found by fitting exponential functions to the measurements along the axis and zero-order Bessel functions radially. In the radial directions distinct departures from the J_0 distribution are

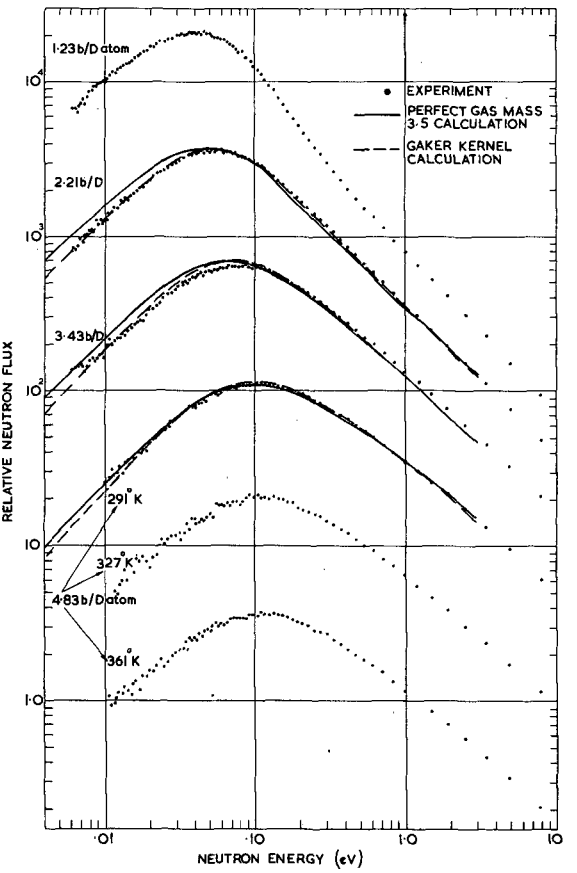

Fig. 2

Experimental and theoretical spectra in heavy water poisoned with boron

found (Fig. 5) and only the central region was used in this fitting procedure. In all cases $\nabla^2\phi/\phi$ was found to be positive. The leakage correction is most serious for the boron solution containing 2.21 b/D atom where $\nabla^2\phi/\phi$ was observed to be 0.011 ± 0.002 cm^{-2} and the ratio of the leakage and absorption terms in the calculation is 4.5% at 0.0253 eV.

3.2. Calculation of the spectra

Spectra were calculated in the diffusion approximation using the SIMPH code [9]. This uses a method first suggested by NELKIN [10] to solve the energy-dependent diffusion equation

$$\left(\Sigma_a(E) - \frac{\nabla^2\phi}{\phi} D(E) + \Sigma_s(E)\right)\phi(E) = \int_0^{E_0} (E' \to E)\phi(E')dE' + \int_{E_0}^{\infty} (E' \to E)\phi_1(E')dE'$$

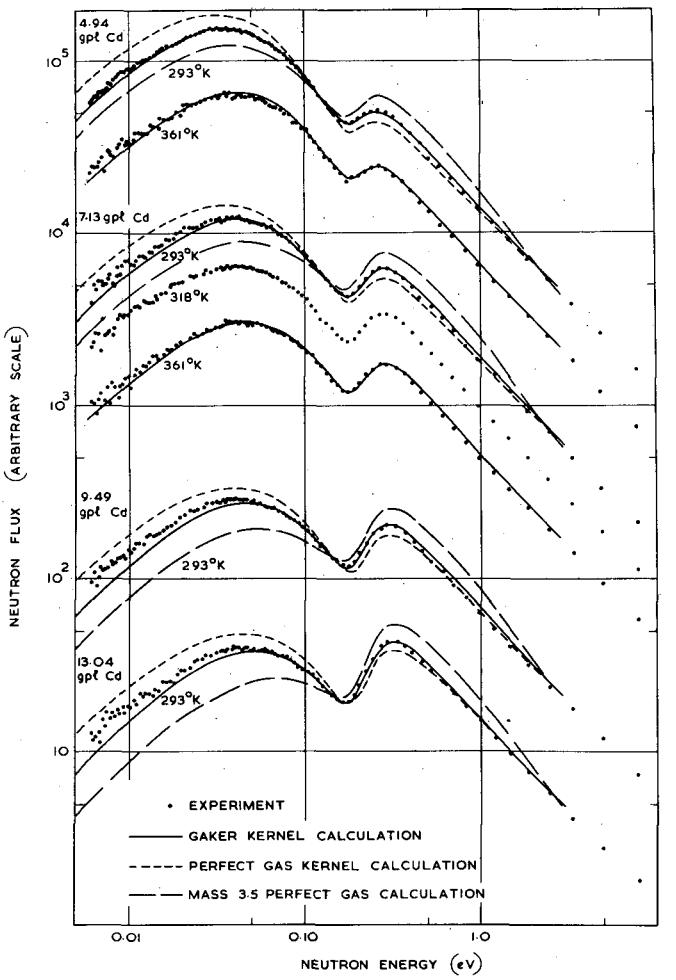

Fig.3

Experimental and theoretical spectra in heavy water poisoned with cadmium

where $\phi_1(E)$ is the slowing-down spectrum from the fast source and is assumed known. The second integral thus takes the place of the source in the equation above.

The scattering kernels available extended to a maximum incident energy of 3 eV. To obtain values above this (needed in calculating the source term) the perfect gas model was used assuming a mixture of mass 2 and mass 16. The diffusion coefficient was obtained as a function of energy from the known experimental values of the total scattering cross-section and from experimental values of $\bar{\mu}$ [11]. The latter had to be extrapolated to obtain values for the highest energies where $\bar{\mu}$ is given by

$$\bar{\mu} = \frac{1}{3}\left(\frac{2}{3A_O} + \frac{4}{3A_D}\right)$$

where A_O and A_D are the atomic masses of oxygen and deuterium respectively.

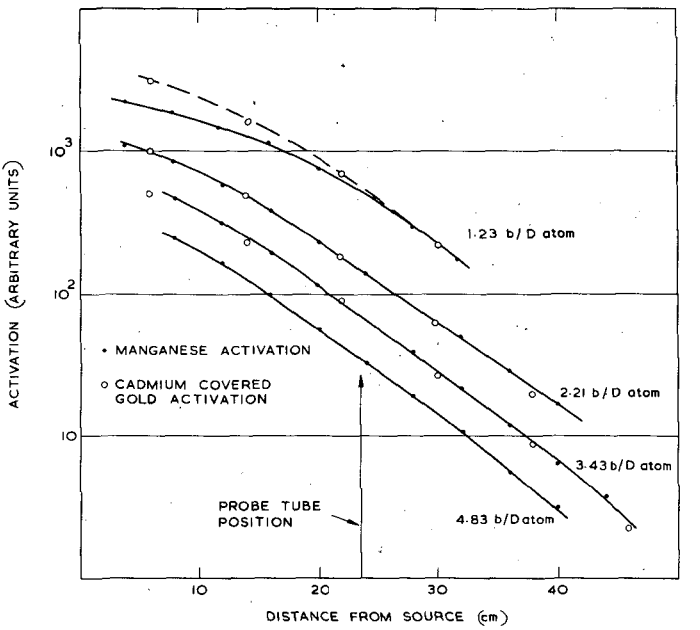

Fig. 4

Gold and manganese activations measured along the axis of the tank in the boron solutions

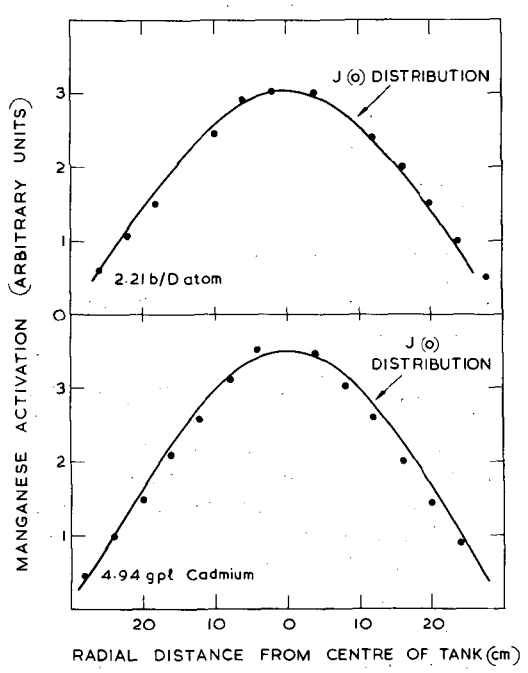

Fig. 5

Radial flux distributions

Before comparing experimental and theoretical spectra they are normalized to equal the rate of neutron loss over the region from 0 to 3 eV, i.e.

$$\int_0^3 \left(\Sigma_a(E) - \frac{\nabla^2\phi}{\phi} D(E)\right)\phi_{exp.}(E)dE = \int_0^3 \left(\Sigma_a(E) - \frac{\nabla^2\phi}{\phi} D(E)\right)\phi_{theor.}(E)dE$$

Normalized values of ϕ_{exp} and ϕ_{theor} should be equal at 3 eV if the neutron conservation condition is satisfied.

Three scattering kernels have been used. Each neglected coherent scattering and treated scattering from oxygen as scattering from a perfect gas of mass 16. The simplest kernel ignores binding and considers the deuterium also as a perfect gas of mass 2. Spectra calculated using this model are included to demonstrate the magnitude of the effect of chemical binding. The second kernel (BROWN and St. JOHN model [12]) uses a gas of mass 3.5 for the deuterium scattering while the third kernel is derived from the modified NELKIN model [13] suggested by HONECK [14] . Cross-sections were calculated from this model in the incoherent approximation using the GAKER code [15] .

Any scattering kernel must satisfy the detailed balance condition (which is usually built into the method of calculation) and must reproduce the experimentally measured total scattering cross-sections. At low energies the second condition cannot be satisfied in the incoherent approximation because of the peak in the observed scattering cross-section. Comparing the total scattering cross-sections from each kernel with experiment, the most sophisticated kernel gives the better fit at high energies and the closest approximation at the coherent peak.

The cadmium solution spectra clearly show the inadequacy of the perfect gas model (Fig. 3). Neutrons with energy just above that of the resonance can lose too much energy in collision with the free atoms and escape down through the resonance resulting in too intense a thermal group. This effect can be partially eliminated by the use of an "effective mass" for the deuterium but this kernel still reproduces spectra in boron solution (1/v absorption) better than in cadmium solution. Now the range of energy transfers is too narrow and the rate of capture in the resonance is too high. The agreement of spectra calculated with the Honeck kernel was reasonable for the boron solutions, although spectra were a little too hard as was also the case for the highly poisoned cadmium solutions. However, the agreement in the resonance energy region is excellent and as discrepancies only appear in the most highly poisoned cadmium solution spectra they cannot be attributed to faulty treatment of the leakage term in the diffusion equation. Spectra at 361°K are also predicted successfully with both the decrease in the magnitude of the thermal group below the resonance and its detailed shape in good agreement with experiment.

3.3. Conclusion

A scattering kernel based on the Honeck model for deuterium in heavy water and calculated in the incoherent approximation is able to predict

spectra in heavy water poisoned with both 1/v and resonance absorbers to better than 10% over the energy range 0.01 to 3.0 eV. For the weaker solutions the agreement is much better than this both at 293 and 361°K. It should be noted that the greatest discrepancies occur for the most strongly poisoned cadmium solutions where there is no possibility of errors occurring in the leakage correction. The differences may thus be safely attributed to imperfections in the kernel. The most significant defects of the model are the assumption of a single frequency to represent the hindered rotation of the molecule and the failure to consider the coherence of the scattering. Calculation of the spectra using a more realistic kernel based on the experimental scattering law [16] is proceeding.

4. SPECTRA AT AN ABSORBING SURFACE IN WATER

4.1. The experiment

The theoretical problem of the angular variation of the flux at a free surface in a moderating medium has been solved analytically for the case of a Maxwellian source distribution of thermal neutrons at an infinite distance from the surface [4, 5]. This source situation is difficult to achieve experimentally, and a fast source has been used in the experiments to be described. The energy spectrum of neutrons emerging along the normal to a water surface has been measured by the pulsed source technique [17, 18] and compared to numerical solutions of the Boltzmann equation assuming isotropic scattering. An earlier experiment by one of the authors [3] studied the angular variation of the spectra at a cadmium surface immersed in water. The results indicated that the spectral shape below 0.1 eV is not very sensitive to angle for values of μ greater than 0.5. (μ is the cosine of the angle between the neutron direction and the outward normal at the surface.) The experiment described here was designed to extend the range of μ to cover grazing angles of emergence and to check whether the cadmium surface experiment was strongly influenced by the source position and the transparency of the cadmium at high energies.

A well-shielded slab of water (60 cm by 60 cm by 15 cm or 20 cm) was mounted so that it could be rotated about a horizontal axis which bisected one face (Fig. 6(a)). Neutrons emerging through a thin aluminium window in the centre of this face at the angle defined by the slab orientation and the fixed 60-m flight path entered the time-of-flight spectrometer. As the slab was rotated it was also moved horizontally in such a way that the neutron source stayed on the normal to the water surface at the point of measurement. The mean relaxation time of the thermal spectra in the slab was 170 μs

periment was strongly influenced by the source position and the transparency of the cadmium at high energies.

A well-shielded slab of water (60 cm by 60 cm by 15 cm or 20 cm) was mounted so that it could be rotated about a horizontal axis which bisected one face (Fig. 6(a)). Neutrons emerging through a thin aluminium window in the centre of this face at the angle defined by the slab orientation and the fixed 60-m flight path entered the time-of-flight spectrometer. As the slab was rotated it was also moved horizontally in such a way that the neutron

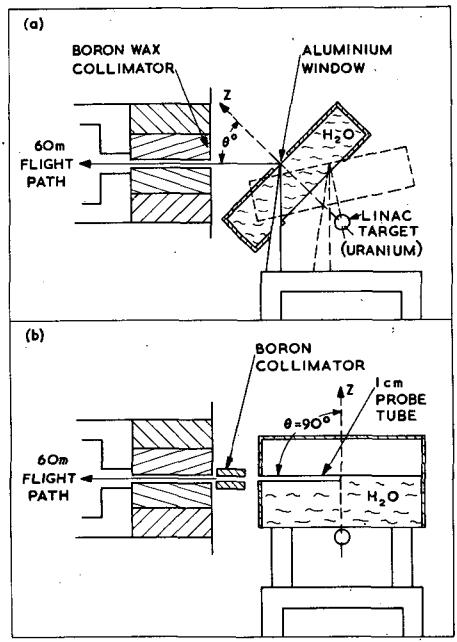

Fig. 6

Experimental arrangements used to study the energy spectra of neutrons emerging from a water surface (a) $0.19 < \mu < 0.74$ (b) $\mu = 0$

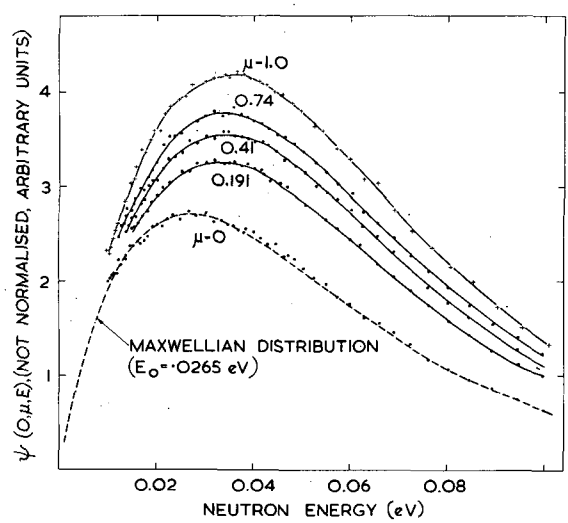

Fig. 7

Observed leakage spectra from a water surface; $\psi(0, 1, E)$ was measured in an earlier experiment [3].

source stayed on the normal to the water surface at the point of measurement. The mean relaxation time of the thermal spectra in the slab was 170 μs and gave a basic time-of-flight resolution of about 3 μs/m. Emergent spectra were measured at three angles for which μ was equal to 0.74, 0.41 and 0.191 respectively (Fig. 7). By using different sized collimators for each angle, the area on the surface seen by the detector was made less than 6 cm by 3 cm in order to minimize the effects of the flux gradient along the surface. The angular dependence of the spectra is not very strong but it can be seen (see Fig. 9) that the mean energies of the spectra decrease as μ decreases. It is of interest to compare the $\mu = 0.74$ spectrum with that measured for $\mu = 0.71$ in the cadmium disc experiment [3]. Below 0.1 eV the spectra are identical (Fig. 8(a)) within the limits set by the possible ex-

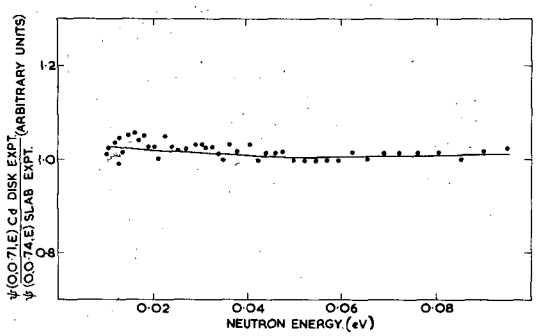

(a)

Fig. 8(a)

A comparison of the neutron spectrum leaving a water surface at approximately 45° as measured in this and an earlier experiment [3]

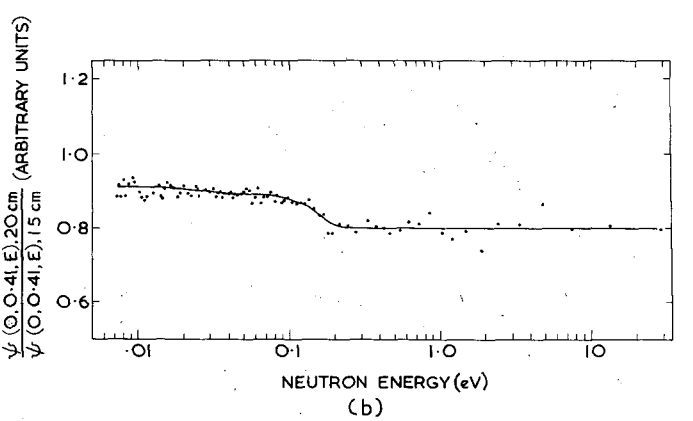

(b)

Fig. 8(b)

A comparison of $\psi(0, 0.41, E)$ for slabs of water of thickness 15 and 20 cm

perimental errors. This implies that the spectral shape below 0.1 eV is determined by the perturbation caused by the boundary and is not sensitive to the source position in the two experiments or to the transparency of the

boundary at high energies as in the cadmium disc experiment. As another test of the same point, the spectra for $\mu = 0.41$ and 0.74 were measured for slabs of thickness 15 cm and 20 cm. The magnitude of the 1/E high-energy component is decreased by increasing the water thickness (Fig. 8(b)) but the spectra below the "joining region" energies are not significantly altered. This again emphasizes that the spectra in this energy region are insensitive to the properties of the source. Although the emergent spectrum for $\mu = 0$ is in practice at a discontinuity an attempt to measure this was made with the experimental geometry shown in Fig. 6(b). A horizontal slab of water is placed over the neutron source, preserving the configuration of the previous experiment, and a neutron beam is extracted down a horizontal probe tube (3 cm wide and 1 cm deep) lying in the water surface. The observed spectrum (Fig. 7) can be fitted reasonably by a Maxwellian distribution with $E_0 = 0.0265$ eV which implies a ratio of neutron temperature to moderator temperature of 1.05. The marked difference between the spectra for $\mu = 0.19$ and zero indicates the special nature of the spectra in the surface, which is to be expected since the flux gradient in this direction is zero.

4.2. Calculation of the spectra

The angular spectra at a water surface have been calculated by solution of the Boltzmann transport equation in the Carlson discrete S_n approximation assuming isotropic scattering. An S_8 calculation in slab geometry was made with the WDSN code [19, 20]. The calculation considered a 15-cm infinite slab of water with a reflecting boundary on the one side and a free surface at the other. A source region having a Maxwellian flux distribution at the moderator temperature was located next to the reflecting boundary and the 15-cm slab was divided into 18 regions with the layers becoming progressively thinner towards the free surface. At the surface, the region in which the angular dependence of the spectra is of interest was 1 mm thick.

A 39 energy group system between 0.001 and 1.0 eV was chosen and group-averaged energy transfer cross-sections were calculated from the scattering law for water [21] using the PIXSE code. Three spectra emergent from the system are shown in Fig. 9. To demonstrate the perturbation introduced by the boundary the spectra have been divided by the source distribution for the calculation which is given by

$$M(E) = \frac{E}{E_0^2} e^{-E/E_0}$$

and the ratios have been set to unity at 0.0265 eV. The spectra are of higher mean energy than the source distribution and become harder as the direction of the neutron approaches the normal to the surface. The same μ-dependence is found in the experimental results (shown on the same figure) which have been normalized in the same way. There is a serious discrepancy between the detailed shape of the experimental and theoretical spectra with the experiments showing the larger deviation from the Maxwellian distribution and disagreeing with theory by 20% at 0.1 eV.

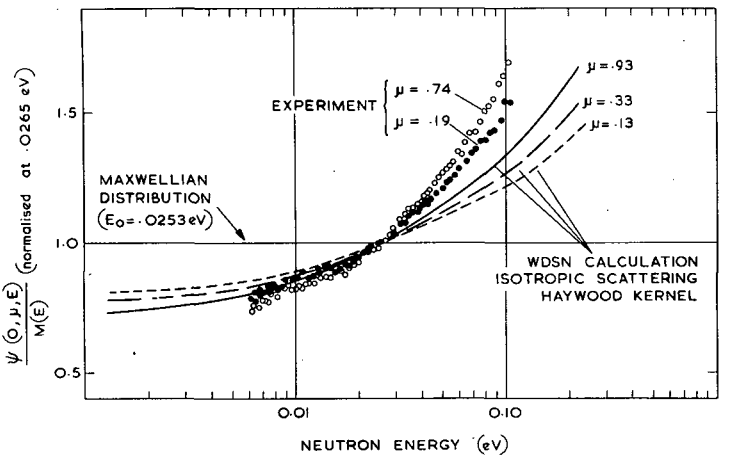

Fig. 9

Experimental and calculated leakage spectra from a water surface. The deviation from a Maxwellian distribution (E_0 = 0.0253 eV) is shown

4.3. Conclusion

The discrepancies between theory and experiment suggest that a transport theory calculation which assumes isotropic scattering cannot predict the angular flux spectra at an absorption discontinuity in water. The scattering kernel was based on a model which has proved to be successful in the prediction of pseudo-infinite medium spectra [22] and it is unlikely that this could be the cause of the disagreement. All the experiments indicate that the source condition is not of great importance to the thermal spectrum shape; however, this will be investigated further. It is not possible to calculate the anomalous spectrum for $\mu = 0$ with the available DSN code because the spectrum changes over a narrow angular range. It has previously been shown [3] that the sharp spectrum change as μ falls to zero cannot be explained analytically on the isotropic scattering assumption.

The angular-dependent energy transfer cross-sections for the moderators are becoming well known from recent experimental and theoretical studies and solutions of the Boltzmann equations utilizing these cross-sections are required for the interpretation of spectra near the strong perturbations.

ACKNOWLEDGEMENTS

We wish to thank Dr. M.J. Poole for his close interest, B. Chidley for preparing the heavy water solutions, D. Jones for the use of foil counting equipment and the Linac operating staff for their close co-operation.

REFERENCES

[1] POOLE, M.J., J. nucl. Energy 5 (1957) 325.
[2] BEYSTER, J.R., WOOD, J.L., LOPEZ, W.M. and WALTON, R.B., Nucl. Sci. Engng 9 (1961) 168.
[3] POOLE, M.J., SCHOFIELD, P. and SINCLAIR, R.N., Exponential and Critical Experiments III IAEA, Vienna (1964) 87-112.
[4] WILLIAMS, M.M.R., Nucl. Sci. Engng 19 (1964) 353-58.
[5] SCHOFIELD, P., AERE Rpt TP 99 (1963).
[6] KLADNIK, I., Proc. 3rd UN Int. Conf. PUAE, 1964, P/708.
[7] PARKS, D.E., BEYSTER, J.R. and WIKNER, N.F., Rpt GA-2437 (1961).
[8] SINCLAIR, R.N. and GOODE, P.D., AERE Rpt PR/NP5 (1963) 9-10.
[9] JONES, R.H. and McLATCHIE, R.C.F., AERE Rpt AERE-M 1355 (1964).
[10] NELKIN, M.S., Nucl. Sci. Engng 2 (1957) 199.
[11] SPRINGER, T., HOFMEYR, Ch., KORNBICHLER, S. and LEMMEL, H.D., Proc. 3rd UN Int. Conf. PUAE, 1964, P/763.
[12] BROWN, H.D. and St. JOHN, D.S., Rpt DP-33 (1954).
[13] NELKIN, M.S., Phys. Rev. 119 (1960) 741.
[14] HONECK, H., Trans. Amer. nucl. Soc. 5 (1962) 47.
[15] HONECK, H. Rpt BNL 5826 (1961).
[16] HAYWOOD, B.C. and THORSON, I.M., Rpt BNL 719, C-32 1 (1962) 26.
[17] BEYSTER, J.R., Rpt GA-3853 (1963).
[18] BECKURTS, K.H., Z. Naturf. 16 (1961) 611.
[19] FRANCESCON, S., AEEW Rpt R 273 (1963).
[20] ASKEW, J.R. and BRISSENDEN, R.J., AEEW Rpt R 161 (1963).
[21] HAYWOOD, B.C., private communication.
[22] JONES, R.H., A compilation of experimental and theoretical neutron spectra, AERE Rpt R 4776 (1964).

MEASUREMENTS OF THE THERMAL NEUTRON SPECTRUM IN THE CORE OF THE FORSCHUNGSREAKTOR FRANKFURT (FRF)

D. ROSSBERG
INSTITUT FÜR KERNPHYSIK DER JOHANN WOLFGANG GOETHE UNIVERSITÄT, FRANKFURT AM MAIN, FEDERAL REPUBLIC OF GERMANY

Abstract — Résumé — Аннотация — Resumen

MEASUREMENTS OF THE THERMAL NEUTRON SPECTRUM IN THE CORE OF THE FORSCHUNGSREAKTOR FRANKFURT (FRF). The thermal neutron spectrum in the core of the FRF was measured using a neutron chopper facility. The FRF is a homogeneous water-boiler reactor (Type L 54 F, Atomics International). Its fuel solution mainly consists of uranyl sulphate (400 g UO_2SO_4/l, enriched in U^{235} to 20%), water and sulphuric acid (concentration 0.4 molar). The absorption cross-section per proton of the solution is 1.85 b.

To extract neutrons from the core, a zirconium scatterer was placed in the central beam tube (through-hole) of the reactor. The scatterer could be positioned at various distances from the core centre. The measured spectra can be described in good approximation by a Maxwellian distribution. The neutron temperatures determined from the spectra are higher than those reported in literature for moderating water systems poisoned by an equivalent amount of absorber. The higher neutron temperature may be explained by assuming an increased effective mass of the moderating protons in the fuel solution. In the joining region between thermal and epithermal energies the spectra differ from those reported for pure water. The cut-off energy of the epithermal spectrum is found to be about $E_n = 5\,kT_n$, T_n being the neutron temperature of the Maxwellian spectrum.

In the course of these measurements the influence of the zirconium scatterer on the neutron spectrum in the extracted beam was investigated. The total neutron cross-section of zirconium in the energy range between 0.002 and 0.1 eV was measured. The results show that only at neutron energies $E_n > 0.02$ eV is the total neutron cross-section of zirconium nearly independent of neutron energy. Below this value coherent scattering in zirconium strongly affects the spectral distribution in the scattered beam.

MESURES DU SPECTRE DES NEUTRONS THERMIQUES DANS LE CŒUR DU RÉACTEUR DE RECHERCHE DE FRANCFORT (FRF). Le spectre des neutrons thermiques dans le cœur de FRF a été mesuré au moyen d'un hacheur de neutrons. FRF est un réacteur homogène à eau bouillante (type L 54 F, Atomics International). Sa solution de combustible est essentiellement composée de sulfate d'uranyle (400 g UO_2SO_4/l, enrichi à 20% en ^{235}U), d'eau et d'acide sulfurique (concentration égale à 0,4 mole par litre). La section efficace d'absorption par proton de la solution est de 1,85 b.

Afin d'extraire les neutrons du cœur, l'auteur a introduit un diffuseur au zirconium dans le canal expérimental central du réacteur. Il était possible de modifier la distance séparant le diffuseur du centre du cœur. On peut dire que les spectres mesurés sont une bonne approximation d'une distribution maxwellienne. Les températures des neutrons, qui ont été déterminées à partir des spectres, sont supérieures à celles qui sont indiquées dans des travaux antérieurs sur des ralentisseurs à eau, empoisonnés par une quantité équivalente d'absorbeurs. Cette différence de température des neutrons peut s'expliquer par le fait que la liaison chimique entre les molécules d'eau, d'une part, et l'acide sulfurique et le sulfate d'uranyle, d'autre part, dans la solution, provoquerait une augmentation de la masse efficace des protons ralentisseurs dans la solution de combustible. Dans la zone de transition entre les énergies thermiques et épithermiques, les spectres diffèrent de ceux qui sont indiqués dans les travaux antérieurs pour l'eau pure. L'énergie de coupure du spectre des neutrons épithermiques s'est avérée être égale à environ $E_n = 5\,kT_n$, T_n étant la température des neutrons du spectre de Maxwell.

L'auteur a cherché à déterminer au cours de ces mesures l'influence du diffuseur au zirconium sur le spectre des neutrons dans le faisceau extrait du cœur. Il a mesuré la section efficace totale du zirconium pour les neutrons dans la gamme des énergies allant de 0,002 eV à 0,1 eV. Les résultats montrent que cette section efficace n'est presque indépendante de l'énergie des neutrons que pour les énergies supérieures à 0,02 eV. Au-dessous de cette valeur, la diffusion cohérente dans le zirconium affecte considérablement la distribution spectrale du faisceau diffusé.

ИЗМЕРЕНИЯ СПЕКТРА ТЕПЛОВЫХ НЕЙТРОНОВ В АКТИВНОЙ ЗОНЕ ИССЛЕДОВАТЕЛЬСКОГО РЕАКТОРА ФРАНКФУРТ (FRF). Спектр тепловых нейтронов в активной зоне реактора FRF измерялся при помощи нейтронного прерывателя. Реактор FRF является гомогенным водяным кипящим реактором (тип L54 F, "Атомикс Интернэшнл"). Топливный раствор для этого реактора состоит главным образом из сульфата-уранила (400 г UO_2SO_4 на 1 л обогащенного до 20% урана-235) воды и серной кислоты (0,4-молярной концентрации). Сечение абсорбции на протон раствора составляет 1,85 барна.

Для извлечения нейтронов из активной зоны в трубку (через отверстие) центрального пучка реактора помещали циркониевый рассеиватель. Этот рассеиватель можно вставить на различных расстояниях от центра активной зоны. Измеренные спектры можно в хорошем приближении описать с помощью максвелловского распределения. Определенные на основании этих спектров температуры нейтронов оказываются более высокими, чем те, о которых сообщалось в литературе для замедляющих водяных систем, которые отравляются эквивалентным количеством поглотителя. Более высокую температуру нейтронов можно объяснить, предположив увеличенную эффективную массу замедляющих протонов в растворе топлива. В прилегающей области между термической и эпитермической энергиями спектры отличаются от тех, о которых сообщалось для чистой воды. Порог энергии эпитермического спектра составляет величину около $E_n = 5\ kT_n$, причем T_n является температурой нейтронов максвелловского спектра.

В ходе этих измерений исследовано влияние циркониевого рассеивателя на нейтронный спектр в извлеченном пучке. Измерено общее сечение нейтронов циркония в диапазоне энергий от 0,002 до 0,1 эв. Результаты показывают, что только при $E_n > 0{,}002$ эв общее сечение нейтронов циркония почти не зависит от энергии нейтронов. Ниже этой величины когерентное рассеяние в цирконии оказывает большое влияние на спектральное распределение в рассеянном пучке.

MEDICION DEL ESPECTRO DE NEUTRONES TERMICOS EN EL CUERPO DEL REACTOR DE INVESTIGACION DE FRANCFORT (FRF). Se ha medido el espectro de neutrones térmicos en el cuerpo del reactor FRF utilizando un selector de neutrones. El FRF es un reactor homogéneo de agua hirviente (tipo L 54 F, Atomics International). Su combustible en solución consiste principalmente en sulfato de uranilo (400 g de UO_2SO_4/l, enriquecido al 20% en ^{235}U), agua y ácido sulfúrico (concentración 0,4 molar). La sección eficaz de absorción protónica de la solución es 1,85 b.

Para extraer los neutrones del núcleo del reactor se colocó un dispersor de circonio en el canal central de irradiación (canal de paso). El dispersor podía colocarse a una distancia variable del centro del núcleo. Los espectros medidos pueden describirse con suficiente aproximación mediante una distribución maxwelliana. La temperatura neutrónica determinada a partir de los espectros es más alta que la indicada en los estudios sobre sistemas moderadores de agua envenenada con una cantidad equivalente de absorbente. Esta elevación de la temperatura neutrónica puede explicarse suponiendo que la masa efectiva de los protones moderadores aumenta en el combustible disuelto. En la región de transición de la energía térmica a la epitérmica, los efectos difieren de los indicados para el agua pura. Se ha comprobado que la energía de corte E_n del espectro epitérmico es del orden de $5\ kT_n$, siendo T_n la temperatura neutrónica correspondiente al espectro maxwelliano.

En el curso de estas mediciones se investigó la influencia del dispersor de circonio en el espectro neutrónico del haz de irradiación procedente del núcleo del reactor. Se midió la sección eficaz neutrónica total del circonio en el intervalo de energía 0,002 - 0,1 eV. Los resultados muestran que la sección eficaz neutrónica total del circonio es prácticamente independiente de la energía neutrónica sólo cuando ésta es superior a 0,02 eV. Por debajo de este valor, la dispersión coherente en el circonio afecta fuertemente la distribución espectral del haz dispersado.

1. INTRODUCTION

Thermal neutron spectra in pure water and in aqueous solutions of absorbers have been investigated in the past years by several authors [1-6]. In the discussion of the results of these measurements the interest is focussed on the relation between neutron temperature and absorption cross-

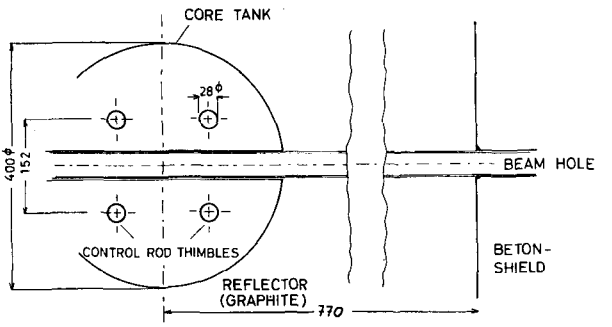

Fig. 1

Horizontal cut through the core and the central exposure tube of the FRF

section per proton in the moderator, and on the form of the neutron energy spectrum in the joining region between thermal and epithermal neutrons.

In this paper the neutron spectrum in the fuel solution of the Forschungsreaktor Frankfurt (FRF) is discussed on the basis of results from spectrum measurements using the chopper technique, which is well known in connection with measurements of this kind [7-10]. In the first sections the experimental arrangement is described, as far as it may affect the reliability of the results.

2. REACTOR AND BEAM HOLE

The FRF is a homogeneous water-boiler reactor (Type L54 of Atomics International). At a maximum power of 50 kW the reactor produces a thermal neutron flux of 7×10^{11} n/cm^2 s in the core centre [11]. The spherical core tank has a diameter of 40 cm. A central exposure tube, out of which the neutrons for the experiments were extracted, extends horizontally through the centre of the core tank (Fig. 1). It has an inside diameter of 36 mm and consists of three coaxial tubes, the inside aluminium tube with 0.9-mm wall thickness, the second aluminium tube with 2-mm wall thickness, and the outside stainless steel tube with 1.6-mm wall thickness and an outside diameter of 47.5 mm. Cooling coils of stainless steel are nearly homogeneously distributed in the core volume. The core tank is surrounded by a graphite reflector. The positions of the vertical control rod thimbles in relation to the exposure tube are shown in Fig. 1. During the experiments the control rods were drawn out completely from the fuel solution.

The fuel solution consists of uranyl sulphate (400 g UO_2SO_4/l, enriched in U^{235} to 20%), water, sulphuric acid (concentration 0.4 M) and some chemical additives, which are unimportant in connection with this paper. The absorption cross-section per proton of the solution is 1.85 b, corresponding to a hydrogen-uranium ratio of 96 in the solution. Taking into account the absorption in the cooling coils one gets an average absorption cross-section of 1.88 b per proton.

3. THE SPECTROMETER EQUIPMENT

The neutron spectrum of the extracted beam was analysed with a chopper, which has been constructed and built by HOFMANN [12]. The rotor has a diameter of 32 cm and consists of high strength aluminium and laminated phenol. Eight curved slit pairs are cut into the neutron stopping material. The start pulse for the time analyser is derived from a light flash, formed by light transmitted through the slits while open for the neutron beam. The slit width at the chopping point is 0.6 mm; the rotational speed of the rotor was varied in the experiments between 470 and 7500 rpm.

To extract neutrons from the core, scatterers were placed in the beam hole. They could be positioned at various distances from the core centre. A collimator inserted into the outer part of the beam hole allowed only those neutrons to reach the detector which were emitted from the scatterer. The alignment of the collimator was checked with the method described by JOHANSSON et al. [9]: The spectrum was measured once with the bare scatterer in the beam hole and again after putting a cadmium sheet in front of the scatterer. The comparison of the counting rates of the two runs ascertained that only neutrons from the scatterer reached the detector. It also has been investigated whether the collimator influences the neutron spectrum in the beam. For this purpose, at a large diameter beam hole of the reactor, the neutron spectrum was measured, first with the beam hole empty and then with the collimator inserted into the hole. No difference between the two spectra could be seen above 10^{-2} eV. At lower energies total reflection of neutrons in the collimator seems to affect the neutron spectrum in the beam.

The neutron detector in the experiments was a bank of six BF_3 proportional counters (Type 40EB70/50G of 20-th Century), which were mounted with their axes perpendicular to the neutron flight direction to give an effective length of 4.1 cm. The neutron flight path between the chopping point and the centre of the detector bank had a length of 6337 ± 2 mm, it was evacuated and shielded against stray neutrons. The detector pulses were fed into a 100 channel time-of-flight analyser.

The measurements yield counting rates P(t) depending on time of flight t, which may be converted into the neutron spectrum $\phi(E)\,dE$ by:

$$\phi(E)\,dE = \text{const.}\frac{P(t)T_c - U}{S(E)b(E)D(ft)}\,E^{-3/2}, \qquad (1)$$

T_c being the dead-time correction, U the background correction, S(E) the sensitivity of the neutron detector, and b(E) a correction factor resulting from the removal of neutrons from the beam by air in the beam hole, aluminium in the vacuum flanges of the drift tube, and the copper walls of the counting tubes. D(ft) is the rotor transmission probability, depending on the product of duty cycle f of the apparatus and neutron time-of-flight. The dead-time correction never exceeded 6% of P(t).

Background was determined at 1.45 eV with a 0.15-mm indium foil and in the thermal region with cadmium in the beam. The background count rate per channel was found to be independent of channel number, thus giving a background correction of about 5% in the epithermal region and of 0.3% in the maximum of the thermal spectrum.

The sensitivity S(E) of the detector was calculated and experimentally checked by measuring neutron spectra with the counter bank and with a thin BF_3 counter, whose efficiency could be assumed to be proportional to $E^{-1/2}$ (after correction for the influence of the copper walls). The agreement between calculation and measurement was good.

The transmission probability of the chopper ("cut-off function") D(ft) was measured in the way reported by STONE and SLOVACEK [7]. No difference could be seen between the transmission curves for thermal and epithermal neutrons within the experimental error of about 3%. The value of the transmission correction in the experiments varied between 0.6 and 1.0.

The energy calibration of the apparatus was performed by transmission measurements with gold (4.9 eV), indium (3.86 and 1.46 eV), cadmium (0.178 eV), and iron ($5 \cdot 10^{-3}$ eV). With the given flight path of 6337 mm, neutron energy is related to time-of-flight by $E = 2.10 \times 10^5 t^{-2}$ (E in eV and t in μs). The respective energy positions of the resonances and the Bragg cut-off in iron were consistent, within experimental error, with the values given in BNL 325 [13].

The energy resolution of the apparatus, due to the opening time of the chopper, the effective length and the time jitter of the detectors, and the channel width of the time analyser varied in the experiments as indicated in Fig. 2. Because of the high resolution of the spectrometer in the energy range of the experiments no resolution corrections have been applied to the measured data.

4. THE SCATTERER TECHNIQUE

The beam scatterer technique is well known from the work of JOHANSSON et al. [9] and from YOUNG et al. [5]. A scatterer, for instance zirconium or lead, is placed in a tube penetrating the assembly. Interpreting the experimental results the scattering cross-section of the scatterer material is assumed to be independent of neutron energy.

To test the validity of this assumption the neutron spectrum from the core was measured under otherwise identical conditions with cylindrical graphite, lead and zirconium scatterers, all of 35-mm diameter and 80-mm length, and in one run with a zirconium scatterer 30 mm in length. The spectra with the 80-mm scatterers are plotted in Fig. 2. It clearly shows the moderation effect of graphite on neutrons in the energy range of the lowest U^{238} resonance at 6.68 eV, as well as large differences between the three spectra in the sub-thermal energy region. Least squares fits of Maxwellian distributions to the data yield the neutron temperature values given in Table I. With graphite and zirconium scatterers, nearly the same neutron temperatures result. According to the energy dependence of the scattering cross-section of lead a hardened spectrum is expected with the lead scatterer, and this was indeed measured.

To investigate more clearly the influence of the zirconium scatterer on the spectrum, the total neutron cross-section of zirconium was measured in the energy range from 2×10^{-3} eV to 10 eV. Figure 3 gives the results. It is seen, that only at energies above 0.02 eV can the cross-section of

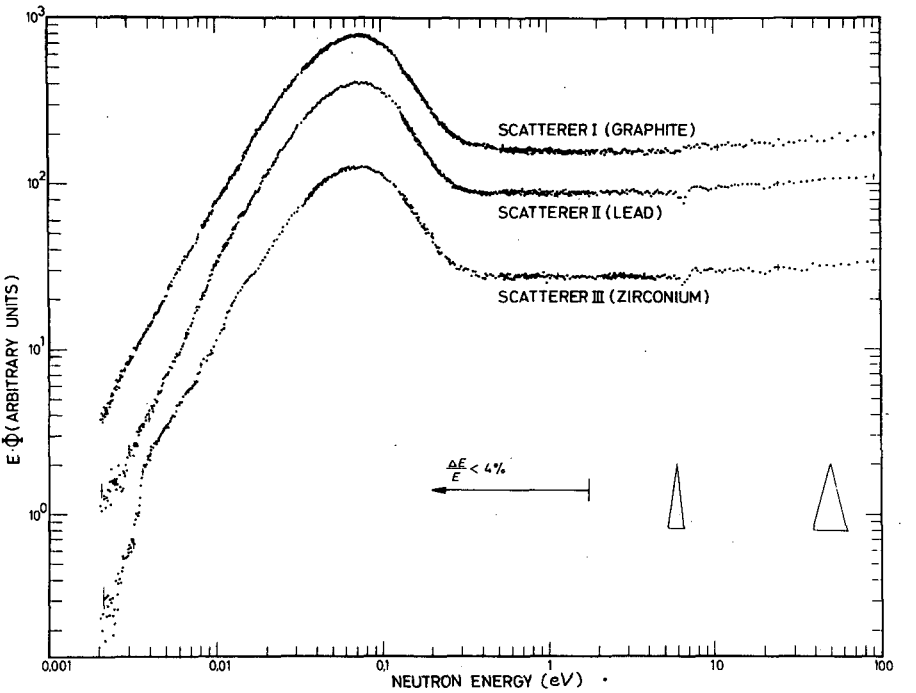

Fig. 2

Neutron spectra Eφ(E) in the core centre, measured with different scatterers
The fuel solution temperature in all runs was 353°K

TABLE I

NEUTRON TEMPERATURE FOR VARIOUS SCATTERERS

Run No.	Scatterer	E_0 (10^{-2} eV)	Neutron temperature $T_n = E_0/k$ (°K)
7	graphite	3.639 ± 1%	423 ± 1%
8	zirconium (80 mm)	3.665 ± 1%	426 ± 1%
19	zirconium (30 mm)	3.666 ± 1%	426 ± 1%
10	lead	3.800 ± 1%	441 ± 1%

Note: In all four runs the fuel solution temperature was 353 ± 3°K.

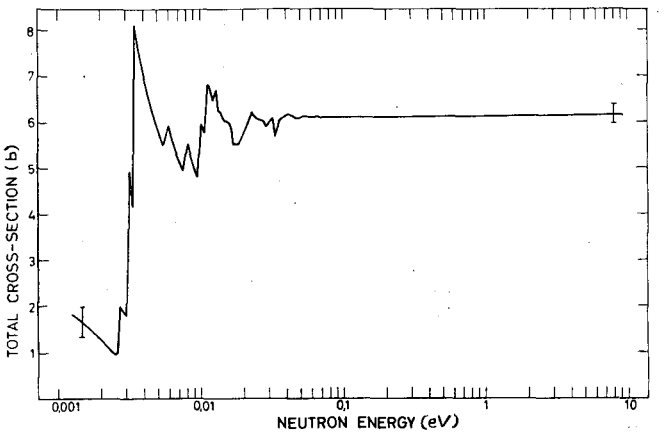

Fig. 3

Total neutron cross-section of zirconium

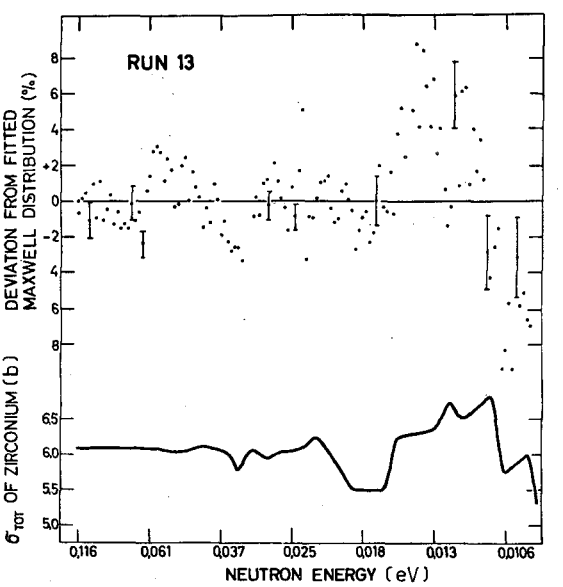

Fig. 4

Run 13: 30-mm zirconium scatterer in the graphite reflector 40 cm from core centre
Deviations of the measured points from the fitted Maxwellian distribution
and total neutron cross-section of zirconium

zirconium be assumed to be independent of neutron energy. In Figs. 4 and 5 the deviations of the measured counting rates from the computed Maxwellian distribution for two runs, both with zirconium scatterer, are plotted, together with the cross-section of zirconium. A correlation between the cross-section curve and the deviations from the Maxwellian curve is obvious,

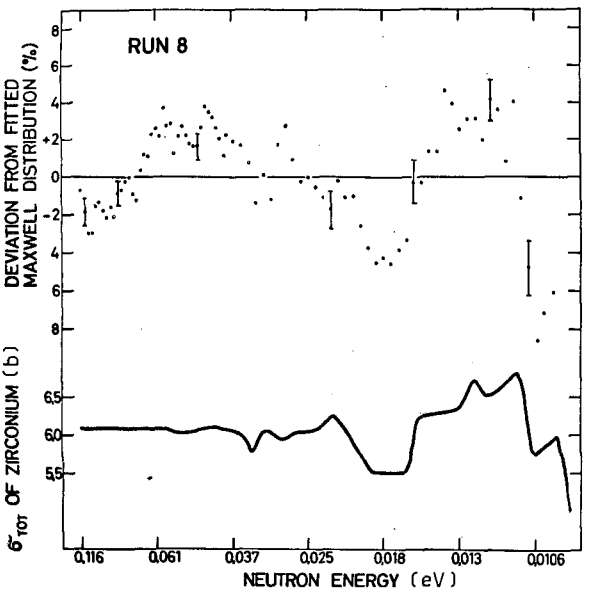

Fig. 5

Run 8: 80-mm zirconium scatterer in the centre of the core
Deviations of the measured points from the fitted Maxwellian distribution
and total neutron cross-section of zirconium

in particular in the energy range below 0.02 eV. Therefore in the following, only data measured in the energy range above 0.02 eV are evaluated in the discussion of the results. At lower energies the zirconium scatterer technique is not suitable for spectrum measurements.

5. RESULTS

Neutron spectrum measurements were performed with the 80-mm zirconium scatterer in the centre of the core at different temperatures of the fuel solution. The measured counting rates were corrected according to Eq. (1), and to determine the neutron temperatures Maxwellian distributions were fitted by the least squares method to the measured points in the range between 0.02 and 0.116 eV. The deviations of the measured points from the calculated Maxwellian curve for one typical run are plotted in Fig. 5. The approximation of the spectra by Maxwellian distributions seems to be rather good, but evidently there are systematical deviations from the Maxwellian distribution, thus indicating the weakness of the temperature concept for this type of hardened spectra.

From the measured-spectra neutron temperatures T_n, the relative increase of neutron temperature over moderator temperature T_m, $(T_n - T_m)/T_m$, and the ratio of thermal to epithermal neutron flux, ϕ_{th}/ϕ_{epi} (1.46 eV), were calculated. The results are given in Table II. The limits of error quoted in Table II are estimated from uncertainties in the correction factors in Eq. (1). The ratio of thermal to epithermal neutron flux derived from the

TABLE II

FUEL AND NEUTRON TEMPERATURES, AND FLUX RATIOS

Run No.	Fuel temperature T_m (°K)	Neutron temperature $T_n = E_0/k$ (°K)	$\frac{T_n - T_m}{T_m}$	ϕ_{th}/ϕ_{epi} (ϕ_{epi} at 1.46 eV)
8	353 ± 3	426 ± 1%	0.207 ± 10%	8.59 ± 0.4
9	334 ± 3	410 ± 1%	0.227 ± 10%	8.53 ± 0.4
23	314 ± 3	388 ± 1%	0.235 ± 10%	8.15 ± 0.4

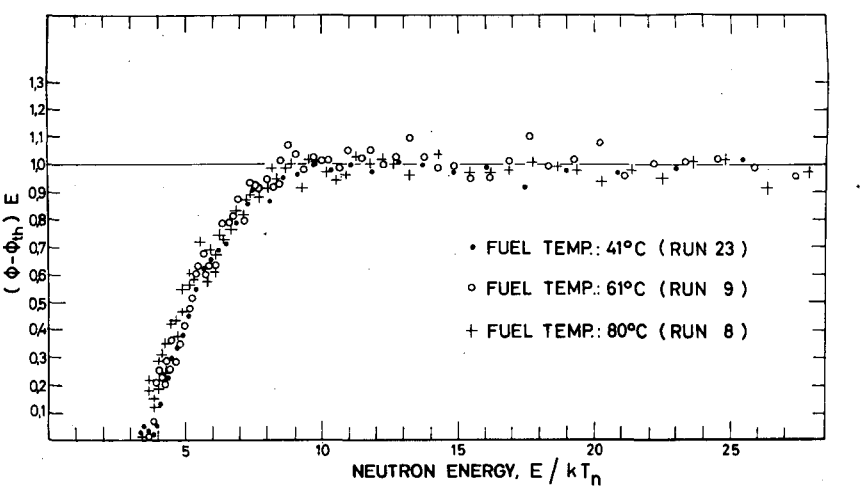

Fig. 6

The joining function for the fuel solution of the FRF

spectra is in agreement with the value measured by STELZER [11] in the same position with foil activation technique.

The relative increase of neutron temperature over moderator temperature is much larger than reported by other authors from measurements in water poisoned by an equivalent amount of absorber (see for instance the summary in [4]). This may be a result of hydration bonds between water molecules and sulphuric acid or uranyl sulphate in the fuel solution, by which the moderation process is hindered, although the acid concentration is only 0.4 M and the hydrogen-uranium ratio is 96.

The influence of diffusion on the measured spectra may be neglected, since the flux gradient at the scatterer position in the core centre is zero and the buckling B^2 at this point is approximately 6×10^{-3} cm^{-2} for thermal and epithermal neutrons [11], thus the term DB^2 being small compared with the macroscopic absorption cross-section of the fuel solution.

By subtracting the fitted Maxwellian distribution from the measured neutron energy spectrum the "joining function" is obtained. In contrast to measurements of other authors in D_2O [9], graphite [14], and water [15], the joining function determined for the neutron spectrum in the fuel solution of the FRF does not increase above the 1/E level in the region of 10 kT_n, as can be seen in Fig. 6. From the measurements, the effective lower limit of the 1/E spectrum was determined to be 5.1 kT_n ± 10% referred to a 1/v absorber.

ACKNOWLEDGEMENTS

The author wishes to acknowledge the contributions made by D. Hofmann in the construction of the neutron chopper and by P. Roeper in developing a computer programme for analysing the data. He is particularly indebted to K. Fiebiger, W. Schütze, and K. Stelzer for many helpful discussions.

REFERENCES

[1] STONE, R.S. and SLOVACEK, R.E., Rpt. KAPL-1916 (1957).
[2] POOLE, M.J., J. nucl. Energy 5 (1957) 325.
[3] BEYSTER, J.R., WOOD, J.L., LOPEZ, W.M. and WALTON, R.B., Nucl. Sci. Engng 9 (1961) 168.
[4] BURKART, E. and REICHARDT, W., Rpt. BNL-719 (1962) 318.
[5] YOUNG, J.C., TRIMBLE, G.D., NALIBOFF, Y.D., HOUSTON, D.H. and BEYSTER, J.R., Nucl. Sci. Engng 18 (1964) 376.
[6] MOSTOVOY, V.I., DIKAREV, V.S., EGIAZAROV, M.B. and SALTIKOV, Yu.S., Rpt. BNL-719 (1962).
[7] STONE, R.S. and SLOVACEK, R.E., Rpt. KAPL-1499 (1956).
[8] MOSTOVOY, V.I., PEVZNER, M.I. and TSITOVICH, A.P., Proc. UN Int. Conf. PUAE 4 (1956) 12.
[9] JOHANSSON, E., LAMPA, E. and SJÖSTRAND, N.G., Ark. Fys. 18 (1960) 513.
[10] BARCLAY, F.R., COATES, M.S., DIMENT, K.M., DURRANI, S.A., GAYTHER, D.B., PITCHER, H.H. and POOLE, M.J., Rpt. BNL-719 (1962) 359.
[11] STELZER, K., Rpt. IKF-1 (1961).
[12] HOFMANN, D., Diplomarbeit Universität Frankfurt am Main (1962).
[13] HUGHES, D.J. and SCHWARTZ, R.B., Rpt. BNL-325 (1958).
[14] COATES, M.S. and GAYTHER, D.B., Rpt. AERE-R 3829 (1961).
[15] BECKURTS, K.H. and WIRTZ, K., Neutron Physics, Berlin (1964) 336.

DISCUSSION

H. POLLAK: You show that there is a correlation between the cross-section for Zr and the spectrum you obtain. What kind of correlation is this?

D. ROSSBERG: The intensity of scattered neutrons is expected to be proportional to the scattering cross-section of the scatterer material. A correlation of this kind is seen in the figures, where the cross-section of zirconium and the deviation of neutron intensity from the fitted Maxwellian are plotted together against energy.

THE EFFECT OF NON-UNIFORM MODERATOR TEMPERATURE ON THE EPITHERMAL NEUTRON SPECTRUM

M.M.R. WILLIAMS
UNIVERSITY OF BIRMINGHAM, UNITED KINGDOM

Abstract — Résumé — Аннотация — Resumen

THE EFFECT OF NON-UNIFORM MODERATOR TEMPERATURE ON THE EPITHERMAL NEUTRON SPECTRUM. The neutron spectrum from a high energy source in an infinite 1/v absorbing medium, possessing a non-uniform temperature variation, is obtained for an arbitrary scattering kernel. The diffusion approximation has been employed to represent the spatial variation of flux, and methods are discussed whereby the full Boltzmann equation can also be used.

The resulting energy spectrum is in the form of an asymptotic series in inverse powers of neutron velocity. The first and second terms in the series are spatially constant and represent the well known 1/E slowing-down flux with a correction for absorption. Succeeding terms depend upon the spatial variation of the physical temperature and contain quantities which are functions of the chemical binding and absorption of the moderator. For constant temperature, the solution becomes identical to that derived some years ago by Corngold for infinite homogeneous media. Numerical results are presented for various moderators and physical temperature variations.

EFFET DE LA TEMPÉRATURE NON UNIFORME DU RALENTISSEUR SUR LE SPECTRE DES NEUTRONS ÉPITHERMIQUES. L'auteur a obtenu le spectre de neutrons émis par une source d'énergie intense dans un milieu absorbant 1/v infini où la température varie de façon non uniforme, pour un noyau de diffusion arbitraire. Il a eu recours à l'approximation de diffusion pour représenter la variation du flux dans l'espace et il discute les méthodes permettant d'utiliser également l'équation de Boltzmann complète.

Le spectre énergétique qui en résulte est de la forme d'une série asymptotique des puissances inverses de la vitesse des neutrons. Les deux premiers termes de la série sont constants dans l'espace et représentent le flux de ralentissement bien connu 1/E corrigé pour tenir compte de l'absorption. Les termes suivants dépendent de la variation de la température dans l'espace et contiennent des quantités qui sont fonction de la liaison chimique et de l'absorption du ralentisseur. Pour une température constante, la solution devient identique à celle à laquelle Corngold était parvenu il y a quelques années pour des milieux homogènes infinis. L'auteur présente des résultats numériques pour divers ralentisseurs et diverses lois de variation de la température.

ВЛИЯНИЕ ТЕМПЕРАТУРЫ НЕОДНОРОДНОГО ЗАМЕДЛИТЕЛЯ НА СПЕКТР НАДТЕПЛОВЫХ НЕЙТРОНОВ. Спектр нейтронов из источника высокой энергии в бесконечной поглощающей среде, подчиняющейся закону 1/v и подверженной неоднородным колебаниям температуры, был получен для произвольного ядра рассеяния. Для представления пространственного изменения потока применяли диффузионную аппроксимацию. Рассматриваются методы, при которых может быть использовано полное уравнение Больцмана.

Результатирующий энергетический спектр имеет вид асимптотического ряда при обратных степенях скорости нейтронов. Первый и второй члены этого ряда являются пространственной константой и представляют хорошо известный замедляющийся поток 1/E с поправкой на поглощение. Последующие члены зависят от пространственных изменений физической температуры и содержат величины, которые являются функциями химической связи и поглощения замедлителя. Для постоянной температуры это решение становится идентичным решению, полученному несколько лет назад Корнгольдом для бесконечной гомогенной среды. Приводятся цифровые результаты для различных замедлителей и вариаций физических температур.

EFECTO DE LA TEMPERATURA NO UNIFORME DEL MODERADOR EN EL ESPECTRO DE NEUTRONES EPITERMICOS. Se determina, para un núcleo de dispersión arbitrario, el espectro neutrónico de una fuente de elevada energía en un medio absorbente infinito, que se ajusta a la ley 1/v con variación no uniforme de la temperatura. Se aplica la aproximación por difusión para representar la variación espacial del flujo, y se examinan métodos que permiten aplicar también la ecuación íntegra de Boltzmann.

El espectro energético resultante presenta la forma de un desarrollo asintótico cuyos exponentes están en razón inversa de la velocidad de los neutrones. El primero y el segundo términos del desarrollo son espacialmente constantes y representan el conocido flujo de moderación 1/E, con una corrección para tener en cuenta la absorción. Los términos siguientes dependen de la variación espacial de la temperatura física y comprenden magnitudes que son función de los enlaces químicos y de la absorción del moderador. Para una temperatura constante la solución es idéntica a la deducida hace algunos años por Corngold para medios infinitos de carácter homogéneo. Se dan resultados numéricos relativos a diversos moderadores y variaciones de la temperatura física.

1. INTRODUCTION

The calculation of the neutron flux, in a medium whose physical temperature depends on position, is of some importance from a practical viewpoint, in connection with nuclear reactors. It is also interesting for purely academic reasons.

The progress made to date in the solution of the Boltzmann equation for media with temperature gradients is not great. This is due to the fact that there is no simple infinite medium problem from which one can gain initial ideas about the energy exchange process. Furthermore, because the physical temperature is a continuous function of position, the cross-sections also become functions of position. Thus, the usual methods of solution of the transport equation are not convenient. KOTTWITZ [1] has solved this problem by considering the simple case of a temperature discontinuity in an infinite medium. However, even this very simple problem has only been solved analytically in the heavy gas approximation. It is well known that the heavy gas model is useful, but it can hardly be expected to give the detail required in many experiments. Some interesting features of the problem of neutron diffusion in a temperature gradient have been discussed by KUŠČER [2] but no analytical method for calculating the flux in an arbitrary temperature gradient has been proposed.

In the present paper we present a method of obtaining the neutron flux in an infinite medium possessing 1/v absorption and any arbitrary temperature gradient or scattering model. The medium contains a high energy, spatially uniform neutron source, so that for $E \gg kt$ the well-known 1/E slowing-down solution persists over the entire medium. By making use of an expansion in inverse powers of neutron velocity and using a representation of the "scattering-in" term of the Boltzmann equation, first derived by CORNGOLD [3], we obtain an exact (as far as diffusion theory will allow) asymptotic expression for the neutron energy spectrum. Results are presented for various moderators and temperature distributions. The extension to transport theory is indicated.

2. THEORY

The equation which describes the neutron flux across a medium with a non-uniform physical temperature distribution may be written, in the diffusion approximation, as:

$$-\nabla\cdot[D(E, T(\underline{r}))\,\nabla\phi(E, \underline{r})] + [\Sigma_a(E, T(\underline{r})) + \Sigma_s(E, T(\underline{r}))]\phi(E, \underline{r}) = \int_0^\infty \Sigma[E' \to E; T(\underline{r})]\phi(E', \underline{r})dE' + S(E, \underline{r}) \tag{1}$$

In general, the solution of this equation presents great difficulties. We shall consider the simplest case of an infinite medium containing a high energy, spatially constant source. Then for $E >> kT$ the spatial variation of the flux, assuming $1/v$ absorption, will be constant, and the energy variation will be of the familiar $1/E$ slowing-down type.

As soon as the neutron energy drops below about 1 eV, the chemical binding and thermal motion of the moderator will affect the slowing-down process. If the temperature of the moderator is non-uniform, the neutron flux will no longer be spatially constant, since variation in the moderating power from point to point will cause a net neutron current.

CORNGOLD (3) has developed an asymptotic solution to Eq. (1) for $1/v$ absorption and $\nabla\phi = 0$, i.e. uniform temperature. His solution is of the form:

$$\xi\Sigma_f E\phi(E) = \sum_{n=0,1/2,1,..}^{\infty} a_n \left(\frac{T}{E}\right)^n \tag{2}$$

where

$$a_n = \sum_{p=0}^{[n]} \tau_n^p \left(-\frac{\Delta}{2}\right)^{2(n-p)} \tag{3}$$

with $\Delta = 2\Sigma_a(T)/\mu\Sigma_f$.

The τ_n^p are functions of temperature and chemical binding, some of which are given in the Appendix of this paper. Corngold's solution is valid down to an energy of about 0.2 eV, but because it is asymptotic, the exact range of validity depends on the magnitudes of the a_n.

To solve Eq. (1) we shall employ a similar asymptotic expansion, namely

$$\xi\Sigma_f E\,\phi(E, \underline{r}) = \sum_{n=0,1/2,1,...}^{\infty} b_n(\underline{r}) \left(\frac{1}{E}\right)^n \tag{4}$$

where the coefficients b_n are space dependent. It is quite clear from the physical aspects of the problem that b_0 is independent of $\underline{r}$, and according to our normalization will be set equal to unity. The remaining $b_n(\underline{r})$ are determined by substitution of Eq. (4) into Eq. (1) and equating coefficients of equal powers of $E^{-1/2}$.

To proceed with the mechanics of the method we require the asymptotic expansions of D(E), $\Sigma_s(E)$ and the collision term $\int \Sigma(E' \to E)\phi(E')dE'$. $\Sigma_s(E)$ may be obtained readily from the short collision time approximation;

$$\Sigma_s(E) = \Sigma_f\left\{1 + \frac{\mu\bar{T}}{2E} + O\left(\frac{T}{E}\right)^3\right\} \tag{5}$$

and the diffusion coefficient may be obtained from

$$D(E) = \frac{1}{3\Sigma_{tr}(E)} = D_f\left\{1 - \frac{\mu\bar{T}}{2E} + \frac{\mu^2\bar{T}^2}{4E^2} + \ldots\right\}, \tag{6}$$

where

$$D_f = 1/3\ \Sigma_f\left(1 - \frac{2}{3A}\right).$$

The only term which presents some difficulty is the one containing the collision operator. However, Corngold has obtained an explicit expression for this, which we may use directly, namely

$$\int_0^\infty \Sigma(E' \to E)\phi(E')dE' = \frac{\pi}{\mu}\sum_{n=0,1,\ldots}^{\infty} \frac{(1-\mu)^n}{n!}\frac{1}{E^n}C_n(E) \tag{7}$$

where

$$C_n(E) = \left[\frac{\partial^n}{\partial y^n}\int_{\alpha(y)E}^{\beta(y)E} \frac{dE'}{E'}S_n(\kappa^2)\phi(E')\right]_{y=1}$$

and

$$\alpha(y) = \left(\frac{\sqrt{y}-\mu}{1-\mu}\right)^2,\quad \beta(y) = \left(\frac{\sqrt{y}+\mu}{1-\mu}\right)^2$$

$$\kappa^2 = 2A\left(E' - \frac{y-\mu}{1-\mu}E\right)$$

$$S_0 = 1,\quad S_1 = 0,\quad S_2 = \frac{\kappa^2\bar{T}}{A},\ \ldots$$

By substituting the asymptotic flux into Eq.(7) we obtain

$$\frac{\pi}{\mu}\sum_{n=0,1,2}^{\infty}\ \sum_{m=0,1/2,1,\ldots}^{\infty}\frac{(1-\mu)^n}{n!}\frac{b_m}{E^n}\left[\frac{\partial^n}{\partial y^n}\int_{\alpha(y)E}^{\beta(y)E}\frac{dE'}{E'}\frac{S_n(\kappa^2)}{(E')^m}\right]_{y=1}$$

The evaluation of the integrals in this expression is easy, if tedious, and we find:

$$\int_0^\infty \Sigma(E'\to E)\phi(E')dE' = \frac{b_0}{E} + \sum_{n=3}^{\infty} I_n\left(\frac{1}{E}\right)^{n/2}$$

where

$$I_3 = b_{1/2}\frac{(1+\mu)^2}{4\mu}\int_{\alpha(1)}^{\beta(1)}\frac{dx}{x^{5/2}}$$

$$I_4 = b_1\frac{(1+\mu)^2}{4\mu}\int_{\alpha(1)}^{\beta(1)}\frac{dx}{x^3} + b_0\overline{T}(1-\mu)^2\frac{(1+\mu)^2}{4\mu}\left\{\frac{\partial^2}{\partial y^2}\left[\int_{\alpha(y)}^{\beta(y)}\frac{dx}{x} - \frac{(y-\mu)}{1-\mu}\int_{\alpha(y)}^{\beta(y)}\frac{dx}{x^2}\right]\right\}_{y=1}$$

$$I_5 = b_{3/2}\frac{(1+\mu)^2}{4\mu}\int_{\alpha(1)}^{\beta(1)}\frac{dx}{x^{3/2}} + \frac{(1+\mu)^2}{4\mu}\,b_{1/2}\overline{T}(1-\mu)^2\left\{\frac{\partial^2}{\partial y^2}\left[\int_{\alpha(y)}^{\beta(y)}\frac{dx}{x^{3/2}} - \frac{(y-\mu)}{1-\mu}\int_{\alpha(y)}^{\beta(y)}\frac{dx}{x^{5/2}}\right]\right\}_{y=1}$$

Now using $\nabla\cdot[D\nabla\phi] = D\nabla^2\phi + \nabla D\cdot\nabla\phi$ and collecting terms in Eq. (1), the following equations for the coefficients $b_n(\underline{r})$ are obtained:

$$-D_f\nabla^2 b_0 = 0 \tag{8}$$

$$-L_f^2\nabla^2 b_{1/2} + \frac{\mu}{\tau^0_{1/2}}b_{1/2} = -\Delta_0 \tag{9}$$

$$-L_f^2\nabla^2 b_1 + \frac{2\mu}{(1+\mu)^2}b_1 = -\Delta_0 b_{1/2} + \frac{2\mu(2-\mu)\overline{T}}{(1+\mu)^2} \tag{10}$$

$$-L_f^2\nabla^2 b_{3/2} + \frac{\mu\tau^0_1}{\tau^0_{3/2}}b_{3/2} = -\frac{1}{2}L_f^2\mu\overline{T}b_{1/2} - \frac{1}{2}L_f^2\mu\overline{\nabla T}\cdot\nabla b_{1/2} - \Delta_0 b_1$$

$$-\frac{\mu}{\tau^0_{1/2}}\left[(2-\mu)\overline{T} - \frac{\tau^0_1}{\tau^0_{3/2}}f\overline{T}\right]b_{1/2} \tag{11}$$

where $L_f^2 = D_f/\Sigma_f$, $\Delta_0 = \Sigma_a(T)\sqrt{T}/\Sigma_f$, $\tau_{3/2}^1 = f\sqrt{T}/T$.

Thus, we have a set of inhomogeneous diffusion equations, with constant coefficients. These may be solved recursively, the solution of one determining the source for the next.

The form of Eq. (8) is implicit in our definition of b_0. Thus, we require the general solution of the equation

$$\nabla^2 y - k^2 y = S(\underline{r})$$

for an infinite medium. This is a standard form and

$$y(\underline{r}) = -\int d\underline{r}' \frac{\exp[-k\,|\underline{r}-\underline{r}'|]}{4\pi\,|\underline{r}-\underline{r}'|} S(\underline{r}')$$

specializing to variation in the x-direction only, this reduces to

$$y(x) = -\frac{1}{2k}\int_{-\infty}^{\infty} S(x')\exp[-k|x-x'|]\,dx'$$

Equations (8), (9) and (10) are written in the simpler notation:

$$\nabla^2 b_{1/2} - k_{1/2}^2 b_{1/2} = \frac{\Delta_0}{L_f^2} \tag{12}$$

$$\nabla^2 b_1 - k_1^2 b_1 = \frac{\Delta_0}{L_f^2} b_{1/2} - \frac{2\mu(2-\mu)\sqrt{T}}{(1+\mu)^2 L_f^2} \tag{13}$$

$$\nabla^2 b_{3/2} - k_{3/2}^2 b_{3/2} = S_{3/2} \tag{14}$$

where

$$S_{3/2} = \frac{\Delta_0 b_1}{L_f^2} + \frac{\mu}{L_f^2 \tau_{1/2}^0}\left[(2-\mu)\sqrt{T} - \frac{\tau_1^0}{\tau_{3/2}^0} f\sqrt{T}\right] b_{1/2} + \frac{\mu\sqrt{T}}{2}\nabla^2 b_{1/2} + \frac{1}{2}\mu\nabla\sqrt{T}\cdot\nabla b_{1/2}$$

and

$$k_{1/2}^2 = \frac{\mu}{\tau_{1/2}^0 L_f^2}, \quad k_1^2 = \frac{2\mu}{(1+\mu)^2 L_f^2}, \quad k_{3/2}^2 = \frac{\mu\tau^1}{\tau_{3/2}^0 L_f^2}$$

We find, therefore

$$b_{1/2} = -\frac{\Delta_0}{\mu}\tau^0_{1/2} \tag{15}$$

$$b_1 = \frac{\Delta_0^2}{2\mu^2}\frac{(1+\mu)^3}{(1-\frac{1}{3}\mu)} + \frac{2\mu(2-\mu)}{(1+\mu)^2 L_f^2}\frac{1}{2k_1}\int_{-\infty}^{\infty} e^{-k_1|x-x'|}\,\overline{T}(x')dx' \tag{16}$$

$S_{3/2}$ simplifies to

$$S_{3/2} = \frac{\Delta_0^3}{2\mu^2 L_f^2}\frac{(1+\mu)^3}{(1-\frac{1}{3}\mu)} + \frac{\Delta_0}{L_f^4}\frac{2\mu(2-\mu)}{(1+\mu)^2}\frac{1}{2k_1}\int_{-\infty}^{\infty} e^{-k_1|x-x'|}\,\overline{T}(x')dx'$$

$$-\frac{\Delta_0}{L_f^2}\left[(2-\mu) - \frac{\tau_1^0}{\tau_{3/2}^0} f\right]\overline{T}(x)$$

Thus

$$b_{3/2} = -\frac{1}{2k_{3/2}}\int_{-\infty}^{\infty} S_{3/2}(x')e^{-k_{3/2}|x-x'|}\,dx' \tag{17}$$

3. ADJACENT HALF-SPACES

As an example, we consider the problem of two adjacent half-spaces at different temperatures; thus

$$T = T_1, \quad x > 0$$

$$T = T_2, \quad x < 0$$

Now for $x > 0$

$$\frac{1}{2k}\int_{-\infty}^{\infty} e^{-k|x-x'|}\,\overline{T}(x')dx' = \frac{\overline{T}_1}{k^2} + \frac{1}{2k^2}(\overline{T}_2 - \overline{T}_1)e^{-kx} \tag{18}$$

and for $x < 0$

$$\frac{1}{2k}\int_{-\infty}^{\infty} e^{-k|x-x'|}\,\overline{T}(x')dx' = \frac{\overline{T}_2}{k^2} + \frac{1}{2k^2}(\overline{T}_1 - \overline{T}_2)e^{+kx} \tag{19}$$

Thus for $x > 0$

$$b_1 = \frac{\Delta_0^2}{2\mu^2} \frac{(1+\mu)^3}{(1-\frac{1}{3}\mu)} + (2-\mu)[\bar{T}_1 + \tfrac{1}{2}(\bar{T}_2 - \bar{T}_1)e^{-k_1 x}] \tag{20}$$

The calculation of $b_{3/2}$ is a little more complicated and the result, for $x > 0$ is

$$b_{3/2} = -\frac{\Delta_0^3}{\mu^3}\tau_{3/2}^0 - \frac{\Delta_0}{\mu} f[\bar{T}_1 + \tfrac{1}{2}(\bar{T}_2 - \bar{T}_1)e^{-k_{3/2}x}]$$

$$-\frac{\Delta_0(2-\mu)\tau_{3/2}^0}{2\mu}(\bar{T}_2 - \bar{T}_1)\left(\tau_1^0 - \frac{2}{(1+\mu)^2}\tau_{3/2}^0\right)^{-1}(e^{-k_1 x} - e^{-k_{3/2}x}) \tag{21}$$

The final form of the flux for $x > 0$ is:

$$\xi\Sigma_f E\phi(E, x) = 1 + \frac{b_{1/2}(x)}{E^{1/2}} + \frac{b_1(x)}{E} + \frac{b_{3/2}(x)}{E^{3/2}} + \ldots \tag{22}$$

We note that for $x \to \infty$, $\phi(E)$ tends to the infinite medium value derived by Corngold.

For the spectrum in the half-space $x < 0$ we make the substitution $\bar{T}_2 \leftrightarrow \bar{T}_1$ and set $x = -x$.

4. NEUTRON CURRENT

The neutron current J is related to the gradient of the flux as follows

$$\xi\Sigma_f EJ(E, x) = \xi\Sigma_f ED(E, x)\frac{d\phi(E, x)}{dx}$$

$$= \frac{D(E, x)}{E}\frac{db_1(x)}{dx} + \frac{D(E, x)}{E^{3/2}}\frac{db_{3/2}(x)}{dx} + \ldots \tag{23}$$

for $x > 0$:

$$\frac{db_1}{dx} = -\tfrac{1}{2}(2-\mu)(\bar{T}_2 - \bar{T}_1)k_1 e^{-k_1 x}$$

$$\frac{db_2}{dx} = \frac{\Delta_0}{2\mu} f(\bar{T}_2 - \bar{T}_1)k_{3/2}e^{-k_{3/2}x}$$

$$+ \frac{\Delta_0(2-\mu)\tau_{3/2}^0}{2\mu} \frac{(\bar{T}_2 - \bar{T}_1)}{\left[\tau_1^0 - \frac{2}{(1+\mu)^2}\tau_{3/2}^0\right]}(k_1 e^{-k_1 x} - k_{3/2}e^{-k_{3/2}x})$$

5. REACTION RATE

The reaction rate of a 1/v absorber, with a cut-off at E_c can easily be calculated from the integral

$$R(x) = \int_{E_c}^{\infty} \frac{1}{v} \phi(E, x) dE$$

which from Eq.(22) becomes

$$\frac{R(x)}{R_f} = 1 + \tfrac{1}{2} \frac{b_{1/2}(x)}{E_c^{1/2}} + \tfrac{1}{3} \frac{b_1(x)}{E_c} + \tfrac{1}{4} \frac{b_{3/2}(x)}{E_c^{3/2}} + \ldots$$

R_f being the reaction rate in the pure 1/E flux and unaffected by moderator absorption or chemical binding.

6. MODERATOR MODELS

The results obtained above are illustrated for a crystal and a liquid, each being compared with the corresponding gas model.

The only parameter involved in the calculation, which depends on the chemical binding, is $\overline{T}$, the effective temperature of the scattering model. For a crystal this is given directly in terms of the phonon frequency spectrum.

$$\overline{T} = \tfrac{1}{2} \int_0^{\infty} f(\omega)\, \omega \coth \frac{\omega}{2T} d\omega$$

We shall discuss three forms of $f(\omega)$ for graphite to determine the sensitivity of the epithermal spectrum to the model, Thus, we shall consider: (1) Einstein model where $\Theta_E = 2000°K$; (2) Debye model where $\Theta_D = 2000°K$ and (3) Egelstaff model (E.G.1) where $\Theta = 2550°K$.

To describe the liquid we chose the "effective width" model, proposed by EGELSTAFF and SCHOFIELD [4]. Three cases are considered:

(1) Standard effective width model

$$\overline{T} = T(1 + \tfrac{1}{4} q^2)$$

$$q = q_0 = 3.7$$

(2) As for case (1), but with q a function of T

$$q = q_0 \left(\frac{T_0}{T} \right)^{1/2}$$

where $q_0 = 3.7$ at $T_0 = 293°K$. This can be shown to give a reasonable form to the effective width model for low temperatures, and for high temperatures $q \to 0$, in agreement with the gas model.

(3) As for case (1), but with the addition of an optical mode,

$$\overline{T} = (1-\beta)\overline{T}q + \beta\overline{T}_{op}$$

In this case $\overline{T}q$ is given by the expression in case (1), and $\overline{T}_{op}$ is given by the Einstein model with $\Theta_E = 4700°K$. The value of β, which is the weight of the optical mode, is taken to be 0.2.

7. DISCUSSION AND CONCLUSIONS

To compare the various models, we have plotted the reaction rate of a 1/v absorber as a function of position across the temperature discontinuity. Because of the limited range of validity of the asymptotic expansion it was necessary to introduce a cut-off at 0.35 eV; this is equivalent to finding the reaction rate of a 1/v absorber in a cadmium cover. The choice of 0.35 eV was made, not only because it corresponds to a practical thickness of cadmium (~ 0.01 in), but because only terms up to, and including, $E^{-3/2}$ were used in calculating the epithermal flux. It was not possible, therefore, to go to values of 0.2 eV as used by Corngold in his work. Corngold used terms through $E^{-7/2}$, which was possible because of the relative simplicity of the coefficients b_n. In the present work, the b_n are functions of position, and rapidly become very tedious to calculate.

Figure 1 shows the reaction rates in a moderator of unit nuclear mass. Various models have been used for the chemical binding. The gas model has the smallest reaction rate and a relatively small variation with position in going from 293 to 500°K. On the other hand, our effective width and modified effective width models have higher reaction rates (order of 12%) and a very much greater variation with position.

The effective width model, for which $q^2 \propto T^{-1}$, has a larger reaction rate than the gas but shows much the same variation with position. This is not surprising since the amplitude of the spatially varying terms in the $b_n(\underline{r})$ are proportional to $\overline{T}_1 - \overline{T}_2$. For the effective width model this leads to

$$\overline{T}_1 - \overline{T}_2 = (T_1 - T_2) + \frac{1}{4}(T_1 q_1^2 - T_2 q_2^2).$$

If $q^2 T$ is constant, then clearly this reduces to the gas model value. We may conclude that the spatial variation of the flux (or reaction rate) depends quite sensitively on the model and on its temperature variation.

Figure 2 shows reaction rates for a moderator of nuclear mass 12, in particular graphite, under various assumptions about the phonon frequency spectrum. The gas model is shown for comparison.

As far as variation with position is concerned, the crystal models show a behaviour which is very different from that in a liquid. In the present case

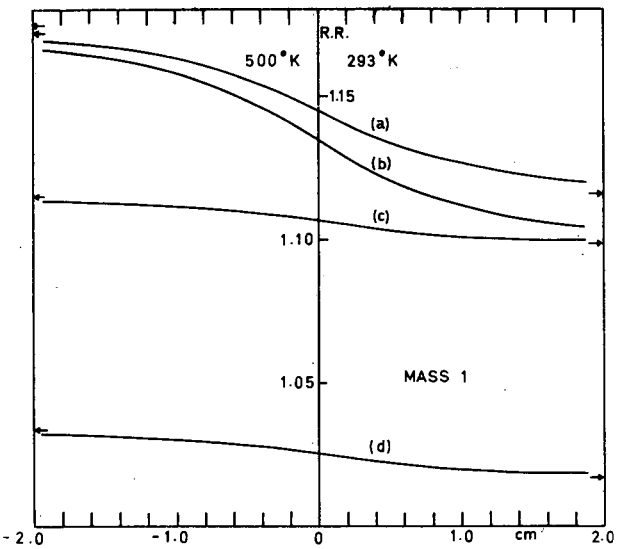

Fig. 1

Reaction rate of 1/v absorber in mass one moderator
(a) Effective width plus optical mode
(b) Effective width independent of temperature
(c) Effective width $q^2 \propto T^{-1}$
(d) Gas model
The arrows indicate asymptotic values.

it is the gas which shows the largest variation with position, and the bound models which predict a very small change in traversing the temperature discontinuity. This phenomenon may be explained easily if we consider the value of $\overline{T}$ for the Einstein model, namely

$$\overline{T} = \tfrac{1}{2}\,\Theta_E \coth\left(\frac{\Theta_E}{2T}\right)$$

Now if $\Theta_E/2T$ is greater than about 2, the "coth" term is essentially unity and $\overline{T} \doteq \frac{1}{2}\,\Theta_E$ irrespective of the value of the physical temperature. This is what occurs in the present example, for which $\Theta_E/2T_1 = 2$ and $\Theta_E/2T_2 = 3.4$, thus the values of $\overline{T}_1$ and $\overline{T}_2$ are 1002 and 1037°K, respectively. Similar behaviour occurs in the other models, although to a lesser extent. The small differences in shape may, however, be sufficient to distinguish one model from another.

One important observation which may be drawn from the present analysis is that the relaxation lengths involved, i.e. $k_{1/2}^{-1}$, k_1^{-1} and $k_{3/2}^{-1}$ are independent of the chemical binding and are functions of the moderator nuclear mass number only. In fact, these quantities are not relaxation lengths in the usual sense of "re-thermalization", i.e., they are not discrete space eigenvalues of the diffusion equation. This is not unexpected for the following reasons. One usually associates relaxation lengths with

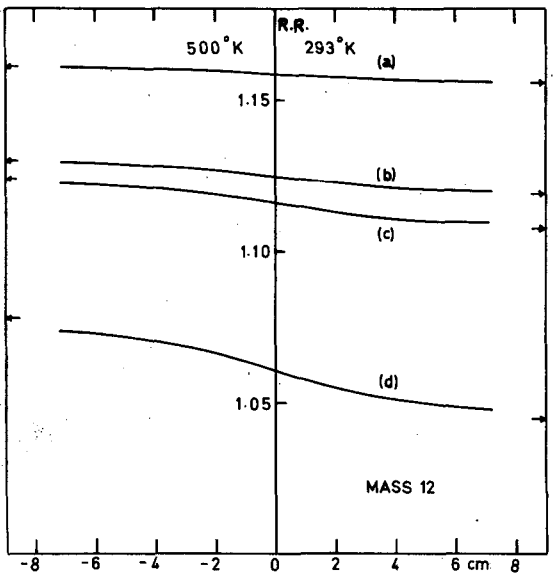

Fig. 2

Reaction rate of 1/v absorber in mass twelve moderator.
(a) Einstein crystal, $\Theta_E = 2000°K$
(b) Debye crystal, $\Theta_D = 2000°K$
(c) Egelstaff model E.G.I, $\Theta = 2550°K$
(d) Gas model
The arrows indicate asymptotic values.

discrete eigenvalues of the Boltzmann (or diffusion) equations; these discrete eigenvalues are in some way essentially concerned with the thermal or Maxwellian part of the spectrum and depend on quantities such as M_2, etc. The asymptotic part of the spectrum on the other hand is governed mainly by the continuum of eigenvalues. That this must be correct can be seen intuitively if we allow the temperature of the medium to go to zero. Then the discrete eigenvalues disappear and only the continuum remains to describe the energy spectrum. The concept of associating the continuum of eigenvalues with the slowing-down or epithermal part of the spectrum has received very little attention and certainly deserves further investigation.

To summarize; we have developed an analytical solution for the flux in an arbitrary temperature gradient in any moderator. It appears that measurements of the epithermal flux across a temperature discontinuity can provide useful information on the scattering law and discriminate between different models.

REFERENCES

[1] KOTTWITZ, D.A., Nucl. Sci. Engng 7 (1960) 345.
[2] KUŠČER, I., Proc. Brookhaven Conf. on Neutron Thermalization, BNL 719 4 (1962) 1255.
[3] CORNGOLD, N., Ann. Phys. 6 (1959) 368.
[4] EGELSTAFF, P. and SCHOFIELD, P., Nucl. Sci. Engng 12 (1962) 260.

APPENDIX I

THE τ_n^p COEFFICIENTS

$$\tau_{1/2}^0 = \frac{1+\mu}{1-\frac{1}{3}\mu}, \quad \tau_1^0 = \tfrac{1}{2}\,\frac{(1+\mu)^3}{1-\frac{1}{3}\mu}, \quad \tau_1^1 = (2-\mu)\overline{T}$$

$$\tau_{3/2}^0 = \frac{1}{6}\,\frac{(1+\mu)^6}{(1-\frac{1}{3}\mu)(1+\frac{1}{3}\mu+\frac{1}{3}\mu^2-\frac{1}{15}\mu^3)}$$

$$f = \frac{19}{6}\,\frac{(1+\frac{2}{3}\mu-\frac{10}{57}\mu^2-\frac{7}{57}\mu^4+\frac{2}{57}\mu^5)}{(1-\frac{1}{3}\mu)(1+\frac{1}{3}\mu+\frac{1}{3}\mu^2-\frac{1}{15}\mu^3)}$$

APPENDIX II

EXTENSION TO TRANSPORT THEORY

The extension of the method described in the text can be readily applied to transport theory. Thus, we have to consider the more general equation

$$\mu\,\frac{\partial\phi(E,x,\mu)}{\partial x} + [\Sigma_s(E,x)+\Sigma_a(E,x)]\,\phi(E,x,\mu) = \int_0^\infty \Sigma(E'\to E;x)\,\phi_0(E',x)\,dE'.$$

where for simplicity we have used plane geometry and isotropic scattering
Expanding the angular flux in the form

$$E\phi(E,x,\mu) = \sum_{n=0}^{\infty} \frac{a_n(x,\mu)}{E^{n/2}}$$

leads to the following set of equations for the $a_n(x,\mu)$.

$$\mu\,\frac{\partial a_0(x,\mu)}{\partial x} + \Sigma_f a_0(x,\mu) = \alpha\, a_{0,0}(x)$$

$$\mu\,\frac{\partial a_1(x,\mu)}{\partial x} + \Sigma_f a_1(x,\mu) + \Sigma_{a0} v_0 a_0(x,\mu) = \beta\, a_{1,0}(x)$$

$$\mu\,\frac{\partial a_2(x,\mu)}{\partial x} + \Sigma_f a_2(x,\mu) + \frac{\Sigma_f \overline{T}}{2A}\, a_0(x,\mu) + \Sigma_{a0} v_0 a_1(x,\mu) = \gamma\, a_{2,0}(x) + \overline{T}\,\delta\, a_{0,0}(x)$$

$$\mu \frac{\partial a_3(x,\mu)}{\partial x} + \tilde{\Sigma}_f a_3(x,\mu) + \frac{\Sigma_f \overline{T}}{2A} a_1(x,\mu) + \Sigma_{a0} v_0 a_2(x,\mu) = s a_{3,0}(x) + \overline{T} t a_{1,0}(x)$$

etc., where the coefficients $\alpha, \beta, \gamma, \delta, s, t$ are defined by

$$E\int_0^\infty \Sigma(E' \to E)\phi(E')dE' = \alpha a_{0,0} + \frac{\beta}{E^{1/2}} a_{1,0} + \frac{1}{E}(\gamma a_{2,0} + \overline{T}\delta a_{0,0})$$

$$+ \frac{1}{E^{3/2}}[s a_{3,0} + \overline{T} t a_{1,0}] + \ldots$$

These equations may be solved recursively, and are amenable to solution by the infinite medium Fourier transform technique. It is found that, in addition to the purely exponential terms in the solution, integral transient terms appear. In the case of the temperature discontinuity problem these transients are important near the interface.

There is an interesting point which it is relevant to discuss here concerning the accuracy of diffusion theory for these problems. As in the case of normal, uniform temperature problems, diffusion theory is valid provided the angular distribution of the flux can be represented by a linear expression in $\cos\theta$; this corresponds to $\nabla\phi$ being small. Now the gradient of the neutron flux in our non-uniform moderator is directly dependent on the gradient of the physical temperature ∇T, thus if ∇T is zero then $\nabla\phi$ is also, by definition of the problem. However, we have already shown that a large ∇T does not necessarily mean a large variation of flux with position. This was particularly evident in crystalline materials in which the binding was very tight. In this case then, diffusion theory will be valid over a larger physical temperature gradient. In hydrogenous moderators, on the other hand, the reverse effect occurs and we might be forced to use transport theory sooner than expected.

DISCUSSION

P. SCHOFIELD: First, I would like to disclaim any responsibility for the so-called "effective width model", which is referred to in section 6 of the paper. The form of frequency distribution on which it is based was devised to account for the diffusive motions in liquid moderators*, that is for something like 1% of the degrees of freedom. That this functional form could be used to represent the whole of $\rho(\epsilon)$ and so give a one-parameter set of scattering laws was suggested by Egelstaff, and this "model" has been used for calculation in water-moderated systems. It is only when one tries to "improve" the model by inclusion of a realistic representation of the molecular vibration that its inadequacy becomes apparent. This is to be discussed in a forthcoming publication. Although the model may be a useful

* SCHOFIELD, P., article on neutron scattering in: Fluctuation Relaxation and Resonance in Magnetic Systems, (TER HAAR, D., Ed.) Oliver and Boyd (1962).

theoretical toy for investigation of thermalization effects, using it to draw conclusions about the properties of a particular real moderator should be strongly discouraged.

A second point I would like to stress is a general one relating to these asymptotic expansions of the spectrum in inverse powers of E. In the literature, the expansion is usually written as a series in (T/E). This is misleading since in the approximations which are used to obtain the series the temperature does not enter explicitly; the important parameter is the "effective temperature" $\bar{T}$ (i.e. 2/3 × the mean kinetic energy of the atoms of the moderator). Thus even at T = 0 for a bound moderator the asymptotic expansions are valid.

The crucial dependence on $\bar{T}$ was illustrated in Williams' paper.

J. SHERWIN: Have the measurements on differentially heated graphite stacks made at Harwell any relevance to your paper?

M. M. R. WILLIAMS: Unfortunately not, because the spectra involved are purely thermal ones and possess no "1/E" tail.

H. POLLAK: Did you take account of the anisotropy of the media in your resolution of the diffusion equation, or is the medium an isotropic one?

M. M. R. WILLIAMS: The medium is isotropic as far as its physical form is concerned; however, I have included anisotropic scattering through the usual transport approximation.

ЭКСПЕРИМЕНТАЛЬНОЕ ИЗУЧЕНИЕ ПРОЦЕССА ТЕРМАЛИЗАЦИИ НЕЙТРОНОВ ВО ВРЕМЕНИ В ГРАФИТЕ И БЕРИЛЛИИ

В.И. МОСТОВОЙ, И.П. САДИКОВ, А.А. ЧЕРНЫШОВ, С.Н. ИШМАЕВ, М.С. ЮДКЕВИЧ и В.З. НОЗИК
ГОСУДАРСТВЕННЫЙ КОМИТЕТ ПО ИСПОЛЬЗОВАНИЮ АТОМНОЙ ЭНЕРГИИ СССР, ИНСТИТУТ АТОМНОЙ ЭНЕРГИИ ИМ. И.В. КУРЧАТОВА, МОСКВА, СССР

Abstract — Résumé — Аннотация — Resumen

EXPERIMENTAL STUDY OF THE NEUTRON-THERMALIZATION PROCESS IN TIME IN GRAPHITE AND BERYLLIUM. A description is given of an experimental facility for studying the establishment of an equilibrium neutron energy spectrum in various media. Short pulses of fast neutrons were produced in the moderators under study by means of a high-current electron linear accelerator. At various intervals following the production of the fast-neutron pulse, the neutron spectra were measured in a beam extracted from the moderator by means of a mechanical chopper phased to the operation of the accelerator. The optimum resolution in spectrum measurement was 2.5 μs/m and the minimum uncertainty in the measurement of slowing-down time was 3.5 μs.

Results are given for the measurement of non-stationary spectra in graphite ($B^2 = 8.9 \times 10^{-3}$ cm^{-2}) and in beryllium ($B^2 = 9.7 \times 10^{-3}$, 24×10^{-3}, 43×10^{-3} cm^{-2}) for slowing-down times of between 30 and about 2500 μs. The results measured in beryllium were compared with calculations of non-stationary spectra performed with double-differential cross-sections computed on the basis of experimental data on the energy spectrum of Be lattice vibrations.

The chemical binding and the thermal agitation of the atoms of the moderator were found to have a marked effect on the speed at which the neutron spectrum approaches the equilibrium spectrum even at times of about 30 μs, which corresponds to an average spectrum energy of about 1 eV for graphite and about 0.2 eV for beryllium. The total time needed to establish an equilibrium neutron spectrum was about 2000 μs in graphite and about 1000 μs in beryllium. The shape assumed by the neutron spectrum in small beryllium blocks is determined to a considerable extent by the effects of coherent scattering, the latter leading to the formation of so-called neutron traps which slow up the establishment of an equilibrium energy spectrum.

ÉTUDE EXPÉRIMENTALE DU PROCESSUS DE THERMALISATION DES NEUTRONS EN FONCTION DU TEMPS DANS LE GRAPHITE ET LE BÉRYLLIUM. Les auteurs décrivent une installation expérimentale permettant d'étudier le processus de formation d'un spectre énergétique des neutrons à l'état d'équilibre dans divers milieux. Pour obtenir des bouffées de neutrons rapides de courte durée dans les ralentisseurs considérés, on a utilisé un accélérateur linéaire de neutrons à courant intense. Le spectre des neutrons dans le faisceau à l'extérieur du ralentisseur était mesuré à des temps différents après la bouffée de neutrons rapides, au moyen d'un hacheur fonctionnant sur les mêmes phases que l'accélérateur. Le meilleur pouvoir de résolution obtenu pour la mesure du spectre était de 2,5 μs/m; l'indétermination minimale dans la mesure du temps de ralentissement s'élevait à 3,5 μs.

Les auteurs indiquent les résultats auxquels ils sont parvenus en mesurant les spectres non stationnaires dans le graphite ($B^2 = 8,9 \cdot 10^{-3}$ cm^{-2}) et dans le béryllium ($B^2 = 9,7 \cdot 10^{-3}$, $24 \cdot 10^{-3}$, $43 \cdot 10^{-3}$ cm^{-2}) pour des temps de ralentissement de 30 à environ 2500 μs. Les résultats des mesures relatives au béryllium sont comparés aux calculs des spectres non stationnaires qui ont été effectués en utilisant des sections efficaces doublement différentielles déterminées sur la base des données expérimentales concernant le spectre énergétique des oscillations du réseau de Be.

Le lien chimique entre les atomes du ralentisseur et leur mouvement thermique exerce une influence sensible sur la vitesse à laquelle le spectre des neutrons approche l'état d'équilibre, même pour des temps de l'ordre de 30 μs, ce qui correspond à une énergie moyenne du spectre d'environ 1 eV pour le graphite et de 0,2 eV pour le béryllium. Le temps nécessaire pour que le spectre des neutrons parvienne à l'état d'équilibre

est pour le graphite d'environ 2000 μs et pour le béryllium de l'ordre de 1000 μs. La formation du spectre des neutrons dans les blocs de béryllium de petites dimensions est déterminée dans une grande mesure par les effets de la diffusion cohérente qui provoque l'apparition de «pièges» à neutrons et de ce fait ralentit ce processus.

ЭКСПЕРИМЕНТАЛЬНОЕ ИЗУЧЕНИЕ ПРОЦЕССА ТЕРМАЛИЗАЦИИ НЕЙТРОНОВ ВО ВРЕМЕНИ В ГРАФИТЕ И БЕРИЛЛИИ. Описана экспериментальная установка для изучения процесса установления равновесного энергетического спектра нейтронов в различных средах. Короткие импульсы быстрых нейтронов в изучаемых замедлителях создавались с помощью сильноточного линейного ускорителя электронов. Спектры нейтронов в пучке, выведенном из замедлителя, измерялись в различные времена после импульса быстрых нейтронов с помощью механического прерывателя, сфазированного с работой ускорителя. Наилучшее разрешение в измерении спектров – 2,5 мксек/м, а минимальная неопределенность в измерении времени замедления – 3,5 мксек.

Приведены результаты измерений нестационарных спектров в графите ($B^2 = 8{,}9 \cdot 10^{-3}$ см$^{-2}$) и в бериллии ($B^2 = 9{,}7 \cdot 10^{-3}$, $24 \cdot 10^{-3}$, $43 \cdot 10^{-3}$ см$^{-2}$) в диапазоне времен замедления от 30 мксек до ~2500 мксек. Результаты измерений в бериллии сравниваются с расчетами нестационарных спектров, которые выполнены с использованием дважды дифференциальных сечений, вычисленных на основе экспериментальных данных об энергетическом спектре колебаний решетки Be. Химическая связь и тепловое движение атомов замедлителя оказвают заметное влияние на скорость приближения спектра нейтронов к равновесному даже при временах ~30 мксек, что соответствует средней энергии спектра ~1 эв для графита и ~0,2 эв для бериллия. Полное время, необходимое для установления равновесного спектра нейтронов, в графите ~2000 мксек и в бериллии ~1000 мксек.

Формирование спектра нейтронов в блоках бериллия малого размера существенным образом определяется эффектами когерентного рассеяния, которое приводит к образованию так называемых нейтронных ловушек, замедляющих процесс установления равновесного энергетического спектра.

ESTUDIO EXPERIMENTAL DEL PROCESO DE TERMALIZACION DE NEUTRONES EN EL GRAFITO Y EN EL BERILIO, EN FUNCION DEL TIEMPO. Los autores describen una instalación experimental para estudiar la formación de un espectro energético de neutrones en equilibrio, en diversos medios. Mediante un acelerador lineal de neutrones de elevada intensidad se produjeron en los moderadores estudiados impulsos breves de neutrones rápidos. Los espectros neutrónicos se midieron a diversos intervalos después de emitida dicha ráfaga de neutrones en un haz extraído del moderador mediante un interruptor mecánico en fase con el acelerador. El poder de resolución óptimo en la medición del espectro fue de 2,5 μs/m y la indeterminación mínima en la medición del tiempo de moderación, 3,5 μs.

Los autores presentan resultados correspondientes a la medición de espectros no estacionarios en grafito ($B^2 = 8{,}9 \cdot 10^{-3}$ cm^{-2}) y en berilio ($B^2 = 9{,}7 \cdot 10^{-3}$, $24 \cdot 10^{-3}$, $43 \cdot 10^{-3}$ cm^{-2}) para tiempos de moderación comprendidos entre 30 μs y unos 2500 μs. Los resultados obtenidos para el berilio se comparan con cálculos de espectros no estacionarios realizados con secciones eficaces de captura doblemente diferenciales, determinados sobre la base de datos experimentales relativos al espectro energético de las vibraciones en el reticulado de Be.

Se observó que la unión química y la agitación térmica de los átomos del moderador ejercen una gran influencia sobre la velocidad a la cual el espectro neutrónico se aproxima al equilibrio, aun para tiempos del orden de 30 μs, que corresponden a una energía espectral media de aproximadamente 1 eV para el grafito y alrededor de 0,2 eV, para el berilio. El tiempo total necesario para que el espectro neutrónico alcance el equilibrio fue de unos 2000 μs en el grafito y del orden de 1000 μs en el berilio. La forma que adopta el espectro neutrónico en pequeños bloques de berilio queda determinada en gran medida por los efectos de la dispersión coherente, que provoca la aparición de «trampas» neutrónicas, frenando así el proceso.

1. ВВЕДЕНИЕ

Экспериментальное изучение процесса термализации нейтронов во времени дает ценную информацию о влиянии химической связи и теплового движения атомов на формирование равновесного спектра нейтронов в за-

медлителе. Результаты таких экспериментов позволяют проверять различные математические методы расчета нейтронных спектров и достоверность используемых в этих расчетах данных о дважды дифференциальных сечениях рассеяния нейтронов.

Изучение нестационарных спектров важно также для дальнейшего развития метода нестационарной диффузии [1,2] , который является в настоящее время одним из основных методов исследования нейтронно-физических параметров замедлителей и размножающих сред. Сведения о формировании во времени равновесного спектра нейтронов представляют большой интерес для анализа данных по нестационарной диффузии. Они позволяют более точно определить ограничения и возможности этого метода.

Данные по нестационарным спектрам важны также в связи с созданием более совершенных импульсных источников холодных и тепловых нейтронов, необходимых для исследований по нейтронной физике, физике твердого тела и др. .

До последнего времени экспериментальные работы по нестационарным спектрам касались, главным образом, измерения их интегральных характеристик: так называемого коэффициента диффузионного охлаждения (C) и связанной с ним константы термализации (τ_{th}). В материалах Брукхейвенской конференции по термализации (1962 г.) опубликована работа Бернарда и др. [3] по прямому измерению нестационарных спектров в графите. Измерения выполнены с разрешением ~70 мксек в интервале времен замедления 300 ÷ 1000 мксек, который относится к заключительному этапу термализации.

В 1964 году группой американских исследователей опубликованы измерения нестационарных спектров в бериллиевой системе малых размеров [4]. Представленные в этой работе результаты относятся к большим временам замедления и имеют предварительный характер.

В публикуемой работе приведены результаты измерений нестационарных спектров, выполненных в графитовой и бериллиевых системах различных размеров, в широком диапазоне времен замедления. Результаты измерений в бериллии сравниваются с расчетами нестационарных спектров, которые выполнены с использованием дважды дифференциальных сечений, рассчитанных на основе экспериментальных данных об энергетическом спектре колебаний решетки Be.

2. МЕТОДИКА ИЗМЕРЕНИЙ И ОБРАБОТКА ЭКСПЕРИМЕНТАЛЬНЫХ РЕЗУЛЬТАТОВ.

Схема экспериментальной обстановки изображена на рис.1. Пучок электронов линейного ускорителя с помощью магнитной системы с поперечным полем отклонялся и фокусировался на свинцовую мишень, находящуюся внутри исследуемого замедлителя, создавая короткие (~0,6 мксек) вспышки быстрых нейтронов с максимальной частотой 100 гц . Спектры нейтронов измерялись в различные моменты времени после вспышки быстрых нейтронов методом времени пролета с помощью механического прерывателя, сфазированного с работой линейного ускорителя. Фазирование осуществлялось путем запуска ускорителя в определенный момент времени от стартового сигнала, приходящего с механического прерывателя. Мо-

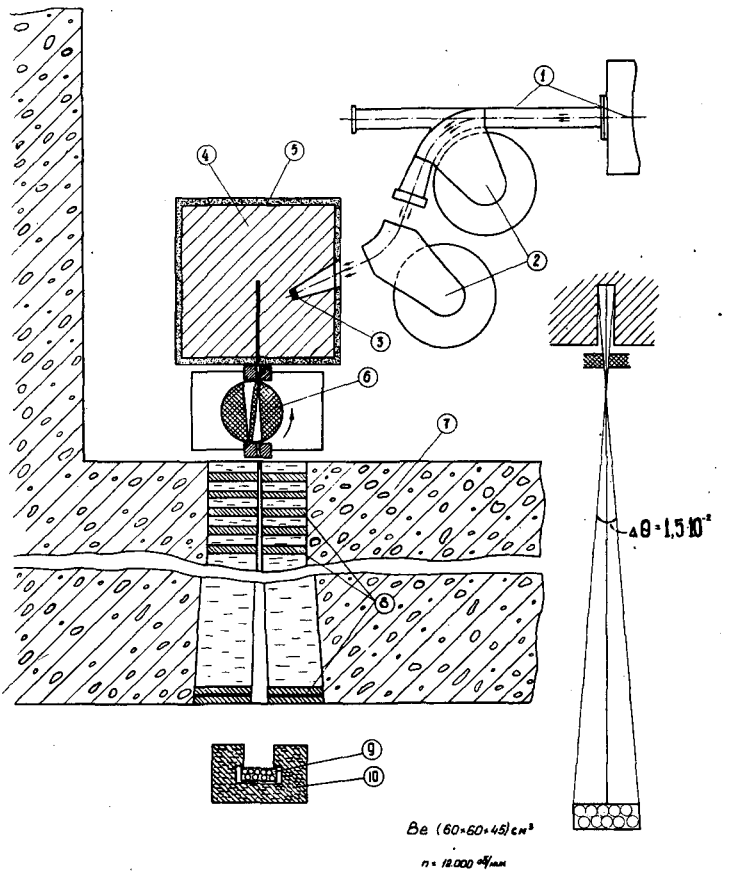

Рис.1

Экспериментальная установка.
1 – линейный ускоритель, 2 – магнитная отклоняющая система, 3 – свинцовая мишень, 4 – исследуемый замедлитель, 5 – карбид бора и кадмий, 6 – прерыватель, 7 – биологическая защита ускорителя, 8 – коллиматор, 9 – детектор, 10 – водный раствор борной кислоты.

мент открытия щели прерывателя фиксировался с помощью импульса, возникавшего от метки, предварительно записанной на магнитной дорожке ротора. Схема задержки, стабилизированная кварцем, позволяла в широких пределах через 1 мксек менять время сдвига T между запуском ускорителя и моментом открытия щели прерывателя. Постоянство скорости вращения механического прерывателя поддерживалось специальной электронной схемой стабилизации, опорная частота которой задавалась кварцевым генератором. Все это позволило определять величину временного сдвига T с точностью ±0,5 мксек.

Ротор прерывателя диаметром 150 мм был изготовлен из стеклопластика с 5% добавкой бора. Он имел две щели расходящегося профиля (рис.2), которые обеспечивали постоянство функции пропускания во всем исследуемом диапазоне энергий. Было изготовлено несколько прерыва-

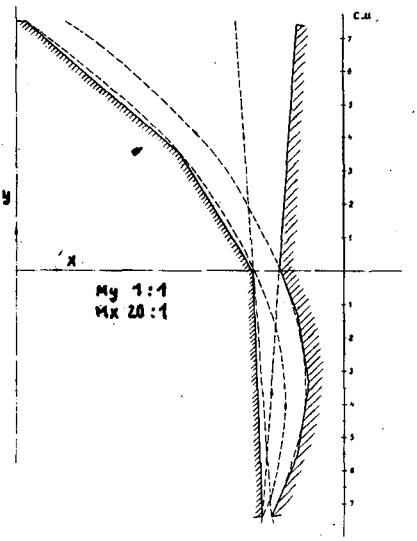

Рис.2

Профиль щели прерывателя.

телей, отличающихся шириной щели. Это позволяло выбирать оптимальное соотношение между разрешением и светосилой в конкретных условиях измерений. Минимальная длительность нейтронного импульса составляла 2,5 мксек при скорости вращения 12 000 об/мин. На расстоянии $\mathscr{L} = 4$ м от прерывателя располагался детектор нейтронов, состоящий из 10 пропорциональных счетчиков BF_3 диаметром 38 мм каждый.

Для иллюстрации на рис.3 представлены типичные экспериментальные спектры, получаемые на каналах временного анализатора. Первые каналы анализатора ($n_к < 40$) регистрируют фон, обусловленный, в основном, быстрыми нейтронами, проходящими сквозь защиту. Видно, что фон существенен только в измерениях спектров при малых временах сдвига T.

После вычета фона экспериментальные спектры нормировались в соответствии с показаниями монитора, шириной канала временного анализатора и длительностью нейтронного импульса.

Дополнительной трудностью при измерении нестационарных спектров является трансформация спектра, возникающая при движении нейтронов от дна полости в замедлителе до прерывателя. Измеряемый непосредственно в эксперименте трансформированный спектр нейтронов $\tilde{\Phi}(v,t)$ связан с интересующим нас спектром нейтронов в призме $\Phi(v,t)$ преобразованием координат:

$$\Phi(v,t) = \tilde{\Phi}\left(v, t+\frac{\ell}{v}\right), \qquad (1)$$

где v — скорость нейтрона; t — время, отсчитываемое от момента вспышки ускорителя; ℓ — расстояние от дна полости в замедлителе до прерывателя.

Для того, чтобы из измеренной скорости счета на каналах временного анализатора получить истинный спектр нейтронов $\Phi(v,t)$, необходимо, кроме указанного преобразования координат, учесть еще ряд обыч-

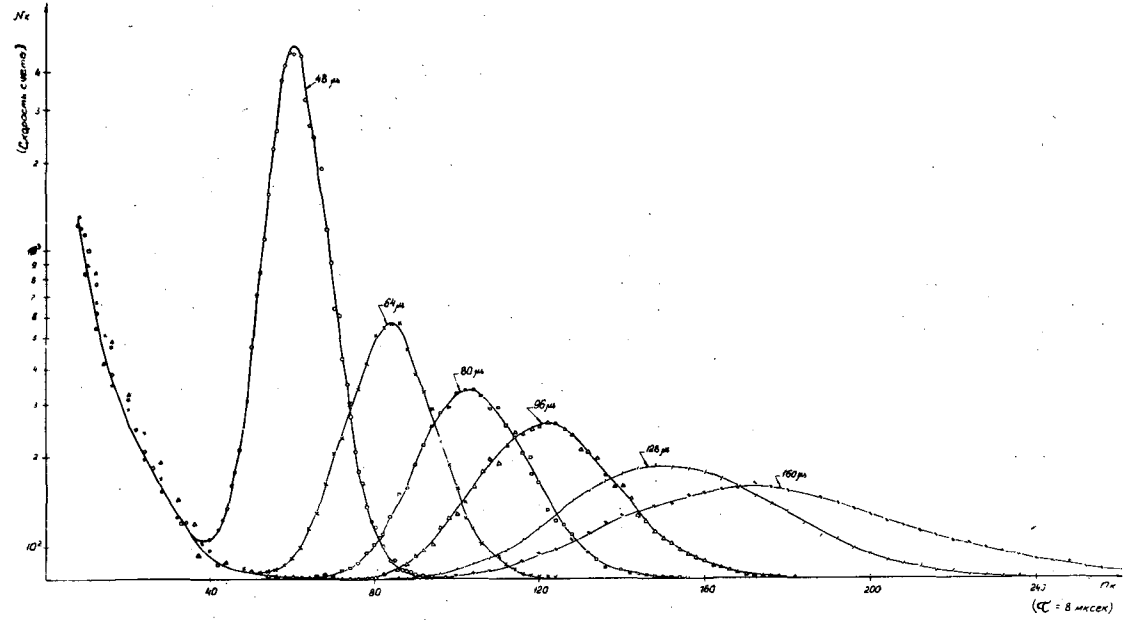

Рис.3

Экспериментальные спектры.

ных аппаратурных поправок: эффективность детектора, поглощение нейтронов в воздухе и конструкционных материалах, пропускание прерывателя. Эффективность детектора была определена экспериментально. Функция пропускания прерывателей, как показали специальные измерения, не зависела от скорости нейтронов во всей исследованной области энергий.

3. МЕТОДИКА РАСЧЕТА НЕСТАЦИОНАРНЫХ СПЕКТРОВ

Расчет спектра нейтронов проводился в P_1 –приближении. Распределение нейтронов $N(E, \vec{r}, t)$ разлагалось по собственным функциям пространственной задачи. Тогда кинетическое уравнение сводится к системе интегро-дифференциальных уравнений для энергетического спектра каждой гармоники $n(E, t)$:

$$\begin{aligned} \frac{\partial n}{\partial t} &= v\mathcal{J}(E,t) + \int \Sigma_s(E' \to E)\, v' n(E', t)\, dE' - \Sigma_t(E) v n(E,t) + Qn(E) \\ \frac{\partial \mathcal{J}}{\partial t} &= -\frac{1}{3} B^2 v n(E,t) + \int \Sigma_s^{(1)}(E' \to E)\, v' \mathcal{J}(E', t)\, dE' - \Sigma_t(E) v\, \mathcal{J}(E) + Q_{\mathcal{J}}(E), \end{aligned} \qquad (2)$$

$\mathcal{J}(E,t)$ – спектр тока нейтронов; $\Sigma_s(E \to E')$ и $\Sigma_s^{(1)}(E \to E')$ – нулевой и первый угловые моменты дважды дифференциального сечения рассеяния; B^2 – собственное число рассматриваемой гармоники.

По энергии в системе (2) осуществлялся переход к многогрупповому представлению. Ширина группы менялась $\sim \overline{E}$, что позволило с помощью 40 групп охватить достаточно широкую область энергий и одновременно получить хорошее разрешение при малых энергиях, где проявляются когерентные эффекты. По времени задача решалась методом Рунге-Кутта [5]. Расчет производился для основной пространственной гармоники.

Дифференциальные сечения рассчитывались в некогерентном гауссовском приближении по программе "ПРАССИВ" [6], [7]. Спектр колебаний решетки Be был взят из работы [8], где он получен из экспериментов по рассеянию нейтронов. Упругое сечение при малых энергиях рассчитывалось с учетом когерентных эффектов.

Полное сечение близко к рассчитанному Бандари [9] и совпадает с измеренным экспериментально [10]. Хорошее совпадение вычисленного и измеренного сечений в области за последним бреговским скачком свидетельствует о том, что сечение неупругого рассеяния при этой энергии рассчитано верно.

4. РЕЗУЛЬТАТЫ ИЗМЕРЕНИЙ В БЕРИЛЛИЕВОЙ СИСТЕМЕ БОЛЬШИХ РАЗМЕРОВ

Спектры нейтронов были измерены в призме размерами $(60 \times 60 \times 45)$ см^3. Бериллиевая призма таких размеров является достаточно большой, чтобы утечка нейтронов из нее не оказывала существенного влияния на процесс

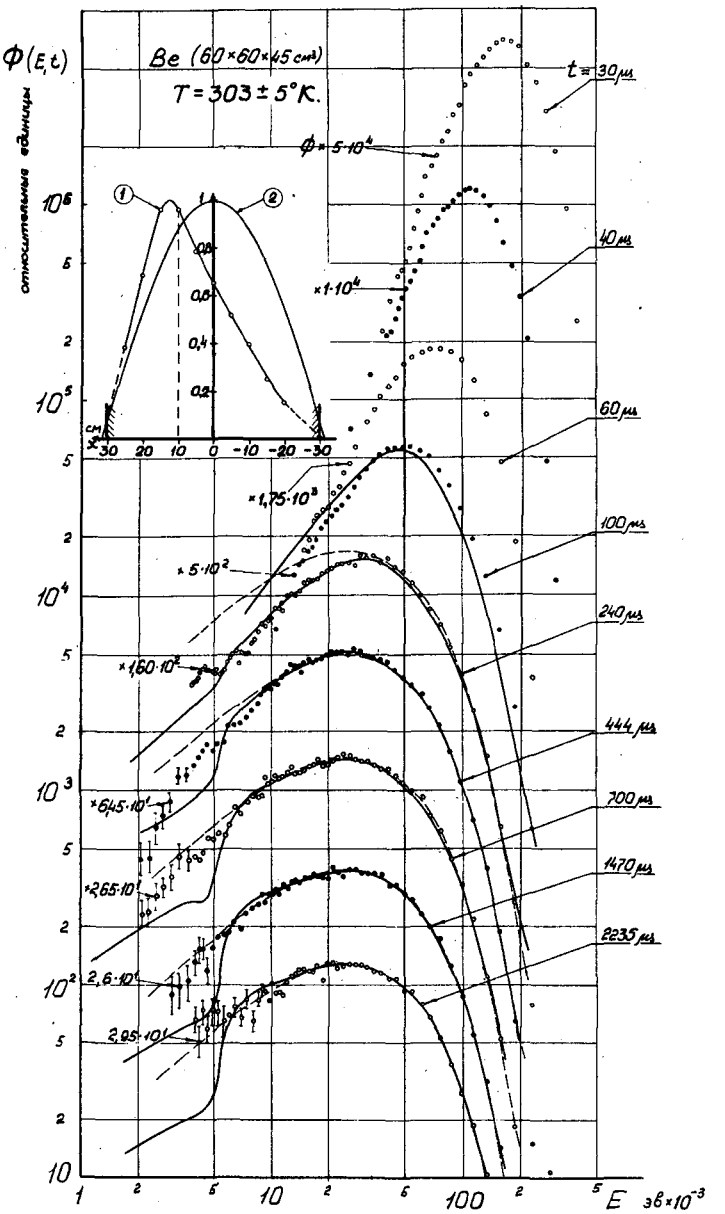

Рис. 4

Эволюция спектра нейтронов
в Be $(60 \times 60 \times 45)$ см^3 во времени:
——— расчет;
- - - - распределение Максвелла;
$KT = KT_{ср} = 26{,}1$ мэв.
1 – распределение плотности тепловых нейтронов, измеренное медными индикаторами вдоль оси x;
2 – асимптотическое пространственное распределение $\left(A\cos\frac{\pi x}{\alpha}\right)$

термализации. Пространственное распределение плотности тепловых нейтронов в призме, измеренное с помощью медных фольг, отличалось от равновесного (косинусо-идального) распределения и имело максимум вблизи источника (см.рис.4а), находящегося в точке с координатами: x = 11 см, y = 6,3 см, Z = 8 см. Пучок нейтронов через канал сечением 1 × 10 см² выводился в направлении оси x из точки с координатами: x = 11 см, y = 0 и Z = 0*.

Спектры нейтронов были измерены при 16 различных значениях временного сдвига (T): 24, 28, 32, 48, 56,64, 80, 96, 128, 192, 256, 320, 480, 768, 1536 и 2540 мксек. Эти измерения позволили получить $\Phi(E,t)$ в интервале времен замедления от 30 мксек до 2210 мксек.

На рис.4 представлена эволюция энергетического спектра нейтронов в бериллии во времени.

В области малых времен замедления, когда энергия нейтрона много больше энергии межатомных связей и тепловых колебаний атомов в кристаллической решетке, процесс замедления можно рассматривать происходящим на свободных и покоящихся ядрах (для Be: $K\theta_D \simeq 0{,}1$ эв.) Для этого случая в работах [11] [12] было получено приближенное выражение для спектра замедляющихся нейтронов от импульсного источника. На рис.5 и в табл.1 приведена зависимость средней энергии нейтронов $\langle E \rangle$ в бериллии от времени замедления, найденная из экспериментальных спектров. Наклонные прямые представляют $\langle E(t) \rangle$, вычисленные для свободных и покоящихся ядер по результатам работы [11]. Видно, что в пределах исследованной области малых времен замедления экспериментальные значения $\langle E \rangle$ лежат заметно выше расчетных. Этот результат свидетельствует о том, что кристаллические связи и тепловое движение атомов Be начинают влиять на процесс замедления при достаточно высоких энергиях нейтронов, заметно превышающих 0,2 эв. Расчеты дважды дифференциального сечения показывают, что переход к рассеянию на свободных и покоящихся ядрах в Be происходит при энергиях ~1 эв.

Дальнейшее формирование равновесного спектра нейтронов качественно происходит следующим образом. Спустя ~200 мксек после нейтронного импульса большая часть спектра совпадает с распределением Максвелла с $KT_{ср} = 0{,}026$ эв, но в области малых энергий экспериментальные точки лежат заметно ниже. Это отклонение уменьшается с течением времени — происходит сравнительно медленное заполнение низкоэнергетической части спектра. При ≃1000 мксек спектр нейтронов в бериллии имеет практически максвелловский вид с температурой среды во всей области энергий выше ~5 мэв.

На рис.4 показаны также спектры, полученные расчетным путем (сплошные кривые). В качестве источника был взят экспериментальный спектр при t = 60 мксек, который заведомо не был искажен разрешением по времени замедления. При сравнении с экспериментом расчетные спектры нормировались по полной плотности нейтронов.

Некоторое различие, наблюдаемое при t = 100 мксек, указывает, повидимому, на то, что использованное сечение дает завышенный средний

---

* В процессе измерения наблюдалось некоторое непостоянство температуры бериллия, обусловленное выделением тепла на мишени. Поэтому температура исследуемого материала известна с некоторой неопределенностью (T = 30° ±5° C).

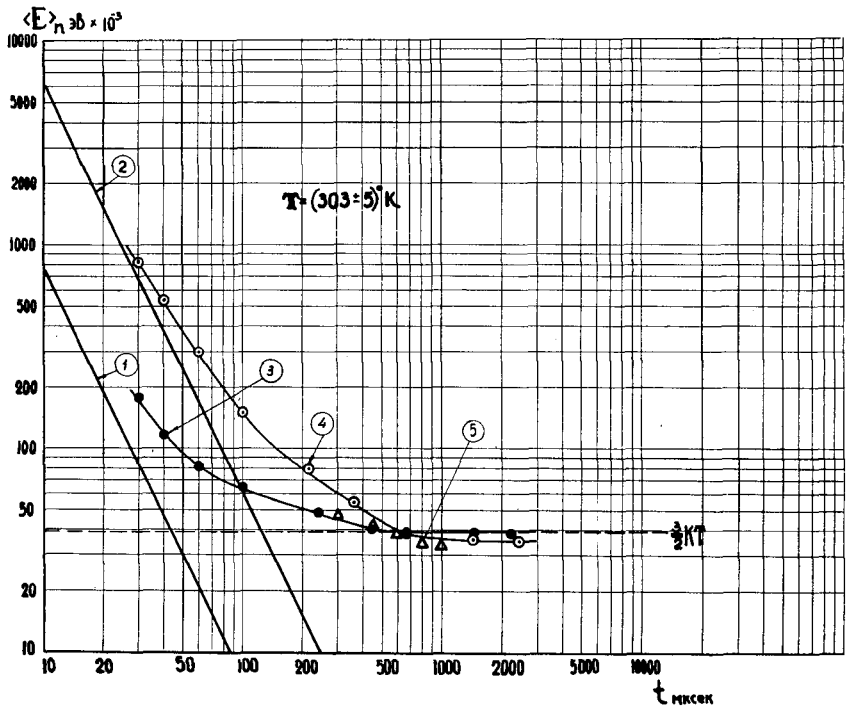

Рис.5

Зависимость средней энергии плотности нейтронов от времени замедления.
1 – расчет [11] для Be; 2 – расчет [11] для графита;
3 – экспериментальные данные для Be (60 × 60 × 45)см^3;
4 – экспериментальные данные для графита (60 × 60 × 45)см^3;
5 – экспериментальные данные для графита [3]
$B^2 = 6{,}43 \cdot 10^{-3}$ см$^{-2}$.

сброс энергии при рассеянии. Отчасти это расхождение может быть связано с влиянием высших пространственных гармоник. При больших временах согласие расчета с экспериментом удовлетворительное, за исключением области ниже последнего брегговского скачка ($E < 5$ мэв). Поток "холодных" нейтронов в измеренном спектре может быть несколько завышен за счет влияния градиента потока, т.к. спектр измерялся в точке, где при больших временах градиент отличен от нуля (см. рис. 4а).

Средняя энергия нейтронов (рис. 5) при больших временах медленно приближается к асимптотическому значению $\langle E \rangle_{ac} = 3/2$ KT, которое равно средней энергии равновесного спектра в среде бесконечных размеров.*

Результаты эксперимента и расчеты показывают, что область, в которой измерение средней энергии нейтронов со временем может быть описано с помощью одного параметра – времени термализации (τ_{th}), ограничивается значениями $\langle E \rangle$ очень мало отличающимися от асимптотического (не более, чем на несколько процентов).

* Начало координат находится в центре призмы.

Таблица 1

Be $\rho = 1{,}85$ г/см^3; $T = 303 \pm 5^\circ$ K

Размеры сборки	(60×60×45) см^3									(30×30×45)			(30×25×21)		
t мксек	30	40	60	100	240	444	700	1470	2236	420	680	930	230	420	680
$\langle E \rangle_n$ *) эв	0,1773	0,1159	0,0822	0,0650	0,0493	0,0398	0,0391	0,0393± ±0,0008	0,0387± ±0,0011	0,0392 ± ±0,0004	0,0394 ± ±0,0005	0,0397 ± ±0,0007	0,0405 ± ±0,0002	0,0390 ± ±0,0003	0,0386 ± ±0,0006
$\int n(E)\,dE$ **)	$3{,}472 \cdot 10^5$	$2{,}480 \cdot 10^5$	$2{,}339 \cdot 10^5$	$2{,}743 \cdot 10^5$	$2{,}336 \cdot 10^5$	$1{,}530 \cdot 10^5$	$1{,}006 \cdot 10^5$	$2{,}719 \cdot 10^4$	$9{,}169 \cdot 10^3$	$2{,}552 \cdot 10^4$	$1{,}149 \cdot 10^4$	$5{,}119 \cdot 10^3$	$2{,}480 \cdot 10^4$	$8{,}048 \cdot 10^3$	$2{,}049 \cdot 10^3$

*) Указаны статистические ошибки измерений.

**) Немонотонный ход $\int n(E)\,dE$ связан с тем, что спектры нейтронов измерены в точке, удалённой на расстоянии ~10 см от источника.

Таблица 2

ГРАФИТ $(60 \times 60 \times 45)$ см^3 $\rho = 1{,}67$ г/см^3; $T = 303 \pm 5°$ K

t мксек	30	40	60	I00	2I5	360	663	I430	2455
$\int_0^\infty \Phi(E)dE$	I6048	94249	46517	I3525	4I25	I825	699	I80	38
$\int_0^\infty n(E)dE$	52525	36316	2I900	I0685	4750	2580	I23I	309	65
$\langle E \rangle_\Phi = \frac{\int_0^\infty \Phi(E)E\,dE}{\int_0^\infty \Phi(E)dE}$ *)	0,8957	0,6I73	0,3403	0,I687	0,0845	0,0670	0,05I5 ± ± 0,00I5	0,0494± ± 0,002I	0,0488± ± 0,0022
$\langle E \rangle_n = \frac{\int_0^\infty n(E)E\,dE}{\int_0^\infty n(E)dE}$ *)	0,8220	0,5350	0,2960	0,I477	0,0704	0,0552	0,0397 ± ± 0,00I2	0,0358± ± 0,00I5	0,0352± ± 0,00I6

*/Указаны статистические ошибки измерений.

Качественно процесс термализации в различных замедлителях можно характеризовать временем, необходимым для установления полного равновесия. Проведенные исследования показывают, что для бериллия это время $\simeq 1000$ мксек.

5. ИЗМЕРЕНИЕ НЕСТАЦИОНАРНЫХ СПЕКТРОВ В БЕРИЛЛИЕВЫХ БЛОКАХ МАЛЫХ РАЗМЕРОВ

Для выснения влияния утечки нейтронов из кристаллического замедлителя на процесс формирования равновесного энергетического распределения были проведены измерения нестационарных спектров нейтронов в малых блоках бериллия размерами $(30 \times 30 \times 45)$ см^3 и $(30 \times 25 \times 21)$см^3. Эти исследования выполнены при сравнительно больших временах замедления, когда энергетический спектр нейтронов должен быть близок к равновесному. Пучок выводился из центра системы, где градиент потока равен нулю. Поэтому, измеряемый спектр был близок к спектру скалярного потока нейтронов. Следует отметить, что в системах таких небольших размеров за счет сильной утечки в процессе замедления высшие пространственные гармоники быстро затухают и должно установиться равновесное пространственное распределение нейтронов. На рис.6 и 7 приведены результаты измерений. С уменьшением размеров бериллиевой системы в области малых энергий обнаруживаются немонотонные отклонения спектра от максвелловского распределения. Причем эти отклонения проявляются особенно отчетливо в блоке Be наименьшего размера $(30 \times 25 \times 21)$ см^3. На рисунках представлена также зависимость от энергии транспортного сечения $\sigma_{tr}(E)$ для Be. Видно, что появление провалов и пиков в нейтронном спектре в точности следует за ходом σ_{tr} с энергией. Это связано с тем, что из блока малых размеров преимущественно вытекают нейтроны, для которых коэффициент диффузии $D = (\lambda_{tr}/3)\,v$ имеет наибольшее значение.

В результате происходит относительное обогащение спектра нейтронами, энергия которых соответствует максимумам в σ_{tr}. Как показано в работе [13], этот эффект "нейтронных ловушек" имеет существенное значение при анализе экспериментов, проводимых методом нестационарной диффузии в кристаллических замедлителях.

Расчетные спектры также содержат указанные немонотонности, которые хорошо согласуются с особенностями экспериментальных спектров. В области "нейтронной ловушки" при 8 мэв рассчитанный поток несколько выше измеренного, что может быть связано с уменьшением сечения рассеяния вследствие эффекта экстинкции.

Расчет показывает, что спектр при $t = 680$ мксек еще не асимптотический. Для установления полного равновесия необходимо время ~ 1800 мксек, что значительно больше, чем в среде больших размеров. Средняя энергия асимптотического спектра оказывается равной 1,36 КТ.

Расчеты асимптотических спектров, проведенные Иха [14], дают несколько меньшее значение $\langle E \rangle_{ac}$, что может быть связано с использованием в работе [14] дебаевской модели для кристалла бериллия.

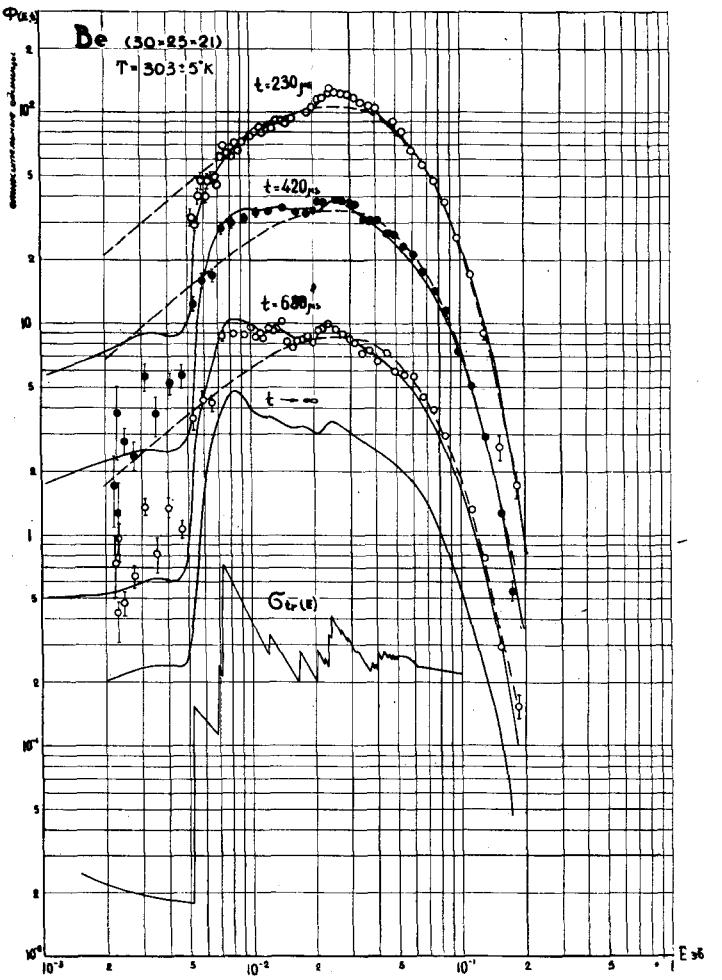

Рис.6

Нестационарные спектры нейтронов в Be (30 × 25 × 21) см³:
——— расчет;
- - - - $\Phi(E) \sim E e^{-E/KT_{ср}}$ $KT_{\varphi} = 26{,}1$ мэв

6. ИЗМЕРЕНИЕ НЕСТАЦИОНАРНЫХ СПЕКТРОВ В ГРАФИТЕ

Измерения спектров в графите были выполнены в системе размеров (60 × 60 × 45) см³ в тех же экспериментальных условиях, в которых производились измерения в бериллии. Результаты измерений $\Phi(E,t)$ представлены на рис.8. По измеренным спектрам была найдена средняя энергия нейтронов, значения которой приведены в табл.2 и показаны на рис.5.

В графите при малых временах замедления $\langle E \rangle$, полученное в эксперименте, ближе к значению, вычисленному для свободных и покоящихся ядер, чем в случае бериллия. Однако и для графита заметно отличие от

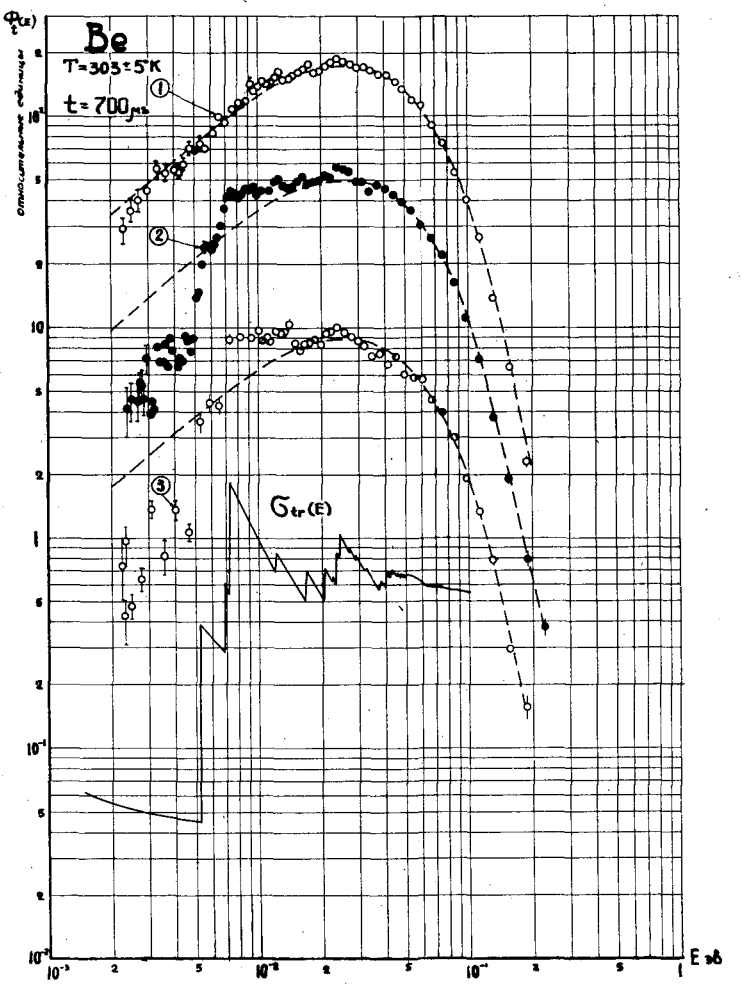

Рис.7
Влияние утечки на форму спектра в Be:
1 – (60 × 60 × 45) см³, 2 – (30 × 30 × 45) см³;
3 – (30 × 25 × 21) см³, - - спектр Максвелла.
$KT_{ср}$ = 26,1 мэв.

расчета, свидетельствующее о влиянии химической связи и теплового движения даже при $\langle E \rangle \sim 1$ эв. В связи с этим интересно отметить результаты работы [15], в которой изучалось влияние теплового движения на начальную фазу термализации. Выполненные расчеты показывают, что тепловое движение практически не будет сказываться только при энергии ~3 эв.

На рис.9 форма спектра, измеренная при t = 30 мксек, сопоставляется с вычисленной для свободных и покоящихся ядер графита, согласно работе [16]. Формы спектров близки, если иметь в виду, что вид экспериментального спектра может быть несколько искажен за счет неточностей при введении поправок на разрешение установки.

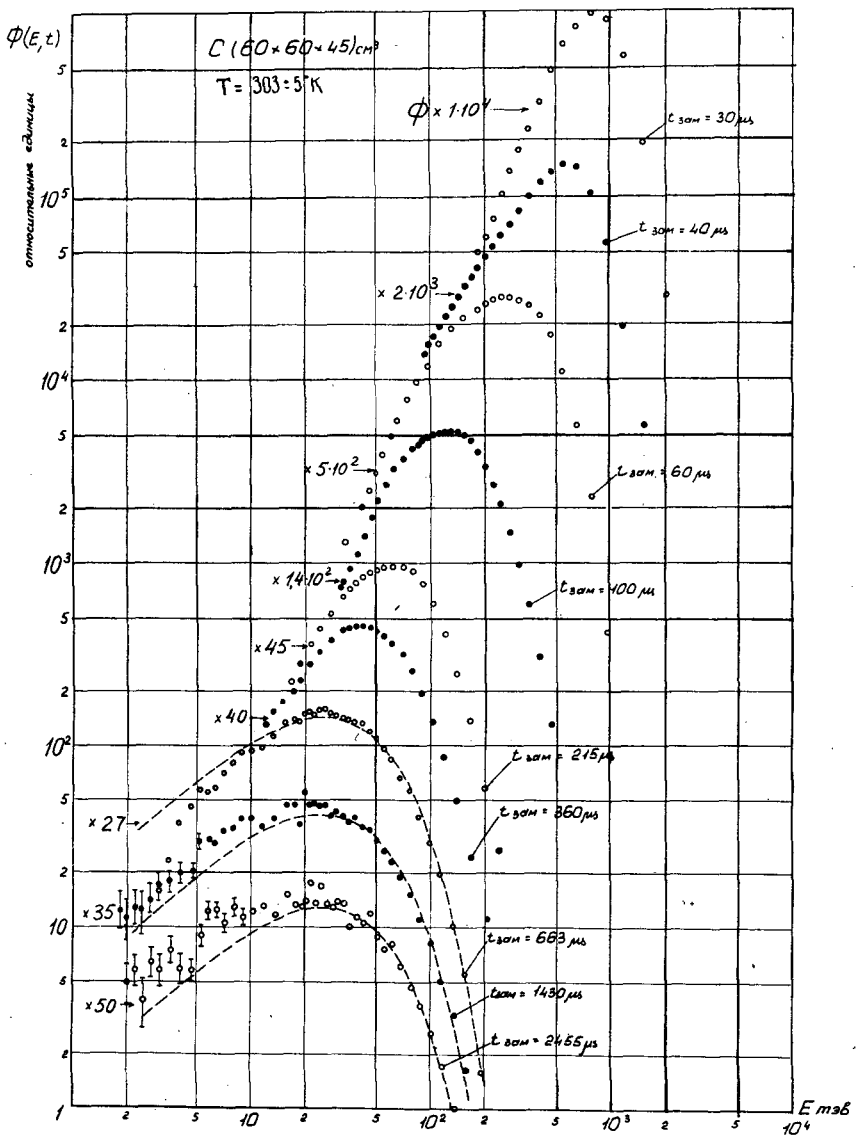

Рис. 8

Эволюция спектра нейтронов в графите (60 × 60 × 45) см³ во времени:
- - - распределение Максвелла; $KT_{ср} = 26{,}1$ мэв.

Из сопоставления рис. 4 и 8 видно, что характер приближения спектра нейтронов к равновесию в графите в общих чертах таков же, как и в бериллии. Однако в связи с большой величиной утечки, равновесный спектр нейтронов в графите отличается от максвелловского вида. На его форму заметное влияние оказывает эффект диффузионного охлаждения. Вследствие этого при больших временах замедления $\langle E \rangle$ оказывается меньше

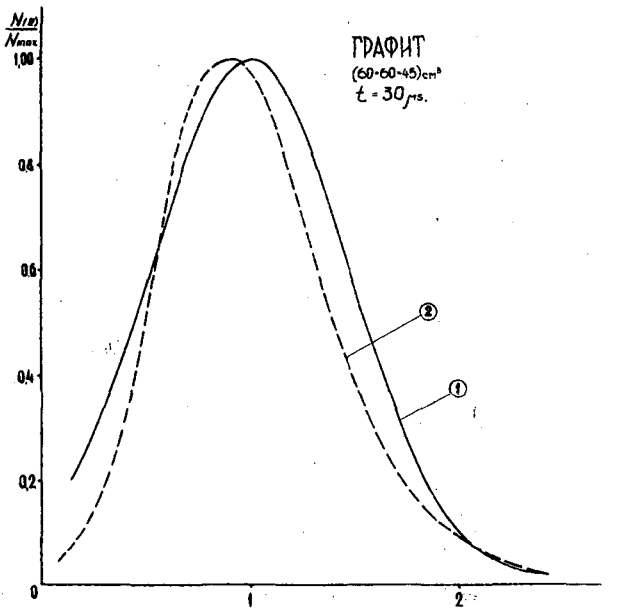

Рис.9

Форма спектра нейтронов в графите при t −30 мксек:
1 − расчет [16]; 2 − эксперимент.

равновесного значения для среды бесконечных размеров −3/2 КТ (рис.5). Из имеющихся экспериментальных данных трудно точно оценить асимптотическое значение <E> поскольку нет полной уверенности, что при t = 2400 мксек достигнут асимптотический вид спектра. Из проведенных измерений следует, что полное время термализации в графите составляет не менее 2000 мксек, что согласуется с результатами работы [17].

На рис.5 показаны значения <E>, полученные в упоминавшейся работе [3], в которой выполнены измерения спектров нейтронов в графитовой призме с $B^2 = 6{,}43 \cdot 10^{-3}$ см². Видно, что, несмотря на больший размер системы, экспериментальные точки, полученные в работе [3], лежат систематически ниже значений <E>, измеренных нами. Одной из возможных причин имеющегося расхождения является, вероятно, некоторое различие температур среды в обоих измерениях. Однако только этим обстоятельством нельзя объяснить полностью наблюдаемых расхождений.

На рис.10 сопоставляются зависимость средней энергии от времени в графите, полученная в данном эксперименте и рассчитанная в работе [18] с использованием сечения рассеяния, вычисленного по модели Паркса. Видно, что рассчитанные спектры заметно мягче, чем экспериментальные, хотя времена, необходимые для достижения равновесия − близки. В некоторой степени имеющееся расхождение можно объяснить за счет того, что при расчете не учитывалось влияние когерентных эффектов на утечку нейтронов из среды ограниченных размеров.

Основное различие в замедляющих и термализующих свойствах графита и бериллия связано с различием масс их ядер. Это можно видеть,

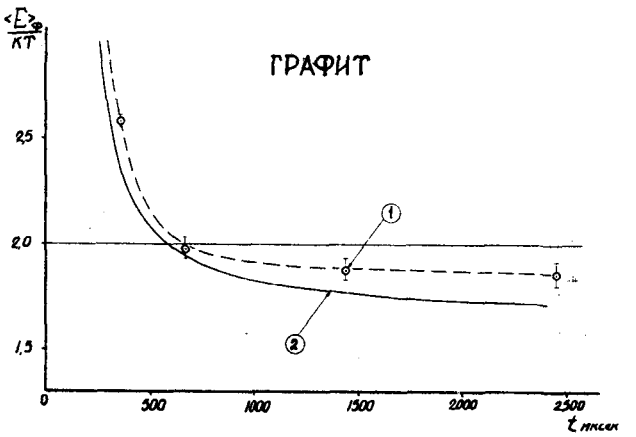

Рис.10

Средняя энергия потока нейтронов в графите как функция времени: 1 – эксперимент ($B^2 = 8{,}9 \cdot 10^{-3}$ см$^{-2}$); 2 – расчет [18] ($B^2 = 9{,}59 \cdot 10^{-3}$ см$^{-2}$).

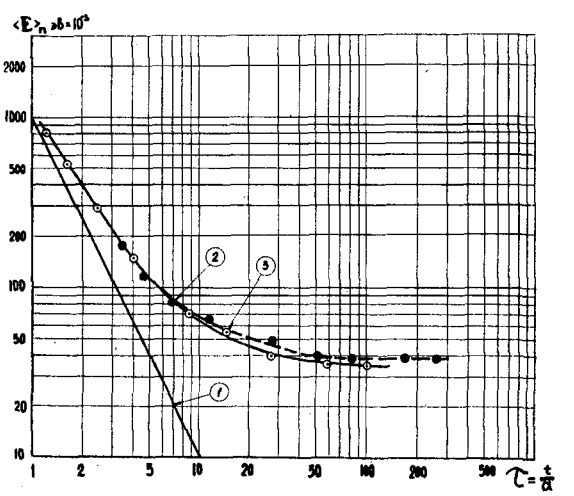

Рис.11

Зависимость $\langle E(\tau) \rangle$ для графита и бериллия: 1 – расчет; 2 – бериллий; 3 – графит.

если сопоставить результаты по $\langle E \rangle$ в масштабе "приведенного" (относительного) времени $\tau = t/a$, где значение a берется таким, чтобы при рассеянии на свободных и покоящихся ядрах $\langle E(\tau) \rangle$ не зависело от массы. Используя аналитическое выражение для спектра нейтронов, рассеянных на свободных и покоящихся ядрах [11], можно найти:

$$a^2 = \frac{m}{2}\left(\frac{2}{\xi}+1\right)\frac{2}{\xi}\cdot\lambda_s^2 ,$$

где m – масса нейтрона, ξ – средняя логарифмическая потеря энергии при столкновении, λ_s – длина рассеяния. На рис.11 представлена зависимость

$\langle E(\tau)\rangle$ для графита и бериллия. Видно, что кривые для C и Be идут близко, хотя и заметно некоторое расхождение, обусловленное, по-видимому, различием в асимптотических значениях $\langle E\rangle$.

В заключение, выражаем свою признательность М.И. Певзнеру и персоналу линейного ускорителя за предоставленную возможность проведения данных экспериментов на ускорителе. Мы благодарны Г.В. Яковлеву, А.А. Осочникову, В.В. Лысову, А.П. Цитовичу и С.К. Сотникову за создание и наладку всей необходимой радиоэлектронной аппаратуры.

ЛИТЕРАТУРА

[1] АНТОНОВ А.В. и др. Доклад на I Женевской конференции по мирному использованию атомной энергии. Женева, 1955.
[2] DARDEL G.F. Trans. Roy. Inst. Techn., n. 75 Stokholm (1954).
[3] BARNARD E. et al. Proc. of the Brookhaven conf. on neutron thermalization, 1962.
[4] FULLWOOD R.R. et al. Nucl. Sc. and Eng., 18, n.1. (1964).
[5] КОЛЛАТЦ Л. Численные методы решения дифференциальных уравнений, ИЛ, М. (1953).
[6] МАЙОРОВ Л.В., ТУРЧИН В.Ф., ЮДКЕВИЧ М.С. Доклад на III-й Женевской конференции, 1964.
[7] ТУРЧИН В.Ф. "Атомная энергия", 1965.
[8] SINCLAIR R.N. Симпозиум по неупругому рассеянию нейтронов в твердых телах и жидкостях. Чок-Ривер, 1962.
[9] BHANDARI R.C. J. Nucl. Energy 6, (1957) 104.
[10] HUGHES D.J. Neutron Cross Section BNL 325, 1955.
[11] ДЯДЬКИН И.Г., БАТАЛИНА Э.П. "Атомная энергия", 10 (1961) 5.
[12] KOPPEL J. Nucl. Sc. and Eng., 8 (1960) 157.
[13] SAUSSURE G.de. Proc. of the Brookhaven conf. on neutron thermalization, 1962.
[14] IHA S.S. Nucl. Energy, A, 12 (1960) 89.
[15] WILLIAMS M. Nucl. Sc. and Eng., 19 n.2 (1964).
[16] КАЗАРНОВСКИЙ М.В. Диссертация. ФИАН СССР (1955).
[17] STARR E., de VILLIERS. Proc. of the Brookhaven conf. on neutron thermalization, 1962.
[18] GHATAK A., HONECK H. Nucl. Sc. and Eng., 21 (1965) 227.

ЭКСПЕРИМЕНТАЛЬНОЕ ИЗУЧЕНИЕ ПРОЦЕССА ТЕРМАЛИЗАЦИИ НЕЙТРОНОВ ВО ВРЕМЕНИ В ВОДОРОДОСОДЕРЖАЩИХ ЗАМЕДЛИТЕЛЯХ

С.Н.ИШМАЕВ, В.И. МОСТОВОЙ, И.П.САДИКОВ и А.А.ЧЕРНЫШОВ
ГОСУДАРСТВЕННЫЙ КОМИТЕТ ПО ИСПОЛЬЗОВАНИЮ АТОМНОЙ ЭНЕРГИИ СССР, ИНСТИТУТ АТОМНОЙ ЭНЕРГИИ им.И.В.КУРЧАТОВА, МОСКВА
СССР

Abstract — Résumé — Аннотация — Resumen

EXPERIMENTAL STUDY OF THE PROCESS OF NEUTRON THERMALIZATION IN TIME IN AQUEOUS MODERATORS. Using a method described in another paper presented at this Symposium, the authors measured non-stationary neutron spectra in zirconium hydride and in water at room temperature as a function of slowing-down time, with a resolution of 3.5 μs.

The spectra measured in a large ZrH prism ($B^2 = 3.8 \times 10^{-2}$ cm^2) belong to a slowing-down time range ($t > 30$ μs) in which the mean neutron energy is less than 0.13 eV and the energy exchange between neutron gas and the medium is caused mainly by the excitation of acoustic lattice vibrations. In this range thermalization proceeds at a comparatively slow rate and the time required to establish an equilibrium neutron spectrum is of the order of 400 μs. In a small ZrH assembly ($B^2 \simeq 20 \times 10^{-2}$ cm^{-2}) a strong diffusion-cooling effect is observed. The spectra measured at long slowing-down times are found to differ considerably from the Maxwellian distribution with the temperature of the medium. The time required to establish an equilibrium energy distribution increases with decreasing system size.

The neutron energy spectra in water ($B^2 = 2.56 \times 10^{-2}$ cm^{-2}) are presented for slowing-down times of over 13 μs, where distortions from resolution are insignificant. The shape of the spectrum is only fully consistent with the Maxwellian distribution at room temperature after about 100 μs following a fast neutron burst. The time required to establish an equilibrium neutron spectrum in this experiment is three to four times longer than the values calculated by various other authors. The possible reasons for this discrepancy are discussed.

ÉTUDE EXPÉRIMENTALE DU PROCESSUS DE THERMALISATION DES NEUTRONS EN FONCTION DU TEMPS DANS LES RALENTISSEURS CONTENANT DE L'EAU. A l'aide de la méthode que les auteurs ont décrite dans un autre mémoire présenté au Colloque, ils ont mesuré, en fonction du temps de ralentissement, les spectres non stationnaires des neutrons dans l'hydrure de zirconium et dans l'eau à la température ambiante, avec un pouvoir de résolution de 3,5 μs.

Les spectres ont été déterminés au moyen d'un prisme de ZrH de grande dimension ($B^2 = 3{,}8 \cdot 10^{-2}$ cm^{-2}) pour des temps de ralentissement supérieurs à 30 μs; pour ces valeurs du temps, l'énergie moyenne des neutrons est inférieure à 0,13 eV et l'échange d'énergie entre le gaz neutronique et le milieu s'opère essentiellement du fait de l'apparition d'oscillations acoustiques dans le réseau; en outre, le processus de thermalisation suit un rythme relativement lent et le temps nécessaire pour obtenir un spectre de neutrons à l'état d'équilibre est de l'ordre de 400 μs. Dans un assemblage à ZrH de petite dimension ($B^2 \simeq 20 \cdot 10^{-2}$ cm^{-2}) on constate un puissant effet de refroidissement par diffusion. Les spectres mesurés pour des temps de ralentissement prolongés diffèrent sensiblement de la distribution maxwellienne à la température ambiante. Le temps requis pour obtenir une distribution équilibrée de l'énergie augmente avec la réduction des dimensions dy système.

Les auteurs présentent les spectres énergétiques des neutrons dans l'eau ($B^2 = 2{,}56 \cdot 10^{-2}$ cm^{-2}) pour des temps de ralentissement supérieurs à 13 μs où les déformations provoquées aux dépens du pouvoir de résolution sont insignifiantes. La forme du spectre ne concorde entièrement avec la distribution maxwellienne à la température ambiante qu'après un délai d'environ 100 μs après la bouffée de neutrons rapides. Dans l'expérience, le temps nécessaire à la formation d'un spectre de neutrons à l'état d'équilibre était de trois à quatre fois supérieur à celui qu'indiquent les calculs effectués par différents auteurs. Les causes possibles de ces divergences font l'objet d'un examen critique.

ЭКСПЕРИМЕНТАЛЬНОЕ ИЗУЧЕНИЕ ПРОЦЕССА ТЕРМАЛИЗАЦИИ НЕЙТРОНОВ ВО ВРЕМЕНИ В ВОДОРОДОСОДЕРЖАЩИХ ЗАМЕДЛИТЕЛЯХ. С помощью методики, описанной в

другом докладе авторов на данную конференцию, измерены нестационарные спектры нейтронов в гидриде циркония и воде при комнатной температуре с разрешением 3,5 мксек по времени замедления.

Спектры, измеренные в призме из ZrH большого размера ($B^2 = 3{,}8 \cdot 10^{-2}$ см^2), относятся к области времен замедления ($t > 30$ мксек), где средняя энергия нейтронов ниже 0,13 эв и обмен энергией между нейтронным газом и средой происходит, в основном, за счет возбуждения акустических колебаний решетки. В этой области процесс термализации идет сравнительно медленно и время, необходимое для установления равновесного спектра нейтронов, оказывается порядка 400 мксек.

В сборке из ZrH малого размера ($B^2 \simeq 20 \cdot 10^{-2}$ см^2) проявляется сильный эффект диффузионного охлаждения. Спектры, измеренные при больших временах замедления, сильно отличаются от максвелловского распределения с температурой среды. Время, необходимое для установления равновесного энергетического распределения, возрастает с уменьшением размеров системы.

Энергетические спектры нейтронов в воде ($B^2 = 2{,}56 \cdot 10^{-2}$ см$^{-2}$) представлены для времен замедления больших 13 мксек, где искажения за счет разрешения незначительны. Форма спектра полностью совпадает с распределением Максвелла при комнатной температуре лишь спустя ~100 мксек после вспышки быстрых нейтронов.

Наблюдаемое в эксперименте время установления равновесного спектра нейтронов в 3–4 раза больше, чем дают расчеты, выполненные различными авторами. Обсуждаются возможные причины расхождений.

ESTUDIO EXPERIMENTAL DEL PROCESO DE TERMALIZACION DE NEUTRONES EN FUNCION DEL TIEMPO EN MODERADORES ACUOSOS. Con ayuda del método descrito en otra memoria presentada a este Simposio, los autores han medido en función del tiempo de moderación los espectros neutrónicos no estacionarios en hidruro de circonio y en agua a temperatura ambiente, con un poder de resolución de 3,5 μs.

Los espectros medidos en un prisma de ZrH de gran tamaño ($B^2 = 3{,}8 \cdot 10^{-2}$ cm^2) pertenecen a un intervalo de tiempos de moderación ($t > 30$ μs) en el cual la energía media de los neutrones es inferior a 0,13 eV y el intercambio de energía entre el gas neutrónico y el medio se debe fundamentalmente a la excitación de vibraciones acústicas en el reticulado. Dentro de este intervalo, la termalización se desarrolla a un ritmo comparativamente lento y el tiempo necesario para obtener un espectro neutrónico de equilibrio es del orden de 400 μs. En montajes de ZrH de pequeñas dimensiones ($B^2 \simeq 20 \cdot 10^{-2}$ cm^{-2}) se observa un marcado efecto de enfriamiento por difusión. Los espectros medidos para tiempos de moderación prolongados difieren considerablemente de la distribución maxwelliana correspondiente a la temperatura ambiente. El tiempo necesario para lograr una distribución energética de equilibrio aumenta a medida que disminuyen las dimensiones del sistema.

Los autores presentan espectros energéticos de neutrones en agua ($B^2 = 2{,}56 \cdot 10^{-2}$ cm^{-2}) para tiempos de moderación superiores a 13 μs, donde las deformaciones debidas a la resolución son insignificantes. La forma del espectro sólo concuerda con la distribución maxwelliana a temperatura ambiente, al cabo de unos 100 μs después de emitida una ráfaga de neutrones rápidos. El tiempo necesario para que el espectro de neutrones alcance el equilibrio es, en este experimento, tres a cuatro veces más prolongado que los valores calculados por diversos autores. En la memoria se analizan los posibles motivos de esta discrepancia.

Методика измерений нестационарных спектров нейтронов в замедлителях изложена в отдельном докладе [1]. На рис. 1 изображена схема экспериментальной установки.

В отличие от кристаллических замедлителей – графита и бериллия, исследованных в работе [1], изучение процесса термализации нейтронов во времени в водородосодержащих веществах представляет собой более сложную в экспериментальном отношении задачу. Существенно меньшие значения времен замедления и термализации нейтронов в водородосодержащих средах по сравнению с бериллием и графитом предъявляют высокие требования к временному разрешению при измерении нестационарных спектров. В данной работе приводятся результаты измерений нестационарных спектров в гидриде циркония и воде, выполненные с разрешением по времени замедления 3,5 мксек.

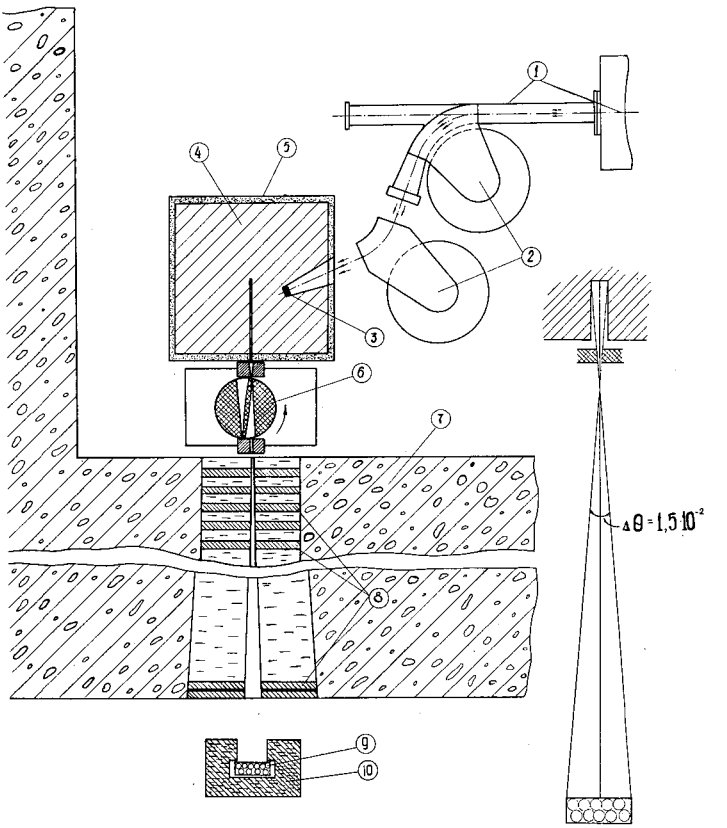

Рис. 1

Экспериментальная установка.
1 — линейный ускоритель; 2 — магнитная отклоняющая система; 3 — свинцовая мишень; 4 — исследуемый замедлитель; 5 — карбид бора и кадмий; 6 — прерыватель; 7 — биологическая защита ускорителя; 8 — коллиматор; 9 — детектор нейтронов; 10 — водный раствор борной кислоты.

ИЗМЕРЕНИЕ НЕСТАЦИОНАРНЫХ СПЕКТРОВ В ГИДРИДЕ ЦИРКОНИЯ

До настоящего времени в литературе не было опубликовано работ, посвященных изучению нестационарных спектров нейтронов в ZrH, хотя особенности в термализующих свойствах этого замедлителя хорошо известны [2], [3]. Замедляющая способность резко уменьшается, когда энергия нейтронов (E) становится меньше 0,13 эв.

В области энергий, больших 0,13 эв, замедляющая способность, в основном, связана с возбуждением оптических колебаний решетки ZrH, при этом нейтрон теряет энергию квантами в 0,13 эв. При $E < 0{,}13$ эв сброс энергии идет только за счет возбуждения акустических колебаний решетки, причем здесь эффективная масса рассеивателя велика и передача энергии незначительна, вследствие чего процесс термализации нейтронов в этой области энергий должен протекать сравнительно медленно. Измерение

нестационарных спектров нейтронов с разрешением 3,5 мксек позволило достаточно подробно исследовать этот этап термализации.

Спектры нейтронов были измерены в двух призмах из ZrH размерами $(30 \times 28 \times 25)$ см^3 и $(25 \times 25 \times 7)$ см^3*. Призмы собирались из прессованных плиток $(50 \times 50 \times 100)$ мм^3, средняя плотность которых равнялась 4,84 г/см^3. Соотношение атомов циркония и водорода в исследованном материале составляло 1:1,88 ($ZrH_{1,88}$).

1. Большая призма (30 × 28 × 25) см^3

Измерения в большой системе были проведены с целью изучения процесса термализации, когда влияние утечки нейтронов из замедлителя невелико. Спектры нейтронов были измерены в диапазоне времен замедления от 30 до 1100 мксек. Источник нейтронов был расположен в точке с координатами $x = 2$ см, $y = 6$ см, $z = 8$ см (начало координат в центре призмы), а пучок нейтронов выводился в направлении оси x через полость сечением (1×8) см^2 из центра призмы: $x = y = z = 0$. При этом градиент потока нейтронов в направлении пучка в этом месте призмы был близок к нулю, вследствие чего изучаемый спектр должен соответствовать спектру скалярного потока. Энергетическое распределение нейтронов в каждой точке при наличии градиентов потока нейтронов определяется не только процессом термализации, но и диффузией нейтронов. При этом влияние диффузии будет минимальным там, где лапласиан потока близок к нулю. Точка, в которой обычно измерялись спектры, находилась на таком расстоянии от источника, где это условие примерно выполняется.

Полученные энергетические спектры нейтронов в различные моменты времени представлены на рис.2. Видно, что исследованный интервал времен охватывает заключительный этап замедления, когда средняя энергия нейтронов ниже 0,13 эв. Анализ изменений, происходящих в спектре нейтронов со временем, позволяет отметить некоторые особенности процесса формирования равновесного спектра в ZrH. Так же, как в графите и бериллии [1], жесткая часть спектра совпадает с равновесным распределением гораздо раньше, чем область низких энергий, где приближение к равновесию происходит значительно медленнее. При $t > 400$ мксек во всем диапазоне исследованных энергий спектр нейтронов может быть описан распределением Максвелла, температура которого ($kT = 24{,}3$ мэв) оказывается несколько ниже температуры замедлителя ($kT_{ср} = 26{,}5 \pm 0{,}4$ мэв) за счет диффузионного охлаждения.

На рис.3 и табл.1 представлено изменение средней энергии нейтронов со временем. Видно, что время, необходимое для установления равновесия в ZrH, составляет 300 + 400 мксек. Влияние диффузионного охлаждения для системы данного размера невелико.

2. Малая призма (25 × 25 × 7) см^3

Измерения спектров в системе малого размера были выполнены с целью изучения влияния утечки на процесс формирования нейтронного спектра в гидриде циркония. Следует отметить, что в ZrH должен наиболее четко

---

* В предварительных измерениях нестационарных спектров нейтронов принимал участие Андрющенко Н.Н.

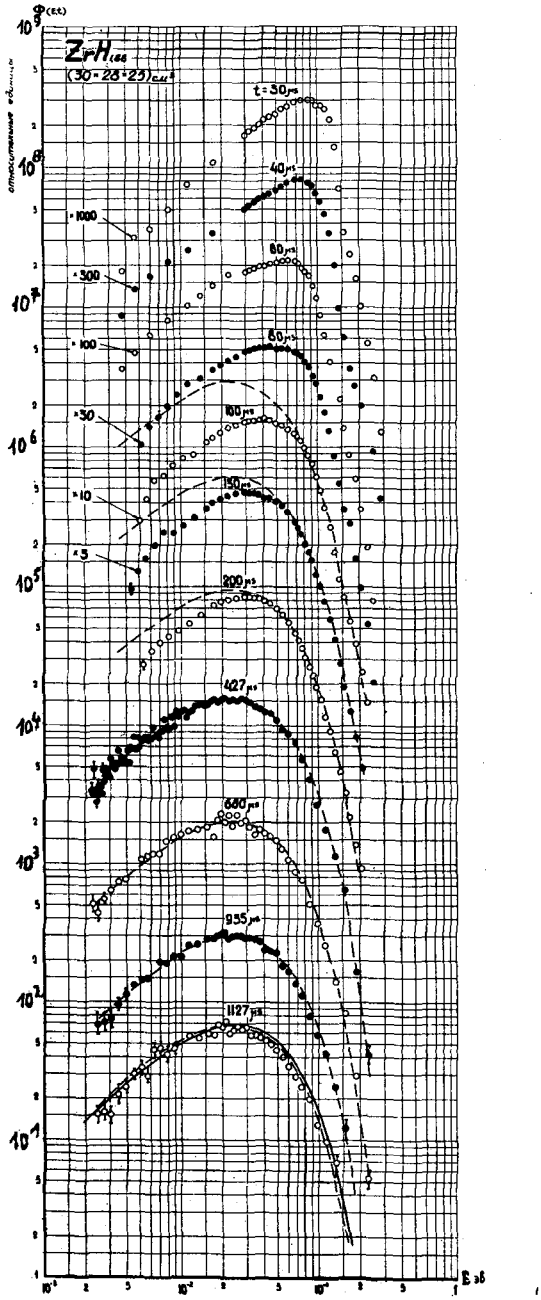

Рис. 2

Эволюция спектра нейтронов в $ZrH_{1.88}$ $(30 \times 30 \times 25)$ см^3

– – – распределение Максвелла: $\Phi(E) \sim E \cdot e^{-\frac{E}{kT}}$

$kT = 24{,}3$ мэв;

—— распределение Максвелла с $kT_{ср} = 26{,}5$ мэв.

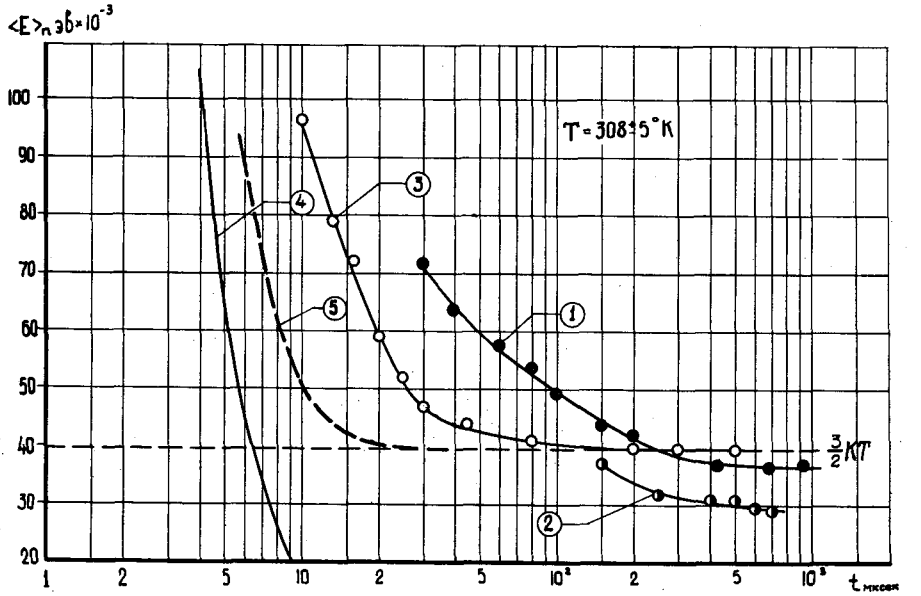

Рис.3

Зависимость средней энергии нейтронов от времени:
1 – $ZrH_{1.88}$ (30 × 28 × 25) см³;
2 – $ZrH_{1.88}$ (25 × 25 × 7) см³; 3 – H_2O (30 × 30 × 45) см³;
4 – расчет для свободных покоящихся ядер [11]; 5 – расчет [8].

проявиться эффект диффузионного охлаждения спектра. Это обусловлено двумя обстоятельствами. Во-первых, транспортное сечение в ZrH с уменьшением энергии быстро возрастает, что усиливает зависимость коэффициента диффузии нейтронов от энергии и приводит к увеличению неравномерности утечки нейтронов разных энергий из системы. Во-вторых, обмен энергией между нейтронным газом и средой (который стремится восстановить равновесие, нарушаемое утечкой) в областях ниже 0,13 эв в гидриде циркония происходит сравнительно медленно.

Исследование спектров нейтронов в системах малых размеров представляет значительный интерес также в связи с вопросом о возможности существования нулевой энергетической гармоники при больших значениях геометрического фактора B^2 [4]. Оно предпочтительно и с точки зрения выполнения теоретических расчетов нестационарных спектров с использованием различных моделей. Это обусловлено тем обстоятельством, что в случае малой системы достаточно решать нестационарное кинетическое уравнение только для основной пространственной гармоники.

Измерения были выполнены в системе размером (25 × 25 × 7) см³ ($B^2 \approx 0{,}2$ см$^{-2}$) в интервале времен замедления от 150 до 700 мксек. Для уменьшения потерь нейтронов при замедлении исследуемая система помещалась в кадмиевый экран толщиной 0,7 мм и окружалась отражателем из гидрида циркония. Специальными измерениями было установлено, что отражатель не искажает спектр тепловых нейтронов. С целью повышения светосилы в данных измерениях использовался прерыватель с широкой

Таблица 1

$ZrH_{1,88}$ $\rho = 4{,}84$ г/см^3 $T = 308 \pm 5^\circ$ K

Геометр. размеры.	(30 x 28 x 25) см^3										(25 x 25 x 7) см^3					
t мксек.	30	40	60	80	100	150	200	427	680	935	150	250	400	500	600	700
$\int_0^t n(E)dE$	$7{,}05\cdot10^7$	$6{,}26\cdot10^7$	$5{,}24\cdot10^7$	$4{,}28\cdot10^7$	$3{,}57\cdot10^7$	$2{,}52\cdot10^7$	$1{,}74\cdot10^7$	$3{,}39\cdot10^6$	$4{,}43\cdot10^5$	$6{,}44\cdot10^4$	$5{,}17\cdot10^5$	$1{,}93\cdot10^5$	$3{,}11\cdot10^4$	$9{,}47\cdot10^3$	$2{,}93\cdot10^3$	$9{,}71\cdot10^2$
$\langle E\rangle_n$ *) $= \frac{\int_0^t n(\varepsilon)E\,dE}{\int_0^t n(\varepsilon)E\,dE_{26\cdot10^{-3}}}$	71,81	63,93	57,45	53,63	49,19	43,80	42,34	36,98± ±0,11	36,63± ±0,18	37,00± ±0,31	37,26± ±0,11	31,81± ±0,18	31,11± ±0,20	30,80± ±0,21	29,41± ±0,23	28,86± ±0,3

*) Указаны статистические ошибки измерений.

щелью, время открытия которой составляло −110 мксек. Поскольку время жизни нейтронов в исследуемой системе было равно 86 мксек, оказалось необходимым при обработке экспериментальных данных учитывать смещение максимума нейтронного импульса, обусловленное экспоненциальным убыванием потока нейтронов, падающих на прерыватель.

Полученные спектры представлены на рис.4. Точки, нанесенные в виде двойных кружков, в области малых энергий получены путем экстраполяции экспериментальных данных в область больших времен замедления. На рис.3 и в табл.1 указаны значения средней энергии нейтронов, вычисленные по измеренным спектра. Видно, что влияние утечки действительно приводит к сильному охлаждению нейтронного газа в призме. Уже при временах замедления ~150 мксек средняя энергия нейтронов оказывается заметно меньше энергии теплового движения ($3/2\,кT_{ср} = 39{,}8$ эв). С течением времени это отличие растет и достигает при больших временах ~40%.

Анализируя изменение формы спектра, можно заметить, что во всех спектрах жесткая часть может быть описана распределением Максвелла с $кT = 20{,}5$ эв, что значительно ниже температуры среды ($кT_{ср} = 26{,}5$ эв). Доля медленных нейтронов в спектре непрерывно возрастает, приводя к постепенному уменьшению средней энергии нейтронов. Сопоставление результатов измерений в большой и малой системах показывает, что установление равновесия в призме малого размера происходит более медленно. Аналогичный эффект наблюдался также при измерении нестационарных спектров в бериллиевых блоках малых размеров. Эти факты подтверждают вывод о том, что время, необходимое для установления основной энергетической гармоники, возрастает с увеличением B^2.

ИЗМЕРЕНИЕ НЕСТАЦИОНАРНЫХ СПЕКТРОВ В ВОДЕ

До последнего времени экспериментальное изучение процесса термализации нейтронов в воде от импульсного источника быстрых нейтронов ограничивалось экспериментами Дарделла, определявшего среднюю энергию нейтронов по пропусканию через серебряный фильтр [5], и работой Меллера и Сьестранда [6], измерявших временное распределение γ-лучей захвата в воде, отравленной кадмием и гадолинием. В этих работах определялась константа термализации, которой характеризовалась скорость установления равновесного спектра нейтронов в воде. В работе [7] Бекуртсом исследовались асимптотические спектры нейтронов в воде в зависимости от геометрического параметра системы (B^2).

Согласно теоретическим расчетам, в которых исследовалась временная эволюция нейтронных спектров [8], [9], [10], время, необходимое для установления равновесия между нейтронным газом и водой, составляет 20 ÷ 30 мксек.

Созданная в ИАЭ им. И.В. Курчатова установка с разрешением 3,5 мксек по времени замедления позволила исследовать процесс термализации нейтронов в воде более детально, чем это было сделано в указанных работах.

Измерения были выполнены в водяной системе размером $(30\times30\times45)$ см^3 в диапазоне времен от 10 до 1000 мксек. Источник нейтронов распола-

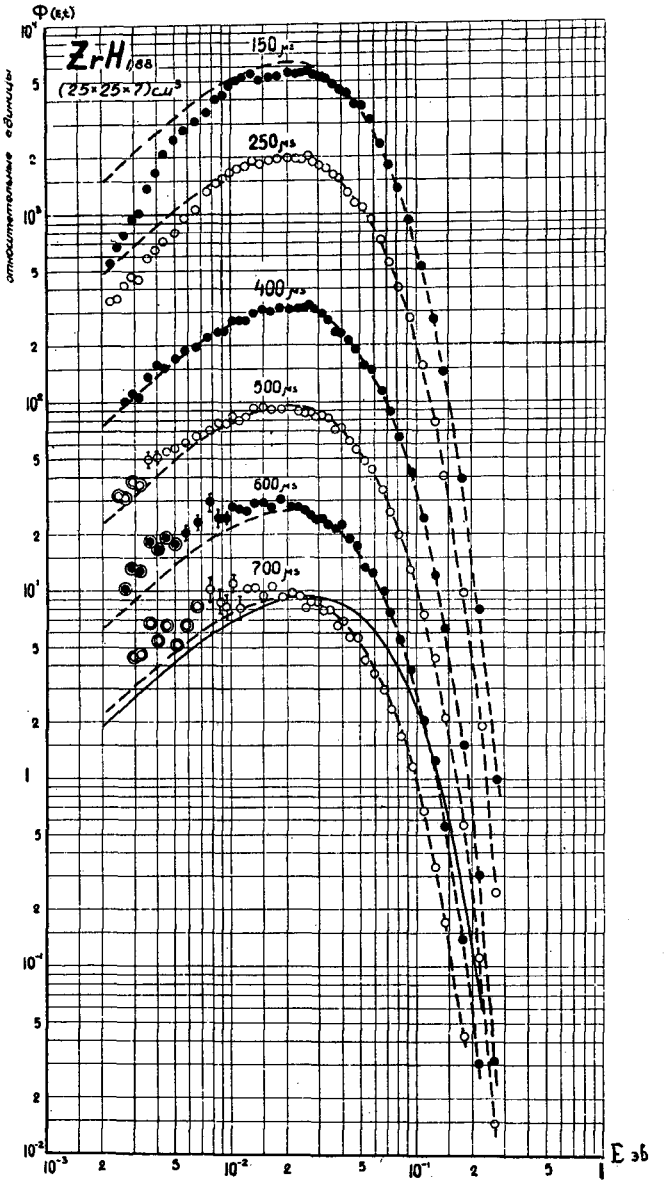

Рис. 4

Нестационарные спектры нейтронов в $ZrH_{1,88}$ (25 × 25 × 7) см³;

– – – распределение Максвелла $\Phi(E) \sim E \cdot e^{-\frac{E}{kT}}$

кТ = 20,5 мэв;

—— распределение Максвелла с $kT_{ср}$ = 26,5 мэв.

гался внутри системы с координатами x = 10 см, y = 3 см, z = 7,5 см, пучок нейтронов выводился из точки x = 10 см, y = z = 0 через полость размером 1 × 8 см².

Исследуемый поток нейтронов может быть представлен в виде поверхности $\Phi(t,t_K)$, где t – время замедления, а $t_K = (\ell/v)$ – время пролета, определяемое скоростью нейтрона. Как указывалось в работе [1], на опыте измеряются лишь отдельные сечения этой поверхности, которые удовлетворяют условию $t + (\ell/\ell)\, t_K = T = \text{const}$. На рис.5 для иллюстрации приве-

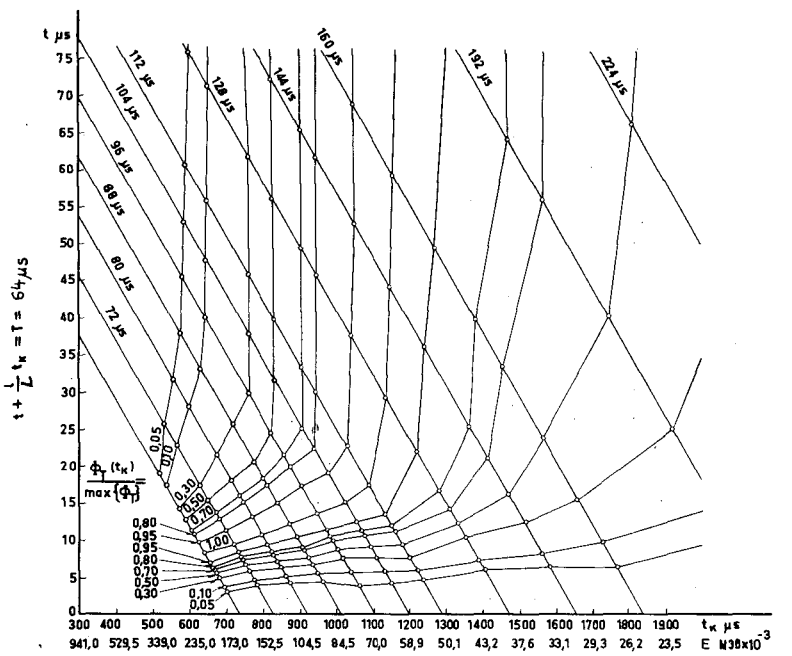

Рис.5

Проекция поверхности $\frac{\Phi(t,t_K=\frac{\ell}{v})}{\max \Phi_T(t_K)}$ на плоскость (t,t_K):

t_K – время пролета; t – время замедления. $T = t + \frac{\ell}{\ell} t_K$;
ℓ – расстояние от точки, в которой измеряется спектр нейтронов, до прерывателя.

дена часть этой поверхности, относящаяся к области малых времен замедления нейтронов в воде. Поверхность изображена в виде проекции на плоскость (t,t_K) лини й равной высоты", причем для удобства все измеренные скость (t,t_K) "линий равной высоты", причем для удобства все измеренные спектры отнормированы на одинаковое значение в максимуме. Из рис.5 можно видеть, в какой области изменения переменных измерена функция $\Phi(t,E)$. Граница надежности экспериментальных данных со стороны малых t определяется разрешением по времени замедления. Специальные измерения спектров в этой области, выполненнные при различной длительности открытия щели прерывателя, показали, что искажения спектра (его уширение) за счет разрешения невелико. Так, при T = 64 мксек уширение спектра не должно превышать 10–20%. На рис.6 показано изменение по-

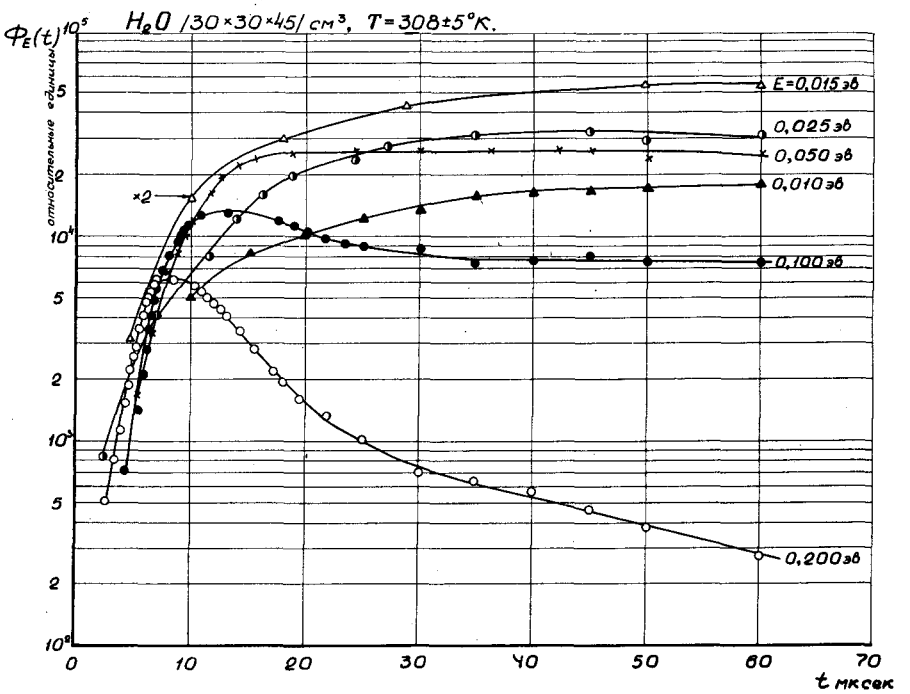

Рис.6

Изменение со временем потоков нейтронов различных энергетических групп в H_2O (30×30×45) см³.

тока нейтронов различных энергий со временем (сечения поверхности Ф(t,E) при E = const); на рис.7 изображена форма энергетического спектра нейтронов в различные моменты времени замедления (сечения поверхности Ф(t,E) при t = const).

В табл.2 и на рис.3 приведены значения средней энергии нейтронов для различных времен замедления, вычисленные из представленных энергетических распределений. Рассмотрение поведения Ф(t,E) во времени показывает, что изменение формы энергетического спектра нейтронов в процессе термализации в воде характеризуется теми же особенностями, которые отмечались ранее при анализе результатов для графита, бериллия [1] и гидрида циркония. Однако при малых временах замедления спектр нейтронов в H_2O оказывается значительно более мягким даже по сравнению с ZrH, что обусловлено большей величиной сброса энергии нейтроном при рассеянии на молекуле H_2O. Равновесный спектр хорошо описывается распределением Максвелла с температурой, соответствующей температуре среды, т.к. утечка нейтронов из данной системы незначительна.

Весьма неожиданным результатом является довольно большое значение времени, необходимого для установления полного равновесия. Практически форма спектра перестает изменяться лишь через ~100 мксек после вспышки быстрых нейтронов. Это в 3÷4 раза больше, чем дают расчеты, выполненные в выше отмеченных работах [8], [9], [10], с использованием довольно реалистических моделей воды. Сопоставление экспериментальных значе-

Таблица 2

H_2O $(30 \times 30 \times 45)$ см^3 $T = 308 \pm 5°$ K

t мксек.	I3,3	I5	20	25	30	45	80	200	300	500
$\int n(\varepsilon)\,dE$	$2{,}73 \times 10^6$	$2{,}82 \times 10^6$	$2{,}94 \times 10^6$	$3{,}12 \times 10^6$	$3{,}26 \times 10^6$	$3{,}40 \times 10^6$	$3{,}52 \times 10^6$	$2{,}31 \times 10^6$	$1{,}34 \times 10^6$	$4{,}52 \times 10^5$
$\langle E \rangle_n$ *) эВ $\times 10^{-3}$	78,83	71,98	58,84	51,92	46,93	44,14 ± ±0,08	41,19 ± ±0,12	39,80 ± ±0,13	39,76 ± ±0,14	39,67 ± ±0,16

*) Указаны статистические ошибки измерений.

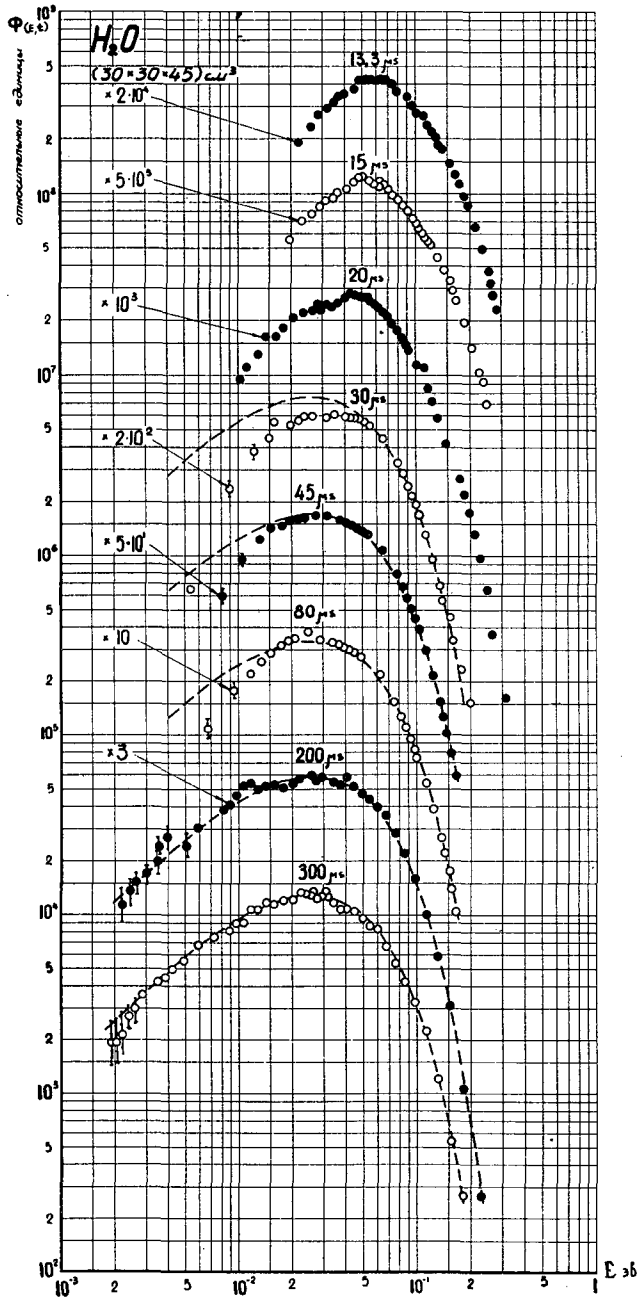

Рис. 7

Нестационарные спектры нейтронов в H_2O ($30 \times 30 \times 45$) см^3.

– – – – $\Phi(E) \sim E \cdot e^{-\frac{E}{kT}}$, $kT_{ср} = 26{,}5$ мэв.

ний $\langle E \rangle(t)$ с расчетом, выполненным в работе [8], дано на рис.3. Видно очень существенное различие. Можно указать на два обстоятельства, которые могли привести к завышению времени термализации в данном опыте. Первым обстоятельством является возмущение, вносимое каналом для вывода нейтронного пучка из замедлителя. Поскольку ширина канала соизмерима с длиной термализации нейтронов в воде, то наличие полости приводит к заметному уменьшению плотности среды в области, где формируется измеряемый спектр нейтронов. Второй причиной завышения времени термализации может служить влияние диффузии нейтронов. Так как точка, в которой измерялся спектр нейтронов, удалена от источника на 8 см, то диффузия приводит к некоторому возрастанию интегральной плотности нейтронов в данной точке в течение всего периода термализации (табл.2 и рис.6). В этом случае сильная зависимость коэффициента диффузии нейтронов в H_2O от скорости должна приводить к ужестчению измеряемого спектра.

Однако грубые оценки показывают, что эти эффекты, по-видимому, не могут привести к столь значительному увеличению времени установления равновесия. Тем не менее для выяснения вопроса необходимо проведение дополнительных экспериментов с целью проверки указанных эффектов. Представляет также интерес выполнение теоретических расчетов нестационарных спектров в воде с учетом геометрии эксперимента.

Авторы благодарны В.В. Головневу, О.Я. Ермолаеву, Е.Ф. Польникову, М.Н. Северову за помощь в проведении экспериментов и обработке результатов, а также Л.А. Толмачевой — за составление программы обработки экспериментальных данных на машине.

ЛИТЕРАТУРА

[1] МОСТОВОЙ В.И., САДИКОВ И.П., ЧЕРНЫШОВ А.А., ИШМАЕВ С.Н., ЮДКЕВИЧ М.С., НОЗИК В.З., "Экспериментальное изучение процесса термализации нейтронов во времени в графите и бериллии". См.в этом томе.
[2] WHITTEMORE W.L., McREYNOLDS A.W. Phys.Rev., 113,(1959) 806.
[3] YOUNG I.C., YOUNG I.A., HOUGHTON G.K., TRIMBLE G.D., BEYSTER I.R. Nucl.Sci. and Eng., 19, n.2 (1964) 230–241.
[4] G.de SAUSSURE. Proc. of the Brookhaven Conf. on neutron thermalization, 1962.
[5] G.F. von DARDEL. Trans.Roy.Inst.Techn., Stockholm, 75 (1954).
[6] MÖLLER and SJÖSTRAND N.G. Arkiv Fysic, 27, (1964) 501.
[7] BECKURTS K.H. Z.Naturforschung., 16a (1961) 611.
[8] МАИОРОВ Л.В., ТУРЧИН В.Ф., ЮДКЕВИЧ М.С., Доклад на III Международной конференции по использованию атомной энергии в мирных целях. Женева, 1964.
[9] GHATAK A.K. and KRIEGER T.I. Nucl.Sci. and Eng., 21 (1965) 304–311.
[10] GHATAK A.K. and HONECK H.C., Nucl.Sci. and Eng., 21 (1965) 227–239.
[11] ДЯДЬКИН И.Г., БАТАЛИНА Э.П., "Атомная энергия", 10, 5 (1961).

ТЕРМАЛИЗАЦИЯ НЕЙТРОНОВ В СИСТЕМЕ ГРАФИТ-ВОДА ПРИ БОЛЬШИХ ГРАДИЕНТАХ ТЕМПЕРАТУРЫ

Л.В. МАЙОРОВ, В.И. МОСТОВОЙ, Ю.А. САФИН и Г.Я. ТРУХАНОВ
ГОСУДАРСТВЕННЫЙ КОМИТЕТ ПО ИСПОЛЬЗОВАНИЮ АТОМНОЙ ЭНЕРГИИ СССР, ИНСТИТУТ АТОМНОЙ ЭНЕРГИИ им.И.В. КУРЧАТОВА, МОСКВА, СССР

Abstract — Résumé — Аннотация — Resumen

NEUTRON THERMALIZATION IN A GRAPHITE-WATER SYSTEM AT LARGE TEMPERATURE GRADIENTS. Measurements were made of the space-energy distribution of thermal neutrons in a graphite-water system at graphite temperatures of 443-823°K and a water temperature of 303°K. The system investigated consisted of a graphite prism measuring 100 cm × 100 cm × 59.5 cm and an aluminium tank of water measuring 175 cm × 175 cm × 50 cm, separated by a thermal screen. The WWR-2 reactor was used as the external neutron source. Neutron beams were extracted from different points in the graphite and the water in the direction of the neutron flux from the reactor incident on the graphite prism. The neutron spectra in the extracted beams were measured by the time-of-flight method by means of a mechanical chopper with a resolution of 20 μs/m.

The measured spectra were compared with the spectra calculated in accordance with a T-2 programme (P-1 approximation, 40 energy groups), use being made of the differential cross-sections for an ideal gas and the differential cross-sections obtained taking into account the chemical binding. Using the method described in the paper, the authors calculated, on the basis of the measured spectra, the neutron rethermalization cross-section in the graphite and the water as a function of graphite temperature. The experimental results were compared with the data obtained by other authors.

THERMALISATION DES NEUTRONS DANS UN SYSTÈME GRAPHITE-EAU EN PRÉSENCE DE GRADIENTS DE TEMPÉRATURE ÉLEVÉS. Les auteurs ont mesuré la distribution spatiale et la distribution selon l'énergie des neutrons thermiques dans un système graphite-eau pour des températures du graphite de 443 à 823°K et une température d'eau de 303°K. Le système étudié se composait d'un prisme en graphite de 100 cm × 100 cm × 59,5 cm et d'un réservoir d'eau en aluminium de 175 cm × 175 cm × 50 cm, séparés entre eux par un écran thermique. Comme source externe de neutrons ils ont utilisé le réacteur refroidi et ralenti à l'eau VVR-2. Les faisceaux de neutrons émanant de plusieurs points du graphite et de l'eau étaient orientés dans la direction du flux de neutrons allant du réacteur vers le prisme en graphite. Les spectres des neutrons dans les faisceaux extérieurs ont été mesurés par la méthode du temps de vol, à l'aide d'un hacheur ayant un pouvoir de résolution de 20 μs/m.

Les auteurs ont comparé les spectres mesurés à ceux qui ont été calculés au moyen du programme T-2 (approximation P-1, quarante groupes d'énergies) en utilisant les sections efficaces différentielles pour un gaz parfait et les sections efficaces différentielles obtenues en tenant compte du lien chimique. A l'aide de la méthode exposée dans le mémoire, on a calculé, en se fondant sur les spectres mesurés, les sections efficaces de thermalisation des neutrons dans le graphite et dans l'eau en fonction de la température du graphite. Les données expérimentales obtenues sont comparées aux résultats indiqués par d'autres auteurs.

ТЕРМАЛИЗАЦИЯ НЕЙТРОНОВ В СИСТЕМЕ ГРАФИТ-ВОДА ПРИ БОЛЬШИХ ГРАДИЕНТАХ ТЕМПЕРАТУРЫ. Измерено пространственно-энергетическое распределение тепловых нейтронов в системе графит-вода при температурах графита от 443° К до 823°К и температуре воды 303° К. Изучаемая система состояла из графитовой призмы размером 100 × 100 × 59,5 см³ и алюминиевого бака с водой размером 175 × 175 × 50 см³, разделенных тепловым экраном. В качестве внешнего источника нейтронов использовался реактор ВВР-2. Пучки нейтронов выводились из различных точек графита и воды в направлении падающего из реактора на графитовую призму потока нейтронов. Спектры нейтронов в выведенных пучках измерялись методом времени пролета при помощи механического прерывателя с разрешением 20 мксек/м.

Проведено сравнение измеренных спектров со спектрами, вычисленными по программе Т-2 (Р-1 приближение, 40 энергетических групп) с использованием дифференциальных се-

чений для идеального газа и дифференциальных сечений, полученных с учетом химической связи. С помощью метода, изложенного в докладе, по измеренным спектрам вычислены сечения ретермализации нейтронов в графите и воде в зависимости от температуры графита. Полученные экспериментальные результаты сравниваются с данными других авторов.

TERMALIZACION DE NEUTRONES EN UN SISTEMA GRAFITO-AGUA CON ELEVADOS GRADIENTES DE TEMPERATURA. Los autores midieron la distribución espacial de la energía de neutrones térmicos en un sistema grafito-agua con temperaturas de 443 - 823°K en el grafito y 303°K en el agua. El sistema estudiado consistió en un prisma de grafito de 100 cm x 100 cm x 59,5 cm y un tanque de aluminio de 175 cm x 175 cm x 50 cm, lleno de agua, separados mediante una pantalla térmica. Como fuente externa de neutrones se utilizó el reactor WWR-2. De distintos puntos del grafito y del agua se extrajeron haces de neutrones, en una dirección coincidente con la del flujo neutrónico proveniente del reactor. Los espectros neutrónicos de los haces extraídos se midieron por el método del tiempo de vuelo, con ayuda de un interruptor mecánico cuyo poder de resolución es 20 μs/m.

Los espectros medidos se compararon con los calculados conforme a un programa T-2 (aproximación P-1, 40 grupos energéticos), utilizándose las secciones eficaces diferenciales correspondientes a un gas ideal y las secciones eficaces diferenciales obtenidas teniendo en cuenta el enlace químico. Con el método descrito en la memoria y sobre la base de los espectros medidos, los autores calcularon la sección eficaz de retermalización de los neutrones en grafito y en agua, en función de la temperatura del primero. Los resultados experimentales se comparan en la memoria con los datos obtenidos por otros autores.

1. ВВЕДЕНИЕ

Наиболее сильные изменения спектра нейтронов в гетерогенном реакторе происходят там, где резко меняется температура среды или ее замедляющие и поглощающие свойства. Пространственно-энергетическое и угловое распределение нейтронов в этих областях определяется как термализующими, так и транспортными свойствами среды. Поэтому для расчета спектров в этих случаях необходимо иметь не только точные исходные данные по дважды дифференциальным сечениям, но и использовать более точные методы решения кинетического уравнения. Сравнения расчетных спектров с измеренными в области скачка температуры или границы сред является хорошей проверкой точности методики расчета и пригодности используемых дважды дифференциальных сечений для описания процесса формирования спектра тепловых нейтронов.

Описанные в докладе эксперименты были предприняты с целью получения пространственно-энергетического распределения нейтронов в системе графит—вода при наличии скачка температуры между графитом и водой. Полученные данные использовались для апробации численных методов решения кинетического уравнения, а также для получения сечений ретермализации в графите и воде, необходимых для расчетов гетерогенных реакторов в малогрупповом приближении.

2. МЕТОДИКА ЭКСПЕРИМЕНТА

Из различных точек изучаемой системы, в которой создавался скачок температуры, выводились микропучки нейтронов. Спектры нейтронов в этих пучках измерялись методом времени пролета.

В качестве внешнего источника нейтронов был использован водо-водяной реактор ВВР-2, работающий на мощности 2000 квт. Реактор давал возможность получать широкий пучок (50×50) см^2 тепловых нейтронов.

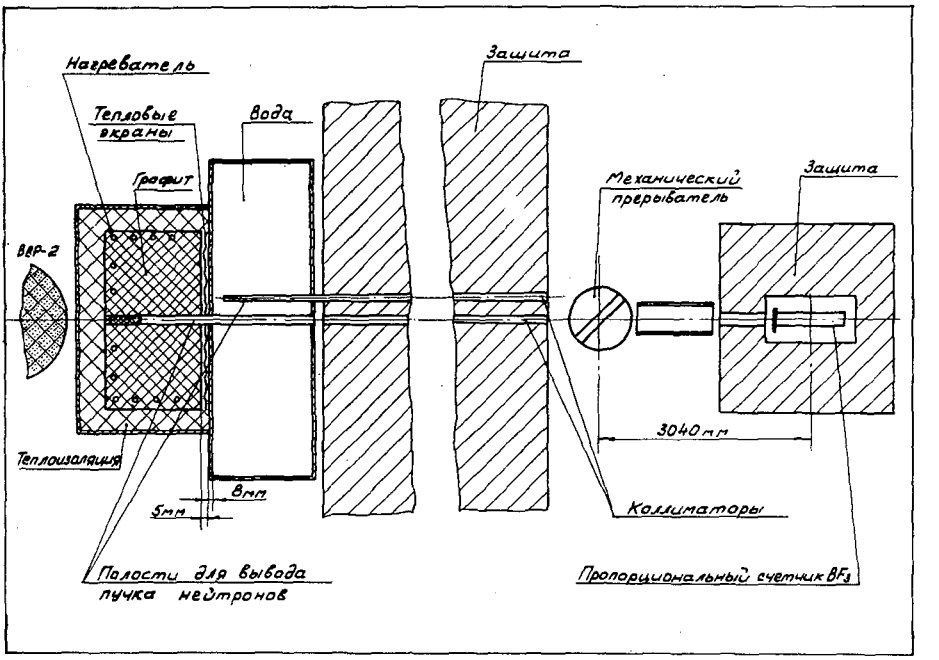

Рис.1

Схема экспериментальной установки.

Схема экспериментальной установки показана на рис.1. Экспериментальная установка состоит из графитовой призмы размерами $(100 \times 100 \times 59{,}5)$ см^3 и бака с водой размерами $(175 \times 175 \times 50)$ см^3.

Графитовая призма нагревалась специальным электрическим нагревателем мощностью 80 квт. Стержни электронагревателя были расположены в специальных отверстиях по периферии с пяти сторон графитовой призмы. Контроль за температурой графита осуществлялся при помощи хромель-алюмелевых термопар.

Между графитовой призмой и баком с водой имелся 5-миллиметровый зазор. В этом зазоре были расположены 3 тепловых экрана, которые обеспечивали тепловую изоляцию графита от воды. Каждый экран имел площадь (100×100) см^2. Ближние к графиту экраны были изготовлены из фольги нержавеющей стали (толщина фольги — 100 микрон), а третий экран выполнен из фольги алюминия (толщина фольги — 200 микрон). Теплоизоляция других граней графитовой призмы осуществлялась при помощи ультралегковесного шамота толщиной 20 см.

Графитовая призма с четырех боковых сторон (поверх теплоизоляции из ультралегковесного шамота) была окружена слоем карбида бора толщиной 20 мм. Вместе с теплоизоляцией и слоем карбида бора она была заключена в герметичный алюминиевый кожух, который при температурах графита выше 600° К заполнялся газообразным азотом для предотвращения окисления графита.

Нейтроны из различных точек графита и воды выводились в направлении падающего из реактора на графитовую призму потока нейтронов. Для

вывода нейтронного пучка из графита служил сквозной канал диаметром 17 мм, проходящий через центр призмы. Он мог дистанционно заполняться графитовыми вставками различной длины. Из воды нейтроны выводились при помощи передвижной алюминиевой трубки с дном.

Для измерения нейтронных спектров был использован механический прерыватель диаметром 150 мм с одной плоскопараллельной щелью шириной 5 мм (ротор механического прерывателя изготовлен из стеклопластика с бором) и 160-канальный временной анализатор. Детектором нейтронов служил торцевой пропорциональный счетчик, наполненный обогащенным газом BF_3 (обогащение $B^{10} \sim 85{,}7\%$) до давления ~593 мм рт.ст. Эффективность детектора для тепловых нейтронов ($v = 2200$ м/сек) составляла ~66%. Разрешение в измерении времени пролета нейтронов составляло 20 мксек/м.

Спектры нейтронов измерялись в точках, расположенных на следующих расстояниях от температурного разрыва.

а) в графите: 0; 5; 10; 20; 45; 95; 195; 295; 395; 495; 595 мм;

б) в воде: 0; 1; 2; 3; 5; 7; 10; 15; 20; 30; 50 и 75 мм.

Измерения проводили при температурах графита 443, 594, 725 и 823° К, температура воды была равна 303° К. Во время измерений температура графита поддерживалась постоянной с точностью ± 7°, а температура воды — с точностью ± 3°.

Спектр нейтронов вычисляли из получаемой скорости счета на каналах временного анализатора по известному соотношению [1], учитывающему функцию пропускания ротора*, эффективность счетчика**, зависимость эффективного пролетного расстояния от энергии нейтронов (за счет смещения эффективного центра регистрации нейтронов в счетчике), зависимость поглощения и рассеяния нейтронов в воздухе на пути от дна полости до детектора и фон нейтронов.

Поправка на разрешение селектора в области тепловых энергий нейтронов, а также поправка на просчеты при регистрации нейтронов не вводились, т.к. они были меньше статистической ошибки измерений. Эффект от нейтронов, испускаемых стенками полости и рассеянных в ней на молекулах воздуха, как показали специальные измерения, был также мал и потому не учитывался.

Обработка экспериментальных данных и описанные ниже расчеты были выполнены на электронно-вычислительной машине М-20.

3. МЕТОДИКА РАСЧЕТА ПРОСТРАНСТВЕННО-ЭНЕРГЕТИЧЕСКОГО РАСПРЕДЕЛЕНИЯ ТЕПЛОВЫХ НЕЙТРОНОВ***

Результаты измерений сравнивались с численным решением кинетического уравнения для потока нейтронов:

---

* Учитывался эффект проницаемости стенок щели ротора.

** Эффективность счетчика определялась экспериментально.

*** Описываемая в этом параграфе методика и расчет были выполнены совместно с Г.Ф. Лиманом.

где $\Phi(z,\mu,v)$ — поток нейтронов скорости v в точке z, которые летят под углом θ ($\mu=\cos\theta$) по отношению к направлению выводимого из системы микропучка.

Сечения рассеяния вычислялись с помощью программ "УПРАС" и "ПРАССИВ" [3] на основании экспериментальных спектров $\rho(\beta)$, полученных в работе [2] для воды и в работе [4] для графита.

Для решения кинетического уравнения (1) использовался следующий метод последовательных приближений:

$$\mu\frac{\partial\Phi^{(n+1)}}{\partial z}+\Sigma_t\Phi^{(n+1)}=Q^{(n+1)}(z,v)+q^{(n)}(z,\mu,v), \tag{2}$$

где

$$Q^{(n+1)}(z,v)=\tfrac{1}{2}\int_{-1}^{1}d\mu\int_{0}^{v_c}\Sigma_{so}(v\leftarrow v')\Phi^{(n+1)}(z,\mu,v')dv'+S(z,\mu,v), \tag{3}$$

$$q^{(n)}(z,\mu,v)=\int_{-1}^{1}d\mu'\int_{0}^{v_c}\left[\Sigma_s(v\leftarrow v',\mu\leftarrow\mu')-\tfrac{1}{2}\Sigma_{so}(v\leftarrow v')\right]\Phi^{(n)}(z,\mu',v')\,dv', \tag{4}$$

$$\Sigma_{so}(v\leftarrow v')=\int_{-1}^{1}d\mu\,\Sigma_s(v\leftarrow v',\mu\leftarrow\mu'). \tag{5}$$

Начальное приближение $q^{(0)}=0$

Схема решения задачи была следующей:

1) Для заданного $q^{(n)}$ решалось уравнение (2), которое предварительно записывалось в форме уравнения Пайерлса:

$$\varphi^{(n+1)}(z,v)=f^{(n)}(z,v)+\int dz'\int dv'K(z,z',v,v')\varphi^{(n+1)}(z',v'), \tag{6}$$

где

$$\varphi(z,v)=\int_{-1}^{1}\Phi(z,\mu,v)d\mu.$$

Уравнение Пайерлса решалось итерационным методом так же, как и в работе [5].

2) По полученному из уравнения (6) потоку $\varphi^{(n+1)}(z,v)$ вычислялся векторный поток $\Phi^{(n+1)}(z,\mu,v)$:

$$\Phi^{(n+1)}(z,\mu,v)=\Phi(0,\mu,v)\cdot e^{-\int_0^z\Sigma_t\,dz}+\frac{1}{\mu}\int_0^z e^{\frac{1}{\mu}\int_z^{z'}\Sigma_t\,dz''}\left[Q^{(n+1)}(z',v)+q^{(n)}(z',\mu,v)\right]dz'. \tag{7}$$

3) По $\Phi^{(n+1)}$ определялось $q^{(n+1)}$, и процесс последовательных приближений повторялся снова.

При незначительной анизотропии потока можно написать следующее приближенное выражение для векторного потока, учитывающее поправку на анизотропию рассеяния:

Для $\mu=1$, что соответствует условиям данного эксперимента,

$$\Phi(z,1,v)\approx\Phi(o,1,v)\,e^{-\int_0^z\Sigma_t\,dz}+\int_0^z e^{\int_z^{z'}\Sigma_t\,dz''}\left[Q^{(1)}(z',v)+q^{(1)}(z',1,v)\right]dz', \quad (8)$$

$$q^{(1)}(z',1,\mu)\approx\Sigma_t(z',v)\bar{\mu}(z',v)\frac{\partial\Phi^{(1)}(z',1,v)}{\partial\mu}, \quad (9)$$

где $\bar{\mu}$ – средний косинус угла рассеяния нейтронов.

По изложенной методике были вычислены:

$\varphi(z,v)$ – скалярный поток нейтронов без учета анизотропии рассеяния;

$\Phi^{(1)}(z,1,v)$ – векторный поток нейтронов без учета анизотропии рассеяния;

$\Phi(z,1,v)$ – векторный поток нейтронов с поправкой на анизотропию рассеяния ($\bar{\mu}\neq 0$).

4. РАСЧЕТ СЕЧЕНИЙ РЕТЕРМАЛИЗАЦИИ

Пространственно-энергетическое распределение тепловых нейтронов, полученное в эксперименте, анализировалось с помощью метода перекрывающихся групп [6,7]. Скалярный поток нейтронов $\varphi(z,E)$ в любой точке z исследуемой системы представлялся в виде суперпозиции двух равновесных распределений:

$$\varphi(z,E)=\Phi_1(z)\chi_1(E)+\Phi_2(z)\chi_2(E), \quad 0\leqslant E\leqslant E_c, \quad (10)$$

где $\chi_\ell(E)$ – пробные функции, удовлетворяющие условию

$$\int_0^{E_c}\chi_\ell(E)\,dE=1 \quad (\ell=1,2)$$

В соответствии с методом перекрывающихся тепловых групп $\Phi_1(z)$ и $\Phi_2(z)$ удовлетворяют следующим приближенным уравнениям баланса:

$$\begin{aligned} D_1\Delta\Phi_1(z)-\Sigma_{a1}\Phi_1(z)-\Sigma_R^{1\to2}\Phi_1(z)+\Sigma_R^{1\to2}\Phi_2(z)&=-S_2(z),\\ D_2\Delta\Phi_2(z)-\Sigma_{a2}\Phi_2(z)+\Sigma_R^{1\to2}\Phi_1(z)-\Sigma_R^{2\to1}\Phi_2(z)&=-S_1(z), \end{aligned} \quad (11)$$

с граничными условиями

$$\begin{aligned} \Phi_\ell(r_л)&=A\ell\\ \Phi_\ell(r_п)&=B\ell \end{aligned} \qquad (\ell=1,2) \quad (12)$$

($r_л$ и $r_п$ – левая и правая граница зоны), где

$$S_1(z)=\frac{E_s(z)-E_{D1}}{E_{D2}-E_{D1}}\cdot S(z),$$

$$S_2(z) = \frac{E_{D2} - E_s(z)}{E_{D2} - E_{D1}} \cdot S(z) ,$$

$$S(z) = \int_0^{E_c} S(z, E)dE ,$$

$$S(z, E) = \int_{E_c}^{\infty} \varphi(z, E')\Sigma_s (E' \to E)dE .$$

Остальные обозначения соответствуют принятым в [8,9].

Сечения ретермализации $\Sigma_R^{1\to 2}$ и $\Sigma_R^{2\to 1}$ находились следующим образом. Используя данные эксперимента, из уравнения (10) методом наименьших квадратов определялись функции $\bar{\Phi}_1(z)$ и $\bar{\Phi}_2(z)$. Уравнение (11) записывалось в виде:

$$\begin{aligned} \Delta\Phi_1(z, \Sigma_R^{1\to 2}, \Sigma_R^{2\to 1}) - K_1^2 \Phi_1(z, \Sigma_R^{1\to 2}, \Sigma_R^{2\to 1}) = \tilde{f}_1(z), \\ \Delta\Phi_2(z, \Sigma_R^{1\to 2}, \Sigma_R^{2\to 1}) - K_2^2 \Phi_2(z, \Sigma_R^{1\to 2}, \Sigma_R^{2\to 1}) = f_2(z), \end{aligned} \tag{13}$$

$$\begin{aligned} \tilde{f}_1(z) &= -\frac{S_2(z)}{D_1} + \Sigma_R^{1\to 2}\frac{\bar{\Phi}_1(z)}{D_1} - \Sigma_R^{2\leftarrow 1}\frac{\bar{\Phi}_2(z)}{D_1}, \\ \tilde{f}_2(z) &= -\frac{S_1(z)}{D_2} - \Sigma_R^{1\to 2}\frac{\bar{\Phi}_1(z)}{D_2} + \Sigma_R^{2\to 1}\frac{\bar{\Phi}_2(z)}{D_2} . \end{aligned} \tag{14}$$

Затем сечения ретермализации $\Sigma_R^{1\to 2}$ и $\Sigma_R^{2\to 1}$ определялись так, чтобы решение уравнений (13) $\Phi_1\left(z, \Sigma_R^{1\to 2}, \Sigma_R^{2\to 1}\right)$ и $\Phi_2\left(z, \Sigma_R^{1\to 2}, \Sigma_R^{2\to 1}\right)$ наилучшим образом аппроксимировали $\bar{\Phi}_1(z)$ и $\bar{\Phi}_2(z)$.

Функции $\Phi_1\left(z, \Sigma_R^{1\to 2}, \Sigma_R^{2\to 1}\right)$ и $\Phi_2\left(z, \Sigma_R^{1\to 2}, \Sigma_R^{2\to 1}\right)$ линейно зависят от неизвестных параметров $\Sigma_R^{1\to 2}$ и $\Sigma_R^{2\to 1}$.

Поэтому эти параметры можно определить, минимизируя функционал:

$$\mathscr{I} = \int_{r_л}^{r_п} \left\{ \left[\bar{\Phi}_1(z) - \Phi_1(z)\right]^2 + \left[\bar{\Phi}_2(z) - \Phi_2(z)\right]^2 \right\} dz \tag{15}$$

5. РЕЗУЛЬТАТЫ

На рис.2,3,4 и 5 приведены результаты измерений спектров нейтронов $v^2 n(z, \mu, v)$ для $\mu = 1$ и расчетов по изложенной выше методике.

На рис.2 изображены экспериментальный спектр и рассчитанный векторный поток $\Phi^{(1)}(z,1,v)$, умноженный на v, в графите на расстоянии 2,0 см от теплового барьера. Температура графита 592° К, температура воды 303° К. Для той же температуры графита на рис.3 приведены аналогичные

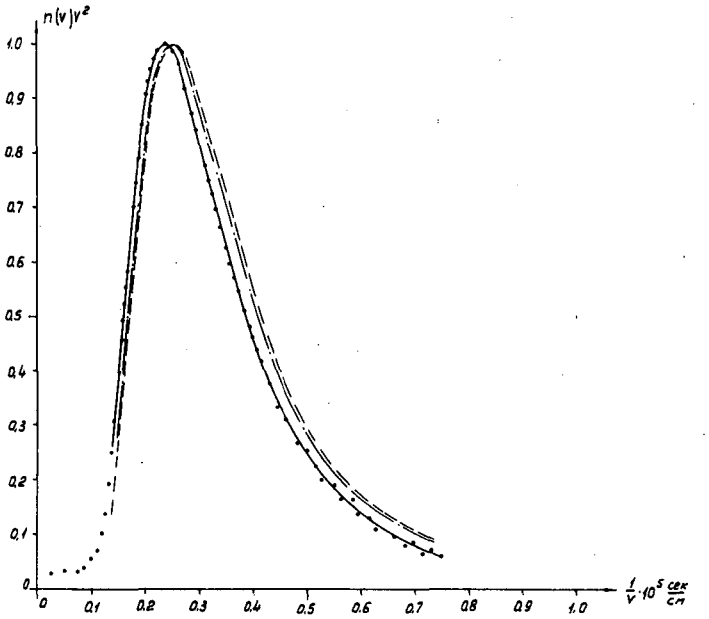

Рис.2

Спектр нейтронов в графите в точке, расположенной на расстоянии 2,0 см от теплового барьера; температура графита 592° К, температура воды 303° К:
о о о о о экспериментальные данные;
———— расчет векторного потока нейтронов с учетом кристаллических эффектов;
– – – – – расчет скалярного потока нейтронов в P_1-приближении по модели одноатомного газа;
— · — расчет скалярного потока нейтронов с учетом кристаллических эффектов.

кривые, изображающие спектры нейтронов в воде на расстоянии 5 мм от теплового барьера. Чтобы показать эффект анизотропии рассеяния в воде на рис.3 также изображена кривая $v\Phi(z,1,v)$.

Экспериментальный и рассчитанный векторные потоки в графите совпадают достаточно хорошо.

На рис.3 видно, что эффект анизотропии рассеяния нейтронов в воде довольно заметен и его следует учитывать, особенно при наличии больших градиентов потока, обусловленных градиентами температуры, поглощения и др.

На тех же рисунках приведены результаты расчета скалярного потока нейтронов по описанной выше методике, которые сравниваются со скалярными потоками, вычисленными в P_1-приближении с использованием модели одноатомного газа.

Как видно, в этих точках в графите и воде различие между обоими расчетами небольшое.

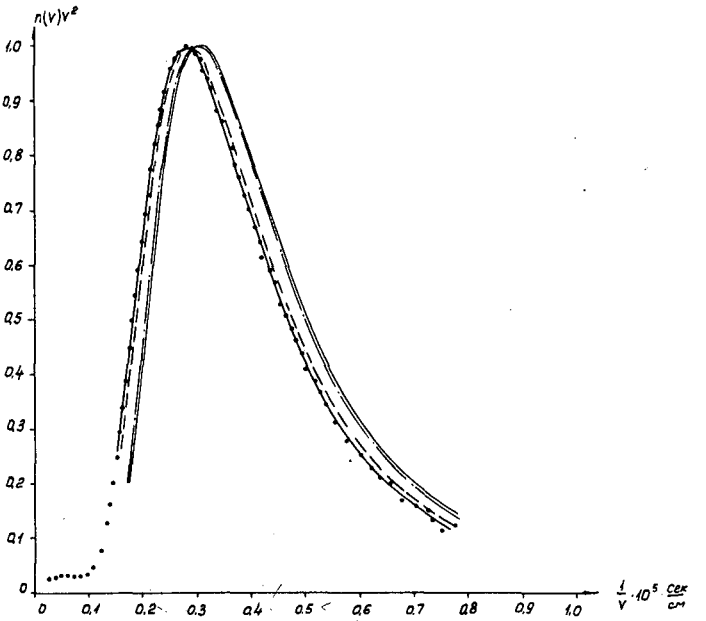

Рис.3

Спектр нейтронов в воде в точке, расположенной на расстоянии 5 мм от теплового барьера; температура графита 592° К; температура воды 303° К:
o o o o o экспериментальные данные;
——— расчет векторного потока нейтронов с учетом химической связи с поправкой на анизотропию рассеяния;
– – – – – расчет векторного потока нейтронов, с учетом химической связи без поправки на анизотропию рассеяния;
— · — расчет скалярного потока нейтронов с учетом химической связи без поправки на анизотропию рассеяния;
——— расчет скалярного потока нейтронов в P_1-приближении по газовой модели.

На рис.6,7 представлены сечения ретермализации в графите и воде в зависимости от температуры графита при постоянной температуре воды (T = 303° K).

Из рис.6 видно, что сечение ретермализации графита существенно зависит от температуры графита и в соответствии с теорией с увеличением температуры приближается к асимптотическому значению $\frac{2A}{(A+1)^2}\Sigma_{s21}$. Сечение ретермализации, полученное Беннетом [9], также возрастает с температурой графита. Однако абсолютная величина полученных им сечений несколько выше. Из рис.6 видно, что результаты Пула [10] лежат ниже как наших данных, так и данных Беннета [9]. Очень слабую зависимость сечения ретермализации от температуры дает расчет по модели свободного газа.

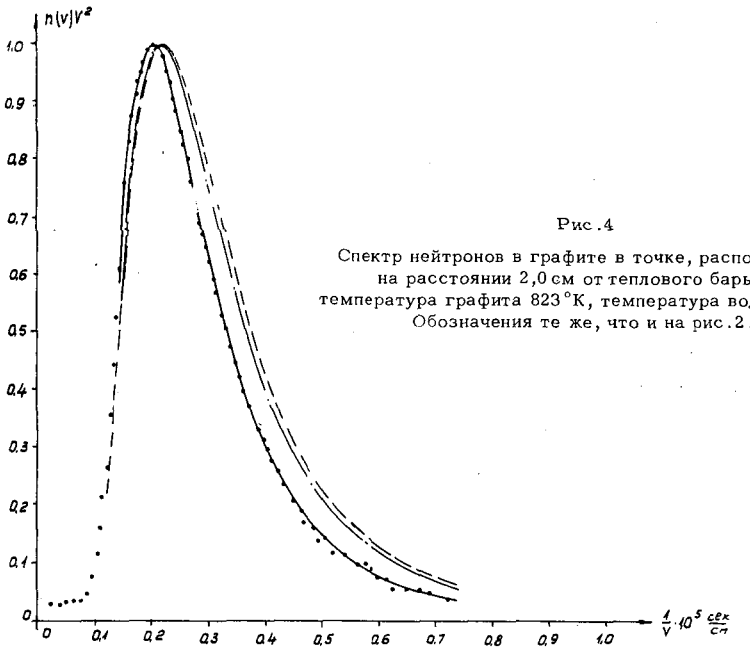

Рис.4

Спектр нейтронов в графите в точке, расположенной на расстоянии 2,0 см от теплового барьера; температура графита 823°К, температура воды – 303°К. Обозначения те же, что и на рис.2.

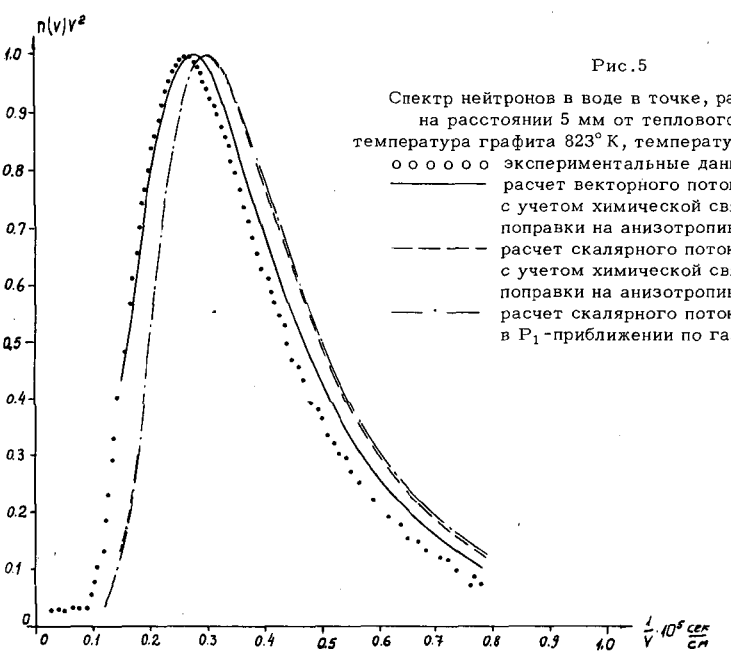

Рис.5

Спектр нейтронов в воде в точке, расположенной на расстоянии 5 мм от теплового барьера; температура графита 823°К, температура воды – 303°К.

ооооооо экспериментальные данные;

———— расчет векторного потока нейтронов с учетом химической связи без поправки на анизотропию рассеяния;

— — — — расчет скалярного потока нейтронов с учетом химической связи без поправки на анизотропию рассеяния;

— · — расчет скалярного потока нейтронов в P_1-приближении по газовой модели.

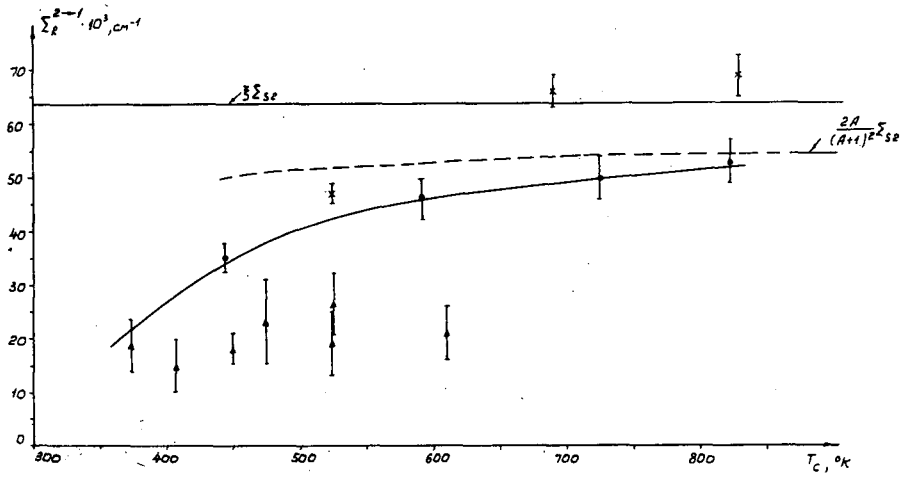

Рис.6

Сечение ретермализации нейтронов в графите:

- ● экспериментальные данные;
- – – – расчет в P_1-приближении по модели одноатомного газа;
- × результаты Беннета [9];
- ▲ результаты Пула и др. [10].

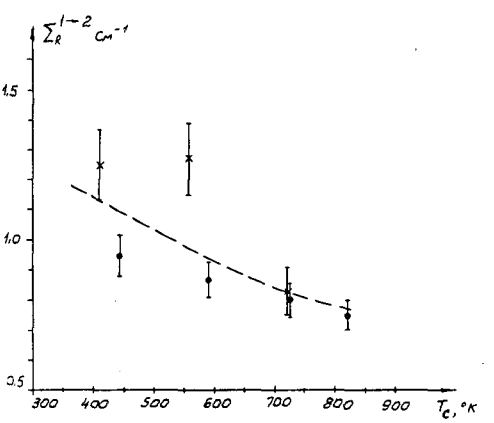

Рис.7

Сечение ретермализации нейтронов в воде.

- o экспериментальные данные;
- – – – расчет в P_1-приближении по газовой модели;
- × результаты Беннета [9].

Сечение ретермализации в воде (рис.7) уменьшается с увеличением температуры графита более медленно, чем это дается моделью свободного газа. Сечения ретермализации, полученные Беннетом [9], несколько отличаются от наших в области температур нейтронов меньше 600° К. Более

подробное сопоставление и анализ результатов различных работ будут даны в отдельной статье.

Авторы благодарны В.Ф.Турчину за любезно предоставленную возможность проведения расчетов сечений рассеяния по его программе "ПРАССИВ".

ЛИТЕРАТУРА

[1] МОСТОВОЙ В.И. и др. Доклад Р/2152 на II Женевской конференции, 1958.
[2] МОСТОВОЙ В.И. и др. Доклад Р/367 на III Женевской конференции, 1964.
[3] МАЙОРОВ Л.В., ТУРЧИН В.Ф., ЮДКЕВИЧ М.С. Доклад Р/360 на III Женевской конференции, 1964.
[4] EGELLSTAFF, P.A., AERE-R 3931 (1962).
[5] HONECK H.C. Nucl.Sci. and Engn., 8, 193 (1960).
[6] KOTTWITZ D.A., Nucl.Sci. and Engn., 7, 345 (1960).
[7] SELENGUT, D.S., Nucl.Sci. and Engn., 9, 94 (1961).
[8] LINDENMEIER G.W., BNL-719 (C-32); IV, (1962), 1271.
[9] BENNETT R.A., BNL-719 (C-32), III, (1962), 838.
[10] POOLE C.G. et al., HL. 63/4053, July 1963.

DISCUSSION

(on the foregoing three papers)

P. ZWEIFEL (Chairman): Was the "vector flux" referred to in paper SM-62/109 the angular flux evaluated for the forward direction, i.e. your direction of measurement?

I. SADIKOV: Yes.

K. H. BECKURTS: I was very surprised by the large time delay you found for the establishment of an asymptotic spectrum in H_2O. I should be interested to know what corrections were applied for the neutron flight time between the medium and the chopper. Could you also perhaps indicate to what extent you believe this result might be influenced by the existence of higher spatial modes?

I. SADIKOV: The results for H_2O surprised us too. A correction was made for the transformation of the spectrum involved in the flight of the neutrons from the moderator to the chopper. Unfortunately, there was not enough time available to discuss in the paper the method of correction used. As far as the influence of the higher spatial harmonics was concerned, this was probably of decisive importance in the conditions in which the experiment was carried out.

P. ZWEIFEL: Did you look for or discover any evidence of "die-away" in your Be experiments which would tie up with the data reported from the Rensselaer Polytechnic Institute?

I. SADIKOV: I am not quite sure whether I understand the term "die-away" correctly. If the question relates to whether in our measurements with Be with the small assemblies we managed to establish an equilibrium condition in time, the answer is that we did not.

E. SILVER: Did you include any measurements of the effects of the phase transition from water to ice on the scattering angular distribution?

I. SADIKOV: No, we did not carry out any measurements of this sort.

ЗАМЕДЛЕНИЕ НЕЙТРОНОВ, ИСПУСКАЕМЫХ ИМПУЛЬСНЫМ ИСТОЧНИКОМ, И СПЕКТРОМЕТРИЯ НЕЙТРОНОВ ПО ВРЕМЕНИ ЗАМЕДЛЕНИЯ

А.А. БЕРГМАН, А.И. ИСАКОВ, М.В. КАЗАРНОВСКИЙ, Ю.П. ПОПОВ и Ф.Л. ШАПИРО
ФИЗИЧЕСКИЙ ИНСТИТУТ им. П.Н. ЛЕБЕДЕВА АН СССР, МОСКВА СССР

Abstract — Résumé — Аннотация — Resumen

MODERATION OF NEUTRONS EMITTED BY A PULSED SOURCE AND NEUTRON SPECTROMETRY BASED ON SLOWING-DOWN TIME. Over the past ten years research has been going on at the P. N. Lebedev Physics Institute on the non-stationary moderation of neutrons in heavy media, the development of a method of neutron spectrometry based on the slowing-down time and the use of this method in studying the energy dependence of the cross-sections of nuclear reactions produced by neutrons with energy up to 30 keV. The authors review this work and discuss the results achieved.

After a brief discussion of the theory of the non-stationary moderation and thermalization of neutrons the authors set forth the results of experimental studies of neutron moderation in graphite, iron and lead, and of neutron thermalization in lead. Using a pulsed neutron source and resonance detectors the distribution of slowing-down times was measured up to a series of fixed values for final neutron energy. The results are compared with theory, which takes into account the thermal motion of the moderator atoms; in the case of lead this thermal motion leads to a measurable spread in the slowing-down times at energies below 10 eV. The relationship between the mean velocity of neutrons in lead and the slowing-down time is measured in the sub-cadmium energy range and a comparison made with multigroup theory. The procedure for determining the energy dependence of neutron reaction cross-sections by slowing-down time is described and the potentialities of this method of spectrometry discussed. There follows a brief discussion of the results obtained in two fields of spectrometric measurement.

Firstly, precise measurement of the relative excitation functions of the following reactions: $He^3(n, p)$, $Li^6(n, \alpha)$, $B^{10}(n, \alpha)$ and $N^{14}(n, p)$ — the most interesting results being the discovery of a constant negative component of the reaction cross-section and indications of the existence of an excited He^4 level.

Secondly, measurement of the energy dependence of averaged radiative capture cross-sections. Measurements carried out on a large number of substances, including separated isotopes, have led to the discovery of hitherto unknown resonance levels with small neutron widths and have made it possible to determine for many nuclei the magnitude of the force function for the capture of neutrons with orbital angular momentum $l=1$.

RALENTISSEMENT DES NEUTRONS ÉMIS PAR UNE SOURCE PULSÉE ET LEUR SPECTROMÉTRIE EN FONCTION DU TEMPS DE RALENTISSEMENT. A l'Institut de physique P. N. Lébédev de l'Académie des sciences de l'URSS, on a procédé, au cours de ces six dernières années, à une série de travaux visant à étudier le ralentissement non stationnaire des neutrons dans les milieux lourds, à élaborer une méthode de spectrométrie des neutrons en fonction du temps de ralentissement et à appliquer cette méthode à l'étude de l'influence que l'énergie exerce sur les sections efficaces des réactions nucéaires provoquées par des neutrons d'une énergie de 30 keV ou moins. Les auteurs donnent un aperçu de ces recherches et en analysent les résultats.

Après avoir examiné brièvement la théorie du ralentissement non stationnaire et de la thermalisation des neutrons, ils indiquent les données fournies par une étude expérimentale du ralentissement des neutrons dans le graphite, le fer et le plomb et par l'étude de leur thermalisation dans le plomb. En utilisant une source de neutrons pulsée et des détecteurs à résonance, ils ont mesuré la distribution des temps de ralentissement pour une série de valeurs déterminées de l'énergie finale des neutrons. Ils comparent les résultats obtenus à la théorie qui tient compte du mouvement thermique des atomes du ralentisseur, lequel provoque, dans le cas du plomb, une dispersion mesurable des temps de ralentissement pour des énergies inférieures à 10 eV. Dans le domaine d'énergies inférieures au seuil cadmium, on a mesuré l'influence du temps de ralentissement sur la vitesse moyenne des neutrons dans le plomb; une comparaison a été faite avec la théorie à plusieurs groupes. Les auteurs décrivent la méthode employée pour déterminer, selon le temps de ralentissement, les variations

de la section efficace des réactions neutroniques en fonction de l'énergie et ils examinent les possibilités d'application et de perfectionnement qu'offre cette méthode de spectrométrie. Ils étudient brièvement les résultats de deux sortes de mesures spectrométriques:

1. Mesures précises portant sur les variations, en fonction de l'énergie, des rapports entre les sections efficaces des réactions $^{3}He(n, p)$, $^{6}Li(n, \alpha)$, $^{10}B(n, \alpha)$ et $^{14}N(n, p)$. Le résultat le plus intéressant de ces expériences a été de découvrir une composante négative constante de la section efficace de ces réactions et de trouver des indices laissant supposer l'existence d'un niveau excité de ^{4}He.

2. Mesures de la variation que subissent les valeurs moyennes des sections efficaces de capture radiative des neutrons par les noyaux, en fonction de l'énergie. Ces mesures, qui ont été faites pour un grand nombre de substances, notamment pour divers isotopes, ont permis de constater l'existence de plusieurs niveaux de résonance à faible largeur neutronique, auparavant inconnues, et de déterminer pour beaucoup de noyaux la valeur de la fonction de force relative à la capture des neutrons à moment orbital $l=1$.

ЗАМЕДЛЕНИЕ НЕЙТРОНОВ, ИСПУСКАЕМЫХ ИМПУЛЬСНЫМ ИСТОЧНИКОМ, И СПЕКТРОМЕТРИЯ НЕЙТРОНОВ ПО ВРЕМЕНИ ЗАМЕДЛЕНИЯ. В Физическом институте им. П.Н.Лебедева АН СССР на протяжении последних 10 лет был выполнен ряд работ по исследованию нестационарного замедления нейтронов в тяжелых средах, развитию метода спектрометрии нейтронов по времени замедления и применению этого метода для изучения энергетической зависимости сечений ядерных реакций, вызываемых нейтронами с энергией до 30 кэв. В настоящем докладе дается обзор этих исследований и обсуждаются их итоги.

В докладе после краткого рассмотрения теории нестационарного замедления и термализации нейтронов излагаются результаты экспериментального изучения замедления нейтронов в графите, железе и свинце и изучения термализации нейтронов в свинце. При помощи импульсного источника нейтронов и резонансных детекторов было измерено распределение времен замедления до ряда фиксированных значений конечной энергии нейтрона. Проведено сравнение полученных результатов с теорией, учитывающей тепловое движение атомов замедлителя, которое в случае свинца приводит к измеримому разбросу времен замедления при энергиях ниже 10 эв. Для подкадмиевой области энергий измерена зависимость средней скорости нейтронов в свинце от времени замедления и проведено сравнение с многогрупповой теорией.

Описана применявшаяся методика определения энергетической зависимости сечений нейтронных реакций по времени замедления и обсуждаются возможности и перспективы этого метода спектрометрии. Кратко обсуждаются результаты спектрометрических измерений, которые велись в двух направлениях. Первое направление – прецизионные измерения энергетической зависимости энергетического хода отношений сечений реакций $He^{3}(n,p)$, $Li^{6}(n,\alpha)$, $B^{10}(n,\alpha)$ и $N^{14}(n,p)$. Наиболее интересный результат этих опытов – обнаружение постоянной отрицательной слагающей сечения реакций и указания на существование возбужденного уровня He^{4}. Второе направление – измерения энергетического хода усредненных сечений радиационного захвата нейтронов ядрами. Измерения, проведенные для большого числа веществ, в том числе разделенных изотопов, привели к обнаружению некоторого числа не известных ранее резонансных уровней с малыми нейтронными ширинами и позволили определить для многих ядер величину силовой функции для захвата нейтронов с орбитальным моментом $l=1$.

MODERACION DE NEUTRONES EMITIDOS POR UNA FUENTE PULSADA Y ESPECTROMETRIA NEUTRONICA BASADA EN EL TIEMPO DE FRENADO. Durante los últimos diez años se han venido realizando en el Instituto de Física P. N. Lebedev investigaciones sobre la moderación no estacionaria de neutrones en medios pesados, el desarrollo de un método de espectrometría neutrónica basada en la medición del tiempo de frenado y la aplicación de este método al estudio de la relación entre la energía y las secciones eficaces de las reacciones nucleares producidas por neutrones con niveles energéticos de hasta 30 keV. En la presente memoria los autores pasan revista a dichos trabajos y analizan los resultados obtenidos.

Después de exponer brevemente la teoría de la moderación y termalización no estacionarias de neutrones, los autores presentan los resultados de estudios experimentales sobre la moderación de neutrones en grafito, hierro y plomo, y sobre la termalización de neutrones en este último metal. Mediante una fuente de neutrones pulsados y usando detectores de resonancia, midieron la distribución de los tiempos de frenado para una serie de valores fijos de energía neutrónica final. En la memoria se comparan los resultados con la teoría, que toma en cuenta la agitación térmica de los átomos del moderador; en el caso del plomo, esta agitación origina una dispersión medible de los tiempos de frenado a energías menores que 10 eV. Dentro del intervalo de energía subcádmica, los autores midieron la relación entre la velocidad media de los neutrones en el plomo y el tiempo de frenado, y compararon los resultados con la teoría de los grupos múltiples. Los autores describen

el procedimiento seguido para determinar, mediante el tiempo de frenado, la relación entre la energía y las secciones eficaces de las reacciones neutrónicas y analizan las posibilidades de este método espectrométrico. Sigue en la memoria un breve análisis de los resultados obtenidos en dos campos de la medición espectrométrica:

En primer lugar, la medición precisa de las funciones de excitación relativas de las siguientes reacciones: $^{3}He(n, p)$, $^{6}Li(n,\alpha)$, $^{10}B(n,\alpha)$ y $^{14}N(n, p)$; los resultados más interesantes son el descubrimiento de una componente negativa constante de la sección eficaz de la reacción e indicios de la existencia de un nivel excitado del ^{4}He.

En segundo lugar, la medición de la relación que existe entre la energía y el valor medio de las secciones eficaces de captura radiativa. Las mediciones realizadas en un gran número de sustancias, incluyendo isótopos separados, han llevado a descubrir niveles de resonancia hasta ahora desconocidos, de limitada anchura neutrónica, y han permitido determinar para numerosos núcleos la magnitud de la función de fuerza correspondiente a la captura de neutrones con un momento angular orbital $l=1$.

1. ВВЕДЕНИЕ

На протяжении последнего десятилетия в Физическом институте имени П.Н. Лебедева АН СССР был выполнен целый ряд исследований с импульсным источником нейтронов, находящимся в тяжелой среде. Теоретически и экспериментально был изучен процесс замедления и термализации нейтронов, испускаемых импульсным источником. Характерная особенность процесса замедления – сравнительная узость мгновенного энергетического распределения в области энергий нейтронов, малых по сравнению с порогом неупругого рассеяния, была использована для разработки метода нейтронной спектрометрии по времени замедления [1, 2]. С помощью спектрометра по времени замедления в свинце было проведено большое количество исследований энергетической зависимости сечений нейтронных реакций в области энергий нейтронов до 30 кэв. Такой спектрометр продолжает использоваться в физическом институте и в настоящее время. Аналогичные установки созданы также в Бомбее [3] и Карлсруэ [4]. В настоящем докладе дается краткий обзор результатов упомянутых выше исследований. Более подробное изложение содержится в работах [5–10].

2. ТЕОРИЯ НЕСТАЦИОНАРНОГО ЗАМЕДЛЕНИЯ И ТЕРМАЛИЗАЦИИ НЕЙТРОНОВ

Спектр нейтронов от стационарного источника, упруго замедляющихся в тяжелой среде (массовое число $A \gg 1$), хорошо описывается возрастной теорией. Согласно этой теории в простейшем случае бесконечной однородной незахватывающей среды с постоянной длиной свободного пробега ℓ скорость нейтронов v и время замедления t однозначно связаны соотношением:

$$\frac{1}{v} = \frac{\xi t}{2\ell} + \frac{1}{v_0}, \qquad (2.1)$$

где ξ – средняя логарифмическая потеря энергии при одном столкновении $\left(\xi \sim \frac{2}{A} \text{ при } A \gg 1\right)$, а v_0 – начальная (при $t=0$) скорость нейтронов. То есть спектр нейтронов от моноэнергетического импульсного источника представляет собой бесконечно узкую линию, перемещающуюся с ростом t в область

меньших скоростей, причем при $t \gg 2\ell/\xi v_0$ энергия нейтронов обратно пропорциональна t^2.

Если начальный спектр не моноэнергетический, то в процессе замедления нейтроны собираются в группу, относительная ширина которой убывает со временем. В этом можно убедиться на примере источника, который в начальный момент испускает нейтроны двух скоростей v_{0_1} и v_{0_2} (пусть $v_{0_1} > v_{0_2}$) с равной интенсивностью. Тогда в каждый последующий момент времени спектр нейтронов будет состоять из двух б-образных линий, и согласно (2.1) относительная ширина такого распределения нейтронов

$$\frac{v_1(t) - v_2(t)}{v_1(t) + v_2(t)} = \left(\frac{1}{v_{0_2}} - \frac{1}{v_{0_1}}\right) \Big/ \left(\frac{\xi t}{\ell} + \frac{1}{v_{0_2}} + \frac{1}{v_{0_1}}\right) \qquad (2.2)$$

стремится к нулю с ростом t.

Такой характер энергетического распределения обусловлен своеобразной "фокусировкой" нейтронов вблизи некоторой средней (убывающей с ростом t) скорости и может быть объяснен на основании следующих качественных соображений. Вероятность соударения нейтрона в единицу времени равна v/ℓ, т.е. (при $\ell = \text{const}$) пропорциональна скорости. Следовательно, пропорционально скорости и среднее относительное изменение скорости в единицу времени. Поэтому, если нейтрон обладает скоростью, меньшей, чем средняя, он будет реже сталкиваться, чем нейтрон со средней скоростью, и относительное изменение скорости за единицу времени у него будет меньше. В результате, спустя некоторое время он попадет в область вблизи средней скорости. Аналогично нейтрон, обладающий скоростью, больше средней, будет чаще сталкиваться, относительное изменение скорости у него будет больше, т.е. спустя некоторое время он также попадет в область средней скорости.

В то же время очевидно, что наряду с подобной фокусировкой вероятностный характер распределения столкновений нейтронов во времени и изменения энергии при каждом столкновении должен вызвать "дефокусировку", которая будет тем сильнее, чем уже нейтронный спектр. Таким образом, в отличие от результатов возрастной теории спектр нейтронов должен со временем стремиться не к бесконечно узкой линии, а к некоторой линии с конечной относительной шириной. Вопрос о форме и ширине этой асимптотической линии обсуждался в ряде работ [11, 12]. К сожалению, точное выражение в замкнутой форме при $\ell = \text{const}$ найти не удается*. Плачек [11] и Валлен [13] нашли моменты асимптотического распределения нейтронов. Казарновским [5, 14] были разработаны методы приближенного расчета нейтронного спектра. Мы не приводим здесь этих формул. Отметим только, что вблизи максимума спектр нейтронов в достаточно тяжелом замедлителе хорошо описывается функцией Гаусса

$$N(v,t)dv = N_0 \frac{\bar{v}}{v} \frac{dv}{v} \exp\left\{-\frac{3A}{4}\left(\frac{\bar{v}}{v} - 1\right)^2\right\}, \qquad (2.3)$$

---

* Это оказывается возможным лишь в нефизическом случае $\ell \sim v$.

где средняя скорость нейтронов $\bar{v}$ и дисперсия скорости D записываются уравнениями:

$$\bar{v} = \frac{\ell(A+1)}{t}; \qquad D = \overline{\left(\frac{\bar{v}}{v} - 1\right)^2} = \frac{2}{3A}. \tag{2.4}$$

Был исследован ряд эффектов, которые могут исказить эти результаты, полученные для идеального замедлителя [5, 6]. Так, примесь тяжелых ядер иной массы приводит к расширению спектра, связанному с дополнительным разбросом скоростей при каждом акте рассеяния. Примесь атомов водорода приводит к тому, что нейтроны, рассеянные на водороде, образуют низкоэнергетический медленно спадающий "хвост" распределения [5].

Учет зависимости длины свободного пробега от скорости, учет поглощения нейтронов, пространственных эффектов и утечки был проведен в работах [5, 6], в которых показано, что в практически интересных случаях эти эффекты не оказывают существенного влияния на ширину нейтронного спектра.

При малых энергиях нейтронов на спектре нейтронов начинают сказываться тепловое движение и химическая связь атомов замедлителя. При $E \gg kT_{эф}$ ($3/2\ kT_{эф}$ – средняя кинетическая энергия атома) дисперсия скоростей оказывается равной

$$D = \frac{2}{3A} + \frac{kT_{эф}}{4E}. \tag{2.5}$$

Относительная величина влияния теплового движения и химической связи на дисперсию имеет, таким образом, порядок величины $AkT_{эф}/E$; влияние на среднюю скорость существенно меньше – порядка $kT_{эф}/E$.

При достаточно больших временах замедления в среде без захвата (или с захватом по закону $1/v$) и без утечки устанавливается максвелловский спектр, соответствующий тепловому равновесию нейтронного газа с замедлителем и не зависящий от свойств среды. В промежуточной области – области термализации – распределение нейтронов, напротив, зависит от деталей закона рассеяния, что крайне усложняет строгое теоретическое рассмотрение. Были развиты сравнительно простые приближенные феноменологические подходы, в которых энергетический спектр разбивался на 2 [15] или более [16] групп. В рамках этих теорий отклонения от теплового равновесия затухают со временем по экспоненциальному закону. Так, например, для средней скорости в трехгрупповом приближении

$$\bar{v}(t) = v(\infty)[1 + ae^{-\lambda_1 t} + be^{-\lambda_2 t}], \tag{2.6}$$

где константы определяются законом рассеяния и, в принципе, могут быть вычислены. Необходимо заметить, что приближение типа (2.6) применимо лишь в том ограниченном случае, когда уравнение переноса нейтронов имеет дискретные собственные значения, помимо нулевого (подробнее см., например, в обзоре [17]).

3. ЭКСПЕРИМЕНТАЛЬНЫЕ ИССЛЕДОВАНИЯ ЗАМЕДЛЕНИЯ И ТЕРМАЛИЗАЦИИ НЕЙТРОНОВ В ТЯЖЕЛЫХ СРЕДАХ

А. Установка

В экспериментах мишень импульсного нейтронного генератора вводилась в середину большой призмы из исследуемого вещества (графит, железо, свинец). Нейтронный генератор представлял собой ускоритель типа Кокрофта-Уолтона на напряжение до 400 кв, в котором осуществлялась реакция $T(d, n)He^4$. Ионы дейтерия получались в источнике типа Пеннинга, работавшем в импульсном режиме с частотой повторения до 1250 гц. Ширина импульса дейтонов из ионного источника составляла ~6 мксек. Дальнейшее укорочение импульса до 0,5 – 1 – 2 мксек. производилось с помощью отклонения ускоренного пучка дейтонов в поле между пластинами специального "электрического затвора". Ионный пучок фокусировался на толстую цирконий-тритиевую мишень; пиковая интенсивность нейтронов составляла $\sim 5 \cdot 10^{11}$ н/сек.

Детекторами нейтронов служили пропорциональные счетчики и ионизационные камеры, содержащие BF_3, слои урана, бора, Li^6F. Для регистрации γ-лучей захвата нейтронов использовались пропорциональные и сцинтилляционные счетчики с кристаллами флюорита или тонкими слоями органических сцинтилляторов. Распределение импульсов от детекторов анализировалось по времени запаздывания относительно вспышки нейтронного генератора с помощью многоканальных временных анализаторов. Наиболее подробно было изучено замедление нейтронов в свинце; измерения проводились с призмой размером примерно $2 \times 2 \times 2{,}3$ м^3 из свинца с паспортной чистотой 99,98%. Дополнительно исследовалось замедление нейтронов в железе и графите; использовались призмы размером соответственно $1{,}2 \times 1 \times 1$ м^3 и $3{,}0 \times 1{,}2 \times 0{,}6$ м^3. Расположение опыта указано на рис.1.

Б. Замедление нейтронов

Зависимость плотности нейтронов от времени замедления измерялась с помощью детектора с эффективностью, пропорциональной $1/v$ (борный или литиевый счетчик). Согласно возрастной теории плотность нейтронов при достаточно больших временах замедления дается соотношением:

$$\rho(t) = const\ e^{-t/T} \cdot t^{-\alpha}, \qquad (3.1)$$

где T – среднее время жизни нейтрона до захвата в замедлителе (предполагается не зависящим от скорости нейтрона);

$$\alpha = \frac{2\omega\ell^2}{3\xi}; \qquad \omega = \frac{\pi^2}{4}\left(\frac{1}{a^2} + \frac{1}{b^2} + \frac{1}{c^2}\right);$$

2a, 2b, 2c – размеры призмы.

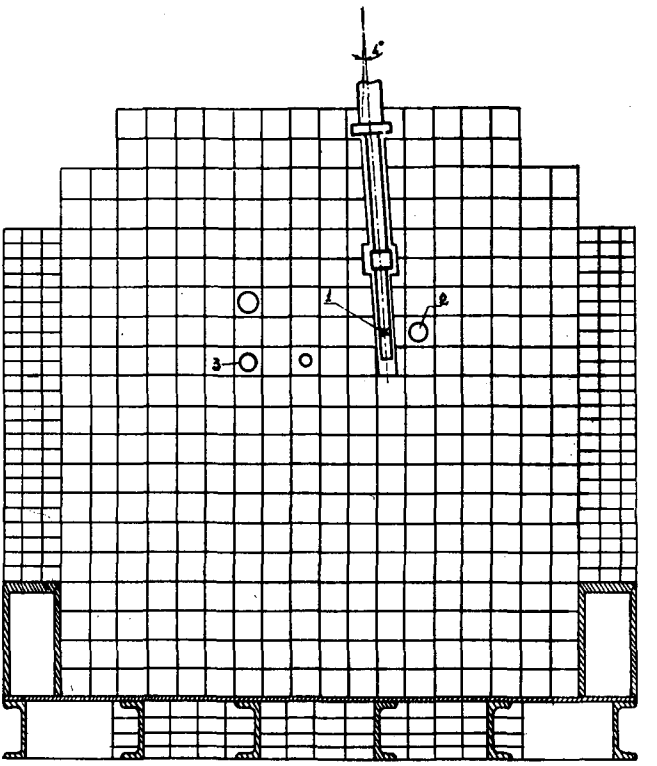

Рис.1

Схема свинцовой призмы:

1 – цирконий-тритиевая мишень; 2 – канал, в котором регистрируется вспышка быстрых нейтронов; 3 – измерительный канал.

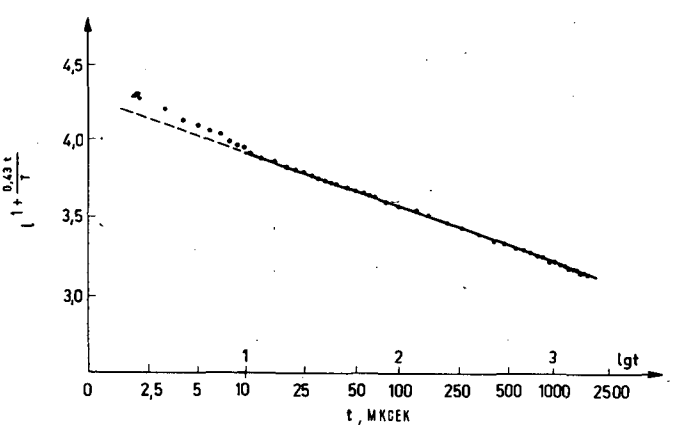

Рис.2

Зависимость плотности нейтронов от времени замедления.

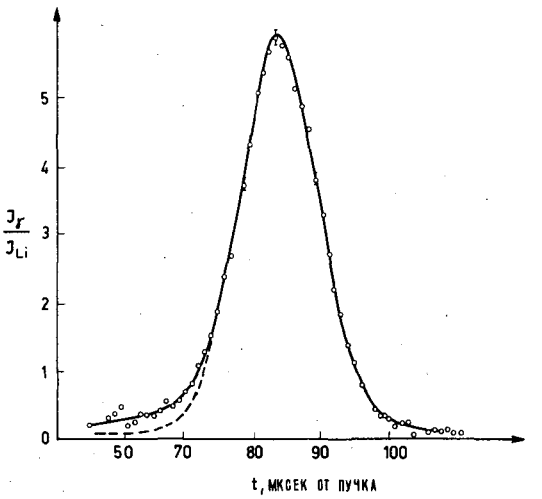

Рис.3

График $\mathscr{I}(t)$ для образца из селена.

Результаты измерений для свинцовой призмы приведены на рис.2. При $t>10$ мксек. точки хорошо удовлетворяют зависимости (3,1). Отклонение при меньших временах связано, как показал анализ, с резонансным захватом нейтронов на уровнях свинца, расположенных в области энергий выше 1 кэв.

Для изучения функции распределения замедляющихся нейтронов использовались резонансные детекторы, т.е. образцы веществ, обладающих изолированными резонансами с шириной Г малой по сравнению с шириной мгновенного спектра нейтронов. Резонансные образцы вместе с детектором захватных гамма-лучей вводились в призму и измерялась зависимость от времени замедления числа нейтронов, поглощаемых образцом в единицу времени. В пределе очень узкого резонанса эта зависимость может быть записана в виде:

$$\mathscr{I}_\gamma(t) = \text{const}\ \rho(t)\, N(E_0, t), \qquad (3.2)$$

где $N(E,t)$ – нормированное ($\int N(E,t)dE = 1$) энергетическое распределение нейтронов в момент времени замедления t.

E_0 – энергия резонанса.

На рис.3 представлен результат измерений с селеновым детектором ($E_0 = 27$ эв) в свинцовой призме. По оси ординат отложено значение

$$\mathscr{I}(t) = \text{const}\ \frac{\mathscr{I}_\gamma(t)}{\rho(t)} \approx N(E_0, t)\,.$$

Кривые такого рода, измеренные для свинцового замедлителя для большого числа резонансов в диапазоне энергий от 0,5 эв до 15 кэв, использовались для определения среднего времени замедления $\bar{t}$ и полуширины распределе-

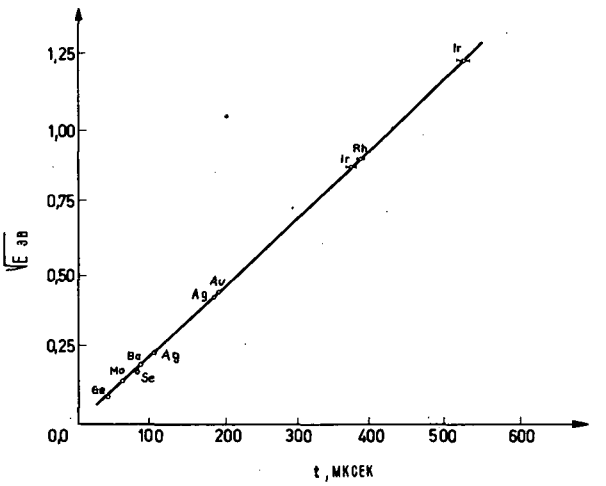

Рис.4

Связь между энергией нейтрона E и средним временем замедления до этой энергии.

ния времен замедления τ. При определении τ вносилась небольшая поправка на ширину кривой резонансного поглощения образца. Полученные результаты приведены на рис.4 и 5. Связь между средним временем замедления и энергией хорошо соответствует выражению (2.1). Полуширины τ описываются выражением

$$\tau^2 = b^2\overline{t}^2 + a^2, \qquad (3.3)$$

где $a^2 = 2 \pm 1$ мксек^2 – постоянная слагающая, определяемая аппаратурным разбросом и разбросом, обусловленным шириной начального распределения нейтронов, которое формируется при неупругом рассеянии первичных 14-мэвных нейтронов в свинце.

Величина b^2 в области энергий $E \gg AkT$ должна согласно (2.5) равняться

$$b^2 = \frac{16 \ln 2}{3A}.$$

Для свинца должно быть $b^2 = 0{,}018$. Из наклона прямой на рис.5 следует значение $b^2 = 0{,}029 \pm 0{,}0015$, что на 60% больше расчетной величины. Анализ возможных причин расхождения привел к выводу, что вероятной основной причиной уширения спектра являются примеси легких ядер к свинцу. Для объяснения ширины и формы наблюдаемых кривых распределения времен замедления необходимо предположить наличие в свинцовой призме водорода в количестве $3{,}5 \cdot 10^{-4}$ атомов H/атом Pb и кислорода в количестве $6 \cdot 10^{-3}$ атомов O/атом Pb. На рис.3 сплошной линией показана форма кривой $\mathcal{J}(t)$, полученная численным расчетом для замедления в свинце, содержащем указанное количество примесей; пунктир — аналогичный расчет

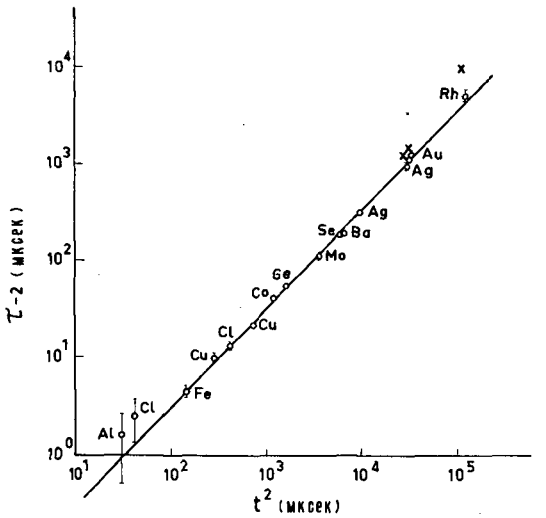

Рис.5

Полуширина τ функции распределения времен замедления в зависимости от среднего времени замедления t:

XXX – измеренные значения τ;
o o o – значения τ после вычитания вклада теплового уширения (пренебрежимо малого при t<100 мксек).

с гауссовой функцией распределения, соответствующей отсутствию в свинце водородной примеси. Как видно, расчетная кривая хорошо описывает эксперимент. Такое же хорошее согласие было получено для резонансов лантана (73 эв), золота (4,9 эв) и иридия (1,3 и 0,65 эв). Для низковольтных резонансов золота и иридия для получения согласия необходимо было учесть второй член выражения (2.5), описывающий влияние теплового движения и химической связи. Влияние этих факторов видно и из рис.5; измеренные полуширины для резонансов Ag, Au и Rh (кресты) располагаются заметно выше прямой, проведенной из области малых времен замедления. Разность $\Delta\tau^2 = \tau^2_{\text{измер}} - \tau^2_{\text{экстраполир}}$ для этих резонансов отложена на рис.6 в функции обратной величины энергии резонанса. Прямая линия соответствует ожидаемой величине $\Delta\tau^2$ согласно выражению (2.5). Как видно, эксперимент хорошо описывается этим выражением.

В опытах с железным и графитовым замедлителями измерения, аналогичные описанным выше, проводились только для резонанса золота с E_0 = 4,9 эв [18]. Как видно из рис.7 и 8, полученные результаты хорошо описываются теорией, причем сколько-нибудь заметного влияния неучтенных примесей не чувствуется. Это и не удивительно, так как при данной концентрации примеси ее влияние на дисперсию пропорционально квадрату отношения массовых чисел замедлителя и примеси, т.е. для железа и графита соответственно в 14 и 300 раз меньше, чем для свинца.

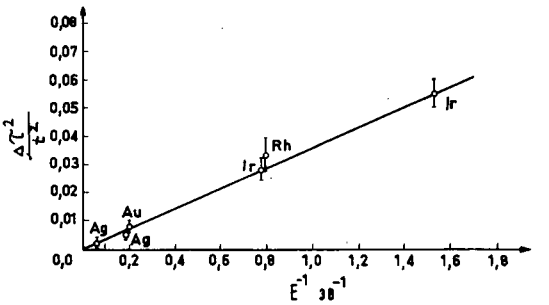

Рис.6

Влияние теплового движения на полуширину функции распределения времен замедления нейтронов до конечной энергии E.
Прямая линия — теоретическая зависимость.

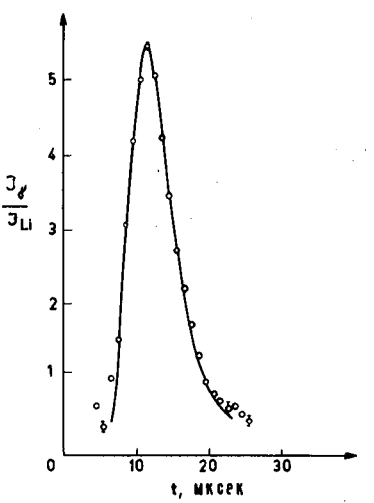

Рис.7

График $\mathcal{J}(t)$ для образца золота в графитовой призме.
Сплошная кривая — теоретический расчет.

B. Термализация

Для изучения термализации нейтронов в свинце было проведено измерение линии поглощения с образцом кадмия. В области малых энергий кадмиевый образец поглощает каждый падающий нейтрон ввиду чего

$$\mathcal{J}_\gamma(t) = \text{const}\,\rho(t)\cdot\bar{v}(t)\,,$$

т.е.

$$\bar{v}(t) = \text{const}\,\frac{\mathcal{J}_\gamma(t)}{\rho\ (t)}\,. \qquad (3.4)$$

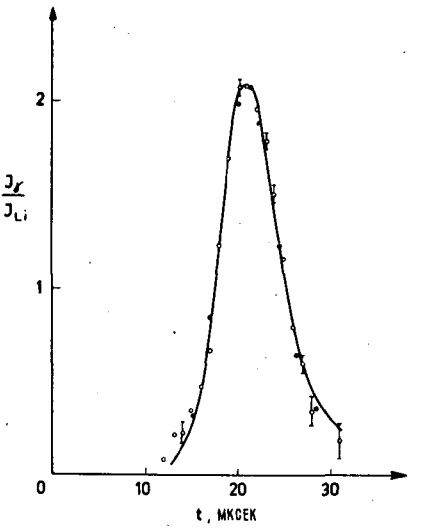

Рис.8

График $\mathcal{I}(t)$ для образца золота в железной призме. Сплошная кривая – теоретический расчет.

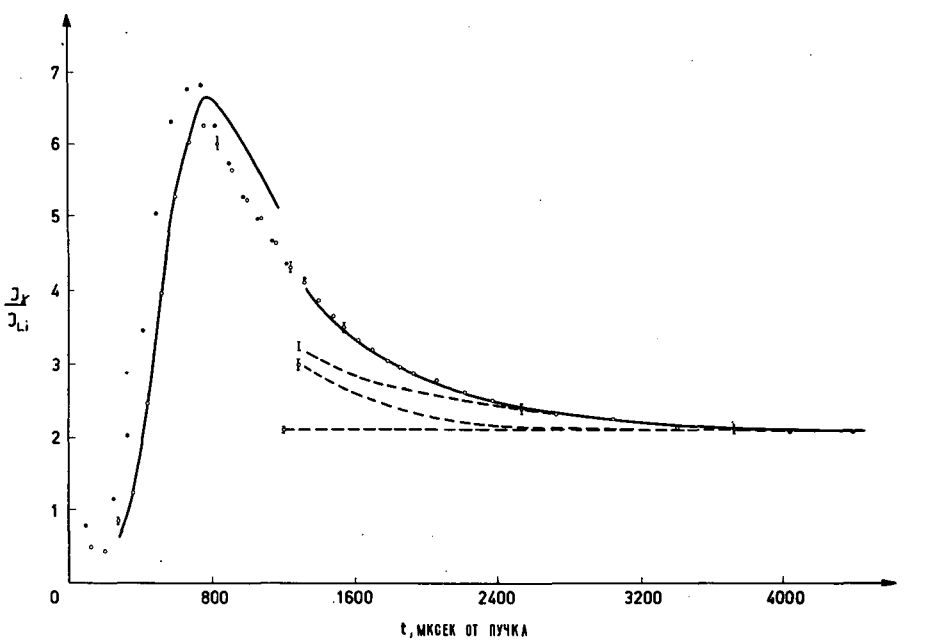

Рис.9

График $\mathcal{I}(t)$ для образца кадмия в свинцовой призме. Черные и светлые кружки – образец Cd толщиной соответственно 1 и 0,5 мм; сплошные кривые – расчет; пунктир – вклад 1-й и 2-й неравновесных групп.

Результаты измерений приведены на рис.9. В области $t<800$ мксек влияние теплового движения и химической связи может быть еще учтено с помощью выражения (2.5), а энергетический спектр может считаться гауссовским. Это позволяет рассчитать теоретическую форму линии поглощения, которая (после соответствующей нормировки) изображена на рис.9 сплошной линией. Нормировочный коэффициент в этом расчете нетрудно связать с константой выражения (3.4), что в свою очередь позволяет определить абсолютную величину асимптотического значения средней скорости нейтронов при больших временах замедления. Для наиболее вероятной скорости отсюда получается значение

$$v_0 = (2{,}21 \pm 0{,}11) \cdot 10^5 \text{ см/сек},$$

что совпадает с вероятной скоростью максвелловского распределения для температуры 300° К равной $2{,}2 \cdot 10^5$ см/сек. Подробности этого эксперимента описаны в работе [7].

Как видно из рис.9, равновесное значение средней скорости устанавливается при временах замедления порядка 4000 мксек. Приближение к равновесию может быть описано выражением (2.6) с константами λ_1 и λ_2, рассчитанными в трехгрупповом приближении по модели тяжелого одноатомного газа. Кенжебаевым [27] были выполнены также расчеты постоянных a и b в рамках той же модели. Результаты расчета удовлетворительно согласуются с экспериментальными данными в области не очень больших времен ($1300 < t < 3600$ мксек), но расходятся при больших временах, что возможно указывает на отсутствие в данном случае ненулевых дискретных собственных значений уравнения переноса нейтронов [17].

4. СПЕКТРОМЕТР НЕЙТРОНОВ ПО ВРЕМЕНИ ЗАМЕДЛЕНИЯ В СВИНЦЕ

Группировка скоростей нейтронов в сравнительно узком интервале вокруг среднего значения $\bar{v}$ в процессе замедления нейтронов в тяжелой среде натолкнула на мысль [1] об использовании этого эффекта для создания нового метода спектрометрии нейтронов – спектрометра по времени замедления.

Энергетическое разрешение такого спектрометра не превышает 30%, что ограничивает область его применения изучением ядер с малой плотностью уровней и измерением сечений захвата, усредненных по резонансам.

Спектрометр подробно описан в Трудах Физического института [6–9]. Он представляет собой свинцовый куб с ребром около 2 м, в центре которого с помощью описанного выше генератора нейтронов создаются вспышки нейтронов с энергией 14 Мэв длительностью 0,5–1 мксек. Для измерения энергетической зависимости сечений исследуемых реакций в один из горизонтальных каналов свинцового куба (рис.1) помещается детектор продуктов реакции и исследуемый образец. С помощью многоканального временного анализатора находится интенсивность испускания продуктов реакции от захвата нейтронов в образце в функции времени замедления $\mathcal{J}_x(t)$. Эта величина получается вычитанием из измерений с образцом фона, измеряемого без образца; вводится также небольшая поправка, учитывающая активацию образца и захват нейтронов, оставшихся от предыдущей вспышки.

В той же точке куба проводятся измерения с пропорциональным счетчиком с тонким слоем бора ($\mathcal{J}_B(t)$). Поскольку сечение реакции $B^{10}(n, \alpha)$ подчиняется закону $1/v$, для тонкого образца мы имеем:

$$\frac{\mathcal{J}_x}{\mathcal{J}_B}(t) = k\langle\sigma_x(E)E^{\frac{1}{2}}\rangle, \qquad (4.1)$$

где скобки означают усреднение по спектру нейтронов в момент времени t.

Можно показать, что в общем случае (образец произвольной толщины, резонансы) имеет место соотношение:

$$\int_{t_1}^{t_2}\frac{\mathcal{J}_x}{\mathcal{J}_B}(t)dt = \frac{Ak}{2\Sigma_s\bar{\ell}}\sum_i\frac{A_{i\,рез}(\ell)}{E_{0i}} \qquad (4.2)$$

где Σ_s – макроскопическое сечение рассеяния замедлителя,

$\bar{\ell}$ – эффективная толщина образца в ядрах на $см^2$, энергия i-того резонанса, $A_{рез}(\ell) = \int_{рез}[1 - \exp(-e\sigma)]\frac{\Gamma\gamma}{\Gamma}dE$.

Применяя соотношение (4.2) к изолированному резонансу или группе резонансов с хорошо известными параметрами или применяя (4.1) к области тепловых энергий, где сечение захвата известно, можно определить градуировочный множитель k. После этого выражения (4.1) и (4.2) могут быть использованы для нахождения сечений захвата и параметров резонансов в остальной области энергий.

Детекторами для регистрации заряженных продуктов реакции (протонов и α-частиц) служили ионизационные камеры и пропорциональные счетчики с тонкими слоями B^{10}, Li^6F, а также наполненные He^3, BF_3, N_2. В случае исследования реакции Cl^{35} (n, p) использовался сцинтилляционный детектор с порошком ZnS(Ag), залитым CCl_4 – прозрачной жидкостью, игравшей роль образца и световода.

Детекторами акта радиационного захвата нейтронов служили пропорциональный счетчик с толстыми стенками и сцинтилляционный счетчик с кристаллом флюорита. Пропорциональный счетчик обладал чувствительностью к γ-лучам, пропорциональной их энергии, т.е. эффективность регистрации акта захвата нейтрона была пропорциональна энергии связи этого нейтрона в ядре, а следовательно, не зависела от спектра захватных γ-лучей.

Опыт использования спектрометра нейтронов по времени замедления позволяет отметить некоторые особенности этого метода:

а) широкий энергетический диапазон дает возможность производить нормировку кривой сечения по низкорасположенным резонансам или тепловой области;

б) рассеяние нейтронов в образце не влияет на уровень фона;

в) спектрометр может быть полезен для реакторостроителей, поскольку он позволяет измерять эффективные резонансные интегралы для отдельных элементов, изотопов, сложных сплавов, определять зависимость этих интегралов от толщины и геометрии образцов;

г) метод характеризуется большой светосилой, причем выигрыш в интенсивности по сравнению с методом времени пролета с тем же источником нейтронов и при том же разрешении составляет 3—4 порядка;

д) измерительная установка сравнительно проста и дешева.

Основным недостатком спектрометра по времени замедления нейтронов в свинце является его плохое разрешение. Кроме того, ухудшение разрешения в киловольтной области, вызванное неупругим рассеянием нейтронов на ядрах свинца, приводит к ограничению сверху диапазона исследования энергией 30—50 кэв.

Последний недостаток может быть ликвидирован, если использовать источник, дающий приблизительно моноэнергетические нейтроны с энергией ниже 570 кэв. Это, по-видимому, позволит повысить верхнюю границу по энергии для спектрометра до нескольких сот кэв. Однако энергетическая полуширина линии ~30% является принципиальным пределом для спектрометров данного типа, если исключить область вблизи начальной энергии нейтронов E_0, в которой дисперсия меньше асимптотической на фактор $(1-E/E_0)$.

5. ИССЛЕДОВАНИЕ СЕЧЕНИЙ РЕАКЦИЙ (n, p), (n, α) и (n, γ)

A. Реакции (n, p) и (n, α)

Трудности градуировки потоков нейтронов в области до 100 кэв не позволяют провести прямого измерения энергетической зависимости сечения реакций в этой области с большой точностью. Поэтому были проведены измерения энергетической зависимости отношения сечений реакций $Li^6(n,\alpha)$, $B^{10}(n,\alpha)$, $He^3(n,p)$ [19] и $N^{14}(n,p)$ [8] в области энергий нейтронов от 0 до 25 кэв с точностью порядка 1% и лучше.

Плохое разрешение спектрометра не могло помешать проведению этих измерений ввиду плавного хода сечения этих реакций. Рис.10—12 иллюстрируют полученные экспериментальные данные. Наиболее интересными результатами этих измерений явилось обнаружение постоянных отрицательных слагающих сечений реакций и получение указаний на существование виртуального возбужденного состояния ядра He^4.

Из общей теории ядерных реакций следует, что в области малых энергий сечение реакции зависит от энергии по закону [20, 21]

$$\sigma_r(E) = (\sigma_r E^{\frac{1}{2}})_0 (E^{\frac{1}{2}} - \alpha + \epsilon E^{\frac{1}{2}} + \ldots), \qquad (5.1)$$

где $-\alpha(\sigma_r E^{\frac{1}{2}})_0$ — упомянутая постоянная отрицательная слагающая сечения,

$$\alpha = \alpha_0 \left[\frac{x_-^2}{g_-} + \frac{(1-x_-)^2}{(1-g_-)} \right], \qquad (5.2)$$

$g = \dfrac{I}{(2I+1)}$ — статистический вес канала реакции со спином канала $\mathcal{I} = I - 1/2$;

x_- — относительный вклад этого канала в тепловое сечение;

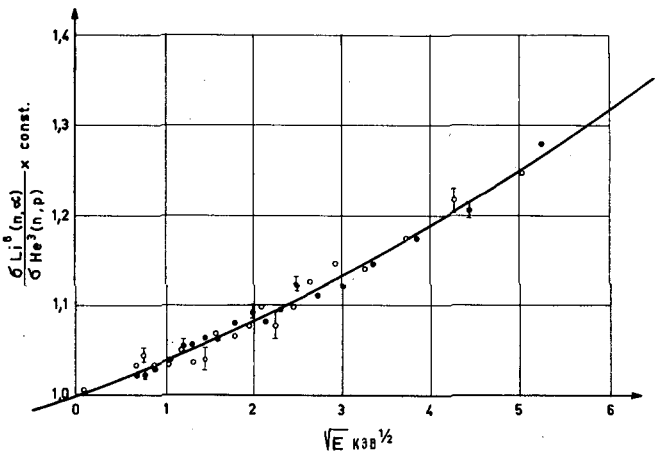

Рис.10

Отношение сечений реакций $Li^6(n, \alpha)$ и $He^3(n, p)$ в функции корня из энергии нейтрона:

светлые кружки – точки 1-й серии измерений; черные кружки – точки 2-й серии измерений; сплошная кривая – парабола $1+\alpha\sqrt{E}+\beta E$, проведенная методом наименьших квадратов по точкам 2-й серии измерений.

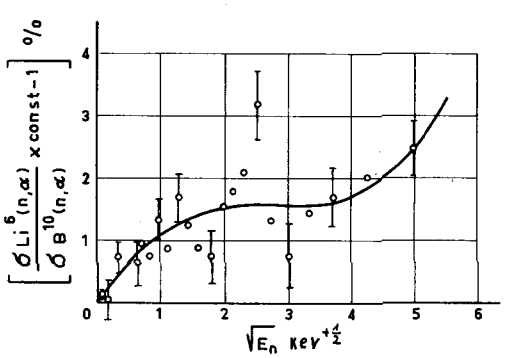

Рис.11

Отклонение отношения сечений реакции $Li^6(n,\alpha)$ и $B^{10}(n, \alpha)$ от его значения в тепловой области.

$$\alpha_0 = \frac{m}{\pi\hbar^2}\left(\frac{A}{A+1}\right)^2 (\sigma_2 E^{\frac{1}{2}})_{E=0} \qquad (5.3)$$

Для отношения сечений двух реакций из (5.1) следует:

$$\frac{\sigma_1(E)}{\sigma_2(E)} = \left(\frac{\sigma_1}{\sigma_2}\right)_{E=0} \cdot [1 + (\alpha_2 - \alpha_1)E^{\frac{1}{2}} + \beta E + \dots] . \qquad (5.4)$$

Экспериментальные данные хорошо описываются выражением (5.4), причем член пропорциональный $E^{1/2}$ играет при малых энергиях основную роль

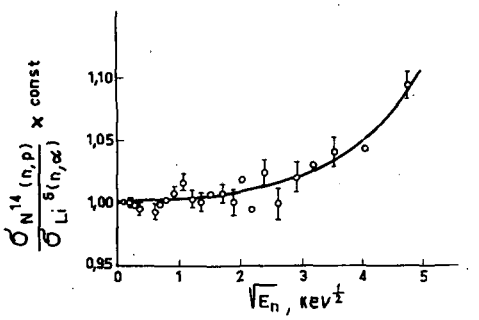

Рис.12

Отношение сечений реакций $N^{14}(n, p)$ и $Li^6(n, \alpha)$.

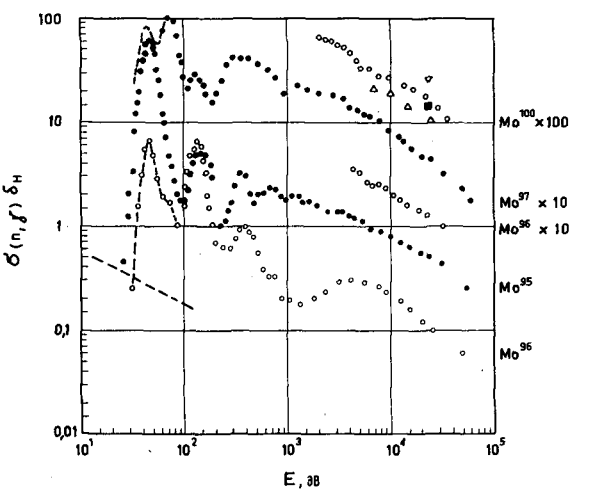

Рис.13

Энергетическая зависимость сечения захвата нейтронов изотопами молибдена:

▽ Хьюмель; ■ Вервье; △ Хьюсон.

в отклонении отношения сечений от константы. Поскольку для Li^6 фактор α мал, оказалось возможным определить величину α для реакций на He^3 и B^{10}. Постоянные слагающие сечений этих ядер были найдены равными соответственно -1,1 и -0,4 барна.

Сравнение измеренной величины α с выражениями (5.2), (5,3) позволило определить вклад спиновых каналов реакций в тепловые сечения реакций $B^{10}(n, \alpha)$ и $He^3(n, \alpha)$. Последняя идет преимущественно по каналу со спином $\mathscr{I}=0$; вклад канала $\mathscr{I}=1$ составляет $6 \pm 6\%$. Это обстоятельство вместе с характером энергетической зависимости сечения реакции $He^3(n, p)$ привело к заключению о существовании уровня He^4 со спином и четностью 0^+, расположенного в районе энергий возбуждения He^4 около 20 Мэв [19]. Этот результат, вызвавший в свое время возражения, сейчас подтверждается экспериментальными исследованиями других авторов [22].

ЗНАЧЕНИЯ РЕЗОНАНСНЫХ ИНТЕГРАЛОВ ПОГЛОЩЕНИЯ

табл.

Элемент	$R_\gamma(1/v)$	$R'_{\gamma\,расч}$	$R'_{\gamma\,эксп}$	R_γ	R_γ (Другие авторы)
Cl	13,5		0,5 ± 0,05	14,1 ± 0,8	12; 12,8±1,7
Sc				10,4 ± 0,4	
V	2,2			2,45 ± 0,02	3,3±0,8; 2,2
Cr	1,36 ±0,1		0,12 ± 0,02	1,5 ± 0,1	2,6±1,1; 1,9
Cr^{50}	7,1 ±0,4		0,3 ± 0,1	7,4 ± 0,4	
Cr^{52}	0,35 ±0,04		0,08 ± 0,01	0,43 ± 0,04	
Cr^{53}	7,9 ±0,7		0,5 ± 0,05	8,4 ± 0,7	
Cr^{54}	<0,13		$<10^{-2}$	<0,13	
Fe	1,1 ±0,03	~0,01	0,12 ± 0,02	1,22 ± 0,04	2,3±0,4; 1,8±0,4; 2,1
Ni	2,1 ±0,09	~0,03	0,07 ± 0,01	2,2 ± 0,1	3,2±0,5; 3,2
Cu	1,65 ±0,01		2,6 ± 0,3	4,2 ± 0,3	3,7±0,8; 2,8±0,5; 4,4±0,2
Br	2,9 ±0,15	78 ±10	12 ± 1 (330 эв)	93 ±10	118±14
Rb	0,32 ±0,03	~0,1	4,2 ± 1,5	4,5 ± 1,5	9,0±2,8; 0,54±0,06
Zr	0,081			1,1 ± 0,2	0,7±0,1; 2,3±0,5; 3,7±0,5; 3
Zr^{90}	0,044			0,2 ± 0,02	
Zr^{91}	0,66			7,3 ± 0,8	
Zr^{94}	0,035			0,23 ± 0,02	
Nb	0,51 ±0,02	8,0 ± 1	1,8 (>1250 эв)	10,3 ± 1,0	8,3; 13±5; 8,3±1,1
Mo	1,2 ±0,05	23,2 ± 3	1,4 ± 0,2 (>800 эв)	26 ± 3	13,8±1,7; 13; 19±2,5
Mo^{95}	6,1			108 ±27	
Mo^{96}	0,53			27 ± 5	
Mo^{97}	0,97			14,5 ± 1,5	
Mo^{98}	0,2 ±0,2	4,5 ± 1	1,8 ± 0,3 (>500 эв)	6,5 ± 1,2	10,9±25; 5,6±1,6

(продолжение табл.)

Элемент	$R_\gamma(1/v)$	$R'_{\gamma расч}$	$R'_{\gamma эксп}$	R_γ	R_γ (Другие авторы)
Mo^{100}	0,2 ±0,2	6,2	1,1 ± 0,2	1,3 ± 0,3	4,0 ± 0,2; 6,2 ± 2,5
Sb	2,5	131 ±15	25 ± 3 (> 50 эв)	158 ±15	106 ± 13; 150
J	3,1	117 ±12	25 ± 3 (> 100 эв)	145 ±12	107 ± 12; 140; 180 ± 30; 154 ± 40
Cs	13	375 ±70	15 ± 2 (> 250 эв)	885 ±70	169 ± 28; 490 ± 80; 420 ± 80; 370 ± 50
La	3,9 ±0,1	9,2 ± 0,9	0,9 ± 0,1 (> 370 эв)	13,9 ± 0,9	11; 11,3; 5,5 ± 2
Pr	5,0 ±0,1	9,7 ± 0,7	2,9 ± 0,3 (> 300 эв)	17,6 ± 0,8	11,3; 23,5 ± 9; 7 ± 3
Eu			72 ± 7 (> 500 эв)		
Eu^{151}			91 ±13 (> 500 эв)		3000
Eu^{153}			50 ± 5 (> 500 эв)		950; 1280 ± 100; 1380 ± 200
Ho	28,6 ±1,3	602 ±64	64 ± 6 (> 130 эв)	695 ±65	
Lu			15 ± 2 (> 1 кэв)		720 ± 70
Ta	9,23 ±0,44		12,6 ± 1,3 (> 1 кэв)		590; 1100 ± 400; 474 ± 62
W	8	303 ±30	27 ± 4 (> 600 эв)	338 ±30	290 ± 35; 340 ± 60
W^{184}	0,9			9,6	
Re	37,8 ±1,8				622
Au	43,5 ±0,1		9,6 ± 0,9 (> 1 кэв)		1558; 1513
Tl	1,50 ±0,22	9,1 ± 1,5	1,5 ± 0,2 (> 600 эв)	12 ± 2	38,4
Tl^{203}	5,0 ±0,4	31 ± 4	4 ± 1 (> 600 эв)	40 ± 5	129
Tl^{205}	0,35 ±0,035		0,4 ± 0,08 (> 600 эв)	0,7 ± 0,1	0,5

Обсуждение других аспектов описанных опытов см. в работах [8, 19]. Исследование резонансов в реакции $Cl^{35}(n, p)$ описано в работе [23].

Б. Реакции (n, γ)

Измерения энергетической зависимости сечения радиационного захвата нейтронов в области энергий от долей эв до ~50 кэв велись в двух направлениях:

а) Изучение ядер с малой плотностью уровней, где разрешение спектрометра позволяет разделять отдельные уровни и обнаруживать новые, в том числе с отрицательной энергией, а также определять резонансные интегралы захвата.

б) Измерение усредненных по резонансам сечений захвата нейтронов в средних и тяжелых элементах и разделенных изотопах.

Были проведены исследования радиационного захвата нейтронов более 50 элементов и разделенных изотопов [24]. В качестве примера на рис.13 приведены кривые сечений для молибдена и его изотопов.

На рис.14 приведена зависимость $\overline{\sigma(n, \gamma)}$ от атомного веса ядра-мишени для средней энергии нейтронов 30 кэв. В зависимости сечения захвата от массового числа четко проявилось влияние замкнутых протонных и нейтронных оболочек, а также влияние четности числа нуклонов в ядре-мишени. Сечения захвата четно-четных изотопов примерно в 5 раз меньше сечений захвата нечетных изотопов. Особенно интересным является то обстоятельство, что сечения нечетно-четных ядер ложатся на одну кривую с сечениями четно-нечетных ядер.

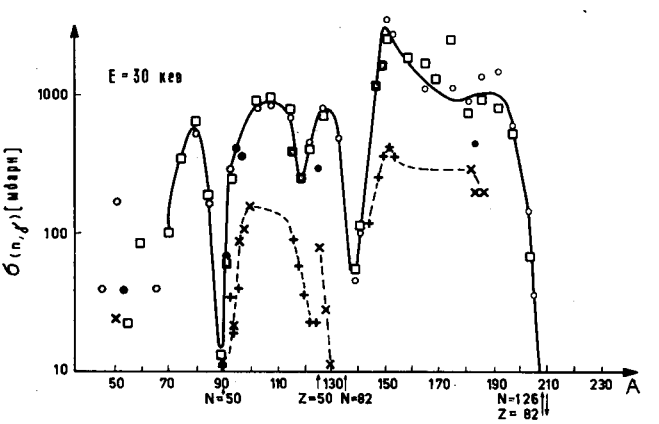

Рис.14

Зависимость усредненного сечения захвата нейтронов с энергией 30 кэв от массового числа ядра-мишени.

Ядро-мишень ч.-ч.	ч.-н.	н.-ч.	
×	●	○	ФИАН
+	■	□	ORNL

Усредненные нейтронные сечения в области энергий ниже 50 кэв обусловлены в основном захватом s- и p-нейтронов. Используя различную энергетическую зависимость вкладов в сечение нейтронов с разными ор-

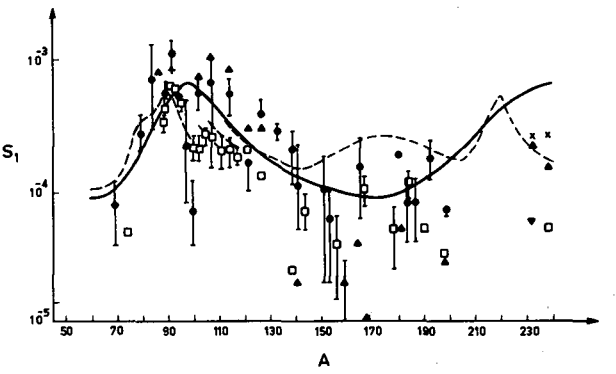

Рис.15

Зависимость силовой функции для p-нейтронов от массового числа ядра-мишени. Сплошная и пунктирная кривые — два варианта теоретических расчетов:

▲ ORNL; × Harwell;
□ DUKE; ▼ ANL;
● ФИАН; + Wisconsin;

битальными моментами, мы проанализировали усредненные сечения захвата с целью определения средних характеристик взаимодействия s- и p-нейтронов (силовых функций $S_0 = (\overline{\Gamma_n^0/D})$ и $S_1 = (\overline{\Gamma_n^1/D})$ и величин $(\Gamma_\gamma/D)_0$ и $(\Gamma_\gamma/D)_1$.

Результаты такого анализа для силовой функции p-нейтронов приведены на рис.15. Хорошее согласие получено с данными Гиббонса и др. [25], анализировавших сечения захвата. В то же время последние результаты группы Дюкского университета [26], опирающиеся в основном на анализ полных сечений, лежат регулярно приблизительно в 2 раза ниже. На рисунке приведены также теоретические кривые зависимости $S_1(A)$, построенные на основании различных вариантов оптической модели ядра. К сожалению, имеющиеся в настоящее время экспериментальные результаты по силовым функциям недостаточно точны для выбора определенного оптического потенциала взаимодействия.

Для существенного улучшения точности определения силовых функций p-нейтронов целесообразно проводить комплексные измерения нескольких *видов усредненных сечений*.

Проведенные измерения позволили получить для широкого круга элементов и отдельных изотопов значения резонансных интегралов поглощения (см. таблицу).

Обращают на себя внимание существенные расхождения в резонансных интегралах Cr, Fe и Ni, полученных "глобальными" методами в измерениях на реакторах и полученных в измерениях энергетической зависимости сечений захвата. Причины расхождений пока указать трудно. Однако к сближению результатов может привести учет в измерениях на реакторах проникновения нейтронов за кадмиевую границу за счет потенциального рассеяния на ядрах образца, вклада примесей, а также учет захвата нейтронов после рассеяния в пределах того же резонанса.

ЛИТЕРАТУРА

[1] ЛАЗАРЕВА Л.Е., ФЕЙНБЕРГ Е.Л., ШАПИРО Ф.Л., ЖЭТФ, 29 (1955) 381.
[2] БЕРГМАН А.А., ИСАКОВ А.И., МУРИН И.Д., ШАПИРО Ф.Л., ШТРАНИХ И.В., КАЗАРНОВСКИЙ М.В., Труды Женевской конференции 1955 г. 4 (1957) 166.
[3] CHANDRAMOLESHWAR K., NAVALKAR M.P., ROMAKRISHNA D.V.S., ROMANA R., SUBBARAMU K.R., Preprint A.E.E. Trombay (1964)
[4] MITZEL F., PLENDL M.S., Nukleonik, 6 (1964) 371.
[5] КАЗАРНОВСКИЙ М.В., Труды ФИАН, 11 (1960) 173.
[6] ШАПИРО Ф.Л., Труды ФИАН, 24 (1964) 3.
[7] ИСАКОВ А.И., Труды ФИАН, 24 (1964) 68.
[8] БЕРГМАН А.А., Труды ФИАН, 24 (1964) 169.
[9] ПОПОВ Ю.П., Труды ФИАН, 24 (1964) 111.
[10] ФРАНК И.М., Труды ФИАН, 24,(1964) 203.
[11] MARSHAK R., Rev. Mod. Phys., 19 (1947) 185.
[12] von DARDEL G.F., Trans. Roy. Inst. Techn., 75 (1954) 1; 94 1; Phys. Rev. 94(1954)1272;
WALLER I., Proc 2"nd ICPUAE, Geneva, 16 (1958) 450;
ERIKSSON K.E., Arkiv. Fys., 16, 1 (1959);
SVARTHOLM N., Trans. Chalmers Univ. Techn. N 164, Göteborg (1955);
KOPPEL J., Nucl. Sci. Eng., 8 (1960) 157;
BOFFI V.C., Ann. of Phys., 27 (1964) 297.
[13] WAHLEN R., Rec. Trav. Inst. Rech. Struct. Matiere (Belgrade, 1955).
[14] КАЗАРНОВСКИЙ М.В., Атомная энергия, 4 (1958) 539. Диссертация (1955). Труды ФИАН, 11 (1959) 175.
[15] ФРАНК И.М., Труды ФИАН, 14 (1962) 117.
von DARDEL G.F., Trans. Roy. Inst. Techn. 75, 1 (1954); Phys. Rev. 94, (1954) 1272.
[16] КАЗАРНОВСКИЙ М.В., ШАПИРО Ф.Л., Сб. "Нейтронная физика", Атомиздат, 1961, стр.169;
КАЗАРНОВСКИЙ М.В., ШАПИРО Ф.Л., СТЕПАНОВ А.В., Вторая Международная конференция по мирному использованию атомной энергии, Женева 1958 г. Доклады советских ученых, т.1, Атомиздат, М., 1959, стр.469.
[17] КАЗАРНОВСКИЙ М.В., Нестационарный перенос нейтронов. Лекции, прочитанные в Междунардной летней школе по физике реакторов, Польша, 1964 г. (в печати).
[18] ИСАКОВ А.И., ЖЭТФ. 41 (1961) 1037.
[19] БЕРГМАН А.А., ИСАКОВ А.И., ПОПОВ Ю.П., ШАПИРО Ф.Л., ЖЭТФ, 33 (1957) 9.
БЕРГМАН А.А., ИСАКОВ А.И., ПОПОВ Ю.П., ШАПИРО Ф.Л., Сб. "Ядерные реакции при малых и средних энергиях" АН СССР, 17 (1958).
БЕРГМАН А.А., ШАПИРО Ф.Л., ЖЭТФ, 40 (1961) 1610.
[20] ШАПИРО Ф.Л., ЖЭТФ, 34 (1958) 1648.
[21] ЛАНДАУ Л.Д., ЛИФШИЦ Е.Д., Квантовая механика, гл.18, Физматгиз, М., 1963.
[22] POPPE C.H., Physics Lett. 2 (1962) 171.
LEFEVRE H., BORCHERS R.R., POPPE C.H., Phys. Rev. 128 (1962) 1328.
WERNTZ C., Phys. Rev. 128 (1962) 1336.
БАЛАШКО Ю.Г., БАРИТ И.Я.,ДУЛЬКОВА Л.С., КУРЕПИН А.Б., Известия АН СССР, серия физическая, 28 (1964) 1124.
TARMIE N., SILBERT M.G., SMITH D.B., LOOS T.S., Phys. Rev., 130 (1963) 1987.
[23] ПОПОВ Ю.П., ШАПИРО Ф.Л., ЖЭТФ, 40 (1961) 1610.
[24] БЕРГМАН А.А., ИСАКОВ А.И., ПОПОВ Ю.П., ШАПИРО Ф.Л., Сб. "Ядерные реакции при малых и средних энергиях" АН СССР, М., 1958, стр.140.
ИСАКОВ А.И., ПОПОВ Ю.П., ШАПИРО Ф.Л., ЖЭТФ, 38 (1960) 989.
КАШУКЕЕВ Н.Т., ПОПОВ Ю.П., ШАПИРО Ф.Л., Journ. Nucl. Energy 14 (1961) 76.
ИСАКОВ А.И., ПОПОВ Ю.П., ШАПИРО Ф.Л., Труды Ташкентской конференции по мирному использованию атомной энергии 1959 г., т.1, 1961, стр.62.
ПОПОВ Ю.П., ШАПИРО Ф.Л., ЖЭТФ, 42 (1962) 988.
КАПЧИГАШЕВ С.П., ПОПОВ Ю.П., Атомная энергия, 15 (1963) 120.
КАПЧИГАШЕВ С.П., ПОПОВ Ю.П., Атомная энергия, 16 (1964) 256.
КОНКС В.А., ПОПОВ Ю.П., ШАПИРО Ф.Л., ЖЭТФ, 46 (1964) 80.
КОНКС В.А., ШАПИРО Ф.Л., ЖЭТФ, 47 (1964) 795.
РОМАНОВ С.А., ШАПИРО Ф.Л., Ядерная физика, 1 (1965) 229.

КОНКС В.А., ФЕНИН Ю.И., Материалы рабочего совещания по взаимодействию нейтронов с ядрами (1964 г.), Дубна, 1964, стр.100.
КАПЧИГАШЕВ С.П., ПОПОВ Ю.П., Материалы рабочего совещания по взаимодействию нейтронов с ядрами (1964 г), Дубна, 1964, стр.104.
[25] GIBBONS J.H., MACKLIN R.L., MILLER P.D., NEILER J.H., Phys.Rev. 122 (1961) 182.
MACKLIN R.L., GIBBONS J.H., IUNADA T., Phys. Rev. 129 (1963) 2695.
[26] SETH K.K., TABONY R.H., BILPUCH E.G., NEWSON H.W., Physics Letters 13 (1964) 70.
[27] КЕНЖЕБАЕВ Ш., "Атомная энергия" (в печати).

DISCUSSION

P. ZWEIFEL (Chairman): Could you explain the meaning of the symbols τ and $\bar{t}$ in your formula $\tau^2 = b^2\bar{t}^2 + a^2$?

Yu. POPOV: The symbol τ is the resonance width at half height as determined mainly by spectrometer resolution. The symbol $\bar{t}$ represents the mean neutron slowing-up time to an energy of E_0, as determined by the position of the resonance peak.

P. ZWEIFEL: Is τ then a reduced width which would be obtained if the resonance width of the detector were zero?

Yu. POPOV: Yes, of course. The value of τ is determined fundamentally by the distribution of neutron speeds around a mean value. Generally speaking, the natural resonance width Γ does not make any appreciable contribution to τ. We made the necessary corrections but these were only of any significant size for the low resonances of rhodium, silver and gold. The uncorrected values of τ for these resonances are indicated by crosses in Fig. 5 of the paper.

K.H. BECKURTS: In your paper you make the suggestion that the energy range of the spectrometer could perhaps be increased by the injection of neutrons below 540 keV, the threshold for inelastic scattering in lead. We considered this possibility some time ago but we found that there is no suitable neutron source of sufficient strength in that energy range. Do you agree with that or have you found a good solution?

Yu. POPOV: Neutron sources at this energy level do generally have low yields. By using slowing-down time spectrometry, however, it is possible to obtain appreciable neutron densities around the specimen, particularly at low slowing-down times. If therefore we perform our measurements in the range of tens and hundreds of keV separately, using neutrons from the (p,n) reaction on heavier targets, it can be hoped that the intensity will be sufficient to guarantee the necessary statistical accuracy. The accelerator will obviously have to produce large currents.

P. ZWEIFEL: I presume you can make measurements of cross-sections very rapidly since you obtain all your points in the same measurement?

Yu. POPOV: Yes, it takes a day to measure the whole cross-section curve for one sample. In the case of heavy nuclei with large cross-sections we can measure two or three samples in a day.

GENERAL DISCUSSION

P. ZWEIFEL (Chairman): I now call on Mr. Jonsson, who would like to make a comment on the results of some recent work in Sweden.

E. JONSSON: This work, which was carried out by E. Johansson, M. Lindberg, J. Mednis and myself at the natural-uranium heavy-water reactor R1 in Stockholm, involved a series of experimental and theoretical investigations on neutron spectra in lattice cells. The neutron spectra were measured with a fast chopper in the energy region 0.01-100 eV. For the calculations the THERMOS code with different scattering models was used.

The following cases were studied:

Case 1: Scalar-flux spectra inside uranium tubes surrounded by D_2O

In these investigations three cells were used, each containing a uranium tube surrounded by D_2O. The tubes were 40 cm long; the inner diameters varied from 14.1 to 42.4 mm and the wall thickness from 1.15 to 9.9 mm. The beam spectra from the lead scatterers, placed inside the tubes, corresponded to the spectra of the angular flux integrated over all angles. The accuracy of the spectra was ±4% over the energy region 0.02-0.2eV.

The THERMOS code was used with three different scattering models for deuterium — the Brown-St. John free gas model ($D_{mass} = 3.595$), the effective-width model, and the Nelkin-Honeck model. For the THERMOS treatment the six nearest fuel rods were included, which made the choice of cell radii less sensitive.

With all three models the code reproduced the thermal spectra within a few per cent. The effective-width model and the Nelkin-Honeck model also yielded reasonable agreement in the epithermal region. The free gas model, however, produced an overestimation of the epithermal level.

Case 2: Scalar flux spectra inside an annular region of H_2O or D_2O placed in one of the tubes above

Inside the largest of the tubes above it was possible to provide for an annular region of moderator, H_2O, D_2O, and mixtures of these were used. This fluid layer was 11.3 mm thick and its temperature was either 22 or 80°C. The neutron spectra were taken from a lead scatterer as above.

With D_2O the spectrum was only slightly softer than in the empty tube, but when the D_2O was replaced by H_2O the spectrum changed considerably. The computed thermal spectra were slightly softer than the chopper spectra, but in the joining region (around the Pu^{239} resonance at 0.3 eV) the calculations yielded too low an estimate of the flux. This effect may be important in plutonium systems.

Case 3: Scalar flux spectra inside a UO_2 tube at temperatures up to 800°C

A cell with a UO_2 tube was also investigated. The UO_2 was heated by the fissions and the temperature rose to 800°C. The results are not yet

available, but it would appear that the spectral shift caused by the temperatures is quite large.

Case 4: Angular flux spectra at various positions in the moderator of a D_2O-uranium cell

In this case the spectra of the angular flux were measured at various positions in a D_2O-uranium cell. Determinations were made in particular of the outgoing flux from a rod.

On the basis of the scalar flux from THERMOS the spectra of the angular flux were calculated for some of the positions used in the experiments. Good agreement was found, which suggests that the THERMOS code reproduces the scalar flux at various positions quite well.

C. A. PRESKITT: Was a P_0 scattering kernel or a P_1 scattering kernel used in this calculation?

H. HONECK: The THERMOS code only includes P_0 scattering kernels.

SYMPOSIUM ON PULSED NEUTRON RESEARCH

HELD AT KARLSRUHE, 10-14 MAY 1965

CHAIRMEN OF SESSIONS

Session I	N.G. SJÖSTRAND	Chalmer University of Technology, Göteborg
Session II	P. SCHOFIELD	Atomic Energy Research Establishment, Harwell
Session III	M. KAZARNOVSKY	P. N. Lebedev Institute of Physics, Moscow
Session IIIA	P. ZWEIFEL	Middle East Technical University, Ankara
Session IV	A. HENRY	Westinghouse Electric Corporation, Pennsylvania
Session V	V. RAIEVSKI	EURATOM, Ispra
Session VI	D. BRETON	Centre d'études nucléaires de Saclay
Session VII	F. STORRER	EURATOM, Brussels
Session VIII	K. WIRTZ	Kernforschungszentrum Karlsruhe

SECRETARIAT OF THE SYMPOSIUM

Scientific Secretaries:	G.R. KEEPIN	Division of Research and Laboratories
	D.W. MAGNUSON	Division of Research and Laboratories
Administrative Secretary:	H.H. STORHAUG	Division of Scientific and Technical Information
Editors:	D. NASTASIA-SCOTTI	Division of Scientific and Technical Information

	M.M. BROWN	Division of Scientific and Technical Information
Records Officer:	T.J. JONES	Division of Languages

IAEA SALES AGENTS

Orders for Agency publications can be placed with your bookseller or any of our sales agents listed below:

ARGENTINA
Comisión Nacional de
Energía Atómica
Avenida del Libertador
General San Martin 8250
Buenos Aires - Suc. 29

AUSTRALIA
Hunter Publications,
23 McKillop Street
Melbourne, C.1

AUSTRIA
Georg Fromme & Co.
Spengergasse 39
Vienna V

BELGIUM
Office international de librairie
30, avenue Marnix
Brussels 5

BRAZIL
Livraría Kosmos Editora
Rua do Rosario, 135-137
Rio de Janeiro

Agencia Expoente Oscar M. Silva
Rua Xavier de Toledo, 140-1° Andar
(Caixa Postal No. 5.614)
São Paulo

BYELORUSSIAN SOVIET SOCIALIST REPUBLIC
See under USSR

CANADA
The Queen's Printer
Ottawa, Ontario

CHINA (Taiwan)
Books and Scientific Supplies
Service, Ltd.,
P.O. Box 83
Taipei

DENMARK
Ejnar Munjsgaard Ltd.
6 Nörregade
Copenhagen K

FINLAND
Akateeminen Kirjakauppa
Keskuskatu 2
Helsinki

FRANCE
Office international de
documentation et librairie
48, rue Gay-Lussac
Paris 5e

GERMANY, Federal Republic of
R. Oldenbourg
Rosenheimer Strasse 145
8 Munich 8

ISRAEL
Heiliger and Co.
3 Nathan Strauss Street
Jerusalem

ITALY
Agenzia Editoriale Internazionale
Organizzazioni Universali (A.E.I.O.U.)
Via Meravigli 16
Milan

JAPAN
Maruzen Company Ltd.
6, Tori Nichome
Nihonbashi
(P.O. Box 605)
Tokyo Central

MEXICO
Librería Internacional
Av. Sonora 206
Mexico 11, D.F.

NETHERLANDS
N.V. Martinus Nijhoff
Lange Voorhout 9
The Hague

NEW ZEALAND
Whitcombe & Tombs, Ltd.
G.P.O. Box 1894
Wellington, C.1

NORWAY
Johan Grundt Tanum
Karl Johans gate 43
Oslo

PAKISTAN
Karachi Education Society
Haroon Chambers
South Napier Road
(P.O. Box No. 4866)
Karachi 2

POLAND
Ośrodek Rozpowszechniana
Wydawnictw Naukowych
Polska Akademia Nauk
Pałac Kultury i Nauki
Warsaw

SOUTH AFRICA
Van Schaik's Bookstore (Pty) Ltd.
Libri Building
Church Street
(P.O. Box 724)
Pretoria

SPAIN
Librería Bosch
Ronda de la Universidad 11
Barcelona

SWEDEN
C.E. Fritzes Kungl. Hovbokhandel
Fredsgatan 2
Stockholm 16

SWITZERLAND
Librairie Payot
Rue Grenus 6
1211 Geneva 11

TURKEY
Librairie Hachette
469, Istiklâl Caddesi
Beyoğlu, Istanbul

UKRAINIAN SOVIET SOCIALIST REPUBLIC
See under USSR

UNION OF SOVIET SOCIALIST REPUBLICS
Mezhdunarodnaya Kniga
Smolenskaya-Sennaya 32-34
Moscow G-200

UNITED KINGDOM OF GREAT BRITAIN AND NORTHERN IRELAND
Her Majesty's Stationery Office
P.O. Box 569
London, S.E.1

UNITED STATES OF AMERICA
National Agency for
International Publications, Inc.
317 East 34th Street
New York, N.Y. 10016

VENEZUELA
Sr. Braulio Gabriel Chacares
Gobernador a Candilito 37
Santa Rosalía
(Apartado Postal 8092)
Caracas D.F.

YUGOSLAVIA
Jugoslovenska Knjiga
Terazije 27
Belgrade

IAEA publications can also be purchased retail at the United Nations Bookshop at United Nations Headquarters, New York, at the news-stand at the Agency's Headquarters, Vienna, and at most conferences, symposia and seminars organized by the Agency.

In order to facilitate the distribution of its publications, the Agency is prepared to accept payment in UNESCO coupons or in local currencies.

Orders and inquiries from countries where sales agents have not yet been appointed may be sent to:

Distribution and Sales Unit, International Atomic Energy Agency,
Kärntner Ring 11, Vienna I, Austria

INTERNATIONAL
ATOMIC ENERGY AGENCY
VIENNA, 1965

ICE: USA and Canada: US $14.00